











Volume 185

Number 1

# THE BIOLOGICAL BULLETIN



AUG 26 1993

Woods Hole, Mass.

---

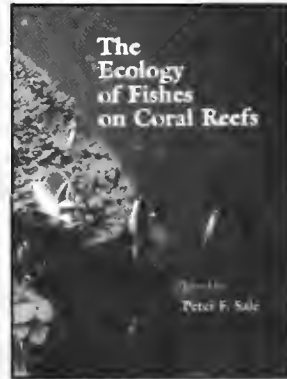
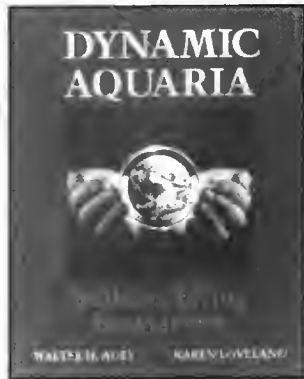
AUGUST 1, 1993

---

Published by the Marine Biological Laboratory

# Marine Science

New and Classic Titles from AP



## Marine Phytoplankton: A Guide to Naked Flagellates and Coccolithophorids

Edited by  
Carmelo R. Tomas

Authored by  
Jane Throndsen and  
Berit Heimdal

### Key Features

- Updates synthesis of modern and historical literature presented by active researchers in the field
- Offers details for identification to species level
- Provides extensive illustrations showing key diagnostic features for identification

August 1993, c. 327 pp., \$79.00 (tentative)  
ISBN: 0-12-693010-4

## Fish Physiology

Volume 12, Parts A and B  
The Cardiovascular System

Edited by  
William S. Hoar,  
Dave J. Randall, and  
Anthony P. Farrell

Part A  
1992, 340 pp., \$85.00/ISBN: 0-12-350435-X

Part B  
1992, 474 pp., \$99.00/ISBN: 0-12-350436-8

## The Ecology of Fishes on Coral Reefs

Edited by  
Peter F. Sale

1991, 754 pp., \$74.95  
ISBN: 0-12-615180-6

## Dynamic Aquaria

Building Living Ecosystems

Walter H. Adey  
Karen Loveland

1991, 643 pp., \$44.95  
ISBN: 0-12-043790-2

## Antarctic Fish Biology

Evolution in a Unique Environment

Joseph T. Eastman

This important volume provides an original synthesis and novel overview of Antarctic fish biology, detailing the evolution of these fish in some of the most unusual and extreme environments in the world. Focusing on one group of fish, the notothenioids, which contains the majority of the current organismal diversity, this book describes a fauna that has evolved in isolation and experienced incredible adaptive radiation by acquiring numerous physiological specializations.

May 1993, 322 pp., \$74.95  
ISBN: 0-12-228140-3

Order from your local bookseller or directly from



**ACADEMIC PRESS**

Order Fulfillment Dept. DM17915  
6277 Sea Harbor Drive, Orlando, FL 32887

CALL TOLL FREE

**1-800-321-5068**

FAX **1-800-336-7377**

Prices subject to change without notice. © 1993 by Academic Press, Inc. All Rights Reserved. KS/AB/MEH — 04083

# THE BIOLOGICAL BULLETIN

PUBLISHED BY  
THE MARINE BIOLOGICAL LABORATORY

## Associate Editors

PETER A. V. ANDERSON, The Whitney Laboratory, University of Florida

DAVID EPEL, Hopkins Marine Station, Stanford University

J. MALCOLM SHICK, University of Maine, Orono

## Editorial Board

WILLIAM D. COHEN, Hunter College

DAPHNE GAIL FAUTIN, University of Kansas

WILLIAM F. GILLY, Hopkins Marine Station,  
Stanford University

ROGER T. HANLON, Marine Biomedical  
Institute,  
University of Texas Medical Branch

CHARLES B. METZ, University of Miami

K. RANGA RAO, University of West Florida

RICHARD STRATHMANN, Friday Harbor Laboratories,  
University of Washington

STEVEN VOGEL, Duke University

SARAH ANN WOODIN, University of South Carolina

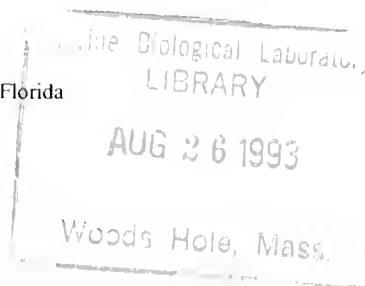
*Editor* MICHAEL J. GREENBERG, The Whitney Laboratory, University of Florida

*Managing Editor* PAMELA L. CLAPP, Marine Biological Laboratory

AUGUST, 1993

Printed and Issued by  
LANCASTER PRESS, Inc.

3575 HEMPLAND ROAD  
LANCASTER, PA





## THE BIOLOGICAL BULLETIN

THE BIOLOGICAL BULLETIN is published six times a year by the Marine Biological Laboratory, MBL Street, Woods Hole, Massachusetts 02543.

Subscriptions and similar matter should be addressed to Subscription Manager, THE BIOLOGICAL BULLETIN, Marine Biological Laboratory, Woods Hole, Massachusetts 02543. Single numbers, \$35.00. Subscription per volume (three issues), \$87.50 (\$175.00 per year for six issues).

Communications relative to manuscripts should be sent to Michael J. Greenberg, Editor-in-Chief, or Pamela L. Clapp, Managing Editor, at the Marine Biological Laboratory, Woods Hole, Massachusetts 02543. Telephone: (508) 548-3705, ext. 428. FAX: 508-540-6902. E-mail: pamcl@hoh.mbl.edu.

---

POSTMASTER: Send address changes to THE BIOLOGICAL BULLETIN, Marine Biological Laboratory, Woods Hole, MA 02543.

Copyright © 1993, by the Marine Biological Laboratory

Second-class postage paid at Woods Hole, MA, and additional mailing offices.

ISSN 0006-3185

---

## INSTRUCTIONS TO AUTHORS

*The Biological Bulletin* accepts outstanding original research reports of general interest to biologists throughout the world. Papers are usually of intermediate length (10–40 manuscript pages). A limited number of solicited review papers may be accepted after formal review. A paper will usually appear within four months after its acceptance.

Very short, especially topical papers (less than 9 manuscript pages including tables, figures, and bibliography) will be published in a separate section entitled "Research Notes." A Research Note in *The Biological Bulletin* follows the format of similar notes in *Nature*. It should open with a summary paragraph of 150 to 200 words comprising the introduction and the conclusions. The rest of the text should continue on without subheadings, and there should be no more than 30 references. References should be referred to in the text by number, and listed in the Literature Cited section in the order that they appear in the text. Unlike references in *Nature*, references in the Research Notes section should conform in punctuation and arrangement to the style of recent issues of *The Biological Bulletin*. Materials and Methods should be incorporated into appropriate figure legends. See the article by Lohmann *et al.* (October 1990, Vol. 179: 214–218) for sample style. A Research Note will usually appear within two months after its acceptance.

The Editorial Board requests that regular manuscripts conform to the requirements set below; those manuscripts that do not conform will be returned to authors for correction before review.

1. **Manuscripts.** Manuscripts, including figures, should be submitted in triplicate. (Xerox copies of photographs are not acceptable for review purposes.) The original manuscript must be typed in no smaller than 12 pitch, using double spacing (including figure legends, footnotes, bibliography, etc.) on one side of 16- or 20-lb. bond paper, 8½ by 11 inches. Please, no right justification. Manuscripts should be proofread carefully and errors corrected legibly in black ink. Pages should be numbered consecutively. Margins on all sides should be at least 1 inch (2.5 cm). Manuscripts should conform to the *Council of Biology Editors Style Manual*, 5th Edition (Council of Biology Editors, 1983) and to American spelling. Unusual abbreviations should

be kept to a minimum and should be spelled out on first reference as well as defined in a footnote on the title page. Manuscripts should be divided into the following components: Title page, Abstract (of no more than 200 words), Introduction, Materials and Methods, Results, Discussion, Acknowledgments, Literature Cited, Tables, and Figure Legends. In addition, authors should supply a list of words and phrases under which the article should be indexed.

2. **Title page.** The title page consists of: a condensed title or running head of no more than 35 letters and spaces, the manuscript title, authors' names and appropriate addresses, and footnotes listing present addresses, acknowledgments or contribution numbers, and explanation of unusual abbreviations.

3. **Figures.** The dimensions of the printed page, 7 by 9 inches, should be kept in mind in preparing figures for publication. We recommend that figures be about 1½ times the linear dimensions of the final printing desired, and that the ratio of the largest to the smallest letter or number and of the thickest to the thinnest line not exceed 1:1.5. Explanatory matter generally should be included in legends, although axes should always be identified on the illustration itself. Figures should be prepared for reproduction as either line cuts or halftones. Figures to be reproduced as line cuts should be unmounted glossy photographic reproductions or drawn in black ink on white paper, good-quality tracing cloth or plastic, or blue-lined coordinate paper. Those to be reproduced as halftones should be mounted on board, with both designating numbers or letters and scale bars affixed directly to the figures. All figures should be numbered in consecutive order, with no distinction between text and plate figures. The author's name and an arrow indicating orientation should appear on the reverse side of all figures.

4. **Tables, footnotes, figure legends, etc.** Authors should follow the style in a recent issue of *The Biological Bulletin* in preparing table headings, figure legends, and the like. Because of the high cost of setting tabular material in type, authors are asked to limit such material as much as possible. Tables, with their headings and footnotes, should be typed on separate sheets, numbered with consecutive Roman numerals, and placed after

the Literature Cited. Figure legends should contain enough information to make the figure intelligible separate from the text. Legends should be typed double spaced, with consecutive Arabic numbers, on a separate sheet at the end of the paper. Footnotes should be limited to authors' current addresses, acknowledgments or contribution numbers, and explanation of unusual abbreviations. All such footnotes should appear on the title page. Footnotes are not normally permitted in the body of the text.

5. **Literature cited.** In the text, literature should be cited by the Harvard system, with papers by more than two authors cited as Jones *et al.*, 1980. Personal communications and material in preparation or in press should be cited in the text only, with author's initials and institutions, unless the material has been formally accepted and a volume number can be supplied. The list of references following the text should be headed Literature Cited, and must be typed double spaced on separate pages, conforming in punctuation and arrangement to the style of recent issues of *The Biological Bulletin*. Citations should include complete titles and inclusive pagination. Journal abbreviations should normally follow those of the U. S. A. Standards Institute (USASI), as adopted by BIOLOGICAL ABSTRACTS and CHEMICAL ABSTRACTS, with the minor differences set out below. The most generally useful list of biological journal titles is that published each year by BIOLOGICAL ABSTRACTS (BIOSIS List of Serials; the most recent issue). Foreign authors, and others who are accustomed to using THE WORLD LIST OF SCIENTIFIC PERIODICALS, may find a booklet published by the Biological Council of the U.K. (obtainable from the Institute of Biology, 41 Queen's Gate, London, S.W.7, England, U.K.) useful, since it sets out the WORLD LIST abbreviations for most biological journals with notes of the USASI abbreviations where these differ. CHEMICAL ABSTRACTS publishes quarterly supplements of additional abbreviations. The following points of reference style for THE BIOLOGICAL BULLETIN differ from USASI (or modified WORLD LIST) usage:

A. Journal abbreviations, and book titles, all underlined (for *italics*)

B. All components of abbreviations with initial capitals (not as European usage in WORLD LIST e.g., *J. Cell. Comp. Physiol.* NOT *J. cell. comp. Physiol.*)

C. All abbreviated components must be followed by a period, whole word components *must not* (i.e., *J. Cancer Res.*)

D. Space between all components (e.g., *J. Cell. Comp. Physiol.*, not *J.Cell.Comp.Physiol.*)

E. Unusual words in journal titles should be spelled out in full, rather than employing new abbreviations invented by the author. For example, use *Rit Vísindafjélag Íslendinga* without abbreviation.

F. All single word journal titles in full (e.g., *Veliger, Ecology, Brain*).

G. The order of abbreviated components should be the same as the word order of the complete title (i.e., *Proc.* and *Trans.* placed where they appear, not transposed as in some BIOLOGICAL ABSTRACTS listings).

H. A few well-known international journals in their preferred forms rather than WORLD LIST or USASI usage (e.g., *Nature, Science, Evolution* NOT *Nature, Lond., Science, N.Y.; Evolution, Lancaster, Pa.*)

6. **Reprints, page proofs, and charges.** Authors receive their first 100 reprints (without covers) free of charge. Additional reprints may be ordered at time of publication and normally will be delivered about two to three months after the issue date. Authors (or delegates for foreign authors) will receive page proofs of articles shortly before publication. They will be charged the current cost of printers' time for corrections to these (other than corrections of printers' or editors' errors). Other than these charges for authors' alterations, *The Biological Bulletin* does not have page charges.



# Helical Swimming in a Freshwater Oligochaete

CHARLES D. DREWES<sup>1</sup> AND CHARLES R. FOURTNER<sup>2</sup>

<sup>1</sup>*Department of Zoology and Genetics, Iowa State University, Ames, Iowa 50011, and*

<sup>2</sup>*Biological Sciences, State University of New York-Buffalo, Buffalo, New York*

**Abstract.** A novel pattern of undulatory swimming is described in the freshwater oligochaete, *Dero digitata* (Family Naididae). Movements are rhythmic (6–12 cycles/s), each cycle consisting of a single, helical body wave that passes from the worm's anterior to posterior end, thus propelling the worm forward. Successive cycles of these waves alternate between right-handed and left-handed helical orientations. Helical swimming in response to posterior tactile stimulation was commonly expressed in all stages of asexual reproduction, including non-fissioning "normal" worms, late prefission worms, and separated anterior or posterior zooids. Swimming also occurred in amputated anterior and posterior body fragments. Reynolds numbers ranged from approximately 50 (in the shortest and slowest worms) to 300 (in the longest and fastest worms). During slow swimming, wave velocities and forward velocities were 37 mm/s and 10 mm/s, respectively; during fast swimming these values were 55 mm/s and 25 mm/s, respectively. Thus, corresponding values of overall "slippage" were 73 and 55%, respectively. Central conduction of swim wave excitation likely involves intersegmental, non-giant fiber pathways that are (1) functionally coupled between anterior and posterior zooids of prefission worms and (2) readily activated by posterior mechanosensory inputs in whole worms and isolated zooids.

## Introduction

Undulatory swimming is a common mode of locomotion for long, narrow, and limbless animals in aquatic environments (Gray, 1953, 1968; Trueman, 1975, 1978; Clark, 1976). Propulsive forces during undulatory swimming are achieved by retrograde passage of rhythmic waves of body bending (Taylor, 1952). In most cases these undulations involve sinusoidal, two-dimensional waves

produced by alternating lateral (*i.e.*, left-right) body bends. Examples include chordates, such as eels and *Branchiostoma* (Lighthill, 1969; Webb, 1976), as well as invertebrates, such as nematodes, polychaetes, and archiannelids (Gray, 1939; Gray and Lissmann, 1964; Clark and Tritton, 1970; Seymour, 1972; Clark and Hermans, 1976).

Notable exceptions to this general pattern are leeches, in which retrograde undulatory waves are produced by alternating dorso-ventral, rather than lateral, bending (Gray *et al.*, 1938; Taylor, 1952; Sawyer, 1986). Another apparent exception is the polychaete *Glycera*, in which a spiral coiling produced by posterior segments is somehow used to propel the animal backward (Stolte, 1932).

In the present study, we describe the undulatory swimming behavior of a freshwater oligochaete, *Dero digitata* (Family Naididae). Its pattern of swimming, which appears unique in comparison to all previously described undulatory swimming in animals, involves rhythmically alternating right-handed and left-handed helical waves that, through retrograde passage, propel the worm forward.

Our aims in this study are to (1) provide a basic description of swimming movements and frame-by-frame analysis of forward progress and wave velocity, (2) compare swim capabilities during various stages of development associated with asexual reproduction, and (3) draw inferences, where possible, regarding neural mechanisms that control swimming. A preliminary report of the study has appeared elsewhere (Drewes and Fourtner, 1990).

## Materials and Methods

The freshwater oligochaete *Dero digitata* (Family Naididae) was obtained from asexually reproducing laboratory cultures, originally collected from Swan Lake, Victoria, BC, Canada (for taxonomy, see Sperber, 1950). Worms were maintained in natural sediments and fed

fragments of wheat kernels. All cultures and experiments were at room temperature (20–22°C).

Various developmental stages were continuously available from cultures, including "normal" (*i.e.*, non-fissioning) worms with resting body lengths  $\approx 10$  mm and late "prefission" worms with resting lengths  $\approx 14$  mm. In the latter worms a midbody fission zone, with adjacent regenerating head and tail segments, divides the body into distinct anterior and posterior zooids (Drewes and Fournier, 1991). In some experiments, prefission worms were severed at the fission plane with microdissection scissors, and swimming capabilities of the two separated zooids were independently examined.

To videotape swimming behavior, individual worms were transferred from cultures to a plastic Petri dish (35 mm D) containing 3.5–4.0 ml of artificial pond water. The dishes were then placed on a glass stage and viewed from below with a Panasonic PV-400 video camera. A field of view ranging from 4.5–20.0 mm on the video monitor was obtained using various combinations of extension tubes, a Canon 100 mm macro lens, and a Wild 2 $\times$  lens extender. Frame speed was 30 frames/s and shutter speed  $1 \times 10^{-3}$  s. A fiber optics illuminator, placed above the dish at an angle of approximately 45°, provided illumination against a dark background. This arrangement provided access to the dish for tactile stimulation of the worm with the tip of a human hair attached to a hand-held probe.

To measure forward progress and swim velocity, a transparent  $1 \times 1$  mm grid pattern was placed between the glass stage and bottom of the Petri dish. Distance measurements were then made directly from the video monitor screen using frame-by-frame replay of swimming episodes. Single-frame images were photographed directly from the monitor with a Polaroid camera.

## Results

### *General description of swimming behavior*

In nature, *Dero digitata* resides in submerged or floating organic debris along the shallow margins of lakes and ponds, where it establishes temporary tubes or burrows, lined with mucus and small particles. Its main mode of locomotion in this environment is peristaltic creeping in which bilaterally symmetrical muscle contractions (circula; and longitudinal), along with actions of ventral chaetae, provide forward or rearward crawling movements. Infrequently, however, worms may exit their tubes and, by initiation of rhythmic swimming movements, enter the surrounding water column.

When placed in a dish devoid of organic debris, worms readily initiate swim movements (Figs. 1, 2), either spontaneously or in response to light tactile stimulation of posterior segments, especially the ciliated gill of the ter-

minial "segment," or pygidium (*cf.* Fig. 2 in Drewes and Fournier, 1991). Tactile-evoked swimming always begins with a stereotyped, J-shaped, ventral flexion of the anterior end (Fig. 1A; frame 1). If this flexion occurs while the ventral surface of the worm is in contact with the bottom of the dish, then the anterior end of the worm is thrust away from the underlying substratum and into the water column. The next phase of movement, usually evident one or two video frames later, is a lateral bending (either to the left or right side) that also occurs in anterior segments and accompanies ventral flexion (Fig. 1A; frame 2). This combination of ventral and lateral flexions, together with a uniform torsion of the body along its midline, comprise the initial stages for forming the first helical wave of a swimming episode.

As the wave of ventral and lateral flexion approaches midbody segments, mainly ventral bending persists in anterior segments. At this time, formation of a single helical wave is essentially achieved, with the wavelength comprising about 30–40% of the worm's body length (Fig. 1B). At a slightly later time, the wave is seen in a midbody position (Fig. 1C).

A diagram of the bending that occurs at the instant a helical wave reaches this midbody position is shown in Figure 1D. Note that lateral bending occurs in segments just posterior and anterior to the helical wave. As shown, bending on one side (left) occurs in posterior segments that are beginning the transition from a straight to a helical configuration. Conversely, bending on the opposite side (right) occurs anterior to the wave, in segments that are reversing this transition (*i.e.*, changing from the helical back to straight configuration).

It should be noted that the body length of all swimming worms appeared substantially reduced in comparison to the body length of resting (non-swimming) worms. In a typical swimming prefission worm (*e.g.*, Fig. 2B) the body length (estimated by tracing along the helical wave formed by the body) was 10 mm. This was about 30% less than the resting body length in prefission worms (14 mm). This reduction in length during swimming appears to involve the entire body and probably derives from a circumferential increase in longitudinal muscle tonus.

When viewed in a line corresponding to the longitudinal axis of head and tail segments, the helical wave in mid-passage appears as a nearly perfect circular loop, the outside diameter of this circle being approximately 1.5 mm. The outer curvature of this loop is mainly formed by the dorsal surface of midbody segments, while the inner curvature is formed by the ventral surface of these segments. Thus, with an optimal combination of focal distance and angle of illumination, the worm's long dorsal chaetae may be visible on the outer curvature of the apex of the helical loop (Fig. 1B) and on the opposing dorsal surface of more straightened anterior and posterior regions (Fig. 1C).



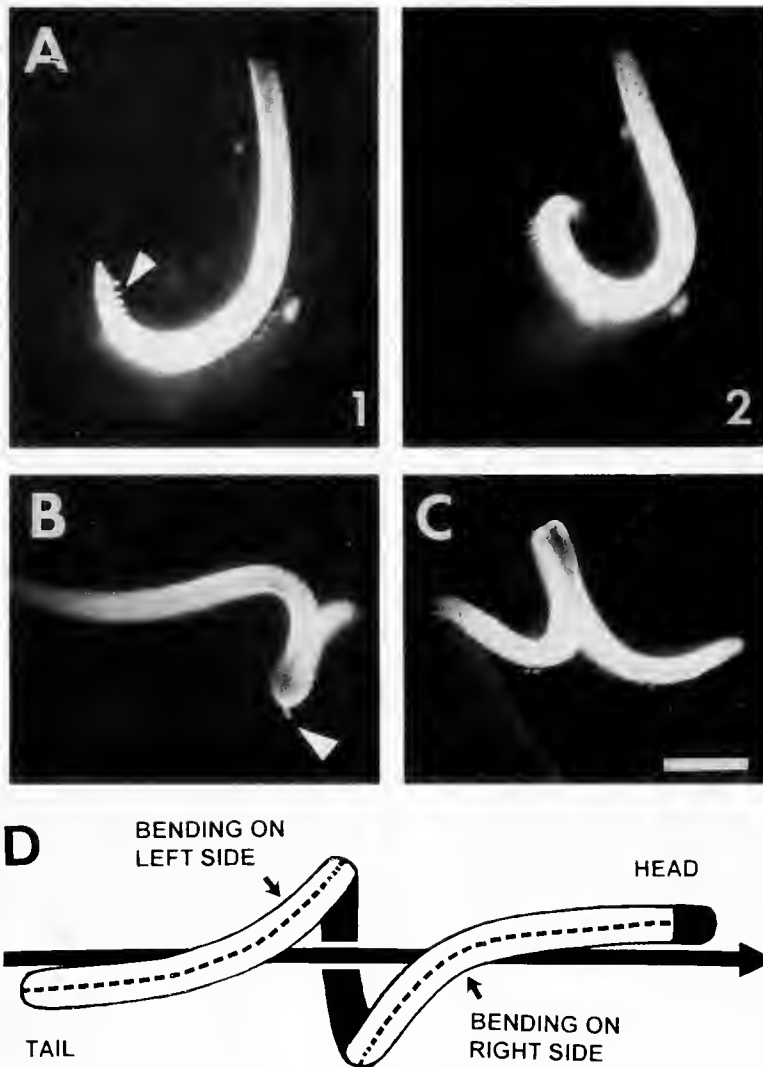


**Figure 1.** Body surface orientation during swimming movements. (A) Initiation of swimming, in response to posterior touch (not shown), begins with a pronounced ventral flexion (J-shape) of the worm's anterior end (frame A1). The arrow shows the brush-like ventral chaetae on the first four anterior segments. Long dorsal chaetae are evident on the outer curvature of the body bend in more posterior segments. In the next frame (A2), continued ventral bending, in combination with lateral bending to the left side, results in formation of the first helical body wave near the worm's anterior end. (B) Dorsal chaetae are visible at the apex of the helical loop (arrow) near the worm's anterior end. (C) With the helical loop in a mid-body position, dorsal chaetae are visible in straightened anterior and posterior segments. The direction of swimming is from left to right in B and C. The scale bar in C is 1 mm and applies to panels A–C. (D) Diagram of bending movements and body surface orientation during passage of a helical wave. The dorsal surface of the worm, labeled as a dotted line, faces away from the central axis of the helix (indicated by the solid arrow). The ventral surface, in black, faces toward the central axis of the helix.

These images indicate that bending movements associated with the formation of each wave are also accompanied by a unidirectional torsion along the worm's longitudinal axis.

Depending on the direction of the initial lateral bending in anterior segments, the first helical loop may be either right-handed or left-handed in orientation. Thus, in the case of initial bending to the worm's right, helical wave

orientation along the worm's longitudinal axis is right-handed. Conversely, with initial bending to the left, the helical wave orientation is left-handed (*e.g.*, see Fig. 1D).

In all cases, movements associated with each subsequent helical wave also begin in anterior segments. However, two important differences should be noted: (1) in contrast to the mechanics of the very first wave, initial movements during the second wave (and all subsequent

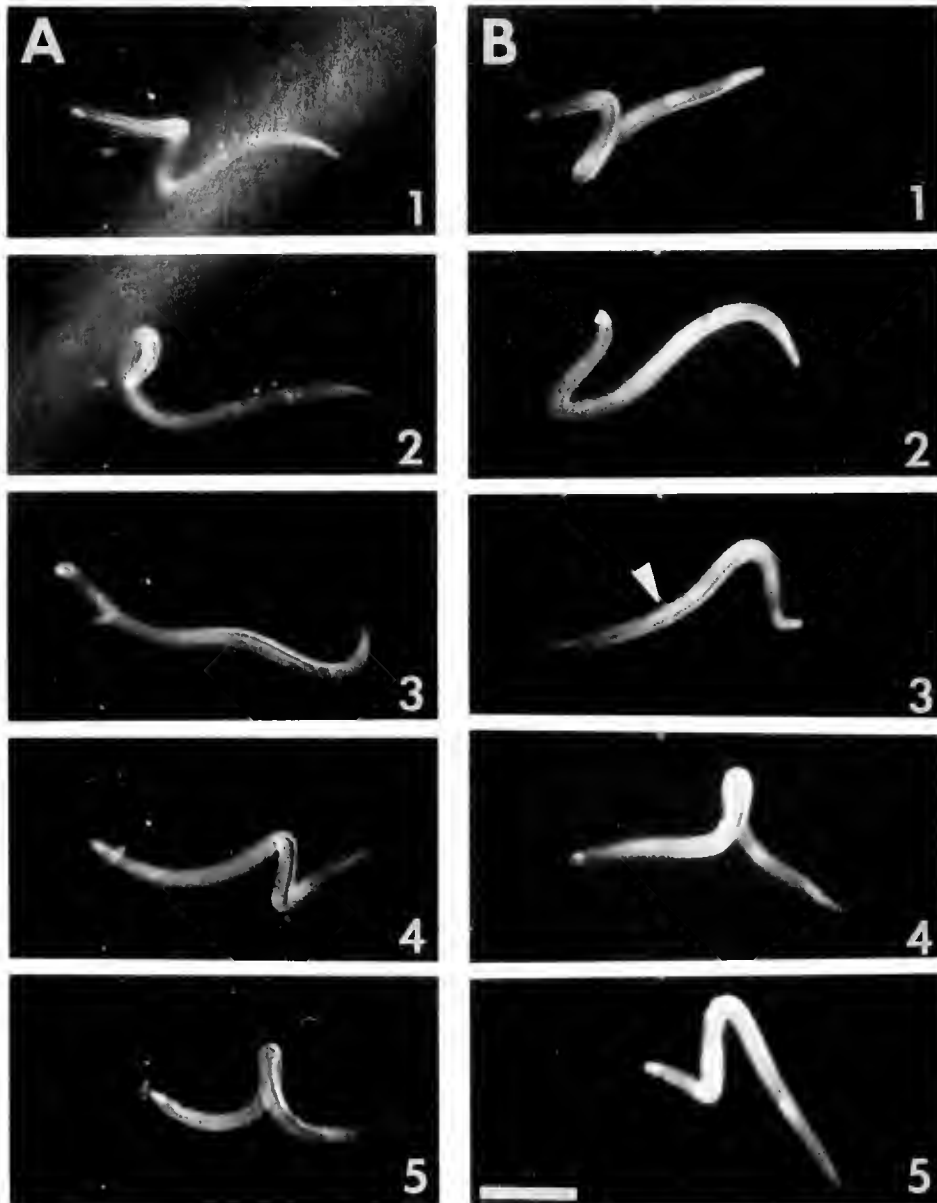


**Figure 2.** Frame-by-frame analysis of swimming movements. (A) Frames 1 and 2 show passage of a left-handed helical wave through middle and posterior segments of a normal worm. No wave is evident in frame 3. In frames 4 and 5, the next helical wave is right-handed in orientation. (B) A right-handed, helical wave is seen in posterior segments of a pre-fission worm (frame 1), but the next wave (frame 3) is left-handed (frame 4). The midbody fission zone is shown in frame 3 (arrow). The direction of swimming is from left to right (*i.e.*, anterior end of worm positioned to the right) for all five frames in A and B. Scale bar = 2 mm).

waves in a single swim episode) involve nearly synchronous ventral and lateral bending in anterior segments, rather than strong ventral bending followed by lateral bending; (2) the orientation of the second and each successive helical wave alternates with the preceding wave. Consequently, swimming in these animals involves rhythmic waves of alternating right-handed and left-

handed helical loops, with each loop appearing in lateral view to form a plane that is roughly perpendicular to, and moving retrograde with respect to, the direction of forward swimming (Fig. 2A).

Essentially the same pattern of swimming was seen throughout all stages of asexual segmental regeneration in late pre-fission worms (*cf.*, Drewes and Fourtner, 1991).

Thus, alternating helical waves progressed without obvious delay or interruption through anterior zooids, across the fission plane, and into posterior zooids (Fig. 2B). In both normal and prefission worms, the number of cycles in each swimming episode appeared highly variable, ranging from two or three to more than 50. One slight difference between swim patterns in prefission and normal worms was that a second helical wave frequently began in anterior segments of late prefission stages before the preceding wave was completed in extreme posterior segments, a situation that seldom occurred in normal worms. This concurrence of two spatially separated waves correlated with the fact that worms at the late prefission stage were about 30% longer than most normal worms.

#### Wave frequency and forward velocity

Frame-by-frame video analysis was used to determine the wave frequency and forward velocity of worms during repeated swimming episodes. Although frequencies in normal worms varied significantly among different swim episodes, wave frequency within a single episode was relatively constant. The mean wave frequency during each episode was determined by dividing the number of consecutive waves (usually 4–10 waves were counted in the field of view) by the number of elapsed video frames. The resulting value was then multiplied by 30 frames/s. Wave frequencies ranged from approximately 6 to 12 waves/s (Fig. 3A).

Forward velocity was determined by measuring the linear distance between the position of the worm's head at the beginning and end of a swimming sequence. This distance was divided by the number of elapsed frames and multiplied by 30 frames/s. Figure 3A shows that forward velocity was directly related to wave frequency. The slope (regression coefficient) of this relationship was 1.72 mm/wave, a distance of about one-third the body length of a normal worm during swimming.

Wave frequency and forward velocity were also determined for prefission worms. Frequencies ranged from approximately 5.5 to 13 waves/s. As in normal worms, a direct relationship was evident between forward velocity and mean frequency (Fig. 3B). However, the slope of this relationship was 2.34 mm/wave, a value significantly greater ( $P < 0.05$ ) than that in normal worms (Fig. 3A). The greater forward progress per cycle may be related to the proportionately longer body length of prefission worms; that is, propulsive forces generated by each wave may act over a longer distance and greater time in prefission worms.

To study whether anterior and posterior zooids were capable of independent swimming, worms in late prefission stages were severed at the fission zone. Swim behavior in anterior and posterior zooids was readily initiated by

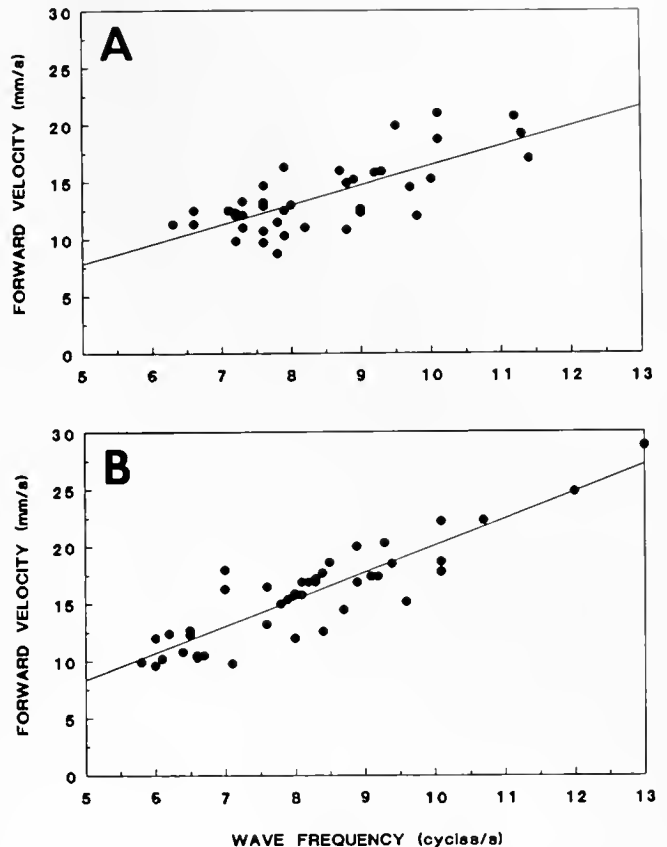


Figure 3. Relationship between forward velocity and wave frequency during swimming in normal and prefission worms. (A) Each point shows the mean velocity from one swim episode in a normal worm (total = 40 episodes from six worms;  $r = 0.73$ ; slope = 1.72). (B) Each point shows the mean swim velocity from one episode in a prefission worm (total = 43 episodes from six worms;  $r = 0.89$ ; slope = 2.34).

touch to the most posterior segments of each zooid. Ranges of wave frequencies in the two zooids were nearly the same as normal worms (Fig. 4A, B). However, the slopes (approximately 1.0 mm/wave in both anterior and posterior zooids) were significantly less ( $P < 0.001$ ) than the slope for intact, prefission worms (Fig. 3B).

Capabilities for swimming were also examined in posterior body halves, obtained by transecting normal worms ( $n = 4$ ) at a midbody position. Each posterior half initiated and sustained independent helical swimming in response to posterior tactile stimulation, just as in posterior zooids from prefission worms. However, forward progress in the posterior halves of normal worms was erratic. This was apparently due to a biomechanical inability of segments just posterior to the transection site to consistently straighten and project in a forward direction immediately after the passage of each propulsive wave. Such straightening occurred in anterior segments of intact normal and prefission worms (see frame 1 in Fig. 2A, B). Nevertheless, the wave frequency in transected posterior halves was

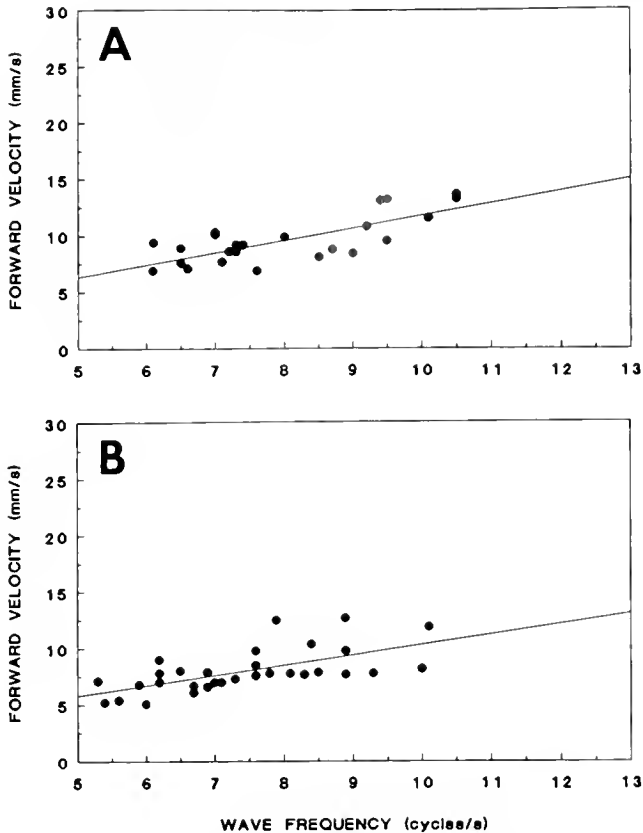


Figure 4. Relationship between forward velocity and wave frequency during swimming in anterior and posterior zooids. (A) Data from 25 swim episodes in five anterior zooids ( $r = 0.74$ ; slope = 1.07). (B) Data from 30 swim episodes in five posterior zooids ( $r = 0.63$ ; slope = 0.91).

comparable to normal worms, varying from 5.5 to 9.5 waves/s.

#### Wave velocity and slippage

Estimates of retrograde wave velocity were obtained by measuring the change in wave position from two successive video frames (Fig. 5A). All wave velocity measurements were (a) made along a line parallel to the longitudinal axis of the worm's body, (b) referenced to the worm's anterior end, and (c) obtained as the wave was in a mid-body position. Such measurements were seldom possible in short, normal worms (or recently fissioned zooids) because the frame rate of the video camera was too slow in relation to wave frequency to capture at least two successive frames showing clear-cut wave positions along the body. However, in long pre-fission worms, these measurements were possible during some swim episodes. Figure 5B shows the direct relationship between retrograde wave velocity and frequency (c/s) in these worms. Wave velocities ranged from 35 to 55 mm/s, values substantially greater than forward velocities of swimming.

Specific values of  $V_{\text{wave}}$  and  $V_{\text{forward}}$  were then used to calculate "slippage" according to the following equation (Gray and Lissmann, 1964):

$$\% \text{ slippage} = \left( \frac{V_{\text{wave}} - V_{\text{forward}}}{V_{\text{wave}}} \right) \times 100$$

From the linear relationship shown in Figure 3B, seven values of  $V_{\text{forward}}$  were interpolated for each unitary value of frequency over the range of 6–12 waves/s. Seven values of  $V_{\text{wave}}$  were similarly interpolated from Figure 5B. These values were then used to calculate "percent slippage" (as above) and "swim efficiency," the latter defined as: (100% – percent slippage), or ( $V_{\text{forward}}/V_{\text{wave}}$ ).

As shown in Figure 6, slippage ranged from 55 to 73% over the normal range of wave frequencies and was approximately 15% less during fast swimming (12 waves/s) than slow swimming (6 waves/s). However, these results assume that  $V_{\text{forward}}$  was uniform throughout a swimming episode. This assumption was tested using frame-by-frame tracking of forward progress of the worm's head during swim episodes (Fig. 7).

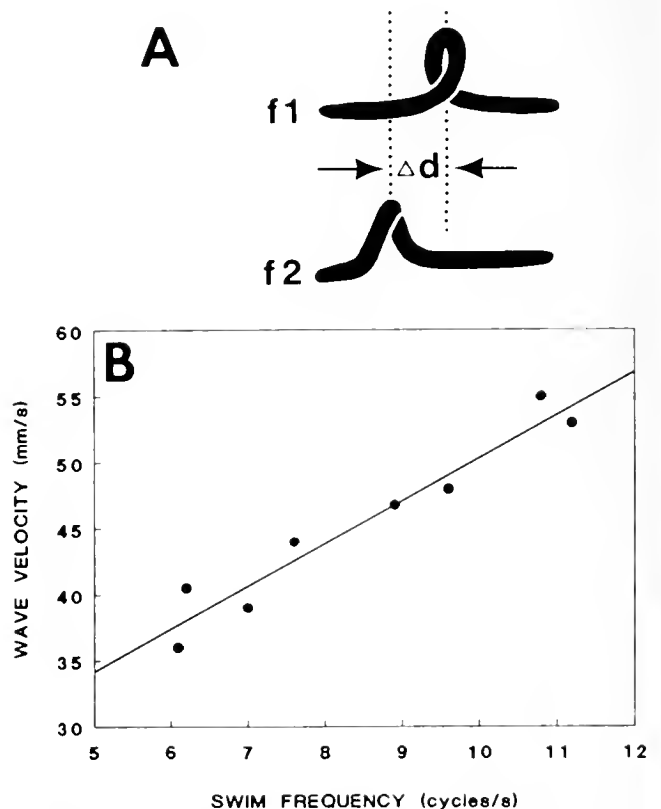


Figure 5. Determination of wave velocity in pre-fission worms. (A) The change in position of the apex of the helical wave, relative to the worm, is measured in two consecutive video frames (f1 and f2). The worm's anterior end is to the right. (B) Data from eight swim episodes in four pre-fission worms indicate that wave velocity is directly related to wave frequency ( $r = 0.97$ ; slope = 3.24).

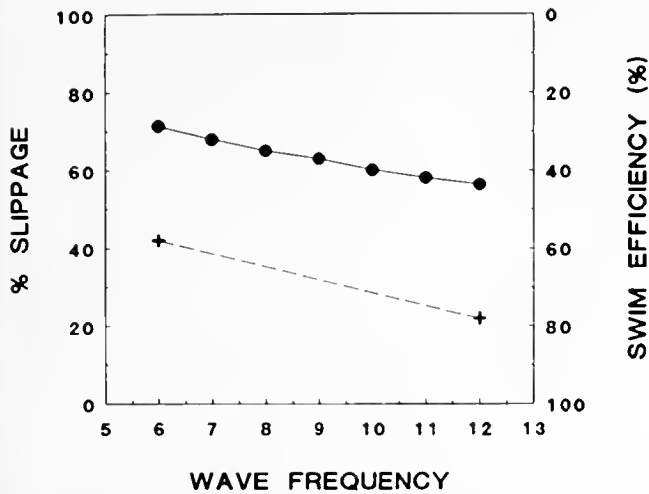


Figure 6. Slippage and swim efficiency at different wave frequencies in preffision worms. Points are derived from the linear slopes shown in Figs. 3 and 5. Filled dots show values of overall slippage. Swim efficiency values for fast and slow swimming are much greater when considering slippage during only the propulsive phase of swimming (+).

In preffision worms, each cycle of swimming showed two distinct phases. One phase, hereafter termed the propulsive phase, was characterized by a rapid and relatively uniform forward progression of the worm's head. The propulsive phase corresponded to video frames in which the helical body wave was in retrograde passage through middle and posterior segments. The second (recovery) phase was characterized by head retrogression and corresponded to the video frame in which the lateral and ventral bending movements required for reformation of the next swim wave occurred in anterior segments.

Forward velocity during the propulsive phase was estimated by tracking head movements in both slow (6 waves/s) and fast (12 waves/s) swimming worms. The results, plotted in Figure 6, suggest that at least half of the overall slippage occurred during the recovery phase and, therefore, may be attributed to movements of head retrogression required for reformation of the swim wave in anterior segments. The remainder of slippage, ranging from approximately 25 to 40% in fast and slow swimming worms, respectively, presumably occurred during the actual propulsive phase of swimming.

Discussion

Undulatory swimming in *Dero* involves retrograde passage of helical body waves and, thus, appears fundamentally different from any other previously described patterns of undulatory locomotion. Unlike two-dimensional, sinusoidal waves that typically involve waves of antagonistic muscle contractions (*i.e.*, either dorsal-lateral or left-right), the propulsive waves for swimming in *Dero*

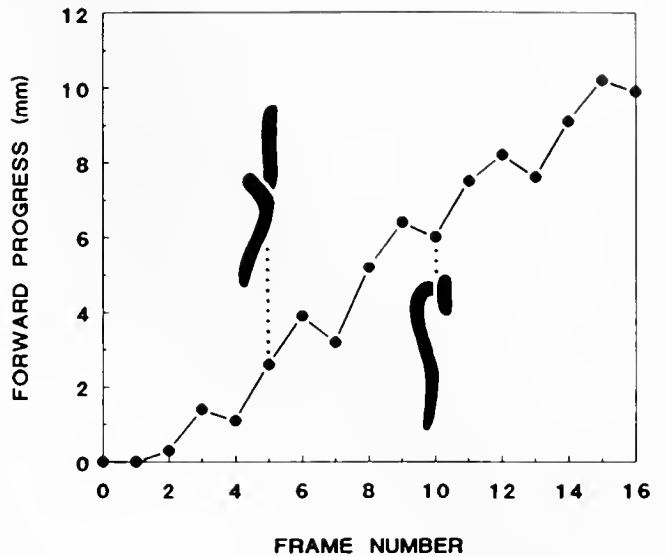


Figure 7. Tracking of forward progress of the head in a preffision worm. Each point shows the linear forward progress of the worm's anterior end, as determined from a video frame. Posterior passage of the helical wave along the body during each cycle of swimming is accompanied by a steep increase in the rate of forward progress (*e.g.*, frames 4-6, 7-9). Reformation of the helical wave at the anterior end (*e.g.*, frames 7, 10, 13) results in head retrogression between each swim cycle.

are three-dimensional and helical in conformation. Based on direct observations of the spatial orientations of body surfaces during helical bending (Fig. 1), as well as estimates of the relative timing and duration of various bending components (Fig. 2), the sequence and phase relationships of requisite bending movements were reconstructed as shown in Figure 8. The illustration applies to any two successive swim cycles (excluding the first cycle) in a typical midbody segment. It should be noted (though not illustrated) that the combination of bending movements for each wave is accompanied by a unidirectional torsion

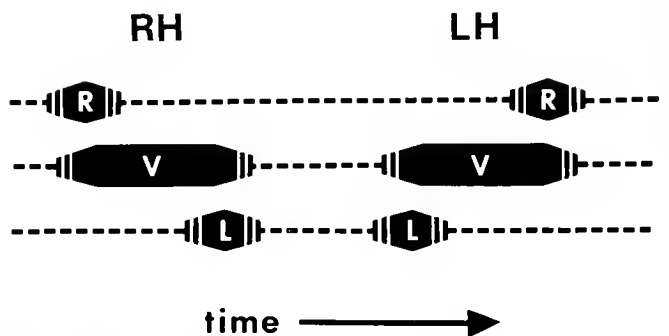


Figure 8. Relative timing of bending movements for a typical midbody segment during two consecutive cycles of helical swimming. A right-handed helical wave (RH) is formed by a combination of right (R), ventral (V), and left (L) bending. Reversal of the bending sequence in the next wave results in a left-handed helical wave (LH).



of the body about the longitudinal axis. The direction of this torsion reverses with each successively alternating helical wave.

Several key features of this sequence are evident: (a) the phase of ventral flexion represents the longest active phase of bending during each cycle and persists through both the left and right flexions that act to straighten the worm; (b) each cycle in a swim episode, beginning with the second cycle, starts with the same direction of lateral bending that terminated the preceding cycle; (c) during formation of each helical wave, lateral and ventral bending begin nearly synchronously, except when anterior segments form the very first wave of a swim episode; and (d) every cycle includes an "inactive" period during which no substantial bending is evident. During this period we assume the worm's body passively, rather than actively, returns to a straightened position. Transition to this position may be enhanced by the maintained increase in longitudinal muscle tonus throughout the body, as previously described.

One behavioral consequence of this pattern is that the orientation of successive waves alternates between right-handed and left-handed helices. The advantages of this alternation are not entirely clear. One likely possibility is that repeated passage of waves in the same direction could result in excessive yaw or pitch, because vectors of the propulsive forces generated by each element of the body wave are, undoubtedly, neither perfectly parallel to the longitudinal axis of the helical coil nor symmetrically distributed in a circumferential pattern around its axis. Alternating orientation of successive helical waves may tend to counterbalance yaw or pitch. Thus, when such effects are averaged over numerous cycles, the result may be relatively straight swimming.

Another possibility relates to the amount of forward progress achieved by passage of each cycle, which represents about 30–40% of the worm's length. Assuming that each helical wave causes a corresponding, though very weak, helical vortex of water displacement during passage, then some stage of the next wave may encounter residual fluid movements associated with the passage of the preceding wave. If such fluid movements are in the same direction as those produced by the next wave, propulsive forces of the moving body wave on the surrounding water may be attenuated. Conversely, greater propulsive force may occur if the next helical wave acts against water that is residually moving in a direction of greater opposition to the body wave.

Helical swimming in *Dero* involves an overall slippage of approximately 50% at maximal swim velocity within the observation arena. These values are comparable to those of larger marine polychaetes that move by lateral undulations, with presumably little or no assistance from parapodial movements (Clark and Hermans, 1976).

Overall slippage in *Dero*, however, appears less than in a wide variety of other animals (nematodes, insect larvae, leeches, and snakes), all using two-dimensional undulatory swimming (Gray and Lissmann, 1964; Taylor, 1952). Nevertheless, several considerations suggest that our calculations of slippage in *Dero* probably represent overestimations.

First, all values of forward progress used to calculate swim velocity assumed straight-line swimming. However, frame-by-frame tracking of head and tail segments showed that, due to periodic yaw and pitch, this assumption was never perfectly met during any swim episode; thus the actual swimming distance was underestimated.

Second, to help ensure that swimming movements occurred in the focal plane of the camera, worms were confined to a 3–4 mm layer of water during all swim episodes. Because swimming was not straight and because the loop formed by helical bending was approximately 1.5 mm in diameter, it is likely that some portions of the worm were briefly near, or actually contacted, the bottom of the dish or water surface during some swim cycles. Thus, there were potential "wall effects" (Vogel, 1981). Such effects could influence forward velocity in two opposing ways: (a) if the helical loop (*i.e.*, that portion of the body generating propulsive force) approached or contacted a rigid surface, then forward velocity would be expected to increase because resistance coefficients are larger as a wall is approached by the loop (Katz and Blake, 1975); (b) if a non-propulsive portion of the body came close to these surfaces, then forward velocity may decrease due to enhanced drag (Taylor, 1972). If the latter effect (which is inversely related to Reynolds number) predominates, then the net result is retardation of the worm's forward progress and an overestimation of slippage for assumed open-water conditions. If the former effect predominates, then the result is enhancement of forward progress and an underestimation of slippage for assumed open-water conditions.

We have recently analyzed forward velocity *versus* wave frequency in normal (non-fissioning) worms under open-water conditions (Drewes and Fortner, unpub.). The slope of this relationship was less than (though not statistically different from) that of normal worms swimming in shallow water (Fig. 3A). This suggests that the two opposing influences on forward velocity generated by "wall effects" were either negligible or essentially counterbalanced one another when worms were swimming in a shallow dish.

For swimming in the fastest and longest fissioning worms the calculated Reynolds number was 300; for this calculation a forward velocity of 30 mm/s and worm body length of 10 mm (during swimming) were used. In comparison, for the slowest and shortest worms (normal) the value was 50; for this calculation a forward velocity of 9 mm/s and worm body length of 6 mm (during swim-

ming) were used. These are similar to Reynolds numbers for swimming in copepods or flight in small insects (Strickler, 1975; Vogel, 1988).

Our results indicated that, in the absence of sediments in which to retreat, helical swimming was readily induced by posterior tactile stimulation. Such swimming was evoked in normal and pre-fission worms, anterior and posterior zooids, or anterior and posterior fragments of normal worms. This suggests that sensory pathways capable of activating swimming are distributed throughout the posterior and middle regions of the body. Previously, electrophysiological studies of *Dero* (Drewes and Fournier, 1991) showed that tactile stimulation in these same regions triggered lateral giant nerve fiber spikes in worms placed on recording grids and covered by a thin film of water. It would be helpful to determine whether touch-evoked lateral giant fiber spiking necessarily precedes or is somehow causally linked to swim initiation in open-water conditions.

Because helical swimming occurs in posterior zooids or isolated posterior fragments, it appears that segmental capabilities for integrating tactile sensory inputs and initiating resultant motor outputs for swimming are widely distributed throughout the body. Normally, however, expression of these outputs in middle and posterior body segments is contingent upon integration of inputs and prior initiation of outputs in cephalic segments. The autonomous expression of a locomotor rhythm at subcephalic levels in body fragments is not unique to oligochaete swimming and appears similar to capabilities for peristaltic crawling in body fragments of earthworms and polychaetes (Friedländer, 1894; Lawry, 1970).

Calculations of retrograde wave velocity (Fig. 5) provide insight into functional properties of intersegmental pathways that coordinate swimming. Clearly, the velocity is variable and correlates directly with wave frequency (c/s). Maximal wave velocity was 55 mm/s, or approximately 1/20 the velocity of the lateral giant nerve fibers and about 1/30 the velocity of the medial giant nerve fibers in this species (Drewes and Fournier, 1991). Therefore it seems highly improbable that either of the two giant fiber pathways directly mediates the retrograde passage of excitation required for helical wave formation.

Future experiments will be directed at examining the adaptive significance of swimming behavior. Because *Dero* appears to maintain a predominantly sessile lifestyle, discovery of intrinsic or extrinsic factors that trigger and modulate swimming may be of special interest.

#### Acknowledgments

We thank Drs. B. Munson and J. Redmond for helpful discussions.

#### Literature Cited

- Clark, R. B. 1976. Undulatory swimming in polychaetes. Pp. 437-446 in *Perspectives in Experimental Biology, Vol. 1, Zoology*, P. S. Davies, ed. Pergamon Press, Oxford.
- Clark, R. B., and D. J. Tritton. 1970. Swimming mechanisms in nereidiform polychaetes. *J. Zool. Lond.* **161**: 257-271.
- Clark, R. B., and C. O. Hermans. 1976. Kinetics of swimming in some smooth-bodied polychaetes. *J. Zool. Lond.* **178**: 147-159.
- Drewes, C. D., and C. R. Fournier. 1990. Corkscrew swimming in an aquatic oligochaete. *Am. Zool.* **30**: 118A.
- Drewes, C. D., and C. R. Fournier. 1991. Reorganization of escape reflexes during asexual fission in an aquatic oligochaete, *Dero digitata*. *J. Exp. Zool.* **260**: 170-180.
- Friedländer, B. 1894. Beiträge zur Physiologie des Centralnervensystems und des Bewegungsmechanismus der Regenwürmer. *Pflüg. Arch. Ges. Physiol.* **58**: 168-206.
- Gray, J. 1939. Studies in animal locomotion. VIII. The kinetics of locomotion of *Nereis diversicolor*. *J. Exp. Biol.* **16**: 9-17.
- Gray, J. 1953. Undulatory propulsion. *Q. J. Microsc. Sci.* **94**: 551-578.
- Gray, J. 1968. Pp. 435-453 in *Animal Locomotion*. Weidenfeld and Nicolson, London.
- Gray, J., and H. W. Lissmann. 1964. The locomotion of nematodes. *J. Exp. Biol.* **41**: 135-154.
- Gray, J., H. W. Lissmann, and R. J. Pumphrey. 1938. The mechanism of locomotion in the leech (*Hirudo medicinalis* Ray). *J. Exp. Biol.* **15**: 408-430.
- Katz, D. F., and J. R. Blake. 1975. Flagellar motions near walls. Pp. 173-184 in *Swimming and Flying in Nature*, Vol. 1, T. Y.-T. Wu, C. J. Brokaw and C. Brennan, eds. Plenum Press, New York.
- Lawry, J. V. 1970. Mechanisms of locomotion in the polychaete, *Harmothoe*. *Comp. Biochem. Physiol.* **37**: 167-179.
- Lighthill, M. J. 1969. Hydrodynamics of aquatic animal propulsion. *Ann. Rev. Fluid Mech.* **1**: 413-445.
- Sawyer, R. T. 1986. Pp. 375-384 in *Leech Biology and Behavior, Vol. 1*. Clarendon Press, Oxford.
- Seymour, M. K. 1972. Swimming in *Arenicola marina* (L.). *Comp. Biochem. Physiol.* **41A**: 285-288.
- Sperber, C. 1950. A taxonomical study of the Naididae. *Zool. Bidr. Uppsala* **28**: 3-296.
- Stolte, H. A. 1932. Analyse aussergewöhnlicher Formen der Bewegung bei einigen bodenbewohnenden Polychäten. *Jen. Z. Naturwiss.* **67**: 199-220.
- Strickler, J. R. 1975. Swimming of planktonic *Cyclops* species (Copepoda, Crustacea): pattern, movements, and their control. Pp. 599-613 in *Symposium on Swimming and Flying in Nature*, Vol. 2, T. Y.-T. Wu, C. J. Brokaw and C. Brennan, eds. Plenum Press, New York.
- Taylor, G. 1952. Analysis of the swimming of long and narrow animals. *Proc. Roy. Soc. (A)* **214**: 158-183.
- Taylor, G. 1972. Low-Reynolds-number flows. Pp. 47-54 in *Illustrated Experiments in Fluid Mechanics*. National Committee for Fluid Mechanics Film Notes. MIT Press, Cambridge.
- Trueman, E. R. 1975. Pp. 107-128 in *The Locomotion of Soft Bodied Animals*. Edward Arnold, London.
- Trueman, E. R. 1978. Locomotion. Pp. 261-269 in *Physiology of Annelids*, P. J. Mill, ed. Academic Press, New York.
- Vogel, S. 1981. Pp. 249-250 in *Life in Moving Fluids*. Willard Grant Press, Boston.
- Vogel, S. 1988. Pp. 105-129 in *Life's Devices*. Princeton University Press, Princeton.
- Webb, J. E. 1976. A review of swimming in *Amphioxus*. Pp. 447-454 in *Perspectives in Experimental Biology, Vol. 1, Zoology*, P. S. Davies, ed. Pergamon Press, Oxford.

# Sag-Mediated Modulated Tension in Terebellid Tentacles Exposed to Flow

AMY S. JOHNSON

*Department of Biology, Bowdoin College, Brunswick, Maine 04011*

**Abstract.** The long, compliant feeding tentacles of the terebellid polychaete *Eupolyornia heterobranchia* not only stretch out over a sandflat substratum but also extend into flow. Tentacles suspended perpendicular to flow responded to increasing velocity by increasing their sag. An analysis of tension in these tentacles, mathematically analogous to that applicable to suspension bridges, shows that sagging permits the tentacles to avoid increases in tension that would otherwise occur as flow increases. Force modulation was achieved by active muscular control rather than by passive material properties. Although these tentacles would certainly break in the experimental flows if they did not sag, the low tension achieved suggests that some other reason, such as limitations on the adherence of cilia and mucus, accounts for the level of tension observed. Because drag is maximum on tentacles oriented perpendicular to flow, reorientation of tentacles, either by sagging or by dangling parallel to flow, additionally reduces tension by reducing drag. Theoretical estimates of drag on tentacles oriented parallel to flow show that they are never in danger of being broken. Drag is sufficient, however, to assist in passive extension of tentacles. While reorientation is a common mode of drag reduction among marine organisms, sagging represents a novel mechanism of mediating structural forces resulting from flow.

## Introduction

Reliance upon a particulate food resource is common among marine invertebrates, and tentacles are among the most versatile of structures used to capture such food. The mechanical demands on tentacles during feeding vary widely depending on the way that tentacles are used, and the mechanical characteristics of the tentacles constrain

the ways that tentacles can be used by animals during feeding.

The mechanical demands on the tentacles used to capture suspended food consist largely of resisting the drag forces exerted upon them by flow. Although there is a range in mechanical characteristics of tentacles specialized for capturing suspended food, typically the tentacles that are used exclusively for suspension feeding are relatively inextensible. Bryozoans, for example, extend a short, stiff crown of tentacles into flow to capture suspended particles.

In contrast, the deposit feeding terebellid polychaetes feed off the surface of the substratum surrounding their tubes by means of numerous, long compliant tentacles. Most terebellids remain within their tubes, so that the area of substratum over which they can feed is limited by the length of their tentacles. During the process of feeding, force is required to pull the tentacles out, to keep them out, and to pull the tentacles back in. Terebellids exert the force to extend their tentacles, at least partially, by means of cilia located in a ventral ciliated food groove. To do this, they flatten the food groove against the substratum and use the cilia to crawl. Mucus in the food groove, in addition to its role in particle adhesion and transport, helps the tentacles to adhere to surfaces. The existence of circular muscles surrounding a fluid-filled tentacular coelom indicates that terebellids may also use internal hydrostatic pressures to help generate the forces required to extend their tentacles.

The present study examines a terebellid polychaete, *Eupolyornia heterobranchia*, that extends tentacles not only over the substratum, but also into flow. *E. heterobranchia* individuals found on False Bay, San Juan Island, Washington suspend their tentacles between layers in dense mats of the sheet-like green alga *Ulva fenestrata* (Fig. 1). The forces exerted on these tentacles include those required to extend the tentacles over the surface of the substratum and flow-induced drag on suspended tentacles.

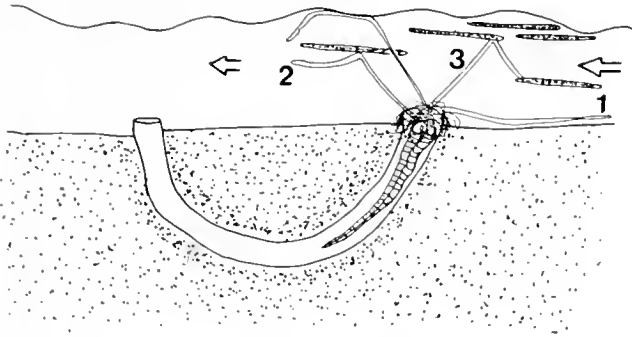


**Figure 1.** Schematic drawing (not to scale) of the terebellid *Eupolymnia heterobranchia* in its natural habitat. Arrow indicates direction of flow. *E. heterobranchia* (1) extends tentacles out over substrata, (2) dangles the ends of tentacles parallel to flow, and (3) suspends tentacles at an angle to flow by attachment either to sheet-like fronds of *Uva fenestrata* or to the water surface.

Tentacles exposed to flow between two points of attachment sag in the direction of flow (Fig. 2), much as the cables of suspension bridges sag in the direction of gravitational forces. The similarity is such that the equations used to analyze tension in the cables of suspension bridges are appropriate for analyzing tension in the tentacles of *E. heterobranchia* oriented perpendicular to flow. Such an analysis is used to address the specific question: how do the behavior and mechanical characteristics of the tentacles of the terebellid polychaete *Eupolymnia heterobranchia* allow them to remain suspended in flow? The results of these experiments represent one step in understanding the association between the mechanical characteristics of feeding tentacles and the way that they are used for feeding.

### Materials and Methods

#### Field site and collection of terebellids

*Eupolymnia heterobranchia* specimens were collected from the False Bay tidal flat on San Juan Island, Washington (48° 29' N; 123° 04' W) at about 0.0 m mean lower low water within areas covered by extensive mats of *Uva fenestrata*. These layered mats occur annually and persist from May through October (Price and Hylleberg, 1982). The unattached thalli of *U. fenestrata* float above the substratum when the flat is submerged. *E. heterobranchia* commonly construct tubes within folds in these floating algal sheets rather than within the mud of the flat. Whether they construct their tubes within the mud or the algal mats, these terebellids suspend their tentacles between the layers of algal thalli and into flow (Fig. 1).

False Bay is characterized by tidally dominated, unidirectional flow. Flow averaged over five days in a slightly more exposed area of False Bay (east side, near site C in

Price and Hylleberg, 1982) was  $0.043 \text{ m s}^{-1}$ ; daily peak velocities ranged between  $0.10$  and  $0.20 \text{ m s}^{-1}$  (Pentcheff, unpubl. data; measured in the field by a Marsh-McBirney electromagnetic flow probe at 6 cm above a rock substratum). Flow over the relatively protected area where *E. heterobranchia* was collected (west side, site D in Price and Hylleberg, 1982) and particularly between the layers of *U. fenestrata*, should be comparable, although somewhat slower.

Once collected, *E. heterobranchia* individuals were maintained at the University of Washington's Friday

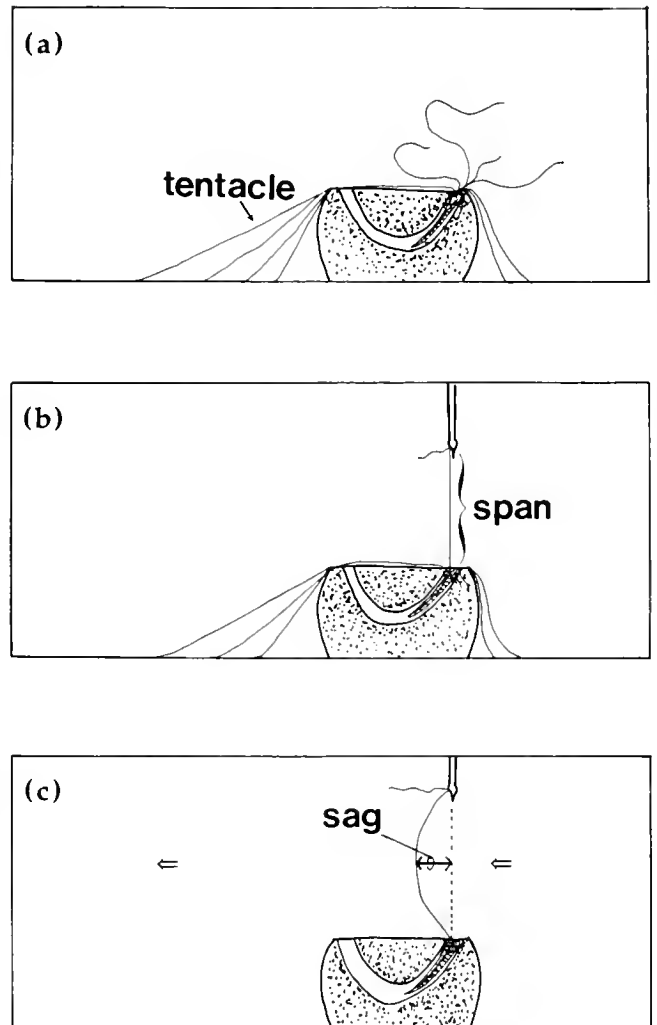


**Figure 2.** Schematic drawing (not to scale) of *Eupolymnia heterobranchia* in a flow tank. (a) Animals were allowed to self-attach a tentacle to the probe (using cilia and mucus). (b) Raising the probe oriented the tentacles perpendicular to flow. Span was the distance between points of attachment. (c) Arrow indicates direction of flow. Sag was the distance between the vertical line drawn between points of attachment and the point of maximum sag.

Harbor Laboratory in circulating seawater tables at around 15°C. When possible, worms were kept in their original tubes. Those specimens of *E. heterobranchia* that lost their original tubes were placed on muddy sediment where they constructed new (flimsier) tubes.

### The parabolic cable equation

The tension (force) in suspended tentacles that results from drag can be estimated with engineering formulas used to calculate tension in the cables of suspension bridges. Tension in the cables of suspension bridges is calculated using the force acting on the cables, the distance (or span) between points of attachment of the cable, and the amount of sag in the cable. Below, I review briefly the standard engineering equations for tension in parabolic cables (those that carry a uniform distributed load; see Steinman, 1942).

The horizontal tension at the points of attachment of a cable is exactly the tension in the cable at the point of maximum sag. At this point, there is only a horizontal component to the tension, and no vertical component. The horizontal tension,  $H$ , is:

$$H = \frac{\omega L^2}{8f} \quad (1)$$

where  $\omega$  for a parabolic cable is the uniform distributed load (a force) per horizontal linear unit,  $L$  is the span distance between points of attachment of the cable, and  $f$  is the sag of the cable. Sag of a cable is defined as the distance between the lowest point and a horizontal line drawn between the points of attachment of the cable.

The maximum tension,  $T$ , in the cable occurs at the points of attachment, where there is the greatest summed contribution from the vertical component of tension. The maximum tension,  $T$ , can be calculated from the horizontal tension,  $H$ , as follows (Steinman, 1942):

$$T = \sqrt{\left(\frac{\omega L}{2}\right)^2 + H^2} \quad (2)$$

Maximum tension can also be expressed as a function of the ratio of span to sag, ( $L/f$ ), by substituting Eqn (1) into Eqn (2) for  $H$ :

$$T = \sqrt{\left(\frac{\omega L}{2}\right)^2 + \left(\left(\frac{\omega L}{8}\right)\left(\frac{L}{f}\right)\right)^2} \quad (3)$$

Similar to the parabolic cable of suspension bridges, where the cable carries a uniformly distributed gravitational load, drag exerts a force that acts along the horizontal distance (projected area) of a tentacle oriented perpendicular to flow and suspended between two points of attachment. Therefore, force, which is  $\omega L$  for the parabolic cable, is drag,  $D$ , in the tentacle-cable equation. The de-

termination of drag on the tentacles of *E. heterobranchia* and its use in the cable equation are described below.

### Drag calculations

Drag is greatest on a tentacle oriented perpendicular to flow (Vogel, 1981). To orient tentacles perpendicular to flow, specimens of *E. heterobranchia*, intact within their tubes, were buried in mud in glass dishes that were placed in the bottom of a recirculating seawater flow tank (similar in design to that of Vogel and LaBarbera, 1978) (Fig. 2a). A micromanipulator was used to lower a probe to the mouth of the worm's tube and, subsequently, to raise the probe after the worm had attached a tentacle using cilia and mucus. In this way, tentacles were oriented perpendicular to the direction of flow, with two points of attachment: one on the probe, the other on the body of the worm (Fig. 2b). The tip ends of these suspended tentacles usually dangled downstream from the point of attachment to the probe (Fig. 2c).

Behavior of the tentacles in response to flow was quantified by photographing each tentacle several times at each velocity with a camera oriented perpendicular to the sag. A known distance on the probe was used to determine scale in all photographs. Span ( $L$ ), sag ( $f$ ), and tentacle length ( $l$ ) were measured off photographs; where span was the distance between points of attachment of a tentacle (Fig. 2b), sag was the distance between the maximum sag (parallel to flow) in that tentacle and a line defined by the two points of attachment (Fig. 2c) and tentacle length was the real length of the tentacle between the points of attachment. The span was set at a minimum by this method (no lower than the tip of the probe), but a tentacle could increase or decrease its span by changing attachment points along the length of the probe.

Drag on tentacles was determined using the standard equation for the drag on a cylinder perpendicular to flow (Vogel, 1981):

$$D = \frac{1}{2}C_D\rho SU^2 \quad (4)$$

where  $D$  is drag,  $C_D$  is the drag coefficient,  $\rho$  is the density of seawater,  $S$  is the projected area of each tentacle perpendicular to flow and  $U$  is the velocity. The projected area,  $S$ , of each tentacle was calculated as  $L \times d$ ; where  $d$  was the tentacle diameter. Tentacle diameter,  $d$ , was measured on 31 living, unstretched tentacles under a compound microscope (mean = 0.10; minimum = 0.05 mm; maximum = 0.13 mm; SE = 0.003 mm). Because diameter could not be measured during experiments in the flow tank, this mean tentacle diameter was used in all calculations of tension, except as described below. A propagation of error analysis using the minimum and maximum diameters measured indicated that this resulted in a maximum error of  $\pm 15\%$  in the tension estimated



for any particular tentacle. The average error from this source was unbiased.

The conventional drag coefficient,  $C_D$ , was estimated from an empirical formula (for Reynolds numbers from unity to  $10^5$ ) for a cylinder oriented perpendicular to flow (White, 1974 cited in Vogel, 1981):

$$C_D = 1 + 10 \text{Re}^{-2/3} \quad (5)$$

where Re is the Reynolds number:

$$\text{Re} = \rho dU/\mu \quad (6)$$

where  $d$  is the diameter of the tentacle and  $\mu$  is the dynamic viscosity of seawater. Unless otherwise specified, all references to drag in this paper refer to the calculation of drag using the variables as described above.

All experimental velocities in the flow tank were determined by timing neutrally buoyant particles. Experiments were conducted at velocities ranging between 0.5 and 7.0  $\text{cm s}^{-1}$ ; these velocities corresponded to Reynolds numbers for the tentacles between 1 and 7. Tentacles did not remain attached to the probe at velocities greater than 7.0  $\text{cm s}^{-1}$ . These velocities fell within the range measured in the field.

#### Use of the cable equation for the tentacles

Drag was used to calculate the maximum tension in the tentacle by substituting  $D$  for  $\omega L$  in Eqn (3):

$$T = \sqrt{\left(\frac{D}{2}\right)^2 + \left(\left(\frac{D}{8}\right)\left(\frac{L}{f}\right)\right)^2} \quad (7)$$

From Eqn 7 it can be seen that tension is a function of drag as well as of the ratio between span and sag ( $L/f$ ).

#### Material tests

The material properties of the tentacles of *E. heterobranchia* were determined by performing force-extension tests on an Instron tensometer (University of British Columbia, Vancouver). Lengths of tentacles, freshly cut off live animals, were fastened to grips, and relaxed by immersion in a solution of 7.5%  $\text{MgCl}_2$ . After relaxation, grips were moved slowly apart until the tentacle was put nearly into tension. The original length of the tentacles between the grips ( $l_0$ ) was determined by reading the value off the Instron to the nearest 0.1 mm. Tentacles were pulled at constant speed of 50  $\text{mm min}^{-1}$  (= a strain rate of between 0.04 and 0.15  $\text{s}^{-1}$ ; mean = 0.09, SE = 0.006) until they broke. Breaking force was measured off the chart paper to the nearest  $\mu\text{N}$ ; breaking length ( $l$ ) was measured off the chart paper to the nearest 0.1 mm. Extension ratio ( $\lambda$ ) was calculated as ( $l/l_0$ ). Extension ratio is useful as an intuitive description of length changes be-

cause  $\lambda = 2$  corresponds to a doubling of length,  $\lambda = 3$  corresponds to a tripling of length, etc. True strain can be determined from the extension ratio as  $\ln \lambda$  (Vincent, 1990). Linear regression analysis revealed that, within the range of strain rates used in these experiments, both breaking force and breaking  $\lambda$  were independent of strain rate [breaking  $\lambda$ :  $f_{(1,24)} = 2.39$ ,  $P$  (that the slope is zero) = 0.14; breaking force:  $f_{(1,24)} = 0.22$ ,  $P = 0.64$ ].

#### Sag-related drag reduction

It is assumed above that the drag of a sagging tentacle is equal to that of a non-sagging tentacle of equal span oriented perpendicular to flow. I used drag on a tentacle perpendicular to flow to isolate the effects of tension-reduction due to the geometry of sagging (the cable equation) from the drag reducing effects of sagging described below. In fact,  $C_D$  (Eqn 5) will be an overestimate of the coefficient of drag for a sagging tentacle because portions of the tentacle are oriented at some smaller (lower drag) angle to flow. The greater the sag of the tentacles, the greater the degree to which the coefficient of drag is overestimated by  $C_D$ . Furthermore, in a constant volume tentacle, diameter will decrease with increasing sag (increasing stretch). The magnitude of these two sag-related mechanisms of drag reduction can be calculated as follows.

The coefficient of drag for a cylinder at some angle to flow,  $C_{D\theta}$ , can be determined from  $C_D$  (for Reynolds numbers to  $10^5$ ; Hoerner, 1965) by:

$$C_{D\theta} = C_D \cos^3\theta \quad (8)$$

where  $\theta$  is the smallest angle between a line perpendicular to flow and the surface of the tentacle. The angle  $\theta$  was obtained at each point on the tentacle by:

$$\theta = \arctangent \frac{d}{dx} \left( \frac{4fx^2}{L^2} \right) \quad (9)$$

where  $x$  is the distance along the span from the origin (at the point of maximum sag) and ( $4fx^2/L^2$ ) is the parabolic equation describing the sagging tentacles (Steinman, 1942). An estimate of the corrected coefficient of drag for the entire tentacle,  $C_{Dc}$ , was obtained by substituting Eqn 9 into Eqn 8 for  $\theta$ , integrating Eqn 8 over the span of the tentacle (*i.e.*, adding up the coefficient of drag for each infinitesimal piece of tentacle) and dividing by the span of the tentacle:

$$\frac{2C_D \int_0^{L/2} \cos^3\theta dx}{L} \quad (10)$$

This is similar to the method used to determine the drag coefficient of a wing from the sum of the local drag coefficients of infinitesimal sections of the wing (Abbott and Von Doenhoff, 1959).

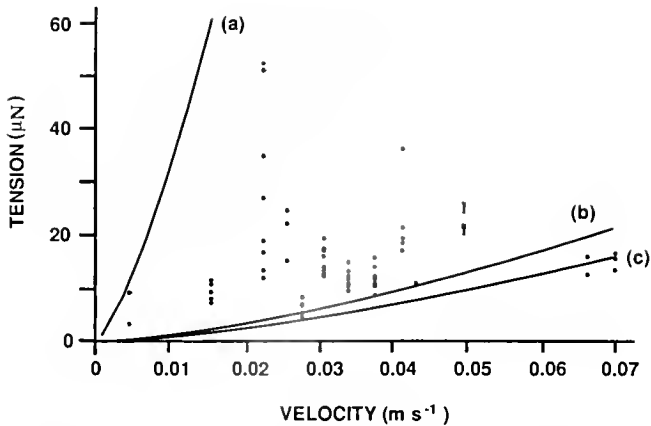


**Figure 3.** Tension ( $\mu\text{N}$ ) of suspended tentacles of *Eupolyornia heterobranchia* as a function of velocity ( $\text{m s}^{-1}$ ). Points indicate data. Tension in these tentacles was independent of velocity. Lines indicate tension calculated from Eqn 7 using the mean span and (a) the highest value for  $L/f$ , (b) the lowest value for  $L/f$ , and (c) the lowest value of  $L/f$  and the drag corrected for either the coefficient of drag or both the coefficient of drag and the tentacle diameter. These lines indicate that tension in the tentacles is reduced by sagging, mostly due to geometry (compare b to a) but also partly due to drag reduction (compare b to c).

A corrected diameter,  $d_c$ , was estimated by assuming that the tentacles maintain a constant volume as they stretch:

$$d_c = d(\lambda)^{-0.5} \quad (11)$$

where  $\lambda$  was determined from the ratio of the total length of the tentacle,  $l$  (measured from the photographs), and the span of the tentacle ( $L = l_0$ ).

## Results

### Tentacles as cables

Calculated drag on suspended tentacles of *Eupolyornia heterobranchia* increased with increasing velocity ( $F_{(1,76)} = 77.1$ ,  $P = 0.0001$ ,  $R^2 = 0.50$ ). Despite this relationship, linear regression analysis indicates that maximum tension (at the points of attachment) was independent of velocity (Fig. 3,  $F_{(1,76)} = 2.67$ ,  $P = 0.11$ ). Maximum tension in the tentacles was between  $0.34 \times 10^{-5}$  N and  $5.2 \times 10^{-5}$  N (mean =  $1.6 \times 10^{-5}$  N,  $n = 78$ ,  $\text{SE} = 0.10 \times 10^{-5}$  N). The results of linear regression analysis using data corrected for just  $C_{Dc}$  ( $F_{(1,76)} = 0.72$ ,  $P = 0.40$ ) as well as both  $C_{Dc}$  and  $d_c$  ( $F_{(1,76)} = 2.38$ ,  $P = 0.13$ ) are consistent with the results of linear regression analysis on the uncorrected data: maximum tension (at the points of attachment) remained independent of velocity.

Tension is a function not only of drag, but also of the ratio between the span and sag of the tentacle (Eqn 7). The independence of tension and velocity indicate that the ratio of span to sag ( $L/f$ ) should decrease as a function

of increasing velocity. The relationship between velocity and ( $L/f$ ) is shown in Figure 4, where curve (a) on Figure 4 represents the linear regression of  $\ln(L/f)$  as a function of  $\ln(\text{velocity})$  plotted on linear axes. Linear regression analysis of  $\ln(L/f)$  with  $\ln(\text{velocity})$  demonstrates that ( $L/f$ ) decreased with increasing velocity ( $F_{(1,76)} = 90.1$ ,  $P = 0.0001$ ,  $R^2 = 0.54$ ).

This relationship could be created by some combination of increasing sag and decreasing span with increasing velocity. Although minimum span was set by the end of the probe, span deviated from this minimum as a terebellid behaviorally moved the point of attachment relative to the end of the probe. Accordingly, span varied between 13.3 and 47.2 mm (mean span = 29.4 mm,  $n = 78$ ,  $\text{SE} = 1.10$ ) and sag varied between 0.160 and 10.3 mm (mean sag = 3.32 mm,  $n = 78$ ,  $\text{SE} = 0.29$ ). Linear regression analysis on the  $\ln$ - $\ln$  relationship between variables reveals that while sag did increase significantly with velocity ( $F_{(1,76)} = 52.9$ ,  $P = 0.0001$ ,  $R^2 = 0.41$ ; for examples, see Fig. 5 and Fig. 6), span was independent of velocity ( $F_{(1,76)} = 1.18$ ,  $P = 0.28$ ).

Individual tentacles initially responded to increases in velocity by increasing sag over a number of seconds ( $<30$

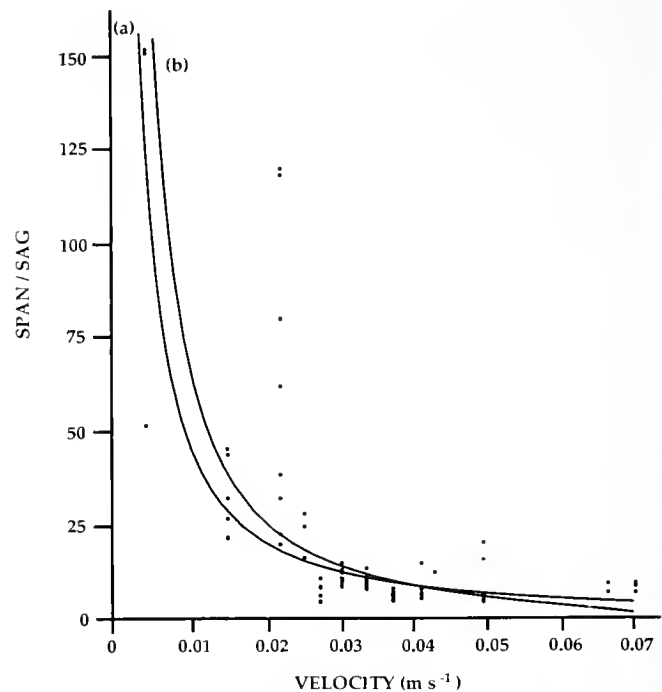


**Figure 4.** The ratio of span-to-sag of suspended tentacles of *Eupolyornia heterobranchia* as a function of velocity ( $\text{m s}^{-1}$ ). Points indicate data. Line (a) indicates the regression from a  $\ln$ - $\ln$  plot of this data; linear regression analysis on  $\ln$ - $\ln$  transformed data indicates that span-to-sag decreased as a function of velocity. Line (b) indicates the theoretical relationship between ( $L/f$ ) and velocity when constant values of tension and span were used in Eqn 12 (means for the data set:  $1.57 \times 10^{-5}$  N and 0.0295 m, respectively).

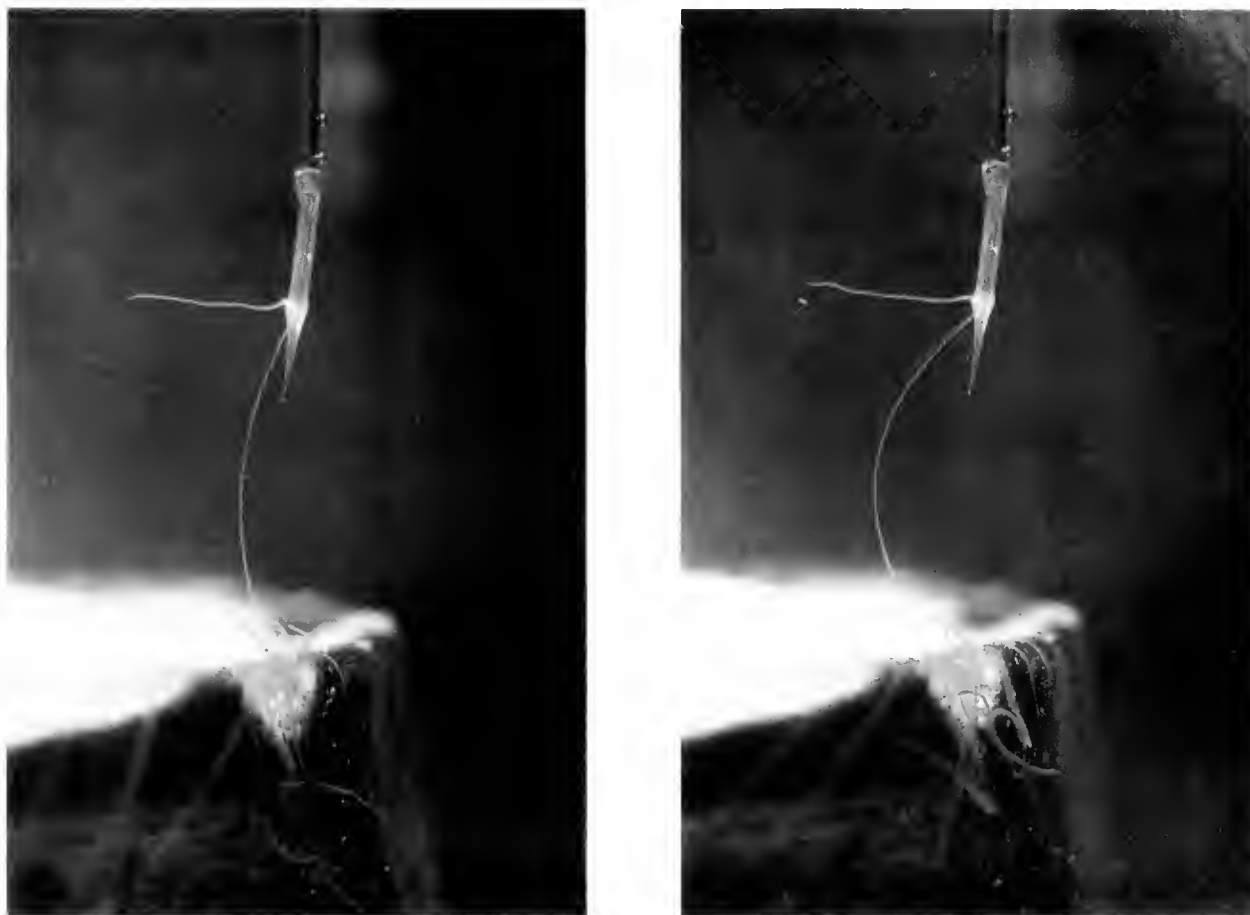


**Figure 5.** Photograph of a tentacle of *Eupolyommia heterobranchia* suspended perpendicular to flow. The tip of the tentacle dangles in the direction of flow, which is from right to left. For scale, span of the tentacle in both photographs is 2.5 cm. The photograph on the left is taken just as the velocity in the flow tank is increased from 1.5 to 3 cm s<sup>-1</sup>. The photograph on the right is of the same tentacle taken several minutes after the increase in velocity. Tentacles respond to increasing velocity by increasing sag.

seconds;  $n = 13$  tentacles). After the initial increase in sag, relatively small increases and decreases in sag occurred while velocity remained constant (Fig. 6).

#### *Mechanical response of tentacles*

A typical force-extension curve for a tentacle of *E. heterobranchia* is shown in Figure 7 (obtained by tracing the result of one force-extension trial directly off the chart paper). A force of  $4.6 \times 10^{-4}$  N more than tripled the length of this tentacle ( $\lambda = 3.5$ ) before breakage. Tentacles broke at forces between  $0.68 \times 10^{-4}$  N and  $7.6 \times 10^{-4}$  N (mean =  $3.5 \times 10^{-4}$  N,  $n = 29$ , SE =  $3.1 \times 10^{-5}$  N). Tentacles broke at  $\lambda$ s ranging from 1.79 to 5.35 (mean = 3.34,  $n = 29$ , SE = 0.17).

The slope of this curve is a measure of the relative stiffness of the tentacle, or its resistance to being extended. The tentacles of *E. heterobranchia* are least stiff at low  $\lambda$ s, requiring relatively little force to extend (Fig. 7a); than at

high  $\lambda$ 's (Fig. 7b). The transition in stiffness (*i.e.*, where the curve deviated from a line tangent to the lower portion of the curve; Fig. 7a) began at  $\lambda$ s in the range 1.66 to 2.48 (mean  $\lambda = 1.93$ ,  $n = 5$ , SE = 0.15) and at forces between  $0.18 \times 10^{-4}$  and  $0.64 \times 10^{-4}$  N (mean =  $0.36 \times 10^{-4}$  N,  $n = 5$ , SE =  $0.08 \times 10^{-4}$  N). Although these tentacles do exhibit strain rate dependent stiffness and stress-relaxation (*sensu* Vincent, 1990) at high  $\lambda$ s, these effects are not seen at low  $\lambda$ s (Johnson, unpubl. data).

The mean maximum tension in suspended tentacles was significantly less than the mean force at which stiffness increased (uncorrected data, ANOVA:  $F_{(1,82)} = 22.4$ ,  $P = 0.0001$ ).

#### **Discussion**

Tentacles of the terebellid polychaete *Eupolyommia heterobranchia* demonstrate a new mechanism of coping with flow forces. Sagging reduces flow-induced tension in ten-

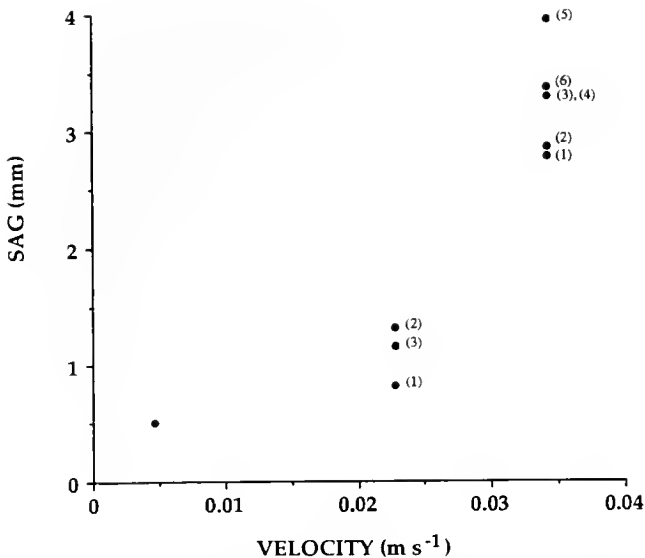


**Figure 6.** Sag (mm) as a function of velocity ( $\text{m s}^{-1}$ ) for one tentacle of *Eupolyornia heterobranchia* that maintained a constant span (mean = 2.8 cm,  $n = 9$ , SE = 1.15) at  $0.005 \text{ m s}^{-1}$ ,  $0.023 \text{ m s}^{-1}$ , and  $0.034 \text{ m s}^{-1}$ . Small numbers indicate the order in which the tentacle was photographed at a specific velocity. Photographs were taken approximately 5 s apart. Tentacles respond to velocity by increasing sag over a number of seconds. Within a velocity sag may also decrease (e.g., 5  $\rightarrow$  6 at  $0.034 \text{ m s}^{-1}$ ) suggesting that muscles are actively involved in regulating sag in the tentacles.

tacles; the largest contributor to this reduction in tension was achieved by closer alignment of force vectors that resist flow (parallel with the length of the tentacle) with force vectors imposed by flow (parallel with the direction of flow). This mechanism has the same ultimate effect as drag reduction by flexibility, streamlining, and reorientation: by modifying the effects of flow forces an organism can function in a wider range of flows (Wainwright and Dillon, 1969; Wainwright *et al.*, 1976; Koehl, 1977, 1984; Vogel, 1984; Denny *et al.*, 1985; Harvell and LaBarbera, 1985; Carrington, 1990). The discussion below analyzes the contribution of sagging and reorientation to tension experienced in the tentacles of *E. heterobranchia*.

The versatile, extensible, and flexible tentacles of terebellid polychaetes commonly occur adjacent to a substratum in low flow, mud, or sand flat environments (reviewed in Fauchald, 1977; Fauchald and Jumars, 1979). Such proximity to a substratum reduces the relative drag experienced for a given freestream flow because of the effect of the boundary layer (slower flows occur adjacent to the substratum). In contrast, the tentacles of the terebellid *E. heterobranchia*, extend not only over a substratum but also out into flow. Although extending tentacles into flow and over fronds of floating algae might increase access to potential food resources, this behavior also increases the exposure of tentacles to drag. Drag will have

conflicting mechanical consequences to tentacles, both positive, including facilitation of tentacle extension, as well as negative, including breakage or dislodgment.

Mechanical analysis, in which tentacles are modelled as the cables of suspension bridges (Eqn 7), reveals the behavioral and mechanical response of these tentacles to drag. For example, Eqn 7 shows that maximum tension in these tentacles (at the points of attachment) was a function not only of drag but also of the ratio between span and sag ( $L/f$ ). Maximum tension was statistically independent of drag, because increasing sag (shown by Figs. 5 and 6) decreased the ratio of span to sag and thus maintained a constant tension despite increasing velocity and, therefore, increasing drag.

Maximum tensions experienced by suspended tentacles were an order of magnitude less than the forces required to break the tentacles, indicating that suspended tentacles that sag are probably never in danger of being broken over the range of velocities at which they remained suspended. One can then ask: would tentacles in this orientation and in these flows break if they didn't sag? To examine this question, tension was calculated using Eqn (7) for tentacles of mean span, keeping ( $L/f$ ) constant over the range of velocities examined. Two extremes, the high-

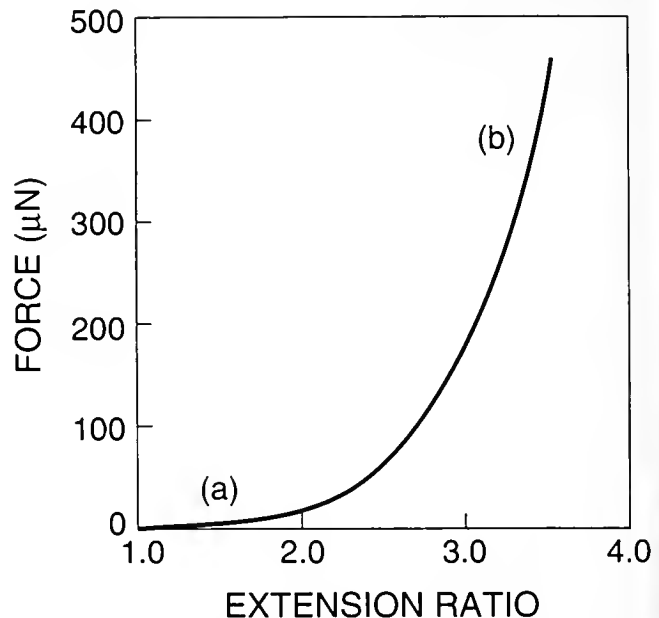


**Figure 7.** Force ( $\mu\text{N}$ ) as a function of extension ratio ( $\lambda$ ) for a relaxed tentacle of *Eupolyornia heterobranchia*. The curve shown in this figure was obtained by tracing the result of one force-extension trial off the chart paper. The slope of this curve is a measure of the relative stiffness of the tentacle. (a) These tentacles are least stiff at the lowest strains, requiring relatively little force to extend; (b) tentacles are most stiff just prior to breakage. Comparison of this curve with tensions and  $\lambda$ s of sagging tentacles indicates that sagging involves active muscles and is not merely a consequence of the passive material properties of the tentacles.

est (150.75) and the lowest (4.54) obtained from this data set, were chosen for  $(L/f)$ . The curves (a) and (b), obtained from the highest and lowest  $L/f$  respectively, were superimposed on the experimental data (Fig. 3: the spans of the tentacles whose data points fall below line b were shorter than the mean tentacle span. Because span contributes not only to this ratio but also to drag, the consequent tension was lower than that obtained from the line calculated from mean span). It can be seen from these calculations that all values for tension obtained from the data are lower than they would be if the tentacles were allowed only a small sag (as in curve 3a). These low-sagging tentacles would be subjected to their mean breaking force of  $3.5 \times 10^{-4}$  N at  $0.053$  m s<sup>-1</sup>, well below the highest velocity at which tentacles remained sagging suspended perpendicular to flow ( $0.07$  m s<sup>-1</sup>). Thus, sagging allows tentacles to remain suspended without breakage at higher flows than would otherwise be possible.

Although sagging potentially avoids breakage, the force in suspended tentacles was an order of magnitude less than that which would break them, suggesting that some other explanation accounts for the particularly low level of tension in suspended tentacles. Perhaps the tentacles sagged passively until they reached an equilibrium between the force imposed on the tentacles and the force with which the material of the tentacles could resist further extension. This mechanism assumes that muscles played no active role in determining the extension of the tentacles. If the tentacles were sagging passively, then a given calculated tension should have produced an extension ratio similar to that produced by a given force for the relaxed tentacle in Figure 7. In fact, although calculated tensions for sagging tentacles were as high as  $5.2 \times 10^{-5}$  N, corresponding to  $\lambda \cong 2.5$  in Figure 7, the greatest  $\lambda$  for sagging tentacles was only  $\lambda = 1.12$ . Thus, tentacles extended too little to be sagging passively: active muscular control must have been involved in controlling sag in the tentacles. Further, suspended tentacles sometimes decreased their sag by as much as 15% when experiencing a constant flow (Fig. 6), also indicating that there is an active muscular contribution controlling sag.

Given that muscles actively control sag in the tentacles, could the observed mean maximum tension correspond to the peak isometric tension of the muscle? Although some invertebrate muscles are somewhat stronger, virtually all muscle exerts a maximum stress of  $0.5$  MN m<sup>-2</sup> (Schmidt-Neilsen, 1983). One can estimate whether the stress in the tentacles exceeds the ability of muscles to hold tentacles in tension by dividing the mean maximum tension ( $1.6 \times 10^{-5}$  N) by an estimate of the cross-sectional area of the muscle in the tentacles ( $3.9 \times 10^{-8}$  m<sup>2</sup>;  $n = 28$ , SE =  $0.9 \times 10^{-8}$  m<sup>2</sup>; Johnson, 1992). The resulting estimate of stress in the muscles of suspended tentacles

( $4.1 \times 10^{-4}$  MN m<sup>-2</sup>) is several orders of magnitude less than that which the muscles can maximally exert.

Thus, *E. heterobranchia* are modulating tension at such low levels in tentacles neither (1) to prevent breakage *per se*, nor (2) as a result of passive material properties of the tentacles, nor (3) because of the limits of peak isometric tension in their muscles. One question arises from these results: is there a functional significance to the level of tension actively maintained in suspended tentacles? The next obvious hypothesis is that *E. heterobranchia* maintain tension in their tentacles below the detachment strength of the mucus and cilia. This hypothesis remains to be tested.

#### *L/f as a function of velocity*

The shape of the relationship between  $(L/f)$  and velocity, described by the curve in Figure 4, suggests that relatively large changes in sag are required to modulate tension at low velocities; whereas relatively small changes in sag result in constant tension at higher velocities. What accounts for the shape of this relationship between  $(L/f)$  and velocity? To address this question, the theoretical relationship between  $(L/f)$  and velocity was determined using constant tension and span by rearranging Eqn (7) to solve for a theoretical  $(L/f)$  as indicated below:

$$\frac{L}{f} = \sqrt{64 \left( \frac{T}{D} \right)^2 - 16} \quad (12)$$

Mean values of tension and span (used in the calculation of  $D$ ) for the data set were used to determine these constants ( $1.57 \times 10^{-5}$  N and  $0.0295$  m, respectively). The result of this calculation is shown by curve (b) in Figure 4. Not surprisingly, comparison of curve (b) with curve (a) in Figure 4 illustrates the earlier statistical results: that these curves represent the sag that is necessary to mediate drag so that tension is modulated under conditions of constant span.

#### *Effects of tentacle orientation on drag*

The above theoretical calculations assumed a constant coefficient of drag and a constant diameter, independent of sag. The above results are thus independent of changes in  $C_D$  and  $d$  that will occur in a sagging tentacle. The following section examines the effects of changes in  $C_D$  and  $d$  to drag reduction (Fig. 3).

Drag on sagging tentacles should be lower than that of a non-sagging tentacle of equal span because tentacles thin as they sag and because portions of the tentacles are oriented at angles less than perpendicular to flow. To examine the potential contribution of sagging to drag reduction, tension was calculated, again using Eqn (7) and the highest and lowest  $L/f$ , but including  $C_{Dc}$  as the coefficient of drag and  $d_c$  as the diameter of these tentacles.

Calculations using the highest  $L/f$ ,  $C_{Dc}$  and  $d_c$  resulted in a line identical to (a); there was no significant drag reduction in a tentacle of such low sag. Calculations using the lowest  $L/f$  with either just  $C_{Dc}$  or both  $C_{Dc}$  and  $d_c$  resulted in curve (c). There are several points that are illustrated by these results: (1) sagging results in drag reduction, especially at high velocities and high sags, (2) drag reduction due to decrease in diameter with increasing sag is negligible, and (3) even at high sags, drag reduction by sag-related reduction in the coefficient of drag contributes much less to reduction of tension than structural alignment of force vectors, especially at low velocities.

An extreme case of orientation relative to flow occurs when tentacles are dangling (*i.e.*, the danglers shown in Fig. 2 and Fig. 5) and thus are oriented parallel to flow. Could a tentacle become long enough and flow fast enough that drag would be sufficient to extend, or even to break, tentacles dangling out into flow? Drag on tentacles oriented parallel to flow can be estimated as approximately half that of tentacles oriented perpendicular to flow (Vogel, 1981). Actual drag should be slightly higher than given by this estimate because tentacles are of finite length. For this reason, I call this estimate "theoretical minimum drag." Figure 8 shows the theoretical minimum drag as a function of velocity for danglers that are 1 cm, 10 cm, and 30 cm long (a reasonable range of lengths for the tentacles of *E. heterobranchia*). Danglers in the low-flow environment of an intertidal flat are never in danger of being broken by drag. When terebellids relax the longitudinal muscles in their tentacles, however, drag is sufficient to contribute to passive tentacle extension. For example, Figure 8 indicates that danglers that are 10 cm long in flow of  $0.10 \text{ m s}^{-1}$  (the lowest peak speed measured) experience forces ( $1.3 \times 10^{-5} \text{ N}$ ) that, while still within the low stiffness region of the force-extension curve, are sufficient to nearly double the length of the average relaxed tentacle (Fig. 7). This mechanism of passive tentacle extension is most effective for longer tentacles in faster flows.

#### Ecological consequences

Quite apart from the mechanical results of this study, the observation that *E. heterobranchia* individuals suspend their tentacles into flow suggests that they are using tentacles to supplement deposit feeding with the capture of suspended food particles. While I have not observed suspension feeding in *E. heterobranchia*, it seems unlikely that it would reject suspended food particles that intercept its suspended tentacles. Although most terebellids are entirely selective deposit feeders (Fauchald and Jumars, 1979), suspension feeding does contribute to the diet of the terebellid *Lanice conchilega* (Buhr, 1976; Buhr and Winter, 1977; Fauchald, 1977). Furthermore, other ter-

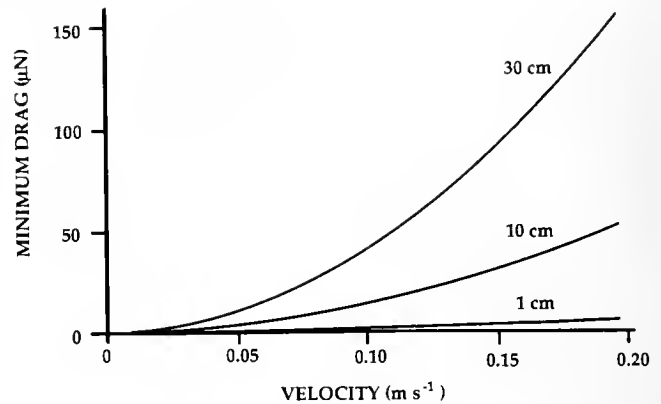


**Figure 8.** Theoretical minimum drag ( $\mu\text{N}$ ) as a function of velocity ( $\text{m s}^{-1}$ ) for 1 cm, 10 cm, and 30 cm long tentacles oriented parallel to flow (danglers). Maximum velocity of  $0.2 \text{ m s}^{-1}$  represents the maximum speed measured at False Bay (Pentcheff, unpub. data). Drag on danglers was always well below the maximum breaking force of tentacles ( $7.6 \times 10^{-4} \text{ N}$ ), but often within the range that would assist in passive extension of tentacles.

ebellids, such as *Loimia medusa* (Ellers, pers. comm.) also extend their tentacles into flow in a manner similar to that which I have described for *E. heterobranchia*.

Flow over the relatively protected area where *E. heterobranchia* is found, and particularly between the layers of *U. fenestrata*, will be slower than that measured by Pentcheff (see Materials and Methods). Furthermore, the angle of tentacles to flow will often be less than perpendicular. Thus, *E. heterobranchia* would be able to suspend tentacles into flow during most of the tidal cycle.

Sagging allows the tentacles to remain suspended in higher flows than would otherwise be possible, presumably increasing the amount of food these tentacles can gather. Feeding would be enhanced by the ability to sag not only because of increased access to suspended material but also because of increased access to food resources deposited upon the prodigious surface area of the stacked thalli of *U. fenestrata*. Thus, sagging increases the ecological range over which these terebellid polychaetes can function.

#### Acknowledgments

The author is deeply appreciative to M. Koehl for her support, advice, and encouragement. Thanks also to J. Gosline, O. Ellers, and R. Emler for helpful discussions and advice; A. O. D. Willows for providing space at Friday Harbor Marine Laboratory; K. Durante, G. Shinn, S. Walker, and W. H. Wilson for field assistance; B. Hale for assistance with data analysis; and D. Pentcheff for use of his unpublished flow data. Special thanks to M. LaBarbera for suggesting the use of the parabolic cable equation and to both him and S. Vogel for being wonderful teachers in the 1981 Biomechanics course at Friday Har-

bor. The quality of this manuscript was improved by two anonymous reviewers. This research was supported, in part, by a Libbie Hyman Memorial Field Scholarship, Northeastern University, and NATO post-doctoral fellowships, N.S.F. Research Planning Grant OCE 90-09763 to A. Johnson and N.S.F. Grants OCE-8352459 and OCE-8510834 to M. Koehl.

### Literature Cited

- Abbott, I. H., and A. E. Von Doenhoff. 1959. *Theory of Wing Sections*. Dover Publications, Inc., New York. 693 pp.
- Buhr, K.-J. 1976. Suspension-feeding and assimilation efficiency in *Lanice conchilega* (Polychaeta). *Mar. Biol.* **38**: 373-383.
- Buhr, K.-J., and J. E. Winter. 1977. Distribution and maintenance of a *Lanice conchilega* association in the Weser Estuary (FRG), with special reference to the suspension-feeding behaviour of *Lanice conchilega*. *Biology of Benthic Organisms. 11th European Marine Biology Symposium*, Galway, Ireland 1976: 101-113.
- Carrington, E. 1990. Drag and dislodgment of an intertidal macroalga: consequences of morphological variation in *Mastocarpus papillatus* Kutzing. *J. Exp. Mar. Biol. Ecol.* **139**: 185-200.
- Denny, M. W., T. L. Daniel, and M. A. R. Koehl. 1985. Mechanical limits to size in wave-swept organisms. *Ecol. Monogr.* **55**: 69-102.
- Fauchald, K. 1977. *The Polychaete Worms. Definitions and Keys to the Orders, Families and Genera*. Natural History Museum of Los Angeles County, Los Angeles. 188 pp.
- Fauchald, K., and P. A. Jumars. 1979. The diet of worms: a study of polychaete feeding guilds. *Oceanogr. Mar. Biol. Ann. Rev.* **17**: 193-284.
- Harvell, C. D., and M. LaBarbera. 1985. Flexibility: a mechanism for control of local velocities in hydroid colonies. *Biol. Bull.* **168**: 312-320.
- Hoerner, S. F. 1965. *Fluid-Dynamic Drag*. Hoerner Fluid Dynamics, Bricktown, NJ.
- Johnson, A. S. 1992. Morphology, mechanics and behavior in feeding with stretchy worm tentacles. *Am. Zool.* **32**: 116A.
- Koehl, M. A. R. 1977. Effects of sea anemones on the flow forces they encounter. *J. Exp. Biol.* **69**: 87-105.
- Koehl, M. A. R. 1984. How do benthic organisms withstand moving water? *Am. Zool.* **24**: 57-70.
- Price, L. H., and J. Hylleberg. 1982. Algal-faunal interactions in a mat of *Ulva fenestrata* in False Bay, Washington. *Ophelia* **21**: 75-88.
- Schmidt-Neilsen, K. 1983. *Animal Physiology: Adaptation and Environment* (3rd ed.). Cambridge University Press, Cambridge. 619 pp.
- Steinman, D. B. 1942. Suspension bridges. Pp. 289-358 in *Movable and Long-span Steel Bridges*, G. A. Hool and W. S. Kinne, eds. McGraw-Hill, New York.
- Vincent, J. 1990. *Structural Biomaterials*. Princeton University Press, Princeton, NJ. 244 pp.
- Vogel, S. 1981. *Life in Moving Fluids*. Willard Grant Press, Boston, MA. 352 pp.
- Vogel, S. 1984. Drag and flexibility in sessile organisms. *Am. Zool.* **24**: 37-44.
- Vogel, S., and M. LaBarbera. 1978. Simple flow tanks for research and teaching. *BioScience* **28**: 638-643.
- Wainwright, S. A., W. D. Biggs, J. D. Currey, and J. W. Gosline. 1976. *Mechanical Design in Organisms*. Princeton University Press, Princeton. 423 pp.
- Wainwright, S. A., and J. R. Dillon. 1969. On the orientation of sea fans. *Biol. Bull.* **136**: 130-139.

# Flow Velocity Induces a Switch From Active to Passive Suspension Feeding in the Porcelain Crab *Petrolisthes leptocheles* (Heller)

GEOFF TRAGER<sup>1,\*</sup> AND AMATZIA GENIN<sup>2</sup>

<sup>1</sup>Bar-Ilan University, Ramat-Gan, Israel, and <sup>2</sup>The H. Steinitz Marine Biology Laboratory, The Interuniversity of Eilat, Israel

**Abstract.** A flow-induced switch in suspension-feeding behavior of the porcelain crab *Petrolisthes leptocheles* was investigated in a laboratory flow tank. Crabs were exposed to two types of experimental water flow to stimulate them to switch from active to passive suspension feeding. In the first experiment, feeding crabs were exposed to a uni-directional accelerating water current, and they switched from active to passive suspension feeding at a mean water velocity of  $3.49 \text{ cm s}^{-1}$ . In the second experiment, crabs were exposed to flow that was fixed at a constant velocity for at least 10 min, and their feeding behavior in this steady flow was observed. This procedure was repeated, using a range of constant-velocity flows that were successively adjusted to increased velocity levels. Crabs exposed to these different constant-velocity flows fed exclusively actively at flows below  $1.5 \text{ cm s}^{-1}$  and exclusively passively at those above  $4.5 \text{ cm s}^{-1}$ . Switches from active to passive feeding occurred throughout the range of constant-velocity flows from  $1.5$  to  $4.5 \text{ cm s}^{-1}$ .

Changes in feeding activity rate induced by an increase in water velocity were measured. The mean activity rate of active feeding (1.05 Hz) was 3.4 times higher than that of passive feeding (0.31 Hz).

The porcelain crab's ability to switch feeding modes in response to increased water velocity probably enhances energetic feeding efficiency in two ways. First, the passive feeding activity rate is lower than the active one and should reduce energetic expenditure. Additionally, the flux of

suspended food increases with water flow velocity, so passive feeders are likely to catch more food per unit time than active feeders do. The ability to switch feeding modes is quite similar to that already described for balanomorph barnacles and appears to represent convergent evolution of flexible feeding behavior in response to variable water flow environment.

## Introduction

Many benthic marine invertebrates can switch their mode of feeding in response to changes in environmental conditions. For example, in the grapsid crab *Gaeticke depressus*, Depledge (1989) observed several feeding modes including scavenging, predation, deposit feeding, and suspension feeding, noting that the particular mode observed depended on the availability of different food types. Turner and Miller (1991) showed that a sufficient water movement would induce deposit-feeding chaetopteric polychaetes to extend their tentacles into the current and switch to suspension feeding. Okamura (1987) inferred a switch from ciliary to tentacular suspension feeding that was induced in bryozoans by particle size and flow velocity. According to foraging theory, such behavioral switches tend to enhance feeding efficiency (as measured in some energy currency, such as net energy gained per unit time, or the ratio of energy gained to energy spent) and thus increase fitness (Schoener, 1971; Pyke, 1984).

In aquatic habitats suspension feeding is a widespread mechanism for obtaining energy and materials from the water column, and representative suspension feeders are found in most major animal phyla (Jorgensen, 1966). Suspension feeders can be generally categorized as either active or passive. Active feeders spend their own metabolic energy to pump water past feeding structures, whereas

Received 6 October 1992; accepted 6 May 1993.

\* Author to whom reprint requests should be addressed. Correspondence address: Dr. Geoffrey C. Trager, The H. Steinitz Marine Biology Laboratory, The Interuniversity of Eilat, P.O. Box 469, Eilat 88103, Israel.



passive feeders rely on the external source of energy in ambient currents for delivery of food particles to feeding structures (LaBarbera, 1984). Some animals, such as barnacles and tunicates, can suspension feed both actively and passively (LaBarbera, 1977).

The passive feeding mode in porcelain crabs has received only brief mention in the literature (e.g., Wicksten, 1973; Kropp, 1981), probably because the velocities of incidental flow induced by aeration devices are typically too low to produce active feeding in laboratory aquaria.

Here, we quantitatively describe a flow-induced switch from active to passive suspension feeding in the porcelain crab *Petrolisthes leptochelēs*. A behavior indexing technique was employed to provide both qualitative information on feeding behavior components and quantitative data on feeding activity rates. These data were amenable to standard time-series analysis (fast Fourier transforms) for quantitative differentiation of active and passive feeding behaviors on the basis of differences in their activity rates (frequencies). Our results supplement the list of species that are known to switch from active to passive suspension feeding when water currents are sufficiently high.

### Materials and Methods

*P. leptochelēs* was collected in the Gulf of Eilat, Red Sea, Israel, from under stones in the shallow subtidal (to 0.5 m depth) off the H. Steinitz Marine Biology Laboratory, the Interuniversity of Eilat, Israel. Specimens were kept in unfiltered, flowing seawater. Experiments were carried out at the Laboratory from January through February 1992 and in February 1993. Throughout all experiments, the water temperature was 25–26°C.

To control water flow precisely, a flow-pattern generator was used. It consisted of a recirculating flow tank (Vogel and LaBarbera, 1978) modified by the addition of computer-controlled water flow. Water movement was produced by computer programs that were interfaced, through a digital-to-analog circuit, with a motor-driven propeller immersed in the flow tank (Fig. 1a). To record behavior and water flow simultaneously, laser optics (Strickler, 1985), fiber optic lamps, close-up lenses, and video equipment were used (Fig. 1b). This video-optical system allowed close-up observation (image magnification from 10 to 30×) of animal motions, as well as visualization of water flow as indicated by the movements of brightly illuminated particles naturally suspended in unfiltered seawater. For videorecording during experiments, all animals were placed on a gravel-filled petri dish which was then positioned on the floor of the flow tank so that the anteroposterior axis of the crab was perpendicular to the axis of flow direction while its mouth faced towards the camera.

Two computer programs were used to produce two types of experimental water flow change. In the first ex-

periment, water was continually accelerated linearly past a suspension feeding crab at a rate of  $0.15 \text{ cm s}^{-2}$ , with a program that produced the repeating pattern of alternating accelerating and decelerating flows shown in Figure 2. The suspension-feeding behavior of one crab at a time was videorecorded during one acceleration period. During the following deceleration period, the crab was removed from the flow tank, and the flow tank motor was shut off. Another crab was placed in the tank, and when feeding began, the motor was turned on to expose the crab to the same accelerating flow stimulus that the previously tested crab experienced. This protocol was repeated until 19 crabs had been tested. The computer program assured that the water flow acceleration stimulus was the same for each crab.

In the second experiment, a different computer program was used to maintain a constant water flow velocity (acceleration = 0) for an extended period. Here, a crab was placed in the flow tank, first in nearly still water (less than  $2 \text{ mm s}^{-1}$ , flow tank motor off), and when feeding began, its behavior was videorecorded for 10 min. Then the crab was removed, the motor was turned on with the computer program at a fixed setting, and flow in the tank was allowed to stabilize (for 1 min) at a steady flow velocity of  $0.5 \text{ cm s}^{-1}$ . The crab was then put back into the tank, and when feeding began, its behavior was videorecorded for another 10 min with flow constantly maintained at  $0.5 \text{ cm s}^{-1}$  (i.e., no change in velocity) throughout the recording period. This procedure was repeated with the same crab, but successively increased, constant velocity flows ( $1.0, 1.5, 2.5, 3.5, 4.5, 5.5,$  and  $6.5 \text{ cm s}^{-1}$ ). Each velocity was maintained for 10 min while feeding behavior was videorecorded. The entire protocol was repeated until 11 crabs had been tested.

Flow velocities local to the animal (from 2 to 6 mm above the distal edges of extended feeding fans) were measured by frame-by-frame tracking of the movements of back-lit particles suspended in flowing water as described by Trager *et al.* (1990).

Time-series data on feeding-motion cycles were obtained by playing back the videorecordings. Components of cyclical feeding behavior were identified, and a numerical value was assigned to each one, producing a behavioral index. For example, crab feeding-fan movements during active suspension feeding consist of three easily identified components (transfer of food particles from the fan to the mouth, upward extension of the fan, and a forward and downward capture stroke) that occur over and over again in the same sequence. These three components were assigned index values 1, 2, and 3, respectively. Behavioral time-series data were taken every 0.04 s (every video frame), over a total period of 81.9 s (more than 50 behavior cycles), by assigning the appropriate index value to the behavioral component observed

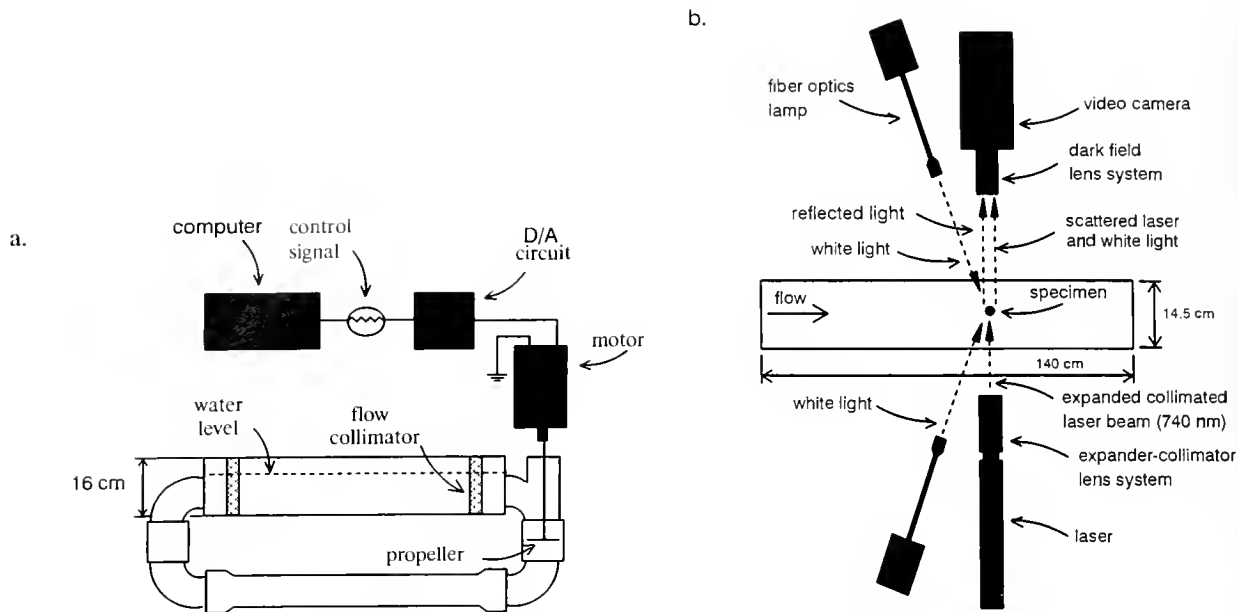


**Figure 1.** Apparatus for controlling water flow. (a) Side view of computer-controlled flume. Computer programs generate digital signals and send them to the digital-to-analog (D/A) circuit, where they are converted to analog signals to the 12 V DC flume motor. This system allows precise repetition of experimental flow regimes. (b) Top view of flow tank showing positioning of video camera, lens system, light sources, optical paths, and specimen. Backlighting was provided, either by a laser in line with the specimen and the video camera or by a fiber optics lamp at an angle of about  $25^\circ$  to a line through the specimen and video camera. The dark-field lens system was used only with the laser. The two backlighting sources were not used simultaneously. Both techniques provide a similar dark-field image in which naturally suspended particles in flowing seawater appear as bright points of light against a dark background, for flow visualization. Frontlighting by fiber optics was also provided for bright-field illumination of moving feeding appendages.

in each consecutive video frame. Plotting the indexed behavioral data against time produces a wave form, or cyclical curve, that illustrates the changes in feeding com-

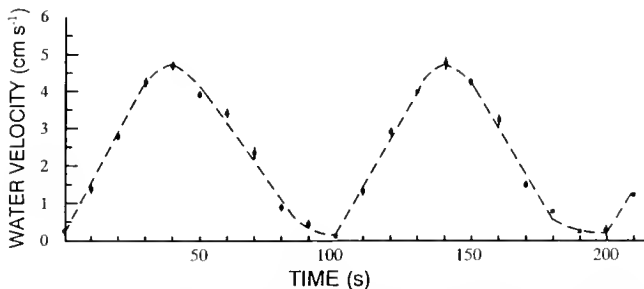


**Figure 2.** Repeating pattern of alternating accelerating and decelerating flows producing replicable, linear, water flow acceleration inducing porcelain crabs to switch from active to passive feeding. Feeding behavior was monitored only while flow accelerated. Flow deceleration simply reset the water velocity back to its original starting level, so that the next animal tested could be exposed to the same flow acceleration stimulus that the previously tested crab experienced. This flow pattern was generated by a triangle-wave signal from a computer program. Each point is the mean velocity of 20 suspended particles tracked from 0.5 s before to 0.5 seconds after the time indicated on the abscissa. Vertical bars show standard errors.

ponents and activity rhythms that concur with changes in flow velocity. The cyclically fluctuating numerical data produced by behavioral indexing are also suitable for analysis with fast Fourier transforms in the frequency domain, so that the distinct activity rates (frequencies of cyclical feeding-fan motions) distinguishing active versus passive feeding could be identified.

## Results

Although active and passive feeding were easy to distinguish on the basis of activity rate and orientation of feeding structures, there was a period of transition during the acceleration experiments when, as water was gradually accelerating, the crabs exhibited intermediate feeding behaviors with characteristics of both modes. These flow-induced behavioral changes, from active to intermediate to passive suspension feeding, are described below.

In very calm water ( $<1 \text{ cm s}^{-1}$ ), the crabs always suspension feed actively, by simultaneously extending both of their setose third maxillipeds to form two extensive spoon-shaped feeding fans (Fig. 3a). Both fully extended fans are then flexed, sweeping rapidly forward, downward, and laterally toward the mouth through a volume of water

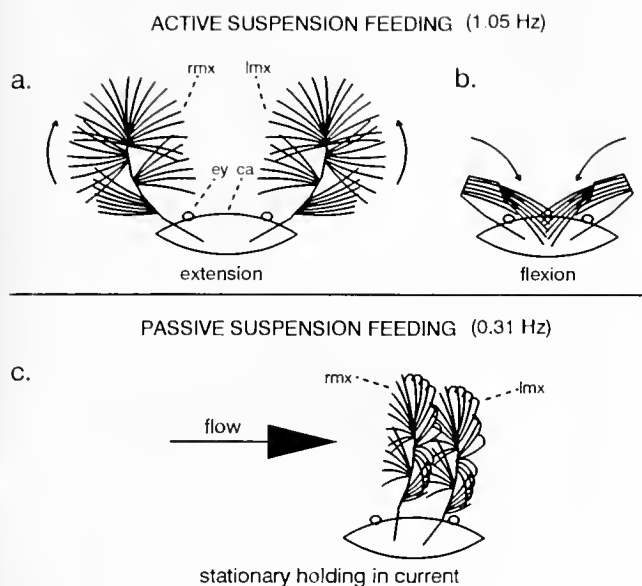


**Figure 3.** Diagram of porcelain crab (front view) carrying out active suspension feeding, which occurs only in slow ambient flow (on average, at flow velocities less than about  $3.5 \text{ cm s}^{-1}$ ), and passive suspension feeding, which occurs only in fast flow (on average, at flow velocities greater than about  $3.5 \text{ cm s}^{-1}$ ). (a) During active feeding, the third maxillipeds are spread laterally and then unflexed so that the setae spread out to form a spoon-shaped fan. Abbreviations: ca, carapace; ey, eye; lmx, left third maxilliped; rmx, right third maxilliped. (b) The next component of active feeding consists of the fan being flexed and sweeping forward, downward, and laterally towards the mouth for removal and transfer of trapped food particles to the mouth. (c) During passive feeding, both feeding fans are held stationary with the concave sides facing into the current. Arrow indicates water flow direction.

(Fig. 3b). Next, the fans contact the second maxillipeds, which remove trapped food particles that are passed to the mouth. This entire sequence is performed repeatedly for as long as active feeding lasts. This feeding behavior is similar to that described by Nicole (1932) for the porcelain crab *Porcellana longicornis*, except that *P. longicornis* usually sweeps its left and right fans alternately, whereas in this study, *P. leptochelae* always swept both fans simultaneously.

When the accelerating water reaches a velocity of about  $1.5$  to  $2 \text{ cm s}^{-1}$ , intermediate behaviors begin with characteristics of both active and passive feeding. The crabs still sweep both fans rapidly and rhythmically, but begin to angle the concave side of the left fan towards the current so that the capture stroke begins in the upstream direction. This is not possible for the right fan because the structure of the third maxillipeds does not permit a sweep (flexion) laterally away from the animal (see Fig. 3). Thus, the right fan, unlike the left fan, continued to repeatedly extend and flex, as in calmer water.

As the water continues to accelerate, the frequency of the cyclical motions for both fans decreases because a

new behavioral component appears. Immediately after fan extension, there is a pause, during which the fan is held fully extended and stationary, with the concave side facing upstream, positioned for passive suspension feeding in the current (Fig. 3c). The duration of this stationary fan-holding behavior steadily increases, up to a point, as the water velocity continues to increase, and the sweep into the current of the left fan is quickly phased out, so that stationary holding is followed by a twisting, forward, downward, and proximolateral flexion similar to that of active feeding. Extension of the fans into the current, holding in a stationary concave-upstream position for a time, and then flexion for particle removal is the typical cycle of passive feeding behavior.

In a few cases, the water was accidentally accelerated very rapidly (e.g., around  $10 \text{ cm s}^{-2}$ ) when the flow system was turned on with the motor already at a high-speed setting. In these cases, the crabs switched from active to passive feeding almost instantaneously, with no evident intermediate behavior. But in the controlled experimental flow that was gradually accelerated (at a rate of  $0.15 \text{ cm s}^{-2}$ ), there was always a period of intermediate behavior. Thus, switch velocity, which is defined here as the ambient water velocity in accelerating flow at which a suspension-feeding animal switches from active to passive feeding, was determined as the point at which the stationary holding component of passive feeding (which is the primary distinguishing characteristic of the passive feeding mode) is longer than 1 s.

The flow-induced behavioral changes from active to intermediate to passive suspension feeding are depicted graphically in an indexed-behavior time-series plot (Fig. 4) that displays both qualitative and quantitative (frequency) information.

The mean switch velocity for all crabs tested in accelerating flow was  $3.49 \text{ cm s}^{-1}$  (Fig. 5). The mean cycle frequencies of active (1.03 Hz) and passive (0.31 Hz) feeding motions are compared in Table I. The passive feeding rate was much more variable than the active feeding rate, and the mean activity rate of actively feeding crabs was 3.4 times greater than that of passively feeding crabs.

In the constant-velocity experiments, all 11 crabs tested fed exclusively in the active mode at velocities less than  $1.5 \text{ cm s}^{-1}$  and exclusively in the passive mode at velocities greater than  $3.5 \text{ cm s}^{-1}$ . Switches from active to passive feeding occurred from  $1.5$  to  $3.5 \text{ cm s}^{-1}$  (Fig. 6). In Figure 6, a crab was considered to have switched to passive feeding if it was observed to perform any passive feeding at all during a 10-min period. Five crabs switched in the middle of an observation period, and two of these switched back and forth several times during that period. For these five crabs that performed both active and passive feeding during an observation period, the mean percent of time

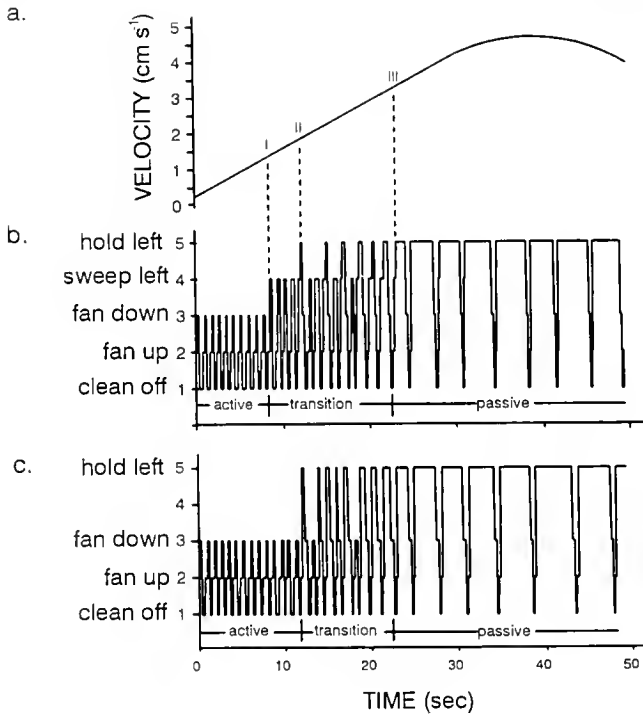


**Figure 4.** Behavioral change from active to intermediate to passive suspension feeding induced by linearly accelerated unidirectional water flow. (a) Linear change in flow velocity inducing the behavioral changes depicted graphically in (b) and (c), which show numerically indexed components of cyclical feeding behavior plotted against time. Each behavioral component and its assigned index value is listed on the ordinate, and the occurrence of any component is indicated by a peak or plateau in the curve at the appropriate level. The length of each horizontal portion of the indexed behavior curve indicates the duration (seconds) of a behavioral component. Steeply inclined rises or drops of the curve show when, from one video frame to the next, a behavioral component has changed. Thus, changes in activity rate (frequency) are indicated by changes in the horizontal distance between curve peaks, and changes in behavioral components are seen as changes in the height of the curve peaks. (b) Indexed behavior time series for the left feeding fan. Active feeding is rapid (0.95 Hz), occurs in slowly moving water, and consists of only 3 components (clean off, fan up, and fan down). The beginning of intermediate behavior, with characteristics of both active and passive feeding, first appears at a velocity of about 1.5 cm s<sup>-1</sup>, when the behavior curve suddenly jumps up to an index value of 4 (sweep left). The time and velocity at which this new component appears is indicated by (I) on the velocity curve. The activity rate also slows down somewhat during this transition period, with the appearance of the "hold left" component [stationary holding of the fan into the current (index value 5); its first appearance is indicated by (II) on the velocity curve]. Strict passive feeding begins at a velocity of about 3.2 cm s<sup>-1</sup> (see III), when the length of the hold left component is greater than 1 s. (c) The right fan shows changes in activity rate that are very similar to those of the left fan, but there is no sweep left (index value 4) component. The activity rate of the right fan during passive feeding is also considerably lower than that of strictly active feeding.

spent in passive feeding was 40.2% (SD = 13.2). The remaining six crabs fed only actively during the entire 10-min observation periods at low velocities, and then

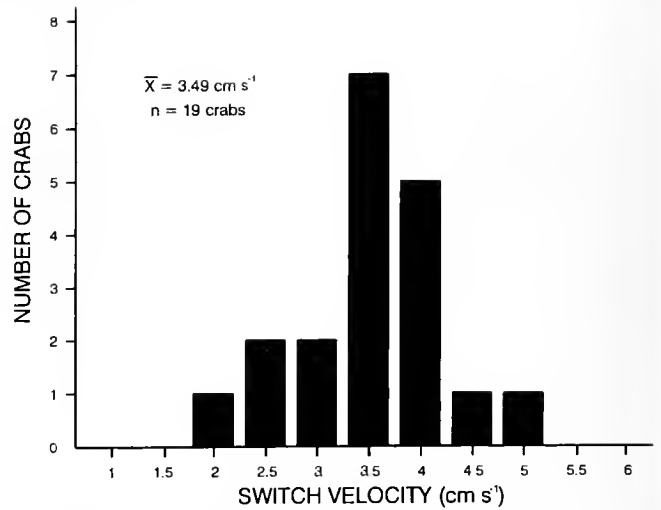


**Figure 5.** Switch velocities (*i.e.*, the ambient water velocities at which crabs switched from active to passive feeding) in unidirectional accelerated flow. Frequency histogram of the number of porcelain crabs in different switch-velocity classes. Each class is the median water velocity indicated on the x axis  $\pm$  0.25 cm s<sup>-1</sup>. Water velocities at the behavioral switch point were measured by calculating the mean velocity of 20 suspended particles video-tracked from 0.5 s before, to 0.5 s after the switch. A switch-velocity value for an individual crab is the average of the left and right fan values.

switched to feeding entirely in the passive mode throughout the observation periods at higher velocities.

Because the flow-induced changes exhibited by all crabs were similar, only two characteristic time series (2048 data points for each feeding fan of one animal) were chosen from the flow acceleration experiments for spectral analysis. Fast Fourier transforms of indexed behavior time series (portions of which are plotted in Fig. 4b and c) show that active and passive feeding behavior can be distinguished by their respective frequencies (Fig. 7). The power spectrum curve in Figure 7, produced by plotting the results of the fast Fourier transforms, indicates the relative importance of different component frequencies

**Table 1**

*Activity rates measured for active and passive suspension feeding in 19 porcelain crabs*

Feeding mode	Mean cycle frequency* (Hz)	Variability (%)	
		Within individuals	Between individuals
Active	1.05	6.4	12.5
Passive	0.31	27.0	19.4

\* Calculated by measuring length (in seconds) of 10 consecutive cycles of active and passive feeding that were recorded on videotape.

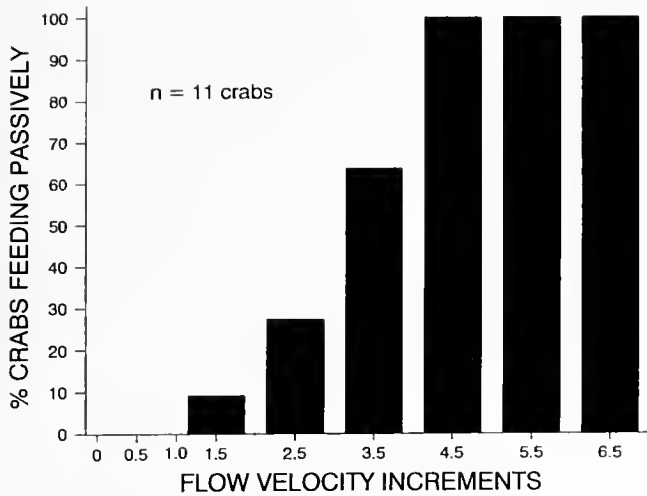


**Figure 6.** Percentage of crabs feeding passively over a range of constant velocity flows. Each constant flow velocity indicated on the  $x$  axis was maintained for 10 min. All crabs fed only actively from 0 to 1.0  $\text{cm s}^{-1}$ . An increasing percentage of crabs switched from active to passive feeding over the range of 1.5 to 4.5  $\text{cm s}^{-1}$ . At flows of 4.5  $\text{cm s}^{-1}$  and above, all crabs fed exclusively in the passive mode.

of feeding-fan movements. Thus, a distinct peak on the power spectrum curve indicates a dominant activity rate, or frequency (on the  $x$  axis directly below the peak), that characterizes a distinct feeding mode. For both the left and right fans, two dominant power spectrum peaks represent the distinct activity rates of active and passive feeding. Several peaks between the active and passive peaks represent intermediate frequency behaviors that occurred during the transition from active to passive feeding.

### Discussion

Not all suspension feeders are able to switch between active and passive modes. The switch may increase feeding efficiency in at least several ways. First, passively feeding crabs are able to depend on an external ambient current to deliver suspended food particles to feeding structures; they therefore do not spend their own metabolic energy to pump water past food-capturing structures. They are also able to orient their feeding appendages optimally with respect to current direction. Baumiller (1988) demonstrated that fluid flux through a concave model filter (a concave-shaped mesh) oriented perpendicular to the flow with the concave side facing upstream was greater than fluid flux through a similarly positioned planar mesh. Spielman and Goren (1968) showed that particle capture efficiency depends on the orientation of filter fibers. These facts together offer an explanation for the consistent passive-feeding orientation of crab feeding fans perpendicular to flow direction, with the concave side facing upstream (see Fig. 3c).

Particle capture rates are also predicted to be higher during passive feeding than during active feeding because passive feeding occurs only in relatively high-velocity flow, when fluid flux—and thus food flux to capture structures—should be greater than in calm water in which active feeding occurs.

Passive feeding is likely to be more efficient than active feeding for another reason. The proportion of total feeding time during which a fan is collecting particles is much greater for a passive feeder than an active feeder. The proportion of total feeding activity time that a fan was

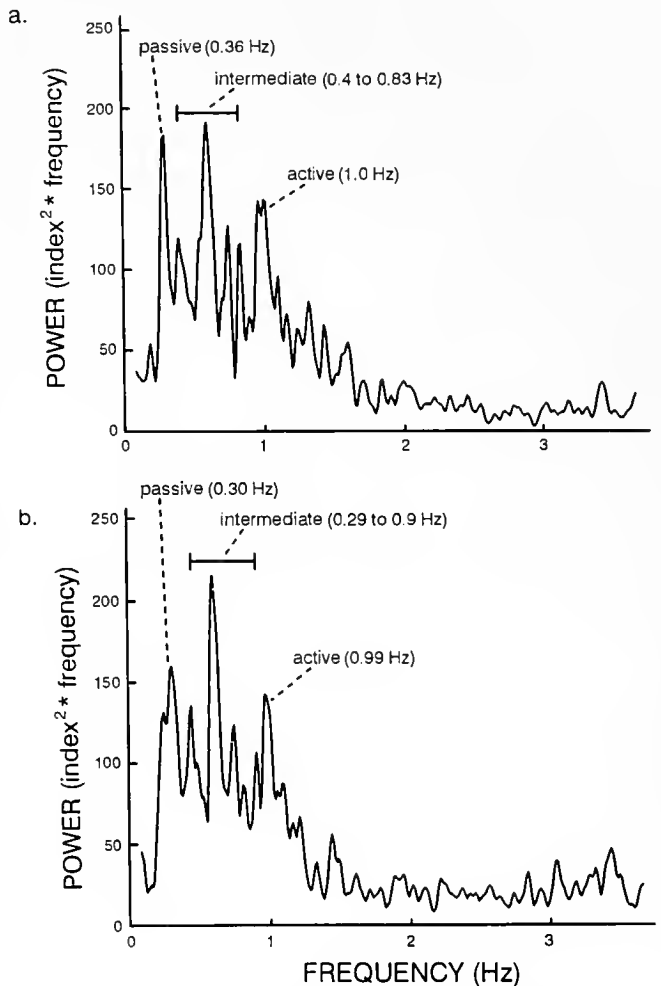


**Figure 7.** Active and passive suspension feeding are distinguished by their respective activity rates, or frequencies: (a) right fan; (b) left fan. Plotting the results of fast Fourier transforms (Press *et al.*, 1986) of indexed time-series data on feeding motion cycles (portions of which are plotted in Figure 4b and 4c) yields two power spectra that indicate the relative importance of the different frequency components of active, intermediate, and passive feeding behavior. In both the right and left fan plots, two distinct power spectrum peaks represent the distinct frequencies that characterize active and passive feeding. Several peaks between the active and passive peaks represent intermediate-frequency transition behaviors with characteristics of both active and passive feeding.

held stationary into the current during passive feeding was 87% (the other 13% of time was occupied by fan flexion, clean off, and extension). During active feeding, however, the fan is trapping particles primarily when a spread-open fan is swept through the water, and this sweep occupied only about 20% of feeding activity time (the other 80% was occupied by folding setae, cleaning them off, and extending the fan for the next sweep). Thus, the ratio of food catching time to food handling time (a reflection of energetic feeding efficiency) is greater for a passive feeder than an active feeder.

Active feeding should be more efficient than passive feeding only when ambient flow is so low that the bulk of the water, and thus the suspended food particles, will move around rather than through a stationary extended fan. This effect has been demonstrated for the barnacle *Semibalanus balanoides* by Trager *et al.* (1990), who showed that a dye stream aimed slightly (2 mm) above the geometrical center of an extended barnacle feeding fan flowed between the filter elements near the fan's center at an ambient flow speed greater than  $3.5 \text{ cm s}^{-1}$ , but was diverted completely around the entire fan at a lower ambient flow speed of  $0.5 \text{ cm s}^{-1}$ . This effect is also predicted by the "leakiness" model of Cheer and Koehl (1987) which describes, as a function of flow speed, bristle spacing, and bristle diameter, how much fluid leaks between the elements of bristled appendages of small organisms, as opposed to how much goes around the entire appendage. When passive feeding becomes less efficient than active feeding (at some ambient flow velocity that can be predicted to be less than, but near, the crab's mean switch velocity of  $3.49 \text{ cm s}^{-1}$ ), a crab must create the relative flow velocity past the filter needed to increase leakiness by actively sweeping its fan rapidly through the water. Therefore, it is the effect of flow velocity on fluid flux (and thus suspended food flux) to the filter that appears to determine the ambient flow velocity at which an animal switches from active to passive feeding.

The factors responsible for the large difference in activity rate between active and passive suspension feeding of porcelain crabs remain obscure. For effective active feeding, the animal must sweep its fans rapidly to pump new water within reach of feeding structures. Thus, a fan not only needs some degree of leakiness for particle capture, but also must have some "non-leakiness" so it can act as a paddle that pushes water past the animal. There are physical and energetic limits on how fast the animal can pump water. Even if these limits are not reached, pumping too fast may result in inefficient processing of the water moving past the animal. This inefficiency might be due not only to the increase in energy cost at a high pumping rate but also to the reduction in particle retention as drag forces increase and allow particles that contact the filter to be carried away by the current. The active

feeding activity rate may represent a trade-off between maximizing flow rate (and thus food flux to the vicinity of the filter) and maximizing food particle capture rate.

The passive feeding activity rate is determined primarily by the length of time a feeding fan is held stationary into the current. In the passive mode, a feeding fan can capture particles without rapid sweeping if it is simply held in position (concave-upstream) for extended periods. Thus, muscular activity rate (and presumably metabolic energy expenditure) is considerably reduced by switching from active to passive feeding when ambient water currents are strong enough.

For the porcelain crab *P. leptochelae* and the barnacle *S. balanoides*, both of which inhabit wave-swept environments, flow velocities are commonly well above the switch velocities of around  $3$  to  $3.5 \text{ cm s}^{-1}$  measured in the laboratory. In this study, field measurements taken every  $0.5 \text{ s}$  over 24 hours with an S4 Interocean current meter, in shallow water ( $0.5 \text{ m}$ ) in the crabs' habitat in the Gulf of Eilat, gave a mean flow speed of  $15.5 \text{ cm s}^{-1}$  ( $\text{SD} = 8.2$ , maximum =  $50.5 \text{ cm s}^{-1}$ ). Moreover, when first taken into captivity, both species began to feed passively if currents were slightly more than  $3 \text{ cm s}^{-1}$ , but did not feed at all for 1 or 2 days if kept in calm water ( $<1 \text{ cm s}^{-1}$ ), then began to feed actively. This suggests that the animals are accustomed to feeding mainly in the passive mode, and a period of starvation is required to induce feeding in the presumably more energy-demanding active mode. In nature, passive feeding may be the dominant mode for these animals because currents are usually sufficiently high. Active feeding in the natural habitat probably occurs only in restricted flow situations, such as tide pools at low tide or very quiet bays and estuaries when tidal currents are weak or absent. In the laboratory, active feeding has appeared to be the dominant mode only because flow velocities in typical observation aquaria are usually lower than the behavioral active-to-passive switch threshold.

Porcelain crabs and balanomorph barnacles demonstrate striking similarities in suspension-feeding structures and behavior. Although the animals are from different major crustacean taxa (Malacostraca and Cirripedia, respectively; Bowman and Abele, 1982), both possess moveable, scoop-shaped, setal feeding nets that can be oriented concave-upstream to current direction. Both are capable of tracking oscillating flow with high precision (Trager *et al.*, 1992), and both can switch from active to passive feeding in the presence of sufficiently rapid water currents. This suggests that other benthic crustacean species with jointed moveable suspension-feeding apparatus (*e.g.*, Hippid sand crabs and suspension-feeding hermit crabs) may also exhibit comparable convergent structural and behavioral adaptations for suspension feeding in variable flow regimes.

### Acknowledgments

We thank David Coughlin for writing the computer programs used to control water flow. Programs for performing fast Fourier transforms were written by Emanuel Boz. A helium-neon laser was provided by J. R. Strickler. We also thank Yair Achituv and the staff at the Bar-Ilan University mechanics and physics workshop for constructing the flow tank and the digital-to-analog electronic circuit. This work was supported by a Wolfson Foundation grant administered by the Israel Academy of Sciences to A. Genin, and a Nussbaum fellowship to G. Trager, through Bar-Ilan University, Ramat-Gan, Israel.

### Literature Cited

- Baumiller, T. K. 1988. Effects of filter porosity and shape on fluid flux: Implications for the biology and evolutionary history of stalked ctenoids. Pp. 786 in *Proc. 6th Int. Echinoderm Biol. Conf.*, R. D. Burke, P. Mladenov, P. Lambert and R. L. Parsley, eds. Victoria, British Columbia.
- Bowman, T. E., and L. G. Abele. 1982. Classification of the recent Crustacea. Pp. 1-27 in *The Biology of Crustacea*, Vol. 1, L. G. Abele, Academic Press, New York.
- Cheer, A. Y. L., and M. A. R. Koehl. 1987. Paddles and rakes: Fluid flow through bristled appendages of small organisms. *J. Theor. Biol.* 129: 17-39.
- Depledge, D. H. 1989. Observations on the feeding behavior of *Gaetice depressus* (Grapsidae: Varuninae) with special reference to suspension feeding. *Mar. Biol.* 100: 253-259.
- Jorgensen, C. B. 1966. *Biology of Suspension Feeding*. Pergamon Press, Oxford. 357 pp.
- Kropp, R. K. 1981. Additional porcelain crab feeding methods (Decapoda, Porcellanidae). *Crustaceana* 40: 307-310.
- LaBarbera, M. 1977. Brachiopod orientation to water movement. I. Theory, laboratory behavior, and field orientations. *Paleobiology* 3: 270-287.
- LaBarbera, M. 1984. Feeding currents and particle capture mechanisms in suspension feeding animals. *Amer. Zool.* 24: 71-84.
- Nicol, E. A. T. 1932. The feeding habits of the Galatheididae. *J. Mar. Biol. Assoc. U.K.* 18: 87-106.
- Okamura, B. 1987. Particle size and flow velocity induce an inferred switch in bryozoan suspension-feeding behavior. *Biol. Bull.* 173: 222-229.
- Press, W. H., B. P. Flannery, S. A. Teukolsky, and W. T. Vetterling. 1986. *Numerical Recipes*. Cambridge University Press, Cambridge. 818 pp.
- Pyke, G. H. 1984. Optimal foraging theory: a critical review. *Annu. Rev. Ecol. Syst.* 15: 523-575.
- Schoener, T. W. 1971. Theory of feeding strategies. *Annu. Rev. Ecol. Syst.* 2: 369-404.
- Spielman, L., and S. L. Goren. 1968. Model for predicting pressure drop and filtration efficiency in fibrous media. *Environ. Sci. Technol.* 2: 279-287.
- Strickler, J. R. 1985. Feeding currents in calanoid copepods: two new hypotheses. *Symp. Soc. Exp. Biol.* 39: 459-485.
- Trager, G. C., D. Coughlin, A. Genin, Y. Achituv, and A. Gangopadhyay. 1992. Foraging to the rhythm of ocean waves: Porcelain crabs and barnacles synchronize feeding motions with flow oscillations. *J. Mar. Biol. Ecol.* 164: 73-86.
- Trager, G. C., J.-S. Hwang, and J. R. Strickler. 1990. Barnacle suspension feeding in variable flow. *Mar. Biol.* 105: 117-127.
- Turner, E. J., and E. C. Miller. 1991. Behavior of a passive suspension feeder (*Phiochactopterus oculatus* (Webster)) under oscillatory flow. *J. Exp. Mar. Biol. Ecol.* 149: 123-137.
- Vogel, S., and M. LaBarbera. 1978. Simple flow tanks for teaching and research. *Bioscience* 28: 638-643.
- Wicksten, M. K. 1973. Feeding in the porcelain crab, *Petrolisthes cinctipes*, (Randall) (Anomura: Porcellanidae). *Bull. So. California Acad. Sci.* 72: 161-162.



## Effects of Flow Speed on Growth of Benthic Suspension Feeders

JAMES E. ECKMAN<sup>1</sup> AND DAVID O. DUGGINS<sup>2</sup>

<sup>1</sup>Skidaway Institute of Oceanography, P.O. Box 13687, Savannah, Georgia 31416, and <sup>2</sup>Friday Harbor Laboratories, 620 University Rd., Friday Harbor, Washington 98250

**Abstract.** In separate experiments in 1991 and 1992, the sensitivities of growth rates of six species of benthic suspension feeder to flow speed were tested in a series of turbulent pipe flows. Species examined were the cheilostome bryozoan *Membranipora membranacea* (1991); the serpulid polychaete *Pseudochitinopoma occidentalis* (1991); and the barnacles *Balanus glandula* (1991), *B. crenatus* (1992), *Semibalanus cariosus* (1992), and *Pollicipes polymerus* (1992). In both experiments, animals were exposed to one of five constant, narrow ranges of speed that varied from about 2–15 cm s<sup>-1</sup>. Growth rates of *Membranipora* and *Pseudochitinopoma* in 1991 declined significantly and monotonically with increasing flow speed, despite evidence that at faster flows there were greater concentrations of suspended food available and higher particulate fluxes. In contrast, there was no detectable relationship between speed and growth of *B. glandula* over the same range of flow speeds in 1991. Results of the 1992 experiment indicated variability in growth responses among three species of barnacle. Growth rates of *S. cariosus* and *P. polymerus* were insensitive to flow speed, whereas growth rates of *B. crenatus* increased from low speeds to a maximum at an intermediate speed of about 8 cm s<sup>-1</sup>, and then tended to decrease at higher speeds. Combined results of the two experiments indicate that the growth response of animals to flow was most obviously related to the relative flow energy of the animal's natural habitat. Growth rates of animals that typically experience relatively weak flows (*P. occidentalis*, *M. membranacea*, and *B. crenatus*) were affected significantly by flow speed, whereas growth rates of animals from comparatively high-energy environments (*B. glan-*

*dula*, *S. cariosus*, and *P. polymerus*) were relatively insensitive to flow speed. In contrast, animal morphology and behavior were not obviously related to growth responses to flow. A key to understanding the impact of flow on a suspension-feeder's growth may be the animal's ability to handle and process particles that have impacted the feeding apparatus and to deliver them to the point of ingestion.

### Introduction

One clear trend that has emerged from many studies of effects of flow speed on both passive and active suspension feeders is that rates of particle capture or growth are lower on both sides of a narrow range of intermediate speeds that appear to be most beneficial. This pattern has been demonstrated for growth of a scallop (Kirby-Smith, 1972) and particle capture by an alcyonacean coral (McFadden, 1986), a sea pen (Best, 1988), a crinoid (Leonard *et al.*, 1988), and a gorgonian coral (Sponaugle and LaBarbera, 1991). There are several causes for this trend. As flow speed increases from near-zero levels, rates of particle encounter with passively deployed filter elements increase (Shimeta and Jumars, 1991), and increased turbulent mixing makes depletion of food particles within the animal's feeding ambit less likely (Wildish and Kristmanson, 1979; Patterson, 1984; Fréchette and Bourget, 1985; Fréchette *et al.*, 1989). At relatively high flow speeds, deformation of filtering structures may reduce the total surface area available for particle capture (Patterson, 1984; Harvell and LaBarbera, 1985; Best, 1988; Shimeta and Jumars, 1991), particles impacting filter elements may be handled or processed with greatly reduced efficiency due to drag effects (Patterson, 1991; Shimeta and Jumars, 1991), or adverse pressure gradients may inhibit process-



ing of water containing suspended particulate food (Wildish *et al.*, 1987).

The trend of maximum particle capture or growth at intermediate flow speeds has not been exhibited in all studies that have addressed the relationship, however. By restricting study to a comparatively narrow range of flow speed on either side of the intermediate speed of maximum growth (nearly always unknown *a priori*), a simpler direct or inverse relationship between speed and particle capture or growth would appear. Thus, a monotonic increase in particle capture with flow speed was noted for a coral (Sebens and Johnson, 1991), but inverse relationships were reported between flow speed and scallop growth (Wildish *et al.*, 1987; Eckman *et al.*, 1989; Wildish and Saulnier, 1992), barnacle growth (Smith, 1946), and particle capture or growth by bryozoans (Okamura, 1984, 1985, 1992).

Despite the attention devoted to this topic of research, some important gaps remain in our understanding of the influence of flow on growth of suspension feeders. First, because prior studies have focused on individual species, it is not yet clear how different species, which have different behaviors and employ different mechanisms of suspension feeding, will respond to the same range of conditions. This knowledge would be useful in determining how assemblages of suspension feeders might become partitioned in space according to flow microhabitat, or in predicting the relative competitive success among species that exhibit differential sensitivities to flow. The relative competitive abilities of suspension-feeding species may well vary among sites depending on their flow energies. Second, for tentaculate suspension feeders (*e.g.*, hydrozoans, bryozoans, gorgonians), there is little evidence that the relationship between flow speed and particle capture (the dependent variable typically evaluated for this diverse guild) translates into identical effects on growth. This result may seem logical, but it has been demonstrated only by Okamura (1992). Moreover, the translation of particle capture to growth may not always be straightforward. For example, for two bryozoans there was a change in direction of the dependence of particle capture rate on flow speed as food-particle size changed over a comparatively narrow range (Okamura, 1987). Consequently, for tentaculate suspension feeders that enjoy a comparatively diverse diet, relationships between flow speed and capture rates of one particle type may not translate faithfully into growth responses.

We therefore carried out two experiments testing effects of flow speed on growth rates of several species of sessile, benthic suspension feeder. Our first experiment, carried out in 1991, involved the cheilostome bryozoan *Membranipora membranacea*, the barnacle *Balanus glandula*, and the serpulid polychaete *Pseudochitinopoma occiden-*

*talis*. These species all feed via a structure that is extended into the flow, beyond the calcareous zoecium, test, or tube that encloses the main body of the colony or animal. However, the behavior and the mechanism for operation of the feeding organ vary among these species, which may affect their relative growth responses to flow. In the first experiment, only the barnacle grew at rates independent of flow speed. Based on this result, we conducted a second experiment in 1992 to determine whether other barnacles from a wide range of habitats showed growth responses similar to that observed in *B. glandula*. This experiment involved the balanoids *B. crenatus* and *Semibalanus cariosus* and the pedunculate species *Pollicipes polymerus*. Finally, to complement these experiments, we also examined the feeding behavior of most of these species as a function of flow speed.

### Materials and Methods

Experiments were conducted at the Friday Harbor Laboratories of the University of Washington. In both experiments, effects of flow speed on growth were determined using animals suspended in pipes characterized by steady, turbulent flows. Relationships describing turbulent flow through a pipe are well known (*e.g.*, Schlichting, 1979; Vogel, 1981), making it comparatively simple to establish, monitor, and describe flow velocities to which animals were exposed.

#### *Experimental apparatus—1991*

Five narrow ranges of flow speed were established within 10 PVC pipes (two replicates per speed). Each pipe was 3-m long and either 2.5 cm or 3.8 cm in radius. All pipes were submerged in a seawater bath within a single tank that was 3.66-m long, 1.22-m wide, and 1.22-m deep. Pipes were aligned in parallel in a single row along the bottom of the tank, and were assigned randomly to different flow speeds. The pipes passed through a water-tight partition inside the tank, 1.22 m from one end. A diaphragm pump continuously supplied the smaller compartment of the tank (the head) with fresh seawater from a depth of 4 m. An overflow pipe in the head tank kept the seawater at a constant depth. The high rate of discharge of the pump (about  $31 \text{ s}^{-1}$ ) mixed water in the head tank thoroughly. An overflow pipe in the other section of the tank (the tail) kept seawater at a constant, lower depth. The resulting constant pressure gradient between the head and tail ends drove steady flows through the pipes. The rate of flow through each pipe was regulated with an adjustable valve located at the discharge end of each pipe.

Six windows (each about  $2.5 \times 4 \text{ cm}$ ) were cut in the wall of each pipe through which were inserted thin strips of plexiglass containing animals used in growth studies

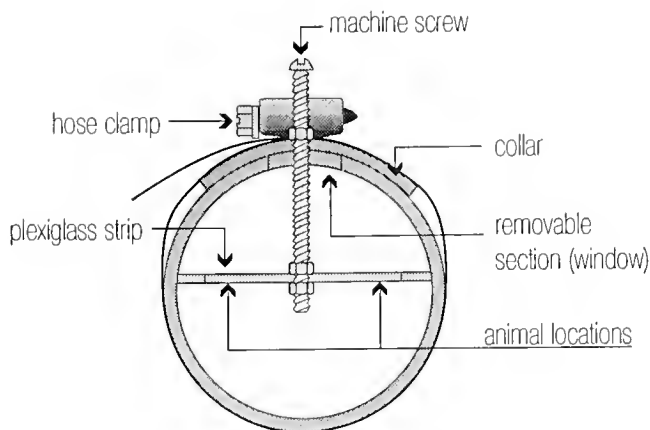


Figure 1. Cross-sectional view of the apparatus used to position suspension feeders within pipe flows. The hose clamp created a nearly watertight seal between the cut-out section of pipe mounted on the collar and the main body of the pipe.

(Fig. 1). The first window was cut 110 cm downstream of the pipe's entrance, and the other five windows were spaced 20-cm apart. The remaining downstream section of each pipe was used in a larval settlement study that will be described elsewhere. Each cut-out section of pipe was glued onto a larger PVC collar that could be clamped onto the pipe to make a nearly watertight seal. This entire assembly was removable. A machine screw passed through a hole in the collar and the section of pipe from which the window was cut (Fig. 1). The screw was used to suspend plexiglass strips containing animals across the diameter of each pipe. Plexiglass strips were 0.16-cm thick, spanning 2 cm in the along-stream dimension and either 5 or 7.6 cm across-stream, depending on the pipe's diameter. Strips were mounted level within pipes (*i.e.*, normal to gravity) such that all animals were facing down.

The growth experiment ran from 6 June–22 November 1991. During this period discharge rates of the pipes ( $Q$ ) were measured on 17 separate dates. Pertinent characteristics of turbulent pipe flows were calculated from pipe discharge rate and radius ( $R$ ) using relationships either given by Schlichting (1979) and Vogel (1981) or derived from equations they presented. The mean flow speed within each pipe ( $U$ ) was

$$U = Q/(\pi R^2) \quad (1)$$

Pipe Reynolds number ( $Re$ ) was

$$Re = U(2R)/\nu \quad (2)$$

where  $\nu$  is the kinematic viscosity of seawater ( $0.01 \text{ cm}^2 \text{ s}^{-1}$ ). The flow speed ( $U_y$ ) at any distance  $y$  from the pipe's wall ( $y = 0$ ) was

$$U_y = U_{\max}(y/R)^{1/n} \quad (3)$$

where  $U_{\max}$  is the maximum flow speed (along the pipe's center line) and

$$n = 6 + 0.6((Re - 4000)/19,000) \quad (4)$$

Eq. (4) was derived from Eq. (20.6) and Fig. (20.3) in Schlichting (1979, p. 599). From Eqs. (3, 4) one can calculate the maximum and minimum ( $U_{\min}$ ) speeds to which feeding organs of animals in any pipe were exposed, assuming that they were a distance at least 10% of the radius away from the pipe wall:

$$U_{\max} = U(1 + 1/n) \quad (5)$$

$$U_{\min} = U_{\max}(0.1)^{1/n} \quad (6)$$

As seawater entered the pipe from the head tank, a boundary layer developed along the pipe's wall. Eqs. (3–6) are valid only for a fully developed flow, which existed at all locations downstream of the distance ( $X_{\text{eq}}$ ) required for the boundary layer to grow to a thickness equal to the pipe's radius. For a turbulent boundary layer, this distance was approximately

$$X_{\text{eq}} = (R/0.37)^{1.25}(U_{\max}/\nu)^{0.25} \quad (7)$$

as derived from Schlichting (1979, his Eq. 21.8).

Table 1 lists flow properties for each of the 10 pipes in the experiment, based on the mean of the 17 separate measurements of discharge rate. In all cases, flow was fully developed before the first animal was encountered 110-cm downstream of each pipe's entrance (*i.e.*,  $X_{\text{eq}} < 110 \text{ cm}$ ). There were five levels of mean speed ( $U$ ) that ranged from about 2–15  $\text{cm s}^{-1}$ . Within each pipe there was little temporal variability throughout the experiment (Table 1); the coefficient of variation (standard deviation/mean) of  $U$  averaged 6.45%. However, due to the radial velocity gradient (Eq. 3), the range of flow speeds experienced by animals within a pipe could have been as great as  $\pm 10\%$ – $15\%$  of  $U$ .

It is important to note that a boundary layer also developed along each plexiglass strip to which animals were attached. Calculations (based on Eq. 21.8 in Schlichting [1979]) indicate that this boundary layer could have been no more than a few millimeters thick, even at the downstream end of each 2-cm-long strip, given the flow velocities in Table 1. Because the feeding structures of animals studied extended even greater distances above the substratum (Eckman and Duggins, 1991; personal observations), the effect of this boundary layer on flow speeds experienced by animals can be ignored, and animals were exposed to speeds reported in Table 1.

#### Experimental protocols—1991

Colonies of *Membranipora membranacea* were obtained after larvae settled onto large strips of plexiglass

Table 1

Average properties of pipe flows, arranged in order of increasing mean flow speed, in the 1991 and 1992 experiments

Pipe No.	$R$ (cm)	$Q$ (cm <sup>3</sup> s <sup>-1</sup> )	$Re$	$U$ (cm s <sup>-1</sup> )	$U_{max}$ (cm s <sup>-1</sup> )	$U_{min}$ (cm s <sup>-1</sup> )	$X_{eq}$ (cm)
1991 Experiment							
7	3.8	85.7	1433	1.9 (.04)	2.2	1.5	71
1	3.8	93.8	1567	2.1 (.03)	2.4	1.6	73
8	2.5	84.8	2124	4.2 (.11)	4.9	3.3	52
3	2.5	92.5	2317	4.6 (.22)	5.3	3.6	53
10	2.5	141	3527	6.9 (.24)	8.1	5.5	59
4	2.5	142	3555	7.0 (.17)	8.2	5.6	59
5	2.5	227	5692	11.2 (.31)	13.0	8.9	67
9	2.5	228	5706	11.2 (.30)	13.1	8.9	67
2	2.5	297	7446	14.7 (.30)	17.1	11.7	71
6	2.5	299	7482	14.7 (.35)	17.1	11.8	71
1992 Experiment							
5	5.1	—	2652	2.6	3.0 (.12)	2.3	111
10	5.1	—	2805	2.8	3.2 (.10)	2.4	112
9	5.1	—	5457	5.4	6.2 (.10)	4.8	133
4	5.1	—	5457	5.4	6.2 (.10)	4.8	133
3	5.1	—	8160	8.0	9.2 (.10)	7.2	147
8	5.1	—	8160	8.0	9.2 (.06)	7.2	147
2	5.1	—	10812	10.6	12.3 (.06)	9.5	157
7	5.1	—	10914	10.7	12.4 (.15)	9.6	157
6	5.1	—	13158	12.9	14.9 (.29)	11.6	165
1	5.1	—	13464	13.2	15.3 (.05)	11.8	166

Pipe No. refers to the relative position of pipes in the tank.  $R$  is inner radius.  $Q$  is discharge rate (not measured in the 1992 experiment).  $Re$  is Reynolds number.  $U$ ,  $U_{max}$  and  $U_{min}$  refer, respectively, to mean flow speed, maximum speed along the centerline, and minimum speed experienced by animals. Standard error (in parentheses) is given for  $U$  in the 1991 experiment and  $U_{max}$  in the 1992 experiment.  $X_{eq}$  is the distance downstream from the entrance required to achieve fully developed flow.

attached to racks suspended at a depth of about 2 m. Strips for deployment in pipes were cut from these larger strips such that each contained two or more colonies < 2 mm in diameter. Colonies on strips were photographed, using a video camera, just before they were placed in pipes on 6 June. Strips were removed from pipes on 25 June, and colonies were rephotographed.

Colonies that had grown to contact other colonies were not analyzed because intraspecific contact interferes with growth (Ellison and Harvell, 1989). Although most of the remaining colonies were circular on 25 June, many others contained invaginations, probably as a result of partial predation (Harvell *et al.*, 1990) inflicted by gastropods introduced into pipes by the pump. To minimize effects of these invaginations on estimates of growth, a "potential growth rate" of each colony was calculated as in Eckman and Duggins (1991). Potential growth was defined as the difference in areas of circles with radii equal to the maximum radius of each living colony (*i.e.*, the farthest distance from ancestrula to colony edge) on 6 and 25 June. Maximum radii were estimated from photographs made on 6 June and measured directly using calipers on 25 June. Use of this method, rather than simple differences in total colony area, allowed us to minimize the influence

of factors such as predation, which would have reduced the size of the colony only at certain points along its edge. Use of this method is further justified since estimates of potential growth rate are strongly correlated with absolute measures of growth rate based on increase in colony area (see Results).

One assumption implicit in the use of this method is that colony growth was isotropic, and not sensitive to flow direction in pipes. To evaluate this assumption quantitatively, we measured maximum dimensions (on 25 June) of 45 haphazardly selected colonies in both across-stream and along-stream directions. The ratio of these dimensions should be 1.0 if growth was insensitive to flow direction.

*Balanus glandula* was obtained after cyprids settled onto large strips of plexiglass attached to rocks in the lower intertidal. Strips for deployment in pipes were cut from these larger strips such that each contained two or more small individuals. Animals on strips were photographed just before being placed in pipes on 1 August. At that time the mean basal diameter of all barnacles was 14.3 mm<sup>2</sup>; the range was 5–31 mm<sup>2</sup>. Strips were removed from pipes on 24 September, and animals were rephotographed. Growth was defined as the increase in basal area of animals

still alive on 24 September. Barnacles that had grown against neighbors were not considered.

*Pseudochitinopoma occidentalis* was obtained after larvae settled onto large strips of plexiglass attached to racks mounted about 20 cm above the bottom at 10-m depth. Strips for deployment in pipes were cut from these larger strips such that each contained two or more small individuals. Animals on strips were photographed just before being placed in pipes on 26 August. At that time the mean length of the calcareous tube of all individuals was 7.1 mm; the range was 2.5–13 mm. Strips were removed from pipes on 22 November, and animals were rephotographed. Growth was defined as the increase in length of the tube of individuals still alive on 22 November.

By using a small head tank and a pump with a high discharge rate, we hoped to ensure that water supplied to pipes was well mixed and that each pipe received the same initial concentration and composition of suspended particulates as food for suspension feeders. However, the possibility of inhomogeneous supply existed. Moreover, because flows varied in strength among pipes, the rates at which particulates settled out of suspension might have varied among pipes, causing differences in food supply. To assess these effects, we twice sampled seawater that exited each pipe and one time each tested for differences in concentrations of chlorophyll, particulate organic carbon (POC), and particulate organic nitrogen (PON).

For chlorophyll, three replicate samples of 1000 ml were collected from each pipe. One replicate was collected from each of the 10 pipes before collecting the next replicate sample. Each sample was filtered through a 0.22- $\mu\text{m}$  glass-fiber filter. Pigments collected on the filter were extracted in acetone, and chlorophyll was measured spectrophotometrically according to Parsons *et al.* (1984).

The number of replicates and the sampling protocol for POC and PON were the same as for chlorophyll. A subsample of each 500-ml seawater sample (volume varied according to the amount of particulates in the sample) was filtered through a 0.22- $\mu\text{m}$  glass-fiber filter that had been baked at 550°C; all glassware was acid-washed. Filters were immediately dried at 65°C and then frozen. Treatment of the filter to remove carbonates was judged unnecessary because the local phytoplankton and zooplankton assemblages contain few individuals with calcareous tests. Masses of C and N on filters were determined using a Perkin-Elmer 2400 Elemental Analyzer and converted to POC and PON concentrations.

#### *Experimental apparatus—1992*

Results of the 1991 experiment prompted us to run a similar experiment in 1992 to evaluate growth responses of three other species of barnacle (*Semibalanus cariosus*,

*Balanus crenatus*, and *Pollicipes polymerus*) to flow speed. Because our original device had been dismantled, we used a different pipe flow apparatus that had been built for another experiment.

Ten straight sections of pipe were used, as in 1991. Each pipe (5.1-cm inner radius) was 307 cm long. The 10 pipes were submerged in a large, round seawater tank (400 cm in diameter, 55 cm deep) that was supplied continuously with fresh, unfiltered seawater. A standpipe in the tank allowed overflow. All pipes were connected directly to a centrifugal pump that supplied each with seawater (at a constant pressure) drawn directly from the tank in which the pipes were submerged. Flow through each pipe was regulated by a valve at the end of each pipe, as in the 1991 experiment. The connecting pipes that led from the pump to the straight sections used in the experiment also had a 5.1-cm inner radius. These connectors varied in length among the 10 pipes from 20–150 cm. To break down the jet of water that exited the pump, two turns were built into the connectors.

Eight windows were cut in each 307-cm-long straight section of pipe. Animals were introduced into pipes through these windows as in the 1991 experiment (Fig. 1). The first window in each pipe was located 46 cm downstream of the beginning of the straight section. The spacing between windows was 30 cm.

We attempted to duplicate the five flow levels used in the 1991 experiment, again with two replicate pipes assigned to each flow level. Flow speeds were not calculated from pipe discharge ( $Q$ ) as in 1991, but instead were measured directly using a 2-axis Marsh-McBirney electromagnetic current meter that was placed on the centerline of each pipe through a window 30 cm from the discharge end. Trials that timed injected dye indicated that the walls of the pipe did not interfere with the magnetic field about the probe enough to affect measurements of current speed, and that measurements obtained with the probe were accurate. Speeds measured with the current meter approximated  $U_{\text{max}}$ , since speed was measured along each pipe's centerline. Other flow parameters were calculated from  $U_{\text{max}}$  using equations presented above, with one exception. The minimum flow speed to which animals were exposed ( $U_{\text{min}}$ ) was calculated assuming that all individuals were at least 20% of the radius away from the pipe wall (in the 1991 experiment a minimum distance of 10% of  $R$  was assumed). This change was justified since barnacles were attached to plexiglass strips by hand in 1992 (see below), and care was taken to place them farther from the pipe wall.

The growth experiment ran from 22 May–30 July 1992. Flows were measured six times during this 69-day period. Table 1 lists flow properties for each of the 10 pipes, based on the mean  $U_{\text{max}}$ . The coefficient of variation in  $U_{\text{max}}$

was <10% for all 10 pipes. Values of  $X_{cq}$  in Table I indicate a problem with the experimental apparatus used in 1992. Depending on flow level, two to four of the eight plexiglass strips containing animals were upstream of the minimum distance required to achieve fully developed flow. Animals on these strips (far from the pipe wall) may have experienced flow speeds somewhat slower on average than animals located further downstream. However, calculations indicate that speeds experienced by animals on these upstream strips would have exceeded  $U_{min}$  shown in Table I, so the range of speeds between  $U_{max}$  and  $U_{min}$  is still an accurate indicator of flow speeds experienced by all animals.

#### Experimental protocols—1992

Small individuals of *Pollicipes polymerus* and *Semibalanus cariosus* were collected from a comparatively high-energy, mid-intertidal zone in the Straits of Juan de Fuca near Clallam Bay, Washington. We collected individuals of both species that had settled onto shells of mussels (*Mytilus edulis* and *M. californianus*), in addition to *P. polymerus* that were attached to plates of larger *S. cariosus*. Relatively small *Balanus crenatus* on discarded aluminum cans were collected from a depth of about 5 m below the public docks of the town of Friday Harbor, Washington. Animals of all three species were returned to the Friday Harbor Laboratories where they were held in seawater tables for several days.

Individuals of all species were glued by hand onto the plexiglass strips that were subsequently placed in pipes. We prepared pieces of mussel shell, aluminum can, or calcareous plate that were about 1 cm<sup>2</sup> and contained one or two individuals of one of the three species. Two or three pieces of each substrate were attached to each plexiglass strip using a submarine adhesive. We positioned each barnacle such that the extended cirral net would be oriented approximately concave into the flow. In addition, *B. crenatus* and *S. cariosus* can rotate the cirrus into this apparently "preferred" orientation (see below). Species were not segregated among strips, and strips were assigned randomly to pipes. We did not use animals that were in contact with other individuals.

Each animal was measured within 2 days of the start of the experiment. The basal area of each individual of *B. crenatus* or *S. cariosus* was calculated from the average of two orthogonal measurements of basal diameter obtained using calipers. At the start of the experiment, the mean basal diameter of *B. crenatus* was 62.8 mm<sup>2</sup>; the range was 17.7–130.5 mm<sup>2</sup>. The mean basal diameter of *S. cariosus* was 52.1 mm<sup>2</sup>; the range was 7.4–139.8 mm<sup>2</sup>. For *P. polymerus* we used calipers to measure the height of the capitulum (distance from the top of the peduncle

to the furthest extension of the plates). At the start of the experiment the mean capitular height was 5.45 mm; the range was 1.6–11.5 mm.

Plexiglass strips were mounted in pipes as in 1991, and animals were exposed to one of the five steady flows from 22 May–30 July. Thereafter, plexiglass strips were returned to seawater tables, and animals were remeasured within several days. Growth is defined as the increase in basal area (*B. crenatus* or *S. cariosus*) or capitular height (*P. polymerus*).

As in the 1991 experiment, pipes were supplied with seawater from a common, presumably well-mixed source so that there would be little variability among pipes in the concentration or composition of suspended particulates supplied to suspension feeders. To assess this variability, on one occasion we sampled the seawater exiting the pipes and tested for differences in concentrations of chlorophyll. Sampling and analytical protocols followed those in the 1991 experiment.

#### Flume observations—1992

To aid in interpreting results of growth experiments, we observed the feeding behavior of all species (except *Pseudochitinopoma occidentalis*) in a range of flows. Qualitative observations of responses of feeding structures were made in a simple recirculating flume of the type described by Vogel and LaBarbera (1978). The main channel of the flume was 200 cm long and 30 cm wide. A flow depth of about 15 cm was used.

Each species was observed separately. Approximately 20–30 individuals or colonies were placed in the center of the flume approximately midway down the channel. We used barnacles attached to small rocks or aluminum cans to elevate them above the flume's developing bottom boundary layer and to expose them to near free-stream flow speeds. For a similar reason, we cut out small pieces of kelp that were encrusted with colonies of *Membranipora membranacea*, used a cyanoacrylate glue to attach them to strips of plexiglass (≈3 cm × 5 cm × 0.3 cm thick), and suspended them in the free-stream flow.

Each species was observed at four to five levels of flow, with flow held constant for at least 10 min before the observations. For any given speed, no differences in feeding behavior were apparent between accelerating and decelerating flows. Because flow in this crude flume was three-dimensional and not fully developed, we measured horizontal flow speeds as close as possible to the animals being observed. To obtain these measurements we used a Marsh-McBirney current meter and also timed the passage of suspended particulates. We consider measured flow speeds to be only approximations.

### Statistical analysis

Regression was used to examine relationships between the mean growth rate of all individuals (or the mean concentration of chlorophyll, POC, or PON) within a pipe and the mean flow speed in the pipe. Mean growth rate was used because individual growth rates within each pipe were not independent, and it would have inflated the degrees of freedom in the regression had individuals been considered separately. The issue addressed by regression, therefore, was whether or not the mean growth rate of a population varied predictably as a function of flow speed.

Prior research on particle capture by suspension feeders suggests that one of two relationships between flow speed and growth would be expected *a priori* (see Introduction): (1) a convex upward relationship in which growth rates are lower on both sides of a narrow range of intermediate speeds that appear to support the highest growth; (2) a monotonically increasing or decreasing relationship. We had no *a priori* reason to expect that any monotonic relationship between growth rate (or concentration) and speed would be linear. Therefore, we searched for a monotonic relationship of the form

$$G = aU^b + c$$

where  $G$  is growth rate (or concentration),  $U$  is mean velocity, and  $a$ ,  $b$ , and  $c$  are constants. We selected constants that produced the maximum  $r^2$  with the constraint that  $0.5 \leq b \leq 3$ . This range was imposed because higher or lower exponents would in some instances produce strongly curved functions especially sensitive to flow speeds near the end of the range; also, growth rates and concentrations predicted from these functions could have been non-sen-

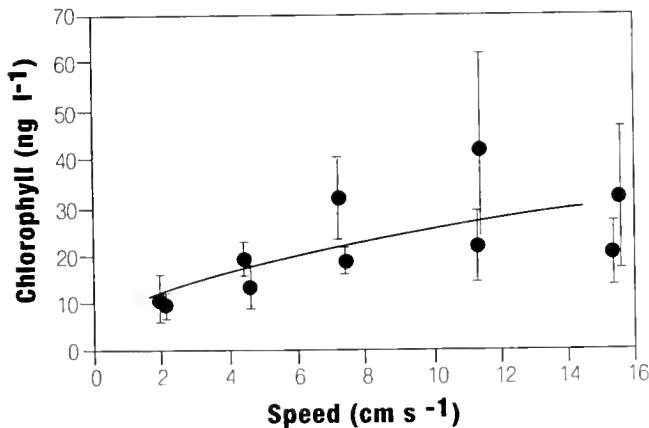


**Figure 2.** Concentrations of chlorophyll as a function of flow speed measured in each pipe in 1991. Each point and error bar represents the mean ( $\pm 1$  SE) of three replicate samples obtained from each pipe. Also shown is the best-fit, significant regression line obtained using the 10 mean values.

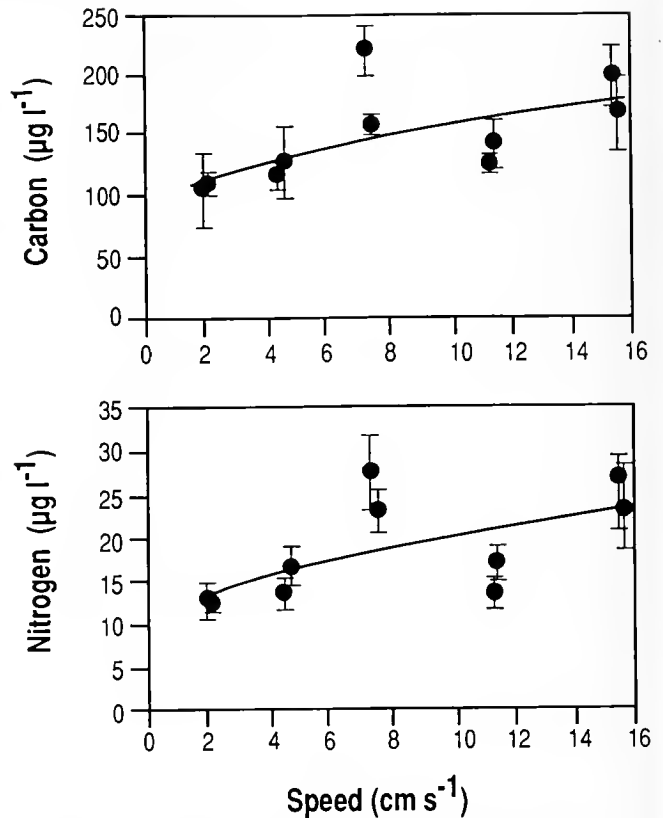


**Figure 3.** Concentrations of POC (top) and PON (bottom) as a function of flow speed measured in each pipe in 1991. Other interpretations as in Figure 2.

sical (e.g., negative growth of calcareous structures or negative concentrations at near-zero flow speeds).

To evaluate whether growth rate was maximal at some intermediate flow speed, we used a 2nd-degree polynomial to regress growth rate against flow speed:

$$G = aU^2 + bU + c$$

with terms as defined above. A 2nd-degree polynomial defines a parabola, and this functional relationship between growth and speed can assume a convex-upward shape as expected *a priori*.

## Results

### 1991 experiment

The concentration of chlorophyll in pipes increased with flow speed by a factor of more than 2 from 2–15  $\text{cm s}^{-1}$  (Fig. 2;  $b = 0.5$ ,  $P = 0.03$ ,  $r^2 = 0.46$ ). The horizontal flux (the product of concentration and velocity) of chlorophyll varied among pipes by a factor of approximately 18 over the 7.5  $\times$  range of flow speeds.

Table II

Numbers of animals per pipe providing measures of growth rate in both experiments

Pipe	1991 Experiment			
	$U$ (cm s <sup>-1</sup> )	M.m.	B.g.	P.o.
7	1.9	8	12	12
1	2.1	8	14	14
8	4.2	2	7	6
3	4.6	8	9	5
10	6.9	4	5	2
4	7.0	6	9	5
5	11.2	7	6	2
9	11.2	1	8	6
2	14.7	4	10	6
6	14.7	4	8	7

Pipe	1992 Experiment			
	$U$ (cm s <sup>-1</sup> )	S.c.	P.p.	B.c.
5	2.6	7	7	7
10	2.8	3	7	5
9	5.4	7	14	6
4	5.4	6	11	7
3	8.0	7	11	6
8	8.0	3	9	8
2	10.6	6	13	9
7	10.7	6	8	8
6	12.9	4	9	9
1	13.2	6	7	5

M.m., *Membranipora membranacea*; B.g., *Balanus glandula*; P.o., *Pseudochitinopoma occidentalis*; S.c., *Semibalanus cariosus*; P.p., *Pollicipes polymerus*; B.c., *Balanus crenatus*.

Concentrations of POC and PON showed nearly identical patterns (Fig. 3), and resembled the variation in chlorophyll with flow speed. Concentrations of POC and PON both doubled as flow speed increased by 7.5 $\times$ , producing about 15-fold differences in C and N fluxes between the weakest and strongest flows. The regression of POC with speed was significant ( $b = 0.5$ ,  $P = 0.05$ ,  $r^2 = 0.39$ ), and that for PON was nearly significant ( $b = 0.5$ ,  $P = 0.06$ ,  $r^2 = 0.38$ ).

Table II lists numbers of animals of all species from which mean growth rate per pipe was estimated. Growth of *Membranipora* was effectively isotropic at all flow speeds. The ratio of cross-stream to along-stream diameter of colonies was indistinguishable from 1.0 at three of five flow speeds (Table III); diverged slightly from unity, but in different directions, at the other two speeds; and at all speeds was within  $\pm 6\%$  of 1.0. Consequently, there was effectively no anisotropic growth that would have biased calculations of potential growth rates. In addition, potential growth rates were strongly correlated with growth rates based on changes in total colony area ( $r^2 = 0.81$ ,  $P < 0.0001$ ,  $n = 50$ ). Potential growth rates of *Membran-*

Table III

Analysis of isotropy in shapes of *Membranipora* colonies

$U$ (cm s <sup>-1</sup> )	$D_{vs}/D_{as}$	$n$	$P$
2	0.967 ( $\pm 0.013$ )	14	*
4	1.010 ( $\pm 0.026$ )	7	NS
7	1.063 ( $\pm 0.016$ )	7	*
11	1.004 ( $\pm 0.029$ )	6	NS
15	0.989 ( $\pm 0.023$ )	11	NS

$U$  is the mean flow speed for each of the five treatments.  $D_{vs}/D_{as}$  gives the mean ratio ( $\pm 1$  SE) of colony diameter measured cross-stream to colony diameter measured along-stream.  $n$  is the number of colonies.  $P$  is the probability that the observed ratio differs from 1.0 (Student's  $t$  test); NS = not significant ( $P > 0.05$ ); \* =  $0.01 < P < 0.05$ .

*ipora* colonies declined monotonically with flow speed (Fig. 4), and the regression was significant ( $b = 1.2$ ,  $P = 0.04$ ,  $r^2 = 0.42$ ).

The large difference in mean colony growth rate between the two replicate pipes at the slowest ("optimal") flow speed (Fig. 4) suggested that conditions in one pipe were anomalously poor. To investigate this possibility we compared probabilities of colony survival among pipes. In both slowest flow pipes, percent colony survival was high (100% and 94%) over the 19-day experiment. The average percent colony survival for all pipes was  $84.2\% \pm 11.3\%$  and was not related to flow speed ( $r^2 = 0.08$ ,  $P = 0.44$ ).

Growth rates of *Balanus glandula* individuals were not detectably sensitive to flow speed over the range studied (Fig. 5). There appeared to be a weak (perhaps 10%), but

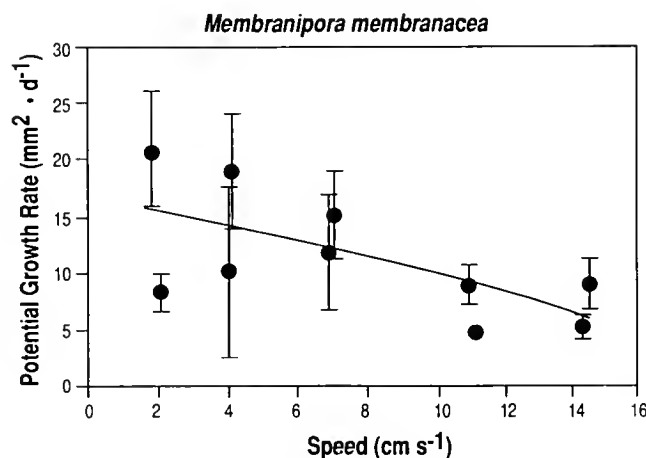


Figure 4. Potential growth rates of *Membranipora membranacea* as a function of the average flow speed measured in each pipe during the 19-day deployment in 1991. Each point and error bar represents the mean growth rate ( $\pm 1$  SE). Also shown is the best-fit, significant regression line obtained using the 10 mean values.

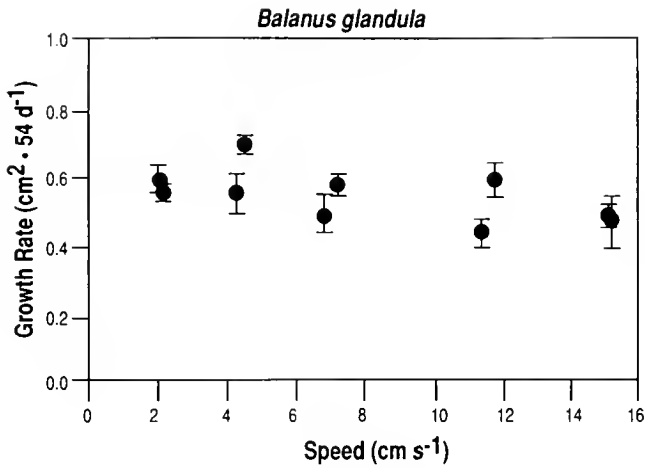


Figure 5. Growth rates of *Balanus glandula* as a function of flow speed during the 54-day deployment in 1991. Other interpretations as in Figure 4. There was no significant best-fit regression.

nonsignificant, monotonic decline in growth rate as speed increased (for all  $b$ : minimum  $P = 0.10$ , maximum  $r^2 = 0.30$ ).

Growth rates of *Pseudochitinopoma* individuals declined monotonically and significantly with flow speed (Fig. 6;  $b = 1.1$ ,  $P = 0.009$ ,  $r^2 = 0.59$ ).

#### 1992 experiment

The concentration of chlorophyll in pipes did not depend on flow speed (Fig. 7). The monotonic regression was not significant (for all  $b$ : minimum  $P = 0.39$ , maximum  $r^2 = 0.095$ ), nor was the polynomial regression.

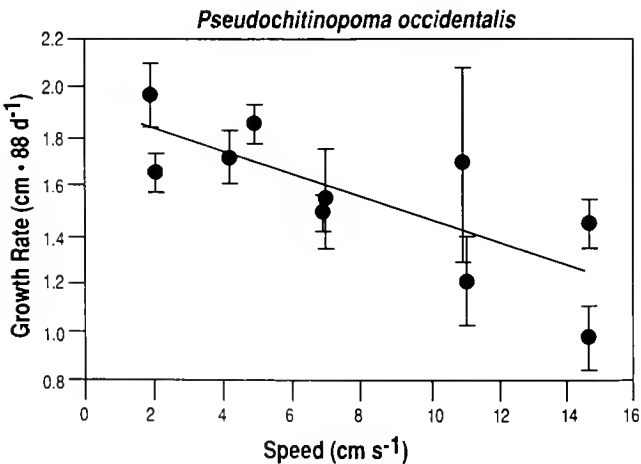


Figure 6. Growth rates of *Pseudochitinopoma occidentalis* as a function of flow speed during the 88-day deployment in 1991. Other interpretations as in Figure 4.

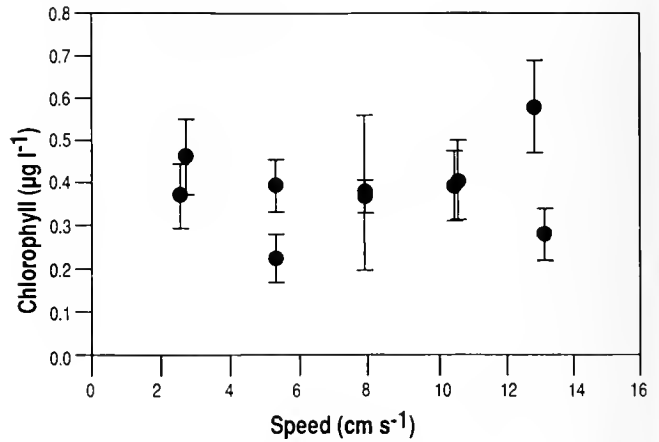


Figure 7. Concentrations of chlorophyll as a function of flow speed in 1992. Other interpretations as in Figure 2. There was no significant best-fit regression.

Therefore, the horizontal flux of chlorophyll varied by a factor of only about 5 over the  $5 \times$  range of flow speeds.

Growth rates of *Semibalanus cariosus* did not depend on flow speed (Fig. 8). The monotonic regression was not significant (for all  $b$ : minimum  $P = 0.17$ , maximum  $r^2 = 0.22$ ), nor was the polynomial regression.

Growth rates of *Pollicipes polymerus* also did not depend on flow speed (Fig. 9). The monotonic regression was not significant (for all  $b$ : minimum  $P = 0.38$ , maximum  $r^2 = 0.10$ ), nor was the polynomial regression.

Growth rates of *Balanus crenatus* appeared to be minimal at the two lowest flow speeds, to increase sharply to a maximum growth rate at  $U \approx 8 \text{ cm s}^{-1}$ , and to decline

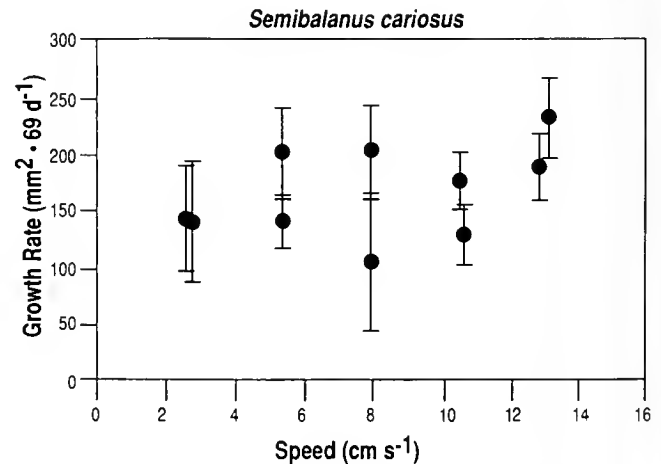


Figure 8. Growth rates of *Semibalanus cariosus* as a function of flow speed during the 69-day deployment in 1992. Other interpretations as in Figure 4. There was no significant best-fit regression.



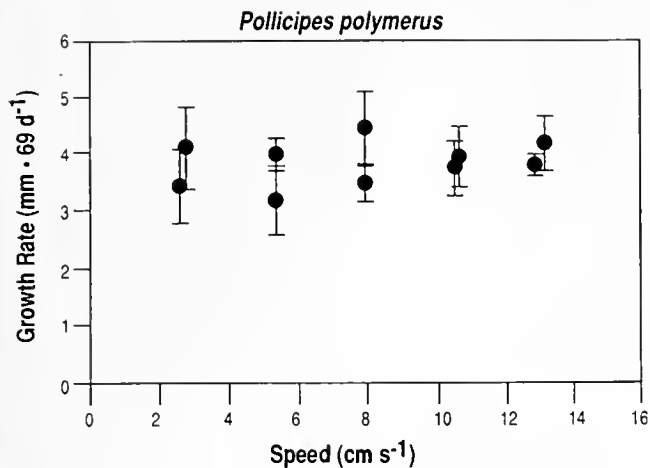


Figure 9. Growth rates of *Pollicipes polymerus* as a function of flow speed during the 69-day deployment in 1992. Other interpretations as in Figure 4. There was no significant best-fit regression.

at higher speeds (Fig. 10). Polynomial regression indicates that this convex-upward trend was weak and not significant at the conventional level of  $P = 0.05$  ( $r^2 = 0.49$ ,  $P = 0.09$ ). However, further evidence of a speed-dependent growth response is supported by results of ANOVA, which indicated that replicate pipe effects were not significant ( $F_{5,60} = 0.63$ ,  $P = 0.68$ ), but that effects of flow level on growth were highly significant ( $F_{4,65} = 3.66$ ,  $P = 0.0095$ ). *A posteriori* multiple comparison tests (T-method—Sokal and Rohlf, 1981, p. 246) indicated that growth rates at  $U = 8 \text{ cm s}^{-1}$  significantly exceeded those at  $U = 2.7$  and  $5.3 \text{ cm s}^{-1}$  ( $\alpha = 0.05$ ).

#### Flume observations of feeding behavior

A detailed description of feeding behaviors as a function of flow speed is given in Table IV. The three balanoid barnacles (*Balanus glandula*, *Semibalanus cariosus*, and *B. crenatus*) all were able to control the cirrus (*i.e.*, actively sweep or hold the cirrus still and erect) over the entire range of flow speeds examined, with little or no deformation of the cirrus by flow. This similarity held despite the wide range of habitats in which these species typically occur. *Balanus glandula* and *S. cariosus* are found in moderate to comparatively high-energy intertidal regions in the Pacific Northwest. These species typically experience oscillatory flows that often have instantaneous speeds far higher than those examined in this study. In contrast, *B. crenatus* lives predominantly in relatively low-energy, subtidal environments. It more typically experiences tidal flows that are not often impacted by wind-generated surface waves. Although tidal currents in the region of the

Friday Harbor Laboratories can be quite strong (Eckman *et al.*, 1989), this species also thrives in areas of comparatively weak flow energy. Animals used in this study were collected from a quiescent environment where even free-stream flows typically are  $<10 \text{ cm s}^{-1}$  (personal observations).

In contrast to the balanoid barnacles, the pedunculate barnacle *Pollicipes polymerus* never swept the cirral net through the water. This species curled the cirrus inward when exposed to stronger flows (a behavior and not a passive deflection of the cirrus by flow) and retracted the cirrus completely at the highest speeds examined. This dissimilarity from the balanoid barnacles held despite the fact that *P. polymerus* lives sympatrically with *S. cariosus* in comparatively high-energy intertidal regions.

The bryozoan *Membranipora membranacea* was able to extend and use the lophophore at flow speeds  $\leq 10 \text{ cm s}^{-1}$ . However, in the face of stronger flows, the lophophore bent and shook noticeably, and was retracted upon contact with moving particles. At the highest speed examined, tentacles were not able to open from the lophophore. *M. membranacea* typically encrusts thalli of kelps. It lives both on the surface-canopy species *Nereocystis luetkeana* and on several understory species whose thalli extend only tens of centimeters above the bottom. Although abundant on plants in high-current regions (personal observations), these essentially flat colonies are submerged deep in the boundary layer that develops on a thallus that typically is aligned somewhat parallel to flow direction. Thus even in high-flow regions, *M. membranacea* on thalli of surface-canopy plants would experience significantly lower flow speeds.

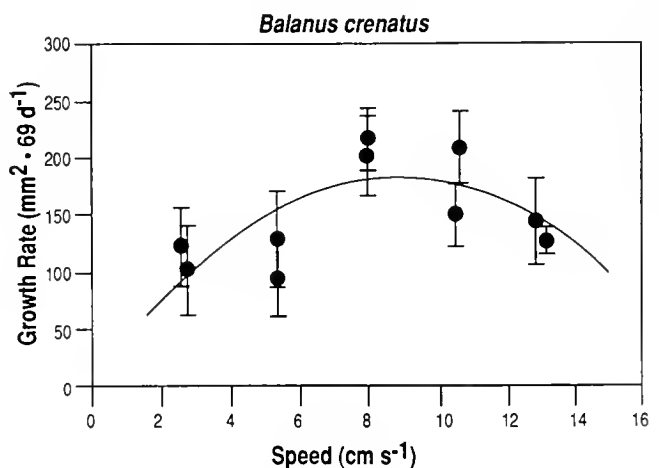


Figure 10. Growth rates of *Balanus crenatus* as a function of flow speed during the 69-day deployment in 1992. Other interpretations as in Figure 4. Also shown is the best-fit, 2nd-degree polynomial regression line obtained using the 10 mean values.

Table IV

Summary of feeding behaviors as a function of flow speed

Flow speed (cm s <sup>-1</sup> )	<i>Balanus glandula</i>	<i>Pollicipes polymerus</i>	<i>Semibalanus cariosus</i>	<i>Balanus crenatus</i>	<i>Membranipora membranacea</i>
2-3	Cirri of all animals sweep continuously ( $\approx 2$ Hz)	(N.O.)	(N.O.)	(N.O.)	Lophophores extended; no deformation of tentacles by flow
4.5-6	Most animals sweep continuously; $\approx 10\%$ pause between sweeps to hold cirrus erect and still for $\approx 1$ s	Cirri of all animals held erect and still; no deformation of cirral net	Cirri of all animals sweeping; cirrus retracts fully into mantle with each beat	Cirri of most animals sweeping; no cirral deformation by flow; rotation of cirrus up to $90^\circ$ into flow is common	Lophophores extended; some weak shaking of tentacles by flow
8-10	Continuous sweeping predominates; $\approx 20\%$ pause briefly between sweeps	Cirri held erect and still; distal portions curled inward slightly (apparently by muscular action)	Many animals pause between sweeps to hold cirrus erect and still for 2-4 s; some animals rotate cirrus up to $90^\circ$ to orient it into flow	As at 4.5-6 cm s <sup>-1</sup>	As at 4.5-6 cm s <sup>-1</sup>
14-18	$\approx 50\%$ sweep constantly; $\approx 50\%$ pause briefly between sweeps; no deformation of cirral net	Increased inward curl of cirri	Most animals pause between sweeps; cirral net not deformed by flow; rotation of cirrus up to $90^\circ$ into flow is common	As at 4.5-6 cm s <sup>-1</sup>	Pronounced bending of tentacles in flow; lophophore retracts on contact with particles in transport
19-21	Most animals pause between sweeps; no deformation of cirral net	(N.O.)	(N.O.)	(N.O.)	Lophophores bent up to $45^\circ$
$\geq 25$	(N.O.)	Cirri almost totally retracted	As at 14-18 cm s <sup>-1</sup>	As at 4.5-6 cm s <sup>-1</sup> , but some deflection of cirrus by flow at peak of extension	Tentacles unable to open from lophophore

(N.O.) = Not Observed at this speed.

The behavior of *Pseudochitinopoma occidentalis* was not observed in flow. This species typically lives in cryptic, subtidal habitats such as the crevices in rocks and the undersides of rock ledges. Consequently, animals of this species normally would experience comparatively slow flow speeds.

### Discussion

Results from the 1991 experiment provide clear evidence that growth rates of *Membranipora* and *Pseudochitinopoma* declined significantly with increasing flow speed. In contrast, over the same range of flow speeds, there was no detectable relationship between speed and growth of *Balanus glandula*, though there was qualitative evidence of a weak inverse relationship. Higher growth rates of the bryozoan and serpulid occurred at weaker flows despite evidence that concentrations of suspended particulate

food may have been lower under these conditions (Figs. 2, 3). By the end of the 1991 experiment, we noted a substantial amount of material deposited on the bottoms of the pipes with weaker flows. Therefore, it is probable that the reduction in concentrations of suspended particles observed twice in the slowest flow pipes was consistent over time, and was caused by gravitational settlement of particles onto the bottom of a pipe, rather than removal of suspended particles by the small number of suspension feeders in each pipe. It is important to recognize that data presented in Figures 2 and 3 may overestimate differences among pipes in concentrations of food available to suspension feeders. Concentrations reported here characterized water exiting the ends of pipes, and gravitational settling would have produced less marked differences approximately halfway down the pipes, where animals were located. However, some differences would have occurred, and growth rates of the bryozoan and serpulid apparently

were greatest under low-flow conditions where food concentrations were also lowest. Had concentrations of suspended food been constant among treatments, we might have seen even stronger effects of flow on growth of these two species.

The 1992 experiment was prompted by the observation that growth of *Balanus glandula* was comparatively insensitive to flow speed, over a moderate range, in contrast to the pronounced sensitivities shown by the bryozoan and serpulid. More specifically, we were interested in determining the extent to which this difference related to the barnacle's behavior, its adaptation to a typically more energetic habitat, and its mechanical and morphological design. Regarding the latter, it seemed possible that barnacles might be generally more capable of feeding efficiently and growing well in a wider range of flows because the cirral net is composed of a rigid exoskeleton operated by a network of internal muscles (though each cirrus is extended hydraulically), and because they use the smaller (1st and 2nd) cirri to handle and process captured particles. These properties distinguish barnacles from many other suspension-feeding invertebrates, like the bryozoan and serpulid, that utilize feeding structures composed of soft tissue, that operate feeding structures mainly hydrostatically, and that process particles adhering to feeding structures primarily using cilia. These properties may render feeding more susceptible to fluid drag forces.

Combined results of the 1991 and 1992 experiments indicate significant differences in growth responses among barnacle species. There was no taxon-wide insensitivity of barnacle growth to flow speed, over even a moderate range of speeds. The interspecific variability relates most obviously to the range of flows that animals typically experience. Barnacles that inhabit comparatively high-energy intertidal environments (*Balanus glandula*, *Semibalanus cariosus*, and *Pollicipes polymerus*) grew well at a wide range of flow speeds (Figs. 5, 8, and 9). In contrast, growth rates of *B. crenatus*, which typically inhabits lower energy, subtidal environments, were significantly affected by flow speed and appeared to be maximal at a fairly weak, intermediate speed (about  $8 \text{ cm s}^{-1}$ ; Fig. 10). This pattern extends beyond the four species of barnacles studied. The bryozoan and serpulid, whose growth rates were lowest in the strongest flows (Figs. 4, 6), also typically inhabit subtidal microhabitats characterized by weaker flow (see above).

The interspecific variability in growth responses among barnacles was not obviously related to feeding behavior. Like the other balanoid barnacles, *Balanus crenatus* was apparently able to sweep with its cirrus over a wide range of flow speeds (Table IV), yet its growth—but not that of the others—was highly sensitive to flow speed.

We therefore conclude that, for each of the six species studied here, growth responses to flow speed were most clearly coupled to the relative flow energy of the animals' natural habitat. Growth response to flow did not reflect the clear similarities in morphology and behavior among some species. The mechanism(s) responsible for the observed differences among species are not obvious from our observations, and warrant further consideration.

Shimeta and Jumars (1991) extended the work of Rubenstein and Koehl (1977) to predict how features of a suspension-feeder's environment and structural aspects of its filtration apparatus combine to determine rates of particle contact with the filter. Their analysis indicates that rates of particle contact with an individual filter element should increase both with flow speed and with the concentration of food particles in suspension. In our experiments, flow speeds increased about  $7.5 \times$ , while food concentrations either remained constant (1992 experiment, Fig. 7) or simultaneously increased by about  $2 \times$  (1991 experiment, Figs. 2, 3). Thus, rates of particle contact with an individual filter element should have increased with speed. Despite this prediction, we observed no monotonic increase in growth rate with increasing flow speed for any of the six species studied, and for two species (*Membranipora membranacea*, *Pseudochitinopoma occidentalis*) we noted an inverse relationship. The most reasonable explanation for this apparent contradiction is that, at speeds studied here, growth rates were governed by a strong inverse relationship between flow speed and efficiency at which particles are retained on the filter apparatus and passed to the point of ingestion. Among these species, the particle-handling abilities of the bryozoan and the serpulid were apparently more sensitive to speed than were those of *B. glandula*, *S. cariosus*, and *P. polymerus*. This heightened sensitivity of particle processing to flow may relate to the way that bryozoans and serpulids use cilia to process particles. An additional factor that may have contributed to the poor growth of the bryozoan and the serpulid in stronger flow is that their feeding apparatus (composed of soft tissue) may have experienced greater deformation in flows than the cirral nets of the barnacles (cf., Patterson, 1984; Harvell and LaBarbera, 1985; Best, 1988; Shimeta and Jumars, 1991; Sponaugle and LaBarbera, 1991).

Some results from our growth study are consistent with many results from prior, shorter term studies that examined effects of flow on particle capture by "tentaculate" suspension feeders (Okamura, 1984, 1985; McFadden, 1986; Best, 1988; Leonard *et al.*, 1988; Sponaugle and LaBarbera, 1991). These studies all noted a maximum feeding rate at a low speed (though not necessarily at the lowest examined) and a strong decline in feeding rate at higher speeds. Our results confirm that at least two other

tentaculate suspension feeders (*M. membranacea* and *P. occidentalis*), and one species of barnacle (*B. crenatus*), exhibit a similar negative performance in strong flows, and that relationships noted previously between flow and particle capture probably translate into similar effects on somatic growth (see also Okamura, 1992).

In contrast to results of many previous studies of particle capture, for five of the six species studied we noted no reduction in growth rate at the lowest flow speeds (*i.e.*, no intermediate speed associated with a seemingly maximal growth rate). We suspect that this difference between our current and many previous results may in part reflect our experimental apparatus and design. The minimum flow speed examined was about  $2 \text{ cm s}^{-1}$ , and our pipe flows were all turbulent. In the absence of flows strong enough to interfere with particle processing, the supply of food to animals at  $2 \text{ cm s}^{-1}$  may have been high enough to ensure maximum growth rates. Moreover, the comparatively efficient mixing of particles in turbulent flows may have prevented an animal's feeding ambit from becoming depleted of food, even at the lowest flow speed. Had we included a flow speed slow enough to establish laminar, and not turbulent, conditions in a pipe, a marked reduction in growth rate might have resulted. At least two of the species studied here (*M. membranacea* and *P. occidentalis*) have no obvious mechanism for avoiding re-filtration of water already depleted of particles in extremely weak flows. A reduction in growth rates of *M. membranacea* was noted when colonies were exposed to laminar flows at speeds  $< 0.5 \text{ cm s}^{-1}$  (Grunbaum, 1992).

Our results help to confirm a conclusion we have drawn previously (Eckman and Duggins, 1991) about the factors that affect growth of *Pseudochitinopoma occidentalis in situ*. This serpulid grew faster in weaker flows found beneath canopies of understory kelps than within more energetic clearings in the canopy. Results of our manipulative experiments implicated flow as one of several factors responsible for this pattern. Our current results confirm that this species of tentaculate suspension feeder is poorly adapted for life in stronger flow environments.

In conclusion, we have shown that there is wide variability among six species of benthic suspension feeder in the sensitivity of growth rate to a fixed range of comparatively moderate flow speeds between about 2 and about  $15 \text{ cm s}^{-1}$ . The growth response of animals to flow related most obviously to the range of flows typically experienced by the animal. Animals that inhabited comparatively weak flow environments showed a strong sensitivity to flow speed, whereas animals from comparatively high-energy environments were relatively insensitive to flow speed. Growth responses to flow did not reflect the clear similarities in morphology and behavior

among some species. We suspect that a key to understanding the impact of flow on a suspension feeder's growth is the animal's ability to handle and process particles that have impacted the feeding structure, and to deliver them to the point of ingestion. Further study of this phenomenon may significantly increase our understanding of the influence of hydrodynamic processes on benthic suspension feeders.

#### Acknowledgments

The considerable efforts of Amy Sewell were instrumental in the completion of this research. Helpful comments on earlier versions of the manuscript were provided by Drs. Carl André, Drew Harvell, Roberta Marinelli, and Don Webb, and by an anonymous reviewer. Dr. Dan Grunbaum assisted with observations on the feeding behavior of *Membranipora* in flow. Dr. Jon Grant provided access to the CHN analyzer at Dalhousie University. Figures were prepared by Anna Boyette and Suzanne McIntosh. We thank A.O.D. Willows, Director of the Friday Harbor Laboratories, and the staff of the Labs for their critical support and assistance. We also thank the Department of Oceanography at Dalhousie University for providing office space for one of us (JEE) during a sabbatical leave. This research was supported by NSF grant OCE-8911116.

#### Literature Cited

- Best, B. A. 1988. Passive suspension feeding in a sea pen: effects of ambient flow on volume flow rate and filtering efficiency. *Biol. Bull.* 175: 332-342.
- Eckman, J. E., and D. O. Duggins. 1991. Life and death beneath macrophyte canopies: effects of understory kelps on growth rates and survival of marine, benthic suspension feeders. *Oecologia (Berl.)* 87: 473-487.
- Eckman, J. E., C. H. Peterson, and J. A. Cahalan. 1989. Effects of flow speed, turbulence, and orientation on growth of juvenile bay scallops *Argopecten irradians concentricus* (Say). *J. Exp. Mar. Biol. Ecol.* 132: 123-140.
- Ellison, A. M., and C. D. Harvell. 1989. Size hierarchies in *Membranipora membranacea*: Do colonial animals follow the same rules as plants? *Oikos* 55: 349-355.
- Fréchette, M., and E. Bourget. 1985. Food-limited growth of *Mytilus edulis* (L.) in relation to the benthic boundary layer. *Can. J. Fish. Aquat. Sci.* 42: 1166-1170.
- Fréchette, M., C. A. Bulman, and W. R. Geyer. 1989. The importance of boundary-layer flows in supplying phytoplankton to the benthic suspension feeder, *Mytilus edulis* L. *Limnol. Oceanogr.* 34: 19-36.
- Grunbaum, D. 1992. Local processes and global patterns: Biomathematical models of bryozoan feeding currents and density dependent aggregations in Antarctic krill. Ph.D. Thesis, Cornell University.
- Harvell, C. D., and M. LaBarbera. 1985. Flexibility: A mechanism for control of local velocities in hydroid colonies. *Biol. Bull.* 168: 312-320.
- Harvell, C. D., H. Caswell, and P. Simpson. 1990. Density effects in a colonial monoculture: experimental studies with a marine bryozoan (*Membranipora membranacea*). *Oecologia (Berl.)* 82: 227-237.

- Kirby-Smith, W. W. 1972. Growth of the bay scallop: the influence of experimental water currents. *J. Exp. Mar. Biol. Ecol.* **8**: 7-18.
- Leonard, A. B., J. R. Strickler, and N. D. Holland. 1988. Effects of current speed on filtration during suspension feeding in *Oligometra serripinna* (Echinodermata: Crinoidea). *Mar. Biol.* **97**: 111-126.
- McFadden, C. S. 1986. Colony fission increases particle capture rates of a soft coral: advantages of being a small colony. *J. Exp. Mar. Biol. Ecol.* **103**: 1-20.
- Okamura, B. 1984. The effects of ambient flow velocity, colony size, and upstream colonies on the feeding success of bryozoa. I. *Bugula stolonifera* Ryland, an arborescent species. *J. Exp. Mar. Biol. Ecol.* **83**: 179-193.
- Okamura, B. 1985. The effects of ambient flow velocity, colony size, and upstream colonies on the feeding success of bryozoa. II. *Conopeum reticulatum* (Linnaeus), an encrusting species. *J. Exp. Mar. Biol. Ecol.* **89**: 69-80.
- Okamura, B. 1987. Particle size and flow velocity induce an inferred switch in bryozoan suspension-feeding behavior. *Biol. Bull.* **173**: 222-229.
- Okamura, B. 1992. Microhabitat variation and patterns of colony growth and feeding in a marine bryozoan. *Ecology* **73**: 1502-1513.
- Parsons, T. R., Y. Maita, and L. M. Lalli. 1984. *A Manual of Chemical and Biological Methods for Seawater Analysis*. Pergamon Press, New York.
- Patterson, M. R. 1984. Patterns of whole colony prey capture in the octocoral, *Alcyonium siderium*. *Biol. Bull.* **167**: 613-629.
- Patterson, M. R. 1991. The effects of flow on polyp-level prey capture in an octocoral, *Alcyonium siderium*. *Biol. Bull.* **180**: 93-102.
- Rubenstein, D. I., and M. A. R. Koehl. 1977. The mechanisms of filter feeding: some theoretical considerations. *Amer. Natur.* **111**: 981-994.
- Schlichting, H. 1979. *Boundary-Layer Theory*, 7th ed., McGraw-Hill Book Co., New York. 817 pp.
- Sebens, K. P., and A. S. Johnson. 1991. Effects of water movement on prey capture and distribution of reef corals. *Hydrobiol.* **226**: 91-101.
- Shimeta, J., and P. A. Jumars. 1991. Physical mechanisms and rates of particle capture by suspension feeders. *Oceanogr. Mar. Biol. Annu. Rev.* **29**: 191-257.
- Smith, F. G. W. 1946. Effect of water currents upon the attachment and growth of barnacles. *Biol. Bull.* **90**: 51-70.
- Sokal, R. R., and F. J. Rohlf. 1981. *Biometry*, 2nd ed., W.H. Freeman & Co., San Francisco. 859 pp.
- Sponaugle, S., and M. LaBarbera. 1991. Drag-induced deformation: a functional feeding strategy in two species of gorgonians. *J. Exp. Mar. Biol. Ecol.* **148**: 121-134.
- Vogel, S. 1981. *Life in Moving Fluids*. Princeton University Press, Princeton, NJ. 352 pp.
- Vogel, S., and M. LaBarbera. 1978. Simple flow tanks for research and teaching. *Bioscience* **28**: 638-643.
- Wildish, D. J., and D. D. Kristmanson. 1979. Tidal energy and sublittoral macrobenthic animals in estuaries. *J. Fish. Res. Board Can.* **36**: 1197-1206.
- Wildish, D. J., and A. M. Saulnier. 1992. The effect of velocity and flow direction on the growth of juvenile and adult giant scallops. *J. Exp. Mar. Biol. Ecol.* **133**: 133-143.
- Wildish, D. J., D. D. Kristmanson, R. L. Hoar, A. M. DeCoste, S. D. McCormick, and A. W. White. 1987. Giant scallop feeding and growth responses to flow. *J. Exp. Mar. Biol. Ecol.* **113**: 207-220.

# Ontogenic Changes in Microhabitat Distribution of Juvenile Bay Scallops, *Argopecten irradians irradians* (L.), in Eelgrass Beds, and Their Potential Significance to Early Recruitment

ZAUL GARCIA-ESQUIVEL AND V. MONICA BRICELJ<sup>1</sup>

*Marine Sciences Research Center, State University of New York, Stony Brook, New York 11794-5000*

**Abstract.** Ontogenetic changes in the vertical distribution of a cohort of juvenile bay scallops, *Argopecten irradians*, on eelgrass, *Zostera marina*, were followed throughout the summer and early fall in two Long Island embayments (New York, USA). Despite site-specific differences in eelgrass height and density, more than 95% of post-settlement scallops remained attached above the bottom until they reached a shell height of about 11 mm. Over a 5-week period, scallops gradually relocated until, at a mean size of 31 mm, all occurred on the bottom. The decline in percent attachment coincided with a 5-fold increase (from 16 to 84  $\mu\text{moles min}^{-1} \text{g muscle dry wt}^{-1}$ ) in the activity of octopine dehydrogenase (proposed here as an index of the scallops' capacity for burst swimming activity), and in maximum rate of increase in the shell aspect ratio. While attached to eelgrass, scallops were nonuniformly distributed, with greatest concentration at mid-canopy. Following disturbance, they rapidly regained above-ground position, attaining asymptotic heights within 3–10 h. This and prior studies suggest that the climbing behavior of the bay scallop is an adaptive response to high predation pressure at small sizes. Enhanced scope for activity (predator avoidance) may enhance survival of scallops at intermediate sizes, when they become too heavy to maintain elevation but have not yet attained effective refuge in size.

## Introduction

Bay scallops, *Argopecten irradians*, which commonly inhabit shallow, sheltered bays along the east coast of the

United States, are closely associated with seagrasses, particularly during their early life history. Planktonic larvae of this species settle and attach by byssus threads, primarily but not exclusively to submerged vegetation such as eelgrass, *Zostera marina* L.; adults occupy a wider range of habitats, including bare, sandy substrata. Thus, dependence on vegetation and habitat restriction appear to decrease with age and size, as has been shown for a variety of marine and freshwater fish that extend their foraging grounds beyond areas with plant cover once they achieve size refuge from predators (Ebeling and Laur, 1985; Werner and Hall, 1988).

In common with other pectinids such as the sea scallop, *Placopecten magellanicus*, bay scallops can attach byssally throughout life, but seldom do so as adults (Belding, 1910; Stanley, 1970). Attachment of juveniles is reversible and dynamic, because *Z. marina* blades have a high turnover rate and elongate rapidly, at a rate of up to 2–5  $\text{cm day}^{-1}$  in the summer (Kemp *et al.*, 1987). In pectinids, byssal attachment and swimming represent antagonistic behaviors (Caddy, 1972). Ontogenetic changes in attachment and swimming capacity of pectinids have been related to morphological, hydrodynamic features of their shells, such as aspect ratio (shell length to height ratio), umbonal angle, and degree of auricle asymmetry (Stanley, 1970; Dadswell, 1990). Burst swimming, which provides scallops with a mechanism to avoid predators, is associated with the production of octopine in rapidly contracting adductor muscle tissue. This end reaction of anaerobic glycolysis, which serves an important role in replenishing  $\text{NAD}^+$  and thus maintaining glycolytic flux during functional anaerobiosis in highly mobile molluscs such as scallops and cephalo-

Received 17 May 1992; accepted 10 May 1993.

<sup>1</sup> Author to whom reprint requests should be addressed.

ods, is catalyzed by octopine dehydrogenase (ODH), an enzyme functionally analogous to lactate dehydrogenase (LDH) (Gade and Grieshaber, 1986). Ontogenetic changes in the activities of glycolytic enzymes such as LDH and pyruvate kinase and their relation to swimming performance have been described in several fish species (*e.g.*, Somero and Childress, 1980), but changes in ODH activity throughout the life cycle of pectinids have not been previously documented.

As reviewed by Brodie *et al.* (1991), prey have evolved two types of defense mechanisms to curtail predation. The first type, predator avoidance mechanisms, involves spatial (*e.g.*, Palmer, 1983; Main, 1987; Werner and Hall, 1988) or temporal (*e.g.*, Kitting, 1985) segregation from predators to minimize the probability of predator-prey encounter. The second type, antipredator mechanisms, increases the probability of survival upon encounter with a predator. Antipredator mechanisms include morphological adaptations such as large size (Crowl, 1990), increased ornamentation or thickening of the shell (Vermeij, 1987), distastefulness, or behavioral responses (*e.g.*, escape response or immobility; reviewed by Main, 1987).

Bay scallops are epifaunal, incapable of complete or prolonged valve closure, and less protected by morphological defenses than other molluscs with heavier, thicker shells; thus they require alternate mechanisms to reduce their vulnerability to predators. Using tethering techniques, Pohle *et al.* (1991) demonstrated that above-ground attachment to the eelgrass canopy gives juvenile bay scallops a significant refuge from benthic predators. Yet the laboratory experiments these investigators conducted using artificial grass suggested that this refuge may be ephemeral because the ability to attach above the bottom decreased markedly over a narrow range of scallop sizes (about 10 to 20 mm). The distributional pattern of the epiphytic, above-bottom habit for juvenile *A. irradians* and the transition to the adult epibenthic habit have not been adequately described in the natural environment and are the focus of the present study.

Information about the rate at which scallops can regain an elevated position and the timing and size at which they lose this ability is important for several reasons. First, it is necessary for determining the relative profitability of different elevations within the eelgrass canopy in terms of growth and survival. Second, it is a prerequisite for predicting the relative vulnerability of scallops to predators during early ontogeny. Third, it is an important consideration in rehabilitating stocks of this commercially exploited species because, in several states on the east coast of the United States, rehabilitation efforts mainly involve planting juveniles in suitable nursery habitat.

This work has three objectives: (1) to describe temporal/ontogenetic patterns in the vertical distribution of bay

scallops in two bays in the Peconic-Gardiners estuary (Long Island, New York, USA) which differ in eelgrass structure; (2) to determine the rate of relocation and the height attained by individual scallops in the eelgrass canopy following disturbance, as well as the effect of scallop density on their climbing behavior in the laboratory; and (3) to relate distributional changes observed in the field to the swimming performance of scallops, as assessed indirectly from shell morphometrics (aspect ratio) and from the activity of octopine dehydrogenase in the adductor muscle.

## Materials and Methods

### Laboratory studies

Juvenile scallops obtained from a local hatchery on 2 May and 1 June 1990 were maintained in a flow-through upweller system at SUNY's Flax Pond Marine Laboratory until ready for use in experiments. These were carried out in rectangular plexiglass tanks (basal area =  $31.5 \times 78.5$  cm) provided with recirculating, filtered (1 to 5  $\mu\text{m}$ ) seawater introduced immediately below the water surface (see Pohle *et al.*, 1991, for a detailed description of the experimental system). Eelgrass shoots were simulated with artificial mimics constructed of buoyant, green polypropylene ribbon (Synthetic Fibers Inc., Newton, PA) 0.5 cm in width, woven into plastic VEXAR mesh at a density of 500 shoots  $\text{m}^{-2}$ , and buried under about 5 cm of clean sand. Seawater was kept at 19° to 23°C and 26 to 28 ppt salinity with a cooling system and freshwater dilutions, respectively. White fluorescent lamps provided artificial 12 h:12 h (light:dark) photoperiod.

A first set of experiments tested the effect of scallop stocking density on the overall success of attachment to vertical substrates. Three experiments were conducted using scallops averaging 9.3 mm in shell height ( $H$ , greatest distance from the umbo to the ventral margin), each with density treatments of 300, 100 and 50 scallops per tank (1213, 404, and 202 scallops  $\text{m}^{-2}$ , respectively) on 11 May ( $\bar{H} \pm \text{SE} = 8.6 \text{ mm} \pm 0.09$ ), 28 June ( $\bar{H} \pm \text{SE} = 10.0 \text{ mm} \pm 0.05$ ), and 1 July ( $\bar{H} \pm \text{SE} = 9.2 \text{ mm} \pm 0.06$ ). Shell height was measured for a subsample of individuals, and scallops were then randomly distributed on the bottom of each tank (water depth = 30 cm; height of eelgrass mimics = 25 cm). The number of scallops attached to blade mimics and tank walls was recorded every 30 min during the first 3 h, every hour during the following 3 h, and at the end of 24 h.

A second set of experiments investigated individual, size-specific climbing behavior. Individually marked scallops were followed over time for 46–49 h. Their vertical position was recorded hourly during the first 5–6 h and at less frequent intervals thereafter. Individuals were

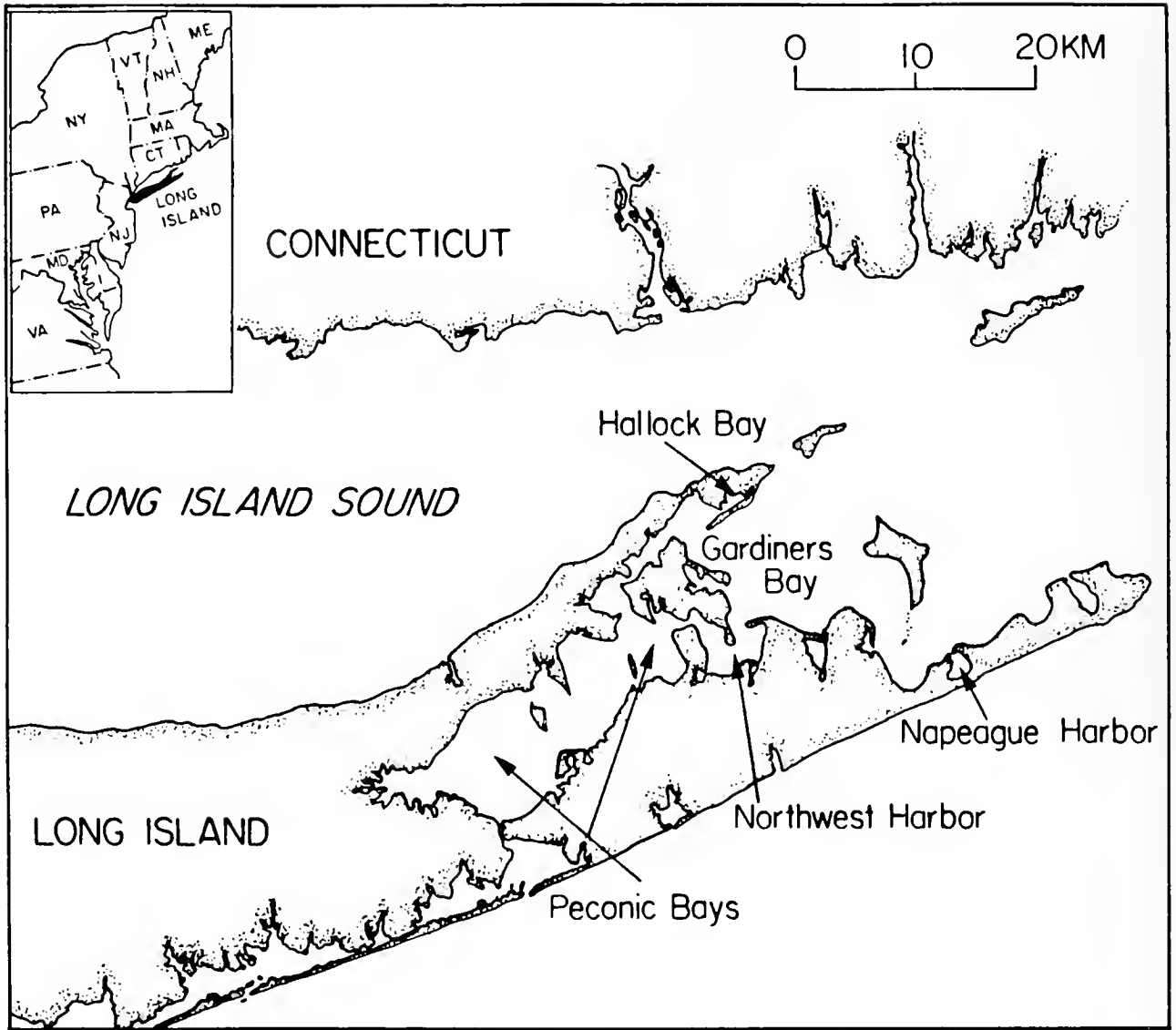


Figure 1. Location of field study sites in eastern Long Island, New York.

identified with numbered, plastic-coated, miniature wire markers glued with Krazy Glue® to the upper valve at least 1 day before running experiments. For each trial, 20–22 scallops of a given size class were released into each of three experimental tanks (density = 89 scallops  $m^{-2}$ ) containing eelgrass shoot mimics 50 cm in length. Three scallop size classes were tested on the following dates: 13.2 mm (SE = 0.07) scallops on 8 and 10 June, 5.7 mm (SE = 0.04) scallops on 11 and 13 June, and 7.2 mm (SE = 0.04) scallops on 14 and 16 June. The coefficient of variation in scallop sizes within any given experimental tank never exceeded 13%. A preliminary experiment showed that the height attained by 7-mm scallops did not differ significantly between one tank containing eelgrass

mimics, canopy height = 50 mm and density = 500 shoots  $m^{-2}$ , and two tanks containing natural, transplanted eelgrass, canopy height = 50 cm and density = 224 shoots  $m^{-2}$  (ANOVA at 48 h,  $F = 1.104$ ,  $df = 2, 61$ ,  $P = 0.338$ ).

#### Field studies

*Vertical distribution of natural set.* The vertical distribution of naturally occurring juvenile bay scallops within the *Z. marina* canopy was characterized throughout the summer and early fall of 1990 in two bays in eastern Long Island, New York, which contrasted in eelgrass shoot density and canopy height: Napeague Harbor (NAPH, 41°01' N, 72°03' W) and Northwest Harbor (NWH,



41°01' N, 72°15' W) (Fig. 1). Both study sites are shallow (about 1 m deep in NAPH and 2–3 m in NWH), well-mixed, and characterized by gentle slopes, sandy substrate, and fairly extensive eelgrass (*Z. marina*) beds, which supported productive bay scallop populations prior to the occurrence of "brown tides" in the region (Hickey, 1977; Eckman, 1987; Bricelj *et al.*, 1987). They have also been the target of scallop reseeding efforts in recent years (C. Smith, pers. comm., Cornell Sea Grant Coop. Extension, NY; Tettelbach and Wenzel, 1991).

Eelgrass densities at the study sites were estimated in the second week of September by counting the number of shoots contained in 25-cm<sup>2</sup> quadrats randomly deployed within the survey area. Surface water temperatures were recorded with a hand-held thermometer ( $\pm 0.5^\circ\text{C}$ ).

Although scallop settlement was first observed in NWH in mid-July, sampling for determination of growth rate, vertical position, and percent attachment of the scallop population on eelgrass did not begin until 26 July, when scallops averaged 4.5 mm in shell height and could thus be readily sampled by divers. Sampling continued until 10 October at NWH and extended between 16 August and 19 September at NAPH. In each harbor, an area well within the eelgrass meadow was sampled weekly. The size of the area was about 200 m<sup>2</sup> in NWH and about 50 m<sup>2</sup> in NAPH.

At each sampling, divers collected 100 to 150 juvenile scallops by swimming along set transects. Using rulers, the divers obtained *in situ* measurements ( $\pm 0.5$  cm) of the vertical position (height of attachment above bottom) of each individual on the eelgrass blade, and the total length of the blade. Scallops found on the bottom were assigned a position of 0 cm. The organisms were placed into numbered, perforated plastic boxes and brought to shore, where their individual shell height was measured with digital calipers ( $\pm 0.01$  mm).

Subsamples of 30 to 100 scallops (depending on size) were transported live in coolers to the laboratory, where they were immediately frozen and stored at  $-70^\circ\text{C}$  until further analysis. These scallops were individually weighed (total wet body weight) using an analytical balance ( $\pm 0.1$  mg), and lyophilized. Soft tissues were then dissected and weighed using a Cahn electrobalance ( $\pm 1$   $\mu\text{g}$ ) or analytical balance, depending on scallop size. Shell height and length (greatest anteroposterior dimension) were determined prior to dissection in order to calculate the aspect ratio.

*Octopine dehydrogenase activity.* Lyophilized tissues were stored with dessicant at  $-70^\circ\text{C}$  until used for enzyme assays. The adductor muscle of individual scallops (including both catch and phasic portions) was dissected out, weighed, and used for determination of octopine dehydrogenase (ODH, EC 1.5.1.11) activity, because more than

97% of the total activity in whole scallop homogenates is found in this tissue (Baldwin and Opie, 1978).

Powdered muscle samples (*ca.* 1 mg) were homogenized with a sonicator probe (Bronwill, Biosonik III) in 1 ml of 100 mM Tris-HCl buffer (pH 7.5) containing Triton x-100 (1% v/v). Homogenates were cooled in ice/water (0–2°C) during, and for a 30-min incubation period following, sonication. They were then centrifuged for 30 min at 1°C and 16,000  $\times g$ . The supernatant was decanted and assayed for ODH activity at 25°C by following changes in absorbance at 340 nm due to the oxidation of NADH, using a Milton Roy Spectronic 1201 spectrophotometer equipped with a thermal cell controlled by an external, recirculating water bath. Activity was determined by dividing the rate of change in absorbance by the extinction coefficient ( $\epsilon_{340} = 6.23 \text{ mM}^{-1} \text{ cm}^{-1}$ ) as described by Fersht (1985). All determinations were made in duplicate, using 50  $\mu\text{l}$  of tissue extract in a total extraction volume of 1 ml, and were completed within several hours of tissue preparation. The composition of the reaction mixture and the concentration of the reactants were those reported to yield maximum enzyme activities (Baldwin and Opie, 1978): 1 mM sodium pyruvate, 0.1 mM NADH, 10 mM L-arginine and 100 mM tris-maleate buffer (pH 7.0). No controls were run for nonspecific activity because previous studies have demonstrated that in scallops, including *A. irradians*, the contribution of lactate dehydrogenase to the oxidation of NADH is negligible (Baldwin and Opie, 1978; Grieshaber, 1978; de Zwaan *et al.*, 1980; and Chih and Ellington, 1983).

*Relocation experiments.* Experiments designed to test the ability of juvenile scallops to relocate (climb and reattach) to eelgrass blades following dislodgement were carried out in Northwest Harbor and within sandy habitat in Hallock Bay (41°02' N 75°15' W; mean depth at low tide = 0.5 m; tidal range = 0.75 m) (Fig. 1).

The first relocation experiment was carried out in NWH on 9 August using scallops collected from natural populations at this site. Divers collected 150 scallops ( $\bar{H} = 8.6$ , SE = 0.13) after determining their individual position on eelgrass as described earlier. Scallops were measured at the shore, individually numbered, and held in ambient bay seawater until released (within about 1 h of collection). Scallops were freely broadcast on the bottom of a previously marked plot within the eelgrass bed, where no predators were present. A diving survey around and inside the plot was carried out the following day (24 h after release) and the vertical position of each recovered individual was recorded.

A second relocation experiment was conducted using hatchery-reared scallops (10 mm), which were transported from the Flax Pond Laboratory to Hallock Bay (1.5 h) in coolers containing ice packs layered with wet newspaper.

Unmarked scallops were released by divers on 28 August within a 30-cm<sup>2</sup> area at the center of sandy plots (1 m × 2 m) within an eelgrass meadow averaging 32 cm in canopy height and 249 shoots m<sup>-2</sup> in density. No natural scallop set was observed at this site in the year of the study. The perimeter of the plots was delimited by a galvanized chain (4.8 mm = 3/16 in. diam.), and plot location was marked with bright fluorescent subsurface buoys (Fig. 2 in Pohle *et al.*, 1991). Three hundred scallops were released in each of four experimental plots, and the percent attachment and vertical position of recaptured scallops were recorded after 3 h (plot 1), 5 h (plot 2) and 24 h (plots 3 and 4). Diver surveys covered a total area of 12 m<sup>2</sup> (a 2-m<sup>2</sup> plot plus a 10-m<sup>2</sup>-perimeter area located 1 m around each plot). Plots were thus sampled destructively, rather than repeatedly over time, to avoid disturbance by divers.

### Statistical analysis

Except where otherwise indicated, statistical analyses followed standard procedures described by Sokal and Rohlf (1981). Percent attachment data obtained from the three stocking density trials were pooled for each time interval and scallop density (50, 100, and 300 scallops per tank). Differences in arcsine-transformed percent attachment values obtained every hour between 1 and 6 h and at the end of 24 h were analyzed with a repeated one-way ANOVA (Wilkinson, 1990).

Differences in height attained on eelgrass mimics with scallop size were analyzed by a two-step procedure. The first step consisted of *a posteriori* multiple comparisons of the mean height attained by scallops (three trials pooled for each size) at 1, 3, 5, 10, 24, and 46–49 h. A Tukey-Kramer test was used on scallop sizes that had homogeneous variances (13.2-mm scallops), and the Games and Howell test was used for those with heterogeneous variances (5.7- and 7.2-mm scallops). In the second step, the position of smaller scallops (5.7 and 7.2 mm) was (1 n + 1)-transformed to correct for heterogeneity of variances, and the mean height of the scallops on eelgrass was compared using a repeated two-way ANOVA (Wilkinson, 1990) with scallop size and aquaria as factors. Time treatments were selected on the basis of results of the multiple comparisons tests and fulfillment of criteria for homoscedasticity among samples ( $F_{\max}$  test).

The degree of association between shell height and elevation of scallops attached to eelgrass blades in the field was measured with the Pearson product-moment correlation coefficient. All data gathered throughout the summer were included in this analysis, but excluding scallops found on the bottom, *i.e.*, at height = 0. The height attained, calculated as a fraction of total blade length to

normalize data for differences in canopy height between bays, was used to test for differences between the relative vertical distribution of scallops from NWH and NAPH, using the Mann-Whitney test for two independent samples.

Data from the relocation experiment conducted in Hallock Bay were analyzed by the *a posteriori* Games and Howell approximate test for equality of means, with height attained at each sampling time as the dependent variable. For the relocation experiment carried out in NWH, the nonparametric Wilcoxon signed-rank test for paired comparisons was used to test for differences in the mean position of scallops at the time of collection and 24 h following release.

## Results

### Laboratory studies

Scallop stocking density, over the range tested in this study, had no significant effect on percent attachment to eelgrass mimics ( $P = 0.293$ , repeated one-way ANOVA). Percent attachment averaged 80% 2 h after release and 85% by the end of 24 h, irrespective of stocking density.

Although scallops swam actively during the first 15 min following release into the experimental tanks, very few (< 1%) attached to the blades by swimming onto them. Swimming generally resulted in vertical rather than horizontal displacement. Scallops primarily gained an elevated position by crawling, as reported by Pohle *et al.* (1991). Downward crawling was never observed, suggesting that scallops may display negative geotaxis at this stage of their life cycle. Tracking of individual trajectories showed that, until they attained their final attachment position, scallops occasionally fell off the blades and had to re-initiate their ascent; but on average, over all trials, only 13% (range = 5 to 29%) fell to the bottom during ascent. Climbing behavior consistently showed two phases: rapid crawling during the first 4–5 h after broadcasting on the bottom, followed by a slowing or complete cessation of crawling. Mean crawling rates, calculated over the first 4 h for animals that did not fall during ascent, were 4.5 cm h<sup>-1</sup> (SE = 0.8,  $n = 156$ ) for small scallops (5.7- and 7.2-mm size classes) and 1.2 cm h<sup>-1</sup> for 13-mm scallops (SE = 0.2,  $n = 41$ ).

Laboratory experiments showed that the vertical distribution of scallops on eelgrass mimics was markedly affected by size. Within a 50-cm canopy, small scallops ( $\bar{H} = 5.7$  and 7.2 mm) reached a near-average asymptotic elevation of 20.4 and 18.8 cm respectively, 10 h after being released into the tanks (Fig. 2); larger scallops (13.2 mm) reached a near-asymptotic height of 6.0 cm after 11 h. Mean height attained by small scallops after 1 h was significantly different from that achieved after 24 h and

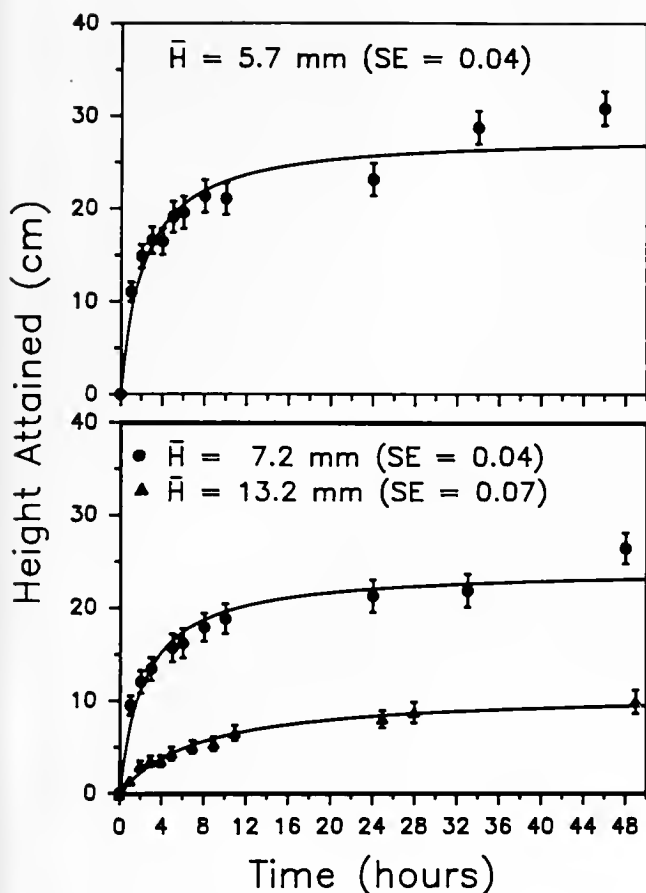


Figure 2. Temporal changes in the mean height above bottom attained by *Argopecten irradians* of three different size classes on eelgrass mimics in the laboratory (mean blade height = 50 cm). Data points are fitted to a rectangular hyperbolic function ( $Y = aX/b + X$ ). Vertical bars represent 95% confidence intervals.

46–48 h (for 7.2- and 5.7-mm scallops, respectively), but not before ( $P < 0.01$ , Games and Howell approximate test for equality of means with unequal variances, Table IB). A Tukey-Kramer test of multiple comparisons also indicated significant differences ( $P < 0.01$ ) in the mean position of larger (13 mm) scallops after 1, 3, or 24 h (Table IB). No significant size effects ( $P = 0.428$ ) were found in the mean height attained by 5.7- and 7.2-mm scallops, or in that attained by scallops of the same size class located in different aquaria ( $P = 0.376$ , Table IA).

Mean elevation of small scallops ( $\leq 7.2$  mm) coincided with mid-canopy height (0.57 of blade height;  $SD = 0.286$ ,  $n = 126$ ), whereas 22% of the scallop population was found near the top (upper 1/10) of the canopy, and none at the base of shoot mimics. In general, however, scallops were distributed throughout most of the length of eelgrass mimics at the end of 48 h (from 2.5 to 48 cm above bottom).

### Field studies

*Vertical distribution of natural set.* A single cohort of first-year *A. irradians* occurred in both embayments throughout this study (July–October), as indicated by unimodal size-frequency distributions obtained in NWH and NAPH over time. No significant new recruitment of post-settlement scallops was observed during late summer and early fall at either study site, except for a few new recruits ( $< 4\%$  of the total) observed in NAPH in early September, although spawning in these embayments is known to extend throughout June and July (Bricelj *et al.*, 1987). Growth parameters (changes in total body weight

Table I

Results of repeated two-way analysis of variance for comparison of mean heights attained by *Argopecten irradians* on eelgrass mimics

A.	Source of variation	Degrees of freedom	MS	F	Significance
	Between subjects				
	Size	1	2.043	0.632	NS
	Aquaria	2	3.185	0.985	NS
	Size $\times$ aquaria	2	8.321	2.573	NS
	Error	124			
	Within subjects				
	Time	5	21.173	62.309	***
	Time $\times$ size	5	0.139	0.409	NS
	Time $\times$ aquaria	10	0.327	0.963	NS
	Time $\times$ size $\times$ aquaria	10	0.513	1.509	NS
	Error	620	0.340		

### B.

#### *A posteriori* multiple comparisons

	5.7-mm scallops					
Time (h)	1	3	5	10	24	46
Height attained (mm)	10.7	16.1	18.5	20.4	22.4	29.9
	7.2-mm scallops					
Time (h)	1	3	5	10	24	48
Height attained (mm)	9.5	13.4	15.7	18.8	21.2	26.4
	13.2-mm scallops					
Time (h)	1	3	5	9	25	49
Height attained (mm)	1.3	3.1	3.8	4.7	6.9	8.4

A. Scallop size (5.7 and 7.2 mm) and experimental aquaria (3 per size), with  $n = 20$ –23 scallops each) were used as testing factors. Runs were carried out on separate dates for each size under identical laboratory conditions. Comparisons were based on records for the same individuals at times = 1, 3, 5, 10, 24, and 46–48 h. B. Results of the Games and Howell approximate test for equality of means are shown for 5.7- and 7.2-mm scallops at selected sampling times. The Tukey-Kramer test was used for 13.2-mm scallops. \*\*\* =  $P < 0.001$ , NS = not significant at  $P > 0.05$ .

and dry tissue weight) of scallops collected in NWH are shown in Table II. Surface water temperatures at this site averaged 27°C in August and 23°C in September, attaining maxima during the second week of August. Temperatures at NAPH were within  $\pm 1^\circ\text{C}$  of those recorded at NWH. Shell growth rate throughout the study period averaged 13.3 and 12.5 mm month<sup>-1</sup> at NWH and NAPH respectively. Based on these measured growth rates for juvenile scallops and a duration of 7 days for metamorphosis of dissoconch larvae into 1.5-mm plicated juveniles in NWH (Eckman, 1987), we estimate that initial settlement of this cohort occurred in the second week of July.

Densities of juvenile scallops were determined quantitatively only at NWH on 16 August and 20 September, when they averaged 16 and 14 scallops m<sup>-2</sup> respectively. Although eelgrass shoot density and canopy height were 1.5 times higher in NAPH (mean density  $\pm$  SE = 704  $\pm$  35 shoots m<sup>-2</sup>; mean canopy height  $\pm$  SE = 38  $\pm$  0.5 cm) than in NWH (density = 464  $\pm$  29 shoots m<sup>-2</sup>; canopy height = 23.5  $\pm$  0.3 cm), temporal patterns in the percentage of scallops attached to eelgrass were very similar at both sites (Fig. 3), and therefore did not appear to be strongly influenced by differences in eelgrass structure. In NWH, 100% of the population remained attached to eelgrass blades until the second week of August, when scallops reached 11.2 mm in mean shell height. In NAPH, 100% attachment was also observed until scallops reached 11.3 mm, one week later than in NWH (Fig. 3). A 5-week transitional period followed, during which scallops relocated from their elevated position on eelgrass blades to the bottom. At both sites, more than 90% of new recruits were found on the bottom by the time they reached a mean size of 26–29 mm. Scallops found on the bottom

(h = 0) are included in the calculation of mean heights plotted in Figure 4, showing clearly that in both bays the entire population had relocated to the bottom by the time scallops reached 31 mm.

At NWH, shell growth rate increased from 1.9–2.8 mm week<sup>-1</sup> between 26 July and 30 August, when most of the scallops remained attached to the eelgrass canopy, to 3.1–4.6 mm week<sup>-1</sup> during the period of relocation to the bottom (30 August to 23 September) (Table II), when attachment dropped sharply from 75% to 1%. Maximum shell growth during the first week of September coincided with a reduced rate of growth for soft tissues, which was equal to 30 mg week<sup>-1</sup>, compared to values of 52 and 59 mg week<sup>-1</sup> during the preceding and following weeks respectively (Table II). At NAPH, maximum rate of shell growth (4.5 mm week<sup>-1</sup>) was recorded at the same time as in NWH. Allometric changes in shell shape with growth are evidenced by the sharp increase in the degree of shell elongation, as measured by the aspect ratio, between sizes of 10 and 25 mm, when scallops are gradually shifting from a byssate to a free-living habit (Fig. 5). Near-asymptotic values in this parameter (> 1.05) are attained at larger sizes.

Diver observations indicated that scallops exhibited a marked increase in swimming activity (diver avoidance response) during transition from an elevated position to the bottom, especially during the last week of August and the second week of September. This habitat shift was accompanied by qualitative changes in vegetation characteristics, notably an increase in the incidence of senescent (brown or discolored) *Z. marina* blades. Furthermore, in July, the drift red alga (*Gracilaria verrucosa*, was mostly restricted to the subtidal zone delimited by the lower eel-

Table II

Mean total body weight (TBW), mean dry soft tissue weight (DTW), and shell growth rates of juvenile bay scallops collected from natural populations in Northwest Harbor, New York, between 26 July and 10 October

Date	Temp. (°C)	TBW (mg)		DTW (mg)		Shell growth rate (mm wk <sup>-1</sup> )
		Mean	(SE; n)	Mean	(SE; n)	
26 July	25	—	—	—	—	—
2 Aug.	27	83.3	(53.6; 49)	5.7	(0.4; 50)	2.2
9 Aug.	30	228.6	(15.0; 50)	15.7	(1.1; 48)	1.9
16 Aug.	29	389.4	(27.6; 51)	28.4	(2.2; 51)	2.6
23 Aug.	22	753.8	(53.0; 50)	57.7	(4.2; 48)	2.8
30 Aug.	27	1459.4	(82.8; 48)	109.3	(6.5; 48)	2.2
7 Sept.	25	1954.4	(128.6; 40)	143.8	(8.7; 48)	4.6
13 Sept.	25	2587.2	(177.6; 37)	193.2	(14.4; 37)	3.5
23 Sept.	20	4742.9	(276.2; 34)	342.4	(21.4; 33)	3.1
29 Sept.	22	5858.4	(423.6; 17)	424.8	(33.0; 17)	1.9
10 Oct.	21	8960.4	(538.6; 19)	608.8	(45.6; 16)	3.6

Standard error and sample size are indicated in parentheses.

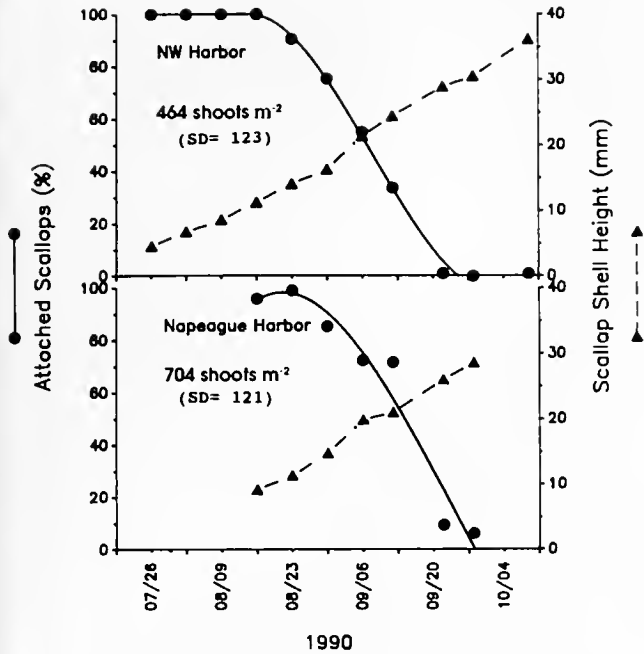


Figure 3. Temporal changes in mean shell height and percent attachment to eelgrass blades of a first-year cohort of *Argopecten irradians* in two eastern Long Island bays, during the summer and early fall of 1990. All standard errors are smaller than the symbol denoting mean shell height. Mean eelgrass (*Zostera marina*) shoot densities within the scallop distributional area are indicated for each harbor.

grass boundary, outside the scallop's main distributional area. However, by the first week of September, *G. verrucosa* was conspicuous throughout the entire scallop zone, intermingled with *Z. marina* or in irregular patches of 1 to 2 m<sup>2</sup>.

Contrary to laboratory results, no significant correlation was found between scallop attachment height (excluding individuals found on the bottom) and scallop size in either NWH ( $r^2 = 0.003$ ,  $P = 0.176$ ) or NAPH ( $r^2 = 0.001$ ,  $P = 0.538$ ). This also differs from the laboratory results of Pohle *et al.* (1991), who found that the relative proportion of scallops attached to the upper vs. lower half of the canopy decreased monotonically between scallop sizes of 6 and 20 mm.

Although scallops were found distributed throughout the eelgrass canopy at both study sites, they clustered primarily at or around mid-blade height, between 0.3 and 0.5 of the canopy height, as indicated by the modes of the frequency distributions shown in Figure 6. This observation is in general agreement with laboratory results. The frequency distributions observed in the field departed significantly from normality (Kolmogorov-Smirnov intrinsic test for goodness of fit,  $D_{\max} = 0.048$  and 0.053 for NWH and NAPH respectively,  $P = 0.01$ ). These distributions were skewed towards the upper canopy and were

leptokurtic ( $g_1 = 0.547$  and 0.151, and  $g_2 = -0.101$  and  $-0.718$  at NWH and NAPH respectively). Skewness was significant only at NWH ( $t = 5.24$ ,  $P < 0.001$ ), but kurtosis was significant at NAPH ( $t = 2.95$ ,  $P < 0.01$ ). The size-specific distribution of scallops, expressed as a fraction of total blade length, differed significantly between the two bays ( $P < 0.001$ , nonparametric Mann-Whitney test for two independent samples). In general, a larger proportion of the scallop population was located in the upper half of the canopy in NAPH than in NWH (about 50 and 30% respectively; Fig. 6).

*Octopine dehydrogenase activity.* Octopine dehydrogenase activity was used as an instantaneous index of the scallops' capacity for burst swimming activity. Within-individual variability in ODH activity, determined by assaying two to three replicate subsamples of ground adductor muscle from each scallop collected on 10 October (mean adductor dry weight = 266 mg), averaged 7%. Lowest mean enzymatic activity ( $16 \mu\text{moles min}^{-1} \text{g}^{-1}$  adductor dry wt<sup>-1</sup>) and lowest variation in activity among similar-sized individuals were measured in early August (Fig. 7), when the entire NWH scallop population ( $\bar{H} = 6.7$  mm) remained attached to the eelgrass canopy (see Fig. 3). Mean ODH activity increased markedly between 30 August and 23 September, during relocation to the bottom, when attachment incidence dropped from

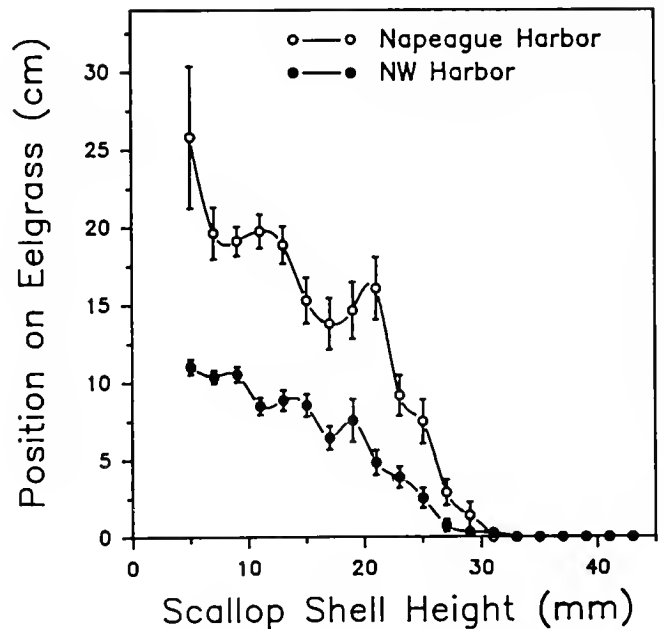


Figure 4. Vertical position (mean height above bottom  $\pm$  SE) of *Argopecten irradians* on eelgrass (*Zostera marina*) blades as a function of shell height, in two eastern Long Island bays. Scallops found on the bottom (height = 0) are included in calculation of the means; eelgrass canopy height = 38 and 23 cm in Napeague and Northwest Harbors respectively.

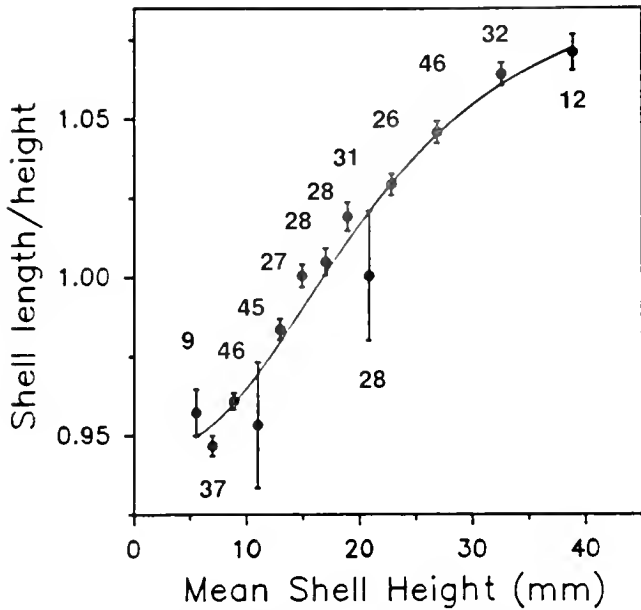


Figure 5. Aspect ratio (AR = mean shell length:height ( $H$ ) ratio  $\pm$  SE) with increasing shell height of a natural population of *Argopecten irradians* collected in Northwest Harbor. Sample size is indicated for each mean value. Fitted curve is described by the equation  $AR = (a - d) / [1 - (H/21.242)^{-0.538} + d]$ , where  $d = 0.944$ .

75% to 1%. Maximum mean values of  $84 \mu\text{moles min}^{-1} \text{g}^{-1}$  were recorded on 23 September, when scallops had reached a mean size of 29 mm, and appeared to decline thereafter.

Over the scallop size range sampled in this study, there was an overall, significant, positive relationship between octopine dehydrogenase activity ( $A$ ) and muscle dry weight ( $W$  in milligrams), as described by the equation:  $A = 9.87$  ( $SE = 3.52$ )  $W^{0.35(SE=0.07)}$  ( $r^2 = 0.81$ ;  $n = 57$ ), determined using SYSTAT iterative nonlinear curve fitting (Wilkinson, 1990). It remains to be determined whether adult scallops exhibit a decline in ODH activities. High individual variability in ODH activity on any given sampling date may be partly attributable to the large variation in scallop sizes. A comparable three-fold range in the weight of the adductor muscles was obtained within any given sampling date throughout the study period.

**Relocation experiments.** Results of the relocation experiment carried out in NWH using individually marked natural set are shown in Figure 8. Forty-three percent of the scallops initially released ( $n_1 = 150$ ,  $\bar{H} = 8.6$  mm) were recovered alive and 7% were found dead (crushed or with empty intact valves) by the end of 24 h. There was no significant difference between the mean position at time zero (collection) and 24 h following dislodgement ( $P = 0.063$ , Wilcoxon signed-rank test for paired comparisons; Fig. 8), although final height was lower than

initial height in 72% of scallops recovered on eelgrass, suggesting that 24 h may have been insufficient to achieve maximum, asymptotic height in this field experiment.

Relocation experiments carried out in Hallock Bay with hatchery-reared scallops ( $\bar{H} = 10$  mm) resulted in rates of attachment similar to those found in the laboratory with scallops of comparable size. Three hours after being released in the field, about 60% of the scallops recovered were attached to eelgrass blades, at a mean height of 8.7 cm (0.3 of canopy height), and these values remained relatively constant thereafter (Fig. 9). Maximum percent attachment and maximum height attained (when expressed as a fraction

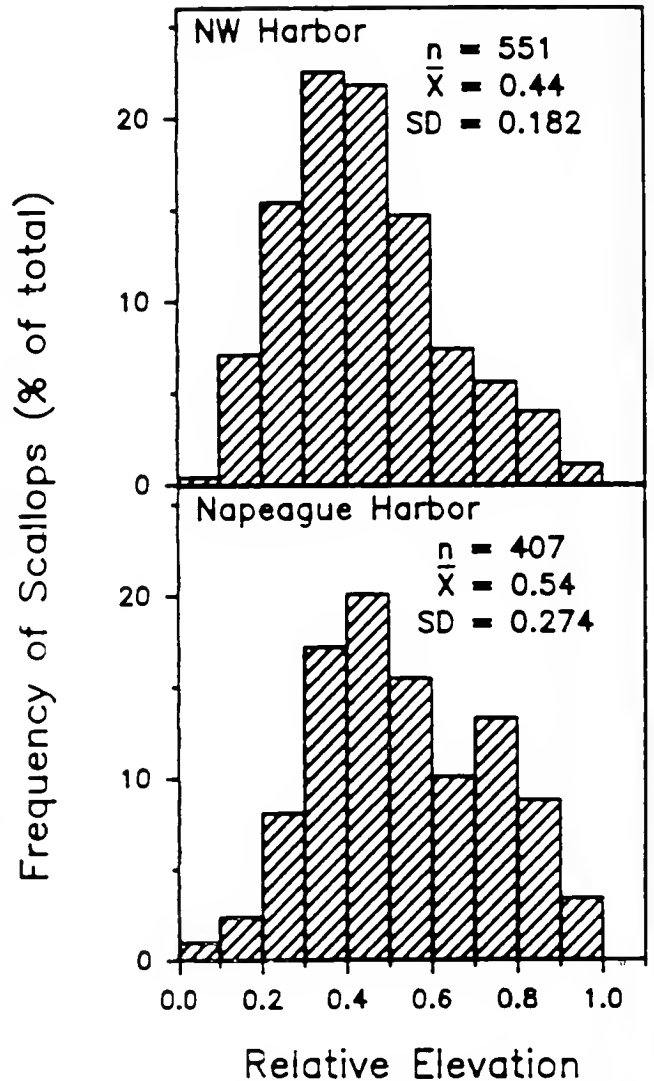


Figure 6. Distribution of juvenile *Argopecten irradians* attached in the eelgrass canopy. Relative elevation is expressed as a fraction of total blade length. All individuals collected above ground during the study are included, since there was no relationship between elevation and size of attached scallops.

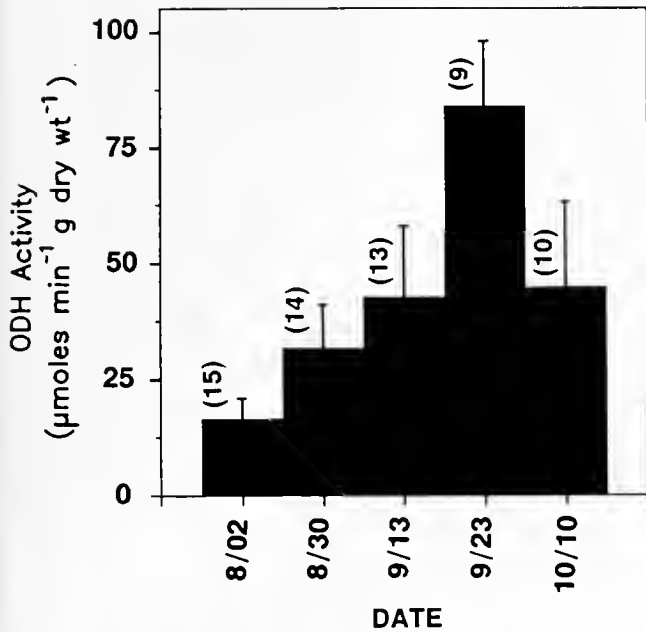


Figure 7. Octopine dehydrogenase activity (in  $\mu\text{moles of substrate min}^{-1} \text{g freeze-dried weight of adductor muscle}^{-1}$ ) of juvenile *Argopecten irradians* collected from a natural population in Northwest Harbor, between 2 August and 10 October. Error bars represent 95% confidence intervals around the mean for each sampling date. Total number of assayed individuals is indicated in parentheses; the 10 October mean includes three values obtained for pooled rather than individual samples.

of total canopy height), were thus lower than those of natural set in NWH and NAPH, and also somewhat lower than those obtained in laboratory trials (Fig. 2). No significant difference was detected between the mean height attained after 3, 5, and 24 h ( $P = 0.178$ ).

### Discussion

Laboratory and field results demonstrate that bay scallops can rapidly gain and maintain above-bottom position in the eelgrass canopy at sizes below *ca.* 10–15 mm. The adaptive significance of this behavior, which allows spatial segregation of juveniles from benthic predators and conspecific adults, may involve (a) enhanced survival through avoidance of predators and burial in unconsolidated sediments; (b) enhanced growth by positioning scallops in an optimum hydrodynamic regime that minimizes exposure to resuspended bottom sediments and maximizes food capture; or (c) a combination of these factors. Seagrasses are known to markedly reduce near-bottom current velocities and water flux (*e.g.*, Fonseca *et al.*, 1983; Eckman, 1987; Irlandi and Peterson, 1991) while generating increased turbulence at the water-canopy interface (Fonseca *et al.*, 1982; Gambi *et al.*, 1990), thus creating steep vertical gradients in the flow regime. Significant

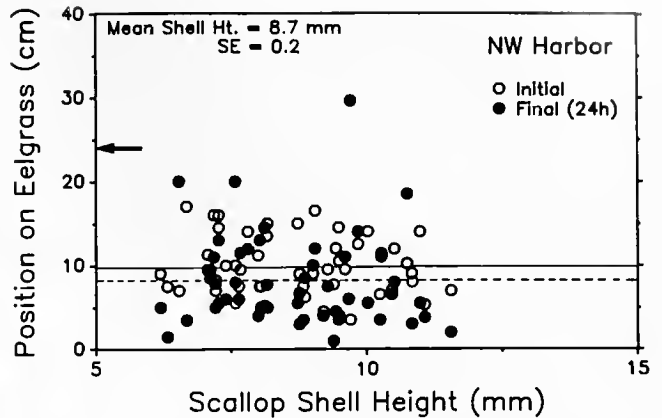


Figure 8. Above-bottom attachment height of individually marked, juvenile *Argopecten irradians* from a natural population in Northwest Harbor, before and after dislodgement from eelgrass blades. Open circles indicate scallop position at the time of initial sampling, and closed circles indicate position 24 h after dislodgement. Mean initial and final heights (9.9 and 8.0 cm) are indicated by solid and dashed horizontal lines respectively. The arrow marks the mean eelgrass canopy height at the study site.

variation in scallop growth rates with elevation within the seagrass bed was found by Ambrose and Irlandi (1992) and Borrero and Bricelj (*in prep.*), an effect that may be related to vertical gradients in food quality and quantity, as well as to flow.

The predator-refuge value of the eelgrass canopy for juvenile bay scallops has been well established (Pohle *et al.*, 1991; Ambrose and Irlandi, 1992). Refuge in elevation is effective in the presence of both nonswimming predators such as green crabs (*Carcinus maenas*), mud crabs (*Dispanopeus sayii*), and spider crabs (*Libinia spp.*) (Pohle *et*

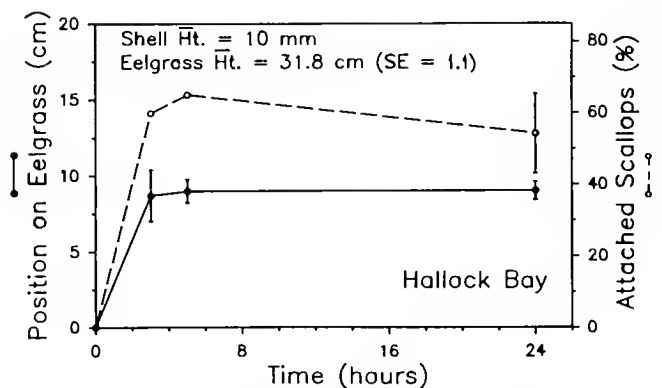


Figure 9. Time-dependent changes in percent attachment and attachment position on eelgrass blades (mean height  $\pm$  SE) of hatchery-reared juvenile *Argopecten irradians* released in Hallock Bay, Long Island. (Total number of scallops recovered = 50 and 66 at 3 and 5 h respectively, and 95 and 60 from each of two plots at 24 h.)



*al.*, 1991) and swimming, portunid crabs (Bauer and Bricelj, unpublished). The existence of a spatial, off-bottom refuge from predators in vegetated habitats was also described for the caridean shrimp *Tozeuma carolinense* (Main, 1987), and several gastropod molluscs. For example, juveniles of the freshwater snail *Planorvelia trivolvis* and all life history stages of *Physella virgata* (both characteristically thin-shelled species) are known to crawl above the water line to avoid predation by crayfish, *Procambrus simulans* (Alexander and Covich, 1991). A similar predator-avoidance strategy was reported for the intertidal marsh periwinkle *Littorina irrorata* (Vaughn and Fisher, 1988).

During the period of attachment to eelgrass, most scallops were found concentrated at about mid-canopy height, with fewer individuals at the tips and bases of eelgrass shoots. In the field, this vertical distribution could reflect preferential aggregation of scallops at mid-height, or it could result from secondary effects such as differential predation pressure or physical disturbance with varying height. The reduction in scallop numbers near-bottom can be readily ascribed to the effects of benthic predation (Pohle *et al.*, 1991), but selective depletion in the upper canopy is harder to explain. Although this region is characterized by higher current velocities and turbulence intensity (Gambi *et al.*, 1990), free-stream velocities at the two study sites were relatively weak, typically attaining maxima  $\leq 10 \text{ cm s}^{-1}$  (Borrero and Bricelj, unpublished), and thus unlikely to cause selective dislodgement of scallops in the upper canopy. Eckman *et al.* (1989) found that juvenile bay scallops commonly experience current speeds  $\geq 17 \text{ cm s}^{-1}$  in seagrass beds in North Carolina, and remain attached to *Zostera* blades at flume velocities of at least  $15 \text{ cm s}^{-1}$ . We cannot, however, rule out the possibility that selective removal of scallops occurs during storm events. The northern puffer, *Sphoeroides maculatus*, a transient predator in some Long Island bays, can preferentially forage for scallops in the upper canopy (Tanikawa and Bricelj, unpublished). Greatest concentration of scallops around mid-canopy, however, was observed in both NWH and NAPH, even though *S. maculatus* was present during the summer of 1990 only in the former embayment.

Eckman *et al.* (1989) found that 5- to 15-mm scallops attained a mean elevation of 3.5 cm within an 8-cm mixed seagrass canopy in Core Sound, North Carolina. In our study, rates of relocation and patterns of microhabitat distribution (attainment of a near-asymptotic mean elevation at about mid-canopy height within 5 to 8 h) were similar for small scallops in the field and in the laboratory. This was the case despite the absence of food, predators, wind and wave action, and epiphytic cover in the laboratory, although fewer scallops (<3%) were found in the

top 1/10 of the canopy in the field than in the laboratory (22%). This similarity suggests that the scallops' distribution on eelgrass results from an adaptive behavior, rather than solely from mortality or disturbance operating after settlement. The findings of Pohle *et al.* (1991) further suggest that predator avoidance is the most likely selection factor for climbing behavior in juvenile scallops, although attachment height may also reflect preference within a vertically heterogeneous flow microenvironment.

The present study demonstrates that scallops between the sizes of about 14 and 29 mm undergo a gradual ontogenetic shift in habitat, from the emergent canopy to the bottom, over a 5-week period. The timing of this transition, which was remarkably similar in two nonadjacent bays, may be influenced by physical constraints that prevent larger scallops from maintaining elevation. Because bay scallops have no buoyancy mechanism and gravitational force scales in proportion to mass, larger scallops are expected to exhibit increasing difficulty in generating sufficient lift and/or strength of byssal adhesion to overcome the force of gravity and support their own weight. Irreversible relocation to the bottom, where predation risk is highest, is observed at a size of about 30 mm and a total body mass of about 5 g (weight in water was not determined in this study). At this size, however, scallops can attain complete refuge from the mud crab, *Dyspanopeus sayi*, a numerically dominant predator in these bays (Strieb, 1992), and partial refuge from other common crab predators (Tettelbach, 1986).

A sharp drop in percent attachment with scallop size is consistent with laboratory results obtained by Pohle *et al.* (1991) at a constant temperature, using eelgrass mimics. Percent attachment of scallops  $\leq 10$  mm was consistently high in both studies, ranging from 97 to 100% in NWH and NAPH, and from 83 to 98% in the study by Pohle *et al.* (1991). High percent attachment was also obtained in our laboratory stocking-density experiments (*e.g.*, 85% for 9-mm scallops), although maximum attachment was only 65% for 10-mm hatchery-reared animals broadcast in Hallock Bay. Variable attachment success may result from differences in condition and scope for activity between hatchery-reared animals and natural set, from selective predatory loss of unattached scallops in the field, or from a combination of both factors. This variability may have important consequences for the survival of cultured juveniles used in reseeding efforts aimed at stock enhancement. An inverse relationship between percent byssal attachment and scallop size (between 40 and 150 mm) was also described, both *in situ* and in the laboratory, in the sea scallop, *Placopecten magellanicus*, a species that attaches primarily to bottom features such as shell and gravel (Caddy, 1972).



Our qualitative observations suggest that swimming activity (escape response) of *Argopecten* increases at intermediate sizes, during the period of transition to the bottom. This corroborates observations made by Tettelbach (1991), who reported that adults and 2- to 7-mm spat of *A. irradians* swam infrequently compared to 15- to 35-mm juveniles. Dadswell (1990) identified three stages in the life history of the longer lived species *Placopecten magellanicus*, including a stage of highest motility at intermediate sizes (30 to 100 mm). Manuel (1992) also observed that juvenile sea scallops (< 10–12 mm) generally remain attached and are more reluctant to swim than larger juveniles. This author identified a discontinuity in the relationship between relative swimming speed and Reynolds number at scallop sizes of 12–16 mm; she attributed reduced swimming capacity below this size to increased drag and greater energy cost associated with swimming below this hydrodynamic threshold. Small juveniles were reported to swim primarily vertically, achieving little horizontal displacement (Manuel, 1992). This type of swimming behavior (vertical ascent), which was also characteristic of small (< 10 mm) *Argopecten* in our study, is expected to be relatively ineffective in avoiding predators, unless elevation allows scallops to be more readily advected away from predators by bottom currents.

In general, scallop species that are active and frequently swim have higher aspect ratios than those that rarely swim and remain byssate throughout life (Stanley, 1970). Furthermore, several scallop species that occur as free-living adults and byssate juveniles display an ontogenetic increase in both umbonal angle and aspect ratio (Stanley, 1970; Gould, 1971). This was confirmed for *Argopecten irradians irradians* in this study, where aspect ratios increased from about 0.95 to 1.07 at sizes between 5 and 43 mm. We are aware of no prior estimates of aspect ratios for juveniles of this subspecies. Our values are comparable to those reported for *Placopecten magellanicus*, a more proficient swimmer than *Argopecten*, over its life cycle (0.90 to 1.05 in the range 15 to 160 mm; Dadswell, 1990). An increase in aspect ratio with growth leads to a decrease in frictional drag and an increase in the lift coefficient of scallops, thus providing an advantage in swimming by partially counteracting the mechanical difficulties associated with increased weight (Gould, 1971).

The increase in swimming activity divers observed while the bay scallops were relocating to the bottom is presumably related to an increase in predator avoidance or dispersal potential and coincided in this study with a marked increase in adductor muscle ODH activity. *A. irradians* relies to a greater extent on anaerobic glycolysis via the octopine pathway to supply energy during burst activity (escape response) than do other scallops such as *Placopecten magellanicus* (de Zwaan *et al.*, 1980) and *Chlamys*

*opercularis* (Grieshaber, 1978). In these species, energy is primarily generated through breakdown of arginine phosphate, and octopine production is largely restricted to the recovery phase following exhaustion. Thus, in *A. i. concentricus*, glycolysis contributes up to 25–88% of ATP production during exhaustive swimming (Chih and Ellington, 1983). Therefore, in this species, ODH per gram of muscle can be interpreted as an index of weight-specific potential for anaerobic metabolism. Enzymatic activity of field-collected scallops showed a 5-fold increase between sizes of 6 and 29 mm, thus following a scaling pattern inverse to that of weight-specific aerobic metabolism, which typically decreases with increasing body size.

Future work should extend measurements of ODH activity to both smaller and larger scallop sizes and increase the sample size, given the large individual variability observed in this study. Ontogenetic changes in ODH activity and differences in scaling with body size between aerobic and anaerobic metabolism have not been previously studied in swimming molluscs. However, increased reliance on anaerobic metabolism for the maintenance of burst-swimming performance with increasing body mass, based on activities per gram of muscle of other glycolytic enzymes, has been described in finfish (Somero and Chil-dress, 1980; Goolish, 1991).

In the present study, mean ODH activity in whole adductor muscle homogenates of *Argopecten irradians* attained a maximum of 84  $\mu\text{moles min}^{-1} \text{g freeze-dried weight}^{-1}$ , a value equivalent to about 17  $\mu\text{moles min}^{-1} \text{g adductor wet wt}^{-1}$ , assuming 80% water content of the adductor muscle. This estimate is lower than the value of 98  $\mu\text{moles min}^{-1} \text{g wet wt}^{-1}$  reported for *A. i. concentricus* of unspecified size (Chih and Ellington, 1983), and somewhat lower than values reported for other pectinids—*i.e.*, 30  $\mu\text{moles min}^{-1} \text{g wet wt}^{-1}$  in *Pecten maximus* and *Chlamys varius* (Zammit and Newsholme, 1976), 58  $\mu\text{moles min}^{-1} \text{g}^{-1}$  in *Pecten alba* (Baldwin and Opie, 1978), and 26  $\mu\text{moles min}^{-1} \text{g}^{-1}$  in *Placopecten magellanicus* (de Zwaan *et al.*, 1980). All literature values cited were measured at 25°C for homogenates of the phasic (striated) adductor muscle, which typically comprises the bulk (about 80%) of total adductor weight (de Zwaan *et al.*, 1980), whereas whole muscle homogenates (catch+ phasic portions) were used in the present study.

In conclusion, the present study, in concert with prior related studies (Pohle *et al.*, 1991; Strieb, 1992), supports the existence of three distinct phases during the bay scallop's early life history. During these phases, juveniles employ three different tactics to increase their survival: (1) development of upward crawling behavior by plicated and early juveniles ( $\leq$  about 11 mm in shell height), enabling

them to rapidly relocate above a minimum threshold height on eelgrass blades to achieve spatial refuge from predators: (2) active escape response, coincident with substantial energy allocation towards shell growth and gradual loss of vertical refuge at intermediate sizes; and (3) attainment of a partial size refuge at sizes exceeding about 30 mm. Mortality rates of natural scallop populations before, during, and after relocation to the bottom are needed to determine the relative value of these successive refugia.

### Acknowledgments

We thank Shino Tanikawa-Oglesby, Max Strieb, and Jim Christie for their assistance in the field; Chris Smith (Cornell Cooperative Extension) for alerting us to the presence of natural scallop set in NWH; the Shinnecock Indian Reservation Hatchery, Southampton, NY, for providing juvenile scallops; Jonathan Zehr and Pat Hassett for their advice on enzyme assays; Francisco Borrero for reviewing this manuscript; and J. K. Winfree of Synthetic Fibers Inc. for donating material for the construction of eelgrass mimics. This project was supported by the NOAA Office of Sea Grant, U.S. Department of Commerce, under grant No. NA90AA-DSG078 to the New York Sea Grant Institute, and by the Living Marine Resources Institute, SUNY at Stony Brook. One of the authors (ZGE) is also indebted to the Consejo Nacional de Ciencia y Tecnologia (CONACYT), Mexico, for support while writing this work. This is Contribution No. 909 from the Marine Sciences Research Center, SUNY Stony Brook.

### Literature Cited

- Alexander, J. E., Jr., and A. P. Covich. 1991. Predation risk and avoidance behavior in two freshwater snails. *Biol. Bull.* **180**: 387-393.
- Ambrose, W. G., Jr., and E. A. Irlandi. 1992. Height of attachment on seagrass leads to trade-off between growth and survival in the bay scallop *Argopecten irradians*. *Mar. Ecol. Prog. Ser.* **90**: 45-51.
- Baldwin, J., and A. M. Opie. 1978. On the role of octopine dehydrogenase in the adductor muscles of bivalve molluscs. *Comp. Biochem. Physiol.* **61B**: 85-92.
- Belding, D. L. 1910. The scallop fishery of Massachusetts: including an account of the natural history of the common scallop. Commonwealth of Massachusetts *Mar. Fish. Ser. No.* **3**: 51 pp.
- Bricelj, V. M., J. Epp, and R. E. Malouf. 1987. Intraspecific variation in reproductive and somatic growth cycles of bay scallops *Argopecten irradians*. *Mar. Ecol. Prog. Ser.* **36**: 123-137.
- Brodie, E. D., Jr., D. R. Formanowicz, and E. D. Brodie III. 1991. Predator avoidance and antipredator mechanisms: distinct pathways to survival. *Ethol. Ecol. & Evol.* **3**: 73-77.
- Caddy, J. F. 1972. Progressive loss of byssus attachment with size in the sea scallop, *Placopecten magellanicus* (Gmelin). *J. Exp. Mar. Biol. Ecol.* **9**: 179-190.
- Chih, C. P., and W. R. Ellington. 1983. Energy metabolism during contractile activity and environmental hypoxia in the phasic adductor muscle of the bay scallop *Argopecten irradians concentricus*. *Physiol. Zool.* **56**: 623-631.
- Crowl, T. A. 1990. Life-history strategies of a freshwater snail in response to stream permanence and predation: balancing conflicting demands. *Oecologia* **84**: 238-243.
- Dadswell, M. J. 1990. Size-related hydrodynamic characteristics of the giant scallop, *Placopecten magellanicus* (Bivalvia: Pectinidae). *Can. J. Zool.* **68**: 778-785.
- de Zwann, A., R. J. Thompson, and D. R. Livingstone. 1980. Physiological and biochemical aspects of valve snap and valve closure responses in the giant scallop *Placopecten magellanicus*. II. Biochemistry. *J. Comp. Physiol.* **137**: 105-114.
- Ebeling, A. W., and D. R. Laur. 1985. The influence of plant cover on surfperch abundance at an offshore temperate reef. *Environ. Biol. Fishes* **12**(3): 169-179.
- Eckman, J. E. 1987. The role of hydrodynamics in recruitment, growth and survival of *Argopecten irradians* (L.) and *Anomia simplex* (D'Orbigny) within eelgrass meadows. *J. Exp. Mar. Biol. Ecol.* **106**: 165-191.
- Eckman, J. E., C. H. Peterson, and J. A. Cahalan. 1989. Effects of flow speed, turbulence, and orientation on growth of juvenile bay scallops *Argopecten irradians concentricus* (Say). *J. Exp. Mar. Biol. Ecol.* **132**: 123-140.
- Fersht, A. 1985. Pp. 176-177 in *Enzyme Structure and Mechanism*. W. H. Freeman, New York.
- Fonseca, M. S., J. S. Fisher, J. C. Zieman, and G. W. Thayer. 1982. Influence of the seagrass, *Zostera marina* L., on current flow. *Estuarine Coastal Shelf Sci.* **15**: 351-364.
- Fonseca, M. S., J. C. Zieman, G. W. Thayer, and J. S. Fisher. 1983. The role of current velocity in structuring eelgrass (*Zostera marina* L.) meadows. *Estuarine Coastal Shelf Sci.* **17**: 367-380.
- Gade, G., and M. K. Grieshaber. 1986. Pyruvate reductases catalyze the formation of lactate and opiens in anaerobic invertebrates. *Comp. Biochem. Physiol.* **83B**: 255-272.
- Gambi, M. C., A. R. Nowell, and P. A. Jumars. 1990. Flume observations on flow dynamics in *Zostera marina* (eelgrass) beds. *Mar. Ecol. Prog. Ser.* **61**: 159-169.
- Goolish, E. M. 1991. Aerobic and anaerobic scaling in fish. *Biol. Rev.* **66**: 33-56.
- Gould, S. J. 1971. Muscular mechanics and the ontogeny of swimming in scallops. *Paleontology* **14**: 61-94.
- Grieshaber, M. K. 1978. Breakdown and formation of high energy phosphates and octopine in the adductor muscle of the scallop, *Chlamys opercularis* (L.) during escape swimming and recovery. *J. Comp. Physiol.* **126**: 269-276.
- Hickey, M. T. 1977. Age, growth, reproduction and distribution of the bay scallop, *Acquiptecten irradians irradians* (Lamarck), in three embayments in eastern Long Island, New York, as related to the fishery. M.S. Thesis, C.W. Post College, Long Island University, New York, 101 pp.
- Irlandi, E. A., and C. H. Peterson. 1991. Modification of animal habitat by large plants: mechanisms by which seagrasses influence clam growth. *Oecologia* **87**: 307-318.
- Kemp, W. M., L. Murray, J. Borum, and K. Sand-Jensen. 1987. Diel growth in eelgrass *Zostera marina*. *Mar. Ecol. Prog. Ser.* **41**: 79-86.
- Kitting, C. L. 1985. Adaptive significance of short-range diel migration differences in a seagrass-meadow snail population. Pp. 227-243 in *Migration: Mechanisms and Adaptive Significance*, M.A. Rankin, ed. *Contrib. Mar. Sci.* **27**.
- Main, K. L. 1987. Predator avoidance in seagrass meadows: prey behavior, microhabitat selection, and cryptic coloration. *Ecology* **68**: 170-180.

- Manuel, J. 1992.** The effect of size and hydrodynamics on the ability of juvenile scallops (*Placopecten magellanicus*) to use jet propulsion for swimming. M.S. Thesis, Acadia University, Canada.
- Palmer, A. R. 1983.** Growth rate as a measure of food value in thalid gastropods: assumptions and implications for prey morphology and distribution. *J. Exp. Mar. Biol. Ecol.* **73**: 95-124.
- Pohle, D. G., V. M. Bricelj, and Z. Garcia-Esquivel. 1991.** The eelgrass canopy: an above-bottom refuge from benthic predators for juvenile bay scallops *Argopecten irradians*. *Mar. Ecol. Prog. Ser.* **74**: 47-59.
- Sokal, R. R., and F. J. Rohlf. 1981.** *Biometry*, 2nd ed. W.H. Freeman, San Francisco. 859 pp.
- Somero, G. N., and J. J. Childress. 1980.** A violation of the metabolism-size scaling paradigm: activities of glycolytic enzymes in muscle increase in larger-size fish. *Physiol. Zool.* **53**: 322-337.
- Stanley, S. M. 1970.** Relation of shell form to life habits in the Bivalvia. *Geol. Soc. Am. Mem.* **125**: 1-296.
- Strieb, M. D. 1992.** The effects of prey size, prey density and eelgrass habitat characteristics on predation of post-settlement bay scallops, *Argopecten irradians*. M.S. Thesis, Marine Sciences Research Center, State University of New York, Stony Brook, NY. 145 pp.
- Tettelbach, S. T. 1986.** Dynamics of crustacean predation on the northern bay scallop, *Argopecten irradians irradians*. Ph.D. Dissertation, University of Connecticut. 229 pp.
- Tettelbach, S. T. 1991.** Seasonal changes in a population of northern bay scallops, *Argopecten irradians irradians* (Lamarck, 1819). Pp. 164-175 in *An International Compendium of Scallop Biology and Culture*, S.E. Shumway and P.A. Sandifer, eds., World Aquaculture Workshops, 1, Baton Rouge, LA.
- Tettelbach, S. T., and P. Wenzel. 1991.** Reseeding efforts and the status of bay scallop populations in New York following the appearance of brown tide. Natl. Shellfish. Assoc. Annual Meeting, June 23-27, 1991, Portland, Maine. p. 273 (Abstract).
- Vaughn, C. C., and F. M. Fisher. 1988.** Vertical migration as a refuge from predation in intertidal marsh snails: a field test. *J. Exp. Mar. Biol. Ecol.* **123**: 163-176.
- Vermeij, G. J. 1987.** Armor and locomotion in bivalved animals. Chapter 11 in *Evolution and Escalation: An Ecological History of Life*, Princeton University Press, New Jersey.
- Werner, E. E., and D. J. Hall. 1988.** Ontogenetic habitat shifts in bluegill: the foraging rate-predation risk trade-off. *Ecology* **69**: 1352-1366.
- Wilkinson, L. 1990.** *SYSTAT: The System for Statistics*. SYSTAT Inc., Evanston, IL.
- Zammit, V. A., and E. A. Newsholme. 1976.** The maximum activities of hexokinase, phosphorylase, phosphofructokinase, glycerol phosphate dehydrogenases, lactate dehydrogenase, octopine dehydrogenase, phosphoenolpyruvate carboxykinase, nucleoside dihydrophosphate kinase, glutamate-oxalacetate transaminase and arginine kinase in relation to carbohydrate utilization in muscles from marine invertebrates. *Biochem. J.* **160**: 447-462.

# Highly Derived Coelomic and Water-Vascular Morphogenesis in a Starfish with Pelagic Direct Development

DANIEL A. JANIES AND LARRY R. McEDWARD

*University of Florida, Department of Zoology, Gainesville, Florida 32611*

**Abstract.** The coelomic development of the starfish *Pteraster tessellatus* (order Velatida, family Pterasteridae) is fundamentally different from that reported for all other asteroids. Coeloms arise from seven separate enterocoels that evaginate from different regions of the archenteron. The water-vascular coelomic system develops from the first five enterocoels (homologous to hydrocoel lobes) which extend radially, in a transverse orientation, from the central region of the archenteron. All other coelomic compartments derive from two enterocoels that evaginate later in development from posterior regions of the archenteron. This mode of coelom formation in *P. tessellatus* leads directly to the adult organization. We hypothesize that this altered pattern of coelomogenesis evolved from the pattern that occurs in the larvae of other spinulosacean asteroids, by a rotation in the site of origin of the anterior enterocoels relative to the archenteron. The altered pattern of coelomogenesis accounts for most of the unusual features of development in *P. tessellatus*: parallel embryonic and adult axes of symmetry, transverse orientation of the juvenile disk, absence of bilateral symmetry, absence of purely larval structures, and the lack of a metamorphosis. We conclude, contrary to previous interpretations, that *P. tessellatus* does not have a larval stage and thus represents the only described case of truly direct development in the asteroids.

## Introduction

The development of *Pteraster tessellatus* is morphologically different from that of all other starfish (McEdward, 1992). *P. tessellatus* has pelagic development but does not pass through the typical asteroid larval forms, the bipin-

naia or the brachiolaria. Important features that distinguish *P. tessellatus* from other asteroids include: absence of specialized larval attachment structures (brachiolar arms and adhesive disc); accelerated development of the water-vascular system and the use of podia for attachment to the substratum at settlement; radial rather than bilateral symmetry; parallel rather than orthogonal embryonic and adult axes of symmetry; a transverse orientation of the juvenile disc; and complex morphogenesis of a supradorsal membrane.

McEdward (1992) concluded that this set of unusual developmental features in *P. tessellatus* characterized a novel type of pelagic larva in the Asterozoa. Subsequent observations led to an intriguing, but more radical, alternative interpretation: *P. tessellatus* completely lacks a larval stage and undergoes direct development (see text box: Definitions). Direct development, in which the embryo develops progressively into the juvenile, with no intervening larval features, has not been reported previously in the asteroids. Documentation of direct development would greatly expand the range of developmental diversity among starfish and would have important implications for the study of the evolution of echinoderm life cycles (McEdward and Janies, 1993).

Evaluation of the hypothesis of direct development requires additional information about the morphology of the developmental stages. Is the asteroid larval body plan present during development in *P. tessellatus*? Specifically, do internal structures develop in a bilaterally symmetrical arrangement, as is typical of starfish larvae, or is the body radially symmetrical, as is suggested by external morphology? Are there independent morphogenetic axes for early (larval) development and later (juvenile) development? Do the coeloms arise and develop in the pattern that is typical among asteroid larvae? Are there any purely

larval (transitory) structures in the development of *P. tessellatus*?

Definitions (after McEdward and Janies, 1993)

**Embryo**—the stages of development between fertilization and the completion of gastrulation.

**Larva**—the intermediate stages in development, produced by post-gastrulation morphogenesis, and eliminated by metamorphosis to the juvenile; these intermediate stages must possess transitory structures that are not involved in, and are not necessary for, morphogenesis of the juvenile.

**Mesogen**—the intermediate stages, transitional between the embryo and the juvenile, in the direct type of development; characterized by a complete absence of larval structures.

**Juvenile**—the developmental stages subsequent to the attainment of the definitive (adult) body plan, but prior to reproductive maturity.

**Metamorphosis**—the morphological transition from the larval body plan to the adult body plan.

**Indirect development**—development that involves a larval stage and a metamorphosis.

**Direct development**—development that lacks a larval stage and a metamorphosis; the juvenile develops progressively (directly) from the embryo, through a series of intermediate stages that are transitional towards the juvenile and do not involve the morphogenesis of any larval structures.

**Developmental pattern**—a set of characters (*e.g.*, development type, habitat, nutrition), each with discrete, mutually exclusive states (*e.g.*, indirect or direct; pelagic or benthic; feeding or nonfeeding) that describes features of the life cycle.

This paper describes some aspects of internal development in *P. tessellatus*, with emphasis on coelom formation and morphogenesis of the water-vascular system. Comparison with the typical pattern of indirect development via pelagic, feeding bipinnarian and brachiolarian larvae, as well as with development via modified pelagic, nonfeeding (lecithotrophic) brachiolarian larvae, reveals the coelomic and water-vascular development in *P. tessellatus* to be completely novel among asteroids. These findings, together with unusual external features of development (McEdward, 1992), lead us to conclude that *P. tessellatus* does not develop through a bilateral larval stage, nor does it undergo a metamorphosis. *P. tessellatus* represents the only known case of truly direct development in the asteroids.

### Materials and Methods

Adults of the starfish *Pteraster tessellatus* Ives, 1888 (Order Velatida, Family Pterasteridae) were collected using SCUBA, from subtidal populations (5 to 20 m) at several sites near the Bamfield Marine Station (48°49'N, 125°08'W) in Barkley Sound, Vancouver Island, British Columbia, Canada, and from depths of 15 to 30 m near the Friday Harbor Laboratories (48°32'N, 123°0'W) in the San Juan Archipelago, Washington. Adults of *P. tes-*

*sellatus* were induced to spawn by intracoelomic injection of 2 to 5 ml ( $10^{-4}$  M) of the hormone 1-methyl adenine. Eggs (about 1000–1400  $\mu$ m in diameter) were released within 1 to 3 h after injection. The eggs developed without artificial insemination and were cultured as described by McEdward (1992).

### Microscopy and 3-D reconstruction

Specimens were fixed for scanning electron microscopy (SEM) in cold osmium tetroxide (2% for 1 h) in 0.45  $\mu$ m filtered seawater, rinsed twice in distilled water, dehydrated through a graded ethanol series (30%, 50%, 70%, 15 min each), and stored in 70% ethanol. In preparation for drying, specimens were dehydrated stepwise to absolute ethanol (90%, 100%, 15 min. each), then infiltrated with hexamethyldisilazane (HMDS, Sigma Chemical Co.) for several hours. Specimens were air-dried at room temperature (Nation, 1983) in a dust-free chamber, sputter-coated with gold-palladium, and stored under desiccation.

Specimens were fixed for serial histological sectioning in Bouin's fluid (24 h), dehydrated through a graded ethanol series for 15 min in each concentration (30%, 50%, 70%), and stored in 70% ethanol. Later, specimens were dehydrated to absolute ethanol (90%, 100% 15 min each, 100% overnight), transferred to absolute ethanol with eosin y for 30 min, transferred to xylene for 30 min, infiltrated with a graded series of paraplast-xylene mixtures (at 56°C under vacuum), then embedded in paraplast. Embedded specimens were serially sectioned at 7 or 12  $\mu$ m, and stained in hematoxylin-eosin. Some specimens were partially sectioned. The tissue remaining in the block was prepared for SEM by dissolving the paraplast in xylene and drying the tissue with HMDS, as described above.

Serial sections (about 80 per mesogen) were examined and photographed with a compound light microscope. Three-dimensional reconstruction was achieved as follows. Sequential sections were aligned visually for tracing. The outer edges of the body wall, coelomic compartments, and developing gut were traced as color-coded contours onto paper with the aid of a camera lucida drawing tube. The tracings were marked with a set of fiducial points for alignment during digitization. The x, y, and z coordinates of points along the contours were entered in a computer with a digitizing tablet and stored as ASCII files. These coordinate data were then plotted as a graphic image of each section and stored as a bitmapped file of raw eight-bit color pixel data. Digitization and data conversion were done with programs written for this purpose (commented Pascal source code for DOS systems can be obtained from McEdward). Entire series of sections (bitmapped files) were imported into the program NIH Image 1.44 (a public domain program for Apple Macintosh computers available over Internet by anonymous ftp from zippy.nimh.



**Figure 1.** Early development of the *Pteraster tessellatus* embryo. A. SEM of early (1d) blastula showing irregular pattern of cleavages and blastomeres of various sizes. B. Histological section of 1d 12h wrinkled blastula showing deep folds in blastular wall and blastocoel. C. Longi-

nih.gov [128.231.98.32]). The regions bounded by endodermal and mesodermal contours in each section were filled with color to allow production of solid (rather than "wire-frame") reconstructions. These filled images were saved as a series of files in TIFF format. Stacking and projecting routines (based on a brightest point algorithm) in NIH Image were used to create 3-D reconstructions. Selected layers, such as the ectoderm could be removed by adjustment of the transparency bounds allowing visualization of internal structures.

## Results

### *Overview of development in Pteraster tessellatus*

External features of development were described by McEdward (1992). Here we summarize that description and add some additional observations. The pattern of early cleavages was irregular and resulted in blastomeres of various sizes without a regular arrangement (Fig. 1A). As cleavage progressed the blastomeres became smaller, and the surface of the embryo acquired a smooth appearance. The wall of the blastula was thrown into deep folds resulting in a wrinkled blastula stage (Fig. 1B). McEdward (1992) had reported that, during gastrulation, initiation of archenteron formation in *P. tessellatus* was correlated with the loss of folding of the blastular wall in the vegetal hemisphere of the embryo. Our study confirmed that subsequent enlargement of the archenteron was accompanied by a progressive loss of folding of the blastular wall, from the equatorial region to the animal pole of the embryo. These observations suggest that the formation of the archenteron may be due primarily to involution and not ingression. The gastrula elongated along the animal-vegetal axis and acquired an ovoid body form, just before hatching at 3 days. Within 1 to 2 days of hatching, an ectodermal depression produced a groove completely around the circumference that divided the body into anterior and posterior regions (Fig. 3A).

The oral surface of the juvenile corresponded to the anterior region of the mesogen (= animal pole of the embryo), and the aboral surface of the juvenile corresponded to the posterior end of the mesogen (= embryonic vegetal pole and blastopore) (Fig. 2). Consequently, the juvenile disc developed in a transverse orientation with respect to the anterior-posterior and animal-vegetal axes. All of the stages of development were characterized by radial, rather than bilateral, symmetry. Morphogenesis of the supra-

tudinal section of 2d 5h gastrula showing the large archenteron and small blastocoelic space. The posterior end, as indicated by the blastopore is oriented to the left. D. Transverse section, perpendicular to the anterior posterior axis of a 4d 16h elongate mesogen, showing five lateral pouches evaginating simultaneously from the equatorial region of the archenteron.

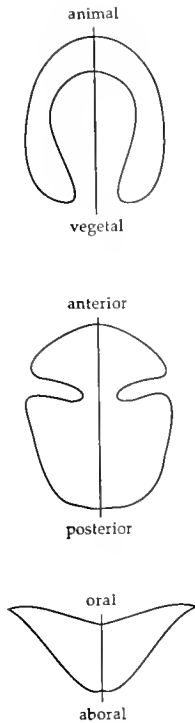


Figure 2. Diagram illustrating the orientation of the axes of symmetry of developmental stages of *Pteraster tessellatus*. Top, animal-vegetal axis of the embryonic stages, zygote to gastrula; middle, anterior-posterior axis of the mesogen; bottom, oral-aboral axis of the juvenile and adult starfish.

dorsal membrane began at 5 to 8 days with the formation of five broad marginal bulges around the circumference of the body, immediately posterior to the groove (Fig. 3A, 4A). The marginal bulges became bilobed at 8 to 10 days (Fig. 4A, O) and eventually divided to produce a total of 10 distinct marginal lobes at 16 days. Five additional lobes developed at the aboral pole of the body at 11 to 13 days. All 15 lobes fused at 17 to 19 days, resulting in a complete supradorsal membrane above the aboral body wall (McEdward, 1992, pp. 181–183). In the adult, the supradorsal membrane encloses a space, the nidamental chamber, that protects, ventilates, and perhaps nourishes young in pterasterids that brood (McClary and Mladenov, 1990). Functional podia, arranged in five clusters, emerged from the circumferential groove at 9 days, long before the development of juvenile arms (at 2.5 months). Early development of the podia is important because the mesogen of *P. tessellatus* lacks the brachiolar arms and adhesive disk of other pelagic nonfeeding larvae (Fig. 3A, 4A). Podia of *P. tessellatus* are used for attachment to the substratum at settlement at 10 to 12 days. Each podial cluster initially consisted of a pair of podia and a terminal podium. Three to four additional pairs of podia were added by 28 days. The juvenile mouth did not form until the second month, and distinct arms were not present in most

*P. tessellatus* juveniles until the third month (McEdward, 1992).

#### Internal development of *Pteraster tessellatus*

**Gastrulation.** At 2 to 3 days of development in *P. tessellatus*, the archenteron widened within the gastrula. The interior of the ovoid stage contained a large archenteron that extended from the blastopore at the posterior (= vegetal) end all the way to the anterior (= animal) end. The archenteron nearly filled the interior of the body, causing the ectodermal and mesendodermal cell layers to lie close together and greatly reduced the blastocoelic space (Fig. 1C). The blastopore closed between days 3 and 4 resulting in a completely closed archenteron sac. The archenteron did not join with the animal ectoderm to form a stomodeal opening. *P. tessellatus* produces large, yolky mesogens that do not feed on particulate food.

**Morphogenesis of the water-vascular system.** At 4 days, five lateral coelomic pouches (enterocoels) evaginated simultaneously from the equatorial region of the archenteron (Fig. 1D, 3E–H). The five enterocoels were arranged symmetrically around the circumference of the archenteron in a transverse plane (*i.e.*, perpendicular to the anterior-posterior axis of the mesogen; Fig. 2, 7III B). These five enterocoels were hydrocoelic in nature because they became the coelomic lining of the water-vascular system (*i.e.*, radial canals, podia, ampullae, and circumoral ring canal). Initially, these hydrocoel lobes were broad, simple evaginations from the archenteron (Fig. 1D). The hydrocoel lobes elongated as they extended radially towards the ectodermal body wall. The hydrocoel lobes remained connected to the archenteron throughout much of the development of the water-vascular system. The hydrocoel lobes and their relationship to the archenteron are evident in transverse section (Fig. 3E–H) and in 3-D reconstruction (Fig. 5A, B). A diagram of the typical adult asteroid water-vascular coelomic system, perihemal coelomic system, hemal system, and axial complex (Fig. 6) and a table of terminology used in this paper, cross referenced to that of Hyman (1955), (Fig. 8) are provided to aid in visualizing the morphogenesis of *P. tessellatus*.

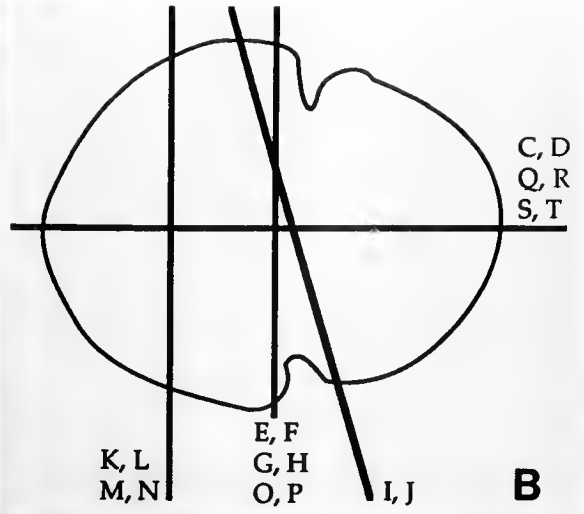
At 5 days, the distal ends of the hydrocoel lobes began to contact the overlying ectoderm (Fig. 3E, F). At the time and location of this contact, the ectoderm began to fold inward to produce the circumferential groove. The groove formed just anterior to the hydrocoel, so that the contact with the hydrocoel lobes occurred along the posterior wall of the groove (Fig. 3C–J).

The proximal and central portions of each hydrocoel lobe developed into a radial canal. The distal part of each hydrocoel lobe widened and then bifurcated to form the coelomic lining of the first pair of podia (Fig. 3G, H). The coelomic lining of each terminal (unpaired) podium de-





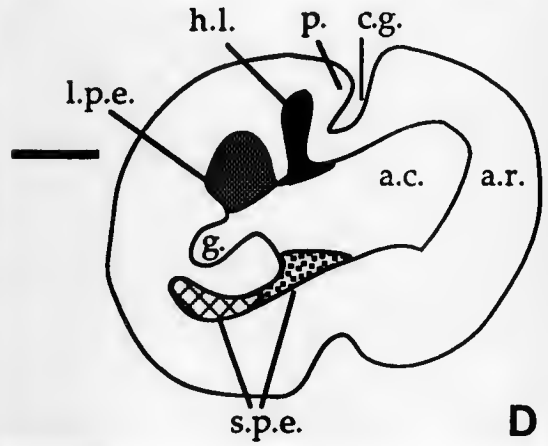
**A**



**B**



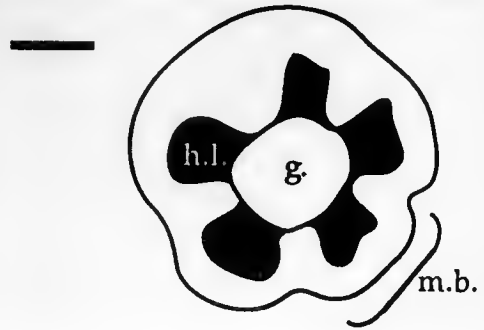
**C**



**D**



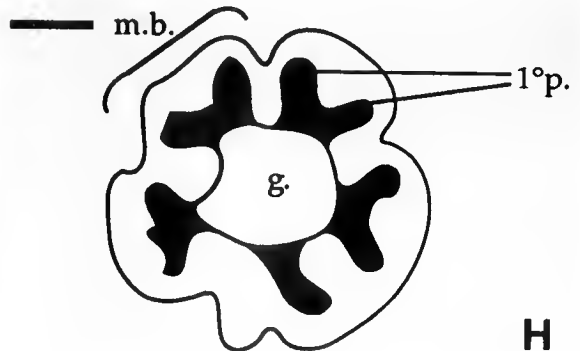
**E**



**F**



**G**



**H**



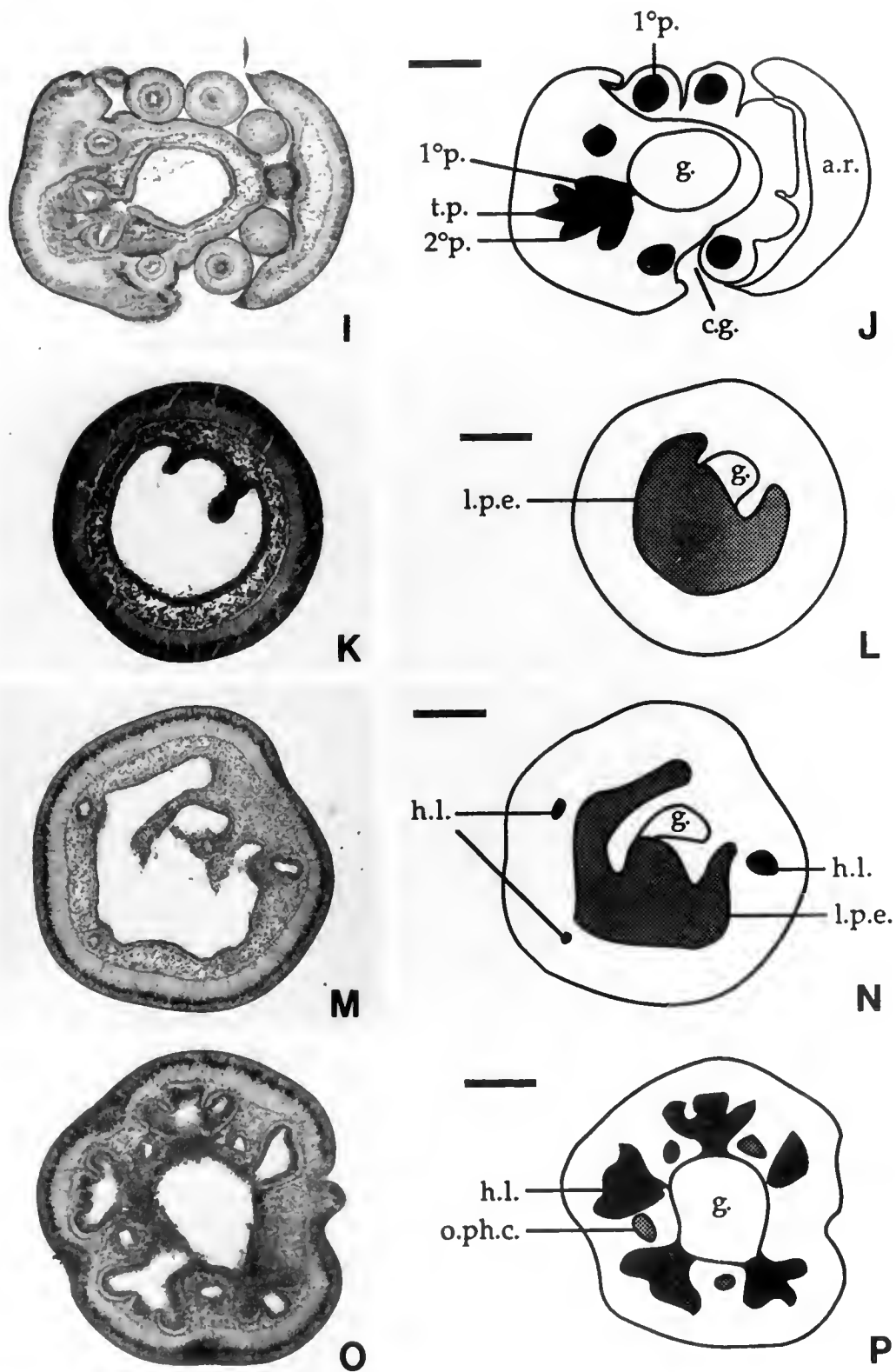
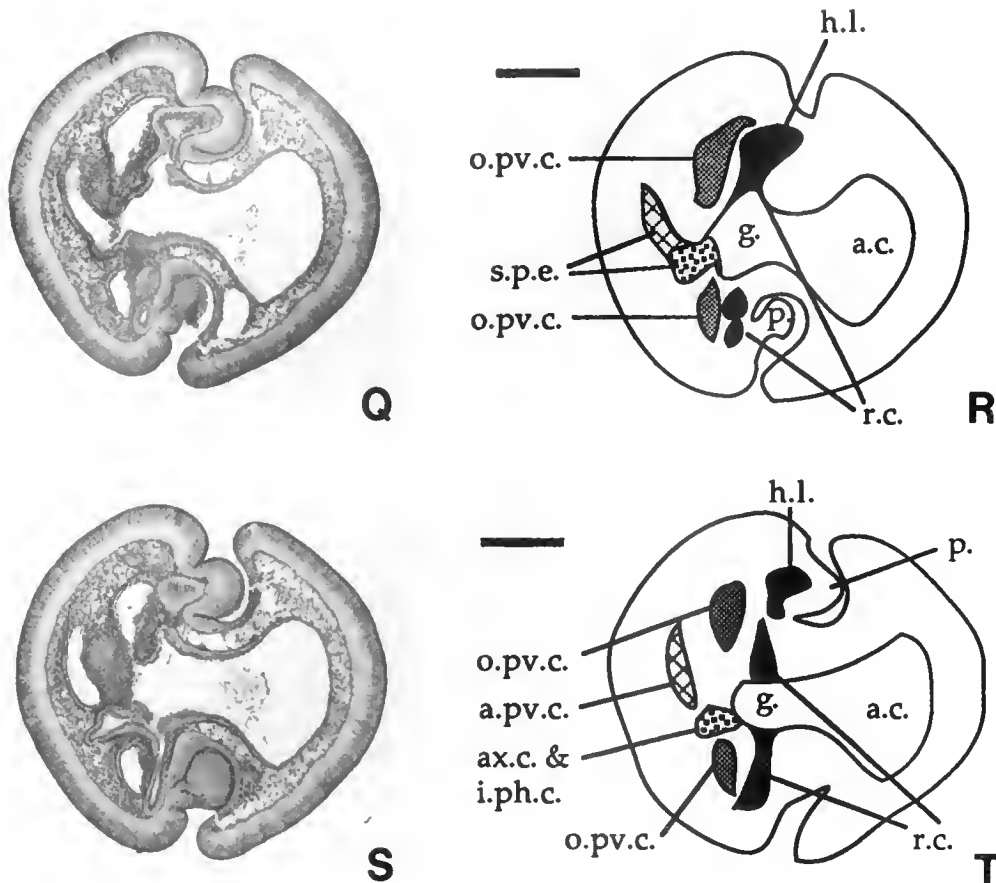


Figure 3. (Continued)



**Figure 3.** Internal morphogenesis of the early (about 6–8d) mesogen of *Pteraster tessellatus*. Magnification is the same in all panels and scale bar equals 0.2 mm. In all lateral views the posterior of the mesogen is oriented to the left. A. SEM, lateral view of 6d mesogen, showing circumferential groove dividing anterior and posterior body regions. Podia are visible in the circumferential groove. B. Drawing of lateral view of mesogen in panel A showing location and orientation of planes of section for the following panels of this figure. C–T. Paired light micrographs and interpretive diagrams of histological sections. See Table 1 for abbreviations. C, D. Longitudinal section of 6d mesogen showing origin of the enterocoels from the archenteron and relationship of circumferential groove to the hydrocoels. E, F. Transverse section of 5d 8h mesogen showing the first five evaginations (hydrocoels) in pentaradial symmetry around the circumference of the archenteron and their early contact with the overlying ectoderm. G, H. Transverse section of 6d mesogen showing the bifurcation of the distal part of each hydrocoel lobe that forms the coelomic lining of the first pair of podia. I, J. Oblique section of 7d mesogen showing the coelomic lining of the terminal unpaired podium forming as an extension from the cleft of the original bifurcation and the coelomic lining second pair of podia evaginating between the terminal podium and the first pair. K, L. Transverse section through a 5d 8h mesogen showing the large posterior enterocoel evaginating as a large crescent shape from the extreme posterior region of the archenteron. M, N. Transverse section of 6d mesogen showing the large posterior enterocoel encircling the gut and enveloping the posterior side of the hydrocoel lobes. O, P. Transverse section of 6d mesogen showing four of the five initial small pouches growing orally from the oral perivisceral coelom between the hydrocoel lobes to originate the outer oral perihemal ring coelom. Q, R. Longitudinal section of 6d 16h mesogen showing the enterocoels, especially the small posterior enterocoel and its mixed set of fates of the (*i.e.*, axocoelic and somatocoelic). S, T. Longitudinal section of 6d 16h mesogen (same mesogen as section in Q, R) showing the somatocoelic derivative (the aboral perivisceral coelom) separating from the distal region of the small posterior enterocoel and moving to the extreme posterior of the body. The proximal region of the small posterior enterocoel develops into the inner oral perihemal ring coelom and likely contributes to the coelomic and hemal axial complex, such as the axial coelom and madreporic vesicle.

Table 1

Abbreviations used in Figures 3 and 4

Abbreviation	Description
1°p.	coelomic lining of the primary podia of the water-vascular system
2°p.	coelomic lining of the secondary podia of the water-vascular system
a.	ampulla of the podia of the water-vascular system
a.c.	anterior compartment of the archenteron
a.p.v.c.	aboral perivisceral coelom
a.r.	anterior region of the mesogen
ax.c.	axial coelom
c.g.	circumferential groove
co.r.c.	circumoral ring canal of the water-vascular system
g.	gut
h.l.	hydrocoel lobe of the water-vascular system
hp.c.	hydropore canal
i.ph.c.	inner oral perihemal ring coelom
l.c.	lateral canal of the water-vascular system
l.p.e.	large posterior enterocoel
m.b.	marginal bulge of the mesogen
o.ph.c.	outer oral perihemal ring coelom
o.p.v.c.	oral perivisceral coelom
p.	ectodermal covering of the podia
r.c.	radial canal of the water-vascular system
s.p.e.	small posterior enterocoel
l.p.	coelomic lining of the terminal podium of the water-vascular system

veloped as an extension from the cleft of the original bifurcation. At 7 days, the coelomic lining of the second pair of podia evaginated between the terminal podium and the first pair (Fig. 3I, J). In the region of the hydrocoel lobes, the ectoderm of the circumferential groove thickened, enveloped the developing coelomic linings, and produced the epidermal covering of the podia. In subsequent development, additional pairs of podia were added immediately proximal to the terminal podium as the radial canals elongated (Fig. 4M, N).

The five hydrocoel lobes remained connected to the gut but were otherwise independent of each other during the early development of the radial canals and podia. Later, these five independent evaginations were connected by a coelomic tube (ring canal) that encircled the gut. At 8 to 9 days, each radial canal separated from the archenteron by a constriction of the oral side of its proximal end. Concurrently, the aboral portion of the proximal end of each radial canal produced small lateral evaginations in the transverse plane of the body. These evaginations grew around the circumference of the archenteron, met in the interradia, and fused to complete the circumoral ring canal (Fig. 4E–N, 5B).

The ampullae developed by an expansion of the coelomic lining on the aboral side of each podium. By 8 days, the ampullae of the first two pairs of podia had greatly

enlarged and extended up against the oral perivisceral coelom (Fig. 4C, D). At 8 to 9 days, the hydropore canal developed as a long tubular invagination from the aboral ectoderm in the extreme posterior region of the body. It extended orally and joined with the developing circumoral ring canal (Fig. 4E, F, I, J, K, L, S, T, and 5B). The hydropore canal was an ectodermal structure that was conspicuous in early development because it stained very deeply. We assumed the hydropore canal gave rise to the stone canal of the adult as is typical of asteroids although we did not trace its development beyond 12 days.

The completion of the major water-vascular components (circumoral ring canal, radial canals, podia with expanded ampullae, and hydropore canal) at 8 to 9 days corresponded to the time at which a mesogen possessed functional podia that could be extended from the body and used to adhere to the substratum. In laboratory cultures, settlement occurred as early as 1 to 2 days after the completion of a functional water-vascular system (McEdward, 1992).

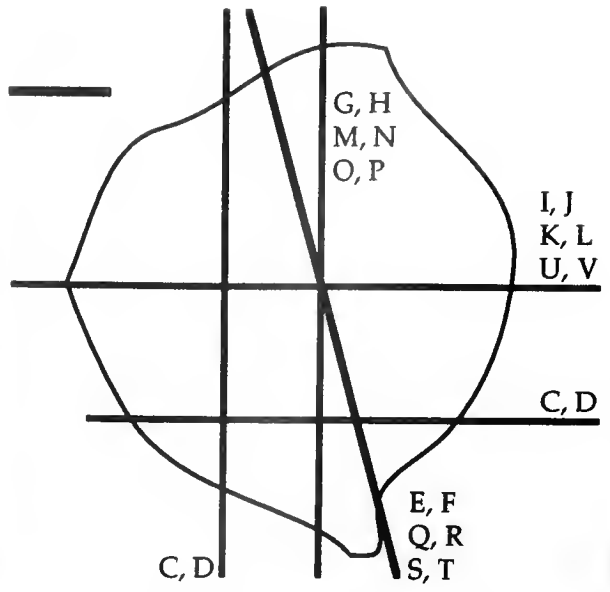
*Formation of the perivisceral coeloms and axial complex.* Soon after the evagination of the hydrocoel lobes from the archenteron, two additional enterocoelic evaginations appeared (Fig. 3C, D, K, L, Q–T, 5A, B): (1) a large posterior enterocoel (= 6th of 7 enterocoels) whose fate was to become the oral perivisceral coelom which in turn produced the outer oral perihemal ring coelom in the juvenile; and (2) a small posterior enterocoel (= 7th of 7 enterocoels) that formed the axial and inner oral perihemal coeloms and the aboral perivisceral coelom.

The large posterior enterocoel developed from the extreme posterior region of the archenteron at 4 to 5 days. Initially, this enterocoel had the shape of a very large crescent lying in a plane transverse to the anterior-posterior axis of the mesogen (Fig. 3K, L, 5A). By 5 days, this large posterior enterocoel assumed the adult location of the oral perivisceral coelom: it encircled the gut and enveloped the posterior side of the hydrocoel (especially the ampullae of the podia) (Fig. 4C, D; 3M, N; 5A). At 6 days, the oral perivisceral coelom developed five small pouches that grew orally (= anteriorly) between the hydrocoel lobes in interradial positions (Fig. 3O, P). These processes then grew laterally and fused in the radii to form the outer oral perihemal ring coelom (Fig. 4O, P).

At 4 to 6 days, the small posterior enterocoel evaginated from the archenteron posterior to the hydrocoel and slightly anterior to site of evagination of the large posterior enterocoel (Fig. 3C, D, M, N; 5A). The small posterior enterocoel subdivided into a complex set of coeloms. At 6 days, the aboral perivisceral coelom separated from the distal region of the small posterior enterocoel and moved to the extreme posterior of the body (Fig. 3Q–T; 5A). The proximal region of the small posterior enterocoel formed a crescentic coelom near the aboral, inner surface of the



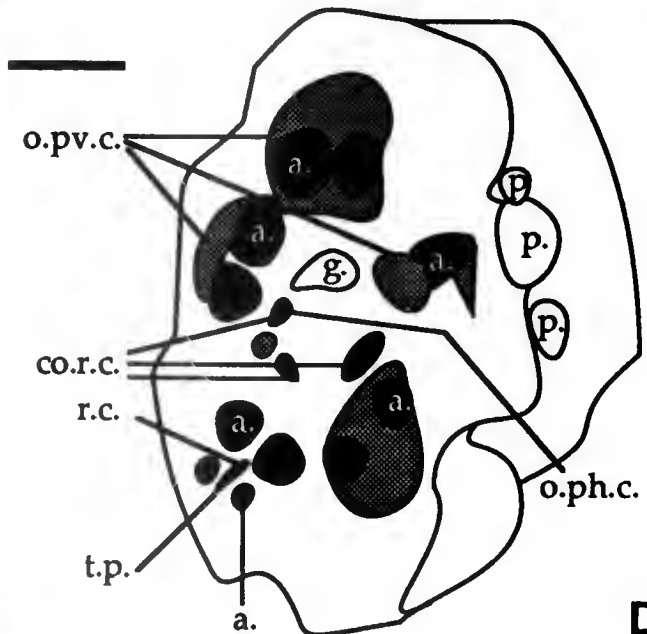
**A**



**B**



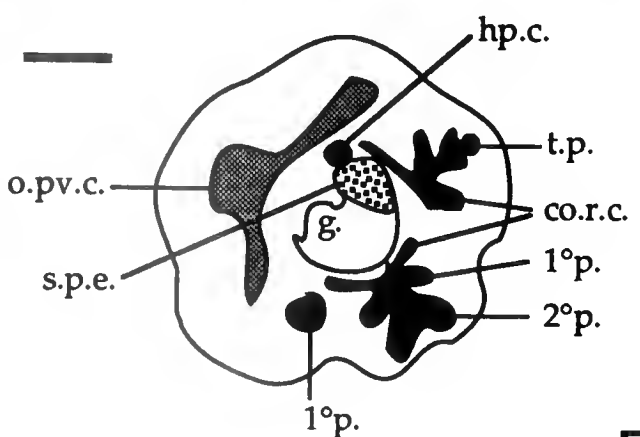
**C**



**D**

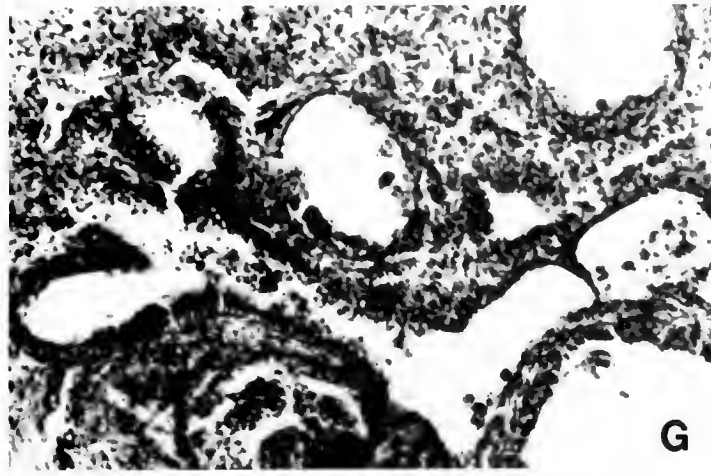


**E**

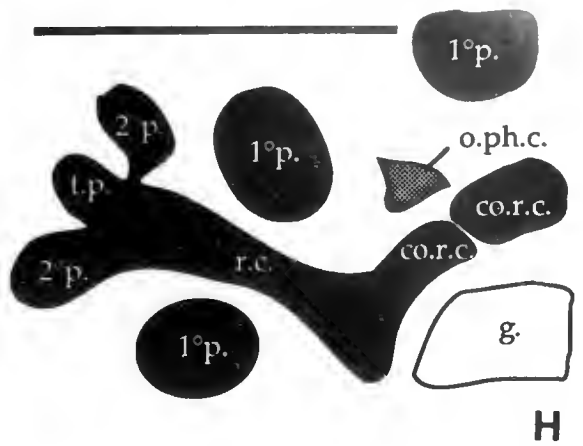


**F**

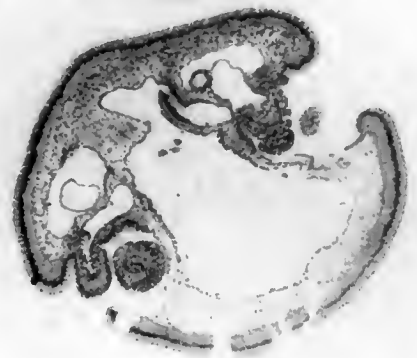
Figure 4.



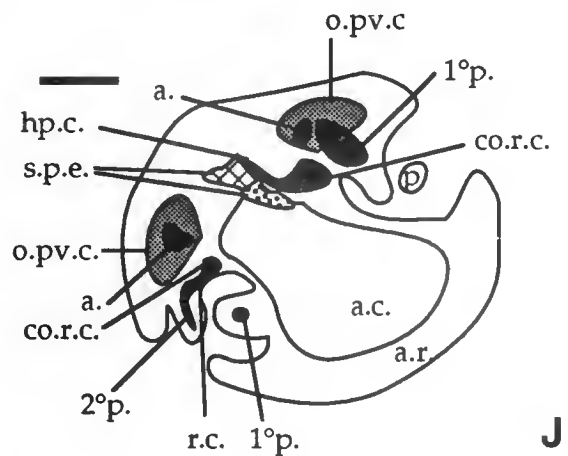
G



H



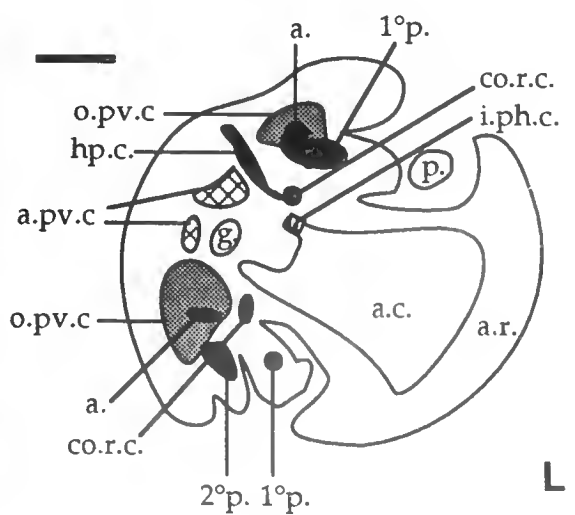
I



J

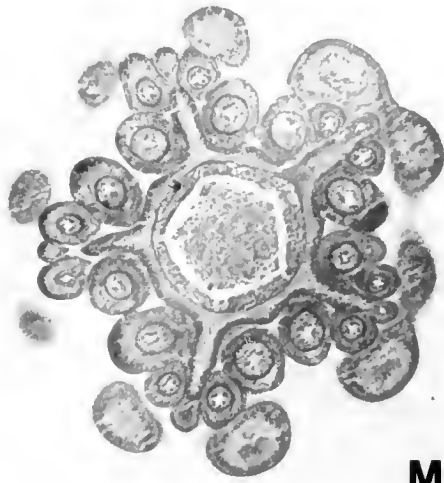


K

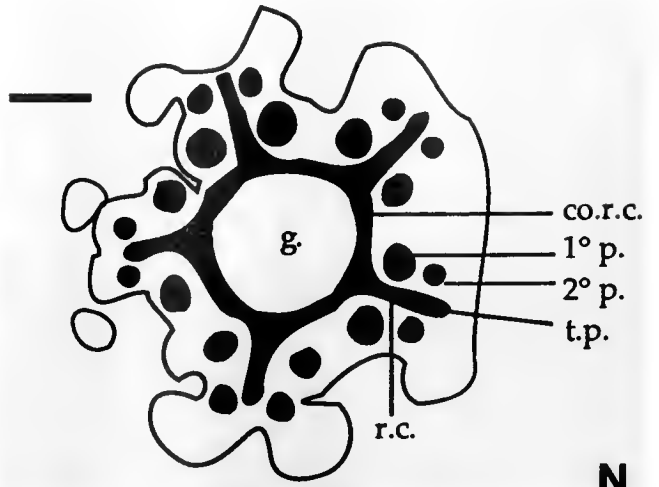


L

Figure 4. (Continued)



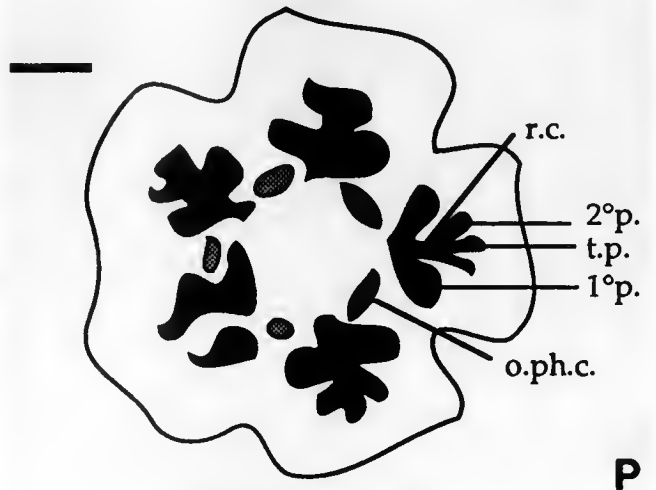
M



N



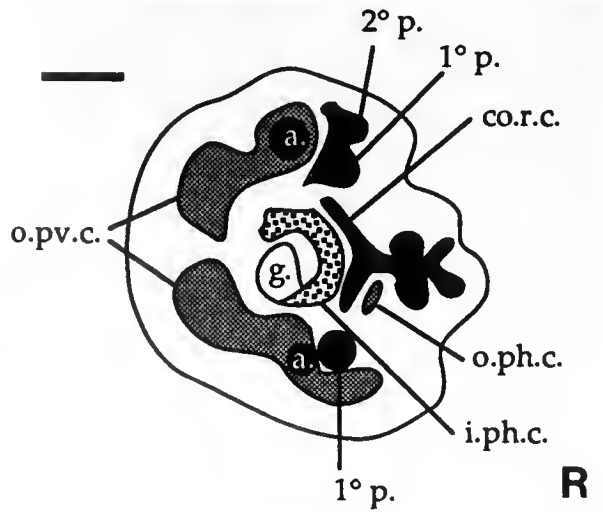
O



P



Q



R

Figure 4. (Continued)

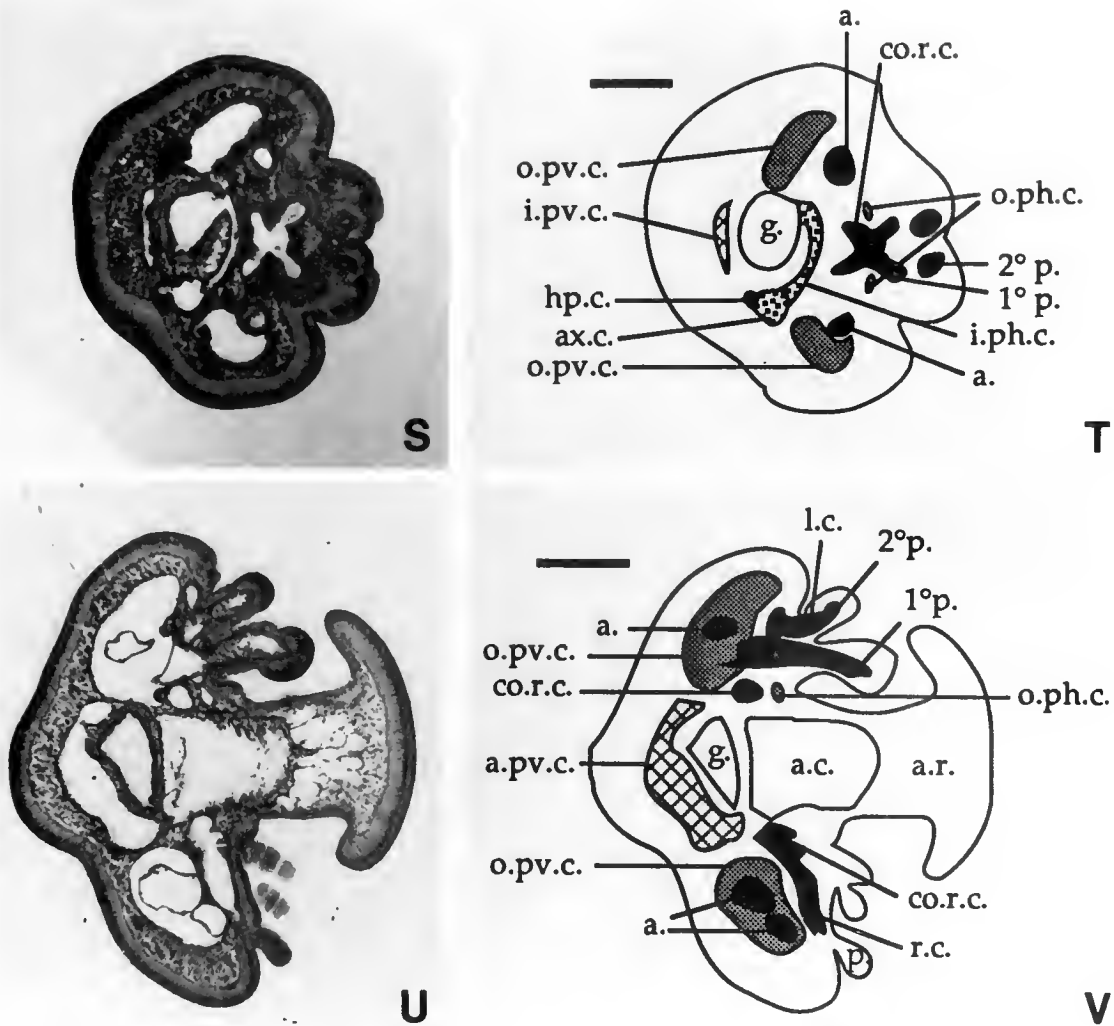


**Figure 4.** Morphogenesis of the late ( $\approx 9$ –11d) mesogen of *Pteraster tessellatus*. Magnification is equal in all panels (except G, H) and all scale bars equal 0.2 mm. In all lateral views the posterior of the mesogen is oriented to the left. See Table 1 for abbreviations. A, SEM, lateral view of 9d mesogen showing five marginal bulges and well developed podia. B, Drawing of lateral view of mesogen in panel A showing location and orientation of planes of section for the following panels of this figure. C, D, SEM and interpretive diagram of 9d mesogen sectioned in two planes and oriented obliquely to the viewer. Transverse face revealing the oral perivisceral coelom and elements of the hemal and water-vascular system in the oral region of the mesogen, especially the ampullae of the podia. Longitudinal face revealing an ampulla and the ectodermal covering of a cluster of podia. E–V, Paired light micrographs and interpretive diagrams of histological sections. E, F, Slightly oblique section of 9d mesogen showing the proximal lateral evaginations of the radial canals that fuse to form the circumoral ring canal of the water-vascular system. Also, the proximity of the hydropore canal to the small posterior enterocoel is visible. G, H, Transverse section at high magnification of an 8d ambulacrum revealing the proximal lateral evaginations of the radial canals that form the circumoral ring canal and showing the early development of a portion of the outer oral perihemal ring coelom. I, J, K, L, Two longitudinal sections from the same 10d mesogen. These illustrate the ectodermal origin of the hydropore canal, its confluence with the middle region of the small posterior enterocoel to form part of the axial complex, and the connection of the hydropore canal to the circumoral ring canal. M, N, Transverse section through the completed water-vascular system of an 11d mesogen. O, P, Transverse section through the same 11d mesogen as in panels M, N. This section is slightly aboral to M, N and hence reveals the outpockets of the oral perivisceral coelom that form the outer oral perihemal ring coelom. Q, R, Oblique section through 9d mesogen showing formation of the crescentic shaped inner oral perihemal ring coelom from the proximal region of the small posterior enterocoel. This view illustrates the proximity of the inner oral perihemal ring coelom with the circumoral ring canal of the water-vascular system. S, T, Oblique section of 7d 16h mesogen showing the formation of the axial complex from the confluence between the inner oral perihemal ring coelom and the hydropore canal. U, V, Longitudinal section of 11d mesogen showing an adult internal organization. At this stage the anterior compartment is in the process of transferring the contents of the anterior region of the mesogen to the gut in order to fuel development.

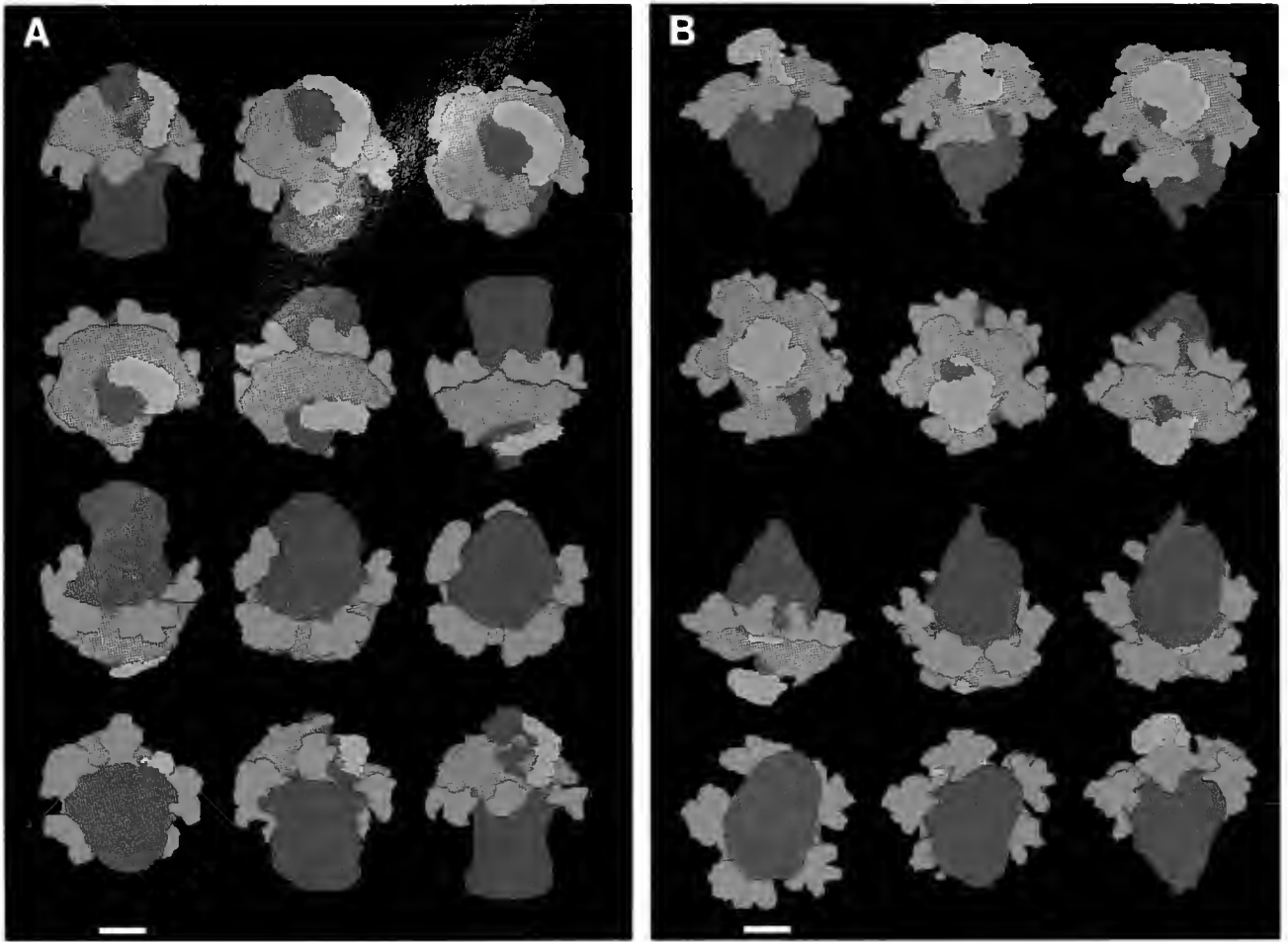


**Figure 5.** Two 3-D reconstructions of internal features (mesoderm and endoderm) of two stages (a. 6d, b. 9d) of a *Pteraster tessellatus* mesogen. Each half page panel contains a montage of 12 views of a single specimen as a series of 30° rotations through a total of 360°. The rotational sequence begins in the upper left and progresses across the top row to the right. Subsequent rows are also read left to right. The initial (upper left) and final (lower right) views are oriented with the posterior of the mesogen up. The identity of each structure is color keyed as follows: red = water-vascular coelomic lining, green = gut and anterior compartment, yellow = small posterior enterocoel, blue = large posterior enterocoel, and purple = hydropore. Scale bar = 0.2 mm.

circumoral ring canal of the water-vascular system (Fig. 4Q, R). This crescentic coelom developed into the inner oral perihemal ring coelom. The middle region of the small posterior enterocoel was confluent with the hydropore canal (Fig. 3Q–T; 4E, F, I–L, S, T). The region of contact between these coeloms likely formed some substructures of the coelomic and hemal axial complex, such as the axial coelom and madreporic vesicle. However, a comprehensive and definitive description of the development of the axial complex will require substantial additional study.

*Development of the gut and anterior compartment.* A great deal of coelomic morphogenesis occurred in *P. tessellatus* while the seven enterocoels remained confluent via the central portion of the archenteron. Masterman

(1902) described a similar arrangement of connected enterocoels and archenteron as a “mesenteron” in *Henricia sanguinolenta* (formerly *Cribella oculata*). This term is useful in describing the internal development of *P. tessellatus*. At 4 to 5 days, in *P. tessellatus*, despite the confluence among all seven of the enterocoels, the gut (endoderm) was histologically differentiated from the coelomic (mesodermal) regions of the mesenteron. The gut was delineated as a deeply staining, thickened epithelial region located posterior to the five hydrocoel lobes and in between the two posterior enterocoels (Fig. 3C, D, Q–T; 5A, B).

The region of the mesogen anterior to the circumferential groove was filled peripherally with yolk and fibrous material, but also contained an epithelial layer that en-



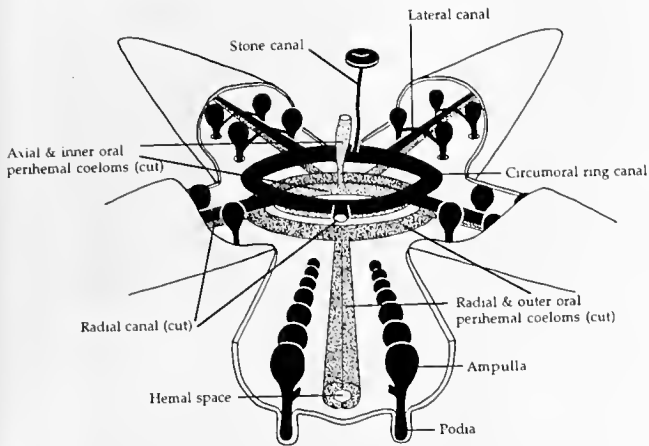


**Figure 6.** Drawing of the internal anatomy of a typical adult asteroid showing the arrangement of water-vascular and perihemal coelomic systems as well as components of the hemal system. See Figure 8 for an interpretation of the stippling.

closed a large, central internal compartment (Fig. 3C, D, Q–T; 4I–L). The epithelial compartment was not the product of enterocoely but was simply the anterior of the archenteron produced by gastrulation. Hence we do not believe it is properly termed a coelom but rather an anterior compartment of the gut. The anterior compartment remained confluent with the gut region of the archenteron throughout juvenile development. Identifiable structures did not develop in the anterior region of the mesogen and its blastocoelic contents were depleted during development (Fig. 4U, V).

### Discussion

*P. tessellatus* is radially symmetrical throughout development, lacks all larval structures, and does not undergo a metamorphosis. In addition, the coeloms arise from seven separate enterocoels that evaginate from different regions of the archenteron. The water-vascular coelomic system develops from the first five enterocoels (homologous to hydrocoel lobes) that extend radially, in a transverse orientation, from the central region of the archenteron. All other coelomic compartments develop from two enterocoels that evaginate later in development from posterior regions of the archenteron. This mode of coelom formation in *P. tessellatus* leads directly to the adult organization. From these results, we conclude that *P. tessellatus* represents the first case of truly direct development described in the asteroids.

Did direct development evolve through modification of the typical pattern of asteroid larval development? The considerable morphological and ecological diversity of asteroid larvae seems to argue against the idea of a typical larva or typical pattern of development. However, only a

single component of development, coelomogenesis, underlies all of the important features characterizing direct development in *P. tessellatus*: radial symmetry, transverse disc, parallel embryonic and adult axes, and lack of larval organization. If there is a general pattern of coelom development among asteroids, or if the starfish most closely related to *P. tessellatus* share common features of coelomogenesis, then there would be a basis from which to explore the morphogenetic changes that could lead to the evolution of direct development. In the following sections, we analyze the literature on asteroid larvae and conclude that there are extremely conservative features of coelomic development. Then we present a hypothesis to explain the evolution of the highly modified coelomogenesis that we have described in *P. tessellatus*.

### Patterns of asteroid coelomogenesis

*Asteroids with indirect development and pelagic feeding larvae.* Development from small eggs (about 100–200  $\mu\text{m}$  in diameter) via feeding bipinnarian and feeding brachiolarian larvae is the ancestral pattern in asteroids (Strathmann, 1974, 1978; McEdward and Janies, 1993). In species with feeding bipinnarian larvae, the coeloms develop from a pair of enterocoels that evaginate from the tip of the archenteron (Fig. 71A–B) (e.g., *Asterias rubens*, Gemmill, 1914; see also reviews by Hörstadius, 1939; Hyman, 1955; Chia and Walker, 1991). The enterocoels develop into three pairs of coeloms (from anterior to posterior: axocoels, hydrocoels, and somatocoels) (Fig. 71C). The somatocoels pinch off from the enterocoels as separate coeloms early in larval development, but the axocoels and hydrocoels are often confluent via small coelomic tubes and hence are considered axohydrocoels by some (Hyman, 1955). However, each coelomic sac or region can be considered to have a separate role in organogenesis (Fig. 7, 8). By the brachiolarian stage, the left and right axocoels fuse in the anterior region of the larva to form a single coelom (axocoel) in the shape and orientation of an inverted U (Fig. 71D) (Gemmill, 1914). The axocoel extends anteriorly into the preoral lobe, which is defined by its location anterior to the larval mouth. This portion of the axocoel is termed the preoral coelom (or anterior coelom). The preoral coelom extends into the lumen of the brachiolar arms (Barker, 1978), if present.

*Paxillosids with indirect development and pelagic feeding larvae.* Asteroids in the order Paxillosida with pelagic feeding development have only a bipinnarian stage. These are termed, “non-brachiolarian larvae” because they lack brachiolar arms and the associated coelomic projections (Oguro *et al.*, 1976). Despite this, these larvae undergo the typical pattern of coelomogenesis (described above and in Fig. 71A–D) and have a well-developed preoral coelom that extends anteriorly into the preoral lobe of

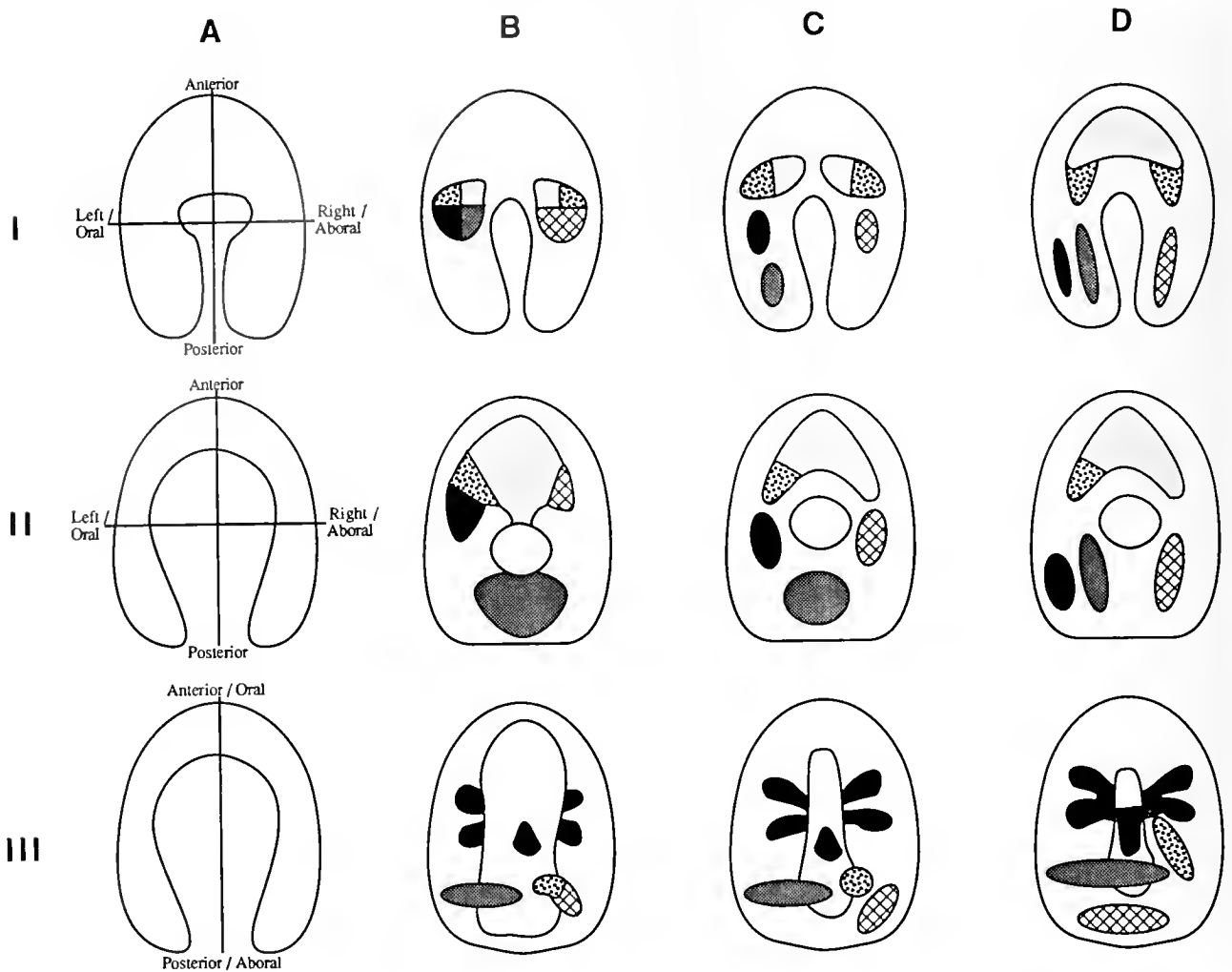


**Figure 7.** Comparison of coelomic origin and fates during development (A through D) in different asteroids (I, II, and III). All drawings are oriented as dorsal views of longitudinal sections with the anterior end up. A key to the stippling indicating coelomic fates is provided in figure 8. I A-D. Ancestral pattern of coelomogenesis via feeding bipinnaria and feeding brachiolarian larval stages. II A-D. Coelomogenesis in the nonfeeding brachiolarian larvae of the superorder Spinulosacea (e.g. the families Solasteridae and Echinasteridae). III A-D. Coelomogenesis in *Pteraster tessellatus*.

the bipinnaria (e.g., *Astropecten scoparius*, Oguro *et al.*, 1976, p. 561, 566; *Luidia clathrata* Komatsu *et al.*, 1991, p. 497).

*Paxillosids with indirect development and pelagic non-feeding larvae.* In several asteroid clades, feeding larvae have been replaced by nonfeeding larvae (Strathmann, 1974, 1978). Some species of the order Paxillosida develop from moderately large (about 300–500  $\mu\text{m}$  in diameter) yolky eggs via pelagic nonfeeding larvae. These are termed barrel-shaped larvae because they have a highly simplified external morphology. Barrel-shaped larvae lack brachiolar apparatus and are likely derived from paxillosids with feeding bipinnaria only (Komatsu *et al.*, 1988; McEdward and Janies, 1993). Although few details of internal development are known, coelom formation in barrel-shaped

larvae is similar to the ancestral pattern because it includes the formation of a U-shape and an anterior coelom (Komatsu, 1975, p. 54; 1982, p. 202; Komatsu and Nojima, 1985, p. 276).

*Asteroids with indirect development and benthic non-feeding larvae.* *Asterina gibbosa* (MacBride, 1896) and *Leptasterias hexactis* (Chia, 1968) develop from large yolky eggs (about 500  $\mu\text{m}$  and 800  $\mu\text{m}$ , respectively) via benthic, simplified, nonfeeding brachiolaria. Coelomogenesis in these species is only slightly modified from the ancestral pattern. A single, large enterocoel evaginates from the anterior tip of the archenteron. This unpaired coelomic sac expands anteriorly and laterally, then extends backwards with a pair (left and right) of short, posterior projections, thus producing the characteristic U-shaped







Pattern	Cavity	Adult fate in the terminology of this paper	Adult fate in the terminology of Hyman, 1955
	Preoral coelom	Resorbed	Resorbed
	Axocoel	Inner oral perihemal coelom Axial perihemal coelom	Inner oral hyponeural sinus Axial sinus
	Hydrocoel	Water-vascular system	Water-vascular system
	Somatocoel	Oral perivisceral coelom Outer oral and radial perihemal coeloms	Hypogastric coelom Outer oral and radial hyponeural sinuses
	Somatocoel	Aboral perivisceral coelom	Epigastric coelom
	Archenteron	Gut	Gut

Figure 8. Key to the stippling patterns used in the coding of internal cavities and their adult fates in figures 3, 4, 6, 7, and 10. This information is cross referenced to the terminology of Hyman (1955).

coelom. The lateral projections eventually give rise to separate coelomic regions (primarily a sagittally oriented hydrocoel on the left side of the larval body and a somatocoel on each side of the larva). The anterior region of the unpaired U-shaped coelomic sac extends into the lumen of the brachiolar arms and is considered homologous to the preoral coelom of feeding larvae (Erber, 1985; Strathmann, 1988).

*Asteroids with indirect development and pelagic non-feeding larvae.* Several asteroids develop from large eggs (about 1000  $\mu\text{m}$  in diameter) via pelagic nonfeeding brachiolarian larvae (distributed in the orders: Forcipulata, Valvatida, Spinulosida, and Velatida; see Fig. 9) (McEdward and Janies, 1993). There are several studies of internal structure in these larvae (e.g., *Fromia ghardaqana*, Mortensen, 1938; *Crossaster papposus* Gemmill, 1920; *Henricia sanguinolenta*, Masterman, 1902; and *Solaster endeca* Gemmill, 1912). The early pattern of anterior and hydrocoelic coelomogenesis of these brachiolaria is identical to that of the benthic brachiolaria.

*Features of coelomogenesis in taxa closely related to Pteraster tessellatus.* In an echinasterid, *Henricia sanguinolenta* (Masterman, 1902), and two solasterids, *Solaster endeca* (Gemmill, 1912) and *Crossaster papposus* (Gemmill 1916, 1920), for which there is detailed information on internal features of development, the archenteron constricts into unpaired anterior, middle, and posterior portions (Fig. 7IIA, B). The anterior portion and the posterior portion of the archenteron are presumptive coelom, whereas the middle portion is presumptive gut (Masterman, 1902; Gemmill, 1912, 1920; Hyman, 1955, p. 298). The axocoels, hydrocoels, and right somatocoel develop from the unpaired anterior coelom, as is typical in non-feeding larval development (Fig. 7IIB-D), but the left so-

matocoel develops from the posterior enterocoel (Fig. 7IIB, C) in proximity to its definitive larval location. The anterior, unpaired enterocoel develops from the anterior portion of the archenteron (Fig. 7IIA-II B). Two long lateral projections extend posteriorly from the anterior enterocoel, producing a U-shaped coelom. In spite of these modifications, many characteristics of the ancestral pattern of asteroid development occur in these species. (1) A hydrocoel pinches off from the left lateral region of the U-shaped coelom. (2) a somatocoel (adult aboral perivis-

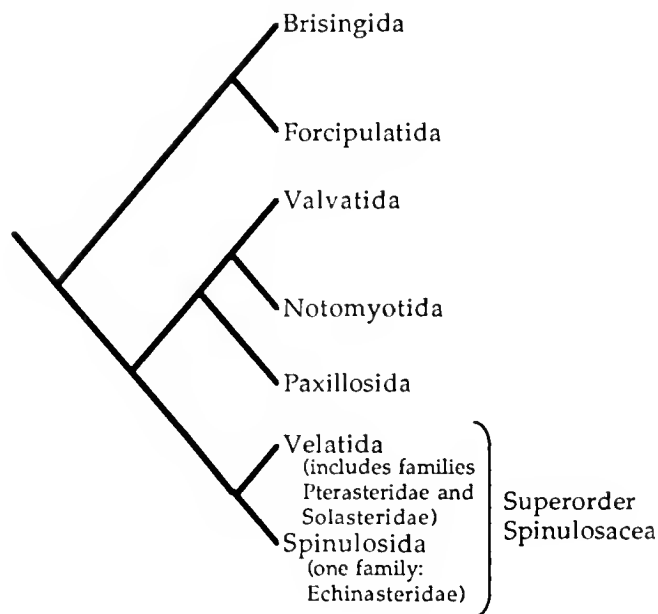


Figure 9. A cladogram of asteroid orders based on Blake (1987). The taxonomic location of the families of the superorder Spinulosacea. This group includes *Pteraster tessellatus* and close relatives.

ceral coelom) forms from the posterior portion of the right side of the U-shaped coelom, (3) the left anterior region of the U-shaped coelom forms the axocoel (adult perihemal coelom of the axial complex and the inner oral perihemal ring coelom), and (4) a preoral coelom lines the brachiolar arms (Fig. 7IIB-D).

One striking difference in the pattern of coelomogenesis in solasterids and echinasterids is a radical departure from the ancestral pattern of coelom development: there has been a change in the site of origin of the left somatocoel. This heterotopic modification, which produces multiple (*i.e.*, anterior and posterior) enterocoels, is a synapomorphy of the asteroids of the superorder Spinulosacea (O. Spinulosida = family Echinasteridae and O. Velatida includes families Solasteridae, Pterasteridae; see Blake, 1987) (Fig. 9).

The evolution of posterior enterocoely dissociated the origin of the left somatocoel from the anterior region of the archenteron, in the lineage leading to *P. tessellatus*. We believe that this modification of coelomogenesis was a necessary precursor to the radical rearrangements of coelomogenesis that occurred in *P. tessellatus* to produce direct development. This was an important preadaptation for the novel positioning and acceleration of water-vascular morphogenesis that occurred in the evolution of pterasterids. Because *P. tessellatus* lacks the bilateral pattern of enterocoely and has instead a radial and transverse pattern, the terms "left" and "right" are inappropriate. Although Gemmill (1912, 1916, 1920) and Masterman (1902) referred to the posterior coelom of the spinulosaceans as the "left posterior coelom" because of homology with the left somatocoel of other asteroid larvae, we refer to this cavity, which is also found in *P. tessellatus*, as the large posterior coelom.

*Unity and diversity in asteroid coelomic development.* In spite of considerable diversity in external larval morphology, the pattern of coelomic development among asteroids is very conservative, regardless of shifts from feeding to nonfeeding, or from pelagic to benthic development. On the basis of the similarity in anterior coelomic development, Erber (1985) argued that a preoral coelom develops in the anterior region of the larva in all asteroids and that, therefore, a homologous brachiolaria stage occurs throughout the Asterozoa, including species in which brachiolar arms are absent (*e.g.*, paxillosids and *P. tessellatus*). Erber's criterion for brachiolarian development is sufficiently general to include all known asteroids, yet it also leads to at least two conclusions that we believe are false. First, Erber (1985) concluded that paxillosids have a "brachiolarian" stage of development. However, as stated earlier, paxillosids develop as feeding bipinnaria or nonfeeding simplifications thereof—they are not brachiolaria nor are they derived from (*i.e.*, homologous with) brachiolaria (Komatsu *et al.*, 1988). Second, Erber (1985)

assumed that the mode of coelom formation in *P. tessellatus* would be identical to that of its close relatives, the echinasterids and solasterids. This assumption was based, in part, on the prevailing interpretation of the evolution of the "larva" of *P. tessellatus*. Fell (1967, p. S71) considered the absence of brachiolar structures in *P. tessellatus* to be the result of minor simplifications of the external structures of a typical pelagic nonfeeding brachiolarian larva.

In all larval types, most of the anterior of the larva (including the preoral coelomic structures) is resorbed at metamorphosis (Fig. 8). This resorption is accomplished by translocation of the larval structures to the oral side of the juvenile rudiment, followed by histolysis and transfer to the juvenile digestive tract (Chia and Burke, 1978). The postmetamorphic (juvenile and adult) fates of the larval coeloms are highly conservative among asteroids, as illustrated by a comparison of figures 7I and 7II. The left side of the axocoel forms the perihemal coelom of the axial complex and the inner oral perihemal ring coelom (Fig. 7, 8) (Hyman, 1955; Dawydoff, 1948). The left hydrocoel forms the entire coelomic lining of the water-vascular system. The left somatocoel, by growing dorsal and ventral extensions medial to the hydrocoel, forms the oral perivisceral coelom. The outer oral perihemal ring coelom forms from small interradial evaginations of the oral perivisceral coelom. The right axohydrocoel is mostly resorbed at metamorphosis yet becomes the madreporic vesicle (an aboral component of the axial complex) in some species (Hyman, 1955). The right somatocoel lies on the side of the gut opposite the hydrocoel (*i.e.*, on the aboral side of the juvenile) and forms the aboral perivisceral coelom.

Given the conservative nature of asteroid coelomogenesis, analysis of the evolution of direct development can be focused on the transition from the larval pattern of coelomogenesis in the nonfeeding brachiolaria of taxa closely related to *P. tessellatus* (*e.g.*, *Solaster* and *Henricia*) to the highly derived pattern of *P. tessellatus*.

#### *What evolutionary changes in morphogenesis occurred to transform a brachiolarian larva into a mesogen?*

Direct development is characterized by the morphogenesis of the juvenile from the embryonic stages and by the complete absence of larval structures in development (McEdward and Janies, 1993). The prevailing view is that evolution of direct development must involve the loss of larval features from the life cycle by the suppression or elimination of larval programs in development (Fell, 1945; Raff, 1987). This hypothesis accurately describes the resultant differences between solasterid or echinasterid brachiolarian larvae and the mesogen of *P. tessellatus*. However, this hypothesis offers little insight into the processes by which the ancestral ontogeny has been modified to

yield the derived ontogeny. One result of eliminating larval features is that juvenile features arise earlier in ontogeny. Direct development cannot evolve simply by accelerating developmental processes. Direct development requires spatial, as well as temporal, changes in morphogenesis because the juvenile must develop from an embryonic rather than a larval organization. We propose that direct development evolved in *P. tessellatus* largely via a series of topological changes in coelomogenesis. These heterotopic changes allowed the embryo (gastrula) to develop into a juvenile coelomic organization, thereby eliminating the larval stage and producing a "recession of metamorphosis" (*sensu* Fell, 1945, see also Raff, 1987).

*A hypothesis of coelomic rearrangement.* The altered pattern of coelomogenesis underlies all of the important features that characterize direct development in *P. tessellatus*. A relatively simple change in the topology of early coelomic development can account for the loss of bilateral symmetry, loss of the preoral lobe, and the development of the coelomic systems in their adult orientation. The arrangement of hydrocoelic lobes from the archenteron establishes radial symmetry and accounts for the transverse orientation of the juvenile disc and the parallel embryonic and adult axes.

We believe that the radical rearrangement of coeloms in *P. tessellatus* evolved by means of a 90° rotation of the anterior enterocoels from the spinulosacean pattern, relative to the animal-vegetal axis of the archenteron (Fig. 10). This rotation shifted the hydrocoel from its ancestral location on the left side of the body (Fig. 10A) to a central location on the longitudinal (animal-vegetal) axis of the body (Fig. 10B). Consequently, the hydrocoel lobes (radial canal precursors) develop in a transverse plane around the archenteron in *P. tessellatus* (Fig. 10C) rather than in the sagittal orientation typical of all asteroid larvae (Fig. 7I, II).

In conjunction with this hypothesized rotation, the ancestral axocoels fused with the ancestral right somatocoel, and the preoral coelom was lost (Fig. 10B). The site of evagination of the large posterior enterocoel in the spinulosacean pattern was unaffected by the relocation of the anterior enterocoels (Figs. 7, 10).

Our hypothesis has several points in its favor. First, it is consistent with the interpretation of the small posterior enterocoel of *P. tessellatus* as homologous to fused left and right axocoels and right somatocoel of the solasterids and echinasterids (Figs. 7II, III; 10C). The mixed coelomic fates of the small posterior enterocoel in *P. tessellatus* (axial and inner oral perihemal ring coeloms and aboral perivisceral coelom) are the basis for this interpretation (Fig. 8).

Second, the rotation hypothesis is supported by the observation that a 90° rotation to the right (flexion *sensu* Gemmill, 1912) occurs at metamorphosis in all asteroids

with indirect development. Metamorphic flexion shifts the coeloms from the larval arrangement into the juvenile arrangement. We argue that an analogous rotation of the positional information specifying sites of enterocoel formation occurred in the lineage leading to *P. tessellatus*. This effectively shifted the specification of the post-metamorphic coelomic arrangement into the very early stages of development. The result was direct development of the coeloms in the juvenile orientation from the archenteron of the embryo (Figs. 7III; 10). It is not surprising that conservative and fundamental features of asteroid metamorphosis, such as the transformation of coeloms from the larval to the adult organization, should be co-opted into a derived pattern of development in which coeloms arise in their adult orientation.

Third, the rotation hypothesis is attractive in its simplicity; a single alteration of the map for enterocoel formation can explain the derivation of a highly modified pattern of coelomogenesis in the evolution of direct (non-larval) development.

Differences in the site of the origin of enterocoels have occurred in other asteroids. In addition to the solasterids and the echinasterids that were discussed above, there are other documented cases of the heterotopic origin of a posterior coelom: *Patiriella regularis* (Byrne and Barker, 1991, p. 334, 341) and *Marthasterias glacialis* (Gemmill, 1916). Although heterotopy seems to be a rare event, on the basis of the limited developmental diversity that has been documented in asteroids, its occurrence illustrates that the presumptive fates of the regions of the archenteron can be modified evolutionarily.

Our rotation hypothesis leads to a new interpretation of some of the features of *P. tessellatus*. The yolky anterior region of the mesogen has traditionally been interpreted as a preoral lobe (*e.g.*, Chia, 1966; Fell, 1967 p. S71). If rotation of the coeloms occurred as we have suggested, then the anterior region of *P. tessellatus* is not homologous to the preoral lobe of a brachiolarian larva, because it lacks the only defining characteristics of a preoral lobe, namely the preoral extension of the anterior coelom into brachiolar apparatus. We believe that, in *P. tessellatus*, the evolution of fused coelomic regions from opposite sides of the solasterid or echinasterid larva involved the loss of the intervening preoral coelom (Fig. 10B). In our interpretation, the site of origin of the former preoral coelom would correspond to the lateral region of the archenteron, posterior to the hydrocoelic lobes and anterior to the site of formation of the small posterior coelom (this point is denoted by the \* on Fig. 10B). The yolky anterior region of the developing *P. tessellatus* is located on the oral surface of the juvenile; it probably functions only as a nutritional store. The extension of the archenteron into the anterior region of the mesogen likely serves as a conduit to deliver nutrients to the gut and is not a preoral coelom.

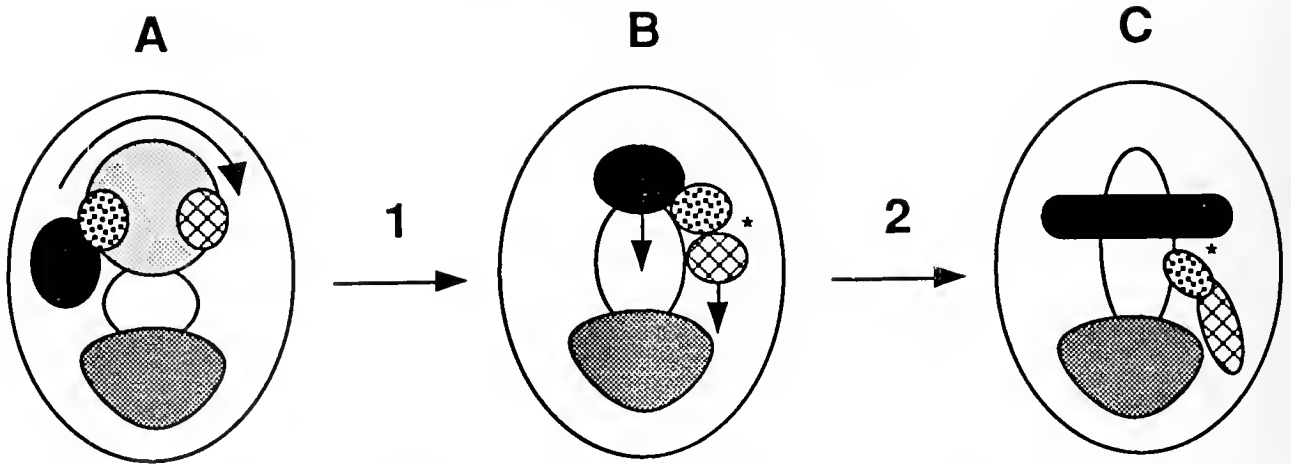


**Figure 10.** A hypothesized evolutionary sequence of coelomic rearrangements (dorsal view) from the spinulosacean pattern of development (A) to that of *Pteraster tessellatus*. Step 1 involves a simple 90° rotation of the ancestral anterior enterocoels relative to the animal-vegetal axis of the archenteron. This shifted the hydrocoel from its ancestral location on the left side of the spinulosacean embryo (A) to a central location in a hypothesized intermediate form (B). Also in step 1, the ancestral axocoel shifted from an anterior-left-central position (A) to an anterior-right-central position where it fused with the ancestral right somatocoel (B) and became the small posterior enterocoel of *P. tessellatus* (C). This fusion was likely facilitated by the loss of the preoral coelom as noted by the \* in stages B and C. Step 2 shows the transition from the hypothesized intermediate form (B) to *P. tessellatus* (C). This could be accomplished by a heterotopic change in the point of origin of the enterocoels from the anterior of the archenteron to the central and posterior locations seen in *P. tessellatus* (C). In this hypothesis the anterior of the archenteron of *P. tessellatus* is a novel feature and not a vestige of a preoral coelom. The posterior site of evagination of the spinulosacean large posterior enterocoel was unaffected by the relocation of the anterior enterocoels.

#### *Comparative morphogenesis in asteroids as a system for studying the evolution of development*

*P. tessellatus* provides an important system for analysis of major evolutionary changes in development, particularly morphogenesis and early pattern formation (e.g., establishment of body axes and symmetry). The alterations in developmental mechanisms associated with the evolution of direct development have recently been approached through a combination of cellular methods (e.g., cell lineage specific gene-expression, cell lineage tracing) and species comparisons (e.g., Jeffrey and Swalla, 1991; Wray and Raff, 1990). Raff (1992) proposed that remodeling of development via changes in the primordial morphogenetic axes of the egg is important in shifts from indirect to direct development. We postulate that just such changes have occurred in the evolution of direct development in *P. tessellatus*. We have documented radical topological changes associated with morphogenesis of juvenile coeloms directly from the embryonic archenteron, rather than from the bilaterally arranged series of larval coeloms. An important component of those changes involved the elimination of larval bilateral symmetry. In solasterid and echinasterid asteroids, larval morphogenesis involves the establishment of a bilateral symmetry that replaces the embryonic radial symmetry. At metamor-

phosis, a new axis of radial symmetry is established for the morphogenesis of the juvenile body. In *P. tessellatus*, the axis of primary embryonic symmetry (radial) is retained as the axis of radial symmetry in the juvenile throughout the development of the mesogen. We postulate that the loss of the larval phase of development and morphogenesis of the juvenile from the embryonic organization may be due, in part, to the elimination of the system for specifying larval left-right and larval dorsal-ventral polarity in the egg and early embryo. Loss of such polarity information would result in a radially symmetrical morphogenetic framework on which to build juvenile coelomic systems and other structures. The relationship between the first cleavage plane and the dorsal-ventral axis is variable among echinoids (Henry *et al.*, 1992), and this has had a mechanistic role in evolutionary changes in development (Henry and Raff, 1990; Henry *et al.*, 1990). These recent findings invite the investigation of changes of morphogenetic axes among asteroids. A comparison of the polarity characteristics of solasterid, echinasterid, and pterasterid eggs and embryos might yield important insights into structural patterning in early development and the mechanisms underlying its evolutionary modification.

Some starfish do not free spawn, but rather brood large yolky nonfeeding young on the benthos. These young de-

velop through larval stages with brachiolarian arms and an adhesive disc, but are not released from the mother until after metamorphosis. Morphological simplification of young might be expected in species with benthic brooding because larvae may be released from selection pressures for effective settlement structures. The morphogenesis of internal structures in brooded asteroids is unknown, so the diversity of developmental modifications that may occur as a result of brooding are not appreciated. An understanding of this diversity is important for assessing whether the evolution of brooding results in specializations and simplifications of morphology and development that are effectively irreversible (as is the case with the loss of feeding larvae, Strathmann, 1978). Alternatively, the evolution of benthic development could eliminate some of the selective pressures on larvae, providing the evolutionary flexibility to generate novel patterns of morphogenesis and thus to allow the re-evolution of pelagic development in new ways despite the loss of larval structures.

Most species of the family Pterasteridae that have been studied hold their eggs under the supradorsal membrane and brood young long into juvenile development. Larval attachment structures were likely lost in the pterasterids after the lineage became very specialized brooders in the deep-sea. Direct development was likely the result of selection for general developmental efficiency, through the elimination of nonfunctional larval features, during a very long history of brooding (see McEdward and Janies, 1993; McEdward, unpubl.). Pelagic development is likely a derived trait in this family.

The comparative study of development among spinulosacean asteroids can directly address the ecological context of evolutionary shifts from indirect to direct development, as well as transitions between pelagic and benthic development. Specifically, comparisons of development among the pelagic brachiolarian larvae from the outgroups Solasteridae and Echinasteridae, the young of a brooding pterasterid, and the pelagic mesogen of *P. tessellatus* would provide a rare opportunity to investigate the role of the evolution of development in the important ecological transition from a nondispersive to a dispersive life history.

Changes in development in conjunction with paedomorphic shifts in the life cycle have potential for the evolution of new body plans. The newly discovered deep-sea concentricycloid echinoderms are characterized by a unique water-vascular geometry of dual circumoral rings (Baker *et al.*, 1986; Rowe *et al.*, 1988). The novel pattern of morphogenesis of the circumoral ring canal in *P. tessellatus*, combined with progenesis, may have provided a mechanism for the evolution of the unique water-vascular geometry of the concentricycloids (Janies and McEdward, in press). We postulate that proximal lateral evaginations

of the radial canal could be duplicated at an early developmental stage to produce dual circumoral ring canals. The duplicated formation of circumoral rings was a likely a key innovation in the evolution of the concentricycloids (Janies and McEdward, in press).

### Acknowledgments

SEM facilities were provided by the University of Florida, Interdisciplinary Center for Biotechnology Research and the Department of Zoology. Histology facilities were provided by L. Guillette. R. Shammami, T. George, and L. Becht entered sectional data for the reconstructions. A. Griffin and S. McWeeney assisted with preparation of some specimens for SEM. Photographic printing and the illustration in Figure 6 were done by D. Harrison.

Funding was provided by the University of Florida Division of Sponsored Research (#89100245, #90012443, and DSR-B) to LRM, The Aylesworth Foundation for the Advancement of Marine Science Scholarship, to DAJ, and the National Science Foundation (OCE 9115549) to LRM.

A. O. D. Willows, Director, provided space and facilities at the Friday Harbor Laboratories and J. McIhnerney, Director, provided space and facilities at the Bamfield Marine Station. D. Duggins, C. Staude, S. Carson, and G. Gibson helped collect starfish.

### Literature Cited

- Barker, M. F. 1978. Structure of the organs of attachment of brachiolaria larvae of *Stichaster australis* (Verrill) and *Coscinasterias calamaria* (Gray) (Echinodermata: Asteroidea). *J. Exp. Mar. Biol. Ecol.* 33: 1-36.
- Baker, A. N., F. W. E. Rowe, and H. E. S. Clark. 1986. A new class of Echinodermata from New Zealand. *Nature* 321: 862-864.
- Blake, D. B. 1987. A classification and phylogeny of post-Paleozoic sea stars (Asteroidea: Echinodermata). *J. Nat. Hist.* 21: 481-528.
- Byrne, M., and M. F. Barker. 1991. Embryogenesis and larval development of the asteroid *Patriella regularis* viewed by light and scanning electron microscopy. *Biol. Bull.* 180: 332-345.
- Chia, F.-S. 1966. Development of a deep-sea cushion star, *Pteraster tessellatus*. *Proc. Cal. Acad. Sci.* 34: 505-510.
- Chia, F.-S. 1968. The embryology of a brooding starfish, *Leptasterias hexactis* (Stimpson). *Acta Zool.* 49: 321-364.
- Chia, F.-S., and R. D. Burke. 1978. Echinoderm metamorphosis: fate of larval structures. Pp. 219-234 in *Settlement and Metamorphosis of Marine Invertebrate Larvae*, F.-S. Chia and M. E. Rice eds. Elsevier, New York.
- Chia, F.-S., and C. W. Walker. 1991. Echinodermata: Asteroidea. Pp. 301-340 in *Reproduction of Marine Invertebrates*, A. Giese, J. S. Pearse, and V. B. Pearse, eds. Boxwood, Pacific Grove, CA.
- Dawydoff, C. 1948. Embryologie des échinodermes. Pp. 278-363 in *Traité de Zoologie*, P.-P. Grassé, ed. Masson, Paris.
- Erber, W. 1985. The larval coelom as a significant feature of bipinnaria and brachiolaria in asteroid ontogeny. A critical approach. *Zool. Anz.* 215: 329-337.
- Fell, H. B. 1945. A revision of the current theory of echinoderm embryology. *Trans. Roy. Soc. N. Z.* 75: 73-101.



- Fell, H. B. 1967. Echinoderm ontogeny. Pp. S60-S85 in *Treatise on Invertebrate Paleontology, Part 5, Echinodermata*, R. C. Moore, ed. Geological Society of America and Kansas University Press, Lawrence.
- Gemmill, J. F. 1912. The development of the starfish *Solaster endeca* Forbes. *Trans. Zool. Soc. Lond.* **20**: 1-71.
- Gemmill, J. F. 1914. The development and certain points in the adult structure of the starfish *Asterias rubens*, L. *Phil. Trans. Roy. Soc. Lond. (B)* **205**: 213-294.
- Gemmill, J. F. 1916. Notes on the development of the starfishes *Asterias glacialis* O. F. M.; *Cribrella oculata* (Link) Forbes; *Solaster endeca* (Retzius) Forbes; *Stichaster roseus* (O. F. M.) Sars. *Proc. Zool. Soc. Lond.* **39**: 553-565.
- Gemmill, J. F. 1920. The development of the starfish *Crossaster papposus*, Müller and Troschel. *Q. J. Microsc. Sci.* **64**: 155-190.
- Henry, J. J., and R. A. Raff. 1990. Evolutionary change in the process of dorsolateral axis determination in the direct developing sea urchin, *Heliocidaris erythrogramma*. *Dev. Biol.* **141**: 55-69.
- Henry, J. J., G. A. Wray, and R. A. Raff. 1990. The dorsolateral axis is specified prior to first cleavage in the direct developing sea urchin *Heliocidaris erythrogramma*. *Development* **110**: 875-884.
- Henry, J. J., K. M. Klueg, and R. A. Raff. 1992. Evolutionary dissociation between cleavage, cell lineage and embryonic axes in sea urchin embryos. *Development* **114**: 931-938.
- Hörstadius, S. 1939. Über die Entwicklung von *Astropecten aranciaeus* L. *Pubbl. Staz. Zool. Napoli* **17**: 221-312.
- Hyman, L. H. 1955. *The Invertebrates, Vol. 4, Echinodermata* McGraw-Hill, New York. 763 pp.
- Janies, D. A., and L. R. McEdward. 1994. A hypothesis for the evolution of the concentricycloid water-vascular system. In *Reproduction and Development of Marine Invertebrates*, W. H. Wilson, Jr., S. A. Stricker and G. L. Shinn, eds. Johns Hopkins Press, Baltimore, MD. (In Press).
- Jeffery, W. R., and B. J. Swalla. 1991. An evolutionary change in muscle lineage of an asexual ascidian embryo is restored by interspecific hybridization with a urodele ascidian. *Dev. Biol.* **145**: 328-337.
- Komatsu, M. 1975. On the development of the sea-star, *Astropecten latespinosus* Meissner. *Biol. Bull.* **148**: 49-59.
- Komatsu, M. 1982. Development of the sea-star *Ctenopleura fisheri*. *Mar. Biol.* **66**: 199-205.
- Komatsu, M., and S. Nojima. 1985. Development of the sea-star, *Astropecten gisselbrechti* Doderlein. *Pac. Sci.* **39**: 274-282.
- Komatsu, M., M. Murase, and C. Oguro. 1988. Morphology of the barrel-shaped larva of the sea-star, *Astropecten latespinosus*. Pp. 267-272 in *Echinoderm Biology*, R. D. Burke, P. V. Mladenov, P. Lambert, and R. L. Parsley, eds. A. A. Balkema, Rotterdam.
- Komatsu, M., C. Oguro, and J. M. Lawrence. 1991. A comparison of development in three species of the genus, *Luidia* (Echinodermata: Asteroidea) From Florida. Pp. 489-498 in *Biology of Echinodermata*, T. Yanagisawa, I. Yasumasa, C. Oguro, N. Suzuki, and T. Motokawa, ed. A. A. Balkema, Rotterdam.
- MaeBride, E. W. 1896. The development of *Asterina gibbosa*. *Q. J. Microsc. Sci.* **38**: 339-411.
- Masterman, A. T. 1902. The early development of *Cribrella oculata* (Forbes) with remarks on echinoderm development. *Trans. R. Soc. Edin.* **40**: 373-418.
- McClary, D. J., and P. V. Mladenov. 1990. Brooding biology of the sea-star *Pteraster militaris* (O. F. Muller): energetic and histological evidence for nutrient translocation to brooded juveniles. *J. Exp. Mar. Bio. Ecol.* **142**: 183-199.
- McEdward, L. R. 1992. Morphology and development of a unique type of pelagic larva in the starfish *Pteraster tessellatus* (Echinodermata: Asteroidea). *Biol. Bull.* **182**: 177-187.
- McEdward, L. R., and D. A. Janies. 1993. Life cycle evolution in asteroids: What is a larva? *Biol. Bull.* **184**: 255-268.
- Mortensen, T. 1938. Contributions to the study of the development and larval forms of echinoderms IV. D. Kgl. Danske Videnske Selsk. Skrifter, Naturv. og Math. Afd., 9 Række, VII. 3.
- Nation, J. L. 1983. A new method using hexamethyldisilazane for preparation of soft insect tissue for scanning electron microscopy. *Stain Technol.* **58**: 347-351.
- Oguro, C., M. Komatsu, and Y. Kano. 1976. Development and metamorphosis of the sea-star *Astropecten scoparius* Valenciennes. *Biol. Bull.* **151**: 560-573.
- Raff, R. A. 1987. Constraint, flexibility and phylogenetic history in the evolution of direct development in sea urchins. *Dev. Biol.* **119**: 6-19.
- Raff, R. A. 1992. Direct-developing sea urchins and the evolutionary reorganization of early development. *BioEssays* **14**: 211-218.
- Rowe, F. W. E., A. N. Baker, and H. E. S. Clark. 1988. The morphology, development and taxonomic status of *Xyloplax* Baker, Rowe, and Clark (1986) (Echinodermata: Concentricycloidea), with the description of a new species. *Proc. R. Soc. Lond. B.* **223**: 431-439.
- Strathmann, R. R. 1974. Introduction to function and adaptation in Echinoderm larvae. *Thalassia Jugoslav.* **10**: 321-339.
- Strathmann, R. R. 1978. The evolution and loss of feeding larval stages of marine invertebrates. *Evolution* **32**: 894-906.
- Strathmann, R. R. 1988. Functional requirements and the evolution of developmental patterns. Pp. 55-61 in *Echinoderm Biology*, R. D. Burke, P. V. Mladenov, P. Lambert, and R. L. Parsley, eds. A. A. Balkema, Rotterdam.
- Wray, G. A., and R. A. Raff. 1990. Novel origins of lineage founder cells in the direct-developing sea urchin *Heliocidaris erythrogramma*. *Dev. Biol.* **141**: 41-54.



# Larval Development (with Observations on Spawning) of the Pencil Urchin *Phyllacanthus imperialis*: a New Intermediate Larval Form?

RICHARD RANDOLPH OLSON<sup>1,2,3</sup>, J. LANE CAMERON<sup>2,4</sup>, AND CRAIG M. YOUNG<sup>2</sup>

<sup>1</sup>Australian Institute of Marine Science, P.M.B. 3, Townsville, Queensland 4810, Australia, <sup>2</sup>Harbor Branch Oceanographic Institution, 5600 Old Dixie Hwy., Ft. Pierce, FL 33450, <sup>3</sup>Department of Zoology, University of New Hampshire, Durham, NH 03801, and <sup>4</sup>DAMES & MOORE, 500 Market Place Tower, 2025 First Avenue, Seattle, WA 98121.

**Abstract.** Information for understanding the evolutionary shift from feeding to nonfeeding in echinoderm larvae can be gained from species whose larval development pattern appears to be intermediate between these extremes. In this paper we report the development of one such species.

The pencil urchin *Phyllacanthus imperialis* spawned synchronously with the mass spawning of scleractinian corals at Lizard Island, Australia, in two consecutive years. Their large yolky eggs (507  $\mu\text{m}$  diameter) developed into nonfeeding echinopluteus larvae with two pairs of larval arms. The arms were identified as postoral and posterodorsal, which are the first and third pairs in typical echinoplutei. A larval skeleton was present, with skeletal rods extending the length of the arms. Five primary podia of the juvenile rudiment appeared at 2 days of age. Metamorphosis of the larvae and settlement began 4 days after fertilization. Histological examination of 2-day-old larvae revealed the presence of a developing gut, but no mouth opened in what would be the oral region of a typical echinopluteus, or the oral surface of the juvenile rudiment in older larvae. Like other cidaroid larvae, this species showed no evidence of an amniotic invagination.

The larva of *P. imperialis* appears to be a transitional form between the morphology of feeding and nonfeeding echinoid larvae. Traces of the ciliary band in the oral region and the presence of arms typical of the echinopluteus larva indicate its evolutionary past, whereas the large egg size and absence of a mouth hint at its future. This larval form provides insights into developmental changes that

occur during the shift from planktotrophy to lecithotrophy in echinoid larvae.

## Introduction

The causes and consequences of the evolutionary shift from feeding to nonfeeding larvae has become a popular topic in recent years (Raff, 1987; Parks *et al.*, 1988; Wray and Raff, 1991; Amemiya and Emlet, 1992; McMillan *et al.*, 1992). Among echinoids, feeding larvae (planktotrophs) are considered to be the ancestral form, and non-feeding larvae (lecithotrophs) are thought to be more derived (Strathmann, 1974). Within this group of echinoderms, the shift from planktotrophy to lecithotrophy is believed to have evolved independently as many as 14 times (Emlet, 1990; *cf.* Strathmann, 1974). Although the potential costs and benefits of direct development have been well discussed (Vance, 1973; Christiansen and Fenchel, 1979; Obrebski, 1979), the reasons for shifts in developmental mode are not completely understood.

Planktotrophy among echinoid larvae is known to be correlated with egg size (Emlet *et al.*, 1987). Of the 276 echinoids reviewed by Emlet (1990), 66% have planktotrophic development and develop from small eggs (<350  $\mu\text{m}$ ), whereas 20% have lecithotrophic development and develop from larger eggs (>500  $\mu\text{m}$ ).

Before our study, only three echinoids had been reported with planktonic larvae that do not fall into one of these two groups; *Brisaster latifrons*, which has a feeding echinopluteus that develops from an egg 345  $\mu\text{m}$  in diameter (Strathmann, 1979); *Clypeaster rosaceus* (egg diameter = 280  $\mu\text{m}$ ), whose larvae are facultative planktotrophs, having the echinopluteus form (Emlet, 1986);

and *Peronella japonica* (egg diameter = 276  $\mu\text{m}$ ), which produces a lecithotrophic "pluteus" with only two arms, but shows normal development of the echinus rudiment (Okazaki and Dan, 1954). Here we report a fourth "intermediate" larval form.

The pencil urchin *Phyllacanthus imperialis* is a member of the order Cidaroida, which is believed to be the most primitive extant echinoid order (Paul and Smith, 1984). It is common on coral reefs throughout the Indo-west Pacific but, being nocturnal and cryptic, is rarely seen even at night. Mortensen (1938), who collected *P. imperialis* in the Red Sea, reported its egg to be 500  $\mu\text{m}$  in diameter, but was unsuccessful in attempting *in vitro* fertilization. In this paper we provide the first description of the larva and development of *P. imperialis*, which has the echinopluteus form but is lecithotrophic.

### Materials and Methods

Gametes of *P. imperialis* were obtained from adults collected at Lizard Island, Australia, during the summers of 1986 and 1987. Urchins were spawned in the days following collection by injecting 5 to 10 ml of 0.55 M KCl into the coelomic cavity. Eggs were fertilized within 1 h of spawning. Embryos and larvae were maintained in an open 3-l beaker at room temperature (29–31°C) without stirring. For histological and morphological examination, embryos and larvae were preserved in Bouin's solution at 20 h and 2, 3, and 4 days after fertilization. To preserve the larval skeleton, a few larvae were preserved in buffered 10% formalin. Embryos and larvae were prepared for scanning electron microscopy (SEM) by dehydration in a graded series of ethyl alcohol through amyl acetate, dried at the critical point ( $\text{CO}_2$ ), gold coated, then examined and photographed using a Novascan 30 scanning electron microscope. Larvae for histological examination were dehydrated to 50% ethyl alcohol, then embedded in JB-4 embedding medium (Polysciences, Inc.). Sequential sections 2–3  $\mu\text{m}$  thick were cut with glass knives and stained with Richardson's stain. Larval skeletal pieces were exposed by corrosion of the soft tissues with 5% sodium hypochlorite (household bleach) from 4-day larvae fixed in buffered formalin.

### Results

#### Spawning

On the Great Barrier Reef of Australia, adult *P. imperialis* are usually cryptic and nocturnal and are rarely encountered even on night dives. However, on the night of 20 November 1986, approximately 20 *P. imperialis* were collected by divers in an area less than 10 m in diameter. This was 4 days after the full moon and the same night as the mass spawning of acroporid scleractinian cor-

als (cf. Babcock *et al.*, 1986). Numerous *P. imperialis* were observed "perched" on the tops of coral heads or mounds of rubble; one male *P. imperialis* was observed spawning. In the days following collection, spawning was induced in these urchins by injecting them with 0.55 M KCl. Freshly spawned eggs were yellow-tan and embedded in a clear gelatinous outer coating that was viscous and sticky. Spawning eggs were held together by this coating to form a strand of eggs that floated directly to the surface as it was released. Mean egg diameter was 507  $\mu\text{m}$  (SD = 31.9,  $n = 10$ ).

Additional urchins were collected on 9 December (five), and 13 December (three). None of these urchins spawned when injected with KCl; examination of their excised gonads revealed that all were spent.

The following year (1987) a few adult *P. imperialis* were observed early in November shortly after the full moon. The density of urchins was considerably lower, and the urchins were not as exposed as had been noted the previous year. Approximately 10 urchins were collected over several nights, but only males produced viable gametes upon injection with KCl. The few females that did respond to KCl injection released masses of what appeared to be undifferentiated yolk material. Urchins collected in late November also were not ripe. No male *P. imperialis* collected at this time spawned when injected, and those females that did spawn produced egg-like irregularly shaped masses of yolk. Urchins collected on 2, 3, 4, and 8 December and injected with KCl all responded similarly. Full moon occurred on 5 December in 1987. On the morning of 9 December, two females injected with KCl released large numbers of eggs, the majority of which were spherical and uniform in size. About a third of these eggs were successfully fertilized. The following day (10 December) two remaining females were spawned, and virtually all of their eggs were uniform in size and shape. Fertilization of these eggs was nearly 100%.

#### Development

Oocytes were opaque (yellow-tan in color) and floated at the surface of the water in their culture beakers. A distinct fertilization membrane was noted 15 min after the introduction of sperm. First cleavage was observed 15 min later—*i.e.*, 30 min after fertilization (Table I). Ten hours after fertilization the embryos were ciliated blastulae rotating within the fertilization membrane and were still floating. Twenty hours after fertilization the embryos were hatched swimming gastrulae, still opaque yellow-tan in color, and floating (Figs. 1, 5). It was not noted whether gastrulation occurred before hatching. Twenty-four hours after fertilization there was considerable variation in the morphology of the larvae, ranging from embryos that were nearly rectangular with one pair of arm rudiments (Fig.

Table 1

*Development schedule of Phyllacanthus imperialis*

Time since fertilization	Stage
30 min	First cleavage
10 h	Ciliated blastula
24 h	Swimming gastrula, some 2 arms
48 h	4 short arms
72 h	Arms elongating, rudiment visible
96 h	Attachment
100 h	Arms break off
116 h	Fully formed juvenile

2) to larvae that were beginning to develop four equal-length arms (as seen at 2 days old; Fig. 3). A few of these larvae were swimming just below the surface of the water. The first evidence of development of the echinus rudiment was apparent within the oral field of these early four-armed plutei (Fig. 3). A band of cilia, extending along the margins of the arms and coursing up onto the preoral lobe, can be seen to be just beginning to form on these larvae (Fig. 3). Three days after fertilization four-armed plutei with well-developed echinus rudiments (Fig. 4) were distributed throughout the culture vessel. Purple pigment granules appeared around the preoral lobe of the larvae and along the arms. Many larvae 3 days old had begun to settle on the bottom and sides of the culture beaker. At this point virtually no larvae remained at the surface of the water. Six days after fertilization all larvae had settled and metamorphosed into juvenile urchins. These juveniles were maintained for another 3 weeks in the beaker without further care (changing of water or feeding).

#### *Description of embryology*

Details of the first few hours of development were not observed, but observations on fixed embryos revealed that there was no wrinkling of the blastula or gastrula. Approximately 15 h after fertilization a typical smooth gastrula was formed by invagination of the blastular wall at the vegetal pole (Fig. 5). Histological sections of gastrulae, 20 h after fertilization, are reminiscent of the typical gastrula of feeding echinoid larvae. The ectodermal wall is relatively thin and there is a distinct blastocoel surrounding the archenteron. At this time the archenteron extends approximately one-third the length of the blastocoel with the distal tip bending toward the ventral surface of the embryo at an angle of approximately 45° (Fig. 5). The timing of mesenchyme migration into the blastocoel was not observed, but in embryos 20 h old, a large clump of mesenchyme cells was aggregated around the tip of archenteron (Figs. 1, 5) and around its base (Fig. 5). Though the archenteron bends toward the ventral surface of the

larva, a stomodeal invagination (larval mouth) never formed. In histological sections of gastrulae, large numbers of intracellular yolk-like granular inclusions can be seen within the mesenchymal, endodermal, and ectodermal cells of the embryo (Figs. 5, 6). The cells of the embryonic wall and the archenteron are distinctly columnar, with their nuclei arranged distally within the cells. The remainder of the cellular inclusions other than yolk-like bodies are also located near the nucleus; the yolk-like bodies are stacked into columns that are generally directed toward the center of the gastrula (Figs. 5, 6). The blastopore is unusually wide, with the opening (110 μm) being almost one-quarter the diameter of the entire embryo (Fig. 5).

Histological cross sections through the preoral lobe of early plutei show the hydropore opening on the dorsal surface of the larva, and that the hydrocoel, juvenile gut, and perivisceral coelom have all formed (Fig. 7; compare Fig. 15a). Cross sections taken near the posterior of these larvae show the extent of development of the water vascular system with the lumens of the primordial tube feet having formed. Except for the perivisceral coelom, all coelomic spaces are filled with cellular and yolky-vesicle inclusions (Figs. 7, 8, 9, 10). The epidermis of the larva is a single layer of cells nearly cuboidal in form.

#### *Three- and four-day-old larvae*

At 3 days the larva is fully formed (Fig. 4), and the juvenile rudiment is very conspicuous. A single continuous ciliary band runs up and down the length of each arm. At the juncture of the posterodorsal arms the ciliary band courses up onto what appears to be the vestige of the preoral lobe (Fig. 11). The preoral lobe has undergone a torsion of nearly 45° to the left, as evidenced by the twisting of the ciliary band on the preoral lobe (Fig. 11), and the ciliary band disappears along the distal edge of the preoral lobe (Fig. 11). Oblique sections though 3-day plutei show an extensive convoluted juvenile gut and fully formed tube feet (Figs. 9, 10). Juvenile spines and pedicellaria are also present (Figs. 4, 13, and 14), giving the impression that 3-day-old larvae are in reality juvenile rudiments with somewhat shortened larval arms. This is similar to the larvae of *Euclidaris thoursi* as described by Emler (1988).

The juvenile rudiment, with five primary podia, develops out of the left side of the larva (Figs. 4, 11, 12, 13). There is no evidence of a juvenile mouth on the oral surface of the rudiment (Fig. 12). The posterior of the larva shows a striking bilateral symmetry (Fig. 14). With cross-polarized light, the larval skeleton was observed to extend to the tips of the arms (Fig. 16). The extent of development of the larval skeleton within the body of the larva was obscured by the development of juvenile skeletal struc-

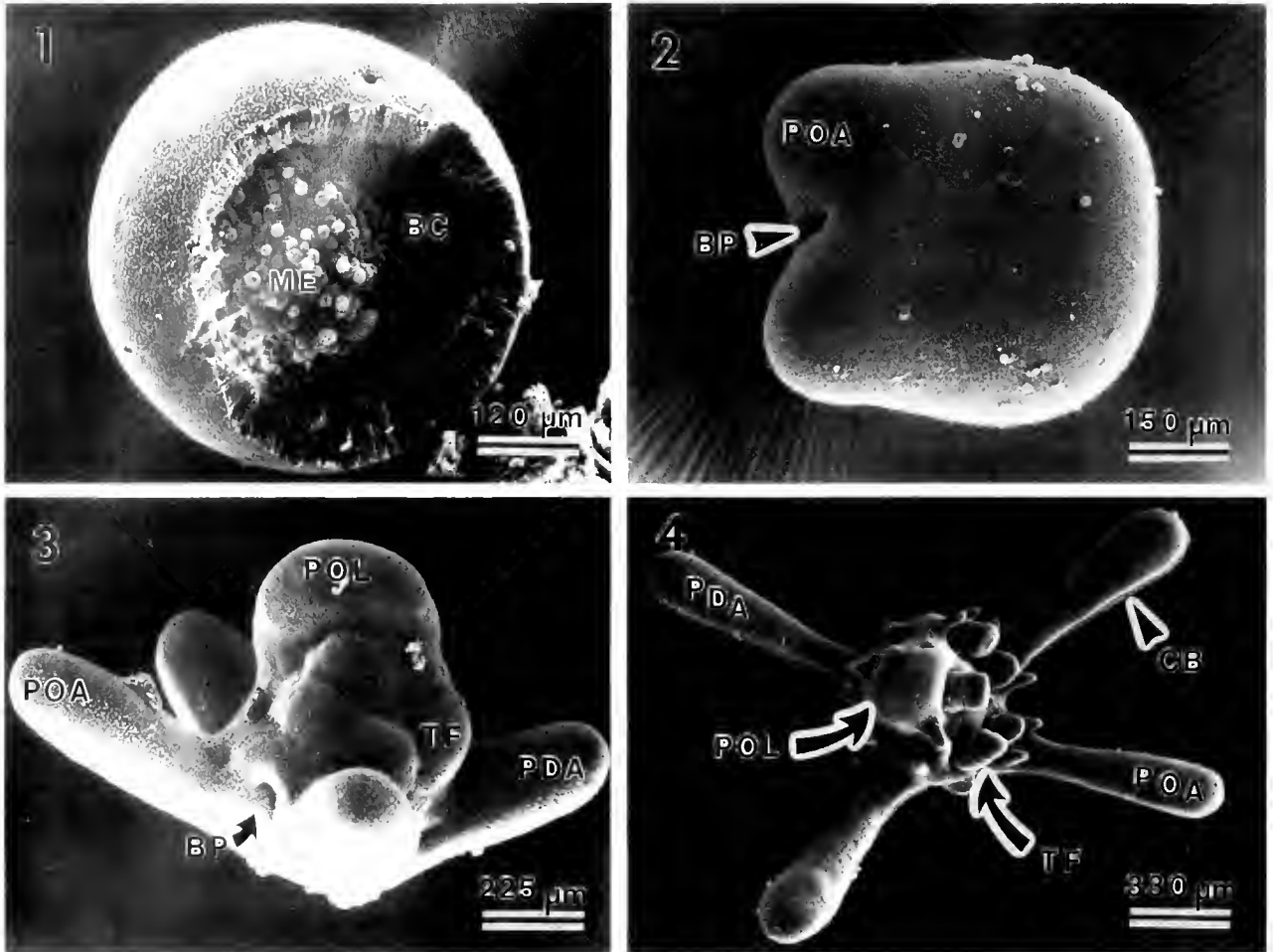


**Figure 1.** Scanning electron micrograph of a fractured gastrula of *Phyllacanthus imperialis* showing mesenchyme cells (ME) aggregated around the base of the archenteron. Note the small blastocoel (BC).  
**Figure 2.** One-day-old embryo showing rudiments of post-oral arms (POA) and blastopore (B).  
**Figure 3.** Two-day-old larva. PDA, posterodorsal arms; TF, tube foot; POL, preoral lobe.  
**Figure 4.** Anterior view of 3- to 4-day-old larva. The preoral lobe has undergone torsion nearly 45° to the left from its orientation in a typical pluteus. CB, ciliary band.

tures and the general opacity of the preoral lobe. Scanning electron micrographs of arm rods showed them to be fenestrated approximately 1 mm in length with a lattice-like plate at the base (Fig. 17). The larvae of *P. imperialis* swim in a typical echinopluteus fashion with the anterior-posterior axis oriented vertically and the posterior directed downwards much like the orientation of a falling badminton shuttlecock (Fig. 13).

#### *Metamorphosis and description of juvenile urchin*

Metamorphosis of the echinopluteus includes the formation of juvenile structures such as tube feet, spines, and pedicellaria, and the resorption of larval tissues. In the majority of echinoids with an echinopluteus larvae, the first appearance of juvenile structures is within the

vestibule, which is an invagination that forms on the left side of the larva. In cidaroids, there is no vestibule (Emlet, 1988), but juvenile structures develop on the left side of the echinopluteus in the same general location as on other echinoid larvae. The onset of metamorphosis can be observed when juvenile structures are visible on the exterior of an echinopluteus larva. These juvenile structures are called the "echinus rudiment."

Settlement and metamorphosis of *P. imperialis* larvae began 4 days after fertilization. Larvae settled by attaching themselves to the side or bottom of the culture vessel with their tube feet splaying their arms out radially. Within 4 h the tissue at the tips of the arms began to retract, exposing the ends of the skeletal rods. Six hours after attachment the tissue on all arms pulled back to the main body of the larva. Over the next 4 h the four arm rods

broke off at their bases. Periodic upward jerking movement of the spines may have facilitated this breakage. Twenty hours after attachment all resemblance to the larval form was lost and small juvenile urchins remained.

Perhaps because the 4-day-old larva was virtually a fully formed juvenile urchin, little morphological change appears to have occurred either internally or externally at this point. Although numerous juveniles survived and formed large numbers of spines, there was still no evidence of a mouth on urchins 21 days old. The nutritional needs of the young urchins are probably met from remaining stored nutrients or possibly through uptake of dissolved organic matter; this is similar to the early development reported for *Heliocidaris erythrogramma* (Williams and Anderson, 1975).

### Discussion

The larva of *P. imperialis* is unlike any previously described echinoid larva. Its external form is surprisingly similar to a feeding echinopluteus, yet it is completely lecithotrophic. The larva most similar to *P. imperialis* is that of the Japanese sand dollar, *Peronella japonica*, which develops from an egg of 276- $\mu\text{m}$  diameter into an echinopluteus-like larva with two, three, or four arms (Okazaki and Dan, 1954). The larva of *P. japonica* lacks a preoral region and does not retain pluteal bilateral symmetry (Okazaki and Dan, 1954; Mortensen, 1921). *Phyllacanthus parvispinus*, a congener also from Australia, has larger eggs (700  $\mu\text{m}$ ) that develop into little more than opaque spheres on which five primary podia appear just before settlement (Parks *et al.*, 1989).

In a review of the evolution of direct development in sea urchins, Raff (1987) identified four patterns of development that could describe the transition from the feeding pluteus to complete direct development (as in brooded embryos). These patterns, which he loosely correlated with egg size, are (1) typical feeding pluteus (100  $\mu\text{m}$  egg), (2) partial pluteus, non-feeding (300  $\mu\text{m}$  egg), (3) direct development with a floating larva (500  $\mu\text{m}$  egg), and (4) brooded by mother, complete direct development (1300  $\mu\text{m}$  egg).

The larva of *P. imperialis* has features of both groups 2 and 3. It still has the echinopluteus form, placing it in group 2, but the buoyancy of the larva and size of the egg place it closer to group 3. Overall, it seems to be a more reduced larval form than *Peronella japonica* (Okazaki and Dan, 1954) in that it is more yolky; however, it is not as reduced as *Asthenosoma ijimai* (Amemiya and Emler, 1992), which shows only the slightest of echinopluteus traits (*i.e.*, little more than primary tube feet and two pairs of "para-arms").

Raff (1988) suggested that three major developmental changes occur in the shift to lecithotrophic direct devel-

opment in echinoderms. First, egg size increases; second, typical pluteus structures are lost; and third, the appearance of juvenile features is accelerated.

The pattern of development observed in *P. imperialis* is consistent with all three of these criteria. The eggs of *P. imperialis* are larger than those of planktotrophs, and some pluteal structures (such as the second and fourth pairs of arms and the mouth) do not develop. Finally there is the rapid (when compared to planktotrophic forms) appearance of juvenile features. At 48 h after fertilization, the juvenile gut is forming (Fig. 7), the primary podia are visible externally (Figs. 11, 12, 13) even though the larval arms have only just begun to develop, and juvenile spines and pedicellaria are well formed.

An important question in considering the apparent shift from planktotrophy to direct development in echinoids is whether the loss of pluteus features occurs before, at the same time as, or after an increase in egg size and a loss of feeding ability. In *P. imperialis* many larval features have been retained despite the increase in egg size and loss of feeding ability. However, there is clear evidence for the disappearance of other pluteus features. The ciliary band, which is well developed along the arms, is greatly reduced on the preoral lobe (Fig. 11), and not all pluteus arms form. With the loss of feeding, the generation of water currents around the oral region is presumably no longer necessary; these currents are known to facilitate particle capture. It would be interesting to examine the effectiveness and structure of the preoral cilia in *Clypeaster rosaceus*, which is a yolky facultative planktotroph that arises from 280- $\mu\text{m}$  eggs. Since it has no obligatory need for particulate food material (although it does gain from feeding), are its preoral cilia reduced?

It is unlikely that the pluteus form in *P. imperialis* is secondarily derived from a brooded embryo (Strathmann, 1974; however, see McEdward (1992) for an argument of re-evolution of pelagic larval development in an asteroid). The retention of pluteus-like features in the larvae of *P. imperialis* may be insignificant from the perspective of the evolution of a form of lecithotrophic direct development. More likely, the pattern of development displayed by *P. imperialis* provides insight into the transition from a feeding larva to a nonfeeding larva and into the relative importance of certain larval characters in making such a transition.

In addition to its unique development pattern, *P. imperialis* also shows an interesting pattern of spawning behavior. At least at Lizard Island, this species spawns and the larvae develop coincidentally with the scleractinian corals of the Great Barrier Reef. In this region, more than 100 species of scleractinian corals mass spawn over the course of three nights between the full and last-quarter moons in late spring (Babcock *et al.*, 1986). These are joined by many species of other taxa such as polychaetes

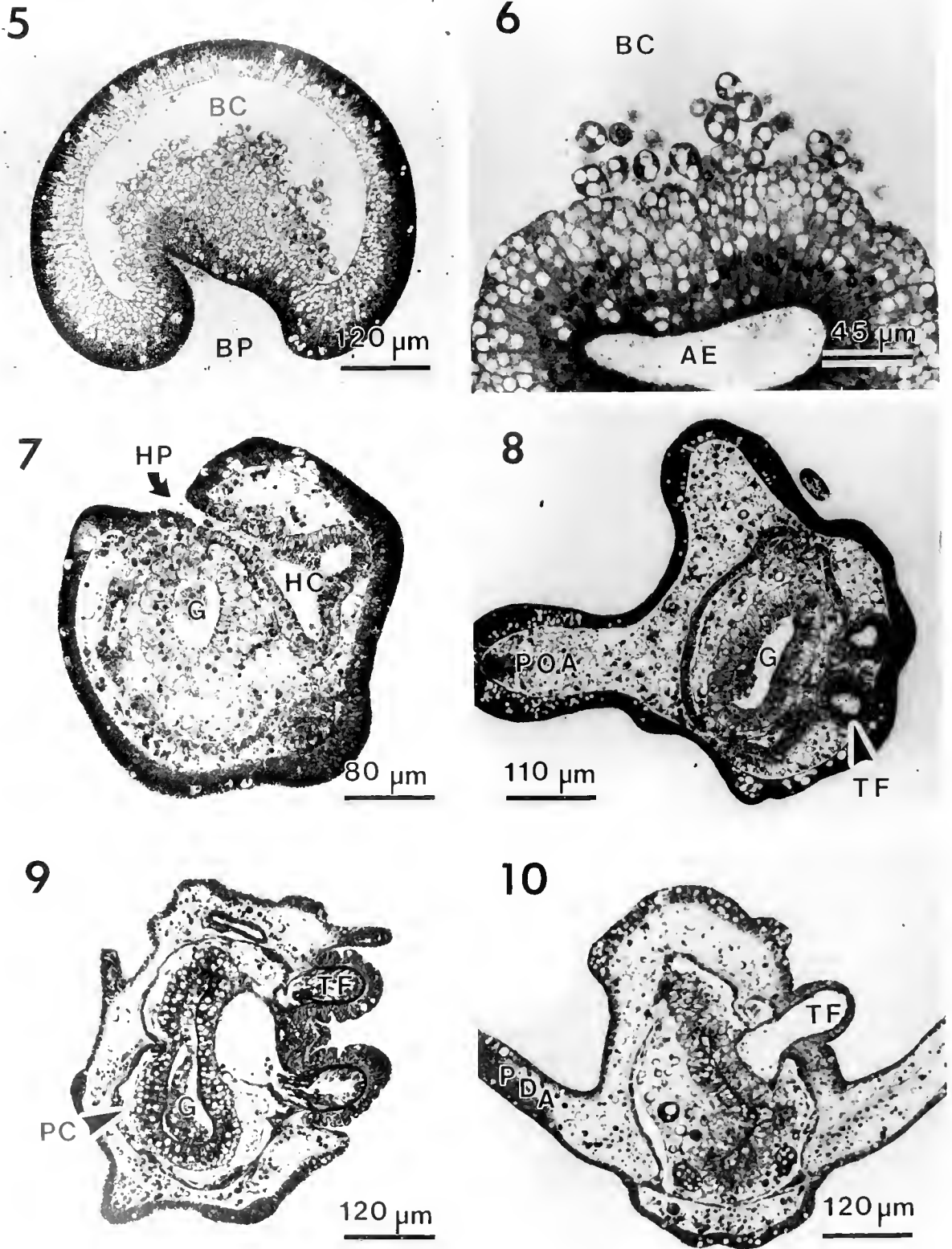
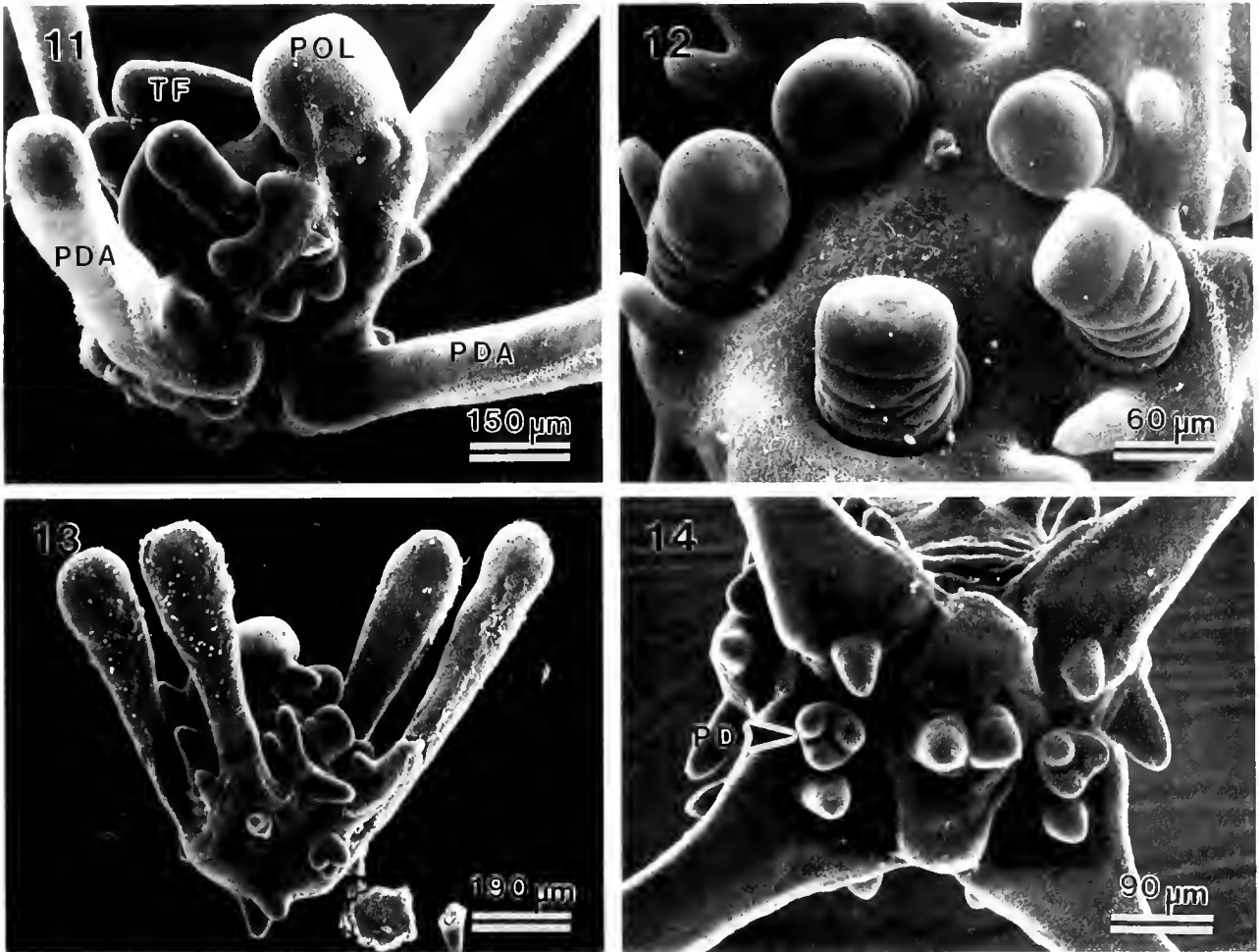


Figure 5. Light micrograph (LM) section of the gastrula of *P. imperialis*. Note blastopore (BP) and blastocoel (BC).

Figure 6. LM close-up of the tip of the archenteron (AE), showing migration of yolk-filled mesenchyme cells into the blastocoel (BC).





**Figure 11.** Dorsal view of 3- to 4-day-old larva. Note ciliary band which diminishes as it extends up onto the preoral lobe.

**Figure 12.** View of the "oral region" of the juvenile rudiment from a 3-day-old larva showing absence of mouth.

**Figure 13.** Swimming orientation of 3- and 4-day-old larva.

**Figure 14.** Posterior view of a larva that is ready to settle. Note the presence of juvenile spines and pedicellaria (PD).

(P. Hutchings, pers. comm.) and holothurians (RRO pers. observation). In the two years that we observed *P. imperialis*, its spawning coincided with that of the corals, and similar to corals, it settled out of the water column 4 to 6 days after fertilization (Babcock and Heyward, 1986). Additionally, both *P. imperialis* larvae and coral

larvae are initially quite buoyant and develop near the surface of the water.

It would be easy to speculate that direct development as observed in *P. imperialis* could be a response to selective pressures that have caused this species and corals to converge on a similar pattern of development. However, direct

**Figure 7.** LM cross section through the preoral lobe of 2-day-old larva. HY, hydropore; HC, hydrocoel; G, gut. See Figure 15a for reference.

**Figure 8.** LM cross section through the body of a 2-day-old larva. POA, preoral arm; G, gut; TF, tube foot. See Figure 15a for reference.

**Figure 9.** LM sagittal section through the preoral lobe of a 3-day-old larva. See Figure 15b for reference.

**Figure 10.** LM sagittal section through the preoral lobe and arms of a 3-day-old larva. See Figure 15b for reference.

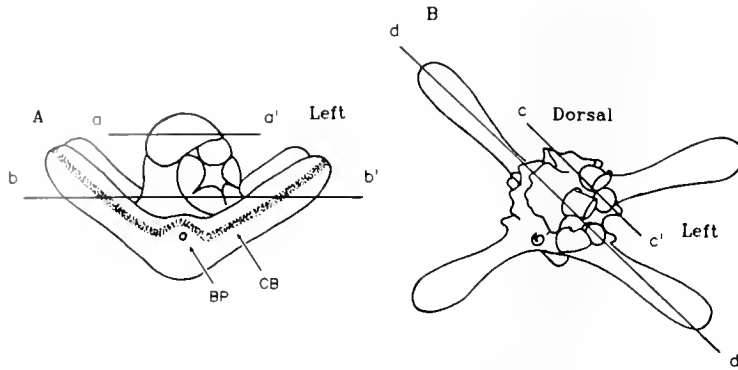


Figure 15. Diagrammatic representation of locations of light micrograph sections shown in Figure 7 (a:a'), Figure 8 (b:b'), Figure 9 (c:c') and Figure 10 (d:d').

lecithotrophic development in echinoids is not limited to the Great Barrier Reef, or even to tropical regions. *Phyl-lacanthus parvispinus* (Raff, 1987) and *Heliocidaris ery-*

*throgramma* (Williams and Anderson, 1975) produce larvae that are ecologically similar to *P. imperialis*, yet these species live in temperate habitats where the corals are not present.

It is difficult to determine exactly why a species undergoes mass spawning (Babcock *et al.*, 1986); however, further examination of the spawning behavior of *P. imperialis* across a broader geographic region might show patterns that point more clearly to the exact environmental cues that trigger such behavior. This type of study might also show whether the pattern of development exhibits any geographic variation that could provide insights into the evolutionary reasons for an invertebrate to shift its pattern of development from feeding to nonfeeding.

#### Acknowledgments

This project was supported in part by a Harbor Branch postdoctoral fellowship. We thank the Lizard Island Research Station for providing field facilities and the Australian Institute of Marine Science for logistical support. Field assistance was provided by A. R. Davis, E. M. Leydecker, R. Z. McPherson, M. B. Olson, K. Osborne, L. Sullivan, and P. Watts. Special thanks to P. Dixon for videotaping metamorphosis and to P. Linley for assisting with SEM. This paper has benefited from discussions with R. Emlet and R. Raff. Harbor Branch Oceanographic Institute Contribution #965. University of New Hampshire, Center for Marine Biology Contribution #281.

#### Literature Cited

- Amemiya, S., and R. B. Emlet. 1992. The development and larval form of an echinothurioid echinoid, *Asthenosoma ijimai*, revisited. *Biol. Bull.* 182: 15-30.
- Babcock, R. C., G. D. Bull, P. L. Harrison, A. J. Heyward, J. K. Oliver, C. C. Wallace, and B. L. Willis. 1986. Synchronous spawnings of 105 scleractinian coral species on the Great Barrier Reef. *Mar. Biol.* 90: 379-394.
- Babcock, R. C., and A. J. Heyward. 1986. Larval development of certain gamete-spawning scleractinian corals. *Coral Reefs* 5: 111-116.

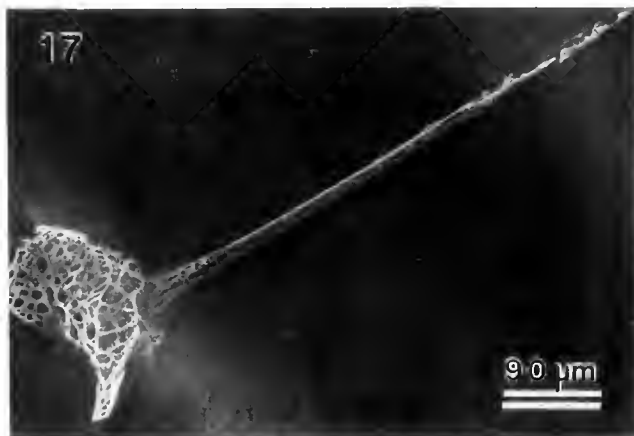
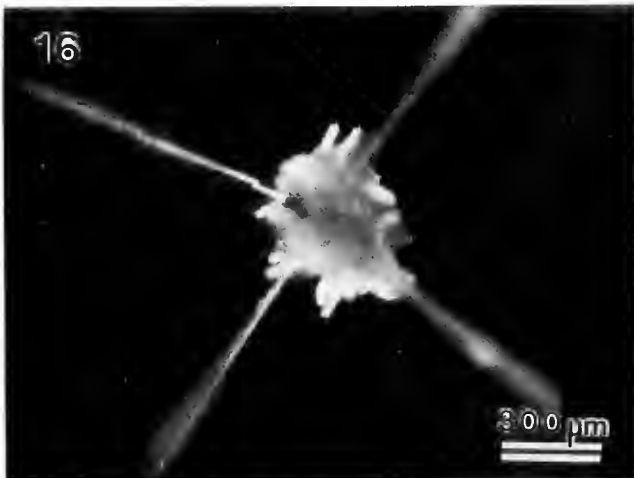


Figure 16. Light micrograph of the larval skeleton of *P. imperialis* highlighted with cross-polarized light.

Figure 17. S.E.M. of a skeletal rod from one arm of a 4-day-old larva of *P. imperialis*.



- Christiansen, F. B., and T. M. Fenchel. 1979. Evolution of marine invertebrate reproductive patterns. *Theor. Popul. Biol.* **16**: 267-282.
- Emlet, R. B. 1986. Facultative planktotrophy in the tropical echinoid *Clypeaster rosaceus* (Linnaeus) and a comparison with obligate planktotrophy in *Clypeaster subdepressus* (Gray) (Clypeasteroidea: Echinoidea). *J. Exp. Mar. Biol. Ecol.* **95**: 183-202.
- Emlet, R. B. 1988. Larval form and metamorphosis of a "primitive" sea urchin, *Eucidaris thouarsi* (Echinodermata: Echinoidea: Cidaroida), with implications for developmental and phylogenetic studies. *Biol. Bull.* **174**: 4-19.
- Emlet, R. B. 1990. World patterns of developmental mode in echinoid echinoderms. Pp. 329-335 in *Advances in Invertebrate Reproduction*, Vol. 5, M. Itoshi and O. Yamashita, eds. Elsevier Science, Amsterdam.
- Emlet, R. B., L. R. McEdward, and R. R. Strathmann. 1987. Echinoderm larval ecology viewed from the egg. Pp. 55-136 in *Echinoderm Studies*, Vol. 2, M. Jangoux and J. M. Lawrence, eds. Balkema, Rotterdam.
- McEdward, L. R. 1992. Morphology and development of a unique type of pelagic larva in the starfish *Pteraster tessellatus* (Echinodermata: Asteroidea). *Biol. Bull.* **182**: 177-187.
- McMillan, W. O., R. A. Raff, and S. R. Palumbi. 1992. Population genetic consequences of developmental evolution in sea urchins (genus *Heliocidaris*). *Evolution* **46**: 1299-1312.
- Mortensen, T. 1921. *Studies of the Development and Larval Forms of Echinoderms*. G.E.C. Gad., Copenhagen.
- Mortensen, T. 1938. Contributions to the study of the development and larval forms of echinoderms IV. Kgl. Dan. Vidensk. Selsk., Skr. Naturvid. Math. Afd. (9), 7(3): 1-59.
- Obrebski, S. 1979. Larval colonizing strategies in marine benthic invertebrates. *Mar. Ecol. Prog. Ser.* **1**: 293-300.
- Okazaki, K., and K. Dan. 1954. The metamorphosis of partial larvae of *Peronella japonica* Mortensen, a sand dollar. *Biol. Bull.* **106**: 83-99.
- Parks, A. L., B. A. Parr, J. Chin, D. S. Leaf, and R. A. Raff. 1988. Molecular analysis of heterochronic changes in the evolution of direct developing sea urchins. *J. Evol. Biol.* **1**: 27-44.
- Parks, A. L., B. W. Bisgrove, G. A. Wray, and R. A. Raff. 1989. Direct development in the sea urchin *Phyllacanthus parvispinus* (Cidaroida): Phylogenetic history and functional modification. *Biol. Bull.* **177**: 96-109.
- Paul, C. R. C., and A. B. Smith. 1984. The early radiation and phylogeny of echinoderms. *Biol. Rev.* **59**: 443-481.
- Raff, R. A. 1987. Constraint, flexibility, and phylogenetic history in the evolution of direct development in sea urchins. *Dev. Biol.* **119**: 6-19.
- Raff, R. A. 1988. Direct developing sea urchins: a system for the study of developmental processes in evolution. Pp. 63-69 in *Echinoderm Biology*, R. Burke, P. Mladenov, P. Lambert, R. Parsley, eds. Balkema Press.
- Strathmann, R. R. 1974. Introduction to function and adaptation in echinoderm larvae. *Thalassia Jugos.* **10**: 321-339.
- Strathmann, R. R. 1979. Echinoid larvae of the Pacific northeast (with a key and comment on an unusual type of planktotrophic development). *Can. J. Zool.* **57**: 610-616.
- Vance, R. R. 1973. On reproductive strategies in marine benthic invertebrates. *Am. Nat.* **107**: 339-352.
- Williams, D. H. C., and D. T. Anderson. 1975. The reproductive system, embryonic development, larval development, and metamorphosis of the sea urchin *Heliocidaris erythrogramma* (Val.) (Echinoidea: Echinometridae). *Aust. J. Zool.* **23**: 371-403.
- Wray, G. A., and R. A. Raff. 1991. The evolution of developmental strategy in marine invertebrates. *Trends Res. Ecol. Evol.* **6**: 45-50.

# Ultrastructure of the Coeloms of Auricularia Larvae (Holothuroidea: Echinodermata): Evidence for the Presence of an Axocoel

ELIZABETH J. BALSER<sup>1</sup>, EDWARD E. RUPPERT<sup>1</sup>, AND WILLIAM B. JAECKLE<sup>2</sup>

<sup>1</sup>*Department of Biological Sciences, 132 Long Hall, Clemson University, Clemson, South Carolina 29634-1903, and* <sup>2</sup>*Smithsonian Environmental Research Center, PO Box 28, Edgewater, Maryland 21037-0028*

**Abstract.** A hallmark feature of echinoderm larvae is the development of the left anterior coelom. This coelom, called the axohydrocoel, consists of the morphologically distinct, but undivided, left axocoel and hydrocoel. The axocoelic portion forms a duct that opens to the exterior via a pore on the dorsal surface of the animal. Holothuroid larvae are thought to lack an axocoel, but develop an anterior coelom, duct, and pore that are regarded as parts of the hydrocoel. New ultrastructural data, however, show that holothuroid auricularia larvae possess an axocoel and hydrocoel united together into an axohydrocoel. During development the anterior coelom consists of an interconnected left somatocoel, hydrocoel, and axocoel. The left somatocoel separates from the axohydrocoel and subdivides into left and right somatocoels. The somatocoels and hydrocoel region of the axohydrocoel are lined by a monociliated mesothelium having characteristics of transporting epithelia. The axocoel epithelium, like that of asteroid larvae, is composed of mesothelial podocytes. A duct connects the *axocoel* directly to the open dorsal pore and is lined with a columnar transporting epithelium. The occurrence of a specialized podocyte-lined cavity between the surface pore and the hydrocoel in echinoderm larvae is indicative of an axocoel. That similar structures occur in auricularia larvae supports the identification of an axocoel in holothuroids.

## Introduction

Holothuroids with indirect development typically have a planktonic feeding auricularia larva that undergoes

metamorphosis to produce a pentactula, or pelagic juvenile. In most holothuroids, the juvenile settles shortly after metamorphosis and assumes an adult lifestyle. The auricularia larva is restricted to the family Synaptidae in the order Apodida and to the families Holothuriidae and Stichopodidae in the order Aspidochirotida (Smiley *et al.*, 1991).

Auricularia larvae have a large blastocoel that houses the J-shaped gut, the paired body coeloms, and the left anterior coelom. In most larval asteroids, ophiuroids, and echinoids, a right anterior coelom is also present, but its developmental fate varies among groups. It reportedly either fuses with the right somatocoel, becomes the pulsatile vesicle (dorsal sac, madreporic vesicle) of the heart, or disappears at metamorphosis (Hyman, 1955; Hendler, 1991; Pearse and Cameron, 1991). The right anterior coelom does not develop in holothuroids and crinoids, which are believed to lack a pulsatile vesicle (Hyman, 1955; Holland, 1991; Smiley *et al.*, 1991).

The left anterior coelom is a unifying feature of echinoderm larvae and, despite differences in specific details of morphogenesis, is positionally and anatomically similar in five of the six extant classes (Hyman, 1955; Dan, 1968; Ruppert and Balsler, 1986; for review see chapters 4–8 in Giese *et al.*, 1991); no information exists on the larval development of the Concentricycloidea. In echinoderm larvae, with the reported exception of holothuroids (Smiley *et al.*, 1991), the left anterior coelom represents a fusion of the left axocoel and hydrocoel (Bury, 1885, 1889; Ruppert and Balsler, 1986; Giese *et al.*, 1991). Hyman (1955), drawing principally on the work of earlier researchers, emphasized this connection and retained the term axohy-

drocoel. The axohydrocoel is open, if only transiently, to the larval somatocoels and to the exterior via a duct and dorsal pore.

Holothuroid auricularia larvae develop an anterior coelom, duct, and pore, but are believed to lack any vestige of an axocoel (Hyman, 1955; Smiley, 1986, 1989). If holothuroids do not have an axocoel, then the anterior coelom, unlike that of other echinoderms, consists only of the hydrocoel and the somatocoel primordium. The left somatocoel arises from the anterior coelom and later divides forming the right and left larval somatocoels. A recent study of the development of the aspidochirotid *Stichopus californicus* (Smiley, 1986) suggests that the left anterior coelom and duct consists solely of the hydrocoel and the somatocoel primordium. Based primarily on the ultrastructure of the madreporic vesicle and the hypothesis that adult holothuroids lack any axoelic derivatives (Smiley, 1986, 1989), Smiley *et al.* (1991) conclude that holothuroid auriculariae have no "identifiable axocoel as part of their complement of coelomic primordia at any stage of development."

Several ultrastructural examinations of axocoelic derivatives in adult echinoderms (Bachmann and Goldschmid, 1978; Welsch and Rehkämper, 1987; Balsler, 1990; Balsler *et al.*, 1993, unpubl. data) and one of the axohydrocoel of a larval asteroid (Ruppert and Balsler, 1986) indicate that podocytes typify the lining of the axocoel. This study was undertaken to search for podocytes and other evidence of an axocoel in holothuroid larvae and is part of a larger investigation that attempts to reconstruct the phylogeny of extant echinoderms using a distinctive echinoderm organ, the axial gland, as a systematic character. Specific objectives of this investigation include examination of the ultrastructure of the larval coeloms of *Holothuria grisea* and different species of field-collected auricularia larvae. A comparison of the coeloms of these larvae with those, particularly the axohydrocoel, of other echinoderms will be used to test the hypothesis that an axocoel is present in holothuroid auricularia larvae.

### Methods and Materials

Auricularia larvae of the holothuriid *Holothuria grisea* were obtained from fertilization of freely spawned gametes. Adults were collected in June 1992 from rock rubble beneath the Ft. Pierce South Seaway Bridge and transported to the Smithsonian Marine Station at Link Port, Ft. Pierce, Florida. Specimens were kept in buckets of unaerated seawater until spawning occurred. Fertilized eggs were washed and transferred to culture dishes with clean seawater. Cultures were maintained at 26°C and provided daily with clean water and the marine alga *Isochrysis galbana* (Tahitian strain) as food.

During the spring and summer of 1992, auricularia larvae were collected from the waters off Grand Bahama Island (approx. 23°N 79.8°W) and from the Gulf Stream off the coast of Florida (approx. 26.5°N 78.8°W). Auriculariae were hand-sorted from plankton tows conducted aboard the R/V *Sunburst* of the Smithsonian Marine Station at Link Port and aboard the R/V *Seadiver* during expeditions 3 (4/27/92) and 4 (6/22/92) headed by Dr. Tammy Frank, Harbor Branch Oceanographic Institution, Ft. Pierce, Florida. Larvae were identified as apodids or aspidochirotids based on the presence or absence of wheel ossicles. Within the order Apodida, only synaptids have an auricularia larva, and only larvae in this family possess wheel ossicles (*e.g.*, Smiley *et al.*, 1991). Based on larval characters, further classification of the aspidochirotids was not possible.

Morphological data for *H. grisea* and field-collected auriculariae were acquired from living larvae and from light and electron microscopy of plastic-embedded specimens. Live auriculariae were photographed with a Zeiss Photomicroscope II loaded with T-max (Kodak) black and white film. Serial developmental stages of *H. grisea* larvae were fixed for microscopy using 2.5% glutaraldehyde in Millonig's phosphate buffer adjusted to 1080 milliosmoles with NaCl. Post fixation in 1.0% OsO<sub>4</sub> in 0.2 M Millonig's buffer was followed by alcohol dehydration, propylene oxide and Epon 812 infiltration, and embedment in Epon 812 (Electron Microscopy Sciences). Field-collected auricularia larvae were prepared for microscopy by the same method.

Serial thick (1 μm) and representative thin sections were cut with a Porter-Blum Sorvall or Reichert-Jung Ultratrac E ultramicrotome. Thick sections were stained with aqueous 1% toluidine blue in 0.5% borax and were observed and photographed with a Zeiss Photomicroscope I. Thin sections were stained with aqueous uranyl acetate followed by lead citrate and examined either with a Zeiss EM 9S or a Hitachi 600 electron microscope.

### Results

#### *Coelomic organization*

The development from fertilized egg to auricularia larva of *H. grisea* follows that described for other indirect-developing holothuroids (*e.g.*, Smiley *et al.*, 1991). The first 24 h postfertilization are marked by the formation of a uniformly ciliated blastula that hatches from the egg envelope and further develops into a gastrula. Gastrulation is followed by differentiation of the archenteron into a gut and a single unpaired anterior coelom. This anterior coelom arises from the apex of the archenteron and is the primordium of all other larval coeloms. Between the second and third day of development, the archenteron bends

toward and fuses with the ventral epidermis to form the mouth. At the same time, the anterior coelom produces a duct, which grows towards the dorsal surface and eventually opens at a pore just to the left of the larval midline. By day 4, the now recognizable auricularia larva has an unbroken epidermal ciliary band and a complete functional gut (Fig. 1). The gut is C-shaped and consists of a ventral mouth and anus separated by an esophagus, stomach, and intestine. In addition to the gut, the blastocoel is occupied by mesenchymal cells and by the anterior coelom (Figs. 1, 2).

Data from a developmental series of *H. grisea* auricularia larvae and from field-collected larvae show that the anterior coelom forms an undivided cavity consisting initially of three morphologically distinct regions (Figs. 1, 3). These regions are the primordia of the hydrocoel, the axocoel, and the paired somatocoels. The somatocoel primordium grows posteriorly along the left side of the large bulbous stomach and eventually separates from the original anterior coelom (Figs. 1, 3, 6). This cavity later subdivides (Fig. 6) to form both the left and right somatocoels flanking the larval stomach (Dan, 1968; Smiley *et al.*, 1991).

The remaining two regions of the anterior coelom, located dorsal to the gut, correspond to the axohydrocoel found in other echinoderm larvae (Fig. 3). The medial lobe, or hydrocoel, extends toward the middle of the larva and grows to encircle the esophagus. This lobe gives rise to the water vascular system of the pentactula and adult.

The third lobe, or axocoel, is situated between the hydrocoel and the dorsal pore and includes the duct connecting the axohydrocoel to the exterior (Figs. 3, 4, 5). The axocoel varies in size among examined species. In *H. grisea*, the axocoel appears to be restricted to the duct and a few cells at the proximal inner end of the duct. In field-collected aspidochirotids and apodids, the axocoel cavity, which is largest in the synaptids, is oval and extends either anteriorly or concentrically from the inner part of the duct (Figs. 4, 5). Dissimilarity in the size of the axocoel may be a reflection of differences in the size of the auricu-

larium of each species. *H. grisea* auriculariae are considerably smaller (0.75 mm in length 15 days postfertilization) than field-collected aspidochirotids (1–3 mm in length) and synaptids (up to 5 mm in length).

### Coelomic ultrastructure

Following morphogenesis of the duct and its connection to the exterior, further growth and differentiation of the anterior coelom results in the three ultrastructurally distinct, but continuous cavities representing the somatocoel primordium, the hydrocoel, and the axocoel. The mesothelium lining all three lobes of the anterior coelom is composed of monociliated cells that rest on a continuous basal lamina and are interconnected by cellular junctions. Ultrastructural dissimilarities in the lining of each cavity are principally differences in cellular junctions, apical microvilli, and basal modifications. Although differentiation is evident, at the latest developmental stage of auricularia examined, the epithelium of each region had not yet acquired all the characteristics of juvenile mesothelia. For example, the hydrocoel and the somatocoel primordial cells lack basal myofilaments typical of cells lining the juvenile water vascular system and body cavity.

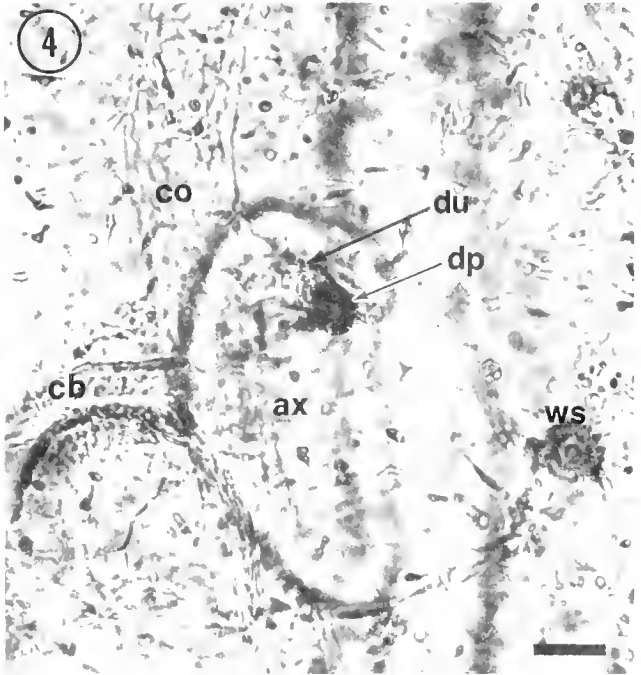
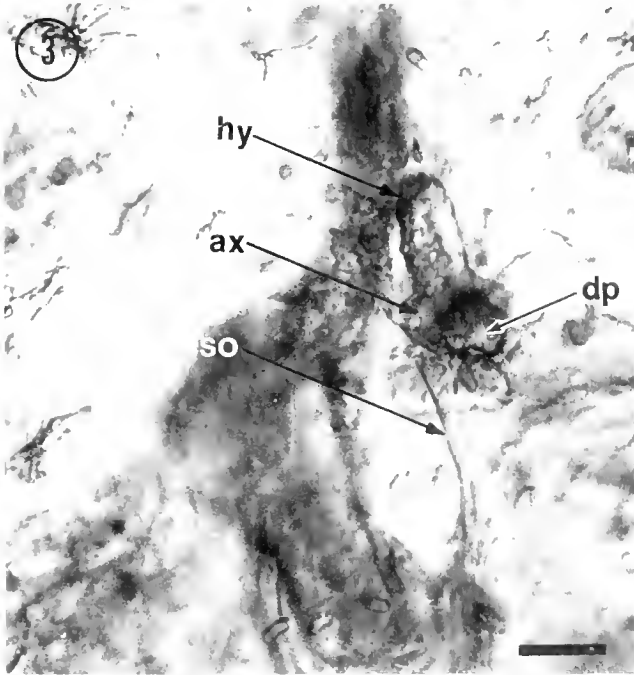
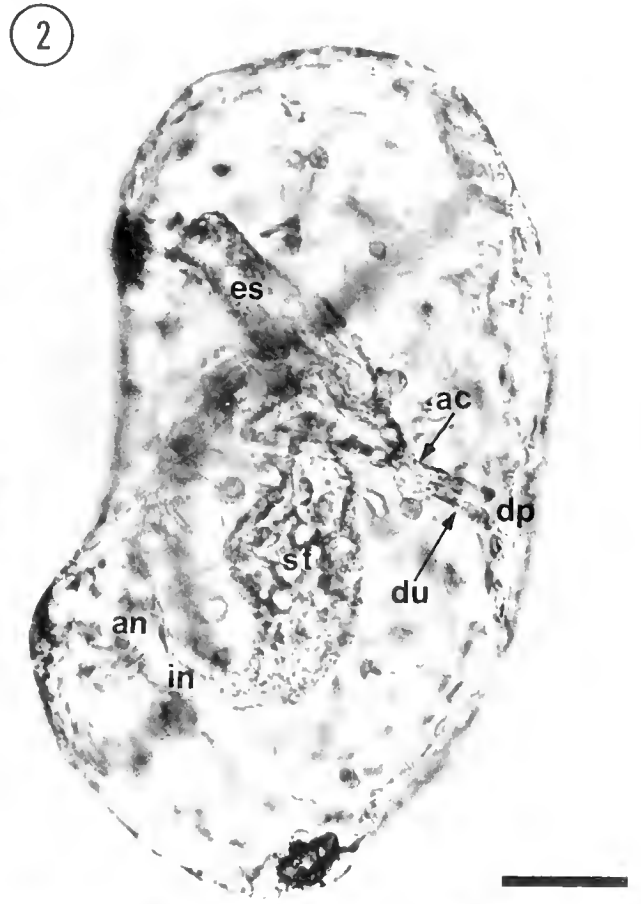
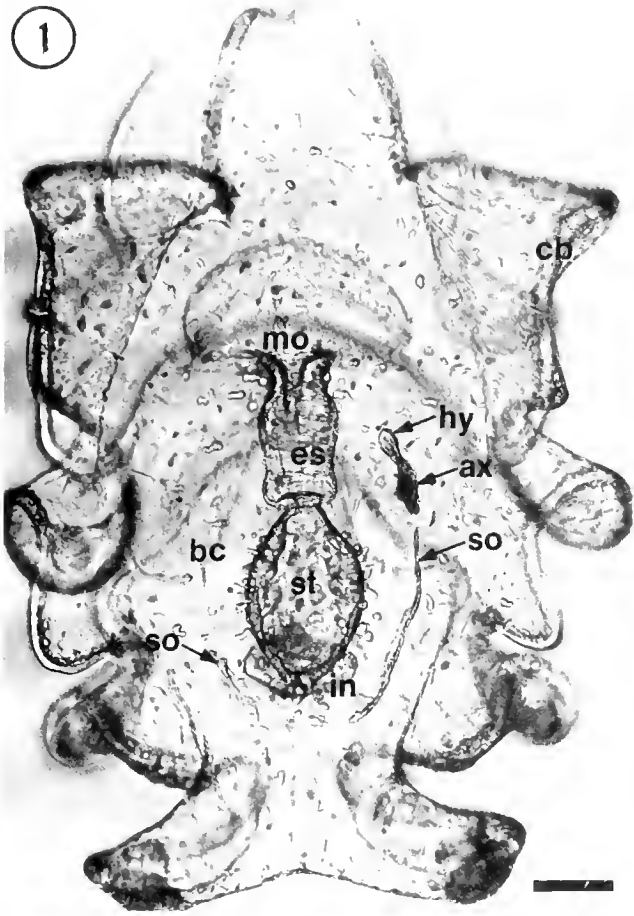
After the somatocoel primordium loses its connection to the anterior coelom, the initially oval cavity becomes elliptical and asymmetrical as it grows posteriorly along the length of the stomach. The cellular lining of the medial surface of the coelom closest to the stomach becomes flat and squamous, while that of the lateral surface remains columnar (Fig. 7). Regardless of shape, somatocoel cells are characterized by apical adhering and septate junctions, scattered apical microvilli, extensive paracellular spaces, and basal, vertebrate-like, tight junctions (Figs. 8, 9, 10). Not all somatocoel cells are coupled by basal tight junctions. In some cases, only basal adhering junctions were observed or basal junctions were absent (Fig. 9). The paracellular spaces often extend to the basal junctions or to the basal lamina. The lateral membranes lining these spaces possess coated pits, endocytic pits, and invagina-

**Figure 1.** Ventral view of a field-collected aspidochirotid auricularia. The axohydrocoel consists of the axocoel (ax) and hydrocoel (hy). This coelom is situated on the left dorsal side of the animal at the level of the junction between the esophagus (es) and the stomach (st). The somatocoels (so), which are initially connected to the axohydrocoel, lie lateral to the stomach. Scale bar = 0.1 mm; bc, blastocoel; cb, ciliated band; in, intestine; mo, mouth.

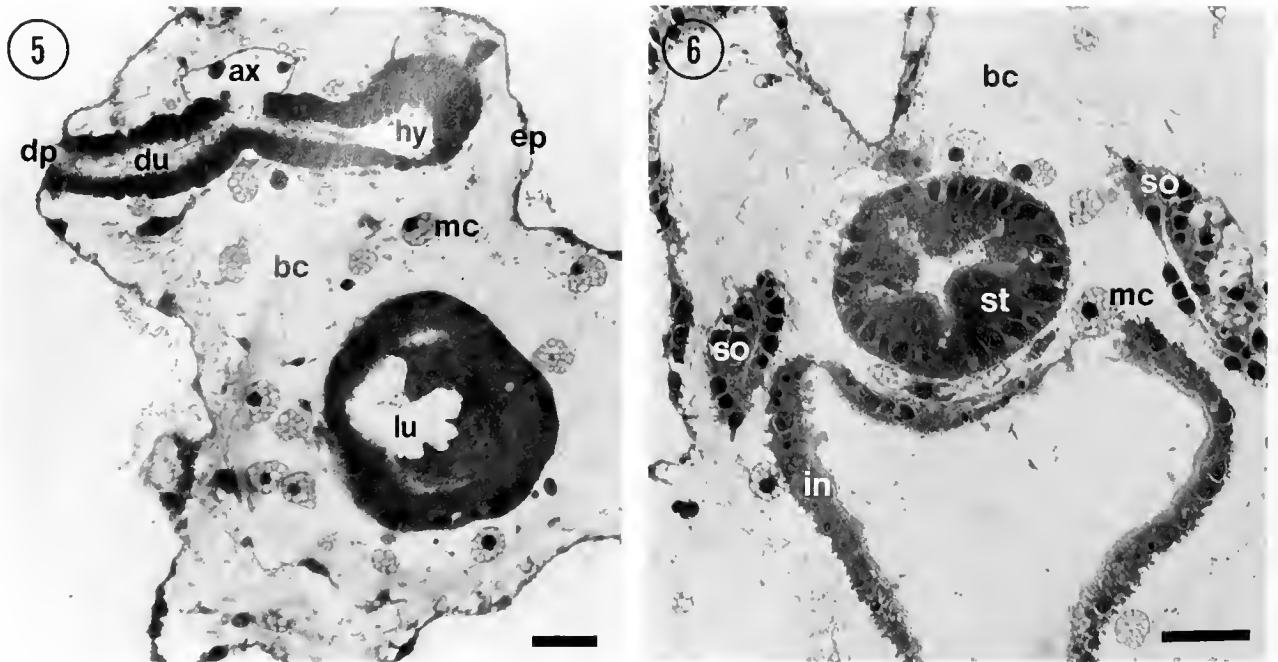
**Figure 2.** Lateral view of a 7-day-old larva of *H. grisea*. At this stage of development, the anterior coelom (ac) consists of the duct (du) and the undivided and undifferentiated left axocoel, hydrocoel, and somatocoel primordium. The duct provides an open connection between the anterior coelom and the dorsal pore (dp). Scale bar = 0.05 mm; an, anus; es, esophagus; in, intestine; st, stomach.

**Figure 3.** Dorsal view of the coeloms of a field-collected aspidochirotid auricularia larva showing the interconnected left axocoel (ax), hydrocoel (hy), and somatocoel (so). Scale bar = 0.05 mm; dp, dorsal pore.

**Figure 4.** Dorsal view of the axocoel (ax), duct (du), and pore (dp) of a field-collected synaptid auricularia larva. Scale bar = 0.05 mm; cb, ciliary band; co, coelom (hydrocoel?); ws, wheel ossicle.



Figures 1-4. Light micrographs of living auricularia larvae.



Figures 5-6. Light micrographs of tangential sections through the larval coeloms of a field-collected aspidochirotid auricularia.

Figure 5. Shows axocoel (ax) and hydrocoel (hy). The axocoel consists of a thin-walled cavity and a ciliated axocoelic duct (du), which opens at the dorsal pore (dp) on the left dorsal side of the animal. Scale bar = 0.01 mm; bc, blastocoel; ep, epidermis; lu, lumen of the stomach; mc, vesiculated mesenchyme cell.

Figure 6. The somatocoels (so) lie lateral to the stomach (st) and the upper intestine (in). Scale bar = 0.025 mm; bc, blastocoel; mc, vesiculated mesenchyme cell.

tions suggestive of transfer tubules (Fig. 8). Somatocoel cells, like those of the other coelomic mesothelia, are monociliated (Fig. 7). The cytoplasm contains coated vesicles, numerous other vesicles, mitochondria, and a large nucleus.

The hydrocoel lobe of the axohydrocoel is lined by squamous and cuboidal epithelial cells joined by apical adhering junctions followed by septate junctions (Figs. 11, 13). Basally, the lateral membranes are extensively interdigitated and are interconnected by tight junctions (Figs. 12, 14). The cytoplasm is replete with basal mitochondria, putative lysosomes, and vesicles. The nucleus is basal and is elongated. Apical microvilli were infrequently observed.

The defining feature of the axocoel mesothelium is the presence of podocytes (Figs. 15-19). Podocytes are epithelial cells that exhibit basal modifications forming foot processes, or pedicels (Figs. 16, 18, 19). Pedicels rest on the underlying basal lamina and provide breaks, or fenestrations, in an otherwise continuous epithelium. Pedicels are bridged by the extracellular matrix of the underlying basal lamina (Figs. 18, 19). In addition to the basal lamina, some pedicels are bridged by diaphragms similar to filtration-slit membranes found across the pores of the fen-

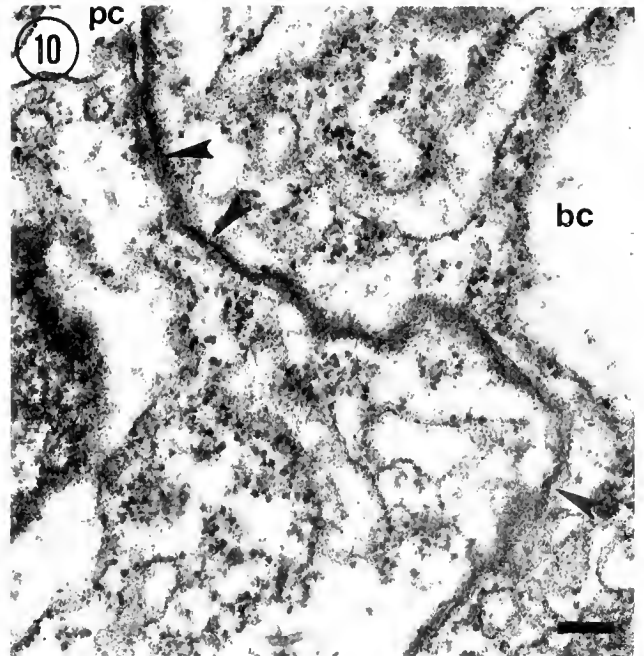
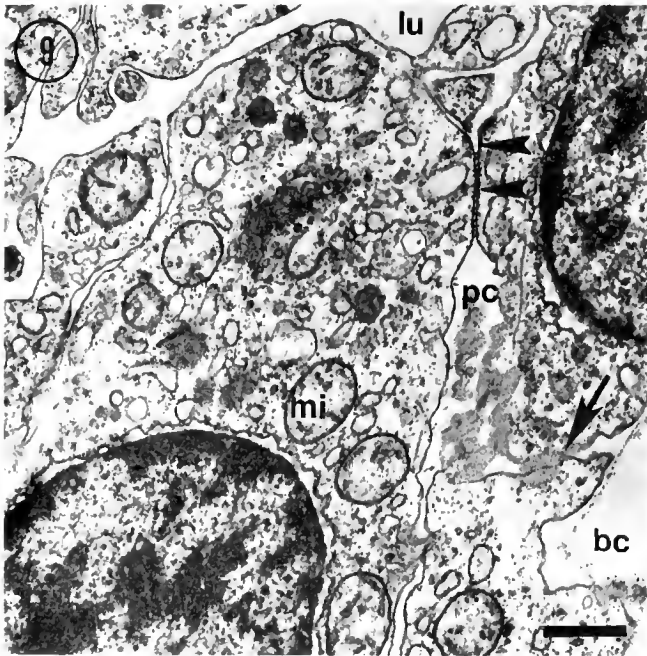
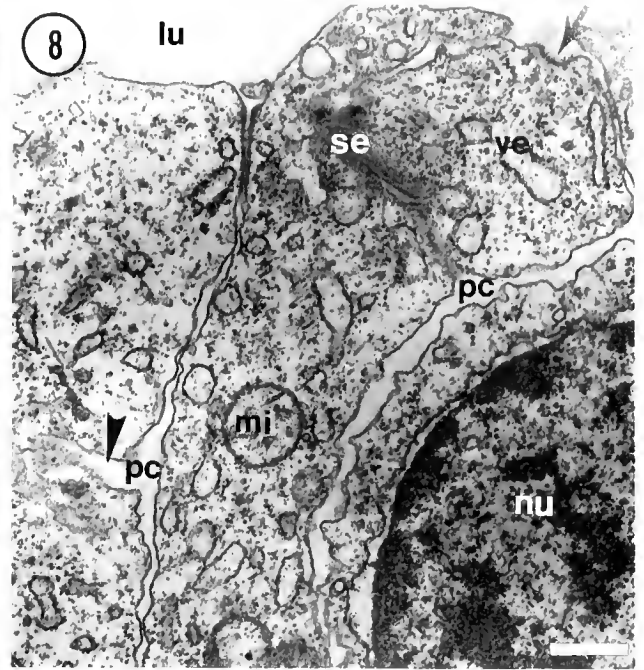
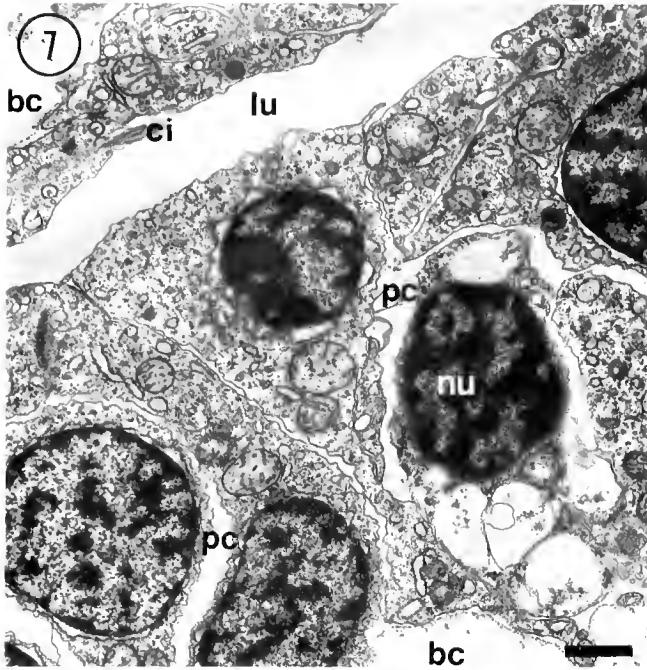
estrated epithelia associated with the vertebrate nephron (Bulger, 1983). The cell bodies of podocytes are generally interconnected only by adhering junctions, but short septate junctions were occasionally observed connecting podocytes to hydrocoel or somatocoel cells or to axocoelic duct cells (Fig. 17). In addition to scattered microvilli (Fig. 17), the apical membrane possesses a single cilium and endocytic and coated pits. The cytoplasm contains vesicles, mitochondria, lysosomes, and a large circular nucleus (Figs. 16, 17).

Columnar monociliated epithelial cells line the lumen of the axocoelic duct which directly connects the axocoel lobe of the axohydrocoel to the dorsal pore (Fig. 20). The apices of these cells have a single cilium, many microvilli (Figs. 20, 21), and coated pits. Coated vesicles, numerous other vesicles, mitochondria, putative lysosomes, and a basal nucleus were observed (Fig. 21). Apical adhering and subapical septate and basal tight junctions are typical of this epithelium (Figs. 22, 23).

### Discussion

The left axohydrocoel develops similarly in all echi- noderm larvae except crinoids (Hyman, 1955; Balsler and





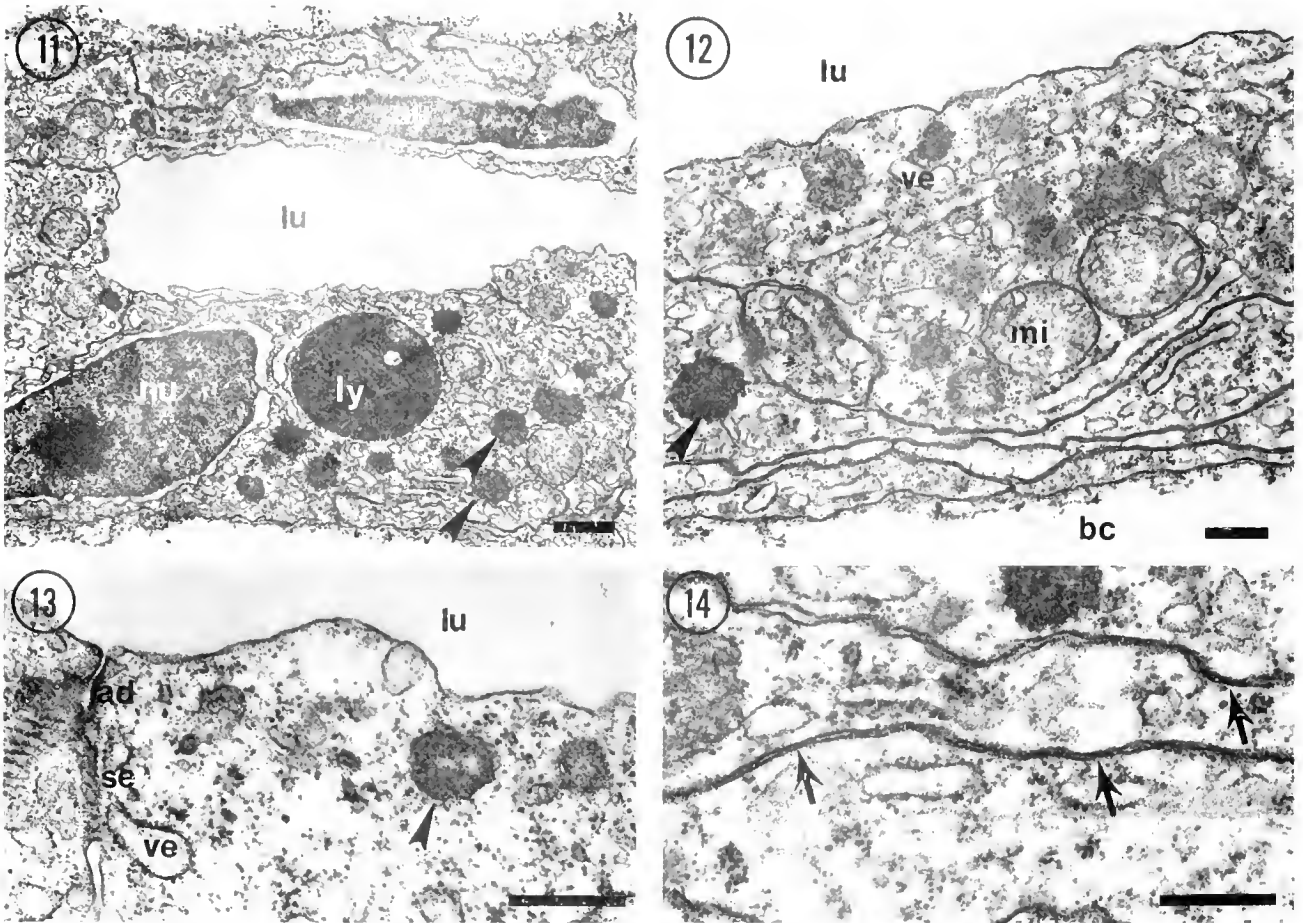
Figures 7-10. Transmission electron micrographs of sections through the somatocoels of aspidochiroid auriculariae.

Figure 7. The epithelium lining the lumen (lu) of the somatocoel is composed of squamous and columnar monociliated cells. Scale bar = 1.0  $\mu$ m; bc, blastocoel; ci, cilium; nu, nucleus; pc, paracellular space.

Figure 8. Large paracellular spaces (pc) lead to channels suggestive of transfer tubules (arrowhead). Scale bar = 0.5  $\mu$ m; lu, lumen of somatocoel; mi, mitochondrion; nu, nucleus; se, grazing section through a subapical septate junction; ve, vesicle; arrow indicates apical coated pit.

Figure 9. Somatocoel epithelial cells are joined by apical adhering junctions followed by subapical septate junctions (arrowheads). Basal junctions are absent between some cells (arrow). Scale bar = 0.5  $\mu$ m; bc, blastocoel; lu, lumen of somatocoel; mi, mitochondrion; pc, paracellular space.

Figure 10. The basal portion of some somatocoel cells are interconnected by tight junctions. Arrowheads indicate points of membrane contact. Scale bar = 0.1  $\mu$ m; bc, blastocoel; pc, paracellular space.



Figures 11–14. Transmission electron micrographs of tangential sections of the hydrocoel region of the axohydrocoel of field-collected synaptid auriculariae.

**Figure 11.** Hydrocoel epithelial cells have elongated nuclei (nu), numerous putative small (500–750 nm in diameter) lysosomes (arrowheads), and larger lysosomes (ly). Scale bar = 1  $\mu\text{m}$ ; lu, lumen of hydrocoel.

**Figure 12.** Hydrocoel epithelial cells show extensive basal interdigitation. Basally located mitochondria (mi) are often associated with these digitations. Scale bar = 0.5  $\mu\text{m}$ ; bc, blastocoel; lu, lumen; ve, vesicle; arrowhead indicates putative lysosome.

**Figure 13.** Apical adhering junctions (ad) are followed by septate junctions (se). Scale bar = 0.5  $\mu\text{m}$ ; lu, lumen; ve, vesicle; arrowhead indicates putative lysosome.

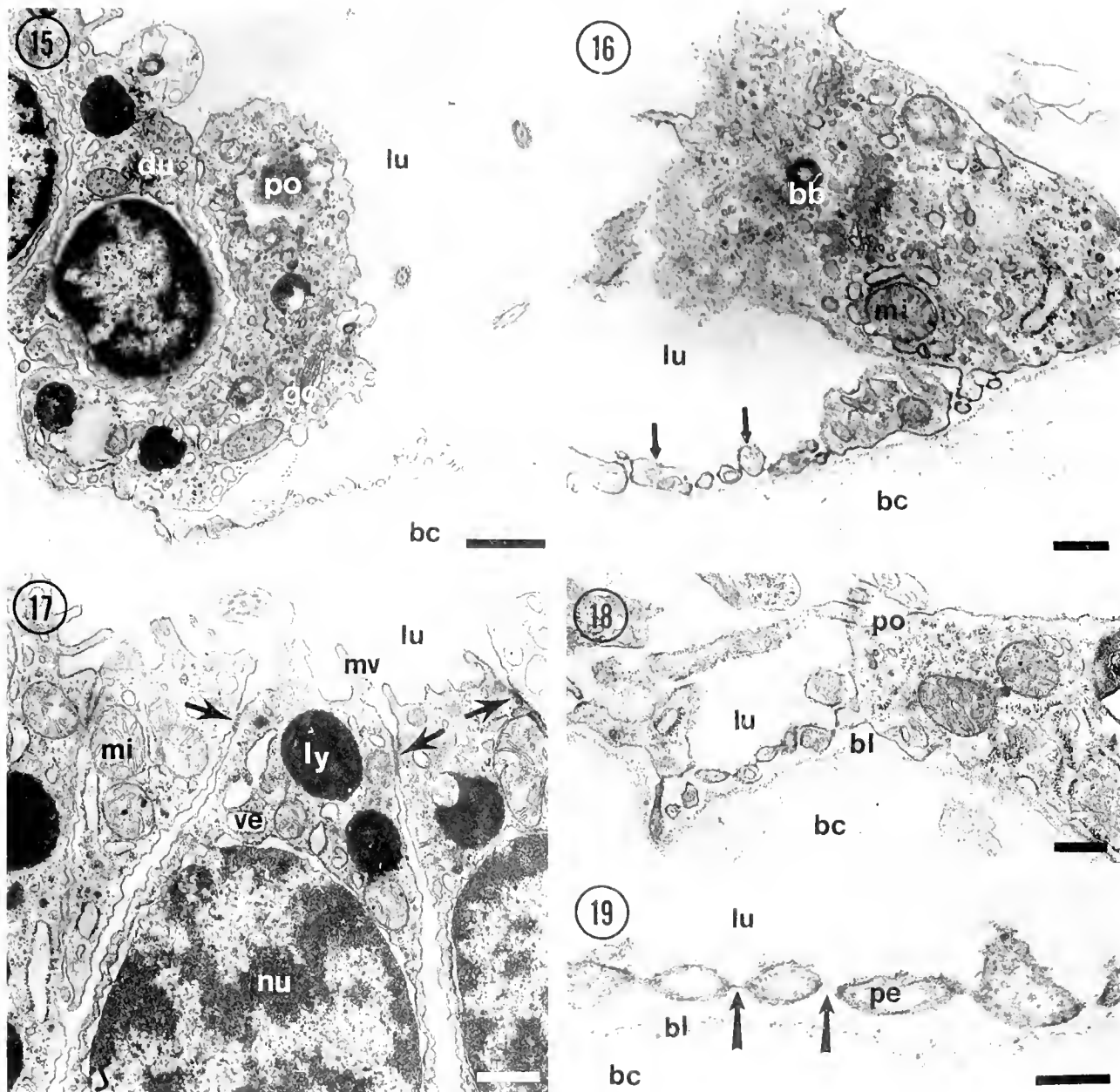
**Figure 14.** Basal junctions are similar to vertebrate tight junctions. Arrows indicate definitive points of membrane contact. Scale bar = 0.5  $\mu\text{m}$ .

Ruppert, 1993). Crinoids differ from other echinoderms because the archenteron separates into anterior and posterior cavities. The anterior cavity gives rise to the enteric sac and the axohydrocoel. The posterior cavity gives rise to the left and right somatocoels. A connection, which is maintained in the adult, is secondarily established between the somatocoels and the axohydrocoel.

In noncrinoid larvae, the left anterior coelom separates from the archenteron and is the primordium of the paired somatocoel, hydrocoel, and axocoel. The somatocoel primordium eventually loses its connection to the anterior coelom, but the axocoel and hydrocoel remain united.

The axohydrocoel establishes a duet that opens to the exterior via the dorsal pore. In crinoids, asteroids, ophiuroids, and echinoids, the undivided axohydrocoel and its union with the exterior are retained through metamorphosis via the stone canal and madreporic pores. The adult stone canal, which may originate from the axocoel, provides a link between the axial gland coelom and the hydrocoel-derived water vascular coelom. The madreporite opens internally into the ampulla (an axocoelic derivative), which joins the axial coelom to the stone canal. A stone canal and madreporite and, according to Erber (1983), a rudimentary ampulla all develop in juvenile





Figures 15-19. Transmission electron micrographs of podocytes lining the axocoel region of the axo-hydrocoel of several different auricularia larvae.

Figure 15. Longitudinal section of the axocoel of a field-collected aspidochirotid larva shows the transition of the cuboidal mesothelium of the duct (du) to the mesothelial podocytes (po) lining the lumen (lu) of the axocoel. Scale bar = 1  $\mu$ m; bc, blastocoel; go, Golgi body.

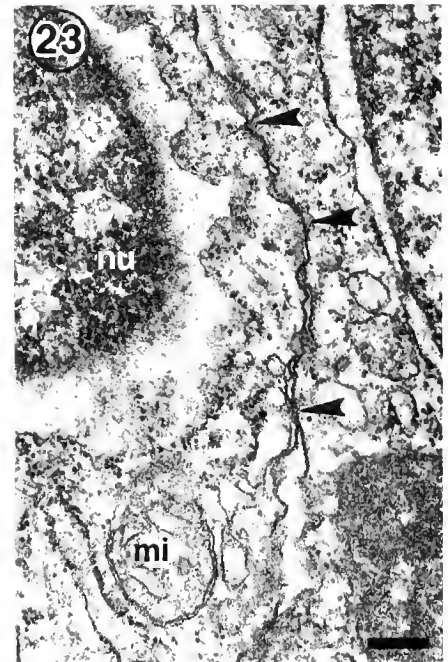
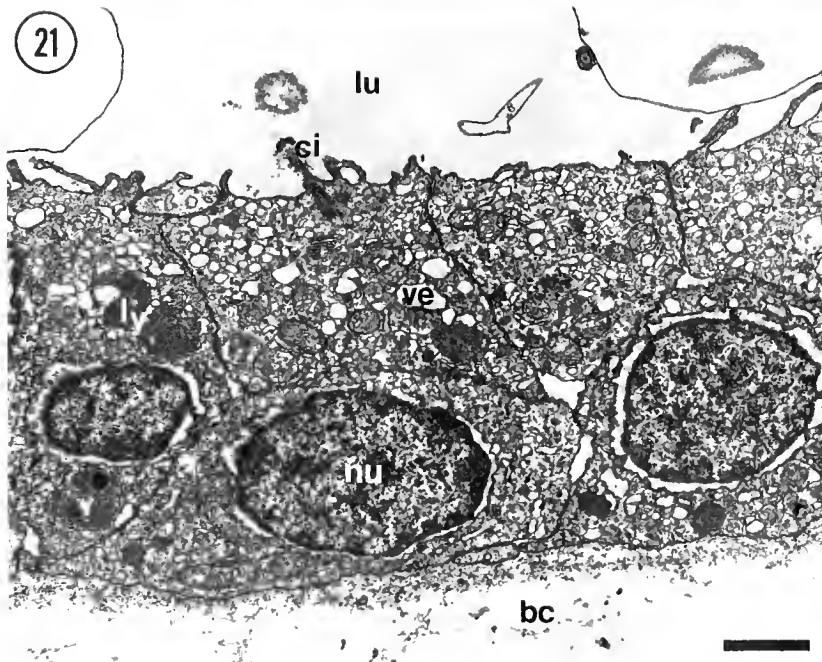
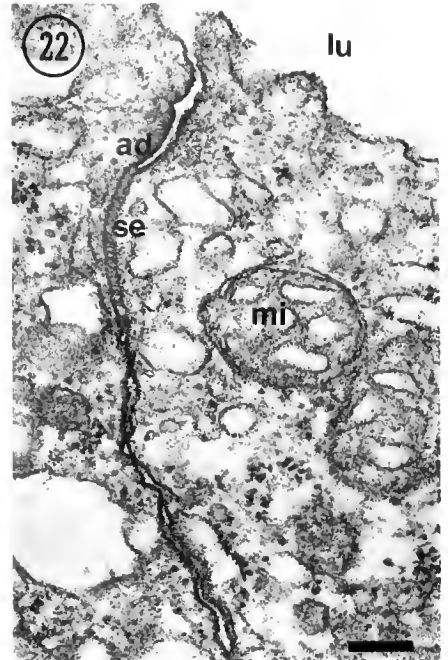
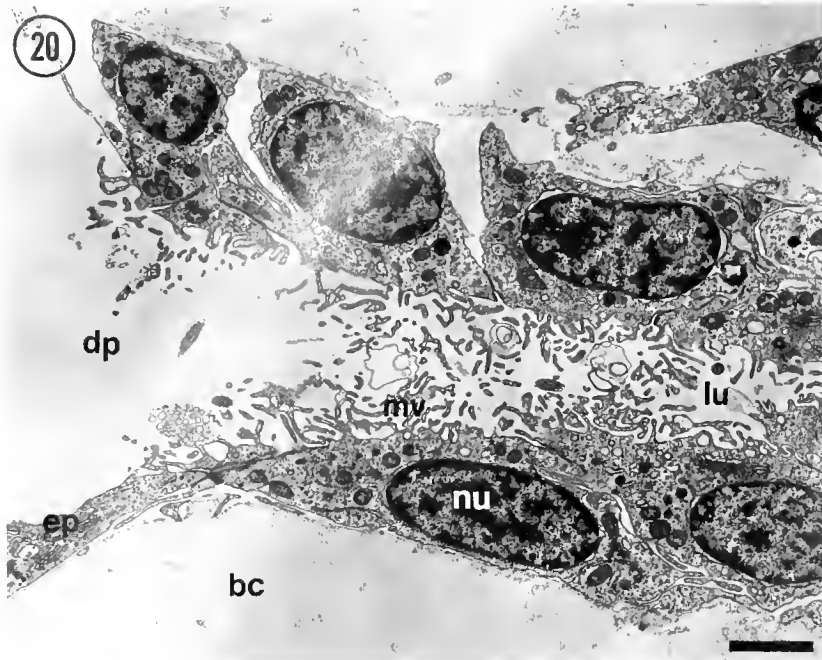
Figure 16. Field-collected synaptid auricularia podocyte. Podocytes are defined by the presence of foot processes or pedicels (arrows). Scale bar = 0.5  $\mu$ m; bb, ciliary basal body; bc, blastocoel; lu, axocoel lumen.

Figure 17. Apical region of podocytes in a held-collected aspidochirotid auricularia showing apical junctions (arrows) and microvilli (mv). Scale bar = 0.5  $\mu$ m; lu, lumen; ly, lysosome; mi, mitochondrion; nu, nucleus; ve, vesicle.

Figures 18-19. Basal region of field-collected aspidochirotid auricularia podocytes (po) showing pedicels that provide gaps or fenestrations (arrows) in an otherwise continuous epithelium. Pedicels that are not joined by filtration slit membranes are bridged only by the basal lamina (bl) supporting this mesothelium. Between pedicels the lumen (lu) of the axocoel and the blastocoel (bc) are separated only by these extracellular connective tissue layers.

Figure 18. Scale bar = 0.5  $\mu$ m.

Figure 19. Scale bar = 0.25  $\mu$ m.



Figures 20–23. Transmission electron micrographs of the axocoelic duct of an *H. grisea* larva (20) and a field-collected synaptid auricularia larva (21–13).

Figure 20. Longitudinal section through the duct that opens to the exterior via the dorsal pore (dp). Duct cells are cuboidal monociliated epithelial cells that have basal nuclei (nu) and apical microvilli (mv). Scale bar = 2  $\mu\text{m}$ ; bc, blastocoel; ep, epidermis; lu, lumen of duct.

Figure 21. Cells lining the duct lumen (lu) possess numerous apical cellular vesicles (ve) and putative lysosomes (ly). Scale bar = 2  $\mu\text{m}$ ; bc, blastocoel; ci, cilium; nu, nucleus.

Figure 22. Shows apical adhering (ad) and septate (se) junctions. Scale bar = 0.25  $\mu\text{m}$ ; lu, lumen; mi, mitochondrion.

Figure 23. Shows basal tight junctions. Arrowheads indicate areas of membrane contact. Scale bar = 0.25  $\mu\text{m}$ ; mi, mitochondrion; nu, nucleus.

holothuroids, but the fate of the larval axocoel reported here is unknown at present.

The ultrastructure of holothuroid larval somatocoels is similar to that of asteroid larvae (unpubl. data) and suggests a transportive function for this epithelium. The presence of paracellular spaces extending from the basal lamina towards the cell apex and the absence of basal junctions in some areas suggest that this epithelium is transporting substances from the blastocoel into the cell or indirectly into the coelom (Berridge and Oschman, 1972). This hypothesis is supported by the presence of apical septate junctions, putative transfer tubules, endocytic and coated pits on the lateral membranes, and numerous vesicles.

The ultrastructure of the hydrocoel also indicates a transporting function. Deeply folded lateral and basal membranes and associated basal mitochondria are typical of osmoregulatory epithelia (Berridge and Oschman, 1972). The presence of occluding apical septate junctions and basal tight junctions and the paucity of apical microvilli suggest that the presumed transport is basally located.

Like that of asteroid larvae, (Ruppert and Balsler, 1986), the holothuroid axocoel mesothelium is composed, in part, of podocytes. The presence of podocytes and of the open ciliated duct to the exterior indicates a pressure-driven filtration system and suggests an excretory function (Ruppert and Smith, 1988). Although, at present, no physiological data are available, we predict that blastocoelic fluid is filtered across the basal lamina underlying the podocytes, through the fenestrations between pedicels, and into the coelomic cavity of the axohydrocoel. Modification of the primary urine could be accomplished by the axohydrocoel and duct mesothelium. The occurrence of apical microvilli, endocytic and coated pits, and numerous apical vesicles suggests that the duct epithelium is transporting substances from the lumen.

Results presented in this paper indicate that holothuroid auricularia larvae possess a left axohydrocoel morphologically similar to that of other echinoderm larvae. In contrast, Smiley *et al.* (1991) argue that holothuroids do not have an axocoel and, thus, the anterior coelom is composed of the hydrocoel and the somatocoel primordia only. They base this hypothesis principally on the unusual ultrastructure of the madreporic vesicle and the presumed lack of axocoelic derivatives in the adult (*i.e.*, the axial gland). Unlike the madreporic vesicle (dorsal sac, pulsatile vesicle), which is a muscular sac in other echinoderms, the madreporic vesicle of holothuroids, as described by Smiley (1986), is a syncytium and probably functions in the secretion of the madreporite ossicles.

Smiley (1989) speculates that axocoelic functions such as larval attachment are assumed by the hydrocoel and that the axocoel of other echinoderms arose from differ-

entiation of the epithelium forming the buccal podia. He supports this idea with the fact that the pentactula (as well as juveniles of direct developers) use the buccal podia as attachment organs. The undivided, undifferentiated holothuroid axohydrocoel is regarded as a hydrocoel only. In his view, the axocoel of other echinoderms evolved later from the plesiomorphic holothuroid "hydrocoel."

The discovery of a morphologically distinct region of the holothuroid larval axohydrocoel, combined with the positional and ultrastructural agreement of that region with the axocoelic portion of the left axohydrocoel of other echinoderms, reopens the question of an axocoel in holothuroids. Data presented here show that holothuroid auricularia larvae develop an axohydrocoel, axocoelic duct, and open dorsal pore. The position of the axocoel and duct between the dorsal pore and hydrocoel, the connection of the axocoel to other larval coeloms, and the presence of podocytes indicate the existence of an axocoel in holothuroid larvae.

#### Acknowledgments

We thank Dr. Tammy Frank for the opportunity to collect holothuroid larvae during her Harbor Branch Oceanographic Institution (Ft. Pierce, Florida) trawling expeditions. We are grateful to Dr. Mary Rice and the staff at the Smithsonian Marine Laboratory at Link Port, Ft. Pierce, Florida, for providing the laboratory space, equipment, and plankton samples that made much of this work possible. Supported by NSF Grant #9006599 to E. E. Ruppert.

#### Literature Cited

- Bachmann, S., and A. Goldschmid. 1978. Fine structure of the axial gland of *Sphaerechinus granularis*. *Cell Tiss. Res.* **193**: 107-123.
- Balsler, E. J. 1990. The fine structure of the axial complex in the brittlestars *Ophiothrix angulata* and *Ophuactis savignyi*. *Am. Zool.* **30**: 114A.
- Balsler, E. J., and E. E. Ruppert. 1993. Ultrastructure of axial vascular and coelomic organs in comasterid feather stars (Crinoidea: Echinodermata). *Acta Zool.* **74**:87-101.
- Berridge, M. J., and J. L. Oschman. 1972. Pp. 1-91 in *Transporting Epithelia*. Academic Press, New York.
- Bulger, R. E. 1983. The urinary system. Pp. 869-912 in *Histology Cell and Tissue Biology*, L. Weiss, ed. Elsevier Science Publ. Co., New York.
- Bury, H. 1885. The metamorphosis of echinoderms. *Q. J. Microsc. Sci.* **38**: 45-131.
- Bury, J. I. 1889. Studies in the embryology of echinoderms. *Q. J. Microsc. Sci.* **29**: 407-449.
- Dan, K. 1968. Echinodermata. Pp. 280-315 in *Invertebrate Embryology*. M. Kume and K. Dan, eds. Prosveta Press, Belgrade.
- Erber, W. 1983. Zum Nachweis des Axialkomplexes bei Holothuriern. *Zool. Scripta.* **12**: 305-313.
- Giese, A. C., J. S. Pearse, and V. B. Pearse, eds. 1991. *Reproduction of Marine Invertebrates: Echinoderms and Lophophorates*, Vol. 6. The Boxwood Press, California. 808 pp.

- Hendler, G. 1991. Echinodermata: Ophiuroidea. Pp. 356-479 in *Reproduction of Marine Invertebrates: Echinoderms and Lophophorates*, Vol. 6. A. C. Giese, J. S. Pearse, and V. B. Pearse, eds. The Boxwood Press, California.
- Holland, N. D. 1991. Echinodermata: Crinoidea. Pp. 247-292 in *Reproduction of Marine Invertebrates: Echinoderms and Lophophorates*, Vol. 6. A. C. Giese, J. S. Pearse, and V. B. Pearse, eds. The Boxwood Press, California.
- Hyman, L. H. 1955. *The Invertebrates: Echinodermata*, Vol. 4. MacGraw-Hill Book Co., New York. 763 pp.
- Pearse, J. S., and R. A. Cameron. 1991. Echinodermata: Echinoidea. Pp. 514-624 in *Reproduction of Marine Invertebrates: Echinoderms and Lophophorates*, Vol. 6. A. C. Giese, J. S. Pearse, and V. B. Pearse, eds. The Boxwood Press, California.
- Ruppert, E. E., and E. J. Balsler. 1986. Nephridia in the larvae of hemichordates and echinoderms. *Biol. Bull.* 171: 188-196.
- Ruppert, E. E., and P. R. Smith. 1988. The functional organization of filtration nephridia. *Biol. Rev.* 63: 231-258.
- Smiley, S. 1986. Metamorphosis of *Stichopus californicus* (Echinodermata: Holothuroidea) and its phylogenetic implications. *Biol. Bull.* 171: 611-631.
- Smiley, S. 1989. The phylogenetic relationships of holothurians: a cladistic analysis of the extant echinoderm classes. Pp. 69-84 in *Echinoderm Phylogeny and Evolutionary Biology*, C. R. C. Paul and A. B. Smith, eds. Oxford Science Publ., England.
- Smiley, S., F. S. McEuen, C. Chafee, and S. Krishnan. 1991. Echinodermata: Holothuroidea. Pp. 664-732 in *Reproduction of Marine Invertebrates: Echinoderms and Lophophorates*, Vol. 6. A. C. Giese, J. S. Pearse, and V. B. Pearse, eds. The Boxwood Press, California.
- Welsch, U., and G. Rehkamper. 1987. Podocytes in the axial gland of echinoderms. *J. Zool.* 213: 45-50.

## Lime-Twig Glands\*: A Unique Invention of an Antarctic Entoproct\*\*

PETER EMSCHERMANN

*Fakultät für Biologie der Universität Freiburg, Biologie für Mediziner,  
Schänzlestr. 1, D 7800 Freiburg i.Br. BRD*

**Abstract.** Specialized glands that release formed secretions of a complex structure are known from several invertebrate phyla. A novel type of such an extrusive organ has been detected in the newly described Antarctic entoproct *Loxosomella brochobola* Emschermann, 1993 and is reported here. The specialized extrusive organs known from other invertebrates are generally unicellular, but these entoproctan glands are multicellular organs. The structured secretion of these glands is an extracellular product homologous to the body cuticle and is discharged in long sticky, hollow threads. In evolutionary convergence to the glutinant spirocysts of the Anthozoa, these threads are assumed—like set out single lime-twigs—to trap larger prey organisms inaccessible to the ciliary feeding current of the entoproct. Specialized glands of this kind have not been known previously in Entoprocta. This “invention” by a nanoplankton feeder must be seen as a specific adaptation to life in an environment that is poor in nanoplankton. *L. brochobola* was found exclusively on the inner, abfrontal surface of the tube-shaped, calcareous colonies of the bryozoon *Porella malouinensis* and shares this microhabitat only with some smaller predators, such as the hydrozoan *Halecium* sp.; no other ciliary feeders are present.

### Introduction

Based on the structure and function of their products, three major types of glands that extrude formed secretions

\* Lime-twigs, used even today in some countries to catch song-birds, are foot-long twigs or willow rods smeared with bird-lime (sticky plant extracts e.g., from mistletoe berries). Such lime-twigs, singly or in groups, are suspended in trees, fixed in hedges or simply stuck into the earth, and small birds adhere to them by their plumage.

\*\* These investigations have been supported by the Deutsche Forschungsgemeinschaft.

Received 11 January 1993; accepted 6 May 1993.

have been described in invertebrate animals. In all cases, these glands are unicellular. First, the well-known stinging and gluing cells (or nemato- and spirocysts) are the characteristic weapons of cnidarian polyps and medusae, especially arranged in batteries along their tentacles. These unicellular glands produce the most complicated glandular products in the animal kingdom: *i.e.*, intracellular capsules containing an invaginated, heavily convoluted, ejective tubule. Upon irritation, the capsule discharges a harpoon-like thread—poisonous or sticky—within a few milliseconds (Holstein, 1981; Tardent and Holstein, 1982; Holstein and Tardent, 1984).

The second type of such highly specialized gland cells are the colloblasts of the Ctenophora. The fishing tentacles of these predatory animals are laden with these glutinous cells that release sticky secretion granules. These, after secretion, remain fixed to the resilient cytoskeleton by bundles of microtubules, and so hold the stuck prey fast (Franc, 1978).

Finally, the so-called rhabdite and rhabdoid-forming gland cells, less spectacular in structure, occur in a variety of worm-like animal phyla, such as the Platyhelminthes (especially the Turbellaria) (Smith *et al.*, 1982), Gnathostomulida (Rieger and Meinitz, 1977), Gastrotricha (Rieger *et al.*, 1974), Nemertinea (Jennings and Gibson, 1969), and Archiannelida among annelids (Martin, 1978). Rhabdite cells are usually scattered over the epithelium covering the body surface or, in nemertineans, the proboscis. They release bundles of rhabdites, and are presumably under nervous control. Rhabdites are rod-like, membrane-bound bodies of lamellar ultrastructure. Upon extrusion by exocytosis, they contact the water and swell, either forming a protective gelatinous sheath around the animal, or enhancing the animal's adhesion to the substratum, or as in nemertineans, aiding the adhesion of prey to the pro-

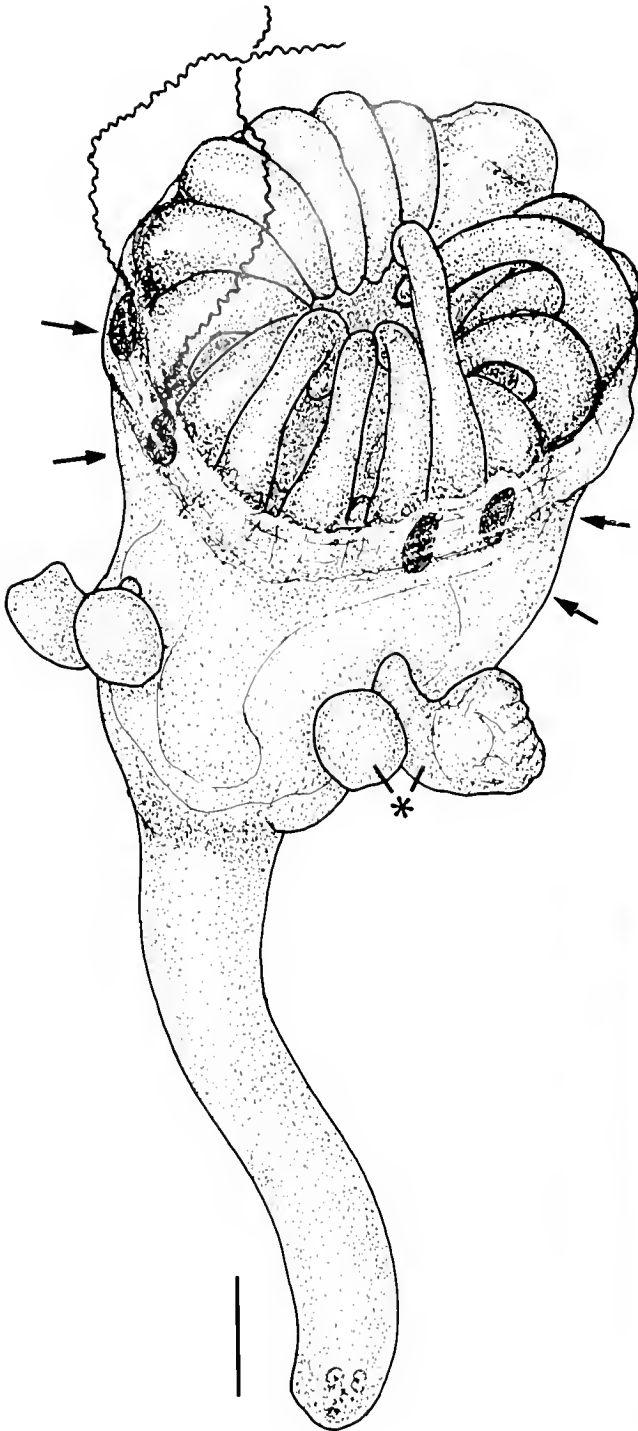


**Figure 1.** *Loxosomella brochobola* n.sp. seen from the oral side. The four lime-twig glands (arrows) are visible, and the pair at the left have discharged. Four zooid buds (\*) of different ages are seen at either side on the anterior body wall (Scale bar: 100  $\mu$ m).

boscis epithelium. Generally, animals with rhabdite cells are small, freely mobile predators that can readily benefit from such extrusive glands.

The newly detected extrusive organs of the Antarctic entoproct *Loxosomella brochobola* Emschermann, 1993 differ considerably from the above types in their genesis, as well as in their dimensions, structure, extruding mechanism, and function.

### Materials and Methods

The entoproct species bearing lime twig glands is a newly described species of Loxosomatidae discovered during the 1989/90 German Antarctic Expedition to the Weddell Sea (Emschermann, 1993). The animals were found exclusively at two locations in the northeastern Weddell Sea, at depths between 250 and 300 m, occurring in small groups of individuals only at the inner, abfrontal side of the tube-shaped colonies of the bryozoan *Porella malouinensis*. About 500 specimens were collected. Small numbers of specimens were kept alive on their original substratum and were examined under the stereo microscope, but these animals could not survive for longer than about 5–8 days under the conditions available aboard ship.

### Fixation and narcotization

Most of the specimens were fixed. For general morphological investigation, 4% formalin in seawater was used. For histological purposes, fixation was at room tem-

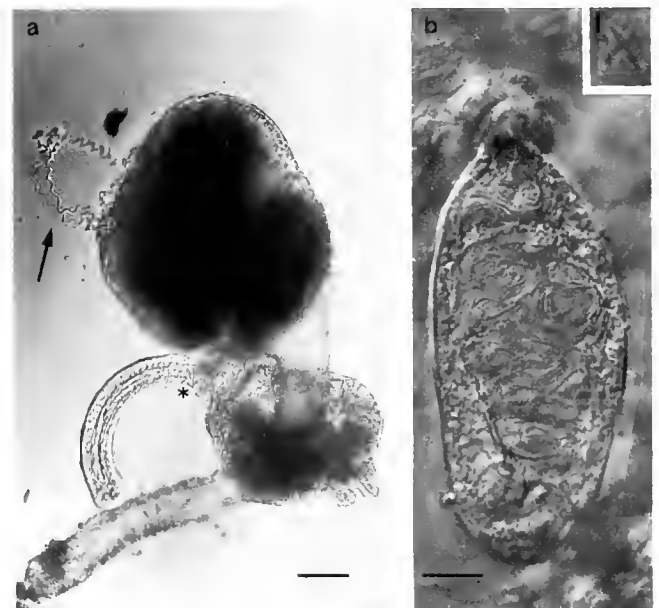


**Figure 2.** a: Specimen with its tentacles withdrawn and the lime-twig threads ejected (arrow). A large bud (\*) is seen at the base of the calyx; b: Isolated lime-twig gland with its invaginated, heavily coiled, dischargeable thread. At the bottom of the gland, in the marginal cytoplasm, one of the four nuclei is in focus. Inset: Optical cross section of the invaginated, hollow cuticular thread (diameter 3  $\mu$ m) with its cruciform lumen visible (Scale bars: a: 100  $\mu$ m; b: 10  $\mu$ m; Inset: 1  $\mu$ m).





**Figure 3.** Electron micrograph of a mature lime-twig capsule in longitudinal section. The coiled, invaginated extrudible tubule (arrows) is visible in the bottle-shaped gland, and a mucous cell (\*) is seen in the epidermis. The circled area is shown in higher magnification in Figures 4a and c (Scale bar: 10  $\mu$ m).

perature in a 2.5% buffered glutaraldehyde solution. Most of the animals were narcotized before fixation, which preserved them in an expanded state. A two-step narcotization gave the best results. First, several grains of the local anesthetic amyleine hydrochloride [Stovaine<sup>R</sup> Rhone Poulenc = 1 methyl-1-(dimethylaminomethyl)-propylbenzoate (hydrochloride)] were added to the jar containing the loxosomatids in about 3 ml of seawater. As soon as the animals were fully expanded, the seawater was replaced by an isotonic solution of  $MgCl_2$ . Amyleine blocks nervous conduction, whereas  $Mg^{++}$  ions prevent autonomous muscular contraction.

The glutaraldehyde fixation was unsatisfactory because, after narcotization, it caused a precipitation, and an adequate postfixation and embedding of the material was impossible aboard ship. Narcotized specimens fixed in formalin were excellently preserved for the general morphological and light microscopical investigation that was carried out in the laboratory at Freiburg. Fortuitously, the formalin-fixed samples turned out to be usable even for electron microscopy. But the preservation of most intracellular membranes, especially of ER-membranes and mitochondria, was not satisfactory, and most of the contents of vesicular compartments of the cells were washed

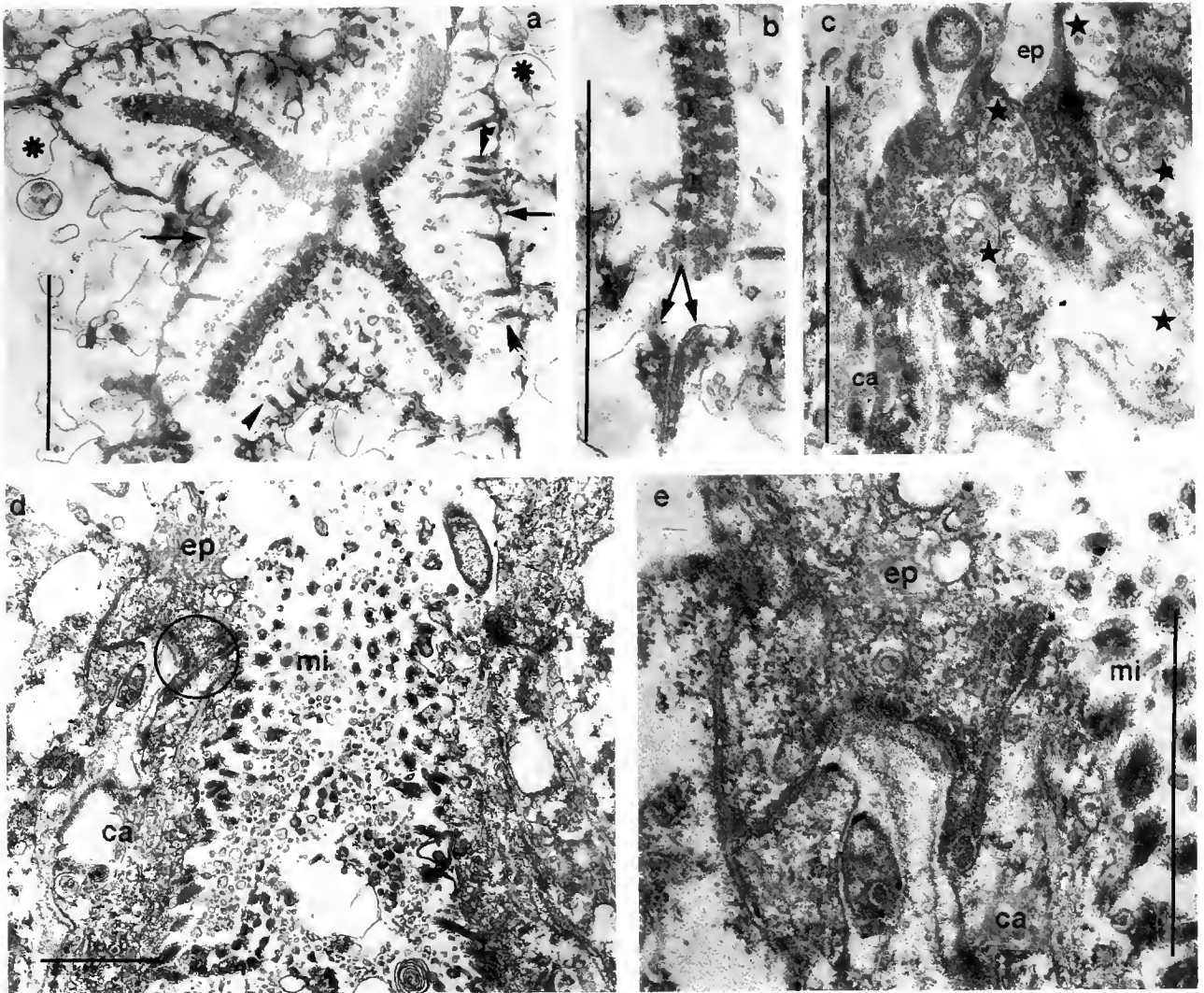


**Figure 4.** a: Cross section of the extrudible hollow thread; the cuticular core (arrows) is traversed by epithelial microvilli (arrowheads), and the cruciform luminal surface of the cuticular tube is decorated by the blister-like microvilli tips (double arrowheads); secretion vesicles (\*) are seen attached to the cytoplasmic side of the cuticular core. At the four edges of the cuticular core the membranes of the four adjacent capsular cells, connected by desmosomes, can be seen. b: Edge of one arm of the x-shaped cross section shown in a, demonstrating the subcuticular membranes of two adjacent capsular cells connected by desmosomes (arrows). c: Sectioned subepidermal nerve fibers (\*) beside the capsular neck, partly filled with synaptic vesicles; ca: capsular cell; ep: epidermal cell. d: Longitudinal section through the neck of a lime-twig capsule; at either side (circled area) desmosome-stabilized junctions between capsular cells (ca) and adjacent epidermal cells (ep) are seen; mi: microvillous border of capsular cells in the mouth funnel. e: Circled area of d in higher magnification showing interdigitations and desmosomes between capsular cell (ca) and epidermal cell (ep) (Scale bars: 1  $\mu$ m).

out, presumably because the material had been stored aboard ship in the fixative for several months before postfixation and embedding.

#### Microscopy

Microscopical investigations were carried out in Freiburg because shipboard microscopical work at

higher magnification turned out to be impossible. The light microscopical evaluation of the material was carried out with Zeiss-Nomarski interference contrast equipment. For ultrastructural examination, the specimens, after postfixation in buffered 2% OsO<sub>4</sub>, were embedded in Epon, sectioned with a diamond knife, and examined under a Zeiss EM 9A electron microscope.



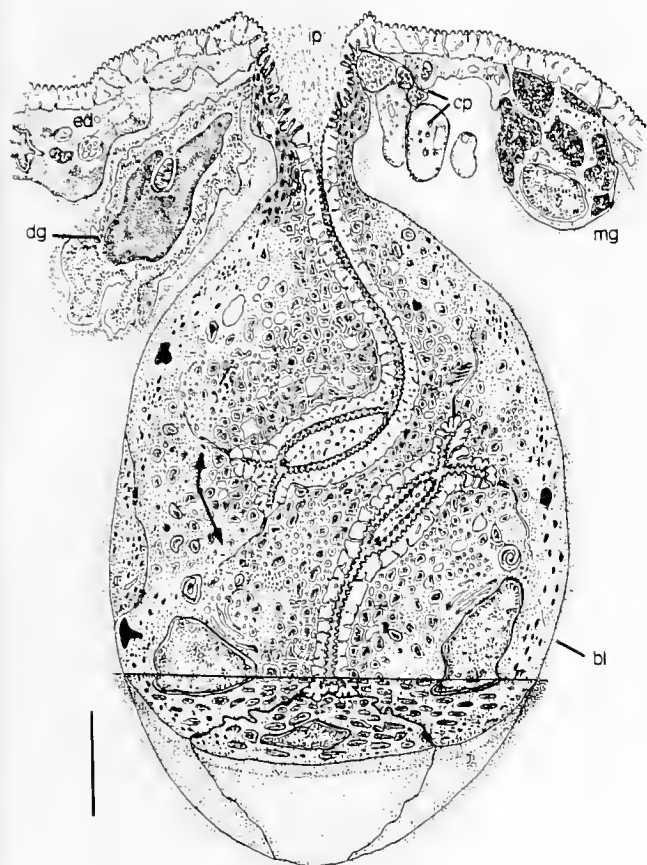


**Figure 5.** Scheme of an immature lime-twig capsule (reconstructed from serial sections). The already slightly coiled, invaginated cuticular tubule and, in cross sections of the latter, at the edges of the arms parts of the twisted membranes of the capsular cells (double arrow) can be seen; at the bottom, the borders of three of the four capsular cells and their nuclei are visible. bl: thickened basal lamina; cp: sectioned paracapsular nervous processes (shown at higher magnification in Fig. 4c); dg: remains of a degenerating discharged capsule; ed: epidermis covered by cuticle; ip: invagination pit with microvillous border, not covered by the tough cuticle (rupture zone); mg: epidermal mucous cell (Scale bar: 10  $\mu$ m).

### Observations

In their normal expanded posture, living zooids of *Loxosomella brochobola* have the peduncle slightly curved, with the oral side of the calyx tilted upward. Seen from above in this position, four large whitish-blue opaque blister-like structures are conspicuous, two on either side of the mouth between the bases of the second and third, and the third and fourth oral tentacles (Fig. 1). Spontaneously, or sometimes upon irritation, long (300–400  $\mu$ m), delicate, helically twisted threads can be ejected from these enigmatic blisters (Figs. 1, 2a). These stretchable sticky threads, hardly visible under the stereo microscope, are as long, or somewhat longer, than the expanded tentacles.

Floating outside the tentacular crown, they remain anchored with their proximal ends in the cells from which they originate. Under the light microscope, the mature extrusive organs are comparatively large, ovoid epithelial capsules, about 80  $\mu$ m long and 45  $\mu$ m wide (Fig. 2b), situated in the outer edge of the peritentacular epidermal fold (Fig. 1). At higher magnification, each capsule appears to be tightly filled by a highly coiled hollow thread or tube (Fig. 2b), the narrow lumen of which is cruciform in optical cross section (Fig. 2b, inset). The capsular cytoplasm is reduced to a narrow marginal layer with four nuclei in its basal portion (Figs. 2b, 5).

### Cellular structure of the lime twig capsule

In electron microscopic sections, the capsule appears bottle shaped (Fig. 3). In its central part, embedded in mainly vesicular contents, numerous sections of the coiled extrudible thread can be seen. The thread is roughly rectangular to X-shaped in cross section, about 3  $\mu$ m thick, and consists of an invaginated cuticular tube (Figs. 4a, 5). Its wall structure is exactly the same as that of the entoproctan epidermal cuticle: a tough glycoprotein layer traversed by epithelial microvilli (Emschermann, 1982). The inner surface of this cuticular tube, facing its cruciform lumen, is decorated by the densely staining, knob-like tips of the microvilli. On its cytoplasmic side, the cuticular tubule, below the subcuticular cell membranes, is densely coated with vesicles (Fig. 4a)—probably Golgi vesicles, as can be inferred by the presence of Golgi complexes in young, differentiating capsular cells (see Fig. 10). These vesicles are partly filled with electron-dense contents (Figs. 4a, 5, 9, 10). The membranes of four adjacent capsular cells connected by the remains of desmosomes (Fig. 4a, b) can be seen at the four edges of the cross-sectioned cuticular core of the invaginated tube. These cellular borders usually cannot be followed for a longer distance, as they are lost in the confusion of vesicle membranes around the tubule (Fig. 5).

In serial longitudinal sections, the four nuclei visible with the light microscope can be demonstrated in the capsular base (Fig. 5). The marginal cytoplasmic rim of the capsular cells has a fine granular structure and is rich in lumpy electron-dense material, possibly degenerating rough ER and storage vacuoles; in contrast, the density of secretion vesicles in this peripheral area is considerably decreased (Figs. 3, 5). Sometimes single multilamellar bodies, probably degenerating membrane complexes or fixation artifacts, can be observed. Because the formaldehyde fixation was inadequate, the remains of mitochondria could only occasionally be identified.

Apically, the capsule constricts like a bottle-neck (Figs. 3, 5) and, in this narrow zone of junction, the capsular

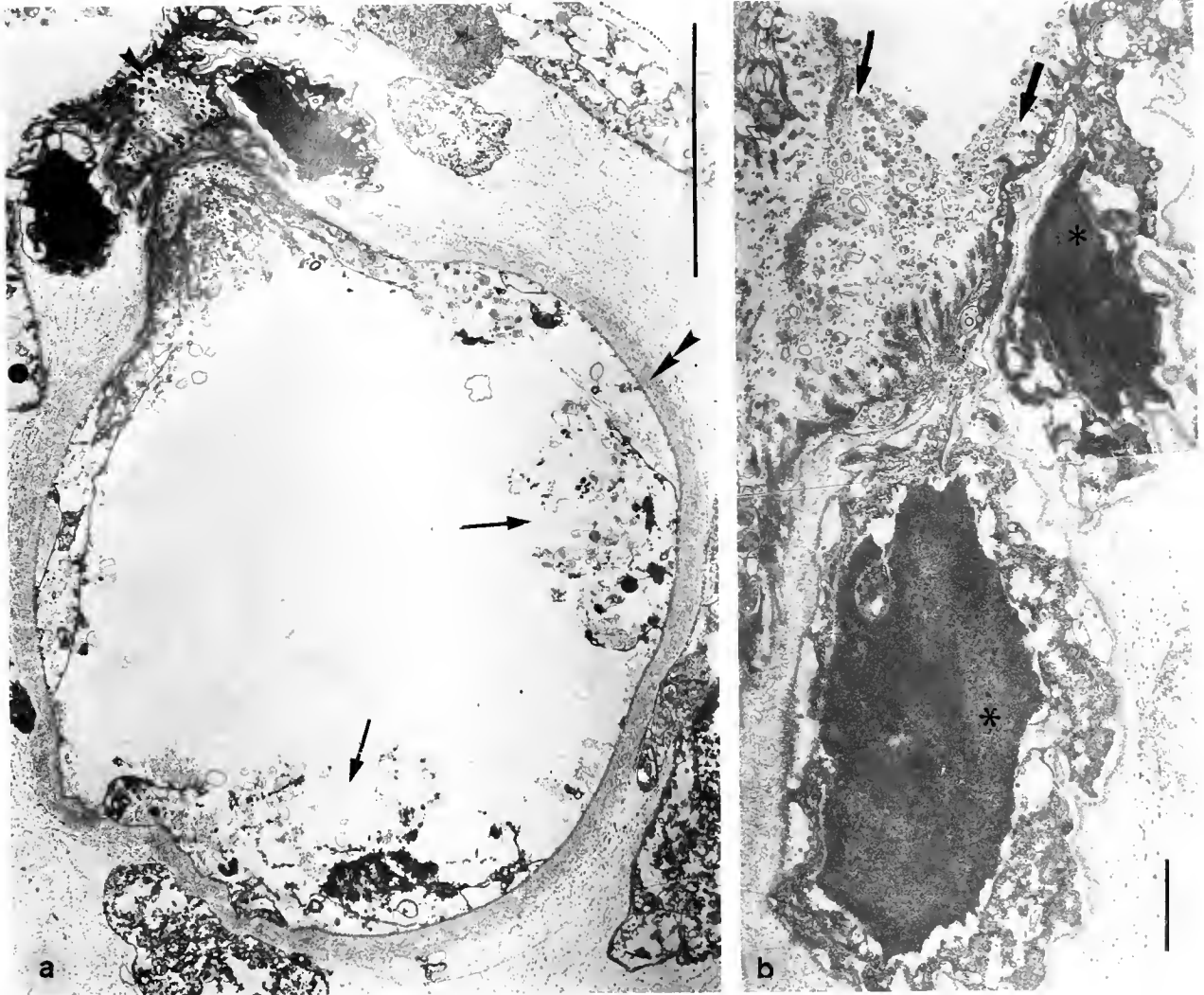


**Figure 6.** a: Electron micrograph of a discharged, empty lime-twig capsule; remnants of the marginal cytoplasm are seen in the capsular lumen (arrows); the invagination pit (arrowhead) is flanked at either side by the adjacent electron-dense residue of a degenerating capsule; the thickened basal lamina (double arrow heads) and a mucous cell in the body epidermis (\*) are also visible. b: Longitudinal sections through two degenerating, residual bodies of lime-twig capsules (\*) at higher magnification; with their upper ends they take part in the formation of the mouth funnel (arrows) of a younger lime-twig capsule. (Scale bars: a: 10  $\mu\text{m}$ ; b: 1  $\mu\text{m}$ ).

cells are connected to the adjacent, flattened epidermal cells by interdigitations and desmosomes (Fig. 4d, e). Specialized supporting cells—comparable, for example, to the supporting cells of enidarian nematocysts—are absent, as are sensory receptors at the capsular apex. The invagination area of the extrusive tubule is a narrow funnel-shaped pit in the epidermal surface. At the pit's outer margin, the tough body cuticle transforms abruptly into a loose mucous layer (a prospective rupture zone; *cf.*, Extrusion Mechanism). Apical membranes of the capsular

cells in this zone are lined by dense, branched microvilli. At the bottom of this pit, at the beginning of the invaginated tubule, the mucous layer is again replaced by the normal cuticular structure (Figs. 4d, 5, 7).

Towards the body cavity, each capsule is surrounded by a robust two-layered basal lamina (Figs. 5, 6, 7) consisting of an electron-dense inner layer about 30 nm thick, the normal subepidermal basement membrane, and a considerably thicker (300–400 nm) outer layer, which in tangential sections seems to have a filamentous structure.

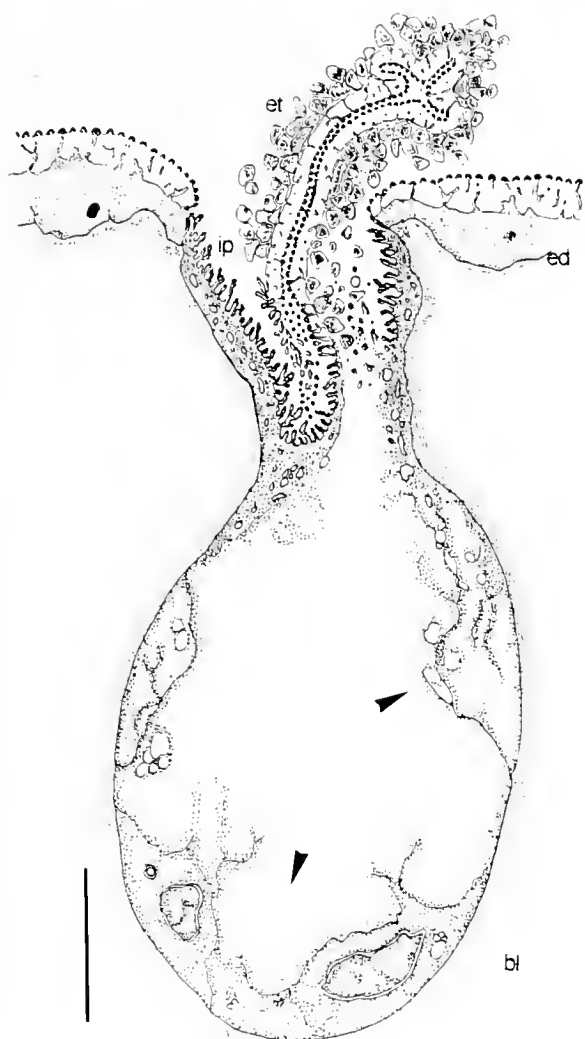


**Figure 7.** Scheme of a discharged lime-twig capsule; remnants of the marginal cytoplasm of the capsular cells (arrow heads) and, at the bottom, two of the nuclei are visible; bl: thickened basal lamina; ed: body epidermis covered by cuticle; et: extruded lime twig thread, discharged by a rupture of the apical cell membrane (at the right); ip: invagination pit with microvillous border, not covered by the tough cuticle (rupture zone) (Scale bar: 10  $\mu$ m).

In shrunken, discharged capsules this outer layer is about twice as thick (700–800 nm) and shows an increased electron density (Fig. 6a).

In several sections, beside the capsular neck, transversely sectioned single subepithelial nerve fibers can be seen (*cf.* Emschermann, 1982, 1985), some of which contain small vesicles resembling presynaptic vesicles (Figs. 4c, 5). However, additional indications of a synaptic connection between these nerve processes and the capsular cells, as well as any evidence of a nervous control of the lime-twig glands, are lacking.

*Discharged capsules* appear somewhat shrunken, but not collapsed (Figs. 6, 7). They are empty except for remains of the marginal cytoplasm and, basally, the degenerating nuclei. The extruded cuticular tubule is not evaginated (*i.e.*, everted like a glove finger as in the cnidarian spiro- and nematocysts), or released by exocytosis, as in rhabdocysts, rather it is ejected through a rupture of the apical cell membrane in the funnel area not covered by cuticle (Figs. 7, 8). After its ejection, the unfolded thread remains covered by a dense coat of the secretion vesicles described above (Figs. 7, 8). Gradually, the latter swell and give off their contents, forming a sticky mucous cover around the unfolding thread (Fig. 8).

Discharged lime-twig capsules are not reloaded. Sometimes, especially in older specimens, large electron-dense complexes of degenerating cells occur; usually from one to three of them at either side of the capsular neck (Figs. 5, 6). They look like extremely shrunken capsules. With their apical ends, these cell complexes take part in the formation of the mouth funnel of the adjacent capsule. These complexes are characterized by pycnotic nuclei and are surrounded by the same robust, but heavily folded basal lamina (Fig. 6b) as the mature capsules. Because these pycnotic complexes contain no trace of an invaginated thread, they are interpreted as degenerating residual bodies of older discharged capsules.

#### *The extrusion mechanism*

I observed neither nervous synaptic connections nor receptor structures associated with the capsular cells themselves (such as the cnidocil of the cnidarian nematocyst), nor specialized adjacent receptor cells. Therefore, the lime-twig thread probably is discharged automatically—for example through a rapid swelling of the mucous contents of the capsule as soon as the latter is mature—rather than by an external stimulus. Presumably triggered by an increased internal pressure, the apical cell membrane ruptures at its point of minimal resistance, *i.e.*, in the invagination funnel where it is not stabilized by an overlying cuticle (Figs. 5, 6b, 7). From the increased thickness and density of the basal lamina in the discharged capsule (Fig. 6a), one might infer that the outer filamentous layer of the lamina acts as an elastic coat and a buttress against the internal pressure.

#### *Development and replacement of lime-twig capsules*

Extrusive capsules in *Loxosomella brochobola* are already present in young, undetached buds. Later, in the adult, discharged capsules are replaced by new ones. In the vicinity of a capsule, sometimes enlarged, bulging ep-



**Figure 8.** a: Lime-twig thread, fixed during discharge but before its total unfolding, hidden under adhering masses of secretion vesicles except at the top right. Visible at the bottom (arrow head) is the rim of the capsular extrusion opening; at the top right (\*), between the secretion masses, the distal-most coiled part of the lime-twig thread is visible. b: Electron microscopic section through a loop of an ejected lime-twig thread; the cuticular core (arrows) is still covered by partly empty secretion vesicles (\*); inset: Part of an extruded lime-twig thread at higher light microscopic magnification (a and inset in b Nomarski contrast; scale bars: a: 100  $\mu\text{m}$ ; b and inset: 10  $\mu\text{m}$ ).

ithelial cells can be found (Figs. 3, 5, 6, 11b). Like the mucous cells of unknown function that occur in all loxosomatids (Emschermann, 1982; 1994) and are scattered between the normal, uniform epidermal cells in the tentacles and the periatrinal fold (Fig. 11a), these paracapsular cells in *L. brochobola* are characterized by large, tightly packed vacuoles full of an electron-dense, granular mucopolysaccharide material and by well-developed rough ER and Golgi complexes in the narrow plasmatic domains between them. Such epidermal mucous cell clusters in the vicinity of discharged capsules quite probably give rise to replacement lime-twig organs.

I have found different developmental stages of lime-twig capsules in most of the specimens examined. Capsule differentiation starts from a rosette of four enlarged epidermal cells (Fig. 9c, inset) bulging out slightly below the underside of the epidermal layer. They contain the same

large electron-dense vacuoles as the mucous cells mentioned above (Fig. 9a). Judging from their arrangement, these clusters each seem to arise from single "mother-cells," probably the above epidermal mucous cells.

The ejectible thread initially differentiates as a central cuticular pit which, step by step, invaginates centrally between the four prospective capsular cells. By the time a short finger-like cuticular tube has invaginated, increasingly small vesicles with electron-dense, non-granular contents are deposited around this growing tube, attached to the subcuticular cell membrane. Simultaneously the initial large vacuoles with their granular contents disappear (Figs. 9, 10). As the tubule increases in length, the four capsular cells twist around each other on their longitudinal axis, in the process curling the tubule into spiral loops (Fig. 5). In a later stage, the membranes between the four capsular cells seem to disappear, thus forming a

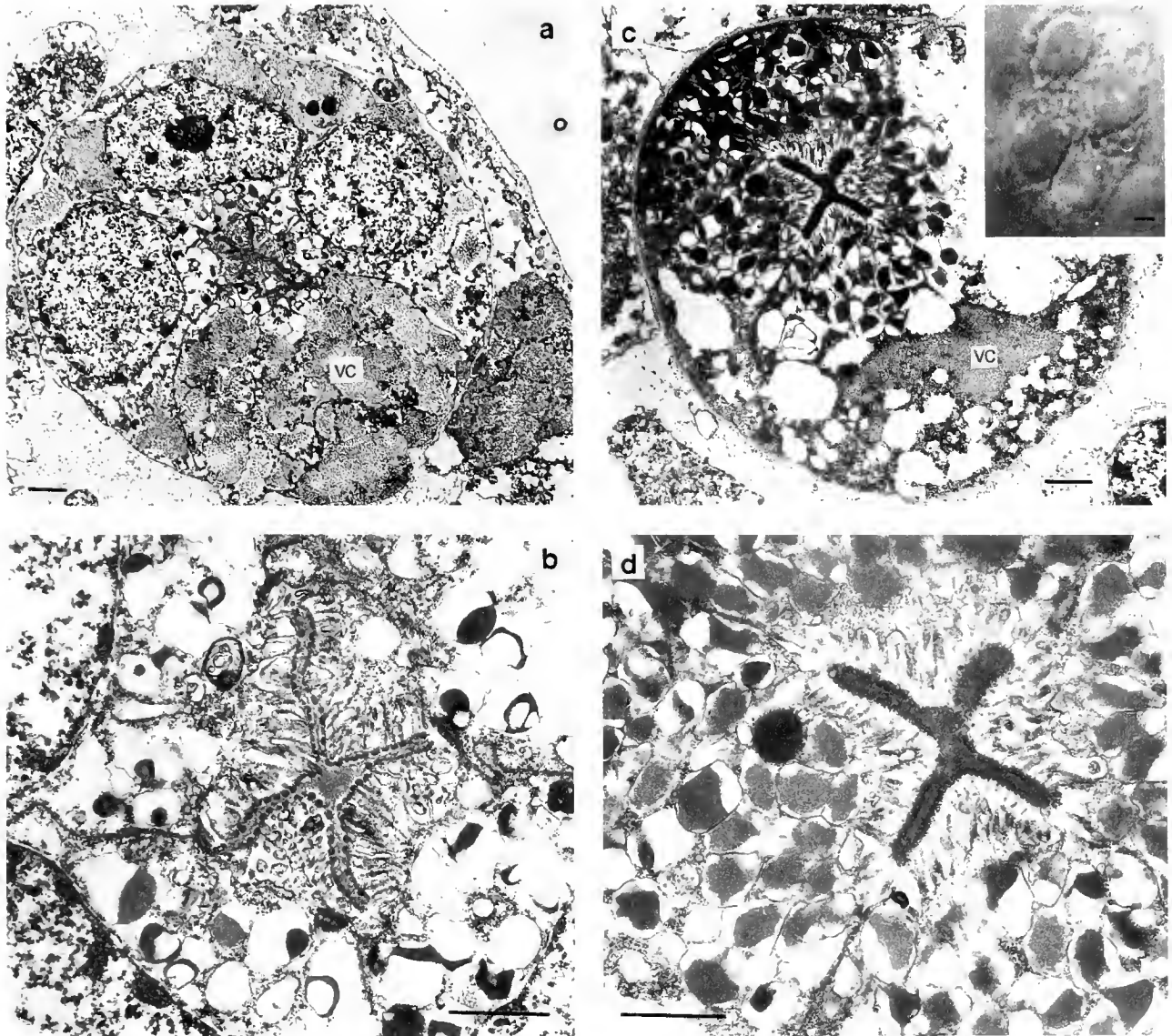


**Figure 9.** Electron microscopic cross sections of developing lime-twig glands. a: Early stage; in three of the capsular cells the nuclei are visible; in the fourth capsular cell are large storage vacuoles (vc). At the top right, bordered by the dotted line, are extremely flattened epidermal cells covered by the cuticle. b: Enlarged central part of a, with the developing extrudible tubule already surrounded by a few secretion vesicles and its luminal surface decorated by microvillous tips. c: Older stage of a developing capsule, the storage mucopolysaccharide vacuoles (vc) gradually disappearing and the electron-dense secretion vesicles increasing in number; d: enlarged central part of c, the cuticular tube surrounded by numerous secretion vesicles; inset in c a developing capsule in optical cross section appearing under light microscopy as a rosette of four enlarged epidermal cells (Scale bars: 1  $\mu$ m).

tetranuclear syncytium that surrounds the ever more coiling extrusive thread.

#### Functions, Origin, and Phylogenetic Relevance of the Lime-Twig Glands

The lime-twig capsules have been observed to extrude their threads, but the actual functioning of these sticky

threads has not yet been seen in living specimens of *Loxosomella brochobola*. Because these glands are arranged at either side of the mouth, they are most likely to be associated with feeding. As possible alternative or additional functions of these entoproctan extrusive glands, defense or locomotion might be taken into consideration. But this last role can be excluded in a sessile species that



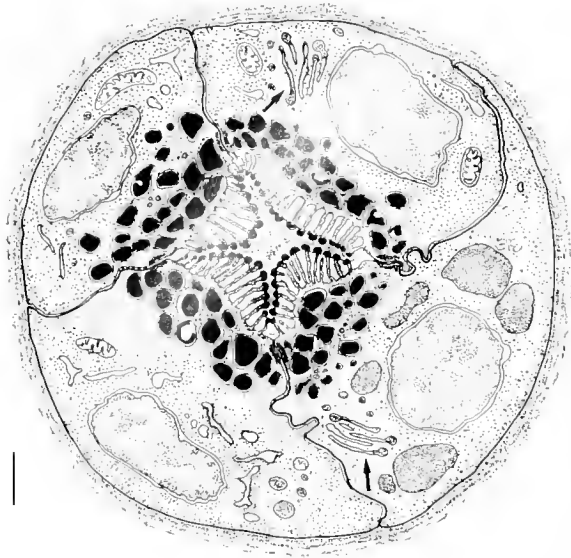


**Figure 10.** Schematic cross section through the basal region of a developing lime-twig gland: the cell at the right contains some early storage vacuoles. The arrows point to Golgi complexes (Scale bar: 1  $\mu\text{m}$ ).

lives irreversibly fixed to its substratum, and the limited number and localized arrangement of the lime twig capsules in a restricted body area speaks at least against their major defensive function. Most probably, the sticky threads act as lime-twigs, trapping larger planktonic food particles or sedentary organisms, both these being inaccessible to the entoproctan ciliary feeding apparatus. From time to time the threads with any adhering matter might be swallowed.

Indeed, *Loxosomella brochobola* was found living within bryozoan tubes in an environment that is extremely poor in nanoplankton, the normal food of *Loxosomatids*. This microhabitat is shared only with some smaller sessile predators such as the hydrozoan *Halecium* sp.; other ciliary feeders were absent. The stomach contents of about 100 specimens examined was consistent with the assumption that *L. brochobola*, at least facultatively, lives as a predator. In 50% of these specimens the stomachs were empty; the stomachs of the rest contained: a very few small, planktonic pennate diatoms; some larger cells, possibly ciliates and the eggs of other small invertebrates; occasional batches of conglomerated small (diameter about 10–12  $\mu\text{m}$ ), brownish-green corpuscles looking like plastids; a great variety of unidentifiable large skeleton fragments of diatoms; and single frustules of larger, non-planktonic pennate and central diatoms up to a size of 90  $\mu\text{m}$ .

Another observation is consistent with *Loxosomella brochobola* catching single larger food particles with its

lime-twig threads rather than being a true ciliary feeder: the tentacular cilia of this species, on average 30–40  $\mu\text{m}$  long, are conspicuously shorter than in most other *Loxosomatids* of comparable size. For example, in *Loxosomella antarctica*, a species living at the same locations but in other, more exposed habitats, the tentacular cilia have a length of 50–60  $\mu\text{m}$  on average. A comparison of the stomach contents of these two species revealed that the latter species feeds predominantly on microcellular material, such as bacteria and small algae. Even where larger sedentary diatoms were abundant and settled on the *Loxosomatid* stalks, they were found only occasionally in its digestive tract.

On the other hand, one would expect to find remains of the swallowed lime-twig threads in the gut of the lime-twig-fishing species; but tangled filamentous material (diameter about 2  $\mu\text{m}$ ) could be detected in the digestive tract of only a few specimens (30% of those with a filled gut), and these tangled threads could not be reliably identified as lime-twig threads, because they did not show the characteristic X-shaped cross section in the light microscope. Of course, the swallowed lime twigs may have already lost their original structure through digestion.

The multicellular or syncytial lime-twig cysts represent a new type of extrusive organ, unique in the animal kingdom. As evidenced by their genesis and structure, they are not homologous to other extruding glands such as the cnidarian spirocysts or the rhabdite-forming cells, and probably represent an isolated apomorphic character of this particular entoproctan species.

These highly specialized organs are most likely derived from mucous glands that occur in great variety in the epidermis of most *Loxosomatidae*, the most primitive group of Entoprocta. Mucous glands are seen in the calyx epithelium of the adult (Nielsen, 1966a, b; Emschermann, 1982, 1985, 1994), as well as in the larval episphere epithelium (Jägersten, 1964); but they seem to be generally lacking in higher, colonial entoproctan families. Mostly these entoproctan mucous glands are unicellular (Fig. 11a, b), and appear dispersed between normal epidermal cells. In some species, such unicellular glands aggregate to pluricellular, stratified plaques (Fig. 11c), which can secondarily invaginate to form subepithelial mucus alveoli, e.g., in *Loxosomella thethyae*, where conspicuous pearl-like alveolar glands (Fig. 12a) are arranged all around the tentacular crown (Salensky, 1877; Nielsen, 1988b). This type of invaginated mucous gland presumably presents the evolutionary basis for the formation of highly specialized glandular organs such as the enigmatic giant, bell-shaped aboral gland of *Loxosommella vivipara* (Nielsen 1966b; Emschermann, 1994) (Fig. 12b) and the lime twig capsules of *Loxosomella brochobola*, described here.

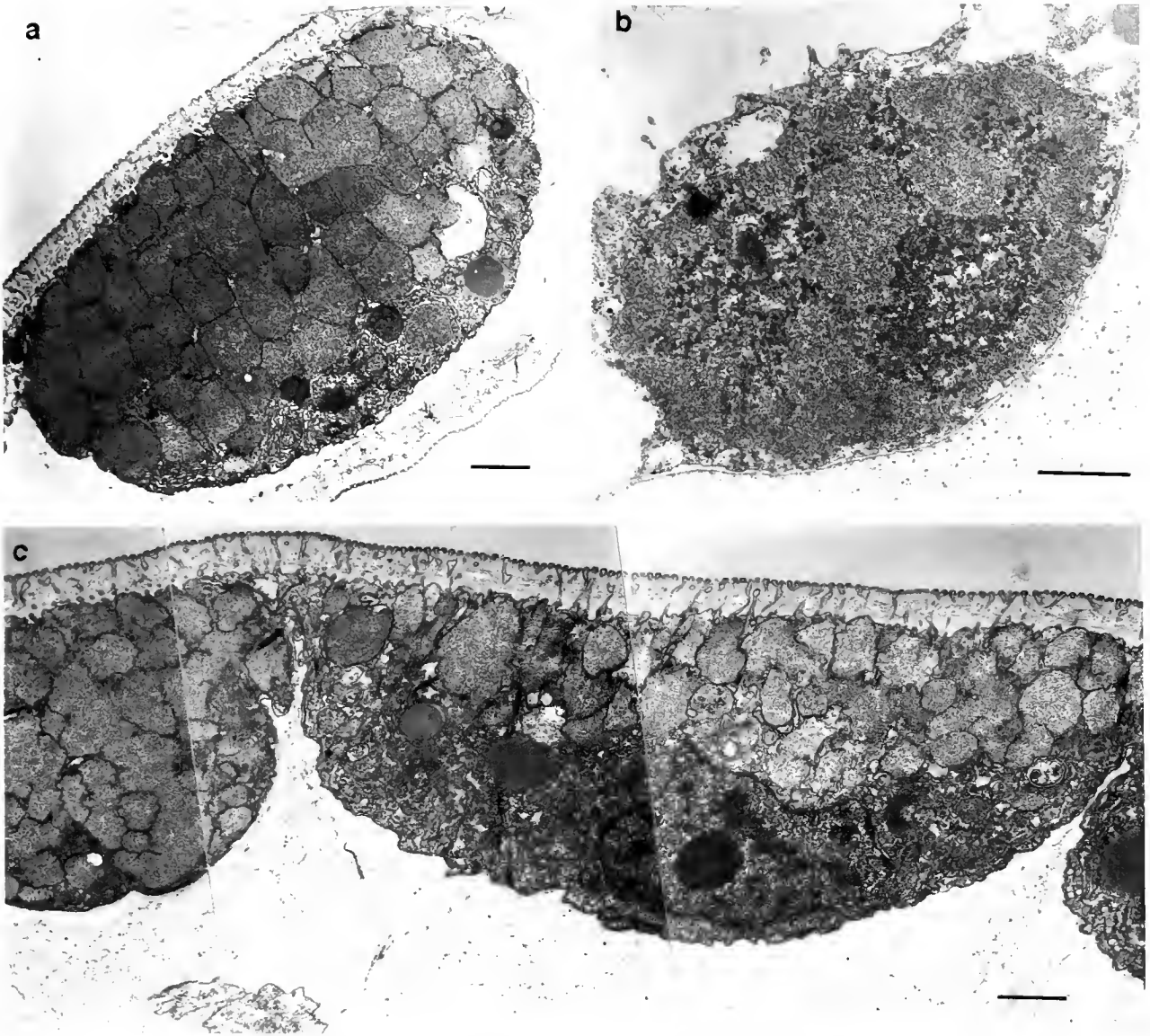


Figure 11. Epidermal mucous cells of Loxosomatidae. Single mucous cells of (a) *Loxosomella crassicauda* Salensky, 1877, and (b) *Loxosomella brochobola* (c) Stratified mucous plaque of *Loxosomella thethyae* Salensky 1877 (Scale bar: 1  $\mu$ m).

### Acknowledgments

I thank Mrs. S. Collatz for her skillful technical assistance and for taking most of the electron micrographs.

### Literature Cited

- Emschermann, P. 1982. Les Kamptozoaires. État actuel de nos connaissances sur leur anatomie, leur développement, leur biologie et leur position phylogénétique. *Bull. Soc. Zool. France* **107**: 317–344.
- Emschermann, P. 1985. Kamptozoa. In *Lehrbuch der Zoologie, vol. 2. Systematik*, R. Siewing, ed. Gustav Fischer, Stuttgart.
- Emschermann, P. 1993. On Antarctic Entoprocta—nematocyst-like organs in a loxosomatid, adaptive developmental strategies, host specificity, and bipolar occurrence of species. *Biol. Bull.* **184**: 153–185.
- Emschermann, P. 1994. Kamptozoa. In *Lehrbuch der speziellen Zoologie*, W. Westheide und R. Rieger, eds. Gustav Fischer, Stuttgart (in press).
- Franc, J. M. 1978. Organization and function of ctenophore colloblasts: an ultrastructural study. *Biol. Bull.* **155**: 527–541.
- Holstein, Th. 1981. The morphogenesis of nematocytes in hydra and forskälia. *J. Ultrastruct. Res.* **75**: 276–290.
- Holstein, Th., and P. Tardent. 1984. An ultrahigh-speed analysis of exocytosis: nematocyst discharge. *Science* **223**: 830–833.



**Figure 12.** a Alveolar, subepithelial mucous gland (\*) from *Loxosomella thethyae* Salensky, 1877 (inset, arrows point to the glands); b highly specialized, giant, bell-shaped mucous gland from *Loxosomella vivipara* Nielsen, 1964. This enigmatic, double-walled gland, situated in the aboral part of the peritentacular rim (see Inset, arrow), consists of an outer ring of about 16 cells and an inner one of 10–20 cells; its glandular lumen is filled by a mucous plug (Scale bars: a: 10  $\mu\text{m}$ ; b and Insets: 100  $\mu\text{m}$ ).

- Jägersten, G. 1964. On the morphology and reproduction of entoproct larvae. *Zool. Bidrag (Uppsala)* 36: 295–314.
- Jennings, J. B., and R. Gibson. 1969. Observations on the nutrition of seven species of rhynchoceolan worms. *Biol. Bull.* 136: 405–433.
- Martin, G. G. 1978. A new finding of rhabdites: mucus production for ciliary gliding. *Zoomorphologie* 91: 235–248.
- Nielsen, C. 1966a. On the life cycle of some loxosomatidae (Entoprocta). *Ophelia* 3: 221–247.
- Nielsen, C. 1966b. Some Loxosomatidae (Entoprocta) from the Atlantic coast of the United States. *Ophelia* 3: 249–275.
- Rieger, R. M., E. Ruppert, G. E. Rieger, and C. Schoepfer-Sterrer. 1974. On the fine structure of gastrotrichs with description of *Chordodasyis antennatus*, sp.n. *Zool. Scr.* 3: 219–237.

- Rieger, R. M., and M. Mainitz. 1977. Comparative fine structure study of the body wall in Gnathostomulida and their phylogenetic position between platyhelminthes and aschelminthes. *J. Zool. Syst. Evolut.-forsch.* 5: 9–34.
- Salensky, M. 1877. Etudes sur les Bryozoaires entoproctes. *Ann. Sci. Nat. sér. 6, Zool.* 5: 1–60.
- Smith III, J., S. Tyler, M. B. Thomas, and R. M. Rieger. 1982. The morphology of turbellarian rhabdites: phylogenetic implications. *Trans. Am. Microsc. Soc.* 101: 209–228.
- Tardent, P., and Th. Holstein. 1982. Morphology and morphodynamics of the stenotele nematocyst of *Hydra attenuata* Pall. (Hydrozoa, Cnidaria). *Cell Tissue Res.* 224: 269–290.



# Antho-RFamide Immunoreactivity in Neuronal Synaptic and Nonsynaptic Vesicles of Sea Anemones

JANE A. WESTFALL<sup>1,\*</sup> AND CORNELIS J. P. GRIMMELIKHUIJZEN<sup>2</sup>

<sup>1</sup>*Department of Anatomy and Physiology, Kansas State University, Manhattan, Kansas 66506,*  
and <sup>2</sup>*Zentrum Für Molekulare Neurobiologie, Universität Hamburg,*  
*Martinistr. 52, 2000 Hamburg 20, Germany*

**Abstract.** Antho-RFamide is a neuropeptide isolated from the sea anemone *Anthopleura elegantissima*. Antho-RFamide immunoreactivity was localized in four different populations of neuronal vesicles in the tentacle nerve plexus of *Anthopleura*. Small, opaque, neuronal vesicles, averaging 49 nm in diameter, were gold-labeled at two-way synapses. Heterogranular vesicles, averaging 184 nm in diameter, were gold-labeled in a neuronal swelling adjacent to a muscle cell process. These vesicles were similar in size to a third class of gold-labeled dense-cored vesicles. A fourth class of immunogold-labeled vesicles observed in neuronal swellings had light cores and averaged 129 nm in diameter. Using 5-nm gold particles, we observed a heavy labeling of the granular cores of the dense-cored vesicles, suggesting that the immunoreactivity is specific to the vesicle core. The ultrastructural demonstration of Antho-RFamide immunoreactivity in interneuronal synaptic vesicles, together with the immunofluorescence and electrophysiological studies of other investigators, suggest that Antho-RFamide plays a role in neurotransmission in sea anemones.

## Introduction

Phe-Met-Arg-Phe-NH<sub>2</sub> (FMRFamide) and Arg-Phe-NH<sub>2</sub> (RFamide) immunoreactivity is present in the nervous system of many invertebrate species, including coelenterates, suggesting a neurotransmitter or neuromodulatory function for peptides related to FMRFamide (Boer *et al.*, 1980; Grimmelikhuijzen *et al.*, 1992). A FMRFam-

ide-like peptide, Antho-RFamide (<Glu-Gly-Arg-Phe-NH<sub>2</sub>), isolated from the sea anemone *Anthopleura elegantissima* (Grimmelikhuijzen and Graff, 1986) and the sea pansy *Renilla köllikeri* (Grimmelikhuijzen and Groeger, 1987), has been demonstrated to play a role in neurotransmission or neuromodulation in sea anemones (McFarlane *et al.*, 1987, 1991; McFarlane and Grimmelikhuijzen, 1991) and sea pansies (Ancil and Grimmelikhuijzen, 1989). Antho-RFamide immunoreactivity has been found in neurons in the ectoderm of tentacles, in the oral disk, and in neurons located near the endodermal muscles of the sea anemone *Calliactis parasitica* (Grimmelikhuijzen *et al.*, 1988, 1992), but the subcellular location of the peptide is unknown.

Using the immunogold-labeling technique and an antiserum against RFamide, we have located RFamide-immunoreactive material in dense-cored vesicles in both neurites and nerve terminals of the freshwater coelenterate *Hydra littoralis* (Koizumi *et al.*, 1989). The chemical nature of this immunoreactive material is, however, unknown, except that it contains a C-terminal dipeptide amide similar to Arg-Phe-NH<sub>2</sub>. The aim of the present study was to determine the ultrastructural localization of a known sea anemone neuropeptide, Antho-RFamide, in neurons of *Anthopleura elegantissima*. Synaptic and nonsynaptic release sites have been demonstrated previously in sea anemones (Westfall, 1970, 1973; Peteya, 1973a, b; Quaglia, 1976; Quaglia and Grasso, 1986). FMRFamide-like immunoreactivity has been demonstrated in large dense-cored vesicles in the hydromedusa *Aglantha digitale*, but is not present in small clear vesicles at synapses (Singla and Mackie, 1991). In this study, we provide evidence for the presence of Antho-RFamide-like material in both synaptic and nonsynaptic granular vesicles.

Received 10 March 1993; accepted 12 May 1993.

\* To whom correspondence should be sent.

Abbreviations: BSA, bovine serum albumin; ddH<sub>2</sub>O, double distilled water; PBS, phosphate buffered saline.

### Materials and Methods

The tentacles of *Anthopleura elegantissima* (Bio-Marine Laboratories, Venice, California) were extirpated and extended with succinyl choline chloride, as suggested by C. DellaCorte, or placed directly in cold fixative for 1 or 2 h. A solution of 4% paraformaldehyde and 0.1% glutaraldehyde in 0.1 M phosphate-buffered saline (PBS; pH 7.6, 0.3 M NaCl) was used to fix various lengths of tentacles, which were rinsed in the same buffer, postfixed for 1 h in 1% OsO<sub>4</sub>, dehydrated in ethanol, rinsed in acetone, and embedded in a mixture of Epon and Araldite.

Thin sections of tentacles were cut with a diamond knife and mounted on Formvar-coated 100-mesh nickel grids. The sections were rinsed in doubly distilled water (ddH<sub>2</sub>O), then exposed to saturated sodium metaperiodate for 30 min to open antigenic sites. After a ddH<sub>2</sub>O rinse, the sections were exposed to normal goat serum diluted 1:20 with PBS-Tween-BSA buffer to block nonspecific antigenic sites. They were incubated for 1 h with rabbit antiserum # 177IV or 177IVA against Antho-RFamide diluted 1:500 with buffer. After rinsing in buffer, the sections were immunogold stained for 1 h in goat anti-rabbit IgG conjugated to 5-, 10-, or 15-nm gold particles, which were diluted in buffer 1:40. After rinsing in buffer with BSA, then in PBS, they were postfixed for 15 min in 2% glutaraldehyde in PBS and rinsed in ddH<sub>2</sub>O. The sections were further stained in 7% uranyl acetate in 70% ethanol, then in Reynold's lead citrate. The grids with sections were lightly coated with carbon and examined in a transmission electron microscope.

Antiserum 177 was raised in a rabbit against the sequence Tyr-Gln-Gly-Arg-Phe-NH<sub>2</sub> (Bachem, Bubendorf, Switzerland), which was coupled by carbodiimide to bovine thyroglobulin (Grimmelikhuijzen and Graff, 1986). Antiserum 177IVA was obtained by affinity chromatography of antiserum 177IV over a column containing Arg-Trp-NH<sub>2</sub> (Bachem) coupled to Sepharose. Cyanobromide-activated Sepharose was obtained from Pharmacia, and the coupling reaction was carried out according to a protocol supplied by the manufacturer. Antiserum 177IVA did not cross react with Antho-RWamide I (<Glu-Ser-Leu-Arg-Trp-NH<sub>2</sub>) or Antho-RWamide II (<Glu-Gly-Leu-Arg-Trp-NH<sub>2</sub>), as suggested by light microscopic examination of sphincter muscle sections of the sea anemone *Calliactis parasitica*, which is rich in Antho-RWamide immunoreactive neurons. Although Antho-RFamide antisera 177IV and 177IVA labeled the same type of small opaque vesicles at interneuronal synapses in the tentacles

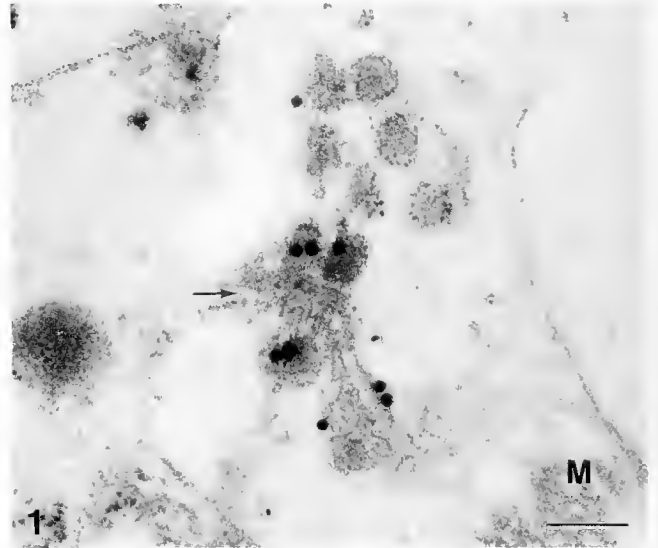


**Figure 1.** Antho-RFamide immunoreactivity in opaque vesicles on both sides of a two-way synapse in the tentacle nerve plexus of *Anthopleura elegantissima*. Note transverse filaments (arrow) in the synaptic cleft and 15-nm gold particles associated with the granular content of the neuronal vesicles. An adjacent muscle cell (M) lacks gold label. Scale bar = 0.1  $\mu$ m.

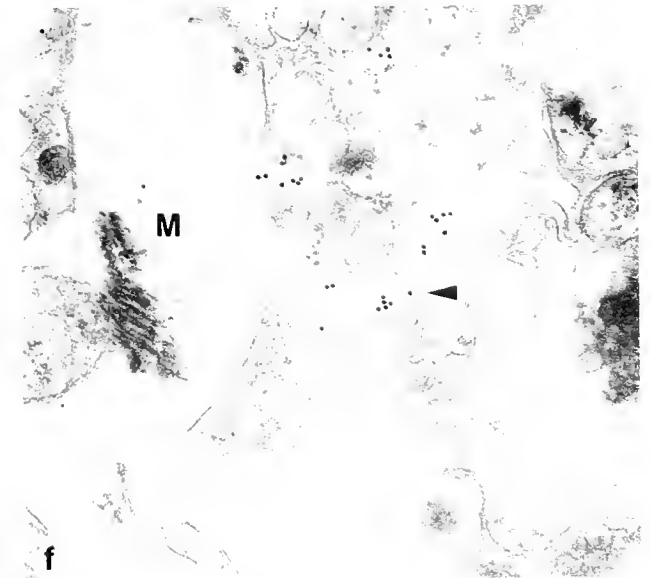
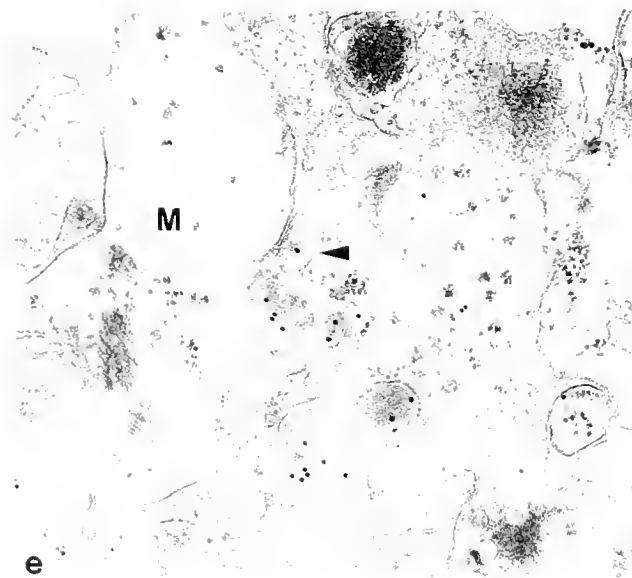
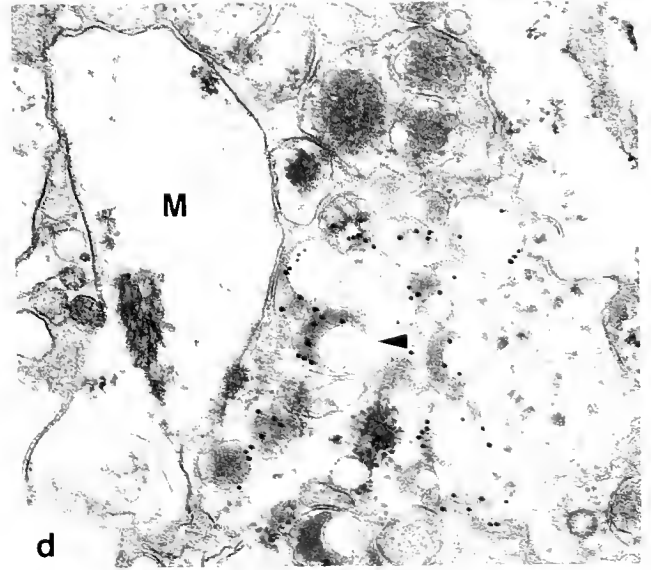
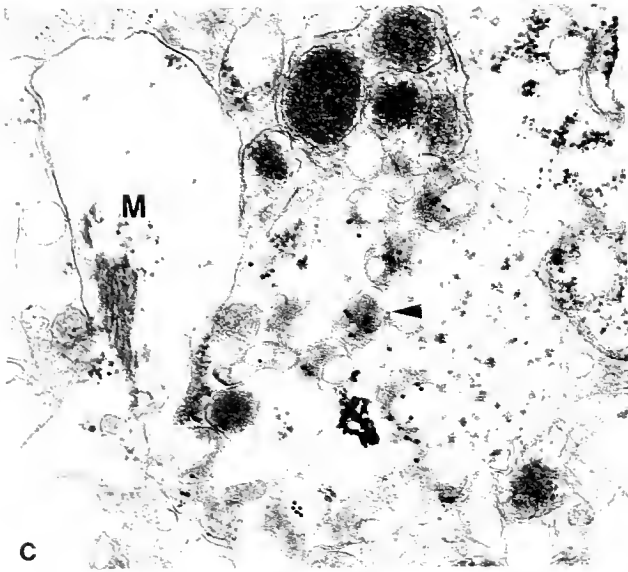
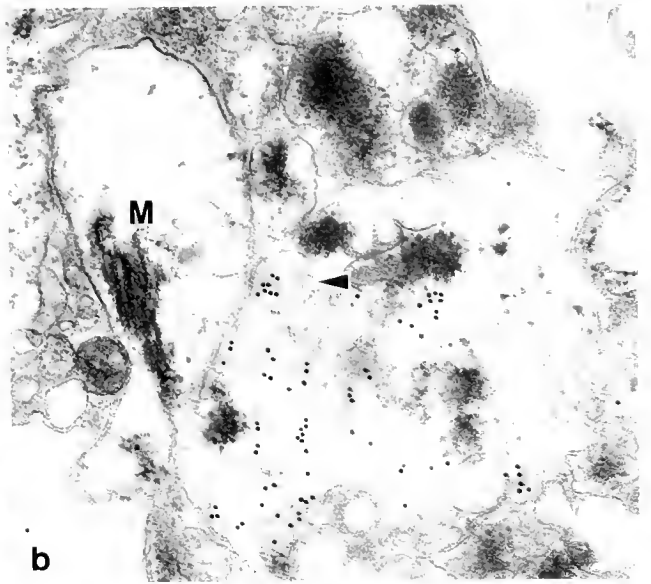
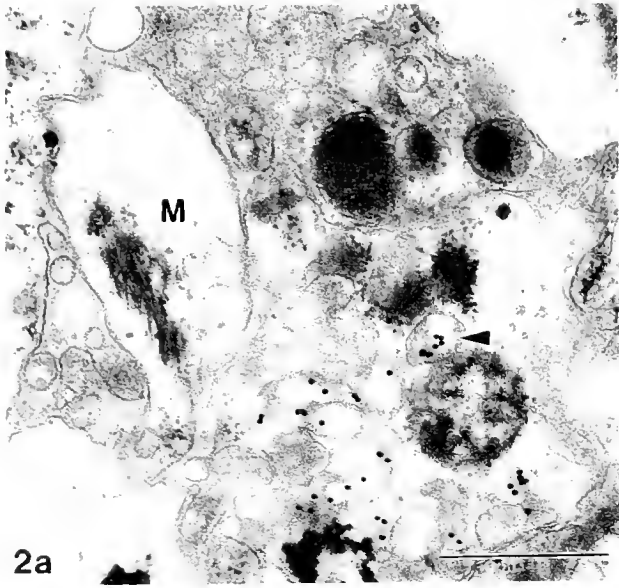
of *Anthopleura elegantissima*, most of the experiments were done with 177IV.

Control sections of the tentacle were exposed to Antho-RFamide antiserum (1:500) that had been incubated overnight in 10  $\mu$ g/ml of Antho-RFamide (Bachem, Bubendorf, Switzerland). Vesicle comparisons were made by measuring 10 or more vesicles of each type and analyzing the data with ANOVA.

### Results

Immunogold labeling of thin sections incubated with antisera against Antho-RFamide revealed gold particles in a variety of granular vesicles in the tentacle nerve plexus of the sea anemone *Anthopleura elegantissima*. Two-way (symmetrical) synapses containing labeled opaque vesicles were observed between neurons in two different tentacles. The paired synaptic membranes were characterized by paramembranous densities extending approximately 0.27  $\mu$ m in length and by an 18-nm-wide cleft containing a series of transverse filaments. In one synapse, gold-labeled opaque vesicles with an average diameter of  $49.15 \pm 2.33$  nm were found in close contact with both sides of the synaptic cleft (Fig. 1). Vesicles in two other symmetrical

**Figure 2.** Heterogranular vesicles (arrowheads) with 1-8 or more gold particles label consistently in six serial sections of a single nerve process (a-f). Note absence of gold label in adjacent muscle cell (M) contacted by at least one labeled vesicle (e). Scale bar = 0.5  $\mu$ m.



synapses were labeled on only one side of the synaptic complex. The 15-nm gold particles were located mainly over the opaque centers of the vesicles, but occasionally they were present on the synaptic and vesicular membranes.

Serial thin sections revealed immunogold labeling in six successive profiles of a nerve cell process with granular vesicles averaging  $184.43 \pm 5.11$  nm in diameter (Fig. 2a–f). The contents of these vesicles were heterogeneous. Some of the vesicles contained pale vacuolate spheres associated with granular crescents. We have termed such vesicles *heterogranular* to distinguish them from the more homogeneously granular, dense-cored vesicles described below. The successive profiles of the nerve process that was traced serially were in close contact with a cytoplasmic extension of a muscle cell, but no paired membrane thickenings indicative of a synaptic complex were present. In one section, a labeled vesicle appeared in close proximity to the muscle cell membrane (arrowhead, Fig. 2e), suggesting a possible paracrine release site. Although we have counted as many as eleven 15-nm gold particles in a single heterogranular vesicle, many vesicles had fewer or no gold particles.

A third population of gold-labeled neuronal vesicles contained a homogeneous dense core and a prominent halo between core and membrane (Fig. 3). The cores were approximately 120 nm in diameter and had a 20-nm halo in the nonflared region of the membrane. Often, the vesicular membrane was irregularly flared, probably as a result of fixation, making measurements difficult. The 10 dense-cored vesicles that we measured were  $181.20 \pm 6.11$  nm in diameter and were similar in size to the heterogranular vesicles. One to five 15-nm gold particles were present in some core profiles, whereas other particles occasionally were located on the vesicular membrane. Therefore, we used 5-nm gold particles to localize the labeled area more specifically. With the smaller sized gold, we counted 30 or more particles in several granular cores and only an occasional particle on the membrane (Fig. 4). This demonstrated that the Antho-RFamide-like material was confined to the granular cores.

Some neuronal swellings contained light-cored vesicles with irregular halos (Fig. 5). These vesicles tended to be smaller than the dark dense-cored vesicles and had an average diameter of  $129 \pm 4.47$  nm. We have termed this fourth population of vesicles *light-cored vesicles*.

Not all neurites containing granular vesicles were labeled, but this was to be expected because sea anemone neurons produce at least 16 different neuropeptides (Grimmelikhuijzen *et al.*, 1992).

We did not observe immunogold staining of granular vesicles in the control sections, which were exposed to primary antibody that had been incubated overnight with

Antho-RFamide (Fig. 6). In order to validate this control, we compared granular vesicles in serial sections of a nerve process (Figs. 5, 6).

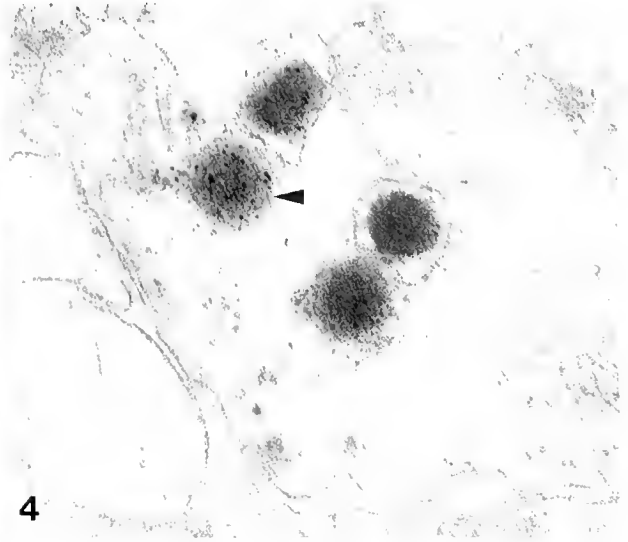
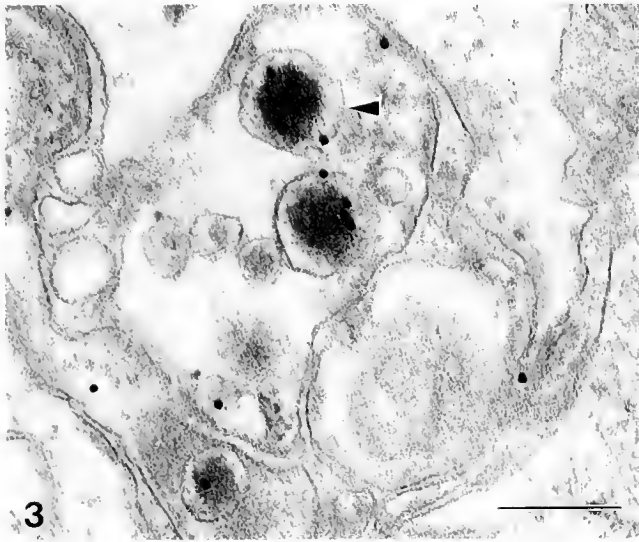
### Discussion

In the sea pansy *Renilla köllikeri*, Antho-RFamide causes tonic rachidial contractions in a dose-dependent fashion and hence is believed to play a role in neuromuscular transmission (Anctil and Grimmelikhuijzen, 1989). On the other hand, in the sea anemone *Calliaetis parasitica*, Antho-RFamide increases the frequency and amplitude of spontaneous contractions in endodermal muscles and also excites the slow conduction systems 1 and 2, which are believed to be neuronal, suggesting that the peptide may act at neuro-neuronal synapses (McFarlane *et al.*, 1987, 1991). Antho-RFamide also increases spontaneous contractions of isolated tentacles of the sea anemone *Actinia equina* (McFarlane and Grimmelikhuijzen, 1991). In the present ultrastructural study on the tentacle nerve plexus of the sea anemone *Anthopleura elegantissima*, Antho-RFamide immunoreactivity was present in small opaque vesicles associated with both sides of a two-way synapse. Our demonstration of gold-labeled interneuronal synapses therefore adds morphological support to the hypothesis that Antho-RFamide acts as a neurotransmitter at neuro-neuronal synapses in sea anemones.

FMRamide-like immunoreactivity has been demonstrated in neurons of the gastropod *Helix pomatia*, where granular vesicles of different sizes and homogeneity were selectively labeled by gold particles (Elekes and Ude, 1993). This variability in size and content of gold-labeled granular vesicles was also observed in the sea anemone *Anthopleura elegantissima* when antisera to Antho-RFamide were used. Based on granular size and appearance, neuronal vesicles containing Antho-RFamide material in the tentacle nerve plexus can be divided into at least four distinct subpopulations.

In *Helix*, many immunogold-labeled granular vesicles are present a short distance from the synaptic contact, which is usually aligned with clear vesicles that lack the gold marker and therefore lack peptides (Elekes and Ude, 1993). In contrast, in the sea anemone, gold-labeled opaque vesicles were present at interneuronal synaptic loci, supporting the concept that peptidergic neurotransmission is phylogenetically primitive (Grimmelikhuijzen *et al.*, 1992).

Symmetrical synapses with vesicles that are 50–100 nm in diameter and contain occasional electron-dense centers have been observed in the sea anemone *Metridium* (Westfall, 1970). The 49-nm opaque vesicles we found at symmetrical synapses are similar to those observed pre-

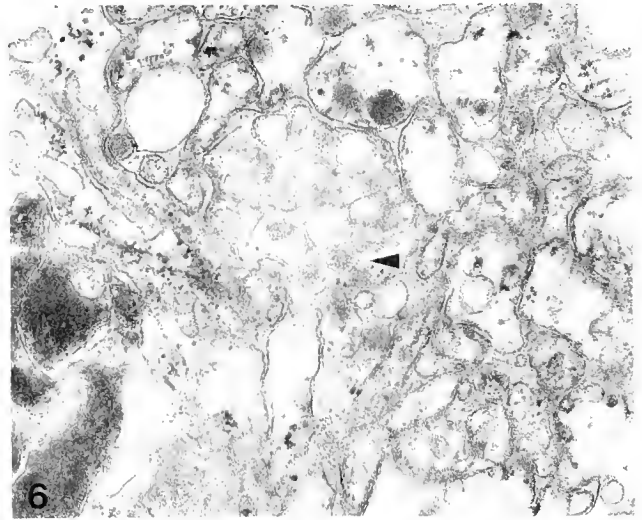
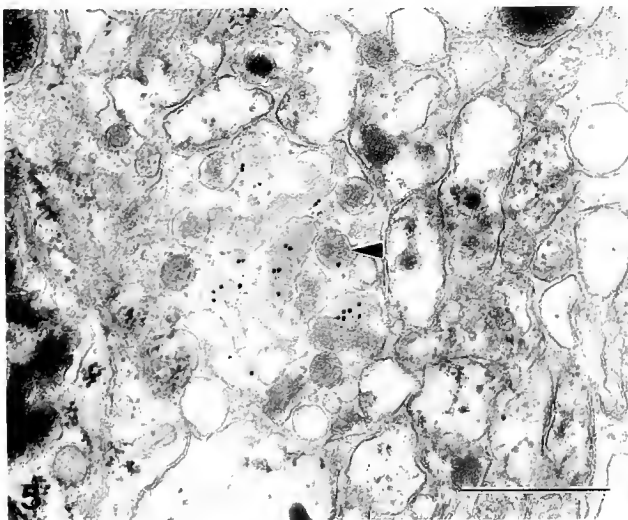


Figures 3 and 4. Comparison of dense-cored vesicles (arrowheads) labeled with 15-nm gold (Fig. 3) and 5-nm gold (Fig. 4) provides evidence that Antho-RFamide immunoreactivity is specifically located in the granular cores. Scale bar = 0.2  $\mu\text{m}$ .

viously in *Metridium*. Symmetrical synapses in coelenterates were first reported in the rhopalia of the jellyfish *Cyanea* (Horridge *et al.*, 1962; Horridge and Mackay, 1962) and were thought to transmit neuronal activity in two directions. The bidirectional nature of these chemical synapses in *Cyanea* motor neurons has been demonstrated electrophysiologically by Anderson (1985). The synaptic vesicles in the scyphozoan bidirectional synapses are relatively translucent with only a slight graininess and are 90–125 nm in diameter (Anderson and Grünert, 1988). Variations in size and core densities may be a result of

the coelenterate species studied and the fixation method used.

Not all granular vesicles in the nerve plexus of sea anemone tentacles are gold-labeled with antisera to Antho-RFamide, suggesting that additional putative transmitter substances may also be present. Each profile of a neurite contains only one type of granular vesicle. Electrophysiological experimentation has shown that a variety of other known sea anemone neuropeptides excite or inhibit tentacle contractions (Grimmelikhuijzen *et al.*, 1992; Carstensen *et al.*, 1992, 1993). Moreover, most of these



Figures 5 and 6. Comparison of experimental (Fig. 5) and control (Fig. 6) serial thin sections of a neuronal process with light-cored vesicles (arrowheads) provides further evidence of the specificity of antisera to Antho-RFamide for some neuronal granular vesicles. Scale bar = 0.5  $\mu\text{m}$ .

neuropeptides are produced by different sets of tentacle neurons (Grimmelikhuijzen, unpub.). Thus, the number of types of neuronal vesicles present in sea anemone tentacles remains unresolved, as does the number of types of putative transmitter substances, suggesting that neurotransmission in sea anemones may be highly complex.

### Acknowledgments

Contribution No. 93-300-J of the Kansas Agricultural Experiment Station. We thank Dr. C-Z. Yu and K. L. Sayyar for technical help and Dr. S. ThyagaRajan for statistical analysis. This study was funded by NSF grant IBN-9120161 and NIH grant NS-10264 to J. A. Westfall and by the Bundesministerium für Forschung und Technologie and the Deutsche Forschungsgemeinschaft to C.J.P. Grimmelikhuijzen.

### Literature Cited

- Anctil, M., and C. J. P. Grimmelikhuijzen. 1989. Excitatory action of the native neuropeptide Antho-RFamide on muscles in the pennatulid *Renilla köllikeri*. *Gen. Pharmacol.* **20**: 381-384.
- Anderson, P. A. V. 1985. Physiology of a bidirectional, excitatory, chemical synapse. *J. Neurophysiol.* **53**: 821-835.
- Anderson, P. A. V., and U. Grünert. 1988. Three-dimensional structure of bidirectional, excitatory chemical synapses in the jellyfish *Cyanea capillata*. *Synapse* **2**: 606-613.
- Boer, H. H., L. P. C. Schot, J. A. Veenstra, and D. Reichelt. 1980. Immunocytochemical identification of neural elements in the central nervous systems of a snail, some insects, a fish, and a mammal with an antiserum to the molluscan cardio-excitatory tetrapeptide FMRF-amide. *Cell Tissue Res.* **213**: 21-27.
- Carstensen, K., K. L. Rinehart, I. D. McFarlane, and C. J. P. Grimmelikhuijzen. 1992. Isolation of Leu-Pro-Pro-Gly-Pro-Leu-Pro-Arg-Pro-NH<sub>2</sub> (Antho-RPamide), an N-terminally protected, biologically active neuropeptide from sea anemones. *Peptides* **13**: 851-857.
- Carstensen, K., I. D. McFarlane, K. L. Rinehart, D. Hudman, F. Sun, and C. J. P. Grimmelikhuijzen. 1993. Isolation of <Gln-Asn-Phe-His-Leu-Arg-Pro-NH<sub>2</sub> (Antho-RPamide II), a novel, biologically active neuropeptide from sea anemones. *Peptides* **14**: 131-135.
- Elekes, K., and J. Ude. 1993. An immunogold electron microscopic analysis of FMRFamide-like immunoreactive neurons in the CNS of *Helix pomatia*: ultrastructure and synaptic connections. *J. Neurocytol.* **22**: 1-13.
- Grimmelikhuijzen, C. J. P., and D. Graff. 1986. Isolation of pGlu-Gly-Arg-Phe-NH<sub>2</sub> (Antho-RFamide), a neuropeptide from sea anemones. *Proc. Natl. Acad. Sci. USA* **83**: 9817-9821.
- Grimmelikhuijzen, C. J. P., and A. Groeger. 1987. Isolation of the neuropeptide pGlu-Gly-Arg-Phe-amide from the pennatulid *Renilla köllikeri*. *FEBS Lett.* **211**: 105-108.
- Grimmelikhuijzen, C. J. P., D. Graff, and A. N. Spencer. 1988. Structure, location and possible actions of Arg-Phe-amide peptides in coelenterates. Pp. 199-217 in *Neurohormones in Invertebrates*, M. C. Thorndyke and G. J. Goldsworthy, eds. Cambridge University Press, Cambridge.
- Grimmelikhuijzen, C. J. P., K. Carstensen, D. Darmer, A. Moosler, H.-P. Nothacker, R. K. Reinscheid, C. Schmutzler, H. Vollert, I. D. McFarlane, and K. L. Rinehart. 1992. Coelenterate neuropeptides: structure, action and biosynthesis. *Am. Zool.* **32**: 1-12.
- Horridge, G. A., and B. Mackey. 1962. Naked axons and symmetrical synapses in coelenterates. *Q. J. Microsc. Sci.* **103**: 531-541.
- Horridge, G. A., D. M. Chapman, and B. Mackey. 1962. Naked axons and symmetrical synapses in an elementary nervous system. *Nature* **193**: 899-900.
- Koizumi, O., J. D. Wilson, C. J. P. Grimmelikhuijzen, and J. A. Westfall. 1989. Ultrastructural localization of RFamide-like peptides in neuronal dense-cored vesicles in the peduncle of *Hydra*. *J. Exp. Zool.* **249**: 17-22.
- McFarlane, I. D., and C. J. P. Grimmelikhuijzen. 1991. Three anthozoan neuropeptides, Antho-RFamide and Antho-RWamides I and II, modulate spontaneous tentacle contractions in sea anemones. *J. Exp. Biol.* **155**: 669-673.
- McFarlane, I. D., D. Graff, and C. J. P. Grimmelikhuijzen. 1987. Excitatory actions of Antho-RFamide, an anthozoan neuropeptide on muscles and conducting systems in the sea anemone *Calliactis parasitica*. *J. Exp. Biol.* **133**: 157-168.
- McFarlane, I. D., P. A. V. Anderson, and C. J. P. Grimmelikhuijzen. 1991. Effects of three anthozoan neuropeptides, Antho-RWamide I, Antho-RWamide II and Antho-RFamide on slow muscles from sea anemones. *J. Exp. Biol.* **156**: 419-431.
- Peteya, D. J. 1973a. A light and electron microscope study of the nervous system of *Ceriantheopsis americanus* (Cnidaria, Ceriantharia). *Z. Zellforsch.* **141**: 301-317.
- Peteya, D. J. 1973b. A possible proprioceptor in *Ceriantheopsis americanus* (Cnidaria, Ceriantharia). *Z. Zellforsch.* **144**: 1-10.
- Quaglia, A. 1976. Osservazioni sul sistema nervoso degli antozoi. *Boll. Zool.* **43**: 397-398.
- Quaglia, A., and M. Grasso. 1986. Ultrastructural evidence for a peptidergic-like neurosecretory cell in a sea anemone. *Oebalia* **13**: 147-156.
- Singla, C. L., and G. O. Mackie. 1991. Immunogold labelling of FMRFamide-like neuropeptide in neurons of *Aglantha digitale* (Hydromedusae: Trachylina). *Can. J. Zool.* **69**: 800-802.
- Westfall, J. A. 1970. Synapses in a sea anemone *Metridium* (Anthozoa). *Electron Microscopy Proc. Int. Congr. 7th, Société Française de Microscopie Electronique, Paris* **3**: 717-718.
- Westfall, J. A. 1973. Ultrastructural evidence for neuromuscular systems in coelenterates. *Am. Zool.* **13**: 237-246.



## Hemoglobin Structure and Function in the Rat-Tailed Sea Cucumber, *Paracaudina chilensis*

SHIRLEY M. BAKER<sup>†</sup> AND NORA B. TERWILLIGER

*Oregon Institute of Marine Biology, University of Oregon, Charleston, Oregon 97420 and  
Department of Biology Eugene, Oregon 97403*

**Abstract.** The rat-tailed sea cucumber, *Paracaudina chilensis*, has abundant hemoglobin-filled hemocytes in its perivisceral coelom, water vascular system, and hemal system. The perivisceral oxyhemoglobin consisted of 34 kDa dimers and molecules with an apparent molecular weight of *ca.* 50 kDa. The perivisceral hemoglobin had a high oxygen affinity with a  $P_{50}$  of 1.5 mm Hg at 15°C. It exhibited cooperative oxygen binding with a Hill coefficient of 1.26 to 1.86. Oxygen affinity appeared to be pH dependent, but the effect was not significant. The heat of oxygenation was  $-11.2$  kcal mol<sup>-1</sup>. At high hemoglobin concentrations, the perivisceral hemoglobin oxygen affinity was lower and the apparent pH effect and cooperativity were increased. Perivisceral and water vascular hemoglobins had spectral characteristics similar to those of other invertebrate and vertebrate hemoglobins. The perivisceral hemoglobin appeared to be electrophoretically heterogeneous and was structurally distinguishable from water vascular hemoglobin. The oxygen affinity of water vascular hemoglobin was not different from that of the perivisceral hemoglobin in spite of the difference in structure and location in the animal. The exceptionally high oxygen affinity hemoglobin of *P. chilensis*, a burrowing sea cucumber, may be adaptive to this animal's oxygen-limited habitat.

### Introduction

Two orders of Holothuroidea, Dendrochirotida and Molpadiida, possess hemoglobin (Hb) in nucleated he-

mocytes (Howell, 1886; Hyman, 1955). Hemocytes may be present in one or more of the three holothurian body cavity systems: the perivisceral coelom, the water vascular system, and the hemal system. The perivisceral coelom, largest in volume, extends the length of the animal between the body wall and the digestive tract. The water vascular system includes the ring canal encircling the pharynx, the buccal podia ampullae, the polian vesicle, and the stone canal, which terminates in the coelom as a perforated madreporic plate. A mesh of contractile sinuses in the gut mesenteries and a ring around the pharynx constitute the hemal system (Hyman, 1955). The rat-tailed sea cucumber, *Paracaudina chilensis*, order Molpadiida, has abundant Hb in all three body cavities. The Hb is contained in nucleated hemocytes, 10–12  $\mu$ m in diameter and 4–6  $\mu$ m in thickness (Kawamoto, 1927).

Hyman (1955) considered the three body cavities in holothurians morphologically continuous, allowing exchange of blood cells and fluid. However, the existence of holothurian species with Hb in only one system suggests that the compartments are not continuous, at least with respect to the passage of hemocytes (Manwell and Baker, 1963; Roberts *et al.*, 1984). In holothurians with hemocytes in more than one system, the Hbs may or may not be electrophoretically distinguishable (Manwell and Baker, 1963; Terwilliger and Terwilliger, 1988). While all three body cavities of *P. chilensis* contain hemocytes, differences in hemocyte cell counts and the presence of other cell types specific to one compartment (Kawamoto, 1927) indicate that the body cavities may not be continuous in this species as well. The presence of dissimilar Hbs in distinct areas of an animal provides the possibility of complementary oxygen affinities and thus an oxygen transfer system (Manwell, 1960; Weber, 1980). Such oxygen transfer systems have been proposed to occur in some polychaetes (Terwilliger, 1974; Mangum *et al.*, 1975) and

Received 23 October 1992; accepted 4 May 1993.

<sup>†</sup> Present address: The College of William and Mary, Virginia Institute of Marine Science, School of Marine Science, Gloucester Point, VA 23062.

Abbreviations: Hb, hemoglobin; kDa, kiloDaltons; n, number of determinations;  $n_H$ , Hill coefficient of cooperativity;  $P_{50}$ , pressure of half saturation;  $P$  = calculated level of significance.



sipunculans (Manwell, 1960; Terwilliger *et al.*, 1985; Mangum and Burnett, 1987). Oxygen affinities of Hbs from separate compartments in holothurians have not been compared.

Molpadiid Hbs generally have relatively high oxygen affinities ( $P_{50} = 3.5$  to  $4.0$  mm Hg at pH 7.5 and  $20^{\circ}\text{C}$ ) and show cooperative oxygen binding (Hill coefficients,  $n_H = 1.45$  to  $1.60$ ) (Terwilliger and Read, 1972; Bonaventura and Kitto, 1973). The Hb properties may be correlated with the oxygen-limited habitat of these burrowing sea cucumbers. The only information on *P. chilensis* Hb function is a 1928 investigation by Kawamoto, who found that the Hb had a relatively lower oxygen affinity ( $P_{50} = 8.0$  mm Hg at  $20^{\circ}\text{C}$ ) and negative cooperativity ( $n_H = 0.82$ ). Hemoglobin concentration, pH, and other conditions used in the study were not reported. The absorption spectra reported for *P. chilensis* Hbs are similar to those of other Hbs, but the peaks were interpreted as shifted 4 nm towards the red with respect to vertebrate and other invertebrate Hbs (Kobayashi, 1932).

The structures of holothurian Hbs have been extensively examined and show interesting features compared to other Hbs. Holothurian Hbs are usually 34 kDa dimers that reversibly form tetramers or higher aggregates (6S) upon deoxygenation (Terwilliger and Read, 1970, 1972; Bonaventura and Kitto, 1973; Terwilliger, 1974; Bonaventura *et al.*, 1976). Aggregation states of holothurian Hbs may also vary with Hb concentration, association occurring at high Hb concentrations and dissociation at low concentrations (Bonaventura and Kitto, 1973; Terwilliger, 1975). Perivisceral Hb of *P. chilensis* has recently been separated into three globin fractions and the complete amino acid sequence of globin I determined (Suzuki, 1989). The sequence shows 59% homology with a major globin from another molpadiid sea cucumber, *Molpadia arenicola* (Mauri, 1985). Like other holothurian Hbs, *P. chilensis* Hb has a blocked n-terminus and an n-terminal extension of 9–10 residues relative to vertebrate globins.

Little more has been reported on the function of *P. chilensis* Hb since the studies by Kawamoto (1928) and Kobayashi (1932). One objective of this study, therefore, was to examine in detail the oxygen binding properties of the perivisceral Hb, including a determination of whether it is sensitive to homotropic or heterotropic effectors. We also compared the structure and function of Hbs from the perivisceral coelom and water vascular system.

### Materials and Methods

Specimens of *Paracaudina chilensis* (Müller) (10–40 g wet weight) were collected from the low intertidal zone of the protected muddy-sand beach at Sunset Bay, Coos Bay, Oregon. Animals were dissected immediately or kept

in sand filled aquaria under running seawater at the Oregon Institute of Marine Biology until use.

Perivisceral fluid was collected by slicing the animals along an interambulacral region and collecting the fluid in an ice-cold dish. Water vascular fluid was collected from the bright red polian vesicle which had been first rinsed to remove perivisceral fluid and then carefully removed from the animal.

Hematocrits were determined on perivisceral fluid according to Davidsohn (1962), and colorimetric determinations of total Hb content were performed according to the cyanmethemoglobin method (Sigma Procedure No. 525). Hematocrit and total Hb results were used to calculate the mean corpuscular Hb concentration (MCHC) (Davidsohn, 1962).

The fluids were centrifuged in a Sorvall RC2B refrigerated centrifuge at  $121 \times g$  for 10 min at  $4^{\circ}\text{C}$  to pellet the hemocytes. The hemocytes were washed three times in a saline buffer based on the ionic composition of seawater: 50 mM  $\text{Mg}^{++}$ , 10 mM  $\text{Ca}^{++}$ , 10 mM  $\text{K}^{+}$ , 540 mM  $\text{Cl}^{-}$ , 418 mM  $\text{Na}^{+}$ , 29 mM  $\text{SO}_4^{-}$ , 0.01 ionic strength Tris-HCl, pH 7.6. The hemocytes were gently lysed with a sintered glass homogenizer in a 1:100 dilution of saline buffer. Cell debris was pelleted by centrifugation at  $13,300 \times g$  for 10 min.

Hemoglobin was separated from small molecules and potential organic modulators by gel filtration on a Sephadex G-100 column ( $24.0 \times 1.8$  cm) in equilibrium with saline buffer. Changes of buffer for studies of the pH effect were accomplished by dialyzing the supernatant against saline buffer of the desired pH. Hemoglobin concentration was determined using a millimolar extinction coefficient at 578 nm of 14.2 (Terwilliger and Read, 1970).

Water vascular Hb was prepared essentially as described for the perivisceral sample except that the small volume of supernatant was not chromatographed in order to avoid diluting the sample. Perivisceral Hb, when used in comparisons with water vascular Hb, was prepared in the same manner.

Oxygen equilibrium experiments were performed as in Benesch *et al.* (1965) using tonometers equipped with 1 cm path length cuvettes and a Beckman DU 70 spectrophotometer. For concentrated samples (0.318 mM heme) and water vascular samples, tonometers equipped with 1 mm path length cuvettes, requiring only 0.3 ml of sample, were employed.

Oxygen binding characteristics of stripped and unstripped perivisceral Hb were compared. Stripped Hb was prepared as described above but was not dialyzed. Unstripped Hb was not separated from other molecules by gel filtration. Instead, unstripped Hb was prepared by diluting the supernatant of lysed cells with saline buffer, to the same Hb concentration as that of the stripped Hb. Stripped Hb was also examined in the presence of 0.15

mM organic phosphates: adenosine 5'-triphosphate (ATP), disodium salt; 2,3-diphospho-D-glyceric acid (2,3-DPG), pentasodium salt; and inositol hexaphosphoric acid (IHP), dodecasodium salt (Sigma Chem. Co.). When IHP was tested, the Hb sample was first dialyzed against a Tris-HCl buffer containing 550 mM  $\text{Cl}^-$  and 500 mM  $\text{Na}^+$ , because the addition of IHP to saline buffer resulted in precipitation.

For structural studies, hemocytes were obtained as described above. After centrifugation, washing, and lysing of the cells, the red supernatant was chromatographed on a Sephadex G-100 column ( $100 \times 1.8$  cm) in equilibrium with a 0.1 M sodium chloride, 0.1 M sodium phosphate buffer, pH 7.4. Spectra of elution fractions were measured with either a Zeiss PMQ-II or a Beckman DU-70 spectrophotometer.

Hemoglobins were analyzed by non-denaturing polyacrylamide gel electrophoresis (PAGE) and sodium dodecyl sulfate polyacrylamide gel electrophoresis (SDS PAGE). PAGE was carried out on oxy-, carboxy-, cyanmet-, and met-Hb samples on 1.5 mm slab gels, 7.5% acrylamide, with a discontinuous buffer system, pH 8.9 (Tris-glycine) as a cathodal buffer, and pH 8.1 (Tris-HCl) as the anodal buffer (Davis, 1964). Hemoglobins were prepared for SDS PAGE by incubation in 2% SDS, 5% mercaptoethanol, and 1 mM phenylmethylsulfonyl fluoride (PMSF) at 100°C for 1.5 min. Samples were electrophoresed on 1.5 mm slab gels, 12.5% acrylamide, with a continuous buffer system of pH 8.5 (Laemmli, 1970).

Analyses of variance were performed to test the significance of regressions of  $\log P_{50}$  and  $n_H$  versus pH. The slopes of none of the regressions were significantly different from zero ( $P = 0.099-0.989$ ). Therefore, for comparisons between treatments, oxygen binding data obtained at different pH were pooled. Results are reported as mean  $\pm$  standard deviation. Analyses of variance and Student's *t*-tests were performed to test the null hypotheses that treatment means were equal. For those analyses of variance in which the null hypothesis was rejected, Ryan's Q multiple comparison test was performed to determine between which treatment means differences existed. Statistical analyses were performed using Minitab (Minitab, Inc.).

## Results

Hematocrits of perivisceral fluid from 14 individuals of *Paracaudina chilensis* ranged from 0.6 to 3.5% with a mean of 1.5%. Hemoglobin concentration of the perivisceral fluid ranged from 0.04 to 0.74 g Hb  $\text{dl}^{-1}$  with a mean of 0.32 g Hb  $\text{dl}^{-1}$ . The mean corpuscular Hb concentration (MCHC) was 20.1 g  $\text{dl}^{-1}$  with a range from 4.5 to 34.0 g  $\text{dl}^{-1}$ . The means and ranges of these values are comparable to those of other holothurians (Roberts *et al.*, 1984).

The perivisceral Hb of *P. chilensis* has spectral characteristics similar to those of other Hbs, with no shift in wavelength observed. Spectral characteristics of water vascular Hb were indistinguishable from those of perivisceral Hb.

Oxygen binding properties of the perivisceral Hb at three temperatures and three heme concentrations are shown in Figures 1 and 2. The perivisceral Hb had a high oxygen affinity with a  $P_{50}$  of  $1.5 \pm 0.3$  mm Hg at 15°C. The oxygen binding was cooperative, with a Hill coefficient,  $n_H$ , greater than one under all experimental conditions examined ( $n_H = 1.26-1.86$ ). Although the slopes of the regressions of  $\log P_{50}$  versus pH were not significantly different from zero, there was a trend towards a slight normal pH dependence between pH 7.0 and pH 8.1;  $\Delta \log P_{50}/\Delta \text{pH}$  ranged from  $-0.08$  to  $-0.44$  as a function of temperature and heme concentration. The oxygen affinity of perivisceral Hb was significantly different at all three temperatures examined ( $P = 0.000$ ) while the cooperativity was not ( $P = 0.683$ ). Oxygen affinity decreased with increasing temperature. The heat of oxygenation,  $\Delta H$ , calculated using the Van't Hoff equation, and including the heat of solution of oxygen in water, was  $-11.2$  kcal  $\text{mol}^{-1}$  (Fig. 3). Both oxygen affinity and cooperativity of perivisceral Hb were significantly different at all three heme concentrations examined ( $P = 0.000$ ).

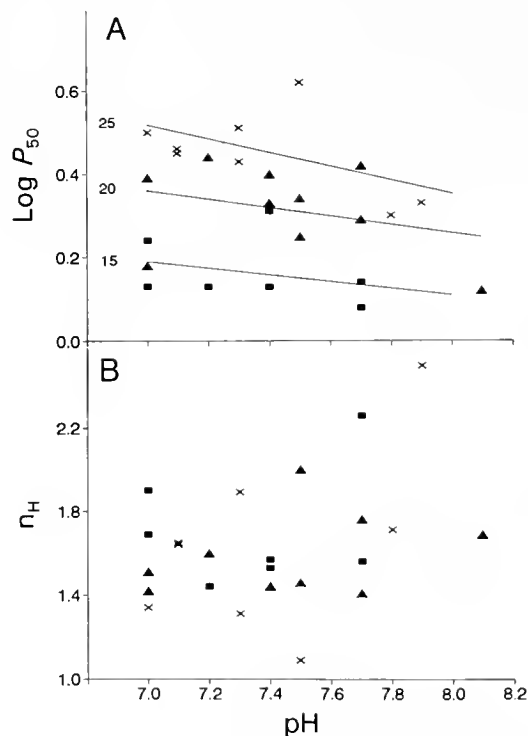


Figure 1. Oxygen affinity (A) and cooperativity (B) of perivisceral Hb of *Paracaudina chilensis* as a function of pH. Hemoglobin concentration, 0.057 mM heme. ■, 15°C; ▲, 20°C; ×, 25°C.

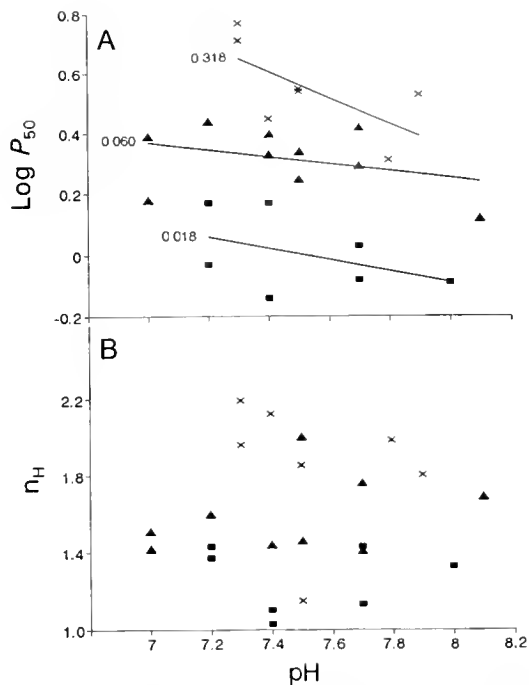


Figure 2. Oxygen affinity (A) and cooperativity (B) of perivisceral Hb of *Paracaudina chilensis* as a function of pH. Temperature, 20°C. ■, 0.018 mM heme; ▲, 0.060 mM heme; ×, 0.318 mM heme.

and 0.001, respectively). Oxygen affinity was lowest ( $P_{50} = 3.8 \pm 1.3$  mm Hg) and cooperativity most pronounced ( $n_H = 1.86 \pm 0.34$ ) at 0.318 mM heme, the highest Hb concentration examined (Fig. 4).

The oxygen affinities of stripped perivisceral Hb, unstripped Hb, and Hb to which ATP or 2,3 DPG had been added, were not significantly different ( $P = 0.165$ ) (Table I). The oxygen affinity of Hb to which IHP had been added was not significantly different from that of the control ( $P = 0.790$ ). The results of this experiment, in which a buffer free of calcium and magnesium was used, suggest that either IHP and divalent cations have opposite effects or divalent cations do not affect *P. chilensis* Hb oxygen affinity. Given the insensitivity of *P. chilensis* Hb to ATP and DPG, the latter is the most likely possibility.

Water vascular Hb had oxygen affinity and cooperativity values which were not significantly different from oxygen binding data obtained from perivisceral Hb samples treated in the same way ( $P = 0.690$  and 0.600 for  $P_{50}$  and  $n_H$ , respectively) (Table I).

The result of gel chromatography on Sephadex G-100 of perivisceral oxyHb is shown in Figure 5. The main Hb peak, HbII, corresponded to a protein with an apparent molecular mass of 34 to 36 kDa. The curve was asymmetric with a leading shoulder peak, HbI, that had an apparent molecular mass of about 50 kDa. *Cucumaria miniata* oxyHb chromatographed as a 34–36 kDa sym-

metrical peak on the same column. Chromatography of Hb samples from 12 animals indicated that different individuals had slightly different ratios of HbI and HbII. There were no apparent spectral differences between the two peaks. When dilute HbI and HbII were rechromatographed separately on the same column, each maintained its elution position, suggesting the peaks were neither associating nor dissociating.

Electrophoresis of perivisceral HbI and HbII on PAGE at pH 8.9 showed differences in banding patterns in both met and cyanmet ligand states (Fig. 6). Although we are unable at present to interpret the bands as subunits or multiples thereof, the two fractions are different under these conditions. Each fraction had an apparent subunit molecular weight, as determined by SDS-PAGE, of about 17 kDa. Only one band was resolved on SDS-PAGE for each peak as well as for a mixture of the two samples. Electrophoretic properties of unpurified perivisceral and water vascular carboxyHbs were compared by PAGE (Fig. 7, top). Both samples appeared to have several Hb bands and one non-heme containing band in common. One additional Hb band was evident in the water vascular Hb sample. Heme-containing bands were red prior to staining with Coomassie Brilliant Blue. After staining, an additional band, #5, was present which was equal in Coomassie staining intensity to the heme-containing bands (Fig. 7,

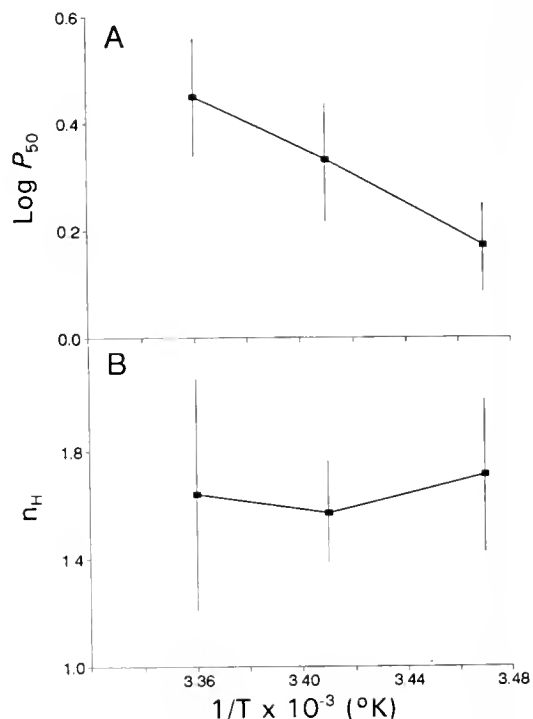


Figure 3. The effect of temperature on oxygen affinity (A) and cooperativity (B) of perivisceral Hb of *Paracaudina chilensis* expressed as a van't Hoff plot. Hemoglobin concentration, 0.057 mM heme.

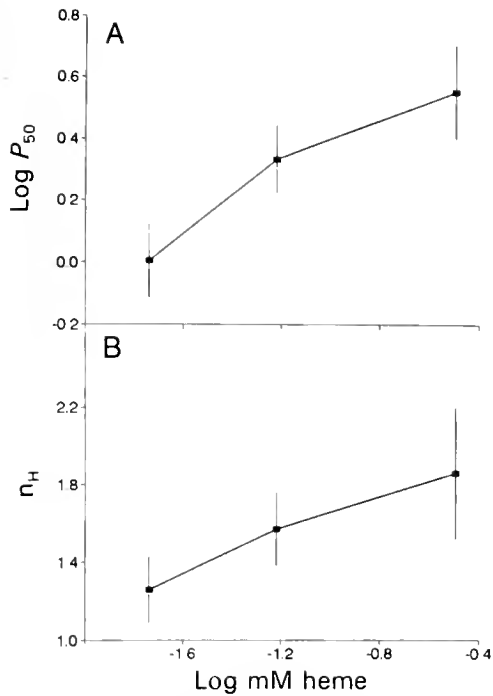


Figure 4. Concentration effect. Oxygen affinity (A) and cooperativity (B) of *Paracaudina chilensis* perivisceral Hb in relation to Hb concentration. Temperature, 20°C.

top). When the heme-containing protein bands from PAGE were cut out and re-electrophoresed on SDS-PAGE, only one 17 kDa band was observed (Fig. 7, bottom). The non-heme-containing bands in both perivisceral and water vascular samples electrophoresed in SDS-PAGE as 16 kDa components.

Table I

Oxygen affinity and cooperativity of Hb of *Paracaudina chilensis*

Condition	n	P <sub>50</sub> <sup>a</sup>	n <sub>H</sub> <sup>a</sup>
Perivisceral Hb in saline buffer <sup>b</sup>			
unstripped	4	3.0 ± 0.54	1.86 ± 0.24
stripped	4	2.1 ± 0.37	1.66 ± 0.28
stripped, 0.15 mM ATP	4	3.5 ± 1.36	1.71 ± 0.17
stripped, 0.15 mM 2,3-DPG	2	2.5	1.78
Perivisceral Hb in buffer free of Ca <sup>++</sup> and Mg <sup>++</sup> <sup>c</sup>			
stripped	3	3.1 ± 0.70	1.85 ± 0.22
stripped, 0.15 mM IHP	4	3.2 ± 0.28	1.80 ± 0.09
Hb in saline buffer <sup>d</sup>			
perivisceral	6	2.3 ± 0.14	2.01 ± 0.19
water vascular	6	2.2 ± 0.55	1.89 ± 0.50

<sup>a</sup> Mean ± standard deviation.

<sup>b</sup> pH 7.5–7.7, 20°C, 0.061 mM heme.

<sup>c</sup> pH 7.5, 20°C, 0.059 mM heme.

<sup>d</sup> pH 7.3–7.7, 20°C, 0.060 mM heme.

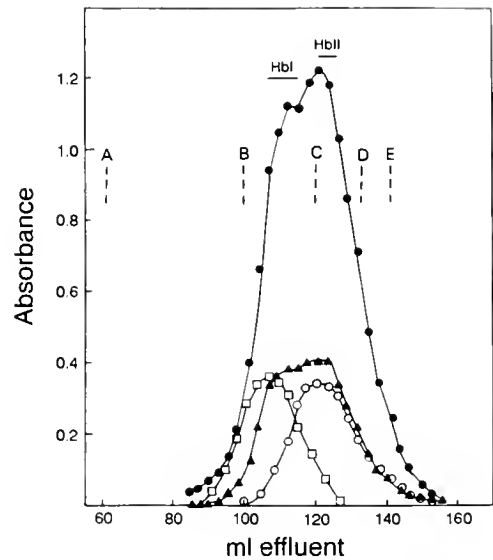


Figure 5. *Paracaudina chilensis* perivisceral Hb chromatographed on Sephadex G-100 column. Buffer, 0.1 M sodium phosphate, pH 7.4. Absorbance at 280 nm (●) and 540 nm (▲). Peak Hb-I rechromatographed, absorbance at 418 nm (□); Peak Hb-II rechromatographed, absorbance at 418 nm (○). Void volume: A, Blue dextran. Calibrants: B, Bovine serum albumin; C, *Cucumaria minuta* oxyHb; D, α-chymotrypsinogen; E, Sperm whale myoglobin.

## Discussion

One novel feature of the perivisceral Hb of *Paracaudina chilensis* is that the molecular weight is heterogeneous in the oxy-state. While other holothurian oxyHbs consist entirely of 34 to 36 kDa dimers in the oxy-state (Roberts *et al.*, 1984), *P. chilensis* oxyHb consisted of 34 kDa di-

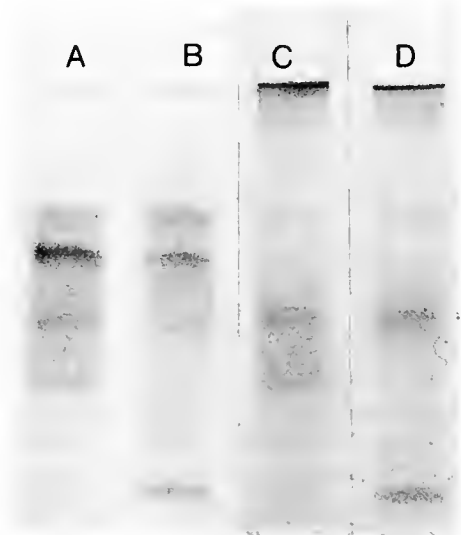


Figure 6. PAGE of *Paracaudina chilensis* perivisceral Hbs, pH 8.9. A, cyanmet HbI; B, cyanmet HbII; C, met HbI; D, met HbII.

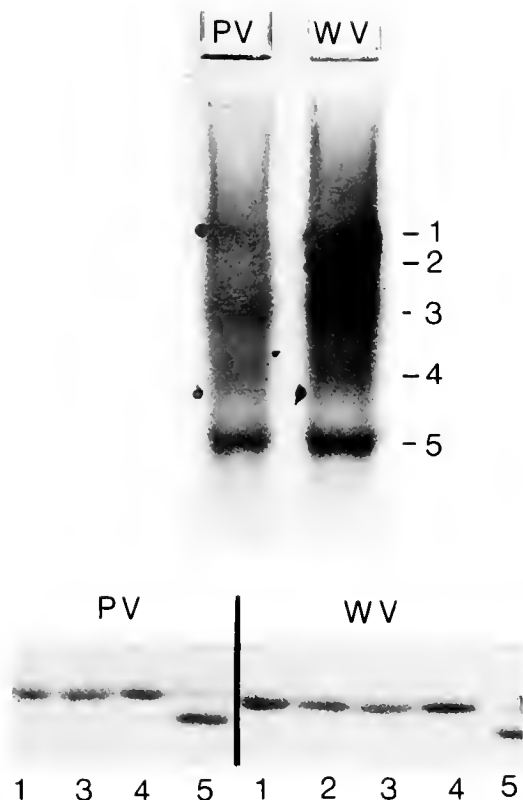


Figure 7. Electrophoretic comparison of *Paracaudina chilensis* perivisceral and water vascular Hbs. Upper, perivisceral (PV) and water vascular (WV) Hbs on pH 8.9 PAGE. Lower, SDS PAGE. PV 1, 2, 3, 4, heme-containing slices from PV PAGE; PV 5 non-heme band from PV PAGE; WV 1, 2, 3, 4, heme-containing slices from WV PAGE; WV 5, non-heme band from WV PAGE.

mers as well as molecules with an apparent molecular weight of 50 kDa (see also Terwilliger and Terwilliger, 1988). The 34 kDa (Hb II) and the 50 kDa (Hb I) fractions were electrophoretically distinguishable. Several holothurian Hbs aggregate to tetramers in the deoxy-state. For example, *Cucumaria miniata* Hb is a dimer of 36 kDa in the oxy-state and aggregates to a tetramer of 55 kDa in the deoxy-state (Bonaventura and Kitto, 1973; Terwilliger, 1975). In our study, *C. miniata* Hb, which has an oxygen affinity about five times lower (Terwilliger, 1975) than that of *P. chilensis* Hb, showed no evidence of aggregation under the column conditions used. This indicates that the column was sufficiently oxygenated to prevent aggregation due to a deoxy-state. Therefore, the apparent 50 kDa Hb in *P. chilensis* is not the result of aggregation in the deoxy-state. The presence of a possible tetrameric oxyHb in a holothurian echinoderm is especially interesting in light of the predominance of the tetrameric aggregation state in the vertebrate Hbs. The subunit molecular weight is similar to that calculated by Suzuki (1989) from the amino acid sequence data.

We found that *P. chilensis* Hb had a very high oxygen affinity with a  $P_{50}$  of  $1.5 \pm 0.29$  mmHg (pH 7.0–7.7, 15°C, 0.058 mM heme). In our studies the Hill coefficient was always greater than one ( $n_H = 1.26$ –1.86). Our data agree with others: almost all holothurian Hbs, even those with multiple components (e.g., *Molpadia arenicola* and *M. öölitica*), have Hill coefficients greater than one (Terwilliger and Read, 1972; Bonaventura and Kitto, 1973). The Hill coefficient that we found for *P. chilensis* Hb is consistent with homotropic interactions within a dimer (Chiancone *et al.*, 1981; Royer *et al.*, 1985; Terwilliger and Terwilliger, 1988).

The increase in oxygen affinity upon dilution for *P. chilensis* Hb has also been observed for several vertebrate Hbs. This phenomenon has been explained by a rapid association-dissociation equilibrium between dimer and tetramer (Rossi-Fanelli *et al.*, 1964; Antonini and Brunori, 1971). The concentration effect is particularly noticeable in lamprey Hb, which has a ligand-linked association from monomer to tetramer upon deoxygenation (Briehl, 1968). Hemoglobins from the polychaete *Glycera* and several other holothurians are examples of invertebrate Hbs displaying a concentration effect (Mizukami and Vinogradov, 1972; Terwilliger, 1975). The concentration effect exhibited by *P. chilensis* Hb is of similar magnitude as that of other Hbs, at least at low Hb concentrations. Bonaventura and Kitto (1973) report that dilution of *M. arenicola* Hb to low pigment concentrations tends to dissociate the oxy-dimers to oxy-monomers. If *P. chilensis* Hb dissociates to monomers upon dilution as well, the monomer may have a higher affinity than the dimer. A physiological implication of the concentration effect is that, because the concentration of Hb in *P. chilensis* hemocytes (MCHC) is higher than that used in our oxygen binding studies, the oxygen affinity of Hb in the hemocytes is probably lower than that determined *in vitro*.

It would be interesting to learn whether the apparent pH dependence of oxygen affinity in *P. chilensis* becomes significant at physiological Hb concentrations. Only one other holothurian Hb, that of *Molpadia arenicola*, is reported to exhibit pH sensitivity in the kinetics of ligand binding (Bonaventura *et al.*, 1976). Cooperativity of *P. chilensis* Hb is more pronounced at the highest Hb concentration, and may be greater *in vivo* than *in vitro*.

Invertebrate Hbs are generally insensitive to organic phosphates (Terwilliger and Terwilliger, 1988; Scholnick and Mangum, 1991). Nonetheless, because of the possibility of a tetrameric oxyHb in *P. chilensis* and the phylogenetic relationship between echinoderms and vertebrates, both deuterostomes, we looked for possible effects of organic modulators known to influence vertebrate tetrameric Hb. There were no observable effects of the organic phosphates, ATP, 2,3-DPG, or IHP, on oxygen binding. This insensitivity may be due to blocking of the

n-termini of the Hb chain of *P. chilensis*, and as seen in several other holothurian Hbs (Kitto *et al.*, 1976; Suzuki, 1989).

The heat of oxygenation of *P. chilensis* Hb is similar to that of most other invertebrate and vertebrate Hbs. Hemoglobins from the perivisceral coelom and the water vascular system of *P. chilensis* were not distinguishable by absorbance spectra. However, these two compartments appear to contain different Hbs whose subunits differ in charge but not size as determined electrophoretically. This information suggests that the compartments are discontinuous, at least with respect to hemocytes. At the same Hb concentration, the oxygen affinities of Hbs from the two compartments are indistinguishable, indicating that an oxygen transfer system is unlikely in this animal. Although Hb concentration parameters were not measured for water vascular fluid, it was darker red than the perivisceral fluid, suggesting a higher Hb concentration. If the Hb concentration in water vascular hemocytes is higher than that in perivisceral hemocytes, then the water vascular Hb may have a lower oxygen affinity *in vivo* due to the concentration effect on oxygen affinity.

*Paracaudina chilensis* lives buried up to 50 cm deep in direct contact with black, muddy sand smelling of hydrogen sulphide. The posterior "tail" is extended to the surface of the substrate and oxygen is obtained via oxygenated water inspired through the anus into the respiratory trees. The body wall of the animal is so thin that the internal organs and dark red coelomic fluid are visible through the skin (Kawamoto, 1928; present authors, pers. obs.). It appears then that *P. chilensis* lives in an oxygen-limited habitat that could potentially draw oxygen away from the sea cucumber.

The oxygen affinity of *P. chilensis* Hb ( $P_{50} = 2.1$  mmHg at 20°C) is higher than that of most other holothurian Hbs ( $P_{50} = 3.5$ –10.0 mmHg at 20°C) (Terwilliger and Terwilliger, 1988). The oxygen affinity is comparable, however, to those of many other invertebrates that inhabit intertidal, microoxic substrates. For example the polychaetes, *Enoplobranchius sanguineus* (Mangum *et al.*, 1975) and *Notomastus latericeus* (Wells and Warren, 1975), and the phoronids, *Phoronopsis viridis* (Garlick *et al.*, 1979), *Phoronis mulleri* (Weber, 1980), and *Phoronis architecta* (Vandergon and Colacino, 1989), have  $P_{50}$  values from 1.3 to 3.0 mmHg. The fact that many invertebrates living intertidally in microoxic substrates have Hbs with exceptionally high oxygen affinities suggests that the high oxygen affinity is adaptive to the habitat. One function of the high oxygen affinity of Hb of these burrowing animals may be to minimize the loss of oxygen to an oxygen-sink habitat. Such a function is proposed for the Hb of the polychaete *Cirriformia tentaculata* which has Hb oxygen affinity and concentration similar to that of *P. chilensis* (Dales and Warren, 1980). The Hb of *P. chi-*

*lensis* may be a storage molecule, the high oxygen affinity serving to retain oxygen even though the thin body wall is surrounded by sand of low oxygen tension.

### Acknowledgments

The authors wish to acknowledge the contribution of Dr. Robert C. Terwilliger to this study. This study was supported by NSF grant 8511150 to RCT and NBT and by an American Heart Association, Oregon Affiliate, summer science research fellowship and an International Women's Fishing Association Scholarship Trust grant to SMB. We would like to thank Dr. L. Burnett, University of Charleston, for the use of his small tonometers. C. P. Mangum and two anonymous reviewers made helpful comments on the manuscript. This is Oregon Institute of Marine Biology Contribution Number 92-02.

### Literature Cited

- Antonini, E., and M. Brunori. 1971. *Frontiers of Biology, Volume 21, Hemoglobin and Myoglobin in Their Reactions with Ligands*. American Elsevier, New York.
- Benesch, R., G. MacDuff, and R. E. Benesch. 1965. Determination of oxygen equilibria with a versatile new tonometer. *Anal. Biochem.* **11**: 81–87.
- Bonaventura, C., J. Bonaventura, B. Kitto, M. Brunori, and E. Antonini. 1976. Functional consequences of ligand-linked dissociation in hemoglobin from the sea cucumber *Molpadia arenicola*. *Biochem. Biophys. Acta* **428**: 779–786.
- Bonaventura, J., and G. B. Kitto. 1973. Ligand-linked dissociation of some invertebrate hemoglobins. Pp. 493–506 in *Comparative Physiology*. L. Bolis, K. Schmidt-Nielsen, and S. H. P. Maddess, eds. North-Holland Publishing Company, Amsterdam.
- Briehl, R. W. 1968. The relation between the oxygen equilibrium and aggregation of subunits in lamprey hemoglobin. *J. Biol. Chem.* **238**: 2361–2366.
- Chiancone, E., P. Vecchini, D. Verzili, F. Ascoli, and E. Antonini. 1981. Dimeric and tetrameric hemoglobins from the mollusc *Scapharca maquivalvis*: structural and functional properties. *J. Mol. Biol.* **152**: 577–592.
- Dales, R. P., and L. M. Warren. 1980. Survival of hypoxic conditions by the polychaete *Cirriformia tentaculata*. *J. Mar. Biol. Assoc. U. K.* **60**: 509–516.
- Davidsohn, I. 1962. The blood. Pp. 61–262 in *Clinical Diagnosis by Laboratory Methods*. I. Davidsohn and B. B. Wells, eds. W. B. Saunders Company, Philadelphia.
- Davis, B. 1964. Disc electrophoresis—II. Method and application to human serum proteins. *Ann. N. Y. Acad. Sci.* **121**: 404–427.
- Garlick, R. L., B. J. Williams, and A. F. Riggs. 1979. The hemoglobins of *Phoronopsis viridis*, of the primitive invertebrate phylum Phoronida: characterization and subunit structure. *Arch. Biochem. Biophys.* **194**: 13–23.
- Howell, W. H. 1886. Presence of haemoglobin in the echinoderms. *Studies Biol. Lab. Johns Hopkins Univ.* **3**: 289–291.
- Hyman, L. H. 1955. *The Invertebrates, Volume IV, Echinodermata*. McGraw-Hill Book Company, New York.
- Kawamoto, N. 1927. The anatomy of *Caudina chilensis* (J. Müller) with especial reference to the perivisceral cavity, the blood and water vascular systems in their relation to the blood circulation. *Sci. Rep. Tohoku Univ. Fourth Ser. (Biol.)* **2**: 239–264.

- Kawamoto, N. 1928.** Oxygen capacity of the blood of certain invertebrates which contains haemoglobin. *Sci. Rep. Tohoku Univ. Fourth Ser. (Biol.)* 3: 561-575.
- Kitto, G. B., D. Erwin, R. West, and J. Omnaas. 1976.** N-terminal substitution of some sea cucumber hemoglobins. *Comp. Biochem. Physiol.* 55: 105-107.
- Kobayashi, S. 1932.** The spectral properties of haemoglobin in the holothurians, *Caudina chilensis* (J. Müller) and *Molpadia roretzii* (v. Marenzeller). *Sci. Rep. Tohoku Univ. Fourth Ser. (Biol.)* 7: 211-227.
- Laemmli, H. 1970.** Cleavage of structural proteins during assembly of the head of bacteriophage T4. *Nature* 227: 680-685.
- Mangum, C. P., and L. E. Burnett. 1987.** Response of sipunculan hemerythrins to inorganic ions and CO. *J. Exp. Zool.* 244: 59-65.
- Mangum, C. P., B. R. Woodin, C. Bonaventura, B. Sullivan, and J. Bonaventura. 1975.** The role of coelomic and water vascular hemoglobin in the annelid family Terebellidae. *Comp. Biochem. Physiol.* 51: 281-294.
- Manwell, C. 1960.** Histological specificity of respiratory pigments—II. Oxygen transfer systems involving hemerythrins in sipunculid worms of different ecologies. *Comp. Biochem. Physiol.* 1: 277-285.
- Manwell, C., and C. M. A. Baker. 1963.** A sibling species of sea cucumber discovered by starch gel electrophoresis. *Comp. Biochem. Physiol.* 10: 39-53.
- Mauri, F. C. 1985.** The structural and functional studies of an echinoderm hemoglobin. PhD dissertation, University of Texas at Austin.
- Mizukami, H., and S. N. Vinogradov. 1972.** Oxygen association equilibria of *Glycera* hemoglobins. *Biochem. Biophys. Acta* 285: 314-319.
- Roberts, M. S., R. C. Terwilliger, and N. B. Terwilliger. 1984.** Comparison of sea cucumber hemoglobin structures. *Comp. Biochem. Physiol.* 77: 237-243.
- Rossi-Fanelli, A., E. Antonini, and A. Caputo. 1964.** Hemoglobin and myoglobin. *Adv. Protein Chem.* 19: 73-222.
- Royer, W., W. Love, and F. F. Fenderson. 1985.** Cooperative dimeric and tetrameric clam haemoglobins are novel assemblages of myoglobin folds. *Nature* 316: 277-280.
- Scholnick, D. A., and C. P. Mangum. 1991.** Sensitivity of hemoglobins to intracellular effectors: primitive and derived features. *J. Exp. Zool.* 259: 32-42.
- Suzuki, T. 1989.** Amino acid sequence of a major globin from the sea cucumber *Paracaudina chilensis*. *Biochim. Biophys. Acta* 998: 292-296.
- Terwilliger, N. B., R. C. Terwilliger, and E. Schabtach. 1985.** Intracellular respiratory proteins of Sipuncula, Echiura, and Annelida. Pp. 193-225 in *Blood Cells of Marine Invertebrates: Experimental Systems in Cell Biology and Comparative Physiology*, W. D. Cohen, ed. Alan R. Liss, Inc., New York.
- Terwilliger, R. C. 1974.** Oxygen equilibria of the vascular and coelomic hemoglobins of the terebellid polychaete, *Pista pacifica*. Evidence for an oxygen transfer system. *Comp. Biochem. Physiol.* 48: 745-755.
- Terwilliger, R. C. 1975.** Oxygen equilibrium and subunit aggregation of a holothurian hemoglobin. *Biochem. Biophys. Acta* 386: 62-68.
- Terwilliger, R. and K. Read. 1970.** The hemoglobins of the holothurian echinoderms, *Cucumaria miniata* Brant, *Cucumaria piperata* Stimson and *Molpadia intermedia* Ludwig. *Comp. Biochem. Physiol.* 36: 339-351.
- Terwilliger, R. C., and K. Read. 1972.** The hemoglobin of the holothurian echinoderm, *Molpadia oölitica* Pourtales. *Comp. Biochem. Physiol.* 42: 65-72.
- Terwilliger, R. C., and N. B. Terwilliger. 1988.** Structure and function of holothurian hemoglobins. Pp. 589-595 in *Echinoderm Biology. Proceedings of the Sixth International Echinoderm Conference*, R. D. Burke, P. V. Mladenov, P. Lambert, and R. L. Parsley, eds. A. A. Balkema, Rotterdam.
- Vandergon, T. L., and J. M. Colacino. 1989.** Characterization of hemoglobin from *Phoronis architecta* (Phoronida). *Comp. Biochem. Physiol.* 94B: 31-39.
- Weber, R. E. 1980.** Functions of invertebrate hemoglobins with special reference to adaptations to environmental hypoxia. *Am. Zool.* 20: 79-101.
- Wells, R. M. G., and L. M. Warren. 1975.** The function of the cellular haemoglobins in *Capitella capitata* (fabricius) and *Notomastus latericus* (Capitellidae: polychaeta). *Comp. Biochem. Physiol.* 52: 737-740.



# Effect of Dietary Protein Content on Growth of Juvenile Mussels, *Mytilus trossulus* (Gould 1850)

D. A. KREEGER<sup>1</sup> AND C. J. LANGDON

*Hatfield Marine Science Center, Department of Fisheries and Wildlife, Oregon State University, Newport, Oregon 97365*

**Abstract.** Juvenile mussels, *Mytilus trossulus*, were fed for 3 weeks on either low-protein (LP) algae, high-protein (HP) algae, or a combination of LP algae and protein microcapsules (PM). Growth rates of mussels fed a satiation ration of 27.5% body weight (bw; ash-free dry weight of algae/ash-free dry tissue weight of mussels) per day of LP algae (28% protein percent weight per weight) were significantly ( $P < 0.05$ ) lower than growth rates of mussels fed a satiation ration (27.5% bw d<sup>-1</sup>) of HP algae (43% protein weight per weight). However, growth rates of mussels fed LP algae (27.5% bw d<sup>-1</sup>) supplemented with one of three different rations (6, 12 and 18% bw d<sup>-1</sup>) of PM increased proportionally to PM ration size. Mussels fed a diet containing LP algae with the highest level of PM supplementation grew at rates that were not significantly different from those of mussels fed a diet of HP algae alone. Growth rates of mussels fed LP algae alone were not improved if the ration of LP algae was increased (34.1% bw d<sup>-1</sup>), indicating that the positive growth response of mussels fed PM supplements was due to an increase in dietary protein content and not simply due to an overall increase in food (energy) availability. In addition, mussels fed LP algae had O/N ratios >18, indicating that they were conserving dietary protein from catabolism; whereas mussels fed protein-rich diets had O/N ratios <10, indicating that they were catabolizing dietary protein. These results suggest that dietary protein contents below 40% w/w and dietary C/N ratios above 10 can qualitatively limit growth rates of juvenile *M. trossulus*.

## Introduction

The availability of nitrogen frequently affects productivity in marine systems (Dugdale, 1967; Riley, 1972;

Mann, 1982; Roman, 1983; Tenore and Chesney, 1985; Asmus, 1986; Rice *et al.*, 1986). A large portion of nitrogen in marine habitats can cycle through populations of suspension-feeding animals, such as bivalve molluscs (Jordan and Valiela, 1982; Dame *et al.*, 1984, 1985; Kautsky and Evans, 1987; Dame and Dankers, 1988; Asmus and Asmus, 1991). The bioavailability of nitrogen and protein for suspension-feeding bivalves in natural habitats is not well documented and may be especially low for many species that use suspended detritus as a food source. Newell (1965) first reported that the bivalve *Macoma balthica* utilizes the microbial coating of detrital particles as a source of dietary protein, and this potential protein source for macroinvertebrates has been cited repeatedly (for reviews, see Fenchel, 1972; Sieburth, 1976; Tenore, 1977), but most of the nitrogen associated with detritus is now known to consist of nonmicrobial humic geopolymers, which are indigestible (Rice, 1982; Crosby *et al.*, 1990; Hicks *et al.*, 1991). Crosby *et al.* (1990) reported, for example, that oysters, *Crassostrea virginica*, were able to assimilate nitrogen of bacteria with an efficiency of 57.2%, but the oyster's assimilation efficiency for detritus-associated nitrogen was only 3.4%.

The importance of nitrogen limitation in the nutrition of suspension-feeding bivalves has not been clearly established. Hawkins and Bayne (for reviews, see Hawkins and Bayne, 1991, 1992) determined nitrogen and carbon budgets of *Mytilus edulis* fed <sup>15</sup>N- and <sup>14</sup>C-labeled *Phaeodactylum tricorutum* and concluded that mussels in their natural environment may be more limited by carbon than nitrogen, in part because mussels were found to be very efficient in recycling nitrogen within their tissues. In support of this conclusion, Flaak and Epifanio (1978) reported that growth rates of oysters, *C. virginica*, increased when they were fed algal diets containing a greater proportion of carbohydrate than protein. In contrast, the dietary protein content of experimental diets has been positively cor-

Received 15 January 1993; accepted 4 May 1993.

<sup>1</sup> Present address: Plymouth Marine Laboratory, Prospect Place, The Hoe, Plymouth, Devon PL1 3DH, United Kingdom.

related with growth of juvenile Manila clams, *Tapes japonica* (Langton *et al.*, 1977; Gallagher and Mann, 1981); *C. virginica* (Webb and Chu, 1982); and *Ostrea edulis* (Enright *et al.*, 1986b). Settlement of larval *C. gigas* was also improved by increasing the protein content of algal diets (Utting, 1986).

Most research on bivalve nutrition has focused on quantitative requirements for energy and nitrogen rather than on qualitative requirements for specific amino acids (for reviews, see Newell, 1979; Bayne and Newell, 1983; Hawkins and Bayne, 1991, 1992; Langdon and Newell, 1992). Few attempts have been made to identify the specific nutritional requirements of suspension-feeders, primarily because it is technically difficult to define and manipulate the biochemical composition of their diet. Unlike macroconsumers, which are commonly fed pelletized artificial diets, suspension-feeders require microscopic particles that are more difficult to prepare. Consequently, dietary protein requirements of bivalve suspension-feeders have had to be inferred by correlating growth and survival rates with dietary protein content of algal diets, even though it is often uncertain whether the observed response was caused by protein content *per se* or by variation in undetermined, nonprotein constituents of algal diets.

In this study, protein microcapsules were used to manipulate dietary protein content, thus allowing unequivocal determination of the effect of dietary protein content on growth of a suspension-feeding bivalve, the mussel *Mytilus trossulus*. The advantage of using microencapsulated diets is that their biochemical composition can be accurately measured and controlled, unlike that of algal diets, which is dependent on culture age and conditions (Sakshaug and Holm-Hansen, 1977; Webb and Chu, 1982; Fabregas *et al.*, 1985, 1986; Utting, 1985; Martin-Jezequel *et al.*, 1988; Fernandez-Reiriz *et al.*, 1989; Thompson *et al.*, 1989, 1990). PM have been shown to be filtered and digested by oysters, *C. virginica* (Chu *et al.*, 1982) and *C. gigas* (Langdon, 1989; Langdon and DeBevoise, 1990), and mussels, *M. trossulus* (Kreeger, 1992), but the ability of bivalves to utilize PM for growth has not been previously reported.

### Materials and Methods

Growth rates were first measured and compared among groups of juvenile mussels, *Mytilus trossulus*, which were fed diets of algae that were isocaloric but different in protein content, to determine whether mussel growth could be correlated with algal protein content, as has been shown for other bivalve species (Langton *et al.*, 1977; Gallagher and Mann, 1981; Webb and Chu, 1982; Enright *et al.*, 1986b). Second, direct evidence for the effect of dietary protein content on mussel growth was obtained by comparing growth of mussels fed on high-protein (HP) algae to growth of mussels fed on an equivalent ration of low-

protein (LP) algae, which was supplemented with protein microcapsules (PM). The effect of differences in energy availability due to different supplementary rations of PM was examined in a separate control treatment in which the ration of LP algae was increased to make it isocaloric with the highest PM-supplemented ration.

### Preparation of microalgae

The alga *Isochrysis galbana* (clone T-ISO) is widely cultured as a nutritious food for suspension-feeding bivalves (Epifanio, 1979; Ewart and Epifanio, 1981; Webb and Chu, 1982; Enright *et al.*, 1986a; Whyte, 1987; Whyte *et al.*, 1989) and was fed to mussels in this study. Cultures were nonsterile but monospecific. Algae were initially cultured at 18°C, aerated (no CO<sub>2</sub> enrichment) with f/2 nutrients (Guillard and Ryther, 1962), in 1.5-l flasks that were then used to inoculate 20-l carboys. The nitrogen content of the nutrient medium of 20-l carboy cultures was adjusted to provide either 200% (nonlimited nitrogen) or 40% (limited nitrogen) of the nitrogen of f/2 medium. High-nitrogen and low-nitrogen cultures contained 150 and 30 ppm (1.765 and 0.353 mg-at N l<sup>-1</sup>) NaNO<sub>3</sub>, respectively.

Biochemical and physical characteristics of both LP (from low-nitrogen cultures) and HP (from high-nitrogen cultures) algae were measured throughout the culture period; measurements included cell concentration, volume, ash-free dry weight (AFDW), and proximate biochemical composition. Algal cell concentrations (number per milliliter) were measured in triplicate using a Coulter Counter (Coulter Electronics, Model ZB1). A Channelyzer (Coulter Electronics, Model 256) was used to examine the spectrum of cell volumes of each algal sample. In healthy cultures, cell sizes were normally distributed, allowing determination of modal cell volume (in cubic micrometers) by finding the volumetric channel with the greatest number of particles (precision approximately  $\pm 0.4 \mu\text{m}^3$ ). Algal AFDW was routinely measured by filtering four samples, containing known numbers of cells, through preweighed and pre-ashed (450°C, 2 d) Whatman GF/C filters, rinsing each with 10 ml 0.5 M ammonium formate to remove seawater, and conducting weight-on-ignition analyses (dried 60°C, 2 d; ashed 450°C, 2 d).

The volume and AFDW of algal cells was found to vary with culture age and conditions and, because diets used for the growth experiment required careful control of energy content, algae could not be fed to mussels simply on the basis of cell concentration. AFDW is more closely related to caloric content than either live or dry weight (Brey *et al.*, 1988), and so algal diets were rationed daily according to AFDW using a linear regression to predict algal AFDW from measured cell volume. Each day of the experiment, both cell concentrations (cell number ml<sup>-1</sup>) and modal cell volumes ( $\mu\text{m}^3 \text{ cell}^{-1}$ ) of 5- to 7-day-old

LP and HP algal cultures were determined and used to calculate volumetric cell concentrations (units =  $\mu\text{m}^3 \times 10^7 \text{ ml}^{-1}$ ). Volumetric cell concentrations were then used to predict concentrations of algal AFDW, based on a highly significant ( $P < 0.0001$ ) linear regression between cell volume (units =  $\mu\text{m}^3 \text{ cell}^{-1}$ ) and AFDW (units =  $\text{mg} \times 10^{-8} \text{ cell}^{-1}$ ), as follows:

$$\text{AFDW} = (0.258 \times \text{cell volume}) - 0.146. \quad (1)$$

Appropriate volumes of LP or HP algal culture were dispensed into stock flasks of the feeding system and diluted to a total volume of 3 l with filtered ( $0.7 \mu\text{m}$ ) seawater.

Algal protein content was routinely measured in triplicate. A known volume of algal culture containing  $10^8$  cells was centrifuged ( $800 \times g$ , 5 min) to form a pellet, rinsed with 10 ml 0.5 M ammonium formate to remove seawater, and dried at  $60^\circ\text{C}$  for 2 days. The pellet was resuspended in 2 ml 0.5 M NaOH, sonicated (Braun-Sonic, Model 2000) for 10 s to disrupt cell walls, heated at  $90^\circ\text{C}$  for 30 min, and left to stand overnight at room temperature. The suspension was then centrifuged ( $1500 \times g$ , 15 min), and 100  $\mu\text{l}$  of the supernatant was transferred to an acid-washed (10%  $\text{HNO}_3$ ) and baked ( $450^\circ\text{C}$ , 24 h) 5-ml test tube. The protein content was analyzed spectrophotometrically using a test kit (Pierce, BCA 23225) based on the procedure of Lowry *et al.* (1951), and standardized with purified algal protein (see Kreeger, 1992, for purification method). Color development in this assay was rapid and continuous over at least a 24-h period; therefore, the absorbance was measured with a spectrophotometer twice, and a linear correction factor was calculated for each sample to correct absorbances for differences in time intervals between analysis of samples and standards. The carbohydrate content of centrifuged and dried (as described above) LP and HP algae was measured using the procedure described by Dubois *et al.* (1956), which was standardized with oyster glycogen (Sigma G-8751, Type II). The lipid content of LP and HP algae was determined gravimetrically after extracting dried algal samples twice with 7.5 ml 1:2 chloroform/methanol, followed by treatment of the combined extract with 5 ml 0.7% weight per volume (w/v) NaCl (Folch *et al.*, 1957; and see "proximate analysis" below). Tripalmitin (Sigma T-5888) was used as a standard in lipid determinations.

The caloric content of LP and HP algae was determined by microbomb calorimetry (L. Wootton, Center for Estuarine and Environmental Studies, Horn Point Laboratory, University of Maryland, Cambridge, MD) of four replicate, freeze-dried samples of each type. LP and HP algae were not statistically (Student's *t* test,  $P > 0.05$ ) different in caloric content. Six replicate samples each of LP and HP algae were also analyzed for their elemental carbon, hydrogen, and nitrogen (CHN) composition (R. L. Petty, Marine Science Institute Analytical Laboratory, University of California, Santa Barbara, CA).

### Preparation of protein microcapsules

Approximately 10 g dry weight of PM was produced from purified crab (*Cancer irroratus*) protein using the technique described by Langdon (1989). The proximate biochemical composition of PM was determined using methods described by Kreeger (1992). The elemental CHN composition and caloric content of PM were also analyzed, as described above for microalgae. The amino acid composition of PM was analyzed to assess the nutritional quality of encapsulated protein and to ensure that the encapsulation process did not selectively destroy amino acids, based on comparison with the amino acid composition of nonencapsulated crab protein. The amino acid compositions of purified protein from *I. galbana* and from tissues of *M. trossulus* were also analyzed for comparisons.

Amino acids were analyzed by B. Robbins at the Central Services Laboratory, Center for Gene Research and Biotechnology, Oregon State University, Corvallis, OR. Proteins were hydrolyzed in either 1% phenol dissolved in 6 N HCl for 24 h at  $110^\circ\text{C}$ , or in 0.2% 3-(2-aminoethyl) indole HCl in 4 N methane sulphonic acid (MSA) for 20 h at  $110^\circ\text{C}$  under vacuum. After hydrolysis, samples were freeze-dried. Hydrolysates were reconstituted in Sodium DiLuent (Beckman, PN 239440), separated on a Spherogel ion exchange column (Beckman 126), and derivatized with ninhydrin reagent (Beckman, Trione). The absorbances were then detected at 570 nm with a tungsten lamp (Beckman, 166). MSA hydrolysis resulted in little loss of tryptophan (tryptophan was lost from samples hydrolyzed with HCl). Amino acid analyses were standardized with Pierce Standard H (Pierce, 20089); Pierce Standard B (Pierce, 20087) was used as a standard for tryptophan analysis.

### Description of experimental diets

Growth of juvenile *M. trossulus* over a 3-week period was compared among groups of mussels fed eight different diets: (1) LP algae delivered at a ration of 27.5% bw (body weight, ash-free dry algal weight/ash-free dry mussel tissue weight)  $\text{d}^{-1}$ , (2) LP algae (34.1% bw  $\text{d}^{-1}$ ), (3) LP algae (27.5% bw  $\text{d}^{-1}$ ) and PM (6.07% bw  $\text{d}^{-1}$ ); (4) LP algae (27.5% bw  $\text{d}^{-1}$ ) and PM (12.1% bw  $\text{d}^{-1}$ ); (5) LP algae (27.5% bw  $\text{d}^{-1}$ ) and PM (18.2% bw  $\text{d}^{-1}$ ); (6) HP algae (27.5% bw  $\text{d}^{-1}$ ); (7) HP algae (27.5% bw  $\text{d}^{-1}$ ) and PM (6.07% bw  $\text{d}^{-1}$ ); and (8) no food (starved control). The standard algal ration of 27.5% bw  $\text{d}^{-1}$  (except Diets 2 and 8) was chosen based on results from a preliminary growth experiment in which juvenile mussels were fed for 3 weeks on either LP or HP algae, each of which was delivered to separate groups of mussels at 10 different rations (from 0 to 55% bw  $\text{d}^{-1}$ ). Mussels fed HP algae in the preliminary experiment grew significantly ( $\alpha = 0.05$ ) faster than mussels fed LP algae at all rations; however, greatest differences

in growth rates between mussels fed LP and HP algae were observed when algae were delivered to mussels at a ration of 27.5% bw d<sup>-1</sup>. A higher ration of either LP or HP algae resulted in the production of pseudofeces by mussels and a small decrease in mussel growth rate. The "satiation" ration of 27.5% bw d<sup>-1</sup> of algae was therefore used as a standard algal ration in the present experiment. Dietary rations were adjusted weekly according to estimated changes in mussel AFDTWs, which were predicted from mussel live weights by regression analysis. Starved mussels (Diet 8) were used as a control for uptake of naturally occurring particles or dissolved organic material.

LP and HP algae were fed to mussels in Diets 1 and 6, respectively, to verify preliminary findings that mussels grew better when fed HP algae than when fed LP algae. PM were fed to mussels in combination with LP algae in Diets 3, 4, and 5 to determine whether differences in growth rates of mussels fed LP and HP algae resulted from differences in the protein content of the algae. The PM ration of 12.1% bw d<sup>-1</sup> delivered to mussels in combination with LP algae (Diet 4) was estimated to balance the difference in protein content between LP and HP algae (Diets 1 and 6), so that mussels fed Diet 4 were provided with the same overall amount of protein for potential assimilation (bioavailable protein) as mussels receiving only HP algae (Diet 6). Rations of PM were calculated based on their potential assimilation, because mussels typically assimilate PM with lower efficiency (e.g., 30%; Kreeger, 1993) than microalgae (e.g., 75%; Bayne and Newell, 1983). Rations of bioavailable protein associated with delivered rations of LP and HP algae were calculated to be 5.73 and 8.78% bw d<sup>-1</sup>, respectively, by multiplying the delivered ration of 27.5% bw d<sup>-1</sup> by the expected assimilation efficiency for mussels fed microalgae (75%; Bayne and Newell, 1983) and by the respective protein contents of LP and HP algae (27.8 and 42.6% w/w; see Results). The difference between these estimated values for bioavailable protein (3.05% bw d<sup>-1</sup>) was termed the replacement protein ration (RPR). To calculate the ration of PM that would need to be delivered to mussels to equal RPR (12.1% bw d<sup>-1</sup>, Diet 4), it was necessary to divide RPR by both the assimilation efficiency for PM determined for *M. trossulus* during spring (30%; Kreeger, 1993) and the protein content of PM (84%, see Results). Estimated rations of bioavailable protein in Diets 1–7 are calculated in Table I and summarized in Figure 1a. Supplements of PM in Diets 3 and 5 were calculated to equal 0.5 RPR and 1.5 RPR, respectively (Table I; Fig. 1, top). PM were also added at 0.5 RPR to HP algae in Diet 7 to determine whether capsule supplements could further increase mussel growth, even when the algal diet was high in protein content (Fig. 1, top).

This experimental design was chosen so that growth differences among mussels fed diets containing PM supplements could be unequivocally attributed to dietary

Table I

Estimation of the ration of dietary protein measured as percentage of body weight (bw) per day, w/w ash-free dry, potentially assimilated by (i.e., bioavailable to) *Mytilus trossulus* fed seven experimental diets

Diet	Ration delivered to mussels			Protein potentially assimilated by mussels from ration		
	Algae	PM <sup>a</sup>	Total	Algae <sup>b</sup>	PM <sup>c</sup>	Total <sup>d</sup>
1. LP	27.5	—	27.5	5.73	—	5.73
2. LP + LP	34.1	—	34.1	7.11	—	7.11
3. LP + 0.5 RPR	27.5	6.07	33.6	5.73	1.53	7.26
4. LP + 1.0 RPR	27.5	12.1	39.6	5.73	3.05	8.78
5. LP + 1.5 RPR	27.5	18.2	45.7	5.73	4.58	10.31
6. HP	27.5	—	27.5	8.78	—	8.78
7. HP + 0.5 RPR	27.5	6.07	33.6	8.78	1.53	10.31

Diets were composed of low-protein *Isochrysis galbana* (LP) or high-protein *I. galbana* (HP), with or without protein microcapsules (PM). The ration of PM required to balance the difference in bioavailable protein between diets of LP and HP algae is the replacement protein ration (RPR).

<sup>a</sup> Rations of PM were calculated to balance the difference in protein content between LP and HP *I. galbana* when fed at 27.5% bw d<sup>-1</sup>.

<sup>b</sup> Protein that was potentially assimilated from *I. galbana* by mussels was estimated by multiplying the delivered algal ration by both a typical assimilation efficiency of mussels fed on microalgae (75%; Bayne and Newell, 1983) and measured algal protein contents (different for LP and HP *I. galbana*; see Table IV).

<sup>c</sup> Protein that was potentially assimilated from PM by mussels was estimated by multiplying the delivered PM ration by both the assimilation efficiency of juvenile mussels fed on PM (assumed to be 30%, based on data for adult mussels during spring; Kreeger, 1993) and the measured protein content of PM (84% w/w, Table IV).

<sup>d</sup> The total potentially assimilated protein ration in each diet was calculated by summing potentially assimilated protein from algae and PM components of each diet.

protein content and not to qualitative variation among nonprotein components of the diet. As a control treatment to assess whether mussel growth was affected by an increase in dietary caloric content in PM-supplemented diets, the ration of LP algae in Diet 2 (34.1% bw d<sup>-1</sup>) was increased above the standard algal ration (27.5% bw d<sup>-1</sup>). This caloric supplement was calculated to approximately equal the bioavailable (potentially assimilated) energy in the highest ration of PM (18.2% bw d<sup>-1</sup> of PM, Diet 5) and was termed the replacement energy ration (RER). RER was calculated to be 108 J mg<sup>-1</sup> d<sup>-1</sup> by multiplying the delivered ration of PM in Diet 5 (18.2% bw d<sup>-1</sup>) by both the measured capsule energy content (19.7 J mg<sup>-1</sup>, see Results) and the assimilation efficiency for PM by mussels during spring (30%; Kreeger, 1993). RER was then divided by both the energy content of LP algae (21.8 J mg<sup>-1</sup>, see Results) and a typical assimilation efficiency for mussels fed on algae (75%; Bayne and Newell, 1983) to calculate the ration of LP algae (6.6% bw d<sup>-1</sup>) required to provide the same bioavailable energy as the capsule

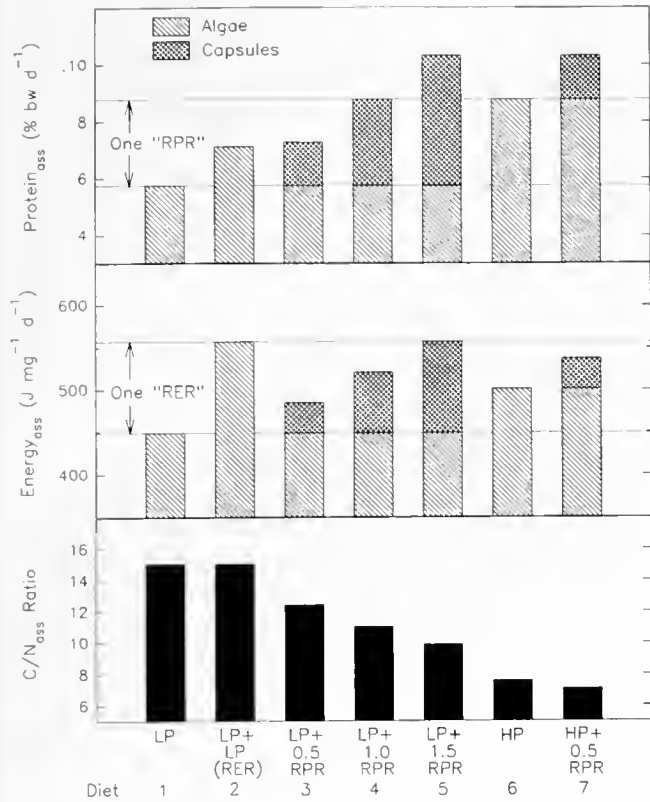


Figure 1. Protein content, energy content, and C/N ratio of the proportions of Diets 1–7 estimated to have been assimilated by (*i.e.*, bioavailable for) *Mytilus trossulus*. Diets were composed of low-protein *Isochrysis galbana* (LP) or high-protein *I. galbana* (HP), with or without protein microcapsules (PM). RPR refers to the replacement protein ration, and RER refers to the replacement energy ration.

supplement in Diet 5. Bioavailable energy contents of experimental diets are calculated in Table II and summarized in Figure 1, middle. Ratios for bioavailable C/N of diets were calculated using results from elemental analysis of PM and both LP and HP algae (Table III; Fig. 1 bottom).

#### Measurement of mussel growth rates

One week prior to the experiment, which was conducted during May 1992, six hundred juvenile *M. trossulus* (shell height = 9–16 mm, wet weight = 100–450 mg) were collected from a genetically characterized (Kreeger, 1992) population in Yaquina Bay, Oregon. Juvenile mussels rather than adults were used in this study so that all tissue production would be somatic and not influenced by changes in mussel reproductive condition, which could affect dietary protein utilization in adults (Kreeger, 1993). Mussels were acclimated in a continuous flow of sand-filtered (approximately 50  $\mu\text{m}$ ) seawater at ambient temperature (13–16°C). During acclimation, mussels were fed  $10^4$  cells  $\text{ml}^{-1}$  (approximate final concentration) of

HP *I. galbana* (T-ISO) until 24 h before experimentation; no food was delivered after that time. At the start of the experiment, 480 mussels were removed from the acclimation system, cleaned of epiphytes and byssus threads, and randomly divided into 24 groups of 20 individuals. The shell of each mussel was dried and numbered using a diamond-tipped etching pen. Individual shell heights (anteroposterior axis) and live weights were measured.

Mussels were reared for 3 weeks at 16–18°C in a series of 24 (three replicates per diet treatment) 4-l polycarbonate beakers, with each beaker containing a group of 20 mussels in 3 l of seawater. The position of tanks on the laboratory bench was assigned randomly. Sand-filtered ambient seawater was cartridge-filtered to 0.7  $\mu\text{m}$  and delivered under constant pressure to a 200-l reservoir tank, which had a float valve at its inflow to maintain a constant head pressure (Fig. 2). Seawater was then gravity delivered to each beaker at a constant rate of 1 l  $\text{h}^{-1}$  beaker $^{-1}$ , controlled with a needle valve at the inflow of each beaker. Water exited each beaker through an outflow port to waste.

Table II

Estimation of the ration of dietary energy measured in joules (per milligram of ash-free mussel tissue) per day, potentially assimilated by (*i.e.*, bioavailable to) *Mytilus trossulus* fed on seven experimental diets

Diet	Ration delivered to mussels			Energy potentially assimilated by mussels from ration		
	Algae	PM <sup>a</sup>	Total	Algae <sup>b</sup>	PM <sup>c</sup>	Total <sup>d</sup>
1. LP	27.5	—	27.5	449	—	449
2. LP + LP	34.1	—	34.1	557	—	557
3. LP + 0.5 RPR	27.5	6.07	33.6	449	35.9	485
4. LP + 1.0 RPR	27.5	12.1	39.6	449	71.5	521
5. LP + 1.5 RPR	27.5	18.2	45.7	449	108	557
6. HP	27.5	—	27.5	501	—	501
7. HP + 0.5 RPR	27.5	6.07	33.6	501	35.9	537

Diets were composed of low-protein *Isochrysis galbana* (LP) or high-protein *I. galbana* (HP), with or without protein microcapsules (PM). The ration of PM required to balance the difference in bioavailable protein between diets of LP and HP algae is the replacement protein ration (RPR).

<sup>a</sup> Rations of PM were calculated to balance the difference in protein content between LP and HP *I. galbana* when fed at 27.5%  $\text{bw d}^{-1}$ .

<sup>b</sup> Energy that was potentially assimilated from *I. galbana* by mussels was estimated by multiplying the delivered algal ration by both a typical assimilation efficiency of mussels fed on microalgae (75%; Bayne and Newell, 1983) and measured algal energy contents (21.8 and 24.3  $\text{J mg}^{-1}$  for LP and HP *I. galbana*, respectively, Table IV).

<sup>c</sup> Energy that was potentially assimilated from PM by mussels was estimated by multiplying the delivered PM ration by both the assimilation efficiency of juvenile mussels fed on PM (assumed to be 30%, based on data for adult mussels during spring; Kreeger, 1993) and the measured energy content of PM (19.7  $\text{J mg}^{-1}$ , Table IV).

<sup>d</sup> The total potentially assimilated energy in each diet was calculated by summing potentially assimilated energy from algae and PM components of each diet.

Table III

Estimates of the C/N ratios of the portion of Diets 1–7 potentially assimilated by (i.e., bioavailable to) *Mytilus trossulus* (C/N<sub>ass</sub> ratios) fed on seven experimental diets

Diet	Potentially assimilated ration (% bw d <sup>-1</sup> )						C/N <sub>ass</sub> ratio
	Algae		PM		Total diet		
	C <sup>a</sup>	N <sup>a</sup>	C <sup>b</sup>	N <sup>b</sup>	C <sup>c</sup>	N <sup>c</sup>	
1. LP	12.0	0.801	—	—	12.0	0.801	15.0
2. LP + LP	14.9	0.995	—	—	14.9	0.995	15.0
3. LP + 0.5 RPR	12.0	0.801	0.836	0.224	12.8	1.03	12.4
4. LP + 1.0 RPR	12.0	0.801	1.67	0.446	13.7	1.25	11.0
5. LP + 1.5 RPR	12.0	0.801	2.51	0.672	14.5	1.47	9.86
6. HP	11.7	1.55	—	—	11.7	1.55	7.55
7. HP + 0.5 RPR	11.7	1.55	0.836	0.224	12.5	1.77	7.06

Diets were composed of low-protein *Isochrysis galbana* (LP) or high-protein *I. galbana* (HP), with or without protein microcapsules (PM). The ration of PM required to balance the difference in bioavailable protein between diets of LP and HP algae is the replacement protein ration (RPR).

<sup>a</sup> The elemental composition of the potentially assimilated (PA) ration of algae was calculated by multiplying the PA algal ration by the elemental carbon (C) and nitrogen (N) weight percent composition of the algae (Table IV).

<sup>b</sup> The elemental composition of the PA ration of PM was calculated by multiplying the PA ration of PM by the measured C and N weight percentage content (Table IV).

<sup>c</sup> Total dietary C and N contents were calculated by summation of algal and PM values.

Beakers were aerated to facilitate mixing and suspension of food particles. Diets 1–7 were delivered continuously at 125 ml h<sup>-1</sup> from a 3-l flask to the inflow of each beaker using one of 21 separate peristaltic-pump channels. A stock suspension of each diet was prepared in each 3-l flask and continuously mixed with a magnetic stir-bar.

At the start of the experiment, 50 additional juvenile mussels were removed from the acclimation system, and their live weights and shell heights were determined. Each mussel's tissue was dissected into an individual preweighed and pre-ashed (450°C) vial for analysis of its ash-free dry tissue weight (AFDTW), using standard weight-on-ignition procedures (dried at 60°C, 2 d; ashed at 450°C, 2 days). Since AFDTW is a better measure of organic content than live or dry weight (Brey *et al.*, 1988), linear regression was then used to derive predictive formulae for mussel AFDTW from measures of live weight and shell height, and these formulae were used to estimate the initial AFDTW of each mussel used in the experiment.

Live weights and shell heights of individual mussels were measured weekly. After these measurements were recorded for the final week, tissues were individually dissected from one-half of the surviving mussels of each treatment and analyzed for their AFDTW using weight-on-ignition analysis (as described previously). The proxi-

mate biochemical composition of the remaining mussels in each treatment was analyzed to determine whether protein ration affected the protein content of mussel tissues (see below). Changes in shell height, live weight, and AFDTW over the 3-week period were then calculated for individual mussels within each treatment. For both live weight and AFDTW data, each mussel's instantaneous growth rate (IGR) was calculated as follows:

$$\text{IGR} = [(\ln W_f - \ln W_i)]/21 \text{ d.} \quad (2)$$

where  $W_f$  and  $W_i$  refer to final and initial mussel weight, respectively. Growth in shell height was expressed as a percentage change in height. Individual changes in shell height, live weight, and AFDTW during the 3-week experiment were compared statistically among replicates ( $n = 3$ ) and diet treatments ( $n = 8$ ) using nested ANOVA procedures (Sokal and Rohlf, 1969). Percentage increases in shell height were arcsine square root transformed (Sokal and Rohlf, 1969). No significant variation among replicates was found in any analysis, so the replicates were pooled and treatments were analyzed by one-way ANOVA and Tukey's multiple range procedures (Sokal and Rohlf, 1969).

#### Determination of O/N ratios for mussels

Rates of oxygen consumption and nitrogen excretion were measured for each group of mussels, and O/N ratios were calculated. O/N ratios are useful indicators of the relative catabolism of dietary protein (ratio <10) versus carbohydrate (ratio >20). After mussels were added to experimental beakers on the first day of the experiment, they were allowed to purge their guts for 24 h, during

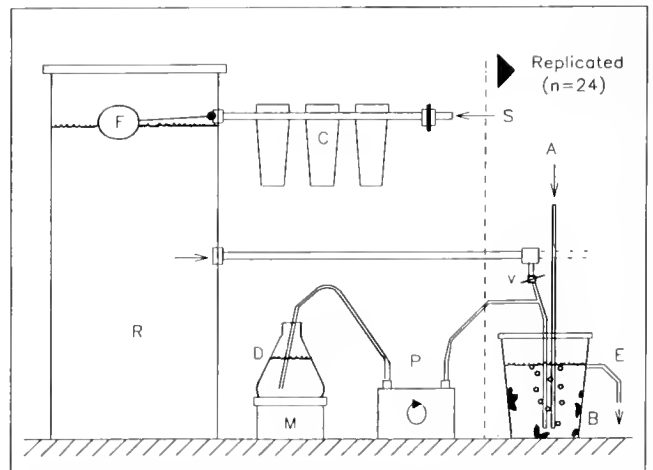


Figure 2. The continuous-flow rearing system used in the mussel growth experiment. S = seawater, C = cartridge filters, F = float valve, R = reservoir tank, D = experimental diet, M = magnetic mixer, P = peristaltic pump, V = needle valve, A = air, B = bivalves, and E = effluent.



which they received only filtered ( $0.7 \mu\text{m}$ ) seawater. For each group of 20 mussels, routine rates of oxygen consumption and ammonia nitrogen excretion were then measured during the same day. The same procedure was repeated on the final day of the experiment.

Rates of oxygen consumption were measured for each group by transferring the mussels from their experimental beaker to a 400-ml respirometer chamber (Strathkelvin, RC 400) which contained filtered ( $0.7 \mu\text{m}$ ) seawater. The respirometer chamber was partially immersed in a recirculating water bath (Forma Scientific Bath and Circulator, Model 2067) that maintained a constant water temperature of  $15^\circ\text{C}$ . After adding mussels to the chamber, the chamber was sealed, all air bubbles were removed, and an oxygen probe from a Strathkelvin oxygen meter (Model 781) was used to monitor internal  $\text{O}_2$  concentration. The oxygen meter was calibrated with air-saturated water, and zero oxygen concentration was determined with a freshly prepared solution of 200 mg sodium sulfite (anhydrous) in 100 ml  $0.01 M$  disodium tetraborate. Mussels rapidly opened their shell valves after being placed in the chamber and, after all appeared active, both oxygen concentration (milliliters per liter) and time were recorded, and recorded again after 15–30 min. This procedure was repeated for each group of animals. In addition, at five different times during the measurement period, oxygen consumption rates of microorganisms (present in respiration chambers) were measured, using a group of "dummy" mussels (empty shells that had been glued together with silicone) that had previously been held in the acclimation tank. Rates of oxygen consumption (milliliters per hour) were calculated using standard procedures, corrected for microbial activity, and expressed in gram-atomic units per AFDTW ( $\mu\text{g-at O}_2 \text{ h}^{-1} \text{ g}^{-1}$ ) for each group of mussels. Seawater in the respirometer chamber was replaced between each oxygen measurement to prevent accumulation of excreta and to keep dissolved oxygen concentrations from falling below 60% saturation.

Excretion of ammonia-nitrogen was measured by transferring mussels to sealed 1-l Nalgene jars containing 500 ml of filtered ( $0.7 \mu\text{m}$ ) seawater for an incubation period of 2–4 h. Initial and final times were recorded to calculate total elapsed time for each measurement. Three additional chambers, without mussels, received  $\text{NH}_3\text{SO}_4$  standards of known concentration. Three chambers also contained dummy mussels. At the start of the incubation period, 50 ml was removed from each of the six control chambers and fixed with 2 ml 10% w/v phenol in 95% ethanol. The pH of each sample was lowered to  $<8$  by addition of  $500 \mu\text{l}$  of  $1 M$  HCl to facilitate retention of ammonia in solution. At the end of the incubation period, a 100-ml sample was removed from each chamber and pH-adjusted with 1 ml of  $1 M$  HCl. Each sample was then vacuum filtered (5 psi) through a  $0.45\text{-}\mu\text{m}$  membrane filter to remove particulate material (a small amount of feces

was occasionally produced). Fifty milliliters of the filtrate was removed from each sample and fixed with phenol as described above. The concentration of ammonia in each sample was analyzed using the method of Solorzano (1969) and standardized with samples that contained known levels of  $\text{NH}_3\text{SO}_4$ . Increases in the gram-atomic weight of ammonia in chambers with living mussels were then corrected for background concentrations of ammonia and for microbial activity, using ammonia concentrations measured in chambers containing dummy mussels. Rates of ammonia excretion of each group of mussels were then calculated and expressed relative to total group AFDTW ( $\mu\text{g-at NH}_4^+\text{-N h}^{-1} \text{ g}^{-1}$ ).

Gram-atomic and weight-specific rates of oxygen consumption and ammonia-nitrogen excretion were directly compared among groups of mussels. At the start of the experiment, oxygen consumption rates, nitrogen excretion rates, and O/N ratios were averaged among the three replicate groups of mussels from each dietary treatment and compared statistically among treatments by one-way ANOVA to determine whether there were any initial differences in physiological parameters among treatments. This analysis was repeated at the conclusion of the experiment to determine whether the protein content of diets fed to mussels over the 3-week experimental period affected the manner in which mussels catabolized protein.

#### *Proximate analysis*

At the end of the experiment, approximately five randomly selected tissue samples from each group of mussels were combined and freeze-dried. After drying, tissue samples were ground into a powder with a mortar and pestle, and the powder was weighed. Each combined tissue sample was then resuspended in 4.5 ml (final volume) distilled  $\text{H}_2\text{O}$  and homogenized for 15 s at maximum speed (Ultra Turrax, Model SDT 1810). From each homogenate, 2 ml was transferred to a second vial for lipid extraction and analysis, using a method modified from Folch *et al.* (1956). Lipids were twice extracted with 7.5 ml 1:2 chloroform/methanol and 2-min bath sonication (Braun-Sonic, Model 52). Supernatants were collected by centrifugation ( $800 \times g$ , 10 min) and combined, and 5 ml 0.7% NaCl was added. The mixture was then vortexed at maximum speed for 30 s and allowed to stand overnight at  $4^\circ\text{C}$ . After settlement, samples were centrifuged ( $800 \times g$ , 15 min), and 4 ml of the lower organic phase was carefully withdrawn by pipet and added to a baked ( $450^\circ\text{C}$ , 2 d) and preweighed 7-ml vial. The samples were then dried for 2 days at  $60^\circ\text{C}$  to remove organic solvents. Vials were weighed after drying and amounts of lipid in original samples were calculated, after correction for losses determined with tripalmitin (Sigma, T-5888) standards that underwent the same process of lipid extraction and drying as tissue samples.



The remainder of each tissue homogenate (2.5 ml) was treated with 4 ml of 5% trichloroacetic acid (TCA), vortexed for 30 s (Vortex-Genie, Model 12-812), heated at 90°C for 30 min, cooled in an ice bath for 30 min, and centrifuged at  $1500 \times g$  for 20 min. The supernatant was withdrawn and 1 ml used for spectrophotometric determination of carbohydrate using the procedure described by Dubois *et al.* (1956), standardized with oyster glycogen (Sigma, Type II, G-8751) that had been subjected to the same extraction process as the tissue samples. The pellet was further treated with 3 ml 0.5 M NaOH, vortexed for 10 s, heated at 90°C for 30 min, and allowed to stand overnight at room temperature. Samples were then centrifuged ( $1500 \times g$ , 10 min), and the protein concentration of the supernatant was determined spectrophotometrically using a test kit based on the procedure of Lowry *et al.* (1951) (Pierce, BCA 23225). The protein content of the initial tissue homogenate was calculated from standard absorbances of purified mussel protein (for procedure, see Kreeger, 1992) that had been treated identically to the samples. Average protein, lipid, and carbohydrate contents in mussel tissues from each beaker were calculated from arcsine square root transformed data and compared statistically among treatments using ANOVA and Tukey's HSD multiple range tests (Sokal and Rohlf, 1969).

## Results

### Characteristics of microalgae

The alga *I. galbana* (clone T-ISO) was successfully cultured in low-nitrogen (40% of the nitrogen of *f/2* medium,  $30 \text{ mg NaNO}_3 \text{ l}^{-1}$ ) and high-nitrogen (200% of the nitrogen of *f/2* medium,  $150 \text{ mg NaNO}_3 \text{ l}^{-1}$ ) enriched seawater. Further reductions in nitrogen concentration below  $30 \text{ mg NaNO}_3 \text{ l}^{-1}$  caused algal cultures to collapse after 6 days of growth. Temporal changes in cell concentrations of low-nitrogen and high-nitrogen cultures are shown in Figure 3a. Both types of algae grew exponentially during the first week of culture (Fig. 3, top). After 7 days, LP (low-nitrogen cultures) algae reached stationary phase; whereas HP (high-nitrogen cultures) algae grew exponentially until about day 10, when stationary phase was reached (Fig. 3, top). Cell concentrations of LP algal cultures were consistently lower than those of HP algal cultures (Fig. 3, top). Both the age and the nitrogen concentration of the culture were highly significant ( $P < 0.0001$ ) predictors of cell concentration, as determined by multiple regression (adjusted  $R^2 = 0.38$ ).

During the culture period, both LP and HP algae increased in cell size, although LP algal cells were usually larger than HP algal cells of similar culture age (Fig. 3, middle). A multiple regression (adjusted  $R^2 = 0.51$ ) for predicting cell volume indicated that both nitrogen concentration and culture age were significant ( $P < 0.0001$ ) variables affecting cell volume. Cell volumes of LP and

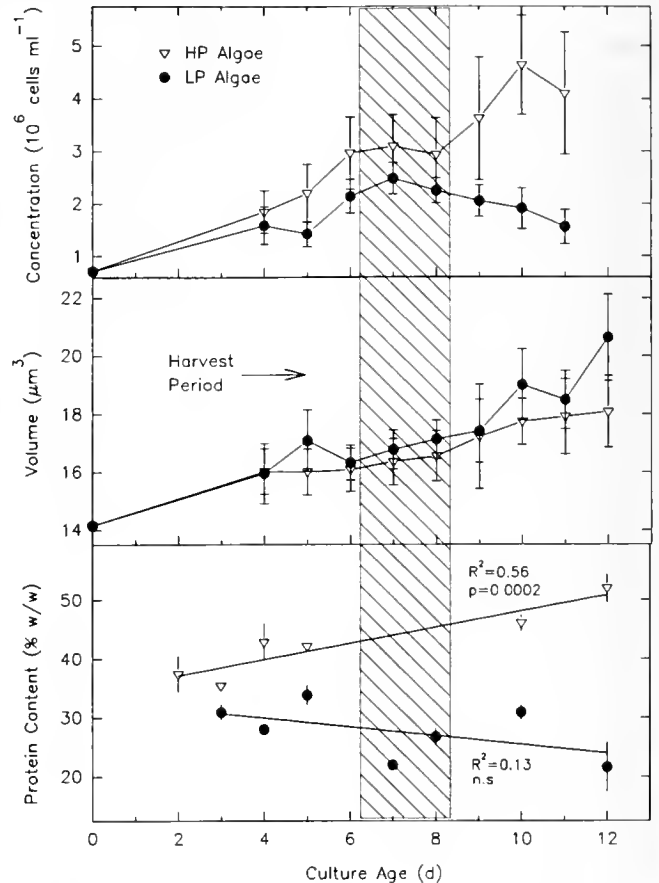


**Figure 3.** Temporal changes in the mean ( $\pm 95\%$  confidence interval) concentration (top), volume (middle), and protein content (bottom) of *Isochrysis galbana* (T-ISO) cells cultured in low-nitrogen (LP) or high-nitrogen (HP) media.

HP algae were averaged ( $\pm$ SE) for the entire culture period and were  $18.0 \pm 2.3 \mu\text{m}^3$  ( $n = 127$ ) and  $17.6 \pm 1.5 \mu\text{m}^3$  ( $n = 93$ ), respectively. As with cell volume, cell AFDW also increased with culture age and nitrogen concentration and averaged ( $\pm$ SE)  $28.0 \pm 13.1 \text{ pg cell}^{-1}$  ( $n = 33$ ) and  $29.3 \pm 12.9 \text{ pg cell}^{-1}$  ( $n = 29$ ) for LP and HP algae, respectively. Equal weight-specific rations of LP and HP algae to be fed to mussels in the growth experiment were calculated from a highly significant ( $P < 0.0001$ ) linear regression equation ( $R^2 = 0.94$ ) for prediction of cell AFDW from cell volume measurements (see Methods).

The biochemical composition and energy content of algae cultured on low-nitrogen and high-nitrogen media are summarized in Table IV. No significant differences ( $P > 0.05$ ) were found between LP and HP algae in their percentage (dry w/w) ash composition; however, LP algae had a significantly ( $P < 0.0001$ ) lower protein content (27.8% w/w) than HP algae (42.6% w/w). Carbohydrate and lipid contents were significantly ( $P = 0.002$  and  $P = 0.006$ , respectively) greater in LP algae (25.1% and 22.0%, respectively) than in HP algae (20.2% and 17.1%,

**Table IV**

Biochemical composition (percentage total dry weight) and energy content (per unit dry weight) of protein microcapsules (PM), low-protein (LP) *Isochrysis galbana* (T-ISO), and high-protein (HP) *I. galbana*

Parameter	Percentage content <sup>a</sup> (Mean ± SE)			Student's <i>t</i> test <i>P</i> value (LP algae vs. HP algae)
	PM	LP algae	HP algae	
Ash	4.18 ± 1.49 ( <i>n</i> = 3)	23.8 ± 1.1 ( <i>n</i> = 5)	19.7 ± 1.4 ( <i>n</i> = 6)	NS
Carbohydrate	0.49 ± 0.15 ( <i>n</i> = 11)	25.1 ± 0.6 ( <i>n</i> = 7)	20.2 ± 0.3 ( <i>n</i> = 7)	<i>P</i> = 0.002
Lipid	ND ( <i>n</i> = 5)	22.0 ± 0.6 ( <i>n</i> = 7)	17.1 ± 0.6 ( <i>n</i> = 7)	<i>P</i> = 0.006
Protein	83.7 ± 3.9 ( <i>n</i> = 10)	27.8 ± 0.8 ( <i>n</i> = 25)	42.6 ± 1.1 ( <i>n</i> = 26)	<i>P</i> < 0.0001
Carbon	45.9 ± 1.8 ( <i>n</i> = 5)	58.4 ± 3.5 ( <i>n</i> = 6)	56.5 ± 5.9 ( <i>n</i> = 6)	NS
Nitrogen	12.3 ± 0.2 ( <i>n</i> = 5)	3.89 ± 0.27 ( <i>n</i> = 6)	7.51 ± 0.22 ( <i>n</i> = 6)	<i>P</i> < 0.0001
C/N ratio	3.73 ± 0.05 ( <i>n</i> = 5)	15.0 ± 1.5 ( <i>n</i> = 6)	7.55 ± 0.87 ( <i>n</i> = 6)	<i>P</i> < 0.0001
(J mg <sup>-1</sup> ) (Mean ± SE)				
Energy content	19.7 ± 0.3 ( <i>n</i> = 5)	21.8 ± 2.3 ( <i>n</i> = 3)	24.3 ± 0.6 ( <i>n</i> = 4)	NS

Statistical differences between algae types were assessed with *t*-tests on arcsine square root transformed percentages.

NS = not significant ( $\alpha = 0.05$ ); ND = not detected.

<sup>a</sup> Except for C/N ratio, which is the percentage carbon composition divided by the percentage nitrogen composition, and energy content, which has units of joules per milligram.

respectively). Interestingly, LP and HP algae did not differ significantly ( $P > 0.05$ ) in carbon content; whereas HP algae contained significantly ( $P < 0.0001$ ) greater nitrogen (7.51%) than LP algae (3.89%), which resulted in a significantly ( $P < 0.0001$ ) lower C/N ratio in HP algae (7.55) than in LP algae (15.0). The energy content of LP and HP algae did not differ significantly (Table IV).

Cell protein content is plotted as a function of time in the bottom portion of Figure 3 for LP and HP algae. A multiple regression analysis ( $R^2 = 0.53$ ) with culture age and nitrogen concentration as variables suggested that algal protein content was significantly ( $P = 0.003$ ) correlated with culture nitrogen concentration, but not significantly ( $P > 0.05$ ) correlated with culture age. Separate linear regressions for LP and HP algae, however, indicated that protein content of HP algae significantly ( $P = 0.0002$ ) increased with culture age; whereas the protein content of LP algae was not significantly ( $P > 0.05$ ) correlated with culture age. Only 5- to 7-day-old cultures of LP and HP algae were harvested for mussel growth experiments.

#### Characteristics of protein microcapsules

The biochemical composition and energy content of PM used in this study are summarized in Table IV. The

average protein content (percent weight per weight) was 83.7%. Carbohydrate content was less than 1% w/w, and no measurable lipid was recovered gravimetrically. Ash accounted for 4.2% of the capsule weight. The nitrogen content of PM was 12.3%, which, if multiplied by the standard protein/nitrogen conversion factor of 6.25, gives a substantially lower estimate of capsule protein content (76.9%) than that measured analytically (83.7%). The reason for this discrepancy is unclear; however, the test kit for protein (Pierce BCA) may have overestimated capsule protein content (for a discussion of error associated with this method, see Zamer *et al.*, 1989). The carbon content of PM was measured to be 45.9% (Table IV), which, when expressed relative to nitrogen content, resulted in a C/N ratio of 3.73. The energy content of PM was 19.7 J mg<sup>-1</sup>, which was not significantly (ANOVA,  $P > 0.05$ ) different from the energy content of either LP or HP algae (21.8 and 24.3 J mg<sup>-1</sup>, respectively).

Amino acid compositions of mussel protein, algal protein, crab protein, and crab PM are given in Table V. With the exception of cysteine, all amino acids were present in all protein samples. Cysteine was poorly represented in both purified crab protein and crab PM, but it is not thought to be essential for mussels (see Discussion). To facilitate a comparison of protein quality between PM

**Table V**

Percent relative concentration of amino acids in protein hydrolysates from different sources

Amino acid	Percent relative concentration in protein hydrolysate				Percent relative to mussel protein	
	Algal protein	Crab protein	Crab PM	Mussel protein	In algal protein	In crab PM
THR*	7.13	8.23	7.34	8.16	87.4	90.0
VAL*	4.88	5.07	4.65	4.30	>100	>100
MET*	2.40	1.68	2.03	2.01	>100	>100
ILE*	4.20	4.59	6.90	4.17	>100	>100
LEU*	9.26	6.19	7.17	6.98	>100	>100
PHE*	4.53	3.98	3.80	3.32	>100	>100
LYS*	5.21	6.85	10.3	7.82	66.6	>100
HIS*	1.96	2.23	2.06	1.74	>100	>100
TRP*	0.761	0.544	0.567	0.467	>100	>100
ARG*	4.38	4.75	4.47	5.11	85.7	87.5
ASP	13.0	15.9	15.3	15.7	82.8	97.5
SER	6.78	6.72	6.34	8.53	79.5	74.3
GLU	9.62	14.7	12.0	11.8	81.5	>100
PRO*	4.74	3.14	2.24	4.20	>100	53.3
GLY	8.67	6.03	5.72	5.68	>100	>100
ALA	9.05	6.51	6.09	5.81	>100	>100
CYS	0.697	0.270	ND	1.39	50.2 <sup>a</sup>	0 <sup>a</sup>
TYR	2.77	3.14	2.99	2.85	97.2	>100

PM = protein microcapsules; ND = not detected.

\* Potentially essential amino acids.

<sup>a</sup> Cysteine was suspected to have been lost during purification of algal and crab protein.

and algal protein, the amount of each amino acid in each protein type was expressed relative to the amount measured in mussel tissue protein (Table V). In both algal protein and PM, the relative concentration of all potentially essential amino acids except lysine was estimated to be greater than 85% of the relative concentration in mussel protein. Lysine was present in algal protein at a relative concentration equivalent to only 67% of that in mussel protein.

#### Growth of mussels fed experimental diets

Shell heights and live weights of juvenile *M. trossulus* did not differ significantly (ANOVA,  $P > 0.05$ ) among the 24 experimental groups at the beginning of the experiment; however, within 1 week, significant differences in mussel growth rates were measured among mussels fed on the eight different diet types. Only growth rates calculated for the total 3-week period are given (Table VI). Nested ANOVAs indicated that mussel growth rates were statistically similar among the three replicates in each dietary treatment; therefore, shell height, live weight, and AFDTW measures of growth were combined for each set of three replicates and analyzed among diet treatments with one-way ANOVAs and Tukey's HSD multiple range tests.

Mussels fed LP *I. galbana* (T-ISO) (Diet 1) grew at significantly ( $P < 0.05$ ) lower rates than mussels fed HP *I. galbana* (Diet 6), when delivered at satiation rations of 27.5% bw d<sup>-1</sup>. Based on shell height, live weight, and AFDTW, growth rates of mussels fed LP algae (Diet 1) were 51, 56, and 53%, respectively, of corresponding growth rates of mussels fed HP algae (Diet 6). Starved control mussels (Diet 8) failed to grow, demonstrating that mussels were unable to derive sufficient nutrients from their culture medium (e.g., dissolved organic material, "background" particulate material) to exceed maintenance requirements. Mortality did not vary significantly (ANOVA,  $P > 0.05$ ) among dietary treatments.

Growth rates of mussels fed LP algae were significantly improved when the ration of LP algae was supplemented with PM (Table VI). Furthermore, there was a proportional increase in mussel growth rate with progressively higher supplements of PM to the LP algal diet. The instantaneous growth (live weight) rate of mussels fed LP algae with the highest supplement of PM (Diet 5;  $17.0 \times 10^{-3} \text{ d}^{-1}$ ) was statistically equal to that of mussels fed only HP algae (Diet 6;  $17.5 \times 10^{-3} \text{ d}^{-1}$ ). Similarly, instantaneous AFDTW growth rates were not significantly ( $P > 0.05$ ) different among groups of mussels fed either LP algae with a 1.0 RPR capsule supplement (Diet 4;  $48.0 \times 10^{-3} \text{ d}^{-1}$ ), LP algae with a 1.5 RPR capsule supplement (Diet 5;  $47.1 \times 10^{-3} \text{ d}^{-1}$ ), or HP algae alone (Diet 6;  $53.3 \times 10^{-3} \text{ d}^{-1}$ ) (Table VI). Supplements of PM added to HP algae (Diet 7) did not improve mussel growth rates com-

Table VI

Increase in shell height, live weight, and ash-free dry tissue weight (AFDTW) of juvenile *Mytilus trossulus* fed eight experimental diets

Diet	Mortality (%)	Increase in shell height (%)	Instantaneous growth rate ( $\times 10^{-3} \text{ d}^{-1}$ )	
			Live weight	AFDTW
1. LP	9.6 ± 3.6	5.81 ± 0.27 <sup>C</sup>	9.73 ± 0.59 <sup>D</sup>	28.0 ± 1.95 <sup>C</sup>
2. LP + LP (RER)	12.2 ± 6.4	5.90 ± 0.37 <sup>C</sup>	10.3 ± 0.71 <sup>CD</sup>	29.9 ± 2.23 <sup>C</sup>
3. LP + 0.5 RPR	6.5 ± 2.3	7.92 ± 0.31 <sup>BC</sup>	13.4 ± 0.74 <sup>C</sup>	36.8 ± 2.86 <sup>BC</sup>
4. LP + 1.0 RPR	17.8 ± 9.7	7.30 ± 0.38 <sup>C</sup>	13.8 ± 1.10 <sup>BC</sup>	48.0 ± 4.85 <sup>AB</sup>
5. LP + 1.5 RPR	0.6 ± 5.0	10.8 ± 0.46 <sup>AB</sup>	17.0 ± 0.87 <sup>AB</sup>	47.1 ± 3.58 <sup>AB</sup>
6. HP	12.6 ± 5.1	11.5 ± 0.42 <sup>A</sup>	17.5 ± 0.86 <sup>A</sup>	53.3 ± 3.23 <sup>A</sup>
7. HP + 0.5 RPR	4.2 ± 8.1	11.4 ± 0.52 <sup>A</sup>	17.6 ± 1.00 <sup>A</sup>	54.7 ± 4.35 <sup>A</sup>
8. Starved	5.6 ± 8.6	0.02 ± 0.01 <sup>D</sup>	1.49 ± 0.46 <sup>E</sup>	-15.5 ± 2.49 <sup>D</sup>

LP and HP refer to low-protein algae and high-protein algae, respectively. RER refers to the replacement energy ration, and RPR refers to the replacement protein ration. For each growth parameter, values having common superscripted letters among dietary treatments are not statistically different (ANOVA,  $P < 0.05$ ). Values reported are means ± SE ( $n = 3$  per value).

pared to those of mussels fed only HP algae (Diet 6; Table VI). Growth of mussels that were fed LP algae at a ration of 34.1% bw d<sup>-1</sup> (LP + LP; Diet 2) did not grow significantly ( $\alpha > 0.05$ ) faster than mussels fed LP algae at 27.5% bw d<sup>-1</sup> (Diet 1; see Table VI). This result confirms the findings of a preliminary experiment in which growth of mussels fed on algal rations reached an asymptote at a ration of 27.5% bw d<sup>-1</sup>, and growth rates did not increase at higher rations. These latter results clearly indicate that growth of mussels fed on LP algae was not limited by ration size.

The instantaneous growth (live weight) rate ( $\text{IGR}_{\text{lw}}$ ) of mussels is plotted versus the estimated C/N ratio of the assimilated (bioavailable) portion of each diet ( $\text{C/N}_{\text{ass}}$  ratio) in Figure 4.  $\text{C/N}_{\text{ass}}$  ratios were slightly different than the C/N ratios of the diets actually delivered to mussels ( $\text{C/N}_{\text{tot}}$  ratio) because PM were assumed to be assimilated with lower efficiency (e.g., 30%; Kreeger, 1993) than microalgae (e.g., 75%, Bayne and Newell, 1983).  $\text{C/N}_{\text{tot}}$  ratios were 15.0, 15.0, 10.4, 8.44, 7.39, 7.55, and 6.51 for Diets 1–7, respectively; whereas estimated  $\text{C/N}_{\text{ass}}$  ratios were 15.0, 15.0, 12.4, 11.0, 9.86, 7.55, and 7.06 for Diets 1–7, respectively (Table III). Mussel growth rates were inversely related to estimated  $\text{C/N}_{\text{ass}}$  ratios between 10 and 15; whereas growth rates appeared to be independent of  $\text{C/N}_{\text{ass}}$  ratios less than 10 (Fig. 4). A linear regression of  $\text{IGR}_{\text{lw}}$  as a function of  $\text{C/N}_{\text{ass}}$  ratio was highly significant ( $P < 0.0001$ ) over the range of  $\text{C/N}_{\text{ass}}$  ratios between 7.1 and 15.0. Additional regressions indicated that  $\text{IGR}_{\text{lw}}$  was also significantly ( $P < 0.01$ ) correlated with  $\text{C/N}_{\text{tot}}$  as well as with the estimated total and bioavailable protein ration in the mussel's diet.

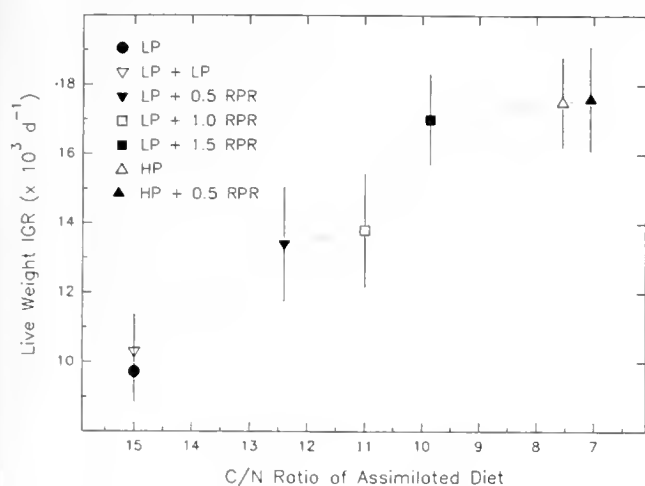


**Figure 4.** Mean ( $\pm 95\%$  CI) instantaneous live weight growth rate ( $IGR_w; \times 10^{-3} d^{-1}$ ) of juvenile *Mytilus trossulus* as a function of the estimated C/N ratio of the assimilated portion of Diets 1–7. LP and HP refer to low-protein algae and high-protein algae, respectively. RPR refers to the replacement protein ration, and RER refers to the replacement energy ration.

Despite highly significant differences in growth rates of mussels fed different diets, mussel tissue biochemical composition was not appreciably altered by ration composition. Initially, the protein content of all mussels was 53% (Table VII). After 3 weeks, the protein content of mussel tissues varied significantly (ANOVA,  $P < 0.05$ ), ranging from 34% to 56%, among dietary treatments; however, tissue protein content was not clearly correlated with dietary protein content, and differences were only marginally significant. The lowest tissue protein contents were measured in mussels that were fed LP algae (Diet 1), and the highest tissue protein contents were measured in mussels fed LP algae with either 0.5 RPR or 1.0 RPR protein capsules (Diets 3 and 4). Lipid content was significantly (ANOVA,  $P < 0.05$ ) greater in tissues of mussels fed LP algae alone (Diet 1) than in any other group of mussels, including the starved controls (Table VII)—a result that is questionable given the high variability associated with lipid values for mussels fed Diet 1. No significant (ANOVA,  $P > 0.05$ ) differences were found in carbohydrate contents among mussels fed different diets (Table VII).

Oxygen consumption rates of mussels at the start of the experiment did not differ significantly (ANOVA,  $P > 0.05$ ) among the 24 groups and averaged  $116 \mu\text{g-at O}_2 \text{ h}^{-1} [\text{g AFDTW}]^{-1}$  (Table VIII). After the 3-week rearing period, however, rates of oxygen consumption were lower in all groups ( $9.3\text{--}75.3 \mu\text{g-at O}_2 \text{ h}^{-1} \text{ g}^{-1}$ ). Mussels fed LP diets generally had higher rates of oxygen consumption than mussels fed HP diets but, due to high variability in rates, differences were not significant ( $P > 0.05$ ) among groups fed Diets 1–7 (Table VIII). Starved controls

**Table VII**

*Proximate biochemical composition of the tissues of juvenile Mytilus trossulus after being fed for 3 weeks on eight experimental diets and at the start (initial) of the growth experiment*

Diet	Percentage composition (Mean $\pm$ SE; $n = 3$ )		
	Protein	Lipid	Carbohydrate
Initial	53.3 $\pm$ 4.5	NM	8.00 $\pm$ 0.20
1. LP	34.1 $\pm$ 2.7 <sup>B</sup>	29.7 $\pm$ 3.2 <sup>A</sup>	10.86 $\pm$ 0.20
2. LP + LP (RER)	44.3 $\pm$ 2.6 <sup>AB</sup>	17.1 $\pm$ 0.6 <sup>B</sup>	11.36 $\pm$ 1.30
3. LP + 0.5 RPR	50.0 $\pm$ 1.6 <sup>A</sup>	19.2 $\pm$ 0.4 <sup>B</sup>	10.12 $\pm$ 0.17
4. LP + 1.0 RPR	55.7 $\pm$ 3.1 <sup>A</sup>	17.1 $\pm$ 0.7 <sup>B</sup>	10.23 $\pm$ 0.06
5. LP + 1.5 RPR	43.6 $\pm$ 0.7 <sup>AB</sup>	16.8 $\pm$ 0.3 <sup>B</sup>	8.39 $\pm$ 0.84
6. HP	41.1 $\pm$ 0.9 <sup>AB</sup>	16.8 $\pm$ 0.2 <sup>B</sup>	8.08 $\pm$ 0.92
7. HP + 0.5 RPR	47.5 $\pm$ 1.4 <sup>AB</sup>	16.3 $\pm$ 0.4 <sup>B</sup>	9.56 $\pm$ 0.34
8. Starved	43.7 $\pm$ 2.1 <sup>AB</sup>	16.8 $\pm$ 0.1 <sup>B</sup>	9.03 $\pm$ 0.32

LP and HP refer to low-protein algae and high-protein algae, respectively. RER refers to the replacement energy ration, and RPR refers to the replacement protein ration. For each of the protein, lipid, or carbohydrate contents (percent dry weight), values having common superscripted letters among dietary treatments are not statistically different (ANOVA,  $P < 0.05$ ).

NM = not measured; samples lost.

consumed only  $9.3 \mu\text{g-at O}_2 \text{ h}^{-1} \text{ g}^{-1}$ , which was significantly ( $P < 0.05$ ) lower than rates of oxygen consumption by mussels fed Diets 1 ( $72.8 \mu\text{g-at O}_2 \text{ h}^{-1} \text{ g}^{-1}$ ) and 3 ( $75.3 \mu\text{g-at O}_2 \text{ h}^{-1} \text{ g}^{-1}$ ). Rates of ammonia nitrogen excretion were greatest in mussels fed LP algae with the greatest supplementation of PM (Diet 5;  $7.01 \mu\text{g-at NH}_4^+\text{-N h}^{-1} \text{ g}^{-1}$ ) (Table VIII). The only significant (ANOVA,  $P < 0.05$ )

**Table VIII**

*Rates of oxygen consumption and nitrogen excretion and O/N ratios of juvenile Mytilus trossulus at the beginning and end of the growth experiment*

Diet	Oxygen consumption ( $\mu\text{g-at O}_2 \text{ h}^{-1}$ [g AFDTW] $^{-1}$ )	Nitrogen excretion ( $\mu\text{g-at NH}_4^+\text{-N h}^{-1}$ [g AFDTW] $^{-1}$ )	O/N ratio
Initial	116 $\pm$ 9.8	6.14 $\pm$ 0.39	18.9 $\pm$ 1.0
1. LP	72.8 $\pm$ 11.7 <sup>A</sup>	3.44 $\pm$ 0.38 <sup>B</sup>	21.2 $\pm$ 5.5 <sup>A</sup>
2. LP + LP (RER)	66.8 $\pm$ 15.4 <sup>AB</sup>	3.60 $\pm$ 0.08 <sup>AB</sup>	18.6 $\pm$ 4.8 <sup>A</sup>
3. LP + 0.5 RPR	75.3 $\pm$ 25.7 <sup>A</sup>	6.68 $\pm$ 1.30 <sup>AB</sup>	11.3 $\pm$ 4.3 <sup>AB</sup>
4. LP + 1.0 RPR	41.8 $\pm$ 3.7 <sup>AB</sup>	6.06 $\pm$ 1.02 <sup>AB</sup>	6.90 $\pm$ 1.36 <sup>AB</sup>
5. LP + 1.5 RPR	51.2 $\pm$ 9.4 <sup>AB</sup>	7.01 $\pm$ 0.91 <sup>A</sup>	7.30 $\pm$ 1.53 <sup>AB</sup>
6. HP	31.5 $\pm$ 8.6 <sup>AB</sup>	6.09 $\pm$ 0.50 <sup>AB</sup>	5.17 $\pm$ 1.81 <sup>B</sup>
7. HP + 0.5 RPR	54.5 $\pm$ 7.1 <sup>AB</sup>	5.43 $\pm$ 0.09 <sup>AB</sup>	10.0 $\pm$ 1.4 <sup>AB</sup>
8. Starved	9.30 $\pm$ 7.38 <sup>B</sup>	4.97 $\pm$ 0.38 <sup>AB</sup>	1.87 $\pm$ 1.37 <sup>C</sup>

LP and HP refer to low-protein algae and high-protein algae, respectively. RER refers to the replacement energy ration, and RPR refers to the replacement protein ration. For each parameter, values having common superscripted letters among dietary treatments are not statistically different (ANOVA,  $P < 0.05$ ). Values reported are mean  $\pm$  SE ( $n = 3$  per measurement, except  $n = 24$  for initial readings).

difference in nitrogen excretion among treatment groups was between mussels fed Diet 5 and mussels fed on LP algae alone (Diet 1;  $3.44 \mu\text{g-at NH}_4^+\text{-N h}^{-1} \text{g}^{-1}$ ).

Even though rates of oxygen consumption and nitrogen excretion did not vary substantially among treatments, differences in O/N ratios among treatments were more discernible (Table VIII, Fig. 5). At the beginning of the experiment, no significant differences were detected in O/N ratios among the 24 groups of mussels, and the initial mean O/N ratio was 18.9, indicating that carbohydrates and perhaps lipids were being catabolized preferentially compared to protein. In contrast, after the 3-week experimental period, O/N ratios of mussels fed diets rich in protein (e.g., Diets 4–6) were reduced to less than 8, reflecting greater catabolism of protein than carbohydrates (Fig. 5). Due to high variability among replicates (statistical resolution of differences in O/N ratios among treatments was poor, see Table VIII), however, O/N ratios of mussels fed LP algae alone (Diets 1 and 2) were significantly ( $P < 0.05$ ) greater than those of mussels fed on HP algae alone (Diet 6). Due to very low rates of oxygen consumption, starved mussels (Diet 8) had an O/N ratio of 1.9, which was statistically ( $P < 0.05$ ) lower than that of fed mussels.

### Discussion

Much is now known about quantitative and caloric dietary effects on feeding, assimilation efficiency, and growth of bivalve molluscs because quantitative aspects of bivalve diets (e.g., algal cell concentration) are easily manipulated (for reviews, see Bayne and Newell, 1983; Hawkins and Bayne, 1992; Langdon and Newell, 1992; Newell and Langdon, 1992). Previous findings (Gallager and Mann, 1981; Langdon and Waldoock, 1981; Langdon, 1982; Webb and Chu, 1982; Enright *et al.*, 1986b; Utting, 1986) indicated, however, that qualitative aspects of diets are also important in determining growth of bivalves. For example, it has commonly been observed that bivalves grow more quickly when fed mixtures of several algal species than when fed monospecific diets (Epifanio, 1979, 1982; Webb and Chu, 1982), presumably because the quality of mixed-species diets is more balanced. The qualitative nutritional requirements of suspension-feeding animals are poorly known compared to those of macrophagic marine animals, because there are technical difficulties in manipulating the composition of microparticulate diets.

The effect of diet quality on suspension-feeding bivalves has previously been studied primarily by comparison of algal diets that vary in biochemical composition. Two related approaches have been used. First, bivalves have been fed different algal species that vary in biochemical composition, and bivalve assimilation or growth has then been correlated with qualitative attributes of the diets

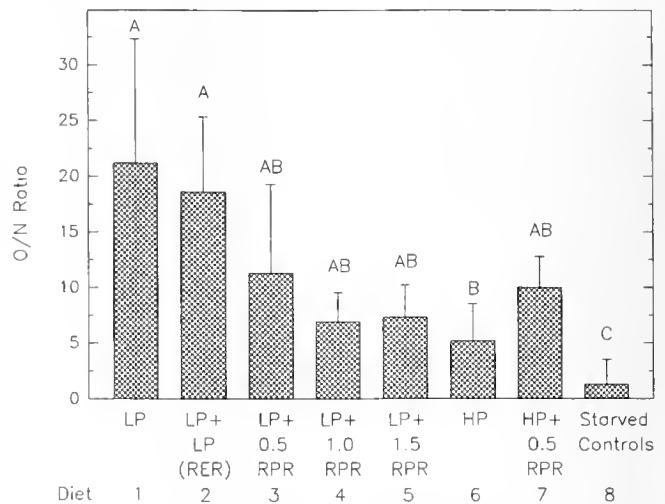


**Figure 5.** O/N ratios (mean  $\pm$  95% CI) of juvenile *Mytilus trossulus* after being fed for 3 weeks on Diets 1–7 composed of low-protein (LP) or high-protein (HP) algae, with or without protein microcapsules. Mussels in dietary treatment 8 were starved. RER refers to the replacement energy ration, and RPR refers to the replacement protein ration. Values having common letters are not significantly (ANOVA,  $P < 0.05$ ) different.

(Flaak and Epifanio, 1978; Webb and Chu, 1982; Enright *et al.*, 1986a; Whyte *et al.*, 1989). Alternatively, growth rates have been compared among bivalves fed monospecific algal diets that vary in biochemical composition due to manipulation of algal culture conditions such as (1) availability of inorganic carbon (Pruder and Bolton, 1979), (2) light intensity or wavelength (Flaak and Epifanio, 1978; Gallager and Mann, 1981; Thompson *et al.*, 1989, 1990), (3) age at which cells are harvested (Sakshaug and Holm-Hansen, 1977; Fabregas *et al.*, 1985, 1986; Utting, 1985; Whyte, 1987; Fernandez-Reirez *et al.*, 1989), and (4) nutrient concentrations in culture media (Sakshaug and Holm-Hansen, 1977; Gallager and Mann, 1981; Utting, 1985; Enright *et al.*, 1986b). The latter approach was used in this study: nitrogen concentrations of cultures of the alga *I. galbana* (clone T-ISO) were manipulated, and the consequent nutritional value of nitrogen-limited algae was determined for the mussel *M. trossulus*.

Reduction of the nitrogen concentration of the culture medium has been shown to lower cellular protein content during both exponential and stationary growth phases of algae (Utting, 1985; Enright *et al.*, 1986b). In this study, nitrogen limitation in cultures of *I. galbana* effectively reduced cell protein content regardless of the age of the culture (Fig. 3, bottom). Algae cultured in f/2 medium (Guillard and Ryther, 1962) in which the nitrogen concentration was reduced by 60%, to  $0.353 \text{ mg-at NaNO}_3\text{-N l}^{-1}$ , contained only 65% of the protein of algae grown in a medium having twice the standard nitrogen concentration ( $1.765 \text{ mg-at NaNO}_3\text{-N l}^{-1}$ ). Similarly, Utting (1985) reported a 30% reduction in the cell protein content

of *I. galbana* when the nitrogen concentration of the culture medium was lowered by 94%.

Other researchers have reported that the biochemical composition of algae can vary with culture age (Sakshaug and Holm-Hansen, 1977; Fabregas *et al.*, 1985, 1986; Utting, 1985; Whyte, 1987; Fernandez-Reiriz *et al.*, 1989). The protein content of algal cells can either decrease or increase with culture age, depending on species and conditions (Utting, 1985; Whyte, 1987; Fernandez-Reiriz *et al.*, 1989). In this study, the cellular protein content of HP *I. galbana* significantly increased during the first 12 days of culture. HP algae did not reach stationary phase until about the 10th day of culture, and the protein content remained high during this phase. The protein content of LP *I. galbana* tended to decline after stationary phase was reached on day 7, but this decrease was not significant.

Algae were routinely harvested for delivery to mussels between days 5 and 7 of culture because during this period LP and HP cultures consistently appeared healthy, as judged visually by the normality of their cell-size distributions. Cell volumes ( $14\text{--}21\ \mu\text{m}^3$ ) of *I. galbana* were generally smaller than those reported by other workers (e.g.,  $46\text{--}74\ \mu\text{m}^3$ , Enright *et al.*, 1986a;  $14\text{--}34\ \mu\text{m}^3$ , Riisgard, 1988), although cell volumes of both LP and HP algae increased significantly with age. Furthermore, algal cells cultured under low-nitrogen conditions were always slightly larger than those of the same age cultured under high-nitrogen conditions. The purpose of measuring cell volume in this study was to allow accurate prediction of cell AFDW. Cell volume was measured with high precision (low coefficients of variation), and the linear regression equation relating algal volume to AFDW was highly significant. The range of cell volume, 14 to  $21\ \mu\text{m}^3$ , corresponded to a range in cell AFDW of between 35 and  $53\ \text{pg cell}^{-1}$ , which was greater than the cell dry weight of  $29.7\ \text{pg cell}^{-1}$  for *I. galbana* (clone T-ISO) reported by Brown (1991). Because cell volume (and therefore AFDW) varied with both time and protein content, it was important to dispense algal rations for mussels based on cell volume (and therefore AFDW) and not simply on cell concentration; otherwise the diets might have differed by up to 50% in energy content. No significant (Student's *t* test,  $P > 0.05$ ) differences were measured in the energy content (per unit dry weight) of LP and HP algae in this study, which confirms a similar report for *I. galbana* by Utting (1985).

Growth rates of juvenile *M. trossulus* were significantly greater when mussels were fed HP *I. galbana* rather than an equal ration of the LP algae. For example, mussels fed LP algae at a ration of  $27.5\% \text{ bw d}^{-1}$  grew in shell height, live weight, and AFDW at rates (5.8, 9.7, 28.0, respectively) that were only 50–55% of those of mussels fed an equivalent ration of HP algae (11.5, 17.5, 53.3, respectively). These results supported findings from a preliminary experiment in which growth rates of mussels fed LP

algae at 10 different rations were approximately 50% of growth rates of mussels fed equivalent rations of HP algae.

A standard algal ration of  $27.5\% \text{ bw d}^{-1}$  was used in this study because a preliminary experiment showed that this ration supported the highest growth rates of mussels, and that rations above  $27.5\% \text{ bw d}^{-1}$  caused mussels to produce pseudofeces. An increase in the ration of LP algae from the standard ration (Diet 1) to  $34.1\% \text{ bw d}^{-1}$  (Diet 2) did not improve mussel growth rates. This finding, together with results from the preliminary experiment (see above), indicate that the difference in growth rates between mussels fed LP and HP algae was a result of differences in diet quality rather than diet quantity or ration size. This correlation between the growth rate of juvenile *M. trossulus* and the protein content of algal diets agrees with previous findings for other bivalve species (Langton *et al.*, 1977; Gallager and Mann, 1981; Webb and Chu, 1982; Enright *et al.*, 1986b). Gallager and Mann (1981), for example, reported that algae with low protein content were inferior to algae of higher protein content in supporting growth of juvenile Manila clams, *Tapes japonica*. Increases in the protein content of algal diets have also been shown to improve settlement of larval *Crassostrea gigas* (Utting, 1986).

As with all previous studies in which bivalve growth has been correlated with algal composition, it is not possible to conclude, based only on data from LP and HP diets (Diets 1, 2, and 6), that algal protein content was directly responsible for variation in mussel growth rates among experimental diets, because nonprotein nutritional constituents of these diets may have co-varied with protein content. In Diets 3, 4, and 5, however, the ration of dietary protein for *M. trossulus* was manipulated independently of algal composition by addition of supplements of microencapsulated protein to LP and HP algal diets. Therefore, the effect of dietary protein content on mussel growth was directly examined without altering algal biochemical composition. Supplementation of LP algae with PM significantly improved the growth rate of juvenile mussels compared to that of mussels fed LP algae alone, which clearly demonstrates that juvenile *M. trossulus* used PM for growth. PM delivered at the highest ration in combination with LP algae supported mussel growth equivalent to that of mussels fed HP algae, and so completely compensated for the lower growth rates of mussels fed LP algae alone. Similar experiments have been used to examine the nutritional requirements of macrophagous marine animals (Kanazawa, 1982; Wilson, 1989). Few researchers, however, have conducted this type of experiment with bivalve suspension-feeders (Gabbott *et al.*, 1976; Langdon and Waldock, 1981; Chu *et al.*, 1982).

PM were composed of approximately 84% protein (based on biochemical analysis). PM have been shown to be filtered, digested, and assimilated by mussels (Kreeger, 1992, 1993). To be of value as a growth supplement,



encapsulated protein must not only be bioavailable, but must also have a balance of essential amino acids that meets the qualitative requirements of the consumer. For many animals, the essential amino acids have been identified as threonine (THR), valine (VAL), methionine (MET), isoleucine (ILE), leucine (LEU), phenylalanine (PHE), lysine (LYS), histidine (HIS), tryptophan (TRP), and arginine (ARG) (Lehninger, 1976; Deshimaru, 1982; Bishop *et al.*, 1983). Unfortunately, the essential amino acid requirements of bivalve molluscs have not been fully ascertained, primarily due to problems in developing a defined diet for suspension-feeders, but are generally believed to be similar to those of other animals (Bishop *et al.*, 1983). Harrison (1975), for example, reported that the California mussel, *M. californianus*, had a dietary requirement for the same 10 amino acids listed above, and perhaps also for proline (PRO).

All of the amino acids considered to be essential for bivalves were substantially present in both algal protein and PM made from crab protein, with two exceptions. The concentration of LYS in protein from *I. galbana* was only 67% of the relative concentration measured in protein from *M. trossulus*. Brown (1991) similarly reported that LYS concentrations in protein from the same clone of *I. galbana*, as well as from 15 other species of microalgae, were lower than the relative concentrations of LYS in protein derived from larval *C. gigas*. The only amino acid for which PM apparently had a deficiency was cysteine (CYS). CYS may have been oxidized during TCA purification of the crab protein (Allen, 1981) because the CYS concentration in purified crab protein was only one-sixth that found before purification. This loss was not considered crucial because *M. edulis* is reported to be capable of converting MET into CYS (Allen and Awapara, 1960).

A nutritious protein has an amino acid profile similar to that in the tissues of the consumer organism (Phillips and Brockway, 1956). Both algal protein and crab PM contained relative concentrations of essential amino acids that were comparable to the amino acid profile of protein purified from *M. trossulus*. Relative concentrations of essential amino acids have been quantitatively compared between bivalve suspension-feeders and their algal diets by calculation of an essential amino acid index (EAAI) (Brown and Jeffrey, 1992). If the quality of a dietary protein is high, the EAAI will be greater than 90; EAAI values less than 70 indicate that the dietary protein is qualitatively poor (Brown and Jeffrey, 1992). Assuming that *M. trossulus* requires 11 essential amino acids (including PRO), then the EAAI calculated for *I. galbana* protein and crab PM were 109 and 105, respectively, which indicates that the quality of protein in these dietary constituents was indeed sufficient for supporting the growth of mussels.

One difficulty in conducting bivalve growth experiments with artificial diets is that bacteria commonly multiply rapidly in the culture system. Thus, it can be unclear

whether bivalve growth is significantly affected by the utilization of bacteria associated with the artificial diets (*e.g.*, Langdon and Bolton, 1984; Langdon and Siegfried, 1984). Considerable recent evidence indicates that some suspension-feeding bivalves are able to derive nutrition from free-living bacteria in the water column or bacteria attached to suspended particulate material (Birkbeck and McHenry, 1982; Wright *et al.*, 1982; Crosby *et al.*, 1990; Langdon and Newell, 1990; Baldwin and Newell, 1991; Douillet, 1991). Leakage rates of PM in this study were low (*e.g.*, 0.5–2% d<sup>-1</sup>, Kreeger, 1992) compared to rates previously reported from PM (*e.g.*, 5–40% d<sup>-1</sup>; Langdon, 1989; Langdon and DeBevoise, 1990). Therefore, mussels probably did not obtain additional nutrients either by taking up the leaked nutrients directly or by ingesting capsule-derived nutrients indirectly in the form of microorganisms. Furthermore, mussels were reared in a continuous flow of filtered (0.7 µm) seawater with eight water volume changes per day, which probably helped to keep the concentrations of microorganisms low. Kreeger and Langdon (1993) reported, for example, that bacteria did not contribute to <sup>14</sup>CO<sub>2</sub> respiration in a similar continuous-flow system in which *M. trossulus* were fed <sup>14</sup>C-labeled PM. Starved control mussels either did not grow or lost weight, which suggests that fed mussels derived food primarily from their experimental diets. Because bacteria apparently did not contribute to mussel nutrition in this study, we concluded that dietary protein content was indeed the qualitative dietary factor of LP algae that was limiting the growth of mussels fed only LP algal diets.

Compared to mussels fed LP algae, mussels fed diets rich in protein for 3 weeks tended to have more protein and less lipid and carbohydrate in their tissues, although the differences were only marginally significant. O/N ratios of mussels fed on LP algae at either 27.5 or 34.1% bw d<sup>-1</sup> were 21.2 and 18.6, respectively, suggesting that these mussels were primarily catabolizing carbohydrates and conserving protein for anabolism. In contrast, mussels fed diets with greater protein content (*e.g.*, HP algae or LP algae with PM supplements) had significantly lower O/N ratios (*e.g.*, 5–10), which suggests that dietary protein was being preferentially catabolized. Starved mussels had O/N ratios below theoretical minimums, probably because their oxygen consumption had decreased to standard rates while nitrogen excretion continued at higher rates during stress (Bayne, 1973a, b; Gabbott and Bayne, 1973). If dietary protein content led to both significantly lower growth rates and higher O/N ratios in mussels fed LP algae compared with HP algae, then the high O/N ratios (*e.g.*, 19) of mussels at the beginning of the experiment indicate that growth rates of juvenile *M. trossulus* in Yaquina Bay, Oregon, may have been limited by dietary protein bioavailability at the time they were sampled (May 1992).

C/N ratios of the bioavailable portion of diets (C/N<sub>ass</sub> ratios; based on estimated assimilation by mussels) varied



from 7.1 to 15.0 and were similar to overall C/N ratios of diets delivered to mussels (C/N<sub>tot</sub> ratios; 6.5 to 15.0). Hawkins and Bayne (1992) reported that *M. edulis* requires an average dietary C/N<sub>tot</sub> ratio of 16 in order to meet its maintenance requirements for carbon and nitrogen, and they suggested that C/N<sub>tot</sub> ratios below 16, such as those typically recorded during algal blooms, may cause transient nutritional limitation by utilizable carbon. In this study, however, the growth rates of juvenile *M. trossulus* were highest at the lowest C/N<sub>tot</sub> ratios (e.g., 6.5–7.5 for Diets 6 and 7) and became progressively lower as dietary C/N<sub>ass</sub> ratios increased above 9.9. Similarly, Gallagher and Mann (1981) reported that growth of juvenile clams, *Tapes japonica*, was greatest when diets had C/N<sub>tot</sub> ratios between 8.4 and 10.5 and that ratios above 10.5 negatively affected growth. Thus, high dietary C/N<sub>tot</sub> ratios (e.g., >10–16) could cause mussel growth to be limited by available nitrogen and protein in the diet.

Little is known about C/N ratios of natural diets for suspension-feeding bivalves. In natural seston, these ratios are likely to vary widely during the year in association with phytoplankton blooms, storm events, or variation in allochthonous food sources. Seasonal changes in concentrations of particulate organic material (POM) and particulate "bioavailable" protein in the seston of Yaquina Bay, Oregon, were reported by Kreeger (1993), and are used to estimate dietary C/N ratios for *M. trossulus* *in situ*. Assuming that 16% of protein is nitrogen and 50% of POM is carbon, then C/N ratios of seston in Yaquina Bay are estimated to vary from 6 (during summer) to 17 (during winter), which is about equal to the experimental range of dietary C/N<sub>tot</sub> ratios used in the growth experiment. Dietary protein availability could, therefore, affect growth rates of juvenile *M. trossulus* in Yaquina Bay at certain times of the year, such as during winter when concentrations of bioavailable protein are lowest (Kreeger, 1993).

In summary, growth of juvenile *M. trossulus* can be significantly affected by variation in dietary protein content at rations at which mussels are satiated, and possibly at lower rations as well. Growth rates of mussels in this study were directly related to dietary protein content (and the estimated bioavailable, assimilated portion) over the range 28 to 43% dry w/w, and inversely related to dietary C/N ratios (and C/N ratios of estimated bioavailable, assimilated portions) over the range 6.5 to 15.0. Cross-linked walled protein microcapsules were found to be beneficial dietary supplements for mussels fed on nitrogen-limited, cultured algae, and they were capable of fully compensating for algal protein deficiencies. Future studies of this kind will be necessary to ascertain the overall nutritional requirements of bivalves. This knowledge will contribute to a better understanding of both the trophic ecology of natural populations of these animals and the ingredients

necessary to produce balanced, inexpensive diets for bivalve aquaculture.

### Acknowledgments

We thank A. J. S. Hawkins, K. Y. Kreeger, and B. L. Bayne for comments on this manuscript. This research was supported by Oregon Sea Grant, National Oceanographic and Atmospheric Administration, Office of Sea Grant, Department of Commerce, Grant No. NA 85AA-D-SG095 under Project R/AQ-56 to C. J. Langdon. Additional support was provided to D. A. Kreeger by a Graduate School Fellowship from Oregon State University, a Brucefield-Reynolds Scholarship from the Hatfield Marine Science Center, and a Mastin Grant from the Department of Fisheries and Wildlife, Oregon State University.

### Literature Cited

- Allen, G. 1981. Conversion of cysteine residues to stable derivatives. Pp. 28–29 in *Sequencing of Proteins and Peptides*. North-Holland Publishing Company, New York.
- Allen, K., and J. Awapara. 1960. Metabolism of sulfur amino acids in *Mytilus edulis* and *Rangia cuneata*. *Biol. Bull.* 118: 173–182.
- Asmus, R. 1986. Nutrient flux in short-term enclosures of intertidal sand communities. *Ophelia* 26: 1–18.
- Asmus, R. M., and H. Asmus. 1991. Mussel beds: limiting or promoting phytoplankton? *J. Exp. Mar. Biol. Ecol.* 148: 215–232.
- Baldwin, B. S., and R. I. E. Newell. 1991. Omnivorous feeding by planktotrophic larvae of the eastern oyster *Crassostrea virginica*. *Mar. Ecol. Prog. Ser.* 78: 285–301.
- Bayne, B. L. 1973a. Aspects of the metabolism of *Mytilus edulis* during starvation. *Neth. J. Sea Res.* 7: 399–410.
- Bayne, B. L. 1973b. Physiological changes in *Mytilus edulis* L. induced by temperature and nutritive stress. *J. Mar. Biol. Ass. U. K.* 53: 39–58.
- Bayne, B. L., and R. C. Newell. 1983. Physiological energetics of marine Mollusca. Pp. 407–515 in *The Mollusca*, Vol. 4, A. S. M. Saleuddin, and K. M. Wilbur, eds. Academic Press, New York.
- Birkbeck, T. II., and J. G. McIlenerney. 1982. Degradation of bacteria by *Mytilus edulis*. *Mar. Biol.* 72: 7–15.
- Bishop, S. H., L. L. Ellis, and J. M. Burcham. 1983. Pp. 243–327 in *The Mollusca*, Vol. 1, P. W. Hochachka, ed. Academic Press, New York.
- Brey, T., II. Rumohr, and S. Ankar. 1988. Energy content of macrobenthic invertebrates: general conversion factors from weight to energy. *J. Exp. Mar. Biol. Ecol.* 117: 271–278.
- Brown, M. R. 1991. The amino-acid and sugar composition of 16 species of microalgae used in mariculture. *J. Exp. Mar. Biol. Ecol.* 145: 79–99.
- Brown, M. R., and S. W. Jeffrey. 1992. Biochemical composition of microalgae from the green algal classes Chlorophyceae and Prasinophyceae. 1. Amino acids, sugars and pigments. *J. Exp. Mar. Biol. Ecol.* 161: 91–113.
- Chu, F., K. L. Webb, D. Hepworth, and M. Roberts. 1982. The acceptability and digestibility of microcapsules by larvae of *Crassostrea virginica*. *J. Shellfish Res.* 2: 29–34.
- Crosby, M. P., R. I. E. Newell, and C. J. Langdon. 1990. Bacterial mediation in the utilization of carbon and nitrogen from detrital complexes by *Crassostrea virginica*. *Limnol. Oceanogr.* 35(3): 625–639.

- Dame, R. F., and N. Dankers. 1988. Uptake and release of materials by a Wadden Sea mussel bed. *J. Exp. Mar. Biol. Ecol.* **118**: 207-216.
- Dame, R. F., R. G. Zingmark, and E. Haskin. 1984. Oyster reefs as processors of estuarine materials. *J. Exp. Mar. Biol. Ecol.* **83**: 239-247.
- Dame, R. F., T. G. Wolaver, and S. M. Libes. 1985. The summer uptake of nitrogen by an intertidal oyster reef. *Neth. J. Sea Res.* **19**: 265-268.
- Deshimaru, O. 1982. Protein and amino acid nutrition of the prawn *Penaeus japonicus*. Pp. 106-123 in *Proceedings of the 2nd International Conference on Aquaculture Nutrition: Biochemical and Physiological Approaches to Shellfish Nutrition*, G. Pruder, C. Langdon, and D. Conklin, eds. Louisiana State University, Baton Rouge, LA.
- Douillet, P. A. 1991. Beneficial effects of bacteria on the culture of larvae of the Pacific oyster *Crassostrea gigas* (Thunberg). Ph.D. Dissertation, Oregon State University. 185 pp.
- Dubois, M., K. A. Gilles, J. K. Hamilton, P. A. Rebers, and F. Smith. 1956. A colorimetric method for the determination of sugars and related substances. *Anal. Chem.* **28**: 350-356.
- Dugdale, R. C. 1967. Nutrient limitation in the sea: dynamics, identification, and significance. *Limnol. Oceanogr.* **12**: 685-695.
- Enright, C. T., G. F. Newkirk, J. S. Craigie, and J. D. Castell. 1986a. Evaluation of phytoplankton as diets for juvenile *Ostrea edulis* L. *J. Exp. Mar. Biol. Ecol.* **96**: 1-13.
- Enright, C. T., G. F. Newkirk, J. S. Craigie, and J. D. Castell. 1986b. Growth of juvenile *Ostrea edulis* L. fed *Chaetoceros gracilis* Schutt of varied chemical composition. *J. Exp. Mar. Biol. Ecol.* **96**: 15-26.
- Epifanio, C. E. 1979. Growth in bivalve molluscs: nutritional effects of two or more species of algae in diets fed to the American oyster *Crassostrea virginica* (Gmelin) and the hard clam *Mercenaria* (L.). *Aquaculture* **18**: 1-12.
- Epifanio, C. E. 1982. Phytoplankton and yeast as foods for juvenile bivalves: a review of research at the University of Delaware. Pp. 292-304 in *Proceedings of the 2nd International Conference on Aquaculture Nutrition: Biochemical and Physiological Approaches to Shellfish Nutrition*, G. Pruder, C. Langdon, and D. Conklin, eds. Louisiana State University, Baton Rouge, LA.
- Ewart, J. W., and C. E. Epifanio. 1981. A tropical flagellate food for larval and juvenile oysters, *Crassostrea virginica* Gmelin. *Aquaculture* **22**: 297-300.
- Fabregas, J., C. Herrero, B. Cabezas, and J. Abalde. 1985. Mass culture and biochemical variability of the marine microalga *Tetraselmis suecica* Kylin (Butch.) with high nutrient concentration. *Aquaculture* **49**: 231-244.
- Fabregas, J., C. Herrero, B. Cabezas, and J. Abalde. 1986. Biomass production and biochemical composition in mass cultures of the marine microalga *Isochrysis galbana* Parke at varying nutrient concentrations. *Aquaculture* **53**: 101-113.
- Fenchel, T. 1972. Aspects of decomposer food chains in marine benthos. *Sond. Verh. Deuts. Zool. Ges.* **65**: 14-22.
- Fernández-Reiriz, M. J., A. Perez-Camacho, M. J. Ferreira, J. Blanco, M. Planas, M. J. Camps, and U. Labarta. 1989. Biomass production and variation in the biochemical profile (total protein, carbohydrates, RNA, lipids and fatty acids) of seven species of marine microalgae. *Aquaculture* **83**: 17-37.
- Flaak, A. R., and C. E. Epifanio. 1978. Dietary protein levels and growth of the oyster *Crassostrea virginica*. *Mar. Biol.* **45**: 157-163.
- Folch, J., M. Lees, and G. H. Sloane-Stanley. 1957. A simple method for the isolation and purification of total lipids from animal tissue. *J. Biol. Chem.* **226**: 497-509.
- Gabbott, P. A., and B. L. Bayne. 1973. Biochemical effects of temperature and nutritive stress on *Mytilus edulis* L. *J. Mar. Biol. Ass. U.K.* **53**: 269-286.
- Gabbott, P. A., D. A. Jones, and D. H. Nicols. 1976. Studies on the design and acceptability of microencapsulated diets for marine particle feeders. II. Bivalve molluscs. Pp. 127-141 in *Proceedings of the 10th European Marine Biology Symposium*, G. Personne and E. Jaspers, eds. Universa Press, Wetteren.
- Gallager, S. M., and R. Mann. 1981. The effect of varying carbon/nitrogen ratio in the phytoplankton *Thalassiosira pseudonana* (3H) on its food value to the bivalve *Tapes japonica*. *Aquaculture* **26**: 95-105.
- Guillard, R. R. L., and J. Ryther. 1962. Studies of marine planktonic diatoms. I. *Cyclotella nana* and *Detonula confervacea*. *Can. J. Microbiol.* **8**: 229-239.
- Harrison, C. 1975. The essential amino acids of *Mytilus californianus*. *Veliger* **18**: 189-193.
- Hawkins, A. J. S., and B. L. Bayne. 1991. Nutrition of marine mussels: factors influencing the relative utilizations of protein and energy. *Aquaculture* **94**: 177-196.
- Hawkins, A. J. S., and B. L. Bayne. 1992. Physiological interrelations, and the regulation of production. Pp. 171-222 in *The Mussel Mytilus: Ecology, Physiology, Genetics and Culture*, E. Gosling, ed. Elsevier, London.
- Hicks, R. E., C. Lee, and A. C. Marinucci. 1991. Loss and recycling of amino acids and protein from smooth cordgrass (*Spartina alterniflora*) litter. *Estuaries* **14**: 430-439.
- Jordan, T. E., and I. Valiela. 1982. A nitrogen budget of the ribbed mussel, *Geukensia demissa*, and its significance in nitrogen flow in a New England salt marsh. *Limnol. Oceanogr.* **27**: 75-90.
- Kanazawa, A. 1982. Penaeid nutrition. Pp. 87-105 in *Proceedings of the 2nd International Conference on Aquaculture Nutrition: Biochemical and Physiological Approaches to Shellfish Nutrition*, G. Pruder, C. Langdon, and D. Conklin, eds. Louisiana State University, Baton Rouge, LA.
- Kautsky, N., and S. Evans. 1987. Role of biodeposition by *Mytilus edulis* in the circulation of matter and nutrients in a Baltic coastal ecosystem. *Mar. Ecol. Prog. Ser.* **38**: 201-212.
- Kreeger, D. A. 1992. Utilization of dietary protein by the mussel, *Mytilus edulis trossulus*. Ph.D. Dissertation, Oregon State University. 209 pp.
- Kreeger, D. A. 1993. Seasonal patterns in the utilization of dietary protein by the mussel *Mytilus trossulus*. *Mar. Ecol. Prog. Ser.* (in press).
- Langdon, C. J. 1982. New techniques and their application to studies of bivalve nutrition. Pp. 305-320 in *Proceedings of the 2nd International Conference on Aquaculture Nutrition: Biochemical and Physiological Approaches to Shellfish Nutrition*, G. Pruder, C. Langdon, and D. Conklin, eds. Louisiana State University, Baton Rouge, LA.
- Langdon, C. J. 1989. Preparation and evaluation of protein microcapsules for a marine suspension-feeder, the Pacific oyster *Crassostrea gigas*. *Mar. Biol.* **102**: 217-224.
- Langdon, C. J., and E. T. Bolton. 1984. A microparticulate diet for a suspension-feeding bivalve mollusc, *Crassostrea virginica*. *J. Exp. Mar. Biol. Ecol.* **353**: 1-21.
- Langdon, C. J., and E. A. DeBevoise. 1990. Effect of microcapsule type on delivery of dietary protein to a marine suspension-feeder, the oyster *Crassostrea gigas*. *Mar. Biol.* **104**: 437-443.
- Langdon, C. J., and R. I. E. Newell. 1990. Utilization of detritus and bacteria as food sources by two bivalve suspension-feeders, the oyster

- Crassostrea virginica* and the mussel *Geukensia demissa*. *Mar. Ecol. Prog. Ser.* **58**: 299-310.
- Langdon, C. J., and R. I. E. Newell. 1992. Digestion and nutrition. Chapter 6 in *The Eastern Oyster, Crassostrea virginica*, A. Eble, V. S. Kennedy, and R. I. E. Newell, eds. Maryland Sea Grant Publication, (in press).
- Langdon, C. J., and C. A. Siegfried. 1984. Progress in the development of artificial diets for bivalve suspension-feeders. *Aquaculture* **39**: 135-153.
- Langdon, C. J., and M. J. Waldo. 1981. The effect of algal and artificial diets on the growth and fatty acid composition of *Crassostrea gigas* spat. *J. Mar. Biol. Ass. U.K.* **61**: 431-448.
- Langton, R. W., J. E. Winter, and O. A. Roels. 1977. The effect of ration size on growth and growth efficiency of the bivalve mollusc *Tapes japonica*. *Aquaculture* **12**: 283-292.
- Lehninger, A. L. 1976. *Biochemistry*, 2nd ed. Worth, New York. 1104 pp.
- Lowry, O. H., N. J. Rosebrough, A. L. Farr, and R. J. Randall. 1951. Protein measurement with the folin phenol reagent. *J. Biol. Chem.* **193**: 265-275.
- Mann, K. H. 1982. *Ecology of Coastal Waters, a Systems Approach*. Blackwell, Oxford.
- Martin-Jezequel, V., S. A. Poulet, R. P. Harris, J. Moal, and J. F. Samain. 1988. Interspecific and intraspecific composition and variation of free amino acids in marine phytoplankton. *Mar. Ecol. Prog. Ser.* **44**: 303-313.
- Newell, R. 1965. The role of detritus in the nutrition of two marine deposit feeders, the prosobranch *Hydrobia ulvae* and the bivalve *Macoma balthica*. *Proc. Zool. Soc. Lond.* **144**: 25-45.
- Newell, R. C. 1979. *Biology of Intertidal Animals*. Marine Ecological Surveys, Faversham, U. K., 781 pp.
- Newell, R. I. E., and C. J. Langdon. 1992. Mechanism and physiology of larval and adult feeding. Chapter 5 in *The Eastern Oyster, Crassostrea virginica*, A. Eble, V. S. Kennedy, and R. I. E. Newell, eds. Maryland Sea Grant Publication, (in press).
- Phillips, A. M., and D. R. Brockway. 1956. The nutrition of trout. II. Protein and carbohydrate. *Prog. Fish-Cult.* **18**: 159-164.
- Pruder, G. D., and E. T. Bolton. 1979. The role of CO<sub>2</sub> enrichment of aerating gas in the growth of an estuarine diatom. *Aquaculture* **17**: 1-15.
- Rice, D. L. 1982. The detritus nitrogen problem: new observations and perspectives from organic geochemistry. *Mar. Ecol. Prog. Ser.* **9**: 153-162.
- Rice, D. L., T. S. Bianchi, and E. H. Roper. 1986. Uptake and internal distribution of exogenously supplied amino acids in the Pacific oyster, *Crassostrea gigas* (Thunberg). *Aquaculture* **66**: 19-31.
- Riisgard, H. U. 1988. Efficiency of particle retention and filtration rate in 6 species of northeast American bivalves. *Mar. Ecol. Prog. Ser.* **45**: 217-223.
- Riley, G. A. 1972. Patterns of production in marine ecosystems. Pp. 91-112 in *Ecosystem Structure and Function*, J. A. Wiens, ed. Oregon State University Press, Corvallis, OR.
- Roman, M. R. 1983. Nitrogenous nutrition of marine invertebrates. Pp. 347-384 in *Nitrogen in the Marine Environment*, E. J. Carpenter and D. G. Capone, eds. Academic Press, New York.
- Sakshaug, E., and O. Holm-Hansen. 1977. Chemical composition of *Skeletonema costatum* (Grev.) Cleve and *Pavlova (Monochrysis) lutheri* (Droop) Green as a function of nitrate-, phosphate-, and iron-limited growth. *J. Exp. Mar. Biol. Ecol.* **29**: 1-34.
- Sieberth, J. M. 1976. Bacterial substrates and productivity in marine ecosystems. *Ann. Rev. Ecol. Syst.* **7**: 259-285.
- Sokal, R. R., and F. J. Rohlf. 1969. *Biometry*. W. H. Freeman, San Francisco.
- Solorzano, L. 1969. Determination of ammonia in natural waters by the phenylhypochlorite method. *Limnol. Oceanogr.* **14**: 799.
- Tenore, K. R. 1977. Food chain pathways in detrital feeding benthic communities: a review, with new observations on sediment resuspension and detrital recycling. Pp. 37-53 in *Ecology of Marine Benthos*, B. C. Coull, ed. University of South Carolina Press.
- Tenore, K. R., and E. J. Chesney, Jr. 1985. The effects of interaction of rate of food supply and population density on the bioenergetics of the opportunistic polychaete, *Capitella capitata* (type 1). *Limnol. Oceanogr.* **30**: 1188-1195.
- Thompson, P. A., M. E. Levasseur, and P. J. Harrison. 1989. Light-limited growth on ammonium vs. nitrate: what is the advantage for marine phytoplankton? *Limnol. Oceanogr.* **34**: 1014-1024.
- Thompson, P. A., P. J. Harrison, and J. N. C. Whyte. 1990. The influence of irradiance on the fatty acid composition of phytoplankton. *J. Phycol.* **26**: 278-288.
- Utting, S. D. 1985. Influence of nitrogen availability on the biochemical composition of three unicellular marine algae of commercial importance. *Aquacult. Eng.* **4**: 175-190.
- Utting, S. D. 1986. A preliminary study on growth of *Crassostrea gigas* larvae and spat in relation to dietary protein. *Aquaculture* **56**: 123-138.
- Webb, K. L., and F.-L. E. Chu. 1982. Phytoplankton as a food source for bivalve larvae. Pp. 272-291 in *Proceedings of the 2nd International Conference on Aquaculture Nutrition: Biochemical and Physiological Approaches to Shellfish Nutrition*, G. Pruder, C. Langdon, and D. Conklin, eds. Louisiana State University, Baton Rouge, LA.
- Whyte, J. N. C. 1987. Biochemical composition and energy content of six species of phytoplankton used in mariculture of bivalves. *Aquaculture* **60**: 231-241.
- Whyte, J. N. C., N. Bourne, and C. A. Hodgson. 1989. Influence of algal diets on biochemical composition and energy reserves in *Patinopecten yessoensis* (Jay) larvae. *Aquaculture* **78**: 333-347.
- Wilson, R. P. 1989. Amino acids and proteins. Pp. 112-148 in *Fish Nutrition*, J. E. Halver, ed. Academic Press, New York.
- Wright, R. T., R. B. Coffin, C. P. Erising, and D. Pearson. 1982. Field and laboratory measurements of bivalve filtration of natural marine bacterioplankton. *Limnol. Oceanogr.* **27**: 91-98.
- Zamer, W. E., J. M. Shick, and D. W. Tapley. 1989. Protein measurement and energetic considerations: comparisons of biochemical and stoichiometric methods using bovine serum albumin and protein isolated from sea anemones. *Limnol. Oceanogr.* **34**: 256-263.

# Hemolymph Insulin-Like Peptides (ILP) Titters and the Influence of ILP and Mammalian Insulin on the Amino Acid Incorporation in the Mantle Collar *In Vitro* in *Helisoma* (Mollusca)

V. M. SEVALA, V. L. SEVALA, AND A. S. M. SALEUDDIN

*Department of Biology, York University, North York, Ontario, Canada M3J 1P3*

**Abstract.** In *Helisoma duryi*, the periostracum is the outermost organic layer of the shell and it is secreted by the mantle collar. Addition of porcine insulin (0.1  $\mu\text{g/ml}$ ) to the incubation medium increases the incorporation of labeled amino acids in the mantle collar *in vitro*. The immunoblotting technique revealed two immunoreactive insulin bands with a molecular weight of 16 and 7 kDa in the hemolymph. Partial purification of insulin-like peptides from the hemolymph by gel filtration chromatography showed that only one fraction containing approximately 7 kDa polypeptide stimulated the incorporation of amino acids into the mantle collar as well as into the periostracum in a dose-dependent manner. In laboratory populations of *Helisoma*, snails with two different shell growth rates can be recognized: fast and slow. Hemolymph titers of insulin-like peptide are low in fast-growing snails ( $2.3 \pm 0.25$  mIU/ml) and higher in slow-growing snails ( $7.8 \pm 0.46$  mIU/ml). When a piece of shell at the edge is removed, a structurally identical new piece is formed within either two days (fast regeneration) or a longer period of seven days (slow regeneration). Hemolymph titers of insulin-like peptide undergo fluctuations during the period of shell regeneration, but a general pattern can be recognized. The titers are low when the shell deposition rate is high and vice versa. We suggest that the insulin-like peptide in the hemolymph is involved in shell growth or shell regeneration.

## Introduction

Insulin-like peptides (ILP) are found in a number of invertebrate species from different phyla (Thorpe and

Duve, 1984). In several members of the phylum Mollusca, ILP have been detected in the cells belonging to the digestive system and in the central nervous system (CNS). Many similarities exist between molluscan ILP and mammalian insulin at both the structural and functional levels (Ebberink *et al.*, 1989).

In the freshwater pulmonate *Lymnaea stagnalis*, three genes encoding molluscan insulin-related peptides MIP I, MIP II, and MIP V have been sequenced (Smit *et al.*, 1988, 1991, 1992). The *in situ* hybridization technique using cDNA has shown that the neurosecretory light green cells (LGC) contained the mRNA encoding these peptides (van Minnen and Schallig, 1990; Smit *et al.*, 1991). In this species, LGC regulate shell and body growth (Geraerts, 1976).

The neurosecretory mediodorsal cells (MDC) of freshwater snails *Helisoma* spp. (*H. duryi*, *H. tenne*, and *H. trivolvis*) are homologous to the LGC of *Lymnaea*, and are also involved in shell growth (Saleuddin and Kunigelis, 1984). Using porcine and human insulin antisera, immunoreactive ILP have been detected in the MDC and hemolymph of *Helisoma* (Saleuddin *et al.*, 1991; Khan *et al.*, 1992). Fine structural studies suggest that the synthetic activity of the MDC, and the rate of release profiles of neurosecretory granules of the MDC axon terminals, reflect the growth rates of the animal (Khan and Saleuddin, 1992).

Among laboratory populations of *Helisoma*, snails with two distinct shell growth rates can be found: fast and slow. Also present are the non-growers whose shell increments are extremely small. A brain extract from a fast-growing snail contains a factor that will stimulate shell growth in slow-growing snails (Kunigelis and Saleuddin, 1978).

The organic periostracum is the pliable outermost layer of the molluscan calcareous shell. Its formation must precede the formation of the calcareous layer. The mantle edge, which secretes the periostracum, can be cultured *in vitro*. A brain-derived factor increases incorporation of labeled amino acids into the periostracum *in vitro* (Kunigelis and Saleuddin, 1985).

In *Helisoma* when a piece of shell is removed from the edge, a new piece is secreted filling the damaged area (Wong and Saleuddin, 1972; Kunigelis and Saleuddin, 1983). Snails undergoing shell regeneration, where rapid transport of calcium and proteins is involved, are suitable for monitoring the hormones involved in shell formation and shell regeneration.

In the present experiments, ILP titers in the hemolymph in snails of known growth rates and in shell-regenerating snails were measured by a radioimmunoassay using human insulin antiserum. The effects of porcine insulin and *Helisoma* ILP on the amino acid incorporation into periostracum by the mantle collar *in vitro* were also studied.

## Materials and Methods

### Animals

Specimens of *H. duryi* were raised in 70-l glass aquaria in dechlorinated tap water at 22°C under a 12L:12D photoperiod. Boiled lettuce, fish-food, and blackboard chalk (source of calcium) were supplied as food *ad libitum*. Adult snails, 6–8-month-old and 10–12 mm shell diameter, were used for studies.

### Shell growth monitoring

Adult snails were marked individually with an identifying number, and a reference line parallel to the growing edge was painted on the shell using a water-soluble polymer acrylic paint with a very fine artist's paint brush. The number and reference line were dried and coated with lacquer containing nylon (nail polish). Shell growth was measured optically as the distance between the reference line and the growing edge using a calibrated micrometer on a Wild M5 stereomicroscope. The shell growth was monitored daily. Based on daily growth increments, the rate of shell deposition was calculated, representing the "net daily increase" in the "mean shell area" deposited and expressed as mean daily linear shell deposition rate (MDLSDR). These snails were grouped into fast growers, slow growers, and non-growers based on the growth rates as outlined by Kunigelis and Saleuddin, 1978.

### Shell damage

Snails with known shell growth rates were used. A piece of shell about 4 × 4 mm was carefully removed at the growing edge of a snail, using a fine rotating blade (Dremel

Tools, Wisconsin), without injuring the underlying mantle tissue. After the shell was damaged, shell regeneration was monitored every day for two weeks. Shell growth ceased until shell regeneration was completed. Previous studies showed that the mantle collars of *Helisoma* cultured *in vitro* synthesized the periostracum. In this experiment, the incorporation of tritium-labeled amino acids into the mantle collar and periostracal proteins was measured both in the presence and absence of insulin.

### Periostracum synthesis *in vitro*

The mantle collars were dissected from snails of known growth rates under aseptic conditions in physiological saline (40 mM NaCl, 3 mM KCl, 3 mM CaCl<sub>2</sub>, 1 mM MgCl<sub>2</sub>, 14 mM NaHCO<sub>3</sub>, 0.2 mM NaH<sub>2</sub>PO<sub>4</sub>), pH 7.2, osmolality 115 mOsm/l, containing antibiotics and an antimycotic [100 IU/ml penicillin and streptomycin and 0.25 µg/ml fungizone (GIBCO, Canada)] and cultured *in vitro* according to the procedure of Kunigelis and Saleuddin (1985). The culture medium contained 55 parts sterile distilled water and 45 parts Medium 199 (GIBCO) containing 25 mM Hepes buffer, Hank's salts, and L-glutamine, osmolality 140 mOsm/l and pH 7.1 A tritiated amino acid mixture (leucine, lysine, phenylalanine, proline, and tyrosine; specific activity 57 Ci/mmol) (Amersham, Canada) was used at a concentration of 1 µCi/ml culture medium. The culture medium was filtered through 0.2 µm sterile disposable filter units and subsequently 100 IU/ml penicillin and streptomycin and 0.25 µg/ml fungizone were added. A mantle collar was placed dorsal surface uppermost in 1.0 ml medium in each well of a sterile 24-well dish (Costar, Cambridge, Massachusetts) at 22°C. In some experiments porcine insulin (0.01–2.0 µg/ml) was added to the culture medium. After 48 hours of incubation, the mantle collars formed periostracum which was collected with a glass pipette. The mantle collar and periostracum were homogenized separately in 100 µl and 200 µl distilled water, respectively. Aliquots of 25 µl of homogenate were spotted onto squares of filter paper (2 × 2 cm; Whatman No. 42) and allowed to dry at room temperature. The amount of label incorporation into proteins was determined by the method of Bramhall *et al.* (1969). Briefly, proteins were precipitated by soaking in 7.5% chilled trichloroacetic acid and heated to 80°C for 30 min to remove non-proteinaceous material. The TCA was removed by rinsing in 50% ethanol in diethyl ether followed by diethyl ether, and the papers were air dried before transferring to a vial containing 10 ml of scintillation cocktail (ACS) (Amersham, Canada). The vials were dark-adapted and counted in a Packard A3000 Scintillation counter. Subsequently, the papers were washed in acetone, air dried, and the protein present on these filter papers determined by using the method of

Bramhall *et al.* (1969). Incorporation of amino acid was expressed as DPM per microgram protein.

#### Hemolymph collection and extraction

Snails were wiped and all traces of mucus were removed using absorbent tissue. They were then bled on a piece of parafilm by puncturing the heart with a No.10 surgical blade. About 100  $\mu$ l hemolymph was collected in 1.5 ml microcentrifuge tubes from each snail. Hemolymph samples were centrifuged at 10,000  $\times g$  for 10 min and supernatants were stored at  $-80^{\circ}\text{C}$  until use.

#### Gel filtration

Hemolymph was subjected to gel filtration G-75 (Pharmacia; Particle size 40-120  $\mu\text{m}$ ) column of 75  $\times$  2 cm equilibrated with 0.06 M phosphate buffer (pH 7) at a flow rate of 0.3 ml/min. The column was calibrated with proteins of known molecular weight. Approximately 5 ml of hemolymph from snails of various growth rates was lyophilized and reconstituted with 2 ml of buffer, then loaded onto the column. The elution of protein was monitored at 280 nm. Fractions (3.5 ml) were collected, 500  $\mu$ l of each fraction was vacuum dried and subjected to RIA for the presence of insulin-like peptides.

#### Bioassay

The partially purified hemolymph fractions from the gel filtration column containing ILPs (approximately 17, 7, and 2 kDa) were lyophilized and tested *in vitro* for possible stimulation of incorporation of labeled amino acids into TCA precipitable mantle collar and periostracal proteins. The mantle collars were cultured *in vitro* with or without insulin-like peptides (250  $\mu$ IU equivalents/ml). After 48 h of incubation, mantle collars and periostracum were removed, homogenized separately in 200  $\mu$ l and 100  $\mu$ l of distilled water, respectively. Aliquots were spotted on filter papers and processed according to the procedure of Bramhall *et al.* (1969), as described earlier. Furthermore, various doses (0, 100, 250, 500  $\mu$ IU equivalents/ml) of the 7-kDa insulin immunoreactive fraction were also tested *in vitro* for the stimulation of  $^3\text{H}$ -labeled amino acid incorporation into mantle and periostracal proteins.

#### Radioimmunoassay

The hemolymph titers of ILP were determined with a commercially available kit that uses antiserum against human insulin (Diagnostic Products, Los Angeles, California). The assay is based on competitive binding of ILP present in the samples and  $^{125}\text{I}$ -labeled insulin. Immobilized insulin antibody is supplied in polypropylene tubes. In each of these tubes, 100  $\mu$ l hemolymph sample and

500  $\mu$ l labeled insulin (0.03  $\mu\text{Ci/ml}$ ) were incubated for 18 h at  $22^{\circ}\text{C}$ . After being carefully decanted, the tubes were counted for 1 min in 10 ml ACS in a Packard A300 Scintillation Counter. The amount of ILP present in samples was determined by comparing the observed counts to a standard curve. The limit of detection of insulin was 1  $\mu$ IU using this procedure. A series of hemolymph and tissue extracts were prepared to compare the competition curve of human insulin with that of the *Helisoma* ILP. The dilution curves for snail ILP ran parallel to the human insulin standard curve (Fig. 1). Thus the relative concentration of *Helisoma* ILP can be determined with this assay. Because we do not know the absolute amount of *Helisoma* ILP in any sample, the titers are expressed as mIU equivalents of insulin.

#### Immunoblotting

The proteins present in the hemolymph and brain extracts were analyzed by sodium dodecyl sulphate gradient (11-23%) polyacrylamide gel electrophoresis employing the "phorcast" gel system (Amersham, Canada). At the end of the electrophoretic run, the proteins were transferred to nitrocellulose (0.2  $\mu\text{m}$ ) (Bio-Rad, Canada) by using Bio-Rad mini trans blot electrophoresis cell at  $4^{\circ}\text{C}$  for 16 h with a constant current of 40 mA. The transfer buffer consisted of 25 mM Tris pH 8.3, 192 mM glycine, 20% methanol. Immediately following the transfer, the blots were placed in a phosphate buffer saline, pH 7.4, containing 5% bovine serum albumin and 0.05% Tween 20 (PBST) for 45 min at  $22^{\circ}\text{C}$ . The membranes were then

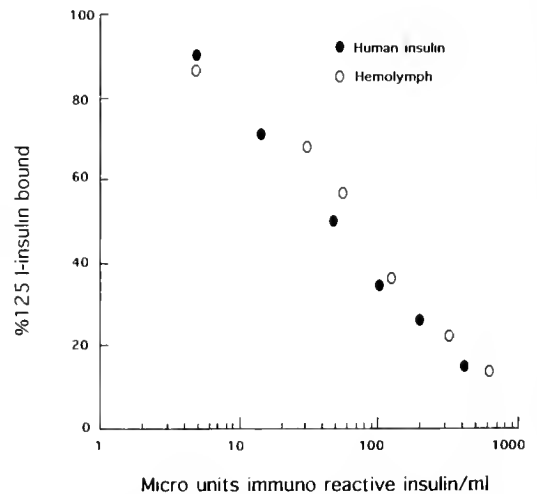


**Figure 1.** Standard curve showing competitive inhibition of  $^{125}\text{I}$ -insulin binding to anti-insulin with unlabeled human insulin (5, 15, 50, 100, 200, and 400  $\mu$ l) and with samples of hemolymph (5, 10, 25, 50, 100, and 200  $\mu$ l) collected from fast-growing snails and adjusted to 0.1 ml prior to the assay. The amount of insulin present in the hemolymph samples was determined from the insulin standard curve.

incubated with bovine insulin antibody raised in guinea pigs (Sigma Chemical Co.) diluted 1:1000 for 1 h, rinsed three times in PBST, followed by incubation with a secondary antibody (anti-guinea pig IgG) conjugated to alkaline phosphatase (1:1000 dilution). The membranes were washed three times in PBST. Finally, the enzyme was localized by 0.033% nitro blue tetrazolium with 0.0165% 5-bromo-4-chloro-3-indolyl-phosphate (Promega, Wisconsin) as a substrate. The presence of an insulin-like molecule was indicated by blue bands on the membrane. The specificity of the antisera used was verified by appropriate controls involving (1) the omission of the primary antiserum, (2) the omission of the secondary antiserum, (3) preincubation of the primary antiserum with bovine insulin, and (4) replacement of the primary antiserum with pre-immune rabbit serum. Under all these control treatments no immunoreactive material was detected on the nitrocellulose membrane.

### Statistical analysis

The results were tested for significance using ANOVA and the difference between means was also tested by Student's *t*-test as described by Sokal and Rohlf (1973).

## Results

### Effect of insulin on protein synthesis in mantle

The influence of porcine insulin on periostracum formation by the mantle collar *in vitro* was determined by assaying the rate of incorporation of a mixture of tritiated

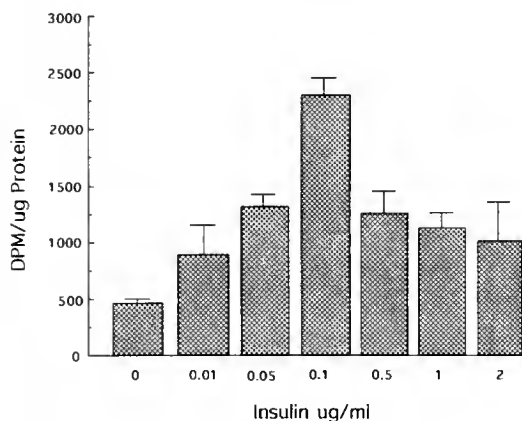


**Figure 2.** Dose response curve showing the *in vitro* incorporation of  $^3\text{H}$ -labeled amino acids into TCA precipitable protein of the mantle collar of *Helisoma*. The mantle collars from snails of known growth rates were dissected and cultured in the medium with and without the indicated dose of insulin for 48 h. The mantle collars were processed (see Methods) to measure the amount of label incorporation into mantle collar protein and the results shown are pooled data (mean  $\pm$  SEM) from three experiments. For each experiment at least 9–11 controls and 9–11 treated mantle collars per insulin dose were assayed.

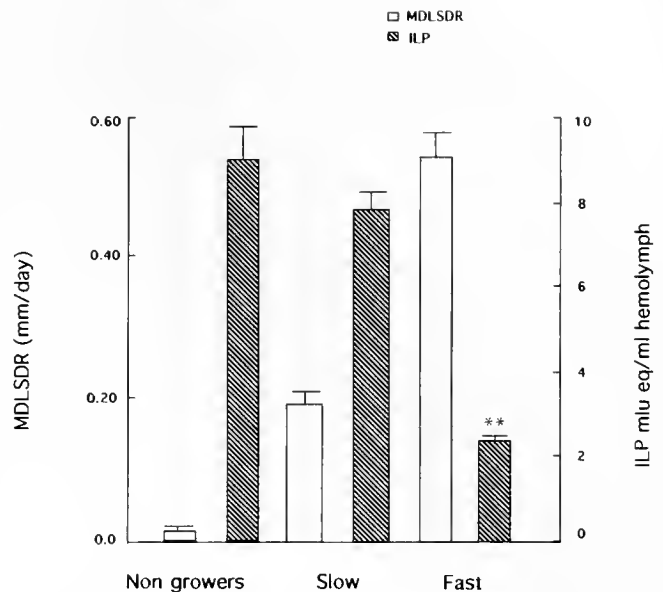


**Figure 3.** A comparison of ILP titers and mean daily linear shell deposition rates (MDLSDR) in non-growing, slow, and fast growing snails. The snails were monitored for shell deposition over a 3–4 week period. Based on daily growth increments, the rate of shell deposition was calculated, which represents the "net daily increase" in the "mean shell area" deposited and expressed as mean daily linear shell deposition rate (MDLSDR) (mm/day). The hemolymph samples were collected from snails after determining their shell growth rates and were used for assaying the ILP titers. The ILP titers are significantly lower in fast growing snails than in non-growing and slow-growing snails (\*\*,  $P < 0.01$ ). Columns indicate the mean of  $n = 15$ , bars the SEM from three separate experiments.

amino acids in the mantle collar. At a concentration of  $0.1 \mu\text{g/ml}$  of insulin, the rate of amino acid incorporation was two-fold higher than at  $0.01 \mu\text{g/ml}$  (Fig. 2).

### ILP titers and shell growth

Daily shell deposition rates have been compared with ILP titers of the hemolymph (Fig. 3). ILP titers are significantly lower in fast-growing snails than in nongrowing and slow-growing snails ( $P < 0.01$ ). However, the ILP titers of slow and nongrowing snails did not differ significantly ( $P > 0.5$ ).

### Rate of shell regeneration

When a piece of shell edge is removed the damaged area is rapidly replaced by a piece of regenerated shell which is first visible 6–8 h following shell damage. Shell regeneration is restricted to the damaged area only. The rate of shell regeneration varied among regenerating snails. Snails that had repaired more than 50% of the damaged shell within 24 h were classified as fast-regenerating snails, while those that took longer than 24 h were slow regen-



erating snails. Normally, fast regenerating snails completed shell repair in two days, while slow regenerating snails took up to seven days to complete shell regeneration (Fig. 4).

#### ILP titers during shell regeneration

ILP titers in the hemolymph of both fast and slow regenerating snails fluctuated considerably not only during the period of shell regeneration but also over the 14-day study period. In fast regenerating snails, the ILP titer during the initial phase of regeneration (first 17 h) was about 3 mIU/ml of hemolymph. This level was maintained until day 3 when the titer dropped to about 2 mIU/ml of hemolymph. This decrease was followed later (after day 9) by a significant increase to 6 mIU/ml at day 14 after the shell growth had virtually stopped (Fig. 5).

In slow regenerating snails, ILP titers showed a different profile. In these snails at the initial phase of regeneration (17 h), the ILP titer was significantly higher than in fast regenerating snails ( $P < 0.01$ ). However, the ILP titer decreased as the rate of shell regeneration accelerated. The ILP titers then increased, coincidentally with the fall of shell regeneration rates (Fig. 5). The ILP titers did not significantly differ between slow and fast regenerating snails from 11 days after injury, and at day 14 the ILP

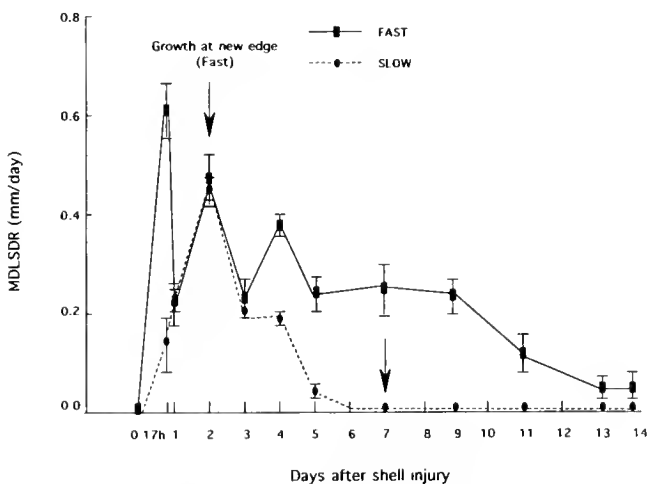


**Figure 4.** MDLSDR in fast- and slow-growing snails. The shell growth in snails was monitored for 3–4 weeks to establish shell deposition rates. Following shell growth rate determination, the shell was carefully injured at time zero. These snails were further monitored for 2 weeks to determine shell regeneration of injured area and the resumption of normal growth at the edge. Based on daily growth increments, the rate of shell deposition was calculated, which represents the “net daily increase” in the “mean shell area” deposited and expressed as mean daily linear shell deposition rate (MDLSDR). Results indicate the mean of  $n = 16$  from three experiments. Arrows indicate the time of completion of shell regeneration. Shell growth at the new edge resumes beyond this point. Note that for slow-growing snails the rate of shell regeneration is not only slower, but no new shell growth occurred following the completion of regeneration.

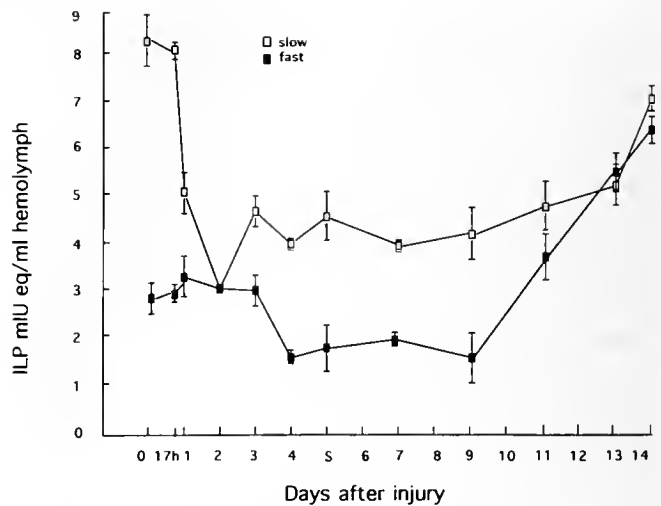


**Figure 5.** ILP titers following shell injury in the snails with known shell growth rates. The snails were monitored over a 3–4 week period and MDLSDR were calculated. A shell area of approximately  $4 \times 4$  mm was carefully removed from these snails at time zero. Following this removal, shell regeneration and the resumption of normal shell growth were monitored daily for 2 weeks. Hemolymph samples from these snails were collected at different times following shell removal and assayed by RIA to determine the ILP titers. Each individual was sampled only once during the experiment and results shown indicate the mean of  $n = 16$ , bars indicate the SEM from three experiments. The titer in slow-regenerating animals is significantly higher than in fast-regenerating animals (\*\*,  $P < 0.01$ ) except on days 2 and 13 after shell removal.

titer returned to the initial level of about 7 mIU/ml of hemolymph.

#### Immunoblotting

Immunoblots prepared by SDS-PAGE from the hemolymph samples using bovine anti-insulin showed two immunoreactive ILP bands whose apparent molecular weights were 16 and 7 kDa, as determined by comparison with the mobility of known molecular weight markers (Fig. 6).

#### Gel filtration

Three peaks of insulin-like immunoreactive-peptide-containing fractions were identified from the eluates of gel filtration as detected by RIA. The apparent molecular weights of the peptides were estimated by calibrating the column with standards of known molecular weights and were found to be 17, 7, and 2 kDa from the hemolymph (Fig. 7). The fractions containing these peptides were pooled and tested for their ability to stimulate the incorporation of tritiated amino acids into TCA precipitable proteins of the mantle collar and periostracum. The data presented in Figures 8 and 9 show that only one fraction containing ILP of 7 kDa significantly stimulated the

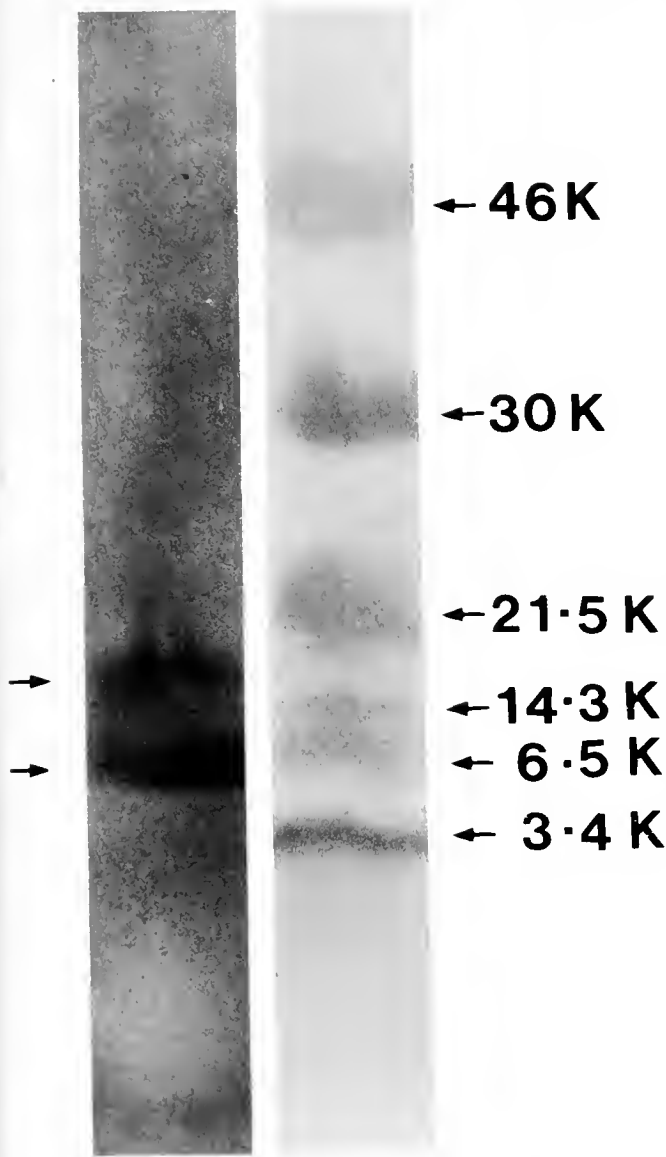


**Figure 6.** Immunoblot of SDS-PAGE of hemolymph from snails (left lane). The hemolymph samples from a mixed population of snails of known growth rates were subjected to SDS-gel electrophoresis and the fractionated proteins were subsequently transferred to nitrocellulose membrane. The membranes were incubated with the primary antiserum (anti-bovine insulin, 1:1000 dilution) for 1 h, rinsed in phosphate buffered saline, pH 7.4, containing 5% bovine serum albumin and 0.05% Tween 20 (PBST) followed by secondary antiserum conjugated to alkaline phosphatase (1:1000 dilution). The membranes were washed and the sites of IgG binding was visualized with nitro blue tetrazolium and 5-bromo-4-chloro-3-indolyl phosphate. Arrows indicate ILPs (16 and 7 kDa) in *Helisoma* hemolymph. The molecular weights of the insulin immunoreactive bands were estimated by running the following known molecular weight protein standards (Amersham) on the same gel (right lane): Ovalbumin 46000, carbonic anhydrase 30000, trypsin inhibitor 21500, lysozyme 14300, aprotinin 6500, and insulin (b) chain 3400.

incorporation of labeled amino acids into mantle collar and periostrical proteins ( $P < 0.05$ ;  $P < 0.01$ , respectively). Furthermore, Figures 10 and 11 demonstrate that addition

of the 7-kDa-containing fraction to the culture medium increases incorporation of tritiated amino acids into TCA precipitable proteins of mantle collar and periostracum in a dose-dependent manner up to a dose of 250  $\mu$ IU/ml.

### Discussion

In many mollusks, shell growth is incremental and is influenced by various internal and external factors (Lutz and Rhoads, 1980). The molluscan shell, which includes an organic outer periostracum, is secreted by the mantle collar. Saleuddin and Kunigelis (1984) showed that when the mantle collar was maintained in organ culture, the periostracum formed *in vitro* was structurally similar to that formed *in vivo*. A crude extract of CNS from a fast growing snail stimulated *in vitro* periostracum formation and increased amino acid incorporation into the mantle collar of a slow-growing snail. In this study, addition of up to 0.1  $\mu$ g/ml porcine insulin to the incubation medium stimulated amino acid incorporation into the mantle collar. Higher concentrations of insulin were not stimulatory, however; inhibitory effects of higher doses of insulin on protein synthesis are not uncommon (de Pablo *et al.*, 1985). Because this study did not specifically include the effect of insulin either on the incorporation of amino acid in the periostracum or on the periostracum formation

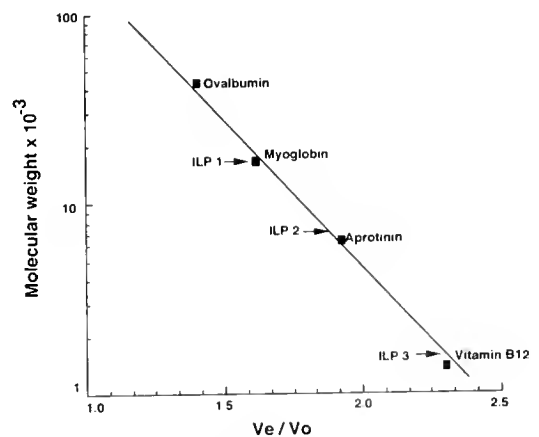


**Figure 7.** Molecular weight determinations of ILP by gel filtration. A mixture of standard proteins was applied to G-75 column ( $2 \times 75$  cm) and eluted at 0.3 ml/min with 0.06 M phosphate buffer. Five ml of hemolymph collected from a mixed population of (80) snails of known growth rates was extracted, lyophilized (see Methods), and reconstituted with 2 ml of buffer, and applied onto the column. ILPs were eluted with phosphate buffer. Fractions (3.5 ml) were collected and 500  $\mu$ l of each fraction was vacuum dried, reconstituted with 100  $\mu$ l of distilled water, and then subjected to RIA for the presence of insulin-like peptides. The following standard proteins were used to calibrate the column: ovalbumin 46000, myoglobin 17000, aprotinin 6500, and vitamin B12 1400 dalton. The arrows indicate the  $V_e/V_o$  (elution volume/void volume) ratios for ILPs in the hemolymph of *Helisoma*. The fractions containing the ILPs were further tested *in vitro* for the stimulation of incorporation of  $^3$ [H]-labeled amino acids into TCA precipitable mantle collar and periostracal proteins of *Helisoma*.

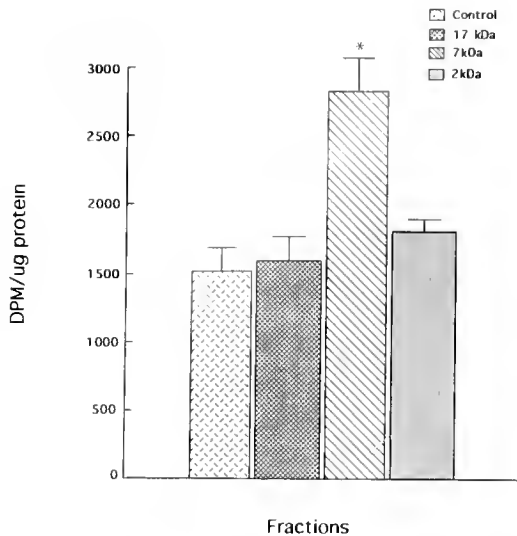


**Figure 8.** The effect of partially purified hemolymph insulin immunoreactive fractions on amino acid incorporation into the TCA precipitable mantle collar protein of *Helisoma*. Three peaks of immunoreactivity (17 kDa, 7 kDa, and 2 kDa) were found in the chromatographic fractions collected from hemolymph eluate as detected by RIA. All of these fractions were tested *in vitro* for the stimulation of incorporation of  $^3\text{H}$ -labeled amino acids into TCA precipitable protein of the mantle collar of *Helisoma*. The mantle collars from different snails of known growth rates were dissected and cultured *in vitro* with and without the immunoreactive fractions (250  $\mu\text{IU/ml}$ ) obtained from the gel filtration column. The mantle collars were processed to measure the label incorporation into mantle collar proteins (see Methods). The 7 kDa ILP significantly stimulated amino acid incorporation into mantle collar protein (\*,  $P < 0.05$ ). Columns in the figure indicate the mean of  $n = 12$ , bars the SEM from three experiments.

itself, the definitive role of insulin on periostracum formation can only be conjectured. Thus it is possible that insulin/ILP could be acting on the mantle collar as a general metabolic stimulator rather than as a specific shell growth factor. Saleuddin *et al.* (1991) showed that injections of microgram quantities of porcine insulin-stimulated shell growth, whereas injection of porcine anti-insulin inhibited shell growth in *Helisoma*.

Geraerts (1976) suggested that a factor from the neurosecretory light green cells (LGC) in *Lymnaea stagnalis* is involved in body and shell growth. It is now known that LGC produce three insulin-related peptides MIP I, MIP II, and MIP V (Smit *et al.*, 1988, 1991, 1992). MIP I has been implicated as a growth hormone. However, direct evidence of the involvement of MIPs as stimulators of shell growth has not been documented. In *Helisoma*, the neurosecretory mediadorsal cells (MDC), which are homologous to LGC of *Lymnaea*, contain immunoreactive insulin-like material that is released into the medium when the CNS is treated with high potassium or 4-aminopyridine (Khan *et al.*, 1992; Khan and Saleuddin, 1992). The synthetic activity of the MDC and the observed

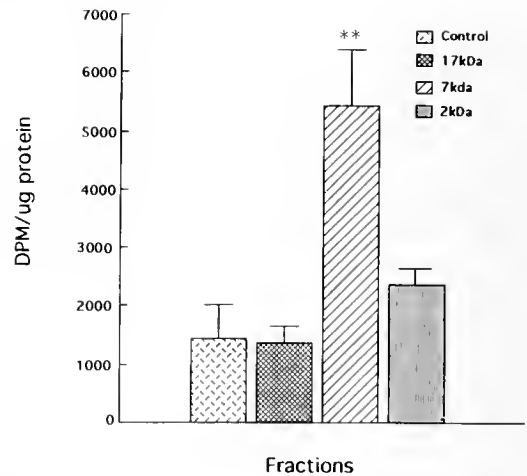


**Figure 9.** The effect of partially purified hemolymph insulin immunoreactive fractions on the stimulation of incorporation of  $^3\text{H}$ -labeled amino acids into TCA precipitable periostracal protein of *Helisoma*. The mantle collars were cultured *in vitro* (similar to Fig. 8) for 48 h and the periostracum produced was collected with a glass pipette and processed (see Methods) for assaying the  $^3\text{H}$  amino acid incorporation into periostracal protein. The 7 kDa ILP significantly stimulated the amino acid incorporation into periostracal protein (\*\*,  $P < 0.01$ ). Columns indicate the mean of  $n = 12$ , bars the SEM from three experiments in triplicate.

release of the ILP at the median lip nerve (neurohemal area) correlate well with shell-growth periods (Khan and Saleuddin, 1992).

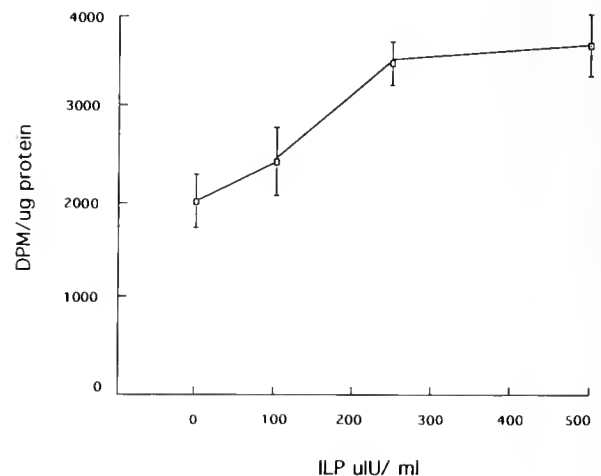


**Figure 10.** The dose-response curve for the stimulation of incorporation of  $^3\text{H}$ -labeled amino acids into TCA precipitable mantle collar protein of *Helisoma* by the partially purified 7 kDa insulin immunoreactive fraction. The mantle collars were cultured *in vitro* with various doses of 7 kDa ILP (0, 100, 250, 500  $\mu\text{IU/ml}$ ) and amino acid incorporation into mantle collar proteins was determined (see Methods). Results shown are pooled data from two separate experiments in triplicate and for each experiment at least 12–15 controls and 10–15 treated mantle collars per dose were assayed.

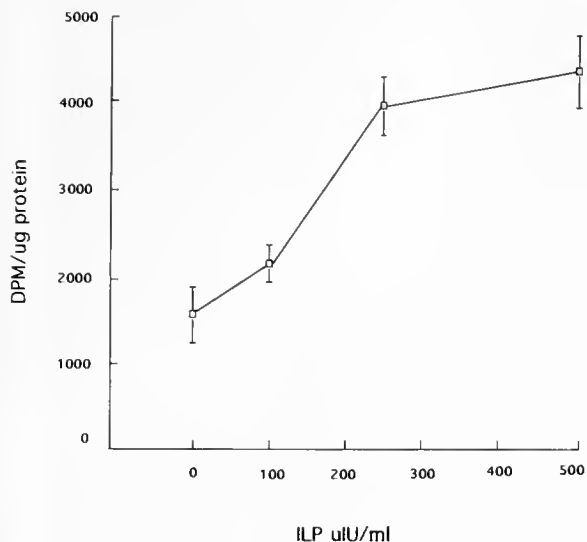


**Figure 11.** The dose-response curve for the stimulation of incorporation of  $^3\text{H}$ -labeled amino acids into TCA precipitable periostracal proteins of *Helisoma* by the partially purified 7 kDa hemolymph insulin-like immunoreactive fraction. The mantle collars were cultured *in vitro* with various doses of 7-kDa ILP (0, 100, 250, and 500  $\mu\text{IU/ml}$ ) and the periostraca formed were processed for assaying the  $^3\text{H}$ -labeled amino acid incorporation into periostracal proteins (see Methods). Results shown are pooled data from two separate experiments in triplicate and in each experiment at least 12–15 controls and 10–15 treated periostraca per dose were assayed.

We have identified ILP in the hemolymph in *Helisoma*. Furthermore we have measured the titers of ILP in the hemolymph of snails with different shell-growth rates and also during the period of shell regeneration. The difference in titers during shell growth or shell regeneration suggests that ILP is involved in these two processes. Although ILP titers were measured by an RIA using anti-human insulin, the titers reflect the relative concentrations of ILP, because the competition curve for *Helisoma* ILP showed a linear relationship to human insulin standards (Fig. 1). In another terrestrial pulmonate, *Otala lactea*, we were able to detect ILP in the hemolymph, hepatopancreas, and CNS, but did not investigate its physiological function (unpub. data). Gomot *et al.* (1992) found insulin immunoreactive neurosecretory cells in the CNS of *Helix aspersa*. Caution of these cells causes a reduction in body weight. Gomot (pers. comm.) reports that injections of microgram quantities of bovine insulin cause juvenile *Helix aspersa* to grow significantly larger than controls over a six-week period.

In this paper, ILP concentrations in the hemolymph were measured by an immunoassay procedure. This technique is based upon recognition of an antigenic determinant of the hormone molecule with specific antibodies raised against the hormone. Furthermore, this technique does not take into account the biological effects of the hormone on target cells or tissues and thus is unable to

distinguish between biologically active and inactive forms of the antigen. Equally significant is the fact that immunoassay techniques fail to distinguish between isohormones with different functions working on separate target tissues (Robertson and Bidney, 1990). For example, the immunoassay used in this study identified the total ILP in the hemolymph without discriminating between ILP from various sources, such as the hepatopancreas or the CNS. The ILP from the hepatopancreas could be involved in sugar metabolism, whereas we believe the ILP from the CNS is a shell-growth factor.

Many mollusks show a daily rhythm of shell deposition. Within laboratory populations of *Helisoma*, fast and slow shell regeneration rates can be recognized over a 14-day period of monitoring. Interestingly, the shell regeneration rates and the hemolymph ILP titers are inversely related. The high titers of ILP associated with slow shell regeneration rates may be due to ILP, which is immunoreactive but lacks bioactivity. A similar situation has been reported in the case of parathyroid hormone (Martin *et al.*, 1977). It is equally possible that the antiserum used in this study recognized degraded hormone fragments with antigenic determinants that are intact.

Partial purification of *Helisoma* hemolymph ILPs by gel filtration showed that only one insulin immunoreactive fraction containing 7-kDa polypeptide stimulated amino acid incorporation in the mantle collar as well as in the periostracum. The presence of high and low molecular weight ILPs in the hemolymph of *Helisoma* may represent the precursor molecule and the degraded fragments of ILP, respectively. It will be interesting to know whether the bioactive ILP fraction is high in fast-growing snails but low or not detectable in slow-growing snails. Both low and high molecular weight immunoreactive insulin materials were present in the hepatopancreas of oysters (de Martinez *et al.*, 1973) and in the gut, hepatopancreas and hemolymph of lobsters (Sanders, 1983).

In *Helisoma*, studies using bioassay, RIA, partial purification, and immunoblotting confirm that ILP (7 kDa) can stimulate periostracum formation by stimulating protein synthesis in the mantle collar *in vitro* and that it is involved in shell growth. In vertebrates it is well established that insulin and related peptides (IGFs) not only regulate glycogen, lipid and protein synthesis but also growth and differentiation (Kahn, 1985; Froesch *et al.*, 1985; Rosen, 1987; de Pablo *et al.*, 1990). The prothoracicotropic hormone (PTTH) in insects, which occurs in multiple forms and which shows some structural similarity with vertebrate insulin, is involved in growth (Mizoguchi *et al.*, 1990). It remains to be seen whether ILP in *Helisoma* is structurally similar to MIPs of *Lymnaea* or to other ILP or to vertebrate insulin. Experiments are currently under way to elucidate the gene structure of ILP in *Helisoma* using cDNA recombinant techniques.

### Acknowledgments

This work was supported by Natural Sciences and Engineering Research Council of Canada. We thank Dr. B. G. Loughton for critically reading the manuscript.

### Literature Cited

- Bramhall, S., N. Noack, M. Wu, and J. R. Loewenberg. 1969. A simple colorimetric method for determination of protein. *Anal. Biochem.* **31**: 146-148.
- Ebberink, R. H. M., A. B. Smit, and J. Van Minnen. 1989. The insulin family: evolution of structure and function in vertebrates and invertebrates. *Biol. Bull.* **177**: 176-182.
- Froesh, E. R., Chr. Schmid, J. Schwander, and J. Zapf. 1985. Actions of insulin-like growth factors. *Ann. Rev. Physiol.* **47**: 443-467.
- Geraerts, W. P. M. 1976. Control of growth by the neurosecretory hormone of the light green cells of the fresh water snail *Lymnaea stagnalis*. *Gen. Comp. Endocrinol.* **29**: 61-71.
- Gomot, A., L. Gomot, C. R. Marchand, C. Colard, and J. Bride. 1992. Immunocytochemical localization of insulin-related peptide(s) in the central nervous system of the snail *Helix aspersa* Muller: involvement in growth control. *Cell. Mol. Neurobiol.* **12**: 21-31.
- Kahn, C. R. 1985. Current concepts of the molecular mechanism of insulin action. *Ann. Rev. Med.* **36**: 429-45.
- Khan, H. R., B. Griffond, and A. S. M. Saleuddin. 1992. Insulin-like peptide(s) in the central nervous system of the snail *Helisoma duryi*. *Brain Res.* **580**: 111-114.
- Khan, H. R., and A. S. M. Saleuddin. 1992. Neurosecretion of the mediodorsal cells of the central nervous system of the snail *Helisoma duryi*. *Cell Tissue Res.* **268**: 131-139.
- Kunigelis, S. C., and A. S. M. Saleuddin. 1978. Regulation of shell growth in the pulmonate gastropod *Helisoma duryi*. *Can. J. Zool.* **56**: 1975-1980.
- Kunigelis, S. C., and A. S. M. Saleuddin. 1983. Shell repair rates and carbonic anhydrase activity during shell repair in *Helisoma duryi* (Mollusca). *Can. J. Zool.* **61**: 597-602.
- Kunigelis, S. C., and A. S. M. Saleuddin. 1985. Studies on the *in vitro* formation of periostracum in *Helisoma duryi*: the influence of brain. *J. Comp. Physiol.* **13**: 177-183.
- Lutz, R. A., and D. C. Rhoads. 1980. Growth patterns within the molluscan shell. Pp. 203-254 in *Skeletal Growth of Aquatic Organisms*, D. C. Rhoads and R. A. Lutz, eds. Plenum Press, New York.
- de Martinez, N. R., M. C. Garcia, M. Salas, and J. L. R. Candela. 1973. Proteins with insulin like activity isolated from oyster (*Ostrea edulis* L.) hepatopancreas. *Gen. Comp. Endocrinol.* **20**: 305-311.
- Martin, K. J., K. A. Hruska, J. Lewis, C. Anderson, and E. Slatopolsky. 1977. The renal handling of parathyroid hormone role of peritubular uptake and glomerular filtration. *J. Clin. Invest.* **60**: 808-814.
- Minnen, J. V., and H. Schallig. 1990. Demonstration of insulin-related substances in the central nervous system of pulmonates and *Aplysia californica*. *Cell. Tissue Res.* **260**: 381-386.
- Mizoguchi, A., M. Hatta, S. Sato, H. Nagasawa, A. Suzuki, and H. Ishizaki. 1990. Developmental change of bombyxin content in the brain of the silk moth *Bombyx mori*. *J. Insect. Physiol.* **36**: 655-664.
- dè Pablo, F., E. Hernandez, F. Collia, and J. A. Gomez. 1985. Untoward effects of pharmacological doses of insulin in early chick embryos: through which receptors are they mediated? *Diabetologica* **28**: 308-318.
- dè Pablo, F., L. A. Scott, and J. Roth. 1990. Insulin and insulin-like growth factor I in early development: peptides, receptors, and biological events. *Endocrine Rev.* **4**: 558-577.
- Robertson, W. R., and S. P. Bidney. 1990. The *in vitro* bioassay of peptide hormones. Pp. 121-157 in *Peptide Hormone Secretion. A Practical Approach*, J. C. Hutton and K. Siddle, eds. Oxford University Press, Oxford, New York, Tokyo.
- Rosen, O. M. 1987. After insulin binds. *Science* **237**: 1452.
- Saleuddin, A. S. M., and S. C. Kunigelis. 1984. Neuroendocrine control mechanisms in shell formation. *Am. Zool.* **24**: 911-916.
- Saleuddin, A. S. M., H. R. Khan, M. Sevala, and V. L. Sevala. 1991. Hormonal control of confirmed shell growth in the snail *Helisoma duryi* (Mollusca: Gastropoda). Pp. 161-165 in *Mechanisms and Phylogeny of Mineralization in Biological Systems*, S. Suga and H. Nakahara, eds. Springer-Verlag, Tokyo.
- Sanders, B. 1983. Insulin-like peptides in the lobster *Homarus americanus* I. Insulin immunoreactivity. *Gen. Comp. Endocrinol.* **50**: 366-373.
- Smit, A. B., E. Vreugdenhil, R. H. M. Ebberink, W. P. M. Geraerts, J. Klootwijk, and J. Joosse. 1988. Growth-controlling molluscan neurons produce the precursor of an insulin-related peptide. *Nature* **33**: 535-538.
- Smit, A. B., W. P. M. Geraerts, I. Meester, H. V. Heerikhuizen, and J. Joosse. 1991. Characterization of a cDNA clone encoding molluscan insulin-related peptide II of *Lymnaea stagnalis*. *Eur. J. Biochem.* **199**: 699-703.
- Smit, A. B., S. F. T. Thijsen, W. P. M. Geraerts, I. Meester, H. V. Heerikhuizen, and J. Joosse. 1992. Characterization of a cDNA clone encoding molluscan insulin-related peptide V of *Lymnaea stagnalis*. *Mol. Brain Res.* **14**: 7-12.
- Sokal, R. R., and F. J. Rohlf. 1973. *Introduction to Biostatistics*. W. H. Freeman, San Francisco.
- Thorpe, A., and H. Duve. 1984. Insulin- and glucagon-like peptides in insects and molluscs. *Mol. Physiol.* **5**: 235-260.
- Wong, V., and A. S. M. Saleuddin. 1972. Fine structure of normal and regenerated shell of *Helisoma duryi*. *Can. J. Zool.* **50**: 1563-1568.

## A Light-Independent Magnetic Compass in the Leatherback Sea Turtle

KENNETH J. LOHMANN AND CATHERINE M. FITTINGHOFF LOHMANN

*Department of Biology, Coker Hall, CB-3280, University of North Carolina, Chapel Hill, North Carolina 27599*

*Diverse animals can orient to the earth's magnetic field (1–6), but the mechanism or mechanisms underlying magnetic field detection have not been determined. Behavioral (7–9) and neurophysiological (10–12) results suggest that the transduction process underlying magnetic compass orientation in vertebrates is light-dependent, a finding consistent with theoretical models proposing that magnetoreception involves a modulation of the response of retinal photoreceptors to light (13, 14). We report, however, that leatherback sea turtle (*Dermochelys coriacea*) hatchlings orient to the geomagnetic field in complete darkness. Thus, light-dependence is not a universal feature of vertebrate magnetic compasses.*

Immediately after emerging from underground nests on oceanic beaches, sea turtle hatchlings enter the sea and swim toward the open ocean in a migration lasting several days. Hatchlings leaving the east coast of Florida quickly establish easterly courses that lead them away from land and toward the Gulf Stream current (15–17). Previous laboratory experiments have demonstrated that hatchling loggerhead turtles (*Caretta caretta*) will orient to the earth's magnetic field (2). To determine whether leatherbacks have a similar ability and whether the transduction mechanism underlying magnetic compass orientation in sea turtles is dependent on light, we investigated the orientation of hatchling leatherbacks swimming in darkness.

Hatchling leatherback sea turtles were obtained from nests deposited on beaches in the vicinity of Fort Pierce, Florida. Nests were examined daily. When a depression formed in the sand above a nest (indicating that the eggs had hatched and that emergence would probably occur that night), several hatchlings were removed, placed into a darkened styrofoam cooler, and transported to the lab-

oratory. Orientation was assessed in a circular water-filled arena surrounded by a Rubens cube coil (18) (Fig. 1) that could be used to reverse the direction of the horizontal component of the ambient magnetic field. Experiments were conducted in a light-tight room between sundown and sunrise, the time when most hatchlings normally enter the sea (19, 20). To eliminate the light emanating from computers and power supplies, all electronic equipment was removed from the room. As an additional precaution against unexpected light sources (*e.g.*, bioluminescence), an observer periodically sat silently beside the coil while experiments were in progress. Following dark-adaptation of one hour or longer, three different observers were unable to perceive any light in the room despite systematic searches and efforts to elicit bioluminescent flashes by stirring the water.

While in darkness, hatchling leatherbacks tested in the earth's magnetic field were significantly oriented in an eastward direction (Fig. 2a). In contrast, hatchlings tested in darkness under reversed field conditions oriented in approximately the opposite direction (Fig. 2b). The two distributions are significantly different, indicating that the ambient magnetic field influenced the orientation of hatchling leatherbacks swimming in darkness.

These results demonstrate that leatherbacks are able to detect the geomagnetic field in the absence of visible light. We conclude that the transduction mechanism underlying magnetic compass orientation is not light-dependent in all vertebrate species.

The magnetic compass of sea turtles could rely on a mechanism different from that used by other vertebrates. The functional characteristics of the loggerhead turtle compass and those of magnetic compasses in two other vertebrate classes, however, appear identical. Like the magnetic compass of birds (5) and of shoreward-orienting newts (4), the loggerhead compass is axial and based on

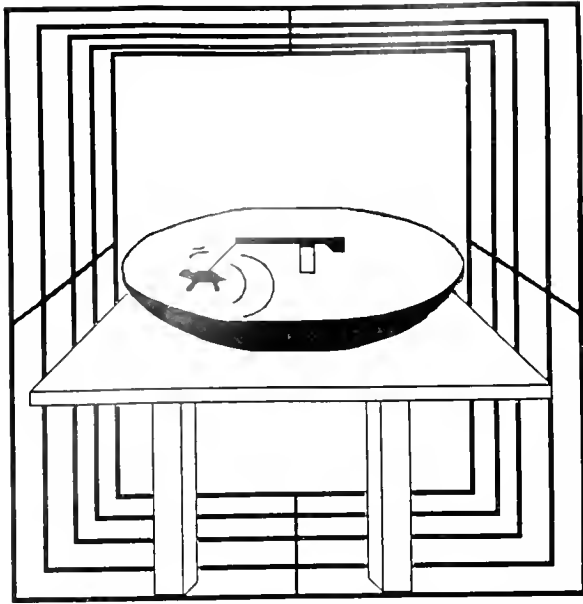


**Figure 1.** The orientation arena was an inverted fiberglass satellite dish (1.02 m diameter) filled with water. The arena was surrounded by a Rubens cube coil 130 cm on a side. Prior to testing, each hatchling was placed into a nylon-Lycra harness that encircled the turtle's carapace without impeding swimming (15). The harness was connected by a short monofilament line to a lever arm mounted on a 360° rheostat. The rheostat was positioned on a post in the center of the orientation arena (2). The lever arm was free to rotate within the horizontal plane and could easily be pulled clockwise or counterclockwise by a swimming turtle. The arm thus tracked the direction toward which the hatchling swam. The central rheostat was wired to a computer in an adjacent room, which recorded the orientation of the turtle every 30 s with an accuracy of  $\pm 2^\circ$ . Thus, the orientation of turtles swimming in darkness could be tracked.

**Methods:** Detailed descriptions of methods are provided in ref #2. Each hatchling was tested once on either its first, second, or third night of captivity. Each trial began in the earth's field (coil off) with a dim light hanging in magnetic east so that hatchlings quickly established a course toward the light (2). The light was provided because hatchlings emerging from their nests at night under natural conditions find the sea using light cues associated with the ocean surface (25); light reflected from the ocean may also provide a directional cue necessary for hatchlings to initiate a seaward course (2, 26). After one hour, the light was turned off and the turtles were permitted to swim in darkness either in the unaltered magnetic field (*i.e.*, the coil remained off) or in a reversed field (*i.e.*, the coil was turned on 10–20 s after the light was turned off). Ten minutes after the light was turned off, the computer began recording the orientation of each hatchling at 30-s intervals. Thus, orientation data were collected only while the turtles were swimming in darkness. Between trials, we periodically altered the position of the power supply relative to the arena to reduce the chance that subtle sounds or vibrations could serve as an orientation cue; such positional changes, however, had no discernible effect on orientation.

field line inclination, rather than on field polarity (21). The possibility therefore exists that all three compasses are based on a common underlying mechanism.

One hypothesis for magnetic field detection in vertebrates proposes that particles of the mineral magnetite

transduce geomagnetic stimuli to the nervous system (22). Although magnetite particles have been detected in cephalic tissues of sea turtles (23) and in numerous other animals known to orient magnetically (22), no direct neurophysiological evidence has been obtained demonstrating a link between magnetite and magnetic field detection in any multicellular organism.

A second hypothesis of magnetoreception has been proposed for elasmobranch fishes. These animals possess sensitive electroreceptors that may endow them with a magnetic compass sense based on electromagnetic induction (24). Because electroreceptors have not been found in reptiles, however, an induction-based mechanism appears unlikely for sea turtles. Moreover, the elasmobranch induction hypothesis requires consistent movement through the earth's magnetic field, yet hatchlings successfully oriented magnetically while tethered and nearly stationary (Fig. 1).

A third hypothesis proposes that magnetoreception occurs in photoreceptors through a transduction process requiring light (7, 13, 14). Our results demonstrate that light is not necessary for magnetic orientation in marine turtles. The results are therefore not consistent with current models of light-dependent magnetoreception. Further research will be required to determine whether the light-independent magnetic compass of sea turtles relies on different

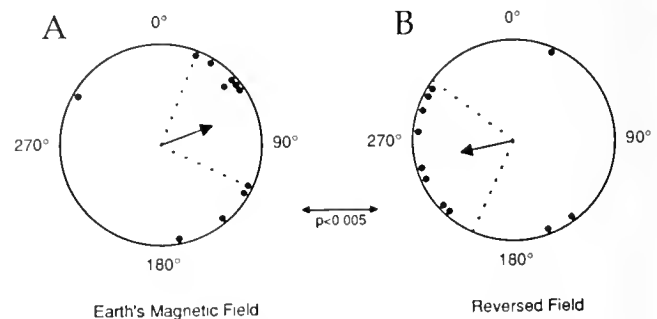


**Figure 2.** Results of magnetic orientation experiments with hatchling leatherbacks tested in darkness. (A) Mean angles of hatchlings tested in the earth's magnetic field. The group was significantly oriented with a mean angle of  $70^\circ$  (Rayleigh test:  $r = 0.55$ ,  $Z = 3.33$ ,  $P < 0.05$ ). (B) Mean angles of hatchling leatherbacks tested in darkness in a reversed field. The group was significantly oriented with a mean angle of  $255^\circ$  (Rayleigh test:  $r = 0.53$ ,  $Z = 3.09$ ,  $P < 0.05$ ). The arrow between the two distributions indicates they are significantly different (Watson test:  $U^2 = 0.300$ ,  $P < 0.005$ ). Arrows in the center of each circle indicate the mean angle of the group; the arrow length is proportional to the magnitude of the mean vector  $r$ , with the radius of the circle corresponding to  $r = 1$ . Dashed lines indicate the 95% confidence interval for the mean angle (27).

**Methods:** Procedures used in analyzing orientation data are described in detail in ref #2, except that: (i) the accuracy of measurements in this study was improved to  $\pm 2^\circ$ , and (ii) to avoid tiring leatherback hatchlings (an endangered species) before release, we terminated experiments as soon as a turtle completed its first oriented swimming period; the mean angle of this period (2) was the hatchling's orientation angle.



receptors than the apparently light-dependent magnetic compasses of birds (5, 9) and newts (7), or whether all three compasses in fact share a common underlying mechanism.

### Acknowledgments

We thank Jay Callaway for developing the data acquisition software, Mike Salmon and Jeanette Wyneken for discussions of experimental protocols, and Erik Martin and Robert Ernest for assistance in locating leatherback turtle nests. The work was supported by NSF grants IBN-9120338 and BNS-87-07173. Endangered species research was authorized under Florida DNR special permit TP 073.

### Literature Cited

- Lohmann, K. J., and A. O. D. Willows. 1987. Lunar-modulated geomagnetic orientation by a marine mollusk. *Science* **235**: 331-334.
- Lohmann, K. J. 1991. Magnetic orientation by hatchling loggerhead sea turtles (*Caretta caretta*). *J. Exp. Biol.* **155**: 37-49.
- Quinn, T. P. 1980. Evidence for celestial and magnetic compass orientation in lake migrating sockeye salmon fry. *J. Comp. Physiol. A* **137**: 243-248.
- Phillips, J. B. 1986. Two magnetoreception pathways in a migratory salamander. *Science* **233**: 765-767.
- Wiltschko, W., and R. Wiltschko. 1988. Magnetic orientation in birds. Pp. 67-121 in *Current Ornithology*, vol. 5, Johnston, R. F., ed. Plenum Press, New York.
- Burda, H., S. Marhold, T. Westenberger, R. Wiltschko, and W. Wiltschko. 1990. Magnetic compass orientation in the subterranean rodent *Cryptomys hottentotus*. *Experientia* **46**: 528-530.
- Phillips, J. B., and S. C. Borland. 1992. Behavioural evidence for use of a light-dependent magnetoreception mechanism by a vertebrate. *Nature* **359**: 142-144.
- Phillips, J. B., and S. C. Borland. 1992. Wavelength specific effects of light on magnetic compass orientation of the eastern red-spotted newt *Notophthalmus viridescens*. *Ethol. Ecol. Evol.* **4**: 33-42.
- Wiltschko, W., and R. Wiltschko. 1981. Disorientation of inexperienced young pigeons after transportation in total darkness. *Nature* **291**: 433-434.
- Olcese, J., S. Reuss, and P. Semm. 1988. Geomagnetic field detection in rodents. *Life Sci.* **42**: 605-613.
- Semm, P., D. Nohr, C. Demaine, and W. Wiltschko. 1984. Neural basis of the magnetic compass: interactions of visual, magnetic and vestibular inputs in the pigeon's brain. *J. Comp. Physiol. A* **155**: 283-288.
- Semm, P., and C. Demaine. 1986. Neurophysiological properties of magnetic cells in the pigeon's visual system. *J. Comp. Physiol. A* **159**: 619-625.
- Leask, M. J. M. 1977. A physicochemical mechanism for magnetic field detection by migrating birds and homing pigeons. *Nature* **267**: 144-145.
- Schulten, K., and A. Windemuth. 1986. Model for a physiological magnetic compass. Pp. 99-106 in *Biophysical Effects of Steady Magnetic Fields*, G. Maret, N. Boccarda, and J. Kiepenheuer, eds. Springer-Verlag, Berlin.
- Salmon, M., and J. Wyneken. 1987. Orientation and swimming behavior of hatchling loggerhead turtles (*Caretta caretta* L.) during their offshore migration. *J. Exp. Mar. Biol. Ecol.* **109**: 137-153.
- Carr, A. 1986. Rips, FADS, and little loggerheads. *BioScience* **36**: 92-100.
- Carr, A. 1986. New perspectives on the pelagic stage of sea turtle development. *NOAA Tech. Memorandum NMFS-SEFC* **190**: 1-36.
- Rubens, S. M. 1945. Cube-surface coil for producing a uniform magnetic field. *Rev. Sci. Instrum.* **16**: 243-245.
- Witherington, B. E., K. A. Bjorndal, and C. M. McCabe. 1990. Temporal pattern of nocturnal emergence of loggerhead turtle hatchlings from natural nests. *Copeia* **4**: 1165-1168.
- Bustard, H. R. 1967. Mechanism of nocturnal emergence from the nest in green turtle hatchlings. *Nature* **214**: 317-318.
- Light, P., M. Salmon, and K. J. Lohmann. 1993. Geomagnetic orientation of loggerhead sea turtles: evidence for an inclination compass. *J. Exp. Biol.* (in press).
- Kirschvink, J. L., D. S. Jones, and B. J. MacFadden. 1985. *Magnetite Biomineralization and Magnetoreception in Organisms*. Plenum Press, New York.
- Perry, A., G. B. Bauer, and A. E. Dizon. 1985. Magnetoreception and biomineralization of magnetite in amphibians and reptiles. Pp. 439-453 in *Magnetite Biomineralization and Magnetoreception in Organisms*, J. L. Kirschvink, D. S. Jones and B. J. MacFadden, eds. Plenum Press, New York.
- Kalmijn, A. J. 1978. Experimental evidence of geomagnetic orientation in elasmobranch fishes. Pp. 347-353 in *Animal Migration, Orientation, and Homing*, K. Schmidt-Koenig and W. T. Keeton, eds. Springer-Verlag, Berlin.
- Mrosovsky, N., and S. F. Kingsmill. 1985. How turtles find the sea. *Z. Tierpsychol.* **67**: 237-265.
- Mrosovsky, N. 1978. Orientation mechanisms of marine turtles. Pp. 413-419 in *Animal Migration, Navigation, and Homing*, K. Schmidt-Koenig and W. T. Keeton, eds. Springer-Verlag, Berlin.
- Batschelet, E. 1981. *Circular Statistics in Biology*. Academic Press, London.



**The Marine  
Biological  
Laboratory  
Woods Hole  
Massachusetts**

**Ninety-Fifth Report  
for the Year 1992  
One-Hundred and Fourth Year**

**Officers of the Corporation**

---

Denis M. Robinson, *Honorary Chairman of the Board  
of Trustees*

Sheldon J. Segal, *Chairman of the Board of Trustees*

Robert E. Mainer, *Vice Chairman of the Board of  
Trustees*

James D. Ebert, *President of the Corporation*

John E. Burris, *Director and Chief Executive Officer*

Robert D. Manz, *Treasurer*

Neil Jacobs, *Clerk of the Corporation*

## **Contents**

---

Report of the Chairman .....	R1
Report of the Director .....	R2
Report of the Treasurer .....	R6
Financial Statements .....	R8
Report of the Library Director .....	R18
Educational Programs	
Summer Courses .....	R21
Short Courses .....	R25
Summer Research Programs	
Principal Investigators .....	R30
Other Research Personnel .....	R31
Library Readers .....	R33
Institutions Represented .....	R34
Year-Round Research Programs .....	R38
Honors .....	R45
Board of Trustees and Committees .....	R48
Laboratory Support Staff .....	R51
Members of the Corporation	
Life Members .....	R53
Regular Members .....	R54
Associate Members .....	R65
Certificate of Organization .....	R68
Articles of Amendment .....	R68
Bylaws .....	R68

## Report of the Chairman

---

The year 1992 was one of historic and exciting change for the Marine Biological Laboratory. In August, the MBL's Board of Trustees voted to adopt major changes in the governance of the Laboratory, and in September we welcomed the Laboratory's newest director and CEO, John E. Burris.

### New Governance Structure

The decision to modify the governance of the MBL came after discussions at a Trustees retreat in 1991 and a year of careful study and work by members of an Ad Hoc Committee on Governance, in consultation with the MBL community. When fully constituted, the MBL's new Board of Trustees will be composed of 18 members drawn from a wide community of distinguished, influential, and experienced individuals. The Board will be a fiduciary body, the guardian of the MBL mission. It will have strong fundraising capabilities, be independent and self regenerating, set policies, and appoint and evaluate the CEO. Board members provide to the laboratory a broad range of valuable experience and will be able to address the institution's challenges with wisdom and objectivity.

A Nominating Committee of the Board will seek eligible candidates for Board membership and the candidates will be elected by the full Board. Six of the Trustees will be selected by the Board from a list of nominees—all scientists and MBL Corporation members—compiled by the MBL Corporation. Other members of the Board may also be chosen from the scientific community at large.

The Corporation will continue to play the crucial role of providing governance on the scientific direction of the MBL. Drawing from its membership, the Corporation will establish a Science Council that will provide advice and counsel on scientific affairs to the MBL's director and to the Board of Trustees. Members

of the Science Council will represent all aspects of scientific life at the MBL.

Finally, an independent Board of Overseers will be established. This group will consist of distinguished scientists—not necessarily members of the MBL Corporation—who will serve as advisors to the Director and to the Board.

### New Director Appointed

After a year-long search, I was pleased to announce in July the appointment of John E. Burris to serve as Director and CEO of the Marine Biological Laboratory. Dr. Burris received his Ph.D. in marine biology from Scripps Institution of Oceanography in 1976. He came to the MBL from the National Research Council of the National Academy of Sciences where he served most recently as Executive Director of the Commission on Life Sciences. He brings to his new role as MBL's Director a broad range of experience in science policy and administration, and as a university faculty member and researcher in marine biology and physiological ecology.

While welcoming John to his new position, I'd also like to pay tribute and offer thanks on behalf of the Laboratory to John's predecessor, Harlyn Halvorson. He served with distinction as Director of the MBL from September 1987 to July 1992. Under Harlyn's leadership the laboratory celebrated a milestone event of June 20, 1992, with the opening of the new Marine Resources Center. Harlyn's dedication and commitment to the Marine Resources project never faltered. He worked all over the country, indeed around the world, garnering support for this effort. We owe Harlyn great thanks as our Director and as the visionary who made this new building possible.

—Sheldon J. Segal

## Report of the Director and Chief Executive Officer

It is with great pleasure that I recount the past year at the Marine Biological Laboratory and contemplate its future, for in my first nine months at the Laboratory I have come to appreciate its many resources and its potential. The greatest of these resources is the human one—the staff, the scientists, the students, and the community. Next is the environment of the MBL—an institution composed of a variety of well-run research laboratories surrounded by waters rich in biological diversity.

What did 1992 bring to the Marine Biological Laboratory?

### *Marine Resources Center*

Our most visible achievement of 1992 was the June 20th opening of the MBL's new Marine Resources Center. Senators Edward M. Kennedy and John Kerry, Congressman Gerry Studds, and NIH Deputy Director Jay Moskowitz participated in the opening ceremonies, which were attended by more than 500 members of the MBL and Woods Hole communities. We owe a great debt of gratitude to Harlyn Halvorson, for his tireless efforts towards making this milestone project a reality.

The new Marine Resources Center provides state-of-the-art engineering systems and advanced laboratory and mariculture facilities, as well as a collaborative veterinary program through the University of Pennsylvania's Laboratory for Marine Animal Health, directed by Donald Abt. Dr. Alan M. Kuzirian has been appointed Acting Director of the new Center. The MRC is reporting early successes in maintaining a



Steve Rosenthal

healthier and more reliable supply of marine organisms. For example, a new generation of dogfish has been born and is thriving in our circulating seawater tanks. Species requiring cold seawater are now available to researchers into the summer months as a result of improved chilled seawater holding facilities. Warmer-water species such as toadfish and scup are being maintained in the facility well past the time when they would have departed Woods Hole waters for warmer climes. A colony of sea worms is also being raised under uniform conditions to produce reliable, standardized bioassays in environmental monitoring.

The challenge facing the MBL is to maximize the use of this wonderful facility. We need to use it not only to



Stephen Rose

Congressman Gerry Studds, Senators John Kerry and Edward M. Kennedy, and MBL Director Harlyn Halvorson at the Opening of the MBL's Marine Resources Center.

maintain organisms caught locally, but also to culture organisms from egg to egg to assure a reliable and genetically and nutritionally defined set of experimental organisms. The facility has extensive capabilities for mariculture and biomedical research, providing exciting potential for expanding the Laboratory's research and educational programs.

### *Year-Round Research*

The MBL's year-round community remains a strong group of investigators, as evidenced by their continued ability to obtain funding through peer-reviewed grants even in these tight times. Some examples of these successes include:

- The Ecosystems Center, jointly directed by John Hobbie and Jerry Melillo, won a large, multi-year award from the National Science Foundation to support a Land-Margin Ecosystems Research program. This research measures the effects of human habitation on fragile coastal zone ecosystems by studying changes in food webs and water quality. The Center is also continuing its research in tropical forests to evaluate the effects of deforestation and air pollution on these rapidly changing environments with grants from the Texaco and Exxon corporations.

- Investigators in the Center for Architectural Dynamics in Living Cells continue to explore the mechanisms and structural dynamics of cell division, differentiation, and motility in living cells. Center scientists are developing an automated polarized light microscope that will document cell architecture on the molecular level. Dr. Shinya Inoué, the Director of the Center, was awarded the E.B. Wilson Award in November, the American Society for Cell Biology's highest honor. As this report goes to press, we have learned that Dr. Inoué was also elected to membership in the National Academy of Sciences.

- The Center for Molecular Evolution, directed by Mitchell Sogin, received national media coverage recently for a dramatic discovery made there in 1992: that the fungi are more closely related to animals than they are to plants. This is a radical departure from accepted classification systems where the fungi have either been grouped with plants or given separate kingdom status. Work at the Center is funded by the NIH and the G. Unger Vetlesen Foundation.

- Lionel Jaffe and his colleagues Peter Smith and Andrew Miller have expanded and diversified funding for the National Vibrating Probe Facility and the Calcium Aequorin Imaging Laboratory. Recent exciting results in these two facilities have provided new insights on the blood-brain barrier, as well as the movement of calcium in newly fertilized eggs.

### *Summer Research at the MBL*

In 1992, more than 300 scientists from around the world came to the MBL to perform research and collaborate with their peers. Using the latest biomedical technologies, their work has implications on studies of aging, diabetes, cognition and memory, mariculture, pollution, vision, and tissue bioadhesives. A series of evening lectures, including the traditional Friday Evening Lecture Series, symposia, and brown bag lunches facilitated the exchange of ideas among our eminent researchers.

Of particular note, summer researchers Sergei Kuznetsov, George Langford, and Dieter Weiss found evidence that a myosin-like motor is responsible for the actin-dependent movement of organelles in squid giant axons. These investigators propose a "dual filament system" to account for the movement of organelles during fast axonal transport. According to their hypothesis, both actin filament-based and microtubule-based motility systems work together to produce and regulate the movement of organelles within the axon. The breakdown of these kinds of transport systems in nerve cells is thought to be involved in various degenerative diseases such as amyotrophic lateral sclerosis.

### *Educational Program*

The MBL's exceptional educational program continued its strong tradition of providing graduate students and postdoctoral fellows with innovative courses in the life sciences. In 1992, 347 students and 200 faculty and lecturers from more than 200 universities and research institutions participated.

In addition to the wide range of core courses at the MBL, 1992 marked the return of the Mariculture course. The course now uses a basic science approach to address the problems of maintaining and culturing marine organisms used in biological research.

The MBL's Information Systems Division teamed up with the National Library of Medicine to provide a one-week course for 30 students in Medical Informatics. Workshops were also designed to teach the MBL community how to use the NLM software. These programs will continue for the next three years.

The MBL was also chosen to host the first course in Fundamental Issues in Vision Research: Molecular and Biological Approaches. This two-week laboratory and lecture course, sponsored by the NIH's National Eye Institute, demonstrated the challenging problems in vision research available to graduate students. Several



MBL summer investigators participated in planning and teaching this course.

### *Fellowship Programs*

The MBL's Fellowship and Scholarship programs received strong support in 1992. More than \$103,000 was available, enabling 16 young investigators and students to participate in the MBL's research and educational programs. The fellowship program was enhanced again this year by a weekly luncheon seminar series in which our young scholars shared their research with the MBL community. Our fellows were also honored at the annual Chamber Music Concert, which in 1992 featured the renowned Tokyo String Quartet.

Ten journalists participated in the 7th annual Science Writing Fellowships Program at the MBL. The one-week hands-on laboratory in cell and molecular biology techniques was again a great success. For the second year, a journalist was sent to the Toolik Lake research site on the north slope of Alaska's Brooks Range, to work with scientists from the MBL's Ecosystems Center.

### *Library*

The MBL/WHOI Library has made significant progress towards its goal of serving as a conduit for, rather than being exclusively a repository of, scientific knowledge, thanks largely to support from the Andrew Mellon Foundation and the Howard Hughes Medical Institute. A fiber optic data network has been installed, which will provide access to the Internet, electronic mail and bulletin boards, and limited access to our journal collection to scientists working around the world. The U.S. Department of Education included the MBL/WHOI Library in its constellation of officially designated research libraries.

### *Construction*

As I write this report, work has begun on a number of construction and renovation projects at the Laboratory. The Lillie research laboratory is in the early stages of being renovated, the result of a \$575,000 matching grant from the National Science Foundation. Although major components of the project won't begin until the fall of 1993, the first phases of the project—the removal of asbestos from some of the research laboratories—is underway. Included in the renovations are a central air conditioning system, forced ventilation

into the labs, a new freight elevator, and a larger-capacity standby electrical power generator.

The Brick Apartment Dormitory is undergoing its first major renovations since it was constructed in 1923. When completed in the summer of 1993, the building will be more energy-efficient and modern. Asbestos will have been removed and a new boiler and bathroom facilities in the dorm wing installed.

December 22, 1992 marked the end of an era for the MBL's Supply Department, when the old shingled supply building was razed to make room for the Lab's new Collection Support Facility. The CSF will occupy basically the same footprint as the old supply building. It will contain a small boat maintenance facility and a diving support facility on the first floor, and a 500 kWatt emergency generator for the new MRC on the second.

### *Special Events and Public Programs*

In 1992, the MBL continued to offer outreach programs to the general public. Three weeks of ELDERHOSTEL programming was offered, and the sessions, which included courses on evolution, ichthyology, biochemistry, and genetics, were met with great enthusiasm by the students. The MBL also continued its acclaimed Falmouth Forum winter series of lectures, presentations, and concerts. Among our 1992 Forum participants was Pulitzer Prize winning author, David McCullough.

### *The Future*

The preceding chronicles the recent concrete achievements of the Laboratory, but it doesn't capture adequately the excitement we all feel about the future. As the times change in biomedical and biological research, the MBL is well-positioned to take advantage of the changes. In education, for instance, where everyone is bemoaning the expense of equipment and laboratories, and where institutions are closing down laboratory courses, we continue to be able to offer modern courses with state-of-the-art equipment. Our rotating faculty and the generous loans of equipment from scores of different vendors are crucial in our ability to do this, as is the generous support we receive from the federal government and private organizations such as the Howard Hughes Medical Institute, the MacArthur Foundation, and the Burroughs Wellcome Fund. We know that our courses are filling a need, as indicated by the increased number of applications for all of them in the summer of 1993.

In an era when young scientists are finding it progressively more difficult to get started and to obtain funding, we have expanded our fellowship program. Again we see the demand for such programs; applications for fellowships more than doubled in 1993 from 1992.

The future of the MBL is indeed bright for our researchers as well. Our new Marine Resources Center and the soon-to-be renovated Lillie research laboratory will provide an improved physical setting where our

scientists may pursue a variety of new research opportunities.

I feel fortunate to have assumed the directorship of the Marine Biological Laboratory, long recognized as one of the world's most important biological laboratories, at this propitious moment. I look forward to working with all of you in the years to come.

—John E. Burris



## Report of the Treasurer

Financially, 1992 will be remembered as the year of transition. With the "changing of the guard" in leadership and the change in governance comes the challenge and opportunity for strengthening the financial future of the MBL.

We finished 1992 with an excess of support and revenues over expenses in the unrestricted current funds of \$275,968. After mandatory and non-mandatory transfers, the net result was a decrease in our unrestricted current fund balance of \$8,451.

This modestly successful result meant that for the first time in a number of years we did not have to use unrestricted quasi-endowment funds to support current operations.

This is a heartening result, but it must be tempered by the observation that this is before a depreciation expense of \$722,959. Like most other not-for-profit organizations, the MBL does not charge depreciation expense to operations. Until the MBL funds

### MBL ENDOWMENT FUNDS 1992

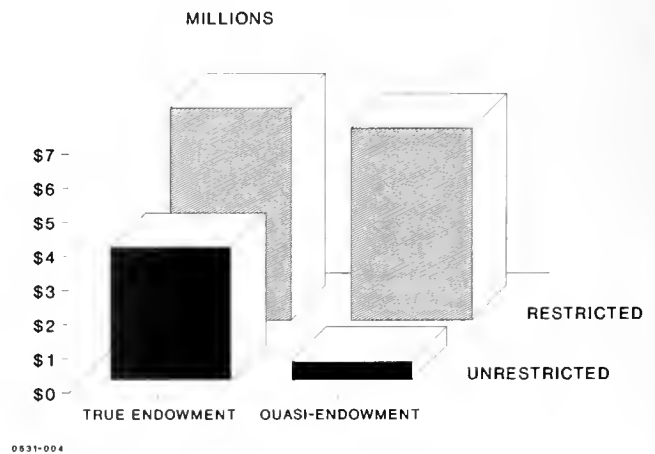


Figure 2

### TOTAL ENDOWMENT FUND BALANCE

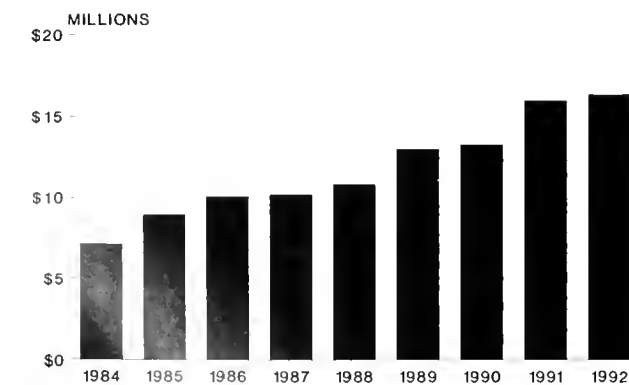


Figure 1

depreciation of operations, there can be no use of the word "surplus."

1992 saw the completion of the Marine Resources Center, and the growth of our plant fund balances from about \$10 million in at the end of 1991 to almost \$20 million at the end of 1992.

Our endowment funds (Figs. 1 and 2) increased slightly from \$15.9 million to \$16.3 million, almost all of this increase resulting from gifts. The total return before fees on our portfolios in 1992 ranged between 5% and 5.8%; clearly, we need to improve on this performance, and we shall endeavor to do so through the efforts of the Investment Committee.

Support and Revenues increased from \$20.8 million in 1991 to \$21.1 million in 1992, due primarily to increasing grant support of research and education. Private gift support decreased due primarily to a lull in receipt of major multi-year grants. This decrease masks

## MBL ANNUAL CAMPAIGN



Figure 3

the robust success of the Annual Campaign (Fig. 3), and other unrestricted gift support. These grew by \$110,000 in 1992, an increase of 34% over the previous year. Revenue from deferred support—drawdowns on previously received gifts—increased by \$436,000 from 1991. This reflects the continuing spend-down of monies received primarily from the Howard Hughes Medical Institute to support the educational and library programs.

Our expenditures increased by \$900,000 with most of the increase coming in the research and education programs as well as administration.

Housing and Dining operations continue to do well, contributing \$158,000 of depreciation expense to the Housing Renewals and Replacements fund. This has allowed us to undertake major upgrades of our housing plant, both through capital expenditures from our Repairs and Replacement fund, and through borrowing.

In 1992 the MBL borrowed \$2,600,000 at favorable tax-exempt rates through the Massachusetts Industrial Finance Agency (MIFA). We use this money to refinance existing debt on our cottages, to renovate the Brick Apartments, and to modernize research facilities in the Crane wing of the Lillie/Crane building. Through this borrowing, and the generous support of donors, we were able to match a \$575,000 award from the National Science Foundation to undertake a \$1,800,000 project for the renovation of scientific facilities.

Looking to 1993 we have a realistically balanced budget that reflects the continued determination to maintain the current level of services at the Laboratory in the most cost-effective manner possible. We can expect the financial stabilization witnessed in 1992 to continue while we take advantage of new funding opportunities. The MBL's long tradition of innovation in fostering the development of scientists and the stimulation of intellectual breakthroughs means that an investment here will yield superior returns.

—Robert D. Manz

# Financial Statements

---

Coopers  
& Lybrand

certified public accountants

## REPORT OF INDEPENDENT ACCOUNTANTS

To the Trustees of  
Marine Biological Laboratory  
Woods Hole, Massachusetts

We have audited the accompanying balance sheet of Marine Biological Laboratory as of December 31, 1992 and the related statement of support, revenues, expenses and changes in fund balances for the year then ended. We previously examined and reported upon the financial statements of the Laboratory for the year ended December 31, 1991, for which condensed statements are presented for comparative purposes only. These financial statements are the responsibility of the Laboratory's management. Our responsibility is to express an opinion on these financial statements based on our audit.

We conducted our audit in accordance with generally accepted auditing standards. Those standards require that we plan and perform the audit to obtain reasonable assurance about whether the financial statements are free of material misstatement. An audit includes examining, on a test basis, evidence supporting the amounts and disclosures in the financial statements. An audit also includes assessing the accounting principles used and significant estimates made by management, as well as evaluating the overall financial statement presentation. We believe that our audit provides a reasonable basis for our opinion.

In our opinion, the financial statements referred to above present fairly, in all material respects, the financial position of Marine Biological Laboratory at December 31, 1992, and its support, revenues, expenses and changes in fund balances for the year then ended in conformity with generally accepted accounting principles.

Our audit was conducted for the purpose of forming an opinion on the basic financial statements taken as a whole. The supplemental schedules of support, revenues, expenses and changes in fund balances for current funds (Schedule I), endowment funds (Schedule II) and plant funds (Schedule III) as of December 31, 1992 are presented for purposes of additional analysis and are not a required part of the basic financial statements. Such information has been subjected to the auditing procedures applied in the audit of the basic financial statements and, in our opinion, is fairly stated, in all material respects, in relation to the basic financial statements taken as a whole.

Boston, Massachusetts  
April 16, 1993

Coopers & Lybrand

MARINE BIOLOGICAL LABORATORY

BALANCE SHEETS

December 31, 1992

(with comparative totals for 1991)

	<u>1992</u>	<u>1991</u>	LIABILITIES AND FUND BALANCES	<u>1992</u>	<u>1991</u>
ASSETS					
Cash	\$ 499,514	\$ 373,365	Current portion of long-term debt (Note F)	\$ 65,000	\$ 60,000
Restricted cash	6,667	6,994	Accounts payable and accrued expenses	1,278,535	822,084
Investments, at market (Note C)	1,628,270	1,778,770	Deferred income	250,490	308,019
Accounts receivable, net of allowance for doubtful accounts of \$8,000 and \$6,000	541,546	458,275	Total current liabilities	1,594,025	1,190,103
Receivables due for costs incurred on grants and contracts	625,857	691,118	Accounts payable (Note E)	208,167	587,579
Other assets	180,927	239,970	Long-term debt (Note F)	2,535,000	1,140,000
Total current assets	3,482,781	3,548,492	Deferred support (Note G)	3,663,698	4,437,140
Restricted cash (Note E)	285,094	587,579	Annuities payable	184,553	152,416
Investments, at market (Notes C and D)	18,236,843	18,298,679	Total long-term liabilities	6,591,418	6,317,135
Deposits with trustee (Note F)	1,548,810	126,116	Commitments (Note E)	8,185,443	7,507,238
Fixed assets (Notes E):			Total liabilities	12,857	21,398
Land	689,660	689,660	Current unrestricted fund balances		
Buildings	27,716,029	17,535,524	Endowment fund balances:	548,061	543,049
Equipment	3,024,613	2,933,618	Quasi-endowment unrestricted	3,884,134	3,735,253
Construction in progress	131,078	6,214,181	Endowment, income for unrestricted purposes	6,219,233	6,049,007
Less accumulated depreciation	(10,707,699)	(10,050,276)	Endowment, income for restricted purposes	5,629,395	5,590,516
	20,853,681	17,322,707	Quasi-endowment restricted	16,280,823	15,917,825
			Total endowment funds		
			Plant fund balances:		
			Unrestricted	19,708,718	10,034,642
			Repairs and replacement reserve	196,470	188,289
			Restricted	22,898	6,214,181
			Total plant funds	19,928,086	16,437,112
			Total liabilities and fund balances	\$44,407,209	\$39,883,573
Total assets	\$44,407,209	\$39,883,573			

The accompanying notes are an integral part of the financial statements.

MARINE BIOLOGICAL LABORATORY

STATEMENT OF SUPPORT, REVENUES, EXPENSES AND CHANGES IN FUND BALANCES

for the year ended December 31, 1992  
(with comparative totals for 1991)

	Current Funds										1991 Total All Funds
	Unrestricted		Endowment Funds		Plant Funds		1992 Total All Funds		1992 Total All Funds		
	Operating Fund	Auxiliary Enterprises	Total	Restricted	Unrestricted	Restricted	Unrestricted	Restricted			
<b>SUPPORT AND REVENUES:</b>											
Grant reimbursements of direct costs				\$5,982,265							\$ 5,982,265
Grant for capital additions			\$3,530,621								4,032,660
Recovery of indirect costs				485,247							4,032,660
Tuition	1,302,795	\$1,798,403	3,101,198	173,733							4,835,681
Fee for services	406,212		406,212	521,698							3,319,506
Investment income	5,239,628	1,798,403	7,038,031	7,162,943							485,247
	428,711		428,711	954,248							3,274,931
Gifts (Note G)	453,970		453,970	319,472							3,212,277
Change in deferred support (Note G)	882,681		882,681	1,273,720		\$ 280,320					927,910
	97,429		97,429	334,481		280,320					18,233,634
Miscellaneous revenue	6,219,738	1,798,403	8,018,141	8,771,144		280,320					1,678,279
Total support and revenues											773,442
											2,451,721
											446,383
											269,003
											21,131,738
<b>EXPENSES:</b>											
Research				6,019,891							6,019,891
Instruction				1,526,154							1,526,154
Scholarships, fellowships and stipends				394,544							394,544
Services	1,982,001	1,422,736	3,404,737	487,886							3,892,623
Administration	2,606,112	145,641	2,751,753	10,000							2,761,753
Plant operations	1,585,953		1,585,953	40,805							1,785,659
Depreciation											722,959
Other				243,571							246,981
Total expenses	6,174,066	1,568,377	7,742,443	8,722,851							17,350,564
Excess (deficit) of support and revenues over expenses	45,672	230,026	275,698	48,293		280,320					3,781,174
Net realized gain on investments				78,636	\$ 23,038	898,719					1,000,393
Net unrealized gain (loss) on investments				(77,518)	(23,216)	(835,402)					(936,136)
Net gain (loss) on investments				1,118	(178)	63,317					64,257
Transfers	(54,213)	(230,026)	(284,239)	(49,411)	5,190	14,349					—
Net change in fund balances	(8,541)	—	(8,541)	—	5,012	357,986					3,845,431
Fund balances, beginning of year	21,398	—	21,398	—	543,049	15,374,776					32,376,335
Fund balances, end of year	12,857	—	12,857	—	548,061	\$15,732,762					\$36,221,766

The accompanying notes are an integral part of the financial statements.



## Marine Biological Laboratory

### Notes to Financial Statements

#### A. Purpose of the Laboratory:

The purpose of Marine Biological Laboratory (the "Laboratory") is to establish and maintain a laboratory or station for scientific study and investigations, and a school for instruction in biology and natural history.

#### B. Significant Accounting Policies:

##### *Basis of Presentation—Fund Accounting*

In order to ensure observance of limitations and restrictions placed on the use of resources available to the Laboratory, the accounts of the Laboratory are maintained in accordance with the principles of fund accounting. This is the procedure by which resources are classified into separate funds in accordance with specified activities or objectives. Separate accounts are maintained for each fund; however, in the accompanying financial statements, funds that have similar characteristics have been combined into fund groups. Accordingly, all financial transactions have been recorded and reported by fund group.

Externally restricted funds may only be utilized in accordance with the purposes established by the donor or grantor of such funds. However, the Laboratory has full control over the utilization of unrestricted funds. Restricted gifts, grants, and other restricted support are accounted for in the appropriate restricted funds. Restricted current funds are reported as revenue as the related costs are incurred (see Note G).

Endowment funds are subject to restrictions which require that the principal be invested in perpetuity. Related investment income is available for use for restricted or unrestricted purposes by the Laboratory depending on donor restrictions. Quasi-endowment funds have been established by the Laboratory for the same purposes as endowment funds; however, the principal of these funds may be expended for various restricted and unrestricted purposes.

##### *Fixed Assets*

Land, buildings and equipment purchased by the Laboratory are recorded at cost. Donated fixed assets are recorded at fair market value at the date of the gift. Depreciation is computed using the straight-line method, beginning the month after the asset is placed in service, over the asset's estimated useful life. Estimated useful lives are generally three to five years for equipment and 20 to 40 years for buildings and improvements. When assets are sold or retired, the cost and accumulated depreciation are removed from the accounts and any resulting gain or loss is included in income for the period.

##### *Contracts and Grants*

Revenues associated with contracts and grants are recognized in the statement of support, revenues, expenses and changes in fund balances as the related costs are incurred (see Note G). Reimbursement of indirect costs relating to government contracts and grants is based on negotiated indirect cost rates. Any over or underrecovery of indirect costs is recognized through future adjustments of indirect cost rates.

##### *Investments*

Investments purchased by the Laboratory are carried at market value. Money market securities are carried at cost plus accrued interest, which approximates market value. Donated investments are recorded at fair market value at the date of the gift. Land held for sale included in investments is carried at the initially recorded market value of \$330,000. For determination of gain or loss upon disposal of investments, cost is determined based on the first-in, first-out method.

The Laboratory is the beneficiary of certain investments reported in the endowment funds which are held in trust by others. The Laboratory's continuing right to these funds is subject to review every ten years by an independent committee. The market values of such investments are \$4,743,257 and \$4,717,315 at December 31, 1992 and 1991, respectively.

##### *Investment Income and Distribution*

The Laboratory follows the accrual basis of accounting except that investment income is recorded on a cash basis. The difference between such basis and the accrual basis does not have a material effect on the determination of investment income earned on a year-to-year basis.

Investment income includes income from a pooled investment account, which income is allocated to the participating funds on the market value unit basis (Note D).

##### *Annuities Payable*

Amounts due to donors in connection with gift annuities are determined based on remainder value calculations which at December 31, 1992 assumed a rate of return of 10%, maximum payout terms of 18 years, and an interest payout rate of 8%.

##### *Tax-Exempt Status*

The Laboratory is exempt from federal income tax under Section 501(c)3 of the Internal Revenue Code.

## R12 Annual Report

### C. Investments.

The following is a summary of the cost and market value of investments at December 31, 1992 and 1991:

	<i>Market</i>		<i>Cost</i>	
	<u>1992</u>	<u>1991</u>	<u>1992</u>	<u>1991</u>
Certificate of deposit	\$ 47,700	\$ 258,351	\$ 46,745	\$ 258,351
Money market securities	1,952,867	1,767,300	1,952,867	1,767,300
U.S. Government securities	1,788,066	1,456,944	1,771,308	1,423,722
Corporate fixed income	8,968,745	8,387,547	8,533,859	7,718,034
Common stocks	6,764,488	7,864,060	4,173,965	4,589,520
Real estate	343,247	343,247	343,247	343,247
Total investments	<u>\$19,865,113</u>	<u>\$20,077,449</u>	<u>\$16,821,991</u>	<u>\$16,100,174</u>

Investments by fund group and related portfolios for the years ended December 31, 1992 and 1991 are as follows:

<i>Current Funds</i>				
Certificates of deposit	\$ 47,700	\$ 258,351	\$ 46,745	\$ 258,351
Money market securities	1,400,000	1,200,000	1,400,000	1,200,000
Library funds	180,570	320,419	183,548	317,557
Total	<u>1,628,270</u>	<u>1,778,770</u>	<u>1,630,293</u>	<u>1,775,908</u>

	<i>Market</i>		<i>Cost</i>	
	<u>1992</u>	<u>1991</u>	<u>1992</u>	<u>1991</u>
<i>Endowment and Quasi-Endowment</i>				
General endowment trust fund	3,755,124	3,735,252	2,897,718	2,707,869
Library endowment trust fund	988,133	982,063	753,904	635,203
Ecosystem funds	4,507,857	4,488,315	3,756,446	3,411,559
Pooled funds	6,910,904	6,608,044	5,806,114	5,253,616
Instruction fund	1,731,578	2,141,758	1,634,269	1,972,772
Real estate	343,247	343,247	343,247	343,247
Total	<u>18,236,843</u>	<u>18,298,679</u>	<u>15,191,698</u>	<u>14,324,266</u>
Total investments	<u>\$19,865,113</u>	<u>\$20,077,449</u>	<u>\$16,821,991</u>	<u>\$16,100,174</u>

### D. Accounting for Pooled Investments:

Certain endowment fund assets are pooled for investment purposes. Investment income from the pooled investment account is allocated on the market value unit basis, and each endowment fund subscribes to or disposes of units on the basis of the market value per unit at the beginning of the calendar quarter within which the transaction takes place. The unit participation of the funds at December 31, 1992 and 1991 is as follows:

	<u>1992</u>	<u>1991</u>
Quasi-endowment unrestricted	4,260	4,618
Quasi-endowment restricted	8,717	8,644
Endowment, income for restricted purposes	40,345	39,458
Endowment, income for unrestricted purposes	79	—
Total	<u>53,401</u>	<u>52,720</u>

Pooled investment activity on a per-unit basis was as follows:

	<u>1992</u>	<u>1991</u>
Unit value at beginning of year	\$128.42	\$108.90
Unit value at end of year	128.66	128.42
Increase in realized and unrealized appreciation	.24	19.52
Net income earned on pooled investments	5.71	5.15
Total return on pooled investments	<u>\$ 5.95</u>	<u>\$ 24.67</u>

E. Deposits and Commitments for Construction Programs:

As of December 31, 1992, the Laboratory has \$285,094 in restricted cash for the construction of the new Collection Support Facility and \$1,548,810 in Deposit with Trustees for the renovations of laboratories and housing facilities. On December 31, 1992, the Laboratory was contractually obligated for approximately \$1,616,288 of additional expenditures in connection with its current building program. The expenditures are covered by funding commitments.

F. Long-Term Debt:

Long-term debt at December 31, 1992 amounted to \$2,600,000. The aggregate amount of principal due for each of the next five fiscal years is as follows:

1993	\$ 65,000
1994	65,000
1995	75,000
1996	75,000
1997	80,000
Thereafter	<u>2,240,000</u>
	2,600,000
Less current portion	<u>65,000</u>
Total	<u>\$2,535,000</u>

In 1992, the Laboratory issued \$1,100,000 Massachusetts Industrial Finance Authority (MIFA) Series 1992A Bonds and \$1,500,000 MIFA Series 1992B. These bonds pay varying annual interest rates and Series 1992 A and B Bonds mature on December 1, 2012. The Series 1992 A and B Bonds are collateralized by a first mortgage on certain Laboratory property.

A portion of Series 1992B Bonds were issued for the purpose of refunding the \$1,330,000 MIFA Series 1989 Bonds, which pay varying annual interest rates and mature on October 31, 2011. The amount of Series 1989 principal outstanding at December 31, 1992 was \$1,140,000. The Laboratory has on deposit investments of \$1,306,172 with Shawmut Bank N.A., as trustee for the MIFA Series 1989 Bonds, for redemption February 1993.

In compliance with the 1992 MIFA bond indentures, the Laboratory has on deposit with State Street Bank and Trust, as trustee for Series 1992 Bonds, investments for construction projects in the amount of \$1,548,810. In 1991, the Laboratory was required to have on deposit \$126,116 for a debt service reserve fund.

Under the most restrictive covenant of long-term debt, the Laboratory's operating surplus (before transfers), interest, expense and transfers from the quasi-endowment for debt service must equal or exceed all debt service payments.

G. Restricted Current Funds Deferred Support:

The Laboratory defers revenue on current restricted funds until the related costs are incurred. Amounts received in excess of expenses are recorded as deferred support. The following summarizes the activity of the deferred support account:

	<u>1992</u>	<u>1991</u>
Balance at beginning of year	\$4,437,140	\$4,774,618
Additions:		
Gifts, endowment income and grants received	7,997,702	7,832,555
Net unrealized gains (losses)	(77,518)	121,308
Net realized gains	78,636	5,102
Transfers	—	36,777
Deductions:		
Funds expended under gifts and grants	8,722,851	8,333,220
Transfers	49,411	—
Balance at end of year	<u>\$3,663,698</u>	<u>\$4,437,140</u>

Deferred restricted gifts of \$453,970 and \$475,874 were expended in 1992 and 1991, respectively, for the support of indirect costs attributable to the Laboratory's instruction programs.

H. Retirement Plan:

The Laboratory participates in the defined contribution pension plan of TIAA-CREF (the "Plan"). The Plan is available to permanent employees that have completed two years of service. Under the Plan, the Laboratory contributes 10% of total compensation for each participant. Contributions amounted to \$502,215 in 1992 and \$495,848 in 1991.

## R14 Annual Report

---

I. Pledges:

As of December 31, 1992, the Laboratory has outstanding pledges of \$737,146 of which \$681,728 is restricted (unaudited). Pledges are not included in the financial statements since it is not practicable to estimate the net realizable value of such pledges. These pledges are scheduled to be paid over the next three years in the amounts of \$509,969, \$169,177, and \$58,000, respectively.

J. Interfund Borrowings

Current unrestricted fund interfund borrowings at December 31 are as follows:

	<u>1992</u>	<u>1991</u>
Due to restricted endowment fund	\$(118,755)	\$ (4,150)
Due to restricted quasi-endowment funds	(50)	(150,000)
Total	<u>\$(118,805)</u>	<u>\$(154,150)</u>

K. Financial Accounting Standard No. 106:

In December 1990, the Financial Accounting Standards Board (FASB) released Statement No. 106, "Employers' Accounting for Postretirement Benefits Other Than Pensions." This new standard requires employers to accrue, during the years that the employee renders the necessary service, the expected cost of benefits to be provided during retirement, and will apply to years beginning after December 15, 1994. The Laboratory is currently analyzing and interpreting the provisions of the Statement as it relates to its current and planned benefits program and its funding options. It is anticipated that adoption of this accounting standard will result in the Laboratory recording a significant liability.

## MARINE BIOLOGICAL LABORATORY

## STATEMENT OF SUPPORT, REVENUES, EXPENSES AND CHANGES IN FUND BALANCES

## CURRENT FUNDS

for the year ended December 31, 1992

	<i>Current Unrestricted Funds</i>			<i>Current Restricted Fund</i>	<i>Total</i>
	<i>Operating Fund</i>	<i>Auxiliary Enterprises Fund</i>	<i>Total</i>		
<b>SUPPORT AND REVENUES:</b>					
Grant reimbursements of direct costs				\$5,982,265	\$5,982,265
Recovery of indirect costs	\$3,530,621		\$3,530,621		3,530,621
Tuition				485,247	485,247
Fees for services:					
Dormitories		\$ 974,076	974,076		974,076
Dining hall		824,327	824,327		824,327
Library	439,822		439,822		439,822
<i>Biological Bulletin</i>	223,811		223,811		223,811
Research services	459,233		459,233	173,733	632,966
Marine resources	179,929		179,929		179,929
Investment income	406,212		406,212	521,698	927,910
	<u>5,239,628</u>	<u>1,798,403</u>	<u>7,038,031</u>	<u>7,162,943</u>	<u>14,200,974</u>
Gifts	428,711		428,711	954,248	1,382,959
Change in deferred support	453,970		453,970	319,472	773,442
	<u>882,681</u>	<u></u>	<u>882,681</u>	<u>1,273,720</u>	<u>2,156,401</u>
Miscellaneous revenue	97,429		97,429	334,481	431,910
Total support and revenues	<u>6,219,738</u>	<u>1,798,403</u>	<u>8,018,141</u>	<u>8,771,144</u>	<u>16,789,285</u>
<b>EXPENSES:</b>					
Research				6,019,891	6,019,891
Instruction				1,526,154	1,526,154
Scholarships, fellowships and stipends				394,544	394,544
Services:					
Dormitories		745,787	745,787		745,787
Dining hall		676,949	676,949		676,949
Library	736,347		736,347	302,135	1,038,482
<i>Biological Bulletin</i>	189,098		189,098		189,098
Research services	622,731		622,731	179,904	802,635
Marine resources	433,825		433,825	5,847	439,672
Administration:					
Administration	2,254,935	145,641	2,400,576	10,000	2,410,576
Sponsored projects administration	351,177		351,177		351,177
Plant operations	1,585,953		1,585,953	40,805	1,626,758
Other				243,571	243,571
Total expenses	<u>6,174,066</u>	<u>1,568,377</u>	<u>7,742,443</u>	<u>8,722,851</u>	<u>16,465,294</u>
Excess of support and revenues over expenses	<u>45,672</u>	<u>230,026</u>	<u>275,698</u>	<u>48,293</u>	<u>323,991</u>
Net unrealized gain on investments				78,636	78,636
Net realized (loss) on investments				(77,518)	(77,518)
Net gain on investments				1,118	1,118
<b>TRANSFERS AMONG FUNDS:</b>					
Debt service		(60,000)	(60,000)		(60,000)
Acquisition of fixed assets	(91,313)	(12,026)	(103,339)		(103,339)
Repairs and replacement		(158,000)	(158,000)		(158,000)
Endowment transfer				200,000	200,000
Capitalization of income				(219,539)	(219,539)
Other	37,100		37,100	(29,872)	7,228
Total transfers among funds	<u>(54,213)</u>	<u>(230,026)</u>	<u>(284,239)</u>	<u>(49,411)</u>	<u>(333,650)</u>
Net change in fund balances	<u>(8,541)</u>	<u></u>	<u>(8,541)</u>	<u></u>	<u>(8,541)</u>
Fund balances, beginning of year	<u>21,398</u>	<u></u>	<u>21,398</u>	<u></u>	<u>21,398</u>
Fund balances, end of year	<u>\$ 12,857</u>	<u></u>	<u>\$ 12,857</u>	<u></u>	<u>\$ 12,857</u>

## MARINE BIOLOGICAL LABORATORY

## STATEMENT OF SUPPORT, REVENUES, EXPENSES AND CHANGES IN FUND BALANCES

## ENDOWMENT FUNDS

for the year ended December 31, 1992

	<i>Unrestricted</i>	<i>Restricted</i>			<i>Total Restricted</i>	<i>Total</i>
		<i>Income for Unrestricted Purposes</i>	<i>Income for Restricted Purposes</i>	<i>Quasi-Endowment</i>		
<b>SUPPORT AND REVENUES:</b>						
Gifts		\$ 128,755	\$ 151,140	\$ 425	\$ 280,320	\$ 280,320
Total support and revenues		128,755	151,140	425	280,320	280,320
Net realized gain on investments	\$ 23,038	189,911	323,933	384,875	898,719	921,757
Net unrealized (loss) on investments	(23,216)	(169,785)	(304,847)	(360,770)	(835,402)	(858,618)
Net gain (loss) on investments	(178)	20,126	19,086	24,105	63,317	63,139
<b>TRANSFERS AMONG FUNDS:</b>						
Capitalization of income	5,190			214,349	214,349	219,539
Endowment transfers				(200,000)	(200,000)	(200,000)
Total transfers among funds	5,190			14,349	14,349	19,539
Net change in fund balances	5,012	148,881	170,226	38,879	357,986	362,998
Fund balances, beginning of year	543,049	3,735,253	6,049,007	5,590,516	15,374,776	15,917,825
Fund balances, end of year	\$ 548,061	\$ 3,884,134	\$ 6,219,233	\$ 5,629,395	\$15,732,762	\$16,280,823

## MARINE BIOLOGICAL LABORATORY

## STATEMENT OF SUPPORT, REVENUES, EXPENSES AND CHANGES IN FUND BALANCES

## PLANT FUNDS

for the year ended December 31, 1992

	<i>Unrestricted</i>		<i>Restricted</i>	<i>Total</i>
	<i>Unrestricted</i>	<i>Repairs and Replacements Reserve</i>		
SUPPORT AND REVENUES:				
Grant for capital additions			\$4,032,660	\$ 4,032,660
Gifts			15,000	15,000
Other revenue			14,473	14,473
Total support and revenues			<u>4,062,133</u>	<u>4,062,133</u>
EXPENSES:				
Depreciation	\$ 722,959		\$ 722,959	722,959
Plant operations		\$ 158,901	158,901	158,901
Other	3,410		3,410	3,410
Total expenses	<u>726,369</u>	<u>158,901</u>	<u>885,270</u>	<u>885,270</u>
Excess (deficit) of support and revenues over expenses	<u>(726,369)</u>	<u>(158,901)</u>	<u>(885,270)</u>	<u>4,062,133</u>
TRANSFERS AMONG FUNDS:				
Debt service	60,000		60,000	60,000
Acquisition of fixed assets	107,495		107,495	107,495
Capital additions, net of disposals	10,232,950		10,232,950	(10,232,950)
Repairs and replacements	—	158,000	158,000	158,000
Other transfers	—	9,082	9,082	(20,466)
Total transfers among funds	<u>10,400,445</u>	<u>167,082</u>	<u>10,567,527</u>	<u>(10,253,416)</u>
Net change in fund balances	<u>9,674,076</u>	<u>8,181</u>	<u>9,682,257</u>	<u>(6,191,283)</u>
Fund balances, beginning of year	<u>10,034,642</u>	<u>188,289</u>	<u>10,222,931</u>	<u>6,214,181</u>
Fund balances, end of year	<u>\$19,708,718</u>	<u>\$ 196,470</u>	<u>\$19,905,188</u>	<u>\$ 22,898</u>





## Report of the Library Director

### *The Library*

The Library's work during 1992 concentrated on the journal collection, the book collection, the rare book room, cataloging, and cooperative relationships.

### *The journal collection*

The journal collection is the heart of the Library's service. The MBL/WHOI Library, in common with all academic research libraries, is working to sustain the collection as far as possible, despite a 12% annual escalation in scientific journal prices over the past decade. Given present national trends in research funding, sustaining the collection calls for innovative cooperation with the publishing industry. Working with Elsevier publishers, the Library was successful in restoring an important journal, *Brain Research*, that was discontinued in 1991.

However, the spiraling cost of the journal collection is a long-term problem, and each year the Library is faced with difficult choices. After extensive review by a panel of 50 scientists, the journal collection was reduced by 32 titles in 1992. Most of the discontinued journals were in clinical and medical areas. These reductions were partially offset by the addition of seven other journals: *Molecular Microbiology*, *Physical Review E*, *Water Environment Research*, the *Canadian Journal of Fisheries and Aquatic Sciences*, *Perspectives on Science*, *Issues in Science and Technology*, and *Serial Sources for the Biosis Previews*.

### *The book collection*

The MBL/WHOI book collection was reviewed to strengthen it and to increase its utility. The Joint MBL/WHOI Library Advisory Committee defined the role of the collection as follows: "... to collect, for general use, those volumes of seminal and enduring value supporting the major scientific fields in which the scientific community is active. The collection should provide a scientist who is proficient in a given field with entry to other disciplines and with broad reviews of techniques and current directions supporting his or her own work."

To meet this purpose, the book collection should be developed with care and should become more available. Some 19% of the collection—7000 books or roughly 30 for every scientist in Woods Hole—are in circulation, including half of the books acquired in the last 3 years. The books are withdrawn for an average of two and a half years, and one book has been taken out for twenty-one.

To remedy this situation, the Joint MBL/WHOI Library Advisory Committee has approved a one-year checkout policy to improve the accessibility of the book collection. A project was started in the fall of 1992 to recall all Library books and check out those that scientists still needed for a one-year period. This project has allowed us to locate and catalog many books that had been held indefinitely in laboratories and offices. The recall project has a long way to go, but it is progressing steadily and will be completed by the end of 1993.

The early winter months brought severe storms to Woods Hole. Strong winds drove rain under the roof of the Lillie building, causing leaks onto the book collection. The wet books, 100 volumes, were frozen and dried; all but two were returned in good condition to the shelves. All books have been moved from the area under the leaks, and a capital project has been approved, subject to funding, for repair of the roof.

### *The Rare Book Room*

The Library's Rare Book Room is an MBL treasure. This year the collection has been enhanced by the donation of a number of old and rare volumes. Through a gift from Cambridge Scientific Abstracts, we have photographed over 100 Leuckart charts, which have also been made into 35-mm slides that can be useful teaching aids. The slides are currently being digitized for easy transfer in electronic format. Our complete collection of these rare wall charts is now maintained in a specially constructed cabinet that preserves them in an acid-free environment in the Rare Book Room.

The rare book collection is currently being placed in the Library catalog. The audio tapes of Friday Evening Lectures, Falmouth Forum, and other lectures have been cataloged and filed. Furniture in the Agassiz Room has been restored, and the framed photographic collection has been identified, covered with UV paper, and hung in related groups in the Agassiz Room and the Rare Book Room. A new cherry filing cabinet has been added to the Agassiz Room to house the biographical files of scientists who have worked at the MBL. The off-season displays in the Lillie Building lobby are maintained by the staff of the Rare Book Room.

### *Cataloging*

The Library worked to make electronically available information more complete and accurate. The catalogs in the Library's computer, the CLAMS system, have been brought up-to-date. The currently subscribed-to serials have been added to the serials catalog, and those journals acquired through the exchange of *The Biological Bulletin* with other institutions are being added. The book collection has been entered into the system, with the exception of expeditions and a few difficult monographic series that require specialized cataloging. The Library began automation of the book circulation process in the fall. Year-round patrons now have a book card, and circulation has been transferred to the automated system.

### *Cooperative relationships*

The Library's membership in the Boston Library Consortium flourished during the year. Among other benefits, this membership provides us with no-cost access to the journal collections of 12 academic libraries in the Boston area. This access privilege is in active use, saving Woods Hole scientists \$20,000 annually in direct charges for articles obtained from other libraries. The addition of a networked document scanning station (ARIEL), financed in part by a grant, has added interlibrary document delivery over the Internet to our services. This station makes it possible electronically to obtain high resolution document images from Boston libraries.

The lowered cost and improved response of these agreements and systems have made it possible to fashion a reciprocal agreement with Brandeis University to develop our collections in concert. Under this agreement, the institutions each agree to retain certain journals. Tables of contents of these journals will be sent monthly to the partner library, and documents from these journals will be delivered with the goal of 24-hour response time.

Other Library activities included the successful September open house, publication of a handy booklet for users of electronic services, and a new program of presentations by Woods Hole scientists that give the Library staff insight into research in the institutions they serve.

### *The Information Systems Division*

The Information Systems Division (ISD) has been extremely productive over the past year, completing projects in Library systems, data networks, classroom and laboratory support, and instruction in Medical Informatics.

### *Library systems*

The bibliographic search system, based on CD-ROM technology, was upgraded and made reliable. The system now makes five bibliographical data bases available, including Aquatic Sciences and Fisheries Abstracts; Life Sciences Abstracts; National Library of Medicine's Medline Service; and The Wilson Disc General Science Index. The fifth and latest is GeoRef, a bibliographic compendium of geological literature from 1785 to the present. The system can now send selected abstracts to scientists' desks by e-mail, or it can directly download the abstracts onto floppy discs on office

computers. All of these services are available over the Internet to Woods Hole scientists anywhere in the world as part of the Library's basic, no-cost service. The majority of bibliographic searches now come to the Library's systems over the Internet rather than from the local terminals in the Library lobby.

The Information Systems Division has gone beyond these services to develop an electronic menu presenting a variety of services at MBL and at other institutions. It is possible to order specimens, equipment, or Chemistry Room supplies; to directly access grant programs at NSF, NIH, NASA, and DOD; to access catalogs of libraries around the world; or to learn about MBL's course offerings, services, and rates through this Library "front end." All Library patrons can have access to this service by talking with the Librarian.

#### *The data network*

The MBL data network has been extended to all campus buildings, including the Marine Resources Center. A new computer was procured to handle increased electronic mail traffic. Equipment to isolate data transmissions is being installed so that laboratories and classrooms do not load the MBL network with their internal traffic. The network was available with 99.8% reliability during 1992.

#### *Classroom and laboratory support*

In 1992, the Information Systems Division became responsible for MBL computing support to courses, wherever that was needed. This involved the installation, and subsequent removal, of 80 networked computers for four courses. As part of the grant from

the National Library of Medicine (NLM) for Medical Informatics training, ISD was called on for selection and installation of 30 personal computers, and for full technical support of a one-week course taught by NLM in early June. More recently the Ecosystems Center has asked the ISD to take care of the computer network in their laboratories.

#### *Instruction in medical informatics*

This year was the first of a grant from the National Library of Medicine to support instruction in Medical Informatics. Following the formal course given by the NLM, the Information Systems Division continued to teach medical informatics to summer course sessions and to audiences at special short courses. These Medical Informatics sessions attracted 150 individuals.

Loeb 308 is being prepared for use as a computer-ready classroom. The computers and software, network connections, and special air handling equipment will assist several courses during the summer as well as the Medical Informatics program.

#### *The Coming Year*

The Library is grateful for the support of the MBL science community and for the help of its many friends. Our goals for the coming year include sustaining the journal collection, improving its housing, and developing electronic delivery of articles from the collection directly to scientists' desks. We look forward to 1993-1994 as another active and productive year.

—David L. Stonehill



## Educational Programs

### *Summer Courses*

#### ***Biology of Parasitism: Modern Approaches*** (June 14–August 15)

##### *Course Director*

John Boothroyd, Stanford University School of Medicine

##### *Associate Director*

Richard Komuniecki, University of Toledo

##### *Faculty*

Jean-François Dubremetz, INSERM, France  
 Alan Fairlamb, London School of Hygiene and Tropical Medicine, UK  
 Fred Finkelman, USUHS/Herbert School of Medicine  
 Kasturi Haldar, Stanford University School of Medicine  
 Joe Urban, United States Department of Agriculture

##### *Instructor*

Richard E. Davis, San Francisco State University

##### *Teaching Assistants*

Patricia Dorn, Stanford University School of Medicine  
 Emilio Duran, University of Toledo  
 Ashraf El Meanawy, University of Cairo Medical School, Egypt  
 Heidi Elmendorf, Stanford University School of Medicine  
 Suzanne Morris, USUHS/Herbert School of Medicine  
 Steven L. Reiner, University of California, San Francisco  
 Keith Smith, London School of Hygiene & Tropical Medicine, UK  
 Martine Soete, INSERM, France

##### *Course Assistants*

Michele Klingbeil, University of Toledo  
 Michelle Rathman, Stanford University

##### *Students*

Thomas Allen, Oregon Health Science University  
 Prasanta Chakraborty, Washington University  
 Claire Chougnat, INSERM, France  
 Johanna Daily, Beth Israel Hospital

Hans Hagen, Keele University, UK  
 Norton Heise, Escola Paulista de Medicina, Brazil  
 Hans-Juergen Hoppe, Oxford University, UK  
 Kuo-Yuan Hwa, Johns Hopkins University  
 Aslog Jansson, Uppsala University, Sweden  
 Assan Jaye, ILRAD, Kenya  
 Adrian Lawrence, Albert Einstein College of Medicine  
 Jose Lima Filho, Harvard School of Public Health  
 Ingrid Loeffler, Michigan State University  
 Michael McIntosh, Hahnemann University  
 Fernando Monroy, University of New Mexico  
 Carlos Moreno, New York University Medical Center  
 Sharon Moshitch, Weizmann Institute of Science, Israel  
 Hagir Suliman, Virginia Tech  
 Lakshmi Venkatakrishnaiah, Medical University of South Carolina  
 Ying-zi Yang, CUNY Medical School

#### ***Embryology: Cell Differentiation and Gene Expression in Early Development*** (June 20–July 31)

##### *Course Directors*

Eric H. Davidson, California Institute of Technology  
 Michael Levine, University of California, San Diego  
 David R. McClay, Duke University

##### *Faculty*

Marianne Bronner-Fraser, University of California, Irvine  
 Andrew R. Cameron, California Institute of Technology  
 Scott E. Fraser, California Institute of Technology  
 Janet Heasman, Wellcome/CRC Institute, UK  
 Steven L. McKnight, Carnegie Institution of Washington  
 Noriyuki Satoh, Kyoto University, Japan  
 Paul Sternberg, California Institute of Technology  
 Christopher C. Wylie, Wellcome/CRC Institute, UK

##### *Faculty Adjunct*

David Epel, Stanford University

##### *Teaching Assistants*

Mary K. Anderson, Johns Hopkins University/Carnegie Institute of Washington

Helen Chamberlin, California Institute of Technology  
Michael Dunn, Massachusetts General Hospital  
Michael Figdor, California Institute of Technology  
Suresh J. Jesuthasan, Oxford University, UK  
Carole LaBonne, Harvard University  
Jeffrey R. Miller, Duke University  
Talma Y. Scherson, University of California, Irvine  
John Shih, California Institute of Technology  
Stephen Small, University of California, San Diego  
Sergei Sokol, Harvard University  
Tanya Whitfield, Wellcome/CRC Institute, UK  
Robert W. Zeller, California Institute of Technology

#### *Lecturers*

William McGinnis, Yale University  
Randy Moon, University of Washington

#### *Speakers*

Don Fischman, Cornell University Medical College  
Nancy Hopkins, Massachusetts Institute of Technology  
Alexander Johnson, University of California, San Francisco  
Andrew P. McMahon, Roche Institute  
James Posakony, University of California, San Diego  
Claudio Stern, Oxford University, UK

#### *Course Administrator*

Jane Rigg, California Institute of Technology

#### *Course Coordinator*

Linda Huffer, Marine Biological Laboratory

#### *Course Assistants*

Cheryl Booth, University of Wisconsin  
Alex Goldberg, Washington University

#### *Students*

Yuping Cai, Michigan State University  
Isabelle Desjeux, Edinburgh University, Scotland  
Corrella Detweiler, Max-Planck Institute, Germany  
Carmen Domingo, University of California, Berkeley  
Marie-Anne Felix, Institut Jacques Monod, France  
Gabor Forgacs, Clarkson University  
Rudiger Fritsch, Max-Planck Institute, Germany  
Tony Frudakis, University of California, Berkeley  
Eleonore Fusco, Massachusetts Institute of Technology  
Maureen Gannon, Cornell University Medical College  
Uta Grieshammer, Boston University  
Catriona Logan, Duke University  
Lily Lou, Yale University  
John Matese, Duke University  
Anna Myat, Imperial Cancer Research Fund, UK  
Lesley Narburgh, St. George's Hospital Medical School, UK  
Zoe Pettway, University of California, Irvine  
David Pleasure, Children's Hospital of Philadelphia  
Paola Polosa, University of Bari, Italy  
Reinhard Schroder, Freiburg University, Germany  
Mark Van Doren, University of California, San Diego  
Paul Vrana, American Museum of Natural History  
Daniel Wagner, University of Texas Anderson Cancer Center  
Cindy Wilson, University of California, Irvine  
Stella Zannini, Stazione Zoologica "A Dohrn", Italy  
Hong Zhang, Case Western Reserve University

## *Microbial Diversity (June 14–July 30)*

---

#### *Course Directors*

John Breznak, Michigan State University  
Martin Dworkin, University of Minnesota

#### *Course Coordinator*

Richard M. Behmlander, University of Minnesota

#### *Course Assistant*

Pamela Contag, Stanford University Medical School

#### *Teaching Assistants*

Joseph P. Calabrese, West Virginia University  
S. Courtney Frasch, University of Minnesota  
Jörg Overmann, University of British Columbia, Canada  
Daniel R. Smith, University of Minnesota

#### *Instructor*

Howard Gest, Indiana University

#### *Lecturers*

Steve Block, Rowland Institute for Science  
Colleen Cavanaugh, Harvard University  
Paul Dunlap, Woods Hole Oceanographic Institution  
Dale Gehringer, Woods Hole Oceanographic Institution  
Steve Goodwin, University of Massachusetts, Amherst  
Brian Howe, Woods Hole Oceanographic Institution  
Holger Jannasch, Woods Hole Oceanographic Institution  
Shadid Khan, Albert Einstein School of Medicine  
Edward Leadbetter, University of Connecticut, Storrs  
Michael Madigan, University of Southern Illinois  
Sandra Nierzwicki-Bauer, Rensselaer Polytechnic Institute  
Bernhard Schink, University of Konstanz, Germany  
Mitchell Sogin, Marine Biological Laboratory  
Karl Stetter, University of Regensburg, Germany  
Sidney Tamm, Boston University Marine Program, MBL  
John Waterbury, Woods Hole Oceanographic Institution  
Carl Woese, University of Illinois

#### *Students*

Valerie Bernan, Lederle Labs  
Jennifer Byrnes, Harvard University  
Francesco Canganella, University of Tuscia, Italy  
Susan Childers, University of Connecticut, Storrs  
Maria Ganeva, Sofia University, Bulgaria  
John Gibson, Florida State University  
Antje Hofmeister, Philipps-University—Marburg, Germany  
Scott Kroken, University of Wisconsin  
Ariel Kusmaro, Tel Aviv University, Israel  
Edouard Miambi, Center ORSTOM/DGRST, Congo  
Margarita Miroshnichenko, Moscow State University, Russia  
Tommy Nielson, Aarhus University, Denmark  
Lorraine Olendzenski, University of Massachusetts, Amherst  
Martin Polz, Harvard University  
Michael Renner, Michigan State University  
Karl Rusterholtz, Merck Sharp & Dohme Research Lab  
Heinrich Sandmeier, University of Basel, Switzerland  
Dirk Schuler, Max-Planck Institute, Germany  
Angelica Seitz, University of Connecticut, Storrs  
Robert Shannon, Indiana University

***Neural Systems & Behavior (June 14–August 7)******Course Directors***

Ronald L. Calabrese, Emory University  
Martha Constantine-Paton, Yale University

***Faculty***

Thomas Abrams, University of Pennsylvania  
Robert Douglas, University of British Columbia, Canada

***Scholars-in-Residence***

Larry Abbott, Brandeis University  
Mary E. Hatten, College of Physicians & Surgeons at Columbia University  
William T. Newsome, Stanford University

***Instructors***

Alexander Borst, Max-Planck-Institut für Biologische Kybernetik, Germany  
Holly Cline, University of Iowa  
Sally Hoskins, City College of New York  
Alan Kay, University of Iowa  
John Koester, Columbia University  
Richard B. Levine, University of Arizona  
Eduardo Macagno, Columbia University  
Robert Malinow, University of Iowa  
Michael Nusbaum, University of Alabama, Birmingham  
Mu-Ming Poo, Columbia University  
Leslie Stevens, Albert Einstein College of Medicine  
Janis C. Weeks, University of Oregon  
Angela Wenning, Universität Konstanz, Germany

***Lecturers***

Gwendal Le Masson, Brandeis University  
William M. Roberts, University of Oregon  
Edgar T. Walters, University of Texas Medical School

***Guest Lecturers***

Robert Barlow, Jr., Syracuse University  
John Dowling, Harvard University

***Teaching Assistants***

Yolonda Alston, Benedict College  
Melissa J. Coleman, University of Alabama, Birmingham  
Yang Dan, Columbia University  
Lise Eliot, Baylor College of Medicine  
Cole Gilbert, Cornell University  
Juergen Haag, Max-Planck-Institut für Biologische Kybernetik, Germany  
Dawn Lewis, Albert Einstein College of Medicine  
Ann Lohof, Columbia University  
Brian J. Norris, University of Alabama, Birmingham  
Andrea Novicki, University of Oregon  
Glen Prusky, Yale University  
David J. Sandstrom, University of Oregon  
Laura Wolszon, Columbia University

***Course Coordinator***

Miriam Ashley, University of California, Irvine

***Course Assistant***

Kyle Lennon, Atlanta, GA

***Students***

Lisa Boulanger, Wesleyan University  
Mary Boyle, University of California, San Diego  
Beatrice Casanovas, University of Bordeaux, France  
Peter Dayan, Salk Institute  
Joseph Erlichman, Dartmouth Medical School  
Daniel Feldman, Stanford University School of Medicine  
Maribel Feliciano, University of Connecticut, Storrs  
Maria Feller, AT&T Bell Laboratories  
Lisa Foa, Deakin University, Australia  
Timothy Gershon, Columbia University  
Erin Jacobs, University of California, Los Angeles  
Juan Jorge-Rivera, Brandeis University  
Lisa Kelly, University of Ottawa, Canada  
Carole Landisman, Rockefeller University  
Stephen Macknik, Harvard Medical School  
Zachary Mamen, University of California, San Diego  
David Raizen, University of Texas Southwestern Medical School  
Jeffrey Reznic, New York University  
Christine Rose, University of Kaiserslautern, Germany  
Stephan Wurden, University of Konstanz, Germany

***Neurobiology (June 14–August 15)******Course Directors***

Leonard K. Kaczmarek, Yale University School of Medicine  
Irwin B. Levitan, Brandeis University

***Faculty***

Hana Asmussen, University of Virginia Medical School  
Gary Banker, University of Virginia  
Arlene Chiu, Beckman Research Institute  
Judith A. Drazba, NIH/NINDS  
Keith Elmslie, Case Western Reserve University  
Steve Goldstein, HHMI/Brandeis University  
Richard Horn, Jefferson Medical College  
Stephen Jones, Case Western Reserve University  
Bechara Kachar, NIH/NIDCD  
Julie A. Kauer, Duke University Medical School  
Richard Kramer, Columbia University  
Lonny Levin, Johns Hopkins University  
John Marshall, Yale University School of Medicine  
Andrew I. Matus, Friedrich Miescher Institute, Switzerland  
Sally Moody, University of Virginia School of Medicine  
Angus C. Nairn, Rockefeller University  
Marina Picciotto, The Pasteur Institute, France  
Randall Reed, HHMI/Johns Hopkins Medical School  
Thomas Reese, NIH/NINDS  
Peter H. Reinhart, Duke University Medical Center  
Talvinder Sihra, University of Dundee, Scotland  
Carolyn Smith, NIH/NINDS

***Lecturers***

George Augustine, University of Southern California  
David Brautigam, Brown University  
Xandra Breakefield, Massachusetts General Hospital  
William Catterall, University of Washington  
Pietro DeCamilli, Yale University  
Michael Greenberg, Harvard University

Lloyd Greene, New York University  
Michael R. Hanley, University of California, Davis  
Ed Hawrot, Brown University  
Robert Horvitz, Massachusetts Institute of Technology  
Richard Haganir, Johns Hopkins School of Medicine  
Christopher Miller, Brandeis University  
Linda Nowak, Cornell University  
Dale Purves, Duke University  
Edward D. Salmon, University of North Carolina, Chapel Hill  
Chris Walsh, Harvard University

*Course Assistants*

Ethan Treistman, University of North Carolina, Chapel Hill  
Cecilia Armstrong, University of Pennsylvania

*Students*

Pavle Andjus, University of Belgrade, Yugoslavia  
Cynthia Cowden, University of Wisconsin  
Ann Marie Craig, University of Virginia  
Matthew Dalva, Duke University  
Atsushi Miyawaki, University of Tokyo, Japan  
Klaus Raming, Hohenheim University, Germany  
Enrique Saldana, University of Salamanca, Spain  
Hilary Smith, University of North Carolina, Chapel Hill  
Camilla Tornoe, Cambridge University, UK  
Ferdinand Vilim, Columbia University  
Elisabeth Walcott, University of California, Irvine  
Kevin Wickman, Mayo Foundation

***Physiology: Cellular and Molecular Biology***

***(June 13–July 25)***

---

*Course Director*

Thomas D. Pollard, Johns Hopkins Medical School

*Faculty*

Robert Jensen, Johns Hopkins Medical School  
Michael E. Mendelsohn, Harvard Medical School/Brigham & Women's Hospital  
Andrew Murray, University of California, San Francisco  
Edward D. Salmon, University of North Carolina, Chapel Hill  
Cynthia Stauffacher, Purdue University  
Murray Stewart, Medical Research Council, UK  
Katherine Swenson, Duke University Medical School  
Edwin Taylor, University of Chicago  
Ron Vale, University of California, San Francisco  
Katherine L. Wilson, Johns Hopkins University School of Medicine

*Instructors*

William B. Busa, Johns Hopkins University  
Margaret A. Titus, Duke University Medical Center

*Teaching Assistants*

Michael Glotzer, University of California, San Francisco  
John R. Jordan, University of Utah, Salt Lake City  
Jennifer Kalish, Johns Hopkins Medical School  
Helen Kent, Medical Research Council, UK  
C. Martin Lawrence, Purdue University  
Sarah O'Neill, Brigham & Women's Hospital/Harvard Medical School  
Stephen F. Parsons, University of North Carolina, Chapel Hill

Homero L. Rey, University of California, Berkeley  
Yan Zhu, Brigham & Women's Hospital/Harvard Medical School

*Lecturers*

Paula Fitzgerald, Merck Corporation  
William Garrard, University of Texas, Dallas  
Don Gill, University of Maryland, College Park  
Reid Gilmore, University of Massachusetts Medical School  
Pascal Goldschmidt-Clermon, Johns Hopkins University  
Jonathan Horowitz, Duke University  
Laurinda Jaffe, University of Connecticut, Storrs  
Jack Johnson, Purdue University  
Paul Lazarow, Mt. Sinai Medical  
Jennifer Lippencott-Schwartz, National Institutes of Health  
Lee Makowski, Boston University  
Peter Novak, Yale University  
Robert Palazzo, Marine Biological Laboratory  
Howard Schachman, University of California, Berkeley  
Pam Silver, Princeton University  
Rick Steinhardt, University of California, Berkeley

*Course Assistants*

Daniel Pollard, Baltimore, MD  
Katie Pollard, Baltimore, MD  
Michael Salmon, Chapel Hill, NC

*Students*

Carol Bascom, Tufts University  
Ellen Brisch, University of Kansas, Lawrence  
Darien Cohen, Dartmouth College  
Hugh Crenshaw, Duke University  
Mario Delmar, SUNY, Syracuse  
Haiyan Deng, Harvard University  
Matthew Frerking, University of California, Davis  
Vicki Goodman, Duke University  
Robin Hammell, Robert Wood Medical School  
Edward Hinchcliffe, University of Minnesota, Minneapolis  
Joseph Kelleher, Johns Hopkins Medical School  
Errol Kolen, University of Missouri, Columbia  
Bodo Lange, University of Manchester, UK  
Annick Le Gall, Cornell University Medical College  
Edward Leonard, University of Pittsburgh Medical School  
Eileen Luque, SUNY, Syracuse  
Deborah Miller, University of Massachusetts, Amherst  
John Murray, Albert Einstein Medical College  
Dana Nojima, University of Minnesota, Minneapolis  
Valerie Pierce, University of Chicago  
Frances Reis, University of Idaho, Moscow  
Normand Richard, University of California, Riverside  
William Robinson, New England Aquarium  
Baerbel Rohrer, University of Calgary, Canada  
Beth Schomer, Stanford University  
Jing Shang, Yale University  
Sidney Shaw, University of North Carolina, Chapel Hill  
Elspeth Stewart, ICRF Clare Hall Laboratories, UK  
Douglas Swank, University of Pennsylvania  
Penny Tavormina, University of Virginia  
Kenan Turnacioglu, University of Pennsylvania  
James Whaley, University of Illinois, Urbana  
Ben Whitlock, Ohio State University  
Lily Wong, University of Virginia  
Lin Wu, Scripps Research Institute  
Jane Ye, Dartmouth College



## Short Courses

### ***Advanced Workshop on Recombinant DNA Methodology (July 6–July 10)***

---

#### *Instructors*

Robert E. Farrell, Jr., Exon-Intron, Inc.  
 Greg Leppert, Exon-Intron, Inc.  
 Charles Vaslet, CAV Consulting

#### *Students*

Isabel Baanante, University of Barcelona, Spain  
 Thomas Borgese, City University of New York  
 Meredith Hullar, Marine Biological Laboratory  
 Robert Lauzon, Albany Medical College  
 Tim Mukoda, United States Air Force  
 Annie Pardo, Universidad Nacional Autonoma, Mexico  
 Karen Ridge, Humana Hospital-Michael Reese  
 Gary Schneider, Loyola University Medical School  
 Earl Weidner, Louisiana State University, Baton Rouge  
 Zhaohui Yang, Marine Biological Laboratory

### ***Advances in Mariculture: Techniques and Future Directions for Providing Marine Organisms for Biological Research (May 17–29)***

---

#### *Course Director*

Roger Hanlon, Marine Biomedical Institute

#### *Course Manager*

Philip Alatalo, Woods Hole Oceanographic Institution

#### *Faculty*

Jelle Atema, Boston University Marine Program, MBL  
 David Bengtson, University of Rhode Island, Kingston  
 Patricia Bubucis, Sea Research Foundation  
 Robert Bullis, Marine Biological Laboratory  
 Elizabeth Clarke, University of Miami  
 Linda Davis, Woods Hole Oceanographic Institution  
 Michael Feldgarden, Yale University  
 Patrick Gaffney, University of Delaware, Lewes  
 Scott M. Gallagher, Woods Hole Oceanographic Institution  
 Dian Gifford, University of Rhode Island, Narragansett  
 Robert Guillard, Bigelow Laboratory for Ocean Sciences  
 Herb Hdu, Wiscasset, ME  
 Holger Jannasch, Woods Hole Oceanographic Institution  
 Rick Karney, Martha Vineyard Shellfish Group, Inc.  
 Alan Kuzirian, Marine Biological Laboratory  
 Donal Manahan, University of Southern California, Los Angeles  
 Judy McDowell, Woods Hole Oceanographic Institution  
 Phil Presley, Carl Zeiss, Inc.  
 Stephen Spotte, Sea Research Foundation  
 Michael Syslo, State Lobster Hatchery & Research Station  
 Stephen Ward, U.S. Fish and Wildlife Service

#### *Students*

Imad Ghossoub, University of Southern Mississippi  
 Dana Krueger, Harvard University  
 Carole Lanteigne, Aquarium & Marine Center, Canada

Amoy Lum Kong, Institute of Marine Affairs, Trinidad and Tobago  
 Darlene Manning, Dalhousie University, Canada  
 Joan Manuel, Dalhousie University, Canada  
 David Remsen, Marine Biological Laboratory  
 Nicholas Roden, Exxon Biomedical Sciences, Inc.  
 Mark Rosenqvist, Aquatic Research Organisms  
 Tina Schappach, MCI Telecommunications  
 Benedikte Vercaemer, Dalhousie University, Canada

### ***Analytical and Quantitative Light Microscopy in Biology, Medicine, and Materials Science (May 14–22)***

---

#### *Course Directors*

Edward D. Salmon, University of North Carolina, Chapel Hill  
 Greenfield Sluder, Worcester Foundation for Experimental Biology  
 David E. Wolf, Worcester Foundation for Experimental Biology

#### *Faculty*

Brad Amos, Medical Research Council, UK  
 Steven M. Block, Rowland Institute for Science  
 Richard Cardullo, University of California, Riverside  
 Gordon Ellis, University of Pennsylvania  
 Harvey Florman, Worcester Foundation for Experimental Biology  
 Jeff Gelles, Brandeis University  
 Anthony Moss, Worcester Foundation for Experimental Biology  
 Rudolf Oldenbourg, Marine Biological Laboratory  
 Kenneth R. Spring, National Institutes of Health

#### *Lecturer*

Shinya Inoué, Marine Biological Laboratory

#### *Teaching Assistants*

Neil Glikzman, University of North Carolina, Chapel Hill  
 Christine McKinnon, Worcester Foundation for Experimental Biology

#### *Course Coordinator*

Frederick Miller, Worcester Foundation for Experimental Biology

#### *Course Assistants*

Robert Knudson, Marine Biological Laboratory  
 Phong Tran, University of North Carolina, Chapel Hill

#### *Students*

John Axelson, Holy Cross College  
 Sandy Chang, Rockefeller University  
 Jean-Yves Chatton, National Institutes of Health  
 Ronald Cohn, Syntex Research  
 William Crowe, University of Texas, Galveston  
 Fernando Delaville, Thomas Jefferson University  
 Dimiter Dimitrov, National Institutes of Health  
 Stephen Doty, Hospital for Special Surgery  
 Deborah Fyngenson, Princeton University  
 Peder Gashberg, Panum Institute, Denmark  
 Craig Giroux, Wayne State University  
 Norman Harris, Louisiana State University  
 Ulrich Kersting, National Institutes of Health  
 Kimberly Kotz, Mayo Clinic  
 Donald O'Malley, SUNY, Stony Brook

Joseph Neary, VA Medical Center  
Charles Pak, National Institutes of Health  
Harold Payne, Case Western Reserve University  
Robert Prusch, Gonzaga University  
Andreas Stemmer, MRC, UK  
Kathy Suprenant, University of Kansas, Lawrence  
Ole Thastrup, Zymogenetics  
Joseph Unthank, Indiana University  
Janice Voltzow, Harvard University  
Henry Yu, Duke University

### ***Basic Workshop on Recombinant DNA Methodology (June 29–July 3)***

---

#### *Instructors*

Robert E. Farrell, Jr., Exon-Intron, Inc.  
Greg Leppert, Exon-Intron, Inc.  
Charles Vaslet, CAV Consulting

#### *Students*

Isabel Baanante, University of Barcelona, Spain  
David Beggs, Northern Ireland Horticultural and Plant Breeding  
Station, Armagh  
Thomas Borgese, City University of New York  
Lotta Chi, CP Li Biomedical Research Corp.  
Judith Grassle, Rutgers University  
Connie Hart, Woods Hole Oceanographic Institution  
Meredith Hullar, Marine Biological Laboratory  
Daniel Johnson, Bowman Gray School of Medicine  
Alan Kuzirian, Marine Biological Laboratory  
Tim Mukoda, United States Air Force  
Annie Pardo, Universidad Nacional Autonoma, Mexico  
Gary Schneider, Loyola University Medical School  
Dean Schraufnagel, University of Illinois, Chicago  
Jacob Sznajder, Humana Hospital-Michael Reese  
Lewis Tilney, Marine Biological Laboratory  
Michael Tytell, Bowman Gray School of Medicine  
Earl Weidner, Louisiana State University  
Zhaohui Yang, Marine Biological Laboratory

### ***Fundamental Issues in Vision Research (August 16–29)***

---

#### *Course Directors*

David S. Papermaster, University of Texas Health Science Center  
John N. Dowling, Harvard University

#### *Faculty*

Robert Barlow, Syracuse University  
Robert W. Baughman, Harvard Medical School  
George B. Benedek, Massachusetts Institute of Technology  
Eliot L. Berson, Massachusetts Eye and Ear Infirmary  
Martin Breitman, Mt. Sinai Hospital, Canada  
Debra Carper, NEI/NIH  
Judah Folkman, Children's Hospital Medical Center  
Ilene K. Gipson, Schepens Eye Research Institute  
Paul A. Hargrave, University of Florida, Gainesville  
John R. Hassell, The Eye & Ear Institute of Pittsburgh  
Fielding Hejtmancik, National Institutes of Health  
Paul N. Hoffman, The Johns Hopkins Hospital

Ehud Kaplan, Rockefeller University  
Jerry R. Kuszak, Rush Presbyterian St. Luke's Medical Center  
Wen Hwa Lee, Institute of Biotechnology  
Ellen Liberman, NEI/NIH  
Thomas F. Linsenmayer, Tufts University Medical School  
Robert Paul Malchow, University of Illinois College of Medicine  
Richard H. Masland, Massachusetts General Hospital  
Robert S. Molday, University of British Columbia, Canada  
Jeremy Nathans, Johns Hopkins University School of Medicine  
Harry A. Quigley, Johns Hopkins Hospital  
James Rae, Mayo Foundation  
Robert R. Rando, Harvard Medical School  
Elio Raviola, Harvard Medical School  
Harris Ripps, University of Illinois College of Medicine  
Paul Russell, NEI/NIH  
Barbara G. Schneider, University of Texas Health Science Center  
Abe Spector, Columbia University  
Tung-Tien Sun, New York University Medical Center  
Guo-Ming Wang, Columbia University  
Charles Zuker, University of California, San Diego

#### *Students*

Jacqueline Biscardi, University of North Carolina, Chapel Hill  
Luzie Brown, Oregon Regional Primate Research Center  
Suzanne Bruhn, Harvard Medical School  
Qian Chen, Tufts University  
Heather Fabry, University of California  
John Gardner, Fox Chase Cancer Center  
Kenneth Giuliano, Carnegie Mellon University  
Brian Jiang, New York University  
Amy Johnson, Columbia University  
Diana Kania, SUNY, Buffalo  
Francis LaRosa, Boston University  
Richard LeBaron, La Jolla Cancer Research Foundation  
Wan-Cheng Li, University of Washington  
Mingyao Liu, University of Maryland  
Qiang Lu, Brandeis University  
Tomoko Nakayama, Whitehead Institute  
Ron Pelton, Vanderbilt University  
Elizabeth Roquemore, Johns Hopkins University  
Mary Woo, Scripps Research Institute  
Yimin Yan, University of Pittsburgh

### ***Medical Informatics (May 31–June 6)***

---

#### *Course Director*

Homer Warner, University of Utah

#### *Faculty*

Paul Clayton, Columbia University  
Peter Haug, University of Utah  
David J. Lipman, National Library of Medicine  
Donald A. B. Lindberg, National Library of Medicine  
Daniel R. Masys, National Library of Medicine  
Robert Sideli, Columbia University

#### *Course Assistant*

Sylvia Jessen, University of Utah

#### *Students*

James Baggott, Hahnemann University  
Gerald Bashein, University of Washington, Seattle

Gary Berman, Albert Einstein College of Medicine  
 Janine Blackman, University of Maryland, Baltimore  
 Athos Bousvaros, Children's Hospital  
 Mona Coutts, University of North Carolina, Chapel Hill  
 Stephen Dubin, Drexel University  
 Peter Ellis, Brown University  
 Michael Fisher, University of Maryland, Baltimore  
 Peter Fleming, Cleveland Clinic Foundation  
 Cathy Harbert, Howard Hughes Medical Institute  
 Linda Jacknowitz, West Virginia University  
 John Kelly, American Medical Association  
 Michael Kessler, American Board of Quality Assurance  
 Michael Krall, Oregon Health Sciences University  
 Lisa Kregel, Case Western Reserve University  
 Rosanne Labree, McLean Hospital  
 Carol LeLonek, University of Buffalo  
 Saul Malozowski, Food & Drug Administration  
 Karen Martinez, Catawba Memorial Hospital  
 Peter Mathews, Kaiser Permanente  
 Julie McGowan, University of Vermont, Burlington  
 Ana Nunez, Hahnemann University  
 Michael Rissinger, New York University  
 Barbara Schultz, VA Medical Center  
 Anthony So, University of California, San Francisco  
 Zoe Stavri, Massachusetts General Hospital  
 Bryan Thompson, Lovelace Medical Foundation  
 Monica Unger, Northeastern Ohio University  
 George Wesley, Office of the Inspector General, Washington, DC

## ***Methods in Computational Neuroscience***

***(August 2–29)***

### *Course Directors*

James M. Bower, California Institute of Technology  
 Christof Koch, California Institute of Technology

### *Faculty*

Paul R. Adams, HHMI, SUNY, Stony Brook  
 Richard Andersen, Massachusetts Institute of Technology  
 Joseph J. Atick, Rockefeller University  
 William Bialek, NEC Research Institute  
 Avis Cohen, University of Maryland, College Park  
 Rodney James Douglas, MRC Anatomical Neuropharmacology  
 Unit, UK  
 Nancy Kopell, Boston University  
 Rodolfo R. Llinás, New York University Medical Center  
 Eve Marder, Brandeis University  
 Michael V. Mascagni, Supercomputing Research Center  
 Kenneth D. Miller, California Institute of Technology  
 John Rinzel, National Institutes of Health  
 Idan Segev, Hebrew University, Israel  
 Terrence Sejnowski, The Salk Institute

### *Teaching Assistants*

David Beeman, University of Colorado, Boulder  
 David Berkowicz, Yale University Medical School  
 Ojvind Bernander, California Institute of Technology  
 Dieter Jaeger, California Institute of Technology  
 Maurice Lee, California Institute of Technology

## ***Computer Managers***

Maneesh Sahani, California Institute of Technology  
 Charles F. Stevens, Salk Institute  
 John Uhley, California Institute of Technology

## ***Students***

Erik Cook, Baylor University  
 Adelle Coster, University of New South Wales, Australia  
 Sharon Crook, University of Maryland, College Park  
 Winrich Freiwald, Tübingen University, Germany  
 Alberto Herrera-Becerra, Universidad Nacional Autónoma, Mexico  
 Martin Huber, Phillips-University-Marburg, Germany  
 Michael Irizarry, Massachusetts General Hospital  
 Ranu Jung, Case Western Reserve University  
 Brandt Kehoe, California State University  
 Ilan Lampl, Hebrew University, Israel  
 Mitchell Maltenfort, Rehabilitation Institute of Chicago  
 Ference Mechler, New York University  
 Jill Nicolaus, University of Chicago  
 Harmon Nine, University of Michigan, Ann Arbor  
 Monica Paolini, University of California, San Diego  
 Yifat Prut, Hebrew University, Israel  
 Iris Reuveni, Ben Gurion University of the Negev, Israel  
 Emilio Salinas, National University, Mexico  
 Eyal Seidemann, Tel Aviv University, Israel  
 Nangiavaram Sekar, University of Iowa, Iowa City  
 Micah Siegel, Yale University  
 Mark Tommerdahl, University of North Carolina, Chapel Hill  
 Yi-Xiong Zhou, McGill Vision Research Center, Canada

## ***Microinjection Techniques in Cell Biology***

***(May 26–June 1)***

### *Course Director*

Robert Silver, Cornell University

### *Faculty*

Suzanne Chandler, Cornell University  
 Donald Chang, Hong Kong University of Science & Technology,  
 Hong Kong  
 Douglas Kline, Kent State University  
 Joanne Kline, Kent State University  
 Patricia Wadsworth, University of Massachusetts, Amherst

### *Students*

David Brauer, United States Department of Agriculture  
 Roger Buchanan, National Institutes of Health  
 Thomas Burke, Ohio State University  
 Hattie Gresham, University of Missouri, Columbia  
 Gupta Kalpana, University of Ottawa, Canada  
 Karen Hedberg, University of Oregon, Eugene  
 Lynne Lucher, Illinois State University  
 Katrina Marsh, Queen's Medical Centre, UK  
 Thomas Martin, University of Wisconsin, Madison  
 James McGill, Duke University  
 Thomas Reese, National Institutes of Health  
 Frieda Reichsman, University of Massachusetts, Amherst  
 Paulo Serodio, New York University  
 Donald Siwek, VA Hospital

Steve Sorota, Columbia University  
James Swanson, Old Dominion University  
Johanna Talavera, Boston University  
Suresh Tiwari, University of Kansas, Lawrence

### ***Rapid Measurement of Neurotransmitter Signals in the Central Nervous System Using In Vivo Electrochemistry (August 19–24)***

---

#### *Course Directors*

Greg Gerhardt, University of Colorado, Denver  
Paul Moore, University of Colorado, Denver

#### *Faculty*

Alain Gratton, Douglas Research Hospital, Canada  
Michael Palmer, University of Colorado, Denver  
William Proctor, University of Colorado, Denver

#### *Technicians*

Paula Bickford, University of Colorado, Denver  
Scot Brock, University of Colorado, Denver  
Mike Doherty, McGill University, Canada  
Marilyn Friedemann, University of Colorado, Denver  
Ron Maloney, University of Colorado, Denver  
Mike Parrish, University of Colorado, Denver  
Steve Robinson, University of Colorado, Denver  
Scott Robinson, University of Colorado, Denver

#### *Students*

Abdel Abdel-Rahman, East Carolina University  
Juan Advis, Rutgers University  
Kurt Batsche, SUNY, Stony Brook  
Thomas Clark, U.S. Army Aeromedical Research  
Dennis Dahl, University of Texas, Dallas  
Audrey Davis, George Washington University  
Matthew Davidson, University of Oregon, Eugene  
Michele Dwyer, Smith College  
Siegward Elsas, University of California, Berkeley  
Michael Hörner, I. Zoologisches Institut, Germany  
Robert Huber, Karl-Franzens-Universität Graz, Austria  
Robert Leipheimer, Youngstown State University  
Tamala Mallett, Meharry Medical College  
Dorothy Pooock, Concordia University, Canada  
David Rothblat, Hahnemann University  
Claude Rouillard, Hospital de l'Enfant-Jesus, Canada  
Charles Stewart, Franklin & Marshall College  
James Suojanen, New England Deaconess Hospital  
Tina Thompson, University of Texas Southwestern  
Ruth Weissenborn, University of St. Andrews, Scotland

### ***Workshop on Molecular Evolution (August 2–14)***

---

#### *Director*

Mitchell L. Sogin, Marine Biological Laboratory

#### *Faculty*

Marlene Belfort, New York State Department of Health  
Daniel Davison, University of Houston

Michael Donoghue, University of Arizona, Tucson  
Doug Ernisse, University of Michigan, Ann Arbor  
Joseph Felsenstein, University of Washington, Seattle  
Walter Gilbert, Harvard University  
Martin Kreitman, University of Chicago  
Laura Landweber, Harvard University  
Bernd Franz Lang, University of Montreal, Canada  
David Maddison, University of Arizona, Tucson  
Marcella McClure, University of California, Irvine  
Roger Milkman, University of Iowa, Iowa City  
Gary Olsen, University of Illinois, Urbana  
Monica Riley, Marine Biological Laboratory  
Terry Speed, University of California, Berkeley  
David Swofford, Smithsonian Museum Support Center  
Bruce Walsh, University of Arizona, Tucson

#### *Course Assistant*

Brendan Reilly, Software Editing Corporation

#### *Students*

Rashid Aman, National Museums of Kenya, Nairobi  
Linda Amaral, Woods Hole Oceanographic Institution  
Wendy Bailey, Yale University  
Charles Baker, Kewalo Marine Laboratory  
Ulrike Beemelmans, University of Cologne, Germany  
Joy Bergelson, Washington University  
David Bermudes, Yale University  
Nancy Bowers, Pennsylvania State University  
Barry Campbell, Queen's University, Canada  
David Carmean, University of California, Davis  
Carlos Cerpa, University of Montreal, Canada  
Belinda Chang, Harvard University  
Bernard Cohen, University of Glasgow, Scotland  
Julio Collado-Vides, Massachusetts Institute of Technology  
Jan Conn, University of Florida, Gainesville  
Eric Delwart, Stanford University Medical Center  
Floyd Dewhirst, Forsyth Dental Center  
Megan Eskey, NASA Ames Research Center  
David Faguy, Queen's University, Canada  
Thomas Friedl, University of Bayreuth, Germany  
Manohar Furtado, Northwestern University Cancer Center  
Steven Gagnon, Laval University, France  
Anne Gerber, Washington University  
Manuel Glynias, Cleveland Clinic Research Institute  
John Gosink, University of Washington, Seattle  
Jotun Hein, Aarhus University, Denmark  
Stephen Hinton, Exxon Corporate Research Laboratories  
Wen-Yen Kao, University of Wisconsin, Milwaukee  
Laura Katz, Cornell University  
Michelle Kelly-Borges, Harbor Branch Oceanographic Institute  
Hans-Peter Klenk, Max-Planck-Institut, Germany  
Richard Kliman, Rutgers University  
Stuart Kuhstoss, Lilly Research Laboratories  
Bernard Labedan, University of Paris-Sud, France  
Damian Labuda, University of Montreal, Canada  
Benedicté Lafay, Station Zoologique, France  
Joyce Lewis, Colorado State University  
Ee Lin Lim, Woods Hole Oceanographic Institution  
François Lutzoni, Duke University  
Kersti MacInnes, Los Alamos National Laboratory  
Katrina Mangin, University of California, Santa Cruz  
Gerogiana May, University of Minnesota, St. Paul  
James McLaughlin, Massachusetts General Hospital

Helen McVeigh, Natural History Museum, UK  
Annabel Miles, James Cook University of North Queensland,  
Australia  
Christine Miller, University of Cincinnati  
Yue Ming, Michigan State University  
Sharon Mitchell, USDA/ARS  
Miklos Muller, Rockefeller University  
Jan Pawlowski, University of Geneva, Switzerland  
Marian Peris, University of California, Los Angeles  
William Piel, Harvard University  
Norman Pieniazek, Centers for Disease Control  
James Pierce, Dupont Merck Pharmaceutical Company

Frank Robert, Idaho National Engineering Laboratory  
Andres Ruiz-Linares, Stanford University  
Robert Setterquist, University of Houston  
Robert Sheehy, University of Arizona, Tucson  
Emmanuel Skoufos, University of Minnesota, Minneapolis  
Ralph Tanner, University of Oklahoma, Norman  
Steven Thompson, Washington State University  
Maira van Staaden, Karl-Franzens-University Graz, Austria  
Todd Wareham, Memorial University of Newfoundland, Canada  
Lee Weigt, Smithsonian Tropical Research Institute, Panama  
Lisa White, University of Houston  
Hong Xie, Smith College



## Summer Research Programs

### *Principal Investigators*

Adams, James A., University of Maryland Eastern Shore  
 Akeson, R., University of Cincinnati  
 Alkon, Daniel L., National Institutes of Health  
 Allen, Nina S., Wake Forest University  
 Armstrong, Clay, University of Pennsylvania  
 Armstrong, Peter B., University of California, Davis  
 Arnold, John M., University of Hawaii  
 Augustine, George J., Duke University Medical Center

Baker, Robert, New York University Medical Center  
 Baldrige, William H., McMaster University Medical School, Canada  
 Barlow, Jr., Robert B., Syracuse University  
 Bearer, Elaine, Brown University  
 Beauge, Luis, Instituto M. y M. Ferreyra, Argentina  
 Bennett, M. V. L., Albert Einstein College of Medicine  
 Bezanilla, Francisco, University of California, Los Angeles  
 Bezprozvanny, Ilya, University of Connecticut Health Center  
 Bingham, Eula, University of Cincinnati  
 Bloom, George S., The University of Texas Southwestern Medical Center, Dallas  
 Bodznick, David, Wesleyan University  
 Borgese, Thomas A., Lehman College, City University of New York  
 Boron, Walter, Yale University School of Medicine  
 Borst, David, Illinois State University  
 Bowlby, Mark R., Harvard Medical School  
 Boyer, Barbara C., Union College  
 Brady, Scott T., The University of Texas Southwestern Medical Center, Dallas  
 Brown, Joel, Albert Einstein College of Medicine  
 Buchanan, Roger A., National Institutes of Health  
 Burdick, Carolyn J., Brooklyn College of the City University of New York  
 Burger, Max M., Friedrich Miescher Institut, Switzerland

Chaet, A. B., University of West Florida  
 Chang, Donald C., Baylor College of Medicine  
 Chanson, Marc, Albert Einstein College of Medicine  
 Chappell, Richard L., Hunter College of the City University of New York  
 Charlton, Milton, University of Toronto, Canada  
 Clay, John, National Institutes of Health  
 Cohen, Lawrence B., Yale University School of Medicine

Cohen, William D., Hunter College of the City University of New York  
 Cooperstein, Sherwin J., The University of Connecticut Health Center  
 Cuppoletti, John, University of Cincinnati College of Medicine

D'Avanzo, Charlene, Hampshire College  
 De Weer, Paul, University of Pennsylvania  
 Di Polo, Reinaldo, IVIC, Venezuela  
 Doroshenko, Peter, Duke Medical Center  
 Dowling, John E., Harvard University

Eckberg, William R., Howard University  
 Ehrlich, Barbara E., University of Connecticut Health Center  
 Eisthen, Heather L., Indiana University

Farbman, Albert, Northwestern University  
 Fein, Alan, University of Connecticut Health Center  
 Fink, Rachel, Mount Holyoke College  
 Fishman, Harvey M., The University of Texas Medical Branch, Galveston  
 Florin-Christensen, Jorge, University of Cincinnati

Gadshy, David, The Rockefeller University  
 Garner, Harold, National Institutes of Health  
 Garber, Sarah S., University of Alabama, Birmingham  
 Garnick, Rita Anne, Fordham University College at Lincoln Center  
 Gesteland, Robert C., University of Cincinnati College of Medicine  
 Gilland, Edwin H., Harvard University  
 Giuditta, Antonio, University of Naples, Italy  
 Goldman, Robert D., Northwestern University Medical School  
 Grant, Philip, National Institutes of Health  
 Griff, Edwin R., University of Cincinnati  
 Gyoeva, Fatma, Institute of Protein Research, Russia

Haimo, Leah, University of California, Riverside  
 Hans, Michael, Max-Planck-Institut für Biophysikalische Chemie, Germany  
 Hegde, Ashok N., Columbia University  
 Helluy, Simone, Wellesley College  
 Hernandez-Cruz, Arturo, Instituto de Fisologia Celular, UNAM, Mexico  
 Highstein, Steven M., Washington University School of Medicine  
 Hill, Susan D., Michigan State University

Holz, George G., IV, Howard Hughes Medical Institution,  
Massachusetts General Hospital  
Hoskin, Francis C. G., Illinois Institute of Technology

Ip, Wallace, University of Cincinnati College of Medicine

Johnston, Daniel, Baylor College of Medicine  
Josephson, Robert K., University of California, Irvine

Kaneshiro, Edna, University of Cincinnati  
Kaplan, Barry B., Western Psychiatric Institute and Clinic  
Kaplan, Ilene M., Union College  
Khan, Shahid, Albert Einstein College of Medicine/National Institutes  
of Health

Khan, Sohaib, University of Cincinnati College of Medicine  
Knowlton, Robert, Jefferson Medical College  
Koide, Samuel S., The Population Council  
Kravitz, Edward, Harvard Medical School  
Kremer, James N., University of Southern California  
Kumar, Ajit, George Washington University School of Medicine  
Kuznetsov, Sergei, Moscow State University, Russia

Landowne, David, University of Miami  
Langford, George, Dartmouth College  
Laufer, Hans, The University of Connecticut  
Lauzon, Robert J., Albany Medical College  
Liman, Emily R., Harvard Medical School  
Lipicky, Raymond J., Food & Drug Administration  
Lisman, John, Brandeis University  
Linás, Rodolfo R., New York University Medical Center

Malchow, Robert Paul, University of Illinois at Chicago College of  
Medicine  
Martin, Rainer, University of Ulm, Germany  
Metuzals, Janis, University of Ottawa, Canada  
Misevic, Gradimir, University Hospital of Basel, Switzerland

Nagle, Ronald L., Albert Einstein College of Medicine  
Nasi, Enrico, Boston University School of Medicine  
Nelson, Leonard, Medical College of Ohio  
Noe, Bryan D., Emory University School of Medicine

Obaid, Ana Lia, University of Pennsylvania School of Medicine

Pant, Harish, NINDS, National Institutes of Health  
Parysek, Linda, University of Cincinnati Medical School  
Patterson, David J., University of Bristol, UK

Quigley, James P., SUNY, Stony Brook

Rakowski, Robert F., University of Health Sciences/The Chicago  
Medical School  
Ratner, Nancy, University of Cincinnati  
Reese, Thomas S., NINDS, National Institutes of Health  
Render, JoAnn, University of Illinois  
Rieder, Conly L., Wadsworth Center for Laboratories & Research  
Ripps, Harris, University of Illinois College of Medicine  
Rome, Lawrence, University of Pennsylvania  
Ross, William, New York Medical College  
Ruderman, Joan V., Harvard Medical School  
Russell, John M., University of Texas Medical Branch

Salzberg, Brian M., University of Pennsylvania School of Medicine  
Schmidt, Joachim, Emory University

Segal, Sheldon, The Population Council  
Severin, Fedor F., Institute of Protein Research, Russia  
Shibley, Michael T., University of Cincinnati College of Medicine  
Silver, Robert B., Cornell University, N.Y. State College of Veterinary  
Medicine  
Siwicki, Kathleen K., Swarthmore College  
Sloboda, Roger D., Dartmouth College  
Smith, David V., University of Cincinnati College of Medicine  
Sperelakis, Nicholas, University of Cincinnati College of Medicine  
Spirin, Alexander S., Academy of Sciences of Russia  
Spray, David C., Albert Einstein College of Medicine  
Steinacker, A., Washington University School of Medicine  
Stemmer, Andreas, Medical Research Council, UK  
Sweeney, H. Lee, University of Pennsylvania School of Medicine

Tanguy, Joelle, Northwestern University  
Telzer, Bruce, Pomona College  
Treisman, Steven N., Worcester Foundation for Experimental  
Biology  
Trejo-Borowski, Amy V., Northwestern University  
Trinkaus, John P., Yale University  
Troll, Walter, New York University Medical Center  
Tytell, Michael, Bowman Gray School of Medicine of Wake Forest  
University

Ueno, Hiroshi, Osaka Medical College, Japan

Vallee, Richard, Worcester Foundation for Experimental Biology

Wadsworth, Patricia, University of Massachusetts  
Watson, Win, University of New Hampshire  
Wehner, Rudiger, University of Zurich, Switzerland  
Weidner, Earl, Louisiana State University  
Weiss, Dieter, Technical University, Munich, Germany  
Wonderlin, William F., West Virginia University  
Wood, Emma R., University of British Columbia, Canada

Yeh, Jay Z., Northwestern University Medical School  
Yoshioka, Tohru, Waseda University, Japan

Zigman, Seymour, University of Rochester School of Medicine &  
Dentistry  
Zottoli, Steven J., Williams College  
Zou, Dong-Jing, Biocenter, Basel University, Switzerland  
Zuazaga de Ortiz, Conchita, University of Puerto Rico  
Zukin, R. Suzanne, Albert Einstein College of Medicine

## *Other Research Personnel*

Ahl, Jonna, University of Hartford  
Alston, Yolonda, Benedict College  
Altamirano, Anibal A., University of Texas Medical Branch,  
Galveston  
Andrews, S. Brian, National Institutes of Health  
Araneda, Ricardo, Albert Einstein College of Medicine  
Ascher, Philippe, Ecole Normale Supérieure, France

Bartley, Annette, Hunter College of CUNY  
Benech, Juan Claudio, Instituto de Investigaciones Biológicas  
Clemente Estable, Uruguay  
Bezprozvannaya, Svetlana, University of Connecticut Health Center  
Bhattacharyya, Anita, University of Cincinnati  
Bittner, George D., University of Texas, Austin



Bommert, Kurt, Max-Planck-Institute for Brain Research, Germany  
 Bouhassira, Eric, Albert Einstein College of Medicine  
 Brackenbury, Robert, University of Cincinnati Medical Center  
 Breitwieser, Gerda E., Johns Hopkins University School of Medicine  
 Buelow, Neal, Syracuse University  
 Bullock, Luce, University of Rochester

Callaway, Joseph C., New York Medical College  
 Chludzinski, John, NINDS, National Institutes of Health  
 Chun, Jong Tai, Western Institute and Psychiatric Clinic  
 Clare, Everton, City College of New York  
 Cohen, Avrum, Yale University School of Medicine  
 Cohen, Darien L., Dartmouth College  
 Cohen, Matthew, Yale University  
 Collin, Carlos, NINDS, National Institutes of Health  
 Corda, David, University of Pennsylvania  
 Correa, Ana H., University of California, Los Angeles  
 Couch, Ernest, Texas Christian University  
 Cox, Daniel, Wake Forest University  
 Crispino, Marianna, University of Naples, Italy  
 Crutcher, Keith, University of Cincinnati  
 Cruz, Rena, Lehman College, CUNY

Danae, Hadi, University of Connecticut  
 Davis, Adam, Yale University  
 DeBello, William, Duke University Medical Center  
 Deffenbaugh, Max, Massachusetts Institute of Technology  
 Dermietzel, Rolf, Universitat Regensburg, Germany  
 Drazba, Judith, NINDS, National Institutes of Health  
 Dudley, Nathaniel, Hampshire College

Edwards, M. Kaye, Haverford College  
 Ehrlich, Michelle, Princeton University  
 Engman, James A., University of Cincinnati

Falk, Chun Xiao, Yale University School of Medicine  
 Felle, Hubert, Botanical Institute I, University Giessen, Germany  
 Florin-Christensen, Monica, University of Cincinnati  
 Flucher, Bernhard E., National Institutes of Health  
 Folwell, Mary Grace, Swarthmore College  
 French, Robert J., University of Calgary, Canada  
 Frenkel, Krystyna, New York University Medical Center

Gallant, Paul, NINDS, National Institutes of Health  
 Gerosa, Daniela, Friedrich Miescher-Institut, Switzerland  
 Gill-Kumar, Pritam, Food & Drug Administration  
 Goldman, Anne E., Northwestern University  
 Gomez, Maria, Boston University School of Medicine  
 Gomez Lagunas, Froylan, University of Pennsylvania  
 Gould, Robert, New York State Institute of Basic Research  
 Grassi, Daniel, Ft. Lauderdale, Florida  
 Greenblatt, Daniel, Brandeis University

Hammar, Kassia, NINDS, National Institutes of Health  
 Harper, David, University of British Columbia, Canada  
 Hershko, Avram, Technion, Israel  
 Herzog, Erik, Syracuse University  
 Hitt, Austin, University of West Florida  
 Hogan, Emilia, Yale University School of Medicine  
 Holmgren, Miguel, University of Health Sciences/The Chicago  
 Medical School  
 Hunt, James, Duke Medical Center

Ito, Etsuro, NINDS, National Institutes of Health

Johnson, Michelle R., Howard University  
 Johnston, Jennifer, Dartmouth College  
 Juneja, Renu, The Population Council

Kaftan, Edward, University of Connecticut Health Center  
 Kammerer, Richard, Friedrich Miescher-Institut, Switzerland  
 Kehoe, Jacques, Ecole Normale Supérieure, France  
 Kelly, Mary E., Syracuse University  
 Kirino, Yutaka, Kyushu University, Japan  
 Klein, Kathryn, Emory University School of Medicine  
 Knudsen, Knud D., Food & Drug Administration  
 Konnerth, Arthur, Max-Planck-Institute, Germany  
 Krause, Todd L., University of Texas, Austin  
 Kudo, Yoshihisa, Mitsubishi Kasei Life Sciences Institute, Japan  
 Kuhns, William, Hospital for Sick Children, Canada

Lasser-Ross, Nechama, New York Medical College  
 Lauzon, Cindy, Albany Medical College  
 Leidigh, Christopher, Albert Einstein College of Medicine  
 Leopold, Philip L., University of Texas Southwestern Medical Center  
 Leung, Doreen Siu Yi, Hong Kong University of Science &  
 Technology, Hong Kong  
 Lim, Jong, New York University Medical Center  
 Lin, Jen-Wei, New York University Medical Center  
 Liu, Lei, University of Connecticut  
 Locke, Rachel, Washington University School of Medicine  
 Lorenzoni, Patrizia, Friedrich Miescher Institut, Switzerland  
 Lu, Jin, University of Texas Medical Branch  
 Luca, Frank, Harvard Medical School

Mangel, Stuart, University of Alabama School of Medicine  
 McCartney, Brooke, Duke University  
 McPhie, Donna, National Institutes of Health/Georgetown University  
 Moir, Robert, Northwestern University  
 Monterrubio, Jose, University of Puerto Rico  
 Moreira, Jorge, NINDS, National Institutes of Health  
 Morrell, Candy M., University of Maryland Eastern Shore  
 Morrison, Paul, University of Glasgow, Scotland

Noe, Jennifer R., Emory University

O'Neil, Peggy, Illinois State University  
 Oka, Kotaro, NINDS, National Institutes of Health  
 Olds, James L., National Institutes of Health

Perez, Reynaldo, University of Puerto Rico  
 Perozo, Eduardo, Jules Stein Eye Institute, University of California,  
 Los Angeles  
 Pethig, Ronald, University of Wales, UK  
 Petri, Victoria, Albert Einstein College of Medicine  
 Plotner, Robert, University of Texas Medical Branch, Galveston  
 Powers, Maureen, Vanderbilt University  
 Pumplin, David W., University of Maryland, Baltimore

Rayos, Nancy, Hunter College  
 Reese, Barbara, NINDS, National Institutes of Health  
 Regehr, Wade, University of Pennsylvania  
 Richards, Kathryn S., Emory University  
 Rook, Martin B., Albert Einstein College of Medicine  
 Rothenberg, Mark, Emory University  
 Rusciano, Dario, Friedrich Miescher Institut, Switzerland

Sakakibara, Manabu, Toyohashi University of Technology  
 Salyapongse, Aimee, Wesleyan University

Sanchez, Ivelisse, Hunter College of CUNY  
 Sartain, Julie Ann, Illinois State University  
 Schiffmann, Dietmar, University of Wurzburg, Germany  
 Sheller, Rebecca, University of Texas  
 Shibuya, Ellen, Harvard Medical School  
 Shrier, Alvin, McGill University, Canada  
 Sigg, Daniel, University of California, Los Angeles  
 Slater, N. Travis, Northwestern University  
 Stanley, Elis, NINDS, National Institutes of Health  
 Stockbridge, Lisa, National Institutes of Health  
 Stockbridge, Norman, Food & Drug Administration  
 Stokes, Darrell R., Emory University  
 Stoyanovsky, Detcho, University of Connecticut Health Center  
 Sugimori, Mutsuyuki, New York University Medical Center  
 Sumanovski, Lazar, University Hospital of Basel, Switzerland  
 Swandulla, Dieter, Max-Planck-Institut, Germany  
 Swank, Douglas, University of Pennsylvania

Takagi, Hiroshi, Waseda University, Japan  
 Tang, Akaysha, Yale University School of Medicine  
 Terasaki, Mark, NINDS, National Institutes of Health  
 Tsau, Yang, Yale University School of Medicine  
 Tseng, Daniel, Northwestern University  
 Tsukimura, Brian, Illinois State University  
 Tucker, Meryl Y., Albany Medical College

Vargas, Fernando, Food & Drug Administration

Weiler, Reto, University of Oldenburg, Germany  
 Werman, Robert, Hebrew University, Israel  
 Wu, Jian-Young, Yale University School of Medicine

Yang, Zhaohui, University of Pennsylvania School of Medicine

Zakevicius, Jane, University of Illinois at Chicago College of Medicine  
 Zavilowitz, Joseph, Albert Einstein College of Medicine  
 Zigman, Bunnie R., University of Rochester School of Medicine &  
 Dentistry

## ***Library Readers: General***

Adelberg, Edward A., Yale Medical School

Babitsky, Steven, Falmouth, MA  
 Barrett, Dennis, University of Denver  
 Barry, Susan F., University Hospital  
 Browne, Robert, Wake Forest University

Candeles, Graciela C., University of Puerto Rico  
 Carriere, Rita M., Brooklyn, New York  
 Clarkson, Kenneth L., AT&T Bell Labs  
 Cobb, Jewel Plummer, California State University  
 Cohen, Ira S., SUNY, Stony Brook  
 Cohen, Leonard A., American Health Foundation

Dixon, Keith E., Flinders University  
 Dube, Francois, University of Quebec at Rimousky, Canada  
 DuBrul, Ernest F., University of Toledo  
 Duncan, Thomas K., Nichols College

Eglinton, Aisling, New England Fisheries, World Trade Center  
 Eisen, Herman N., Massachusetts Institute of Technology  
 Epstein, Herman T., Brandeis University

Farmanfarmaian, A., Rutgers University  
 Frenkel, Krystyna, New York University Medical Center  
 Friedler, Gladys, Bunting Institute  
 Fussell, Catherine, University of Pennsylvania

Gabriel, Mordecai L., Brooklyn College  
 German, James, The New York Blood Center  
 Gilbert, Daniel L., National Institutes of Health  
 Goldfarb, Ronald H., Pittsburgh Cancer Institute  
 Goldstein, Moise H., The Johns Hopkins University  
 Goward, Samuel N., University of Maryland  
 Grossman, Albert, New York University Medical Center  
 Guttenplan, Joseph, New York University Dental Center

Harrington, John P., University of South Alabama  
 Hill, Richard W., Michigan State University  
 Humphreys, Tom, University of Hawaii

Inoue, Sadyuki, McGill University, Canada

Kaltenbach, Jane, Mount Holyoke College  
 Kaminer, Benjamin, Boston University School of Medicine  
 Klemow, Kenneth, Wilkes University  
 Kline, Richard Paul, Columbia University

Lee, John J., City College of CUNY  
 Levitz, Mortimer, NYU Medical Center

Marine Biocontrol Co., Sandwich, MA  
 Marine Research, Falmouth, MA  
 Martin, Donald Creagh, Conrad Jobst Tower  
 McCoy, Floyd, Associated Scientists of Woods Hole  
 Michaelson, James, MGH Cancer Center  
 Mooseker, Mark S., Yale University  
 Morrell, Leyla DeToledo, Rush Medical College

Olins, Ada L., University of Tennessee  
 Olins, Donald E., University of Tennessee  
 Ostrer, Harry, NYU Medical Center

Prosser, C. Ladd, University of Chicago  
 Prusch, Robert D., Gonzaga University

Ramamurthy, Baskar, Indian Institute of Science  
 Robinson, Denis, Marine Biological Laboratory  
 Rose, Birgit, University of Miami School of Medicine  
 Rosenbluth, Jack, NYU School of Medicine  
 Rosenfeld, Allan, Columbia University School of Medicine  
 Roth, Lorraine, Brookline, MA  
 Russell-Hunter, W. D., Syracuse University

Schippers, Jay, New York, NY  
 Schweitzer, Nicola, Imperial College, UK  
 Scott-Connor, Harry, Madison, MS  
 Selby, Cecily Cannan, NYU  
 Shepro, David, Boston University  
 Shriftman, Mollie Starr, N. Nassau Health Center  
 Silva, Robert, Marine Research  
 Spiegel, Evelyn, Dartmouth College  
 Spotte, Stephen, Sea Research Foundation & Marine Sci. Inst.  
 Stephenson, William K., Earlham College  
 Sweet, Frederick, Washington University School of Medicine  
 Szent-Györgyi, Andrew, Brandeis University

Trager, William, The Rockefeller University

Van Holde, Kensal E., Oregon State University

Warren, Leonard, Wistar Institute

Weir, Gray E., Naval Historical Center

Wilbur, Charles G., Colorado State University

Wittenberg, Beatrice, Albany Medical College

Wittenberg, Jonathan, Albert Einstein College of Medicine

### ***Library Readers: Desks***

Anderson, Everett, Harvard Medical School

Boyer, John, Union College

Chambers, Edward L., University of Miami

Collier, Marjorie McCann, Saint Peters College

Clark, Arnold M., Woods Hole, MA

Copeland, Eugene, Woods Hole, MA

Cohen, Seymour, Woods Hole, MA

Edds, Louise L., Ohio University

Ellington, Athleen, University of Massachusetts

Fussell, Catherine P., Pennsylvania School of Medicine

Gehrke, Lee, Massachusetts Institute of Technology

Gray, Richard A., Baylor College of Medicine

Haubrich, Robert, Denison University

Herskovits, Theodore T., Fordham University

Johnston, Dan, Baylor College of Medicine

Kelly, Robert E., University of Illinois, Chicago

King, Kenneth, Woods Hole, MA

Korf, Bruce R., Boston, MA

Krane, Stephen, Massachusetts General Hospital

Laderman, Aimlee D., Yale University

Leighton, Joseph, Peralta Cancer Research Institute

Lorand, Laszlo, Northwestern University

Mauzerall, David, Rockefeller University

Mizell, Merle, Tulane University

Morrell, Frank, Rush Medical Center

Narahashi, Toshio, Northwestern University

Nickerson, Peter A., SUNY, Buffalo

Pappas, George D., University of Illinois, Chicago

Person, Philip, Flushing, NY

Rao, T. S., Donapaula, Gao-India

Rickles, Frederick R., University of Connecticut Health

Rosati, Floriana, Siena, Italy

Roth, Jay, Woods Hole, MA

Shepard, Frank, Falmouth, MA

Sonnenblick, Benjamin, Rutgers University

Spector, Abraham, Columbia University

Spiegel, Evelyn, Dartmouth College

Spiegel, Melvin, Dartmouth College

Sundquist, Eric, United States Geological Survey

Sydlik, Mary Ann, SUNY, Geneseo

Tilney, Louis, University of Pennsylvania

Tilney, Molly, University of Pennsylvania

Tsuji, Frederick, Scripps Institute

Tweedell, Kenyon S., University of Notre Dame

Webb, H. Marguerite, Woods Hole, MA

Weir, Gary E., U.S. Naval Historical Center

### ***Library Readers: Rooms***

Cariello, Lucio, Stazione Zoologica, Italy

D'Alessio, Giuseppe, Via Mezzocannone, Italy

Filley, O. D., Filley & Co.

Goldman, Robert, Northwestern University Medical School

Hines, Michael, Duke University

Ilan, Joseph, Case Western Reserve University

Ilan, Judith, Case Western Reserve University

Moore, John W., Duke University

Patterson, David, University of Sydney, Australia

Rabinowitz, Michael, MBL/Harvard Medical School

Reynolds, George T., Princeton University

Sheetz, Michael P., Duke University

Speck, William, Case Western Reserve University

Spirin, Alexander, Academy of Sciences, Russia

Stuart, Ann E., University of North Carolina, Chapel Hill

Tykocinski, Mark L., Case Western Reserve University

Weissmann, Gerald, NYU Medical Center

Yoshioka, Tohru, Waseda University, Japan

Zweig, Ron, Ecologic

### ***Domestic Institutions Represented***

Alabama, University of, Birmingham

Alabama, University of, School of Medicine

Albany Medical College

Albert Einstein College of Medicine

American Board of Quality Assurance

American Medical Association

American Museum of Natural History

Aquatic Research Organisms

Arizona State University

Arizona, University of

AT&T Bell Laboratories

Axon Instruments, Inc.

Barry Controls

Baylor College of Medicine

Beckman Instruments, Inc.

Becton Dickinson IS

Benedict College

Bigelow Laboratories for Ocean Studies

Bio-Rad Laboratories

Boston University

Boston University Marine Program

Boston University School of Medicine

Bowman Gray School of Medicine of Wake

Forest University

Brandeis University

Brandeis University, HHMI

Brinkmann Instruments, Inc.

Brooklyn College of the City University of

New York

- Brown University  
Brown University School of Medicine  
BTX  
Buffalo, University of
- C. P. Li Biomedical Research Corp.  
California Institute of Technology  
California Institute of Technology, Beckman Institute  
California State University, Fresno  
California, University of, Berkeley  
California, University of, Davis  
California, University of, Irvine  
California, University of, Los Angeles  
California, University of, Riverside  
California, University of, San Diego, HHMI  
California, University of, San Francisco  
Cambridge Technology  
Carnegie Mellon University  
Case Western Reserve University  
Catawba Memorial Hospital  
CAV Consulting  
Center for Disease Control  
Chicago Medical School, University of Health Sciences  
Chicago, Rehabilitation Institute of  
Chicago, University of  
Children's Hospital, Boston  
Children's Hospital, Philadelphia  
Children's Hospital Medical Center  
Cincinnati, University of  
Cincinnati, University of, College of Medicine  
Cincinnati, University of, Medical Center  
City College of New York  
Clarkson University  
Cleveland Clinic Foundation  
Cleveland Clinic Research Institute  
Codonics  
Colorado, University of, Boulder  
Colorado, University of, Health Science Center  
Columbia Graduate School of Arts & Sciences  
Columbia University  
Columbia University, College of Physicians & Surgeons  
Columbia University for Medical Informatics  
Connecticut, University of, Health Center  
Connecticut, University of, Storrs  
Cornell University  
Cornell University Medical College  
Cornell University, N.Y. State College of Veterinary Medicine  
Costar Corporation  
Coy Laboratory Products  
CUNY Medical School
- Dage MTI, Inc.  
Dartmouth College  
Dartmouth Medical School  
David Kopf Instruments  
Delaware, University of  
Digital Equipment Corporation
- Drexel University  
Dummond Scientific  
Duke University  
Duke University Medical Center  
Dupont Merck Pharmaceutical Company
- E. I. duPont de Nemours & Co. (Inc.)  
East Carolina University  
Eastman Kodak Company  
EG & G Instruments  
Emory University  
Emory University School of Medicine  
ENRM VA Hospital  
Eppendorf, Inc.  
Ericomp, Inc.  
Exon-Intron, Inc.  
Exxon Biomedical Sciences, Inc.
- Fisher Scientific  
Florida Medical Entomology Lab, Gainesville  
Florida State University  
Florida, University of, College of Medicine  
Food & Drug Administration  
Fordham University College at Lincoln Center  
Forsyth Dental Center  
Fox Chase Cancer Center  
Franklin & Marshall College  
Frederick Haer & Company
- General Valve Corporation  
George Washington University  
George Washington University School of Medicine  
GIBCO/BRL Life Technologies, Inc.  
Gilson Medical Electronics, Inc.  
Gonzaga University  
Grass Instrument Company
- Hahnemann University  
Hahnemann University School of Medicine  
Hamamatsu Photonic Systems  
Hampshire College  
Harbor Branch Oceanographic Institution  
Harvard Community Health Plan  
Harvard Medical School  
Harvard Medical School/Brigham & Women's Hospital  
Harvard School of Public Health  
Harvard University  
Haverford College  
Hawaii, University of  
Hitachi  
Hofer Scientific  
Hoffman-La Roche, Inc.  
Holy Cross College  
Honeywell Corporation  
Hospital for Special Surgery  
Houston, University of  
Howard Hughes Medical Institution, Massachusetts General Hospital  
Howard University
- Humana Hospital  
Hunter College  
Hunter College of the City University of New York
- ICN Radiochemicals (Division of ICN Biomedicals, Inc.)  
Idaho National Engineering Laboratory  
Idaho, University of  
Illinois Institute of Technology  
Illinois State University  
Illinois, University of  
Illinois, University of, College of Medicine  
Indec Systems Corporation  
Indiana University  
Indiana University Medical Center  
Inovision Corporation  
Institute of Biotechnology  
International Equipment Company  
Iowa, University of  
ISCO, Inc.
- James Madison University  
Jefferson Medical College  
JEOL  
Johns Hopkins Hospital  
Johns Hopkins University  
Jouan, Inc.  
Jules Stein Eye Institute, University of California, Los Angeles
- Kansas, University of  
Kent State University  
Kewalo Marine Laboratories  
Kramer Scientific Corporation
- Lab Line Instruments, Inc.  
Lab Products  
La Jolla Cancer Research Foundation  
Laser Science  
Lederle Laboratories  
Lehman College, City University of New York  
Leica, Inc.  
Lilly Research Laboratories  
Lister Hill National Center for Biomedical Communications  
Los Alamos National Laboratory  
Louisiana State University  
Louisiana State University Medical College  
Lovelace Medical Foundation  
Loyola University Medical School  
Ludlum Measurements, Inc.
- M. D. Anderson Cancer Center  
MCI Telecommunications  
Maryland, University of, Baltimore  
Maryland, University of, Eastern Shore  
Maryland, University of, Medical School  
Massachusetts Eye and Ear Infirmary, Berman-Gund Laboratory  
Massachusetts General Hospital

- Massachusetts Institute of Technology  
 Massachusetts, University of, Amherst  
 Mayo Clinic  
 Mayo Foundation  
 Medical College of Ohio  
 Medical Systems Corporation  
 McLean Hospital  
 Meharry Medical College  
 Merck Sharp & Dohme Research Laboratories  
 Meridian Instruments  
 Miami, University of  
 Michigan State University  
 Michigan, University of  
 Micro Video Instruments  
 Miles Inc., Diagnostics Division  
 Millipore Corporation  
 Minnesota, University of  
 Missouri, University of, School of Medicine  
 Missouri, University of, Columbia  
 MJ Research  
 Molecular Probes  
 Mount Holyoke College
- NACVIS Systems  
 NAOS Marine Laboratory  
 NAPA Permanente Medical Group  
 Narishige USA, Inc.  
 NASA Ames Research Center  
 National Institutes of Health  
 National Institutes of Health/NCI  
 National Institutes of Health/NEI  
 National Institutes of Health, NHLBI  
 National Institutes of Health/NIDCD  
 National Institutes of Health/NINDS  
 National Library of Medicine  
 Nebraska, University of  
 NEC Research Institute  
 Neuro Data Instrument Corporation  
 New Brunswick Scientific Company, Inc.  
 New England Aquarium  
 New England Deaconess Hospital  
 New Hampshire, University of  
 New Mexico, University of  
 New York Medical College  
 New York State Department of Health  
 New York State Institute of Basic Research  
 New York, State University of  
 New York, State University of, Albany  
 New York, State University of, Buffalo  
 New York, State University of, Stony Brook  
 New York, State University of, Syracuse  
 New York University  
 New York University Medical Center  
 Newport Corporation  
 Nikon, Inc.  
 Nikon Instruments  
 North Carolina, University of  
 North Carolina, University of, Chapel Hill  
 Northeast Ohio University College of Medicine  
 Northwestern University  
 Northwestern University Cancer Center  
 Northwestern University Medical School
- Office of the Inspector General  
 Ohio State University  
 Oklahoma, University of  
 Old Dominion University  
 Olympus Corporation  
 Opti-Quip  
 Oregon Health Sciences University  
 Oregon Regional Primate Research Center  
 Oregon, University of  
 Owl Scientific
- Pennsylvania State University  
 Pennsylvania, University of  
 Pennsylvania, University of, School of Medicine  
 Perceptics Corporation  
 Perkin-Elmer Corporation  
 Pharmacia, Inc.  
 Photometrics, Ltd.  
 Photon Technology International  
 Physitemp Instruments, Inc.  
 Pittsburgh Eye and Ear Institute  
 Pittsburgh, University of  
 Pittsburgh, University of, School of Medicine  
 Pomona College  
 Population Council, The  
 Princeton University  
 Puerto Rico, University of  
 Purdue University
- R & M Biometrics, Inc.  
 Radiomatic Instruments & Chemical Company, Inc.  
 Research Precision Instruments  
 Rhode Island, University of  
 RMC  
 Robbins Scientific Corp.  
 Rochester, University of  
 Rochester, University of, School of Medicine & Dentistry  
 Rockefeller University  
 Rowland Institute for Science  
 Rush Presbyterian St. Luke's Medical Center  
 Rutgers University
- Salk Institute, The  
 San Francisco State University  
 Savant Instruments, Inc.  
 Schepens Eye Research Institute, Inc.  
 Scientific Systems  
 Scripps Research Institute  
 Shandon-Lipshaw  
 Shimadzu Scientific Instruments, Inc.  
 Smith College  
 Smithsonian Institution Museum  
 Sony Medical Electronics  
 South Carolina, University of, Medical School  
 Southern California, University of  
 Southern Mississippi, University of  
 Stanford University  
 Stanford University School of Medicine, Beckman Center  
 Stoelting Company
- Strategene  
 Supercomputing Research Center  
 Sutter Instrument Company  
 Swarthmore College  
 Syntex Research  
 Syracuse University
- Technical Manufacturing Corporation  
 Technical Products International, Inc.  
 Technical Video, Ltd.  
 Texas Christian University  
 Texas, University of  
 Texas, University of, Austin  
 Texas, University of, Health Science Center  
 Texas, University of, Medical Branch, Galveston  
 Texas, University of, Medical School, Houston  
 Texas, University of, Southwestern Medical Center, Dallas  
 Thomas Jefferson University  
 Toledo, University of  
 Tufts University  
 Tufts University Medical School  
 Tufts University School of Veterinary Medicine  
 Turner Designs
- UMDNJ, Robert Wood Medical School  
 USDA, ARS, ERRC  
 Uniformed Services University of the Health Sciences, Hebert School of Medicine  
 Union College  
 United States Air Force  
 United States Department of Veteran Administration, Affairs Medical Center  
 United States Fish & Wildlife Service  
 Universal Imaging Corporation  
 Utah, University of  
 Utah, University of, School of Medicine
- Vanderbilt University  
 Vanderbilt University School of Medicine  
 Vermont, University of  
 Video Scope International, Ltd.  
 Virginia/Maryland Regional College  
 Virginia, University of  
 Virginia, University of, Medical School  
 Vital Images
- Wadsworth Center for Laboratories & Research  
 Wake Forest University  
 Warner Instrument Corporation  
 Washington State University  
 Washington, University of  
 Washington University  
 Washington University School of Medicine  
 Waters Chromatography Division  
 Wayne State University  
 Wellesley College  
 Wesleyan University  
 West Florida, University of  
 West Virginia University

West Virginia University Health Sciences  
Center  
Western Psychiatric Institute and Clinic  
Whitehead Institute  
Williams College  
Wisconsin, University of, Madison

Wisconsin, University of, Milwaukee  
Woods Hole Oceanographic Institution  
Worcester Foundation for Experimental  
Biology  
Xybion Corporation

Yale University  
Yale University School of Medicine  
Youngstown State University  
  
Carl Zeiss, Inc.  
Zymogenetics Corporation

## Foreign Institutions Represented

Aarhus University, Denmark  
Academy of Sciences, Russia  
Academy of Sciences, Institute of Protein  
Research, Russia  
Aquarium & Marine Center, Canada  
  
Barcelona, University of, Spain  
Bari, Università di, Italy  
Basel, University of, Switzerland  
Basel, University of, Biocenter, Switzerland  
Bayreuth, Universitaet, Germany  
Belgrade, University of, Yugoslavia  
Ben Gurion, University of, Israel  
Bordeaux, University of, France  
Botanical Institute I. University Giessen,  
Germany  
Bristol, University of, United Kingdom  
British Columbia, University of, Canada  
  
Cairo, University of, Medical School, Egypt  
Calgary, University of, Canada  
CINEVESTAV-IPN, Mexico City, Mexico  
CNRS, Station Zoologique, France  
Concordia University, Canada  
  
Dalhousie University, Canada  
Deakin University, Australia  
Douglas Research Hospital, Canada  
  
Ecole Normale Supérieure, France  
Edinburgh University, United Kingdom  
Escola Paulista de Medicina, Brasil  
  
Freiburg Institut für Biologie, Germany  
Friedrich Miescher Institut, Switzerland  
  
Geneve, Université de, Switzerland  
Glasgow, University of, Scotland  
  
Hebrew University, Israel  
Hong Kong University of Science &  
Technology, Hong Kong  
Hospital de l'Enfant-Jésus, Canada  
Hospital for Sick Children, Canada  
  
ILRAD, Kenya  
Imperial Cancer Research Fund, United  
Kingdom  
INSERM, France  
Institut fuer Zoologie, Germany  
Institut J. Monod, France

Institute of Marine Affairs, West Indies  
Institute of Zoophysiology, Germany  
Instituto de Fisologia Celular, UNAM,  
Mexico  
Instituto de Investigaciones Biologicas  
Clemente Estable, Uruguay  
Instituto M.y.M. Ferreyra, Argentina  
I.V.I.C., Venezuela  
I. Zoologisches Institut, Germany  
  
James Cook University of North Queensland,  
Australia  
  
Kaiserlautern, University of, Germany  
Karl-Franzens-Universität, Austria  
Keele University, UK Institut for Tropical  
Medicine, Germany  
Koln, University of, Germany  
Konstanz, University of, Germany  
Kyoto University, Japan  
  
Laval, Université dekl, Canada  
  
Manchester, University of, United Kingdom  
Max-Planck-Institut, Germany  
Max-Planck-Institut für Biologische  
Kybernetik, Germany  
Max-Planck-Institut für Biophysikalische  
Chemie, Nikolausberg, Germany  
Max-Planck-Institut für Brain Research,  
Germany  
Max-Planck-Institut für  
Entwicklungsbiologie, Germany  
McGill University, Canada  
McGill Vision Research Center, Canada  
McMaster University Medical School,  
Canada  
Medical Research Council, United Kingdom  
Mexico, University of, Mexico  
Montreal, University of, Canada  
Moscow State University, Russia  
MRC Anatomical Neuropharmacology Unit  
MRC Laboratory of Molecular Biology,  
United Kingdom  
  
Naples, University of, Italy  
National Museums, Kenya  
National University, Mexico  
Newfoundland, Memorial University of,  
Canada

New South Wales, University of, Australia  
Northern Ireland Department of Agriculture,  
Ireland  
  
Oldenburg, University of, Germany  
ORSTOM/DGRST Center, Congo  
Osaka Medical College, Japan  
Ottawa, University of, Canada  
Oxford University, United Kingdom  
  
Panum Institute, Denmark  
Paris-Sud, Université, France  
Pasteur Institute, France  
Pembroke College, United Kingdom  
Philipps-Universität, Germany  
  
Queen's Medical Centre, United Kingdom  
Queens University, Canada  
  
Regensburg, Universität, Germany  
  
St. Andrews University, Scotland  
St. George's Hospital Medical School, United  
Kingdom  
Salamanca, University of, Spain  
Sofia University, Bulgaria  
Stazione Zoologica, Italy  
Sydney, University of, Australia  
  
Technion, Israel  
Tel Aviv University, Israel  
Tokyo, University of, Japan  
Toronto, University of, Canada  
Toyohashi University of Technology  
Tübingen, University of, Germany  
Tuscia, University of, Italy  
  
Ulm, University of, Germany  
University Hospital of Basel, Switzerland  
Uppsala Biomedical Center, Sweden  
  
Wales, University of, United Kingdom  
Waseda University, Japan  
Weizmann Institute of Science, Israel  
Wellcome Research Laboratories, United  
Kingdom  
Wurzburg, University of, Germany  
  
Zurich, University of, Switzerland

## Year-Round Research Programs



### *Architectural Dynamics in Living Cells Program*

Established in 1992 this program focuses on architectural dynamics in living cells—the timely and coordinated assembly and disassembly of macromolecular structures essential for the proper functioning, division, motility, and differentiation of cells; the spatial and temporal organization of these structures; and their physiological and genetic control. The program is also devoted to the development and application of powerful new imaging and manipulation devices that permit such studies directly in living cells and functional cell-free extracts. The Architectural Dynamics in Living Cells Program promotes interdisciplinary research and consists of resident core investigators and a cadre of adjunct members.

#### *Staff*

Inoué, Shinya, Distinguished Scientist  
Oldenbourg, Rudolf, Associate Scientist  
Stemmer, Andreas, Visiting Assistant Scientist

### *Boston University Marine Program*

#### *Faculty*

Atema, Jelle, Professor of Biology, Program Director  
Humes, Arthur G., Professor of Biology Emeritus  
Tamm, Sidney L., Professor of Biology  
Valiela, Ivan, Professor of Biology

#### *Staff*

Hahn, Dorothy, Senior Administrative Secretary  
Kean, Kristen, Program Assistant  
Schillizzi, Cynthia, Program Manager

#### *Visiting Faculty and Investigators*

Collette, Bruce, NMFS National Museum of Natural History,  
Washington, DC  
Cuomo, Carmela, Yale University  
D'Avanzo, Charlene, Hampshire College

Hinga, Kenneth, University of Rhode Island  
Kaufman, Les, Edgerton Research Lab, New England Aquarium  
Kremer, James, University of Southern California  
McFall-Ngai, Margaret, Scripps Institute of Oceanography  
McPhee, Linda, postgraduate WHMS student from Ontario  
Muscatine, Leonard, University of California, Los Angeles  
Peckol, Paulette, Smith College  
Rietsma, Carol, SUNY, New Paltz  
Sardet, Christian, Villefranche-sur-Mer, France  
Seeler, Jacob, University of Texas Southwestern Medical Center  
Simmons, William, Visiting Lecturer, Boston University  
Wainright, Sam, Rutgers University  
Ward, Nathalie, Center for Coastal Studies

#### *Research Staff*

Basil, Jennifer, Postdoctoral Investigator  
Breithaupt, Thomas, Postdoctoral Investigator  
Chang, Patrique, Visiting Investigator  
Dudley, Judy, Visiting Research Assistant  
Eisthen, Heather, Grass Fellow  
Deiner, Michael, Visiting Research Assistant  
Foreman, Kenneth, Research Associate  
Hammes, Michelle, Research Assistant  
Langton, Lori, Research Assistant  
MacDonald, Robin, Research Assistant  
Miller, Caroline, Visiting Lab Assistant  
Seely, Brad, Visiting Research Assistant  
Tamm, Signhild, Senior Research Associate  
Voigt, Rainer, Research Associate

#### *Teaching Assistants*

Asmutis, Regina, Course Assistant  
Bushman, Paul, Woods Hole Marine Semester Coordinator  
Farley, Lynda, Course Assistant  
Gomez, George, Course Assistant  
Karavanich, Christy, Course Assistant  
Lowe, Brian, Course Assistant  
O'Brien, Todd, Course Assistant  
Schlezinger, David, Course Assistant



*Graduate Students*

Alber, Meryll  
 Anderson, John  
 Bohachevsky, Boris  
 Bryden, Cynthia  
 Bushmann, Paul  
 Cowan, Diane  
 Farley, Lynda  
 Gomez, George  
 Hersh, Douglas  
 Joy, Jennifer  
 Karavanich, Christy  
 LaMontagne, Michael  
 Lavalli, Kari  
 Lindner, Kate  
 Lowe, Brian  
 McPhee, Linda (postgrad. Ontario)  
 Mosiach, Simon  
 O'Brien, Todd  
 Portnoy, John  
 Schlezinger, David  
 Tamse, Armando  
 Usup, Gires  
 White, David

*Undergraduate Students Fall 1992*

Alterman, Randy  
 Bayha, Keith  
 Bechtel, Jamlá  
 Benning, Linda  
 Brown, Timothy (Wesleyan)  
 Bowman, Liza  
 Castro, Natalia  
 Conlon, Jeffrey  
 Crooks, Wendy  
 Davidson, Stacie  
 DeSantis, Krystal  
 DePalma, James  
 Ellison, Rob  
 Emerson, Lyndal  
 Esham, Kristina  
 Ettinger, Brian  
 Fox, Ellen  
 Harding, Jennifer  
 Harmer, Tara  
 Hoffner, Jude (Wesleyan)  
 Horgan, Edward  
 Kachra, Tasleem (Brandeis)  
 Keyser, Alisa  
 Kim, Hong  
 Kotwas, Kristin  
 Lentine, Maria  
 Lombard, Benjamin  
 Maron, Christopher  
 Pedersen, Jennifer  
 Peralta, Michelle  
 Pimental, Helenium  
 Pretto, Christopher  
 Rader, Lauren  
 Rulison, Steve  
 Suarez, Mark  
 Szczepankiewicz, Peter  
 Vanmarke, Kristien

Vavpetic, Lisa  
 Wanger, Jolle  
 Wingertner, Scott  
 Yang, Grace

*Summer Undergraduate Interns*

Barak, Jeri  
 Berg, Kathleen  
 Collins, Glynnis  
 Cordray, Diane  
 Flick, Kevin  
 Guilfoyle, Kerry Jo  
 Harrison, John  
 Herr, Barbara  
 Kirkendall, Ellen  
 Owen, Jennifer  
 Rollenhagen, Julianne  
 Watt, Melissa

*Laboratory of Jelle Atema*

Organisms use chemical signals as their main channel of information about the environment. These signals are transported in the marine environment by turbulent currents, viscous flow, and molecular diffusion. Receptor cells extract signals through various filtering processes. Currently, the lobster with its exquisite sense of taste and smell, is our major model to study the signal filtering capabilities of the whole animal and its narrowly tuned receptor cells. Research focuses on amino acids (food signals) and pheromones (courtship and dominance), neurophysiology of receptor cells, behavior guided or modulated by chemical signals, and computational models of odor plumes and neural filters.

*Laboratory of Arthur G. Humes*

Research interests include systematics, development, host specificity, and geographical distribution of copepods associated with marine invertebrates. Current research is on taxonomic studies of copepods from invertebrates in the tropical Indo-Pacific area, and poecilostomatoid and siphonostomatoid copepods from deep-sea hydrothermal vents and cold seeps.

*Laboratory of Sidney Tamm*

Research interests include cell physiology and motility, cytoskeleton, ciliary and flagellar motion, and trophic ecology of gelatinous zooplankton. Current research is on neural and ionic control of ciliary feeding and escape behaviors of marine invertebrates, distribution of calcium channels and calcium sensors in ctenophore cilia, geotactic mechanisms and sensory receptors in ctenophores, jellies with jaws (macro-ciliary teeth and actin bundles in *Beroë*), and rotary motors and fluid membranes in symbiotic protozoa.

*Laboratory of Ivan Valiela*

Our major research activity involves the Waquoit Bay Land Margin Ecosystems Research Project. This work examines how human activity in coastal watersheds (including landscape use and urbanization) increases nutrient loading to groundwater and streams. Nutrients in groundwater are transported to the sea, and, after biogeochemical transformation, enter coastal waters. There, increased nutrients bring about a series of changes. The Waquoit Bay LMER is designed to help us to understand and model the coupling of land use

and consequences to receiving waters, and to study the processes involved.

A second long-term research topic is the structure and function of salt marsh ecosystems, including the processes of predation, herbivory, decomposition, and nutrient cycling.

### *Center for Molecular Evolution*

The major research effort of this laboratory is the structure analysis of ribosomal RNA. Similarities between small subunit ribosomal RNA sequences are used to infer the evolutionary history of eukaryotic microorganisms and to design molecular probes for studies in marine ecology.

#### *Staff*

Sogin, Mitchell L., Director and Senior Scientist  
Gunderson, John, Research Associate  
Hinkle, Greg, Postdoctoral Fellow  
Leipe, Detlev, Postdoctoral Fellow  
Morrison, Hillary, Research Associate/Postdoctoral fellow

### *The Ecosystems Center*

The Center was established in 1975 to promote research and education in ecosystems ecology. Twelve senior scientific staff and 43 research assistants and support staff study the terrestrial and aquatic ecology of a wide variety of ecosystems ranging from Brazil (carbon cycling and trace gas emissions from tropical forests and pastures) to the Alaskan Arctic (long-term studies of the response of tundra, lake, and stream biota to change) to the Harvard Forest (long-term studies of the effects of disturbance in forest ecosystems) to Massachusetts Bay (rates of denitrification). Many projects, such as those dealing with sulfur transformations in lakes and nitrogen cycling in the forest floor, investigate the movements of nutrients and make use of the Center's mass spectrometry laboratory (directed by Brian Fry) to measure the stable isotopes of carbon, nitrogen, and sulfur. The research results are applied wherever possible to questions of the successful management of the natural resources of the earth. In addition, the ecological expertise of the staff is made available to public affairs groups and government agencies who deal with such problems in acid rain, ground water contamination, and possible carbon dioxide-caused climate change.

#### *Staff*

Hobbie, John E., Co-Director	Jones, David
Melillo, Jerry M., Co-Director	Kicklighter, David
Bahr, Michele	Laundre, James
Castro, Mark	Martin, Daniel
Chapman, Jonathan	McGuire, A. David
Deegan, Linda	Miliefsky, Michele
Donovan, Suzanne	Murray, Georgia
Dornblaser, Mark	Nadelhoffer, Knute
Downs, Martha	Newkirk, Kathleen
Drumme, Todd	O'Hara, Patricia
Fry, Brian	Padien, Daniel
Garratt, Robert	Pallant, Julie
Geyer, Heidi	Parmentier, Nancy
Giblin, Anne	Peterson, Bruce
Griffin, Elisabeth	Rastetter, Edward
Helfrich, John	Redmond, Leslie
Hopkinson, Charles	Regan, Kathleen
Hullar, Meredith	Repert, Deborah
Jesse, Martha	Ricca, Andrea

Scanlon, Deborah  
Schwamb, Carol  
Shaver, Gaius

Stuedler, Paul  
Tholke, Kristin  
Tucker, Jane

#### *Postdoctorals*

Johnson, Loretta  
McKane, Robert

Neill, Christopher  
Peterjohn, William

#### *Visiting Scholars*

Normann, Bosse, University of Umeå, Sweden

#### *Consultants*

Bowles, Francis  
Bowles, Margaret  
Schwarzman, Elisabeth

### *Laboratory for Marine Animal Health*

The laboratory provides diagnostic, consultative research, and educational services to the institutions and scientists of the Woods Hole community concerned with marine animal health. Diseases of wild, captive, and cultured animals are investigated.

#### *Staff*

Abt, Donald A., Director and The Robert R. Marshak Term Professor of Aquatic Animal Medicine and Pathology, School of Veterinary Medicine, University of Pennsylvania  
Bullis, Robert A., Research Assistant Professor of Microbiology, University of Pennsylvania  
Lawrence, Wade B., Research Assistant Professor of Pathology, University of Pennsylvania  
Leibovitz, Louis, Director Emeritus  
McCafferty, Michelle, Histology Technician, University of Pennsylvania  
Moniz, Priscilla C., Secretary  
Smolowitz, Roxanna M., Research Associate in Pathology, University of Pennsylvania  
Wadman, Elizabeth A., Microbiology Technician, University of Pennsylvania

### *Laboratory of Aquatic Biomedicine*

This laboratory investigates leukemias of soft shell clams. Monoclonal antibodies developed by this laboratory and techniques in molecular biology are used to investigate the differences between normal and leukemic cells and their ontogeny. The impact of pollutants on leukemogenesis is currently being studied with an emphasis on regional superfund sites.

#### *Staff*

Reinisch, Carol L., Investigator, MBL, and Chairperson Department of Comparative Medicine, Tufts University School of Veterinary Medicine  
Leland, Christian, Laboratory Assistant

### *Laboratory of Cell Biochemistry*

This laboratory uses cell and molecular biological methods to study the regulation of gene expression in marine fish. Current emphasis is on gene products involved in hepatic heme biosynthesis and

utilization. These processes are affected by hormonal, nutritional, and pharmacological agents as well as xenobiotics, and carcinogens. In addition, free heme is a feedback regulator of its biosynthesis. The principal site at which these agents act to control the rate of heme production is 5-aminolevulinic synthase (ALS), the first enzyme of the pathway. However, it has not been possible to define the mechanisms that lead to enzyme induction or repression. Marine fish are attractive for that purpose because they have similar regulatory features for heme biosynthesis but lack some of the hepatic processes that have confounded studies in mammals. Evidence to date strongly indicates that expression of fish ALS is regulated at a post-transcriptional stage. Cloned cDNAs have been isolated for both the housekeeping and erythroid forms of ALS, and the sequence of the e-type cDNA encodes an iron regulatory element that controls the rate of mRNA translation. It is expected that these studies of the fish ALS system will give new insights into the control of heme biosynthesis in vertebrate organisms, including man. Primary cultures of fish hepatocytes provide the experimental material for this work, and an additional interest of this laboratory is in establishing these cell cultures as a nonmammalian model for biomedical research.

#### *Staff*

Cornell, Neal W., Senior Scientist  
Abilock, Rigele, Research Assistant  
Bruning, Grace, Research Assistant  
Stukey, Jetley, Laboratory Assistant

#### *Visiting Scientist*

Fox, T. O., Harvard Medical School

### ***Laboratory of Developmental Genetics***

This research group studies the early gene control of cellular differentiation pathways (cell lineage determination) in the embryos of tunicates and other marine invertebrate species.

#### *Staff*

Whittaker, J. Richard, Senior Scientist  
Crowther, Robert, Research Associate  
Loescher, Jane L., Research Assistant  
Meedel, Thomas H., Assistant Scientist

#### *Visiting investigators*

Collier, J. R., Brooklyn College  
Lee, James J., Columbia University, College of Physicians & Surgeons

### ***Laboratory of Judith P. Grassle***

Studies on the population genetics and ecology of marine invertebrates living in disturbed environments, especially of sibling species in the genus *Capitella* (Polychaeta). Flume studies on bivalve and polychaete larval habitat selection.

#### *Staff*

Grassle, Judith P., Senior Scientist  
Mills, Susan W., Research Assistant

### ***Laboratory of Harlyn O. Halvorson***

Over the past year, we have isolated a large number of actinomycetes and sporeformers from various marine environments

like deep sea cores and sediments. Our intention is to characterize these bacteria at the molecular level and to look for biologically active components. Protocols based on DNA fingerprinting and quantitative hybridizations have been developed to differentiate marine sporeformers from one another, as well as from terrestrial sporeformers. The hybridization data has shown that the bacterial isolates are not closely related to one another.

Numerical taxonomic methods are also being used to cluster the various isolates. The physiologically interesting sporeformers will also be characterized by physical mapping using rare-cutting restriction endonucleases.

#### *Staff*

Halvorson, Harlyn O., Principal Investigator  
Chikarmane, Hemant, Assistant Scientist  
VanLooy, Lori, Research Assistant

#### *Visiting Investigators*

Anderson, Porter, University of Rochester  
Keynan, Alex, Hebrew University, Jerusalem, Israel  
Kornberg, Hans, Christ's College, Cambridge, UK  
Vincent, Walter, University of Delaware  
Yashphe, Jacob, Hebrew University, Jerusalem, Israel  
Wainwright, Norman

### ***Laboratory of Shinya Inoué***

Study of the molecular mechanism and control of mitosis, cell division, cell motility, and cell morphogenesis, with emphasis on biophysical studies made directly on single living cells, especially developing eggs in marine invertebrates. Development of biophysical instrumentation and methodology, such as polarization optical and video microscopy and digital image processing techniques, and exploration of their underlying theory are an integral part of the laboratory's effort.

#### *Staff*

Inoué, Shinya, Distinguished Scientist  
Knudson, Robert, Instrument Development Engineer  
Oldenbourg, Rudolf, Assistant Scientist  
Stemmer, Andreas, Visiting Assistant Scientist  
Stukey, Jetly, Research Assistant  
Woodward, Bertha M., Laboratory Manager

#### *Visiting investigators*

Bajer, Andrew, University of Oregon  
Burgos, Mario, Universidad Nacional de Cuyo—Conicet  
Febvre, Colette, Station Zoologique, Villefranche-sur-Mer, France  
Febvre, Jean, Station Zoologique, Villefranche-sur-Mer, France  
Sardet, Christian, Station Zoologique, Villefranche-sur-Mer, France

### ***Laboratory of Alan M. Kuzirian***

Research in this laboratory explores the functional morphology and ultrastructure of various organ systems present in opisthobranch mollusks. The program includes mariculture of the nudibranch, *Hermisenda crassicornis*, with emphasis on developing reliable culture methods for rearing and maintaining this animal as a research resource. Studies include optimization of adult and larval nutrition, control of facultative pathogens and disease, development of morphologic criteria for staging larvae and juveniles, and

metamorphic induction. Morphologic studies stress the ontogeny of neural and sensory structures, and neurochemicals associated with the photic and vestibular systems that have been used as models systems in learning and memory studies.

Concurrent with these studies is the development of a new technique to obtain and reconstruct serial block face images (SBFI) of epoxy-embedded or cryoprepared tissues sectioned or freeze-fractured/freeze-etched inside an SEM by an *in situ* miniature ultramicrotome.

Additional collaborative research includes histochemical investigations on strontium's role in initiating calcification in molluscan embryos (shell and statoliths), as well as immunocytochemical labeling of cell-surface and secretory product antigens using monoclonal and polyclonal antibodies on *Hermisenda* sensory and neurosecretory neurons in cell culture. Systematic and taxonomic studies of nudibranch mollusks are also of interest.

*Staff*

Kuzirian, Alan M., Associate Scientist  
Tamse, Catherine T., Research Assistant

**Laboratory of Andrew L. Miller and  
Lionel F. Jaffe**

This laboratory investigates the role played by calcium ions in a wide range of fundamental cell processes; in developing eggs, in differentiated tissues, and in cell extracts. This is possible through the use of aequorin, a bioluminescent protein complex. Aequorin can either be microinjected into cells or transgenically expressed without disturbing function or development. The pattern of luminescence that is emitted by an aequorin-loaded cell reveals changing patterns and levels of free calcium within the cell (or its progeny). Photons are collected and correlated with dynamic cellular events by an imaging system developed in our laboratory. This technique has some substantial advantages over other methods of imaging intracellular calcium and as a result supports an extensive collaborative research effort. The laboratory is currently studying cytokinesis in frog and fish eggs; cell cycle control in sea urchin and surf clam eggs; polarity expression in frog eggs; tip growth in pollen tubes; injury and degeneration in neurons; mechanisms of fertilization in sea urchins; differentiation in slime molds; and calcium release in cell extracts from frog eggs. The laboratory is supported by the NSF to both pursue biological questions and to develop the aequorin-based imaging technique.

*Staff*

Miller, Andrew L., Assistant Scientist  
Karpus, Eric, Design Engineer  
Jaffe, Lionel F., Senior Scientist

*Visiting Investigators*

Alexander, Steve, Wadsworth Center  
Bearer, Elaine, Brown University  
Browne, Carole, Wake Forest University  
Felle, Hubert, University of Giessen  
Fishman, Harvey M., University of Texas Medical Branch  
Fluck, Richard A., Franklin and Marshall College  
Hepler, Peter, University of Massachusetts  
Krause, Todd L., University of Texas  
Metuzals, Janis, University of Ottawa, Canada  
Sardet, Christian, Ville-Franche-sur-Mer, France  
Swenson, Katherine, Duke University Medical School  
Woodruff, Richard, Westchester University

**Laboratory of Rudolf Oldenbourg**

We study physical optics relevant to microscopic imaging and develop advanced instrumentation in light microscopy for the study of structural dynamics in cells and cell components. The current focus of this new laboratory is the development of a novel polarized light microscope that combines polarization optics with new electro-optical components, video, and digital image processing for a fast analysis of specimen anisotropies over the entire viewing field at the highest resolution of the light microscope. Biological mechanisms to be explored with this new instrument range from the emergence and functional role of filamentous structures in living cells, to the generation of ordered domains in liquid crystals and polymer solutions. The laboratory currently investigates the fine structure of myofibrils and the mechano-elastic properties of virus liquid crystals.

*Staff*

Oldenbourg, Rudolf, Associate Scientist

**Laboratory of Robert E. Palazzo**

This laboratory studies the biochemical regulation of cellular events during meiosis and mitosis. An integral part of the research effort is the design of reconstitution systems that faithfully execute cell cycle-dependent events under defined conditions. Current cell biological, immunochemical, biochemical, and microscopic methodologies are employed. Using marine eggs as a material source, assays have been developed that allow the study of germinal vesicle breakdown, aster formation, and reactivation of isolated mitotic apparatus *in vitro*. Current focus of the laboratory is on the identification of cell cycle-dependent regulatory events with major emphasis on protein phosphorylation and other post-translational modifications. The ultimate goal is the identification of key enzymes and target substrates that are involved in the regulation of cell division and are highly conserved during evolution.

*Staff*

Palazzo, Robert E., Assistant Scientist  
Dawson, Tim, Undergraduate Research Assistant  
Peng, Gang, Postdoctoral Associate  
Przybyla, Beata, Graduate Research Assistant  
Sun, Yong, Postdoctoral Associate  
Vogel, Jacalyn, Research Assistant

*Visiting investigators*

Eckberg, William, R., Howard University  
Heins, Susanne, Maurice E. Muller Institute, Basel, Switzerland  
Rieder, Conly, L., Wadsworth Center for Labs and Research

**Laboratory of Nancy Rafferty**

This laboratory investigates the role of the lens cytoskeleton and its associated proteins in maintenance of lens shape, in lens accommodation and development of cataract when the cytoskeleton is disrupted. Studies include an assessment of the role of cytosolic free calcium on homeostasis of the lens cytoskeleton, the localization of various cytoskeletal proteins in lens epithelium, and determination of the relative amounts of soluble actin to filamentous actin in lens cells during aging. Most of these studies employ a fish model using primary cultures of lens epithelium and electron and immunofluorescence microscopy.

*Staff*

Rafferty, Nancy S., Scientist, Northwestern University  
Rafferty, Keen A., Research Associate

**Laboratory of Monica Riley**

Research in this laboratory focuses on the molecular evolution and gene expression in the bacterium *Escherichia coli*. In a collaborative effort, a database containing information on the intermediary metabolism and biochemical pathways of *E. coli* is being developed. When completed, this database is expected to contain information on each metabolic reaction, the enzyme, the reactants, products, cofactors, activators, inhibitors, kinetics, equilibrium constants, binding constants, etc.

Related research is on the evolution of the *E. coli* DNA and organization of the genes in the chromosome. Comparative nucleotide and amino acid sequence data provide information on the evolutionary relationships of *E. coli* genes to other genes in the *E. coli* genome and to homologous genes in related bacteria.

*Staff*

Riley, Monica, Senior Scientist  
Farquhar, Karyn, Research Assistant

**Laboratory of Sensory Physiology**

Since 1973, the laboratory has conducted research on various aspects of vision. Current studies focus on photoreceptor cells, on their light-absorbing pigments, and on their biochemical reactions initiated by light stimulation. Microspectrophotometric and biochemical techniques are used to study the receptors of both vertebrates (amphibia, fish, and mammals) and invertebrates (horseshoe crab and squid).

*Staff*

Harosi, Ferenc, Director, Associate Scientist, MBL, and Boston University School of Medicine  
Szuts, Ete, Associate Scientist, MBL, and Boston University School of Medicine

*Visiting investigators*

Erickson, Martha, Brandeis University  
Evans, Barbara I., University of Oregon, Eugene  
Greenblatt, Daniel, Brandeis University  
Hawryshyn, Craig W., University of Victoria, B. C., Canada  
Kleinschmidt, Jochen, NYU Medical Center  
Singarajah, Kandar, V., Federal University of Paraiba, Brazil

**Laboratory of Neuroendocrinology**

This laboratory studies the molecular and cellular bases of two neural programs that regulate different important behaviors in the model mollusk *Aplysia*. Research is conducted on the mechanisms of the neuronal circadian oscillators located in the eyes. These circadian oscillators drive the circadian activity rhythm of the animal, which is concerned with the daily timing of food gathering and of prolonged rest. Additional research is conducted on a group of neuroendocrine cells that produce a peptide, "egg-laying hormone," that initiates egg laying and associated behaviors. The laboratory is interested in how the three-dimensional shape of this peptide hormone allows a highly specific interaction with its receptor and the intracellular processes

that are triggered by it. In another project, the laboratory has discovered and is continuing research on a novel second messenger enzyme, an NADase, in the oocytes of *Aplysia*, that generates cyclic ADPR, a Ca<sup>2+</sup>-mobilizing product.

*Staff*

Strumwasser, Felix, Director  
Cox, Rachel L., Senior Research Assistant  
Elder, Peggy, Laboratory Assistant  
Groelle, Holly, Postdoctoral Fellow  
Heisermann, Gary, Postdoctoral Fellow  
Hellmich, Mark, Postdoctoral Fellow  
Lewis, Karen, Laboratory Assistant  
Vogel, Jackie, Research Assistant

**Laboratory of Osamu Shimomura**

Biochemical studies of the various types of bioluminescent systems. Preparation of the improved forms of aequorin for measuring intracellular free calcium.

*Staff*

Shimomura, Osamu, Senior Scientist, MBL, and Boston University School of Medicine  
Shimomura, Akemi, Research Assistant  
Nakamura, Hideshi, Harvard University

**Laboratory of Raquel Sussman**

We investigate the molecular mechanism of DNA damage-inducible functions in *E. coli*. Present studies deal with novel genes that affect radiation-induced mutagenesis and analysis of RecA functions.

*Staff*

Sussman, Raquel, Associate Scientist

**National Vibrating Probe Facility**

The vibrating probe is an instrument that enables an investigator to explore, map, measure, and analyze the patterns of natural ionic currents through living cells, embryos, and even adult organisms. This is done—non-invasively—by measuring the very minute electrical voltage gradients or specific ion gradients generated by those currents within the external medium. Among the current collaborative projects are studies of currents through epithelial cells, *Aplysia* bag cells, cockroach nervous system, injured squid axons, growing pollen tubes, root hairs, and fungi. Investigators are welcome to conduct exploratory studies on their own systems during the summer months. Extensive investigations may be carried out at other times throughout the year. This facility is supported by the Biomedical Research Technology Program, National Center for Research Resources, NIH. Applications for research time should be made to P. Smith.

*Staff*

Jaffe, Lionel, Senior Scientist and Facility Co-Director  
McLaughlin, Jane, Research Assistant  
Sanger, Richard, Senior Electronics Technician  
Shipley, Alan, Research Associate  
Smith, Peter J. S., Co-Director

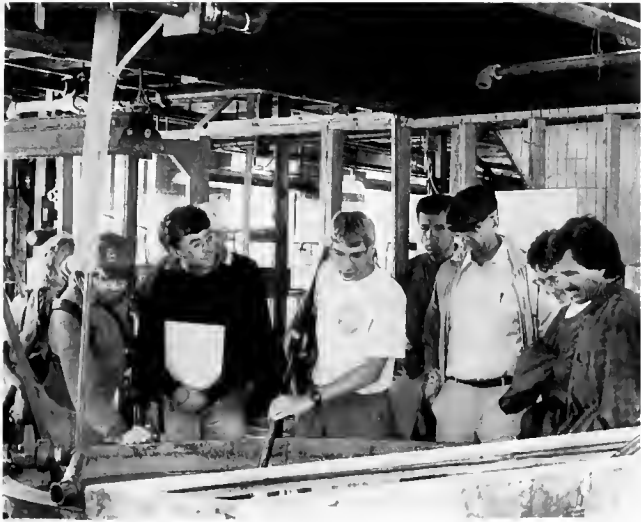
*Visiting investigators*

Allen, Nina, Wake Forest University  
Backie, Iain, Robert Gordon University, Scotland  
Bittner, George, University of Texas, Galveston  
Cox, Daniel, Wake Forest University  
Demarest, Jeff, University of Arkansas  
Fay, Frederic, University of Massachusetts Medical School  
Feijo, José, University of Lisbon, Portugal  
Felle, Hubert, University of Giessen, Germany  
Fishman, Harvey, University of Texas, Galveston  
Ford, Timothy, Harvard University  
Giblin, Anne, Ecosystems, MBL  
Hill, Susan, Michigan State University  
Hoch, Harvey, Cornell University  
Karplus, Eric, MBL

Krause, Todd, University of Texas, Galveston  
Leech, Colin, Howard Hughes Institute, Massachusetts General  
Hospital  
Mitton, Bryce, Massachusetts Institute of Technology  
Morgan, Jim, University of Arkansas  
Nagel, Wolfram, University of Munich, Germany  
Pierson, Elisabeth, University of Siena, Italy  
Wright, Jonathan, McMaster University, Ontario, Canada

***Other Year-Round Investigators and Staff***

Stephens, Raymond E., Principal Investigator  
Szent-Gyorgyi, Gwen, Research Assistant  
Tilney, Lewis G., University of Pennsylvania  
Tilney, Molly S., University of Pennsylvania



## Honors

### Friday Evening Lectures

- Carl Woese, University of Illinois, 26 June "The Revolution in Evolution: Microbiology Comes Into its Own"
- Eric Lander, Whitehead Institute for Biomedical Research, Massachusetts Institute of Technology, 3 July "Dissecting Human Heredity"
- Mary Woolley, Research! America, 10 July "The Problem isn't Science . . . The Problem is Silence: When the People Lead, the Leaders Will Follow . . ."
- Rüdiger Wehner, Universität Zürich, 16, 17 July (Forbes Lectures) "Photoreceptor Twist: A Solution to the False Color Problem" (16 July) "Ant Navigation: How a Small Brain Solves a Complex Task" (17 July)
- Michael Bennett, Albert Einstein College of Medicine, 24 July "From Electric Fishes to Electric Synapses: Gap Junctions Into the Modern Era"
- Stephen Heinemann, The Salk Institute, 31 July "Molecular Biology of the Glutamate Receptors: Structure and Function"
- William Catterall, University of Washington, 7 August (Monsanto Lecture) "From Ionic Currents to Molecules. The Molecular Basis of Electrical Excitability in the Brain"
- Peter Narins, University of California, Los Angeles, 14 August (Lang Lecture) "Biostructural Adaptations for Acoustic and Seismic Communication in Amphibians: Lessons From the Forest"
- Carolyn Cohen, Brandeis University, 21 August "New Twists on an Old Protein Fold: The  $\alpha$ -helical Coiled Coil"
- Richard Rowe, The Faxon Company, 28 August "The Evolution of Scholarly Communications"

### Fellowships

#### Robert Day Allen Fellowship

Sergei A. Kuznetsov, Technische Universität, Germany, and Moscow University, Russia

#### Frederik B. Bang Fellowship Fund

Robert J. Lauzon, Albany Medical College

#### Bakalar Fellowship

Fatima Gyoeva, Russian Academy of Sciences, Institute of Protein Research

#### Frank A. Brown Memorial Readership

Gary E. Weir, Naval Historical Center, Washington, DC

#### Bernard Davis Fellowship

David J. Patterson, University of Sydney, Australia

#### Frank R. Lillie Fellowship

Peter Doroshenko, Duke University Medical Center

#### William Randolph Hearst Fellowship

Eleanore Fusco, Massachusetts Institute of Technology

#### Stephen W. Kuffler Fellowship

Arturo Hernandez-Cruz, Universidad Nacional Autónoma de México, Instituto de Fisiología Celular, México

#### Jacques Loeb Fellowship

Christine R. Rose, University of Kaiserslautern, Germany

#### Nikon, Inc. Fellowship

Andreas Stemmer, MRC Laboratory of Molecular Biology, UK



### H. Burr Steinbach Memorial Fellowship

Ilya Bezprozvanny, University of Connecticut Health Center

### M. G. F. Fuortes Fellowship

Arturo Hernandez-Cruz, Instituto de Fisiologia Celular, UNAM, Mexico

### MBL Summer Fellows

Roger Buchanan, NINDS, National Institutes of Health  
Peter Doroshenko, Duke University Medical Center  
Fedor Severin, Institute of Protein Research, Russia  
Joelle Tanguy, Northwestern University  
Amy V. Trejo, Northwestern University  
Patricia Wadsworth, University of Massachusetts, Amherst  
William Wonderlin, West Virginia University

### Herbert W. Rand Fellowship

Alexander S. Spirin, Institute of Protein Research, Russia

### Science Writing Fellowships

Stephen Braun, Freelance  
Robert Cooke, *Newsday*  
Elizabeth Culotta, Freelance  
Heather Dewar, *The Miami Herald*  
Donald Frederick, National Geographic Society News Service  
David Graham, *San Diego Union-Tribune*  
Jeff Hecht, *New Scientist*  
Rebecca Perl, *Atlanta Journal-Constitution*  
John Schieszer, KPLR-TV, St. Louis, MO  
Cindy Schreuder, *Chicago Tribune*  
Joannie Schrof, *U.S. News & World Report*

### Steps Toward Independence—MBL Summer Fellowships

Ilya Bezprozvanny, University of Connecticut Health Center  
Roger Buchanan, NINDS, National Institutes of Health  
Fatima Gyoeva, Institute of Protein Research, Russia  
Arturo Hernandez-Cruz, Instituto de Fisiologia Celular, UNAM, Mexico  
Sergei Kuznetsov, Technische University, Germany  
Patricia Wadsworth, University of Massachusetts, Amherst

## Scholarships

---

### Alberto Monroy Fellow

Paola Loguercio Polosa, Universita di Bari, Italy

### Bernard Davis Scholarship

Maria Ganeva, Sofia University, Bulgaria  
Ariel Kusmaro, Tel Aviv University, Israel  
Edouard Mambi, Center ORSTOM/DGRST, Congo  
Marganta L. Miroshnichenko, Moscow State University, Russia

### Biology Club of CUNY

Stefan Wurden, Universitat Konstanz, Germany

### Father Arsenius Boyer Scholarship Fund

Atsushi Miyawaki, University of Tokyo, Japan

### C. Lalor Burdick Scholarship

Beatrice Casasnovas, University of Bordeaux, France

### Gary N. Calkins Memorial Scholarship

Lesley J. Narburgh, St. George's Hospital Medical School, UK

### Frances S. Claff Memorial Scholarship

Atsushi Miyawaki, University of Tokyo, Japan

### Edwin Grant Conklin Memorial Scholarship

Lisa C. Foa, Deakin University, Australia

### Lucretia Crocker Endowment Fund

Isabelle M. Desjeux, Edinburgh University, UK  
Marie-Anne Felix, Institut J. Monod, France  
Anna M. Myat, Imperial Cancer Research Fund, UK

### William F. and Irene Diller Scholarship Fund

Stefan Wurden, Universitat Konstanz, Germany

### Caswell Grave Scholarship

Beatrice Casasnovas, University of Bordeaux, France  
Peter S. Dayan, CNL, Salk Institute

### Aline D. Gross Scholarship

Cindy A. Wilson, University of California, Irvine

### Merkel H. Jacobs Scholarship

Lisa C. Foa, Deakin University, Australia  
Christine R. Rose, University of Kaiserslautern, Germany

### Arthur Klorfein Fund Scholarship

Pavle R. Andjus, University of Belgrade, Yugoslavia  
Atsushi Miyawaki, University of Tokyo, Japan  
Enrique Saldana, University of Salamanca, Spain  
Camilla Tornoe, Pembroke College, UK  
Elisabeth C. Walcott, University of California, Irvine

### S. O. Mast Founders Scholarship

Lisa A. Kelly, University of Ottawa, Canada

### Michigan State Scholarship Center for Microbial Ecology Fellow

Jennifer L. Byrnes, Harvard University

### Faith Miller Scholarship

Sergei Kuznetsov, Technische University, Germany, and Moscow University, Russia

**James S. Mountain Memorial Fund Scholarship**

Joseph F. Kelleher, Johns Hopkins University School of Medicine  
 Annick H. Le Gall, Cornell University Medical College  
 Valerie A. Pierce, University of Chicago  
 Ben B. Whitlock, Ohio State University  
 Lin Wu, Scripps Research Institute

**Planetary Biology Internship**

Dirk Schuler, Max-Planck-Institut, Germany  
 Angelica P. Seitz, University of Connecticut, Storrs

**William Townsend Porter Foundation Fellowship**

Darien L. Cohen, Dartmouth College  
 Nathaniel Dudley, Hampshire College  
 Juan C. Jorge-Rivera, Brandeis University  
 Errol R. Kolen, University of Missouri, Columbia  
 Edward E. Leonard, University of Pittsburgh School of Medicine

**Herbert W. Rand Scholarship**

Stefan Wurden, Universität Konstanz, Germany

**Society for Developmental Biology Scholarship**

Maureen A. Gannon, Cornell University Medical College  
 John C. Matese, Duke University

**Society for General Physiologists Scholarships**

Marie-Anne Felix, Institut J. Monod, France  
 Marla B. Feller, AT&T Bell Laboratories  
 Pavle Andjus, Institute of General & Physical Chemistry, Serbia,  
 Yugoslavia  
 Matthew Frerking, University of California, Davis

**Marjorie W. Stetten Fund**

Lisa A. Kelly, University of Ottawa, Canada

**Surdna Foundation Scholarship**

Isabelle M. Desjeux, Edinburgh University, UK  
 Christine R. Rose, University of Kaiserslautern, Germany

**William Morton Wheeler Family Founders' Scholarship**

Beatrice Casasnovas, University of Bordeaux, France

**American Society for Cell Biology**

Carmen R. Domingo, University of California, Berkeley  
 Darien L. Cohen, Dartmouth College  
 Errol R. Kolen, University of Missouri, Columbia  
 Adrian C. Lawrence, Albert Einstein College of Medicine  
 Edward E. Leonard, University of Pittsburgh School of Medicine  
 Zoe Y. Pettway, University of California, Irvine

**American Psychological Association**

Maribel Feliciano, University of Connecticut

***Awards*****Lewis Thomas Award**

Richard Harris, National Public Radio  
 Larry Thompson, Freelance

# Board of Trustees and Committees

## *Corporation Officers and Trustees*

### *Ex officio*

- Honorary Chairman of the Board of Trustees, Denis M. Robinson, Key Biscayne, FL  
Chairman of the Board of Trustees, Sheldon J. Segal, The Population Council, New York, NY  
Vice Chairman of the Board of Trustees, Robert E. Mainer, The Boston Company, Boston, MA  
President of the Corporation, James D. Ebert, Chesapeake Bay Institute, Baltimore, MD  
Director of the Corporation, Harlyn O. Halvorson, Marine Biological Laboratory, Woods Hole, MA<sup>1</sup>  
Director and Chief Executive Officer, John E. Burris, Marine Biological Laboratory, Woods Hole, MA<sup>2</sup>  
Treasurer, Robert D. Manz, Helmer & Associates, Waltham, MA  
Clerk of the Corporation, Kathleen Dunlap, Tufts University School of Medicine, Boston, MA

### *Class of 1996*

- Eloise E. Clark, Bowling Green State University, Bowling Green, OH  
Norman Bernstein, Diane and Norman Bernstein Foundation, Washington, DC  
Martha W. Cox, Nantucket, MA  
John E. Dowling, Harvard University, Boston, MA  
Gerald Fischbach, Harvard University, Boston, MA  
John G. Hildebrand, University of Arizona, Tucson, AR  
Shinya Inoué, Marine Biological Laboratory, Woods Hole, MA  
Neil Jacobs, Hale & Dorr, Boston, MA  
Gerald Weissmann, New York University Medical Center, New York, NY

### *Class of 1995*

- Clay M. Armstrong, University of Pennsylvania Medical School, Philadelphia, PA  
Dieter Blennemann, Carl Zeiss, Inc., Thornwood, NY  
Dick Grace, The Brain Center, New Seabury, MA  
Eric H. Davidson, California Institute of Technology, Pasadena, CA  
Judith P. Grasse, Institute of Marine & Coastal Sciences, Rutgers University, New Brunswick, NJ  
Mary J. Greer, Cambridge, MA  
Franklin M. Loew, Tufts University School of Veterinary Medicine, North Grafton, MA  
Brian M. Salzman, University of Philadelphia School of Medicine, PA  
Robert B. Silver, Cornell University, Ithaca, NY  
J. Philip Trinkaus, Yale University, New Haven, CT

### *Class of 1994*

- Frederick Bay, The Bay Foundation, New York, NY  
Mary-Ellen Cunningham, Grosse Pointe Farms, MI  
Robert D. Goldman, Northwestern University Medical School, Chicago, IL  
Rodolfo R. Llinas, New York University Medical Center, New York, NY  
Robert W. Pierce, Boca Grande, FL  
Thomas D. Pollard, Johns Hopkins University, Baltimore, MD  
Irving W. Rabb, University Place at Harvard Square, Cambridge, MA

\* *ex officio*

<sup>1</sup> to August 31, 1992

<sup>2</sup> from September 1, 1992

- Joan V. Ruderman, Harvard University School of Medicine, Boston, MA  
Joseph Sanger, University of Pennsylvania School of Medicine, Philadelphia, PA  
Ann E. Stuart, University of North Carolina, Chapel Hill, NC

### *Class of 1993*

- Garland E. Allen, Washington University, St. Louis, MO  
Jelle Atema, Marine Biological Laboratory, Woods Hole, MA  
William L. Brown, Weston, MA  
Alexander W. Clowes, University of Washington School of Medicine, Seattle, WA  
Barbara E. Ehrlich, University of Connecticut, Farmington, CT  
Richard E. Kendall, East Falmouth, MA  
Edward A. Kravitz, Harvard Medical School, Boston, MA  
Jerry M. Melillo, Marine Biological Laboratory, Woods Hole, MA  
Henry H. Schmidek, Neurosurgeon, Marion, MA  
Roger D. Sloboda, Dartmouth College, Hanover, NH

### *Emeriti*

- Edward A. Adelberg, Yale University, New Haven, CT  
John B. Buck, Sykesville, MD  
Seymour S. Cohen, Woods Hole, MA  
Arthur L. Colwin, Key Biscayne, FL  
Laura Hunter Colwin, Key Biscayne, FL  
D. Eugene Copeland, Marine Biological Laboratory, Woods Hole, MA  
Sears Crowell, Indiana University, Bloomington, IN  
Alexander T. Daignault, Boston, MA  
William T. Golden, New York, NY  
Teru Hayashi, Woods Hole, MA  
Ruth Hubbard, Cambridge, MA  
Lewis Kleinholz, Reed College, Portland, OR  
Maurice E. Krahl, Tucson, AZ  
Charles B. Metz, Miami, FL  
Keith R. Porter, University of Pennsylvania, Philadelphia, PA  
C. Ladd Prosser, University of Illinois, Urbana, IL  
S. Meryl Rose, Waquoit, MA  
W. D. Russell-Hunter, Syracuse University, Syracuse, NY  
John W. Saunders, Jr., Waquoit, MA  
Mary Sears, Woods Hole, MA  
David Shepro, Boston University, Boston, MA  
Homer P. Smith, Woods Hole, MA  
D. Thomas Trigg, Wellesley, MA  
Walter S. Vincent, Woods Hole, MA  
George Wald, Cambridge, MA

### *Executive Committee of the Board of Trustees*

- Sheldon J. Segal, Chairman  
Frederick Bay, 1994  
John E. Burris\* (effective 9/1/92)  
Mary-Ellen Cunningham, 1994  
James D. Ebert\*  
Ray L. Epstein\*  
Robert D. Goldman, 1994  
Harlyn O. Halvorson\* (through 8/31/92)  
Robert E. Mainer, Vice Chairman  
Robert Manz\*  
Jerry M. Melillo, 1993  
Joseph W. Sanger, 1994  
Roger D. Sloboda, 1993

**Trustee Committees****Audit**

Robert E. Mainer, Chairman  
 Ray L. Epstein\*  
 Pamela Ghetti\*  
 Robert D. Manz\*  
 Joan V. Ruderman  
 Gaius R. Shaver  
 John Speer\*  
 Andrew Szent-Gyorgyi  
 D. Thomas Trigg  
 Stanley W. Watson

**Compensation**

Sheldon J. Segal, Chairman  
 Robert E. Mainer  
 Robert D. Manz

**Development**

Frederick Bay  
 Robert B. Barlow, Jr.  
 John E. Burris\* (effective 9/1/92)  
 James D. Ebert\*  
 Harlyn O. Halvorson\* (through 8/31/92)  
 Rodolfo R. Llinás  
 Luigi Mastroianni  
 Robert Pierce  
 Sheldon J. Segal\*

**Investment**

William L. Brown, Chairman  
 Pamela Ghetti\*  
 William T. Golden

Maurice Lazarus  
 Werner R. Lowenstein  
 Robert D. Manz  
 Irving W. Rabb  
 John Speer\*  
 W. Nicholas Thorndike  
 D. Thomas Trigg

**Long-Range Planning**

Robert D. Manz, Chairman  
 Dieter Blennemann  
 Ray Epstein\*  
 Rodolfo R. Llinás  
 Robert Mainer  
 John Speer\*  
 Andrew Szent-Gyorgyi

**Standing Committees****Buildings & Grounds**

Kenyon S. Tweedell, Chairman  
 Barbara C. Boyer  
 Alfred B. Chaet  
 Lawrence B. Cohen  
 Richard D. Cutler\*  
 William R. Eckberg  
 Alan Fein  
 Ferenc Harosi  
 Donald B. Lehy\*  
 Thomas Meedel  
 Evelyn Spiegel

**Fellowships**

Thoru Pederson, Chairman  
 Martha Constantine-Paton  
 Ray L. Epstein\*  
 Leslie D. Garrick\*  
 Anne E. Giblin  
 George M. Langford  
 José Lemos  
 Eduardo R. Macagno  
 Carol L. Reinisch  
 J. Richard Whittaker

**Housing, Food Service,  
and Child Care**

Thomas S. Reese, Chairman  
 Susan R. Barry  
 Milton Charlton  
 Richard Cutler\*  
 Robert Michael Gould  
 Stephen M. Highstein  
 LouAnn King\*  
 Darrell R. Stokes

**Institutional Animal Care and Use**

Leslie D. Garrick, Chairman  
 Robert A. Bullis  
 Alfred B. Chaet  
 Ray L. Epstein  
 Alan M. Kuzirian  
 Andrew Mattox

**Instruction**

Roger D. Sloboda, Chairman  
 George Augustine, Jr.  
 Ray L. Epstein\*  
 Rachel D. Fink  
 Leslie D. Garrick\*  
 Leah T. Haimo  
 Susan Hill  
 Ronald R. Hoy  
 Hans Laufer  
 Joan V. Ruderman  
 Robert B. Silver  
 Raymond Stephens  
 John B. Waterbury

**Library Joint Management**

John E. Burris, MBL  
 Robert Gagosian, WHOI  
 Larry Ladd, WHOI  
 John Speer, MBL\*  
 David Stonehill, MBL/WHOI

**Library Joint Advisory**

David Shepro, Chairman, MBL  
 John E. Hobbie, MBL  
 Gerald Weissmann, MBL  
 Henry Dick, WHOI  
 Werner Deuser, WHOI  
 Page Valentine, USGS  
 Kevin Friedland, NMFS

**Marine Resources**

Robert D. Goldman, Chairman  
 Donald A. Abt  
 William D. Cohen  
 Richard Cutler\*  
 Donald B. Lehy\*  
 Toshio Narahashi  
 George D. Pappas  
 Roger D. Sloboda  
 Melvin Spiegel  
 Antoinette Steinacher

**Radiation Safety**

Ete Z. Szutz, Chairman  
 David W. Borst  
 Richard L. Chappell  
 Sherwin J. Cooperstein  
 Louis M. Kerr  
 Andrew Mattox\*  
 Robert Rakowski  
 Walter S. Vincent

**Research Services**

Peter B. Armstrong, Chairman  
 Neal W. Cornell  
 Richard Cutler\*  
 Barbara E. Ehrlich  
 Kenneth H. Foreman  
 Joseph Ilan  
 Ehud Kaplan  
 Samuel S. Koide  
 Aimlee D. Laderman  
 Jack Levin  
 Andrew Mattox\*  
 Robert D. Palazzo  
 James P. Quigley  
 Peter J. S. Smith  
 Paul A. Stuedler  
 Mark L. Tykocinski

\* *ex officio*

***Research Space***

Joseph W. Sanger, Chairman  
Paul J. De Weer  
Ray L. Epstein\*  
Leslie D. Garnek\*  
David Landowne  
Hans Laufer  
Eduardo R. Macagno

\* *ex officio*

Jerry M. Melillo  
Joan V. Ruderman  
Robert B. Silver  
Steven N. Treisman  
Ivan Valiela  
Richard Vallee

***Safety***

John E. Hobbie, Chairman  
Lee Bourgojn

Richard Cutler\*  
Edward Enos\*  
Susan Goux  
Louis M. Kerr  
Alan Kuzirian  
Donald B. Lehy\*  
Andrew Mattox\*  
Paul A. Stuedler



## Laboratory Support Staff\*

### Biological Bulletin

Clapp, Pamela L., Managing Editor  
 McCaffrey, Karen  
 Ready, Beth  
 Showalter, Christine M.

### Controller's Office

Speer, John W., Controller

#### Accounting Services

Afonso, Janis E.  
 Binda, Ellen F.  
 Campbell, Ruth B.  
 Davis, Doris C.  
 Ghetti, Pamela M.  
 Gilmore, Mary F.  
 Hobbs, Roger W., Jr.  
 Poravas, Maria

#### Chem Room

Miller, Lisa A.  
 Schorer, Timothy M.  
 Mancevice, Denise M.

#### Purchasing

Hall, Lionel E., Jr.  
 Mancevice, Denise M.  
 Schorer, Timothy M.

### Director's Office

Burris, John E., Director and CEO  
 Halvorson, Harlyn O., Director  
 Epstein, Ray L., Associate Director  
 Burrhus, I. Elaine  
 Catania, Didia

### External Affairs

Carotenuto, Frank C., Director  
 Aspinwall, Duncan P.  
 Berthel, Dorothy  
 Faxon, Wendy P.  
 Lessard, Kelley J.

\*Including persons who joined or left the staff during 1992.

### Associates Program

Armstrong, Ellen P., Liaison  
 DiIorio, Anne E.  
 Price, F. Carol  
 Scanlon, Deborah

### Communications Office

Clapp, Pamela L., Director  
 Kaye-Peterson, Amy  
 Liles, George  
 Ready, Beth

### Gray Museum

Backus, Richard H., Curator  
 Armstrong, Ellen P.  
 Montiero, Eva

### Housing

King, LouAnn D., Conference Center and  
 Housing Manager  
 Johnson, Frances N.

### Telephone Office

Baker, Ida M.  
 Geggatt, Agnes L.  
 Ridley, Alberta W.

### Human Resources

Goux, Susan P., Manager  
 Donovan, Marcia H.

### MBL/WHOI Library

Stonehill, David L., Director, MBL/WHOI  
 Library Center  
 Ashmore, Judith A.  
 Costa, Marguerite E.  
 Mirra, Anthony J.  
 Monahan, A. Jean  
 Nelson, Heidi  
 Nickerson, Ruth L.  
 Pratson, Patricia G.  
 deVeer, Joseph M.

### Copy Service Center

Mountford, Rebecca J., Supervisor  
 Jackson, Jacquelyn F.  
 Mancini, Mary  
 Ridley, Sherie

### Information Systems Division

Norton, Catherine N., Director  
 Hamre, Lynne  
 Kogelnik, Andreas  
 Remsen, David  
 Space, David B.  
 Tollios, Constantine D.

### Safety Services

Mattox, Andrew H., Safety Officer

### Apparatus

Barnes, Franklin D.  
 Haskins, William A.  
 Martin, Lowell V.  
 Nichols, Francis H., Jr.

### Shipping and Receiving

Geggatt, Richard E.  
 Illgen, Robert F.

### Services, Projects, and Facilities

Cutler, Richard D., Manager  
 Enos, Joyce B.  
 Kurland, Charles I

### Building Services and Grounds

Hayes, Joseph N., Superintendent  
 Allen, Wayne D.  
 Anderson, Lewis B.  
 Barnes, Susan M.  
 Beaudoin, Helen  
 Boucher, Richard L.  
 Bowin, Dara  
 Collins, Paul J.  
 Conlin, Henry P.  
 Dorris, John J.  
 Dutra, Roger S., Jr.  
 Gibbons, Roberto G.

Gonsalves, Walter W., Jr.  
Krajewski, Viola I.  
Lynch, Henry L.  
Mancevice, Denise M.  
Mancini, Mary  
McNamara, Noreen  
Rattacasa, Frank D.  
Sabo, Linda P.

*Plant Operations and Maintenance*

Lehy, Donald B., Superintendent  
Baldic, David P.  
Blunt, Hugh F.  
Bourgoin, Lee E.  
Carini, Robert J.  
Fish, David L., Jr.  
Gonsalves, Paul J.  
Gonsalves, Walter W., Jr.  
Hathaway, Peter J.  
Justason, C. Scott  
Lochhead, William M.  
Lunn, Alan G.  
McAdams, Herbert M. III  
Mills, Stephen A.  
Olive, Charles W., Jr.  
Schoepf, Claude  
deVeer, Robert L.

*Instrument Development Lab*

Knudson, Robert A.

*Machine Shop*

Sylvia, Frank E.

*Marme Resources Center*

Enos, Edward G., Jr., Superintendent  
Cipoletta, Charles D.  
Fisher, H. Thomas, Jr.  
Hanley, Janice S.  
Moniz, Priscilla C.  
Monteiro, Dana  
Sayers, Scott  
Sullivan, Daniel A.  
Tassinari, Eugene

*Photolab*

Golder, Linda M.  
Golder, Robert J.

*Sponsored Programs*

Garrick, Leslie D., Administrator  
Chrysler, Dorianne  
Dwane, Florence  
Huffer, Linda  
Lynch, Kathleen F.  
Price, F. Carol

*Electron Microscopy Lab*

Kerr, Louis M.

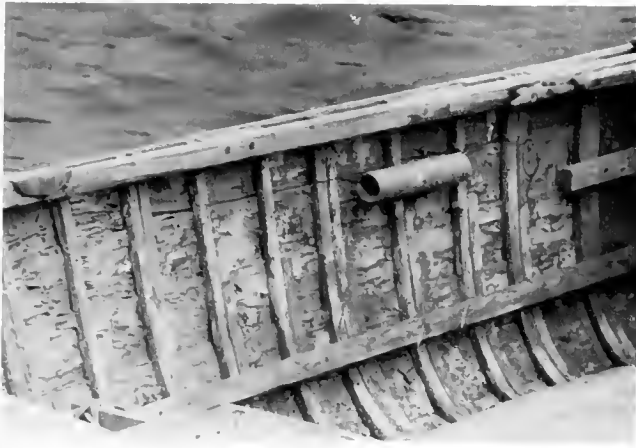
*Temporary Employees*

Cardoza, Laurie A.  
Cserny, Mary  
Elder, Peggy  
Kaufmann, Sandra J.  
Laurencot, Colette  
Lyons, Elaine D.

*Summer Support Staff*

Amon, Tyler C.  
Andrews, Ethan  
Andrews, Mark  
Balmer, Ethan  
Boyer, Cynthia  
Cadieux, C. Brian  
Cardoza, Laurie A.  
Carpenter, Mark  
Chin, Hong  
Clark, Martina  
Cloherty, Sean  
Connor, John H.  
Cutler, Laura  
DeLinks, Audrey  
DeLinks, Elizabeth  
Diachun, Peter  
Donovan, Jason P.

Fiset, Christopher  
Funkhouser, Margaret  
Galvao, Anne Marie  
Hainfeld, David  
Hammond, Jeramie  
Hibbitt, Karen  
Hoerner, Pauline  
Johnson, Paul C.  
Just, Thomas  
Kessler, Anne P.  
Kilpatrick, Brian  
Kociemba, David  
Kovac, Marc  
Krajewski, Chester  
Langton, Lori  
Lovell, Lynne  
Mansfield, Darren  
McCartney, Tegan  
McDonald, Brian  
McLeish, Elizabeth  
McNeill, Jeffrey  
Moorhouse, Laura  
Neeley, Maire  
Nelson, Beth  
Northern, Marc  
O'Connor, Patricia M.  
Regan, John F.  
Remsen, Andrew S.  
Rickles, Andrew  
Rickles, Jason  
Santos, Marcelina  
Shenandoah, Denise  
Shephard, Jennifer  
Sloboda, Aaron  
Smith, Kelli M.  
Swan, Elizabeth  
Torres, Sophie J.  
Towle, Jennifer  
Ulbrich, Ciona  
Varao, John  
Vernaglia, David  
Vogel, Augustus  
Welenc, Karen  
Wetzel, Ernest D.  
Zakaria, Pauzi



## Members of the Corporation\*

### Life Members

**Adelberg, Edward A.**, Provost's Office, Yale University, 115 Hall of Graduate Studies, New Haven, CT 06520  
**Amatnick, Ernest**, 4797 Boston Post Road, Pelham Manor, NY 10803

**Bang, Betsy G.**, 76 F.R. Lillie Road, Woods Hole, MA 02543

**Bartlett, James H.**, Department of Physics, University of Alabama, Box 870324, Tuscaloosa, AL 35487-0324

**Beams, Harold W.**, Department of Biology, University of Iowa, Iowa City, IA 52242

**Bernheimer, Alan W.**, Department of Microbiology, New York University Medical Center, 550 First Ave., New York, NY 10016

**Bertholf, Lloyd M.**, Westminster Village #2114, 2025 E. Lincoln St., Bloomington, IL 61701

**Bodian, David**, 4100 North Charles St., #913, Baltimore, MD 21218

**Bridgman, A. Josephine**, 715 Kirk Rd., Decatur, GA 30030

**Buck, John B.**, 7200 Third Ave., #C020, Sykesville, MD 21784

**Burbanck, Madeline P.**, Box 15134, Atlanta, GA 30333

**Burbanck, William D.**, Box 15134, Atlanta, GA 30333

**Clark, Arnold M.**, 53 Wilson Rd., Woods Hole, MA 02543

**Cohen, Adolph I.**, Department of Ophthalmology, Washington University School of Medicine, St. Louis, MO 63110 (resigned)

**Cohen, Seymour S.**, 10 Carrot Hill Rd., Woods Hole, MA 02543-1206

**Colwin, Arthur**, 320 Woodcrest Rd., Key Biscayne, FL 33149

**Colwin, Laura Hunter**, 320 Woodcrest, Key Biscayne, FL 33149

**Copeland, D. E.**, 41 Fern Lane, Woods Hole, MA 02543

**Corliss, John O.**, P. O. Box 53008, Albuquerque, NM 87153

**Costello, Helen M.**, Carolina Meadows, Villa 137, Chapel Hill, NC 27514

**Crouse, Helen**, Address unknown

**Dudley, Patricia L.**, Department of Biological Sciences, Barnard College, Columbia University, 3009 Broadway, New York, NY 10027

**Edwards, Charles**, 2244 Harbour Court Drive, Longboat Key, FL 34228

**Failla, Patricia M.**, 2149 Loblolly Lane, Johns Island, SC 29455

**Ferguson, James K. W.**, 56 Clarkehaven St., Thornhill, Ontario L4J 2B4 Canada

**Glusman, Murray**, 50 E. 72nd St., New York, NY 10021

**Goldman, David**, 63 Loop Rd., Falmouth, MA 02540

**Graham, Herbert**, 36 Wilson Rd., Woods Hole, MA 02543

**Green, James W.**, 409 Grant Ave., Highland Park, NJ 08904

**Grosch, Daniel S.**, 1222 Duplin Road, Raleigh, NC 27607

**Hamburger, Viktor**, Department of Biology, Washington University, St. Louis, MO 63130

**Hamilton, Howard L.**, Department of Biology, University of Virginia, 238 Gilmer Hall, Charlottesville, VA 22901

**Harding, Clifford V., Jr.**, Wayne State University School of Medicine, Department of Ophthalmology, Detroit, MI 48201

**Haschenmeyer, Audrey E. V.**, 21 Glendon Road, Woods Hole, MA 02543

**Hauschka, Theodore S.**, FD1, Box 781, Damariscotta, ME 04543

**Hisaw, F. L.**, 5925 SW Plymouth Drive, Corvallis, OR 97330

**Hubbard, Ruth**, 21 Lakeview Avenue, Cambridge, MA 02138

**Humes, Arthur G.**, Marine Biological Laboratory, Boston University Marine Program, Woods Hole, MA 02543

**Hurwitz, Charles**, Veterans Administration Hospital, Basic Science Research Laboratory, Albany, NY 12208

**Jones, Meredith L.**, Division of Worms, Museum of Natural History, Smithsonian Institution, Washington, DC 20560

**Karush, Fred**, Department of Microbiology, University of Pennsylvania School of Medicine, Philadelphia, PA 19104-6076

**Kille, Frank R.**, 1111 S. Lakemont Ave. #444, Winter Park, FL 32792

**Kingsbury, John M.**, Department of Plant Biology, Cornell University, Ithaca, NY 14853

**Kleinholz, Lewis**, Department of Biology, Reed College, 3203 SE Woodstock Blvd., Portland, OR 97202

**Laderman, Ezra**, Yale University, School of Music, New Haven, CT 06520

**Lauffer, Max A.**, Address unknown

**LeFevre, Paul G.**, 15 Agassiz Road, Woods Hole, MA 02543

**Levine, Rachmiel**, 2024 Canyon Rd., Arcadia, CA 91006

**Lochhead, John H.**, 49 Woodlawn Rd., London SW6 6PS, England, UK

**Loewus, Frank A.**, Washington State University, Institute of Biological Chemistry, Pullman, WA 99164

**Lofffield, Robert B.**, Department of Chemistry, University of New Mexico School of Medicine, Albuquerque, NM 87131

\* Including action of the 1992 Annual Meeting.



**Magruder, Samuel R.**, 270 Cedar Lane, Paducah, KY 42001  
**Malkiel, Saul**, Allergic Diseases, Inc., 130 Lincoln St., Worcester, MA 01609  
**Mathews, Rita W.**, Box 131, Southfield, MA 01259  
**Miller, James A.**, 307 Shorewood Drive, E. Falmouth, MA 02536  
**Moore, John A.**, Department of Biology, University of California, Riverside, CA 92521  
**Moscona, Arthur A.**, University of Chicago, Department of Molecular Genetics and Cell Biology, 920 East 58th Street, Chicago, IL 60637  
**Mullins, Lorin J.**, University of Maryland School of Medicine, Department of Biophysics, Baltimore, MD 21201

**Nasatir, Maimon, P. O. Box 379, Ojai, CA 93024-0379**

**Pollister, A. W.**, 8 Euclid Ave., Belle Mead, NJ 08502  
**Prosser, C. I. add**, Department of Physiology and Biophysics, Burrill Hall 524, University of Illinois, Urbana, IL 61801  
**Provasoli, Luigi**, Via Stazione 43, 21025 Comerio (VA), Italy  
**Prytz, Margaret McDonald**, Address unknown

**Ratner, Sarah**, Department of Biochemistry, Public Health Research Institute, 455 First Ave., New York, NY 10016  
**Renn, Charles E.**, Address unknown  
**Reynolds, George**, Department of Physics, Princeton University, Jadwin Hall, Princeton, NJ 08544  
**Rice, Robert V.**, 30 Burnham Dr., Falmouth, MA 02540  
**Richards, A. Glenn**, 942 Cromwell Ave., St. Paul, MN 55114  
**Rockstein, Morris**, 600 Biltmore Way, Apt. 805, Coral Gables, FL 33134  
**Ronkin, Raphael R.**, 3212 McKinley St., NW, Washington, DC 20015  
**Rose, S. Meryl**, 32 Crosby Ln., E. Falmouth, MA 02536

**Sanders, Howard**, Woods Hole Oceanographic Institution, Woods Hole, MA 02543  
**Sato, Hidemi**, Faculty of Social Science, Nagano University, Shiminogo, Ueda, Nagano 386-12, Japan  
**Scharrer, Berta**, Department of Anatomy, Albert Einstein College of Medicine, 1300 Morris Park Avenue, Bronx, NY 10461  
**Schlesinger, R. Walter**, University of Medicine and Dentistry of New Jersey, Department of Molecular Genetics and Microbiology, Robert Wood Johnson Medical School, Piscataway, NJ 08854-5635  
**Schmitt, F. O.**, Room 16-512, Massachusetts Institute of Technology, Cambridge, MA 02139  
**Scott, Allan C.**, 1 Nudd St., Waterville, ME 04901  
**Silverstein, Arthur M.**, The Johns Hopkins Hospital Wilmer Institute, Baltimore, MD 21205  
**Smith, Homer P.**, 8 Quissett Ave., Woods Hole, MA 02543  
**Smith, Paul F.**, P. O. Box 264, Woods Hole, MA 02543  
**Sonnenblick, B. P.**, 515A Heritage Hill, Southbury, CT 06488  
**Steinhardt, Jacinto**, 1508 Spruce St., Berkeley, CA 94709  
**Stephens, Grover C.**, Department of Ecology & Evolutionary Biology, School of Biological Sciences, University of California, Irvine, CA 92717

**Taylor, Robert E.**, 20 Harbor Hill Rd., Woods Hole, MA 02543  
**Trager, William**, The Rockefeller University, 1230 York Ave., New York, NY 10021

**Villee, Claude A.**, Harvard Medical School, Parcel B/Room 122, 25 Shattuck Street, Boston, MA 02115  
**Vincent, Walter S.**, 16 F.R. Lillie Rd., Woods Hole, MA 02543

**Wald, George**, 21 Lakeview Ave., Cambridge, MA 02138  
**Waterman, T. H.**, Yale University, Biology Department, Box 6666, New Haven, CT 06511

**Wichterman, Ralph**, 31 Buzzards Bay Ave., Woods Hole, MA 02543  
**Wiercinski, Floyd J.**, 21 Glenview Road, Glenview, IL 60025  
**Wigley, Roland L.**, 35 Wilson Rd., Woods Hole, MA 02543  
**Wilber, Charles G.**, Department of Biology, Colorado State University, Fort Collins, CO 80523

**Zinn, Donald J.**, Department of Zoology, University of Rhode Island, Kingston, RI 02881  
**Zorzoli, Anita**, 18 Wilbur Blvd., Poughkeepsie, NY 12603  
**Zweifach, Benjamin W.**, 8811 Nottingham Place, La Jolla, CA 92037

## *Regular Members*

**Abt, Donald A.**, Marine Biological Laboratory, Laboratory for Marine Animal Health, Woods Hole, MA 02543  
**Acheson, George H.**, 25 Quissett Ave., Woods Hole, MA 02543  
**Adams, James A.**, Department of Natural Sciences, University of Maryland, Eastern Shore, Princess Anne, MD 21853  
**Adelberg, Edward A.**, Provost's Office, 115 Hall of Graduate Studies, Yale University, New Haven, CT 06520  
**Adelman, William J., Jr.**, 160 Locust St., Falmouth, MA 02540  
**Afzelius, Bjorn**, Address unknown  
**Alberte, Randall S.**, Department of Molecular Genetics and Cell Biology, University of Chicago, 1103 E. 57th Street, Chicago, IL 60637  
**Alkon, Daniel**, NINCDS/NIH, Dept. LMNC, Bldg. Park, Rm. 431, Bethesda, MD 20852  
**Allen, Garland E.**, Department of Biology, Washington University, Box 1137, One Brookings Drive, St. Louis, MO 63130-4899  
**Allen, Nina S.**, Department of Biology, Wake Forest University, Box 7325, Winston-Salem, NC 27109  
**Amatnick, Ernest**, 4797 Boston Post Rd., Pelham Manor, NY 10803  
**Anderson, Everett**, Department of Anatomy & Cell Biology, LHRRB, Harvard Medical School, 45 Shattuck St., Boston, MA 02115  
**Anderson, J. M.**, 110 Roat St., Ithaca, NY 14850  
**Anderson, Porter W.**, Department of Pediatrics, University of Rochester Medical Center, Box 690, 601 Elmwood Ave., Rochester, NY 14642  
**Armett-Kibel, Christine**, Dean of Science Faculty, University of Massachusetts, Boston, MA 02125  
**Armstrong, Clay M.**, Department of Physiology, University of Pennsylvania Medical School, Philadelphia, PA 19104-8725  
**Armstrong, Peter B.**, Department of Zoology, University of California, Davis, CA 95616  
**Arnold, John M.**, Pacific Biomedical Research Center, 209A Snyder Hall, University of Hawaii, Honolulu, HI 96822  
**Arnold, William A.**, 102 Balsam Rd., Oak Ridge, TN 37830  
**Ashton, Robert W., Esq.**, Bay Foundation, Eikenberry and Schoolman, 99 Wall St., New York, NY 10005  
**Atema, Jelle**, Boston University Marine Program, Marine Biological Laboratory, Woods Hole, MA 02543  
**Atwood, Kimball C., III**, P. O. Box 673, Woods Hole, MA 02543 (deceased)  
**Augustine Jr., George J.**, Department of Neurobiology, Duke University Medical Center, Durham, NC 27710  
**Ayers, Donald E.**, 4607 1/2 MacArthur Blvd., NW #B, Washington, DC 20007-2533

**Baccetti, Baccio**, Institute of Zoology, University of Siena, 53100 Siena, Italy  
**Baker, Robert G.**, Department of Physiology and Biophysics, New York University Medical Center, 550 First Ave., New York, NY 10016

- Baldwin, Thomas O.**, Department of Biochemistry and Biophysics, Texas A&M University, College Station, TX 77843
- Barlow, Robert B., Jr.**, Institute for Sensory Research, Syracuse University, Merrill Lane, Syracuse, NY 13244-5290
- Barry, Daniel T.**, 1014 Barren Ridge Drive, Seabrook, TX 77586-4002
- Barry, Susan R.**, Department of Physical Medicine and Rehabilitation, ID204, University of Michigan Hospital, Ann Arbor, MI 48109-0042
- Bartell, Clelmer K.**, 2000 Lake Shore Drive, New Orleans, LA 70122
- Bass, Andrew H.**, Seely Mudd Hall, Department of Neurobiology, Cornell University, Ithaca, NY 14853
- Battelle, Barbara-Anne**, Whitney Laboratory, University of Florida, 9505 Ocean Shore Blvd., St. Augustine, FL 32086
- Bauer, G. Eric**, Department of Anatomy, University of Minnesota, Minneapolis, MN 55455
- Bay, Frederick**, Bay Foundation, 99 Wall St., 18th Fl., New York, NY 10005
- Baylor, Edward R.**, P. O. Box 93, Woods Hole, MA 02543
- Baylor, Martha B.**, P. O. Box 93, Woods Hole, MA 02543
- Beams, Harold W.**, Department of Biology, University of Iowa, Iowa City, IA 52242 (deceased)
- Bearer, Elaine L.**, Division of Biology & Medicine, Department of Pathology, Brown University, Box G, Providence, RI 02912
- Beauge, Luis Alberto**, Department of Biophysics, Instituto M.y.M. Ferreyra, Casilla de Correo 389, 5000 Cordoba, Argentina
- Beck, Lyle V.**, 2455 Tamarack Trail, Apt. 8, Bloomington, IN 47408
- Begenisich, Ted**, Department of Physiology, University of Rochester, Medical Center, Box 642, 601 Elmwood Ave., Rochester, NY 14642
- Begg, David A.**, Department of Anatomy & Cell Biology, University of Alberta, Edmonton, Alberta T6G 2H7, Canada
- Bell, Eugene**, Marine Biological Laboratory, Tissue Engineering, Inc., Woods Hole, MA 02543
- Benjamin, Thomas L.**, Department of Pathology, Harvard Medical School, 25 Shattuck St., Boston, MA 02115
- Bennett, M. V. L.**, Albert Einstein College of Medicine, Department of Neuroscience, 1410 Pelham Pkwy. S., Bronx, NY 10461
- Bennett, Miriam F.**, Department of Biology, Colby College, Waterville, ME 04901
- Berg, Carl J., Jr.**, P. O. Box 769, Kilauea, Kauai, HI 96754-0769
- Berlin, Suzanne T.**, 5 Highland St., Gloucester, MA 01930
- Berne, Robert M.**, Department of Physiology, University of Virginia, School of Medicine, Charlottesville, VA 22908
- Bernstein, Norman**, Diane and Norman Bernstein Foundation, Inc., 5301 Wisconsin Ave., #600, Washington, DC 20015-2015
- Bezanilla, Francisco**, Department of Physiology, University of California, Los Angeles, CA 90024
- Biggers, John D.**, Department of Physiology, Harvard Medical School, Boston, MA 02115
- Bishop, Stephen H.**, Department of Zoology, Iowa State University, Ames, IA 50010
- Blaustein, Mordecai P.**, Department of Physiology, School of Medicine, University of Maryland, 655 W. Baltimore Street, Baltimore, MD 21201
- Blennemann, Dieter**, Carl Zeiss, Inc., One Zeiss Drive, Thornwood, NY 10594
- Bloom, George S.**, Department of Cell Biology and Neuroscience, The University of Texas Southwestern Medical Center, 5223 Harry Hines Blvd., Dallas, TX 75235-9039
- Bloom, Kerry S.**, Department of Biology, University of North Carolina, Wilson Hall, CB#3280, Chapel Hill, NC 27599-3280
- Bodznick, David A.**, Department of Biology, Wesleyan University, Lawn Avenue, Middletown, CT 06457
- Boettiger, Edward G.**, 29 Juniper Point, Woods Hole, MA 02543
- Booolotian, Richard A.**, Science Software Systems, Inc., 3576 Woodcliff Rd., Sherman Oaks, CA 91403
- Borgese, Thomas A.**, Department of Biology, Lehman College, CUNY, Bedford Park Blvd., West, Bronx, NY 10468
- Borisy, Gary G.**, Laboratory of Molecular Biology, University of Wisconsin, Madison, WI 53706
- Borst, David W., Jr.**, Department of Biological Sciences, Illinois State University, Normal, IL 61761-6901
- Bosch, Herman F.**, Box 617, Woods Hole, MA 02543
- Bowles, Francis P.**, P. O. Box 674, Woods Hole, MA 02543
- Boyer, Barbara C.**, Department of Biology, Union College, Schenectady, NY 12308
- Brandhorst, Bruce P.**, Department of Biological Sciences, Simon Fraser University, Barnaby, BC V5A 1S6, Canada
- Brinley, F. J.**, Neurological Disorders Program, NINCDS, NIH, 812 Federal Building, Bethesda, MD 20892
- Brown, Joel E.**, Albert Einstein College of Medicine, 506 Kennedy Center, 1400 Pelham Parkway, Bronx, NY 10461
- Brown, Stephen C.**, Department of Biological Sciences, SUNY, Albany, NY 12222
- Brown, William L.**, Retired Chairman, Bank of Boston (01-23-11), 100 Federal St., Boston, MA 02106-2016
- Browne, Carole L.**, Department of Biology, Wake Forest University, Winston-Salem, NC 27109
- Browne, Robert A.**, Department of Biology, Wake Forest University, Box 7325, Winston-Salem, NC 27109
- Bryant, Shirley H.**, Department of Pharmacology and Cell Biophysics, ML 575, University of Cincinnati, Cincinnati, OH 45267
- Bucklin, Anne C.**, Marine Biological Laboratory, Woods Hole, MA 02543
- Bullis, Robert A.**, Marine Biological Laboratory, Woods Hole, MA 02543
- Burd, Gail Deerin**, Department of Molecular and Cell Biology, Life Sciences South, Rm 444, University of Arizona, Tucson, AZ 85721
- Burdick, Carolyn J.**, Department of Biology, Brooklyn College, Bedford Avenue & Avenue H, Brooklyn, NY 11210
- Burger, Max**, Friedrich Miesner Institut Bau 1060 Postfach 2543, Basel 4002, Switzerland
- Burgos, Mario**, IHEM Medical School, UNC Conicet, Casilla de Correo 56, 5500 Mendoza, Argentina
- Burky, Albert**, Department of Biology, University of Dayton, Dayton, OH 45469
- Burris, John E.**, Marine Biological Laboratory, Woods Hole, MA 02543
- Burstyn, Harold L.**, Morrison Law Firm, The Morrison Building, 145 North Fifth Avenue, Mt. Vernon, NY 10550
- Bursztajn, Sherry**, Harvard Medical School, Mailman Research Center, 115 Mill St., Belmont, MA 02178
- Busa, William**, Department of Biology, Johns Hopkins University, 3400 N. Charles St., Baltimore, MD 21218
- Calabrese, Ronald L.**, Department of Biology, Emory University, 1555 Pierce Drive, Atlanta, GA 30322
- Callaway, Joseph C.**, Department of Physiology, New York Medical College, Basic Sciences Bldg., Valhalla, NY 10595
- Cameron, Andrew**, Department of Biology, California Institute of Technology, Pasadena, CA 91125
- Campbell, Richard H.**, Bang-Campbell Associates, Box 47, Woods Hole, MA 02543
- Candelas, Graciela C.**, Department of Biology, University of Puerto Rico, Rio Piedras, PR 00931
- Carew, Thomas J.**, Department of Psychology, Yale University, P. O. Box 11A, Yale Station, New Haven, CT 06520
- Cariello, Lucio**, Biochemistry Department, Stazione Zoologica, Villa Comunale, 80121 Naples, Italy

- Carlson, Francis D.**, Biophysics Department, The Johns Hopkins University, N. Charles St., Baltimore, MD 21218
- Carriere, Rita M.**, Department of Anatomy and Cell Biology, Box 5, SUNY Health Science Center, 450 Clark Ave., Brooklyn, NY 11203
- Case, James**, University of California, Vice Chancellor of Research, Santa Barbara, CA 93106
- Cassidy, Rev. J. D.**, Providence College, Dept. of St. Thomas Aquinas, Providence, RI 02918
- Cavanaugh, Colleen M.**, Harvard University, Biological Laboratories, 16 Divinity Ave., Cambridge, MA 02138
- Cebra, John J.**, Department of Biology, Leidy Labs, G-6, University of Pennsylvania, Philadelphia, PA 19174
- Chaet, Alfred B.**, University of West Florida, Pensacola, FL 32504
- Chambers, Edward L.**, Department of Physiology and Biophysics, University of Miami, School of Medicine, P. O. Box 016430, Miami, FL 33101
- Chang, Donald C.**, Department of Physiology, Baylor College of Medicine, One Baylor Plaza, Houston, TX 77030
- Chappell, Richard L.**, Department of Biological Sciences, Hunter College, Box 210, 695 Park Ave., New York, NY 10021
- Chauncey, Howard H.**, 30 Falmouth St., Wellesley Hills, MA 02181 (deceased)
- Chen, Thomas T.**, Center for Marine Biotechnology, University of Maryland, 600 E. Lombard St., Baltimore, MD 21202
- Chikarmane, Hemant M.**, Marine Biological Laboratory, Woods Hole, MA 02543
- Child, Frank M., III**, Department of Biology, Trinity College, Hartford, CT 06106
- Chisholm, Rex L.**, Department of Cell Biology, Northwestern University Medical School, Chicago, IL 60611
- Citkowitz, Elena**, 410 Livingston St., New Haven, CT 06511
- Clark, Eloise E.**, Vice President, Bowling Green State University, Bowling Green, OH 43403
- Clark, Hays**, 26 Deer Park Drive, Greenwich, CT 06830
- Clark, James M.**, 210 Emerald Lane, Palm Beach, FL 33480
- Clark, Wallis H., Jr.**, Bodega Marine Laboratory, P. O. Box 247, Bodega Bay, CA 94923
- Claude, Philippa**, Primate Center, Capitol Court, Madison, WI 53706
- Clay, John R.**, Laboratory of Biophysics, NIH, Building 9, Room 1E-124, Bethesda, MD 20892
- Clowes, Alexander W.**, Department of Surgery RF-25, University of Washington School of Medicine, Seattle, WA 98195
- Clutter, Mary**, Office of the Director, Room 518, National Science Foundation, Washington, DC 20550
- Cobb, Jewel Plummer**, California State University, 5151 State University Drive, Los Angeles, CA 90032-8500
- Cohen, Avis H.**, Section of Neurobiology and Behavior, Mudd Hall, Cornell University, Ithaca, NY 14853-2702 (resigned)
- Cohen, Carolyn**, Rosenstiel Basic Medical Sciences Research Center, Brandeis University, Waltham, MA 02254
- Cohen, Lawrence B.**, Department of Physiology, Yale University School of Medicine, 333 Cedar Street, New Haven, CT 06510-8026
- Cohen, Maynard**, Department of Neurological Sciences, Rush Medical College, 600 South Paulina, Chicago, IL 60612
- Cohen, Rochelle S.**, Department of Anatomy, University of Illinois, 808 W. Wood Street, Chicago, IL 60612
- Cohen, William D.**, Department of Biological Sciences, Hunter College, 695 Park Ave., Box 79, New York, NY 10021
- Coleman, Annette W.**, Division of Biology and Medicine, Brown University, Providence, RI 01912
- Collier, Jack R.**, Department of Biology, Brooklyn College, Bedford & Avenue H, Brooklyn, NY 11210
- Collier, Marjorie McCann**, Biology Department, Saint Peter's College, 2641 Kennedy Boulevard, Jersey City, NJ 07306
- Cook, Joseph A.**, The Edna McConnell Clark Foundation, 250 Park Ave., New York, NY 10017
- Cooperstein, S. J.**, University of Connecticut Health Center, Department of Anatomy, Farmington Ave., Farmington, CT 06032
- Cornell, Neal W.**, Marine Biological Laboratory, Woods Hole, MA 02543
- Cornwall, Melvin C., Jr.**, Department of Physiology L714, Boston University School of Medicine, 80 E. Concord St., Boston, MA 02118
- Corson, David Wesley, Jr.**, 516 Rice Hope Dr., Mt. Pleasant, SC 29464-9296
- Corwin, Jeffrey T.**, Department of Otolaryngology, University of Virginia Medical Center, Box 430, Charlottesville, VA 22908
- Costello, Walter J.**, Department of Zoology Z/BS, College of Medicine, Ohio University, Athens, OH 45701
- Couch, Ernest F.**, Department of Biology, Texas Christian University, Fort Worth, TX 76129
- Cox, Martha**, William C. Cox Foundation, 190 South Beach Road, Hobe Sound, FL 33455
- Crane, Sylvia E.**, 438 Wendover Drive, Princeton, NJ 08540
- Cremer-Bartels, Gertrud**, Universitats Augenklinik, 44 Munster, Germany
- Crow, Terry J.**, Department of Neurobiology and Anatomy, University of Texas Medical School, Houston, TX 77225
- Crowell, Sears**, Department of Biology, Indiana University, Bloomington, IN 47405
- Crowther, Robert**, Department of Biology, University of New Brunswick, BS 45111, Fredericton, NB, Canada E3B 6E1
- Cunningham, Mary-Ellen**, 62 Cloverly Road, Grosse Pointe Farms, MI 48236
- Currier, David L.**, P. O. Box 2476, Vineyard Haven, MA 02568
- Cutler, Richard**, Marine Biological Laboratory, Woods Hole, MA 02543
- D'Alessio, Giuseppe**, Department of Organic & Biological Chemistry, University of Naples, Via Mezzocannone 16, Naples, Italy 80134
- D'Avanzo, Charlene**, School of Natural Science, Hampshire College, Amherst, MA 01002
- Daignault, Alexander T.**, 29 Quisset Harbor Rd., Falmouth, MA 02540
- Dan, Katsuma**, Tokyo Metropolitan Union, 1-1 Minami-Osawa, Hachioji City 192-03, Japan
- David, John R.**, Tropical Public Health, Harvard School of Public Health, 665 Huntington Ave., Boston, MA 02115
- Davidson, Eric H.**, Division of Biology, 156-29, California Institute of Technology, Pasadena, CA 91125
- Davis, Bernard D.**, Bacterial Physiology Unit, Harvard Medical School, Boston, MA 02115
- Davis, Joel P.**, Seapuit, Inc., P. O. Box G, Osterville, MA 02655
- Daw, Nigel W.**, 5 Old Pawson Rd., Branford, CT 06405
- Deegan, Linda A.**, The Ecosystems Center, Marine Biological Laboratory, Woods Hole, MA 02543
- DeGroof, Robert C.**, 145 Water Crest Dr., Doylestown, PA 18901
- DeHaan, Robert L.**, Department of Anatomy and Cell Biology, Emory University School of Medicine, Atlanta, GA 30322
- DeLanney, Louis E.**, Institute for Medical Research, 2260 Clove Drive, San Jose, CA 95128
- Denkla, Marth B.**, Kennedy-Krieger Institute, Johns Hopkins School of Medicine, 707 North Broadway, Baltimore, MD 21205
- Dentler, William L.**, Department of Physiology & Cell Biology, University of Kansas, 4011 Haworth Hall, Lawrence, KS 66044
- DePhillips, Henry A., Jr.**, Department of Chemistry, Trinity College, 300 Summit Street, Hartford, CT 06106
- DeSimone, Douglas W.**, Department of Anatomy and Cell Biology, Box 439, Health Sciences Center, University of Virginia, Charlottesville, VA 22908

- DeToledo-Morrell, Leyla**, Department of Neurological Sciences, Rush Medical College, Chicago, IL 60612
- Dettbarn, Wolf-Dietrich**, Department of Pharmacology, School of Medicine, Vanderbilt University, Nashville, TN 37127
- De Weer, Paul J.**, Department of Physiology, University of Pennsylvania School of Medicine, Philadelphia, PA 19104-6085
- Dixon, Keith E.**, School of Biological Sciences, Flinders University, Bedford Park, 5042, South Australia, Australia
- Dowling, John E.**, The Biological Laboratories, Harvard University, 16 Divinity St., Cambridge, MA 02138
- DuBois, Arthur Brooks**, John B. Pierce Foundation Laboratory, 290 Congress Ave., New Haven, CT 06519
- Duncan, Thomas K.**, Department of Environmental Sciences, Nichols College, Dudley, MA 01570
- Dunham, Philip B.**, Department of Biology, Syracuse University, Syracuse, NY 13244
- Dunlap, Kathleen**, Department of Physiology, Tufts University Medical School, Boston, MA 02111
- Dunlap, Paul V.**, Department of Biology, Woods Hole Oceanographic Institution, Redfield 316, Woods Hole, MA 02543
- Dworkin, Martin**, Department of Microbiology, University of Minnesota, 1460 Mayo Bldg., Box 196 UMHC, Minneapolis, MN 55455-0312
- Ebert, James D.**, Department of Biology, The Johns Hopkins University, 213 Macaulay Hall, Baltimore, MD 21218
- Eckberg, William R.**, Department of Zoology, Howard University, Washington, DC 20059
- Edds, Kenneth T.**, Department of Anatomical Sciences, SUNY, Buffalo, NY 14214
- Eder, Howard A.**, Albert Einstein College of Medicine, 1300 Morris Park Ave., Bronx, NY 10461
- Edstrom, Joan**, 2515 Milton Hills Dr., Charlottesville, VA 22901
- Egynd, Laszlo G.**, 18 Skyview, Newton, MA 02150
- Ehrlich, Barbara E.**, Division of Cardiology, University of Connecticut Health Center, 263 Farmington Avenue, Farmington, CT 06030
- Eisen, Arthur Z.**, Division of Dermatology, Washington University, St. Louis, MO 63110
- Eisen, Herman N.**, Massachusetts Institute of Technology, E17-128, 77 Massachusetts Ave., Cambridge, MA 02139
- Elder, Hugh Young**, Institute of Physiology, University of Glasgow, Glasgow, Scotland G12 8QQ
- Elliott, Gerald F.**, The Open University Research Unit, Foxcombe Hall, Berkeley Rd., Boars Hill, Oxford, England OX1 5HR
- Englund, Paul T.**, Department of Biological Chemistry, Johns Hopkins School of Medicine, Baltimore, MD 21205
- Epel, David**, Hopkins Marine Station, Pacific Grove, CA 93950
- Epstein, Herman T.**, 18 Lawrence Farm Road, Woods Hole, MA 02543
- Epstein, Ray L.**, 30 Coonamessett Circle, Falmouth, MA 02540
- Erulkar, Solomon D.**, 318 Kent Rd., Bala Cynwyd, PA 19004
- Essner, Edward S.**, Kresge Eye Institute, Wayne State University, 540 E. Canfield Ave., Detroit, MI 48201 (resigned)
- Farb, David H.**, Department of Pharmacology L603, Boston University School of Medicine, Boston, MA 02118
- Farmanfarmaian, A.**, Department of Biological Sciences, Nelson Biological Laboratory, Rutgers University, Piscataway, NJ 08855
- Fein, Alan**, Department of Physiology, University of Connecticut Health Center, Farmington, CT 06032
- Feinman, Richard D.**, Box 8, Department of Biochemistry, SUNY Health Science Center, 450 Clarkson Avenue, Brooklyn, NY 11203
- Feldman, Susan C.**, Department of Anatomy, University of Medicine and Dentistry of New Jersey, New Jersey Medical School, 100 Bergen St., Newark, NJ 07103
- Fessenden, Jane**, 225 Lakeview Ave., Falmouth, MA 02540
- Festoff, Barry W.**, Neurology Service (127), Veterans Administration Medical Center, 4801 Linwood Blvd., Kansas City, MO 64128
- Fink, Rachel D.**, Department of Biological Sciences, Clapp Laboratory, Mount Holyoke College, South Hadley, MA 01075
- Finkelstein, Alan**, Albert Einstein College of Medicine, 1300 Morris Park Ave., Bronx, NY 10461
- Fischbach, Gerald**, Department of Neurobiology, Harvard Medical School, 220 Longwood Ave., Boston, MA 02115
- Fishman, Harvey M.**, Department of Physiology and Biophysics, University of Texas Medical Branch, Galveston, TX 77550
- Flanagan, Dennis**, 12 Gay St., New York, NY 10014
- Fluck, Richard Allen**, Department of Biology, Franklin & Marshall College, Box 3003, Lancaster, PA 17604-3003
- Foreman, K. II.**, Boston University Marine Program, Marine Biological Laboratory, Woods Hole, MA 02543
- Fox, Thomas Oren**, Division of Medical Sciences, Harvard Medical School, 260 Longwood Ave., Boston, MA 02115
- Franzini-Armstrong, Clara**, School of Medicine, University of Pennsylvania, 330 S. 46th Street, Philadelphia, PA 19143
- Frazier, Donald T.**, Department of Physiology and Biophysics, University of Kentucky Medical Center, Lexington, KY 40536
- French, Robert J.**, Health Sciences Center, University of Calgary, Calgary, Alberta, T2N 4N1, Canada
- Freygang, Walter J., Jr.**, 6247 29th St., NW, Washington, DC 20015 (resigned)
- Friedler, Gladys**, Boston University School of Medicine, 80 East Concord Street, Boston, MA 02118
- Fry, Brian**, Marine Biological Laboratory, Woods Hole, MA 02543
- Fulton, Chandler M.**, Department of Biology, Brandeis University, Waltham, MA 02254
- Furshpan, Edwin J.**, Department of Neurophysiology, Harvard Medical School, Boston, MA 02115
- Futrelle, Robert P.**, College of Computer Science, Northeastern University, 360 Huntington Avenue, Boston, MA 02115
- Gabriel, Mordecai**, Department of Biology, Brooklyn College, Brooklyn, NY 11210
- Gadsby, David C.**, Laboratory of Cardiac Physiology, The Rockefeller University, 1230 York Avenue, New York, NY 10021
- Gainer, Harold**, Lab of Functional Neurochemistry, NIH, Bldg. 36, Room 4D-20, Bethesda, MD 20892
- Galatzer-Levy, Robert M.**, 180 N. Michigan Avenue, Chicago, IL 60601
- Gall, Joseph G.**, Carnegie Institution, 115 West University Parkway, Baltimore, MD 21210
- Gallant, Paul E.**, NIH, Bldg. 36, Rm. 2A-29, Bethesda, MD 20892
- Garber, Sarah S.**, Department of Physiology, Medical College of Pennsylvania, 2900 Queen Ln., Philadelphia, PA 19129
- Gascoyne, Peter**, Box 85E, University of Texas, M. D. Anderson Hospital and Tumor Institute, 6723 Bertner Avenue, Houston, TX 77030
- Gelperin, Alan**, Department of Biophysics, AT&T Bell Labs, Room 1C464, 600 Mountain Avenue, Murray Hill, NJ 07974
- German, James L., III**, Lab of Human Genetics, The New York Blood Center, 310 East 67th St., New York, NY 10021
- Gibbs, Martin**, Institute for Photobiology of Cells and Organelles, Brandeis University, Waltham, MA 02254
- Giblin, Anne E.**, Ecosystems Center, Marine Biological Laboratory, Woods Hole, MA 02543

- Gibson, A. Jane**, Department of Biochemistry, Cornell University, Ithaca, NY 14850
- Gifford, Prosser**, 540 N Street, SW, S-903, Washington, DC 20024
- Gilbert, Daniel L.**, Clinical Neuroscience Branch, NINDS, Bldg. 9, Room 1E-124, Bethesda, MD 20892
- Giudice, Giovanni**, Dipartimento di Biologia Evoluzionale e Dello Sviluppo, I-90123, Via Archirafi 21, Università di Palermo, Palermo, Italy
- Giuditta, Antonio**, Department of Animal Physiology, University of Naples, Via Mezzocannone 84, Naples, Italy 80134
- Glynn, Paul**, 2770 Beechwood, Pittsburgh, PA 15217
- Golden, William T.**, American Museum of Natural History, 40 Wall St., Room 4201, New York, NY 10005
- Goldman, Robert D.**, Department of Cell, Molecular and Structural Biology, Northwestern University, 303 E. Chicago Ave., Chicago, IL 60611
- Goldsmith, Paul K.**, NIH, Bldg. 10, Room 9C-101, Bethesda, MD 20892
- Goldsmith, Timothy H.**, Department of Biology, Yale University, New Haven, CT 06510
- Goldstein, Moise H., Jr.**, ECE Department, Barton Hall, Johns Hopkins University, Baltimore, MD 21218
- Goodman, Lesley Jean**, Department of Biological Sciences, Queen Mary College, Mile End Road, London, E1 4NS, England, UK
- Gould, Robert Michael**, Institute for Basic Research in Developmental Disabilities, 1050 Forest Hill Rd., Staten Island, NY 10314
- Gould, Stephen J.**, Museum of Comparative Zoology, Harvard University, Cambridge, MA 02138
- Govind, C. K.**, Life Sciences Division, University of Toronto, 1265 Military Trail, West Hill, Ontario, M1C 1A4, Canada
- Graf, Werner**, Rockefeller University, 1230 York Ave., New York, NY 10021
- Grant, Philip**, 2939 Van Ness Street, N.W., Apt. 302, Washington, DC 20008
- Grass, Ellen R.**, The Grass Foundation, 77 Reservoir Rd., Quincy, MA 02170
- Grassle, Judith**, Institute of Marine & Coastal Studies, Rutgers University, Box 231, New Brunswick, NJ 08903
- Graubard, Katherine**, Department of Zoology, NJ-15, University of Washington, Seattle, WA 98195
- Greenberg, Everett Peter**, Department of Microbiology, College of Medicine, University of Iowa, Iowa City, IA 52242
- Greenberg, Michael J.**, Whitney Laboratory, 9505 Ocean Shore Blvd., St. Augustine, FL 32086-8623
- Greer, Mary J.**, 16 Hillside Ave., Cambridge, MA 02140
- Griffin, Donald R.**, Concord Field Station, Harvard University, Old Causeway Road, Bedford, MA 01730
- Gross, Paul R.**, Center for Advanced Studies, University of Virginia, 444 Cabell Hall, Charlottesville, VA 22903
- Grossman, Albert**, New York University Medical Center, 550 First Ave., New York, NY 10016
- Grossman, Lawrence**, Department of Biochemistry, Johns Hopkins University, 615 North Wolfe Street, Baltimore, MD 21205
- Gruner, John**, Cephalon, Inc., 145 Brandywine Parkway, W. Chester, PA 19380-4245
- Gunning, A. Robert**, P. O. Box 165, Falmouth, MA 02541
- Gwilliam, G. P.**, Department of Biology, Reed College, Portland, OR 97202
- Haimo, Leah**, Department of Biology, University of California, Riverside, CA 92521
- Hall, Linda M.**, Department of Biochemistry and Pharmacology, SUNY, 317 Hochstetter, Buffalo, NY 14260
- Hall, Zack W.**, Department of Physiology, University of California, San Francisco, CA 94143
- Halvorson, Harlyn O.**, 26 Fay Road, Woods Hole, MA 02543
- Hamlett, Nancy V.**, Department of Biology, Harvey Mudd College, 301 E. 12th St., Claremont, CA 91711
- Haneji, Tatsuji**, Chiba University Medical School, 1-8-1, Inohana, Chiba, 280, Japan
- Hanna, Robert B.**, College of Environmental Science and Forestry, SUNY, Syracuse, NY 13210
- Harosi, Ferenc L.**, Laboratory of Sensory Physiology, Marine Biological Laboratory, Woods Hole, MA 02543
- Harrigan, June F.**, 7415 Makaa Place, Honolulu, HI 96825
- Harrington, Glenn W.**, Division of Cell Biology and Biophysics, 403 Biological Sciences Building, University of Missouri, Kansas City, MO 64110
- Harris, Andrew L.**, Department of Biophysics, Johns Hopkins University, 34th & Charles Sts., Baltimore, MD 21218
- Hastings, J. W.**, The Biological Laboratories, Harvard University, 16 Divinity Street, Cambridge, MA 02138
- Hayashi, Teru**, 7105 SW 112 Place, Miami, FL 33173
- Haydon-Baillie, Wensley G.**, Porton Int., 2 Lowndes Place, London, SW1X 8DD, England, UK
- Hayes, Raymond L., Jr.**, Department of Anatomy, Howard University, College of Medicine, 520 W St., NW, Washington, DC 20059
- Hepler, Peter K.**, Department of Botany, University of Massachusetts, Amherst, MA 01003
- Herndon, Walter R.**, University of Tennessee, Department of Botany, Knoxville, TN 37996-1100
- Herskovits, Theodore T.**, Department of Chemistry, Fordham University, John Mulcahy Hall, Room 638, Bronx, NY 10458
- Hiatt, Howard H.**, Department of Medicine, Brigham and Women's Hospital, 75 Francis Street, Boston, MA 02115
- Highstein, Stephen M.**, Department of Otolaryngology, Washington University School of Medicine, St. Louis, MO 63110
- Hildebrand, John G.**, Arizona Research Laboratories, Division of Neurobiology, 603 Gould-Simpson Science Building, University of Arizona, Tucson, AZ 85721
- Hill, Richard W.**, Department of Zoology, Michigan State University, E. Lansing, MI 48824
- Hill, Susan D.**, Department of Zoology, Michigan State University, E. Lansing, MI 48824
- Hillis Llewellya**, Smithsonian Tropical Research Institute, Unit 0948 APO-AA, Miami, FL 34002-0948
- Hillman, Peter**, Department of Biology, Life Sciences & Neurobiology, Hebrew University, Jerusalem 91904, Israel
- Hinegardner, Ralph T.**, Division of Natural Sciences, University of California, Santa Cruz, CA 95064
- Hines, Michael**, Department of Neurobiology, Duke University Medical Center, Box 3209, Durham, NC 27710
- Hinsch, Gertrude, W.**, Department of Biology, University of South Florida, Tampa, FL 33620
- Hobbie, John E.**, Ecosystems Center, Marine Biological Laboratory, Woods Hole, MA 02543
- Hodge, Alan J.**, 3843 Mt. Blackburn Ave., San Diego, CA 92111
- Hoffman, Joseph**, Department of Physiology, School of Medicine, Yale University, New Haven, CT 06515
- Hollyfield, Joe G.**, Baylor School of Medicine, Texas Medical Center, Houston, TX 77030
- Holtzman, Eric**, Department of Biological Sciences, Columbia University, New York, NY 10027
- Hopkinson, Charles S., Jr.**, Marine Biological Laboratory, Woods Hole, MA 02543
- Hoskin, Francis C. G.**, 33 Hyatt Road, Woods Hole, MA 02543
- Houghton, Richard A., III**, Woods Hole Research Center, P. O. Box 296, Woods Hole, MA 02543

- Hoy, Ronald R.**, Section of Neurobiology and Behavior, Cornell University, Ithaca, NY 14853
- Hufnagel, Linda A.**, Department of Microbiology, University of Rhode Island, Kingston, RI 02881
- Hummon, William D.**, Department of Zoology, Ohio University, Athens, OH 45701
- Humphreys, Susie H.**, Food and Drug Administration, HFF-156, Switzer, 200 C Street, SW, Washington, DC 20204-0001
- Humphreys, Tom D.**, University of Hawaii, PBRC, 41 Ahui St., Honolulu, HI 96813
- Hunt, Richard T.**, ICRF, Clare Hall Laboratories, South Mimms Potter's Bar, Herb EN6-3LD, England
- Hunter, Robert D.**, Department of Biological Sciences, Oakland University, Rochester, MI 48309-4401
- Hunter, W. Bruce**, Box 321, Lincoln Center, MA 01773
- Hurwitz, Jerard**, Memorial Sloan Kettering Institute for Cancer Research, 1275 York Avenue, New York, NY 11021
- Huxley, Hugh E.**, Department of Biology, Rosenstiel Center, Brandeis University, Waltham, MA 02154
- Hynes, Thomas J., Jr.**, Meredith and Grew, Inc., 160 Federal Street, Boston, MA 02110-1701
- Han, Joseph**, Department of Developmental Genetics and Anatomy, Case Western Reserve University School of Medicine, Cleveland, OH 44106
- Ingolia, Nicholas**, Department of Physiology, New Jersey Medical School, 100 Bergen St., Newark, NJ 07103
- Inoué, Saduyki**, Department of Anatomy, McGill University Cancer Centre, 3640 University St., Montreal, PQ H3A 2B2, Canada
- Inoué, Shinya**, Marine Biological Laboratory, Woods Hole, MA 02543
- Isselbacher, Kurt J.**, Massachusetts General Hospital Cancer Center, 149 13th Street, Charlestown, MA 02129
- Issidorides, Marietta, R.**, Department of Psychiatry, University of Athens, Monis Petraki 8, Athens, 140 Greece
- Izzard, Colin S.**, Department of Biological Sciences, SUNY, 1400 Washington Ave., Albany, NY 12222
- Jacobs, Neil**, Hale & Dorr, 60 State St., Boston, MA 02109
- Jaffe, Lionel**, Marine Biological Laboratory, Woods Hole, MA 02543
- Jannasch, Holger W.**, Department of Biology, Woods Hole Oceanographic Institution, Woods Hole, MA 02543
- Jeffery, William R.**, Bodega Marine Laboratory, Box 247, Bodega Bay, CA 94923
- Johnston, Daniel**, Division of Neuroscience, Baylor College of Medicine, Baylor Plaza, Houston, TX 77030
- Josephson, Robert K.**, Department of Biological Sciences, University of California, Irvine, CA 92717
- Kabat, E. A.**, Department of Microbiology, College of Physicians and Surgeons, Columbia University, 630 West 168th St., New York, NY 10032 (resigned)
- Kaczmarek, Leonard K.**, Department of Pharmacology, Yale University School of Medicine, 333 Cedar St., New Haven, CT 06510
- Kaley, Gabor**, Department of Physiology, Basic Sciences Building, New York Medical College, Valhalla, NY 10595
- Kaltenbach, Jane**, Department of Biological Sciences, Mount Holyoke College, South Hadley, MA 01075
- Kaminer, Benjamin**, Department of Physiology, School of Medicine, Boston University, 80 East Concord St., Boston, MA 02118
- Kane, Robert E.**, PBRC, University of Hawaii, 41 Ahui St., Honolulu, HI 96813
- Kaneshiro, Edna S.**, Department of Biological Sciences, University of Cincinnati, JL 006, Cincinnati, OH 45221
- Kao, Chien-yuan**, Department of Pharmacology, Box 29, SUNY, Downstate Medical Center, 450 Clarkson Avenue, Brooklyn, NY 11203
- Kaplan, Ehud**, Department of Biophysics, The Rockefeller University, 1230 York Ave., New York, NY 10024
- Karakashian, Stephen J.**, Apt. 16-F, 165 West 91st St., New York, NY 10024
- Karlin, Arthur**, Department of Biochemistry and Neurology, Columbia University, 630 West 168th St., New York, NY 10032
- Katz, George M.**, Fundamental and Experimental Research Labs, Merck Sharp and Dohme, P. O. Box 2000, Rahway, NJ 07065
- Kelly, Robert E.**, Department of Anatomy, College of Medicine, University of Illinois, P. O. Box 6998, Chicago, IL 60680
- Kemp, Norman E.**, Department of Biology, University of Michigan, Ann Arbor, MI 48109
- Kendall, John P.**, Faneuil Hall Associates, 176 Federal Street, 2nd Floor, Boston, MA 02110
- Kendall, Richard E.**, 26 Green Harbor Road, East Falmouth, MA 02536
- Kerr, Louis M.**, Marine Biological Laboratory, Woods Hole, MA 02543
- Keynan, Alexander**, Laboratory for Developmental and Molecular Biology, Department of Biochemistry, Hebrew University of Jerusalem, Givat-Ram, Jerusalem, Israel
- Khan, Shahid M. M.**, Department of Anatomy & Structural Biology, Albert Einstein College of Medicine, 1300 Morris Park Ave., Bronx, NY 10461
- Kiehart, Daniel P.**, Department of Cellular Biology, Duke Medical Center, Box 3709, 307 Naneline Duke Bldg., Durham, NC 27710
- Kirk, Mark D.**, Division of Biological Sciences, University of Missouri, Columbia, MO 65211
- Klotz, Irving M.**, Department of Chemistry, Northwestern University, Evanston, IL 60201
- Knudson, Robert A.**, Marine Biological Laboratory, Instrument Development Lab, Woods Hole, MA 02543
- Koide, Samuel S.**, Population Council, The Rockefeller University, 1230 York Avenue, New York, NY 10021
- Kornberg, Sir Hans**, The Master's Lodge, Christ's College, Cambridge CB2 3BU, England, UK
- Kosower, Edward M.**, address unknown
- Krahl, M. E.**, 2783 W. Casas Circle, Tucson, AZ 85741
- Krane, Stephen M.**, Arthritis Unit, Massachusetts General Hospital, Fruit Street, Boston, MA 02114
- Krauss, Robert**, FASEB, 9650 Rockville Pike, Bethesda, MD 20814
- Kravitz, Edward A.**, Department of Neurobiology, Harvard Medical School, 220 Longwood Ave., Boston, MA 02115
- Kriebel, Mahlon E.**, Department of Physiology, SUNY Health Science Center, Syracuse, NY 13210
- Kristan, William B., Jr.**, Department of Biology B-022, University of California San Diego, La Jolla, CA 92093
- Kropinski, Andrew M. B.**, Department of Microbiology/Immunology, Queen's University, Kingston, Ontario K7L 3N6, Canada
- Kuhns, William J.**, Hospital for Sick Children, Department of Biochemistry Research, Toronto, Ontario M5G 1X8, Canada
- Kuhreber, Willem M.**, Marine Biological Laboratory, Woods Hole, MA 02543 (resigned)
- Kusano, Kiyoshi**, NIH, Bldg. 36, Room 4D-20, Bethesda, MD 20892
- Kuzirian, Alan M.**, Marine Biological Laboratory, Woods Hole, MA 02543
- Laderman, Aimlee**, Yale University School of Forestry, New Haven, CT 06511
- LaMarche, Paul H.**, Eastern Maine Medical Center, 489 State St., Bangor, ME 04401

- Landis, Dennis M. D.**, Department of Developmental Genetics and Anatomy, Case Western Reserve University School of Medicine, Cleveland, OH 44106
- Landowne, David**, Department of Physiology, P.O. Box 016430, University of Miami School of Medicine, Miami, FL 33101
- Langford, George M.**, Department of Biological Sciences, Dartmouth College, 6044 Gilman Laboratory, Hanover, NH 03755
- Lasser-Ross, Nechama**, Department of Cell Biology, New York Medical College, Valhalla, NY 10595
- Laster, Leonard**, University of Massachusetts Medical School, 55 Lake Avenue, North, Worcester, MA 01655
- Laufer, Hans**, Department of Biological Science, Molecular and Cell Biology, Group U-125, University of Connecticut, Storrs, CT 06268
- Lazarow, Paul B.**, Department of Cell Biology and Anatomy, Mount Sinai Medical School, Box 1007, 5th Avenue & 100th Street, New York, NY 10021
- Lazarus, Maurice**, Federated Department Stores, Inc., Sears Crescent, City Hall Plaza, Boston, MA 02108
- Leadbetter, Edward R.**, Department of Molecular and Cell Biology, U-131, University of Connecticut, Storrs, CT 06268
- Lederberg, Joshua**, The Rockefeller University, 1230 York Ave., New York, NY 10021
- Lee, John J.**, Department of Biology, City College of CUNY, Convent Ave. and 138th St., New York, NY 10031
- Lehy, Donald B.**, Marine Biological Laboratory, Woods Hole, MA 02543
- Leibovitz, Louis**, 3 Kettle Hole Road, Falmouth, MA 02540
- Leighton, Joseph**, 2324 Lakeshore Avenue, #2, Oakland, CA 94606
- Leighton, Stephen**, NIH, Bldg. 13 3W13, Bethesda, MD 20892
- Leinwand, Leslie Ann**, Department of Microbiology and Immunology, Albert Einstein College of Medicine, 1300 Morris Park Ave., Bronx, NY 10461
- Lerman, Sidney**, Eye Research Lab, Room 41, New York Medical College, 100 Grasslands Ave., Valhalla, NY 10595
- Lerner, Aaron B.**, Yale University, School of Medicine, New Haven, CT 06510
- Lester, Henry A.**, California Institute of Technology, 156-29, Pasadena, CA 91125
- Levin, Jack**, Veterans Administration Medical Center, 113A, 4150 Clement St., San Francisco, CA 94121
- Levine, Richard B.**, ARL, Division of Neurobiology, University of Arizona, 611 Gould-Simpson Bldg., Tucson, AZ 85721
- Levinthal, Françoise**, 435 Riverside Dr., New York, NY 10025
- Levitan, Herbert**, Department of Zoology, University of Maryland, College Park, MD 20742
- Levitan, Irwin B.**, Department of Biochemistry, Brandeis University, Waltham, MA 02254
- Linck, Richard W.**, Department of Anatomy, Jackson Hall, University of Minnesota, 321 Church Street, S. E., Minneapolis, MN 55455
- Lipicky, Raymond J.**, Department of Cardio-Renal/Drug Prod. Div., FDA, Rm. 16B-45, 5600 Fishers Lane, Rockville, MD 20857
- Lisman, John E.**, Department of Biology, Brandeis University, Waltham, MA 02254
- Liuzzi, Anthony**, 320 Beacon St., Boston, MA 02116
- Llinás, Rodolfo R.**, Department of Physiology and Biophysics, New York University Medical Center, 550 First Ave., New York, NY 10016
- Loew, Franklin M.**, Tufts University School of Veterinary Medicine, 200 Westboro Rd., N. Grafton, MA 01536
- Loewenstein, Birgit R.**, Department of Physiology and Biophysics, R-430, University of Miami School of Medicine, Miami, FL 33101
- Loewenstein, Werner R.**, Department of Physiology and Biophysics, University of Miami, P. O. Box 016430, Miami, FL 33101
- London, Irving M.**, Massachusetts Institute of Technology, Harvard-MIT Division, E-25-551, Cambridge, MA 02139
- Longo, Frank J.**, Department of Anatomy, University of Iowa, Iowa City, IA 52442
- Lorand, Laszlo**, Department of Biochemistry and Molecular Biology, Northwestern University, 2153 Sheridan Road, Evanston, IL 60208
- Luckenbill-Edds, Louise**, 155 Columbia Ave., Athens, OH 45701
- Macagno, Eduardo R.**, 1003B Fairchild, Department of Biosciences, Columbia University, New York, NY 10027
- MacNichol, E. F., Jr.**, Department of Physiology, Boston University School of Medicine, 80 E. Concord St., Boston, MA 02118
- Maglott-Duffield, Donna R.**, American Type Culture Collection, 12301 Parklawn Drive, Rockville, MD 20852-1776
- Maiensehein, Jane Ann**, Department of Philosophy, Arizona State University, Tempe, AZ 85287-2004
- Mainer, Robert**, The Boston Company, One Boston Place, OBP-15-D, Boston, MA 02108
- Malbon, Craig Curtis**, Department of Pharmacology, Health Sciences Center, SUNY, Stony Brook, NY 11794-8651
- Manalis, Richard S.**, Department of Biological Sciences, Indiana University—Purdue University at Fort Wayne, 2101 Coliseum Blvd., E., Fort Wayne, IN 46805
- Mangum, Charlotte P.**, Department of Biology, College of William and Mary, Williamsburg, VA 23185-8795
- Manz, Robert D.**, Helmer and Associates, Suite 1310, 950 Winter St., Waltham, MA 02154
- Margulis, Lynn**, Botany Department, University of Massachusetts, Morrill Science Center, Amherst, MA 01003
- Marinucci, Andrew C.**, 102 Nancy Drive, Mercerville, NJ 08619
- Marsh, Julian B.**, Department of Biochemistry and Physiology, Medical College of Pennsylvania, 3300 Henry Ave., Philadelphia, PA 19129
- Martin, Lowell V.**, 10 Buzzards Bay Ave., Woods Hole, MA 02543 02543
- Martinez, Jr., Joe L.**, Department of Psychology, University of California, Berkeley, 3210 Tolman Hall, Berkeley, CA 94720
- Martinez-Palomo, Adolfo**, Seccion de Patologia Experimental, Cinvesav-ipn, 07000 Mexico, D.F. A.P., 140740, Mexico
- Maser, Morton**, Woods Hole Education Assoc., P. O. Box EM, Woods Hole, MA 02543
- Mastroianni, Luigi, Jr.**, Department of Obstetrics and Gynecology, Hospital of the University of Pennsylvania, 106 Dulles, 3400 Spruce Street, Philadelphia, PA 19104-4283
- Matteson, Donald R.**, Department of Biophysics, University of Maryland School of Medicine, 660 West Redwood Street, Baltimore, MD 21201
- Mautner, Henry G.**, Department of Biochemistry, Tufts University School of Medicine, 136 Harrison Ave., Boston, MA 02111
- Mauzerall, David**, The Rockefeller University, 1230 York Ave., New York, NY 10021
- McCann, Frances**, Department of Physiology, Dartmouth Medical School, Hanover, NH 03755
- McLaughlin, Jane A.**, Marine Biological Laboratory, Woods Hole, MA 02543
- McMahon, Robert F.**, Department of Biology, Box 19498, University of Texas, Arlington, TX 76019
- Meedel, Thomas**, Biology Department, Rhode Island College, 600 Mt. Pleasant Ave., Providence, RI 02908
- Meinertzhagen, Ian A.**, Department of Psychology, Life Sciences Center, Dalhousie University, Halifax, Nova Scotia B3H 451, Canada
- Meiss, Dennis E.**, Immunodiagnostic Laboratories, 488 McCormick St., San Leandro, CA 94577
- McIlillo, Jerry M.**, Ecosystems Center, Marine Biological Laboratory, Woods Hole, MA 02543



- Mellon, DeForest, Jr.**, Department of Biology, Gilmer Hall, University of Virginia, Charlottesville, VA 22903
- Mellon, Richard P.**, P. O. Box 187, Laughlintown, PA 15655
- Mendelsohn, Michael E.**, Cardiovascular Division, Harvard Medical School, 75 Francis Street, Boston, MA 02115
- Metuzals, Janis**, Department of Pathology, University of Ottawa, Ottawa, Ontario K1H 8M5, Canada
- Metz, Charles B.**, 7220 SW 124th St., Miami, FL 33156
- Miledi, Ricardo**, Department of Psychobiology, University of California, Irvine, CA 92717
- Milkman, Roger**, Department of Biology, University of Iowa, Iowa City, IA 52242
- Miller, Andrew L.**, Marine Biological Laboratory, Woods Hole, MA 02543
- Mills, Robert**, 10315 44th Avenue, W 12 H Street, Bradenton, FL 33507-1535
- Misevic, Gradimir**, Department of Research, University Hospital of Basel, Mebelstrasse 20, CH-4031, Basel, Switzerland
- Mitchell, Ralph, DAS**, Harvard University, 29 Oxford Street, Cambridge, MA 02138
- Miyakawa, Hiroyoshi**, Department of Physiology, Yamagata University School of Medicine, Yamagata 990-23, 7990-23 Japan
- Miyamoto, David M.**, Department of Biology, Drew University, Madison, NJ 07940
- Mizell, Merle**, Department of Cell & Molecular Biology, Tulane University, New Orleans, LA 70118
- Moore, John W.**, Department of Neurobiology, Box 3209, Duke University Medical Center, Durham, NC 27710
- Moore, Lee E.**, Department of Physiology and Biophysics, University of Texas Medical Branch, Galveston, TX 77550
- Morin, James G.**, Department of Biology, University of California, Los Angeles, CA 90024
- Morrell, Frank**, Department of Neurological Science, Rush Medical Center, 1753 W. Congress Parkway, Chicago, IL 60612
- Morse, Patricia M.**, University of Washington Marine Labs, 620 University Rd., Friday Harbor, WA 98250
- Morse, Stephen Scott**, The Rockefeller University, 1230 York Ave., Box 2, New York, NY 10021-6399
- Mote, Michael L.**, Department of Biology, Temple University, Philadelphia, PA 19122
- Mountain, Isabel**, Vinson Hall #112, 6251 Old Dominion Drive, McLean, VA 22101-4804
- Muller, Kenneth J.**, Department of Physiology and Biophysics, University of Miami School of Medicine, Miami, FL 33101
- Murray, Andrew W.**, Department of Physiology, University of California, Box 0444, Parnassus Ave., San Francisco, CA 94143-0444
- Murray, Sandra Ann**, Department of Neurology, Anatomy and Cell Science, University of Pittsburgh School of Medicine, Pittsburgh, PA 15261
- Musacchia, Xavier J.**, P.O. Box 5054, Della Vista, AR 72714-0054
- Nabrit, S. M.**, 686 Beckwith St., SW, Atlanta, GA 30314
- Nadelhoffer, Knute**, Marine Biological Laboratory, Woods Hole, MA 02543
- Naka, Ken-ichi**, 2-9-2 Tatsumi Higashi, Okazaki, Japan 444
- Nakajima, Shigehiro**, Department of Pharmacology and Cell Biology, University of Illinois College of Medicine at Chicago, 835 S. Wolcott Ave., Chicago, IL 60612
- Nakajima, Yasuko**, Department of Anatomy and Cell Biology, University of Illinois College of Medicine at Chicago, M/C 512, Chicago, IL 60612
- Narahashi, Toshio**, Department of Pharmacology, Northwestern University Medical School, 303 East Chicago Ave., Chicago, IL 60611
- Nasi, Enrico**, Department of Physiology, Boston University School of Medicine, R-406, 80 E. Concord St., Boston, MA 02118
- Nealson, Kenneth H.**, Great Lakes Research Center, University of Milwaukee, 600 E. Greenfield Ave., Milwaukee, WI 53204
- Nelson, Leonard**, Department of Physiology, CS10008, Medical College of Ohio, Toledo, OH 43699
- Nelson, Margaret C.**, Section of Neurobiology and Behavior, Cornell University, Ithaca, NY 14850
- Nicholls, John G.**, Biocenter, Klingelbergstrasse 70, Basel 4056, Switzerland
- Nickerson, Peter A.**, Department of Pathology, SUNY, Buffalo, NY 14214
- Nicosia, Santo V.**, Department of Pathology, University of South Florida, College of Medicine, Box 11, 12901 North 30th St., Tampa, FL 33612
- Noe, Bryan D.**, Department of Anatomy and Cell Biology, Emory University School of Medicine, Atlanta, GA 30322
- Northcutt, R. Glenn**, Department of Neuroscience, A-001, Scripps Institution of Oceanography, La Jolla, CA 92093-0201
- Norton, Catherine N.**, Marine Biological Laboratory, Woods Hole, MA 02543
- Nusbaum, Michael P.**, Neurobiology Research Center, University of Alabama, Birmingham, Volker Hall, G878S, Birmingham, AL 35294
- O'Herron, Jonathan**, Jonathan & Shirley O'Herron Foundation, One Rockefeller Plaza, New York, NY 10020
- O'Melia, Anne F.**, 16 Evergreen Lane, Chappaqua, New York 10514
- Obaid, Ana Lia**, Department of Neuroscience, University of Pennsylvania School of Medicine, 234 Stemmler Hall, Philadelphia, PA 19104-6074
- Oertel, Donata**, Department of Neurophysiology, University of Wisconsin, 281 Medical Science Bldg., Madison, WI 53706
- Ohki, Shinpei**, Department of Biophysical Sciences, SUNY at Buffalo, 224 Cary Hall, Buffalo, NY 14214
- Oldenbourg, Rudolf**, Marine Biological Laboratory, Woods Hole, MA 02543
- Olds, James L.**, NIH, 9/1W125, Bldg. 9, Bethesda, MD 20892
- Olins, Ada L.**, University of Tennessee-Oak Ridge, Graduate School of Biomedical Sciences, Biology Division ORNL, P. O. Box 2009, Oak Ridge, TN 37831-8077
- Olins, Donald E.**, University of Tennessee-Oak Ridge, Graduate School of Biomedical Sciences, Biology Division ORNL, P. O. Box 2009, Oak Ridge, TN 37831-8077
- Oschman, James L.**, 31 Whittier Street, Dover, NH 03820
- Palazzo, Robert E.**, Department of Physiology & Cell Biology, University of Kansas, Lawrence, KS 66045
- Palmer, John D.**, Department of Zoology, University of Massachusetts, Amherst, MA 01002
- Palti, Yoram**, Rappaport Institution, Technion, POB 9697, Haifa, 31096 Israel
- Pant, Harish C.**, NINCDS/NIH, Laboratory of Neurochemistry, Bldg. 36, Room 4D-20, Bethesda, MD 20892
- Pappas, George D.**, Department of Anatomy, College of Medicine, University of Illinois, 808 South Wolcott St., Chicago, IL 60612
- Pardee, Arthur B.**, Department of Pharmacology, Harvard Medical School, Boston, MA 02115
- Pardy, Roosevelt L.**, School of Life Sciences, University of Nebraska, Lincoln, NE 68588
- Parmentier, James L.**, Cato Research, Ltd., 4364 South Alston Ave., Durham, NC 27713
- Passano, Leonard M.**, Department of Zoology, Birge Hall, University of Wisconsin, Madison, WI 53706



- Pearlman, Alan L.**, Department of Physiology, School of Medicine, Washington University, St. Louis, MO 63110
- Pederson, Thoru**, Worcester Foundation for Experimental Biology, Shrewsbury, MA 01545
- Perkins, C. D.**, 400 Hilltop Terrace, Alevan, MA 01824
- Person, Philip**, Research Testing Labs, Inc., 10000 St. Huntington Station, NY 11746
- Peterson, Bruce J.**, Ecosystems Center, Marine Biological Laboratory, Woods Hole, MA 02543
- Pethig, Ronald**, School of Electromagnetic Engineering Science, University College of N. Wales, Deakin Building, Gwynedd, LL57 1UT, UK
- Pfohl, Ronald J.**, Department of Biology, Miami University, Oxford, OH 45056
- Pierce, Robert W.**, 4851 Shore Lane, P. O. Box 1404, Boca Grande, FL 33921 (deceased)
- Pierce, Sidney K., Jr.**, Department of Zoology, University of Maryland, College Park, MD 20742
- Poindexter, Jeanne S.**, Barnard University, Columbia University, 3009 Broadway, New York, NY 10027-6598
- Pollard, Harvey B.**, NIH, NIDDKD, Lab of Cell Biology & Genetics, Bldg. 8, Rm. 401, Bethesda, MD 20892
- Pollard, Thomas D.**, Department of Cell Biology and Anatomy, Johns Hopkins University, 725 North Wolfe St., Baltimore, MD 21205
- Poole, Alan F.**, Academy of Natural Sciences of Philadelphia, 19th and the Parkway, Philadelphia, PA 19103
- Porter, Beverly H.**, 5542 Windysun Ct., Columbia, MD 21045
- Porter, Keith R.**, Department of Biology, Leidy Laboratories, Rm. 303, University of Pennsylvania, Philadelphia, PA 19104-6018
- Porter, Mary E.**, Department of Cell Biology and Neurology, University of Minnesota, 4-147 Jackson Hall, Minneapolis, MN 55455
- Potter, David**, Department of Neurobiology, Harvard Medical School, Longwood Avenue, Boston, MA 02115
- Potts, William T.**, Department of Biology, University of Lancaster, Lancaster, England, UK
- Powers, Dennis A.**, Hopkins Marine Station, Stanford University, Pacific Grove, CA 93950
- Powers, Maureen K.**, Department of Psychology, Vanderbilt University, Nashville, TN 37240
- Pratt, Melanie M.**, Department of Anatomy and Cell Biology, University of Miami School of Medicine (R124), P. O. Box 016960, Miami, FL 33101
- Prendergast, Robert A.**, Wilmer Institute, Johns Hopkins Hospital, 601 N. Broadway, Baltimore, MD 21287-9142
- Presley, Phillip H.**, Carl Zeiss, Inc., 1 Zeiss Drive, Thornwood, NY 10594
- Price, Carl A.**, Waksman Institute of Microbiology, Rutgers University, P. O. Box 759, Piscataway, NJ 08854
- Prior, David J.**, Department of Biological Sciences, NAU Box 5640, Northern Arizona University, Flagstaff, AZ 86011
- Prusch, Robert D.**, Department of Life Sciences, Gonzaga University, Spokane, WA 99258
- Purves, Dale**, Department of Neurobiology, Duke University Medical School, Box 3209, Durham, NC 27710
- Quigley, James**, Department of Pathology, SUNY Health Science Center, BHS Tower 9, Rm. 140, Stony Brook, NY 11794
- Rabb, Irving W.**, University Place at Harvard Square, 124 Mt. Auburn St., Suite 200, Cambridge, MA 02138
- Rabin, Harvey**, DuPont Merck Pharmaceutical, R&D Division, Exp. Station 328/358, Wilmington, DE 19880
- Rabinowitz, Michael B.**, Marine Biological Laboratory, Woods Hole, MA 02543
- Rafferty, Nancy S.**, Department of Anatomy, Northwestern University Medical School, 303 E. Chicago Avenue, Chicago, IL 60611
- Rakowski, Robert F.**, Department of Physiology and Biophysics, UHS/The Chicago Medical School, 3333 Greenbay Rd., N. Chicago, IL 60064
- Ramon, Fidel**, CINVESTAV, Depto Fisiologia, Apto Postal 14-740, Mexico, D.F., 07000
- Ranzi, Silvio**, Sez Zoologia Se Nat, Via Coloria 26, 120133, Milano, Italy
- Rastetter, Edward B.**, Ecosystems Center, Marine Biological Laboratory, Woods Hole, MA 02543
- Rebhun, Lionel I.**, Department of Biology, Gilmer Hall, University of Virginia, Charlottesville, VA 22901
- Reddan, John R.**, Department of Biological Sciences, Oakland University, Rochester, MI 48309-4401
- Reese, Barbara F.**, NINCDS/NIH, Bldg. 36, Room 3B26, 9000 Rockville Pike, Bethesda, MD 20892
- Reese, Thomas S.**, NINCDS/NIH, Bldg. 36, Room 2A27, 9000 Rockville Pike, Bethesda, MD 20892
- Reiner, John M.**, 111 Emerson St., Apt. 623, Denver, CO 80218 (deceased)
- Reinisch, Carol L.**, Department of Comparative Medicine, Tufts University School of Veterinary Medicine, 200 Westboro Rd., Bldg. 20, North Grafton, MA 01536
- Reynolds, George T.**, Department of Physics, Jadwin Hall, Princeton University, Princeton, NJ 08544
- Rich, Alexander**, Department of Biology, Massachusetts Institute of Technology, Cambridge, MA 02139
- Rickles, Frederick R.**, Department of Medicine, Division of Hematology-Oncology, University of Connecticut Health Center, Farmington, CT 06032
- Riley, Monica**, Marine Biological Laboratory, Woods Hole, MA 02543
- Ripps, Harris**, Department of Ophthalmology, University of Illinois, 1855 W. Taylor Street, Chicago, IL 60611
- Ritchie, Murdoch**, Department of Pharmacology, Yale University School of Medicine, 333 Cedar St., New Haven, CT 06510
- Robinson, Denis M.**, 200 Ocean Lane Drive #908, Key Biscayne, FL 33149
- Rome, Lawrence C.**, Department of Biology, University of Pennsylvania, Philadelphia, PA 19104
- Rosenbaum, Joel L.**, Department of Biology, Kline Biology Tower, Yale University, New Haven, CT 06520
- Rosenbluth, Jack**, Department of Physiology, New York University School of Medicine, 550 First Ave., New York, NY 10016
- Rosenbluth, Raja**, Department of Biological Sciences, Simon Fraser University, Burnaby, BC, V5A 1S6, Canada
- Roslansky, John**, Box 208, 26 Bar Neck Road, Woods Hole, MA 02543
- Roslansky, Priscilla F.**, 57 Buzzards Bay Ave., Woods Hole, MA 02543
- Ross, William N.**, Department of Physiology, New York Medical College, Valhalla, NY 10595
- Roth, Jay S.**, 18 Millfield Street, P. O. Box 285, Woods Hole, MA 02543
- Rowland, Lewis P.**, Neurological Institute, 710 West 168th St., New York, NY 10032
- Ruderman, Joan V.**, Department of Anatomy and Cell Biology, Harvard University School of Medicine, 220 Longwood Ave., Boston, MA 02115
- Rushforth, Norman B.**, Department of Biology, Case Western Reserve University, Cleveland, OH 44106
- Russell-Hunter, W. D.**, Department of Biology, Lyman Hall 012, Syracuse University, Syracuse, NY 13244

- Saffo, Mary Beth**, Institute of Marine Sciences, 272 Applied Sciences, University of California, Santa Cruz, CA 95064
- Sager, Ruth**, Dana Farber Cancer Institute, 44 Binney St., Boston, MA 02115
- Sagi, Amir**, Department of Life Sciences, Ben-Gurion University of the Negev, P.O. Box 653, Bee-Sheva, Israel, 84105
- Salama, Guy**, Department of Physiology, University of Pittsburgh, Pittsburgh, PA 15261
- Salmon, Edward D.**, Department of Biology, Wilson Hall, CB3280, University of North Carolina, Chapel Hill, NC 27599
- Salzberg, Brian M.**, Department of Neuroscience, University of Pennsylvania, 234 Stemmler Hall, Philadelphia, PA 19104-6074
- Sanborn, Richard C.**, 11 Oak Ridge Road, Teaticket, MA 02536 (deceased)
- Sanger, Jean M.**, Department of Anatomy, School of Medicine, University of Pennsylvania, 36th and Hamilton Walk, Philadelphia, PA 19174
- Sanger, Joseph**, Department of Anatomy, School of Medicine, University of Pennsylvania, 36th and Hamilton Walk, Philadelphia, PA 19174
- Sattelle, David B.**, AFRC Unit-Department of Zoology, University of Cambridge, Downing St., Cambridge CB2 3EJ, England, UK (resigned)
- Saunders, John W., Jr.**, P. O. Box 381, Waquoit Station, Waquoit, MA 02536
- Saz, Arthur K.**, Department of Immunology, Georgetown University Medical School, Washington, DC 20007
- Schachman, Howard K.**, Department of Molecular Biology, University of California, Berkeley, CA 94720
- Schatten, Gerald P.**, Integrated Microscopy Facility for Biomedical Research, University of Wisconsin, 1117 W. Johnson St., Madison, WI 53706
- Schatten, Heide**, Department of Zoology, University of Wisconsin, Madison, WI 53706
- Schiff, Jerome A.**, Institute for Photobiology of Cells and Organelles, Brandeis University, Waltham, MA 02254
- Schmeer, Arline C.**, Merceene Cancer Research Institute, Hospital of Saint Raphael, New Haven, CT 06511
- Schmidke, Henry H.**, Department of Neurosurgery, St. Luke's Hospital, 102 Page St., New Bedford, MA 02740
- Schnapp, Bruce J.**, Department of Cellular & Molecular Physiology, Harvard Medical School, 25 Shattuck St., Boston, MA 02115
- Schuel, Herbert**, Department of Anatomical Sciences, SUNY, Buffalo, Buffalo, NY 14214
- Schwartz, James H.**, Center for Neurobiology and Behavior, New York State Psychiatric Institute—Research Annex, 722 W. 168th St., 7th Floor, New York, NY 10032
- Schweitzer, A. Nicola**, School of Medicine, Section of Immunobiology, Yale University, New Haven, CT 06510
- Scotfield, Virginia Lee**, Department of Microbiology and Immunology, UCLA School of Medicine, Los Angeles, CA 90024
- Sears, Mary**, P. O. Box 152, Woods Hole, MA 02543
- Segal, Sheldon J.**, The Population Council, One Dag Hammarskjold Plaza, New York, NY 10036
- Selman, Kelly**, Department of Anatomy, College of Medicine, University of Florida, Gainesville, FL 32601
- Shanklin, Douglas R.**, Department of Pathology, Room 584, University of Tennessee College of Medicine, 800 Madison Avenue, Memphis, TN 38163
- Shapiro, Herbert**, 6025 North 13th St., Philadelphia, PA 19141 (deceased)
- Shashoua, Victor E.**, Ralph Lowell Labs, Harvard Medical School, McLean Hospital, 115 Mill St., Belmont, MA 02178
- Shaver, Gaius R.**, Ecosystems Center, Marine Biological Laboratory, Woods Hole, MA 02543
- Shaver, John R.**, Department of Zoology, Michigan State University, East Lansing, MI 48824
- Sheetz, Michael P.**, Department of Cell Biology, Duke University Medical Center, Box 3709, 385 Nanaline Duke Bldg., Durham, NC 27710
- Shepard, David C.**, P. O. Box 44, Woods Hole, MA 02543
- Shepro, David**, Department of Microvascular Research, Boston University, 5 Cummington St., Boston, MA 02215
- Sheridan, William F.**, Biology Department, University of North Dakota, Box 8238, University Station, Grand Forks, ND 58202-8238
- Sherman, I. W.**, Department of Biology, University of California, Riverside, CA 92521
- Shimomura, Osamu**, Marine Biological Laboratory, Woods Hole, MA 02543
- Shipley, Alan M.**, Marine Biological Laboratory, Woods Hole, MA 02543
- Siegel, Irwin M.**, Department of Ophthalmology, New York University Medical Center, 550 First Avenue, New York, NY 10016
- Siegelman, Harold W.**, Department of Biology, Brookhaven National Laboratory, Upton, NY 11973
- Silver, Robert B.**, Department of Physiology, Cornell University, 822 Veterinary Research Tower, Ithaca, NY 14853-6401
- Siwicki, Kathleen K.**, Biology Department, Swarthmore College, 500 College Ave., Swarthmore, PA 19081
- Sjodin, Raymond A.**, Department of Biophysics, University of Maryland, Baltimore, MD 21201
- Skinner, Dorothy M.**, Oak Ridge National Laboratory, P. O. Box 2009, Biology Division, Oak Ridge, TN 37831
- Slohoda, Roger D.**, Department of Biological Sciences, 306 Gilman, Dartmouth College, Hanover, NH 03755
- Sluder, Greenfield**, Worcester Foundation for Experimental Biology, 222 Maple Ave., Shrewsbury, MA 01545
- Smith, Peter J. S.**, Marine Biological Laboratory, Woods Hole, MA 02543
- Smith, Ralph I.**, Department of Integrative Biology, University of California, Berkeley, CA 94720
- Smith, Stephen J.**, Department of Molecular & Cellular Physiology, Beckman Center, Stanford University School of Medicine, Stanford, CA 94305-5426
- Smolowitz, Roxanne M.**, Laboratory of Marine Animal Health, Marine Biological Laboratory, Woods Hole, MA 02543
- Sogin, Mitchell**, Marine Biological Laboratory, Woods Hole, MA 02543
- Sorenson, Martha M.**, Cicade Universitaria-RFRJ, Department de Bioquimica-ICB/CCS, Rio de Janeiro, RJ 21910, Brasil
- Speck, William T.**, The Presbyterian Hospital in the City of New York, New York, NY 10032-3784
- Spector, Abraham**, Department of Ophthalmology, Columbia University, 630 West 168th Street, New York, NY 10032
- Speer, John W.**, Marine Biological Laboratory, Woods Hole, MA 02543
- Speksnijder, Johanna E.**, Hubrecht Laboratory, Uppsalalaan 8, 3584 CT Utrecht, The Netherlands
- Sperelakis, Nicholas**, Department of Physiology & Biophysics, University of Cincinnati, Cincinnati, OH 45267-0576
- Spiegel, Evelyn**, Department of Biological Sciences, Dartmouth College, Hanover, NH 03755
- Spiegel, Melvin**, Department of Biological Sciences, Dartmouth College, Hanover, NH 03755
- Spray, David C.**, Albert Einstein College of Medicine, Department of Neurosciences, 1300 Morris Park Avenue, Bronx, NY 10461
- Steele, John Hyslop**, Woods Hole Oceanographic Institution, Woods Hole, MA 02543

- Steinacker, Antoinette**, Dept. of Otolaryngology, Washington University, School of Medicine, Box 8115, 4566 S. Euclid Avenue, St. Louis, MO 63110
- Steinberg, Malcolm**, Department of Biology, Princeton University, Princeton, NJ 08544-1014
- Stemmer, Andreas C.**, Marine Biological Laboratory, Woods Hole, MA 02543
- Stetten, Jane Lazarow**, 4701 Willard Road, Poolesville Chase, MD 20815-4635
- Stuedler, Paul A.**, Ecosystems Center, Marine Biological Laboratory, Woods Hole, MA 02543
- Stokes, Darrell R.**, Department of Biology, Emory University, Atlanta, GA 30322
- Stommel, Elijah W.**, Section of Neurology, Dartmouth-Hitchcock Medical Center, 2 Maynard St., Hanover, NH 03756
- Stracher, Alfred**, Department of Biochemistry, SUNY Health Science Center, 450 Clarkson Ave., Brooklyn, NY 11203
- Strehler, Bernard L.**, 2310 Laguna Circle Dr., Agoura, CA 91301-2884
- Strickler, J. Rudi**, Center for Great Lakes Studies, 600 East Greenfield Ave., Milwaukee, WI 53204 (resigned)
- Strumwasser, Felix**, USUHS, Department of Psychiatry, 4301 Jones Bridge Rd., Bethesda, MD 20814-4799
- Stuart, Ann E.**, Department of Physiology, Medical Sciences Research Bldg. 206H, University of North Carolina, Chapel Hill, NC 27599-7545
- Sugimori, Mutsuyuki**, Department of Physiology and Biophysics, New York University Medical Center, 550 First Avenue, New York, NY 10016
- Summers, William C.**, Huxley College of Environmental Studies, Western Washington University, Bellingham, WA 98225
- Suprenant, Kathy A.**, Department of Physiology and Cell Biology, 4010 Haworth Hall, University of Kansas, Lawrence, KS 66045
- Sussman, Maurice**, 72 Carey Lane, Falmouth, MA 02540
- Sussman, Raquel B.**, Marine Biological Laboratory, Woods Hole, MA 02543
- Sweet, Frederick**, Department of OB & GYN, Box 8064, Washington University School of Medicine, 499 South Euclid, St. Louis, MO 63110
- Sydlik, Mary Anne**, Department of Biology, Westfield State College, Westfield, MA 01086
- Szent-Györgyi, Andrew**, Department of Biology, Brandeis University, Bassine 244, 415 South Street, Waltham, MA 02254
- Szent-Györgyi, Gwen P.**, Marine Biological Laboratory, Woods Hole, MA 02543
- Szuts, Ete Z.**, 12 Hamlin Ave., Falmouth, MA 02540
- Tabares, Lucia**, AVDA, Department of Physiology, Sanchez. Prizjuan 4, 411009 Seville, Spain
- Tamm, Sidney L.**, Boston University Marine Program, Marine Biological Laboratory, Woods Hole, MA 02543 (reinstated)
- Tanzer, Marvin L.**, Department of Biostructure & Function, Medical School, University of Connecticut, Farmington, CT 06030-3705
- Tasaki, Ichiji**, Laboratory of Neurobiology, NIMH/NIH, Bldg. 36, Rm. 2B-16, Bethesda, MD 20892
- Taylor, Douglass L.**, Center for Fluorescence Research, Carnegie Mellon University, 4400 Fifth Avenue, Pittsburgh, PA 15213
- Teal, John M.**, Department of Biology, Woods Hole Oceanographic Institution, Woods Hole, MA 02543
- Telfer, William H.**, Department of Biology, University of Pennsylvania, Philadelphia, PA 19104
- Telzer, Bruce**, Thille Building, Pomona College, 175 W. 6th Street, Claremont, CA 91711
- Thorndike, W. Nicholas**, Wellington Management Company, 28 State St., Boston, MA 02109
- Townsel, James G.**, Department of Physiology, Meharry Medical College, Nashville, TN 37208
- Travis, David M.**, 223 Newell Road, Holden, MA 01520-1442
- Treistman, Steven N.**, Worcester Foundation for Experimental Biology, 222 Maple Avenue, Shrewsbury, MA 01545
- Trigg, D. Thomas**, One Federal Street, 9th Floor, Boston, MA 02211
- Trinkaus, J. P.**, Department of Biology, Yale University, New Haven, CT 06511
- Troll, Walter**, Department of Environmental Medicine, College of Medicine, New York University, New York, NY 10016
- Troxler, Robert F.**, Department of Biochemistry, School of Medicine, Boston University, 80 East Concord St., Boston, MA 02118
- Tucker, Edward B.**, Department of Natural Sciences, Baruch College, CUNY, 17 Lexington Ave., New York, NY 10010
- Turner, Ruth D.**, Mollusk Department, Museum of Comparative Zoology, Harvard University, Cambridge, MA 02138
- Tweedell, Kenyon S.**, Department of Biological Sciences, University of Notre Dame, Notre Dame, IN 46656
- Tykocinski, Mark L.**, Institute of Pathology, Case Western Reserve University, 2085 Adelbert Rd., Cleveland, OH 44106
- Tytell, Michael**, Department of Anatomy, Bowman Gray School of Medicine, Wake Forest University, Winston-Salem, NC 27103
- Ueno, Hiroshi**, Department of Medical Chemistry, Osaka Medical College, 2-7 Daigaku-machi, Takatsuki, Osaka 569, Japan
- Valiela, Ivan**, Boston University Marine Program, Marine Biological Laboratory, Woods Hole, MA 02543
- Vallee, Richard**, Cell Biology Group, Worcester Foundation for Experimental Biology, Shrewsbury, MA 01545
- Valois, John**, Marine Biological Laboratory, Woods Hole, MA 02543
- Van Holde, Kensa**, Department of Biochemistry and Biophysics, Oregon State University, Corvallis, OR 97331-6503
- Vogel, Steven S.**, LBM, NIDDK/NIH, Bldg. 10, Rm. 9B04, Bethesda, MD 20892
- Waksman, Byron**, Foundation for Microbiology, 300 East 54th St., New York, NY 10022
- Wall, Betty**, 9 George St., Woods Hole, MA 02543
- Wallace, Robin A.**, Whitney Laboratory, 9505 Ocean Shore Blvd., St. Augustine, FL 32086
- Wang, Ching Chung**, Department of Pharmaceutical Chemistry, University of California, San Francisco, CA 94143
- Wang, Hsien-yu**, Department of Biochemistry, National Defense Medical Center, Taipei, Taiwan, Republic of China
- Wangh, Lawrence J.**, Department of Biology, Brandeis University, 415 South St., Waltham, MA 02254
- Warner, Robert C.**, Department of Molecular Biology and Biochemistry, University of California, Irvine, CA 92717
- Warren, Kenneth S.**, Maxwell Communications Corp., 866 Third Avenue, New York, NY 10022
- Warren, Leonard**, Wistar Institute, 36th and Spruce Streets, Philadelphia, PA 19104
- Waterbury, John B.**, Department of Biology, Woods Hole Oceanographic Institution, Woods Hole, MA 02543
- Watson, Stanley**, Associates of Cape Cod, Inc., P. O. Box 224, Woods Hole, MA 02543
- Wayman, Stephen G.**, Department of Neurology, LCI 708, Yale School of Medicine, 333 Cedar Street, New Haven, CT 06510
- Webb, H. Marguerite**, Marine Biological Laboratory, Woods Hole, MA 02543

- Weber, Annemarie**, Department of Biochemistry and Biophysics, School of Medicine, University of Pennsylvania, Philadelphia, PA 19066
- Weidner, Earl**, Department of Zoology and Physiology, Louisiana State University, Baton Rouge, LA 70803
- Weiss, Dieter G.**, Institut für Zoologie, Technische Universität München, 8046 Garching, FRG
- Weiss, Leon P.**, Department of Animal Biology, School of Veterinary Medicine, University of Pennsylvania, Philadelphia, PA 19104
- Weissmann, Gerald**, New York University Medical Center, 550 First Avenue, New York, NY 10016
- Werman, Robert**, Neurobiology Unit, The Hebrew University, Jerusalem, Israel
- Westerfield, R. Monte**, The Institute of Neuroscience, University of Oregon, Eugene, OR 97403
- Whittaker, J. Richard**, Department of Biology, Bag Service #45111, University of New Brunswick, Fredericton, NB E3B 6E1, Canada
- Wilson, Darcy B.**, San Diego Regional Cancer Center, 3099 Science Park Road, San Diego, CA 92121
- Wilson, T. Hastings**, Department of Physiology, Harvard Medical School, Boston, MA 02115
- Witkovsky, Paul**, Department of Ophthalmology, New York University Medical Center, 550 First Ave., New York, NY 10016
- Wittenberg, Beatrice**, Department of Physiology & Biophysics, Albert Einstein College of Medicine, Bronx, NY 10461
- Wittenberg, Jonathan B.**, Department of Physiology and Biophysics, Albert Einstein College, 1300 Morris Park Ave., Bronx, NY 01461
- Wolken, Jerome J.**, Department of Biological Sciences, Carnegie Mellon University, 440 Fifth Ave., Pittsburgh, PA 15213
- Wonderlin, William F.**, Department of Pharmacology & Toxicology, West Virginia University, Morgantown, WV 26506
- Worden, Mary Kate**, Department of Neurobiology, Harvard Medical School, 220 Longwood Ave., Boston, MA 02115
- Worgul, Basil V.**, Department of Ophthalmology, Columbia University, 630 West 168th St., New York, NY 10032
- Wu, Chau Hsiung**, Department of Pharmacology, Northwestern University Medical School, Chicago, IL 60611
- Wytenbach, Charles R.**, Department of Physiology and Cell Biology, University of Kansas, Lawrence, KS 66045
- Yashphe, Jacob**, Hebrew University, Hadassah Medical School, Jerusalem, Israel, 91010
- Yeh, Jay Z.**, Department of Pharmacology, Northwestern University Medical School, Chicago, IL 60611
- Zigman, Seymour**, School of Medicine and Dentistry, University of Rochester, 260 Crittenden Blvd., Rochester, NY 14620
- Zimmerberg, Joshua J.**, NIH, Bldg. 12A, Room 2007, Bethesda, MD 20892
- Zottoli, Steven J.**, Department of Biology, Williams College, Williamstown, MA 01267
- Zucker, Robert S.**, Neurobiology Division, Department of Molecular and Cellular Biology, University of California, Berkeley, CA 94720
- Zukin, Ruth Suzanne**, Department of Neuroscience, Albert Einstein College of Medicine, 1410 Pelham Parkway South, Bronx, NY 10461

### Associate Members

- |   |                                   |                                  |  |
|---|-----------------------------------|----------------------------------|--|
| Alfano, Dr. Louis                       | Borg, Dr. and Mrs. Alfred F.      | Cobb, Dr. Jewel P.               | Eustis, Mr. and Mrs. Jack              |
| Allen, Mr. and Mrs. Wayne               | Borgese, Dr. and Mrs. Thomas      | Copeland, Dr. and Mrs. D. Eugene | Farnham, Ms. Elizabeth                 |
| Allison, Mr. and Mrs. Douglas F.        | Bowles, Dr. and Mrs. Francis P.   | Cornell, Dr. and Mrs. Neal       | Fausch, Mr. and Mrs. David             |
| Anderson, Mr. and Mrs. Seneca           | Braur, Dr. and Mrs. Mark          | Cowan, Ms. Stacy                 | Fisher, Mr. and Mrs. Frederick S., III |
| Andrews, Dr. Edwin J.                   | Briana, Anthony                   | Cowling, Mr. John                | Folino, Mr. John W., Jr.               |
| Aristide, Ms. Tracy                     | Brown, Mrs. Jennie P.             | Cowling, Dr. Vincent             | Freeman, Mr. and Mrs. Howard           |
| Armstrong, Dr. and Mrs. Richard A.      | Brown, Mrs. Tomas A.              | Crabb, Mr. and Mrs. David L.     | Fribourgh, Dr. James H.                |
| Aspinwall, Mr. and Mrs. Duncan          | Brown, Dr. and Mrs. Thornton      | Crain, Mr. and Mrs. Melvin C.    | Friendship Fund                        |
| Atwood, Mrs. Kimball                    | Buck, Dr. and Mrs. John B.        | Cross, Mr. and Mrs. Norman C.    | Frosch, Dr. and Mrs. Robert A.         |
| Bagley, Mr. Everett E.                  | Burghauer, Dr. Alan H.            | Crossley, Miss Dorothy           | Fye, Mrs. Paul M.                      |
| Bakalar, Mr. and Mrs. David             | Burris, Dr. and Mrs. John E.      | Crossley, Miss Helen             | Garfield, Ms. Eleanor                  |
| Ballantine, Mrs. Elizabeth E.           | Buxton, Mr. and Mrs. Bruce E.     | Crowell, Mrs. Villa              | Garrett, Dr. Patricia                  |
| Bang, Mrs. Betsy G.                     | Canney, Ms. Paula                 | Davis, Mr. and Mrs. Joel P.      | Gault, Ms. Christine                   |
| Bang, Ms. Molly                         | Carlson, Dr. and Mrs. Francis     | DiBerardino, Dr. Marie A.        | Gellis, Dr. and Mrs. Sydney            |
| Banks, Ms. Jamie                        | Carlton, Mr. and Mrs. Winslow G.  | Donnette, Mr. and Mrs. Joseph    | Glazebrook, Mrs. Rebeckah D.           |
| Banks, Mr. and Mrs. William L.          | Case, Mrs. Patricia A.            | Donovan, Mr. and Mrs. David L.   | Glenn, Mr. Gary                        |
| Barlow, Mr. and Mrs. R. Channing        | Chaet, Mr. and Mrs. Alfred        | Douglas, Ms. Jean                | Goldstein, Dr. and Mrs. Moise H., Jr.  |
| Barnes, Mr. John                        | Chandler, Mr. Robert              | Droban, Ms. Suzanne              | Goodwin, Mr. and Mrs. Charles          |
| Benthos, Inc.                           | Child, Dr. and Mrs. Frank M., III | Drumme, Mr. and Mrs. Todd A.     | Grant, Mrs. Rose                       |
| Berg, Mr. and Mrs. C. John              | Chisholm, Dr. Sallie W.           | Dugan, Mr. and Mrs. William P.   | Greer, Mr. and Mrs. W. H., Jr.         |
| Berg, Ms. Linnea                        | Clark, Dr. and Mrs. Arnold M.     | Duplaix, Dr. Nicole              | Griffith, Dr. and Mrs. B. Herold       |
| Bernheimer, Drs. Alan W. and Harriet P. | Clark, Mr. and Mrs. Leroy, Jr.    | Ebert, Dr. and Mrs. James D.     | Grossman, Barbara                      |
| Bigelow, Mr. and Mrs. Robert O.         | Clement, Mrs. Octavia             | Egloff, Mrs. F. R. L.            | Haakonsen, Dr. Harry O.                |
| Bihrlle, Dr. William                    | Cloud, Dr. Laurence P.            | Eliott, Mr. Raymond              | Hadamard, Dr. Antoine F.               |
| Bleck, Dr. Thomas P.                    | Clowes Fund, Inc.                 | Ellis, Dr. and Mrs. David        | Halvorson, Dr. and Mrs. Harlyn O.      |
| Blumenfeld, Dr. Olga                    | Clowes, Dr. and Mrs. Alexander W. | Engles, Mr. and Mrs. George      | Hamstrom, Ms. Mary Elizabeth           |
| Boche, Mr. Robert D.                    | Clowes, Mr. Allen W.              | Esswein, Dr. Arthur              | Harrington, Mr. Robert B.              |
| Bolton, Mr. and Mrs. Thomas C.          | Clowes, Mrs. Margaret             | Estabrooks, Mr. Gordon C.        | Harrington, Mr. Robert D., Jr.         |

- Harvey, Mrs. Janet  
Hastings, Dr. and Mrs. J. Woodland  
Haubrich, Dr. Robert R.  
Hays, Dr. David S.  
Hiatt, Dr. and Mrs. Howard H.  
Hibbitt, Mrs. H. D.  
Hiehar, Dr. Barbara  
Hirschfeld, Mrs. Eleanor M.  
Hodge, Dr. and Mrs. Stuart  
Hodosh, Mrs. Helen  
Holmes, Mrs. George  
Hoskin, Dr. Francis  
Hough, Mr. John T.  
Howard, Mrs. Mary Jean  
Huettner, Dr. and Mrs. Robert J.  
Huettner, Ms. Susan A.  
Inoué, Dr. and Mrs. Shinya  
Jackson, Miss Elizabeth B.  
Jewett, G. F., Foundation  
Jewett, Mr. and Mrs. G. F., Jr.  
Jewett, Mr. and Mrs. Raymond L.  
Jones, Mr. and Mrs. DeWitt C., III  
Jones, Mr. and Mrs. Frederick, II  
Jones, Mr. Frederick S., III  
Jordan, Dr. and Mrs. Edwin P.  
Kahn, Dr. Harry S.  
Karush, Mrs. Sally  
Katz, Mrs. Marcella  
Keoughan, Ms. Patricia E.  
Kivy, Dr. and Mrs. Peter  
Knoble, Ms. Mary  
Knowles, Mr. and Mrs. Sidney A.  
Korgen, Dr. Ben J.  
Kraco, Ms. Karen  
Kravitz, Dr. and Mrs. Edward A.  
Kuffler, Mrs. Phyllis  
Laderman, Mr. Ezra and Dr. Aimee  
Lakian, Mr. and Mrs. John  
Lash, Ms. Rebecca  
Laster, Dr. and Mrs. Leonard  
Laufer, Dr. and Mrs. Hans  
Laufer, Ms. Jessica, and Weiss, Mr. Malcolm  
Laufer, Dr. Marc R.  
Lawrence, Mr. and Mrs. William  
Leach, Dr. and Mrs. Berton J.  
Leahy, Michael  
LeBlond, Mr. and Mrs. Arthur  
Leeson, Mr. and Mrs. A. Dix  
LeFevre, Dr. Marian E.  
Leffler, Dr. Charles W.  
Levitz, Dr. Mortimer  
Light, Mr. and Mrs. Donald W.  
Lindberg, Mr. Lennart  
Livingstone, Jr., Mr. and Mrs. Robert  
Lloyd, Mr. and Mrs. James E.  
Loessel, Mrs. Sarah  
Low, Miss Doris V.  
Mackey, Mr. and Mrs. William K.  
MacLerdy, Mrs. Margaret M.  
Magee, Mrs. J.  
Mahoney, Mrs. J.  
Mann, Mrs. Rosalie  
Mann, Mr. and Mrs. Philip B.  
Mann, Mrs. S. Madeline  
Mast, Dr. and Mrs. Julian B.  
Matuszyna, Mr. and Mrs. Joseph C.  
Masari, Dr. Marisa  
Mason, Mr. and Mrs. Appleton  
Mavor, Mr. and Mrs. James  
Mastroianni, Dr. and Mrs. Luigi, Jr.  
Manzerall, Mrs. Miriam J.  
McElroy, Mrs. Nella W.  
McGonigle, Mr. Paul  
McKoan, Ms. Mary W.  
McMahon, Mr. John J.  
McMurtrie, Mrs. Cornelia Hanna  
Meigs, Mr. and Mrs. Arthur V.  
Meigs, Dr. and Mrs. J. Wister  
Melillo, Dr. and Mrs. Jerry M.  
Mellon, Mr. and Mrs. Richard P.  
Mendelson, Dr. Martin  
Metz, Dr. and Mrs. Charles B.  
Meyers, Mr. and Mrs. Richard  
Mills, Mrs. Margaret A.  
Mixer, Mrs. Florence E.  
Monroy, Mrs. Anna  
Montgomery, Dr. and Mrs. Charles H.  
Montgomery, Mrs. Mary E.  
Morse, Dr. M. Patricia  
Morse, Jr., Mr. and Mrs. Richard  
Munson, Mr. William  
Murchelano, Dr. Robert  
Nace, Mr. Paul F., Jr.  
Nangle, Mr. John E.  
Neill, Mr. William G.  
Nelson, Dr. Pamela  
Netsky, Dr. Martin  
O'Connell, Dr. and Mrs. Clifford  
Olszowka, Dr. Janice S.  
O'Neil, Mr. Thomas  
Ott, Dr. Karen  
Palmer, Mr. and Mrs. David  
Pappas, Dr. and Mrs. George D.  
Parmenter, Dr. Charles  
Pearce, Dr. John B.  
Pearson, Mrs. Helen M.  
Pederson, Dr. and Mrs. Thoru  
Peri, Mr. and Mrs. John B.  
Person, Dr. and Mrs. Philip  
Plough, Ms. Frances  
Plough, Mr. and Mrs. George H.  
Plymouth Savings Bank  
Porter, Dr. and Mrs. Keith R.  
Press, Dr. Frank  
Price, Ms. Carol  
Price, Mr. John S.  
Prosser, Dr. and Mrs. C. Ladd  
Putnam, Mr. and Mrs. Allan Ray  
Putnam, Mr. and Mrs. William A., III  
Quezada, Dr. Fernando  
Rankin, Mrs. Julia S.  
Regan, Reverend Msgr. John J.  
Righter, Mr. and Mrs. Harold  
Riina, Mr. John R.  
Riley, Dr. Monica  
Ripple, Mr. and Mrs. John  
Robbins, Ms. Ann  
Robertson, Mrs. Lola E.  
Robinson, Dr. Denis M.  
Robinson, Mr. John G.  
Robinson, Mr. and Mrs. Marius A.  
Roose, Ms. Elayne  
Root, Mrs. Pauline  
Rosenthal, Ms. Hilde  
Rosett, Mrs. Atholie K.  
Roslansky, Drs. John and Priscilla  
Ross, Dr. Robert  
Ross, Dr. Virginia S.  
Rowe, Dr. Don  
Rubinow, Mrs. Shirley  
Sallet, Mrs. Grace W.  
Sallop, Ms. Linda and Fenlon, Mr. Michael  
Sanidas, Dr. and Mrs. Dennis J.  
Saunders, Dr. and Mrs. John W.  
Sawyer, Mr. and Mrs. John E.  
Scheffler, Ms. Astrid  
Schlesinger, Mrs. R. Walter  
Schwamb, Mr. and Mrs. Peter  
Scott, Mrs. Elsie M.  
Seder, Mr. John  
Selby, Dr. Cecily  
Seliger-Egelson, Ms. Pauline  
Senft, Mrs. Deborah G.  
Shanklin, Dr. and Mrs. D. R.  
Shapiro, Mrs. Harriet  
Sharp, Mr. and Mrs. Robert W.  
Shaver, Dr. John R.  
Sheehy, Mr. David  
Shemin, Mrs. Charlotte  
Shepro, Dr. and Mrs. David  
Silver, Mr. and Mrs. Bertram R.  
Simon, Mr. and Mrs. Stephen A.  
Simonds, Mr. and Mrs. Jonathon O.  
Singer, Mr. and Mrs. Daniel M.  
Smith, Drs. Frederick E. and Marguerite A.  
Smith, Mr. and Mrs. Homer P.  
Smith, Ms. Stacy Cowan  
Solomon, Dr. and Mrs. A. K.  
Speck, Dr. William T.  
Spiegel, Drs. Melvin and Evelyn  
Steele, Mrs. M. Evelyn  
Steele, Dr. Robert E.  
Steinbach, Mrs. Eleanor  
Stephenson, Dr. and Mrs. Wm. K.  
Stetson, Mrs. Judith G.  
Stetten, Mrs. Jane Lazarow  
Stump, Mr. Robert  
Swain, Mr. Albert H.  
Swanson, Dr. and Mrs. Carl P.  
Swift, Mr. and Mrs. E. Kent  
Swift, Mr. and Mrs. Robert  
Swope, Mr. and Mrs. Gerard L.  
Swope, Mrs. Marjorie P.  
Taylor, Mr. James K.  
Taylor, Mrs. Jean G.  
Tebbetts, Mr. and Mrs. Edwin H.  
Thier, Dr. and Mrs. Samuel  
Timmins, Mrs. Linda L.  
Todd, Mr. and Mrs. Gordon F.  
Trager, Mrs. Ida  
Trigg, Mr. and Mrs. D. Thomas  
Troll, Dr. and Mrs. Walter  
Trousos, Miss Natalie  
Ulbrich, Ms. Ciona  
Ulbrich, Mr. and Mrs. Volker  
Valois, Mr. and Mrs. John  
Van Buren, Mrs. Alice H.  
Vincent, Dr. and Mrs. Walter S.  
Vonderhaar, Dr. William  
Voorhis, Mr. Arthur  
Wagner, Mr. Mark  
Waite, Mrs. Charles  
Waksman, Mrs. Joyce  
Walter, Mr. and Mrs. Henry  
Warren, Mrs. Eve  
Weeks, Mr. and Mrs. John T.  
Weiffenbach, Dr. and Mrs. George  
Weissmann, Dr. and Mrs. Gerald  
Wendorff, Ms. Lillian  
Wessel, Dr. Gary  
Wheeler, Dr. and Mrs. Paul S.  
Wheeler, Dr. William M.  
Whitehead, Mrs. Barbara  
Wickersham, Mrs. Joan  
Wigley, Mrs. Roland  
Wigley, Ms. Susan  
Wilber, Mrs. Clare M.  
Willis, Mr. Herbert F.  
Wilson, Mr. and Mrs. Leslie J.  
Winn, Dr. William M.  
Wittenberg, Dr. Beatrice  
Woitkoski, Miss Nancy  
Wolfensohn, Mrs. Sarah A.  
Wolfensohn, Mr. and Mrs. Wolfe  
Woodwell, Dr. and Mrs. George M.  
Zacks, Dr. and Mrs. Sumner  
Zimmerli, Mr. and Mrs. Bruce  
Zinn, Dr. and Mrs. Donald J.

*Gift Shop Volunteers*

Barbara Atwood  
 Patricia Barlow  
 Harriet Bernheimer  
 Glorie Borgese  
 Jennie Brown  
 Shannon Brown  
 Elizabeth Buck  
 Mary Buckley  
 Shirley Chaet  
 Vera Clark  
 Peggy Clowes  
 Jewell Cobb  
 Villa Crowell  
 Janet Daniels  
 Alma Ebert  
 Ellie Gabriel  
 Vi Gifford  
 Rose Grant  
 Edie Grosch  
 Barbara Grossman  
 Jean Halvorson

Helen Hodosh  
 Polly Hyde  
 Sally Karush  
 Brookie Ketchum  
 Ruth Ann Laster  
 Evelyn Laufer  
 Barbara Little  
 Sally Loessell  
 Vinnie Mackey  
 Connie Martyna  
 Mariam Mauzerall  
 Phyllis Myers  
 Florence Mixer  
 Lorraine Mizell  
 Eleanor Nace  
 Arlene Park  
 Bertha Person  
 Dottie Phinney  
 Elizabeth Price  
 Kathryn Price  
 Julia Rankin

Virginia Reynolds  
 Erika Righter  
 Jean Ripps  
 Lola Robinson  
 Lilyan Saunders  
 Elsie Scott  
 Marilyn Shepro  
 Fran Silverstein  
 Marcia Simmons  
 Cynthia Smith  
 Peggy Smith  
 Louise Specht  
 Susie Steinbach  
 Dorothy Stracher  
 Natalie Trousof  
 Mary Ulbrich  
 Barbara Van Holde  
 Alice Veeder  
 Dorothy Ville  
 Clare Wilber

*MBL Tour Guides*

Betsy Bang  
 John Buck  
 Sears Crowell

Teru Hayashi  
 Julie Rankin  
 Lola Robertson

Mary Ulbrich  
 Donald Zinn  
 Margery Zinn

# Certificate of Organization Articles of Amendment Bylaws

## Certificate of Organization

(On File in the Office of the Secretary of the Commonwealth)

No. 3170

We, Alpheus Hyatt, President, William Stanford Stevens, Treasurer, and William T. Sedgwick, Edward G. Gardiner, Susan Mims and Charles Sedgwick Minot being a majority of the Trustees of the Marine Biological Laboratory in compliance with the requirements of the fourth section of chapter one hundred and fifteen of the Public Statutes do hereby certify that the following is a true copy of the agreement of association to constitute said Corporation, with the names of the subscribers thereto:

We, whose names are hereto subscribed, do, by this agreement, associate ourselves with the intention to constitute a Corporation according to the provisions of the one hundred and fifteenth chapter of the Public Statutes of the Commonwealth of Massachusetts, and the Acts in amendment thereof and in addition thereto.

The name by which the Corporation shall be known is  
THE MARINE BIOLOGICAL LABORATORY.

The purpose for which the Corporation is constituted is to establish and maintain a laboratory or station for scientific study and investigations, and a school for instruction in biology and natural history.

The place within which the Corporation is established or located is the city of Boston within said Commonwealth.

The amount of its capital stock is none.

In Witness Whereof, we have hereunto set our hands, this twenty seventh day of February in the year eighteen hundred and eighty-eight, Alpheus Hyatt, Samuel Mills, William T. Sedgwick, Edward G. Gardiner, Charles Sedgwick Minot, William G. Farlow, William Stanford Stevens, Anna D. Phillips, Susan Mims, B. H. Van Vleck.

That the first meeting of the subscribers to said agreement was held on the thirteenth day of March in the year eighteen hundred and eighty-eight.

In Witness Whereof, we have hereunto signed our names, this thirteenth day of March in the year eighteen hundred and eighty-eight, Alpheus Hyatt, President, William Stanford Stevens, Treasurer, Edward G. Gardiner, William T. Sedgwick, Susan Mims, Charles Sedgwick Minot

(Approved on March 20, 1988 as follows.)

I hereby certify that it appears upon an examination of the within written certificate and the records of the corporation duly submitted to my inspection, that the requirements of sections one, two and three of chapter one hundred and fifteen, and sections eighteen, twenty and twenty-one of chapter one hundred and six, of the Public Statutes, have been complied with and I hereby approve said certificate this twentieth day of March A D eighteen hundred and eighty-eight.

Charles Endicott  
Commissioner of Corporations)

## Articles of Amendment

(On File in the Office of the Secretary of the Commonwealth)

We, James D. Ebert, President, and David Shepro, Clerk of the Marine Biological Laboratory, located at Woods Hole, Massachusetts 02543, do hereby certify that the following amendment to the Articles of Organization of the Corporation was duly adopted at a meeting held on August 15, 1975, as adjourned to August 29, 1975, by vote of 444 members, being at least two-thirds of its members legally qualified to vote in the meeting of the corporation:

Voted: That the Certificate of Organization of this corporation be and it hereby is amended by the addition of the following provisions:

"No Officer, Trustee or Corporate Member of the corporation shall be personally liable for the payment or satisfaction of any obligation or liabilities incurred as a result of, or otherwise in connection with, any commitments, agreements, activities or affairs of the corporation.

"Except as otherwise specifically provided by the Bylaws of the corporation, meetings of the Corporate Members of the corporation may be held anywhere in the United States.

"The Trustees of the corporation may make, amend or repeal the Bylaws of the corporation in whole or in part, except with respect to any provisions thereof which shall by law, this Certificate or the bylaws of the corporation, require action by the Corporate Members."

The foregoing amendment will become effective when these articles of amendment are filed in accordance with Chapter 180, Section 7 of the General Laws unless these articles specify, in accordance with the vote adopting the amendment, a later effective date not more than thirty days after such filing, in which event the amendment will become effective on such later date.

In Witness whereof and Under the Penalties of Perjury, we have hereto signed our names this 2nd day of September, in the year 1975, James D. Ebert, President; David Shepro, Clerk.

(Approved on October 24, 1975, as follows:

I hereby approve the within articles of amendment and, the filing fee in the amount of \$10 having been paid, said articles are deemed to have been filed with me this 24th day of October, 1975.

Paul Guzzi  
Secretary of the Commonwealth)

## Bylaws

(Revised August 7, 1992 and December 10, 1992)

### ARTICLE I—THE CORPORATION

A. *Name and Purpose* The name of the Corporation shall be The Marine Biological Laboratory. The Corporation's purpose shall be to establish and maintain a laboratory or station for scientific study and investigation and a school for instruction in biology and natural history

**B. Nondiscrimination** The Corporation shall not discriminate on the basis of age, religion, color, race, national or ethnic origin, sex or sexual preference in its policies on employment and administration or in its educational and other programs.

#### ARTICLE II—MEMBERSHIP

**A. Members.** The Members of the Corporation ("Members") shall consist of persons elected by the Board of Trustees (the "Board"), upon such terms and conditions and in accordance with such procedures, not inconsistent with law or these Bylaws, as may be determined by the Board. At any regular or special meeting of the Board, the Board may elect new Members. Members shall have no voting or other rights with respect to the Corporation or its activities except as specified in these Bylaws, and any Member may vote at any meeting of the Members in person only and not by proxy. Members shall serve until their death or resignation unless earlier removed with or without cause by the affirmative vote of two-thirds of the Trustees then in office. Any Member who has retired from his or her home institution may, upon written request to the Corporation, be designated a Life Member. Life Members shall not have the right to vote and shall not be assessed for dues.

**B. Meetings.** The annual meeting of the Members shall be held on the Friday following the first Tuesday in August of each year, at the Laboratory of the Corporation in Woods Hole, Massachusetts, at 9:30 a.m. The Chairperson of the Board shall preside at meetings of the Corporation. If no annual meeting is held in accordance with the foregoing provision, a special meeting may be held in lieu thereof with the same effect as the annual meeting, and in such case all references in these Bylaws, except in this Article II.B., to the annual meeting of the Members shall be deemed to refer to such special meeting. Members shall transact business as may properly come before the meeting. Special meetings of the Members may be called by the Chairperson or the Trustees, and shall be called by the Clerk, or in the case of the death, absence, incapacity or refusal of the Clerk, by any other officer, upon written application of Members representing at least ten percent of the smallest quorum of Members required for a vote upon any matter at the annual meeting of the Members, to be held at such time and place as may be designated.

**C. Quorum.** One hundred (100) Members shall constitute a quorum at any meeting. Except as otherwise required by law or these Bylaws the affirmative vote of a majority of the Members voting in person at a meeting attended by a quorum shall constitute action on behalf of the Members.

**D. Notice of Meetings.** Notice of any annual meeting or special meeting of Members, if necessary, shall be given by the Clerk by mailing notice of the time and place and purpose of such meeting at least 15 days before such meeting to each Member at his or her address as shown on the records of the Corporation.

**E. Waiver of Notice.** Whenever notice of a meeting is required to be given a Member, under any provision of the Articles or Organization or Bylaws of the Corporation, a written waiver thereof, executed before or after the Meeting by such Member, or his or her duly authorized attorney, shall be deemed equivalent to such notice.

**F. Adjournments.** Any meeting of the Members may be adjourned to any other time and place by the vote of a majority of those Members present at the meeting, whether or not such Members constitute a quorum, or by any officer entitled to preside at or to act as Clerk of such meeting, if no Member is present or represented. It shall not be necessary to notify any Members of any adjournment unless no Member is present or represented at the meeting which is adjourned, in which case, notice of the adjournment shall be given in accordance with Article II.D. Any business which could have been transacted at any meeting of the Members as originally called may be transacted at an adjournment thereof.

#### ARTICLE III—ASSOCIATES OF THE CORPORATION

**Associates of the Corporation.** The Associates of the Marine Biological Laboratory shall be an unincorporated group of persons (including associations and corporations) interested in the Laboratory and shall be organized and operated under the general supervision and authority of the Trustees. The Associates of the Marine Biological Laboratory shall have no voting rights.

#### ARTICLE IV—BOARD OF TRUSTEES

**A. Powers.** The Board of Trustees shall have the control and management of the affairs of the Corporation. The Trustees shall elect a Chairperson of the Board who shall serve until his or her successor is elected and qualified. They shall annually elect a President of the Corporation. They shall annually elect a Vice Chairperson of the Board who shall be Vice Chairperson of the meetings of the Corporation. They shall annually elect a Treasurer. They shall annually elect a Clerk, who shall

be a resident of Massachusetts. They shall elect Trustees-at-Large as specified in this Article IV. They shall appoint a Director of the Laboratory for a term not to exceed five years, provided the term shall not exceed one year if the candidate has attained the age of 65 years prior to the date of the appointment. They shall choose such other officers and agents as they shall think best. They may fix the compensation of all officers and agents of the Corporation and may remove them at any time. They may fill vacancies occurring in any of the offices. The Board shall have the power to choose an Executive Committee from their own number as provided in Article V, and to delegate to such Committee such of their own powers as they may deem expedient in addition to those powers conferred by Article V. They shall, from time to time, elect Members to the Corporation upon such terms and conditions as they shall have determined, not inconsistent with law or these Bylaws.

##### **B. Composition and Election**

(1) The Board shall include 24 Trustees elected by the Board as provided below:

(a) At least six Trustees ("Corporate Trustees") shall be Members who are scientists, and the other Trustees ("Trustees-at-Large") shall be individuals who need not be Members or otherwise affiliated with the Corporation.

(b) The 24 elected Trustees shall be divided into four classes of six Trustees each, with one class to be elected each year to serve for a term of four years, and with each such class to include at least one Corporate Trustee. Such classes of Trustees shall be designated by the year of expiration of their respective terms.

(2) The Board shall also include the Chief Executive Officer, Treasurer and the Chairperson of the Science Council, who shall be *ex officio* voting members of the Board.

(3) Although Members or Trustees may recommend individuals for nomination as Trustees, nominations for Trustee elections shall be made by the Nominating Committee in its sole discretion. The Board may also elect Trustees who have not been nominated by the Nominating Committee.

**C. Eligibility.** A Corporate Trustee or a Trustee-at-Large who has been elected to an initial four-year term or remaining portion thereof, of which he/she has served at least two years, shall be eligible for re-election to a second four-year term, but shall be ineligible for re-election to any subsequent term until one year has elapsed after he/she has last served as a Trustee.

**D. Removal.** Any Trustee may be removed from office at any time with or without cause, by vote of a majority of the Members entitled to vote in the election of Trustees; or for cause, by vote of two-thirds of the Trustees then in office. A Trustee may be removed for cause only if notice of such action shall have been given to all of the Trustees or Members entitled to vote, as the case may be, prior to the meeting at which such action is to be taken and if the Trustee to be so removed shall have been given reasonable notice and opportunity to be heard before the body proposing to remove him or her.

**E. Vacancies.** Any vacancy in the Board may be filled by vote of a majority of the remaining Trustees present at a meeting of Trustees at which a quorum is present. Any vacancy in the Board resulting from the resignation or removal of a Corporate Trustee shall be filled by a Member who is a scientist.

**F. Meetings.** Meetings of the Board shall be held from time to time, not less frequently than twice annually, as determined by the Board. Special meetings of Trustees may be called by the Chairperson, or by any seven Trustees, to be held at such time and place as may be designated. The Chairperson of the Board, when present, shall preside over all meetings of the Trustees. Written notice shall be sent to a Trustee's usual or last known place of residence at least two weeks before the meeting. Notice of a meeting need not be given to any Trustee if a written waiver of notice executed by such Trustee before or after the meeting is filed with the records of the meeting, or if such Trustee shall attend the meeting without protesting prior thereto or at its commencement the lack of notice given to him or her.

**G. Quorum and Action by Trustees.** A majority of all Trustees then in office shall constitute a quorum. Any meeting of Trustees may be adjourned by vote of a majority of Trustees present, whether or not a quorum is present, and the meeting may be held as adjourned without further notice. When a quorum is present at any meeting of the Trustees, a majority of the Trustees present and voting (excluding abstentions) shall decide any question, including the election of officers, unless otherwise required by law, the Articles of Organization or these Bylaws.

**H. Transfers of Interests in Land.** There shall be no transfer of title nor long-term lease of real property held by the Corporation without prior approval of not less than two-thirds of the Trustees. Such real property transactions shall be finally acted upon at a meeting of the Board only if presented and discussed at a prior meeting of the Board. Either meeting may be a special meeting and no less than four weeks shall elapse between the two meetings. Any property acquired by the Corporation after December 1, 1989 may be sold, any mortgage or pledge of real



property (regardless of when acquired) to secure borrowings by the Corporation may be granted, and any transfer of title or interest in real property pursuant to the foreclosure or endorsement of any such mortgage or other real property may be effected by any holder of a mortgage or other interest in real property of the Corporation, with the prior approval of not less than a majority of the Trustees (other than any Trustee or Trustees with a direct financial interest in the transaction being considered for approval) present at a regular or special meeting of the Board at which the mortgage or other interest is granted.

## ARTICLE V—TRUSTEES

A. *Executive Committee* There shall be an Executive Committee of the Board of Trustees which shall consist of not more than eleven (11) Trustees, including *ex officio* Trustees, elected by the Board.

The Chairperson of the Board shall act as Chairperson of the Executive Committee and the Vice Chairperson as Vice Chairperson. The Executive Committee shall meet at such times and places and upon such notice and appoint such subcommittees as the Committee shall determine.

The Executive Committee shall have and may exercise all the powers of the Board during the intervals between meetings of the Board except those powers specifically withheld, from time to time, by vote of the Board or by law. The Executive Committee may also appoint such committees, including persons who are not Trustees, as it may, from time to time, approve to make recommendations with respect to matters to be acted upon by the Executive Committee or the Board.

The Executive Committee shall keep appropriate minutes of its meetings, which shall be reported to the Board. Any actions taken by the Executive Committee shall also be reported to the Board.

B. *Nominating Committee* There shall be a Nominating Committee which shall consist of not fewer than four nor more than six Trustees appointed by the Board in a manner which shall reflect the balance between Corporate Trustees and Trustees-at-Large on the Board. The Nominating Committee shall nominate persons for election as Corporate Trustees and Trustees-at-Large, Chairperson of the Board, Vice Chairperson of the Board, President, Treasurer, Clerk, Director of the Laboratory and such other officers, if any, as needed, in accordance with the requirements of these Bylaws. The Nominating Committee shall also be responsible for overseeing the training of new Trustees. The Chairperson of the Board of Trustees shall appoint the Chairperson of the Nominating Committee. The Chairperson of the Science Council shall be an *ex officio* voting member of the Nominating Committee.

C. *Science Council* There shall be a Science Council (the "Council") which shall consist of Members of the Corporation elected to the Council by vote of the Members of the Corporation, and which shall advise the Board with respect to matters concerning the Corporation's mission, its scientific and instructional endeavors, and the appointment and promotions of persons or committees with responsibility for matters requiring scientific expertise. Unless otherwise approved by a majority of the members of the Council, the Chairperson of the Council shall be elected annually by the Council. The chief executive officer of the Corporation shall be an *ex officio* voting member of the Council.

D. *Board of Overseers* There shall be a Board of Overseers which shall consist of not fewer than five nor more than eight scientists who have expertise concerning matters with which the Corporation is involved. Members of the Board of Overseers may or may not be Members of the Corporation and may be appointed by the Board of Trustees on the basis of recommendations submitted from scientists and scientific organizations or societies. The Board of Overseers shall be available to review and offer recommendations to the officers, Trustees and Science Council regarding scientific activities conducted or proposed by the Corporation and shall meet from time to time, not less frequently than annually, as determined by the Board of Trustees.

E. *Board Committees Generally* The Trustees may elect or appoint one or more other committees (including, but not limited to, an Investment Committee, a Development Committee, an Audit Committee, a Facilities and Capital Equipment Committee and a Long-Range Planning Committee) and may delegate to any such committee or committees any or all of their powers, except those which by law, the Articles of Organization or these Bylaws the Trustees are prohibited from delegating; provided that any committee to which the powers of the Trustees are delegated shall consist solely of Trustees. The members of any such committee shall have such tenure and duties as the Trustees shall determine. The Investment Committee, which shall oversee the management of the Corporation's endowment funds and marketable securities shall include as *ex officio* members, the Chairperson of the Board, the Treasurer and the Chairperson of the Audit Committee, together with such Trustees as may be required for not less than two-thirds of the Investment

Committee to consist of Trustees. Except as otherwise provided by these Bylaws or determined by the Trustees, any such committee may make rules for the conduct of its business, but, unless otherwise provided by the Trustees or in such rules, its business shall be conducted as nearly as possible in the same manner as is provided by these Bylaws for the Trustees.

F. *Actions Without a Meeting* Any action required or permitted to be taken at any meeting of the Executive Committee or any other committee elected by the Trustees may be taken without a meeting if all members of such committees consent to the action in writing and such written consents are filed with the records of meetings. Members of the Executive Committee or any other committee elected by the Trustees may also participate in any meeting by means of a telephone conference call, or otherwise take action in such a manner as may, from time to time, be permitted by law.

G. *Manual of Procedures* The Board of Trustees, on the recommendation of the Executive Committee, shall establish guidelines and modifications thereof to be recorded in a Manual of Procedures. Guidelines shall establish procedures for: (1) Nomination and election of members of the Corporation, Board of Trustees and Executive Committee; (2) Election of Officers; (3) Formation and Function of Standing Committees.

## ARTICLE VI—OFFICERS

A. *Enumeration* The officers of the Corporation shall consist of a President, a Treasurer and a Clerk, and such other officers having the powers of President, Treasurer and Clerk as the Board may determine, and a Director of the Laboratory. The Corporation may have such other officers and assistant officers as the Board may determine, including (without limitation) a Chairperson of the Board, Vice Chairperson and one or more Vice Presidents, Assistant Treasurers or Assistant Clerks. Any two or more offices may be held by the same person. The Chairperson and Vice Chairperson of the Board shall be elected by and from the Trustees, but other officers of the Corporation need not be Trustees or Members. If required by the Trustees, any officer shall give the Corporation a bond for the faithful performance of his or her duties in such amount and with such surety or sureties as shall be satisfactory to the Trustees.

B. *Tenure* Except as otherwise provided by law, by the Articles of Organization or by these Bylaws, the President, Treasurer, and all other officers shall hold office until the first meeting of the Board following the annual meeting of Members and thereafter, until his or her successor is chosen and qualified.

C. *Resignation* Any officer may resign by delivering his or her written resignation to the Corporation at its principal office or to the President or Clerk and such resignation shall be effective upon receipt unless it is specified to be effective at some other time or upon the happening of some other event.

D. *Removal* The Board may remove any officer with or without cause by a vote of a majority of the entire number of Trustees then in office, at a meeting of the Board called for that purpose and for which notice of the purpose thereof has been given, provided that an officer may be removed for cause only after having an opportunity to be heard by the Board at a meeting of the Board at which a quorum is personally present and voting.

E. *Vacancy* A vacancy in any office may be filled for the unexpired balance of the term by vote of a majority of the Trustees present at any meeting of Trustees at which a quorum is present or by written consent of all of the Trustees, if less than a quorum of Trustees shall remain in office.

F. *Chairperson* The Chairperson shall have such powers and duties as may be determined by the Board and, unless otherwise determined by the Board, shall serve in that capacity for a term coterminous with his or her term as Trustee.

G. *Vice Chairperson* The Vice Chairperson shall perform the duties and exercise the powers of the Chairperson in the absence or disability of the Chairperson, and shall perform such other duties and possess such other powers as may be determined by the Board. Unless otherwise determined by the Board, the Vice Chairperson shall serve for a one-year term.

H. *Director* The Director shall be the chief operating officer and, unless otherwise voted by the Trustees, the chief executive officer of the Corporation. The Director shall, subject to the direction of the Trustees, have general supervision of the Laboratory and control of the business of the Corporation. At the annual meeting, the Director shall submit a report of the operations of the Corporation for such year and a statement of its affairs, and shall, from time to time, report to the Board all matters within his or her knowledge which the interests of the Corporation may require to be brought to its notice.

I. *Deputy Director* The Deputy Director, if any, or if there shall be more than one, the Deputy Directors in the order determined by the Trustees, shall, in the

absence or disability of the Director, perform the duties and exercise the powers of the Director and shall perform such other duties and shall have such other powers as the Trustees may, from time to time, prescribe.

*J. President.* The President shall have the powers and duties as may be vested in him or her by the Board.

*K. Treasurer and Assistant Treasurer.* The Treasurer shall, subject to the direction of the Trustees, have general charge of the financial affairs of the Corporation, including its long-range financial planning, and shall cause to be kept accurate books of account. The Treasurer shall prepare a yearly report on the financial status of the Corporation to be delivered at the annual meeting. The Treasurer shall also prepare or oversee all filings required by the Commonwealth of Massachusetts, the Internal Revenue Service, or other Federal and State Agencies. The account of the Treasurer shall be audited annually by a certified public accountant.

The Assistant Treasurer, if any, or if there shall be more than one, the Assistant Treasurers in the order determined by the Trustees, shall, in the absence or disability of the Treasurer, perform the duties and exercise the powers of the Treasurer, shall perform such other duties and shall have such other powers as the Trustees may, from time to time, prescribe.

*L. Clerk and Assistant Clerk.* The Clerk shall be a resident of the Commonwealth of Massachusetts, unless the Corporation has designated a resident agent in the manner provided by law. The minutes or records of all meetings of the Trustees and Members shall be kept by the Clerk who shall record, upon the record books of the Corporation, minutes of the proceedings at such meetings. He or she shall have custody of the record books of the Corporation and shall have such other powers and shall perform such other duties as the Trustees may, from time to time, prescribe.

The Assistant Clerk, if any, or if there shall be more than one, the Assistant Clerks in the order determined by the Trustees, shall, in the absence or disability of the Clerk, perform the duties and exercise the powers of the Clerk and shall perform such other duties and shall have such other powers as the Trustees may, from time to time, prescribe.

In the absence of the Clerk and an Assistant Clerk from any meeting, a temporary Clerk shall be appointed at the meeting.

*M. Other Powers and Duties.* Each officer shall have in addition to the duties and powers specifically set forth in these Bylaws, such duties and powers as are customarily incident to his or her office, and such duties and powers as the Trustees may, from time to time, designate.

## ARTICLE VII—AMENDMENTS

These Bylaws may be amended by the affirmative vote of the Members at any meeting, provided that notice of the substance of the proposed amendment is stated in the notice of such meeting. As authorized by the Articles of Organization, the Trustees, by a majority of their number then in office, may also make, amend or repeal these Bylaws, in whole or in part, except with respect to (a) the provisions of these Bylaws governing (i) the removal of Trustees and (ii) the amendment of these Bylaws and (b) any provisions of these Bylaws which by law, the Articles of Organization or these Bylaws, requires action by the Members.

No later than the time of giving notice of meeting of Members next following the making, amending or repealing by the Trustees of any Bylaw, notice thereof stating the substance of such change shall be given to all Members entitled to vote on amending the Bylaws.

Any Bylaw adopted by the Trustees may be amended or repealed by the Members entitled to vote on amending the Bylaws.

## ARTICLE VIII—INDEMNITY

Except as otherwise provided below, the Corporation shall, to the extent legally permissible, indemnify each person who is, or shall have been, a Trustee, director or officer of the Corporation or who is serving, or shall have served at the request of the Corporation as a Trustee, director or officer of another organization in which the Corporation directly or indirectly has any interest as a shareholder, creditor or otherwise, against all liabilities and expenses (including judgments, fines, penalties, and reasonable attorneys' fees and all amounts paid, other than to the Corporation or such other organization, in compromise or settlement) imposed upon or incurred by any such person in connection with, or arising out of, the defense or disposition of any action, suit or other proceeding, whether civil or criminal, in which he or she may be a defendant or with which he or she may be threatened or otherwise involved, directly or indirectly, by reason of his or her being or having been such a Trustee, director or officer.

The Corporation shall provide no indemnification with respect to any matter as to which any such Trustee, director or officer shall be finally adjudicated in such action, suit or proceeding not to have acted in good faith in the reasonable belief that his or her action was in the best interests of the Corporation. The Corporation shall provide no indemnification with respect to any matter settled or comprised unless such matter shall have been approved as in the best interests of the Corporation, after notice that indemnification is involved, by (i) a disinterested majority of the Board of the Executive Committee, or (ii) a majority of the Members.

Indemnification may include payment by the Corporation of expenses in defending a civil or criminal action or proceeding in advance of the final disposition of such action or proceeding upon receipt of an undertaking by the person indemnified to repay such payment if it is ultimately determined that such person is not entitled to indemnification under the provisions of this Article VIII, or under any applicable law.

As used in the Article VIII, the terms "Trustee," "director," and "officer" include their respective heirs, executors, administrators and legal representatives, and an "interested" Trustee, director or officer is one against whom in such capacity the proceeding in question or another proceeding on the same or similar grounds is then pending.

To assure indemnification under this Article VIII of all persons who are determined by the Corporation or otherwise to be or to have been "fiduciaries" of any employee benefits plan of the Corporation which may exist, from time to time, this Article VIII shall be interpreted as follows: (i) "another organization" shall be deemed to include such an employee benefit plan, including without limitation, any plan of the Corporation which is governed by the Act of Congress entitled "Employee Retirement Income Security Act of 1974," as amended, from time to time, ("ERISA"); (ii) "Trustee" shall be deemed to include any person requested by the Corporation to serve as such for an employee benefit plan where the performance by such person of his or her duties to the Corporation also imposes duties on, or otherwise involves services by, such person to the plan or participants or beneficiaries of the plan; (iii) "fines" shall be deemed to include any excise tax plan pursuant to ERISA; and (iv) actions taken or omitted by a person with respect to an employee benefit plan in the performance of such person's duties for a purpose reasonably believed by such person to be in the interest of the participants and beneficiaries of the plan shall be deemed to be for a purpose which is in the best interests of the Corporation.

The right of indemnification provided in this Article VIII shall not be exclusive of or affect any other rights to which any Trustee, director or officer may be entitled under any agreement, statute, vote of Members or otherwise. The Corporation's obligation to provide indemnification under this Article VIII shall be offset to the extent of any other source of indemnification of any otherwise applicable insurance coverage under a policy maintained by the Corporation or any other person. Nothing contained in the Article shall affect any rights to which employees and corporate personnel other than Trustees, directors or officers may be entitled by contract, by vote of the Board or of the Executive Committee or otherwise.

## ARTICLE IX—DISSOLUTION

The consent of every Trustee shall be necessary to effect a dissolution of the Marine Biological Laboratory. In case of dissolution, the property shall be disposed of in such a manner and upon such terms as shall be determined by the affirmative vote of two-thirds of the Trustees then in office in accordance with the laws of the Commonwealth of Massachusetts.

## ARTICLE X—MISCELLANEOUS PROVISIONS

*A. Fiscal Year.* Except as otherwise determined by the Trustees, the fiscal year of the Corporation shall end on December 31st of each year.

*B. Seal.* Unless otherwise determined by the Trustees, the Corporation may have a seal in such form as the Trustees may determine, from time to time.

*C. Execution of Instruments.* All checks, deeds, leases, transfers, contracts, bonds, notes and other obligations authorized to be executed by an officer of the Corporation in its behalf shall be signed by the Director or the Treasurer except as the Trustees may generally or in particular cases otherwise determine. A certificate by the Clerk or an Assistant Clerk, or a temporary Clerk, as to any action taken by the Members, Board of Trustees or any officer or representative of the Corporation shall as to all persons who rely thereon in good faith be conclusive evidence of such action.

*D. Corporate Records.* The original, or attested copies, of the Articles of Organization, Bylaws and records of all meetings of the Members shall be kept in Massachusetts at the principal office of the Corporation, or at an office of the Corpo-

ration's Clerk or resident agent. Said copies and records shall be kept in the same office. They shall be available at all reasonable times for inspection by any Member for any proper purpose, but not to secure a legal opinion on a purpose other than in the interest of the applicant, as a Member, in the affairs of the Corporation.

E. *Articles of Organization* All reference to the Articles of Organization shall be deemed to refer to the Articles of Organization of the Corporation, as amended and in effect, from time to time.

F. *Transactions with Interested Parties* No contract or transaction of fraud, no contract or other transaction between this Corporation and another corporation or any firm, association, partnership or person shall be void or invalidated by the fact that any Trustee or officer of this Corporation is pecuniarily or otherwise interested in or is a director, member or officer of such other corporation or of such firm, association or partnership, if such person is pecuniarily or otherwise interested

in such contract or other transaction or is in any way connected with any person or person, firm, association, partnership, or corporation pecuniarily or otherwise interested therein; provided that the fact that he or she individually or as a director, member or officer of such corporation, firm, association or partnership in such a party or is so interested shall be disclosed to or shall have been known by the Board of Trustees or a majority of such Members thereof as shall be present at a meeting of the Board of Trustees at which action upon any such contract or transaction shall be taken; any Trustee may be counted in determining the existence of a quorum and may vote at any meeting of the Board of Trustees for the purpose of authorizing any such contract or transaction with like force and effect as if he/she were not so interested, or were not a director, member or officer of such other corporation, firm, association or partnership, provided that any vote with respect to such contract or transaction must be adopted by a majority of the Trustees then in office who have no interest in such contract or transaction.







# CONTENTS

## BEHAVIOR AND BIOMECHANICS

- Drewes, Charles D., and Charles R. Fournier**  
Helical swimming in a freshwater oligochaete . . . 1
- Johnson, Amy S.**  
Sag-mediated modulated tension in terebellid tentacles exposed to flow . . . . . 10
- Trager, Geoff, and Amatzia Genin**  
Flow velocity induces a switch from active to passive suspension feeding in the porcelain crab *Petroliustes leptocheles* (Heller) . . . . . 20

## ECOLOGY AND EVOLUTION

- Eckman, James E., and David O. Duggins**  
Effects of flow speed on growth of benthic suspension feeders . . . . . 28
- Garcia-Esquivel, Zaul, and V. Monica Bricelj**  
Ontogenetic changes in microhabitat distribution of juvenile bay scallops, *Argopecten irradians irradians* (L.), in eelgrass beds, and their potential significance to early recruitment . . . . . 42

## DEVELOPMENT AND REPRODUCTION

- Janies, Daniel A., and Larry R. McEdward**  
Highly derived coelomic and water-vascular morphogenesis in a starfish with pelagic direct development . . . . . 56
- Olson, Richard Randolph, J. Lane Cameron, and Craig M. Young**  
Larval development (with observations on spawning) of the pencil urchin *Phyllacanthus imperialis*: a new intermediate larval form? . . . . . 77

## INVERTEBRATE MORPHOLOGY AND PHYLOGENY

- Balsler, Elizabeth J., Edward E. Ruppert, and William B. Jaeckle**  
Ultrastructure of the coeloms of auricularia larvae (Holothuroidea: Echinodermata): evidence for the presence of an axocoel . . . . . 86
- Emschermann, Peter**  
Lime-twig glands: a unique invention of an Antarctic entoproct . . . . . 97

## NEUROBIOLOGY

- Westfall, Jane A., and Cornelis J. P. Grimmelikhuijzen**  
Antho-RFamide immunoreactivity in neuronal synaptic and nonsynaptic vesicles of sea anemones 109

## PHYSIOLOGY

- Baker, Shirley M., and Nora B. Terwilliger**  
Hemoglobin structure and function in the rat-tailed sea cucumber, *Paracaudina chilensis* . . . . . 115
- Kreeger, D. A., and C. J. Langdon**  
Effect of dietary protein content on growth of juvenile mussels, *Mytilus trossulus* (Gould 1850) . . . 123
- Sevala, V. M., V. L. Sevala, and A. S. M. Saleuddin**  
Hemolymph insulin-like peptides (ILP) titers and the influence of ILP and mammalian insulin on the amino acid incorporation in the mantle collar *in vitro* in *Helisoma* (Mollusca) . . . . . 140

## RESEARCH NOTE

- Lohmann, Kenneth J., and Catherine M. Fittinghoff Lohmann**  
A light-independent magnetic compass in the leatherback sea turtle . . . . . 149
- Annual Report of the Marine Biological Laboratory** R1

Volume 185

Number 2

# THE BIOLOGICAL BULLETIN



Marine Biological Laboratory  
LIBRARY  
NOV 18 1993  
Woods Hole, Mass.

---

OCTOBER, 1993

---

Published by the Marine Biological Laboratory



# VALUABLE BIOLOGICAL RESOURCES



## Antarctic Fish Biology Evolution in a Unique Environment Joseph T. Eastman

This important volume provides original synthesis and novel overview of Antarctic fish biology, detailing the evolution of these fish in some of the most unusual and extreme environments in the world. Focusing on one group of fish, the notothenioids, which contains the majority of the current organismal diversity, this book describes a fauna that has evolved in isolation and experienced incredible adaptive radiation by acquiring numerous physiological specializations. Darwin's

finches and African cichlids may be joined by Antarctic fishes as exemplars of adaptive radiation.

The book's coverage is detailed and comprehensive, and the author clearly recognizes the fact that they are a component of a most interesting and biologically unique ecosystem and environment. Topics in **Antarctic Fish Biology** include past and present environments, fossil records, taxonomic composition of fauna, systematic relationships, diversification, and physiological adaptations.

May 1993, 322 pp., \$74.95/ISBN 0-12-228140-3



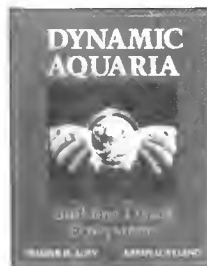
## Herpetology An Introductory Biology of Amphibians and Reptiles George R. Zug

Herpetology has always been one of the most exciting disciplines of zoology. During the past few years the field has continued to grow, yet it has been plagued by scarcity of comprehensive, up-to-date textbooks containing the most important developments. This timely book fills that void. Through skillful synthesis, the author summarizes the diversity in the biology of living amphibians and reptiles and describes the breadth of current

herpetological research. Topics covered include the evolution, classification, development, reproduction, population, and environmental issues surrounding the study of amphibians and reptiles. Designed as an advanced undergraduate textbook, **Herpetology** is a valuable resource for students, practitioners, and interested amateurs alike.

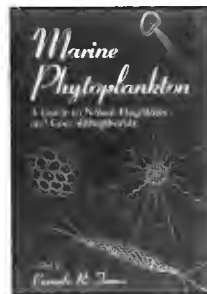
**CONTENTS: Diversity and History:** Amphibians. Origin and Evolution of Amphibians. Reptiles. Origin and Evolution of Reptiles. **As Predators and as Prey:** Diet and Feeding Defense and Escape. **Life Cycle—Reproduction, Development, and Growth:** Modes of Reproduction and Development. Dynamics of Reproduction. **Individuals and the Environment:** Spacing, Movement, and Orientation. Homeostasis—Air, Heat, and Water. **Populations and the Environment:** Population Dynamics. Population and Species Interactions. **Systematics and Classification:** Systematics—Theory and Practice. Caeilians and Salamanders. Frogs. Turtles and Crocodylians. Lizards, Amphisbaenians, and Tuataras. Snakes. Subject Index.

1993, 527 pp., \$50.00/ISBN 0-12-782620-3



## Dynamic Aquaria Building Living Ecosystems Walter H. Adey and Karen Loveland

1991, 643 pp., \$44.95/ISBN 0-12-043790-2



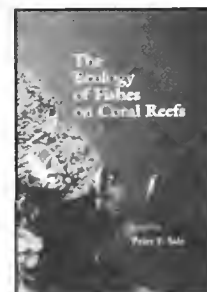
## Marine Phytoplankton A Guide to Naked Flagellates and Coccolithophorids

Edited by  
**Carmelo R. Tomas**  
Authored by  
**Jahn Thronsdén and Berit Heimdal**

**Marine Phytoplankton: A Guide to Naked Flagellates and Coccolithophorids** aids the identification of marine phytoplankton, particularly flagellated and extant coccolithophorid taxa. Because most identifications are routinely done employing light microscopy, the emphasis

is on this means of viewing. More advanced methods, like electron microscopy, are presented where appropriate. Many species are illustrated, and extensive citations encourage entry into the primary literature.

August 1993, 263 pp., \$79.00/ISBN 0-12-693010-4



## Now Available in Paperback! The Ecology of Fishes on Coral Reefs

Edited by  
**Peter F. Sale**

"This is an excellent book that will serve not just as an information and literature reference for future reef fish researchers: it will also serve as a fountain from which all ecologists will draw a cornucopia of ideas."

—BIOSCIENCE

This book provides a comprehensive and up-to-date review of the ecology of coral reef fishes presented by top researchers from North America and Australia. Over the last 20 years, immense strides have been made in our understanding of ecological systems in general and in reef fish ecology in particular. Many of the methodologies that reef fish ecologists use in their studies will be useful to a wider audience of ecologists for the design of their ecological studies. Significant among the impacts of the research on reef fish ecology are the development of nonequilibrium models of community organization, more emphasis on the role of recruitment variability in structuring local assemblages, the development and testing of evolutionary models of social organization and reproductive biology, and new insights into predator—prey and plant—herbivore interactions.

Paperback Reprint: \$39.95  
August 1993, 754 pp./ISBN 0-12-615181-7  
Casebound \$74.95  
1991, 754 pp./ISBN 0-12-615180-6

## Two Volumes in the ISOTOPIC TECHNIQUES IN PLANT, SOIL, AND AQUATIC BIOLOGY Series

### Carbon Isotope Techniques

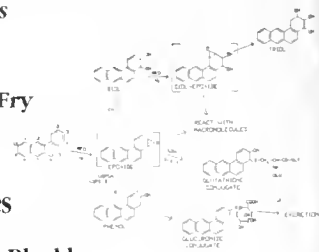
Edited by  
**David C. Coleman and Brian Fry**

Paperback: \$42.95/ISBN 0-12-179731-7  
Casebound \$85.00/ISBN 0-12-179730-9  
1991, 274 pp.

### Nitrogen Isotope Techniques

Edited by  
**Roger Knowles and T. Henry Blackburn**

1992, 311 pp., \$69.95/ISBN 0-12-416965-1



Order from your local bookseller or directly from



**ACADEMIC PRESS**

Order Fulfillment Department DM17915  
6277 Sea Harbor Drive, Orlando, FL 32887

Prices subject to change without notice. © 1993 by Academic Press, Inc. All Rights Reserved. KS/AB/BK—07103

CALL TOLL FREE

**1-800-321-5068**

FAX **1-800-336-7377**

# THE BIOLOGICAL BULLETIN

PUBLISHED BY  
THE MARINE BIOLOGICAL LABORATORY

## Associate Editors

PETER A. V. ANDERSON, The Whitney Laboratory, University of Florida

DAVID EPEL, Hopkins Marine Station, Stanford University

J. MALCOLM SHICK, University of Maine, Orono

## Editorial Board

WILLIAM D. COHEN, Hunter College

DAPHNE GAIL FAUTIN, University of Kansas

WILLIAM F. GILLY, Hopkins Marine Station,  
Stanford University

ROGER T. HANLON, Marine Biomedical  
Institute,  
University of Texas Medical Branch

CHARLES B. METZ, University of Miami

K. RANGA RAO, University of West Florida

RICHARD STRATHMANN, Friday Harbor Laboratories,  
University of Washington

STEVEN VOGEL, Duke University

SARAH ANN WOODIN, University of South Carolina

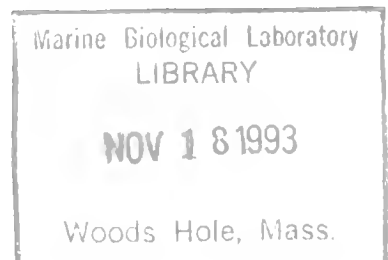
*Editor:* MICHAEL J. GREENBERG, The Whitney Laboratory, University of Florida

*Managing Editor:* PAMELA L. CLAPP, Marine Biological Laboratory

OCTOBER, 1993

Printed and Issued by  
LANCASTER PRESS, Inc.

3575 HEMPLAND ROAD  
LANCASTER, PA



## THE BIOLOGICAL BULLETIN

THE BIOLOGICAL BULLETIN is published six times a year by the Marine Biological Laboratory, MBL Street, Woods Hole, Massachusetts 02543.

Subscriptions and similar matter should be addressed to Subscription Manager, THE BIOLOGICAL BULLETIN, Marine Biological Laboratory, Woods Hole, Massachusetts 02543. Single numbers, \$35.00. Subscription per volume (three issues), \$87.50 (\$175.00 per year for six issues).

Communications relative to manuscripts should be sent to Michael J. Greenberg, Editor-in-Chief, or Pamela L. Clapp, Managing Editor, at the Marine Biological Laboratory, Woods Hole, Massachusetts 02543. Telephone: (508) 548-3705, ext. 428. FAX: 508-540-6902. E-mail: pamcl@hoh.mbl.edu.

POSTMASTER: Send address changes to THE BIOLOGICAL BULLETIN, Marine Biological Laboratory, Woods Hole, MA 02543.

Copyright © 1993, by the Marine Biological Laboratory

Second-class postage paid at Woods Hole, MA, and additional mailing offices.  
ISSN 0006-3185

## INSTRUCTIONS TO AUTHORS

*The Biological Bulletin* accepts outstanding original research reports of general interest to biologists throughout the world. Papers are usually of intermediate length (10–40 manuscript pages). A limited number of solicited review papers may be accepted after formal review. A paper will usually appear within four months after its acceptance.

Very short, especially topical papers (less than 9 manuscript pages including tables, figures, and bibliography) will be published in a separate section entitled "Research Notes." A Research Note in *The Biological Bulletin* follows the format of similar notes in *Nature*. It should open with a summary paragraph of 150 to 200 words comprising the introduction and the conclusions. The rest of the text should continue on without subheadings, and there should be no more than 30 references. References should be referred to in the text by number, and listed in the Literature Cited section in the order that they appear in the text. Unlike references in *Nature*, references in the Research Notes section should conform in punctuation and arrangement to the style of recent issues of *The Biological Bulletin*. Materials and Methods should be incorporated into appropriate figure legends. See the article by Lohmann *et al.* (October 1990, Vol. 179: 214–218) for sample style. A Research Note will usually appear within two months after its acceptance.

The Editorial Board requests that regular manuscripts conform to the requirements set below; those manuscripts that do not conform will be returned to authors for correction before review.

1. **Manuscripts.** Manuscripts, including figures, should be submitted in triplicate. (Xerox copies of photographs are not acceptable for review purposes.) The original manuscript must be typed in no smaller than 12 pitch, using double spacing (including figure legends, footnotes, bibliography, etc.) on one side of 16- or 20-lb. bond paper, 8½ by 11 inches. Please, no right justification. Manuscripts should be proofread carefully and errors corrected legibly in black ink. Pages should be numbered consecutively. Margins on all sides should be at least 1 inch (2.5 cm). Manuscripts should conform to the *Council of Biology Editors Style Manual*, 5th Edition (Council of Biology Editors, 1983) and to American spelling. Unusual abbreviations should

be kept to a minimum and should be spelled out on first reference as well as defined in a footnote on the title page. Manuscripts should be divided into the following components: Title page, Abstract (of no more than 200 words), Introduction, Materials and Methods, Results, Discussion, Acknowledgments, Literature Cited, Tables, and Figure Legends. In addition, authors should supply a list of words and phrases under which the article should be indexed.

2. **Title page.** The title page consists of: a condensed title or running head of no more than 35 letters and spaces, the manuscript title, authors' names and appropriate addresses, and footnotes listing present addresses, acknowledgments or contribution numbers, and explanation of unusual abbreviations.

3. **Figures.** The dimensions of the printed page, 7 by 9 inches, should be kept in mind in preparing figures for publication. We recommend that figures be about 1½ times the linear dimensions of the final printing desired, and that the ratio of the largest to the smallest letter or number and of the thickest to the thinnest line not exceed 1:1.5. Explanatory matter generally should be included in legends, although axes should always be identified on the illustration itself. Figures should be prepared for reproduction as either line cuts or halftones. Figures to be reproduced as line cuts should be unmounted glossy photographic reproductions or drawn in black ink on white paper, good-quality tracing cloth or plastic, or blue-lined coordinate paper. Those to be reproduced as halftones should be mounted on board, with both designating numbers or letters and scale bars affixed directly to the figures. All figures should be numbered in consecutive order, with no distinction between text and plate figures. The author's name and an arrow indicating orientation should appear on the reverse side of all figures.

4. **Tables, footnotes, figure legends, etc.** Authors should follow the style in a recent issue of *The Biological Bulletin* in preparing table headings, figure legends, and the like. Because of the high cost of setting tabular material in type, authors are asked to limit such material as much as possible. Tables, with their headings and footnotes, should be typed on separate sheets, numbered with consecutive Roman numerals, and placed after

the Literature Cited. Figure legends should contain enough information to make the figure intelligible separate from the text. Legends should be typed double spaced, with consecutive Arabic numbers, on a separate sheet at the end of the paper. Footnotes should be limited to authors' current addresses, acknowledgments or contribution numbers, and explanation of unusual abbreviations. All such footnotes should appear on the title page. Footnotes are not normally permitted in the body of the text.

5. **Literature cited.** In the text, literature should be cited by the Harvard system, with papers by more than two authors cited as Jones *et al.*, 1980. Personal communications and material in preparation or in press should be cited in the text only, with author's initials and institutions, unless the material has been formally accepted and a volume number can be supplied. The list of references following the text should be headed Literature Cited, and must be typed double spaced on separate pages, conforming in punctuation and arrangement to the style of recent issues of *The Biological Bulletin*. Citations should include complete titles and inclusive pagination. Journal abbreviations should normally follow those of the U. S. A. Standards Institute (USASI), as adopted by BIOLOGICAL ABSTRACTS and CHEMICAL ABSTRACTS, with the minor differences set out below. The most generally useful list of biological journal titles is that published each year by BIOLOGICAL ABSTRACTS (BIOSIS List of Serials; the most recent issue). Foreign authors, and others who are accustomed to using THE WORLD LIST OF SCIENTIFIC PERIODICALS, may find a booklet published by the Biological Council of the U.K. (obtainable from the Institute of Biology, 41 Queen's Gate, London, S.W.7, England, U.K.) useful, since it sets out the WORLD LIST abbreviations for most biological journals with notes of the USASI abbreviations where these differ. CHEMICAL ABSTRACTS publishes quarterly supplements of additional abbreviations. The following points of reference style for THE BIOLOGICAL BULLETIN differ from USASI (or modified WORLD LIST) usage:

A. Journal abbreviations, and book titles, all underlined (for *italics*)

B. All components of abbreviations with initial capitals (not as European usage in WORLD LIST *e.g.*, *J. Cell. Comp. Physiol.* NOT *J. cell. comp. Physiol.*)

C. All abbreviated components must be followed by a period, whole word components *must not* (*i.e.*, *J. Cancer Res.*)

D. Space between all components (*e.g.*, *J. Cell. Comp. Physiol.*, not *J.Cell.Comp.Physiol.*)

E. Unusual words in journal titles should be spelled out in full, rather than employing new abbreviations invented by the author. For example, use *Rit Vísindafjélagið Íslendinga* without abbreviation.

F. All single word journal titles in full (*e.g.*, *Veliger*, *Ecology*, *Brain*).

G. The order of abbreviated components should be the same as the word order of the complete title (*i.e.*, *Proc.* and *Trans.* placed where they appear, not transposed as in some BIOLOGICAL ABSTRACTS listings).

H. A few well-known international journals in their preferred forms rather than WORLD LIST or USASI usage (*e.g.*, *Nature*, *Science*, *Evolution* NOT *Nature, Lond.*, *Science, N.Y.*; *Evolution, Lancaster, Pa.*)

6. **Reprints, page proofs, and charges.** Authors receive their first 100 reprints (without covers) free of charge. Additional reprints may be ordered at time of publication and normally will be delivered about two to three months after the issue date. Authors (or delegates for foreign authors) will receive page proofs of articles shortly before publication. They will be charged the current cost of printers' time for corrections to these (other than corrections of printers' or editors' errors). Other than these charges for authors' alterations, *The Biological Bulletin* does not have page charges.

# ERRATA

*The Biological Bulletin*, Volume 184, Number 3, pages 322–329

The following corrections should be noted in the paper by Gabriele Gaus *et al.* titled "The sequences of five neuropeptides isolated from *Limulus* using antisera to FMRFamide."

Table 1

Representatives of four classes of FMRFamide-related peptides present in dipteran insects\*

Class	Sequence	Reference
FaGRPs <sup>a</sup>	Asp-Pro-Lys-Gln-Asp-Phe-Met-Arg-Phe-NH <sub>2</sub>	(Schneider and Taghert, 1988)
Myosuppressins <sup>b</sup>	Thr-Asp-Val-Asp-His-Val-Phe-Leu-Arg-Phe-NH <sub>2</sub>	(Nichols, 1992a)
Sulfakinins <sup>c</sup>	Phe-Asp-Asp-Tyr-Gly-His-Met-Arg-Phe-NH <sub>2</sub>	(Nichols, 1992b)
Head peptides <sup>d</sup>	pGlu-Arg-Pro-Pro-Ser-Leu-Lys-Thr-Arg-Phe-NH <sub>2</sub>	(Lea and Brown, 1990)

\* The first three peptides in the list were isolated from *Drosophila melanogaster*; the fourth is from *Aedes aegypti*.

<sup>a</sup> FMRFamide-gene-related peptides; multiple, variable copies processed from a precursor.

<sup>b</sup> Similar C-terminal tetrapeptide, but not encoded on any known FMRFamide gene; peptide shown is *Drosophila* myosuppressin; type of the class is leucomyosuppressin from *Leucophaea maderae*.

<sup>c</sup> Only C-terminal tripeptide is analogous to FaGRPs; peptide shown is drosulfakinin; type of the class is leucosulfakinin.

<sup>d</sup> Only C-terminal dipeptide is analogous to FaGRPs.

The Table shown above replaces the original Table 1 in the paper. Its significance is unchanged; *i.e.*, it illustrates, with selected examples, the four distinct classes of FaRPs that seem to occur in all insect species. The errors are as follows:

- The sulfakinin sequence shown in the original Table 1 was *leucosulfakinin* (pGlu-Ser-Asp-Asp-), rather than *drosulfakinin* (Phe-Asp-Asp-). Moreover, the original reference (Nichols *et al.*, 1988) is to the DNA sequence of *drosulfakinin*; but the processed peptide has also been sequenced (Nichols and Conkright, 1990; Nichols, 1992). The last of these is the most appropriate citation.

- In the original Table 1, the reference to the head peptide is Matsumoto *et al.*, 1989. Indeed, as Lea and Brown (1990) state: "Dr. Shogo Matsumoto, working in our laboratory, developed a purification protocol that yielded three related peptides from heads of *Aedes aegypti*. These were purified to homogeneity and sequenced." Two of these sequences were published in Matsumoto *et al.* (1989), but the head peptide shown in Table 1 was not. The correct citation, now in the revised Table 1, is therefore Lea and Brown (1990). To complete the story, the two sequences presented in Matsumoto *et al.* (1989) are: pGlu-Arg-Pro-Hyp-Ser-Leu-Lys-Thr-Arg-Phe-NH<sub>2</sub> and Thr-Arg-Phe-NH<sub>2</sub>. Note that the first of these is the same as the head peptide in Table 1, except that the proline at position 4 is hydroxylated.

## Literature Cited

- Lea, A. O., and M. R. Brown. 1990. Neuropeptides of mosquitoes. Pp. 181–188 in *Molecular Insect Science*, H. H. Hagedorn, J. E. Hildebrand, M. G. Kidwell, and J. H. Law, eds. Plenum Press, New York.
- Matsumoto, S., M. R. Brown, J. W. Crim, S. R. Vigna, and A. O. Lea. 1989. Isolation and primary structure of neuropeptides from the mosquito, *Aedes aegypti*, immunoreactive to FMRFamide antiserum. *Insect Biochem.* 19: 277–283.
- Nichols, R. 1992a. Isolation and structural characterization of *Drosophila* TDVDHVFLRFamide and FMRFamide containing neural peptides. *J. Mol. Neurosci.* 3: 213–218.
- Nichols, R. 1992b. Isolation and expression of the *Drosophila* drosulfakinin neural peptide gene-product, DSK-1. *Mol. Cell Neurosci.* 3: 342–347.
- Nichols, R., and M. Conkright. 1990. Isolation and characterization of *Drosophila* peptides containing an -ArgPheNH<sub>2</sub> C-terminus. *Soc. Neurosci. Abstr.* 16: 1031.

*The Biological Bulletin*, Volume 185, Number 1, page 42

The following correction should be noted in the paper by Zaul Garcia-Esquivel and V. Monica Bricelj titled "Ontogenic changes in microhabitat distribution of juvenile bay scallops, *Argopecten irradians irradians* (L.), in eelgrass beds, and their potential significance to early recruitment."

The first word of the title should be replaced with the word "Ontogenetic" so that the corrected title now reads: "Ontogenetic changes in microhabitat distribution of juvenile bay scallops, *Argopecten irradians irradians* (L.), in eelgrass beds, and their potential significance to early recruitment."

# A Comparative Study of Reproduction and Development in the Polychaete Family Terebellidae

DAMHNAIT MCHUGH\*

*Department of Biology and Institute of Marine Sciences, University of California,  
Santa Cruz, California 95064*

**Abstract.** The reproduction and development of four species of terebellid polychaetes from the west coast of North America were studied and compared with several other terebellid species to reveal the covariation of life history traits in the group, and assess any limitations on terebellid life history evolution that may be imposed by ancestry or body design. The four species in the present study span the range of reproductive and developmental modes known for the family Terebellidae. *Eupolyornia crescentis* and *Neoamphitrite robusta* are both free spawners that reproduce during discrete 3-month breeding periods. In *E. crescentis*, oogenesis takes from 5 to 8 months and spawning occurs from July to September, maximum oocyte diameter is 210  $\mu\text{m}$ , and fecundity reaches  $\sim 128,500$  during a single breeding period. The *E. crescentis* larva develops near the bottom for about 7 days before settling as a five-setiger juvenile. *Neoamphitrite robusta* reproduces from April to July after a 12-month oogenic cycle; oocytes in this species measure up to 180  $\mu\text{m}$ , and fecundity reaches  $\sim 830,000$ . The two brooders in the study, *Ramex californiensis* and *Thelepus crispus*, brood their larvae in the maternal tube. *T. crispus* reproduces continuously for at least 6 months, and has up to 51,500 larvae in a single brood. The oocytes in this species (400  $\mu\text{m}$ ) give rise to larvae that are brooded to the one-setiger stage and then emerge to undergo a one-day planktonic period before the larvae settle and become juveniles at eight setigers. *Ramex californiensis* reproduces continuously year round; larvae are brooded in cocoons that are laid sequentially in the tube, with up to 44 larvae in a single cocoon. Development from the 410  $\mu\text{m}$  oocytes

is direct, and juveniles have 11 setigers. Unlike *E. crescentis* and *N. robusta*, in which oogenesis is synchronized within individuals to produce a peak of large oocytes during the discrete spawning period, *R. californiensis* and *T. crispus* females have a wide range of oocyte sizes throughout the year.

Correlation analysis and analysis of variance of reproductive and developmental traits of these and several other terebellid species revealed some expected trends. For example, egg size varies according to the mode of reproduction (free spawning, extratubular brooding, or intratubular brooding), and is also correlated with juvenile size. However, egg size does not predict fecundity in terebellids when body size is held constant, and brooding is not restricted to small-bodied species. Indeed, the largest and smallest species in the study brood their larvae intratubularly, suggesting that allometric constraints may not be important in determining mode of reproduction in these polychaetes. The Terebellidae is a diverse family found in all marine habitats, yet all known terebellid larvae are non-feeding; this contrasts with the occurrence of both planktotrophy and lecithotrophy in other polychaete families, and leads to the proposal that larval development in terebellids has been constrained during the evolution of the lineage. The results of this study demonstrate that generalizations regarding complex relationships among life history traits are often inappropriate. The need for more comparative studies of marine invertebrate reproduction and development, and the integration of phylogenetic analyses into the study of life history evolution in marine invertebrates is highlighted.

## Introduction

The great diversity of reproductive and developmental modes exhibited by marine invertebrates presents a chal-

Received 18 December 1992; accepted 14 July 1993.

\* Present address: Department of Invertebrate Zoology, NHB-163, National Museum of Natural History, Smithsonian Institution, Washington, DC 20560.

lenge to evolutionary biologists who seek patterns and trends in life histories. Responses have included models of optimal combinations of life history traits (e.g., Vance, 1973; Christiansen and Fenchel, 1979; Roughgarden, 1989), and theoretical arguments and experimental tests on the adaptive significance of certain traits (e.g., Thorson, 1950; Chia, 1974; Pechenik, 1979; Doyle and Hunte, 1981; Sinervo and McEdward, 1988; Strathmann, 1985; Grant, 1990; Hart, 1992). Several hypotheses regarding the associations between traits have also been investigated using specific cases (e.g., Strathmann *et al.*, 1984; Kabat, 1985; Hess, 1993). However, only a few studies have undertaken statistical analyses of comparative data to assess the covariation of life history traits in marine invertebrate groups (Hines, 1982; Buroker, 1985; Olive, 1985; Emlet *et al.*, 1987; McEdward and Chia, 1991). This contrasts with the numerous investigations into life history evolution of vertebrates, in which the comparative approach has clearly identified relationships among life history traits, and has documented biological constraints and phylogenetic effects on the evolution of life histories (e.g., Trendall, 1982; Stearns, 1983, 1984a, b; Dunham and Miles, 1985; Harvey and Clutton-Brock, 1985; Gittleman, 1986; Saether, 1988; Miles and Dunham, 1992).

While the range of reproductive modes in most marine invertebrate phyla is well known, life history data are scattered and in many cases incomplete, so that comparative data sets are rare. In this study, I combine data from autecological investigations of terebellid polychaetes with my own results for four terebellid species from the west coast of North America to construct a data matrix of life history traits for the family Terebellidae. Despite large variations in size, the body organization is relatively homogenous among all the genera in the family. This feature, as well as the fact that no feeding larvae have been reported in this group, means that the comparisons made in the present study will not be complicated by the covariation of traits with different body forms or different larval nutrition mechanisms. Nonetheless, it is obvious from previous studies of terebellids [*Nicolea zostericola* (Eckelbarger, 1974, 1975, 1976), *Neoleprea streptochaeta* (Duchêne, 1979), *Thelepus setosus* (Duchêne, 1980, 1991), *Eupolymnia nebulosa* (Grémare, 1986; Bhaud *et al.*, 1987; Bhaud and Grémare, 1988; Bhaud, 1991), *Lance conchilega* (Heimler, 1981; Bhaud, 1988, 1991; Smith, 1989a, b), and *Ramex californiensis* (Blake, 1991)], that the Terebellidae, like many other polychaete families, exhibit a high degree of heterogeneity in terms of reproduction and development (Wilson, 1991).

The following life history traits were investigated in *Eupolymnia crescentis* Chamberlin, 1919, *Neoamphitrite robusta* (Johnson, 1901), *Thelepus crispus* Johnson, 1901, and *Ramex californiensis* Hartman, 1944, and gathered from previously published accounts of several other ter-

ebellid species: (1) mode of reproduction, *i.e.*, free spawning, extratubular brooding or intratubular brooding; (2) body size, *i.e.*, maximum body length; (3) maximum oocyte size; (4) maximum fecundity, *i.e.*, maximum number of full-grown oocytes in free spawning species, or maximum number of larvae in a single brood in brooding species; (5) mode of development, *i.e.*, planktonic, mixed, or direct development; (6) stage at juvenile, *i.e.*, the number of setigers present when larvae begin to feed on the adult diet; (7) duration of the breeding season; and (8) breeding strategy, *i.e.*, iteroparous or semelparous. These data were analyzed to reveal the covariation of life history traits in the Terebellidae, and comparisons were made with other polychaetes and marine invertebrates in general. The possible limitations on life history evolution in the Terebellidae, imposed either by ancestry or design, were also examined, and the need for a phylogenetic analysis of the group discussed.

## Materials and Methods

### Species

*Eupolymnia crescentis*, which ranges from Alaska to western Mexico, is common in sandy mud sediments of bays and estuaries of the California coast. *Neoamphitrite robusta*, which is distributed from Alaska to California, is also found in abundance in mud and under rocks of the intertidal zone of the central California coast. *Thelepus crispus* is found in tubes of coarse sand and gravel attached to the undersides of rocks in the intertidal from Alaska to southern California. Apart from the observation that *T. crispus* spawns yellow-orange oocytes onto the sediment surface in July and August on San Juan Island, Washington (Strathmann, 1987), the reproduction and development of these three common species have remained undescribed. The larval development of the fourth species, *Ramex californiensis*, which is restricted in its distribution to the central California coast, is known (Blake, 1991). I have supplemented the observations of Blake (1991) to provide more information about the reproductive biology of this species.

### Reproductive mode

The reproductive mode refers to the degree of parental care provided to fertilized eggs. Eggs may be free spawned to give rise to planktonic larvae, or larvae may be brooded either within the maternal tube or in a gelatinous mass outside the tube. Each species was assigned a reproductive mode according to observations made in the field or in the lab.

### Body size

Maximum body length of each species was recorded from personal observations or from the literature. Length

was chosen as a measure of body size because of its correlation with body volume (e.g., *T. crispus*:  $r^2 = 0.88$ ,  $n = 17$ ,  $P < 0.001$ ), and because it is a parameter that is often reported for terebellids in the literature.

#### *Length of breeding season*

Between April 1990 and May 1992, *E. crescentis* and *N. robusta* were collected intertidally from Bodega Harbor, California. Monthly samples were fixed in 10% seawater-buffered formalin and preserved in 70% ethanol. The coelomic contents from up to 10 females from each sample were examined, and the maximum diameters of 80 oocytes from each female were measured at 100 $\times$  magnification. A year-long time series of oocyte size frequency histograms was constructed for each species to show the pattern of oocyte development and likely breeding season for the population. Oocyte diameter data were log transformed before analysis of variance (ANOVA) to examine the degree of synchrony among samples throughout the year, and among females in each sample; Scheffé's *post hoc* test was used to clarify the reasons for any significant differences (Sokal and Rohlf, 1981). The reproductive period of each species was confirmed by spawning observations in the lab, and by qualitative observations of coelomic contents during a second reproductive season.

*R. californiensis* was sampled intertidally from Dillon Beach, California, almost every month from August 1990 to February 1992. The worms were fixed and preserved as described above, and oocyte size frequency histograms were constructed for bimonthly intervals from August 1990 to June 1991. The number of oocytes in each female was small, therefore all the oocytes found in each female were measured. The presence of broods in tubes from the monthly collections was also noted. *Thelepus crispus* was observed in the field and collected from a variety of locations on San Juan Island, Washington, from July to December, 1991. The presence of egg masses in the field and in the lab was recorded during this time to estimate the length of the reproductive period.

#### *Maximum oocyte size and fecundity*

Maximum oocyte size was recorded from coelomic samples of mature females of each species, and estimates of fecundity for *E. crescentis* and *N. robusta* were made as follows. The number of oocytes in three 2-ml subsamples from a 250-ml suspension of all oocytes removed from weighed, mature females were counted. An estimate of the total number of oocytes in each worm was then extrapolated from the mean number in the subsamples. To estimate fecundity in *R. californiensis*, the number of larvae were counted in all cocoons taken from five tubes from each of three months (April, May, and June, 1991); as the cocoons of *R. californiensis* are deposited as se-

quential broods rather than simultaneously, maximum fecundity was recorded as the highest number of larvae in a single cocoon, *i.e.*, the maximum number of larvae in one brood. In *T. crispus*, a single brood consists of paired, elongated egg masses that are attached to the maternal tube. Entire broods collected in the field in July and October 1991 were blotted and weighed, and the number of embryos in a weighed subsample of each brood was counted. This number was extrapolated to give an estimate of the number of larvae in an entire brood.

#### *Mode of development*

Several adults of *E. crescentis* spawned spontaneously in seawater tables at Bodega Marine Laboratory, California, following collection on August 9, 1991. On August 13, other adults were placed in individual finger bowls in 0.2  $\mu\text{m}$  filtered seawater and induced to spawn by increasing the seawater temperature by about 8 $^\circ\text{C}$  over one hour in direct sunlight, followed by flushing with ambient temperature seawater ( $\sim 16^\circ\text{C}$ ). Fertilizations were made in 0.2  $\mu\text{m}$  filtered seawater and larvae were maintained at Long Marine Laboratory, California, at about 16 $^\circ\text{C}$  with regular water changes. Settled larvae were transferred to 100  $\mu\text{m}$  filtered seawater, and raised in dishes that were covered with microbial films.

Although individuals of *N. robusta* spawned occasionally in the lab during May 1991, attempts to induce synchronous spawning of males and females during two reproductive periods (May, 1991; April and May, 1992) failed. Development in *R. californiensis* has been described by Blake (1991), and was also monitored in October and November, 1990, in this study. Embryos were collected in the field, or from cocoons laid in the lab. Worms and cocoons were maintained in small petri dishes with some sand and nitex mesh in 5  $\mu\text{m}$  filtered seawater at about 14 $^\circ\text{C}$ . For *T. crispus*, development was recorded in October and November, 1991, from broods collected on San Juan Island and raised at Friday Harbor Laboratories, Washington, in 64  $\mu\text{m}$  filtered seawater at about 11 $^\circ\text{C}$ .

#### *Comparative data*

Data on the reproduction and development of seven other terebellids were collected from the literature. When available, the following life history traits were recorded for each species: (1) mode of reproduction, *i.e.*, free spawning, extratubular brooding or intratubular brooding; (2) maximum body length (mm); (3) maximum diameter ( $\mu\text{m}$ ) of coelomic oocytes; (4) maximum fecundity, *i.e.*, maximum number of full grown oocytes in free spawning species, or maximum number of larvae in a single brood in brooding species; these data vary over several orders of magnitude and therefore were log transformed for sta-



tistical analyses; (5) number of days larvae spend in the plankton; (6) stage at juvenile, *i.e.*, the number of setigers present on larvae when they begin to feed on the adult diet; (7) duration of the breeding season (months); and (8) breeding strategy, *i.e.*, iteroparous or semelparous. The relationships between these traits in the family Terebellidae were examined using a correlation matrix. ANOVA was used to determine whether traits differed significantly among the reproductive modes, and multiple regression analysis was used to examine the covariation of some traits when body size is held constant.

## Results

### Present study

**Reproductive mode.** *Eupolyommia crescentis* and *Ncoamphitrite robusta* are both broadcast spawners, as shown by their free-spawning behavior in the lab during July and August, 1991, and May, 1991, respectively. Moreover, no brooded larvae were ever found in the field. *Thelepus crispus* and *Ramex californiensis*, on the other hand, are both brooders. Females of *T. crispus* were collected in the field with several elongated egg masses attached to the interior of the tube. *Ramex californiensis* sequentially lays small cocoons along the length of the inner tube wall.

**Body size.** The maximum body length of the four species ranges from 25 mm in *R. californiensis* to 280 mm in *T. crispus*; *E. crescentis* measures up to 130 mm, and *N. robusta* has a maximum length of 250 mm (Hartman, 1969; pers. obs.). Using the volume of a cone ( $\frac{1}{3}\pi r^2 h$ ) as an estimate of body volume, with body length =  $h$  and body width =  $2r$ , the order of body sizes among the four species remains the same (*R. californiensis*:  $\sim 26 \text{ mm}^3$ ; *E. crescentis*:  $\sim 3400 \text{ mm}^3$ ; *N. robusta*:  $\sim 11,000 \text{ mm}^3$ ; *T. crispus*:  $\sim 12,400 \text{ mm}^3$ ).

**Length of breeding season.** Figure 1 shows the oocyte size frequency histogram for *E. crescentis* from April 1990 to March 1991. Oocytes grow rapidly from about  $50 \mu\text{m}$  in April to begin to accumulate as full-grown oocytes of about  $180 \mu\text{m}$  in diameter from late May, until there is a single peak around  $185 \mu\text{m}$  in August (Fig. 1). The annual spawning period of *E. crescentis* at Bodega Harbor is from July through September, as is indicated from the histograms and confirmed by observations of spawning in the lab; although no sample is available for September 1990, mature females were present in a sample taken in September 1991. No coelomic oocytes were observed in the post-spawning population in October 1990, and it is not until January 1991 that proliferation of primary oocytes begins again. Development from small primary oocytes released into the coelom to full grown oocytes takes from five to eight months in this species. ANOVA tests show significant differences in mean oocyte diameter

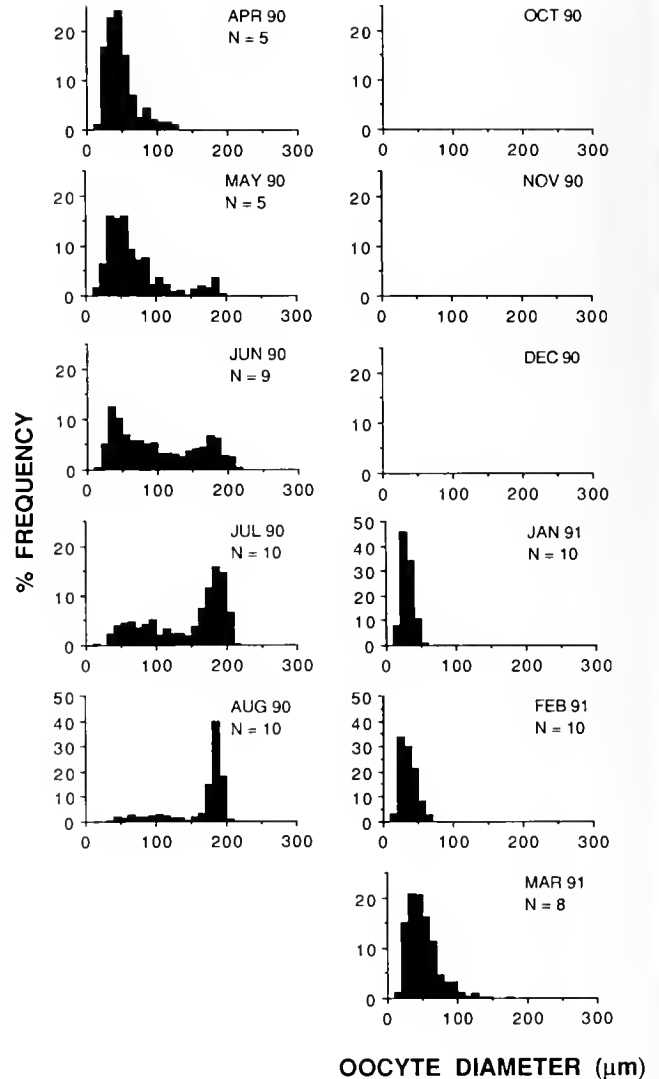


**Figure 1.** Monthly size-frequency histograms of maximum oocyte diameter for *Eupolyommia crescentis* from Bodega Harbor, California, from April 1990 to March 1991. No sample was available for September 1990; 15 worms were examined in each sample from October, November, and December, 1990, but no gametes were seen. N, number of females in each sample.

among females in monthly samples (*e.g.*, June, 1990:  $F = 6.295$ ,  $df = 8$ ,  $P < 0.0001$ ; July, 1990:  $F = 11.50$ ,  $df = 9$ ,  $P < 0.0001$ ; August, 1990:  $F = 12.34$ ,  $df = 9$ ,  $P < 0.0001$ ). However, multiple comparison tests reveal that in August, 1990, the month in which the highest proportion of full-grown oocytes are present in the population, nine of the ten females did not differ significantly in their mean oocyte diameter.

*Ncoamphitrite robusta* shows a different pattern of reproduction in which oogenesis takes a full year, from May to the following April, and mature females with large, full-grown oocytes are present in the population from

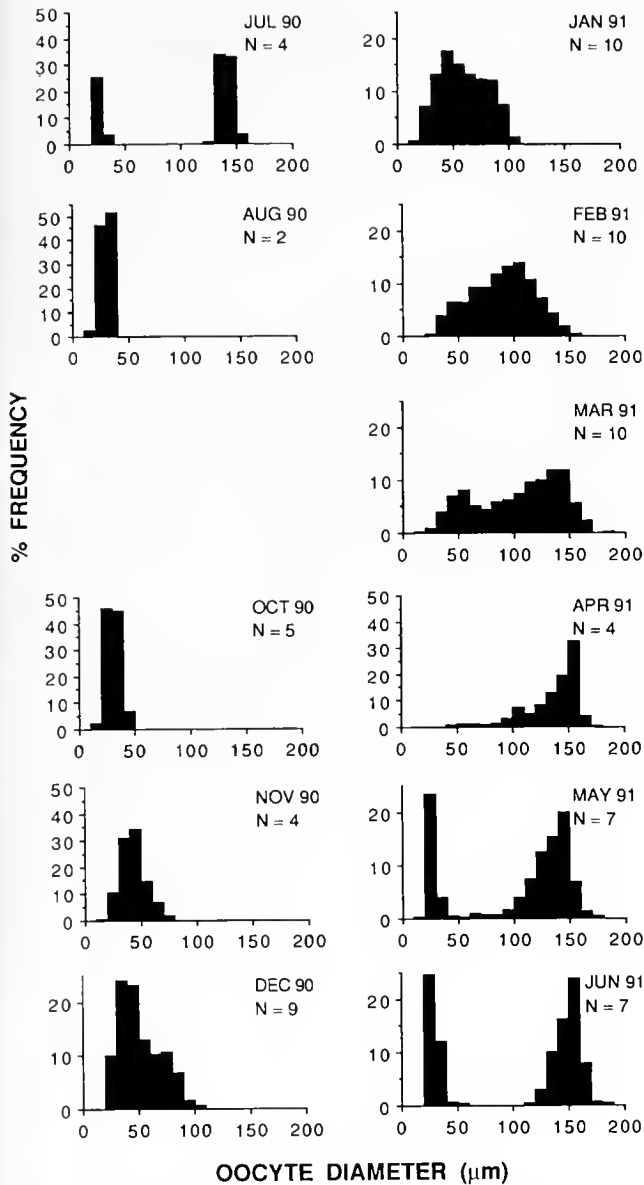


**Figure 2.** Monthly size-frequency histograms of maximum oocyte diameter for *Neoamphitrite robusta* from Bodega Harbor, California, from July 1990 to June 1991. The bimodal peaks for May and June, 1991, and July 1990, reflect differences in oocyte size-frequency distributions among worms in the samples, not within worms. No sample was available for September 1990. N, number of females in each sample.

April through July (Fig. 2). This breeding season coincides with the spawning of some individuals in the lab during May 1991. In the oocyte size frequency histograms for July 1990 through June 1991, July 1990 represents the end of the spawning period. In that sample, a single mature female accounts for the peak of large oocytes, and three other worms in the sample contain a few small oocytes. By August 1990, only two worms out of nine examined contained any gametes, and they each had only very early

stage oocytes. Proliferation of primary oocytes continues in the population from May to March, with steady growth from October into full grown oocytes and spawning the following April through July (Fig. 2). ANOVA tests show significant differences in mean oocyte diameter among females in the monthly samples (e.g., October 1990:  $F = 13.70$ ,  $df = 4$ ,  $P < 0.0001$ ; February 1991:  $F = 12.24$ ,  $df = 9$ ,  $P < 0.0001$ ; June 1991:  $F = 109.80$ ,  $df = 6$ ,  $P < 0.0001$ ), and multiple comparison tests confirm that oogenesis is not tightly synchronized among females at any time throughout the year. Bimodal distributions of oocytes appear in the May and June 1991 samples, and also in the July 1990 sample (Fig. 2). However, in each case, the peak of smaller oocyte sizes is fully accounted for by two or three females that have only 10–30  $\mu\text{m}$  diameter oocytes in the coelom.

In *R. californiensis*, bimonthly samples of females from Dillon Beach all show a wide range of oocyte sizes throughout the year; in each sample there is skewing towards smaller oocytes, with just a small proportion of oocytes  $> 300 \mu\text{m}$  in diameter present (Fig. 3). Intratubular cocoons of larvae of *R. californiensis* were found in samples from every month sampled between June 1990 and February 1992; in many cases females were still with the broods, and they always contained oocytes of various sizes in their coeloms. While the larvae within each cocoon were at the same development stage, the stages of larval development differed among cocoons in a tube, indicating that the cocoons were laid sequentially.

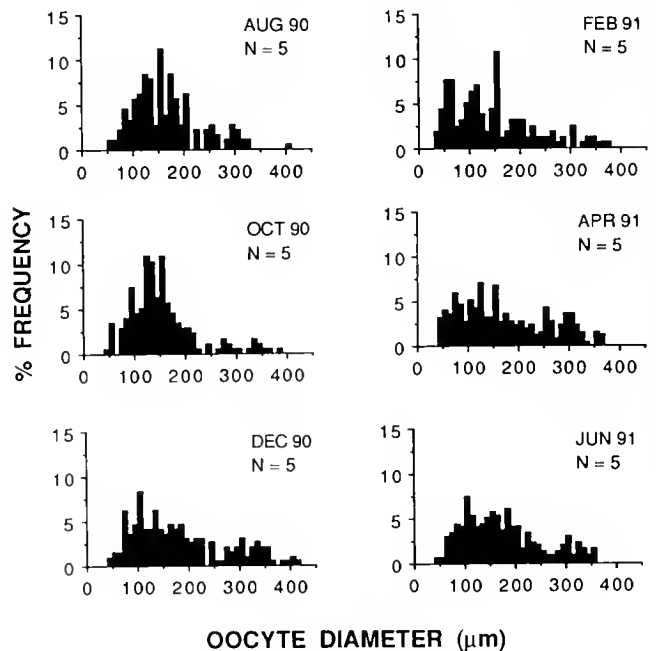


**Figure 3.** Bimonthly size-frequency histograms of maximum oocyte diameter for *Ramex californiensis* from Dillon Beach, California, from August 1990 to June 1991. N, number of females in each sample.

Table I

Maximum coelomic oocyte diameter and maximum fecundity recorded for *Eupolymnia crescentis*, *Neoamphitrite robusta*, *Ramex californiensis*, and *Thelepus crispus*

	Maximum oocyte size ( $\mu\text{m}$ )	Maximum fecundity <sup>†</sup> (n; $\bar{X} \pm \text{S.E.}$ )
<i>Eupolymnia crescentis</i>	210	128,500 (6; 105,430 $\pm$ 12,951)
<i>Neoamphitrite robusta</i>	180	829,833 (5; 404,799 $\pm$ 109,338)
<i>Ramex californiensis</i>	410	44 (15; 29 $\pm$ 2.4)
<i>Thelepus crispus</i>	400	51,555 (4; 28,582 $\pm$ 11,796)

<sup>†</sup> Fecundity in *E. crescentis* and *N. robusta* is the total number of oocytes in gravid females; fecundity in *R. californiensis* and *T. crispus* is the number of larvae in a single brood, i.e., a single cocoon in *R. californiensis*, or a single mass of elongated egg sacs in *T. crispus*; n, sample size;  $\bar{X} \pm \text{S.E.}$ , mean  $\pm$  standard error.

Intratubular egg masses of *T. crispus* were observed in the field in July, October, and November of 1991, and have also been reported in August (Strathmann, 1987). Egg masses were also laid in the lab in November and December of 1991. It appears then that *T. crispus* breeds for at least six months from July to December, and perhaps longer.

*Maximum oocyte size and fecundity.* In all four species, oocytes change from a spherical to a discoid shape as they develop in the coelom, and they round out again when spawned. Table I shows the maximum oocyte diameter recorded from coelomic samples of each species. *Ramex californiensis* and *T. crispus* have the largest oocyte sizes, at 410 and 400  $\mu\text{m}$ , respectively, while *N. robusta* has the smallest (180  $\mu\text{m}$ ); the maximum oocyte size in *E. crescentis* is 210  $\mu\text{m}$ . The maximum fecundity ranges from 44 in a single cocoon of *R. californiensis*, to 829,833 full-

grown oocytes in a mature *N. robusta* female, with *T. crispus* and *E. crescentis* having maximum fecundities of 51,555 and 128,500, respectively (Table I). The high degree of variation in fecundity of each species is due to body size differences among females in each sample. In Table II total spawn or brood volume is expressed as a percentage of total body volume for the four species. This crude estimate shows that reproductive output (percent of total body volume given to a single brood or spawn) in the worms ranges from about 2.37% in *R. californiensis* to about 8.60% in *N. robusta*. *E. crescentis* and *T. crispus* have values of about 6.67% and 5.88%, respectively.

*Mode of development.* Table III summarizes the larval development of *E. crescentis* at about 16°C. Twenty-four hours after fertilization, the larva is about 150  $\mu\text{m}$  long, fully ciliated and free swimming, and has two red eyespots. By about 48 h, the  $\sim 200$   $\mu\text{m}$ -long trochophore stage is reached; the larva possesses an apical tuft, a wide prototrochal band, a telotroch, and a neurotroch. During the third day of development, surface constrictions indicate the onset of segmentation, and the first pair of hooded setae appear. By the end of the third day, larvae possess a pair of hooded setae on each of two segments. Setae and setigers are continually added as outlined in Table III. The ciliated mouth appears when the larvae are about 5 days old and approximately 350  $\mu\text{m}$  long. At this stage the gut outline is already visible, but yolk granules are still found in the gut and body cavity, and it is not until the larva is about 7 days old that the mouth and gut become fully functional. At this stage the larva possesses five setigers, the posterior four of which bear a pair of uncini. The telotroch is lost and the neurotroch is reduced to a ciliary patch behind the mouth. Up to this point in their development the larvae have been mainly near the bottom, and they are not very active swimmers. After this stage, the juveniles crawl around, feeding on microbial films on the bottom of the culture dishes. By 21 days the first tentacle bud is 100  $\mu\text{m}$  long, there are eight setigers, and the first pair of nephridia has begun to develop.

Table II

Estimates of reproductive output for *Eupolymnia crescentis*, *Neoamphitrite robusta*, *Thelepus crispus*, and *Ramex californiensis*

	Single oocyte volume <sup>a</sup> ( $\text{mm}^3$ )	Total oocyte volume <sup>b</sup> ( $\text{mm}^3$ )	Total body volume <sup>c</sup> ( $\text{mm}^3$ )	Total oocyte volume / Total body volume $\times 100$ (%)
<i>Eupolymnia crescentis</i>	$1.766 \times 10^{-3}$	$2.270 \times 10^2$	$3.403 \times 10^3$	6.67
<i>Neoamphitrite robusta</i>	$1.150 \times 10^{-3}$	$9.544 \times 10^2$	$11.062 \times 10^3$	8.60
<i>Ramex californiensis</i>	$14.137 \times 10^{-3}$	0.622	26.180	2.37
<i>Thelepus crispus</i>	$14.137 \times 10^{-3}$	$7.288 \times 10^2$	$12.389 \times 10^3$	5.88

Reproductive output is expressed as the percentage of total body volume that is given to free-spawned or brooded eggs in a single reproductive event.  $a = \frac{4}{3} \pi r^3$ , where  $2r$  is the diameter of a spawned, spherical oocyte in each species;  $b = a \times$  fecundity in each species (see Table I);  $c = \frac{1}{3} \pi^2 h$ , where  $2r$  is the maximum width, and  $h$  is the maximum length of each species.

Table III

*Development of Eupolyornia crescentis larvae raised at approximately 16°C in August 1991*

Days after spawning	Stage of development
1	150 $\mu\text{m}$ ciliated larva; 2 red eyespots appear.
2	200 $\mu\text{m}$ long trochophore larva with apical tuft, a wide prototroch and telotroch; neurotroch also present, and intersecting the telotroch; first segmental constriction appears.
3	250 $\mu\text{m}$ long larva with 1 or 2 setigers, each with a single pair of capillary setae.
4	$\sim$ 300 $\mu\text{m}$ long larva with 2 setigers, the first with 2 pairs capillary setae and the second with a single pair.
5	350 $\mu\text{m}$ long larva with 3 setigers, the first 2 with 2 pairs of capillary and the third with a single pair of capillary setae; prototroch and telotroch are reduced.
6	$\sim$ 350 $\mu\text{m}$ long larva with 4 setigers, the first 3 with 2 pairs of capillary setae, and a single pair of uncini on setigers 2 through 4; neurotroch beginning to disappear posteriorly.
7	$\sim$ 500 $\mu\text{m}$ long juvenile with 5 setigers (4 with uncini) and a fully functional gut; telotroch almost gone and neurotroch further reduced to ciliary patch behind mouth; animals stick to the bottom or sides of the container and slowly sink passively if disturbed.
11	Six setigers, all but the first with a single pair or uncini; all larval ciliation gone.
21	$\sim$ 950 $\mu\text{m}$ long juvenile with 7 to 8 setigers, and the first tentacle bud ( $\sim$ 100 $\mu\text{m}$ long); heavily ciliated lips everted often in feeding; first pair of nephridia visible in the first aseptigerous segment.

The development of *T. crispus* is summarized in Table IV. In this species, larvae hatch from the intratubular egg mass as 350  $\mu\text{m}$  long, one-setiger larvae. While hatching from an egg mass is not tightly synchronized among all larvae, newly hatched larvae are usually at this stage of development. The prototroch, telotroch, and neurotroch are well developed, and there are two eyespots; there is no apical tuft and segmental ciliary bands are absent. Up to the second day post-hatching, larvae have limited swimming abilities, and thereafter they remain on the bottom of the container. The second setiger develops on the third day, and by day four there are three setigers. At 7 days, the prototroch and telotroch have been lost from the 4-setiger larvae, and the neurotroch begins to recede from the posterior end leaving only segmental patches of cilia by day 12. At this stage there are five setigers, each with two pairs of capillary setae. In eight-setiger stages the gut is fully functional and the juveniles form mucus tubes to which sediment particles adhere.

Observations of development in *R. californiensis* in the present study are generally similar to those reported by Blake (1991); larvae undergo direct development, and emerge as eight-setiger, crawl away larvae with three to five tentacles. The mouth and gut become functional at the 11- to 12-setiger stage, approximately 15 days after hatching.

#### Comparative data

Data on reproductive and developmental traits of seven other terebellid species were available in the literature. Combined with the data from the present study, the traits of three intratubular brooders, three extratubular brooders, and six broadcast spawners are represented in Table V [one species, *Eupolyornia nebulosa*, is reported as an extratubular brooder in the Mediterranean and as a broadcast spawner in the English Channel (Grémare, 1986; Bhaud *et al.*, 1987)]. There are 11 species from 9 genera represented in the matrix.

Table IV

*Development of Thelepus crispus larvae raised at approximately 14°C in October and November 1991*

Days after hatching	Stage of development
1	$\sim$ 350 $\mu\text{m}$ long larva with a well-developed prototroch, telotroch, and neurotroch; 2 red eyespots; the first segmental constriction and the first pair of hooded setae develop.
3	Larvae remain on the bottom of the container, the second segmental constrictions appear and the second pair of capillary setae develop on the first setiger.
5	$\sim$ 450 $\mu\text{m}$ long larvae with 3 setigers; tentacle bud beginning to develop.
7	$\sim$ 500 $\mu\text{m}$ long larva with 4 setigers, the first 2 with 2 pairs of capillary setae and a single pair of setae on the third and fourth setigers; prototroch and telotroch are gone, and the neurotroch is receding from the posterior end.
12	Five setigers, each with 2 pairs of capillary setae; neurotroch reduced to segmental patches; first tentacle increasing in length.
26	$\sim$ 800 $\mu\text{m}$ long juvenile with functional gut; 8 setigers, 5 with a pair of uncini; tentacle now $\sim$ 100 $\mu\text{m}$ long, but food ingested by everting lips.

Table V  
 Summary of reproductive and developmental traits of 11 species of the family Terebellidae

	Reproductive mode	Body size (mm)	Maximum oocyte size ( $\mu\text{m}$ )	Maximum fecundity	Days in plankton	Stage at juvenile (setigers)	Breeding season (months)	Breeding strategy	Sources
<i>Ramex californensis</i>	Intratubular brooder	25	410	44	0	11	12	Iteroparous	This study, a
<i>Neoleprea streptochaeta</i>	"	50	600	300	0	10	1	Iteroparous	b
<i>Thalopus crispus</i>	"	280	400	51,555	1	8	6+	Iteroparous	This study
<i>Nicola zostericola</i>	Extratubular brooder	23	300	665	0	6	3	Semelparous	c, d
<i>Eupolyommia nebulosa</i> (Banyuls)	"	50	190	60,000	7.5 <sup>†</sup>	5	3	Iteroparous	e, f, g, h
<i>Thalopus setosus</i>	"	300	220	150,000	1	10	2.5	Iteroparous	i, j
<i>Eupolyommia nebulosa</i> (Dinard)	Broadcast spawner	50	200	—	—	2	1	Iteroparous	e, f, g, h
<i>Amaena occidentalis</i>	"	100	210	21,000	—	—	—	Semelparous	k, l
<i>Eupolyommia crescentis</i>	"	130	210	128,500	7	5	2	—	This study
<i>Xcauphitrite robusta</i>	"	250	180	829,833	—	—	3	—	This study
<i>Lanice conchleosa</i>	"	300	150	160,000	5 (52) <sup>††</sup>	4 (16) <sup>††</sup>	1	Iteroparous	m, n, o, p, q
<i>Amphitrite ornata</i>	"	380	100	—	—	—	3	—	r, s, t

Sources: a = Blake, 1991; b = Duchêne, 1980; c = Eckelbarger, 1974; d = Eckelbarger, 1975; e = Grémare, 1986; f = Bhaud et al., 1987; g = Bhaud and Grémare, 1988; h = Bhaud, 1991; i = Duchêne, 1991; k = Hannan et al., 1977; l = Fauchald, 1983; m = Hermler, 1981; n = Bhaud, 1988; o = Smith, 1989a; p = Smith, 1989b; q = R. I. Smith, pers. comm.; r = Mead, 1897; s = Scott, 1909; t = Scott, 1910. —, indicates no data available; †, value is the average of reported values; ††, values given in parentheses are for the secondary planktonic stage (autophore larva) of this species.

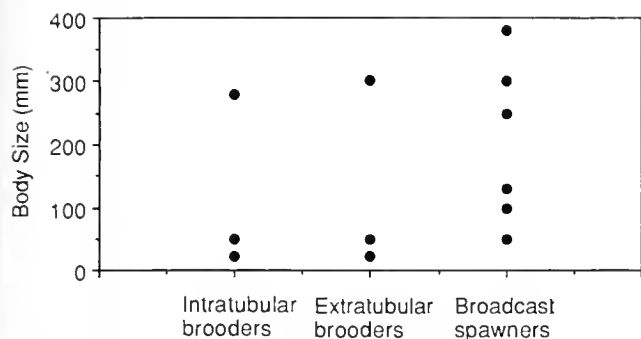


Figure 4. The reproductive modes of terebellids graphed against body size (length in mm).

Size ranges from 23 to 380 mm among all species, with no significant difference in body size among reproductive modes ( $F = 0.518$ ,  $df = 11$ ,  $P < 0.612$ ). Indeed, as Figure 4 illustrates, each of the three reproductive modes are represented in species of vastly differing body sizes. ANOVA reveals a statistically significant difference in the maximum oocyte size among the three reproductive modes ( $F = 19.33$ ,  $df = 11$ ,  $P < 0.0006$ ). The smallest oocyte sizes are associated with the six broadcast spawners, while the largest ones are those of species that brood their larvae in the maternal tube. Fecundity ranges over several orders of magnitude among the species in the study, with the two extremes being *R. californiensis* (44) and *N. robusta* (829,833). While log of fecundity does not differ significantly among the three reproductive modes ( $F = 3.039$ ,  $df = 9$ ,  $P < 0.112$ ), it does differ between brooders with direct development and those with a planktonic stage during development ( $F = 108.03$ ,  $df = 5$ ,  $P < 0.0091$ ).

Three of the species in the study undergo direct development, and in the five species for which planktonic development is known, the larvae remain in the plankton from 1 to about 7.5 days. The length of the planktonic period does not differ according to reproductive mode ( $F = 3.07$ ,  $df = 7$ ,  $P < 0.134$ ), but the stage at which the larval gut becomes fully functional and exogenous food

supplies are taken in (*i.e.*, number of setigers at initial juvenile stage) does ( $F = 6.97$ ,  $df = 8$ ,  $P < 0.027$ ). Larvae from intratubular brooders become independent from yolk supplies at a more developed stage (up to 11 setigers in *R. californiensis*) than either extratubular brooders (5–10 setigers) or broadcast spawners (2–5 setigers).

Free-spawning species and extratubular brooders generally have short, discrete breeding seasons, while two of the intratubular brooding species reproduce continuously for extended periods. However, the length of the breeding season does not differ significantly according to reproductive mode ( $F = 2.25$ ,  $df = 10$ ,  $P < 0.167$ ). Only two species, *Nicolea zostericola* and *Amaeana occidentalis*, are reported to be semelparous; six others are iteroparous.

The matrix of correlation coefficients for the life history traits is shown in Table VI. It shows that fecundity covaries directly with body size, and inversely with egg size. However, there is no significant relationship between body size and oocyte size, and multiple regression analysis shows that egg size does not predict fecundity if body size is held constant ( $F_{(2,5)} = 3.390$ ,  $P < 0.117$ ). Juvenile stage covaries directly with egg size, and inversely with the length of the planktonic period during development. While the relationship is not significant ( $P < 0.054$ ), there is a definite trend towards decreasing planktonic period with increasing egg size. No other correlations among traits are statistically significant.

## Discussion

### Present study

The four species in the present study span the range of reproductive and developmental modes recorded for the family Terebellidae. *Eupolyornia crescentis* and *Neoamphitrite robusta* are both free-spawning terebellids with reproductive periods lasting approximately three months. Interestingly, these two co-occurring species differ in their timing of primary oocyte release, the pattern of oocyte growth, and the timing of spawning. Environmental stimuli control primary oocyte release and rate of oocyte

Table VI

Correlations between reproductive and developmental traits among species of the family Terebellidae

	Body size	Maximum oocyte size	Maximum fecundity	Days in plankton	Stage at juvenile	Breeding season
Body size	1					
Maximum oocyte size	-0.449	1				
Maximum fecundity	<u>0.747</u>	<u>-0.743</u>	1			
Days in plankton	0.106	-0.699	0.671	1		
Stage at juvenile	0.053	<u>0.698</u>	-0.581	<u>-0.778</u>	1	
Breeding season	-0.177	0.312	-0.523	-0.389	0.570	1

$P < 0.05$  for underlined values.

growth in some polychaetes (see Olive, 1984). However, without further study, it is not possible to speculate on how the same environmental stimuli affect *E. crescentis* and *N. robusta* so differently. While reproduction in *E. crescentis* and *N. robusta* populations is not tightly synchronized, fertilization efficiency in these species could potentially be enhanced by the stimulation of conspecifics by spawning individuals, as apparently happened with *E. crescentis* in the lab in August, 1991. Such an effect would presumably be greater in *E. crescentis*, which reaches densities of 3 animals per 10 cm<sup>2</sup> at Bodega Harbor; *N. robusta* is patchy in its distribution, usually occurring in small groups of several adults.

The maximum egg sizes in *E. crescentis* and *N. robusta*, 210 and 180  $\mu\text{m}$ , respectively, are within the range associated with lecithotrophy in polychaetes generally (Schroeder and Hermans, 1975), and are very similar to those reported for other free spawning terebellids, *Eupolymnia nebulosa* (Grémare, 1986) and *Amaeana occidentalis* (Hannan *et al.*, 1977). The number of eggs produced by *E. crescentis* in a single reproductive period is substantially larger than that of *A. occidentalis*, which has a similar body size and egg size (Fauchald, 1983). Fecundity of *N. robusta* is very high compared to reports for other terebellids, and other lecithotrophic polychaetes (Grémare and Olive, 1986), although it should be noted that fecundity is rarely reported for large, free-spawning species.

Larval development in *E. crescentis* is planktonic and non-feeding, and corresponds generally with the primary planktonic larval development of *Lanice conchilega* (Heimler, 1981). Like *L. conchilega*, *E. crescentis* has a demersal metatrochophore, but *E. crescentis* larvae are not good swimmers. Although the dispersal of *E. crescentis* larvae over the seven-day planktonic period observed in this study might be expected to be substantial, it may be restricted due to the habitat of the species. Like many terebellids (Day, 1967; Bhaud, 1991), *E. crescentis* is found in quiet bays where fine sediments are deposited, areas in which offshore/alongshore currents may not exert great influences on larval dispersal. The common high population densities of *E. crescentis* (e.g., Bodega Harbor, California, and South Slough, Oregon) could result from the retention of larvae in the parental habitat. While attempts to raise larvae of *N. robusta* during the present study were unsuccessful, it is predicted, with a maximum egg size of 180  $\mu\text{m}$  and broadcast spawning, that *N. robusta* undergoes development similar to *E. crescentis*, with a comparable planktonic period.

The two brooders in the study, *Ramex californiensis* and *Thelepus crispus*, both brood their larvae in the maternal tube. These two species represent the extremes in body size in this study, 25 and 280 mm, respectively, and the presence of brooding in a worm as large as *T. crispus*

is unexpected (see discussion below). Despite the great differences in body size, these two species share a number of life history traits. Both reproduce continuously, *R. californiensis* year round and *T. crispus* for at least six months. Continuous year-round breeding has never been reported in a terebellid before, although it is known in other brooding polychaetes, for example, the ampharetid *Hypaniola kowalewskii* (Marinescu, 1964). The extratubular brooding terebellids, *Nicolea zostericola*, *Eupolymnia nebulosa*, and *Thelepus setosus* breed over three to four months, but only a single batch of oocytes is produced annually in these species (Eckelbarger, 1975; Bhaud *et al.*, 1987; Duchêne, 1991). This contrasts with *R. californiensis* in which females with broods of larvae have oocytes of all developmental stages present in the coelom at all times of the year. While oogenesis in *T. crispus* was not monitored from month to month, those females found with broods also had oocytes of all sizes in the coelom.

*Ramex californiensis* and *T. crispus* have very similar maximum oocyte sizes, 410 and 400  $\mu\text{m}$ , respectively. Such large eggs are typical of brooding polychaetes (Schroeder and Hermans, 1975) and of some brooding terebellids; however, they are substantially smaller than the maximum egg size of 600  $\mu\text{m}$  reported by Duchêne (1980) for the terebellid, *Neoleprea streptochoeta*. Fecundity in *R. californiensis*, 44, is very small. *Nicolea zostericola*, which is approximately the same size as *R. californiensis* but produces eggs of 300  $\mu\text{m}$ , has a maximum fecundity of 665 for its single, discrete spawning period (Eckelbarger, 1974). Nonetheless, the number of larvae produced by these two species in a lifetime may be comparable, because *R. californiensis* can have up to 11 cocoons at any one time, and apparently lays additional cocoons over time. The fecundity of *T. crispus*, 51,555, is very high compared to other large intratubular brooding polychaetes, like some sabellids (G. Rouse, pers. comm.). It is much smaller than the fecundity of large free-spawning species in the study, *N. robusta*, but the reproductive output of *T. crispus* is closer to the two free-spawning species in the study than to *R. californiensis* (see Table II). Pairing of males and females prior to reproduction, as has been described in *N. zostericola* (Eckelbarger, 1974), has not been observed in either *R. californiensis* or *T. crispus*. However, some special mode of sperm transfer seems necessary in these two species to accommodate fertilization of eggs before cocoon or egg mass formation within the tube. In *R. californiensis*, this speculation is supported by the presence of elongated sperm ( $\sim 10 \mu\text{m}$ ; pers. obs.).

Despite their similar egg sizes, *R. californiensis* and *T. crispus* differ substantially in their dispersal potentials. *Ramex californiensis* undergoes direct development with no planktonic stage, whereas *T. crispus* has a mixed mode of development with brooded larvae that undergo a short-

lived planktonic stage. Development in *R. californiensis* most closely resembles that of *N. streptochoeta*, in which juveniles of 10 setigers emerge from the maternal tube after a lengthy period of intratubular development (Duchêne, 1980). The 11-setiger juveniles of *R. californiensis* can build mucus tubes and feed on detrital matter; they avoid whatever mortality risks of planktonic development there might be. The rate of post-settlement mortality in either species is unknown, however, in *R. californiensis* at least, it is unlikely that there are any negative intraspecific interactions between adults and juveniles as seen in *E. nebulosa* (Bhaud, 1990, 1991), because of the small adult size in this species and the tubicolous habit of newly emerged juveniles.

The mixed development of *T. crispus* is similar to that of *T. setosus* and *E. nebulosa* (Bhaud and Grémare, 1988; Duchêne, 1991). In both species of *Thelepus*, the planktonic period of development is short (~1 day), and *T. crispus* larvae, at least, are poor swimmers. This may restrict the dispersal of the larvae, effectively isolating different populations of the species. The population genetics of *T. crispus*, *R. californiensis*, and *E. crescentis*, species with larval planktonic periods ranging from 0 to 7 days, are being investigated to reveal whether the degree of genetic exchange among populations of each species corresponds with their differing dispersal potentials.

#### Comparative data

Correlation analyses of the matrix of reproductive and developmental traits for the 11 species in the study reveal several expected trends, but also a few that are contrary to widely accepted generalizations regarding the covariation of life history traits. Egg size is an important life history trait; it is an indicator of maternal investment per offspring, is easily measured, and is correlated with several other life history traits in marine invertebrates. Thorson (1950) reported that egg size is correlated with fecundity and development mode in several marine invertebrate groups, and these trends have also been noted for polychaetes in general (Schroeder and Hermans, 1975), and some polychaete families in particular (e.g., Sabellidae: McEuen *et al.*, 1983). Egg volume ranges over two orders of magnitude among the Terebellidae, and the relationship between egg size and mode of reproduction has been noted for several terebellid species in the past (Blake, 1991; Bhaud, 1988). However, this is the first study in which a significant difference in egg size among reproductive modes has been demonstrated for this or any polychaete family. Egg size increases with the degree of parental care provided to the larvae, with intratubular brooders having the largest eggs and free-spawning species the smallest. In echinoderms, egg size is generally correlated with energetic content (Emlet *et al.*, 1987), however, no studies on the

energetic content of terebellid eggs have been published. Nonetheless, from the observations of this study it is expected that egg size (*i.e.*, oocyte diameter) is also correlated with energetic content among terebellid species.

It is usually assumed that for organisms of comparable size, smaller eggs are associated with increased fecundity, and vice versa (Olive *et al.*, 1984). While egg size is a commonly reported variable in studies on reproduction and development, data on fecundity in many marine invertebrate groups are not available, and the trade off between these two life history traits has not often been investigated. The present study is the first in which fecundity of different polychaete species is compared with other reproductive traits. Initial correlation analysis indicates that the trade off between egg size and fecundity is as expected among terebellids; however, multiple regression analysis shows that egg size does not predict fecundity if body size is held constant. In a regression analysis of life history traits in oysters, Buroker (1985) found no significant relationship between egg size and fecundity. These results demonstrate that generalizations regarding the relationship between these two traits are not appropriate until further comparative investigations in other groups are made; the relationship is obviously complex, and may be linked to reproductive effort or larval survivorship, neither of which are well known for polychaetes.

All terebellids in the study undergo external fertilization, *i.e.*, copulation is absent, and there is no evidence of self fertilization in any terebellid species, although rarely hermaphrodites have been observed (e.g., *Ramex californiensis*, pers. obs.; *Pista pacifica*, R. I. Smith, pers. comm.). In *Nicolea zostericola*, which broods its embryos in an extratubular cocoon, males and females pair before spawning and sperm is gathered in the short oral tentacles of the female before mature eggs are passed over the tentacles for fertilization (Eckelbarger, 1974). This is the case also in the intratubular brooder, *Neoleprea streptochoeta* (Duchêne, 1980), but not *Eupolyommia nebulosa*, in which eggs in an extratubular gelatinous mass are fertilized by free sperm in the water (Smith, 1989a). Unfortunately, sperm ultrastructure, which is generally indicative of fertilization mechanism in polychaetes (see Jamieson and Rouse, 1989), has been reported for only one terebellid species, *N. zostericola* (Eckelbarger, 1975). Additional studies of this aspect of terebellid reproduction would provide more insights into the fertilization biology of this group.

While terebellids display a great variety of reproductive modes, one feature shared by the species in this comparative study is the use of endogenous nutrient supplies during larval development. Two terebellid species feed in the plankton, but this occurs during a secondary planktonic stage after metamorphosis (aulophore stage) (Wilson, 1928; Heimler, 1981; Bhaud, 1988). Newly metamor-



phosed juveniles of *Lanice conchilega* and *Loimia medusa* engage in this activity, which is functionally equivalent to larval feeding, *i.e.*, it involves ingestion of plankton and potential increased dispersal during the planktonic feeding period, but morphologically it is a very different process: larval cilia are not used in feeding or in locomotion during the planktonic stage (Heimler, 1981; Bhaud, 1988). Therefore, the planktonic stage must be considered analogous rather than homologous to planktotrophic larva (Bhaud, 1988).

In marine invertebrates generally, planktotrophic larval development has been proposed as the common ancestral condition (Jägersten, 1972; Strathmann, 1978). The evolutionary loss of larval feeding involves the loss of ciliary feeding bands and sometimes the whole larval gut, and the probability of regaining these feeding structures is thought to be so unlikely that a biased transition from planktotrophy to lecithotrophy is expected (Strathmann, 1985). The descendants from a lineage from which larval feeding forms have been lost will be restricted in their options for development modes (Strathmann, 1978, 1985). Once development is constrained, the evolution of other life history traits like egg size and fecundity may also be affected. The present study emphasizes the absence of larval feeding in terebellids, a well-defined polychaete family that is found in all marine habitats. Assuming the monophyly of terebellids, lecithotrophy apparently represents a fixed trait in this group. This contrasts with the occurrence of both planktotrophy and lecithotrophy in other polychaete families (*e.g.*, Spionidae, Cirratulidae, Nereidae, Onuphidae, Dorvilleidae, and Serpulidae) (Wilson, 1991), and suggests that development has been constrained during the evolution of the terebellid lineage. Alternatively, lecithotrophy may be selectively advantageous in terebellids; planktotrophy may be an option that has never been favored. This hypothesis seems implausible given the diversity of habitats occupied by members of the family Terebellidae.

No studies on field mortality rates of terebellid larvae have been published, although Bhaud (1991) reported low mortality rates of *Eupolyornia nebulosa* larvae under lab conditions. Terebellid larvae lack defensive structures seen in some polychaete larvae (Bhaud and Cazaux, 1982; Pennington and Chia, 1984), and they are poor swimmers, in which buoyancy appears to play a major role in the maintenance of a planktonic existence (Nyholm, 1951; pers. obs.). These features of terebellid larvae suggest that they are probably vulnerable to predation in the plankton, with increasing size during development being their only protection. Brooding of larvae is presumably less hazardous than planktonic development, and in terebellids the fertilization efficiency among brooders is thought to be substantially higher than in broadcast spawning species (Eckelbarger, 1974; Duchêne, 1980). Mixed development

involves brooding followed by a planktonic larval period (Pechenik, 1979). Initial brooding likely increases fertilization efficiency and provides protection for the early stages. The maintenance of a planktonic stage, despite the possible increased mortality risks, suggests some selective advantage associated with dispersal or some disadvantage associated with no dispersal; alternatively, functional limits (*e.g.*, space, oxygen requirements) may prohibit brooding of larvae beyond certain stages. In any case, the significantly higher fecundities among terebellids with mixed development compared with those with direct development may compensate for any increased mortality risks associated with planktonic stages.

Juvenile stage (number of setigers), which differs significantly among reproductive modes, is significantly correlated with egg size in terebellids. As larval development in terebellids is apparently dependent on yolk supplies, this relationship between egg size and juvenile stage is not surprising; in the absence of planktonic feeding, larger eggs will give rise to larger, more developed juveniles (Strathmann, 1985). Interestingly, there is no correlation between the number of days during development spent in the plankton and the initial egg size. This is also the case in some cirripedes (Barnes and Barnes, 1965), and it follows the prediction of Strathmann (1977) that the larval period will be independent of egg size, if size at metamorphosis increases with increasing egg size.

If, as previously mentioned, brooding of larvae is the safest mode of development, then all other things being equal, all marine invertebrates would brood their larvae (Emlet *et al.*, 1987). However, among related species, if any of them brood it is usually only the smaller ones (Strathmann and Strathmann, 1982; Strathmann *et al.*, 1984). Numerous studies have confirmed this association of brooding with small body size in a wide variety of groups, including echinoderms (*e.g.*, Menge, 1975), mollusks (Pearse, 1979; Sastry, 1979), and some polychaetes (Knight-Jones and Bowden, 1984). Various hypotheses have been invoked to explain this pattern, and the one based on allometric constraints has been supported by several studies (Strathmann and Chaffee, 1984; Strathmann *et al.*, 1984; McClary and Mladenov, 1989). In organisms of increasing size, fecundity increases disproportionately with the surface area available for brooding, therefore larger animals are less capable of retaining and ventilating all the offspring that they can produce; small animals are less likely to encounter this problem (Strathmann and Strathmann, 1982). Terebellids, however, do not support this hypothesis. Indeed, the terebellids in the present study provide a clear exception to the generalization that large body size may be incompatible with brooding in marine invertebrates. One of the largest species in the study, *Thelepus crispus*, broods its embryos in its tube, as does one of the smallest species in the study, *Ramex*

*californiensis*. While reproductive output is expected to be limited by space in large, tubicolous polychaetes (Hines, 1986), there does not appear to be a substantial limitation in terebellids when large broadcast spawners are compared with a large intratubular brooder in the present study (see Table II). It is possible that large terebellids, and perhaps other sedentary polychaetes, can overcome the suggested constraints of brooding by (i) having a tube that has greater surface area than the body (*i.e.*, longer, wider), or (ii) by ventilating the tube well with peristaltic contractions of the body, as has been described by Dales (1961) for several terebellid species. In some other marine invertebrates, scaling constraints do not provide adequate explanation for the association of brooding with small size; Hess (1993) found no evidence of allometric constraints on brood size in spirorbid polychaetes (1–3 mm in length), and Kabat (1985) showed that brood area does not constrain reproductive output in the small bivalve, *Transenella tantilla* (6 mm shell length).

From the matrix of reproductive and developmental traits, it is clear that brooders show wider ranges of values for all traits than broadcasting species (Table V). This probably reflects the grouping of species with functionally similar reproductive modes that are of different evolutionary origins. Only with a phylogenetic analysis of the family will it be possible to address such issues. With such an analysis we can also begin to evaluate how much of the variation in life history traits is due to phylogenetic effects, and how much is the result of adaptation to different selective environments, as has already been done for some vertebrate groups (*e.g.*, Harvey and Clutton-Brock, 1985; Gittleman, 1986; Miles and Dunham, 1992). Although biases in the data are likely, due to the nonrandom way in which subjects were chosen, and the phylogenetic effects on life history traits can only be speculated upon for now, the results of this study nonetheless show that generalizations about the covariation of life history traits in marine invertebrates need to be viewed with caution. The exceptions to some commonly held assumptions provided by the Terebellidae show that more comparative studies of marine invertebrate reproduction and development are needed to broaden our base for life history theories.

#### Acknowledgments

This paper is dedicated to the memory of Dr. Ralph I. Smith, who introduced me to the terebellids of the central California coast. I am grateful to him, and also to Dr. John S. Pearse for their support, advice, and encouragement throughout this study. I thank them, Drs. G. W. Rouse and P. D. Reynolds, and two anonymous reviewers for critical reviews of the manuscript. Dr. G. Griggs, Director, Long Marine Laboratory and Institute of Marine

Sciences, University of California, Santa Cruz; Dr. J. Clegg, Director, Bodega Marine Laboratory; and Dr. A. O. D. Willows, Director, Friday Harbor Laboratories, graciously provided the use of those facilities. I thank J. Kurpius for assistance with oocyte measurements, B. Steele for help with larval culture and maintenance, G. Pierce for advice on statistics, and S. Edmands, P. Fong, J. Kurpius, E. McHugh, C. E. Mills, P. D. Reynolds, R. I. Smith, and P. Wolfe for accompanying me on field trips. Some collection of data and revisions of the manuscript were made while the author was a Scholar-in-Residence at Hamilton College. Financial support from the following sources is gratefully acknowledged; Biology Independent Study Funds, University of California, Santa Cruz; the Society for Sigma Xi; the Dr. E. H. and E. M. Myers Oceanographic and Marine Biology Trust; the Friends of Long Marine Laboratory; and the Lerner-Gray Fund for Marine Research (American Museum of Natural History).

#### Literature Cited

- Barnes, H., and M. Barnes. 1965. Egg size, nauplius size, and their variation with local, geographical, and specific factors in some common cirripedes. *J. Anim. Ecol.* 34: 391–402.
- Bhaud, M. 1988. The two planktonic larval periods of *Lanice conchilega* (Pallas, 1766) Annelida Polychaeta, a peculiar example of the irreversibility of evolution. *Ophelia* 29(2): 141–152.
- Bhaud, M. 1990. Conditions d'établissement des larves de *Eupolyornia nebulosa*: acquis expérimentaux et observations en milieu naturel; utilité d'une confrontation. *Océanis* 16(3): 181–189.
- Bhaud, M. R. 1991. Larval release from the egg mass and settlement of *Eupolyornia nebulosa* (Polychaeta, Terebellidae). *Bull. Mar. Sci.* 48(2): 420–431.
- Bhaud, M., and C. Cazaux. 1982. Les larves de polychètes des cotes de France. *Océanis* 8: 57–160.
- Bhaud, M., and A. Grémare. 1988. Larval development of the terebellid polychaete *Eupolyornia nebulosa* (Montagu) in the Mediterranean Sea. *Zool. Scripta* 17(4): 347–356.
- Bhaud, M., A. Grémare, F. Lang, and C. Retière. 1987. Étude comparées des caractères reproductifs du terebellien *Eupolyornia nebulosa* (Montagu) (Annélide Polychète) en deux points de son aire géographique. *C. R. Acad. Sci. Paris Série III* 304(5): 119–122.
- Blake, J. A. 1991. Larval development of Polychaeta from the northern California coast V. *Ramex californiensis* Hartman (Polychaeta: Terebellidae). *Bull. Mar. Sci.* 48(2): 448–460.
- Buroker, N. E. 1985. Evolutionary patterns in the family Ostreidae: larviparity vs. oviparity. *J. Exp. Mar. Biol. Ecol.* 90: 233–247.
- Chia, F-S. 1974. Classification and adaptive significance of developmental patterns in marine invertebrates. *Thalassia Jugoslav.* 10: 121–120.
- Christiansen, F. B., and T. M. Fenchel. 1979. Evolution of marine invertebrate reproductive patterns. *Theor. Pop. Biol.* 16: 267–282.
- Dales, R. P. 1961. Oxygen uptake and irrigation of the burrow by three polychaetes: *Eupolyornia*, *Thelepus* and *Neoamphitrite*. *Physiol. Zool.* 34: 306–311.
- Day, J. H. 1967. *A Monograph on the Polychaeta of Southern Africa*. British Museum of Natural History Publications, London.
- Doyle, R. W., and W. Hunte. 1981. Genetic changes in "fitness" and yield of a crustacean population in a controlled environment. *J. Exp. Mar. Bio. Ecol.* 52: 147–156.

- Duchêne, J. C. 1979. Premières données sur la reproduction et la croissance de la polychète *Thelepus setosus* (Terebellidae) en province subantarctique. *Ann. Inst. Océanogr. Paris* 55(2): 145-154.
- Duchêne, J. C. 1980. Premières données sur la reproduction et la croissance de la polychète *Neoleprea streptochoeta* (Terebellidae) en province subantarctique. *Ann. Inst. Océanogr. Paris* 56(2): 109-115.
- Duchêne, J. C. 1991. Growth rate, fecundity and spawning in two subantarctic populations of *Thelepus setosus* (Quatrefages) (Polychaeta: Terebellidae). *Ophelia Suppl.* 5: 313-320.
- Dunham, A. E., and D. B. Miles. 1985. Patterns of covariation in life history traits of squamate reptiles: the effect of size and phylogeny reconsidered. *Am. Nat.* 126: 231-257.
- Eckelbarger, K. J. 1974. Population biology and larval development of the terebellid polychaete *Nicolea zostericola*. *Mar. Biol.* 27: 101-113.
- Eckelbarger, K. J. 1975. A light and electron microscope investigation of gametogenesis in *Nicolea zostericola* (Polychaeta: Terebellidae). *Mar. Biol.* 30: 353-370.
- Eckelbarger, K. J. 1976. Origin and development of the amoebocytes of *Nicolea zostericola* (Polychaeta: Terebellidae) with a discussion of their possible role in oogenesis. *Mar. Biol.* 36: 169-182.
- Emlet, R. B., L. R. McEdward, and R. R. Strathmann. 1987. Echinoderm larval ecology viewed from the egg. *Echinoderm Studies* 2: 55-136.
- Fauchald, K. 1983. Life diagram patterns in benthic polychaetes. *Proc. Biol. Soc. Wash.* 96(1): 160-177.
- Gittleman, J. L. 1986. Carnivore life history patterns: allometric, phylogenetic, and ecological associations. *Am. Nat.* 127: 744-771.
- Grant, A. 1990. Mode of development and reproductive effort in marine invertebrates: should there be any relationship? *Funct. Ecol.* 4(1): 128-129.
- Grémare, A. 1986. A comparative study of reproductive energetics in two populations of the terebellid polychaete *Eupolyornia nebulosa* Montagu with different reproductive modes. *J. Exp. Mar. Biol. Ecol.* 96: 287-302.
- Grémare, A., and P. J. W. Olive. 1986. A preliminary study of fecundity and reproductive effort in two polychaetous annelids with contrasting reproductive strategies. *Int. J. Invert. Reprod. Dev.* 9: 1-16.
- Hannan, C. A., L. W. Hulberg, K. M. Mawn, and J. W. Nybakken. 1977. *A Study to Develop Standard Procedures for Life History Analyses of Benthic Invertebrates for Biological Monitoring in Marine and Estuarine Environments*. Moss Landing Marine Laboratories, California State University Consortium. 217 pp.
- Hart, M. W. 1992. Larval feeding performance and egg size evolution in echinoids. *Am. Zool.* 32(5): 114A.
- Hartman, O. 1969. *Atlas of Sedentary Polychaetous Annelids from California*. Allan Hancock Foundation, University of Southern California. Los Angeles. 812 pp.
- Harvey, P. H., and T. H. Clutton-Brock. 1985. Life history variation in primates. *Evolution* 39(3): 559-581.
- Heimler, W. 1981. Untersuchungen zur Larvalentwicklung von *Lanice conchilega* (Pallas) 1766 (Polychaeta, Terebellomorpha) Teil I: Entwicklungsablauf. *Zool. Jb. Anat.* 106: 12-45.
- Hess, H. C. 1993. The evolution of parental care in brooding spirorbid polychaetes: the effect of scaling constraints. *Am. Nat.* 141: 577-596.
- Hines, A. H. 1982. Allometric constraints and variables of reproductive effort in brachyuran crabs. *Mar. Biol.* 69: 309-320.
- Hines, A. H. 1986. Larval problems and perspectives in life histories of marine invertebrates. *Bull. Mar. Sci.* 39(2): 506-525.
- Jagersten, G. 1972. *Evolution of the Metazoan Life Cycle*. Academic Press, London and New York.
- Jamieson, B. G. M., and G. W. Rouse. 1989. The spermatozoa of the Polychaeta (Annelida): an ultrastructural review. *Biol. Rev.* 64: 93-157.
- Kabat, A. R. 1985. The allometry of brooding in *Transenella tantilla* (Gould) (Mollusca: Bivalvia). *J. Exp. Mar. Biol. Ecol.* 91: 271-279.
- Knight-Jones, P., and N. Bowden. 1984. Incubation and scissiparity in Sabellidae (Polychaeta). *J. Mar. Biol. Assoc. U.K.* 64: 809-818.
- Marinescu, V. P. 1964. La reproduction et le développement des polychètes reliques ponto-casiens du Danube: *Hypaniola kowalewskii* (Grimm) et *Manayunkia caspica*. *Ann. Rev. Roum. Biol. (série Zool.)* 9: 87-100.
- McClary, D. J., and P. V. Mladenov. 1989. Reproductive pattern in the brooding and broadcasting sea star *Pteraster militaris*. *Mar. Biol.* 103: 531-540.
- McEdward, L. R., and F.-S. Chia. 1991. Size and energy content of eggs from echinoderms with pelagic lecithotrophic development. *J. Exp. Mar. Biol. Ecol.* 147: 95-102.
- McEuen, F. S., B. L. Wu, and F.-S. Chia. 1983. Reproduction and development of *Sabella media*, a sabellid polychaete with extratubular brooding. *Mar. Biol.* 76: 301-309.
- Mead, A. D. 1897. The early development of marine annelids. *J. Morphol.* 3(2): 227-326.
- Menge, B. 1975. Brood or broadcast? The adaptive significance of different reproductive strategies in the two intertidal sea-stars *Leptasterias hexactis* and *Pisaster ochraceus*. *Mar. Biol.* 31: 87-100.
- Miles, D. B., and A. E. Dunham. 1992. Comparative analyses of phylogenetic effects in the life-history patterns of iguanid reptiles. *Am. Nat.* 139(4): 848-869.
- Nyholm, K.-G. 1951. Contributions to the life-history of the ampharetid, *Melinna cristata*. *Zool. Bidr. Uppsala* 29: 79-93.
- Olive, P. J. W. 1984. Environmental control of reproduction in Polychaeta. *Fortschr. Zool.* 29: 17-38.
- Olive, P. J. W. 1985. Covariability of reproductive traits in marine invertebrates: implications for the phylogeny of the lower invertebrates. Pp. 42-59 in *The Origin and Relationships of Lower Invertebrates*, Conway Morris, S., D. George, R. Gibson, and H. M. Platt, eds. Oxford University Press.
- Olive, P. J. W., P. J. Morgan, N. H. Wright, and S. L. Zhang. 1984. Variable reproductive output in Polychaeta: options and design constraints. Pp. 399-408 in *Advances in Invertebrate Reproduction*, Vol. 3, W. Engels, ed. Elsevier Science Publications, New York.
- Pearse, J. S. 1979. Polychaeta. Pp. 27-86 in *Reproduction of Marine Invertebrates*, Vol. 5, A. C. Giese and J. S. Pearse, eds. Academic Press, New York.
- Pechenik, J. A. 1979. Role of encapsulation in invertebrate life histories. *Am. Nat.* 114: 859-870.
- Pennington, J. T., and F.-S. Chia. 1984. Morphological and behavioral defenses of trochophore larvae of *Sabellaria cementarium* (Polychaeta) against four planktonic predators. *Biol. Bull.* 167: 168-175.
- Roughgarden, J. 1989. The evolution of marine life cycles. Pp. 270-300 in *Mathematical Evolutionary Theory*, M. Feldman, ed. Princeton University Press, Princeton, New Jersey.
- Saether, B.-E. 1988. Pattern of covariation between life-history traits of European birds. *Nature* 331: 616-617.
- Sastry, A. N. 1979. Pelecypoda (excluding Ostreidae). Pp. 113-292 in *Reproduction of Marine Invertebrates*, Vol. 5, A. C. Giese and J. S. Pearse, eds. Academic Press, New York.
- Schroeder, P. C., and C. O. Hermans. 1975. Annelida: Polychaeta. Pp. 1-214 in *Reproduction of Marine Invertebrates*, Vol. 3, A. C. Giese and J. S. Pearse, eds. Academic Press, New York.
- Scott, J. W. 1909. Some egg-laying habits of *Amphitrite omata* Verrill. *Biol. Bull.* 17: 327-340.
- Scott, J. W. 1910. Further experiments on the methods of egg-laying in *Amphitrite*. *Biol. Bull.* 20: 252-265.
- Sinervo, B. R., and L. R. McEdward. 1988. Developmental consequences of an evolutionary change in egg size: an experimental test. *Evolution* 42(5): 885-899.

- Smith, R. I. 1989a. Observations on spawning behavior of *Eupolyornia nebulosa*, and comparisons with *Lanice conchilega* (Annelida, Polychaeta, Terebellidae). *Bull. Mar. Sci.* **45**(2): 406-414.
- Smith, R. I. 1989b. Notes on gamete production in *Lanice conchilega* (Annelida, Polychaeta, Terebellidae). *Invert. Rep. Dev.* **15**: 7-12.
- Sokal, R. R., and F. J. Rohlf. 1981. *Biometry*. Freeman, New York. 324 pp.
- Spight, T. M., C. Birkeland, and A. Lyons. 1974. Life histories of large and small murexes (Prosobranchia: Muricidae). *Mar. Biol.* **24**: 229-242.
- Stearns, S. C. 1983. The influence of size and phylogeny on patterns of covariation among life-history traits in mammals. *Oikos* **41**: 173-187.
- Stearns, S. C. 1984a. The effects of size and phylogeny on patterns of covariation in the life history traits of lizards and snakes. *Am. Nat.* **123**: 56-72.
- Stearns, S. C. 1984b. The tension between adaptation and constraint in the evolution of reproductive patterns. Pp. 387-398 in *Advances in Invertebrate Reproduction*. Vol. 3. W. Engels, ed. Elsevier Science Publishers, New York.
- Strathmann, M. F. 1987. *Reproduction and Development of Marine Invertebrates of the Northern Pacific Coast. Data and Methods for the Study of Eggs, Embryos, and Larvae*. University of Washington Press, Seattle and London. 670 pp.
- Strathmann, R. R. 1977. Egg size, larval development, and juvenile size in benthic marine invertebrates. *Am. Nat.* **108**: 29-44.
- Strathmann, R. R. 1978. The evolution and loss of feeding larval stages of marine invertebrates. *Evolution* **32**: 894-906.
- Strathmann, R. R. 1985. Feeding and nonfeeding larval development and life-history evolution in marine invertebrates. *Ann. Rev. Ecol. Syst.* **16**: 339-361.
- Strathmann, R. R. 1986. What controls the type of larval development? Summary statement for the evolution session. *Bull. Mar. Sci.* **39**(2): 616-622.
- Strathmann, R. R., and C. Chaffee. 1984. Constraints of egg masses. II. Effect of spacing, size, and number of eggs on ventilation of masses of embryos in jelly, adherent groups, or thin-walled capsules. *J. Exp. Mar. Biol. Ecol.* **84**: 85-93.
- Strathmann, R. R., and M. F. Strathmann. 1982. The relation between adult size and brooding in marine invertebrates. *Am. Nat.* **119**: 91-101.
- Strathmann, R. R., M. F. Strathmann, and R. H. Emson. 1984. Does limited brood capacity link adult size, brooding and simultaneous hermaphroditism? A test with the starfish *Asteria phylactica*. *Am. Nat.* **123**(6): 796-818.
- Thorson, G. 1950. Reproduction and larval development of marine benthic invertebrates. *Biol. Rev.* **25**: 1-45.
- Trendall, J. T. 1982. Covariation of life history traits in the mosquitofish, *Gambusia affinis*. *Am. Nat.* **119**(6): 774-783.
- Vance, R. R. 1973. On reproductive strategies in marine benthic invertebrates. *Am. Nat.* **107**: 339-352.
- Wilson, D. P. 1928. The post-larval development of *Loimia medusa* Sav. *J. Mar. Biol. Assoc. U.K.* **15**: 129-149.
- Wilson, W. H. 1991. Sexual reproductive modes in polychaetes: classification and diversity. *Bull. Mar. Sci.* **48**(2): 500-516.

# Distinct Reproductive Types of Male Spider Crabs *Libinia emarginata* Differ in Circulating and Synthesizing Methyl Farnesoate

AMIR SAGI<sup>1</sup>, ELLEN HOMOLA<sup>2</sup>, AND HANS LAUFER<sup>3</sup>

*Department of Molecular and Cell Biology, University of Connecticut, Storrs, Connecticut 06260 and Marine Biological Laboratory, Woods Hole, Massachusetts 02543*

**Abstract.** Levels of methyl farnesoate in the blood and *in vitro* rates of methyl farnesoate synthesis by the mandibular organ were investigated to determine whether this compound is related to the differences in morphology and reproductive states of distinct types of male spider crabs described by Homola *et al.* (1992) in winter populations. Three male types, selected from a summer population, were investigated in detail: (1) males with relatively large propoduses (claws) and worn exoskeletons (abraded), (2) males with relatively large propoduses and exoskeletons covered with epicuticle (unabraded), and (3) males with small propoduses and unabraded exoskeletons (small).

All males examined had sperm, but abraded males, identical in propodus and body size to unabraded males, had a reproductive system that weighed twice as much. Large-clawed unabraded males had relatively small reproductive systems. Small-clawed males possessed a small reproductive system.

Abraded males possessed larger mandibular organs, containing almost twice the total protein, and their mandibular organs synthesized significantly more methyl farnesoate *in vitro* than did the other types of males. Circulating levels of methyl farnesoate, in the hemolymph of the abraded males, were more than twice as high as the levels detected in any other type of male.

The strong relationship between methyl farnesoate levels, male morphology, and reproductive system development calls for further studies on the role of methyl farnesoate in the regulation of reproduction and morphogenesis in male crustaceans.

## Introduction

The crustacean mandibular organ was first described by Le Roux (1968). Two decades later, Laufer *et al.* (1987) identified a secretory product of this gland, methyl farnesoate, which is found both in the mandibular organ and the hemolymph of the spider crab *L. emarginata*. Methyl farnesoate is the unepoxidated form of the insect juvenile hormone III. In insects, juvenile hormones play several regulatory roles both as gonadotropins (Herman and Bennett, 1975) and morphogens (Wigglesworth, 1970).

Different male types were described in adult spider crab populations using a propodus (claw) to carapace ratio (Tessier, 1960; Hartnoll, 1963; Aldrich, 1974). Recently, different adult male types were described in *L. emarginata* that were collected in the winter (Homola *et al.*, 1992). Those types differ from each other in the appearance of the exoskeleton as well as in relative claw size. Abraded males had larger reproductive systems and higher methyl farnesoate titers compared to the unabraded males (Homola *et al.*, 1992).

The present study examines the size of the mandibular organ, its relative rate of methyl farnesoate synthesis, and level of methyl farnesoate in the circulatory system of *L. emarginata* males collected in the summer. We report the results of a comparative study of methyl farnesoate production and circulation in three male morphs distinctive

Received 12 August 1991; accepted 16 July 1993.

<sup>1</sup> Present address: Department of Life Sciences, Ben-Gurion University, P.O. Box 653, Beer-Sheva, 84105, Israel.

<sup>2</sup> Present address: Bodega Marine Laboratory, University of California, P.O. Box 247, Bodega Bay, CA 94923.

<sup>3</sup> To whom all correspondence should be addressed.

Abbreviations: A, abraded; U, unabraded; S, small; MF, methyl farnesoate.

in their claw size, appearance of the exoskeleton, and development of their reproductive system.

## Materials and Methods

### Animals

Individuals of *Libinia emarginata* were collected in two locations, off the coast 2 km south of Woods Hole, Massachusetts, and 1 km north of Vineyard Haven harbor, Martha's Vineyard, during June and July 1990. Two hundred and four (204) male crabs were individually tagged and held in the facilities of the Marine Biological Laboratory (Woods Hole, MA) in two 4500-liter tanks in the presence of females. Fresh seawater was continuously pumped into the tanks so that the whole volume of water was replaced 2.5 times a day. The crabs were fed fresh or frozen squid twice a day *ad libitum*. Leftover food and other debris was siphoned out of the tanks once a day. Carapace length and propodus length were measured to the nearest millimeter using a vernier caliper. The animals were categorized into three morphs on the basis of log propodus to log carapace ratios, and the appearance of the exoskeleton (Tessier, 1960; Kuris *et al.*, 1987; Homola *et al.*, 1992). The abraded and unabraded morphs were illustrated previously (Homola *et al.*, 1992). Because *L. emarginata* molt in the fall (Hinsch, pers. comm., Hinsch, 1972) and newly molted animals are completely unabraded, the unabraded males collected in the summer had more variation in the state of abrasion of the carapace compared with the winter population (Homola *et al.*, 1992). Therefore the population was classified with respect to the degree of abrasion, and animals with the greatest amount of intact epicuticle were selected and classified as unabraded males. Three distinct types of males were selected from the captured population of 204 males shown in Figure 1: (1) abraded large males (A) with relatively large propodus ( $n = 20$ ), (2) unabraded large males (U) with relatively large propodus ( $n = 20$ ), and (3) unabraded males with a relatively small propodus (S) ( $n = 29$ ).

### The reproductive system of selected male types

Body weight was measured to  $\pm 0.01$  g. The testes, sperm duct, and accessory gland (Homola *et al.*, 1992) were dissected and weighed separately to  $\pm 0.01$  g to determine their wet weight. The reproductive system indices were calculated by dividing the sum of the components of the reproductive system by carapace length and multiplying by 100. A sample of semen from the vas deferens of each crab was examined under a light microscope for the presence of spermatophores.

### *In vitro* methyl farnesoate synthesis by the mandibular organ

The paired mandibular organs were dissected from each male. One organ was removed from the mandibular tendon, homogenized in Pantin's saline (Laufer *et al.*, 1986, 1987), and an aliquot was withdrawn for total protein determination, using the Bradford protein assay (Bradford, 1976). The other organ was incubated attached to the mandibular tendon, so that it would not be damaged during dissection, and transferred to 400  $\mu$ l of media where it was incubated for 2 h at 22–25°C with gentle agitation. The culture medium was Pantin's saline containing 20 mM HEPES (pH 7.4), 3.8 mM dextrose, 0.2% BSA and [methyl<sup>3</sup>]-methionine (specific activity = 200 mCi/mmol, total activity = 40  $\mu$  Ci/ml). Following incubation, the isotope incorporation was stopped by fixing the cells with ethanol. The gland and the culture medium were then homogenized and extracted with 1 ml hexane. Therefore, MF synthesis refers to the sum of the radio-labeled MF secreted into the medium and that which is retained within the gland. The amount of radioactivity in methyl farnesoate in a 100  $\mu$ l sample was determined using liquid scintillation spectrometry. Approximately 90% of the radioactivity in the hexane extract co-eluted with the methyl farnesoate standard on normal phase HPLC (Laufer and Borst, 1988; Homola, 1989).

### Methyl farnesoate levels in the hemolymph

Prior to dissection, hemolymph samples (2 ml) were taken from the base of the walking legs, using a 5-cc syringe with an 18-gauge needle. The samples were transferred to 15-ml glass tubes, on ice, containing 5 ml acetonitrile, and 2 ml 4% NaCl. 25 ng of the cis-trans (non-biological) isomer of methyl farnesoate was added to each tube as an internal standard (Sagi *et al.*, 1991). The samples were extracted with 1 ml hexane. Hemolymph titers of methyl farnesoate were determined according to the method developed by Laufer *et al.* (1986, 1987) and modified by Borst and Tsukimura (1991). Two hundred microliters from the hexane phase was loaded onto a Waters HPLC system using a 5  $\mu$  Econosil silica column (Alltech), two model 501 pumps and a Lambda Max 481 absorbance detector that was set at 218 nm. The running solvent was 1% diethyl ether in hexane flowing at 2.5 ml/min. Peak areas were calculated using Omega software (Version 1.4 Perkin Elmer/Nelson), and hemolymph methyl farnesoate titers were determined with reference to the known amount of the internal standard in the sample.

### Data analysis

The dimensions in mm of the propodus along the lateral margin, and the length of the carapace, were logarith-

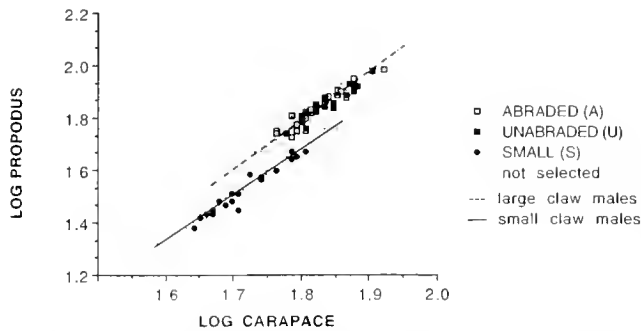


**Figure 1.** Regression analysis of log-transformed carapace and propodus data from a summer population of male *Libinia emarginata*. Three male types were found in the sample; abraded (□) and unabraded (■) males with relatively large propoduses (the upper regression line) and small claw type (●) (the lower regression line). Animals marked not selected (.) were present in the original sample but not used in this study.

mically transformed prior to the analysis of linear regression (Tessier, 1960; Kuris *et al.*, 1987). Assuming that the specific activity of the radiolabeled methyl farnesoate synthesized by the gland is equal to that of the precursor, and that only one labeled methyl group is incorporated into each methyl farnesoate molecule, the *in vitro* synthetic rates of the mandibular organs were calculated and expressed in nanomoles/gland/h as was previously calculated for *Libinia emarginata* (Laufer *et al.*, 1987) and *Procambarus clarkii* glands (Landau *et al.*, 1989).

Pearson correlation coefficients and Waller-Duncan *k*-ratio *t* test were calculated using the Statistical Analysis System (SAS Institute, Cary, North Carolina).

## Results

### Types of male *L. emarginata*

Males (204 individuals), with carapace length greater than 35 mm, were plotted with respect to log propodus versus log carapace (Fig. 1). The population appears to fall into two linear clusters (Homola *et al.*, 1992). The upper regression line represents the large-clawed males while the lower regression line represents unabraded small-clawed males (S). Among the large-clawed males, two distinct classes emerged with respect to exoskeleton texture. Abraded males (A) were quite smooth and were presumed to have molted a long time ago; unabraded males (U) had velvety epicuticle and presumably molted the previous fall.

### Reproductive system and mandibular organ size in the different types of males

The three morphologically distinct male types differ in the relative development of their reproductive systems and mandibular organs (Fig. 2). The largest reproductive

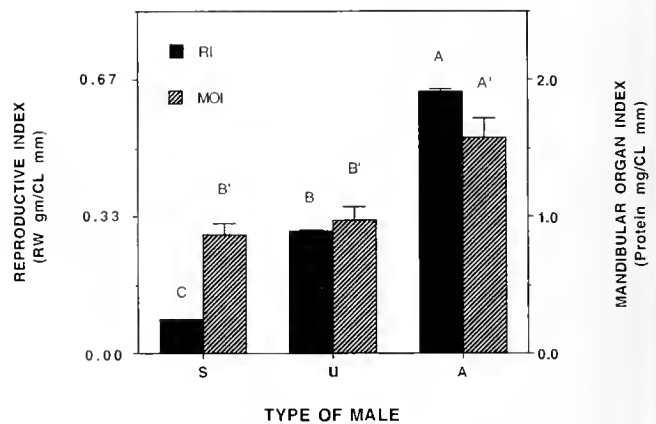


**Figure 2.** The reproductive system and mandibular organ indices in the three types of *Libinia emarginata* males. Abraded (A), unabraded (U), and small-clawed (S). Reproductive system weight (RW), carapace length (CL), reproductive index (RI), mandibular organ index (MOI). The reproductive system weight was normalized for body size and the mandibular organ index is expressed as total mandibular organ protein normalized for body size. Bars represent mean  $\pm$  SEM of at least 17 observations. Bars labeled with different letters are significantly different ( $P \leq 0.001$ ).

system and mandibular organ indices (normalized for body size), were found in the abraded males ( $0.64 \pm 0.2$  and  $1.51 \pm 0.77$ , respectively). The reproductive system and mandibular organ indices were significantly lower in the unabraded males ( $0.3 \pm 0.1$  and  $0.97 \pm 0.43$ , respectively) and were the lowest in the small-clawed unabraded males ( $0.08 \pm 0.01$  and  $0.87 \pm 0.35$ , respectively). Mandibular organ indices were not statistically different in small clawed and unabraded males. The size of the reproductive system (Fig. 3) and mandibular organ (Fig. 4)

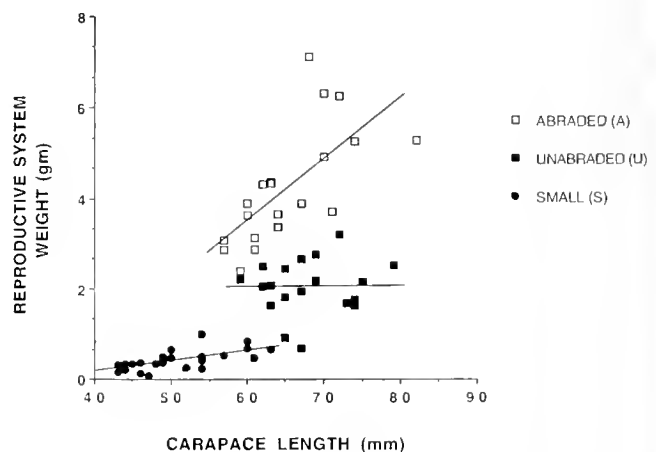


**Figure 3.** Regression analysis of carapace length and reproductive system weight in the three types of *Libinia emarginata* males. Abraded (A) ( $y = -4.61 \pm 0.14x$ ), unabraded (U) ( $y = 1.98 \pm 1.09 \times 10^{-3}x$ ), and small-clawed (S) ( $y = -0.71 \pm 2.26 \times 10^{-2}x$ ).



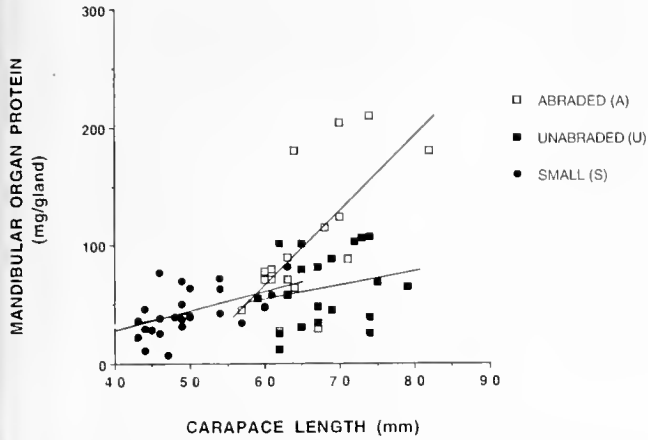


**Figure 4.** Regression analysis of carapace length and total protein in the mandibular organ of three *Libinia emarginata* male types. Abraded (A) ( $y = -313.96 \pm 6.32x$ ), unabraded (U) ( $y = -17.27 \pm 1.19x$ ), and small-clawed (S) ( $y = -38.7 \pm 1.65x$ ).

appear to be significantly correlated with body size in both the abraded (A) and small-clawed (S) males. The Pearson correlation coefficients for reproductive systems and carapaces are: A,  $r = 0.683 P \leq 0.001 n = 20$ , S,  $r = 0.623 P \leq 0.001 n = 29$ , and for the mandibular organs and carapaces A,  $r = 0.676 P \leq 0.002 n = 17$ ; S,  $r = 0.513 P \leq 0.007 n = 26$ . In the unabraded males, the sizes of the mandibular organ and the reproductive system were not found to be significantly correlated with body size, Pearson correlation coefficients for reproductive system and carapace  $r = 0.080 P \leq 0.73 n = 20$ , and for the mandibular organ and carapace  $r = 0.126 P \leq 0.600 n = 19$ .

*Methyl farnesoate synthesis and its levels in the circulation*

The largest mandibular organs, *i.e.*, those having the highest measurements of total protein per gland (Fig. 5), were found in the abraded males ( $101.62 \pm 58.43$  mg). The largest glands synthesized the highest amounts of methyl farnesoate during a 2-h incubation period ( $9.3 \times 10^5 \pm 4.8 \times 10^5$  DPM in methyl farnesoate/gland/2h or  $1.04 \pm 0.54$  nanomoles/gland/h). The smaller glands ( $66.65 \pm 29.29$  mg) of the unabraded males synthesized significantly less methyl farnesoate *in vitro* ( $5.7 \times 10^5 \pm 2.4 \times 10^5$  DPM/gland/2 h, or  $0.64 \pm 0.27$  nanomoles/gland/h), and the small clawed males synthesized the smallest amounts of methyl farnesoate ( $3.3 \times 10^5 \pm 2.0 \times 10^5$  DPM/gland/2 h, or  $0.37 \pm 0.22$  nanomoles/gland/h).

The circulating levels of methyl farnesoate (Fig. 6) were the highest in the abraded males ( $67.20 \pm 16.58$  ng/ml). Methyl farnesoate levels were significantly lower in the hemolymph of the unabraded males ( $29.60 \pm 7.10$  ng/

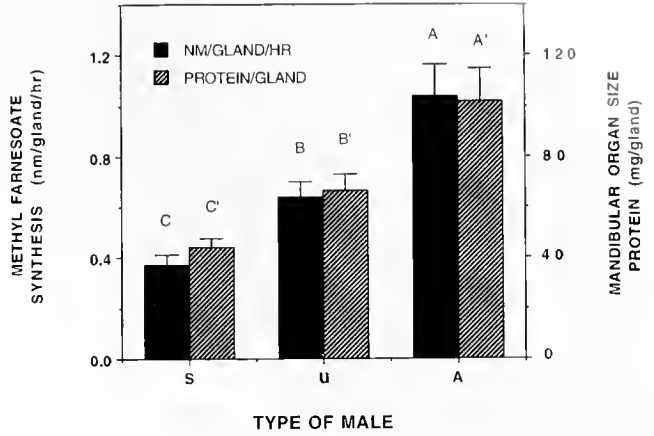


**Figure 5.** Mandibular organ size and its *in vitro* methyl farnesoate synthesis in three *Libinia emarginata* male types. Abraded (A), unabraded (U), and small-clawed (S). Mandibular organ size is expressed in total (mg) protein per gland and its activity is measured by the amount of radiolabeled methyl farnesoate produced by an organ within a one-hour period. The bars represent mean  $\pm$  SEM of at least 17 observations. Bars labeled with different letters are significantly different ( $P \leq 0.001$ ).

ml), despite the fact that these males had similar claw and carapace sizes as did the abraded males. The lowest level of methyl farnesoate was found in the hemolymph of small-clawed males ( $10.70 \pm 5.97$  ng/ml), this value is not statistically different from the level found in the large unabraded males.

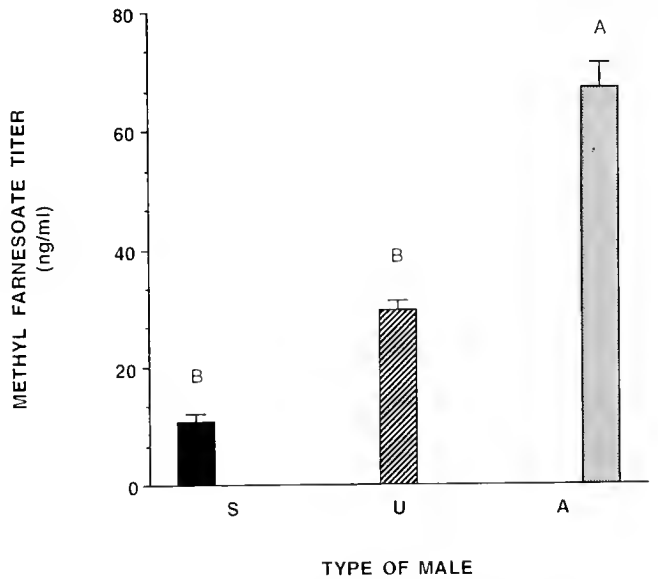


**Figure 6.** Circulating levels of methyl farnesoate in the hemolymph of three *Libinia emarginata* male types. Abraded (A), unabraded (U), and small-clawed (S). Methyl farnesoate concentrations are expressed in ng/ml of hemolymph. The bars represent mean  $\pm$  SEM of at least 17 observations. Bars labeled with different letters are significantly different ( $P \leq 0.001$ ).



## Discussion

### *Distinct male L. emarginata morphs*

Hartnoll (1963) described three types of male spider crabs on the basis of relative claw length. We suggest, on the basis of differences in the appearance of the exoskeleton, that the 'mature' (Hartnoll, 1963) type is composed of two distinct types, unabraded and abraded males (Homola *et al.*, 1992). These male morphs may represent different reproductive states within the life history of *L. emarginata*. This view is supported by the fact that the reproductive systems and the mandibular organs are considerably less developed in unabraded males compared with abraded males of the same size. Males with relatively small propoduses were termed 'pre-pubescent' by Hartnoll (1963). We found such males to possess mature sperm and thus 'pre-pubescent' is physiologically inappropriate; we used the term small-claw male. In the present study we did not investigate smaller males that were termed 'immature' by Hartnoll and may possess different morphological features. This fraction of the population remains to be studied in the future.

### *The life history of male L. emarginata*

The relation of epicuticular loss and reproductive system growth illuminates our understanding of the life history of *L. emarginata*. Our observations of winter populations (Homola *et al.*, 1992) and the observations by Hinsch (pers. comm. and Hinsch, 1972) that large *L. emarginata* males terminally molt in the fall, suggests to us that the abraded crabs investigated are anecdytic and that they last molted two seasons ago approximately 20 months prior to the study (or earlier). Thus, these males have reached full reproductive tract development, positively related to their body size, at least a year following their terminal molt. On the other hand, the unabraded large-clawed males, having similar body sizes but significantly smaller reproductive systems and mandibular organs, are suggested to have had their terminal molt approximately 11 months ago in the previous fall. Unlike the abraded males, the sizes of the mandibular organs and the reproductive tracts in the unabraded males are poorly correlated with body size. The reproductive indices of unabraded males collected in the summer were twice as large as those collected in the winter (1.19 and 0.58, respectively; Homola *et al.*, 1992). Correspondingly, methyl farnesoate titers increased from 5.2 ng/ml in the winter (Homola *et al.*, 1992) to 29 ng/ml in the summer. The facts that (a) the reproductive system of the unabraded male is not as fully developed as is permitted by its body size, (b) their reproductive system is much smaller than the abraded males of the same body size, and (c) their reproductive system indices increased from winter to summer, may

indicate that unabraded males are either in the process of commencement of reproductive augmentation, or are under a state of reproductive arrest.

### *Possible role for methyl farnesoate in the regulation of reproduction and morphogenesis*

The fact that gonadal maturity and high methyl farnesoate synthesis by the mandibular organ and elevated methyl farnesoate in the blood coincide in male *Libinia emarginata* may suggest that all three events occur in parallel due to a higher causal regulation and are thus related, but independent events. It may also suggest a causal relationship, comparable to juvenile hormone and reproduction in insects (Herman and Bennett, 1975; Wigglesworth, 1970). This relationship is suggested by the fact that the most active mandibular organs are in males with the highest levels of methyl farnesoate in their hemolymph, and that these males have the most highly developed reproductive systems. Moreover, Hinsch (1980) observed that gonad size is stimulated by mandibular organ implants. Because methyl farnesoate is the predominant product of the mandibular organ, it is suggested that the relationship between this compound and the gonad index may be viewed as causal. Along these lines it can be suggested that in these crabs, methyl farnesoate may act similarly to juvenile hormone in several insect species, by terminating reproductive diapause and stimulating reproduction (Spielman, 1974; Mitchell, 1981; De Wilde, 1983, for review). The results of the present study call for future direct experimental approach, such as mandibular organ transplantation or methyl farnesoate augmentation, in order to study the causal relationship between methyl farnesoate levels and reproduction.

## Acknowledgments

We thank Dr. Armand Kuris for numerous stimulating discussions and Dr. Jonna Ahl for her critical review of the manuscript. We also thank Dr. Frank Mauri from the Biotechnology Center of the University of Connecticut for his technical advice, and David Koslowsky and Hadi Danai for their assistance. This study was supported by a U. S. Israel Binational Agricultural Research and Development fellowship and by a Fulbright fellowship (to A.S.) and the Sea Grant College program (NOAA), a Research Service Award from the NIH and a Lady Davis fellowship (to H.L.).

## Literature Cited

- Aldrich, J. C. 1974. Allometric studies on energy relationships in the spider crab *Libinia emarginata* (Leach). *Biol. Bull.* **147**: 257-273.
- Borst, D. W., and B. Tsukimura. 1991. Quantification of methyl farnesoate levels in hemolymph by high-performance liquid chromatography. *J. Chromatogr.* **545**: 71-78.

- Bradford, M. 1976.** A rapid and sensitive method for the quantification of microgram quantities of protein utilizing the principle of protein-dye binding. *Anal. Biochem.* **72**: 248-254.
- De Wilde, J. 1983.** Endocrine aspects of diapause in the adult stage. Pp. 357-368 in *Invertebrate Endocrinology*, Vol. 1, R. G. H. Downer and H. Laufer, eds. A. R. Liss, Inc., New York.
- Hartnoll, R. G. 1963.** The biology of Manx spider crabs. *Proc. Zool. Soc. Lond.* **141**: 423-496.
- Herman, W. S., and D. C. Bennett. 1975.** Regulation of oogenesis, female-specific protein production, and male and female reproductive gland development by juvenile hormone in the butterfly, *Nymphalis antiopa*. *J. Comp. Physiol.* **99**: 321-338.
- Ilinsch, G. W. 1972.** Some factors controlling reproduction in the spider crab *Libinia emarginata*. *Biol. Bull.* **143**: 358-366.
- Ilinsch, G. W. 1980.** Effect of mandibular organ implants upon the spider crab ovary. *Trans. Am. Microsc. Soc.* **99**: 317-322.
- Homola, E. M. 1989.** Regulation of methyl farnesoate synthesis in the spider crab, *Libinia emarginata*. M. S. Thesis. University of Connecticut. 85 pp.
- Homola, E., A. Sagi, and H. Laufer. 1991.** Relationship of claw form and exoskeleton condition to reproductive system size and methyl farnesoate in male spider crab *Libinia emarginata*. *Invert. Reprod. Dev.* **20**: 219-225.
- Kuris, M. A., Z. Ra'anan, A. Sagi, and D. Cohen. 1987.** Morphotypic differentiation of male Malaysian giant prawn, *Macrobrachium rosenbergii*. *J. Crust. Biol.* **7**: 219-237.
- Landau, M., H. Laufer, and E. Homola. 1989.** Control of methyl farnesoate synthesis in the mandibular organ of the crayfish *Procambarus clarkii*: evidence for peptide neurohormones with dual functions. *Invert. Reprod. Dev.* **16**: 165-168.
- Laufer, H., and D. Borst. 1988.** Juvenile hormone in crustacea. Pp. 305-313 in *Endocrinology of Selected Invertebrate Types*, Invertebrate Endocrinology, Vol. 2. Alan R Liss, Inc., New York.
- Laufer, H., D. Borst, F. C. Baker, C. Carrasco, M. Sinkus, C. C. Reuter, L. W. Tsai, and D. A. Schooley. 1987.** The identification of a juvenile hormone-like compound in a crustacean. *Science* **235**: 202-205.
- Laufer, H., M. Landau, D. Borst, and E. Homola. 1986.** The synthesis and regulation of methyl farnesoate, a new juvenile hormone for crustacean reproduction. Pp. 135-143 in *Advances in Invertebrate Reproduction*, Vol. 4, M. Porchet, J. C. Andries, and A. Dhainaut, eds. Elsevier Science Publications, Amsterdam.
- Le Roux, A. 1968.** Description d'organes mandibulaires nouveaux chez les crustacés décapodes. *C. R. Hebd. Acad. Sci. Ser. D. Sci. Nat.* **266**: 1414-1417.
- Mitchell, C. J. 1981.** Diapause termination, gonoactivity, and differentiation of host-seeking behaviour from blood feeding behaviour in hibernating *Culex tarsalis* (Diptera: Culicidae). *J. Med. Entomol.* **18**: 386-394.
- Sagi, A., E. Homola, and H. Laufer. 1991.** Methyl farnesoate in the prawn *Macrobrachium rosenbergii*: *in vitro* synthesis by the mandibular organ and titers in the hemolymph. *Comp. Biochem. Physiol.* **99B**: 879-882.
- Spielman, A. 1974.** Effects of synthetic juvenile hormone on ovarian diapause of *Culex pipiens* mosquitoes. *J. Med. Entomol.* **11**: 223-225.
- Tessier, G. 1960.** Relative growth. Pp. 537-560 in *The Physiology of the Crustacea*, Vol. 1, T. H. Waterman, ed. Academic Press, New York.
- Wigglesworth, V. B. 1970.** *Insect Hormones*. W. H. Freeman, San Francisco. 159 pp.

# Spermatophores and Plug Substance of the Marine Shrimp *Trachypenaeus similis* (Crustacea: Decapoda: Penaeidae): Formation in the Male Reproductive Tract and Disposition in the Inseminated Female

RAYMOND T. BAUER AND LIN JUN MIN

*Department of Biology, University of Southwestern Louisiana, Lafayette, Louisiana, 70504*

**Abstract.** Sperm are packaged into many small spermatophores of variable size in the median vas deferens (MVD) of the male. A substance is intermixed with sperm in the proximal coils of the MVD, separating groups of sperm that will be ejaculated as spermatophores. Most of the ejaculatory duct is occupied by a chamber filled with a transparent, viscous fluid termed the "plug substance." When males are artificially ejaculated, spermatophores are emitted, followed by plug substance that quickly solidifies. This latter material fills and stoppers a space on the female, the median pocket, which serves as an antechamber to the apertures of the internalized seminal receptacles, where sperm from ruptured spermatophores are stored. The slit-like openings to the receptacles are functionally divided into a posterior aperture, stoppered by plug substance after insemination, a closed mid-section, and an anterior exit for sperm release during spawning.

Direct insemination by an everted male gonopore is considered more likely than transmission of spermatophores and plug substance via the male gonopod (petasma). In addition to its hypothesized roles during insemination and sperm release, the mass of plug substance (mating plug) may act as a paternity assurance device that prevents subsequent inseminations by other males.

## Introduction

There is considerable variation in the form and complexity of materials transferred from the male to the female during insemination in penaeoid shrimps (Decapoda: Penaeoidea) (Bauer, 1991). Sperm may be packaged in

structurally complicated spermatophores composed of an assortment of accessory substances secreted in the male reproductive tract. The most complex spermatophores are those attached externally to the genital area, or thelycum, of the female, as in the white shrimp, *Penaeus setiferus*, and other species of the subgenus *Litopenaeus* (Pérez Farfante, 1975; Bauer and Cash, 1991; Chow *et al.*, 1991). In contrast, in the rock shrimps, *Sicyonia* spp., sperm in a seminal fluid are produced by the male and transferred to, and stored in, internal seminal receptacles of the female (Clark *et al.*, 1984; Pérez Farfante, 1985; Bauer, 1991, 1992). Other penaeoid shrimps, such as *Trachypenaeus* spp., show intermediate degrees of spermatophore complexity and of internalization of sperm storage (Burkenroad, 1934; Heldt, 1938a, b; Hudinaga, 1941; Malek and Bawab, 1974a, b; Pérez Farfante, 1971, 1982; Champion, 1987; Bauer and Cash, 1991).

Detailed knowledge of the nature and formation of spermatophores and associated substances and of their disposition in the inseminated female is essential to an understanding of the mechanics of insemination, sperm storage, and sperm release during fertilization. In addition, characters associated with spermatophores and the insemination morphology of the male and female are important in analyses of the evolutionary relationships among taxa of penaeoid shrimps, as well as to an evolutionary interpretation of their mating systems (Bauer, 1991).

Observations on the spermatophores, seminal receptacles, and thelyca of various species of *Trachypenaeus* (Penaeidae) have been made by Andrews (1911), Burkenroad (1934), Kubo (1949), Pérez Farfante (1971), and Bauer (1991). The structure of the *Trachypenaeus* sper-

matophore is somewhat unusual among penaeoids in that sperm are packaged into numerous small spherical bundles (Burkenroad, 1934; Bauer, 1991), superficially very similar to spermatophores produced by male brachyuran crabs (Spalding, 1942; Cronin, 1947; Beninger *et al.*, 1988; Hinsch, 1988). However, little detailed information on *Trachypenaeus* spp. is available on the formation and structure of spermatophores, on a male accessory substance that plugs or seals the female seminal receptacles, or on the placement of sperm and "plug substance" in the thelyca and seminal receptacles of females.

In this report, we describe in *Trachypenaeus similis* (Smith) (1) the structure and formation of spermatophores and the plug substance in the male reproduction tract, and (2) the thelycum/seminal receptacle system of the female, especially the placement of sperm and plug substance therein. We discuss alternative hypotheses on the mechanics of insemination, based both on these morphological observations and on observations from artificial ejaculation of living males. We make comparisons of spermatophores and insemination morphology of *T. similis* with that of other penaeoid shrimps and other decapod taxa.

### Materials and Methods

Specimens of *Trachypenaeus similis* were obtained by bottom trawling at night in various locations in the northern Gulf of Mexico. Some material used for dissection and histology was obtained on cruises in 1987 and 1990 within an area at 28–29°N latitude and 88–94°W longitude. From 1989 to 1992, other specimens were trawled from the Mississippi Sound, just off the northwest end of Horn Island, Mississippi. Observations on living shrimps were taken on specimens collected from the Horn Island location and transported in oxygen-saturated water within sealed plastic bags to recirculating seawater facilities at the University of Southwestern Louisiana.

Segments of or entire reproductive tracts of 33 males and the thelycum/seminal receptacle area of 30 females were prepared for histology or paraffin carving. Live specimens, anesthetized with chilling when possible, were injected with and initially preserved in Davidson's solution (Shaw and Battle, 1957). Within a few days of fixation, specimens were washed in running water for 1–2 h and were then taken through a graduated series of alcohol changes (25%, 35%, 50%, 70%) with final storage in 70% ethyl alcohol. Standard alcohol dehydration and toluene infiltration were used to prepare dissected material for embedding in a compound of paraffin and plastic polymers (Galigher and Kozloff, 1971). Sections were stained with Mallory's Triple Stain, using the variation in which sections are rinsed with 1% phosphotungstic acid after staining in acid fuchsin and prior to staining in aniline

blue-orange G mixture (Galigher and Kozloff, 1971). In paraffin carving, material was sectioned to a desired location, deparaffined in toluene, gradually re-infiltrated with 100% ethyl alcohol, and prepared for scanning electron microscopy (SEM) by critical-point drying with carbon dioxide and sputter coating with a 10–20 nm thickness of gold/palladium. Methods for SEM of external morphology are described in Bauer (1987).

Living shrimps were maintained on water tables with recirculating seawater. Adult females were isolated individually and checked daily for molting. Upon molting, females cast off stored sperm and other male products from previous inseminations, and several such females were preserved for SEM 2–3 days after molting. Exuviae of many females (>50) were collected and preserved for later examination. Living males, held ventral side up immersed in seawater in a dish under a stereomicroscope, were artificially ejaculated by squeezing both sides of the posterior cephalothorax at the level of the gonopores with a pair of fine forceps.

Ejaculated spermatophores or fresh dissections of ejaculatory ducts were deposited in a drop of seawater on plastic coverslips coated with polylysine (Mazia *et al.*, 1975). After 5–10 minutes to allow spermatophores and sperm from spontaneously ruptured spermatophores to adhere to coverslip surfaces, coverslips were gently immersed in 4% seawater formalin in petri dishes for fixation of material. Washes with distilled water and a standard alcohol series were made by gently pipetting solutions out of and into the petri dishes. The coverslips with adhering material were then prepared for SEM as described above.

### Results

#### *Gross morphology of the male reproductive tract*

The male reproductive system, situated above the gut and hepatopancreas in the posterior half of the cephalothorax, consists of paired testes, vasa deferentia, and ejaculatory ducts (Fig. 1). The testis on each side is composed of 5–6 lobes, the first with an anterior elongation, and a posterior extension inserted among the coils of the median vas deferens. In freshly sacrificed specimens, a testicular lobe can be teased apart, revealing that each lobe is composed of a single, highly convoluted seminiferous tubule.

The vas deferens can be divided on the basis of gross morphology into proximal, median, and distal portions (Fig. 1). The structure we identify as the proximal vas deferens (PVD) is a very fine duct, difficult to identify in, and illustrate from, gross dissections but apparent in serial sections (Fig. 2). A PVD runs along the mesial edges of the testicular lobes, merging into the proximal part of the median vas deferens at the posterior end of the testis (Fig. 1). The connections between the seminiferous tubules and the PVD were not clearly observed. We refer to the highly

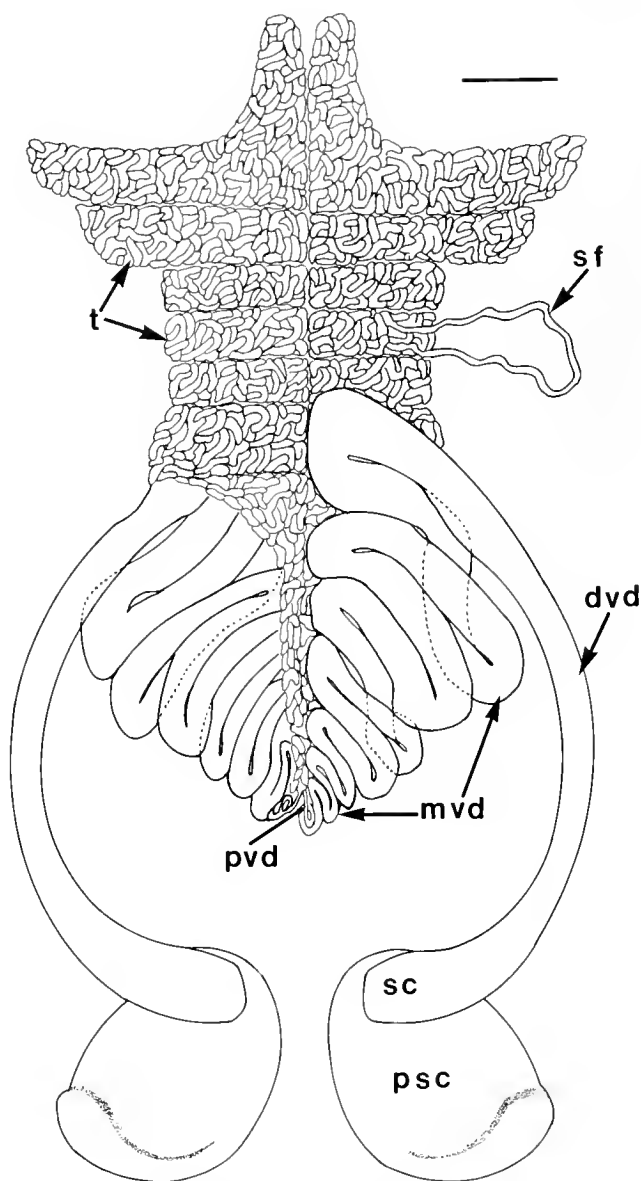


**Figure 1.** Diagram of male reproductive tract of *Trachypenaeus similis*, dorsal view. Testicular tissue covering coils of right median vas deferens (MVD) is not illustrated. In most preserved specimens, the coils of the MVD are usually bunched into a more compact, tangled mass than illustrated in this diagram, with the distal (anterior) coils somewhat below the more proximal (posterior) ones. dvd, distal vas deferens; mvd, coils of median vas deferens; psc, plug substance chamber of ejaculatory duct; pvd, posterior end of proximal vas deferens merging into the median vas deferens; sc, spermatorphore chamber of ejaculatory duct; sf, semi-niferous tubule; t, testicular lobes. Scale bar = 1 mm

coiled portion of the vas as the median vas deferens (MVD), which lies under the posterior part of the testis (Fig. 1). Each MVD begins posteriorly, gradually increasing in diameter distally (anteriorly). The distal vas deferens (DVD) is defined as the long, curved, uncoiled portion of the vas that lies outside of the testicular-MVD

DVD extends to the body wall of the last cephalothoracic segment, descending down ventrally to join the ejaculatory duct in the floor of the cephalothorax.

The ejaculatory duct has two distinct but confluent chambers (Fig. 1). The spermatorphore chamber (SC), an extension of the DVD, is located anteriorly, opening mesially to the outside through the gonopore, situated externally between the mesial edge of the coxa of the fifth (most posterior) pereopod and the sternum of the male. A large chamber, the "plug substance chamber" (PSC), lies posterior to the SC. The PSC is partially divided into two regions, which are continuous mesially. The two chambers of the ejaculatory duct are quite distinct in color and transparency, with the SC bright white or opaque, and the PSC clear or transparent with a yellow tint in living and preserved specimens, respectively.

#### *Spermatorphore structure and formation*

When males are artificially ejaculated, a short cord composed of many spermatorphores is emitted from the gonopores. The spherical spermatorphores, which separate from each other in seawater within seconds to minutes, are quite variable in size (Fig. 6). Each spermatorphore is composed of a group of sperm cells surrounded by a thin film or pellicle (Figs. 3, 4). Undisturbed spermatorphores remain intact in seawater for at least an hour, but rupture easily when moved about or handled, releasing the sperm cells (Figs. 3, 4, 7). Many sperm cells were examined with SEM and light microscopy, and all showed the same external structure of a main body, cap, spike, and a long, delicate filament extending away from the main body (Fig. 7).

A striking decrease in the thickness of the epithelium lining the MVD from the proximal to distal coils (Fig. 5) coincides with spermatorphore formation. In the most proximal coils of the MVD, the epithelium is composed of large cuboidal to columnar cells with distinct nuclei (Fig. 2), and the lumens of these coils are filled with a solid mass of sperm (Figs. 2, 5, 8). In this region, a material, termed here MVD substance, which apparently forms the spermatorphore pellicle, first appears (Fig. 8). In sections stained with Mallory's Triple Stain, the MVD substance appears a pale blue when viewed with light microscopy. The MVD substance increases in volume more distally in the MVD, where it intermingles with sperm, surrounding and separating out groups or packets, which are incipient spermatorphores (Fig. 9).

In the DVD, the epithelium is quite flattened and thin, as in the distal-most part of the MVD (Fig. 5), and the lumen is filled with sperm packets surrounded by MVD substance (Fig. 12). When the wall of the DVD is stripped away to expose the underlying contents, the separate, variably sized groups of sperm are exposed,

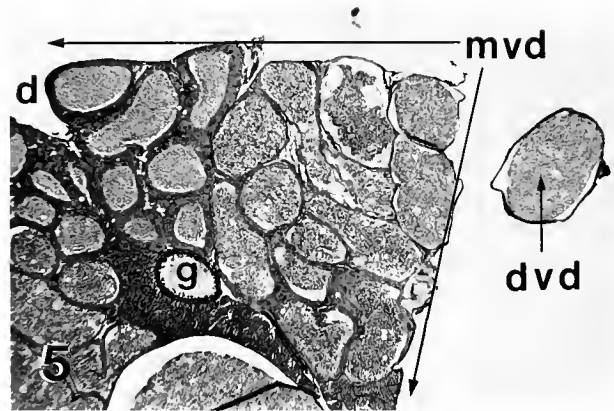
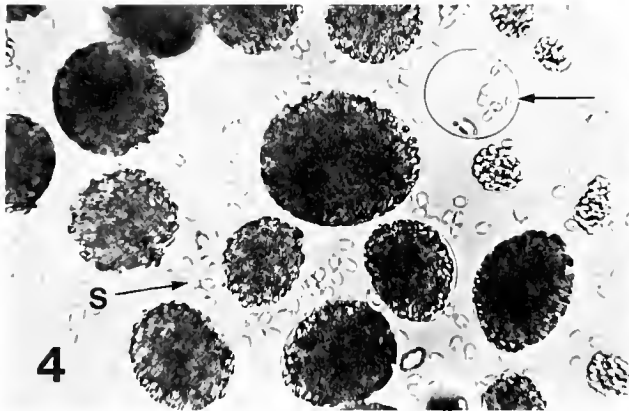
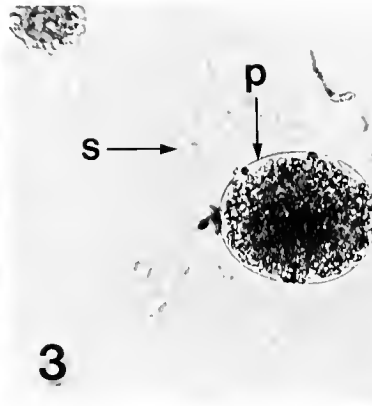
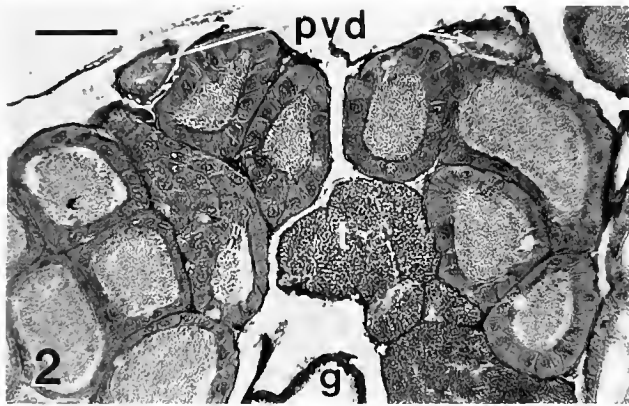


**Figure 2.** Cross section through proximal (posterior) coils of median vas deferens of *Trachypenaeus similis*, showing left and right proximal vasa deferentia (pvd) dorsal to coils. g, gut; t, tissue of posterior extension of testes.

**Figure 3.** Single spermatophore showing pellicle (p) surrounding group of sperm. s, sperm free in water from ruptured spermatophores.

**Figure 4.** Group of spermatophores including one (unlabeled arrow) in which most sperm have escaped, leaving behind a largely unbroken pellicle. s, sperm from ruptured spermatophores.

**Figure 5.** Cross section through coils of median vas deferens (bordered by arrows labeled mvd) of one side approximately halfway along its length, showing proximal-to-distal decrease in duct wall thickness. Note thin-walled distal vas deferens (dvd) lateral to median vas deferens. d, dorsal side of section; g, gut. Scale bar in Figure 2 represents 800  $\mu$ m in Figure 2, 300  $\mu$ m in Figures 3, 4, and 2 mm in Figure 5.

coated by MVD substance (Fig. 10). The MVD substance surrounding the sperm packets is completely continuous with that of adjacent groups of sperm (Figs. 10, 12).

#### *Internal anatomy of and materials in the ejaculatory duct*

Sections through the ejaculatory duct show that the spermatophore chamber (SC) is a continuation of the thin-walled DVD, filled with sperm packets separated by MVD substance (Figs. 11, 13). A large duct, the "plug substance" chamber (PSC), occupies the bulk of the ejaculatory duct (ED) (Figs. 1, 11) and is lined with a well-developed epithelium (Figs. 11, 14). The PSC is partially subdivided with a posterior chamber (Figs. 1, 14), which is confluent

mesially with the main PSC chamber. The PSC and the SC are separated on the mesial side of the ED (Fig. 11), but laterally, in the area of the gonopore, the two chambers are continuous (Fig. 15). Plug substance intrudes into the mass of sperm packets above the posterior gonopore area (Fig. 15), but more anteriorly sperm packets fill the space over the gonopore (Fig. 13).

The interior of the PSC is filled with a material (Figs. 11, 14), appearing a reddish purple when stained with Mallory's Triple Stain and viewed with light microscopy, which is very hard and difficult to section in paraffin-embedded material. When living males are artificially ejaculated, the contents of the PSC flow out of the gonopore after emission of a cord of spermatophores. The PSC material is a viscous, clear, adhesive fluid when first leaving the gonopore. Within



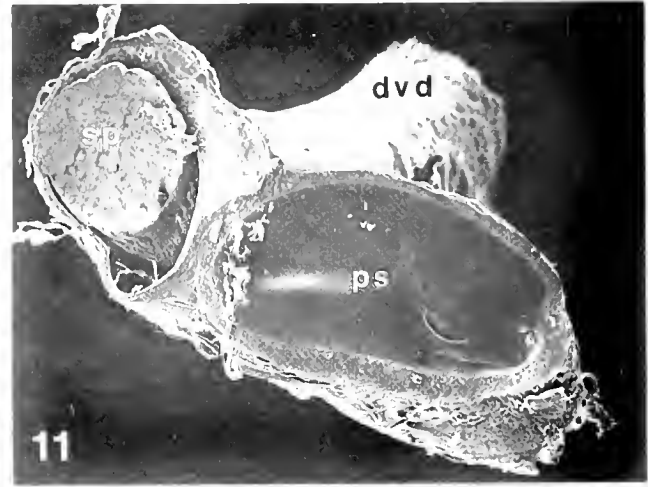
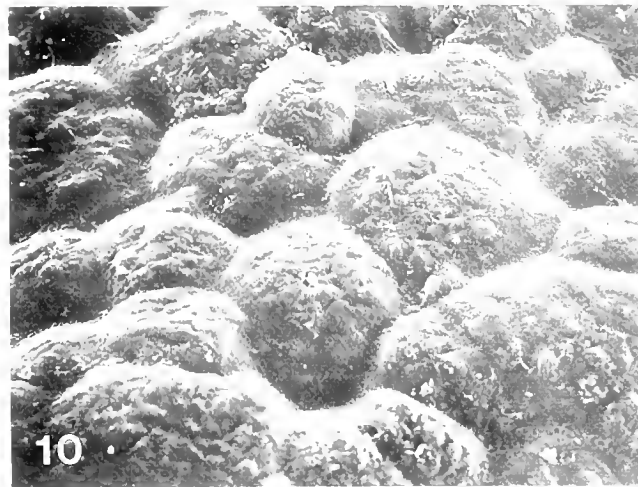
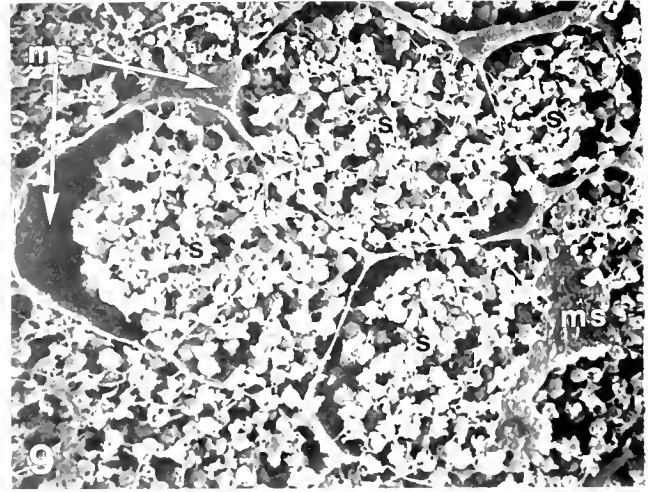
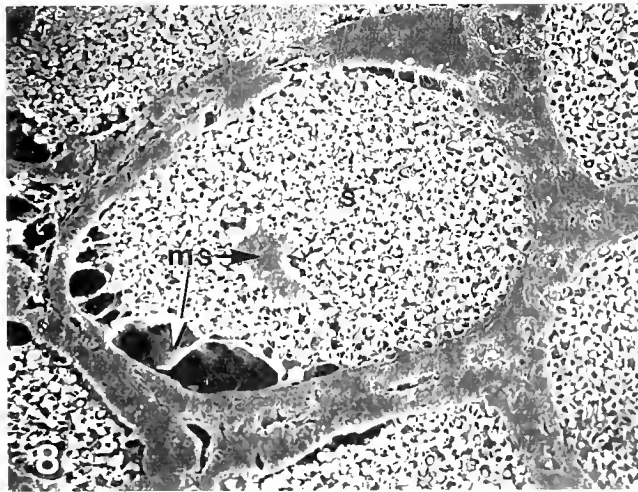
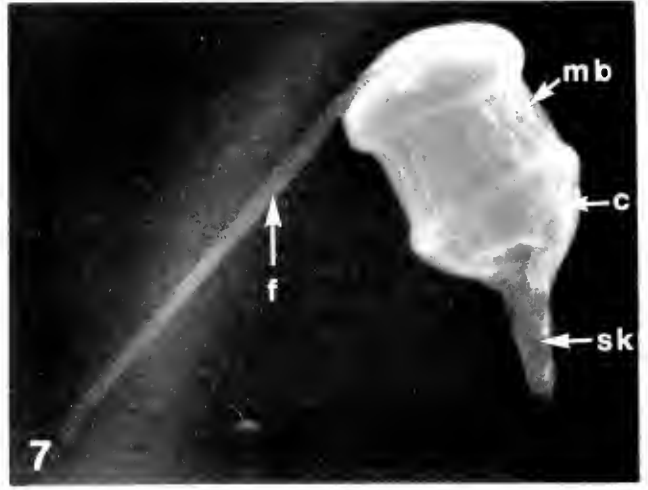
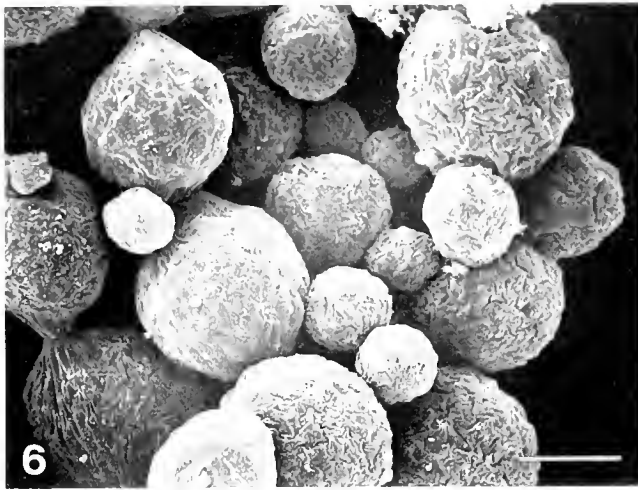


**Figure 6.** Spermatophores of *Trachypenaeus similis* showing variation in size  
**Figure 7.** Sperm cell of *T. similis*: c, cap; f, filament; mb, main body; sk, spike  
**Figure 8.** Section through median vas deferens near proximal end, showing appearance of MVD substance (ms) just inside epithelium and inside solid mass of sperm (s), sperm mass  
**Figure 9.** Section through four adjoining sperm packets separated by MVD substance (ms) in distal (anterior) end of median vas deferens; s, sperm mass  
**Figure 10.** View of outer surface of spermatophores exposed when wall of distal vas deferens was dissected away. Note continuity of MVD substance among spermatophores  
**Figure 11.** Sagittal section taken on mesal side of right ejaculatory duct: dvd, distal vas deferens; ps, plug substance in plug substance chamber; sp, mass of spermatophores in spermatophore chamber. Scale bar in Figure 6 represents 33  $\mu\text{m}$  in Figure 6, 1.4  $\mu\text{m}$  in Figure 7, 35  $\mu\text{m}$  in Figure 8, 18  $\mu\text{m}$  in Figures 9 and 10, and 216  $\mu\text{m}$  in Figure 11

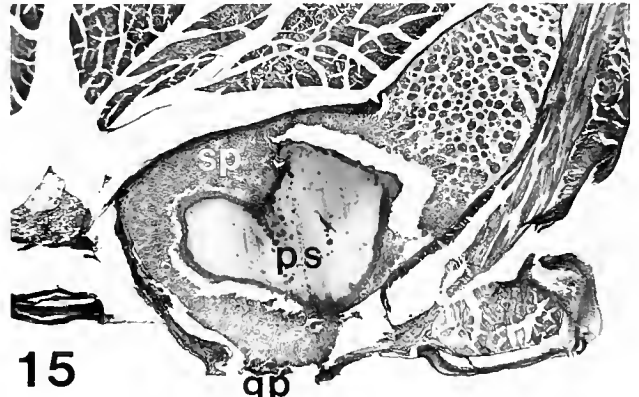
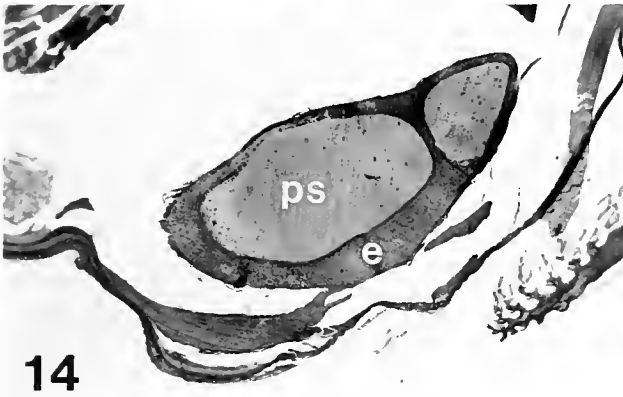
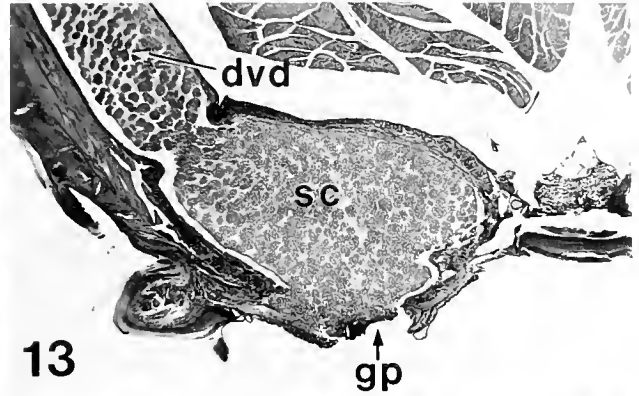
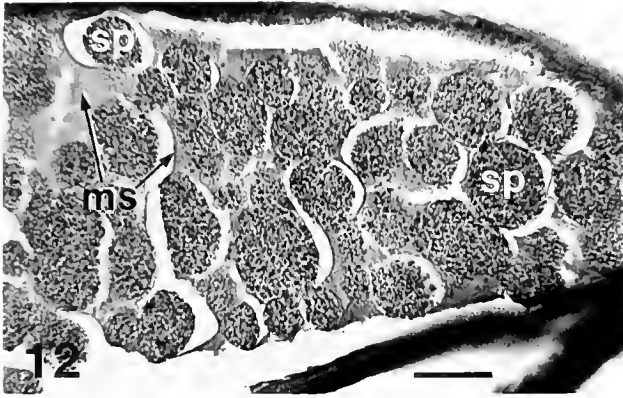


**Figure 12.** Longitudinal section through segment of distal vas deferens. Section was stretched by heating during preparation, separating groups of sperm (spermatophores) from surrounding MVD substance. ms, MVD substance; sp, spermatophores.

**Figure 13.** Cross section through spermatophore chamber (sc) of ejaculatory duct, left side, at level of gonopore (gp). dvd, distal vas deferens.

**Figure 14.** Cross section through plug substance chamber, posterior end, of right ejaculatory duct. e, epithelium; ps, plug substance.

**Figure 15.** Cross section through right ejaculatory duct near posterior end of gonopore. Note plug substance (ps) surrounded by spermatophores (sp). gp, gonopore. Scale bar in Figure 12 represents 300  $\mu$ m in Figure 12 and 2 mm in Figures 13–15.

seconds of emission, it becomes only weakly adhesive, and it changes from a viscous fluid to a soft, malleable, solid mass. It begins a change in transparency and color within seconds, becoming opaque and white within a few minutes. The gross appearance of the PSC material is, after some minutes of exposure to seawater, identical to the material, termed here "plug substance," which plugs and seals the median pocket and seminal receptacles of the female (see below).

#### *Disposition of sperm and plug substance in the inseminated female*

Modifications of the sternum of the penultimate (XIII) and ultimate (XIV) segments of the cephalothorax comprise the genital area, or thelycum, of the female. The

external morphology of the thelycum can be best observed in recently molted, uninseminated females (Fig. 16). On sternite XIV, a pair of flaps (Fig. 16), separated by a longitudinal gap, form the floor of a space, the median pocket (Figs. 18–20). On sternite XIII is the undivided median protuberance, part of which extends posteriorly and dorsal to the sternite XIV flaps. In most inseminated females, the plug substance (PS) from the male can be seen protruding from the median pocket in the transverse gap between the median protuberance and the flaps, and from between the mesial margins of the latter (Figs. 17, 18–20). The PS is quite hard in living females and firmly seals the thelycum flaps together. In contrast, in living or preserved uninseminated females, the flaps can be pulled back and moved quite easily. The PS in the median pocket of the female thelycum has similar staining properties as that



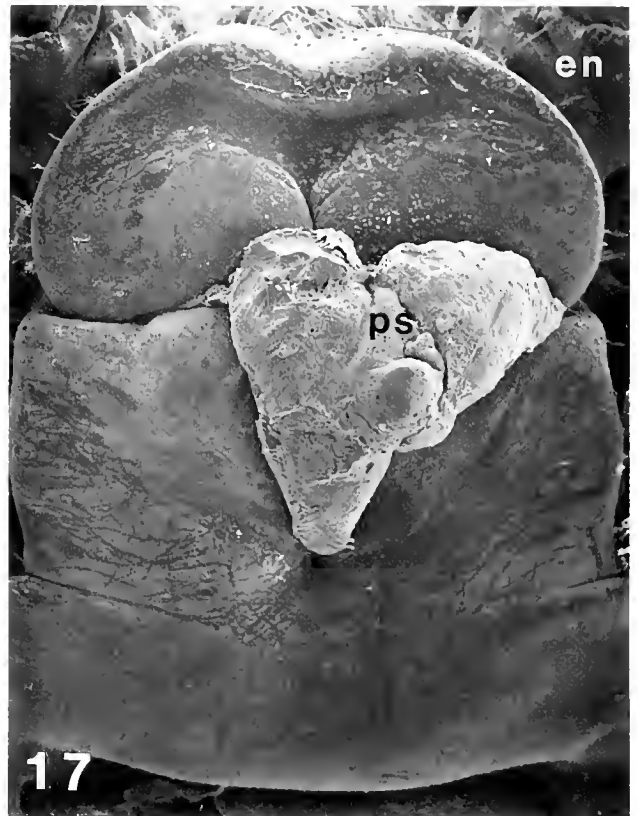
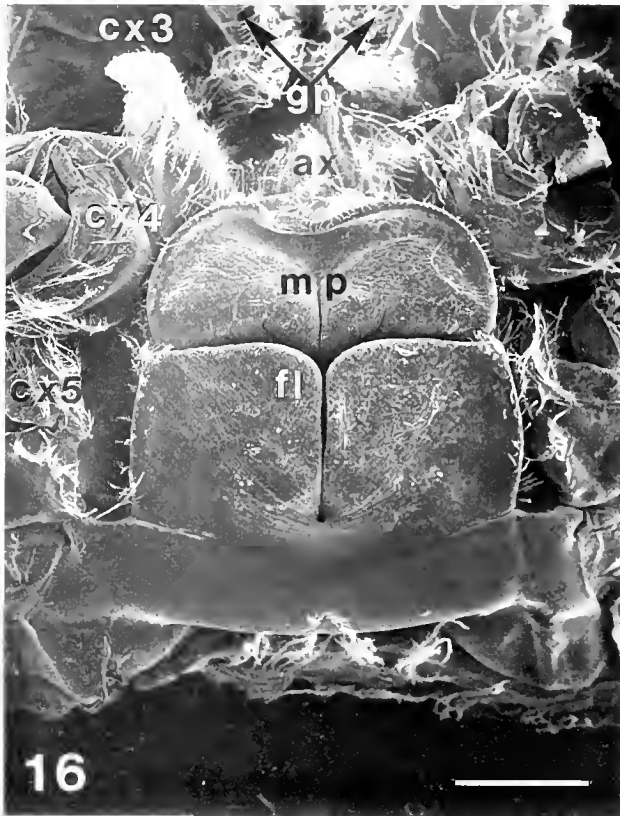


**Figure 16.** Ventral surface of posterior cephalothorax of an unseminated female of *Trachypenaeus similis*, showing thelycum. ax, apex of median protuberance; cx3, cx4, cx5, coxae of third, fourth, and fifth pereopods, respectively. fl, flap; gp, gonopores; mp, median protuberance.

**Figure 17.** Thelycum of unseminated female, showing plug substance (ps) protruding from median pocket. en, endite of coxa of pereopod 4. Scale bar in Figure 16 represents 590  $\mu\text{m}$  in Figure 16 and 421  $\mu\text{m}$  in Figure 17.

in the PSC of the male, as well as comparable physical properties such as hardness and homogeneity of texture in paraffin-carved material viewed with SEM (Figs. 11, 18–20). Examination of exuviae of inseminated females shows that PS remains in the median pocket from the time of insemination until the next molt, at which time it is cast off with the exuviae.

Inside the cephalothorax, dorsal to the thelycum, lie a pair of cuticular invaginations, the seminal receptacles, each with large posterior and smaller anteromesial and anterolateral lobes (Figs. 22–23). The posterior lobes are dorsal to sternite 14, while the anterior lobes lie dorsal and lateral to the median protuberance. Sections through the seminal receptacles showed no spermatophores but rather sperm in a solid mass. Within the sperm mass, small, irregular patches of material, identical in appearance and staining properties to that of the MVD substance of the male, were usually observed in sectioned material. Examination of exuviae show that sperm remaining in the receptacles, often in considerable quantity, are cast off with the cuticular lining of the receptacles when an inseminated female molts.

The opening into each seminal receptacle is a narrow slit between the anteromesial and posterior lobes that extends up to the anterolateral lobe as well. Each seminal receptacle slit (SRS) begins in the roof of the median pocket just posterior to the transverse gap between flaps and median protuberance (Fig. 20), extending anteriorly along the sides of the median protuberance up to about the level of the coxal endite (Fig. 17) of pereopod 4. Sections through the posterior end of the SRS of inseminated females show that the borders of the SRS are separated but that the opening is stoppered with plug substance (Figs. 20, 21). More anteriorly, in the region just anterior to the transverse gap between flaps and median protuberance, the SRS appears functionally closed because its borders, the median protuberance on one side and a fold of the adjacent sternal wall on the other, are tightly pressed together (Figs. 24, 25). The borders of the SRS separate again near its anterior end so that the anterolateral lobe of the seminal receptacle is open to the exterior near the coxal endite of pereopod 4 (Fig. 26). In serial sections through the genital area of several females, sperm were found outside

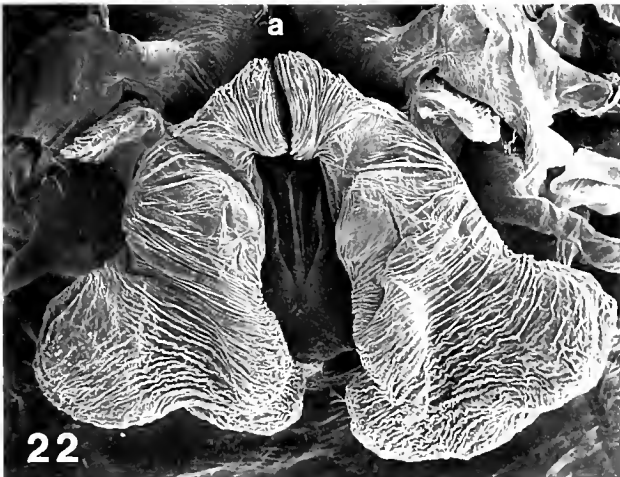
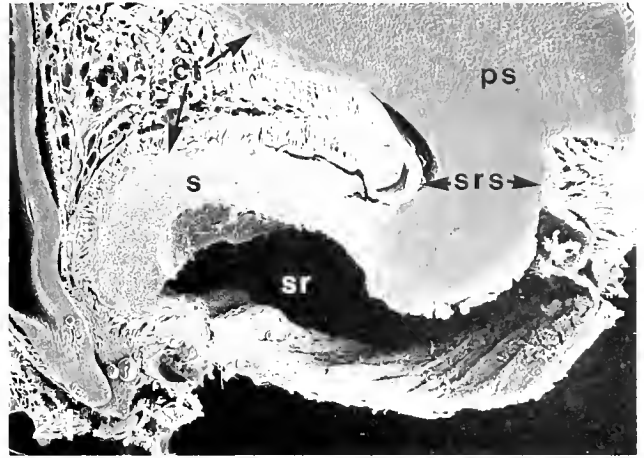
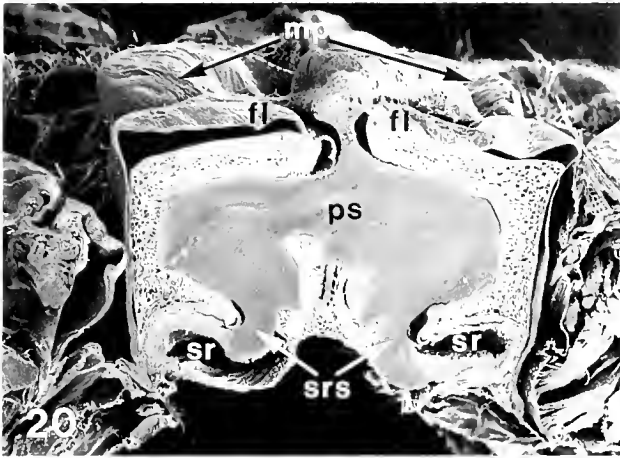
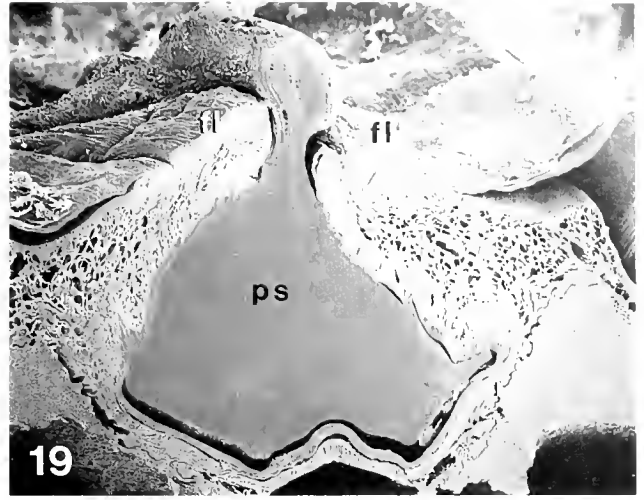
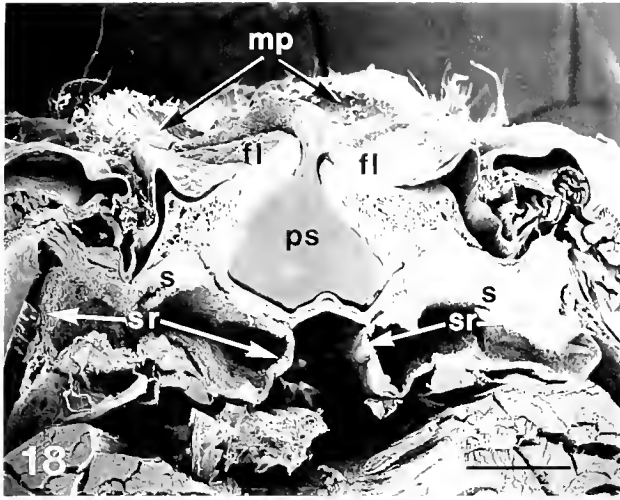


**Figure 18.** Cross section through thelycum of inseminated female of *Trachypenacus similis* at approximately halfway between anterior and posterior ends of transverse slit between flaps (see Figures 16–17 for orientation). Section is viewed from posterior side of animal, ventral (external) surface up. Median pocket is filled with plug substance (ps) that protrudes from between flaps (fl) to exterior. Posterior lobes of seminal receptacles (sr, lateral extent indicated by arrows) inside the cephalothoracic cavity are partially filled with sperm (s). mp, median protuberance.

**Figure 19.** Higher magnification of median pocket filled with plug substance (ps) which protrudes to exterior between flaps (fl) of thelycum.

**Figure 20.** Cross section through thelycum of inseminated female just posterior to transverse gap between flaps (fl) and median protuberance (mp). Orientation same as that for Figure 18. Note plug substance (ps) intruding into each seminal receptacle (sr) from median pocket, plugging each receptacle's slit or opening (srs).

of the seminal receptacles, anterior to the SRS, in the channel or groove (Fig. 27) on each side of the median protuberance up to its apex near the female gonopores (Fig. 16).

### Discussion

The packaging of sperm into numerous small spermatophores, as described here in *Trachypenaeus similis*, is unusual for a penaeoid shrimp. In most species of penaeoids, a single large mass of sperm, surrounded by a variety of accessory materials, is emitted from each male gonopore during ejaculation (Heldt, 1938a, b; Malek and Bawab, 1974a, b; Pérez Farfante, 1975; Champion, 1987; Orsi Relini and Tunesi, 1987; Ro *et al.*, 1990; Bauer and Cash, 1991; Bauer, 1991, Chow *et al.*, 1991). In species with such large, complex spermatophores, the vas deferens is subdivided into two ducts, one containing sperm mass and surrounding capsular substance, the other with one or more accessory materials that serve to attach or seal the sperm mass on or in the thelycum of the female. In *T. similis*, as in other *Trachypenaeus* spp., the vas deferens is a simple undivided tube containing a single material (MVD substance) that participates in the formation of many small spermatophores. The "plug substance" of *T. similis*, appearing only in the ejaculatory duct, is not homologous to accessory materials produced in the median vasa deferentia of other penaeoid shrimps. Observations by Burkenroad (1934) indicate that males of another penaeid, *Xiphocaris kroyeri* (Heller), may have a similar system of many small spermatophores with a plug substance present in the ejaculatory duct, but the details of this system have not yet been described. Only males of the penaeoid genus *Sicyonia* have simpler reproductive tracts in which a simple mass of sperm in a fluid matrix is found in the vas deferens, is emitted from the gonopores, and is stored in the female seminal receptacles without any male accessory substances (Burkenroad, 1934; Bauer, 1991).

Ultrastructural studies on the vasa deferentia of a variety of male decapods have demonstrated the secretion of spermatophore and accessory substances by the epithelium of the vas deferens [majid crab *Libinia emarginata* Leach, Hinsch and Walker, 1974; lobster *Homarus americanus* H. Milne Edwards, Kooda-Cisco and Talbot, 1986; majid crab *Chionoecetes opilio* (O. Fabricius), Ben-

inger *et al.*, 1988; crayfish *Cherax albidus*, Talbot and Beach, 1989; *Penaeus* shrimps, Ro *et al.*, 1990; Chow *et al.*, 1991]. We did not study possible secretion of the material (MVD substance) that appears to form the pellicles of spermatophores in *Trachypenaeus similis*. Secretion of MVD substance might be revealed by ultrastructural studies on the epithelium of the proximal coils of the median vas deferens where this substance first appears.

Males of brachyuran crabs such as *Carcinus maenas* (Linnaeus), *Callinectes sapidus* Rathbun, *Portunus sanguinolentus* (Herbst), *Chionoecetes opilio*, and *Geryon* spp. produce many spermatophores of small size, as in *Trachypenaeus similis*. The epithelium of the vas deferens of these brachyurans secretes a substance or substances that, after intermixing into the sperm mass and surrounding groups of sperm, condenses into the spermatophore pellicle (Spalding, 1947; Cronin, 1947; Ryan, 1967; Beninger *et al.*, 1988; Hinsch, 1988, 1991). Our observations in this study on isolation of packets of sperm by MVD substance suggest a comparable mechanism of spermatophore formation in *T. similis*. We observed peristaltic contractions in the median and distal portions of vasa deferentia excised from freshly sacrificed males, similar to observations made in other decapod species (Ryan, 1967; Ro *et al.*, 1990; suggested from vas deferens ultrastructure by Kooda-Cisco and Talbot, 1986; Talbot and Beach, 1989). Such contractions of the vas deferens wall might serve to intermix MVD substance with the sperm mass in spermatophore formation as well as move all duct contents more distally.

The sperm cells of *Trachypenaeus similis* are similar to those described for other penaeoid shrimps (Clark *et al.*, 1984; Griffin *et al.*, 1988; Felgenhauer and Abele, 1991) except for a novel structure, a long delicate but conspicuous filament on the end of the cell opposite the spike. The filaments were not only visible in sperm released from spermatophores but also apparent within sectioned vasa deferentia, indicating that the filaments were not artifacts nor results of any type of reaction of sperm to seawater.

The distribution of plug substance in the median pocket of the female thelycum, and its emission after the spermatophores in artificially ejaculated males, suggest alternative hypotheses on the mechanics of insemination in *Trachypenaeus similis*. One alternative we propose is that

**Figure 21.** Close-up of cross section through one seminal receptacle from Figure 20. Slit or opening (srs) to receptacle from median pocket is filled with plug substance (ps). Note that cuticle (ct) of median pocket (arrow towards upper right) is continuous with that (arrow towards lower left) of seminal receptacle (sr, empty part of lumen of receptacle). s, sperm mass with bits of darker MVD substance inside receptacle.

**Figure 22.** Dorsal view of left and right seminal receptacles inside cephalothorax. Internal organs and soft tissues were removed by treatment with KOH, leaving only cuticular structures. a, anterior direction.

**Figure 23.** Close-up of left seminal receptacle from Figure 22, rotated 90°. al, anterolateral lobe; am, anteromesial lobe; pl, posterior lobe. Scale bar in Figure 18 represents 492  $\mu\text{m}$  in Figure 18, 230  $\mu\text{m}$  in Figure 19, 402  $\mu\text{m}$  in Figure 20, 126  $\mu\text{m}$  in Figure 21, 466  $\mu\text{m}$  in Figure 22, and 300  $\mu\text{m}$  in Figure 23.

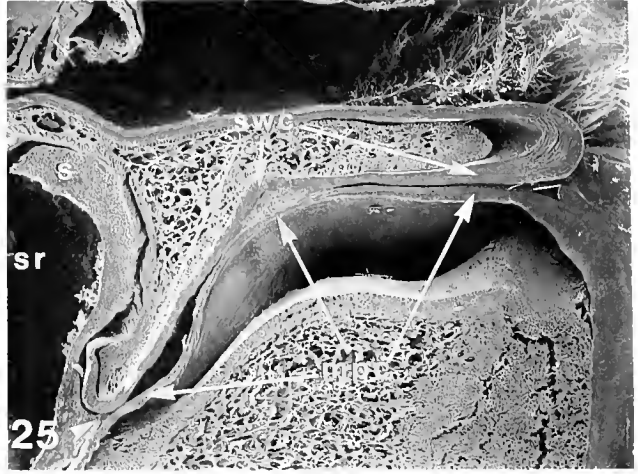
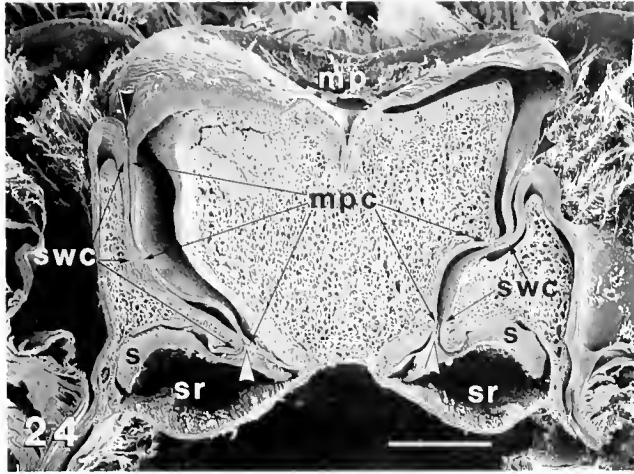


**Figure 24.** Cross section through median protuberance (mp) just anterior to thelycum flaps and median pocket (same orientation as Figures 18 and 20). Unmarked black arrowheads point to locations on external surface which would be open to passageway leading to the slits or openings (unmarked white arrowheads) of seminal receptacles (sr) if passageway were not blocked by abutting cuticles of median protuberance and adjoining sternal wall. mpc, cuticle of median protuberance; s, sperm mass; sr, lumen of seminal receptacle; swc, cuticle of sternal wall.

**Figure 25.** Close-up of blocked passageway between opening to seminal receptacle and external surface. Rotated 90° clockwise from Figure 24, left side (right side of animal). Note bit of sperm mass trapped about midway (middle arrows of mpc and swc) along the closed passageway. Labels same as Figure 24. Scale bar in Figure 24 represents 385 μm in Figure 24 and 179 μm in Figure 25.

the spermatophores are introduced into the median pocket, followed by an injection of plug substance, directly from the male gonopore that is perhaps everted into a papilla during ejaculation. In this scenario, the plug substance would displace the spermatophores from the me-

dian pocket (rupturing them in the process), would force the sperm mass into the posterior ends of the slits that open into the seminal receptacles, and would stopper these openings, preventing backflow and loss of sperm from the receptacles. Alternately, Burkenroad (1934) suggested that

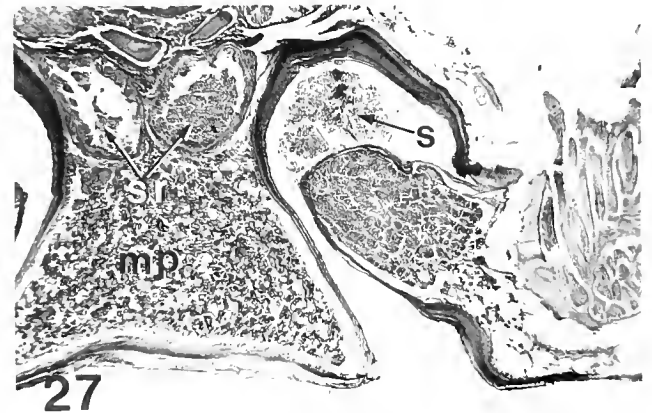
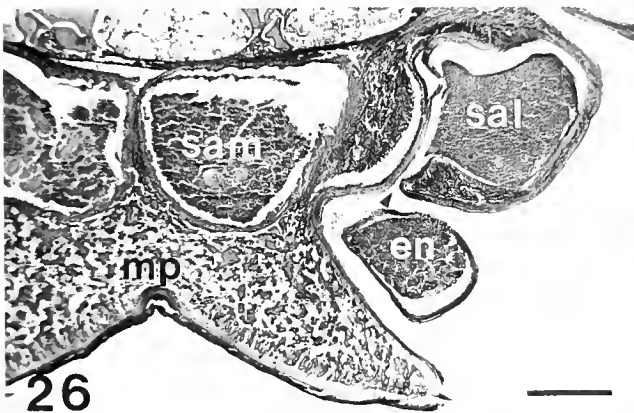


**Figure 26.** Cross section through median protuberance (mp) and area just lateral on right side (section viewed from posterior, dorsal is up in micrograph). Note that opening (small arrowhead) from anterolateral lobe of right seminal receptacle is open to the exterior. en, section through coxal endite of pereiopod 4; sal, sperm mass inside anterolateral lobe; sam, sperm mass inside anteromesial lobe of right seminal receptacle.

**Figure 27.** Cross section through the median protuberance (mp) near its apex. Same orientation as Figure 26. Note sperm (s) outside of seminal receptacles in channel between median protuberance and sternum lateral to it. sr, very anterior ends of anteromesial lobes of seminal receptacles, partially filled with sperm. Scale bar in Figure 26 represents 2 mm in Figures 26 and 27.



the petasma, a semi-closed tubular structure on the male's first pleopods, might function as the injection apparatus, with each of its grooved horns inserting into one of the seminal receptacles during copulation. He hypothesized that spermatophores would first be deposited, and then the petasma would withdraw slightly and deposit the "sperm free secretion" or plug substance into the median pocket. It seems unlikely to us that plug substance, only slightly fluid when first ejaculated, hardening to a soft mass almost immediately, could flow through the petasma and out its narrow terminal channels.

In many vertebrates and invertebrates, hardened or coagulated male products ("mating or copulatory plugs") block the openings to the female reproductive tract after mating (Mann, 1984). Parker (1970) and Thornhill and Alcock (1983), citing examples of mating plugs in various insect species, suggested that one function of mating plugs is to prevent re-insemination of a female once it has mated. Mating plugs ("sperm plugs") have been described in a variety of brachyuran crabs by Hartnoll (1969), who suggested their major role was to prevent loss of sperm from receptacles after copulation. However, Diesel (1991) discussed their possible function as a paternity assurance mechanism in certain brachyurans. In *Trachypenaeus similis*, the male plug substance that blocks access to the seminal receptacles of the females may serve, in addition to preventing loss of sperm from the receptacles after copulation, as a mating plug precluding subsequent inseminations by other males. We have observed during artificial ejaculation of males that the amount of plug substance in and protruding from the median pocket of the female thelycum is approximately that emitted from one ejaculatory duct of one male.

Plug substance may also play an indirect but important role in sperm release from the seminal receptacles. During spawning and concomitant fertilization, which occur separately from mating and insemination in most penaeoids (Anderson *et al.*, 1985; Pillai *et al.*, 1988; Bauer, 1991), sperm being forced out of receptacles by whatever means would be prevented from flowing back out the wrong direction (into the median pocket) by the plug substance that stoppers the receptacle apertures. Sperm must leave the receptacles through what appears to be the only available exits, the openings from the anterolateral lobes of the receptacles. From these exits, sperm would enter the grooves on each side of the median protuberance, streaming forward to just below the gonopores where eggs would be emerging during spawning.

#### Acknowledgments

The senior author (R.T.B.) wishes to thank Dr. Isabel Pérez Farfante for the stimulating and useful discussions on the thelyca and seminal receptacles of *Trachypenaeus*

spp. We wish to thank George Cantrell, captain of the R/V Bill Demoran out of the Gulf Coast Research Laboratory, for his skill and patience in trawling *Trachypenaeus* on our collecting trips to Horn Island, Mississippi. Our participation in cruises on the NOAA vessel R/V Oregon II was quite useful in collecting material used in this study. We thank Dr. Bruce Felgenhauer for alerting us to the polylysine technique used in preparing spermatophores for SEM. We also thank the anonymous reviewers of this manuscript for their helpful suggestions and comments. This research was supported by grants from the National Oceanographic and Atmospheric Administration's Louisiana Sea Grant Program (No. NA89AA-D-SG226) and the Louisiana Educational Quality Support Fund (1989-92-RD-A-20).

#### Literature Cited

- Anderson, S. L., W. H. Clark, Jr., and E. S. Chang. 1985. Multiple spawning and molt synchrony in a free spawning shrimp (*Sicyonia ingentis*, Penaeoidea). *Biol. Bull.* **168**: 377-394.
- Andrews, E. A. 1911. Sperm transfer in certain decapods. *Proc. U.S. Natl. Mus.* **39**: 419-434.
- Bauer, R. T. 1987. Stomatopod grooming behavior: functional morphology and amputation experiments in *Gonodactylus oerstedii*. *J. Crustacean Biol.* **7**: 414-432.
- Bauer, R. T. 1991. Sperm transfer and storage structures in penaeoid shrimps: a functional and phylogenetic perspective. Pp. 183-207 in *Crustacean Sexual Biology*, R. T. Bauer and J. W. Martin, eds. Columbia University Press, New York.
- Bauer, R. T. 1992. Repetitive copulation and variable success of insemination in the marine shrimp *Sicyonia dorsalis* (Decapoda: Penaeoidea). *J. Crustacean Biol.* **12**: 153-160.
- Bauer, R. T., and C. E. Cash. 1991. Spermatophore structure and anatomy of the ejaculatory duct in *Penaeus setiferus*, *P. duorarum*, and *P. aztecus* (Crustacea: Decapoda): homologies and functional significance. *Trans. Am. Microsc. Soc.* **110**: 144-162.
- Beninger, P. G., R. W. Elnor, T. P. Foyle, and P. H. Odense. 1988. Functional anatomy of the male reproductive system and the female spermatheca in the snow crab *Chionoecetes opilio* (O. Fabricius) (Decapoda: Majidae) and a hypothesis for fertilization. *J. Crustacean Biol.* **8**: 322-331.
- Burkenroad, M. D. 1934. The Penaeidea of Louisiana, with a discussion of their world relationships. *Bull. Am. Mus. Nat. Hist.* **68**: 61-143.
- Champion, H. F. B. 1987. The functional anatomy of the male reproductive system in *Penaeus indicus*. *S. Afr. J. Zool.* **22**: 297-307.
- Chow, S., M. M. Dougherty, W. J. Dougherty, and P. A. Sandifer. 1991. Spermatophore formation in the white shrimps *Penaeus setiferus* and *P. vannamei*. *J. Crustacean Biol.* **11**: 201-216.
- Clark, W. H., Jr., A. I. Yudin, F. J. Griffin, and S. Shigekawa. 1984. The control of gamete activation and fertilization in the marine Penaeidae, *Sicyonia ingentis*. Pp. 459-472 in *Advances in Invertebrate Reproduction 3*, W. Engels *et al.*, eds. Elsevier Science Publishers B. V., Amsterdam.
- Cronin, L. E. 1947. Anatomy and physiology of the male reproductive system of *Callinectes sapidus* Rathbun. *J. Morphol.* **81**: 209-239.
- Diesel, R. 1991. Sperm competition and the evolution of mating behavior in Brachyura, with special reference to spider crabs (Decapoda, Majidae). Pp. 145-163 in *Crustacean Sexual Biology*, R. T. Bauer and J. W. Martin, eds. Columbia University Press, New York.
- Felgenhauer, B. E., and L. G. Abele. 1991. Morphological diversity of decapod spermatozoa. Pp. 322-341 in *Crustacean Sexual Biology*.

- R. T. Bauer and J. W. Martin, eds. Columbia University Press, New York.
- Galigher, A. E., and E. N. Kozloff. 1971. *Essentials of Practical Microtechnique*. Lea & Febiger, Philadelphia. 531 pp.
- Griffin, F. J., K. Shigekawa, and W. H. Clark, Jr. 1988. Formation and structure of the acrosomal filament in the sperm of *Sicyonia ingentis*. *J. Exp. Biol.* **246**: 94-102.
- Hartnoll, R. G. 1969. Mating in the Brachyura. *Crustaceana* **16**: 161-181.
- Heldt, J. H. 1938a. La reproduction chez les crustacés décapodes de la famille de pénéides. *Ann. Inst. Oceanogr.* **18**: 31-206.
- Heldt, J. H. 1938b. De l'appareil génital des Penaeidae. Relations morphologique entre spermatophore, thelycum et petasma. *Travaux de la Station Zoologique de Wimereux* **13**: 349-358.
- Hinsch, G. W. 1988. Ultrastructure of the sperm and spermatophores of the golden crab *Geryon fenneri* and a closely related species, the red crab *G. quinqueidens*, from the eastern Gulf of Mexico. *J. Crustacean Biol.* **8**: 340-345.
- Hinsch, G. W. 1991. Structure and chemical content of the spermatophores and seminal fluid of reptantian decapods. Pp. 290-307 in *Crustacean Sexual Biology*, R. T. Bauer and J. W. Martin, eds. Columbia University Press, New York.
- Hinsch, G. W., and M. H. Walker. 1974. The vas deferens of the spider crab, *Libinia emarginata*. *J. Morphol.* **143**: 1-20.
- Hudinaga, M. 1941. Reproduction, development, and rearing of *Penaeus japonicus*. *Jpn. J. Zool.* **10**: 305-393.
- Kooda-Cisco, M., and P. Talbot. 1986. Ultrastructure and role of the lobster vas deferens in spermatophore formation: the proximal segment. *J. Morphol.* **188**: 91-104.
- Kubo, I. 1949. Studies on penaeids of Japanese and its adjacent waters. *J. Tokyo Coll. Fish.* **36**: 1-467.
- Malek, S. R. A., and F. M. Bawab. 1974a. The formation of the spermatophore in *Penaeus kerathurus* (Forskål, 1775) (Decapoda: Penaeidae). I. The initial formation of a sperm mass. *Crustaceana* **26**: 273-285.
- Malek, S. R. A., and F. M. Bawab. 1974b. The formation of the spermatophore in *Penaeus kerathurus* (Forskål, 1775) (Decapoda: Penaeidae). II. The deposition of the main layers of the body and of the wing. *Crustaceana* **27**: 73-83.
- Mann, T. 1984. *Spermatophores*. Springer-Verlag, Berlin. 240 pp.
- Mazia, D., G. Schatten, and W. Sale. 1975. Adhesion of cells to surfaces coated with polylysine. *J. Cell Biol.* **66**: 198-200.
- Orsi Relini, L., and L. Tunesi. 1987. The structure of the spermatophore in *Aristeus antennatus* (Risso, 1816). *Invest. Pesq.* **51**(Supl. 1): 461-470.
- Parker, G. A. 1970. Sperm competition and its evolutionary consequences in the insects. *Biol. Rev. Camb. Philos. Soc.* **45**: 525-567.
- Pérez Farfante, I. 1971. A key to the American Pacific shrimps of the genus *Trachypenaeus* (Decapoda: Penaeidae), with the description of a new species. *U.S. Natl. Mar. Fish. Serv. Fish. Bull.* **69**: 635-646.
- Pérez Farfante, I. 1975. Spermatophores and thelyca of the American white shrimps, genus *Penaeus*, subgenus *Litopenaeus*. *U.S. Natl. Mar. Fish. Serv. Fish. Bull.* **73**: 463-486.
- Pérez Farfante, I. 1982. The geminate shrimp species *Parapenaeus longirostris* and *P. politus* (Crustacea: Decapoda: Penaeoidea). *Quad. Lab. Tecn. Pesca Ancona* **3**: 187-205.
- Pérez Farfante, I. 1985. The rock shrimp genus *Sicyonia* (Crustacea: Decapoda: Penaeoidea) in the eastern Pacific. *U.S. Natl. Mar. Fish. Serv. Fish. Bull.* **83**: 1-78.
- Pillai, M. C., F. J. Griffin, and W. H. Clark, Jr. 1988. Induced spawning of the decapod crustacean *Sicyonia ingentis*. *Biol. Bull.* **174**: 181-185.
- Ro, S., P. Talbot, J. Leong-Trujillo, and A. L. Lawrence. 1990. Structure and function of the vas deferens in the shrimp *Penaeus setiferus*: segments 1-3. *J. Crustacean Biol.* **10**: 455-468.
- Ryan, E. P. 1967. Structure and function of the reproductive system of the crab *Portunus sanguinolentus* (Herbst) (Brachyura: Portunidae). I. The male system. *Proc. Symp. Crustacea, Mar. Biol. Assoc. India* **2**: 506-521.
- Shaw, B. L., and H. I. Battle. 1957. The gross and microscopic anatomy of the digestive tract of the oyster *Crassostrea virginica* (Gmelin). *Can. J. Zool.* **35**: 325-347.
- Spalding, J. F. 1942. The nature and formation of the spermatophore and sperm plug in *Carcinus maenas*. *Q. J. Microsc. Sci.* **83**: 399-422.
- Talbot, P., and D. Beach. 1989. Role of the vas deferens in the formation of the spermatophore of the crayfish (*Cherax*). *J. Crustacean Biol.* **9**: 9-24.
- Thornhill, R., and J. Alcock. 1983. *The Evolution of Insect Mating Systems*. Harvard University Press, Cambridge, Massachusetts. 547 pp.

# Sperm-Specific Basic Proteins in the Holocephalan Fish *Hydrolagus colliei* (Chondrichthyes, Chimaeriformes) and Comparison with Protamines from an Elasmobranch

N. SAPERAS<sup>1,2,3</sup>, M. CHIVA<sup>1,3</sup>, N. C. BOLS<sup>1,4</sup>, D. KULAK<sup>1</sup>, AND H. E. KASINSKY<sup>1,\*</sup>

<sup>1</sup>Department of Zoology, University of British Columbia, Vancouver, British Columbia, Canada V6T 1Z4, and Bamfield Marine Station, Bamfield, British Columbia, Canada V0R 1B0; <sup>2</sup>Institut de Ciències Del Mar, C.S.I.C., 08039 Barcelona, Spain; <sup>3</sup>Department d'Enginyeria Química, Universitat Politècnica de Catalunya, 08028 Barcelona, Spain; and <sup>4</sup>Department of Biology, University of Waterloo, Waterloo, Ontario, Canada N2L 3G1

**Abstract.** Seven basic proteins can be isolated from sperm nuclei of the holocephalan ratfish *Hydrolagus colliei*. Two of these proteins (R3 and m0) are devoid of cysteine, whereas five of them (R1, R2, m1, m2, and m3) contain low levels of this amino acid residue. The proteins R1, R2, and R3 are major ones in the sperm nuclei of *H. colliei*, and they are analogous to basic proteins Z1, Z2, and Z3 (scylliorhinines) from the sperm of the elasmobranch *Scylliorhinus canicula*. However, taking into account the partial sequence of R3 protein and the number of cysteines in R1 and R2, these proteins do not seem to be homologous to the scylliorhinines. A comparison of sperm basic proteins between *H. colliei* (a holocephalan) and *S. canicula* (an elasmobranch) suggests a remarkable divergence of these proteins from a common ancestral pattern during the evolution of Chondrichthyes.

## Introduction

The spermatozoan nucleus usually contains specific proteins that condense the DNA. In most animal spermatozoa, these proteins replace somatic histones. They show a great interspecific variability (Bloch, 1976; Kasinsky, 1989). The sperm-specific basic proteins (SBPs) of some bony fish (called "protamines," "monoprotamines," or "true protamines") have been very well studied at the levels of protein (Ando *et al.*, 1973; McKay *et al.*, 1986;

Saperas *et al.*, 1993, a, b); gene (Dixon *et al.*, 1985); and genetic expression (Iatrou and Dixon, 1978; Hecht, 1989; Oliva and Dixon, 1991). The protamines of other vertebrates, particularly those from amphibians, reptiles, birds, and mammals, have often been considered to be molecules that are related evolutionarily to these protamines (Nakano *et al.*, 1976; Chiva *et al.*, 1987, 1989; Oliva and Dixon, 1991; Takamune *et al.*, 1991). Among the cartilaginous fishes, spermatogenesis in a few species has been studied based on cytochemical staining (Bols and Kasinsky, 1974, 1976) and electrophoresis (Oliveras *et al.*, 1990). However, at the level of biochemical characterization, knowledge of protamines in cartilaginous fish is based entirely on studies of a single species, *Scylliorhinus canicula* (Quero, 1984), the lesser spotted dogfish (also known as the small spotted catshark).

The observations on the changes of nuclear proteins that occur during the spermiogenesis of *S. canicula* show evident differences between this species and bony fish. Gusse and Chevaillier (1978, 1981) observed that two basic "intermediate" proteins, S1 and S2, appear in the early modifications of chromatin structure during spermiogenesis in *S. canicula*. These proteins partially substitute for histones (Chevaillier, 1991), although in more advanced stages they are in turn replaced by other basic proteins (protamines). These authors found four protamines (Z1, Z2, Z3, and S4) called "scylliorhinines" in the spermatozoan nucleus. One of these protamines (Z3) is a protein with 31 amino acid residues, a high percentage of arginine (64.5 mol%), and no cysteine (Sautière *et al.*, 1981; Gusse

Received 16 March 1993; accepted 23 June 1993.

\* Address correspondence to this author at the University of British Columbia.

*et al.*, 1983). This protein is organized in arginine clusters, and its primary structure is comparable with that of the protamines from bony fish. Z1, Z2, and S4 are cysteine-rich protamines and contain 50, 46, and 32 residues, respectively. The first two are rich in arginine, whereas S4 is rich in lysine (Gusse *et al.*, 1983). The sequences of these three molecules do not show a significant number of identities in the position of their residues (Sautière *et al.*, 1984; Martinage *et al.*, 1985; Chevaillier *et al.*, 1987); nor are they comparable to cysteine-rich protamines from mammals. In a general analysis from a comparison of the sequences of these proteins (Sautière *et al.*, 1984; Chevaillier *et al.*, 1987), these authors suggest two important points: (1) Z3 and bony fish protamines probably originated from the same ancestral DNA sequence, before the divergence between cartilaginous and bony fish occurred; (2) Z1, Z2, and S4 probably had an independent origin from different gene families. The studies of the sequence of intermediate protamines S1 and S2 also show that there is no relationship between their sequences and those from sperm protamines (Chauvière *et al.*, 1987, 1989).

In spite of this work, we cannot extend these results to chondrichthyan fish in general because *S. canicula* is the only species of cartilaginous fish that has been studied biochemically. In this work, we examine the sperm proteins of the ratfish (rabbitfish) *Hydrolagus collicii*. This species is a holocephalan (order Chimaeriformes). It was selected because the holocephalans diverged very early from the rest of the cartilaginous fish (Nelson, 1984). They are considered to be more primitive than elasmobranchs (Schaeffer, 1981). Consequently, a comparison between the protamines of *H. collicii* and *S. canicula* may provide valuable information about the common characteristics of these molecules in the early stages of the evolution of fish. We should take into account that the long period of separate evolution between these two groups could result in important differences between their sperm proteins.

## Materials and Methods

### Animals

*H. collicii* testes were obtained in April at the Friday Harbor Laboratories, San Juan Island, Washington, USA; in May at Comox, British Columbia, Canada; and in June at the Bamfield Marine Station, B.C., Canada.

### Nuclei

Nuclei were prepared separately from whole testis, epididymis, and ampulla ductus deferentis after Gusse and Chevaillier (1978) as follows. The tissues were dissected on ice with scissors and homogenized for 30 s in a Sorvall Omnimixer in buffer A (20 mM Tris pH 7.5/0.15 M KCl/0.34 M sucrose) containing either 50 mM benzamidine chloride or 0.5 mM PMSF as a proteolytic inhibitor. The

homogenate was filtered through four layers of cheesecloth and centrifuged at  $4000 \times g$  for 8 min. The resulting sediment (1 vol) was homogenized in 15 vol of buffer A containing proteolytic inhibitor and 0.1% (w/v) Triton X-100 in a Dounce hand homogenizer under the same conditions. The resulting homogenate was underlaid by 15 vol of buffer B (20 mM Tris pH 7.5/0.15 M KCl/1.4 M sucrose) containing the proteolytic inhibitor, and centrifuged for 20 min at  $30,000 \times g$ . The sediment was washed in distilled water and the nuclei (or chromatin) obtained again by centrifugation ( $4000 \times g$ , 8 min). All the procedures were performed in the cold.

### Proteins

Proteins were extracted from nuclei with 0.25 N HCl. In the cases that will be detailed below, nuclear sediments were reduced and alkylated before (or between) the extractions. For *H. collicii*, we applied the method used by Gusse *et al.* (1983) on *S. canicula* to allow the comparison of sperm protamines between both species. Nuclear sediments were reduced with 20 vol of buffer C (50 mM Tris, pH 8.8/10 mM DTT/2 mM disodium EDTA) in a 1-h incubation at  $37^\circ\text{C}$  under  $\text{N}_2$  atmosphere. After centrifugation at  $7700 \times g$  for 10 min, the sediment was alkylated with 25 vol of 12.5 mM iodoacetamide in buffer C for 1 h at the same conditions and centrifuged.

For Figure 1, basic nuclear proteins were prepared from testicular zones. In this case, the micromethod of Louie and Dixon (1972) was used to isolate and extract sperm basic proteins from cell suspensions. We have utilized this method previously, as described in detail by Kasinsky *et al.* (1985).

### Chromatography

Chromatographic separation of proteins by ion exchange columns was performed on CM-52 cellulose (Whatman). Proteins were dissolved in 50 mM acetate buffer (pH 6.0) containing 0.2 M NaCl (Chiva *et al.*, 1987, 1988). In some cases, the proteins extracted from sperm nuclei were reduced and alkylated again before chromatographic separation. Reduction was performed in buffer D (20 mM DTT/8 M urea/0.5 M NaCl) for 1 h at  $37^\circ\text{C}$  under  $\text{N}_2$  atmosphere. Alkylation with 50 mM iodoacetamide in buffer D was done under the same conditions (Gusse *et al.*, 1983). Afterwards, the proteins were dialyzed against acetate buffer/NaCl and loaded onto the columns.

When necessary, fractions collected from CM-cellulose columns were applied on a  $5 \mu\text{m}$  Spherisorb column and purified by reverse-phase high-performance liquid chromatography (HPLC). The column was equilibrated with 0.05% trifluoroacetic acid (TFA) and proteins separated with a gradient of acetonitrile in 0.05% TFA.



### Amino acid analysis

Amino acid analyses were performed as described by Chiva and Mezquita (1983). These analyses were used to determine the molar compositions of proteins. The number of amino acid residues in each protein was inferred from the compositional values and from the electrophoretic mobility in acetic-urea polyacrylamide gels (Daban *et al.*, 1991).

In addition, we used the method described by Creighton (1980) and Hollecker (1989) to determine the integral number of cysteine residues of the molecules. This method has been applied to *H. collicii* protamines as well as to a commercial standard (BPTI, Boehringer Mannheim). The protein was denatured and reduced by incubating in 8 M urea/10 mM DTT/10 mM Tris-HCl pH 8.0/1 mM disodium EDTA for 30 min at 37°C. Afterward, aliquots of the sample were alkylated by adding 0.25 M iodoacetamide, 0.25 M iodoacetate, and varying ratios of iodoacetamide to iodoacetate, respectively. After 15 min at room temperature, the solutions were placed on ice and adequate volumes analyzed in polyacrylamide gels containing 8 M urea, following the low pH discontinuous system of Reisfeld *et al.* (1962).

### N-terminal sequence

The amino-terminal sequence of ratfish protamine R3 was determined by automated Edman degradation with an Applied Biosystems 470A Protein Sequencer, and the phenylthiohydantoin derivatives of amino acid residues were analyzed on an Applied Biosystems 120A on-line HPLC system using a microbore C18 Brownlee column (2.1 × 220 mm) (Saperas *et al.*, 1993b).

### Electrophoresis

The procedure of Panyim and Chalkley (1969) was used for routine electrophoretic analysis of proteins. The gels were stained with 0.25% (w/v) Coomassie blue in methanol/acetic acid/H<sub>2</sub>O (5:1:1 by volume) and destained in the same mixture. Gels were 10 cm long, but sometimes 20-cm gels were used to improve resolution. To count the cysteine residues of the protein molecules, we used the methodology described by Reisfeld *et al.* (1962), but using gels containing 8 M urea.

### Histology

In two specimens, midsagittal sections were dissected from concentric zones of ampullae in the testis (Stanley, 1963). Starting from the ampullogenic zone, a portion of each zone was fixed in 10% neutral-buffered formalin and used for cytochemical analyses (Bols and Kasinsky, 1974, 1976). The remainder of each zone was used to isolate and extract sperm basic proteins from nuclei by the micro-method of Louie and Dixon (1972).

## Results

### Nuclear proteins in testicular and sperm cells

For the electrophoretic analysis of basic nuclear proteins during the course of testicular spermatogenesis, one testis was dissected into concentric zones (A to E). A portion of each zone was examined cytochemically to establish the stages of spermiogenesis present in the tissue that had to be examined by electrophoresis. Spermiogenesis in the ratfish has been divided into seven stages on the basis of nuclear protein cytochemistry (Bols and Kasinsky, 1976). In Figure 1 left, zones A and B are equivalent to cytochemical stages 1 and 2 identified by Bols and Kasinsky (1976), and they contain round spermatids (A) and spermatids just beginning to undergo nuclear elongation (B). Zone C (stages 3–4) is heterogeneous and shows spermatids starting the process of spiralization, as well as those still in the midst of nuclear elongation. In zone D (stages 5–6), spermatids are completing spiralization, while in zone E (stage 7) the testicular sperm cells are organized into tightly packed cysts. None of these zones is completely homogeneous, but each zone (except for C) is enriched for cells at a particular stage of spermiogenesis.

The electrophoretic analysis of basic nuclear proteins from each of these zones is shown in Figure 1, right. This analysis reveals that somatic histones are the main proteins contained in nuclei from early spermiogenic stages, but in the most advanced stages, the spermatid nuclei contain a collection of proteins with higher mobility than histone H4. Three of these proteins appear to be major: they have been designated as R1, R2, R3. The proteins appearing in Figure 1 have been extracted from nuclei with 0.25 N HCl without previous reduction/alkylation of these nuclei. A subsequent reduction/alkylation and extraction of the chromatin did not solubilize any additional proteins.

Nuclei of sperm cells have been isolated separately from epididymis and the anterior and posterior region of the ampulla ductus deferentis. Figure 2 shows the proteins extracted from these nuclei with and without reducing conditions for chromatin. When nuclei are reduced and alkylated, a complex set of proteins can be solubilized with 0.25 N HCl extraction (Fig. 2, lanes b, c, d). The three major bands coincide with R1, R2, and R3 observed in spermiogenic testicular nuclei, but some minor bands also appear in the electrophoretic pattern (arrows in Fig. 2). When nuclei are extracted with 0.25 N HCl without previous reduction, only the protein R3 (Fig. 2, lane e) plus one minor band (named m0 in lane e) can be solubilized. Proteins R1 and R2 can be solubilized from sperm nuclei only after reduction of chromatin (Fig. 2, lane g). In this case, some minor bands also appear in the electrophoretic pattern (designated as m1, m2, and m3 in lane g). We have found these electrophoretic patterns to be highly reproducible with many sperm-nuclei preparations using different proteolytic inhibitors. We conclude

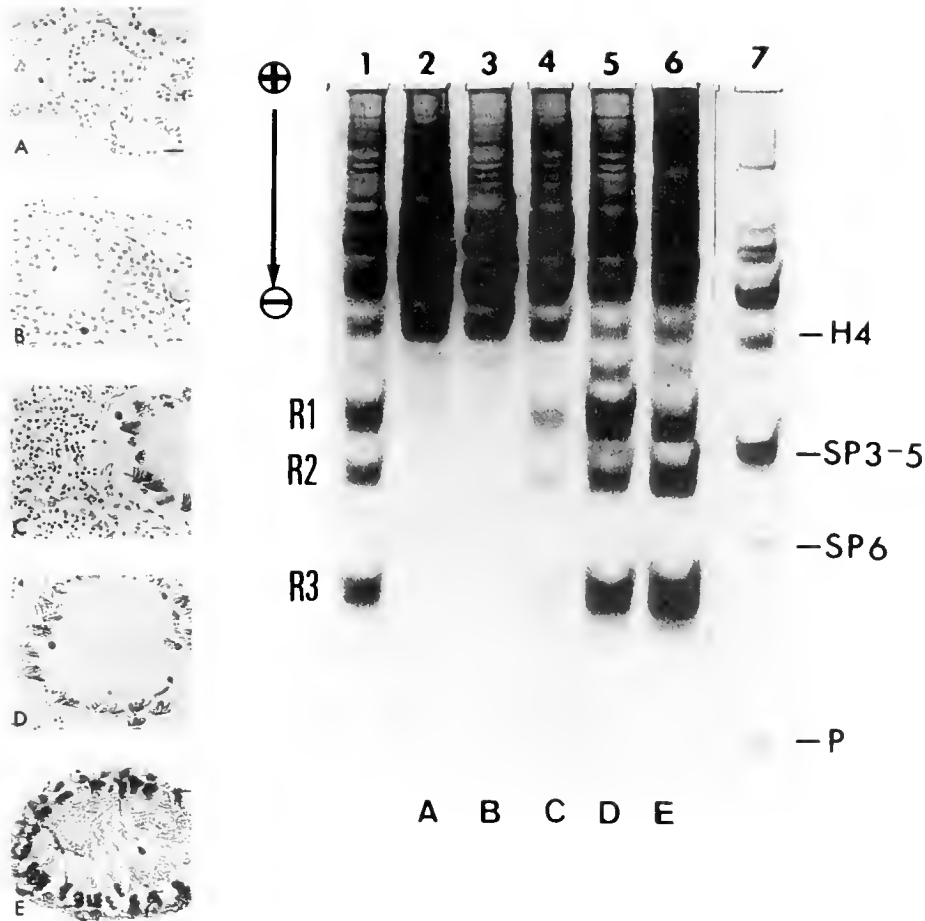


**Figure 1.** Left: Midsagittal sections of *Hydrolagus colliet* testis showing follicles containing different stages of spermiogenesis. Feulgen staining, zones A-D; hematoxylin-eosin staining, Zone E. Zones A and B, spermatids beginning the process of nuclear elongation; Zone C, mixture of spermatids undergoing nuclear elongation and spermatids beginning the process of spiralization; Zone D, spermatids undergoing spiralization; Zone E, sperm organized into tightly packed cysts. Scale (in A) denotes 10 μm for each zone. Right: Electrophoretic profiles of basic proteins extracted with 0.25 N HCl (without reduction) from dissected testicular zones. Lane 1, *H. colliet* whole testis; lanes 2-6, *H. colliet* testicular zones A-E, respectively; lane 7, standards of frog (*Xenopus laevis*) sperm basic proteins (histones and proteins SP 3-5, SP 6) and herring protamine (P). H4 = evolutionary conservative histone H4. Electrophoresis in this and subsequent figures is from top (+) to bottom (-).

that sperm-specific basic protamines of *H. colliet* consist of three major (R1, R2, and R3) and four minor (m0, m1, m2, and m3) proteins. Only two of them (R3 and m0) can be extracted from sperm nuclei without previous reduction. In addition, R1 and R2 reproducibly have a slightly lower mobility when extracted without reduction from testis (Fig. 2, lane f) than when extracted with reduction from epididymal sperm (Fig. 2, lane g).

*Purification and analysis of proteins*

We used sperm cells from epididymis, as well as anterior and posterior parts of the ampulla ductus deferentis, for the purification of ratfish nuclear sperm proteins. Nuclei

were extracted directly with 0.25 N HCl, cleared by centrifugation; and reduced, alkylated, and re-extracted with 0.25 N HCl. The fractions containing proteins solubilized without reduction (R3 and m0) and proteins extracted after reduction (R1, R2, m1, m2, and m3) were precipitated with the addition of six volumes of cold acetone (-20°C overnight), rinsed with acetone, and dried.

The former fraction (R3 and m0) was placed on a CM-cellulose column and proteins were collected in two "peaks" (I and II, and Fig. 3A). Whereas peak II contained the purified protein R3 (Fig. 3, lane II), peak I contained a mixture of R3 and m0 (Fig. 3A, lane I). Proteins from this peak were separated by reverse-phase HPLC. In this system we obtained a series of peaks, some of them con-

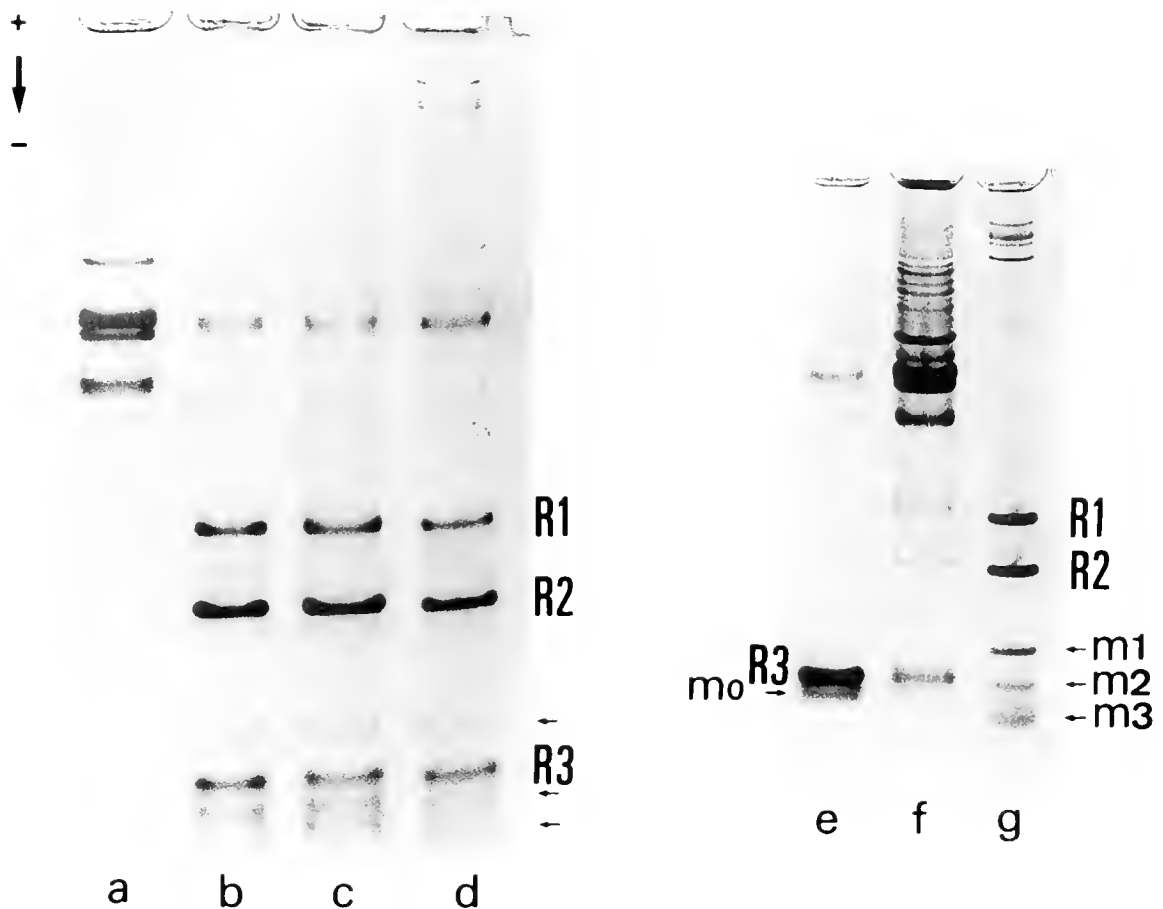


**Figure 2.** Effect of reduction and extraction of sperm basic proteins of *Hydrolagus coliei*. Left: Proteins extracted with 0.25 *N* HCl after reduction and alkylation of sperm nuclei. Lane b, sperm from epididymis; lane c, sperm from the anterior region of ampulla ductus deferentis; lane d, sperm from the posterior region of the ampulla ductus deferentis. Lane a shows a standard of histones from unripe testes of *H. coliei*. Arrows next to lane d indicate minor bands m1, m2, m3. Right: Proteins extracted with 0.25 *N* HCl without previous reduction. Lane e, epididymal sperm nuclei; lane f, testicular nuclei. Lane g shows the pattern when epididymal sperm basic proteins remaining in nuclei after removal of R3 and m0 (with 0.25 *N* HCl, lane e) are re-extracted with 0.25 *N* HCl after reduction/alkylation.

taining the purified proteins R3 and m0 (Fig. 3B). Proteins R3 and m0 from those columns were analyzed for their amino acid content. Compositional values are shown in Table I together with the amino acid composition of non-keratinous protamine Z3 from *S. canicula*. The amino acid content of *H. coliei* R3 is remarkably different from that of *S. canicula* Z3 (see Discussion).

An aliquot of the purified protein R3 was dialyzed extensively against 50 mM  $\text{NH}_4\text{HCO}_3$  and lyophilized. For sequencing purposes, the protein was further purified by reverse-phase HPLC (see Materials and Methods). The 16 N-terminal amino acid sequence for protein R3 obtained by automated Edman degradation (Fig. 4) shows two heterogeneous clusters of basic amino acid residues (RRRH) and (KKRKRK). The comparison of this part of the R3 molecule with the complete sequence of Z3 protamine of *S. canicula* supports the idea emerging from the

amino acid analysis data that there is a large difference between ratfish R3 and dogfish Z3.

The proteins extracted with 0.25 *N* HCl after reduction of sperm nuclei were purified using the same types of chromatography as before. First we separated three fractions (I, II, and III in Fig. 5A) by ion exchange on CM-cellulose. Fraction II contained purified R1, and Fraction III contained R2 (Fig. 5C, lanes c, d). Fraction I contained the rest of R1 plus the minor proteins m1, m2, and m3 (not shown). Proteins from fraction I were purified in reverse-phase HPLC (Fig. 5, B and C) and analyzed compositionally. Table II shows their amino acid composition compared with scylliorhines Z1, Z2, and S4. Although the compositional values are partially similar amongst the ratfish sperm basic proteins and scylliorhines Z1 and Z2, this does not mean that they all belong to the same family of proteins; *i.e.*, ratfish and dogfish proteins need

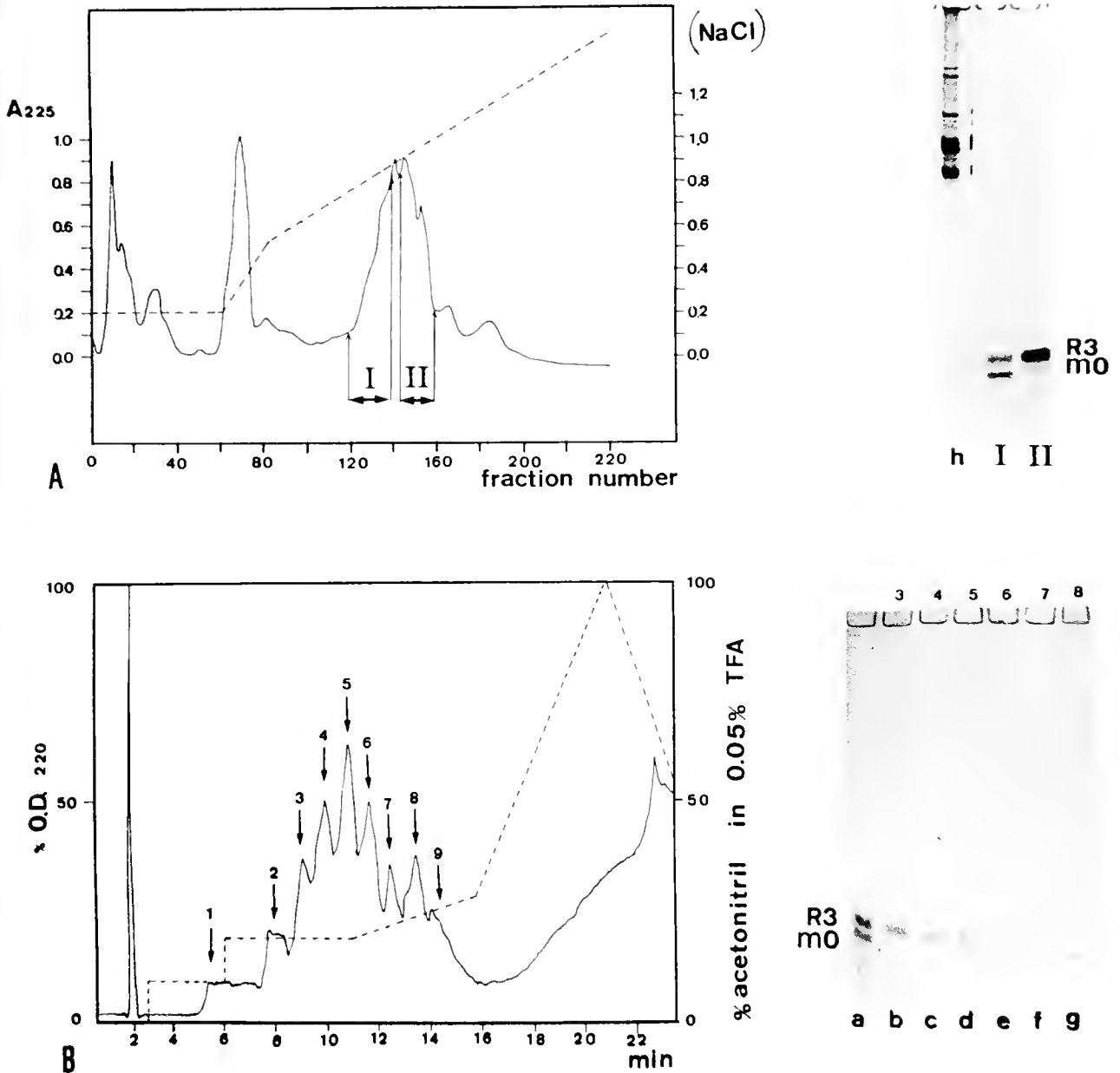


**Figure 3.** Chromatographic purification of R3 and m0 proteins. A. CM-cellulose chromatography of proteins extracted from sperm nuclei without previous reduction. Molarity of NaCl is shown on righthand vertical axis. Fraction II contains the purified protein R3 (see electrophoretic control on right). Lane h shows histones from unripe testes of *Hydrolagus colliet*. B. HPLC of protein contained in peak I from panel A. Fractions 3 and 4 contain R3 protein and fraction 8 contains m0 protein.

not be homologous. In fact, scylliorhines Z1 and Z2 may not be homologous to each other. In spite of possessing comparable amino acid compositions, Z1 and Z2 do not have similar sequences (Chevaillier, 1991). The cysteine content is also significantly different: whereas scylliorhines are very rich in this amino acid residue, protamines R1 and R2 from ratfish (and also the minor protamines m1, m2, and m3) have a poor content of cysteine.

To verify the low content of cysteine in ratfish sperm basic proteins, we applied the method described by Creighton (1980), which relies on the charge differences introduced by specific chemical modification of the amino acid. In Cys residues, the reaction of the thiol group with iodoacetic acid introduces a new acidic group, whereas reaction with neutral iodoacetamide does not change the net charge. Thus, the method consists of adding varying ratios of iodoacetamide to iodoacetate to portions of the protein to generate a com-

Table I

Amino acid composition (mol %) of ratfish sperm basic proteins R3 and m0 compared with Z3 protamine (*S. canicula*) and salmine

Amino acid	R3	m0	Z3 <sup>a</sup>	Salmine <sup>b</sup>
Lys	20.7	23.8	—	—
His	4.3	5.6	—	—
Arg	27.6	23.7	64.5	65.6
Asx	4.6	1.0	—	—
Thr	2.6	4.9	—	—
Ser	7.4	9.3	9.7	12.5
Glx	5.7	7.4	—	—
Pro	6.9	3.5	—	9.4
Gly	4.0	3.5	19.4	6.2
Ala	3.4	2.7	3.2	—
Cys	—	—	—	—
Val	1.9	—	—	6.2
Met	1.6	3.4	—	—
Ile	—	1.8	—	—
Leu	3.8	6.1	—	—
Tyr	—	2.0	3.2	—
Phe	5.3	1.2	—	—
Number of residues	45 ± 4 <sup>c</sup>	—	31	32

<sup>a</sup> After the sequence by Sautière *et al.* (1981).

<sup>b</sup> After the sequence by Ando and Watanabe (1969).

<sup>c</sup> Estimated from the amino acid composition and electrophoretic mobility.

plete spectrum of protein molecules with 0, 1, . . . *N* acidic carboxymethyl groups, where *N* is the integral number of cysteine residues per protein molecule.

In Figure 6A we show the incubation, with different ratios of iodoacetamide to iodoacetate, of a standard bovine pancreatic trypsin inhibitor (BPTI) from Boehringer Mannheim and the incubation, under the same conditions, of testicular protamines R1 and R2 from ratfish (Fig. 6, B and C). In the BPTI control, bands of lower electrophoretic mobility (Fig. 6A, arrows right) correspond to a progressive number of acid-modified cysteine residues. In the case of protamines R1 and R2, it is not possible to infer the presence of more than one Cys per molecule (2 arrows on right of Fig. 6, B and C). This result agrees with the previous one obtained by amino acid analysis.

### Discussion

The holocephalans diverged very early from the other cartilaginous fish and therefore have followed a separate

evolution for a long period of time (Nelson, 1984). This fact makes the comparison between the sperm basic proteins of *S. canicula* (an elasmobranch) and *H. colliei* (a holocephalan) of great interest because the characteristics they share might correspond to the sperm basic proteins in the original type of cartilaginous fish.

### Sperm protamine model

The pattern of sperm basic proteins in ratfish seems to be the same as in *S. canicula*. Both possess a major non-keratinous protamine (R3/Z3) and a couple of comparable major keratinous (cysteine-containing) proteins (R1, R2/Z1, Z2). In both species, the latter basic proteins are not extractable from the spermatozoan without a previous reduction, but they are extractable from the testis. Apart from that, each organism has some peculiarities, as can be seen in S4 from *S. canicula* and in the minor bands m1, m2, and m3 from *H. colliei* (Table II).

In Figure 7 we show the comparison between the electrophoretic patterns of the protamines of these two species. It is interesting to note the parallelism between both patterns and the difference (approximately constant) between the electrophoretic mobility of the proteins of one species and the other. This difference is attributable to the size of the protamines, which are larger in ratfish than in *S. canicula*.

Gusse and Chevallier (1980a, b) showed that dogfish basic proteins Z1 and Z2 (as well as S4) could form a beaded structure with sperm DNA, whereas Z3 would possibly act in higher orders of sperm DNA packing. The presence of a very similar model in *H. colliei* suggests a functional analogy for proteins R1, R2, and R3. This remains to be proved. However, from the evolutionary point of view, one fact clearly stands out: The model of two keratinous basic proteins plus a nonkeratinous basic protein has to be interpreted as an ancestral character shared by cartilaginous fish after their separation from other animals in early vertebrate evolution.

### Characteristics of the molecules

In a series of studies on the scylliorhinines, Gusse, Chevallier, Sautière, and colleagues (Sautière *et al.*, 1981, 1984; Martinage *et al.*, 1985; Chevallier *et al.*, 1987, 1989) sequenced the four protamines of *S. canicula* (Z1, Z2, Z3, and S4), as well as the two intermediate proteins (S1

	1	5	10	15	20	25	30
(a)	A	R R R H S M K K	K R K S	V R R			
(b)	A	R S R S R R S	Y G R G R R R G G R R R R R R R R R R R R R R G G R				

Figure 4. N-terminal sequence of (a) R3 sperm protein from *Hydrolagus colliei* compared with the sequence of (b) Z3 from *S. canicula* (Sautière *et al.*, 1981).

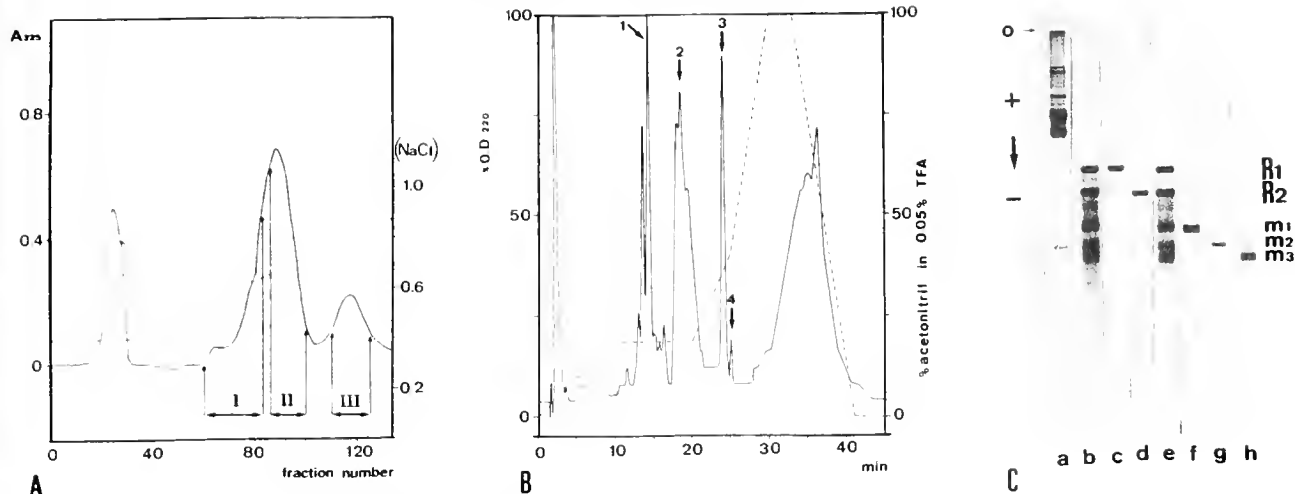


**Figure 5.** Chromatographic purification of R1, R2, m1, m2, and m3 proteins. A. CM-cellulose separation of the complete set of proteins; B. HPLC purification of proteins eluted in fraction I from panel A; C. Electrophoretic control of proteins purified: lane c, protein R1 from fraction II of panel A; lane d, protein R2 from fraction III of panel A; lane f, protein m1 from peak 3 of panel B; lane g, protein m2 from peak 4 of panel B; lane h, protein m3 from peak 1 of panel B. Lanes b and e are the complete set of proteins after 0.25 N HCl extraction and the reduction/alkylation process. Lane a shows a standard of histones and protein R3 from *Hydrolagus collet*.

and S2) that are present in the nuclei of differentiating spermatids but not in nuclei of spermatozoa. The following evolutionary generalizations can be made. First, Z3

is a protamine structurally very similar to the typical true protamines of bony fish (Sautière *et al.*, 1981). These authors suggest that "scylliorhinine Z3 and teleost

**Table II**

*Amino acid composition (mol %) of ratfish R1, R2, m1, m2, and m3 sperm basic proteins compared with keratinous protamines Z1, Z2, and S4 of S. canicula*

Amino acid	R1	R2	m1	m2	m3	Z1 <sup>a</sup>	Z2 <sup>b</sup>	S4 <sup>c</sup>
Lys	12.2	9.9	20.1	21.0	15.6	16.0	13.0	43.7
His	6.9	1.2	6.5	7.7	5.4	4.0	6.5	—
Arg	30.1	39.3	35.4	30.0	29.2	32.0	37.0	21.9
Asx	4.3	1.7	1.5	2.8	1.2	4.0	—	—
Thr	2.8	4.6	—	1.8	4.8	4.0	2.2	—
Ser	4.0	9.7	10.5	4.0	8.7	4.0	4.3	—
Glx	6.0	1.5	6.7	4.9	5.1	2.0	2.2	—
Pro	6.9	3.8	—	4.8	—	6.0	2.2	6.2
Gly	6.4	21.1	7.6	5.2	7.7	2.0	2.2	3.1
Ala	2.7	3.8	—	3.6	9.3	2.0	10.9	9.4
Cys <sup>d</sup>	1.2	1.4	2.0	1.3	1.9	8.0	8.7	12.5
Val	3.5	—	5.1	2.3	7.8	4.0	4.3	3.1
Met	1.2	—	—	1.9	—	—	2.2	—
Ile	3.9	1.7	—	1.1	—	—	2.2	—
Leu	4.5	1.8	2.3	3.3	3.3	8.0	2.2	—
Tyr	2.2	—	1.8	1.0	—	2.0	—	—
Phe	1.2	2.3	—	3.3	—	2.0	—	—
Number of residues:	79 ± 4 <sup>e</sup>	66 ± 2 <sup>e</sup>				50	46	32

<sup>a</sup> After the sequence by Chevallier *et al.* (1987).

<sup>b</sup> After the sequence by Martinage *et al.* (1985).

<sup>c</sup> After the sequence by Sautière *et al.* (1984).

<sup>d</sup> Cys determined as carboxymethyl-cysteine.

<sup>e</sup> Estimated from the amino acid composition and electrophoretic mobility.

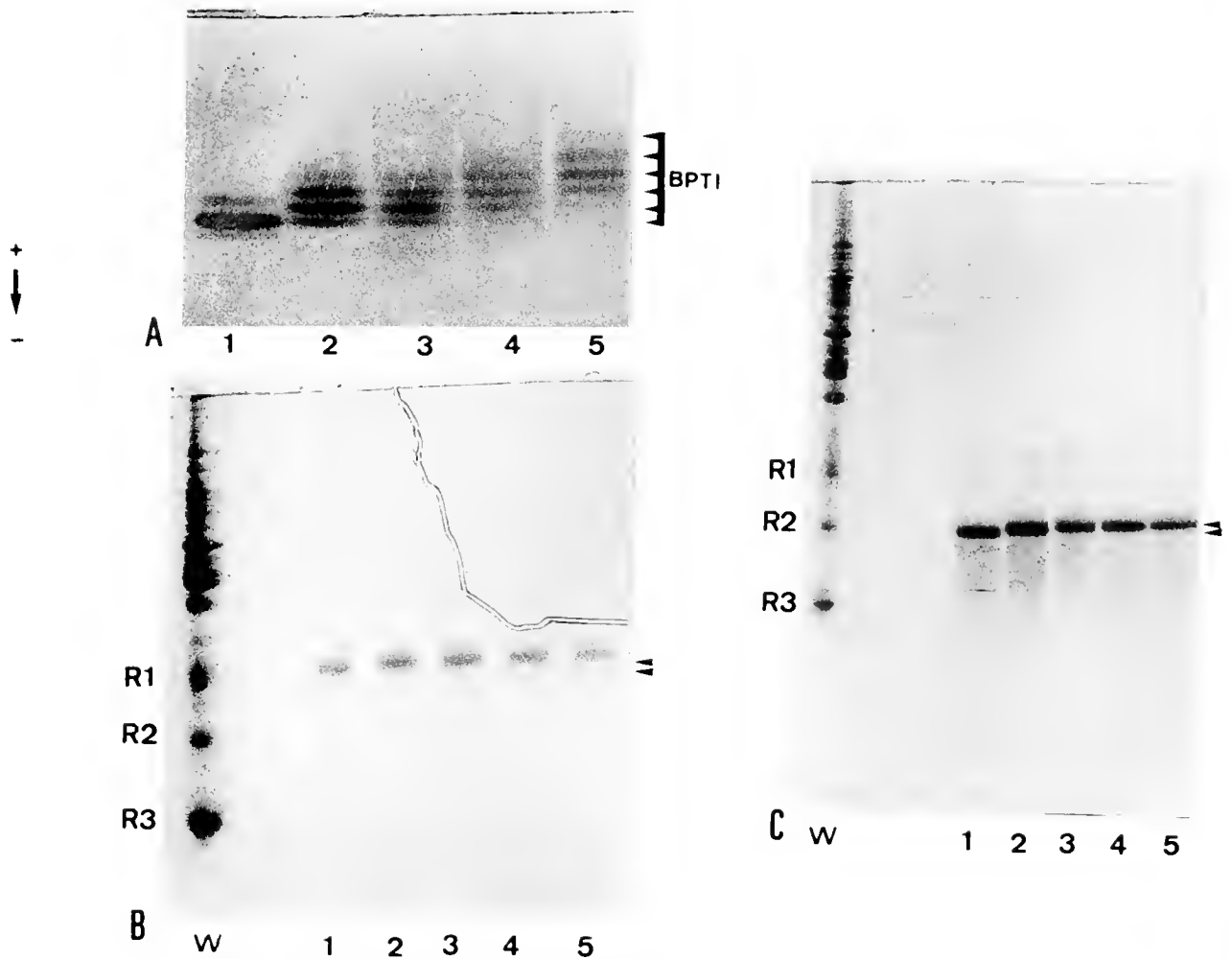


**Figure 6.** Determination of the number of cysteine residues according to the method of Creighton (1980). A. Standard of BPTI (Boehringer Mannheim); B. R1 from *Hydrolagus collieri*; C. R2 from *H. collieri* Reaction with iodoacetamide (1); iodoacetamide/iodoacetate in ratios of 1:1 (2), 1:3 (3), and 1:9 (4); and with iodoacetate (5). W = whole basic protein pattern from *H. collieri* testis.

protamines originated very probably from the same ancestral DNA sequence before the divergence of Chondrichthyes and Osteichthyes during the Devonian period" (Chevaillier *et al.*, 1987). Second, there are very few identities in the sequences of protamines Z1, Z2, and S4. Possibly, these basic proteins have evolved neither from the same single ancestral polypeptide nor from the same gene family. Third, the intermediate basic proteins S1 and S2 are not homologous to the sperm proteins. These data mean that the sperm (and spermiogenic) nuclear proteins from *S. canicula* are coded by a series of genes that express coordinately during spermiogenesis but do not possess a close evolutionary relationship.

The comparison of ratfish protamines with those from *S. canicula* brings out yet a greater variability in this system of molecules. Ratfish R3 protamine differs greatly from *S. canicula* Z3 protamine (Table I). R3 contains a relatively great diversity of amino acid residues (14 dif-

ferent types), contrasted with only five types of residues that constitute Z3. In addition, ratfish is relatively poor in arginine (27.6 mol % versus 64.5 mol % in dogfish), and its N-terminal sequence shows the presence of clusters of heterogeneous basic residues (RRRH, KKKRK) that are not present in Z3, nor in the protamines of bony fish. The minor protamine m0 presents compositional characteristics similar to R3 (Table I).

The comparison between the amino acid composition of R1 and R2 and the scylliorhines Z1 and Z2 (Table II) shows that, globally, all these proteins possess a comparable composition. However, this similarity does not necessarily mean that there is a homology between them. Two points are inconsistent with such a homology: (1) scylliorhines Z1 and Z2 are compositionally similar but their sequences present hardly any identities; (2) there are important deviations in the compositions of R1 and R2 with respect to Z1 and Z2, as can be seen by the larger

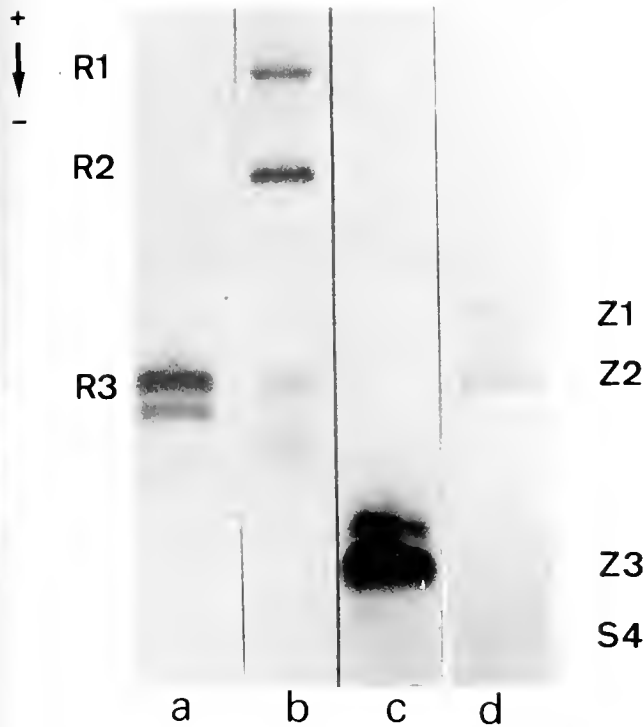


Figure 7. Comparison of electrophoretic patterns of sperm basic proteins from *Hydrolagus collicii* (lanes a, b) and *S. canicula* (lanes c, d); proteins without cysteine (lanes a and c) and cysteine-containing proteins (lanes b and d).

proportion of glycine in ratfish R2 (21.1 mol %) and the presence of a very low percentage of cysteine in both R1 and R2.

The results presented here show a high variability among chondrichthyan protamines, possibly due to an origin from a different pool of genes or, alternatively, to great divergence while retaining the ancestral pattern of two keratinous protamines and one nonkeratinous protamine. Finally, the great difference between proteins R3 from ratfish and Z3 from dogfish calls into question the interpretation (Sautière *et al.*, 1981) that nonkeratinous protamines from Chondrichthyes and typical protamines from bony fish have the same common ancestor.

**Acknowledgments**

We wish to thank Drs. J. A. Subirana and D. Lloris for their helpful support and advice. Doctors Ph. Chevallier and M. Gusse kindly provided us with purified samples of *S. canicula* sperm basic proteins and assisted us with helpful discussions. We are also grateful to C. Buesa from the Servei de Seqüenciació de Proteïnes de la Universitat de Barcelona (Spain). Specimens were obtained with the help of Drs. H. Stanley, M. H. I. Dodd, and the late J. M. Dodd, as well as J. Lee. For assistance with sectioning of testes and cytochemistry, we thank Drs. H. Stanley and

M. MacKay, as well as E. Rosenberg. A number of students and assistants deserve thanks for their efforts in various aspects of this study; these include the late J. Boyko, D. Braille, L. Gutovich, J. Ip, S. Jessa, H. Lau, L. Johnstone, E. Soorany, M. Tsui, and I. Uzuraga. This work was supported in part by a Travel Fellowship from the Ministerio de Educacion y Ciencia, Spain (N.S.); CICYT, Spain (M.C.); and NSERC, Canada (H.E.K.).

**Literature Cited**

Ando, T., and S. Watanabe. 1969. A new method for fractionation of protamines and the amino acid sequence of one component of salmine and the three components of iridine. *Int. J. Protein Res.* **1**: 221-224.

Ando, T., M. Yamasaki, and K. Suzuki. 1973. *Protamines: Isolation, Characterization and Function*. Springer Verlag, New York.

Bloch, D. P. 1976. Histones of sperm. Pp. 139-167 in *Handbook of Genetics*, Vol. 5. R.C., King, ed., Plenum Press, New York.

Bols, N. C., and H. E. Kasinsky. 1974. Cytochemistry of sperm histones in three cartilaginous fish. *Can. J. Zool.* **52**: 437-439.

Bols, N. C., and H. E. Kasinsky. 1976. On the diversity of sperm histones in the vertebrates: II. A cytochemical study of the basic protein transitions during spermiogenesis in the cartilaginous fish *Hydrolagus collicii*. *J. Exp. Zool.* **198**: 109-114.

Chauvière, M., A. Martinage, G. Briand, P. Sautière, and Ph. Chevallier. 1987. Nuclear basic protein transition during sperm differentiation. Amino acid sequence of a spermatid-specific protein from the dogfish *Scylliorhinus caniculus*. *Eur. J. Biochem.* **169**: 105-111.

Chauvière, M., A. Martinage, G. Briand, P. Sautière, and Ph. Chevallier. 1989. Nuclear basic protein transition during sperm differentiation. Primary structure of the spermatid-specific protein S2 from the dogfish *Scylliorhinus caniculus*. *Eur. J. Biochem.* **180**: 329-335.

Chevallier, Ph., A. Martinage, M. Gusse, and P. Sautière. 1987. Amino acid sequence of scylliorhinine Z1 and comparison of the primary structure of the protamines of the dogfish *Scylliorhinus caniculus*. *Biochim. Biophys. Acta* **914**: 19-27.

Chevallier, Ph. 1991. Nuclear protein transitions during sperm differentiation. Pp. 19-25 in *Comparative Spermatology 20 Years After*. B. Baccetti, ed. Raven Press, New York.

Chiva, M., H. E. Kasinsky, M. Mann, and A. Subirana. 1988. On the diversity of sperm basic proteins in the vertebrates: VI. Cytochemical and biochemical analysis in birds. *J. Exp. Zool.* **245**: 304-317.

Chiva, M., H. E. Kasinsky, and J. A. Subirana. 1987. Characterization of protamines from four avian species. *FEBS Letters* **215**: 237-240.

Chiva, M., D. Kulak, and H. E. Kasinsky. 1989. Sperm basic proteins in the turtle *Chrysemus picta*. Characterization and evolutionary implications. *J. Exp. Zool.* **249**: 329-333.

Chiva, M., and C. Mezquita. 1983. Quantitative changes of high mobility group non-histone chromosomal proteins HMG-1 and HMG-2 during rooster spermatogenesis. *FEBS Letters* **162**: 324-328.

Creighton, T. E. 1980. Counting integral numbers of amino acid residues per polypeptide chain. *Nature* **284**: 487-489.

Daban, M., M. Chiva, E. Rosenberg, H. E. Kasinsky, and J. A. Subirana. 1991. Protamines in prosobranchian gastropods (Mollusca) vary with different modes of reproduction. *J. Exp. Zool.* **257**: 265-283.

Dixon, G. H., J. M. Aiken, J. M. Jankowsky, D. I. McKenzie, R. Moir, and J. C. States. 1985. Organization and evolution of the protamine genes of salmonid fish. Pp. 287-314 in *Chromosomal Proteins and Gene Expression*. G. R. Reeck, G. H. Goodwin, and P. Puigdomènech, eds. Plenum Press, New York.

Gusse, M., and Ph. Chevallier. 1978. Étude ultrastructurale et chimique de la chromatine au cours de la spermiogénèse de la rousette *Scylliorhinus caniculus* (L.). *Cytobiologie* **16**: 421-443.



- Gusse, M., and Ph. Chevaillier. 1980a. Electron microscope evidence for the presence of globular structures in different sperm chromatin. *J. Cell Biol.* **87**: 280-284.
- Gusse, M., and Ph. Chevaillier. 1980b. Molecular structure of chromatin during sperm differentiation of the dogfish *Scylliorhinus caniculus* (L). *Chromosoma* **77**: 57-68.
- Gusse, M., and Ph. Chevaillier. 1981. Microelectrophoretic analysis of basic protein changes during spermiogenesis in the dogfish *Scylliorhinus caniculus* (L). *Exp. Cell Res.* **136**: 391-397.
- Gusse, M., P. Sautière, M. Chauvière, and Ph. Chevaillier. 1983. Extraction, purification and characterization of the sperm protamines of the dogfish *Scylliorhinus caniculus*. *Biochim. Biophys. Acta* **748**: 93-98.
- Hecht, N. 1989. Mammalian protamines and their expression. Pp. 347-373 in *Histones and Other Basic Nuclear Proteins*. L. Hnilica, G. Stein, and J. Stein, eds. CRC Press, Boca Raton, Florida.
- Hollecker, M. 1989. Counting integral numbers of residues by chemical modification. Pp. 145-153 in *Protein Structure. A Practical Approach*. T. E. Creighton, ed. IRL Press, Oxford.
- Iatrou, K., and G. H. Dixon. 1978. Protamine messenger RNA: its life history during spermatogenesis in rainbow trout. *Fed. Proc.* **37**: 2526-2533.
- Kasinsky, H. E. 1989. Specificity and distribution of sperm basic proteins. Pp. 73-163 in *Histones and Other Basic Nuclear Proteins*. L. Hnilica, G. Stein, and J. Stein, eds. CRC Press, Boca Raton, Florida.
- Kasinsky, H. E., S. Y. Huang, M. Mann, J. Roca, and J. A. Subirana. 1985. On the diversity of sperm histones in the vertebrates: IV. Cytochemical and amino acid analysis in Anura. *J. Exp. Zool.* **234**: 33-46.
- Louie, A., and G. H. Dixon. 1972. Trout testis cells. I. Characterization by DNA and protein analysis of cells separated by velocity sedimentation. *J. Biol. Chem.* **247**: 5490-5497.
- Martinage, A., M. Gusse, D. Bélaiche, P. Sautière, and Ph. Chevaillier. 1985. Amino acid sequence of a cysteine-rich, arginine-rich sperm protamine of the dogfish *Scylliorhinus caniculus*. *Biochim. Biophys. Acta* **831**: 172-178.
- McKay, D. M., B. S. Renaux, and G. H. Dixon. 1986. Rainbow trout protamines. Amino acid sequences of six distinct proteins from a single testis. *Eur. J. Biochem.* **158**: 361-366.
- Nakano, M., T. Tobita, and T. Ando. 1976. Studies on a protamine (galline) from fowl sperm. 3: The total amino acid sequence of intact galline molecule. *Int. J. Pep. Protein Res.* **8**: 565-578.
- Nelson, J. S. 1984. *Fishes of the World*. 2nd edition. Wiley, New York.
- Oliva, R., and G. H. Dixon. 1991. Vertebrate protamine genes and the histone-to-protamine replacement reaction. *Prog. Nucl. Acid Res. Mol. Biol.* **140**: 25-94.
- Oliveras, C., R. Valdivia, N. Lafuente, D. Kulak, and H. E. Kasinsky. 1990. Electrophoretic analysis of sperm basic proteins in *Schroederichthys chilensis* and comparison with other cartilaginous fish. *Rev. Biol. Mar., Valparaiso* **25**: 99-108.
- Panyim, S., and R. Chalkley. 1969. High resolution acrylamide gel electrophoresis of histones. *Arch. Biochem. Biophys.* **130**: 337-346.
- Quero, J. C. 1984. Scylliorhinidae. Pp. 95-99 in *Fishes of the North-Eastern Atlantic and the Mediterranean*, Vol. 1, P. J. P. Whitehead, M. L. Bauchot, J. C. Hureau, J. Melsen, and E. Tortonese, eds. UNESCO.
- Reisfeld, R. A., U. J. Lewis, and D. E. Williams. 1962. Disk electrophoresis of basic proteins and peptides on polyacrylamide gels. *Nature* **195**: 281-283.
- Saperas, N., D. Lloris, and M. Chiva. 1993a. Sporadic appearance of histones, histone-like proteins, and protamines in sperm chromatin of bony fish. *J. Exp. Zool.* **265**: 575-586.
- Saperas, N., E. Ribes, C. Buesa, G. García-Hegart, and M. Chiva. 1993b. Differences in chromatin condensation during spermiogenesis in two species of fish with distinct protamines. *J. Exp. Zool.* **265**: 185-194.
- Sautière, P., G. Briand, M. Gusse, and Ph. Chevaillier. 1981. Primary structure of a protamine isolated from the sperm of the dogfish *Scylliorhinus caniculus*. *Eur. J. Biochem.* **119**: 251-255.
- Sautière, P., M. Gusse, G. Briand, A. Martinage, and Ph. Chevaillier. 1984. Primary structure of scylliorhinine S4, a protamine isolated from sperm nuclei of the dogfish *Scylliorhinus caniculus*. *Biochim. Biophys. Acta* **791**: 82-86.
- Schaeffer, B. 1981. The xenacanth shark neurocranium, with comments on elasmobranch monophyly. *Bull. Am. Mus. Nat. Hist.* **169**: 1-66.
- Stanley, H. P. 1963. Urogenital morphology in the chimaeroid fish *Hydrolagus collieri*. *J. Morphol.* **112**: 11-127.
- Takamune, K., H. Nishida, M. Takai, and Ch. Katagiri. 1991. Primary structure of toad sperm protamines and nucleotide sequence of their cDNAs. *Eur. J. Biochem.* **196**: 401-406.

# Morphogenesis of Maternal and Paternal Genomes in Fertilized Oyster Eggs (*Crassostrea gigas*): Effects of Cytochalasin B at Different Periods During Meiotic Maturation

FRANK J. LONGO<sup>1</sup>, LORI MATHEWS<sup>1</sup>, AND DENNIS HEDGECOCK<sup>2</sup>

<sup>1</sup>*Department of Anatomy, University of Iowa, Iowa City, Iowa 52242, and* <sup>2</sup>*Bodega Marine Laboratory, P.O. Box 247, Bodega Bay, California 94923*

**Abstract.** Fertilized oyster (*Crassostrea gigas*) eggs, treated with and without cytochalasin B (CB) at varying periods during meiotic maturation, were examined following 7-aminoactinomycin D (7-AAD) and anti- $\beta$  tubulin staining for DNA and microtubular patterns, respectively. Electron microscopic observations of untreated fertilized eggs revealed the development of an extensive network of endoplasmic reticulum during germinal vesicle breakdown. Germinal vesicle breakdown was not accompanied by the disappearance of the nucleolus; the latter persisted morphologically unchanged throughout fertilization. The first meiotic spindle [ $12.4 \pm 1.0 \mu\text{m}$  ( $1 \times 5.4 \pm 0.55 \mu\text{m}$  (diameter (d); metaphase plate))] was oriented with its long axis perpendicular to the egg's surface. In contrast, the second meiotic spindle was approximately one half the size of the first [ $7.4 \pm 0.65 \mu\text{m}$  ( $1 \times 2.91 \pm 0.29 \mu\text{m}$  (d))] and initially oriented with its long axis parallel to the egg's surface. Just prior to anaphase II, the spindle rotated so that its long axis became perpendicular to the egg's surface. Following its incorporation into the egg cytoplasm, the sperm nucleus dispersed but did not form a nuclear envelope until the completion of polar body formation. Just prior to pronuclear migration, an array of microtubules assembled around the female pronucleus, and then regressed; concomitantly, a sperm aster formed in conjunction with the centrosome associated with the developing male pronucleus. Following their migration and apposition with one another, both pronuclei underwent prophase as independent structures. Chromosomes from the male and female pronuclei became

organized on a mitotic spindle in preparation for first cleavage. In zygotes treated with CB continuously or for just meiosis I, anaphase I occurred; however, a polar body failed to form. Consequently, all the diads were retained within the zygote and became situated on a tripolar spindle. In such cases, anaphase II resulted in the production of a variable number of chromosomal aggregations that developed into pronuclei (3 to 6). In contrast, zygotes treated with CB during meiosis II developed spindles characteristic of untreated specimens; however, polar body formation was blocked, resulting in the development of usually two maternal pronuclei. Morphogenesis of *C. gigas* fertilized eggs is discussed in reference to similar processes in other species and with respect to strategies of triploid embryo production using CB.

## Introduction

Considerable emphasis has been given to the genetic manipulation of mollusks, in particular oysters, and its potential contribution to the domestication of aquatic fauna (Allen, 1987; Beaumont and Fairbrother, 1991). Triploid mollusks have been induced using a variety of methods: chemical, pressure, and temperature. Depending on when applied, cytochalasin B (CB) may inhibit the production of the first, second, or both polar bodies (Longo, 1972). Consequently, maternally derived chromosomes, normally segregated from the zygote, are retained, resulting in various states of ploidy. Although the effects of CB in oyster zygotes have been followed by cytological methods and flow cytometry (Allen, 1983; Chaiton and Allen, 1985; Guo *et al.*, 1992a, b), important cellular and developmental biological questions remain

unanswered regarding centrosome activity, spindle organization, and distribution of chromosomes. To establish the efficacy of procedures for chromosome manipulation, detailed analyses of the normal sequence of events during and after fertilization are required. In particular, analysis of components involved with meiotic maturation and pronuclear development and association in oysters may provide a better understanding of cellular and developmental processes in general and new insights into methods for increasing the effectiveness of chromosome manipulation.

Although electron microscopic studies have demonstrated ultrastructural features of oyster gametes (Galtsoff and Philpott, 1960; Galtsoff, 1964; Daniels *et al.*, 1971; Gutierrez *et al.*, 1978; Alliegro and Wright, 1983), we are unaware of studies dealing with the fine structure of gamete interactions and fertilization in this organism. Furthermore, investigations dealing with cellular and developmental aspects of oysters are relatively limited and unfocused (see Longo, 1983). The availability and abundance of both the organism and its gametes, as well as the relative ease of obtaining and handling eggs and embryos, make oysters a potentially ideal system for cellular and developmental studies. However, clear, baseline data regarding the morphology and biochemistry of gametogenesis, fertilization, and early embryogenesis are for the most part lacking, as are defined conditions and parameters to optimize development in this organism.

In a series of studies examining artificially activated oyster eggs for genetic studies, we investigated the course of fertilization events in CB-treated and untreated *Crassostrea gigas* eggs; we used electron microscopy and immunofluorescent techniques for the observation of DNA and microtubular organizations. Our observations bear on the structure and function of the meiotic spindle at first and second meiosis, germinal vesicle breakdown, and pronuclear development and association. These new observations are directly related to mechanisms whereby CB affects polar body formation and embryo ploidy.

### Material and Methods

Mature oysters were obtained during the months from May to July from commercial producers in the vicinity of Bodega Bay, CA, and maintained in aquaria with running seawater at the Bodega Marine Laboratory, Bodega Bay, CA. The animals were stripped of their gametes: eggs were suspended in seawater and sperm were kept "dry" at 4°C until used for fertilization. Eggs were filtered through a 60- $\mu$ m Nytex screen to remove gonadal tissue and debris, washed several times in seawater, and brought to a concentration of approximately  $2 \times 10^5$ /ml. The amount of sperm added to an egg suspension was determined for each experiment to avoid polyspermy. Gen-

erally, 20  $\mu$ l of sperm from stripped testis was diluted into 10 ml seawater, which was then added to a 200-ml egg suspension. Fertilization and early development were carried out at 22°C.

At periodic intervals (3 or 6 min) following the mixing of sperm and eggs, 10-ml samples were taken and fixed (1) for electron microscopy (3% glutaraldehyde, 3% paraformaldehyde, 1% acrolein in seawater at 4°C; Longo and Anderson, 1970); (2) for 7-AAD (Molecular Probes, Eugene, OR) staining of DNA (3% paraformaldehyde and 0.1% glutaraldehyde in seawater at 4°C); and (3) for tubulin staining (50% methanol in 50 mM EGTA, pH 6.8 at -20°C). Preparations for electron microscopy were washed overnight in seawater (two changes), incubated in 0.5% OsO<sub>4</sub> in seawater for 1 h at 0°C, dehydrated in ethanol, and embedded in Spurr's embedding medium. Eggs were thin sectioned, stained with lead citrate and uranyl acetate, and viewed with a Hitachi 7000 EM electron microscope or thick sectioned (0.5 to 1.0  $\mu$ m), stained with toluidine blue, and viewed with brightfield optics.

Specimens for DNA staining were washed overnight in seawater, incubated in a 3:1 solution of ethanol and acetic acid, and washed twice in phosphate buffered saline (PBS). Samples were stored at 4°C in PBS containing 0.02% NaN<sub>3</sub>, reacted with 4 mg/ml NaBH<sub>4</sub> in PBS for 15 min, and stained in 1.5  $\mu$ g/ml 7-AAD in PBS for 10 min. Stained preparations were washed two times in PBS, mounted in glycerol, and viewed with a Nikon inverted microscope fitted for epifluorescence. Specimens were also stained with the DNA intercalating dyes Hoechst 33342 and DAPI as described for 7-AAD. Fluorescent preparations were photographed using Kodak T-max 400 film.

Specimens prepared in cold methanol were washed two times in PBS and incubated in 1% BSA in PBS for 1 h, followed by a 1 h-incubation in anti- $\beta$ -tubulin antibody (Calbiochem, San Diego, CA). Specimens were washed twice in PBS, incubated in FITC-goat antimouse antibody (1/20 dilution) for 1 h, washed in PBS, and mounted and viewed as previously described for 7-AAD specimens.

CB (stock of 1 mg/ml DMSO) was added to egg suspensions to a final concentration of 1  $\mu$ g/ml just prior to insemination, immediately following first polar body formation or during the period (15 min) in which the first polar body is produced in controls. In the latter instance, after exposure to CB, zygotes were washed twice and resuspended in seawater. Controls consisted of fertilized eggs suspended in DMSO at a final concentration of 1  $\mu$ l/ml. Samples of CB-treated eggs were fixed and processed as described above for untreated specimens.

The rates of sperm nuclear and female pronuclear enlargement were determined from specimens stained in 7-AAD. Video images of stained maternal and paternal genomes (about 50/time point) were projected onto a video monitor and their area determined. Specimens (50-60)

stained with antitubulin antibody during polar body formation were projected onto a video monitor and the length and width of the first and second meiotic spindles were measured. Results for nuclear and spindle measurements are presented as means  $\pm$  SD.

## Results

### *Morphogenesis of untreated eggs and zygotes*

**Structure of the unfertilized egg and germinal vesicle breakdown.** The overall morphology of unfertilized eggs after incubation in seawater for 30 to 60 min took two forms: (1) Eggs were highly crenulated, pear-shaped, or both and possessed an intact germinal vesicle. (2) Eggs were essentially spheroidal (about 56  $\mu$ m in diameter) and had germinal vesicles or were at metaphase I of meiosis. In virtually all preparations obtained from stripped ovaries, both germinal vesicle and metaphase I containing oocytes were present in approximately equal numbers. A small percentage (10 to 15%) appeared to be intermediate—*i.e.*, at a stage of germinal vesicle breakdown. Incubation in seawater for longer periods increased the number of eggs at metaphase I, but rarely did it approach 80% after 3-h incubation. Less than 1% of the eggs artificially activated spontaneously and developed beyond metaphase I.

The germinal vesicle was spherical (about 30  $\mu$ m in diameter) and possessed a relatively smooth surface (Fig. 1a, b). Tetrad chromosomes were distinguished in specimens stained with 7-AAD but not in DAPI- and Hoechst-stained specimens because of high background staining (Fig. 1b). A single, large nucleolus was a distinct feature of the germinal vesicle (Fig. 1a).

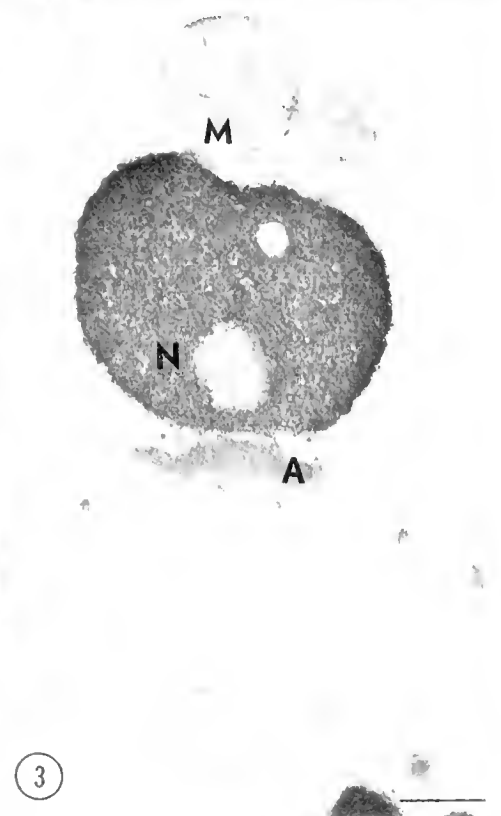
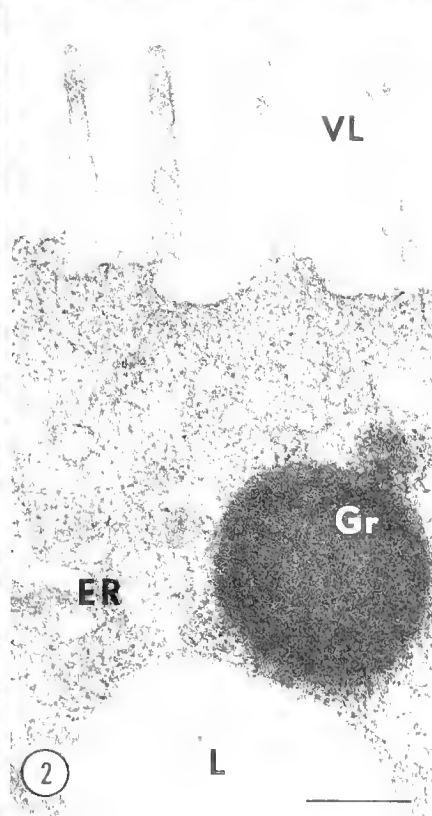
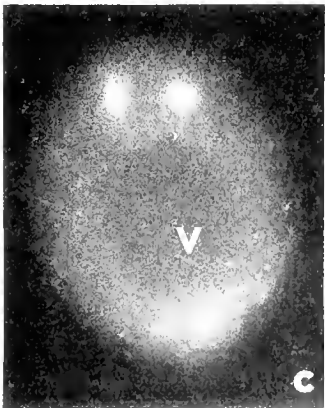
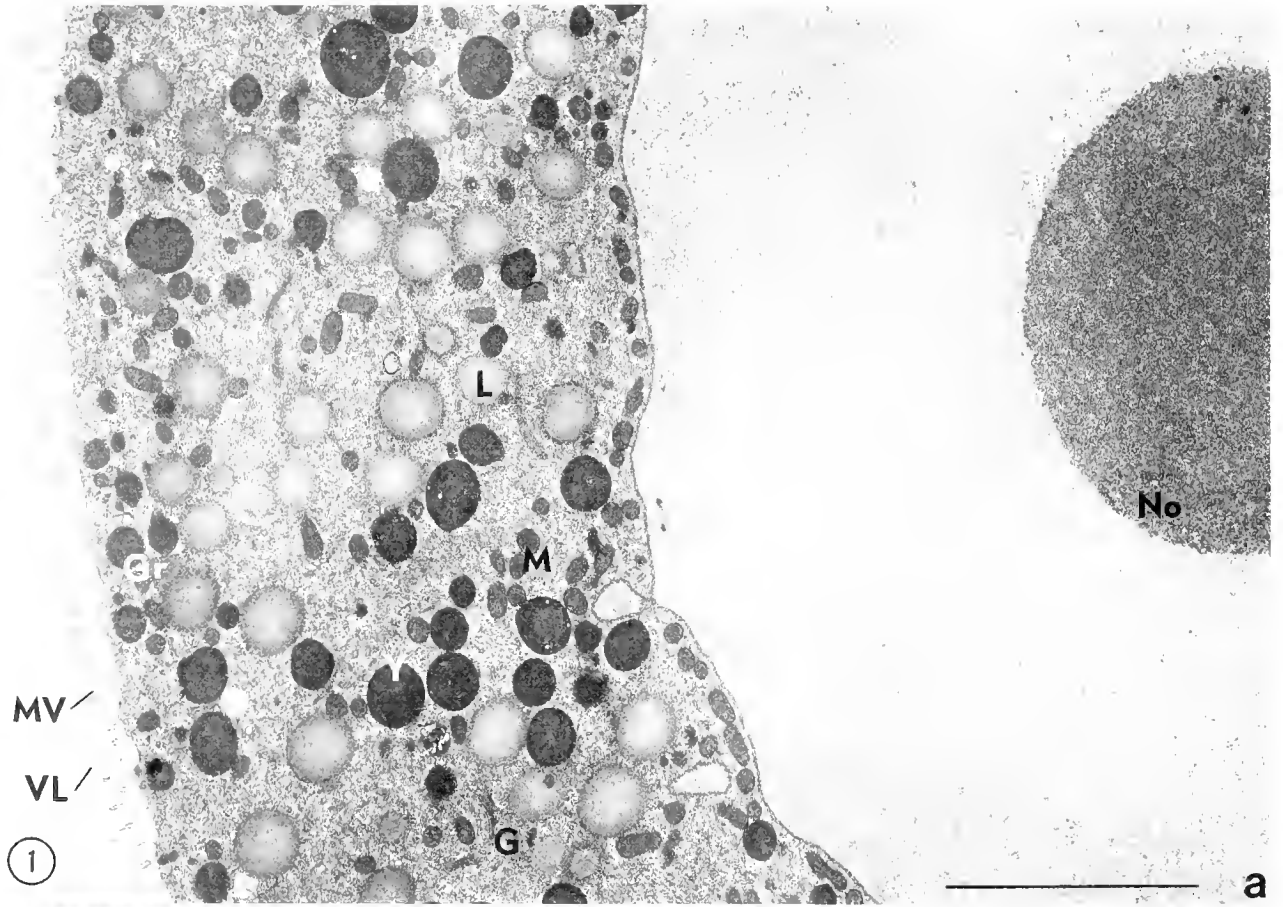
The cytoplasm of eggs having germinal vesicles contained two relatively small, stellate foci of antitubulin staining that were usually positioned at one pole of the germinal vesicle (Fig. 1c). Mitochondria, cisternae of endoplasmic reticulum, Golgi and yolk bodies were distributed apparently at random throughout the egg cytoplasm (Figs. 1a, 2). The endoplasmic reticulum was present as relatively small cisternae that did not form large aggregations or extensive networks. Granules, possessing a homogeneous electron-dense texture, were observed along the egg's periphery (Figs. 1a, 2). The egg surface was reflected into prominent microvilli, about 1  $\mu$ m in length by 0.1  $\mu$ m in diameter (Fig. 2), that projected through a vitelline layer composed of a fine filamentous material. Along the external surface of the vitelline layer was a lamina, perhaps adherent jelly, that was suspended from the tips of the microvilli (Figs. 2, 3).

Germinal vesicle breakdown was initiated spontaneously or apparently as a result of sperm-egg interaction. In the latter case, sperm, having undergone the acrosome reaction, were observed at the tips of microvilli (Fig. 3).

Other than the presence of sperm, germinal vesicle breakdown in fertilized and unfertilized eggs appeared to be morphologically comparable (Fig. 4). There was little, if any, apparent modification in the structure of the nucleolus (Fig. 5). In fact, an intact nucleolus persisted throughout fertilization (see below). The tetrad chromosomes progressively condensed, and this was accompanied by a crenulation of the surface of the germinal vesicle (Figs. 4, 5a; inset 5c). Nuclear pores disappeared and fenestrations developed within the nuclear envelope such that eventually the condensing chromosomes were loosely surrounded by cisternae derived from the nuclear envelope (Fig. 5b, c). Concomitantly, aggregations and anastomosing networks of endoplasmic reticulum became prominent throughout the cytoplasm (Fig. 5c, d; inset 5d).

As the chromosomes condensed, they progressively aggregated onto a plate-like mass in the center of the egg (Fig. 4c). Concomitant with this aggregation, the two stellate foci of antitubulin staining—formerly positioned at one pole of the germinal vesicle—enlarged, became closely associated with the condensing chromosomes, and eventually localized to poles of the first meiotic spindle. The first meiotic spindle then moved peripherally to become positioned within the cortex (Fig. 4e, f). The size and orientation of the first meiotic spindle are particularly noteworthy in contrast to the second (Fig. 4e, f). The long axis of the first meiotic spindle was  $12.4 \pm 1.0 \mu$ m and its diameter at the metaphase plate measured  $5.4 \pm 0.55 \mu$ m. In all specimens examined, the long axis of the spindle was positioned normal to the egg surface.

**Polar body formation.** In those eggs inseminated at metaphase I or the germinal vesicle stage, gamete interaction triggered the continuation of meiotic maturation. At anaphase I, diads disjoined; the most cortically positioned of the two groups of chromosomes became enclosed within the first polar body (Figs. 4g, h; 6). Concomitantly, that portion of the spindle remaining within the zygote regressed. This was followed by the reorganization of the diad chromosomes onto the metaphase plate of the second meiotic spindle (Fig. 6a), which was distinctly different from the first. (1) The size of the second meiotic spindle, both its long axis ( $7.4 \pm 0.6 \mu$ m) and its diameter ( $2.9 \pm 0.29 \mu$ m), were approximately one half that of the first. (2) Its orientation when formed was exactly opposite that of the first; *i.e.*, its long axis was positioned parallel to the egg's surface (Fig. 6b). Just prior to anaphase II, the second meiotic spindle rotated so that its long axis became perpendicular to the egg surface (Fig. 6c, d). Accompanying anaphase II was the formation of the second polar body, which became positioned subjacent or lateral to the first (Figs. 6e, 7). The maternal chromosomes remaining in the zygote swelled and became invested by a



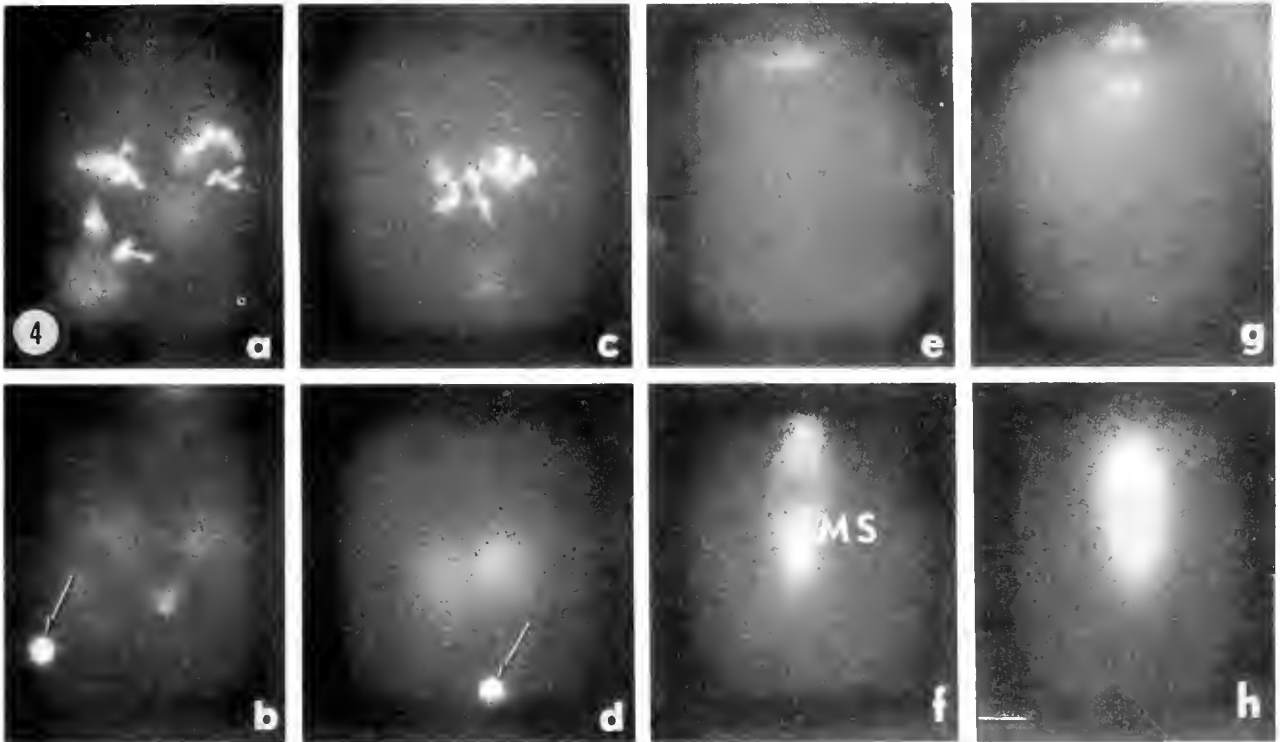


**Figure 4.** Condensation of tetrads and their localization within the egg during metaphase and anaphase I. Progressive stages in the condensation and alignment of tetrads onto the metaphase plate takes place in the midregion of the egg (a, c); the metaphase spindle (MS) then moves to and becomes positioned at one pole of the egg with its long axis perpendicular to the egg's surface (e, f). (b, d) Micrographs of fertilized eggs shown in Figure 4a and c, respectively, at levels to demonstrate incorporated sperm nuclei (arrows). (g, h) Specimen at anaphase I depicting segregating chromosomes (g) and the meiotic spindle (h). (a-e, g) Preparations viewed to show 7-AAD-stained parental genomes. (f, h) Antitubulin-stained meiotic spindles. Scale bar = 10  $\mu$ m.

nuclear envelope to form the female pronucleus (Figs. 6g, h; 7, 11).

In conjunction with the spindle pole remaining in the egg, a system of microtubules assembled and enveloped the developing female pronucleus (Fig. 6 f-g). Accompanying these changes, a sperm aster developed in association with the transforming sperm nucleus (Fig. 6f, g).

With the continued growth of the sperm aster, the system of microtubules associated with the female pronucleus became smaller and eventually disappeared.

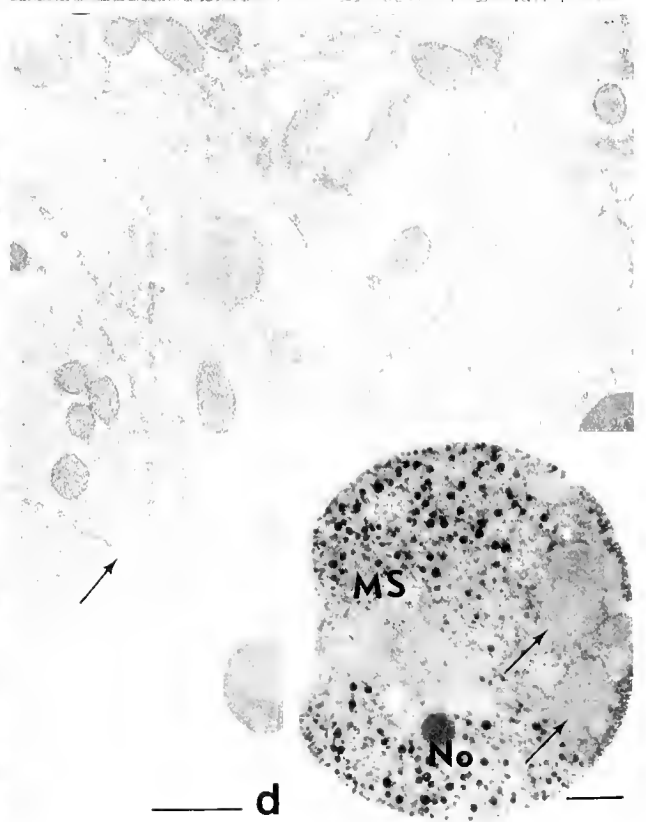
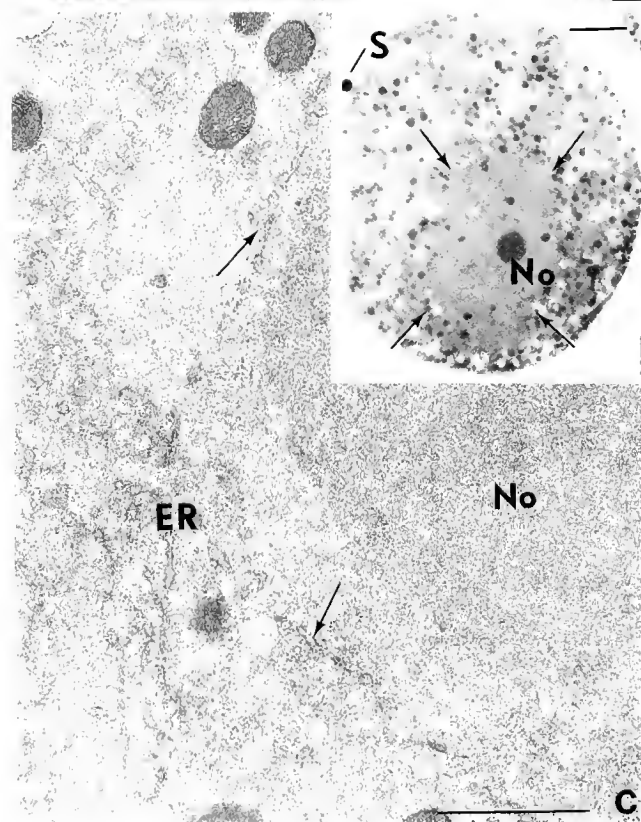
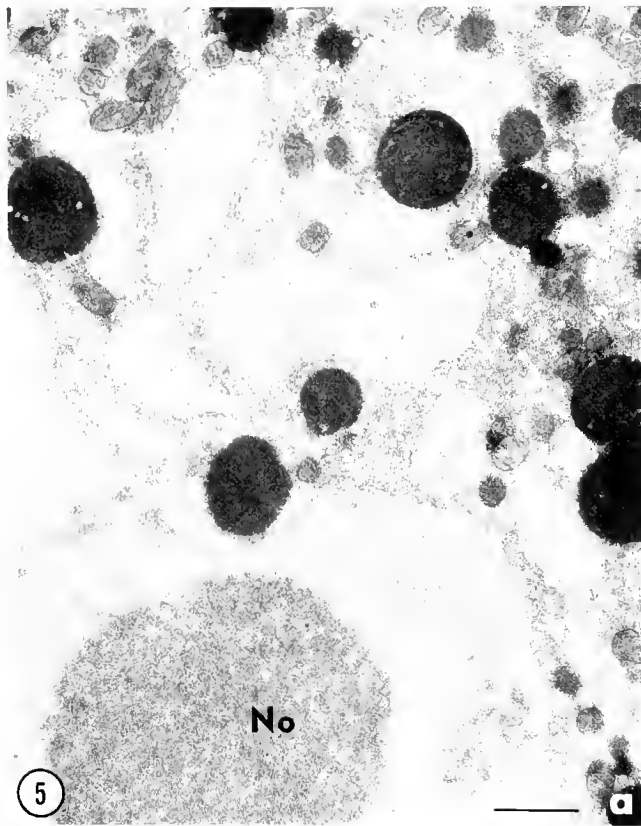
Half-spindles taken into the first and second polar bodies quickly regressed following the formation of each polar body and appeared as fluorescent streaks (Fig. 6b-d). Chromosomes of the first polar body usually failed to dis-

**Figure 1.** Unfertilized oyster eggs containing germinal vesicles. (a) The surface of the germinal vesicle is relatively smooth and devoid of extensive folds. The cytoplasm consists of a fairly homogeneous distribution of yolk (Y), lipid droplets (L), Golgi (G), and mitochondria (M). Although cisternae of endoplasmic reticulum are distributed throughout the egg cytoplasm, they do not form large aggregations as seen in eggs in which the germinal vesicle has broken down (see Fig. 5). Granules (Gr), smaller and with a more homogeneous content than yolk bodies, occupy the cortical region of the egg. (b, c) Fluorescence micrographs of 7-AAD- and antitubulin-stained eggs demonstrating tetrad chromosomes (b) and foci of microtubules (c) at one pole of the germinal vesicle (V). MV, microvilli; VL, vitelline layer; No, nucleolus. Scale bar = 5  $\mu$ m.

**Figure 2.** Cortex of an unfertilized egg depicting microvilli, granules (Gr), lipid droplets (L), elements of the endoplasmic reticulum (ER), and vitelline layer (VL). Structural changes in the egg cortex were not apparent as a result of insemination. Scale bar = 0.5  $\mu$ m.

**Figure 3.** Sperm-egg interaction. The sperm has undergone the acrosome reaction and is in contact with the egg's microvilli. N, sperm nucleus; M, sperm mitochondria; A, basal portion of the sperm acrosome. Scale bar = 0.5  $\mu$ m.





5

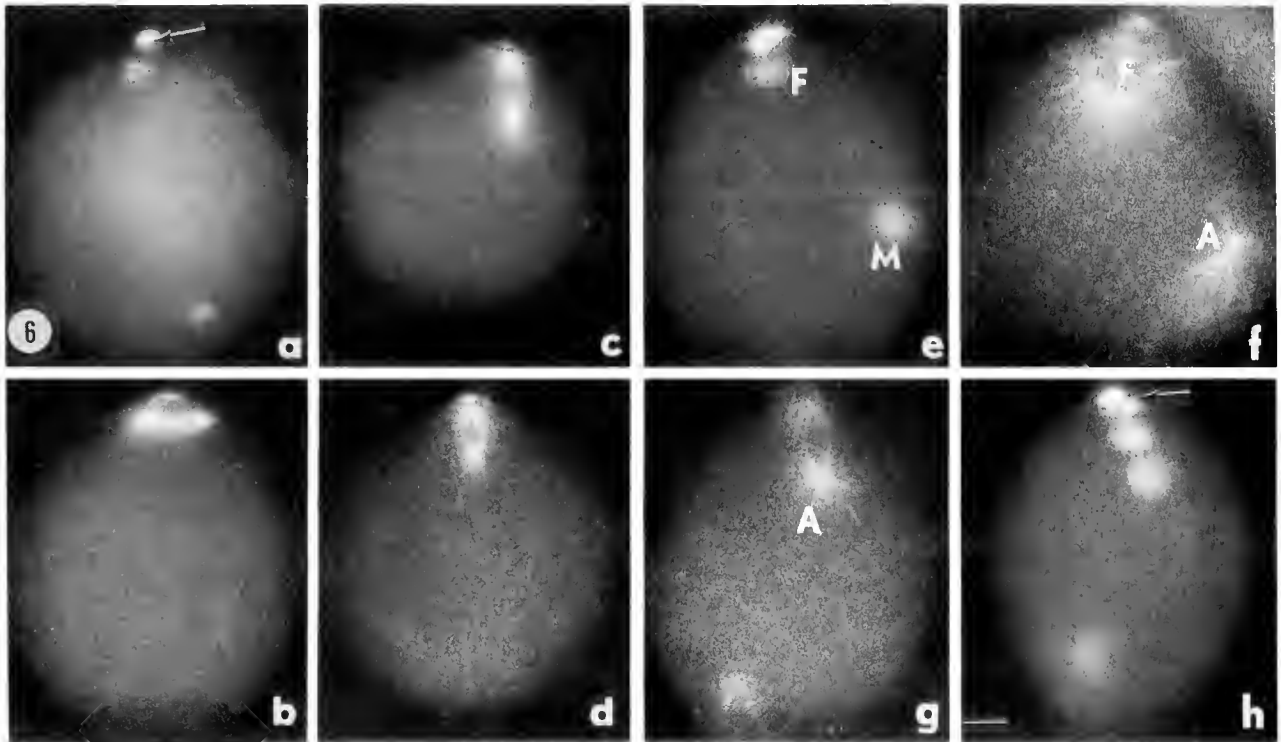


**Figure 6.** Polar body formation. (a–b) Fertilized egg shortly following the formation of the first polar body (arrow). The chromosomes remaining in the egg following anaphase I become organized on the second meiotic spindle, which is significantly smaller than the first and is initially oriented tangential to the egg's surface (b). (c, d) The second meiotic spindle rotates and becomes positioned normal to the egg's surface (c) and undergoes anaphase II (d). (e, f) Fertilized eggs following anaphase II. (e) The maternal (F) and sperm (M) chromatin enlarge to form female and male pronuclei, respectively. (f, g) Microtubule arrays develop in conjunction with the female and male (sperm aster) pronuclei. (g) The microtubule array associated with the female pronucleus (F) eventually regresses with the continued development of the sperm aster (A). (h) Zygote depicting apposed male and female pronuclei and two polar bodies (arrow). Preparations a, e, h are viewed to show 7-AAD staining and the maternal and paternal chromatin; specimens b, c, d, f, g viewed to show antitubulin-stained structures. Scale bars = 10  $\mu$ m.

perse and were not delimited by a nuclear envelope (Fig. 7). In contrast, chromosomes of the second polar body dispersed and were surrounded by a nuclear envelope (Fig. 7).

*Sperm incorporation and male pronuclear development.* Sperm-egg interaction leads to gamete membrane fusion and, as a consequence, the incorporation of the sperm nucleus, mitochondria, and axonemal complex (Figs. 8a–

d). The projection of egg cytoplasm that formed at the site of sperm entry—the fertilization cone—was relatively small, usually just slightly larger than the sperm head. The pore connecting the fertilization cone with the egg cortex widened, thereby allowing the contents of the spermatozoan to move into the cortex (Fig. 8a, b). This was followed by sperm chromatin dispersion: an apparently rapid process in which the condensed, granular chromatin

**Figure 5.** Germinal vesicle breakdown is accompanied by the formation of extensive convolutions of the nuclear envelope (a) and aggregations of endoplasmic reticulum (ER). (b, c) The nuclear envelope loses its pores and is severed at multiple sites to form cisternae (arrows) that are morphologically similar to endoplasmic reticulum. (d and inset) Elongate networks and aggregations of endoplasmic reticulum (arrows) that form in eggs having undergone germinal vesicle breakdown. Aggregations of endoplasmic reticulum are sufficiently large that they are readily discerned as "clear" staining areas in light microscopic preparations (inset d; arrows). A prominent feature of germinal vesicle breakdown in oyster eggs is the retention of an intact nucleolus (No; a–c, insets c and d). Inset c: Stained thick section showing a sperm prior to its incorporation into the egg cortex and an intact nucleolus (No) in the area of the disrupted germinal vesicle (arrows). MS, meiotic spindle. Scale bar = 1  $\mu$ m (Fig. 5a–d); 10  $\mu$ m (insets).



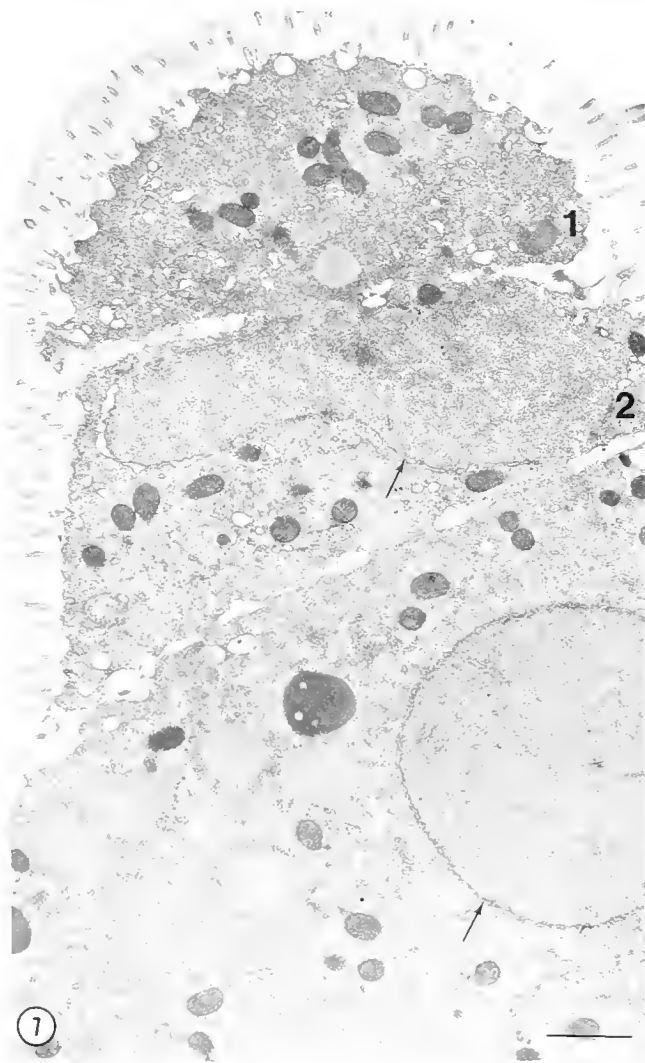


**Figure 7.** First and second polar bodies and female pronucleus of a zygote following meiotic maturation. Chromatin within the second polar body (2) and zygote becomes organized within a nuclear envelope (arrows). Chromatin in the first polar body (1) usually remains devoid of delimiting membranes. Scale bar = 1  $\mu$ m.

became dispersed into an aggregation of fine chromatin filaments (Fig. 8c, d). Analysis of sperm chromatin dispersion revealed that it consisted of basically two phases of enlargement: (1) a slow rate that occurred during germinal vesicle breakdown and polar body formation, and (2) a much faster rate of expansion corresponding with female pronuclear enlargement (Fig. 9). The sperm chromatin remained in a dispersed state, free of a nuclear envelope throughout the period of polar body formation. Concomitant with the formation of the female pronucleus, vesicles and elongate cisternae aggregated along the surface of the dispersed sperm chromatin. These elements fused together and acquired pores to constitute the nuclear envelope (Figs. 10, 11).

*Pronuclear apposition and formation of the first cleavage spindle.* After formation of the pronuclei, the male pronucleus migrated to the female pronucleus, which was either centrally placed within the zygote or situated just subjacent to the first and second polar bodies (Fig. 11). Within the two pronuclei were dense accumulations, structurally reminiscent of the nucleolus derived from the germinal vesicle (Fig. 11c). These structures appeared within the pronuclei with no apparent change in the nucleoli derived from germinal vesicles (Fig. 11b, insets b, c).

With the apposition of the pronuclei, two antitubulin-staining foci appeared; these became the poles of the mitotic spindle (Fig. 12a-c). Simultaneously, the male and female pronuclei underwent prophase; *i.e.*, their chromosomes condensed (Fig. 12) and their nuclear envelopes broke down (Fig. 12e-h). Subsequently, the maternally and paternally derived chromosomes became positioned on the metaphase plate of the mitotic spindle assembled for first cleavage (Fig. 12h). A similar pattern of morphogenesis was also observed in polyspermic eggs. The male pronuclei, each of which possessed a sperm aster (Fig. 12d; see also CB Effects), migrated into association with one another and the female pronucleus. A multipolar spindle formed from this association; the number of poles it possessed was a direct reflection of the extent of polyspermy.

#### *CB effects*

*Continuous exposure to CB.* Many of the processes occurring in zygotes treated with CB were similar to, if not the same as these in the controls; therefore, only those processes directly affected by CB are described here. In the continuous presence of CB, formation of both polar bodies was inhibited. Anaphase I occurred and the projection of cytoplasm normally budded from the egg to form a polar body developed; however, it was not severed from the zygote (Fig. 13a-d). Consequently, all the diad chromosomes were retained within the zygote (Fig. 13c). The spindle regressed and all the chromosomes became reorganized on a tripolar spindle formed within the egg cortex (Fig. 13e-f). The spindle had the shape of an equilateral triangle in which the length of each side was approximately equal to the long axis of spindles that formed at metaphase II in untreated eggs. Interestingly, the tripolar spindle was oriented within the cortex so that a base or an apex was positioned directly subjacent to the cell surface. Chromosome separation followed and a variable number (3-6) of female pronuclei were eventually assembled, most likely as a result of chromosome segregation and aggregation at anaphase II and pronuclear assembly, respectively (Longo, 1972).

*CB application during first polar body formation.* When CB was administered only during the period of first polar

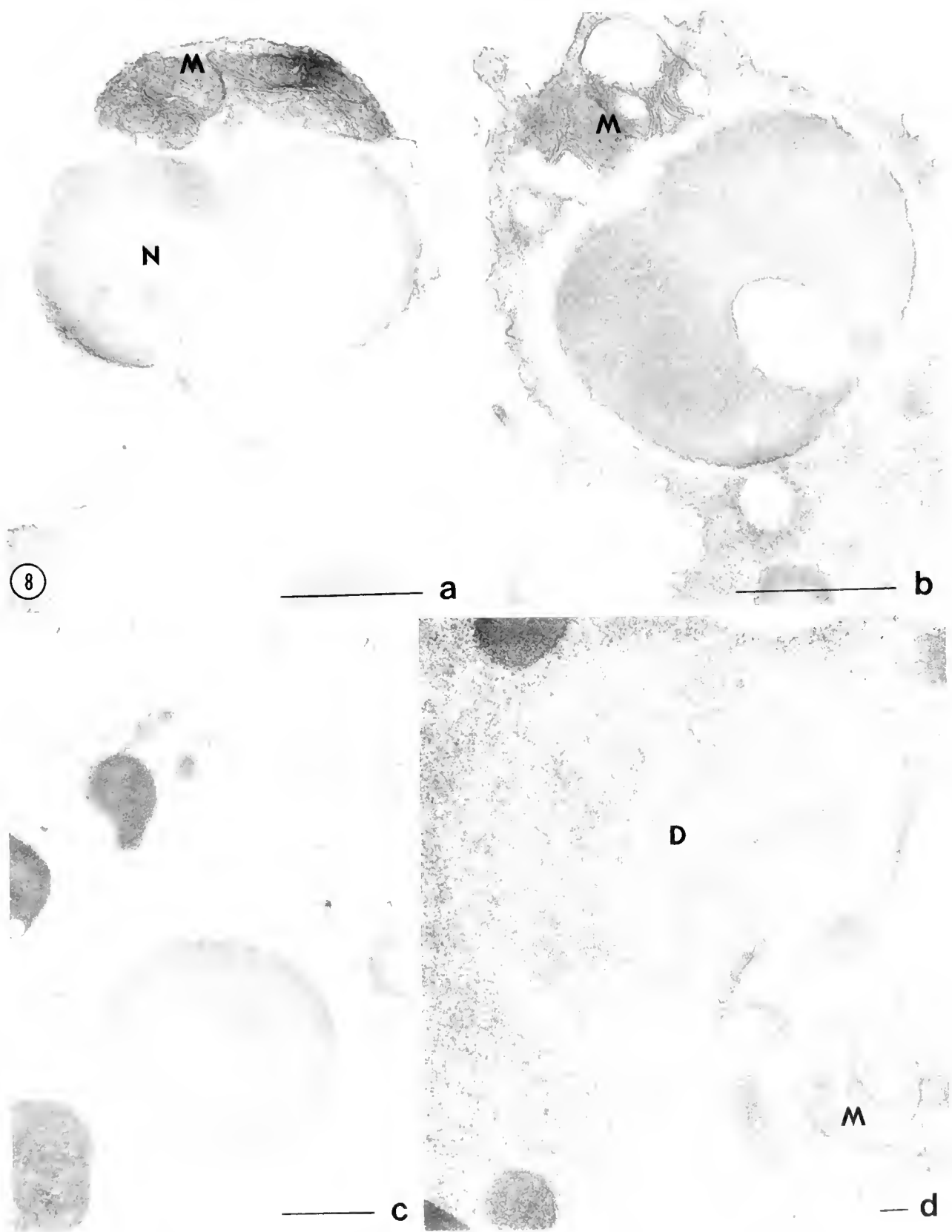
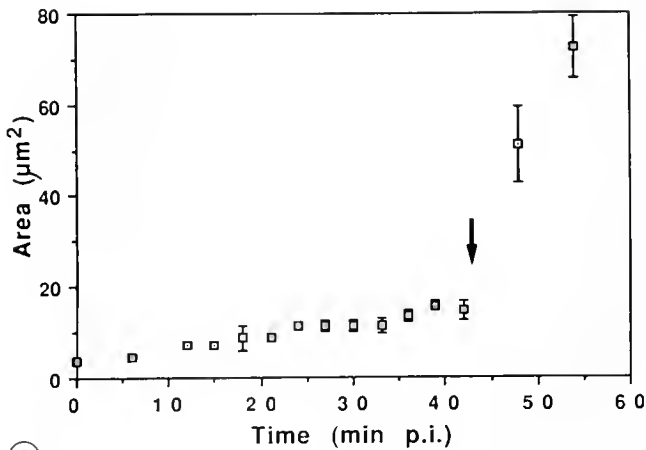


**Figure 8.** (a-d) Sperm incorporation (a, b) A small fertilization cone, essentially encompassing the sperm nucleus (N) and mitochondria (M), forms following gamete membrane fusion. (c, d) Both the sperm nucleus and mitochondria move through this projection of cytoplasm into the egg cortex where the condensed chromatin disperses (c) into an aggregation of fine filaments (d) D, dispersed sperm chromatin. Scale bars 1  $\mu\text{m}$  (Fig. 8a-c), 0.1  $\mu\text{m}$  (Fig. 8d)



9. **Figure 9.** Sperm nuclear enlargement consists of at least two stages: a phase consisting of a relatively slow rate of expansion that occurs during germinal vesicle breakdown and polar body formation [0 to ~40 min postinsemination (p.i.)]. This is followed by a phase of rapid expansion that occurs in conjunction with enlargement of the female pronucleus. The arrow indicates the time meiotic maturation is concluded and development of a maternal pronucleus is initiated.

body formation (15 min), chromosomes normally extruded from the zygote in the first polar body were retained. As in the case of zygotes continuously exposed to CB, all of the maternal chromosomes became positioned on a tripolar spindle (Fig. 14a, b). When CB-treated eggs were washed and resuspended in fresh seawater following the period of first polar formation (20 min after insemination), a polar body did not always form. When it did, it was morphologically similar to the second polar body of control zygotes (Fig. 15a); *i.e.*, it possessed dispersed chromatin surrounded by a nuclear envelope (Fig. 15). In these cases a variable number (3–6) of female pronuclei formed in a manner described above.

**CB application during second polar body formation.** Zygotes treated with CB during formation of the second polar body possessed a first polar body and had their chromosomes organized on second meiotic spindles typical of controls (Fig. 16a, b). In the presence of CB, the spindle rotated so that its long axis became positioned perpendicular to the egg surface (Fig. 16c, d). Anaphase II ensued and a projection of cytoplasm encompassing chromosomes normally expelled with the polar body formed (Fig. 16e). However, the cytoplasm was not severed from the zygote and all of the chromosomes of the second meiotic division were retained (Fig. 16e). Three pronuclei formed within such zygotes, two of maternal origin and one derived from the sperm (Fig. 16f); all underwent prophase as in controls. The condensed chromosomes of all three pronuclei became organized on a single mitotic spindle (Fig. 16g, h).

## Discussion

The observations presented here document changes in fertilized eggs of the Pacific oyster, *Crassostrea gigas*. Meiotic maturation, assembly of the male and female pronuclei, pronuclear association, and subsequent development of the first cleavage spindle in CB-treated and untreated specimens have been observed with both light and electron microscopy.

### Egg structure at fertilization

Essentially two morphological forms of *C. gigas* eggs were present from stripped, ovarian preparations. This variation in overall structure and in meiotic maturation has been noted previously and may be related to the method of gamete acquisition (Longo, 1983). The significance of these two forms with respect to gamete maturation, fertilizability, and potential for development is unclear. Numerous studies (Longwell and Stiles, 1968; Downing and Allen, 1987; Stephano and Gould, 1988; Scarpa and Allen, 1992) have demonstrated that oyster eggs, obtained by stripping, can be fertilized and are capable of embryogenesis. Observations presented here indicate that with the exception of germinal vesicle breakdown and first meiotic spindle assembly, both forms undergo virtually identical processes at fertilization.

It is noteworthy that reports of the timing of various stages of fertilization vary considerably (Galtsoff, 1964; Longwell and Stiles, 1968; Stiles and Longwell, 1973; Stanley *et al.*, 1984; Downing and Allen, 1987). Although parameters for optimal fertilization and early embryogenesis have not been well-defined, temperature and salinity as well as the mode of gamete acquisition no doubt have profound effects on the timing of fertilization events and subsequent development (see Scarpa and Allen, 1992). The use of serotonin to induce germinal vesicle breakdown (Osanaï, 1985) provides a means of obtaining homogeneous populations of eggs so that more synchronous development can be achieved. With respect to events reported here, events in serotonin-treated eggs are essentially the same morphologically as in eggs obtained by stripping (Stephano and Gould, 1988). The timing of fertilization events, however, is related to the meiotic stage of the egg at insemination (Scarpa and Allen, 1992).

Egg structure and the events of *C. gigas* fertilization, involving germinal vesicle breakdown and the formation of the first meiotic spindle, are similar to structures and processes reported for other mollusk eggs (Longo and Anderson, 1969, 1970; Longo, 1983; Komaru *et al.*, 1990; Longo and Scarpa, 1991; see also Dessev and Goldman, 1988; Dessev *et al.*, 1989; Stricker and Schatten, 1989). Notable differences, however, were observed in the present study. Retention of the nucleolus is a consistent feature of *C. gigas* eggs that undergo germinal vesicle breakdown.

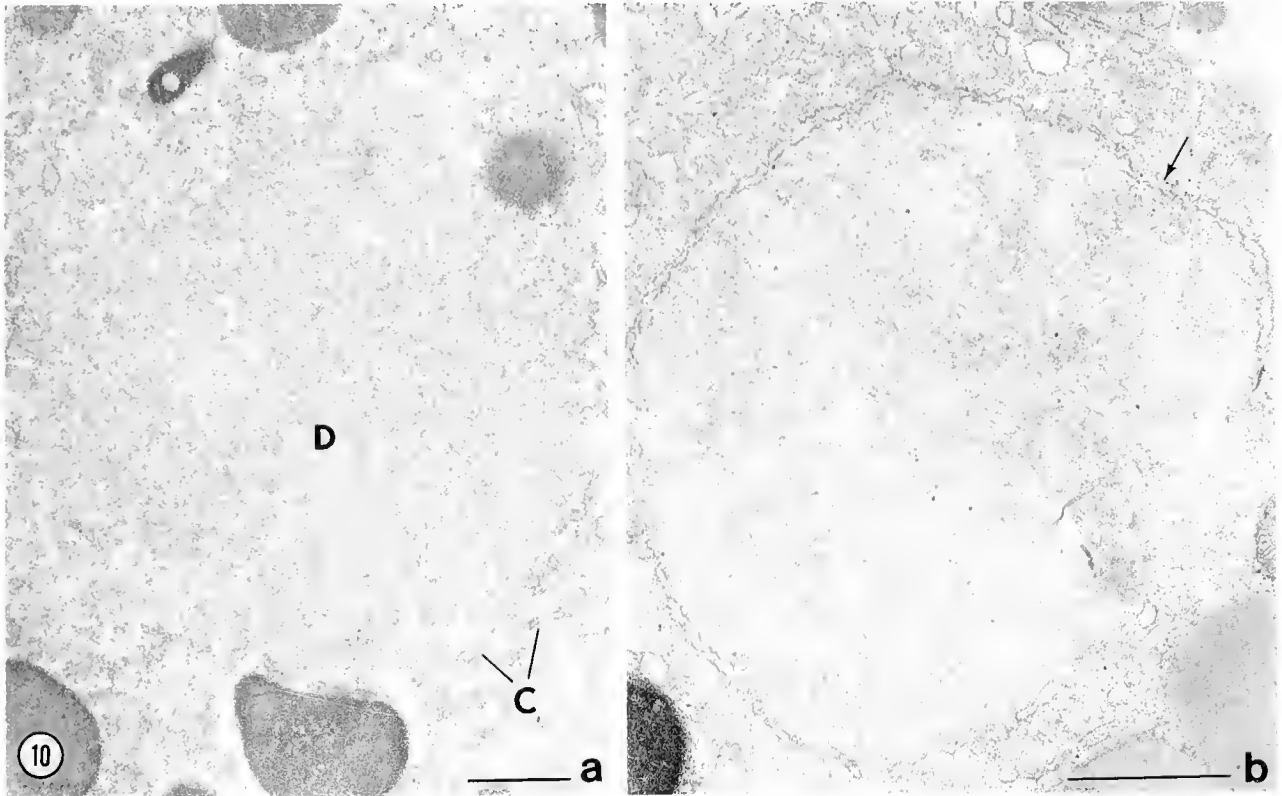


**Figure 10.** (a, b) Formation of the male pronuclear envelope. (a) Following polar body formation, cisternae (C) surround the dispersed sperm chromatin (D) and (b) fuse to form a nuclear envelope (arrow). Scale bar = 1  $\mu\text{m}$ .

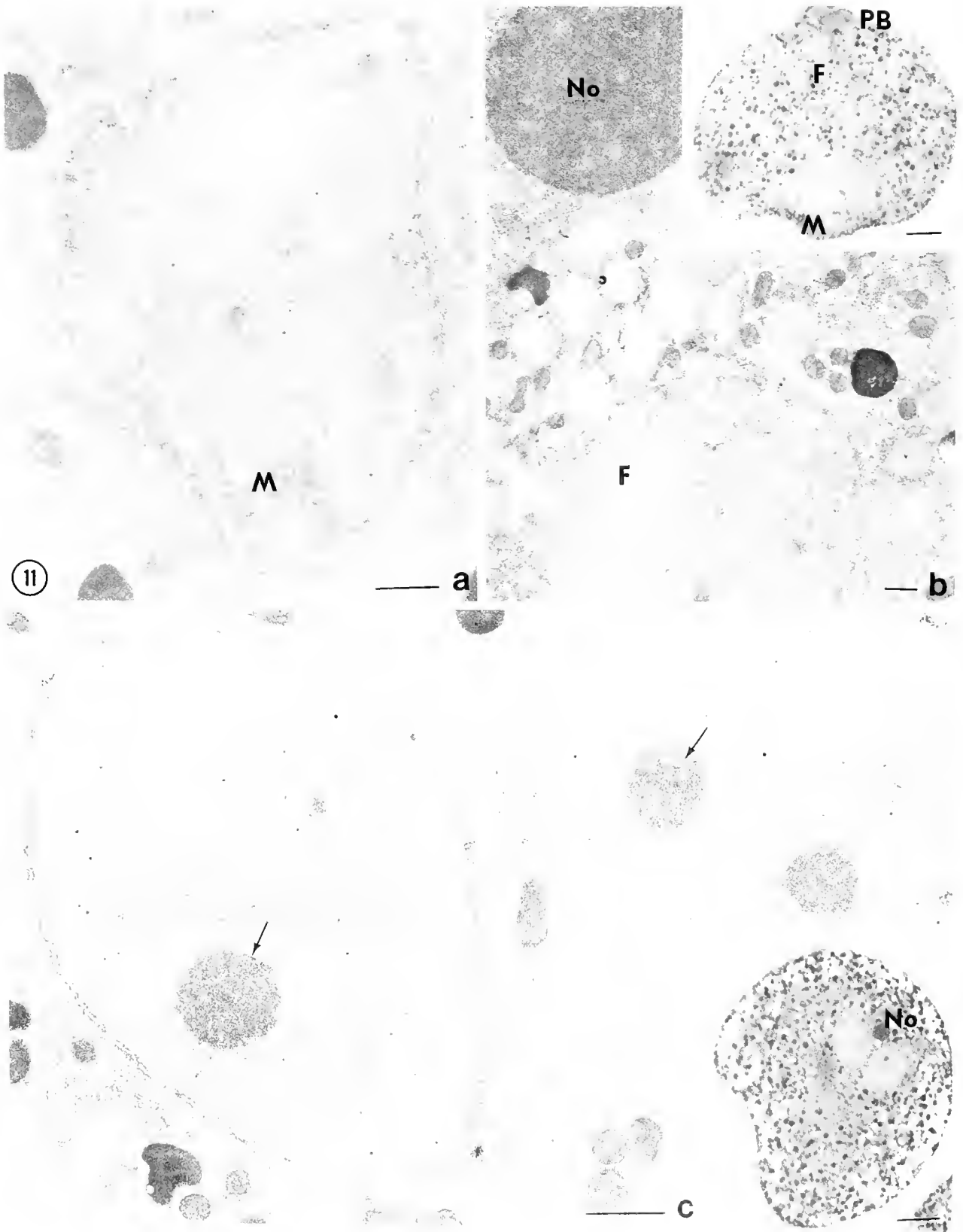
This structure did not appear to diminish appreciably in size throughout the period of fertilization (up to 1 h). In mitotic cells, loss of the nucleolus is due to the cessation of rRNA synthesis, coupled with the continued processing of ribosomal precursors (Anastassova-Kristeva, 1977; Hadjiolov, 1985). Failure of these events presumably would lead to the retention of a nucleolus as seen here.

Major events in the breakdown of the germinal vesicle are the loss of nuclear pore complexes and the vesiculation of the nuclear envelope into cisternae that are structurally reminiscent of elements of the endoplasmic reticulum. Concomitant with the breakdown of the nuclear envelope is the formation of networks and aggregations of endoplasmic reticulum. Although the surface area of the nuclear envelope measures about  $2900 \mu\text{m}^2$ , it is doubtful that all membranous elements comprising the networks and aggregations that appear with germinal vesicle breakdown are, in fact, derived from the nuclear envelope. This impression is based on preliminary observations (F. J. Longo, pers. obs.) indicating that the number and size of endoplasmic reticulum aggregations comprise a greater area than can be accommodated by the nuclear envelope of the germinal vesicle. Hence, we suggest that concomitant with germinal vesicle breakdown, cisternae of en-

doplasmic reticulum throughout the egg are organized into dense aggregations and networks. Cisternae derived from the breakdown of the nuclear envelope may be a part of these membranous arrays.

Alterations in the endoplasmic reticulum seen in *C. gigas* eggs/zygotes are similar to those described for starfish oocytes (Kato *et al.*, 1990) and reminiscent of dynamic changes that occur in the endoplasmic reticulum of sea urchin eggs at fertilization, presumably in relation to the initiation of egg activation (Terasaki and Jaffe, 1991; see also Campanella *et al.*, 1984; Speksnijder *et al.*, 1993). Morphogenic changes of the endoplasmic reticulum may play a similar role in the regulation of fertilization processes in *C. gigas* eggs.

Changes in the surface structure of the egg, *i.e.*, crenated to smooth, appeared to be coupled to nuclear events and are largely inhibited by CB (F. J. Longo, pers. obs.). The cortex of *C. gigas* eggs was similar to that of other spiralian eggs (Rebhun, 1962; Fallon and Austin, 1967; Longo and Anderson, 1969, 1970; Hylander and Summers, 1977). Previous studies (Galtsoff, 1964; Osanai, 1969) refer to either a cortical granule reaction or fertilization envelope formation in *Crassostrea*; such processes were not apparent, nor were changes in microvillar structure and the



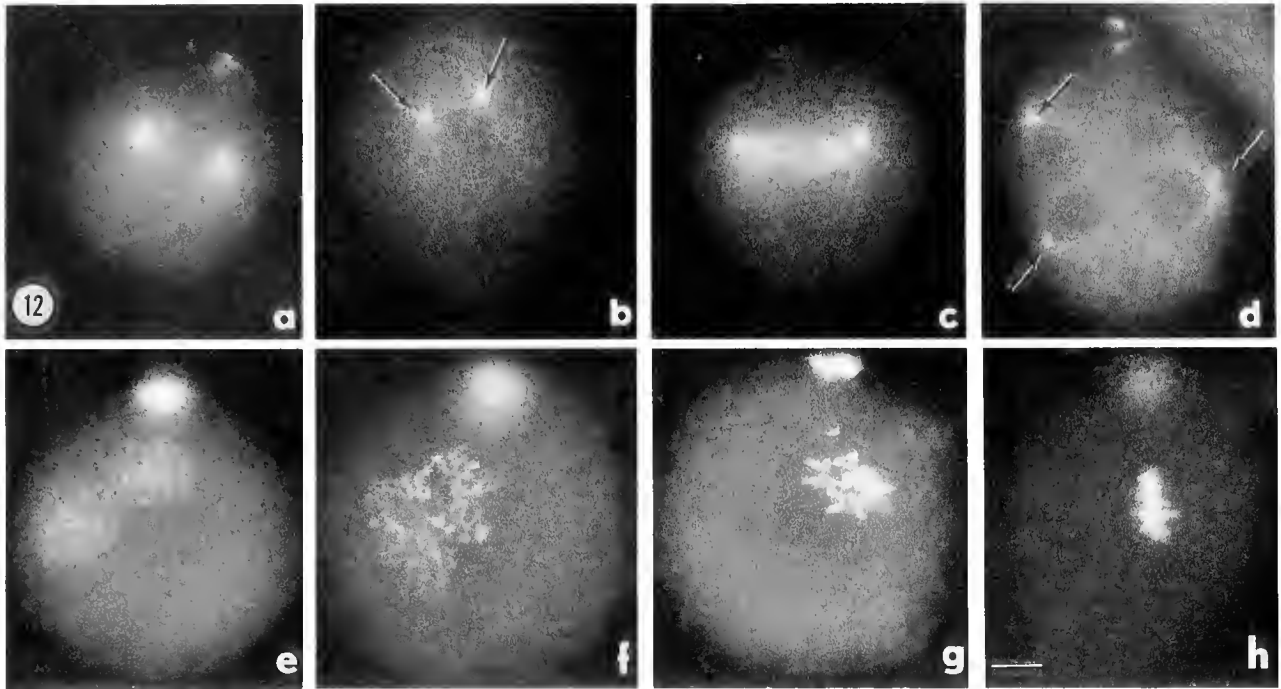


**Figure 12.** Antitubulin- and 7-AAD-stained specimens depicting the development of microtubule arrays (a-d) and the morphogenesis of the maternally and paternally derived chromatin following pronuclear apposition (e-h). (a-c) Stages in the development of the mitotic spindle; the developing spindle poles are shown at the arrows. (d) Polyspermic egg in which each male pronucleus is associated with a developing sperm aster (arrows). (e, f) Apposed male and female pronuclei undergoing chromatin condensation. (g, h) Coalescence (g) and alignment (h) of the paternally and maternally derived chromosomes on the metaphase plate of the first cleavage spindle. P, polar bodies. Scale bar = 10  $\mu\text{m}$ .

vitelline layer obvious with the methods employed here (see also Alliegro and Wright, 1983).

#### *Centrosomes and first and second meiosis*

Observations presented here indicate that germinal vesicle eggs of *C. gigas* possess two foci of radiating microtubules that may be intimately involved in meiotic spindle formation. At the time of germinal vesicle breakdown, they appear to establish the poles of the first meiotic apparatus. Such foci are reminiscent of those observed in starfish oocytes (Schroeder, 1985; Otto and Schroeder, 1984) and in other cell types (see Kalt and Schliwa, 1993) where they organize microtubules during both interphase and mitosis and are referred to as centrosomes.

The first meiotic spindle of *C. gigas* forms in the central portion of the egg and then moves to and becomes positioned perpendicularly to the egg cortex. A similar morphogenesis has been described for vertebrate and invertebrate eggs (Gard, 1992; see Longo, 1983). It is noteworthy that in the present case, migration to and orientation of the spindle within the egg cortex does not appear to be affected by CB. This is in contrast to studies with maturing mammalian oocytes indicating that microfilaments are involved in the centrifugal displacement of the first metaphase spindle (Longo and Chen, 1985; Maro *et al.*, 1986; Van Blerkom and Bell, 1986; Alexandre *et al.*, 1989; Ryabovra *et al.*, 1986).

The size and orientation of the first meiotic spindle of *C. gigas* are comparable to those previously reported and

**Figure 11.** (a-c) Male (M) and female (F) pronuclei prior to (a, b), and following their apposition (c). (b) The nucleolus (No) derived from the former germinal vesicle is situated near the female pronucleus (F). (c) Both the male and female pronuclei accumulate dense aggregations, reminiscent of nucleoli (arrows). Inset b: Male (M) and female (F) pronuclei prior to their migration. The area partially surrounding the male pronucleus and essentially devoid of granular organelles comprises a portion of the sperm aster. Inset c: Apposed male and female pronuclei adjacent to the nucleolus derived from the former germinal vesicle. PB, first and second polar bodies. Scale bar = 1  $\mu\text{m}$  (Fig 11a-c); 10  $\mu\text{m}$  (insets).

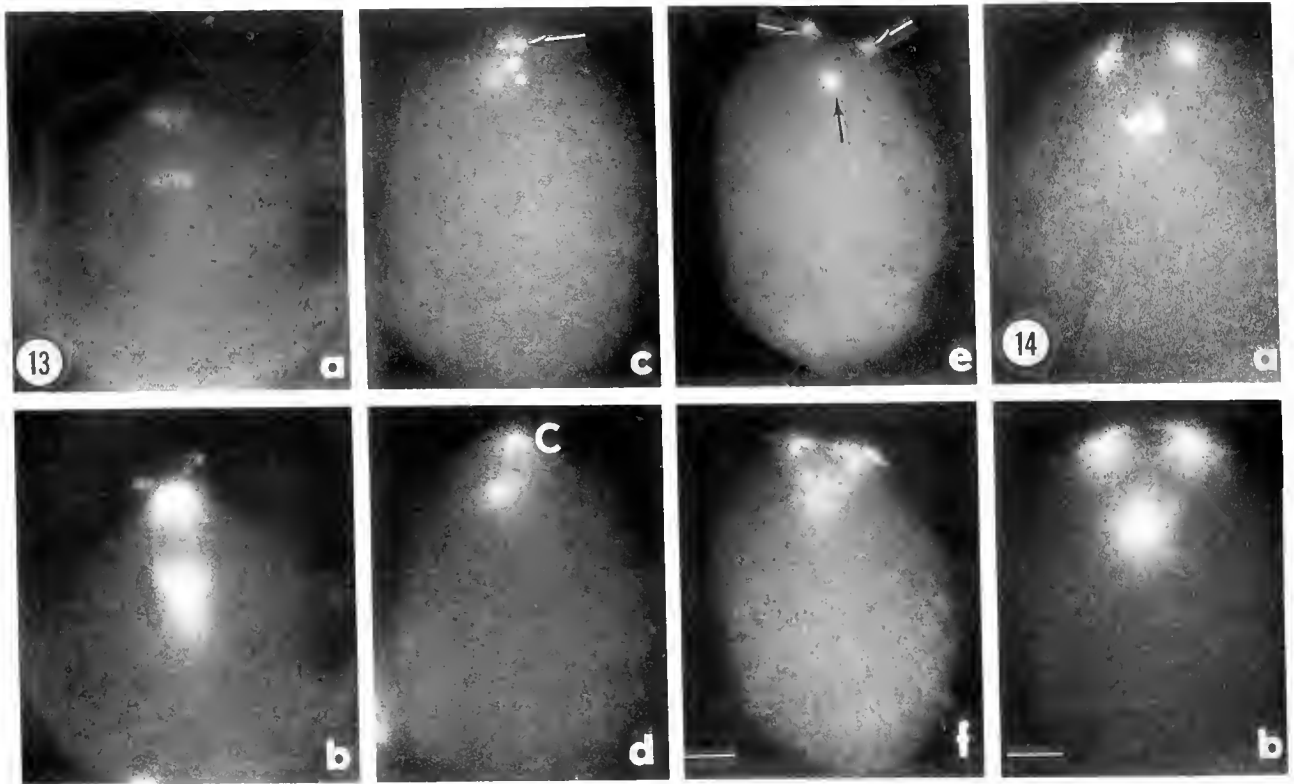


**Figure 13.** (a, c, e) 7-AAD- and antitubulin-stained (b, d, f) eggs treated continuously with cytochalasin B. (a–d) Because first polar body formation is inhibited, the chromosomes (arrows) and the spindle pole (C) normally expelled at meiosis I are retained within the zygote. (e, f) All of the chromosomes (arrows) then become part of a tripolar spindle (f). Scale bar = 10  $\mu$ m.

**Figure 14.** Tripolar spindle that forms in fertilized eggs treated with cytochalasin B during meiosis I. Specimen stained with 7-AAD (a) and antitubulin (b). Scale bar = 10  $\mu$ m.

for other mollusk species that have been examined (Inaba, 1936; Longo and Anderson, 1969, 1970; Kuriyama *et al.*, 1986; Kuraishi and Osanai, 1988). However, the second meiotic spindle differs from the first in both its size and initial orientation. The basis for differences in size and orientation of the second meiotic spindle is not clear. Meiotic spindles oriented parallel to the egg cortex are not uncommon, particularly in mammals (Longo, 1987; see also Gard, 1992). As far as we are aware, differences in spindle size of meiotic eggs are unusual, and how they might be regulated is not clear. An examination of previously published observations of fertilized Japanese oyster eggs does show what may be differences in size and orientation of the first and second meiotic spindles (Inaba, 1936; Kuraishi and Osanai, 1988). Whatever the scheme to explain such differences, it will have to take into account observations that the axes of the tripolar meiotic spindle formed in CB-treated eggs are approximately equal to the spindle length of the second meiotic apparatus. Furthermore, mechanisms underlying spindle orientation have not been established, although microtubules have been

implicated in this process (Hyman, 1989; Kropf *et al.*, 1990; Fernandez *et al.*, 1990; Gard, 1992).

The array of microtubules that develops in conjunction with the forming female pronucleus disappears by pronuclear migration, suggesting that it may have little to do with this process. Concomitant with the increase and regression of the microtubular array associated with the female pronucleus is the development of the sperm aster, which accompanies the male pronucleus in its migration. The sperm aster remains in proximity with the associated pronuclei and with the onset of prophase appears to divide into two foci that form the poles of the cleavage spindle (Sluder *et al.*, 1985; Schatten *et al.*, 1986). This morphogenesis and the disappearance of microtubule arrays associated with the female pronucleus suggest that centrosomes of *C. gigas* embryos are paternally derived as described for other species (Longo and Anderson, 1969, 1970; Kuriyama *et al.*, 1986; Schatten *et al.*, 1986; Sluder *et al.*, 1985, 1989.) The presence of multiple sperm asters in polyspermic oyster eggs, their apparent contribution to the formation of multipolar cleavage spindles, and mi-



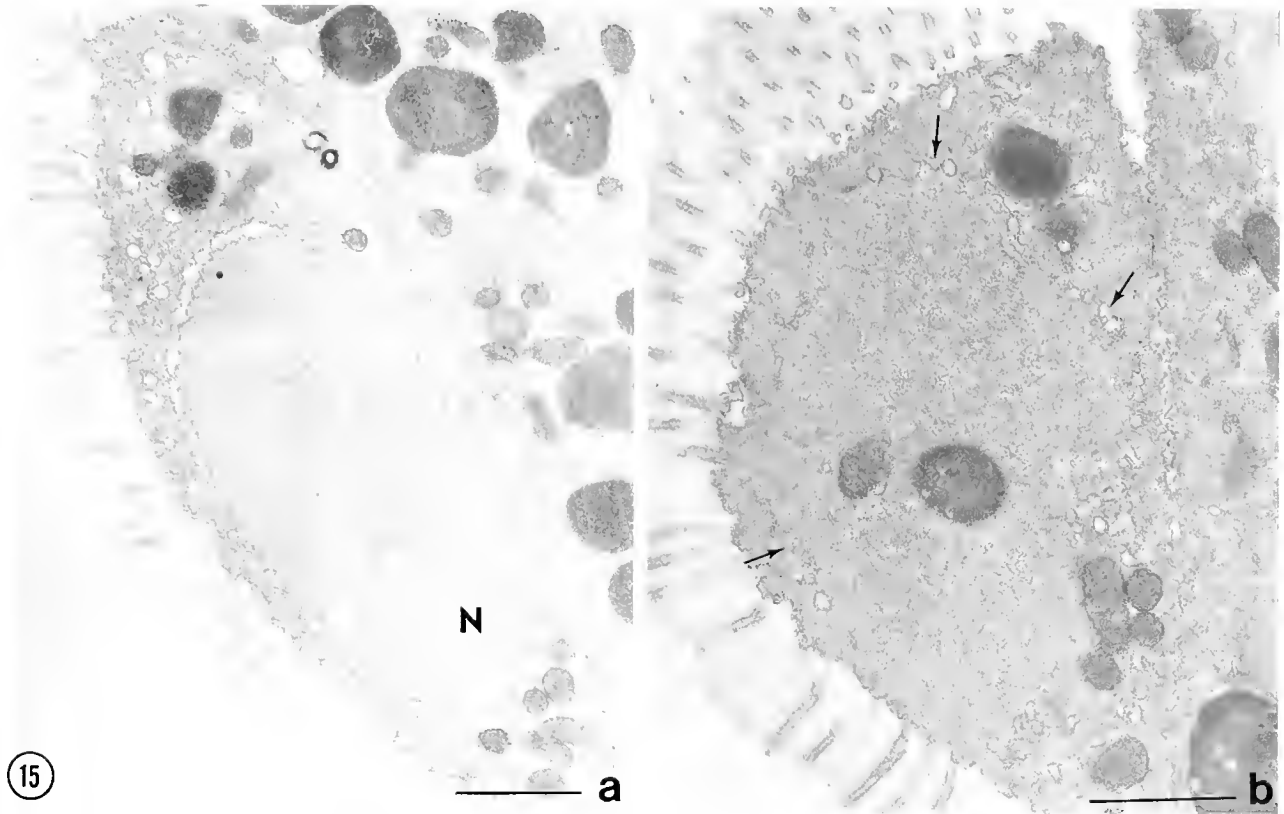


**Figure 15.** Polar bodies formed in eggs treated with cytochalasin B during the period of meiosis I and meiosis II (b). Usually only polar bodies developing at meiosis II possess chromatin that becomes organized into a nucleus. (a) Nucleus (N) in a polar body formed after inhibition of the first polar body. (b) Chromatin of polar bodies that form at the first meiotic division may be surrounded by cisternae (arrows), however, and a nuclear envelope usually fails to form. Scale bar = 1  $\mu$ m.

crotubule dynamics in CB-treated eggs (see below) are consistent with this notion.

#### *Sperm nuclear transformations*

The different rates of sperm nuclear expansion observed here are similar to those that have been previously reported in oysters (Kuraishi and Osanai, 1988; Komaru *et al.*, 1990) and in other mollusks (Da-Yuan and Longo, 1983; Luttmner and Longo, 1988; Longo and Scarpa, 1991). It is noteworthy that during polar body formation in eggs inseminated at an arrested stage of meiosis there is a condensation of the dispersed sperm chromatin (Longo, 1990). Such a size reduction was not noted here, due possibly to the heterogeneity of the population studied or to the presence of a relatively small decrease that went undetected. Inspection of micrographs from published investigations of fertilized oyster eggs reveals images of incorporated sperm nuclei that appear to have condensed following their initial dispersion (Kuraishi and Osanai, 1988; Komaru *et al.*, 1990).

It is not until the completion of meiosis and in conjunction with the assembly of a female pronucleus that a nuclear envelope formed along the periphery of the dispersed sperm chromatin. Nuclear envelope assembly with respect to both the male and female pronuclei involves an aggregation of cisternae along the periphery of the dispersed chromatin and their fusion (Lohka, 1988). The two pronuclei that form are virtually identical in size and structure; however, the female pronucleus is distinguished by its associated microtubule array and proximity to the polar bodies. The male pronucleus is identifiable by its association with the sperm aster. Morphogenesis of apposed male and female pronuclei of oyster zygotes is essentially the same as described for other mollusks (Longo and Anderson, 1969, 1970; Longo and Scarpa, 1991; see Longo, 1983).

#### *CB effects*

Results of the present study are consistent with previous investigations demonstrating that CB application leads to



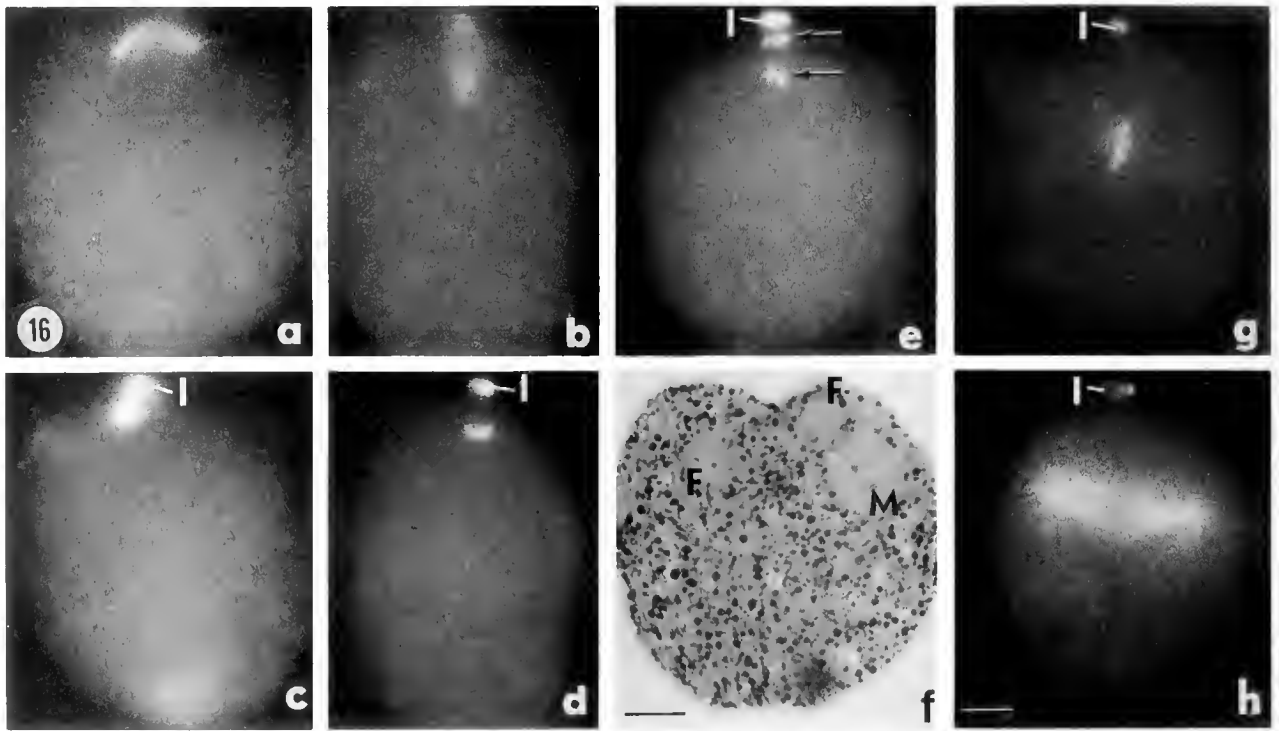


**Figure 16.** Effect of cytochalasin B (CB) on eggs at the second meiotic division. (a-d) When added immediately following first polar body formation, CB does not inhibit the development and changes in orientation of the second meiotic spindle. (a) A spindle forms that is initially positioned parallel to the egg surface; it then rotates to a perpendicular orientation (b) as in untreated eggs. (c, d) Same preparation shown in a and b, respectively, but viewed to show chromosomes stained with 7-AAD. (e, f) After spindle rotation, anaphase II ensues but is not accompanied by the formation of a second polar body. The chromosomes (arrows) retained within the egg develop into pronuclei (F, M), and the meiotic spindle regresses. (g, h) The two female pronuclei and the one male pronucleus that are formed undergo prophase and the chromosomes from all three pronuclei become organized on a single mitotic spindle. 1, first polar body. Scale bar = 10  $\mu\text{m}$ .

polyploidy (Stanley *et al.*, 1981; Downing and Allen, 1987; Allen, 1987; Komaru *et al.*, 1990), particularly when given at two critical periods corresponding to anaphase I and II (Quillet and Panelay, 1986). As shown here and in previous studies with *Spisula* (Longo, 1972), CB has no apparent effect on the elevation of the cytoplasmic projection that becomes a polar body, but does affect its separation from the zygote. This is presumably a result of CB's action on the band of actin filaments comprising the cleavage furrow (Rappaport, 1975). Consequently, the projection that normally would become a polar body is not severed from the zygote, and chromosomes normally segregated from the zygote are retained. Depending on the time and duration of CB application, varying modes and degrees of ploidy result (Allen, 1987; Komaru *et al.*, 1990; Guo *et al.*, 1992a, b).

Recent investigations by Guo *et al.* (1992a, b) indicate that when CB is administered at metaphase I, greater than 50% aneuploids are produced. This result is in excellent agreement with the present study demonstrating that,

when formation of the first polar body is blocked, chromosomes remaining in the zygote become organized on a tripolar, meiotic spindle. Orientation of the tripolar spindle and mechanisms by which it might function may be responsible for the distribution of aneuploidy around peaks with 23–27 and 35–37 chromosomes (Guo *et al.*, 1992a, b). The presence of a tripolar spindle is also consistent with investigations indicating that during meiosis there is a halving of material responsible for the organization of the meiotic spindle (Sluder *et al.*, 1989, 1993). Specifically, the observations presented here indicate that the spindle pole normally expelled with the first polar body is retained and, although it is unable to divide, it is able to participate in the organization of one pole of the tripolar spindle. In contrast, the center normally retained in the zygote following meiosis I divides and presumably is responsible for the organization of two poles of the tripolar spindle. This implies that the centrosome normally taken into the first polar body is affected in some way during the course of meiosis such that it is unable to be-

have in the same manner as the center normally retained within the zygote (Sluder *et al.*, 1989). These observations are consistent with recent experiments in starfish zygotes which demonstrate that the reproductive capacity of maternal centrosomes is degraded during meiosis I (Sluder *et al.*, 1993).

In theory, when only the first or the second polar body is blocked, two female pronuclei are formed; when both polar bodies are inhibited at least four female pronuclei are formed (Longo, 1972; Komaru *et al.*, 1990). Deviations from these values reflect the manner in which the second meiotic spindle becomes organized and the way the maternal chromosomes aggregate and become delimited by a nuclear envelope (Longo, 1972). In the treatments studied here, all the maternally derived pronuclei migrate to and become associated with the male pronucleus. The associated pronuclei then undergo prophase as separate structures, and their chromosomes become associated on a single mitotic spindle. Such an observation is consistent with previous accounts, indicating that centrosomes of the embryo are paternally inherited (Wilson, 1925; Sluder *et al.*, 1989, 1993).

#### Acknowledgments

The assistance of Ms. Tena Perry, Ms. Erin Jacobs, and Mr. Eric Freese is greatly appreciated. Special thanks are extended to Dr. Wallis H. Clark, Jr., for his comments and advice during the course of this investigation. Portions of the study presented here were supported by funds from the NIH. This paper is dedicated to the memory of Dr. Harold W. Beams (Emeritus Professor of Biology, the University of Iowa, Iowa City). His talents as an inspiring teacher and devoted researcher profoundly influenced all those who were privileged to know him. The curiosity and enthusiasm he demonstrated for cell and developmental biology throughout his long and illustrious career inspired us to a greater love of science.

#### Literature Cited

- Alexandre, H., A. Van Canwenberge, and J. Mulnard. 1989. Involvement of microtubules and microfilaments in the control of the nuclear movement during maturation of mouse oocyte. *Dev. Biol.* **136**: 311-320.
- Allen, S. K. 1983. Flow cytometry: assaying experimental polyploid fish and shellfish. *Aquaculture* **33**: 317-328.
- Allen, S. K. 1987. Genetic manipulations—critical review of methods and performances for shellfish. Pp. 127-143 in *Selection, Hybridization, and Genetic Engineering in Aquaculture*, K. Tiews, ed. Vol. II. Heenemann Verlag, Berlin.
- Alliegro, M. C., and D. A. Wright. 1983. Polyspermy inhibition in the oyster, *Crassostrea virginica*. *J. Exp. Zool.* **227**: 127-137.
- Anastassova-Kristeva, M. 1977. The nucleolar cycle in man. *J. Cell Sci.* **25**: 103-110.
- Beaumont, A. R., and J. E. Fairbrother. 1991. Ploidy manipulation in molluscan shellfish: a review. *J. Shellfish Res.* **10**: 1-18.
- Campanella, C., P. Andreucetti, C. Taddei, and R. Talevi. 1984. The modification of cortical endoplasmic reticulum during *in vitro* maturation of *Xenopus laevis* oocytes and its involvement in cortical granule exocytosis. *J. Exp. Zool.* **229**: 283-293.
- Chaiton, J. A., and S. K. Allen. 1985. Early detection of triploidy in the larvae of Pacific oysters, *Crassostrea gigas*, by flow cytometry. *Aquaculture* **48**: 35-43.
- Da-Yuan, C., and F. J. Longo. 1983. Sperm nuclear dispersion coordinate with meiotic maturation in fertilized *Spisula solidissima* eggs. *Dev. Biol.* **99**: 217-224.
- Daniels, E. W., A. C. Longwell, J. M. McNiff, and R. W. Wolfgang. 1971. Ultrastructure of spermatozoa from the American oyster *Crassostrea virginica*. *Trans. Am. Microsc. Soc.* **90**: 275-282.
- Dessev, G., and R. Goldman. 1988. Meiotic breakdown of nuclear envelope in oocytes of *Spisula solidissima* involves phosphorylation and release of nuclear lamin. *Dev. Biol.* **130**: 543-550.
- Dessev, G., R. Palazzo, L. Rebhun, and R. Goldman. 1989. Disassembly of the nuclear envelope of *Spisula* oocytes in a cell-free system. *Dev. Biol.* **131**: 496-504.
- Downing, S. L., and S. K. Allen. 1987. Induced triploidy in the Pacific oyster, *Crassostrea gigas*. Optimal treatments with cytochalasin B depend on temperature. *Aquaculture* **61**: 1-15.
- Fallon, J. F., and C. R. Austin. 1967. Fine structure of gametes of *Nereis limbata* (Annelida) before and after interaction. *J. Exp. Zool.* **166**: 225-242.
- Fernandez, J., N. Olea, V. Tellez, and C. Matte. 1990. Structure and development of the egg of the glossiphonid leech *Theromyzon rude*: re-organization of the fertilized egg during completion of the first meiotic division. *Dev. Biol.* **37**: 142-154.
- Galtsoff, P. S. 1964. The American oyster *Crassostrea virginica* Gmelin. *Fish. Bull. U.S. Fish Wild Res.* **64**: 324-354.
- Galtsoff, P. S., and D. E. Philpott. 1960. Ultrastructure of the spermatozoan of the oyster, *Crassostrea virginica*. *J. Ultrastruct. Res.* **3**: 241-253.
- Gard, D. L. 1992. Microtubule organization during maturation of *Xenopus* oocytes: assembly and rotation of the meiotic spindles. *Dev. Biol.* **151**: 516-530.
- Guo, X., K. Cooper, W. K. Hershberger, and K. K. Chew. 1992a. Genetic consequences of blocking polar body I with cytochalasin B in fertilization eggs of the Pacific oyster, *Crassostrea gigas*. I. Ploidy of resultant embryos. *Biol. Bull.* **183**: 381-386.
- Guo, X., W. K. Hershberger, K. Cooper, and K. K. Chew. 1992b. Genetic consequences of blocking polar body I with cytochalasin B in fertilized eggs of the Pacific oyster, *Crassostrea gigas*. II. Segregation of chromosomes. *Biol. Bull.* **183**: 387-393.
- Gutierrez, M., J. P. Crespo, and E. Pascual. 1978. Ultraestructura de ovocitos y espermatozoides del ostión, *Crassostrea angulata* Lmk. de la costa sudatlántica de España. *Investigacion Pesquera* **42**: 167-178.
- Hadjiolov, A. A. 1985. *The Nucleolus and Ribosome Biogenesis*. Springer-Verlag, New York.
- Hylander, B. L., and R. G. Summers. 1977. An ultrastructural analysis of the gametes and early fertilization in two bivalve molluscs, *Chama macerophylla* and *Spisula solidissima* with special reference to gamete binding. *Cell Tiss. Res.* **182**: 469-489.
- Hyman, A. A. 1989. Centrosome movement in the early divisions of *Caenorhabditis elegans*: A cortical site determining centrosome position. *J. Cell Biol.* **109**: 1185-1193.
- Inaba, F. 1936. Studies on the artificial parthenogenesis of *Ostrea gigas*, Thunberg. *J. Sci. Hiroshima Univ., Ser. B. Div. 1*, **5**: 29-46.
- Kalt, A., and M. Schliwa. 1993. Molecular components of the centrosome. *Trends Cell Biol.* **3**: 118-128.
- Kato, K. II., S. Washitani-Nemoto, A. Hino, and S. Nemoto. 1990. Ultrastructural studies on the behavior of centrioles during meiosis of starfish oocytes. *Dev. Growth Differ.* **32**: 41-49.

- Komaru, A., H. Matsuda, T. Yamakawa, and K. T. Wada. 1990. Chromosome behavior of meiosis-inhibited eggs with cytochalasin B in Japanese pearl oyster. *Nippon Suisan Gakkaishi* 56: 1419-1422.
- Kropf, D. L., A. Maddock, and D. L. Gard. 1990. Microtubule distribution and function in early *Pelvetia* development. *J. Cell Sci.* 97: 545-552.
- Kuraishi, R., and K. Osanai. 1988. Behavior of sperm nuclei in meiotic eggs of the oyster, *Crassostrea gigas*. *Bull. Mar. Biol. Stn. Asamushi* 18: 57-65.
- Kuriyama, R., G. G. Borisy, and Y. Masui. 1986. Microtubule cycles in oocytes of the surf clam, *Spisula solidissima*: a fluorescence study. *Dev. Biol.* 114: 151-160.
- Lohka, M. J. 1988. The reconstitution of nuclear envelopes in cell-free extracts. *Cell Biol. Int. Rep.* 12: 833-848.
- Longo, F. J. 1972. Effects of cytochalasin B on events of fertilization in the surf clam, *Spisula solidissima*. I. Polar body formation. *J. Exp. Zool.* 182: 321-344.
- Longo, F. J. 1976. Ultrastructure aspects of fertilization in Spiralian eggs. *Am. Zool.* 16: 375-394.
- Longo, F. J. 1983. Meiotic maturation and fertilization. Pp. 49-89 in *The Mollusca*, Vol 3. K. M. Wilbur, ed. Academic Press, New York.
- Longo, F. J. 1987. *Fertilization*. Chapman & Hall, New York.
- Longo, F. J. 1990. Dynamics of sperm nuclear transformation at fertilization. Pp. 297-307 in *Fertilization in Mammals*, B. D. Bavister, J. Cummins, and E. R. S. Roldan, eds. Serono Symposium, U.S.A. Norwell, MA.
- Longo, F. J., and E. Anderson. 1969. Cytological aspects of fertilization in the lamellibranch, *Mytilus edulis*. I. Polar body formation and development of female pronucleus. *J. Exp. Zool.* 172: 69-96.
- Longo, F. J., and E. Anderson. 1970. An ultrastructural analysis of fertilization in the surf clam, *Spisula solidissima*. I. Polar body formation and development of the female pronucleus. *J. Ultrastruct. Res.* 33: 495-514.
- Longo, F. J., and D. Y. Chen. 1985. Development of cortical polarity in mouse eggs: involvement of the meiotic apparatus. *Dev. Biol.* 107: 382-394.
- Longo, F. J., and J. Scarpa. 1991. Expansion of the sperm nucleus and association of the maternal and paternal genomes in fertilized *Mulinia lateralis* egg. *Biol. Bull.* 180: 56-64.
- Longwell, A. C., and S. S. Stiles. 1968. Fertilization and completion of meiosis in spawned eggs of the American oyster, *Crassostrea virginica* Gmelin. *Caryologia* 21: 65-73.
- Luttmers, S. J., and F. J. Longo. 1988. Sperm nuclear transformations consist of enlargement and condensation coordinate with stages of meiotic maturation in fertilized *Spisula solidissima* eggs. *Dev. Biol.* 128: 86-96.
- Maro, B., M. H. Johnson, M. Webb, and G. Floch. 1986. Mechanisms of polar body formation in the mouse oocyte: an interaction between the chromosomes, the cytoskeleton, and the plasma membrane. *J. Embryol. Exp. Morphol.* 92: 11-32.
- Osanai, K. 1969. Relation between cortical change and cytoplasmic movement in the oyster egg. *Annu. Rep. Fac. Educ. Iwate Univ.* 29: 39-44.
- Osanai, K. 1985. *In vitro* induction of germinal vesicle breakdown in oyster oocytes. *Bull. Mar. Biol. Stn. Asamushi* 18: 1-9.
- Otto, J. J., and T. E. Schroeder. 1984. Microtubule arrays in the cortex and near the germinal vesicle of immature starfish oocyte. *Dev. Biol.* 101: 274-281.
- Quillet, E., and P. J. Panelay. 1986. Triploidy induction by thermal shocks in the Japanese oyster, *Crassostrea gigas*. *Aquaculture* 57: 271-279.
- Rappaport, R. 1975. Establishment and organization of the cleavage mechanism. *Soc. Gen. Physiol. Ser.* 30: 287-305.
- Rebhun, L. I. 1962. Electron microscope studies on the vitelline membrane of the surf clam, *Spisula solidissima*. *J. Ultrastruct. Res.* 6: 107-122.
- Ryabova, L. V., M. I. Betina, and S. G. Vassetsky. 1986. Influence of cytochalasin B on oocyte maturation in *Xenopus laevis*. *Cell* 19: 89-96.
- Scarpa, J., and S. K. Allen. 1992. Comparative kinetics of meiosis in hybrid crosses of Pacific oyster *Crassostrea gigas* and Suminoe oyster *C. rivularis* with the American oyster *C. virginica*. *J. Exp. Zool.* 263: 316-322.
- Schatten, H., G. Schatten, D. Mazia, R. Balczon, and C. Simerly. 1986. Behavior of centrosomes during fertilization and cell division in mouse oocytes and in sea urchin eggs. *Proc. Natl. Acad. Sci. USA* 83: 105-109.
- Schroeder, T. E. 1985. Cortical expressions of polarity in the starfish oocyte. *Dev. Growth Differ.* 27: 311-321.
- Sluder, G., C. L. Reider, and F. Miller. 1985. Experimental separation of pronuclei in fertilized sea urchin eggs: Chromosomes do not organize a spindle in the absence of centrosomes. *J. Cell Biol.* 100: 897-903.
- Sluder, G., F. J. Miller, K. Lewis, E. D. Davison, and C. L. Rieder. 1989. Centrosome inheritance in starfish zygotes: selective loss of the maternal centrosome after fertilization. *Dev. Biol.* 131: 567-579.
- Sluder, G., F. J. Miller, and K. Lewis. 1993. Centrosome inheritance in starfish zygotes II: Selective suppression of the maternal centrosome during meiosis. *Dev. Biol.* 155: 58-67.
- Speksnijder, J. E., M. Terasaki, W. J. Hage, L. F. Jaffe, and C. Sardet. 1993. Polarity and reorganization of the endoplasmic reticulum during fertilization and endoplasmic segregation in the ascidian egg. *J. Cell Biol.* 120: 1337-1346.
- Stanley, J. G., S. K. Allen, and H. Hudu. 1981. Polyploidy induced in the American oyster, *Crassostrea virginica*, with cytochalasin B. *Aquaculture* 23: 1-10.
- Stanley, J. G., H. Hudu, and S. K. Allen. 1984. Growth of American oysters increased by polyploidy induced by blocking meiosis I but not meiosis II. *Aquaculture* 37: 147-155.
- Stephano, J. L., and M. Gould. 1988. Avoiding polyspermy in the oyster (*Crassostrea gigas*). *Aquaculture* 73: 295-307.
- Stiles, S. S., and A. C. Longwell. 1973. Fertilization, meiosis and cleavage in eggs from large mass spawnings of *Crassostrea virginica* Gmelin, the commercial American oyster. *Caryologia* 26: 253-262.
- Stricker, S. A., and G. Schatten. 1989. Nuclear envelope disassembly and nuclear lamina depolymerization during germinal vesicle breakdown in starfish. *Dev. Biol.* 135: 87-98.
- Terasaki, M., and L. Jaffe. 1991. Organization of the sea urchin endoplasmic reticulum and its reorganization at fertilization. *J. Cell Biol.* 114: 929-940.
- Van Blerkom, J., and H. Bell. 1986. Regulation of development in the fully grown mouse oocyte: chromosome mediated temporal and spatial differentiation of the cytoplasm and plasma membrane. *J. Embryol. Exp. Morphol.* 93: 213-238.
- Wilson, E. B. 1925. *The Cell in Development and Heredity*. MacMillan, Co., New York.

## Histochemical Studies of Jelly Coat of *Marthasterias glacialis* (Echinodermata, Asteroidea) Oocytes

MÁRIO SOUSA<sup>1,\*</sup>, RUI PINTO<sup>3</sup>, PEDRO MORADAS-FERREIRA<sup>2</sup>,  
AND CARLOS AZEVEDO<sup>1</sup>

Laboratories of <sup>1</sup>Cell Biology and <sup>2</sup>Biochemistry of the Institute of Biomedical Sciences, University of Oporto, and <sup>3</sup>the Laboratory of Enzymology of the Institute of Medical Genetics, 4000 Porto, Portugal

**Abstract.** Histochemical studies revealed the presence of two major polysaccharides in the oocyte jelly coat (JC) of *Marthasterias glacialis*: a fibrillar component that contains carboxylic and sulfated groups and a loose component composed of neutral or weakly acidic polysaccharides. When isolated JC was submitted to cellulose acetate electrophoresis (CAE) and then stained with alcian blue, three bands appeared, of which one remained at the origin and two migrated toward the anode. Glycosaminoglycan-like molecules isolated from JC were separated by CAE into three main moving bands, two that present an  $R_f$  similar to that of the intermediary moving band of total JC and one that has an  $R_f$  similar to that of the faster moving band of total JC. These bands also have critical electrolyte points similar to those of total JC. Chondroitinase ABC mainly attacked the faster moving band, whereas protease and hyaluronidase seemed to digest all bands. These results and the  $R_s$  of isolated and standard glycosaminoglycans after mono- and bidimensional CAE suggest that the glycosaminoglycan-like molecules bear some resemblance to chondroitin sulfate, heparan sulfate, and hyaluronic acid.

### Introduction

Complex carbohydrates have been implicated in sperm-egg recognition, binding, and activation in both vertebrates and invertebrates (Miller and Ax, 1990).

The macromolecular structures of the jelly coat (JC) of the echinoderm oocyte have not yet been morphologically

differentiated, despite the importance of this information to the understanding of sperm-egg interaction. In the sea urchin, the oocyte JC was demonstrated to contain a sialo-protein and a fucose sulfate polysaccharide that induces the acrosomal reaction of the sperm (SeGall and Lennarz, 1979). Histochemical studies have also found two major polysaccharides in the JC, neutral and acidic (Jondeung and Czihak, 1982), thus confirming the biochemical results. In the starfishes *Asterias amurensis* and *Asterina pectinifera*, the oocyte JC was also demonstrated to contain two major polysaccharides, a large sulfated glycoprotein that induces the acrosomal reaction and a high-mannose glycoprotein (for a review see Hoshi *et al.*, 1990a, b), but no morphological studies have been made to confirm these biochemical findings.

We characterized the oocyte JC of the starfish *Marthasterias glacialis* by histochemical and electrophoretic methods. Our results show that the JC can be morphologically differentiated into two major polysaccharides that probably contain glycosaminoglycan-like materials.

### Materials and Methods

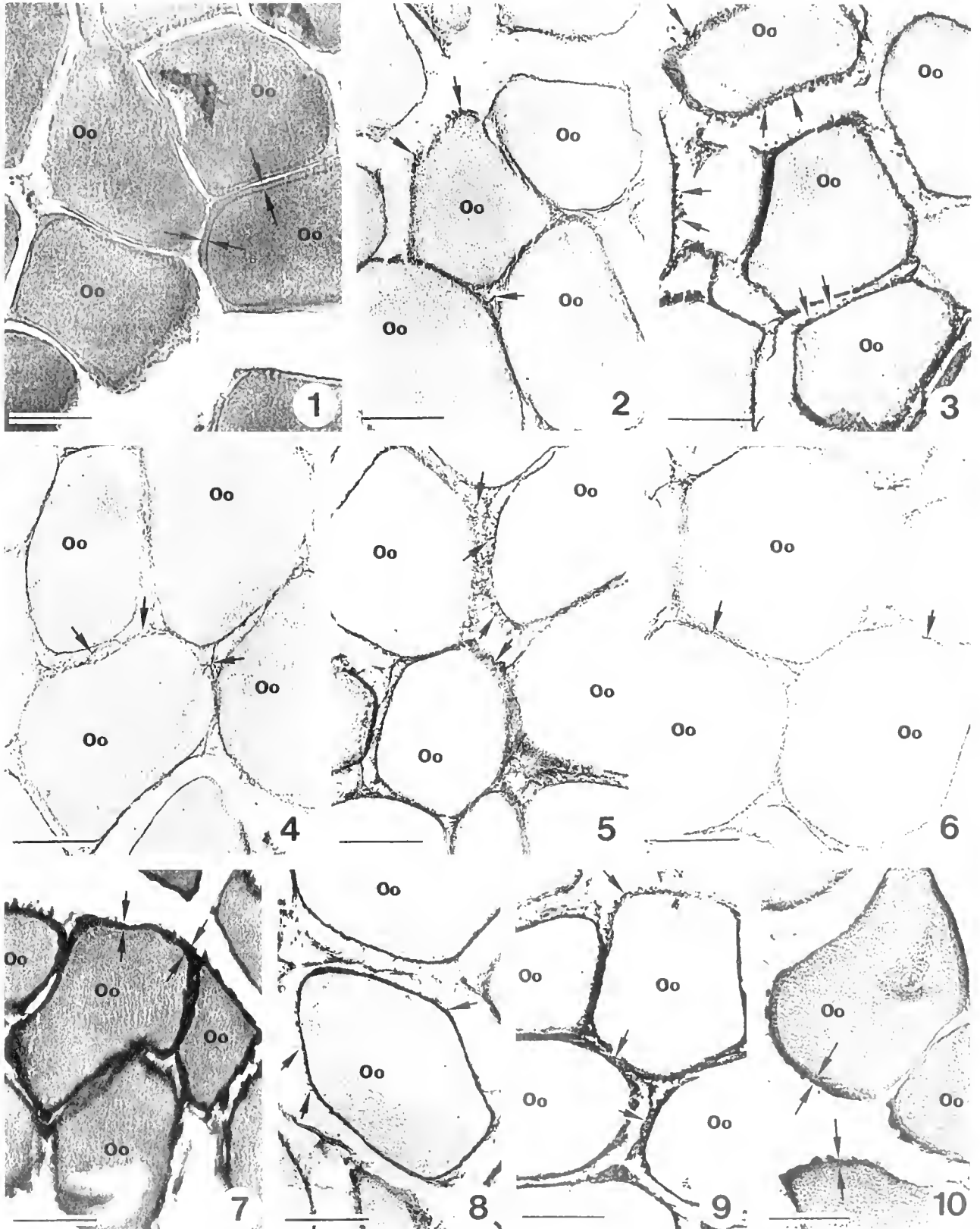
Several specimens of *M. glacialis* were collected in the intertidal zone of the North Atlantic, 30 km north of Oporto, Portugal. The animals were maintained in the laboratory in well-aerated seawater.

For histochemical studies of the jelly coat of the oocyte, mature ovaries were fixed in Bouin's fluid for 24 h, processed through alcohol and benzene, and embedded in paraffin (Ganter and Jollès, 1969). Sections were cut at 7  $\mu$ m. The following histochemical methods were employed, all without counterstaining:

(1) Alcian blue (1%) 8GX (Sigma) staining at pH 0.5 (Ab pH 0.5) according to the method of Lev and Spicer

Received 27 August 1992; accepted 6 July 1993.

\* Address correspondence to this author at the Laboratory of Cell Biology, Institute of Biomedical Sciences, University of Oporto, I.g. Prof. Abel Salazar 2, 4000 Porto, Portugal.



Figures 1-10. Histochemical staining of the jelly coat (JC) of mature oocytes (Oo) in the ovary of *Marthasterus glacialis*. Bar = 50  $\mu$ m.

to demonstrate sulfate groups, and at pH 2.5 (Ab pH 2.5) according to the method of Wagner and Shapiro to demonstrate those acid groups which remain ionized at and above this pH (Lev and Spicer, 1964; Ganter and Jollès, 1969, 1970).

(2) Methylation to modify functional groups (carboxyl and sulfate) of polysaccharides (Ganter and Jollès, 1969, 1970). Sections were collodionized and then immersed in a solution consisting of liquid HCl diluted to 1% with liquid absolute methanol, at 37°C (mild methylation) or at 60°C (active methylation) for 4–12 h. Some of the sections were then saponified to reverse the methylation of carboxylic acids (1% KOH in 70% ethanol at room temperature for 30 min). After methylation or saponification, sections were stained with Ab pH 0.5 and Ab pH 2.5. Methylation was also performed as in Pearse (1968), with 0.1 *N* HCl-absolute methanol for 8–96 h at 37°C (mild) or at 60°C (drastic).

(3) Alcian blue/critical-electrolyte-concentration technique (Ab-CEC) to identify the different negatively charged acidic groups (Scott and Dorling, 1965; Pearse, 1968; Scott, 1985), by using different MgCl<sub>2</sub> concentrations in 3% acetic acid, 0.1% Ab.

(4) The standard periodic acid-Schiff (PAS) reaction for vicinal hydroxyl groups of polysaccharides according to McManus (Pearse, 1968; Ganter and Jollès, 1969, 1970).

(5) Aldehyde fuchsin (AF) staining according to Halmi and Davies (Pearse, 1968; Ganter and Jollès, 1969, 1970) to stain carboxyl and sulfated groups by using basic fuchsin and paraldehyde.

(6) The sequential staining procedures of Ab pH 0.5-PAS and Ab pH 2.5-PAS to differentiate neutral and acidic polysaccharides, and AF-Ab pH 2.5 to distinguish sulfated from weakly acidic polysaccharides (Spicer, 1965; Pearse, 1968; Ganter and Jollès, 1969, 1970).

(7) Mercury-bromophenol blue (Hg-BPB) staining to detect total protein (Pearse, 1968; Ganter and Jollès, 1969, 1970).

The oocyte JC was isolated by the acid method of Matsui *et al.* (1986a). Mature female gonads were cut in Millipore-filtered (0.2 µm) seawater (FSW) at pH 8, and the liberated oocytes were left in FSW until their spontaneous maturation, which is characterized by loss of follicular cells and breakdown of germinal vesicles (Meijer *et al.*, 1984). JC was obtained by washing the oocytes with 20 vol of FSW, resuspending them in 3 vol of FSW, and then lowering the pH to 5.0 with 0.1 *N* HCl. Dejellied oocytes were removed by centrifugation for 5 min at 1500 rpm, and the jelly supernatant was recentrifuged for 30 min at 10,000 rpm at 4°C. The resulting supernatant was adjusted to pH 8.0 with 0.1 *N* NaOH, dialysed against distilled water (Spectra/Por, MW cutoff ×3500) and then lyophilized (SeGall and Lennarz, 1979). Protein concentrations were determined by the method of Lowry *et al.* (1951).

Glycosaminoglycans (GAGs) were isolated from JC according to Whiteman (1972, 1973a,b) as modified by Whiteman and Henderson (1977). To 3 ml of jelly solution (4 mg/ml water), 30 ml of an Ab solution (5 ml of 1% aqueous Ab, 2.65 ml of 2 *M* MgCl<sub>2</sub>, 10 ml of 0.5 *M* Na-acetate pH 5.8, and 82.35 ml water) was added. The GAG-Ab complex was then left to equilibrate for 2 h at room temperature (rt). After centrifuging for 15 min at 5000 rpm, 200 µl of 4 *M* NaCl and 100 µl of methanol were added to the pellet with vortex mixing. Then, 100 µl of 0.1 *M* Na<sub>2</sub>CO<sub>3</sub> and 400 µl of water were added with vortex mixing. The solution was left to equilibrate for 30 min at rt, and then recentrifuged as above. To 600 µl of the clear supernatant, 1.8 ml of ethanol was added. The solution was left for 10 min at rt, and finally centrifuged as above. The precipitate was left to desiccate overnight and then was resuspended in 50 µl of water. After cen-

**Figure 1.** Hemalumen-eosin. The JC is the layer that appears uniformly stained (between arrows) all around the oocytes (Oo).

**Figures 2 and 3.** Alcian blue (Ab) at pH 2.5 to demonstrate the acidic groups that remain ionized at and above this pH, and at pH 0.5 to demonstrate sulfate groups. The JC appears discontinuously stained, giving a mesh-like or fibrillar appearance (arrows). The staining is more intense at pH 0.5 (Fig. 3).

**Figures 4–6.** Ab/critical-electrolyte-concentration technique at 0.0 *M*, 0.2 *M*, and 0.6 *M* MgCl<sub>2</sub> to identify the different negatively charged acidic groups. The JC is discontinuously stained (arrows), revealing a mesh-like or fibrillar component. The staining increases until 0.2 *M* (Fig. 5) and then decreases, becoming almost negative after 0.6 *M* MgCl<sub>2</sub> (Fig. 6).

**Figure 7.** The standard periodic acid-Schiff reaction for vicinal hydroxyl groups of polysaccharides. The JC is intensely and uniformly stained (between arrows).

**Figures 8 and 9.** Aldehyde-fuchsin (AF) to stain carboxyl and sulfated groups, and AF-Ab pH 2.5 to distinguish sulfated from weakly acidic polysaccharides. The JC is discontinuously stained, giving a mesh-like or fibrillar appearance (arrows). Much more fibrillar material appears stained after AF-Ab pH 2.5 (Fig. 9).

**Figure 10.** Mercury-bromophenol blue reaction for total protein. The entire JC appears stained (between arrows).

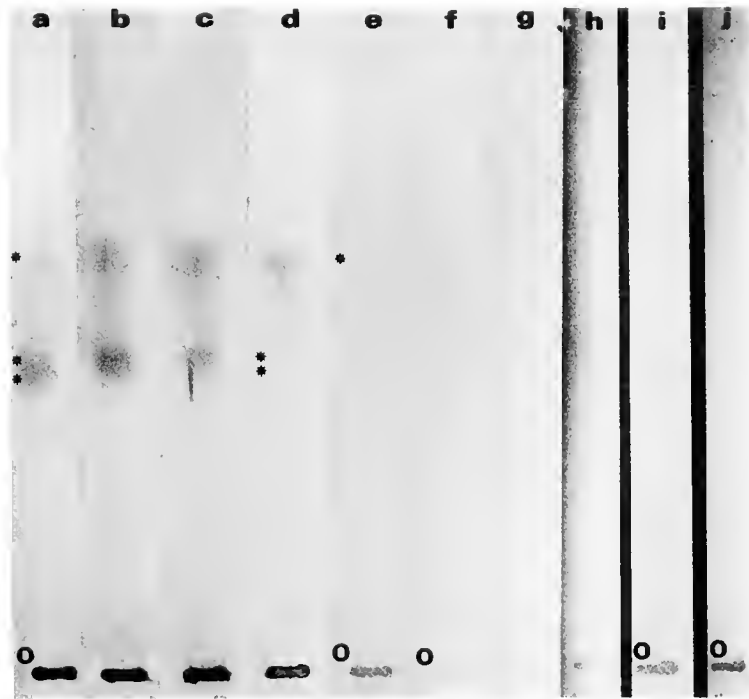


**Figure 11.** Cellulose acetate electrophoresis of total jelly coat. Alcian blue staining (a). Three bands can be observed, of which one remained at the origin (O) and two migrated toward the anode with intermediary (\*\*\*) and faster (\*) mobilities. Alcian blue/critical-electrolyte-concentration technique (Ab-CEC) at different concentrations of  $MgCl_2$ : (b) 0.1 M, (c) 0.2 M, (d) 0.4 M, (e) 0.6 M, (f) 0.8 M, (g) 1 M, and (h) 1.5 M. The critical electrolyte concentration of the intermediary moving band (\*\*\*) is 0.4 M (d) and that of the faster moving band (\*) is 0.6 M (e), whereas the staining of the band at the origin (O) shows an intense decrement after 0.6 M  $MgCl_2$  (f). Only the band at the origin is stained by coomassie blue (i) and standard periodic acid-Schiff (PAS) reaction (j).

trifuging as above, the supernatant was used for electrophoresis.

Concentration of GAGs was determined by the method of Whiteman (1972, 1973a,b). To 25 and 50  $\mu$ l of a 1-mg jelly/ml water solution (in triplicate), 1 ml of the above Ab solution was added. After 4 h at rt, the solution was centrifuged as above, and then 2 ml of ethanol was added to the pellet with vortex mixing. After centrifuging as above, the precipitate was dissociated with 1 ml of 7.5% aqueous SDS by vortex mixing. After 30 min at rt, solutions were read at 678 nm in a Pye-Unicam SP6-550 spectrophotometer. The standard calibration curve was run with a starting solution of chondroitin-4-sulfate, 200  $\mu$ g/ml water, over the range of 0–10  $\mu$ g/ml.

For monodimensional cellulose acetate electrophoresis (CAE), Cellogel sheets, 5.7  $\times$  14 cm, were previously equilibrated in electrophoresis buffer (0.05 M calcium acetate, pH 7.2). Samples (10–20  $\mu$ l/lane, from a 4-mg jelly/ml aqueous solution or from the GAG precipitate) were applied with an LRE applicator (Medizin Technik). Standards were from Sigma and consisted of 1 mg/ml water of keratan sulfate, dermatan sulfate, heparan sulfate, chondroitin sulfate, hyaluronic acid, and heparin. Elec-

trophoresis was performed in an electrophoresis apparatus (EP-166 Medizin Technik) at a constant voltage of 200 V for 1 h (14 V/cm). For bidimensional CAE, Cellogel sheets, 14  $\times$  14 cm, were equilibrated in 0.1 M pyridine, 0.47 M formic acid, pH 3, and the first run was for 1 h at 100 V. For the second dimension, electrophoresis was performed in 0.05 M calcium acetate, pH 7.2, for 2 h at 200 V (Hata and Nagai, 1972). Sheets were then stained with coomassie blue R (Fluka AG) (Cb), PAS, or Ab-CEC. For Ab-CEC (Scott, 1985; Wall and Gyi, 1988), gels were stained overnight and then washed and stored in the same CEC solution without Ab. For general Ab staining, a 0.5% solution in 7% acetic acid was used. For the PAS reaction, acetic acid fixed gels were washed in 3% acetic acid for 15 min, oxidized for 1 h at 4°C with fresh 1% periodic acid in 3% acetic acid, washed three times (5 min each) with water, and stained overnight at 4°C in the Merck Schiff reagent.

For enzymatic treatments, JC or the GAG precipitate was submitted to the following digestions: chondroitinase ABC (Sigma, from *Proteus vulgaris*, 0.55 U/mg) was used at 0.25 and 0.75 U/mg JC for 3 and 24 h at 37°C in 0.1 M Tris-HCl-0.1 M Na-acetate, pH 7.3 (Yanagishita *et al.*,



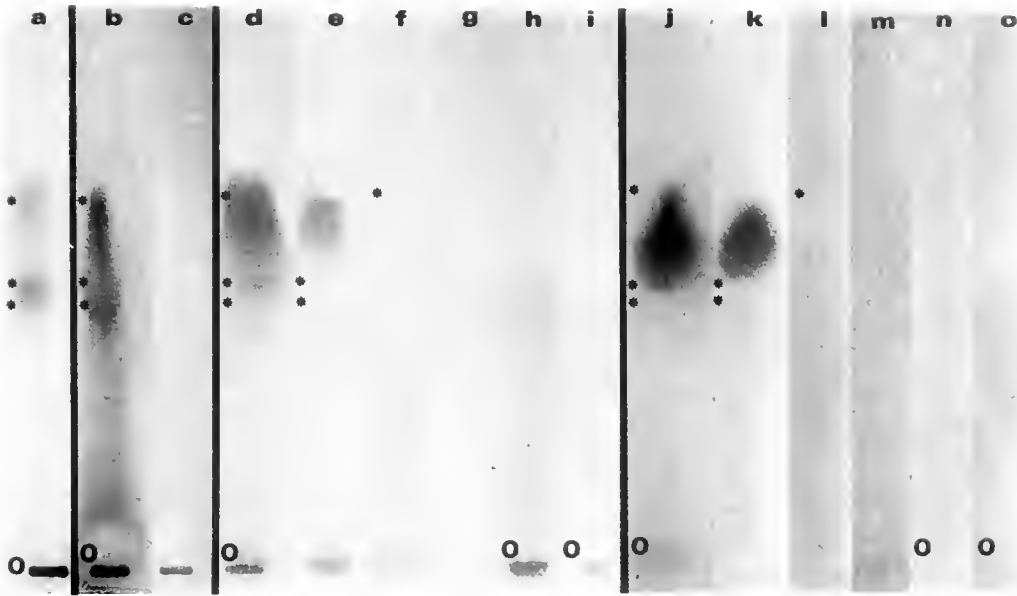


**Figure 12.** Cellulose acetate electrophoresis of total jelly coat after enzymatic digestions. Chondroitinase ABC digestion: Alcian blue staining (a). No changes are observed on the band at the origin (O), or on the intermediary (\*\*\*) and faster (\*) moving bands. Neuraminidase digestion: Alcian blue (b) and standard periodic acid-Schiff (PAS) reaction (c). The intermediary (\*\*\*) and faster (\*) moving bands appear partially digested, producing a smear in which both bands are still visible (b), with no changes apparently having occurred on the band at the origin [O] (b) and (c). Hyaluronidase digestion: (d) through (i). The alcian blue (d) and PAS (i) staining of the band at the origin (O) is decreased, but no changes are noticed (h) with coomassie blue. The intermediary (\*\*\*) and faster (\*) moving bands also seem to be partially digested—their independent configurations changed to a large smear (d). A minimal amount of this smear presents a CEC coincident with that of the intermediary moving band (\*\*\*) [(e), 0.4 M MgCl<sub>2</sub>], whereas most of the smear shows a CEC coincident with that of the faster moving band (\*) [(f), 0.6 M MgCl<sub>2</sub>]. Control strip containing only the enzyme (g). Protease digestion: (j) through (o). A large smear is observed at the level of the intermediary (\*\*\*) and faster (\*) moving bands with alcian blue staining (j). The CEC of this smear is coincident with that of the faster moving band (\*) [(l), 0.6 M MgCl<sub>2</sub>] and not with that of the intermediary moving band (\*\*\*) [(k), 0.4 M MgCl<sub>2</sub>]. The band at the origin (O) appears totally digested—no staining is noticed after alcian blue (j), coomassie blue (n), or PAS (o) staining. Control strip containing only the enzyme (m).

1979; Heinegard and Sommarin, 1987); hyaluronidase (Sigma, from sheep testes, type V, 2000 U/mg) was used at 50, 100, and 200 U/mg JC for 3 and 24 h at 37°C in 0.15 M NaCl, 0.1 M Na-acetate, 0.001 M disodium EDTA, pH 5 (Cowman *et al.*, 1981; Turner and Cowman, 1985; Min and Cowman, 1986); neuraminidase (Sigma, type V, from *Clostridium perfringens*, 1.7 U/mg) was used at 25 and 100 U/mg JC for 24 h at 37°C in 0.1 M Na-acetate pH 5.3 with 0.04 M CaCl<sub>2</sub> (Kudo, 1982; Delgado and Zoller, 1987); trypsin (Sigma, type III, from bovine pancreas, 11,680 U/mg) was used at 10 µg and 0.3 mg/mg JC, protease (Sigma, type VI, from *Streptomyces griseus*, 5 U/mg) and pronase E (Merck, from *Streptomyces griseus*, 95,000 PUK/g) were used at 2 mg/mg JC, all three for 3 and 24 h at 37°C in 0.1 M Tris-HCl, 0.1 M Na-acetate, pH 7.3 (Yanagishita *et al.*, 1979; Grimek and Ax, 1982; Heinegard and Sommarin, 1987; Huey *et al.*, 1990). Digestions were terminated by boiling the samples for 5–10 min (Cowman *et al.*, 1981). Samples were then applied to CAE as above.

## Results

### Light microscopy

Ab discontinuously stained the JC of mature *M. glacialis* oocytes. The reaction was more intense at pH 0.5 than at 2.5 (Figs. 1–3), thus demonstrating on this mesh-like or fibrillar component the presence of both sulfated and carboxylic groups, with the predominance of the former (Lev and Spicer, 1964; Ganter and Jollès, 1969, 1970). Methylation abolished staining with Ab, but sections that were mildly methylated could be partly retained with Ab at both pHs after saponification with KOH. Methylation, which blocks carboxylic and eliminates sulfated groups (Ganter and Jollès, 1969, 1970), did not inhibit Ab pH 0.5 staining after saponification, indicating that this staining is not specific for sulfated groups alone and that the stronger reaction obtained at that pH cannot be assumed to be due to a sulfate-rich polysaccharide. In the presence of MgCl<sub>2</sub> (Ab-CEC), the intensity of Ab staining gradually increased until 0.2 M and then de-



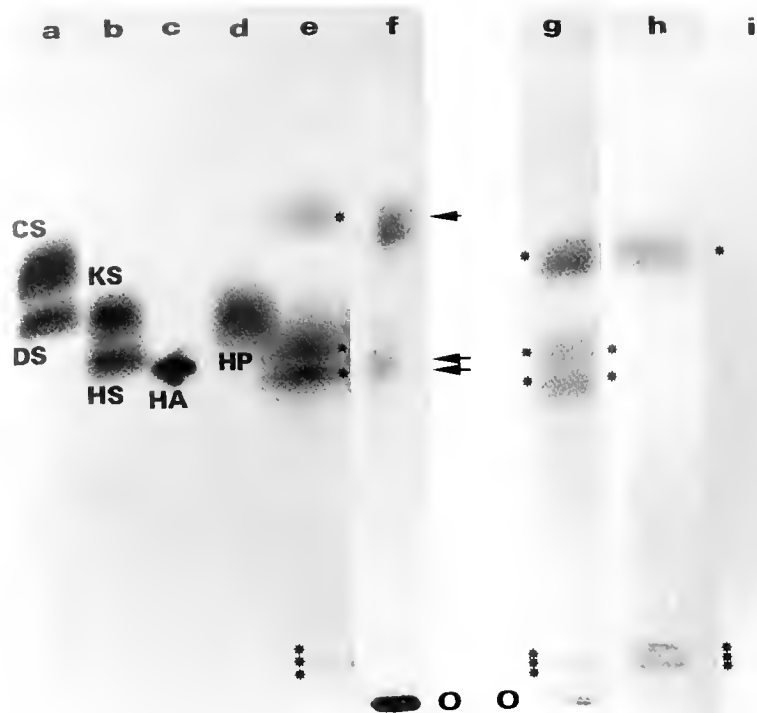


**Figure 13.** Cellulose acetate electrophoresis of GAG-standards [(a) through (d)] and GAG-like molecules [(e) through (i)] after staining with alcian blue [(a) through (f)] and alcian blue/critical-electrolyte-concentration technique (Ab-CEC) at different concentrations of  $\text{MgCl}_2$  [(g), 0.2 *M*, (h), 0.4 *M*, (i), 0.6 *M*  $\text{MgCl}_2$ ]. Standards are (a) chondroitin sulfate (CS) and dermatan sulfate (DS), (b) keratan sulfate (KS) and heparan sulfate (HS), (c) hyaluronic acid (HA), and (d) heparin (HP). Molecules in (e), (g), (h), and (i) were isolated from total jelly coat; molecules in (f) were those of the total jelly coat. Isolated GAG-like molecules separated into three moving bands (e). Two of these bands (\*\*\*) had an  $R_f$  similar to that of the intermediary moving band of total jelly coat [(f), double arrow], and one (\*) had an  $R_f$  similar to that of the faster moving band of total jelly coat [(f), arrow]. A minor component (\*\*\*) can also be seen near or at the origin (O) [(e), (g), (h)]. The intermediary moving bands (\*\*\*) of isolated GAG-like molecules seem to comigrate with HS and HA, whereas the faster moving band (\*) migrates slightly above CS (e). The CEC of the intermediary moving bands (\*\*\*) is 0.4 *M*  $\text{MgCl}_2$  (h) and that of the faster moving band (\*) and the minor bands (\*\*\*) near the origin (O) is 0.6 *M*  $\text{MgCl}_2$  (i).

creased to become almost negative after 0.6 *M* (Figs. 4–6). These results suggest that the Ab-stained material is not highly sulfated and that carboxylic groups predominate, because strong staining was found only in the presence of low  $\text{MgCl}_2$  concentrations (Scott and Dorling, 1965; Scott, 1985).

Contrary to Ab staining, PAS and Ab pH 2.5-PAS uniformly stained the whole jelly layer an intense pink and purple, respectively (Fig. 7), thus revealing the presence of a second macromolecular component made up of neutral or weakly acidic polysaccharides (Pearse, 1968; Ganter and Jollès, 1969, 1970; Rambourg, 1971).

When sections were stained with AF, the fibrillar component of the JC stained purple but, after the sequence AF-Ab pH 2.5, much more fibrillar material appeared stained with intense purple and blue (Figs. 8, 9), which

suggests the presence of both carboxylic and sulfated groups in the fibrillar component of the JC, although with a predominance of the former (Pearse, 1968; Ganter and Jollès, 1969, 1970).

With protein staining, the Hg-BPB reaction gave a strong blue stain to the entire JC (Fig. 10), suggesting that JC polysaccharides may be associated with proteins.

#### *Cellulose acetate electrophoresis*

When JC was submitted to CAE and then stained with Ab, three bands appeared, of which one remained at the origin and two migrated toward the anode (Fig. 11a). With the Ab-CEC staining technique, the bands of intermediary and faster mobilities showed a critical electrolytical point at 0.4 and 0.6 *M*  $\text{MgCl}_2$ , respectively, whereas the staining

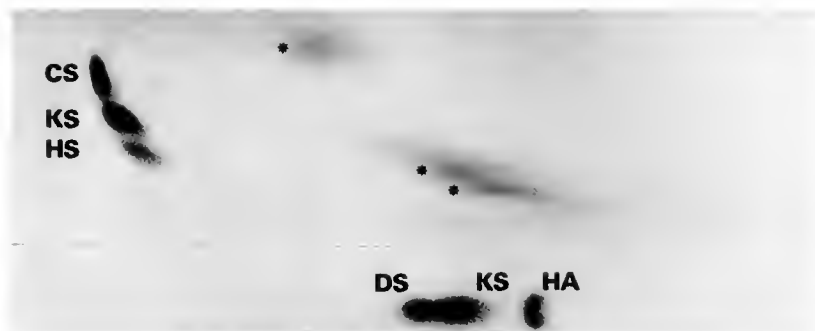


**Figure 14.** Bidimensional cellulose acetate electrophoresis of GAG-like molecules isolated from total jelly coat (alcian blue staining). Standards of first dimension are hyaluronic acid (HA), keratan sulfate (KS), and dermatan sulfate (DS). In this buffer system (pH 3), heparan sulfate (HS) comigrates with KS. Standards of second dimension are HS, KS, and chondroitin sulfate (CS). In this buffer system (pH 7.2), HA comigrates with HS, and DS with KS. Isolated GAG-like molecules separated into three bands, of which two (\*\*) seem to migrate near to HS and HA and then may correspond to the intermediary moving bands (Fig. 13), and one (\*) that migrates near CS and then may correspond to the faster moving band (Fig. 13).

of the band at the origin showed an intense decrement after 0.6 M MgCl<sub>2</sub> (Fig. 11b-h). Only the band that remained at the origin was stained by Cb and PAS (Fig. 11i, j). Protein determination gave a value of 190 μg protein/mg JC, or about 19% of the total JC. These biochemical findings, together with the histochemical results obtained with PAS and Ab pH 2.5-PAS stainings, suggest that the neutral or weakly acidic JC component, as detected on tissue sections, is mainly contained in the band that remained at the origin.

The Ab-CEC staining of tissue sections, which gave a maximum staining of the JC fibrillar material at 0.2 M and an almost absence of staining after 0.6 M MgCl<sub>2</sub>, further suggest that this JC component may have mainly separated after CAE into the two moving bands. All three bands appeared resistant to chondroitinase ABC digestion (Fig. 12a). Neuraminidase seemed to digest the moving band slightly, producing a smear in which both bands are still visible (Fig. 12b, c). After hyaluronidase treatment, Ab and PAS staining of the band at the origin appeared decreased, but no change was noticed with Cb staining. This suggests the presence of both polysaccharides and proteins on that band, with polysaccharides being partially digested by the enzyme (Fig. 12d-i). The two moving bands seemed also to have been partially attacked by hyaluronidase, because their independent configurations changed to a large smear (Fig. 12d). Most of the smear, however, showed a critical electrolyte point coincident with that of the faster moving band, thus suggesting that the intermediary moving band was mainly digested by the enzyme (Fig. 12e, f). Protease seemed to have mainly digested the intermediary moving band, because the moving residual band presents a critical electrolyte point coincident with that of the faster moving band (Fig. 12j-l). However, the configuration of the faster moving band

also changed, producing a large smear band, which suggests that it has been partially attacked by the enzyme (Fig. 12j-l). The band at the origin appeared totally digested by protease, as no staining was noticed after Ab, Cb, and PAS stainings (Fig. 12j-o). This indicates that proteins on this band may be structurally linked to polysaccharides, because digestion of the band enabled polysaccharides to move and escape detection.

Glycosaminoglycan-like materials were isolated from the JC and shown to constitute about 20% of the total JC. After CAE, they separated into three main moving bands, two that present an R<sub>f</sub> similar to that of the intermediary moving band of total JC and one whose R<sub>f</sub> is similar to that of the faster moving band of total JC (Fig. 13). A minor component was also observed near the origin (Fig. 13). This latter finding suggests that the intense Ab staining of the band at the origin of total JC is due not to the presence of a large GAG-like component but to the staining of the weakly acidic groups of the JC PAS-positive component. The presence of GAG-like materials in the same positions as on the main moving bands of total JC was further confirmed by CEC experiments. These experiments showed coincident critical electrolytical points, thus suggesting that the GAG-like materials were extracted from the moving bands (Fig. 13).

In relation to standards, the two intermediary moving bands seemed to comigrate with heparan sulfate and hyaluronic acid, while the faster moving band migrated slightly above chondroitin sulfate (Fig. 13). Similar relationships to standards could also be established after bidimensional CAE (Fig. 14). Chondroitinase ABC mainly attacked the faster moving band, whereas protease and hyaluronidase seemed to have digested all bands (Fig. 15). These results thus suggest that the Ab-precipitated materials from total JC may be proteoglycan-like, containing

GAG-like materials similar to chondroitin sulfate in the faster moving band and heparan sulfate/hyaluronic acid in the intermediary moving bands. The reason that chondroitinase ABC attacked the intermediary moving band and hyaluronidase digested all bands is that they can act in hyaluronate and chondroitin sulfate, respectively (Heinegard and Sommarin, 1987). The lack of a clear  $R_f$  relationship between isolated GAGs and standards may be due to the presence of associated proteins or may indicate that they are only partially similar in structure. The different results obtained with enzymatic digestions of total JC and isolated GAG-like materials may be explained by the different accessibility of enzymes to GAG-like molecules in total JC.

### Discussion

The histochemical study of the JC of *M. glacialis* oocytes revealed the presence of two major types of polysaccharides: an acidic fibrillar material, which seems to contain carboxylic (uronic/sialic) and sulfated groups; and a loose component, which seems to contain neutral or weakly acidic polysaccharides with vic-glycols near carboxylic groups. On the basis of protein staining, these structures may be associated with proteins. As with the starfish, the JC of sea urchin oocytes shows the presence of neutral and acidic polysaccharides that contain carboxylic and sulfated groups in proximity to vicinal hydroxyls, but the JC appears much more sulfated, and its acidic component could not be morphologically distinguished from the neutral component (Jondeung and Czihak, 1982).

SeGall and Lennarz (1979) suggested that the polysaccharide component of the JC of sea urchins is made up of a sialoprotein and a fucose sulfate glycoconjugate. In addition to these two components, the JC was shown to contain small peptides (SAP) that are chemoattractant (e.g., resact) and motility activating for sperm (Garbers, 1989; Suzuki, 1990; Hoshino *et al.*, 1992; Harumi *et al.*, 1992; Suzuki and Yoshino, 1992; Yoshino and Suzuki, 1992; Yoshino *et al.*, 1992). Recently, the fucose sulfate glycoconjugate was shown to contain several proteins that, using SAP-1 as cofactor, induce the acrosomal reaction of the sperm, and a fucose sulfate polymer that is responsible for sperm agglutination (Garbers *et al.*, 1983; Yamaguchi *et al.*, 1989; Shimizu *et al.*, 1990; Mikami-Takei *et al.*, 1991).

In the starfish, the JC was demonstrated to contain a large sulfated glycoprotein (ARIS) and a group of steroidal saponins (Co-ARIS), which induce the acrosomal reaction and the degradation of sperm histones: an oligopeptide (SAP) that participates in the induction of the acrosomal reaction and stimulates sperm respiration; and a high-mannose glycoprotein (Uno and Hoshi, 1978; Ikadai and

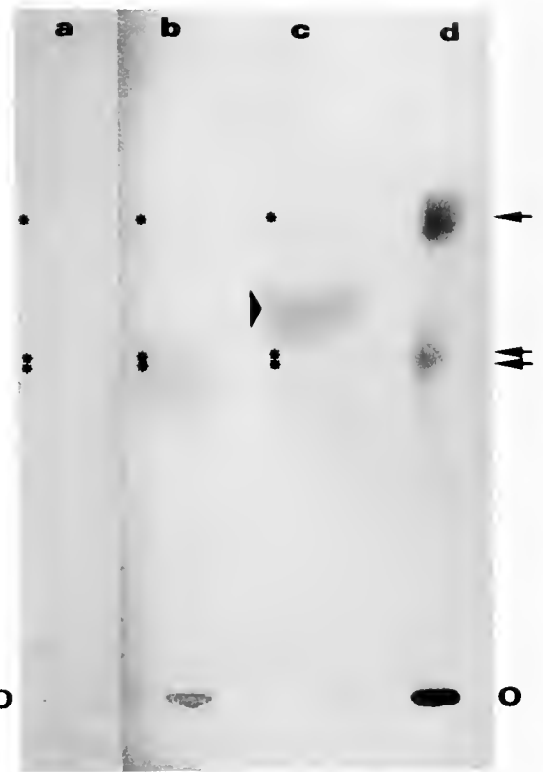


**Figure 15.** Cellulose acetate electrophoresis of GAG-like molecules isolated from total jelly coat after enzymatic digestions (alcian blue staining). (a) Hyaluronidase seems to have digested all bands, because no band appears stained. (b) Chondroitinase ABC seems to have partially digested the band at the origin (O) (because its staining appears decreased) and the intermediary moving band (\*\*), producing a large smear. This enzyme seems to have totally digested the faster moving band (\*), as no band is noticed at that level. (c) Proteinase seems to have attacked all bands, since no band appears stained. The band (arrowhead) that appears between the intermediary (\*\*) and faster (\*) moving bands may represent residual GAG-like materials liberated from the digested bands. (d) Total jelly coat under the same conditions but without enzymatic treatment (O, band at the origin; double arrow, intermediary moving band; arrow, faster moving band).

Hoshi, 1981a, 1981b; Matsui *et al.*, 1986a, 1986b; Endo *et al.*, 1987; Nishiyama *et al.*, 1987a, 1987b; Hoshi *et al.*, 1990a, 1990b; Amano *et al.*, 1992).

Although GAGs are known components of the cumulus of mammalian oocytes, they have not yet been reported in the jelly layer of echinoderm oocytes. Alcian blue, which is known to selectively precipitate GAGs (Reale *et al.*, 1986), specifically stained the outer region and some fibrillar extensions of the JC of *M. glacialis* oocytes (Sousa and Azevedo, 1988) as well as some high molecular weight components extracted from it (Sousa *et al.*, 1992). Based on these results and on the present histochemical experiments on ovary sections, GAGs were isolated from the JC of *M. glacialis* oocytes and qualitatively analyzed by cellulose acetate electrophoresis under different conditions. Taking into consideration the relative migration

rate of these materials and of standard GAGs, as well as their sensitivities to chondroitinase ABC and hyaluronidase digestions, it is possible to suggest that the JC may contain GAG-like molecules that bear some resemblance to chondroitin sulfate, heparan sulfate, and hyaluronic acid. Quantitative experiments are being performed to confirm these findings.

### Acknowledgments

This work was partially supported by CME-INIC and Fund. Eng. A. Almeida. We thank Mr. Vítor Oliveira for technical help and Mr. João Carvalheiro for the iconographic work.

### Literature Cited

- Amano, T., Y. Okita, and M. Hoshi. 1992. Treatment of starfish sperm with egg jelly induces the degradation of histones. *Dev. Growth Differ* 34: 99–106.
- Cowman, M. K., E. A. Balazs, C. W. Bergmann, and K. Meyer. 1981. Preparation and circular dichroism analysis of sodium hyaluronate oligosaccharides and chondroitin. *Biochemistry* 20: 1379–1385.
- Delgado, M. V., and L. C. Zoller. 1987. A quantitative and qualitative cytochemical analysis of glycosaminoglycan content in the zona pellucida of hamster ovarian follicles. *Histochemistry* 87: 279–287.
- Endo, T., M. Hoshi, S. Endo, Y. Arata, and A. Kobata. 1987. Structures of the sugar chains of a major glycoprotein present in the egg jelly coat of a starfish, *Asterias amurensis*. *Arch. Biochem. Biophys.* 252: 105–112.
- Ganter, P., and G. Jollès. 1969. *Histochimie Normale et Pathologique*. Vol. 1. Gauthier-Villars, Paris.
- Ganter, P., and G. Jollès. 1970. *Histochimie Normale et Pathologique*. Vol. 2. Gauthier-Villars, Paris.
- Garbers, D. L. 1989. Molecular basis of signalling in the spermatozoon. *J. Androl.* 10: 99–107.
- Garbers, D. L., G. S. Kopf, D. J. Tubb, and G. Olson. 1983. Elevation of sperm 3':5'-monophosphate concentrations by a fucose-sulfate-rich complex associated with eggs: I. structural characterization. *Biol. Reprod.* 29: 1211–1220.
- Grimek, H. J., and R. L. Ax. 1982. Chromatographic comparison of chondroitin-containing proteoglycan from small and large bovine ovarian follicles. *Biochem. Biophys. Res. Commun.* 104: 1401–1406.
- Harumi, T., K. Hoshino, and N. Suzuki. 1992. Effects of sperm-activating peptide 1 on *Hemicentrotus pulcherrimus* spermatozoa in high potassium sea water. *Dev. Growth Differ.* 34: 163–172.
- Hata, R., and Y. Nagai. 1972. A rapid and micro method for separation of acidic glycosaminoglycans by two-dimensional electrophoresis. *Anal. Biochem.* 45: 462–468.
- Heinegard, D., and Y. Sommarin. 1987. Isolation and characterization of proteoglycans. *Methods Enzymol.* 144: 319–372.
- Hoshi, M., T. Amano, Y. Okita, T. Okinaga, and T. Matsui. 1990a. Egg signals for triggering the acrosome reaction in starfish spermatozoa. *J. Reprod. Fert. Suppl.* 42: 23–31.
- Hoshi, M., T. Amano, Y. Okita, T. Okinaga, and T. Matsui. 1990b. Induction of the acrosome reaction in starfish. Pp. 239–252 in *Mechanism of Fertilization. Plants to Humans*, B. Dale, ed. NATO ASI Series, Series H: Cell Biology, Vol. 45. Springer-Verlag, Berlin.
- Hoshino, K., T. Shimizu, Y. Sendai, T. Harumi, and N. Suzuki. 1992. Differential effects of the egg jelly molecules FSG and SAP-I on elevation of intracellular  $Ca^{2+}$  and pH in sea urchin spermatozoa. *Dev. Growth Differ* 34: 403–411.
- Huey, G., A. Moiin, and R. Stern. 1990. Levels of [ $^3H$ ]glucosamine incorporation into hyaluronic acid by fibroblasts is modulated by culture conditions. *Matrix* 10: 75–83.
- Ikadaï, H., and M. Hoshi. 1981a. Biochemical studies on the acrosome reaction of the starfish, *Asterias amurensis*. I. Factors participating in the acrosome reaction. *Dev. Growth Differ* 23: 73–80.
- Ikadaï, H., and M. Hoshi. 1981b. Biochemical studies on the acrosome reaction of the starfish, *Asterias amurensis*. II. Purification and characterization of acrosome reaction-inducing substance. *Dev. Growth Differ.* 23: 81–88.
- Jondeung, A., and G. Czihak. 1982. Histochemical studies of jelly coat of sea-urchin eggs during oogenesis. *Histochemistry* 76: 123–136.
- Kudo, S. 1982. Ultrastructure and ultracytochemistry of fertilization envelope formation in the carp egg. *Dev. Growth Differ.* 24: 327–339.
- Lev, R., and S. S. Spicer. 1964. Specific staining of sulphate groups with alcian blue at low pH. *J. Histochem. Cytochem.* 12: 309.
- Lowry, O. H., N. J. Rosebrough, A. L. Farr, and R. J. Randall. 1951. Protein measurement with the folin reagent. *J. Biol. Chem.* 193: 265–275.
- Matsui, T., I. Nishiyama, A. Hino, and M. Hoshi. 1986a. Induction of the acrosome reaction in starfish. *Dev. Growth Differ.* 28: 339–348.
- Matsui, T., I. Nishiyama, A. Hino, and M. Hoshi. 1986b. Acrosome reaction-inducing substance purified from the egg jelly inhibits the jelly-induced acrosome reaction in starfish: an apparent contradiction. *Dev. Growth Differ.* 28: 349–357.
- Meijer, L., P. Pondaven, P. Guerrier, and M. Moreau. 1984. A starfish oocyte user's guide. *Can. Biol. Mar.* 45: 457–480.
- Mikami-Takei, K., M. Kosakai, M. Isemura, T. Suyemitsu, K. Ishihara, and K. Schmid. 1991. Fractionation of jelly substance of the sea urchin egg and biological activities to induce acrosome reaction and agglutination of spermatozoa. *Exp. Cell Res.* 192: 82–86.
- Miller, D. J., and R. L. Ax. 1990. Carbohydrates and fertilization in animals. *Mol. Reprod. Dev.* 26: 184–198.
- Min, H., and M. K. Cowman. 1986. Combined alcian blue and silver staining of glycosaminoglycans in polyacrylamide gels: application to electrophoretic analysis of molecular weight distribution. *Anal. Biochem.* 155: 275–285.
- Nishiyama, I., T. Matsui, and M. Hoshi. 1987a. Purification of Co-ARIS, a cofactor for acrosome-inducing substance, from the egg jelly of starfish. *Dev. Growth Differ.* 29: 161–169.
- Nishiyama, I., T. Matsui, Y. Fujimoto, N. Ikekawa, and M. Hoshi. 1987b. Correlation between the molecular structure and the biological activity of Co-ARIS, a cofactor for acrosome reaction-inducing substance. *Dev. Growth Differ.* 29: 171–176.
- Pearse, A. G. E. 1968. *Histochemistry, Theoretical and Applied*. Vols. 1 and 2. J. A. Churchill, London.
- Rambourg, A. 1971. Morphological and histochemical aspects of glycoproteins at the surface of animal cells. *Int. Rev. Cytol.* 31: 57–114.
- Reale, E., L. Luciano, and M. Spitznas. 1986. Histochemical demonstration of hyaluronic acid molecules by alcian blue. *Histochem. J.* 18: 306–316.
- Scott, J. E. 1985. Proteoglycan histochemistry—a valuable tool for connective tissue biochemists. *Collagen Res. Rel.* 5: 541–575.
- Scott, J. E., and J. Dorling. 1965. Differential staining of acid glycosaminoglycans (mucopolysaccharides) by alcian blue in salt solutions. *Histochemie* 5: 221–233.
- SeGall, G. K., and W. J. Lennarz. 1979. Chemical characterization of the component of the jelly coat from sea urchin eggs responsible for induction of the acrosome reaction. *Dev. Biol.* 71: 33–48.
- Shimizu, T., H. Kinoh, M. Yamaguchi, and N. Suzuki. 1990. Purification and characterization of the egg jelly macromolecules, sialo-

- glycoprotein and fucose sulfate glycoconjugate, of the sea urchin *Hemicentrotus pulcherrimus*. *Dev. Growth Differ.* **32**: 473-487.
- Sousa, M., and C. Azevedo. 1988. Ultrastructural and histochemical observations of the cortical reaction in *Marthasterias glacialis* (Echinodermata, Asteroidea). *J. Submicrosc. Cytol. Pathol.* **20**: 629-633.
- Sousa, M., P. Moradas-Ferreira, and C. Azevedo. 1992. Presence of a trypsin-like protease in starfish sperm acrosome. *J. Exp. Zool.* **261**: 349-354.
- Spicer, S. S. 1965. Diamine methods for differentiating mucosubstances histochemically. *J. Histochem. Cytochem.* **13**: 211-234.
- Suzuki, N. 1990. Structure and function of egg-associated peptides of sea urchins. Pp. 271-286 in *Mechanism of Fertilization: Plants to Humans*, B. Dale, ed., NATO ASI Series, Series H: Cell Biology, Vol. 45, Springer-Verlag, Berlin.
- Suzuki, N., and K.-I. Yoshino. 1992. The relationship between amino acid sequences of sperm-activating peptides and the taxonomy of echinoids. *Comp. Biochem. Physiol.* **102B**: 679-690.
- Turner, R. E., and M. K. Cowman. 1985. Cationic dye binding by hyaluronate fragments: dependence on hyaluronate chain length. *Arch. Biochem. Biophys.* **237**: 253-260.
- Uno, Y., and M. Hoshi. 1978. Separation of the sperm agglutinin and the acrosome reaction-inducing substance in egg jelly of starfish. *Science* **200**: 58-59.
- Wall, R. S., and T. J. Gyi. 1988. Alcian blue staining of proteoglycans in polyacrylamide gels using the critical electrolyte concentration approach. *Anal. Biochem.* **175**: 298-299.
- Whiteman, P. D. 1972. A new method for the determination of acid glycosaminoglycans in urine. *Biochem. J.* **127**: 87-88.
- Whiteman, P. 1973a. The quantitative measurement of alcian blue-glycosaminoglycan complexes. *Biochem. J.* **131**: 343-350.
- Whiteman, P. 1973b. The quantitative determination of glycosaminoglycans in urine with alcian blue 8GX. *Biochem. J.* **131**: 351-357.
- Whiteman, P., and H. Henderson. 1977. A method for the determination of amniotic-fluid glycosaminoglycans and its application to the prenatal diagnosis of Hurler and SanFilippo diseases. *Clin. Chim. Acta* **79**: 99-105.
- Yamaguchi, M., M. Kurita, and N. Suzuki. 1989. Induction of the acrosome reaction of *Hemicentrotus pulcherrimus* spermatozoa by the egg jelly molecules, fucose-rich glycoconjugate and sperm-activating peptide I. *Dev. Growth Differ.* **31**: 233-239.
- Yanagishita, M., D. Rodbard, and V. C. Hascall. 1979. Isolation and characterization of proteoglycans from porcine ovarian follicular fluid. *J. Biol. Chem.* **254**: 911-920.
- Yoshino, K.-I., and N. Suzuki. 1992. Two classes of receptor specific for sperm-activating peptide III in sand-dollar spermatozoa. *Eur. J. Biochem.* **206**: 887-893.
- Yoshino, K.-I., T. Takao, Y. Shimonishi, and N. Suzuki. 1992. Sperm-activating peptide type-V (SAP-V), a fifth member of the sperm-activating peptide family, purified from the egg-conditioned media of the heart urchin *Brissus agassizii*. *Comp. Biochem. Physiol.* **102B**: 691-700.

# Ultrastructural Histochemistry of *Marthasterias glacialis* (Echinodermata, Asteroidea) Gametes Before and After Fertilization

MÁRIO SOUSA\* AND CARLOS AZEVEDO

Laboratory of Cell Biology, Institute of Biomedical Sciences, University of Oporto,  
4000 Porto, Portugal

**Abstract.** The gametes of the starfish *Marthasterias glacialis* were studied, both before and after fertilization, using several histochemical methods at the ultrastructural level. Results showed that the oocyte jelly coat (JC) could be morphologically differentiated into a fibrillar network of acidic polysaccharides, probably containing glycosaminoglycans (GAGs), and a loose component made of neutral polysaccharides that occupies the interstices of the former. Results also suggested that it is the fibrillar component of the JC to which the spermatozoon attaches and reacts. Staining of the acrosomal vesicle contents confirmed that the peripheral dense component attaches the spermatozoon to the JC, whereas the central and apical electron-lucent component coats the acrosomal process as it extends through the oocyte investments. The acrosomal process membrane was also shown to be negatively charged. Staining of cortical vesicles confirmed their tripartite compartmentalization: the spiral lamellae fused with the fertilization envelope (FE), transferring its staining to the inner layer of the FE, whereas the matrix could be subdivided into two components—a fibrillar mesh of acidic polysaccharides that fused with the FE and some amorphous aggregates that seem to become dispersed in the perivitelline space.

## Introduction

The components of the oocyte jelly coat (JC) have not yet been differentiated at the morphological level, despite the importance of this information to the understanding

of sperm-egg interaction. In the sea urchin, a sialoprotein and a fucose sulfate polysaccharide that induces the acrosomal reaction of the sperm have been isolated from the oocyte JC (SeGall and Lennarz, 1979), and morphological studies have confirmed the existence of two main JC polysaccharide components (Kidd, 1978; Jondeung and Czihak, 1982; Bonnell and Chandler, 1990). In the starfishes *Asterias amurensis* and *Asterina pectinifera*, a large sulfated glycoprotein, which induces the acrosomal reaction, and a high-mannose glycoprotein have been isolated from the oocyte JC (Hoshi *et al.*, 1990). At the light microscopical level, we have shown that the oocyte JC of the starfish *Marthasterias glacialis* is morphologically differentiated into two main polysaccharides (Sousa *et al.*, 1993), and here we confirm these findings at the ultrastructural level, showing their precise structure, distribution, and histochemical characteristics.

We have also shown that the acrosomal and cortical vesicles of *M. glacialis* gametes contain distinct morphological components that exhibit different destinies after being exocytosed (Sousa and Azevedo, 1986, 1987, 1988a, 1988b, 1989a, 1989b, 1990). Results of the present study further support the view that the compartmentalization of acrosomal and cortical vesicle contents serves to guide different components to different roles during fertilization.

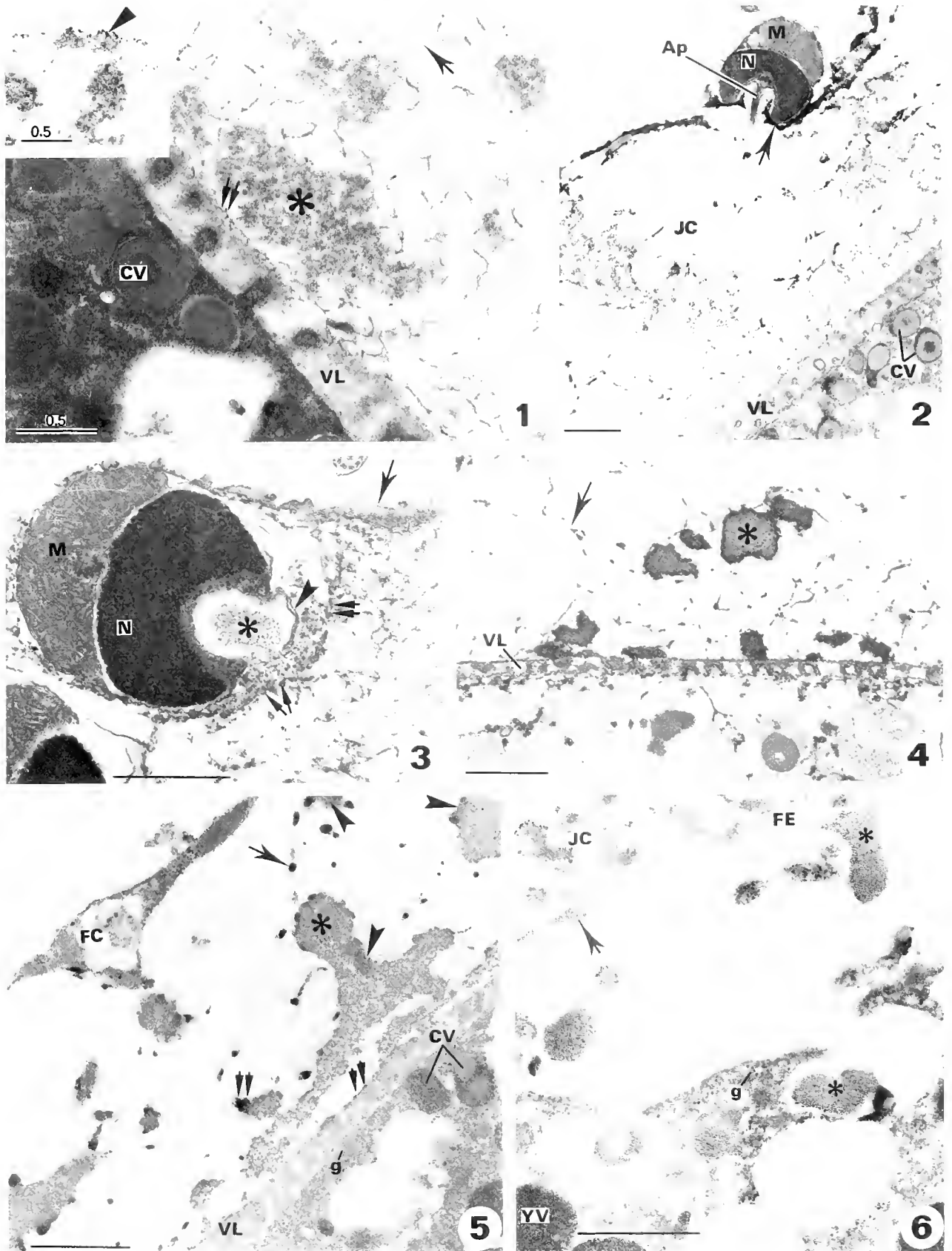
## Materials and Methods

Several specimens of *M. glacialis* were collected in the intertidal zone of the North Atlantic, 30 km north of Oporto, Portugal, and maintained in the laboratory in well-aerated seawater.

Small pieces of ovary and testis, free oocytes and fertilized eggs (Sousa and Azevedo, 1985) were processed for (1) ruthenium red (RR) staining according to Anderson

Received 27 August 1992; accepted 6 July 1993.

\* Address correspondence to this author at the Laboratory of Cell Biology, Institute of Biomedical Sciences, University of Oporto, Lg. Prof. Abel Salazar 2, 4000 Porto, Portugal.



Figures 1-6. Transmission electron micrographs of *Marthasterias glacialis* oocytes with various stains. VL, vitelline layer; CV, cortical vesicles; JC, jelly coat; N, nucleus; M, mitochondrion; YV, yolk vesicles.



(1968); (2) alcian blue (Ab) at pHs 6.9 and 1, with the presence of  $MgCl_2$ , using the staining method of Crawford and Abed (1986); (3) high iron diamine-thiocarbohydrazide-silver proteinate (HID-TCH-SP) sequence according to Spicer *et al.* (1978) and Sannes *et al.* (1979); and (4) cationic cacodylate iron colloid (CCIC) as in Seno *et al.* (1983).

For histochemical studies on grid, the material was fixed in glutaraldehyde made in FSW-Na cacodylate (3:1), pH 7.2, washed, dehydrated, and embedded in Epon. Ultrathin sections were collected on gold grids and stained for (1) tannic acid-uranyl acetate (TA-UA) (Sannes *et al.*, 1978); (2) phosphotungstic acid (PTA)-chromic acid (PTA-CrA) (Rambourg, 1971; Rambourg *et al.*, 1969), PTA-HCl (Weinstock and Leblond, 1971), aqueous PTA (PTA-aq) (Krimmer and Esponda, 1980) and PTA-acetone; (3) periodic acid-thiocarbohydrazide-silver proteinate (PA-TCH-SP) (Thiéry, 1967); (4) periodic acid-silver methenamine (PA-SM) and PA-CrA-SM (Rambourg, 1967; Dawson and Filipe, 1976); (5) CCIC; and (6) HID.

Ultrathin sections were observed in a JEOL 100 CX II transmission electron microscope (TEM) operated at 60 kV.

For scanning electron microscopy (SEM), fixed oocytes were washed in 0.2 M Na-cacodylate pH 7.2, postfixed with 1% osmium tetroxide in the buffer for 2 h at 4°C, dehydrated in ethanol series, critically point dried in carbon dioxide, mounted on specimen stubs with double-coat tape, coated with gold, and examined in a JEOL 35 C SEM.

## Results

In the oocyte JC, RR stained a fibrillar material that delimits both the outer and inner aspects of the JC and spreads between some amorphous aggregates (Fig. 1). With insemination, the amorphous component dissolved, and the exocytosed peripheral dense component of the acrosomal vesicle, now stained by RR, attached the sper-

matozoon to the JC outer border (Fig. 2). Similar results were obtained with Ab pH 7 (Fig. 3). At pH 1, Ab stained the fibrillar component and the periphery of the amorphous aggregates of the JC (Fig. 4). The Thiéry technique stained some globular regions along the fibrillar component of the JC as well as its sites of attachment to the amorphous aggregates and vitelline layer, some regions of the periphery of the amorphous aggregates, and cortical vesicles (Fig. 5). After the cortical reaction, cortical vesicles transferred their staining to the undercoating of the FE (Fig. 6). Silver methenamine labeled the globular and adjacent parts of the fibrillar component of the JC as well as its sites of attachment to the amorphous aggregates and vitelline layer, some portions of the matrix of cortical vesicles (Fig. 7), and the sperm acrosomal vesicle (Fig. 8). With fertilization, no staining was transferred from cortical vesicles to the FE, whereas the stained acrosomal material attached the spermatozoon to the JC and coated the acrosomal process (Fig. 8). TA stained both components of the JC, some regions of the matrix of cortical vesicles, and the peripheral and central electron-lucent component of the acrosomal vesicle (Fig. 9). With fertilization, the stained acrosomal component coated the acrosomal process, and the stained material of cortical vesicles fused with the FE, although without transferring the staining to it (Fig. 10). Similar results were obtained with PTA, although the amorphous component of JC was more difficult to stain, and the acrosomal vesicle did not stain with PTA-HCl and PTA-Aq. No staining was found with the HID and HID-TCH-SP techniques. With the CCIC method, staining was observed only at pH 7. Unreacted oocytes did not show any staining (Fig. 11), but after the cortical reaction some regions of the matrix of cortical vesicles appeared stained, although the labeling was not transferred to the FE (Fig. 12). When applied on grid, CCIC stained the fibrillar component of the JC of unreacted oocytes (Fig. 13).

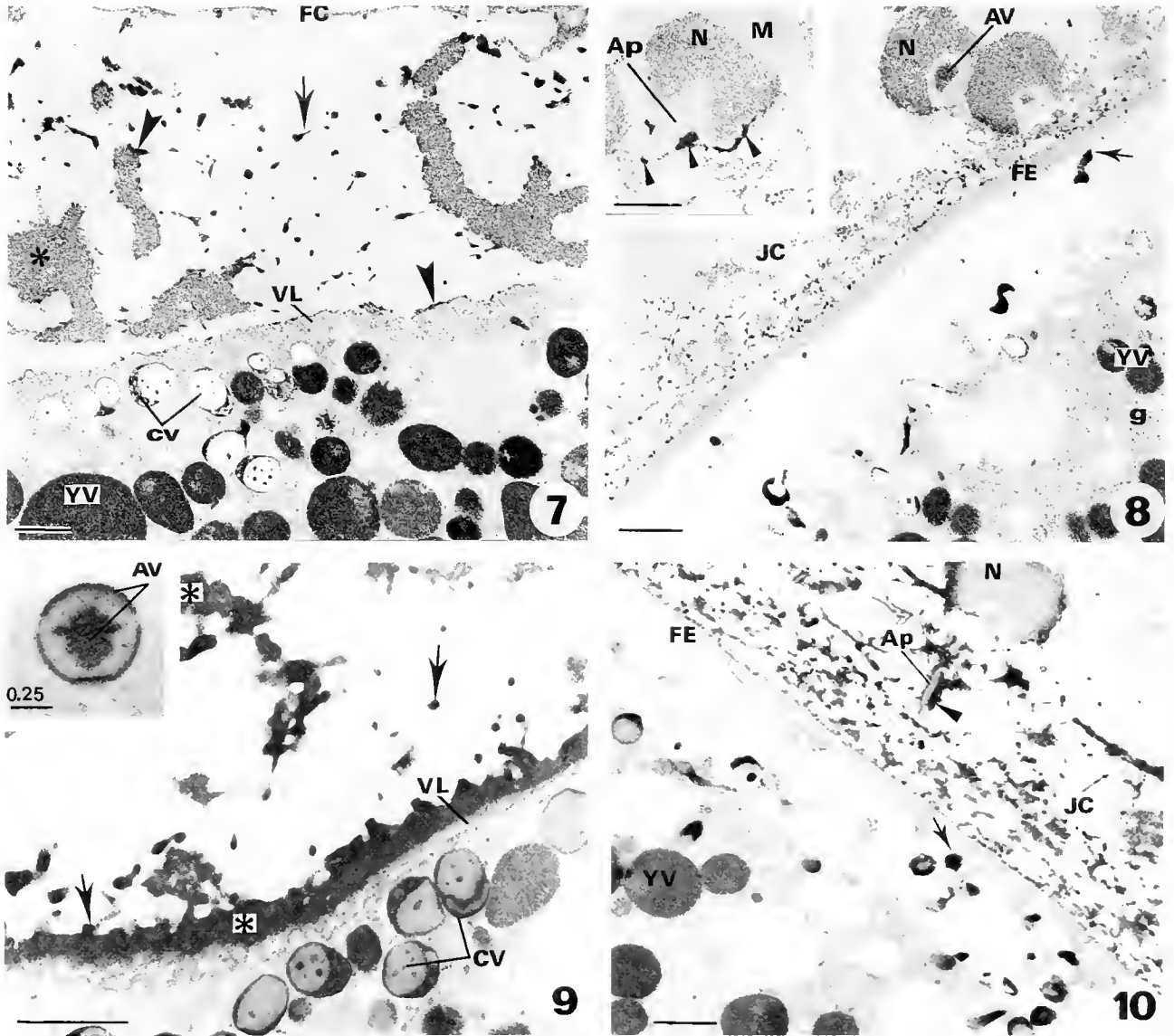
In the spermatozoon, CCIC staining disrupted the plasma membrane, which enabled the label to be found in the periphery of microtubules, in the pericentriolar

**Figures 1-2.** Ruthenium red stain (RR). In the unreacted oocyte (Fig. 1), RR stained a fibrillar material that delimits the outer (arrowhead) and inner (double arrow) regions of the JC and spreads between (arrow) some amorphous aggregates (\*); bar = 0.5  $\mu m$ . At fertilization (Fig. 2), the stained peripheral dense component (arrow) of the acrosomal vesicle attached the spermatozoon to the JC. Ap, acrosomal process; bar = 1  $\mu m$ .

**Figures 3-4.** Alcian blue (Ab) stain; bar = 1  $\mu m$ . At pH 7 (Fig. 3), Ab shows that the spermatozoon reacted over the Ab-stained inner fibrils (double arrows) and not at the large outer stained region (arrow) of the JC fibrillar component. Fused sperm acrosomal and plasma membranes (arrowhead); (\*), precipitated acrosomal contents. At pH 1 (Fig. 4), Ab stained the fibrillar material (arrow) and the periphery of the amorphous (\*) JC components.

**Figures 5-6.** The Thiéry staining technique; bar = 1  $\mu m$ . In the unreacted oocyte (Fig. 5), stain was taken up by some globular regions along the JC fibrillar component (arrow) as well as its sites of attachment (double arrows) to the amorphous aggregates (\*) and VL, some regions at the periphery of the amorphous aggregates (arrowheads), and the CV. FC, follicular cell; g, glycogen. After the cortical reaction (Fig. 6), CV contents (\*) transferred their stain to the undercoat (arrow) of the fertilization envelope (FE).





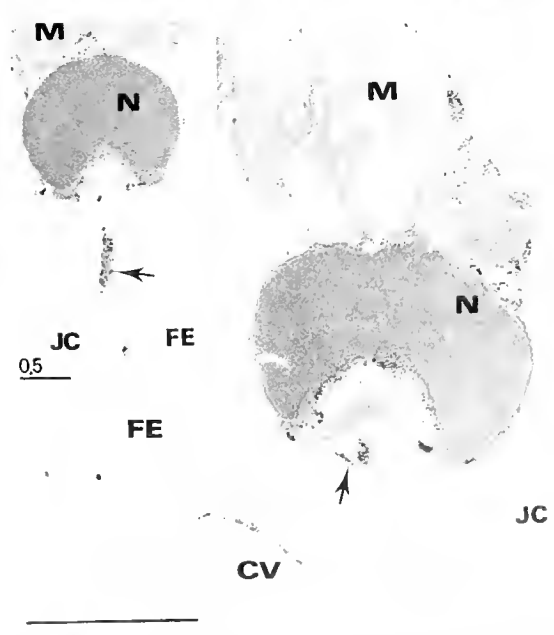
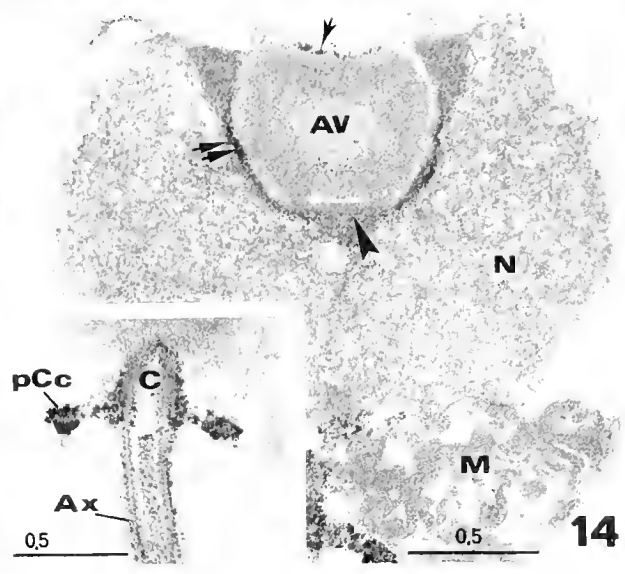
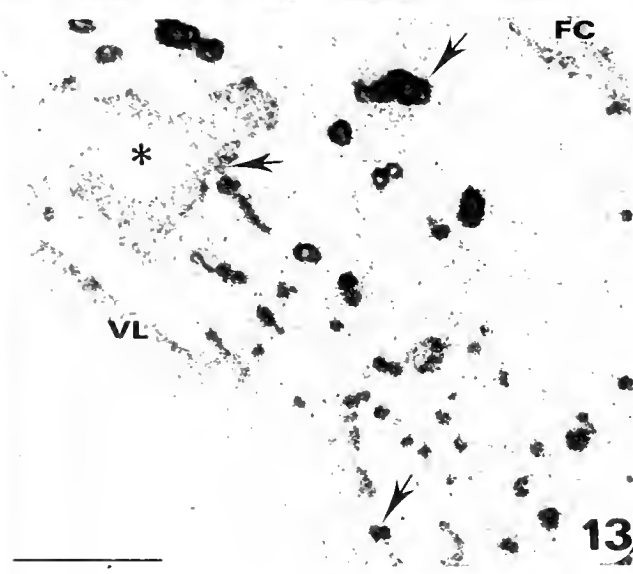
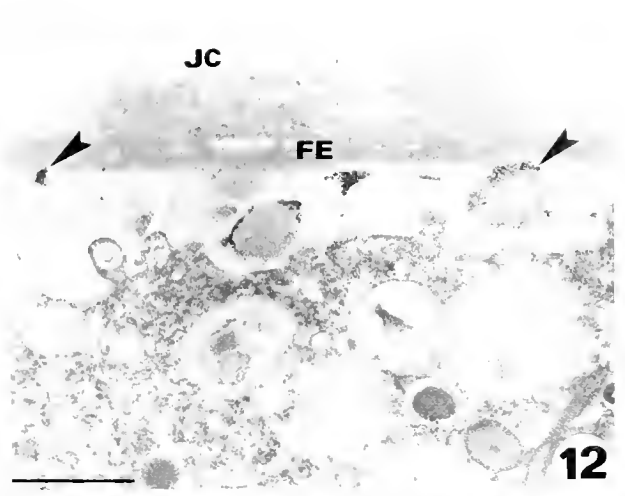
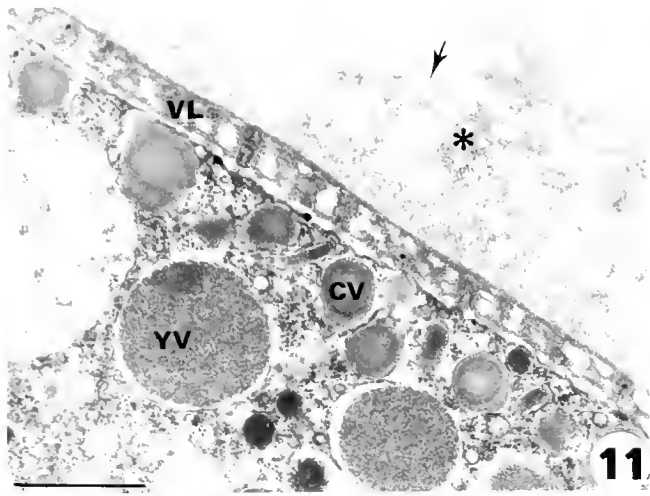
**Figures 7–10.** Transmission electron micrographs of *Marthasterius glacialis* oocytes with various stains. VL, vitelline layer; CV, cortical vesicles; JC, jelly coat; YV, yolk vesicles; N, nucleus; M, mitochondrion; Ap, acrosomal process; FE, fertilization envelope.

**Figures 7–8.** Periodic acid-silver methenamine (PA-SM) stain; bar = 1  $\mu\text{m}$ . In the unreacted oocyte (Fig. 7), stain was taken up by the globular and adjacent parts of the JC fibrillar component (arrow), as well as by its sites of attachment (arrowheads) to the amorphous aggregates (\*) and VL, and by some portions of CV. With fertilization (Fig. 8), no stain was transferred from the CV (arrow) to the FE, whereas the stained acrosomal contents (AV) attached the sperm to the JC and coated the Ap (arrowheads); g, glycogen.

**Figures 9–10.** Tannic acid-uranyl acetate (TA-UA) stain; bar = 1  $\mu\text{m}$ . In the unreacted oocyte (Fig. 9), TA-UA stained the fibrillar (arrows) and amorphous (\*) JC components, some portions of the CV, and the acrosomal vesicle (AV) peripheral and central electron-lucent components. Inset = 0.25  $\mu\text{m}$ . With fertilization (Fig. 10), the AV components (arrowhead) coated the Ap, whereas the component of the CV (arrow) fused with the FE without transferring any staining to it.

complex, and in the acrosome (Fig. 14). The label on intact plasma membrane was minimal, but after the acrosomal reaction the membrane of the acrosomal process appeared intensely labeled (Fig. 15).

When observed by SEM, the JC appeared as a complex network of fibrillar materials with different thicknesses, which probably correspond to the fibrillar component observed by TEM (Fig. 16).



15

Figures 11-15. Transmission electron micrographs of *Marthasterus glacialis* oocytes and spermatozoa stained with cationic cacodylate iron colloid (CCIC) pH 7. VL, vitelline layer; CV, cortical vesicles; JC, jelly coat; YV, yolk vesicles; N, nucleus; M, mitochondrion; FE, fertilization envelope; bar = 1 μm; insets = 0.5 μm.

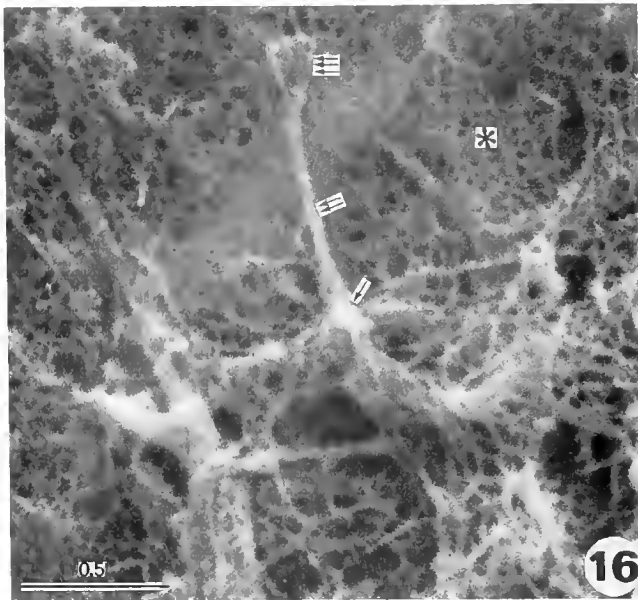


**Figure 16.** When observed by scanning electron microscopy, the jelly coat was seen to be formed by large dense fibrous structures that progressively branched (arrow to triple arrow) to give origin to the inner fine fibrillar network (\*). Bar = 0.5  $\mu$ m.

### Discussion

Despite the intensive biochemical characterization of the echinoderm JC, the differentiation of its components at the ultrastructural level is not well known. In the sea urchin, RR staining distinguished between amorphous and fibrillar components (Kidd, 1978), and Bonnell and Chandler (1990) demonstrated, by platinum replicas, that the fibrillar material corresponded to the fucose-sulfate-rich polysaccharide responsible for inducing the acrosomal reaction of the spermatozoon (SeGall and Lennarz, 1979).

In the present study, RR and Ab stained a fibrillar material in the JC of *M. glacialis* oocytes; this material forms a branched matrix all around the oocyte and contains amorphous aggregates between its interstices. At fertilization, the spermatozoon bound and reacted over the fibrillar material, whereas the amorphous aggregates dissolved as the acrosomal process penetrated the jelly layer.

RR is known to precipitate GAGs, acidic polysaccharides, and polypeptides, but not neutral polysaccharides (Luft, 1966), whereas at neutral pH and in the presence of  $MgCl_2$ , Ab selectively stains GAGs (Reale *et al.*, 1986). Thus the amorphous aggregates probably correspond to neutral polysaccharides and the fibrillar component to acidic polysaccharides, with the possibility that this latter material may contain GAGs. The acidic nature of the fibrillar material was also demonstrated by the presence of surface negative charges, as shown by CCIC staining and by the fact that it bound calcium (Sousa and Azevedo, 1989b). TA and PTA techniques for complex carbohydrates stained both JC components. The absence of staining with HID argues against the presence of sulfated groups in the JC, but this result can also be due to the masking or inaccessibility of those groups. Staining with the Thiéry and silver methenamine techniques for acid glycoproteins showed a more complex composition of both JC components, because only some regions appeared stained. Although fixation and dehydration is likely to lead to artifacts such as shrinkage and solubilization of material and the jelly structure could have been altered during these processes, the effects might have been lessened by RR and Ab stainings. Therefore, the fibrillar and amorphous components of the JC can be assumed to correspond to the major structural components of the jelly layer. In conclusion, results showed that the JC of the starfish oocyte can be morphologically differentiated into two main polysaccharides, thus confirming the previous light microscopical and biochemical (Hoshi *et al.*, 1990; Sousa *et al.*, 1993) findings. The putative existence of GAGs in the JC of *M. glacialis* oocytes is further confirmed in Sousa *et al.* (1993).

In *M. glacialis*, the acrosomal vesicle of the spermatozoon contains ATPase and calcium in the peripheral dense component, and acid and alkaline phosphatases in the central and apical electron-lucent component (Sousa and Azevedo, 1986, 1988a, 1989b). In the present work, this differentiation was further confirmed because RR, Ab, and PA-SM stained the peripheral dense component, which bound the sperm to the JC, whereas TA, PTA, and PA-SM stained the central and peripheral electron-lucent component, which coated the acrosomal process. Simi-

**Figure 11.** The unreacted oocyte did not show any staining in the fibrillar (arrow) and amorphous (\*) JC components.

**Figure 12.** After cortical reaction, some regions of the CV appeared stained (arrowheads), although the labeling was not transferred to the FE.

**Figure 13.** On-grid staining of oocytes labeled the fibrillar (arrows) JC component. FC, follicular cell.

**Figure 14.** In the unreacted sperm, leaked plasma membranes allowed staining of the periphery of microtubules of centrioles (C) and axoneme (Ax), the pericentriolar complex (pCc), the acrosomal-plasma membrane contact zone (arrow), the basolateral periacrosomal material (double arrow), and the inner acrosomal vesicle (AV) membrane (arrowhead).

**Figure 15.** After the acrosomal reaction, the acrosomal process membrane appeared labeled (arrow).

larly, the oocyte cortical vesicles have also been compartmentalized into spiral lamellae, which contain peroxidase activity, and a matrix that was further subdivided into a mesh-like structure that stains with RR, Ab, and AgNO<sub>3</sub> as well as for acid and alkaline phosphatase activities, and contains amorphous aggregates within its holes (Sousa and Azevedo, 1987, 1988b, 1989a, 1990). Although both the mesh-like component and the spiral lamellae fuse with the FE, only the staining carried by the latter is transferred to the inner layer of the FE. Our present results confirmed this tripartite structural and functional nature of cortical vesicles, with acidic polysaccharides and negative charges found to be concentrated in the mesh-like component.

### Acknowledgments

This work was partially supported by CME-INIC and Fund. Eng. A. Almeida. We thank Mr. João Carvalheiro for the iconographic work.

### Literature Cited

- Anderson, W. A. 1968. Cytochemistry of sea urchin gametes. II. Ruthenium red staining of gamete membranes of sea urchins. *J. Ultrastruct. Res.* **24**: 322-333.
- Bonnell, B., and D. Chandler. 1990. Visualization of the *Lytechinus pictus* egg jelly coat in platinum replicas. *J. Struct. Biol.* **105**: 123-132.
- Crawford, B., and M. Abed. 1986. Ultrastructural aspects of the surface coatings of eggs and larvae of the starfish, *Pisaster ochraceus*, revealed by alcian blue. *J. Morphol.* **187**: 23-37.
- Dawson, P. A., and M. I. Filipe. 1976. An ultrastructural application of silver methenamine to the study of mucin changes in the colonic mucosa adjacent to and remote from carcinoma. *Histochem. J.* **8**: 143-158.
- Hoshi, M., T. Amano, Y. Okita, T. Okinaga, and T. Matsui. 1990. Egg signals for triggering the acrosome reaction in starfish spermatozoa. *J. Reprod. Fert. Suppl.* **42**: 23-31.
- Jondeung, A., and G. Cizhak. 1982. Histochemical studies of jelly coat of sea urchin eggs during oogenesis. *Histochemistry* **76**: 123-136.
- Kidd, P. 1978. The jelly and vitelline coats of the sea urchin egg: new ultrastructural features. *J. Ultrastruct. Res.* **64**: 204-215.
- Krimer, D. B., and P. Esponda. 1980. Presence of polysaccharides and proteins in the chromatoid body of mouse spermatids. *Cell Biol. Int. Rep.* **4**: 265-270.
- Luft, J. H. 1966. Fine structure of capillary and endocapillary layer as revealed by ruthenium red. *Fed. Proc.* **25**: 1773-1783.
- Rambourg, A. 1967. An improved silver methenamine technique for the detection of periodic acid-reactive complex carbohydrates with the electron microscope. *J. Histochem. Cytochem.* **15**: 409-412.
- Rambourg, A. 1971. Morphological and histochemical aspects of glycoproteins at the surface of animal cells. *Int. Rev. Cytol.* **31**: 57-114.
- Rambourg, A., W. Hernandez, and C. P. Leblond. 1969. Detection of complex carbohydrates in the Golgi apparatus of rat cells. *J. Cell Biol.* **40**: 395-414.
- Reale, E., L. Luciano, and M. Spitznas. 1986. Histochemical demonstration of hyaluronic acid molecules by alcian blue. *Histochem. J.* **18**: 306-316.
- Sannes, P. L., T. Katsuyama, and S. S. Spicer. 1978. Tannic acid-metal salt sequences for light and electron microscopic localization of complex carbohydrates. *J. Histochem. Cytochem.* **26**: 55-61.
- Sannes, P. L., S. S. Spicer, and T. Katsuyama. 1979. Ultrastructural localization of sulfated complex carbohydrates with a modified iron diamine procedure. *J. Histochem. Cytochem.* **27**: 1108-1111.
- SeGall, G. K., and W. J. Lennarz. 1979. Chemical characterization of the component of the jelly coat from sea urchin eggs responsible for induction of the acrosome reaction. *Dev. Biol.* **71**: 33-48.
- Seno, S., T. Tsujii, and S. Ukita. 1983. Cationic cacodylate iron colloid for the detection of anionic sites on cell surface and the histochemical stain of acid mucopolysaccharides. *Histochemistry* **78**: 27-31.
- Sousa, M., and C. Azevedo. 1985. Acrosomal reaction and early events at fertilization in *Marthasterias glacialis* (Echinodermata: Asteroidea). *Gamete Res.* **11**: 157-167.
- Sousa, M., and C. Azevedo. 1986. Cytochemical study on the spermatozoon and at early fertilization in *Marthasterias glacialis* (Echinodermata, Asteroidea). *Biol. Cell* **56**: 79-84.
- Sousa, M., and C. Azevedo. 1987. Silver staining of the cortical reaction in oocytes of *Marthasterias glacialis* (Echinodermata, Asteroidea). *Can. J. Zool.* **65**: 2607-2611.
- Sousa, M., and C. Azevedo. 1988a. Presence of ATPase and alkaline phosphatase activities in the starfish acrosome. *Cell Biol. Int. Rep.* **12**: 1049-1054.
- Sousa, M., and C. Azevedo. 1988b. Ultrastructural and histochemical observations of the cortical reaction in *Marthasterias glacialis* (Echinodermata, Asteroidea). *J. Submicrosc. Cytol. Pathol.* **20**: 629-633.
- Sousa, M., and C. Azevedo. 1989a. Starfish sperm-oocyte jelly binding triggers functional changes in cortical granules: a study using acid phosphatase and ruthenium red ultrastructural histochemistry. *Histochemistry* **90**: 353-357.
- Sousa, M., and C. Azevedo. 1989b. Ultrastructural localization of calcium in the acrosome and jelly coat of starfish gametes. *Dev. Growth Differ.* **31**: 227-232.
- Sousa, M., and C. Azevedo. 1990. Alkaline phosphatase and peroxidase activities in starfish cortical vesicles before and after cortical reaction. *J. Submicrosc. Cytol. Pathol.* **22**: 97-102.
- Sousa, M., R. Pinto, P. Moradas-Ferreira, and C. Azevedo. 1993. Histochemical studies of jelly coat of *Marthasterias glacialis* (Echinodermata, Asteroidea) oocytes. *Biol. Bull.* **185**: 215-224.
- Spicer, S. S., J. H. Hardin, and M. E. Setser. 1978. Ultrastructural visualization of sulphated complex carbohydrates in blood and epithelial cells with the high iron diamine procedure. *Histochem. J.* **10**: 435-452.
- Thiery, J.-P. 1967. Mise en évidence des polysaccharides sur coupes fines en microscopie électronique. *J. Microsc.* **6**: 987-1018.
- Weinstock, A., and C. P. Leblond. 1971. Elaboration of the matrix glycoprotein of enamel by the secretory ameloblasts of the rat incisor as revealed by radioautography after galactose-<sup>3</sup>H injection. *J. Cell Biol.* **51**: 26-51.

## Abundance of Food Affects Relative Size of Larval and Postlarval Structures of a Molluscan Veliger

R. R. STRATHMANN<sup>1</sup>, L. FENAUX<sup>2</sup>, A. T. SEWELL<sup>1</sup>, AND M. F. STRATHMANN<sup>1</sup>

<sup>1</sup>Friday Harbor Laboratories, University of Washington, 620 University Road, Friday Harbor, Washington 98250 and <sup>2</sup>Observatoire des Sciences de la Mer, CNRS, URA 716, Université Paris VI-INSU-CNRS, 06230 Villefranche-sur-Mer, France

**Abstract.** Veliger larvae of mollusks were predicted to develop a larger velum relative to the larval shell when reared with scarce food. The functional consequences of such developmental plasticity would be (1) greater maximum capacity for capturing particles when food is scarce and (2) greater growth of structures retained in the postlarva when food is abundant. The hypothesis was tested by rearing veligers of the oyster *Crassostrea gigas* at high (near satiating) and low (growth limiting) concentrations of food. Veligers at the measured shell lengths (>200  $\mu\text{m}$ ) had significantly larger velar lobes and longer prototrochal cilia than veligers reared in low concentrations of food. An analogous response to food levels (relatively longer ciliated band when food is scarce) has now been found for larvae as disparate as oyster veligers and sea urchin plutei. These observations suggest that functionally similar examples of developmental plasticity in the growth of larval parts have evolved more than once and may be widespread. An alternative interpretation is that differential mortality or growth in a genetically heterogeneous batch of oyster larvae results in advanced veligers of different forms at different concentrations of food. Both interpretations suggest an adaptive advantage to growing a larger apparatus for clearing particles from suspension when food is scarce and shifting materials to growth of postlarval structures (shell and associated structures) when food is abundant.

### Introduction

The bodies of many larvae are divided into (1) those parts that are useful at settlement or are retained through

metamorphosis and (2) ephemeral larval parts that are not needed for settling and are resorbed at metamorphosis. The ephemeral parts commonly are structures for feeding or defense during a planktonic larval period. Structures for suspension feeding constitute a major part of the ephemeral larval body of many larval forms (Strathmann, 1978; McEdward, 1984; Nielsen, 1987). These structures provide a high maximum clearance rate (Strathmann, 1987b), which is the rate at which a volume of water is cleared of suspended food particles. When suitable food is scarce, a suspension-feeding larva requires a high clearance rate to obtain sufficient nutrition for rapid growth and development. When food is abundant, however, and a high clearance rate would accumulate more food than could be digested, larvae behaviorally reduce their clearance rates or reject many of the captured particles (Strathmann, 1987b). Thus when food is abundant, larvae have a greater capacity for clearing particles from suspension than is needed.

These observations indicate different functional requirements for adaptation of larvae to high or low concentrations of food. When food is scarce, nutritional intake depends on a high clearance rate, and development of a large ephemeral apparatus for capturing particles is advantageous. When food is abundant, such a large ephemeral apparatus is superfluous, and growth should instead be allocated to other structures: those for digestion of food, those for storage of nutrients, or those that will become useful at or after settlement (Strathmann *et al.*, 1992). Because larvae within a population may encounter greatly different concentrations of food, an invariant type of larval development would result in either disadvantageously low clearance rates when food is scarce or an inefficient diversion of growth to unused ephemeral structures when

food is abundant. One solution to this functional problem is developmental plasticity.

Developmental plasticity of this kind is known for the echinoplutei of sea urchins. These larvae grow longer larval arms when food is scarce and shorter arms when food is abundant. The maximum clearance rate depends on the length of the ciliary band (Strathmann, 1987b; Hart, 1991), and longer arms bear longer ciliary bands. Also, when food is abundant, the development of rudiments of postlarval structures is accelerated relative to the external larval body (Boidron-Metairon, 1988; Hart and Scheibling, 1988; Strathmann *et al.*, 1992). These observations on echinoplutei led to the hypothesis that allocation of materials to structures used for larval feeding, as opposed to structures used at or after settlement, depends on the amount of suitable food available to larvae; but we know of no reports of this kind of developmental plasticity in other suspension-feeding larvae.

To test the generality of the above hypothesis, we have studied a larva of different form, feeding mechanism, and phylum, but with a similar functional problem. The veliger larvae of mollusks capture particles by different physical mechanisms than those used by the larvae of echinoderms (Strathmann, 1987b; Gallagher, 1988). Mollusks and echinoderms are distantly related phyla, representing the spiralian and deuterostome lineages. Both molluscan veligers and echinoid plutei have ephemeral structures bearing ciliary bands that capture particles, and both have structures that endure through metamorphosis. In echinoplutei, the ciliary band and arms are only larval, but the echinus rudiment persists through metamorphosis. In veligers, the ciliary bands and velar lobes are ephemeral, but the shell and much of the remaining body persist through metamorphosis. We examined veligers of the oyster *Crassostrea gigas* for developmental plasticity of velar size relative to shell size.

### Materials and Methods

Embryos were obtained from a spawning of nine female and two male oysters conditioned at 18°C at the Westcott Bay Sea Farm, which is north of Puget Sound at the north end of San Juan Island. Larvae were reared at the Friday Harbor Laboratories.

Embryos and larvae were maintained in jars, each containing 2 l of seawater that had been filtered through a 0.45  $\mu\text{m}$  membrane filter. The initial concentration of D-stage larvae at first feeding was 1.1  $\text{ml}^{-1}$ . Cultures were stirred mechanically by paddles pulled at 10 strokes  $\text{min}^{-1}$  (Strathmann, 1987a). The jars were maintained at 20.5 to 23.5°C, except when the water was changed every two days; the new water was briefly 17 to 20°C, and at least once was as low as 15°C.

At every water change, equal numbers of cells of the algae *Isochrysis galbana* (T-ISO) and *Chaetoceros calcitrans* were added to make a total concentration of 3000 cells  $\text{ml}^{-1}$  for low food levels and 30,000 cells  $\text{ml}^{-1}$  for high food levels. There were three replicate jars for each food treatment. The algal species and concentrations were selected on the basis of previous studies. *C. calcitrans* is superior to *I. galbana* as a food for the larvae of *C. gigas* (Waldock and Nascimento, 1979), but both support growth. Sprung (1984) found growth of veligers of *Mytilus edulis* fed *I. galbana* to be maximal at concentrations of 30,000 cells  $\text{ml}^{-1}$  and lower than the maximum at concentrations of 3000 cells  $\text{ml}^{-1}$ . Maximal growth of veligers of *Crassostrea virginica* required additions of algal food to more than 100,000 cells  $\text{ml}^{-1}$  in some experiments (Davis and Guillard, 1958; Rhodes and Landers, 1973), but the concentrations of veligers were greater in these studies than in ours, and therefore more algae may have been removed by grazing. Also, in these studies of *C. virginica*, the minimal additions of food required for maximal growth increased as the veligers developed, but the removal of algae by an increasing rate of larval grazing may be the cause, and the concentration required for the maximal growth of veligers of *Mytilus edulis* did not change (Sprung, 1984). A constant 30,000 cells  $\text{ml}^{-1}$  for the maximal ration was therefore considered adequate and less likely to introduce complications from over-feeding.

Because growth was variable, equal numbers of the largest larvae were taken for measurement from subsamples of equal volume from each jar.

Measurements of shell, velum, and velar cilia were taken from videotapes of larvae recorded through a compound microscope. All measurements were done with Image version 1.22 software by Wayne Rasband at NIH and were provided by the National Technical Information Service.

First, the length and width of the velum were recorded through the 4 $\times$  objective as the larva swam up against a cover glass (Fig. 1A). We restricted the horizontal movements of larvae by placing them within a piece of nylon mesh with openings larger than their bodies. Because the velum is approximately elliptical, its circumference was approximated by  $2\pi[(L/2)^2 + (W/2)^2]^{1/2}$ , in which L and W are the length and width of the velum.

Next, we measured the longest cilia that were observed on videotapes recorded through the 10 $\times$  objective with DIC optics. These were the prototrochal cilia, recorded during their effective strokes as the larva swam upward against the cover glass; they were measured from the velar edge to their tips (Fig. 1C).

The shell was videorecorded and its length measured after the larva had been killed with a drop of 4% formalin



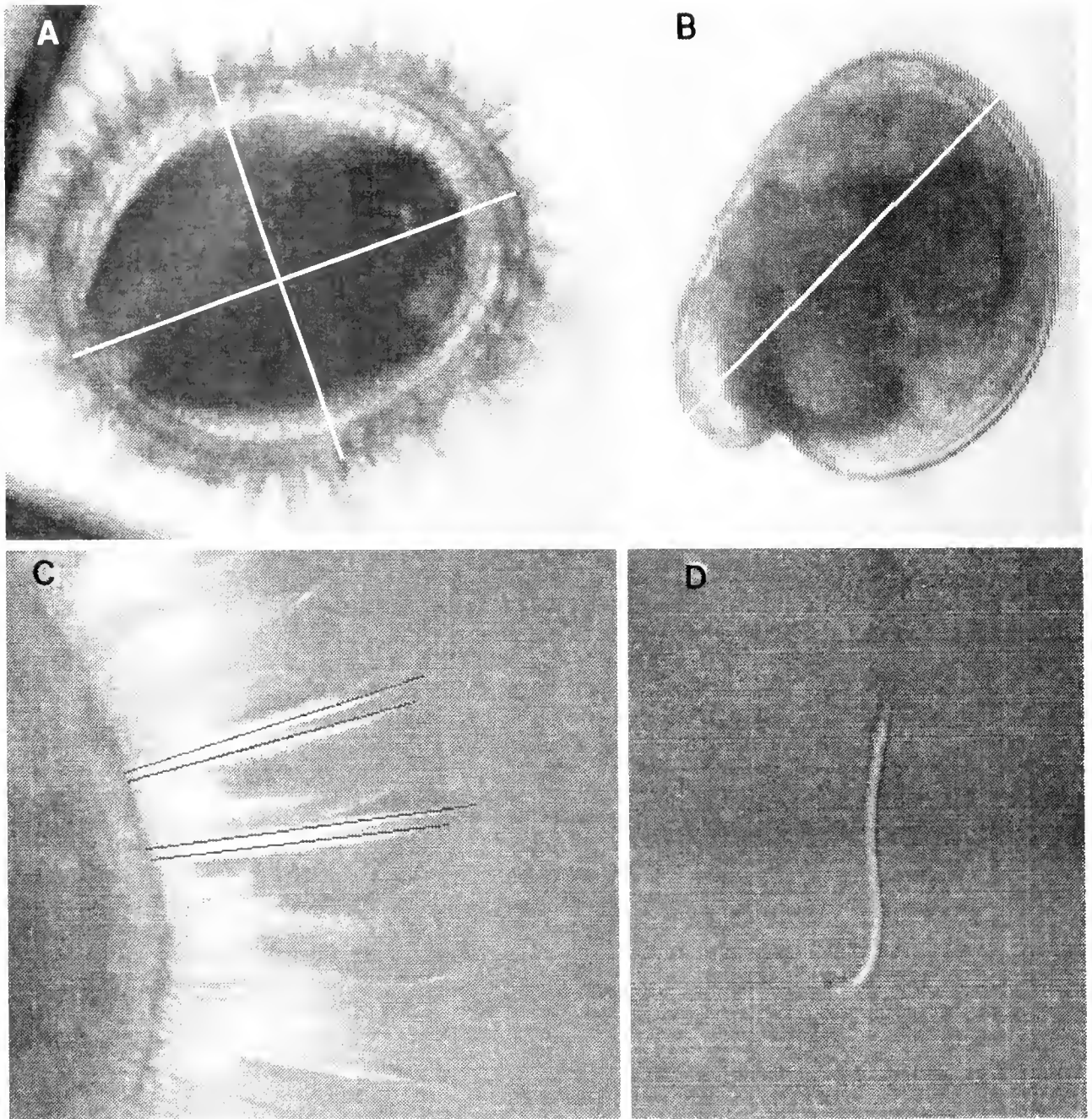


**Figure 1.** Dimensions of veligers of *Crassostrea gigas* measured from videotaped records. (A) Velar length and width (white lines) of larvae swimming upwards in a cage of nylon mesh. (B) Greatest length of the shell (white line). (C) Lengths of prototrochal cilia in their effective strokes (black lines). (D) Dissected prototrochal cilium (length measured along the curve of the cilium from basal body to cilium tip).

buffered with  $\text{CaCO}_3$  in seawater. We measured the greatest length of the shell, from the umbo to the shell edge (Fig. 1B).

Finally, the velum of the formalin-fixed larva was torn with tungsten needles, and the slide was searched for intact

compound cilia, which were videorecorded through the  $10\times$  objective. The longest cilia (Fig. 1D) were measured as a curved line from base to tip. For both methods of measuring cilia, data for cilium lengths were usually the means of five measurements per larva, but sometimes only

three good measurements of a larva's cilia could be obtained from the video-images.

Because videotaped records were inadequate for some measurements on some individual larvae, final sample sizes per jar differed, and the several comparisons of dimensions were therefore made from samples of different sizes.

Jar effects were tested by ANOVA for each measure of the velum or velar cilia, with the jar as a factor and shell length as a covariate in models with and without interaction effects. There were no significant jar effects for any of the four measures of the velum and velar cilia at either high or low concentrations of food. Plots of data for each measure of the velum and velar cilia indicated no differences among jars. Because jar effects were not evident in statistical tests and inspection of plots, veligers from replicate jars were lumped within treatments to increase the degrees of freedom in the analysis of effects of high and low concentrations of food.

Outlying points that might have produced a significant difference based on a few erroneous estimates or abnormal larvae were eliminated from the ANOVAs that tested effects of high and low food levels. These points are the single high value for velum length within the low food treatment in Figure 3, the single low value for length of beating cilium within the high food treatment in Figure 4, and the single low value for length of dissected cilium within the high food treatment in Figure 4.

Effects of food on velar dimensions and cilium lengths were first tested with an ANOVA model with food level as a factor, shell length as a covariate, and the interaction of food level and shell length. In these tests, effects of the interaction were not significant ( $P > 0.70$ ), except for the test for length of beating cilia. Where the interactions were not significant, the  $F$  ratio for the interaction was less than  $2F_{0.50}$  (Paull, 1950), and we therefore tested for effects of food level and shell length without including their interaction in the ANOVA model.

## Results

As expected, larvae at the higher concentration of food grew faster in shell length (Fig. 2) and velar dimensions, and they reached eyespot (Fig. 1B) and pediveliger stages sooner.

More interestingly, larvae reared in a lower concentration of food had velar lobes that were wider, longer, and of greater circumference relative to shell length. When regressions of velar dimensions on shell length were compared, the slopes were similar, but the  $Y$  intercept was lower for larvae with the higher concentration of food, indicating smaller velums at a given shell length (Table I). There was some overlap in the two sets of larvae, how-

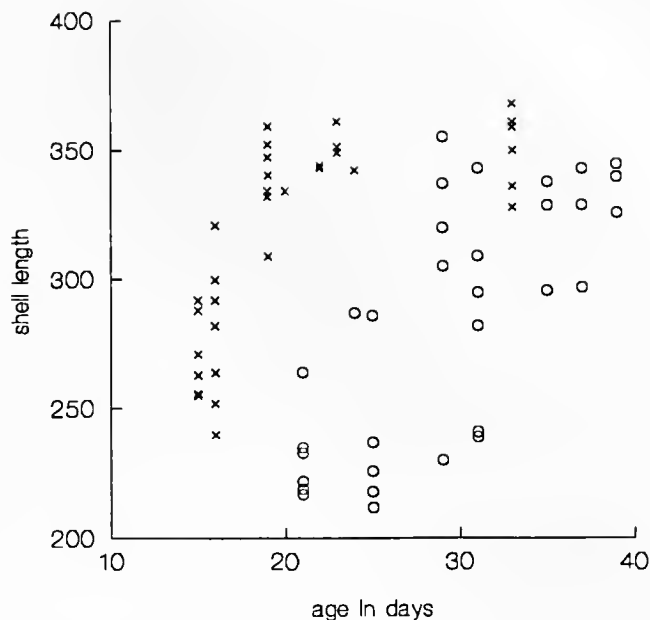


Figure 2. Shell length ( $\mu\text{m}$ ) versus age for sampled veligers at high (x) and low (o) levels of food.

ever (Fig. 3). The effect of the concentration of food was not significant in an ANOVA model that included the interaction between the factor food and the covariate shell length, but because the interactions were not significant, a simpler model without the interaction was used, and an effect of food was then significant for all three measures of velar size at  $P < 0.001$  (ANOVA,  $df$  1, 64).

The lengths of prototrochal cilia measured during their effective strokes were greater, relative to shell length, for larvae reared in a lower concentration of food. Because the position of the cilia in their effective strokes could not be judged when larvae were viewed from above, the data are scattered (Fig. 4A). Nevertheless, the effect of food on cilium length was significant at  $P < 0.02$  (ANOVA,  $df$  1, 64; natural log transformation; interaction of food level and shell length included in the ANOVA model).

The lengths of prototrochal cilia that had been dissected from the larvae were greater relative to shell length for larvae with a lower concentration of food. Because prototrochal cilium lengths vary, and the position of a cilium on the velum could not be judged after the cilia had been removed, there was considerable scatter and overlap in data for larvae with high and low food (Fig. 4B). The effect of food on cilium length was barely significant at  $P < 0.05$  (ANOVA,  $df$  = 1, 63; interaction of food and shell length not included in the ANOVA model because of non-significance).

The measured lengths of cilia were greater for dissected cilia than for beating cilia measured during their effective



Table I

Ordinary least squares regression equations for velar dimensions against shell length with all measurements in  $\mu\text{m}$

	SE intercept	SE coefficient	n	r
Velar width <i>versus</i> shell length				
High food $W = -60.0 + 0.862S$	20.7	0.064	30	0.931
Low food $W = -23.5 + 0.835S$	13.5	0.046	37	0.951
Velar length <i>versus</i> shell length				
High food $L = -25.1 + 1.005S$	23.8	0.073	30	0.933
Low food $L = -9.8 + 1.007S$	14.9	0.051	37	0.958
Velar circumference <i>versus</i> shell length				
High food $C = -122.6 + 2.930S$	62.7	0.194	30	0.944
Low food $C = -49.1 + 2.905S$	38.7	0.132	37	0.966

The outlying point for the low food treatment (Fig. 3B) was omitted.

strokes. This difference may result from the inclusion of basal bodies and the curvature of the cilium in measurements of dissected cilia. It is also possible that measurements along the curve of cilia with software for image analysis exaggerated the lengths of dissected cilia.

The increase in cilium length with velar size was similar whether larvae were reared in high or low concentrations of food (Fig. 5).

### Discussion

Oyster larvae with less food grew velar lobes that were larger relative to the lengths of their shells (Fig. 3). The velar circumference was relatively greater, and therefore the band of prototrochal cilia that produces the current for feeding and swimming was longer. The prototrochal cilia were longer relative to the shell (Fig. 4) but not longer relative to the velar circumference (Fig. 5). The simplest interpretation of the result is that there is a developmental plasticity in velar growth in response to food.

An alternative interpretation is that these differences result from differential mortality or growth of larvae of different genotypes. This alternative would also imply adaptive differences in form, but would attribute these differences to genetic variation in the population rather than to developmental plasticity. This alternative hypothesis can be rejected when mortality rates are sufficiently low and growth rates uniform, as in a previous study of larval sea urchins (Strathmann *et al.*, 1992), but is a possible explanation of treatment effects in most laboratory experiments on marine larvae, including this one.

If there is additive genetic variation in allocation of materials to larval parts, then measurements of growth of a single part, such as the larval shell, would not necessarily represent patterns of genetic variation in growth of the whole larva. For example, absence of strong selection for rapid larval growth is one interpretation of additive genetic

variation in the growth of larval shells (Hilbish *et al.*, 1993). Another possible interpretation is that selection for rapid growth under different food regimes has retarded the loss of heritable variation in growth rate of shells. Abundant food could favor greater allocation to shell growth, and scarce food could favor greater allocation to velar growth. Potential complexities are indicated in Boulding and Hay's (1993) discussion of environmental plasticity and genetic variance for shell shape of intertidal littorines.

Some measurements of the feeding apparatus could be open to interpretations other than differences in growth of shell and velum, but taken together, the measurements indicate differing allocation to the apparatus for capturing food. The velum is extended when it is filled with fluid, and one could argue that hungry larvae simply expanded their velums to a greater extent. It might even be argued that behavioral differences alter the curvature of cilia in their effective strokes; but explanations of this sort cannot be made for cilia dissected from the velum. Because the cilium lengths had about the same relation to velar dimensions for larvae reared with high or low concentrations of food (Fig. 5), the differences in measured sizes indicate differences in growth of the velum as well as of the cilia.

Previous studies of velar function indicate that longer prototrochal cilia and a longer prototrochal band both increase maximum clearance rate (Strathmann and Leise, 1979; Gallager, 1988; Hansen and Ockelmann, 1991). Longer prototrochal cilia also can capture larger particles (Strathmann, 1987b; Hansen, 1991). The differences in larval proportions associated with low or high concentrations of food are therefore those predicted as an adaptive developmental plasticity in response to different concentrations of food. When food is scarce, more growth should be allocated to the apparatus for clearing particles from suspension (prototrochal band, prototrochal cilia). When food is abundant, more growth should be allocated toward

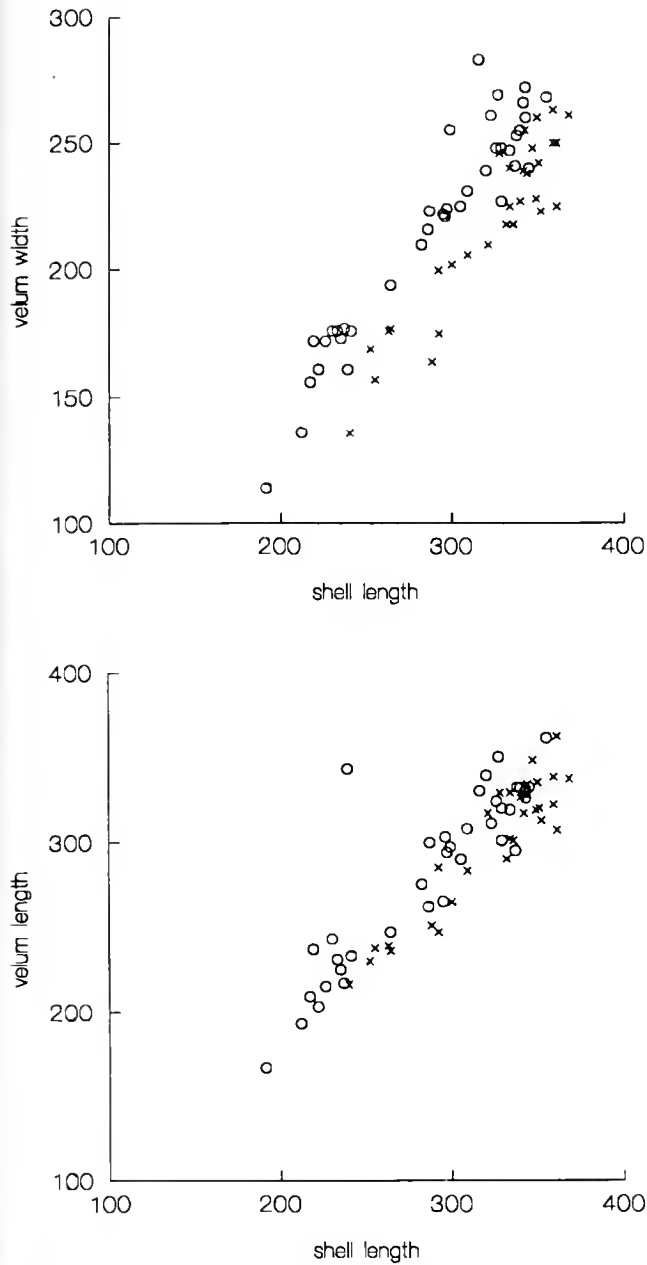


Figure 3. Velar dimensions *versus* shell length with all dimensions in  $\mu\text{m}$ . Symbol for veligers with a high concentration of food is x, with a low concentration is o.

development of postlarval structures (shell and associated structures).

The differences in larval proportions in response to food level were not great but were clearly evident. The consequences for clearance rates cannot be accurately calculated because (1) longer cilia capture particles farther from the base of the cilium, but not necessarily in proportion to the increased length of the cilium; (2) longer cilia can

have greater angular velocities when there are more simple cilia per compound cilium; and (3) longer cilia may remove larger particles from suspension (Strathmann and Leise, 1979; Strathmann, 1987; Gallager, 1988; Hansen, 1991; Hansen and Ockelmann, 1991). Nevertheless, our experiment provides a minimum estimate of the increases in maximum clearance rates that result from a scarcity of food for veligers that have grown to  $300\ \mu\text{m}$  shell length.

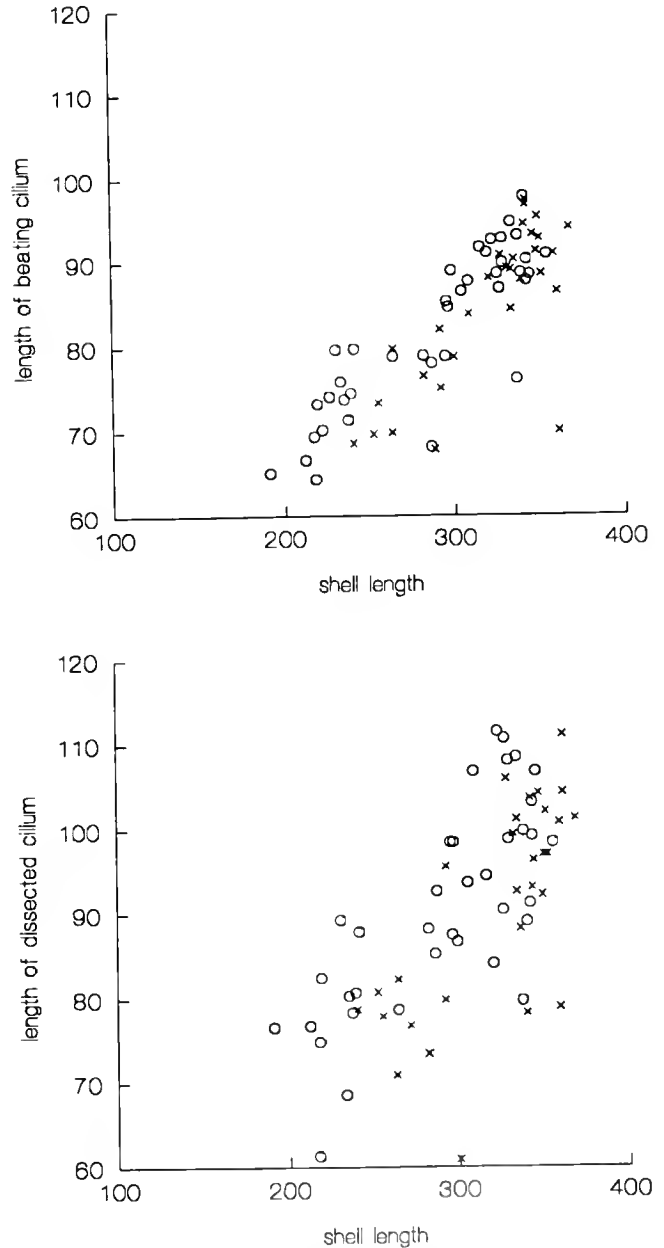
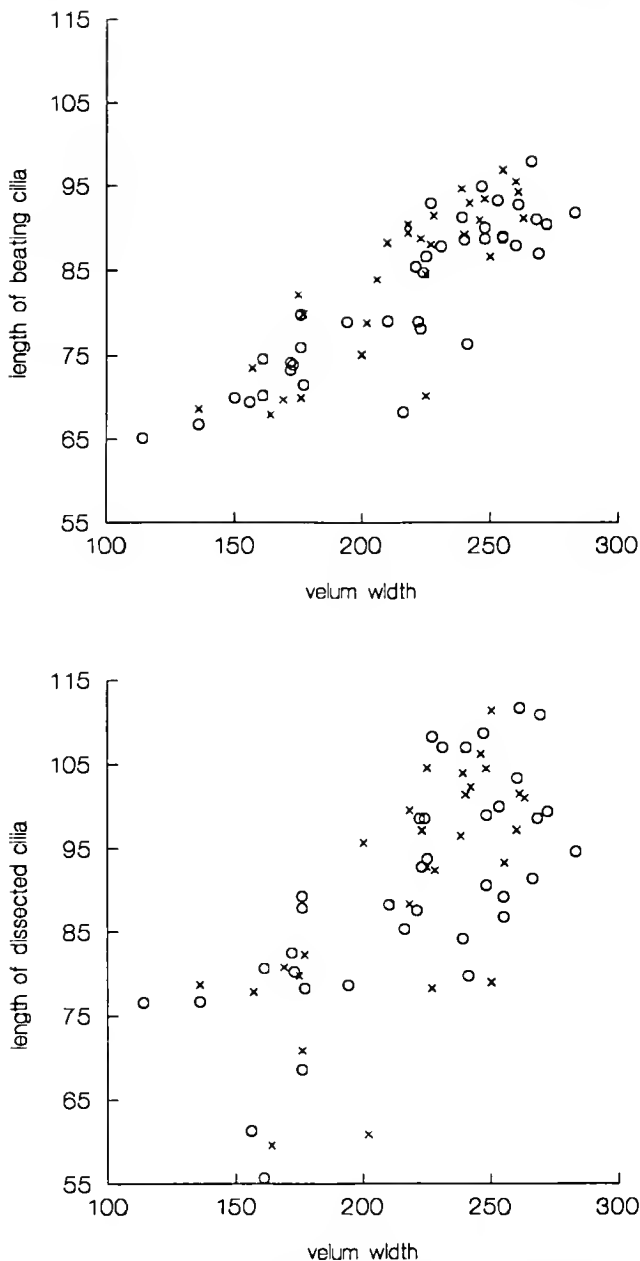


Figure 4. Lengths of prototrochal cilia *versus* shell length with all dimensions in  $\mu\text{m}$ . Top: prototrochal cilia in their effective strokes. Bottom: prototrochal cilia dissected from the velum. Symbol for veligers with a high concentration of food is x, with a low concentration is o.



**Figure 5.** Lengths of prototrochal cilia versus velum width with all dimensions in  $\mu\text{m}$ . Symbol for veligers with a high concentration of food is x, with a low concentration is o.

Expected velar circumference increased from 756 to 822  $\mu\text{m}$  (Table I), or 8.7%. Expected length of beating prototrochal cilia increased from 81.3 to 84.2  $\mu\text{m}$ , and expected length of dissected cilia increased from 87.0 to 91.8  $\mu\text{m}$ , increases of 3.6 and 5.5%. At the least, these differences would increase maximum clearance rate by 13 to 15%. Possible increases in the size of food captured and in the angular velocities of cilia could further increase

the effect of these size differences on maximum clearance rates. It remains to be determined whether more extreme nutritional conditions produce greater variation in the larvae of *Crassostrea gigas*, or whether greater variation in development occurs in species with larger velar lobes or with a more varied natural supply of food.

Laboratory observations on plutei and veligers suggest that wild larvae that grow at lower concentrations of particulate food should develop a relatively larger capacity for capturing food. This prediction is supported by the few field observations available for plutei (Fenaux *et al.*, 1993; L. Fenaux *et al.*, unpub. obs.). Sampling of planktonic veligers could determine whether variations in their proportions are correlated with concentrations of food in nature.

Not all types of larvae exhibit such a clear separation of ephemeral structures for capturing food and structures needed for settlement or postlarval life. Comparative studies can determine the degree to which developmental plasticity in larval proportions depends on this separation.

#### Acknowledgments

This research was supported by NSF grants OCE8922659 and OCE9301665, the Friday Harbor Laboratories, and the Department of Zoology of the University of Washington. M. Billington of the Westcott Bay Sea Farms provided oyster embryos and a culture of *Chaetoceros calcitrans*. T. J. Hilbish, M. J. Greenberg, and anonymous reviewers provided useful comments.

#### Literature Cited

- Boidron-Metairon, I. F. 1988.** Morphological plasticity in laboratory-reared echinoplutei of *Dendraster excentricus* (Eschscholtz) and *Lyttechinus variegatus* (Lamarck) in response to food conditions. *J. Exp. Mar. Biol. Ecol.* **119**: 31-41.
- Boulding, E. G., and T. K. Hay. 1993.** Quantitative genetics of shell form of an intertidal snail: constraints on short-term response to selection. *Evolution* **47**: 576-592.
- Davis, H. C., and R. R. Guillard. 1958.** Relative value of ten genera of micro-organisms as food for oyster and clam larvae. *Fish. Bull. U. S. Fish Wildl. Serv.* **58**: 293-304.
- Fenaux, L., M. F. Strathmann, and R. R. Strathmann. 1993.** Five tests of food-limited growth of larvae in coastal waters by comparisons of rates of development and form of echinoplutei. *Limnol. Oceanogr.* (in press)
- Gallager, S. M. 1988.** Visual observations of particle manipulation during feeding in larvae of a bivalve mollusc. *Bull. Mar. Sci.* **43**: 344-365.
- Hansen, B. 1991.** Feeding behaviour in larvae of the opisthobranch *Philine aperta* II. Food size spectra and particle selectivity in relation to larval behaviour and morphology of velar structures. *Mar. Biol.* **111**: 263-270.
- Hansen, B., and K. W. Ockelman. 1991.** Feeding behaviour in larvae of the opisthobranch *Philine aperta*. I. Growth and functional responses at different developmental stages. *Mar. Biol.* **111**: 255-261.

- Hart, M. W. 1991. Particle captures and the method of suspension feeding by echinoderm larvae. *Biol. Bull.* **180**: 12-27.
- Hart, M. W., and R. E. Scheibling. 1988. Comparing shapes of echinoplutei using principal components analysis, with an application to larvae of *Strongylocentrotus droebachiensis*. Pp. 277-284 in *Echinoderm Biology*. R. D. Burke, P. V. Mladenov, P. Lambert, and R. L. Parsley, eds. Balkema, Rotterdam.
- Hilbish, T. J., E. P. Winn, and P. D. Rawson. 1993. Genetic variation and covariation during larval and juvenile growth in *Mercenaria mercenaria*. *Mar. Biol.* **115**: 97-104.
- McEdward, L. R. 1984. Morphometric and metabolic analysis of the growth and form of an echinopluteus. *J. Exp. Mar. Biol. Ecol.* **82**: 259-287.
- Nielsen, C. 1987. Structure and function of metazoan ciliary bands and their phylogenetic significance. *Acta Zool.* **68**: 205-262.
- Paulk, A. E. 1950. On a preliminary test for pooling mean squares in the analysis of variance. *Ann. Math. Statist.* **21**: 539-556.
- Rhodes, E. W., and W. S. Landers. 1973. Growth of oyster larvae, *Crassostrea virginica*, of various sizes in different concentrations of the chrysophyte, *Isochrysis galbana*. *Proc. Natl. Shellfish. Assoc.* **63**: 53-59.
- Sprung, M. 1984. Physiological energetics of mussel larvae (*Mytilus edulis*). I. Shell growth and biomass. *Mar. Ecol. Prog. Ser.* **17**: 283-293.
- Strathmann, M. F. 1987a. *Reproduction and Development of Marine Invertebrates of the Northern Pacific Coast, Data and Methods for the Study of Eggs, Embryos, and Larvae*. University of Washington Press, Seattle. 670 pp.
- Strathmann, R. R. 1978. The evolution and loss of feeding larval stages of marine invertebrates. *Evolution* **32**: 907-914.
- Strathmann, R. R. 1987b. Larval feeding. Pp. 465-550 in *Reproduction of Marine Invertebrates*, Vol. 9, *General Aspects: Seeking Unity in Diversity*. A. C. Giese, J. S. Pearse, and V. B. Pearse, eds. Blackwell, Palo Alto.
- Strathmann, R. R., L. Fenaux, and M. F. Strathmann. 1992. Heterochronic developmental plasticity in larval sea urchins and its implications for evolution of nonfeeding larvae. *Evolution* **46**: 972-986.
- Strathmann, R. R., and E. Leise. 1979. On feeding mechanisms and clearance rates of molluscan veligers. *Biol. Bull.* **157**: 524-535.
- Waldock, M. J., and I. A. Nascimento. 1979. The triacylglycerol composition of *Crassostrea gigas* larvae fed on different algal diets. *Mar. Biol. Lett.* **1**: 77-86.

# Co-Activation of Antagonistic Motoneurons as a Mechanism of High-Speed Hydraulic Inflation of Prey Capture Appendages in the Pteropod Mollusk *Clione limacina*

TIGRAN P. NOREKIAN AND RICHARD A. SATTERLIE

Friday Harbor Laboratories, University of Washington, Friday Harbor, Washington 98250 and  
\*Department of Zoology, Arizona State University, Tempe, Arizona 85287-1501

**Abstract.** The predatory pteropod mollusk *Clione limacina* catches its prey by using specialized oral appendages called buccal cones. Eversion and elongation of buccal cones is a hydraulic phenomenon. In the cerebral ganglia, two groups of motoneurons have been identified that underlie functionally opposite movements of buccal cones: extrusion and retraction. We suggest that the remarkably rapid inflation of buccal cones (50 ms) is achieved through initial co-activation of antagonistic neurons, which presumably produces high pressure in the head hemocoel prior to buccal cone extrusion. The subsequent sudden inhibition of retractor motoneuron activity results in a very rapid and powerful inflation of the buccal cones. Cerebral interneurons that evoke co-activation are described.

## Introduction

Feeding behavior of the pteropod mollusk *Clione limacina* has been described in several studies (Wagner, 1885; Conover and Lalli, 1972; Litvinova and Orlovsky, 1985; Lalli and Gilmer, 1989; Hermans and Satterlie, 1992). *Clione* is a predatory carnivore that feeds only on actively swimming pteropods of the genus *Limacina* and has highly specialized structures for their capture. To seize the prey, *Clione* rapidly everts six oral appendages, called buccal cones, which then become tentacle-like and grasp the *Limacina* shell, holding it during the subsequent phases of feeding (Fig. 1). The eversion and elongation of buccal cones is a hydraulic phenomenon and is accom-

plished by squeezing hemocoelic fluid into the central cavities of the cones. Buccal cone extrusion is a remarkably rapid reaction and occurs within 50–70 ms (Hermans and Satterlie, 1992). Such speed is not typical for hydrostatic movements in mollusks. The rapid extrusion of the *Clione* buccal cones is thus interesting from mechanical and neurobiological points of view.

Two groups of motoneurons that control the prey-capture movements of buccal cones have been identified in the cerebral ganglia of *Clione* (Norekian and Satterlie, 1993). The first group comprises a number of electrically coupled, normally silent cells called **A** motoneurons, whose activation induces opening of oral skin folds and extrusion of buccal cones. The second group of motoneurons consists of several spontaneously active cells, called **B** motoneurons, whose firing underlies retraction of buccal cones. Constant and stable spontaneous spike activity in **B** neurons maintains buccal cones in the permanently retracted position. When active, **A** neurons produce strong inhibitory inputs to **B** neurons, which terminate **B** neuron firing (Fig. 2A). Obtained data, however, revealed that **A**-to-**B** inhibition is not monosynaptic, and a single spike in an **A** motoneuron was usually ineffective in producing an inhibitory postsynaptic potential in **B** neurons (Norekian and Satterlie, 1993; Fig. 2A).

As previously mentioned, protraction of buccal cones is accomplished by squeezing hemocoelic fluid from the head hemocoel into the central cavities of the buccal cones. The speed at which this occurs depends upon the speed of synchronous activation of different muscle groups involved in buccal cone extrusion and the time required to move the hemocoelic fluid into the cone cavities. One

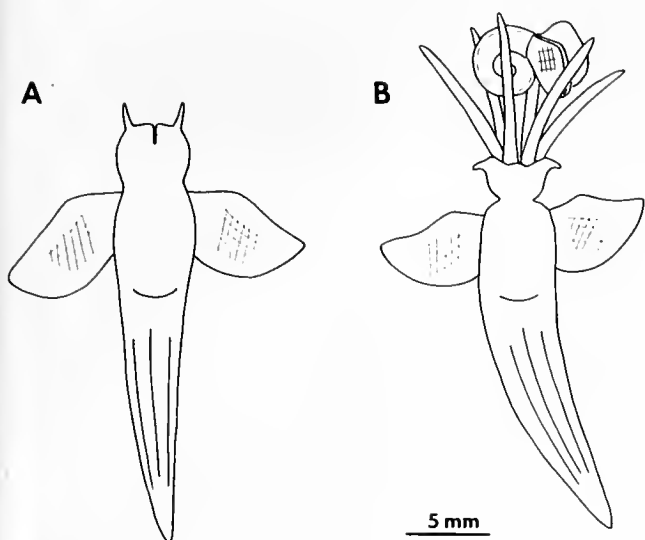


**Figure 1.** (A) Nonfeeding *Clione limacina* with buccal cones withdrawn inside the head and covered by skin folds (lips). (B) *Clione* with extruded buccal cones capturing the prey, *Limacina helicina*.

possible way to achieve this transfer rapidly is to increase pressure in the head hemocoel significantly prior to buccal cone extrusion. The fact that A-to-B inhibition is not monosynaptic, and A and B motoneurons, which underlie antagonistic movements of buccal cones, can be synchronously active, provides a physiological basis for this phenomenon.

### Materials and Methods

Experiments were carried out at Friday Harbor Laboratories, University of Washington, in the summer and at Arizona State University in the winter and spring. Adult specimens of *Clione limacina*, 1–3 cm body length, were collected and held in large beakers of seawater at 5–10°C.

Electrophysiological experiments were performed on preparations consisting of the head, central nervous system, and wings. All nerves running from the central ganglia to the head and to the wings were intact, but body nerves were cut. The preparations were tightly pinned to a Sylgard-coated Petri dish with cactus spines (*Opuntia* sp.). Prior to recording, ganglia were desheathed by bathing the preparation in a 1 mg/ml solution of protease (Sigma type XIV) for approximately 5 min, followed by a 30-min wash.

For intracellular recordings, glass microelectrodes were filled with 2 M potassium acetate and had resistances of 10–20 MΩ. Electrophysiological signals were amplified, displayed, and recorded using conventional techniques. Intracellular stimulation was provided via amplifier bridge circuits. For morphological investigation of recorded neurons, a 5% solution of 5(6)-carboxyfluorescein (Sigma)

prepared in 2 M potassium acetate was iontophoresed via the recording electrodes with 0.5–10 nA negative current pulses for 20–30 min. Resistances of the electrodes were 20–30 MΩ. Injected cells were observed and photographed live in the recording dish with an incident-light fluorescent microscope (Nikon).

Tactile stimulation of the head and lips was provided by a thin polymeric filament, 0.2 mm in diameter. Fifty-six preparations were used in the experiments.

### Results

#### *Co-activation of antagonistic motoneurons*

During simultaneous recordings of A and B neuron activities, common excitatory inputs were recorded in both types of neurons (Fig. 2B, C). Some of these depolarizing inputs were subthreshold for A neuron activity and produced only an increase in B neuron firing. Others evoked a few spikes in A neurons, but were insufficient to initiate A-to-B neuron inhibition, resulting in a short period of co-activation of both types of neurons (Fig. 2B). This kind of neuron activity did not produce notable behavioral responses in the preparations. Buccal cones remained withdrawn inside the head, covered by skin folds (lips). When spontaneous, common inputs were of greater strength and sufficient to initiate prolonged A neuron bursting, they produced co-activation of A and B neurons followed by sudden inhibition of B neurons and continuation of A neuron activity (Fig. 2C). Such strong bursting activity of A neurons, which resulted in inhibition of B neurons, was always correlated with a strong behavioral reaction of the preparation—opening of the oral skin folds (lips) and partial extrusion of buccal cones (schematic drawings in Fig. 2C). In intact animals, buccal cones become tentacular, extending approximately one-half of a body length (Fig. 1B). The necessary compromise of the fluid skeleton prevented full extension of buccal cones in dissected preparations. Nevertheless, all behavioral events underlying buccal cone extrusion could be observed; these include opening of the oral skin folds, general contraction of the head wall muscles, contraction of buccal cone circular muscles, and eventually a partial expansion of the buccal cones (schematic drawings in Fig. 2C).

Initial co-activation of A and B neurons, when followed by inhibition of B neurons and continuation of A neuron activity, typically lasted for around 1 s. The result of A and B neuron co-activation would be the contraction of head wall and neck musculature (A motoneuron activity) with maintained retraction of the buccal cones (B motoneuron activity), that would lead to a significant increase of fluid pressure in the head hemocoel of intact *Clione*. The subsequent sudden inhibition of B neuron activity, with continued activation of A neurons, would result in a very rapid and powerful inflation of the buccal cones.

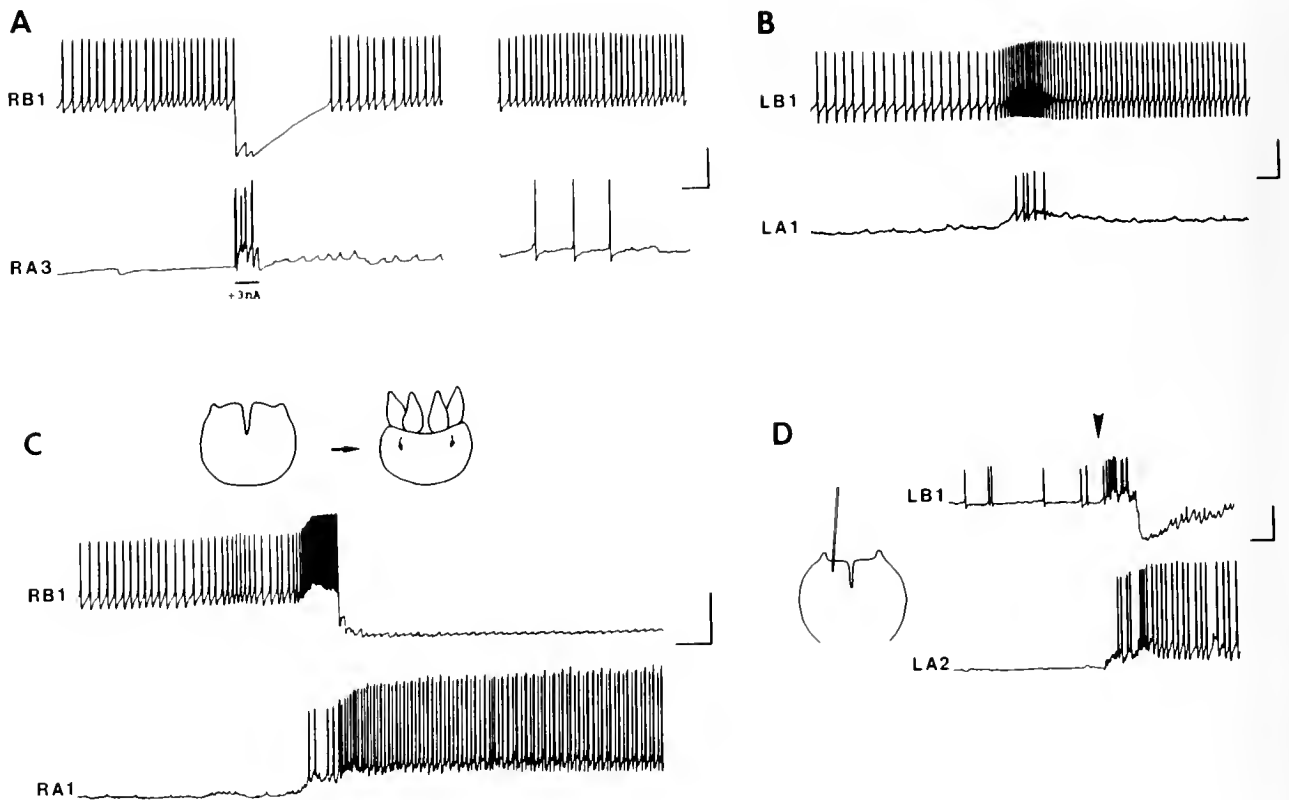


**Figure 2.** (A) Activation of A neurons produced high amplitude inhibitory potentials in B neurons. However, A-to-B inhibition is polysynaptic, and individual spikes in A neurons were usually insufficient to produce inhibitory potentials in B neurons. (B) Spontaneous, common excitatory inputs were recorded in both A and B neurons. (C) When common excitatory inputs were strong enough to produce powerful and prolonged spike activity in A neurons, they evoked initial co-activation of both types of neurons followed by B neuron inhibition with continuation of A neuron firing. This type of neuron activity was closely correlated with the behavioral response of the head as shown by schematic drawings. In silent preparations, buccal cones are withdrawn inside the head and covered by oral skin folds. When bursts of spikes appeared in A neurons and inhibited B neurons, the skin folds moved laterally and the buccal cones were partially extruded. (D) Tactile stimulation of the anterior region of the head, including lips (shown by schematic drawing), produced common excitatory inputs in both A and B neurons. These inputs were sometimes strong enough to initiate co-activation of both types of neurons followed by inhibition of B neurons with continuation of A neuron firing. The moment of stimulation is shown by arrow. Scale bars = 15 mV, 2 s.

Such common excitatory inputs, which are capable of producing co-activation of A and B neurons, can arise from contact with prey. In several studies, it was shown that the capture of *Limacina* by *Clione* was initiated by direct contact with the prey (Conover and Lalli, 1972; Lalli and Gilmer, 1989; Litvinova and Orlovsky, 1985). Tactile stimulus from the prey thus appears to play an important role in initiating extrusion of buccal cones. Tactile stimulation of the anterior part of the head and the lips of *Clione* produced excitatory inputs to both A and B neurons (Fig. 2D). These common excitatory inputs were sometimes strong enough to initiate co-activation of A and B neurons followed by inhibition of B neuron firing and continuation of A neuron activity (Fig. 2D). This kind of neuron activity resulted in the opening of the skin

folds and the partial extrusion of the buccal cones. Therefore, common excitatory inputs to A and B neurons arising from contact with prey can provide a contributory mechanism underlying the high speed of hydrostatic extrusion of buccal cones during prey capture in *Clione*.

#### *Interneurons producing co-activation of A and B motoneurons*

One pair of neurons that produced synchronous excitatory inputs to both A and B motoneurons was identified in the cerebral ganglia. Due to their *coordinating* influence on A and B motoneuron activities, these were designated  $C_{AB}$  neurons. Cell bodies of  $C_{AB}$  neurons were small, 15–30  $\mu\text{m}$  in diameter, and were situated on the anterior



margin of the cerebral ganglia between head nerves N1 and N2 (Fig. 3A). Neurons were silent or had low frequency (0.5 Hz) spontaneous spike activity, with membrane potentials between  $-55$  and  $-60$  mV. Activation of a recorded  $C_{AB}$  neuron by injecting depolarizing current pulses resulted in the appearance of excitatory postsynaptic potentials in **A** motoneurons and biphasic excitatory-inhibitory responses in **B** motoneurons (Fig. 3B). The primary response of **B** motoneurons was a burst of fast excitatory postsynaptic potentials that produced a short burst of increased spike activity (1-s duration, spike frequency up to 10 Hz). The spike burst was followed by a slow hyperpolarizing wave that terminated **B** neuron firing for 10–30 s after  $C_{AB}$  neuron activation. In **A** motoneurons,  $C_{AB}$  neurons produced fast excitatory postsynaptic potentials that were able to induce **A** neuron spike activity (Fig. 3B). Sometimes the spike activity in **A** motoneurons was not strong enough to activate **A**-to-**B** inhibition (Fig. 3B), but at other times it produced fast inhibitory potentials in **B** motoneurons, masking the slow inhibitory response induced directly by  $C_{AB}$  neurons. Thus, the typical response to  $C_{AB}$  neuron activation was initial, brief co-activation of **A** and **B** motoneurons followed by prolonged **B** neuron inhibition, induced by fast **A**-to-**B** inhibitory postsynaptic potentials, slow hyperpolarizing waves, or both.

Connections between  $C_{AB}$  neurons and **A** and **B** motoneurons appear to be monosynaptic. Each spike in a  $C_{AB}$  neuron produced an individual excitatory postsynaptic potential in a recorded **A** motoneuron with a stable, short latency of 2.5 ms (Fig. 4A). Similarly, each  $C_{AB}$  neuron spike produced an individual excitatory postsynaptic potential in a recorded **B** motoneuron with a stable latency

of 4 ms (Fig. 4B). Moreover, spike durations in  $C_{AB}$  neurons, which varied during bursting activity, were reflected in the amplitude of excitatory postsynaptic potentials in **A** and **B** neurons. The second and third spikes in the  $C_{AB}$  neuron were wider than the first spike (Fig. 4A), and as a consequence, the second and third postsynaptic potentials in the **A** neuron had higher amplitudes than the first. In addition, a high  $Mg^{++}$ /high  $Ca^{++}$  seawater (110 mM  $MgCl_2$ , 25 mM  $CaCl_2$ ) did not block postsynaptic potentials in **A** and **B** motoneurons induced by  $C_{AB}$  neurons (Fig. 4C). In high  $Mg^{++}$ /high  $Ca^{++}$  solution, **B** motoneurons demonstrated both components of the biphasic synaptic response, and slow hyperpolarization was detected even after two to three  $C_{AB}$  neuron spikes. Biphasic monosynaptic contacts can be explained by the existence of two types of receptors on the membrane of **B** motoneurons for the same transmitter, or by the release of co-transmitters by the  $C_{AB}$  neurons.

Activation of a single  $C_{AB}$  neuron produced similar responses in ipsilateral and contralateral **A** and **B** motoneurons (Fig. 4C). Carboxyfluorescein injections of  $C_{AB}$  neurons revealed that each neuron had many small, thin processes around the cell body in the ipsilateral ganglion and one large axon running through the paracerebral connective to the contralateral cerebral ganglion (Fig. 5). This paracerebral axon of  $C_{AB}$  neuron appears to underlie the observed contralateral connections.

Contralateral  $C_{AB}$  neurons were electrically coupled. Electrotonic coupling was demonstrated by applying depolarizing or hyperpolarizing square current pulses to one neuron and recording similar but attenuated responses simultaneously in the contralateral neuron (Fig. 6A). Electrical coupling was sufficient to produce 1:1 spike ac-

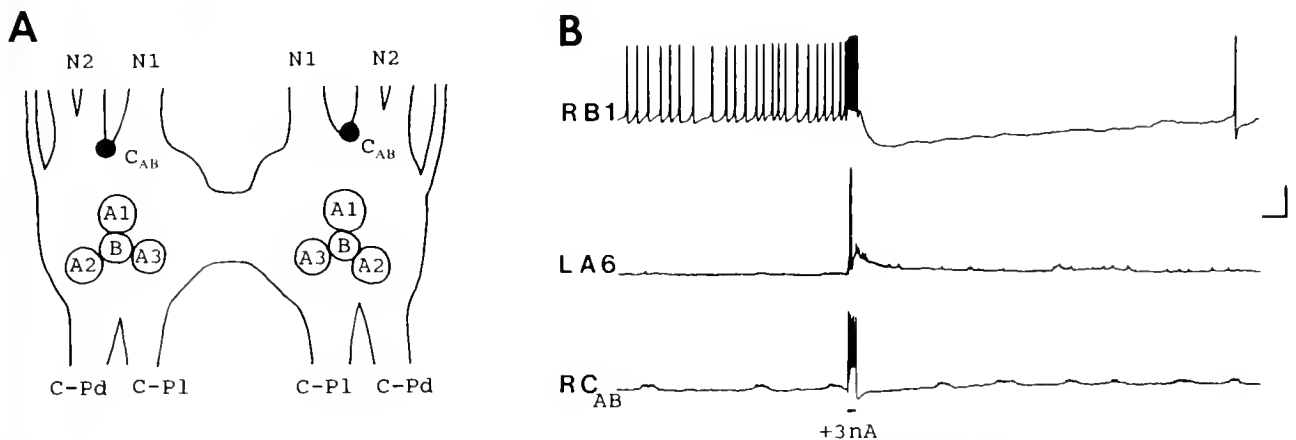


Figure 3. (A) Position of  $C_{AB}$  neuron somata in the cerebral ganglia: N1 and N2—head nerves; C-Pd and C-Pl—cerebro-pedal and cerebro-pleural connectives; some of the **A** and **B** motoneurons are also shown. (B) Effect of  $RC_{AB}$  neuron stimulation on the activities of LA6 and RB1 motoneurons. Notice the initial, short co-activation of **A** and **B** motoneurons and subsequent appearance of a slow hyperpolarizing wave in **B** motoneurons. Scale bars = 15 mV, 2 s.

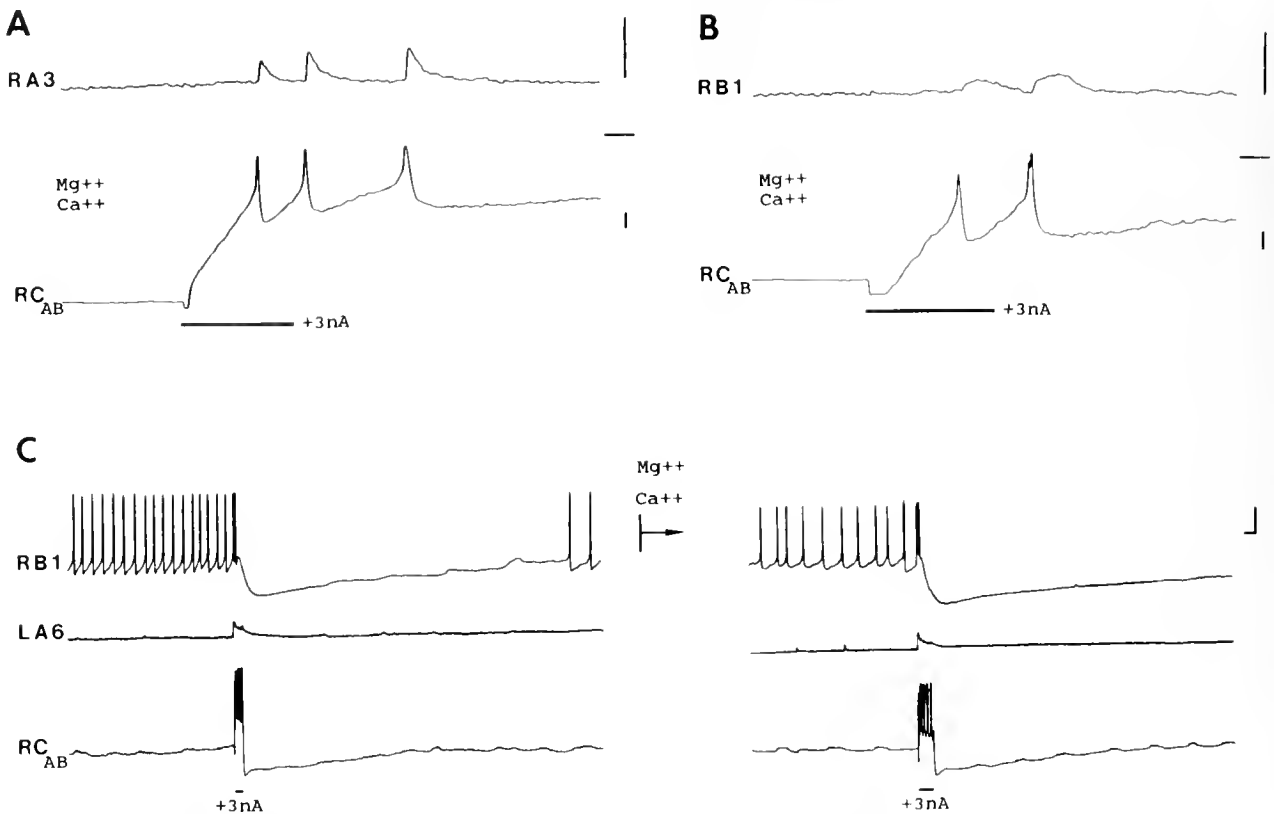


Figure 4. (A, B) Each spike in the  $C_{AB}$  neuron produced individual excitatory postsynaptic potentials in **A** and **B** neurons with stable short latencies even in high  $Mg^{++}$ /high  $Ca^{++}$  solution. Scale bars = 10 mV, 50 ms. (C) High  $Mg^{++}$ /high  $Ca^{++}$  saline did not influence any of the types of postsynaptic potentials in **A** and **B** motoneurons after  $C_{AB}$  neuron activation. Scale bars = 15 mV, 1 s.

tivity in  $C_{AB}$  neurons (Fig. 6A), suggesting that electrical coupling plays an important role in synchronizing activities of contralateral  $C_{AB}$  neurons.

**B** motoneurons did not induce responses in cerebral  $C_{AB}$  neurons, whereas strong activation of **A** motoneurons produced inhibitory inputs in  $C_{AB}$  neurons (Fig. 6B). This connection was not monosynaptic, because individual spikes in **A** neurons did not produce individual inhibitory postsynaptic potentials in  $C_{AB}$  neurons, and only strong burst activity was able to induce  $C_{AB}$  neuron inhibition. These inhibitory inputs presumably serve as negative feedback, preventing reverberation of impulses between the two groups of neurons.

As previously mentioned, mechanical contact with prey produces significant sensory inputs that initiate buccal cone extrusion. Tactile stimulation of the anterior region of the head, including the lips, produced excitatory inputs in  $C_{AB}$  neurons that were able to initiate spike activity in  $C_{AB}$  neurons (Fig. 7). Thus,  $C_{AB}$  neurons, which produce co-activation of **A** and **B** motoneurons, are included in the neuron pathway that underlies the rapid extrusion of buccal cones initiated by mechanical inputs from the prey.

## Discussion

Expansion of the buccal cones of *Clione* is a hydraulic phenomenon accomplished through squeezing of hemocoelic fluid from the head hemocoel into the hemocoelic cavities of the buccal cones. Ordinarily, such hydraulic inflation of tentacular structures is a relatively slow process, as seen in the erection of tentacles in pulmonates, which is dependent on hydrostatic pressure in the cephalopedal sinus (Dale, 1973). In *Clione*, however, buccal cone expansion is extremely fast, occurring in 50 to 70 ms (Hermans and Satterlie, 1992).

There are only a few examples of such fast reactions in mollusks. The best known example, which is behaviorally analogous to *Clione* buccal cone expansion, is the prey capture reaction of squid tentacles, which elongate fully in 15 to 30 ms (Keir, 1985). However, the mechanisms by which the buccal cones and squid tentacles move to grasp their prey are quite distinct. Cephalopod tentacles are muscular hydrostats that do not rely on volume changes in fluid-filled cavities (Kier, 1985). Their elongation is a purely muscular phenomenon, so the speed of

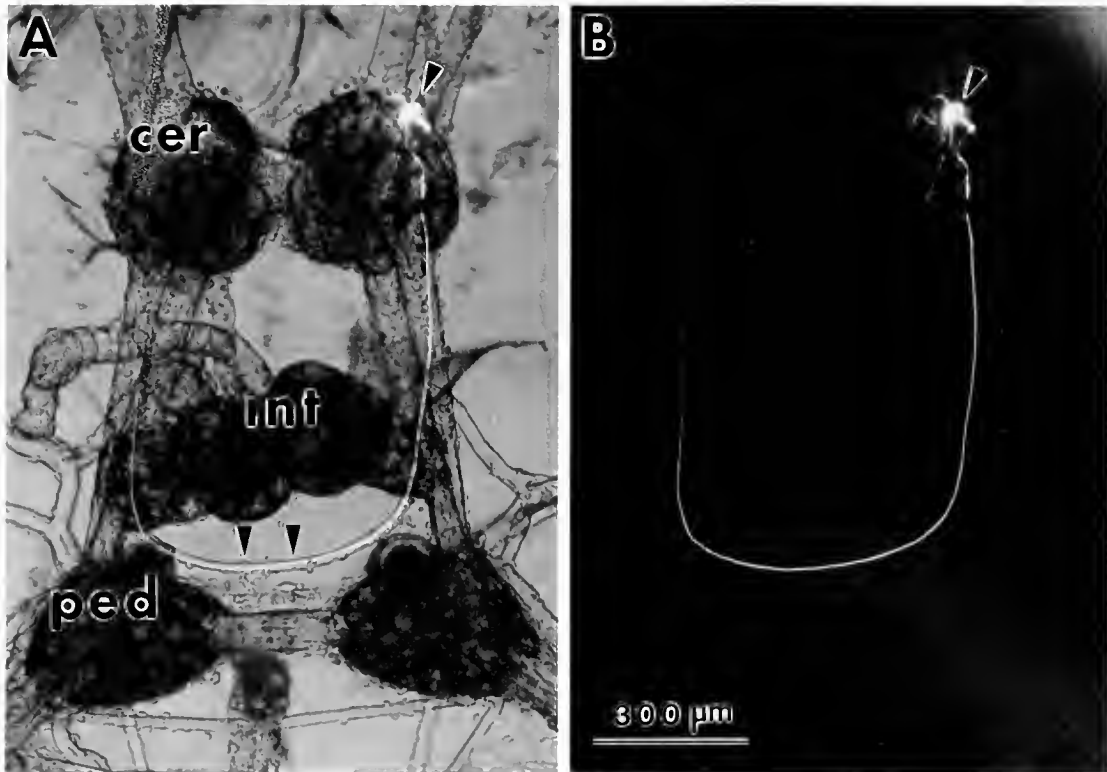


Figure 5. (A, B) Morphology of  $C_{AB}$  neurons revealed by carboxyfluorescein injections. A single arrow shows the position of the cell body of neuron  $RC_{AB}$ . Double arrows show the paracerebral connective; cer—cerebral ganglion, ped—pedal ganglion, int—intestinal ganglia.

their reaction depends only on the speed of muscle contraction. This raises the interesting question of how the *Clione* buccal cones, which are hydrostatic structures, expand at a rate that is within the range of muscular elongation. We propose here that co-activation of functionally reciprocal **A** and **B** motoneuron groups, which evoke protraction and retraction of buccal cones respectively, is critical for their rapid and powerful extrusion.

The time of *Clione* buccal cone expansion depends on the time required for synchronizing the activities of all muscles involved in producing this reaction, and on the time required for moving hemocoelic fluid into the cone cavities. The first factor, synchronization, is a problem because buccal cone expansion requires the contraction of many muscle groups, including head wall muscles, neck muscles, circular muscles of buccal cones, and muscles opening the skin folds. Twenty-six **A** motoneurons whose activity evokes contraction of these muscles have been identified in the cerebral ganglia of *Clione* (Norekian and Satterlie, 1993). Synchronized activity of all **A** neurons is required for initiating buccal cone extrusion. One second of co-activation observed in **A** and **B** motoneurons prior to buccal cone inflation would give time for synchronization of activities of all **A** neurons and all muscle groups participating in this reaction.

The second problem is the necessity to eject hemocoelic fluid into cone cavities as rapidly and forcefully as possible. Two factors appear to contribute to resolving this problem. First, Hermans and Satterlie (1992) demonstrated that expansion of buccal cones is associated with a 23% reduction in head diameter and a distinct circular constriction in the neck region, without any notable contractions of body wall muscles. Lalli (1967) described a muscular diaphragm that surrounds the anterior aorta in the neck region and appears to separate head and body hemocoels. Closure of this diaphragm would allow isolation of the head hemocoel so that rapid contractions of the head and neck muscles could be translated rapidly and efficiently into unidirectional fluid movements into the buccal cones. Second, a method of greatly increasing pressure in the head hemocoel immediately prior to buccal cone inflation would greatly increase the rate of buccal cone inflation. Co-activation of antagonistic **A** and **B** motoneurons, which evokes protraction and retraction of buccal cones respectively, appears to be a mechanism capable of significantly increasing the pressure inside the head prior to buccal cone extrusion. Contraction of all muscles participating in buccal cone extrusion tends to force hemocoelic fluid into the cone cavities while simultaneous contraction of retractor muscles opposes this fluid movement, pre-

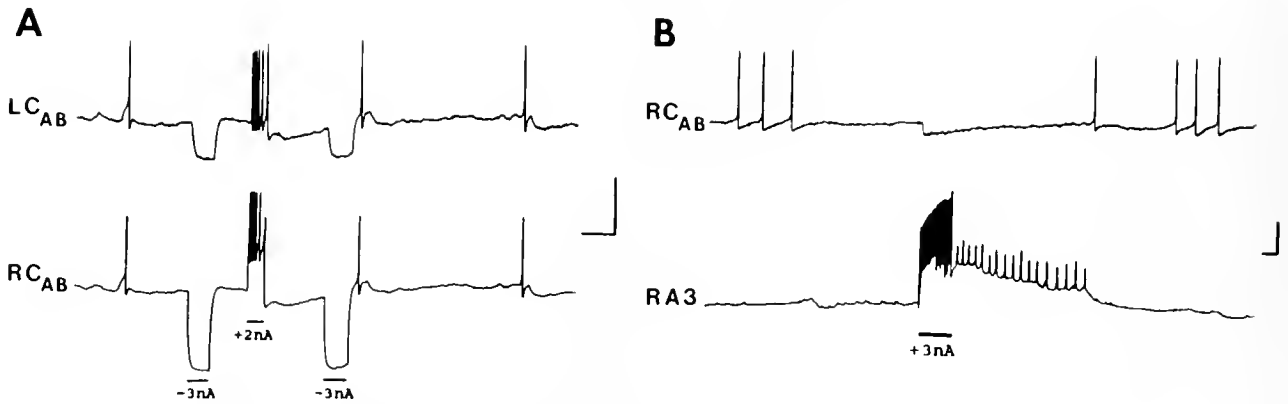


Figure 6. (A) Contralateral C<sub>AB</sub> neurons are electrically coupled as demonstrated by applying depolarizing or hyperpolarizing square current pulses to one neuron and recording similar responses simultaneously in the contralateral neuron. Scale bars = 15 mV, 2 s. (B) Activation of A neurons produced inhibitory inputs in C<sub>AB</sub> neurons. Scale bars = 10 mV, 1 s.

sumably producing a *significant* increase in blood pressure inside the head. Subsequent sudden inhibition of the retractor neurons and, therefore, relaxation of retractor muscles would lead to a very forceful and rapid ejection of hemocoelic fluid from the head into cone cavities and to inflation of buccal cones. Behavioral observations with high-speed cinematographic analyses show an initial bulging of the head immediately prior to buccal cone extrusion (Hermans and Satterlie, 1992), supporting the hypothesis of co-activation of antagonistic muscle groups.

Similar mechanisms underlying powerful and rapid reactions have been found in other animals. In the locust, energy for the jump is stored in the elastic elements of the leg during a short period of co-contraction of hindleg extensor and flexor muscles. A sudden inhibition of flexor activity transfers the stored energy to rapid extension movements of the hindlegs (Heitler and Burrows, 1977). For an analogy based on fluid pressure, we can look at the mammalian heart. During the brief isometric contraction phase of the ventricles, when both sets of ven-

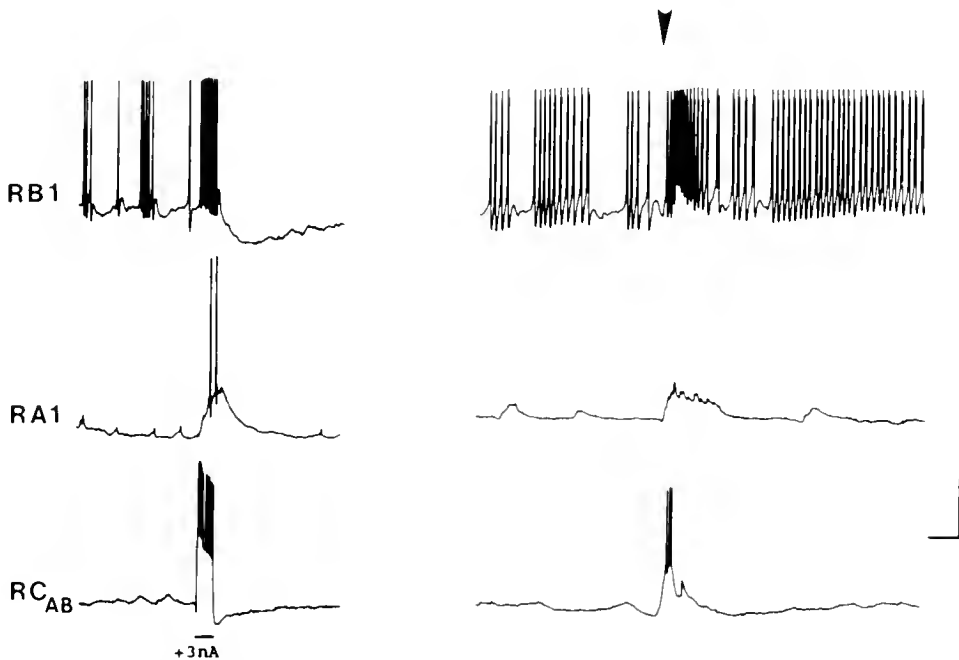


Figure 7. C<sub>AB</sub> neurons were identified based on the reactions they produced in A and B neurons. Tactile stimulation of the anterior region of the head, including lips, produced excitatory inputs in all three types of neurons including neuron C<sub>AB</sub>. The moment of tactile stimulation is shown by the arrow. Scale bars = 20 mV, 2 s.

tricular valves are closed, fluid pressure builds rapidly, thus allowing blood to be more forcefully ejected after opening of the semilunar valves.

### Acknowledgments

We thank Dr. A. O. Dennis Willows, director of Friday Harbor Laboratories, for generous assistance, and Drs. Claudia Mills and Win Watson for collecting animals. This work was supported by NIH grant ROI NS27951.

### Literature Cited

- Conover, R. J., and C. M. Lalli. 1972. Feeding and growth in *Clione limacina* (Phipps), a pteropod mollusc. *J. Expl. Mar. Biol. Ecol.* **9**: 279-302.
- Dale, B. 1973. Blood pressure and its hydraulic functions in *Helix pomatia* L. *J. Exp. Biol.* **59**: 477-490.
- Heitler, W. J., and M. Burrows. 1977. The locust jump. I. The motor programme. *J. Exp. Biol.* **66**: 203-219.
- Hermans, C. O., and R. A. Satterlie. 1992. Fast-strike feeding behavior in a pteropod mollusc, *Clione limacina* Phipps. *Biol. Bull.* **182**: 1-7.
- Kier, W. M. 1985. The musculature of squid arms and tentacles: ultrastructural evidence for functional differences. *J. Morphol.* **185**: 223-239.
- Lalli, C. M. 1967. Studies on the structure and biology of two gymnosomatous pteropods, *Clione kincaidi* Agersborg and *Crucibranchaca macrochura* (Meisenheimer). Ph.D. Dissertation, University of Washington. 175 pp.
- Lalli, C. M., and R. W. Gilmer. 1989. *Pelagic Snails: The Biology of Holoplanktonic Gastropod Mollusks*. Stanford University Press, Stanford, CA.
- Litvinova, N. M., and G. N. Orlovsky. 1985. Feeding behaviour of pteropod mollusc *Clione limacina*. *Bull. Soc. Natur. Moscow, Sect. Biol.* **90**: 73-77 (in Russian).
- Norekian, T. P., and R. A. Satterlie. 1993. Cerebral neurons underlying prey capture movements in the pteropod mollusc, *Clione limacina* I. Physiology, morphology. *J. Comp. Physiol. A* **172**: 153-169.
- Wagner, N. 1885. *Die Wirbellosen des Weissen Meeres: Zoologische Forschungen an der Kuste des Solowetzischen Meerbusens in den Sommermonaten der Jahre*. Verlag Von Wilhelm Engelmann, Leipzig, Germany.

## FMRFamide and GABA Produce Functionally Opposite Effects on Prey-Capture Reactions in the Pteropod Mollusk *Clione limacina*

TIGRAN P. NOREKIAN AND RICHARD A. SATTERLIE

*Department of Zoology, Arizona State University, Tempe, Arizona 85287-1501,\* and Friday Harbor Laboratories, University of Washington, Friday Harbor, Washington 98250*

**Abstract.** The effects of FMRFamide and gamma-aminobutyric acid (GABA) on prey-capture reactions in *Clione* and on cerebral **A** and **B** neurons, which control opposite movements of prey capture appendages, have been studied. FMRFamide hyperpolarized **A** neurons and depolarized and increased spike activity in **B** neurons. FMRFamide thus had a reciprocal effect on **A** and **B** neurons, triggering buccal cone withdrawal. In addition, FMRFamide inhibited swimming, acceleration of which is a component of feeding arousal. Many neurons throughout the central nervous system showed FMRFamide immunoreactivity. Dense networks of immunoreactive fibers were localized in the head wall, buccal mass and in buccal cones, adjacent to striated longitudinal muscle cells. In wings, immunoreactive processes were found mainly in association with smooth retractor muscles. GABA depolarized and activated **A** neurons but hyperpolarized and inhibited **B** neurons. The overall effect of GABA thus resulted in extrusion of buccal cones. Both direct GABA responses and inhibitory postsynaptic potentials (IPSPs) induced in **B** neurons by **A** neuron activity were chloride-mediated. However, picrotoxin and bicuculline did not block IPSPs or direct GABA responses in **B** cells.

### Introduction

The pteropod mollusk *Clione limacina* is a highly specialized carnivore that feeds on shelled pteropod mollusks of the genus *Limacina* (Wagner, 1885; Lalli and Gilmer, 1989). To catch the prey, *Clione* uses three pairs

of oral appendages, called buccal cones, that are normally cone shaped and covered by skin folds. Contact with the prey induces very rapid eversion of the buccal cones, which then become tentacle-like and seize the shell of the prey. The eversion and elongation of buccal cones is primarily due to hydraulic inflation. After capturing its prey, *Clione* uses its buccal cones to position the *Limacina* shell aperture over its mouth and uses two clusters of specialized chitinous hooks and the radula, to extricate the *Limacina* from its shell, swallowing it whole. Feeding behavior of *Clione* also involves a significant increase of locomotory activity: swimming changes from slow to fast (Litvinova and Orlovsky, 1985; Hermans and Satterlie, 1992).

Two groups of motoneurons in the cerebral ganglia of *Clione* have been identified as directly involved in the control of prey-capture reactions (Norekian and Satterlie, 1991a, b, 1993). The first group consists of electrically coupled cells, called **A** neurons, which form an integral network that is silent in nonfeeding animals. Upon activation, **A** neurons evoke opening of the oral skin folds and extrusion of the buccal cones. The second group of motoneurons (**B** neurons) evokes retraction of buccal cones into the head. In nonfeeding animals, **B** neurons show regular spike activity that maintains the buccal cones in the withdrawn position. **A** and **B** neurons thus serve antagonistic functions. When active, **A** neurons induce a powerful inhibitory input to **B** cells, which terminates **B** cell firing. This reciprocal arrangement of firing activities directly determines the behavioral state of the buccal cones. Any changes in the activities of **A** and **B** neuron groups produce significant changes in the behavioral output and are thus very important for realization of feeding behavior.

Received 8 February 1993; accepted 16 July 1993.

\*Mailing address.

**A** and **B** neuron activities and behavioral responses of buccal cones can be controlled or modulated by different neurotransmitters. The roles of various neurotransmitters in realization of specific behaviors have been investigated in a variety of invertebrates. Serotonin, for example, appears to act as a central transmitter-modulator for feeding arousal and activation of feeding behavior (e.g., Lent *et al.*, 1989; Kupfermann and Weiss, 1981). A behavioral role has also been demonstrated for several other neuroactive substances, including the neuropeptide FMRFamide (Murphy *et al.*, 1985; Bulloch *et al.*, 1988; Cooke *et al.*, 1985; Cooke and Gelperin, 1985).

The primary goal of this study is to describe the effects of the neuropeptide FMRFamide and gamma-aminobutyric acid (GABA) on the system of **A** and **B** neurons underlying prey-capture reactions in *Clione*, and on its behavioral output. FMRFamide-containing cells and fibers in the central nervous system (CNS) and peripheral tissues of *Clione* are localized immunohistochemically. These data allow discussion of the role of FMRFamide and GABA in feeding behavior in *Clione*. Preliminary results of some GABA effects have been published (Norkian and Satterlie, 1991a, b).

### Materials and Methods

Behavioral and physiological experiments were carried out at Friday Harbor Laboratories, University of Washington, in the spring and summer. Adult specimens of *Clione limacina*, 1–3 cm in body length, were collected from the breakwater and held in large beakers of seawater at 10–13°C. Morphological work was carried out at Arizona State University.

#### Preparation

Electrophysiological experiments were performed on preparations consisting of the head, central nervous system, and wings. All nerves running from the central ganglia to the head and to the wings were intact, while body nerves were cut. The preparations were tightly pinned to a Sylgard-coated petri dish with cactus spines (*Opuntia sp.*). Prior to recording, ganglia were partially desheathed by bathing the preparation in a 1 mg/ml solution of protease (Sigma type XIV) for approximately 5 min, followed by a 30–60 min wash. The solution in the recording chamber was changed with the aid of a peristaltic pump that allowed constant perfusion of solutions at a rate of 1 ml/min (chamber volume = 5 ml). Solutions were prepared using filtered natural seawater.

#### Electrophysiological recordings

For intracellular recordings, glass microelectrodes were filled with 2 M potassium acetate, and had resistances of

10–20 M $\Omega$ . Electrophysiological signals were amplified, displayed, and recorded using conventional techniques. Intracellular stimulation was provided via amplifier bridge circuits. Electrodes were filled with 3 M potassium chloride for the experiments with high intracellular chloride; chloride leakage from the electrodes caused the required increase in intracellular chloride concentration.

#### Transmitter application

To understand if a recorded neuron was directly sensitive to a neurotransmitter, three methods were used. The first involved chemical isolation of neurons by bathing the preparation in high concentrations of divalent cations. Solutions used included 333 mM magnesium chloride, 2 mM cobalt chloride, and 0.5 mM cadmium chloride. Magnesium chloride solution blocks chemical synaptic connections in the *Clione* preparation as demonstrated in the swimming system (Satterlie, 1989).

The second method included mechanical isolation of identified neurons. In these experiments, the ganglionic sheath was detached from the surface of neurons by exposure to 2 mg/ml protease for 10–15 min. The sheath was then mechanically removed and the preparation washed for 30–60 min. The appropriate neuron was penetrated with a recording microelectrode and slowly pulled from the ganglion. Axons that might still have provided synaptic connections with the CNS were then cut.

The third method involved local application of transmitter directly onto the cell body of the recorded neuron. Microiontophoresis was used for GABA, and diffusion microapplication was used for both FMRFamide and GABA. For microiontophoresis, glass micropipette electrodes with tip diameters of 1  $\mu$ m were filled with a 1 mM solution of GABA prepared in distilled water. The amplitude of negative current pulses used to eject GABA was 10 to 100 nA with durations of 100 to 1000 ms. For diffusion microapplication, glass pipettes with tip diameters of 2–3  $\mu$ m were filled with a 1 mM solution of the transmitter prepared in seawater and the electrode tip placed close to the cell surface. Transmitter was released from the tip of the electrode by diffusion. When the electrode tip was moved away from the recorded neuron, the effects were eliminated. Addition of neurotransmitters and antagonists to the bathing solution was accomplished with a graduated 1 ml pipette. The final concentrations were calculated from the known volume of injected solution and the known volume of the recording dish. For use of GABA antagonists, the preparations were bathed in high Mg<sup>++</sup> saline containing the required concentration of antagonist for 5–15 min. Picrotoxin, bicuculline, bicuculline methbromide, bicuculline methchloride, and pentylene-tetrozole were purchased from Sigma Chemical Company or Research Biochemicals Inc. Picrotoxin, bicuculline



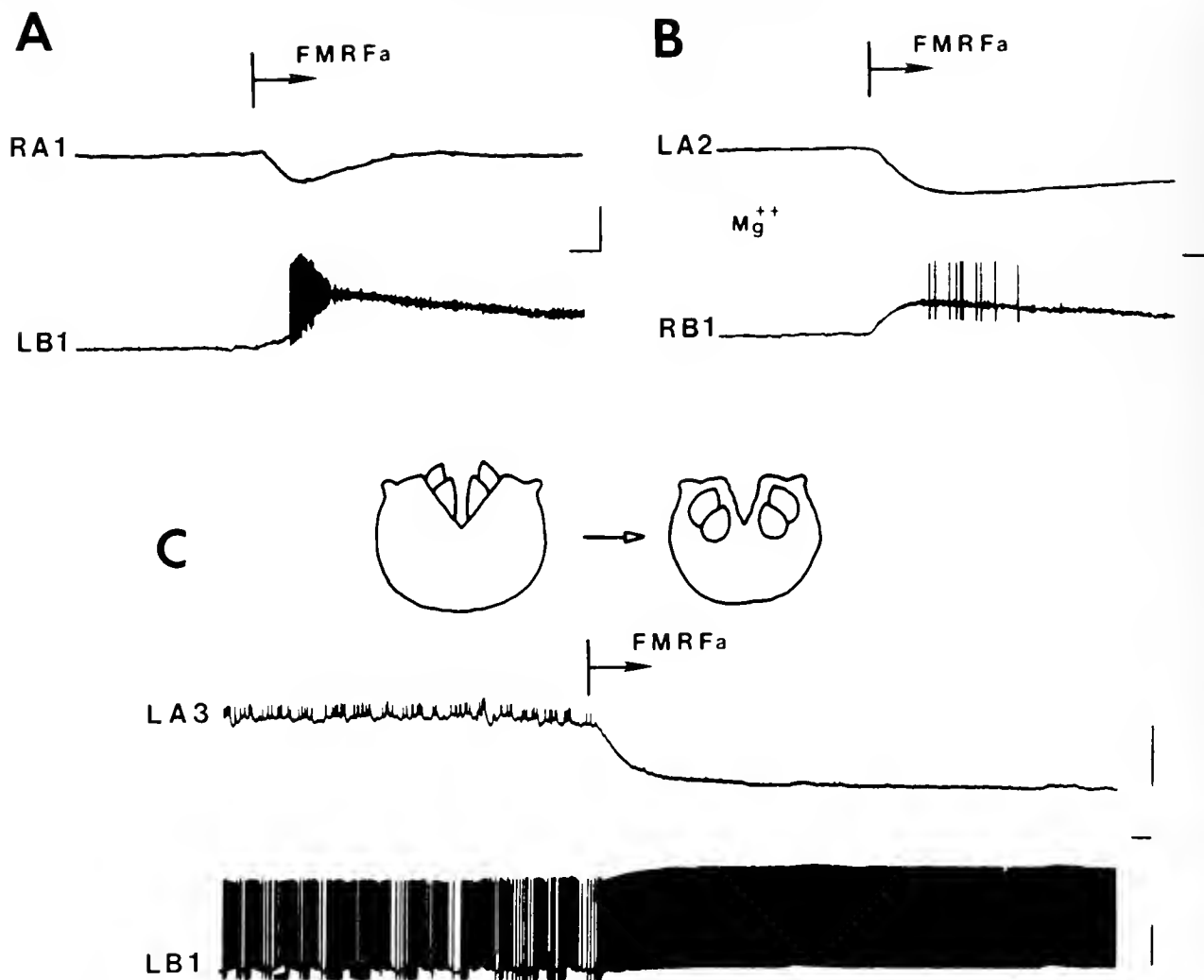


**Figure 1.** Effects of FMRFamide on A and B neurons. (A) Bath-applied  $8 \mu\text{M}$  FMRFamide produced hyperpolarization of an isolated RA1 neuron and depolarization of an isolated LB1 neuron. The peptide was applied in constantly perfused seawater. Scale bars = 15 mV, 3 s. (B) In high  $\text{Mg}^{++}$  seawater, which terminated spontaneous firing of neuron RB1, application of  $10 \mu\text{M}$  FMRFamide also hyperpolarized neuron LA2 and depolarized and activated neuron RB1. Scale bars = 15 mV, 2 s. (C) Application of  $10 \mu\text{M}$  FMRFamide in normal seawater resulted in hyperpolarization of neuron LA3 and a significant increase of spike activity in neuron LB1. The line drawings schematically show the head in dissected preparations before and after FMRFamide application. Before application the buccal cones were slightly relaxed; after application they were completely withdrawn. Scale bars = 15 mV, 2 s.

methbromide, bicuculline methchloride, and pentylenetetrazole were diluted directly in seawater, while bicuculline first was diluted in 0.25 ml of alcohol and then in seawater. All GABA antagonist solutions were prepared immediately before use. In these experiments, GABA was prepared in a solution of the antagonist and applied with the 1-ml pipette. In this way, the final concentration of antagonist was not changed when the GABA was added. The same procedure was performed during tetraethylammonium or 4-aminopyridine (Sigma) and FMRFamide application.

#### *Immunocytochemistry*

Dissected preparations were fixed overnight in 4% paraformaldehyde in phosphate buffer, washed for 12 h in phosphate buffered saline (PBS), and pre-incubated in PBS containing 0.01% Triton X-100 and a 5% solution of goat serum in PBS/Triton X-100. Tissue was incubated in a 1:500 dilution of anti-FMRFamide antibody (INCSTAR) in goat serum/PBS/Triton for 48 h. Following a series of PBS washes, tissue pieces were incubated in a 1:20 dilution of fluorescein-labeled goat anti-rabbit secondary antibody (Kirkegaard & Perry) for 12 h. Another series

of PBS washes was followed by infiltration of a mounting medium consisting of 1 part 50 mM Tris buffer (pH 9.5) and 9 parts glycerol. Tissue pieces were viewed and photographed in whole mount in a Nikon fluorescence microscope with epifluorescence and standard FITC filters.

For electron microscopy the tissue was fixed in 2% glutaraldehyde in phosphate buffer instead of 4% paraformaldehyde. A similar procedure was used for applying the primary antibody. After washing, a peroxidase-labeled avidin-biotin secondary antibody system was used (Vectastain ABC elite kit). The peroxidase was reacted with diaminobenzidine, and the tissue was washed and fixed in 1% osmium tetroxide in phosphate buffer for 1 h. The tissue was washed, dehydrated in an ethanol series and propylene oxide, and embedded in Epon. Thin sections were cut on a Porter-Blum MT-2B microtome and examined in a Philips EM201 electron microscope. To test for the specificity of the FMRFamide immunostaining, two different controls were used. First, primary antibody was omitted from the procedure. Second, primary antibody was incubated overnight with 10  $\mu$ M FMRFamide before use. In both cases, no labeling was detected.

The total number of preparations used in this study was 90.

## Results

### Effects of FMRFamide

FMRFamide, at 1–2  $\mu$ M and above, hyperpolarized the cerebral **A** neurons and depolarized the **B** neurons (Fig. 1). To assess whether **A** and **B** neurons directly responded to FMRFamide, the peptide was tested on isolated somata of identified **A** and **B** neurons. Isolated **A** neurons demonstrated hyperpolarizing responses to ap-

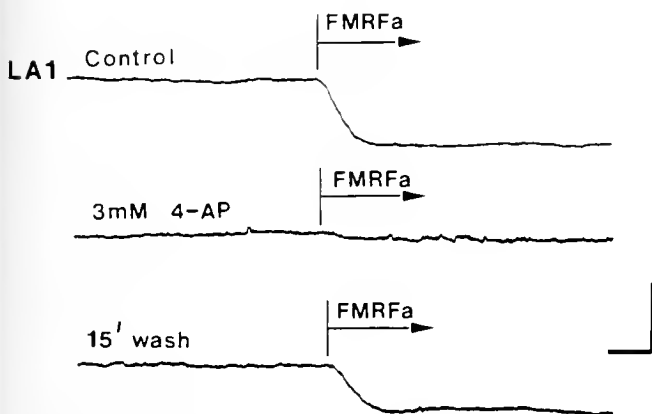


Figure 2. Blocking of FMRFamide hyperpolarizing responses in **A** neurons by 4-aminopyridine. Effects of 50  $\mu$ M FMRFamide on neuron LA1 before, 1 min after 3 mM of 4-AP was applied externally, and after 15 min of washing in seawater. The entire experiment was conducted in high  $Mg^{++}$  seawater. Scale bars = 5 mV, 2 s.



Figure 3. Fast and slow inhibitory postsynaptic potentials recorded in **A** neurons. Scale bars = 15 mV, 2 s.

plication of FMRFamide, but isolated **B** neurons showed depolarizing responses (Fig. 1A). Similar responses were observed in high  $Mg^{++}$  solution (Fig. 1B).

Bath application of FMRFamide in seawater produced hyperpolarization of **A** neurons and a 5- to 10-fold increase of **B** neuron spike activity (Fig. 1C). FMRFamide thus had a reciprocal effect on the activities of **A** and **B** neurons, which was visually correlated with the buccal cones being held in a withdrawn position (Fig. 1C). In all experiments, strong withdrawal reactions of buccal cones were observed for the duration of FMRFamide application.

In addition to FMRFamide and GABA, we also tested the effects of serotonin, dopamine, acetylcholine,  $SCP_B$ , and L-glutamate on the cerebral **A** and **B** neurons. FMRFamide was the only agent that hyperpolarized the **A** neurons; all the others produced depolarization. A neuron hyperpolarization, evoked by bath application of 5–10  $\mu$ M FMRFamide, was 10–15 mV from the normal resting potential of –60 to –65 mV. Tetraethylammonium (TEA) and 4-aminopyridine (4-AP), known to block different voltage-sensitive  $K^+$  currents (see Hille, 1992), antagonized the FMRFamide-evoked hyperpolarization (Fig. 2). Hyperpolarization produced by 50  $\mu$ M FMRFamide was completely blocked by external perfusion of 10 mM TEA or 3 mM 4-AP after 2 min ( $n = 9$ ). This effect was reversed by washing for 15–20 min in seawater.

Two types of inhibitory postsynaptic potentials (IPSPs) were recorded in **A** neurons: fast and slow (Fig. 3). Fast IPSPs had durations of less than 1 s, and amplitudes up to 5 mV; they appeared with frequencies of up to 3 Hz. Slow IPSPs had durations between 20 s and 1 min and amplitudes up to 15 mV. The source of neither type of IPSPs is known, but FMRFamidergic neurons may be involved.

One important component of natural feeding arousal in intact *Clione* is acceleration of swimming. For this reason the effect of FMRFamide on the swimming system was tested. Perfusion of 5  $\mu$ M FMRFamide or higher concentrations completely blocked swimming activity, as noted through behavioral observation of wing movements and by recording electrical activity of swim motoneurons

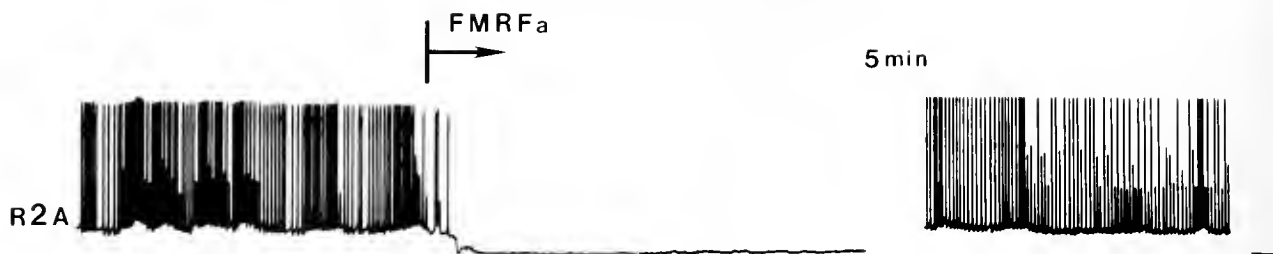


Figure 4. Inhibitory effect of  $10 \mu\text{M}$  FMRFamide on the activity of swim motoneuron R2A, located in the pedal ganglion. Note the hyperpolarization of the motoneuron and disappearance of synaptic inputs. After a 5-min wash, impulse activity was restored. Scale bars = 20 mV, 3 s.

(Fig. 4). FMRFamide produced hyperpolarization of swim motoneurons. It also appeared to inhibit the swim pattern generator (SPG), as evidenced by the loss of the synaptic pattern of activity produced by the SPG in swim motoneurons.

#### FMRFamide immunolocalization in *Clione*

*Central nervous system.* Immunoreactive somata were found on dorsal and ventral surfaces of buccal, cerebral, pedal, and intestinal ganglia (Fig. 5).

*Buccal ganglia.* The buccal ganglia contained two pairs of immunoreactive cells on the ventral anterior surface and a few cells on the dorsal surface. The most conspicuous of the latter cells were a pair of large ( $80 \mu\text{m}$  in diameter) neurons found near the posterior margin (Fig. 5; 6C, D). In addition, an asymmetrical immunoreactive neuron was found on the medial margin of the right buccal ganglion (Fig. 5).

*Cerebral ganglia.* Several immunoreactive cells were found in the cerebral ganglia (Fig. 5). These included two clusters of large cells ( $60\text{--}80 \mu\text{m}$ ) at the anterior margin of the ganglia, which showed stable, weak fluorescence in each preparation. A group of intermediate-size neurons ( $40\text{--}50 \mu\text{m}$ ) was revealed in the middle of each ganglion on the dorsal surface. On the ventral surface, two notable immunoreactive cells with bright fluorescence were revealed in the central part of the ganglia, along with a pair of large cells (up to  $100 \mu\text{m}$ ), showing weak fluorescence, in the posteriolateral margins. Small somata included a tight cluster on the posteriomarginal margin, near the cerebral commissure. Also, a large asymmetrical cell body,  $70 \mu\text{m}$  in diameter, with bright fluorescence, was localized in the posteriomarginal margin of the ganglia.

*Pedal ganglia (Fig. 5).* In the pedal ganglia, two cells showing bright fluorescence were found in the anterior region, and two additional cells were localized in the lateral region of the dorsal surface. Also, a tight cluster of small neurons was revealed in the anteriolateral part of the dorsal surface of each pedal ganglion. On the ventral surface, two labeled neurons were found in the anterior region,

and a group of neurons was localized in the posteriomarginal region. A cluster of small neurons was also revealed in the lateral region of the ganglia.

*Intestinal ganglia (Fig. 5).* Large (up to  $100 \mu\text{m}$  in diameter) immunoreactive cell bodies with asymmetrical positions were localized on the dorsal and ventral surfaces of intestinal ganglia. Also, on the posterior margin of the intestinal ganglia, a pair of symmetrical large neurons showed stable, extremely bright fluorescence in each preparation. These cells sent thick axons into intestinal nerve N12, which innervated the esophagus (according to Wagner, 1885). In addition, two small cell bodies were found in the pleural ganglia. All ganglia contained a dense network of neuropilar immunoreactive processes.

*Head.* The head of *Clione* had a dense network of immunoreactive processes partly originating from immunoreactive fibers that run from cerebral ganglia to the head nerves and cerebro-buccal connectives and from buccal ganglia to the buccal mass. In addition, the buccal mass contained many extraganglionic immunoreactive somata (Fig. 6). Three groups of small immunoreactive cell bodies were found in the middle of the buccal mass, between the hook sacs (Fig. 6). The first group consisted of a pair of symmetrical neurons found on the ventral surface of the buccal mass far from the buccal ganglia. Two other groups included two symmetrical pairs of clusters found on the dorsal surface, closer to the buccal ganglia, and consisted of 3–5 neurons per cluster. Cells from each cluster sent axons to the ipsilateral buccal ganglion. Additional multiple cell bodies were found around the mouth and radula, most associated with the lips (Fig. 6A). A dense network of immunoreactive processes was revealed in the head skin (Fig. 7A) originating from intensely immunoreactive fibers that crossed the whole thickness of the head wall (Fig. 7B).

*Buccal cones.* Buccal cones had a dense network of immunoreactive fibers arranged in a longitudinal, compressed network (Fig. 7C, D). It is important to stress that these immunoreactive fibers were restricted to the oral side of each buccal cone—the side that makes contact with the prey. There are three groups of muscles in the

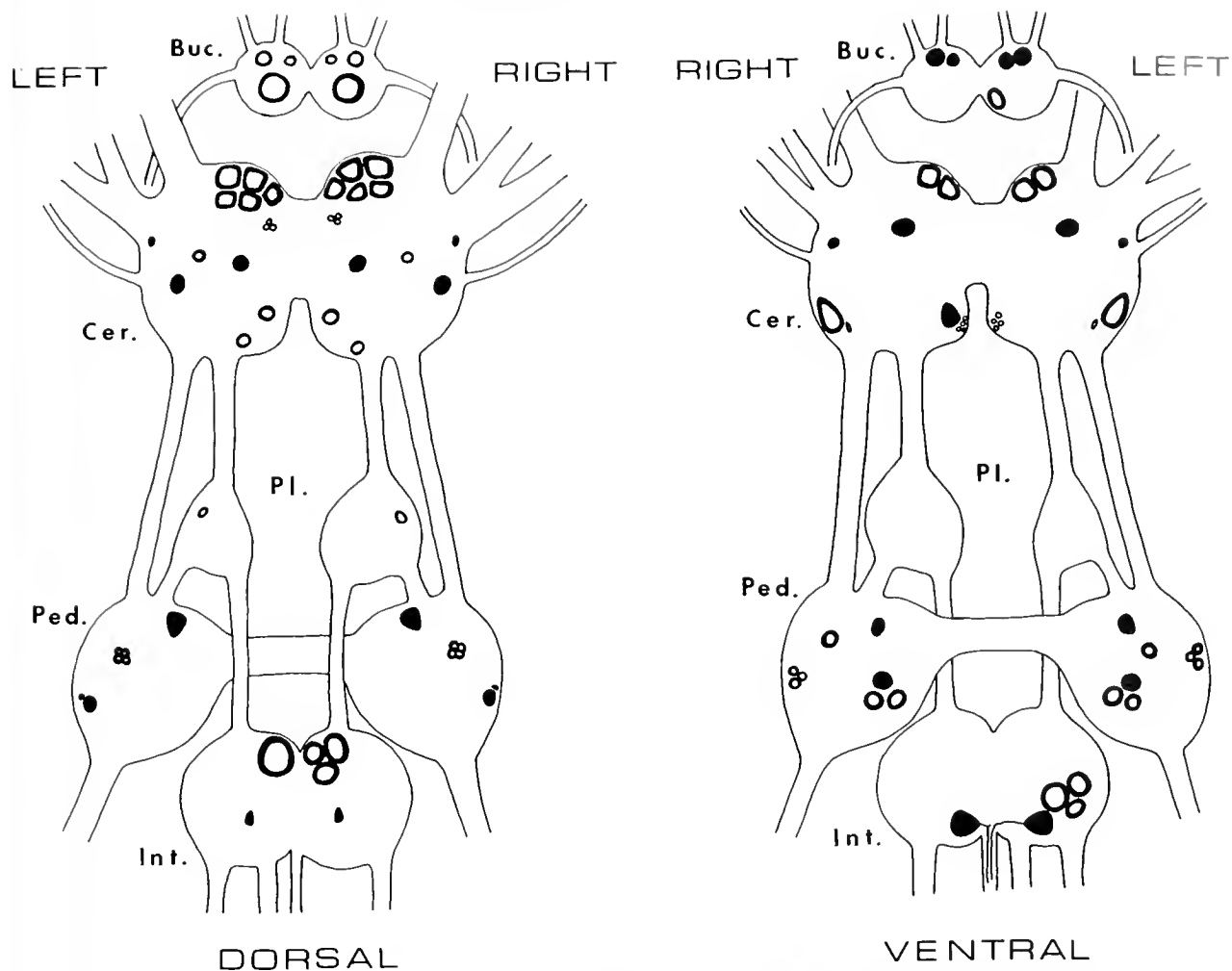


Figure 5. A map of FMRFamide immunoreactive cells on the dorsal and ventral surfaces of central ganglia including buccal (Buc), cerebral (Cer), pedal (Ped), pleural (Pl), and intestinal (Int) pairs. Cells filled in black showed a high level of immunoreactivity; white cells showed a lower level.

buccal cones as revealed by light and electron microscopy: circular smooth muscles and smooth and striated longitudinal muscles (Fig. 8A–C). Immunoreactive processes were primarily associated with bundles of striated longitudinal muscles. Electron microscopical examination of buccal cones revealed immunoreactive terminals adjacent to the striated longitudinal muscle cells (Fig. 8D).

*Wings.* The wings of *Clione* also contained networks of immunoreactive fibers originating from the pedal ganglia and wing nerves (Fig. 9A). Material sectioned for both light (Fig. 9B) and electron microscopy revealed that immunoreactive processes are associated only with retractor muscles of the wings: transverse and longitudinal smooth retractor muscles (classification according to Huang and Satterlie, 1989).

#### Effects of gamma-aminobutyric acid

Gamma-aminobutyric acid (GABA) depolarized and activated the A neurons but hyperpolarized and inhibited

the B neurons (Fig. 10). To test the direct sensitivity of A and B neurons to GABA, they were chemically isolated with high  $Mg^{++}$  or 0.5 mM  $Cd^{++}$  solutions. In all cases, GABA depolarized A neurons and hyperpolarized B neurons (Fig. 10B). Local application of GABA onto the somata of recorded A and B neurons produced similar results (Fig. 10A). Both GABA effects, depolarization of A neurons and hyperpolarization of B neurons, were associated with increases in membrane conductance (Fig. 10C).

Both A and B neurons were very sensitive to GABA. The depolarizing effect of GABA on A neurons was noted with concentrations as low as 0.3  $\mu M$ . Strong activation of spike activity in A neurons was typically produced with GABA concentrations of 1  $\mu M$  and higher. Hyperpolarizing responses were noted in B neurons with GABA concentrations as low as 0.1  $\mu M$ . GABA at a concentration of 1  $\mu M$  had a powerful inhibitory effect on B neurons.

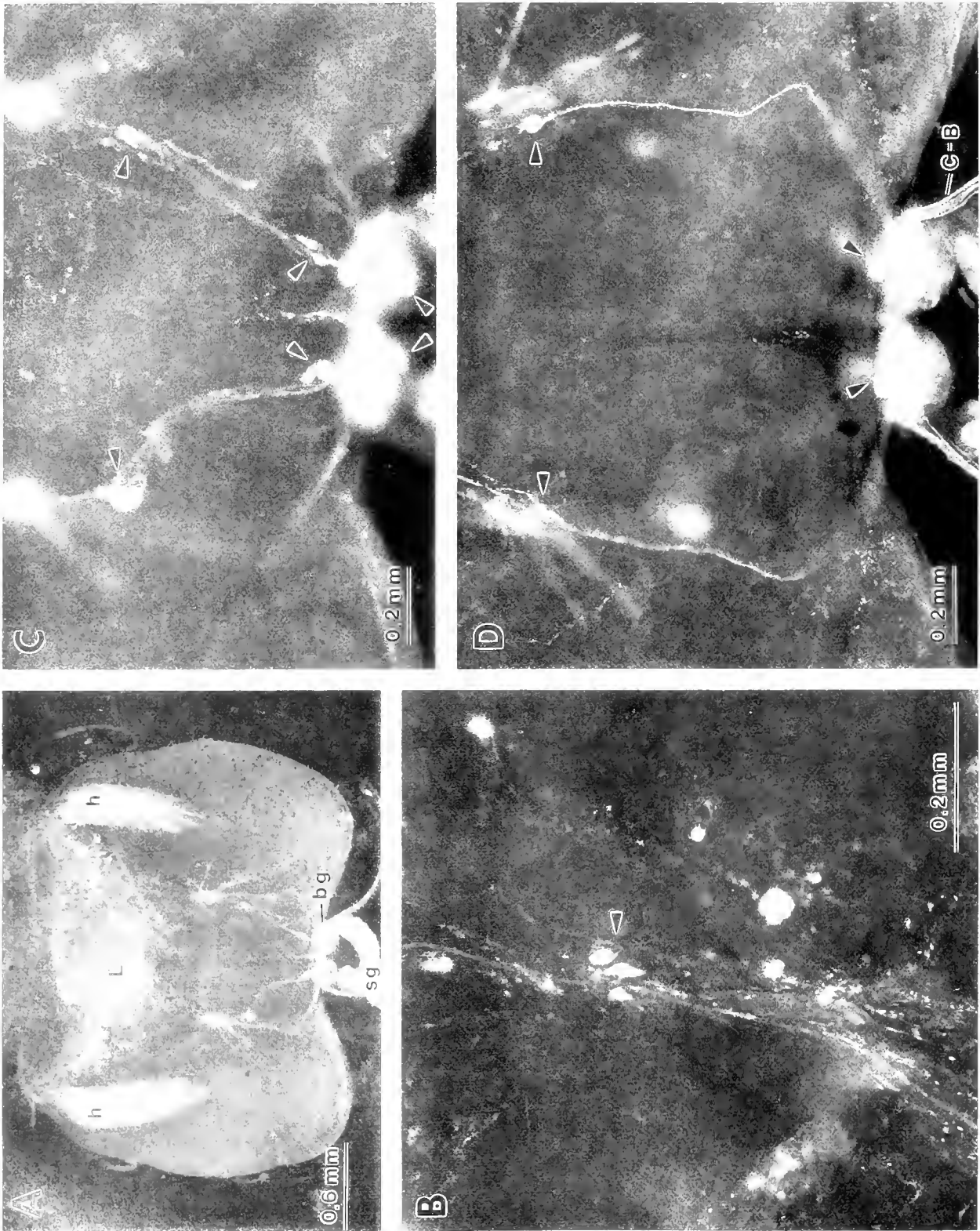


**Figure 6.** Photomicrographs of FMRI amide immunoreactivity in the buccal ganglia and buccal mass. (A) General view of the ventral surface: bg, buccal ganglia; sg, salivary gland; h, hooks; L, lips. (B) Higher magnification of the buccal mass surface showing extraganglionic immunoreactive cell bodies (arrows) and fibers (arrowhead). (C) and (D) dorsal and ventral surfaces of the buccal ganglia and close-by regions of buccal mass; arrows show immunoreactive cell bodies, C-B cerebro-buccal connectives.

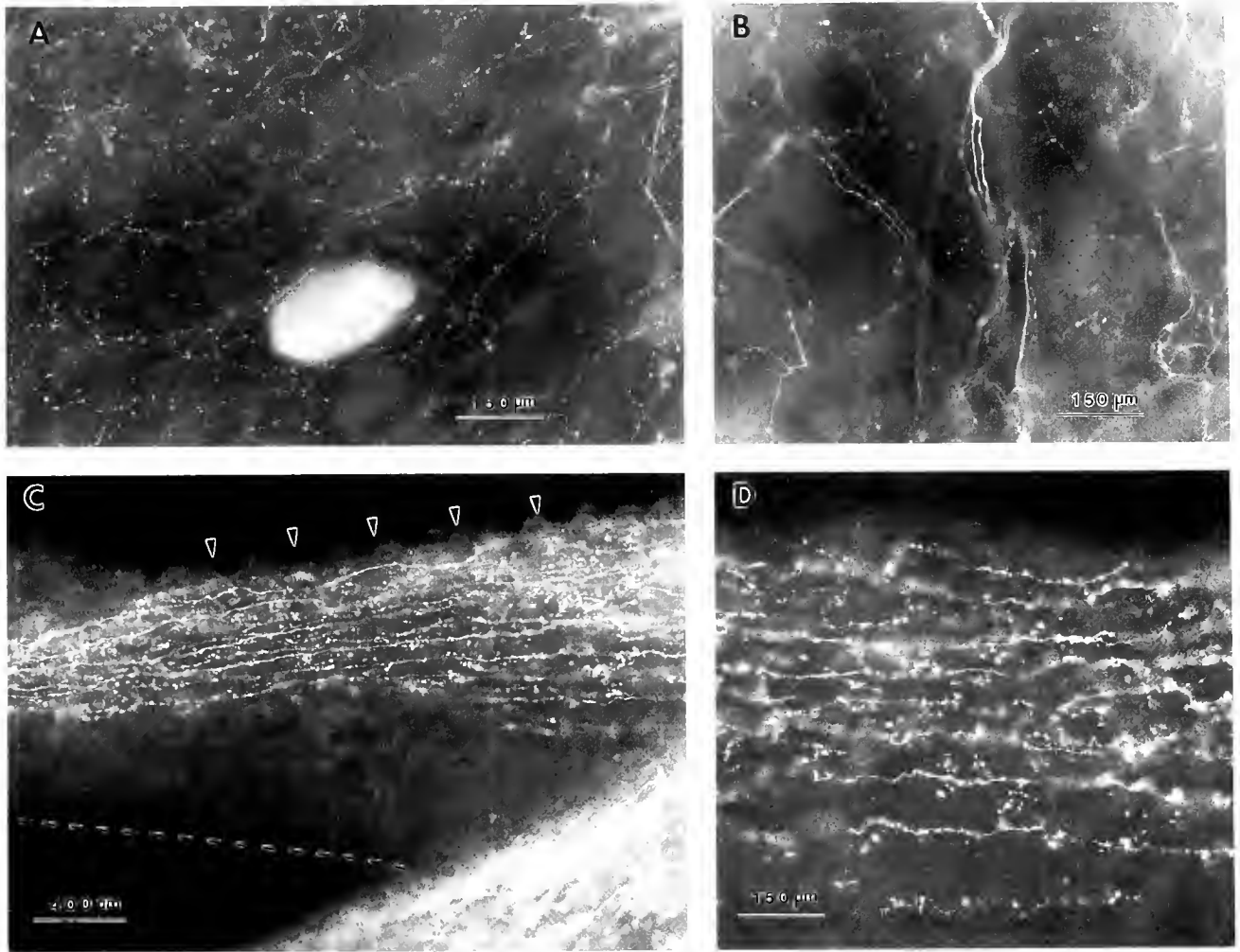


**Figure 7.** FMRFamide immunoreactivity in the head. (A) Network of immunoreactive fibers on the surface of the head skin. (B) Immunoreactive processes run through the entire thickness of the head wall. (C, D) Dense network of longitudinally oriented immunoreactive fibers in buccal cones. Note that fibers are localized only on the internal, oral side of the buccal cone (indicated by arrows). The extent of the external (aboral) side of the cone is indicated by the dashed line in C.

producing hyperpolarizing responses up to 10 mV in amplitude. During GABA application, **B** neurons received two types of inhibitory influence. First, the direct effect of GABA was membrane hyperpolarization. Second, activation of **A** neurons resulted in powerful synaptic inhibition of **B** cells (Fig. 10D).

Bath application of 1  $\mu$ M (or higher) GABA in seawater produced strong activation of **A** neurons and inhibition of **B** neurons (Fig. 10D). GABA thus produced a reciprocal effect on **A** and **B** neurons. The overall behavioral effect of GABA perfusion was the opening of the oral skin folds and protraction of buccal cones. These effects persisted while GABA was present in the recording chamber.

#### *Possible GABAergic nature of IPSPs in B neurons*

GABA was the only transmitter studied that caused hyperpolarization of **B** neurons. Other neurotransmitters

tested—including FMRFamide, serotonin, dopamine, acetylcholine,  $SCP_B$ , and L-glutamate—depolarized **B** neurons. Experiments were therefore conducted to test whether GABA is the transmitter released onto the **B** neurons during **A** neuron activity.

The reversal potentials for GABA-induced hyperpolarization ( $-60 \text{ mV} \pm 3 \text{ mV}$ ,  $n = 7$ ) and **A**-neuron-induced IPSPs ( $-60 \text{ mV} \pm 2 \text{ mV}$ ,  $n = 10$ ) appeared identical and indicated a selective increase in membrane permeability to chloride ions. To increase the intracellular concentration of chloride ions, the recording electrodes were filled with 3 *M* potassium chloride instead of 2 *M* potassium acetate. Leakage of chloride ions from the tip of such electrodes would be expected to cause an increase of intracellular chloride concentration and a shift in the reversal potential of a chloride-mediated response in the



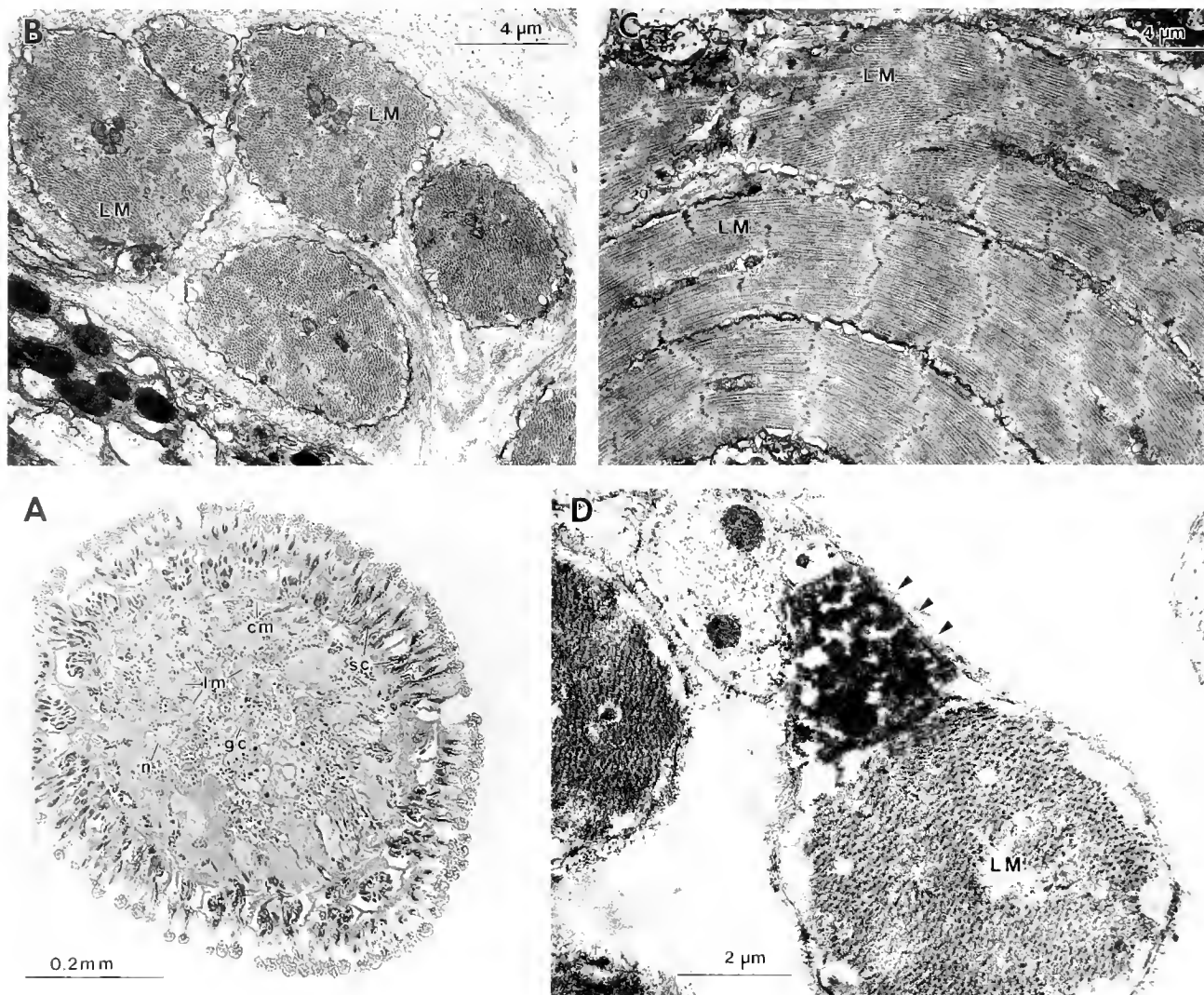


**Figure 8.** Buccal cones. (A) Light photomicrograph of a buccal cone cross section: lm, longitudinal muscles; cm, circular muscles; n, nerve branch; gc, gland cells; sc, secretory cells; the hemocoelic space is not seen since the buccal cone was in a retracted position when fixed. (B) Electron micrograph of a buccal cone cross section: LM, longitudinal muscle cells. (C) Electron micrograph of a buccal cone showing cross-striation of the longitudinal muscle cells. (D) Electron micrograph of a buccal cone cross section showing an immunoreactive terminal (arrows) adjacent to a striated longitudinal muscle cell (LM).

depolarizing direction. Results from one experiment using KCl electrodes placed in **B** neurons are shown in Figure 11A. Just after penetration of the cell, normal IPSPs were recorded following **A** neuron activation. After 10 min, similar stimulation did not produce a change in the **B** neuron membrane potential. Thirty minutes after penetration, **B** neuron IPSPs were reversed, and after 50 min the amplitude of the depolarizing responses was large enough to produce strong activation of the **B** neuron (Fig. 11A). Such experiments suggest that chloride ions are involved in generating the **B** neuron IPSPs.

Similar changes were observed in GABA responses of **B** neurons recorded with KCl electrodes (Fig. 11B). Just after penetration, GABA perfusion produced strong hyperpolarization of **B** neurons. After 10 min, the hyperpolarizing responses disappeared. Twenty to forty minutes after penetration, GABA application began to produce strong depolarization of **B** neurons (Fig. 11B). In several experiments, we tested both IPSPs and GABA responses in the same **B** neuron and observed simultaneous changes in both IPSPs and GABA responses. During these experiments, the baseline membrane potential did not change

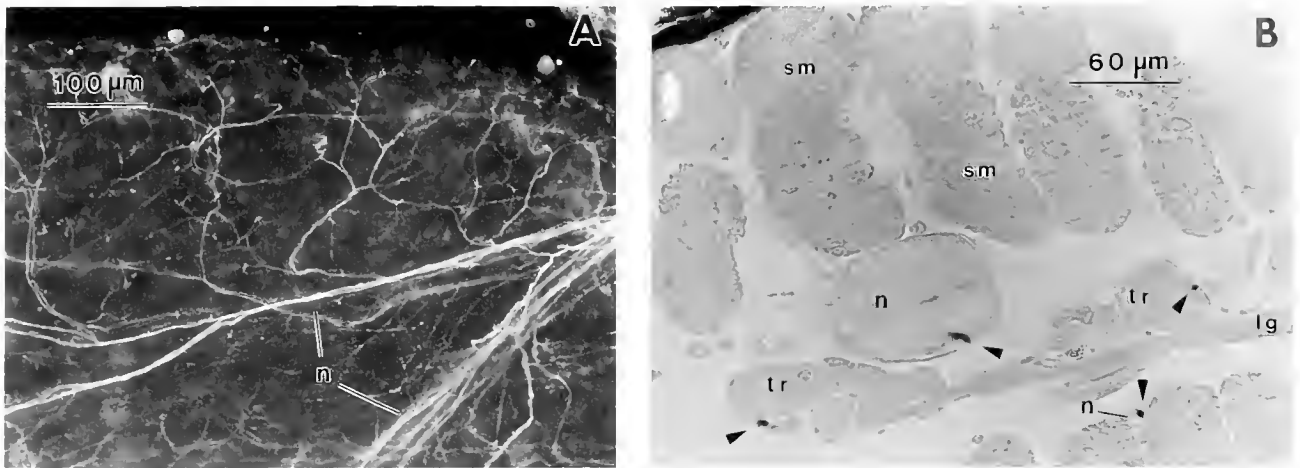


**Figure 9.** FMRamide immunoreactivity of the wings. (A) Immunoreactive fibers (fluorescent secondary antibody) enter the wing through the pedal wing nerve and branch extensively inside the wing: n, two main branches of the wing nerve within the left wing. The optical section is parallel to the dorsal surface of the wing. (B) Transverse section of the wing: arrows show immunoreactive fibers (peroxidase-labeled secondary antibody); sm, swim muscles; tr, transverse retractor muscles; lg, longitudinal retractor muscles; n, nerve.

by more than 4 mV. These data suggest that the **B** neuron IPSPs and GABA responses involve the same ionic mechanism: an increase in chloride permeability.

The final test involved use of different GABA antagonists, specifically including blockers of GABA-activated chloride channels, such as picrotoxin. Picrotoxin did not block **B** neuron IPSPs, even at concentrations of 1 mM. Similarly, bicuculline (a specific blocker of GABA<sub>A</sub> receptors) at concentrations up to 1 mM did not influence the IPSPs. Because these results seemed to contradict the initial suggestion of a GABAergic nature of IPSPs in **B** neurons, the direct GABA responses of **B** neurons were examined. Picrotoxin did not alter the GABA-induced responses (GABA concentration of 10 μM), even in concentrations of 1 mM. GABA-induced hyperpolarizations were also not influenced by pentylenetetrazole, another blocker of GABA-activated chloride channels, even when the concentration was 10 times higher than the GABA concentration. GABA responses were also unaltered by bicuculline at 1 mM, when GABA concentration was 10 μM. These results were repeated in over 35 preparations during three experimental seasons. GABA receptors on **B** neurons thus are not sensitive to the GABA antagonists picrotoxin, pentylenetetrazole, or bicuculline. The data showing that picrotoxin did not block either chloride-dependent GABA responses or IPSPs in **B** neurons strengthen the initial suggestion of the GABAergic nature of **B** neuron IPSPs. However, the question of whether GABA participates in producing IPSPs in **B** neurons cannot be resolved by pharmacological methods. Only identification of particular GABAergic neurons that receive excitatory inputs from **A** neurons and monosynaptically inhibit **B** neurons can give a final answer.

## Discussion

### *FMRFamide*

FMRFamide has potent effects on central neurons of many mollusks. For example, some neurons of *Helix* are excited by FMRFamide, others are inhibited, and some show biphasic responses (Cottrell, 1983; Cottrell *et al.*, 1984; Walker *et al.*, 1981). In *Clione*, FMRFamide depolarized **B** neurons and strongly hyperpolarized **A** neurons. The reversal potential for FMRFamide responses in **A** neurons was about -80 mV, a value that is similar to the theoretical equilibrium potential for K<sup>+</sup> ions in many cells. This would suggest that the FMRFamide responses in *Clione* **A** neurons are potassium mediated, as in other molluscan neurons (Cottrell *et al.*, 1984; Boyd and Walker, 1985; Belardetti *et al.*, 1987; Brussard *et al.*, 1988). Further evidence for a potassium dependency to this response might be that the FMRFamide-induced hyperpolarizations were blocked by TEA and 4-AP, agents that are known to block voltage-activated K<sup>+</sup> currents (Hille, 1992). However, because those agents have not been reported to block ligand or second-messenger-activated K<sup>+</sup> currents, their action here may represent either a novel action on ligand-activated K<sup>+</sup> currents or an indirect effect. We cannot, as yet, distinguish between these possibilities. FMRFamide was the only active agent tested that caused a hyperpolarization in **A** neurons. Two types of naturally occurring IPSPs, fast and slow, were described in **A** neurons, although their source is not known. It is possible that some of the inhibitory inputs are due to activity in FMRFamidergic neurons. Many neurons throughout the central nervous system of *Clione* have been shown to have FMRFamide immunoreactivity, including



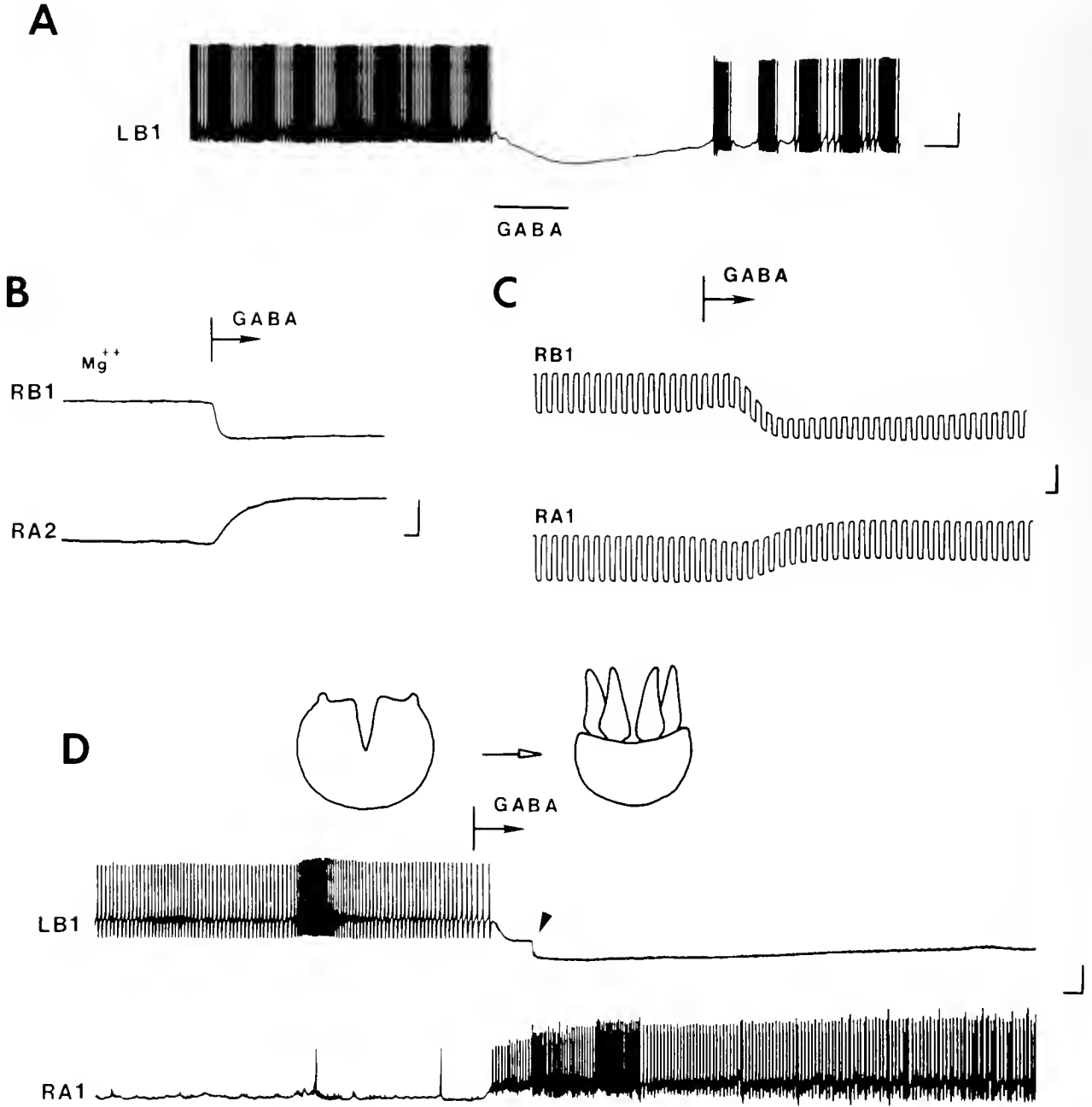


**Figure 10.** Effects of GABA on A and B neurons. (A) Local application of GABA from a glass micro-electrode onto the soma of neuron **LB1**. The duration of the GABA pulse is indicated by the bar. Scale bars = 20 mV, 2 s. (B) Effect of 5  $\mu$ M GABA on neurons **RA2** and **RB1** in high  $Mg^{++}$  solution. Note that GABA depolarizes A neurons and hyperpolarizes B neurons. Scale bars = 10 mV, 1 s. (C) GABA-induced hyperpolarization of B neurons and depolarization of A neurons are associated with the increases in membrane conductance. Two intracellular electrodes were used in these experiments: one for recording membrane potential (shown in figure), and a second for injecting negative current pulses. Current pulses: neuron **RB1**, -1 nA; neuron **RA1**, -2 nA. Scale bars = 10 mV, 2 s. (D) Effect of 2  $\mu$ M GABA on neurons **LB1** and **RA1** in seawater. Note the initial smooth hyperpolarization and the delayed appearance of inhibitory postsynaptic potentials (shown by arrow) in **B1** neuron initiated by A neurons. The drawings above the record indicate observed activity of the head before and after GABA application. Before application skin folds were closed and buccal cones were withdrawn; after application skin folds were open and buccal cones were partially extruded. Scale bars = 20 mV, 2 s.

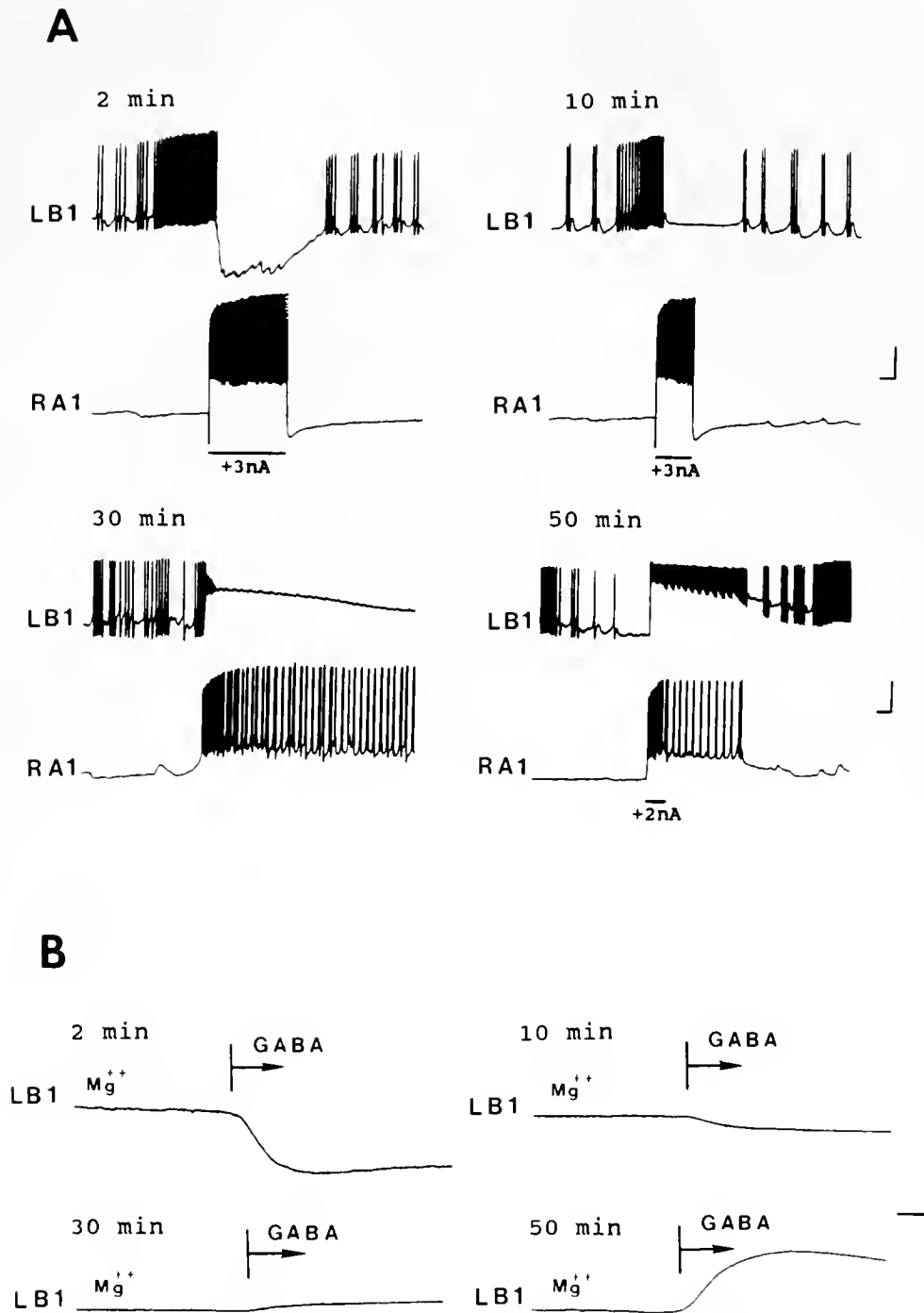


**Figure 11.** Recordings from neuron **LB1** with microelectrodes filled with 3 M KCl. (A) Two minutes after penetrating the **B** neuron, a burst of action potentials in **RA1** produced a hyperpolarizing response; 10 min after penetration, the hyperpolarizing response was eliminated; 30 min after penetration, induced spike activity in **RA1** produced a depolarizing response in **LB1**, 50 min after penetration, the depolarizing **B** neuron response was sufficient to trigger spike activity in **LB1**. Scale bars = 10 mV, 2 s. (B) Direct GABA responses in **LB1** following application of 5  $\mu$ M GABA. The recordings were made in high Mg<sup>++</sup> seawater. The beginning of GABA application is indicated by the vertical bar with the attached arrow. Two minutes after penetration with the KCl electrode, a hyperpolarizing response was induced. This response was reduced at 10 min and reversed at 30 min. Fifty minutes after penetration, GABA perfusion produced a large depolarizing response. Scale bars = 10 mV, 2 s.

cells of the buccal, cerebral, pedal, and intestinal ganglia. The map of FMRFamide immunoreactive neurons can now be used to search for candidate neurons that influence **A** and **B** neuron activities.

The effect of FMRFamide on **A** and **B** neurons is well coordinated to produce inhibition of buccal cone extrusion (hyperpolarization of **A** neurons) and enhancement of buccal cone retraction (depolarization of **B** neurons). The overall behavioral response, withdrawal reaction of the buccal cones, was always observed during FMRFamide perfusion. Similar inhibitory effects of FMRFamide on the components of feeding behavior have been described for several other molluscs. Micromolar concentrations of FMRFamide inhibited patterned motor activity, which underlies feeding behavior, in *Helisoma* buccal ganglia and suppressed activity in salivary gland cells (Murphy *et al.*, 1985; Bulloch *et al.*, 1988). The inhibitory influence of FMRFamide on the feeding motor program was demonstrated in lip-brain preparations of *Limax* (Cooke *et al.*, 1985; Cooke and Gelperin, 1985). FMRFamide also inhibited spontaneous and induced contractions of the anterior gizzard of *Aplysia* (Austin *et al.*, 1983).

Immunolocalization of FMRFamide in cells in buccal ganglia, as well as in extraganglionic neurons in the buccal mass and mouth region, and the dense network of immunoreactive fibers in the buccal muscles suggest a physiological role for this neuropeptide in the regulation of feeding behavior of *Clione*. Similarly, FMRFamide immunoreactivity has been observed in a number of neurons in buccal ganglia and in buccal muscles of *Aplysia* (Lloyd *et al.*, 1987). Of particular interest is localization of intensely immunoreactive fibers in *Clione* buccal cones. FMRFamide immunoreactive terminals were found to innervate cross-striated longitudinal muscle cells, which underlie movements of protracted buccal cones. Contraction of the longitudinal muscles on the oral side of buccal cones would produce catching and holding movements of the cones, which is observed during the acquisition and manipulation phases of feeding behavior. FMRFamide immunoreactive fibers were found only on the oral side of each buccal cone. This localization of immunoreactive processes suggests that FMRFamide participates in control or modulation of buccal cone movements during feeding behavior of *Clione*.

Bath application of FMRFamide also led to the inhibition of swimming, termination of which is a component of withdrawal behavior in *Clione*. FMRFamide immunoreactive nerve fibers, observed in the wings of *Clione*, were associated with retraction musculature. Excitatory effects of FMRFamide on retractor muscles have been demonstrated on the anterior byssus retractor muscle of *Mytilus edulis* (Painter, 1982) and on *Helix* tentacle retractor muscle (Cottrell *et al.*, 1983). FMRFamide there-

fore may act as a mediator involved in inhibitory control of different components of feeding behavior in *Clione*.

#### *Gamma-aminobutyric acid*

GABA has been found to excite some gastropod neurons and to inhibit others (Walker *et al.*, 1975; Yarowsky and Carpenter, 1978; Oomura *et al.*, 1979). Yarowsky and Carpenter (1978) identified five types of responses in *Aplysia* neurons, the most common of which was a fast chloride-mediated hyperpolarization with a reversal potential of  $-58$  mV. Picrotoxin ( $1-100$   $\mu M$ ) and bicuculline ( $10-100$   $\mu M$ ) blocked the chloride-mediated inhibition produced by GABA.

In *Clione*, GABA depolarized and activated **A** neurons and hyperpolarized **B** neurons. The hyperpolarizing response of **B** neurons had a reversal potential of  $-60$  mV and was chloride-mediated. Likewise, IPSPs in **B** neurons, induced by **A** neuron activity, had reversal potentials of  $-60$  mV, and were linked with activation of chloride channels. These data, plus the observation that GABA was the only transmitter tested that inhibited **B** neurons, suggest that GABA might be the transmitter released during the **A**-to-**B** neuron inhibition. GABAergic neurons have been localized by immunohistochemical methods in *Clione* in the cerebral, pedal, and buccal ganglia (Arshavsky *et al.*, 1993).

However, picrotoxin, a blocker of GABA-activated chloride channels (Nistri and Constanti, 1979; Simmonds, 1983; Tallman and Gallagher, 1985), did not block either **B** neuron IPSPs or the direct inhibitory action of applied GABA, even in concentrations of  $1$  mM. Bicuculline, a specific antagonist of inhibitory GABA<sub>A</sub> receptors, also did not block the IPSPs or GABA responses. The fact that bicuculline, picrotoxin, and pentylentetrazole (another tested GABA chloride-channel blocker) did not have any effect on chloride-mediated GABA inhibition in **B** neurons was unusual, but not unique. GABA-activated chloride-conductance increases that are insensitive to picrotoxin have been described in the stomatogastric ganglion of the crab *Cancer pagurus* (Marder and Paupardin-Tritsch, 1978) and in neuromuscular preparations of the spiny lobster, *Panulirus* (Albert *et al.*, 1986). It was also reported that bicuculline had no effect on GABA-mediated IPSPs in the locust (Watson and Burrows, 1987) and did not inhibit the binding of  $^3H$ -GABA to a putative GABA receptor in cockroach nerve cord extracts (Lummis and Sattelle, 1985). The **B** neurons of *Clione* may represent another model for studying such unusual GABA inhibitory responses.

One of the most important aspects of the GABA effect in *Clione* is the coordinated influence on **A** and **B** neurons. GABA depolarized and activated **A** neurons but hyperpolarized **B** neurons, which also received powerful IPSPs

from the activated A cells. The overall effect is to turn off the system that is responsible for buccal cone withdrawal while activating the system that triggers food acquisition. During GABA perfusion, it was always possible to observe opening of the oral skin folds and protraction of the buccal cones.

GABA is usually considered a classical local neurotransmitter, and only a few studies have shown it to have widespread behavioral effects. GABA was shown to have an excitatory effect on patterned feeding motor activity in *Helisoma trivolvis*; GABA activated the central pattern generator in buccal ganglia in quiescent preparations and increased the rate of patterned activity in activated preparations (Richmond *et al.*, 1986). In *Limax*, however, GABA was reported to suppress the feeding motor program in a lip-brain preparation (Cooke *et al.*, 1985). In *Clione*, GABA injection into intact animals strongly activated feeding behavior, including protraction of buccal cones (Arshavsky *et al.*, 1993). Arshavsky *et al.* (1993) also described the excitatory effect of GABA on locomotion, on the feeding rhythm generator of the buccal ganglia, and on cerebral neurons, which appear to be some of the A neurons identified in our previous work (Norekian and Satterlie, 1993).

GABA and FMRFamide thus evoke functionally opposite behavioral effects in *Clione* through coordinated changes in the activities of three groups of neurons. FMRFamide inhibits prey-capture reactions and initiates withdrawal reactions: retraction of buccal cones through hyperpolarization of A neurons and depolarization of B neurons, and inhibition of swimming. GABA, on the contrary, initiates feeding reactions through powerful extrusion of the buccal cones due to strong activation of A neurons and direct inhibition of B neurons.

### Acknowledgments

This work was supported by a Grass Fellowship in Neuroscience to TPN in 1990 and NIH grant RO1 NS27951 to RAS.

### Literature Cited

- Albert, J., C. J. Lingle, E. Marder, and M. B. O'Neil. 1986. A GABA-activated chloride-conductance not blocked by picrotoxin on spiny lobster neuromuscular preparations. *Br J Pharmacol* **87**: 771-779.
- Arshavsky, Y. I., T. G. Deliagina, G. N. Gamkrelidze, G. N. Orlovsky, Y. V. Panchin, L. B. Popova, and O. V. Shupliakov. 1993. Pharmacologically-induced elements of the hunting and feeding behaviour in the pteropod mollusc *Clione limacina* 1. Effects of GABA. *J. Neurophysiol.* **69**: 512-521.
- Austin, T., S. Weiss, and K. Lukowiak. 1983. FMRFamide effects on spontaneous and induced contractions of the anterior gizzard in *Aplysia*. *Can. J. Physiol. Pharmacol.* **61**: 949-953.
- Belardetti, F., E. R. Kandell, and S. A. Siegelbaum. 1987. Neuronal inhibition by the peptide FMRFamide involves opening of S K<sup>+</sup> channels. *Nature* (London) **325**: 153-156.
- Boyd, P. J., and R. J. Walker. 1985. Actions of the molluscan neuropeptide FMRFamide on neurones in the suboesophageal ganglia of the snail *Helix aspersa*. *Comp. Biochem. Physiol.* **81C**: 379-386.
- Brussaard, A. B., K. S. Kits, A. ter Maat, J. van Minnen, and P. J. Moed. 1988. Dual inhibitory action of FMRFamide on neurosecretory cells controlling egg laying behavior in the pond snail. *Brain Res.* **447**: 35-51.
- Bulloch, A. G. M., D. A. Price, A. D. Murphy, T. D. Lee, and H. N. Bowes. 1988. FMRFamide peptides in *Helisoma*. identification and physiological actions at a peripheral synapse. *J. Neurosci.* **8**: 3459-3469.
- Cooke, I., and A. Gelperin. 1985. Mapping and pharmacology of neurotransmitters in the feeding control system of *Limax*. *Soc. Neurosci. Abstr.* **11**: 368.
- Cooke, I., K. Delaney, and A. Gelperin. 1985. Complex computation in a small neural network. Pp. 173-191 in *Memory Systems of the Brain*. N. M. Weinberger, J. L. McGaugh, and G. Lynch, eds. Guilford Press, New York.
- Cottrell, G. A. 1983. Actions of FMRFamide and related peptides on snail neurons. Pp. 213-220 in *Molluscan Neuro-Endocrinology*. J. Lever and H. H. Boer, eds. North-Holland Publ., Amsterdam.
- Cottrell, G. A., N. W. Davies, and K. A. Green. 1984. Multiple actions of a molluscan cardioexcitatory neuropeptide and related peptides on identified *Helix* neurones. *J. Physiol.* **356**: 315-333.
- Cottrell, G. A., M. J. Greenberg, and D. A. Price. 1983. Differential effects of the molluscan neuropeptide FMRFamide and the related Met-enkephalin derivative YGGFMRFamide on the *Helix* tentacle retractor muscle. *Comp. Biochem. Physiol.* **75C**: 373-375.
- Hermans, C. O., and R. A. Satterlie. 1992. Fast-strike feeding behavior in a pteropod mollusc, *Clione limacina* Phipps. *Biol. Bull.* **182**: 1-7.
- Hille, B. 1992. *Ionic Channels of Excitable Membranes*. Sinauer Associates Inc., Sunderland, MA.
- Huang, Z., and A. Satterlie. 1989. Smooth muscle fiber types and a novel pattern of thick filaments in the wing of the pteropod mollusc *Clione limacina*. *Cell Tissue Res.* **257**: 405-414.
- Kupfermann, I. and K. R. Weiss. 1981. The role of serotonin in arousal of feeding behavior of *Aplysia*. Pp. 255-287 in *Serotonin Neurotransmission and Behaviour*. B. L. Jacobs and A. Gelperin, eds. MIT Press, Cambridge.
- Lalli, C. M., and R. W. Gilmer. 1989. *Pelagic Snails. The Biology of Holoplanktonic Gastropod Mollusks*. Stanford University Press, Stanford, CA.
- Lent, C. M., M. H. Dickinson, and C. G. Marshall. 1989. Serotonin and leech feeding behavior: obligatory neuromodulation. *Amer. Zool.* **29**: 1241-1254.
- Litvinova, N. M. and G. N. Orlovsky. 1985. Feeding behaviour of pteropod mollusc *Clione limacina*. *Bull. Moscow Naturalist Soc.* section of Biology **90**: 73-77 (in Russian).
- Lloyd, P. E., M. Frankfurt, P. Stevens, I. Kupfermann, and K. R. Weiss. 1987. Biochemical and immunocytochemical localization of the neuropeptides FMRFamide, SCP<sub>A</sub>, SCP<sub>B</sub>, to neurons involved in the regulation of feeding in *Aplysia*. *J. Neurosci.* **7**: 1123-1132.
- Lummis, S. C. R., and D. B. Sattelle. 1985. Insect central nervous system gamma-aminobutyric acid receptors. *Neurosci. Lett.* **60**: 13-18.
- Marder, E., and D. Paupardin-Tritsch. 1978. The pharmacological properties of some crustacean neuronal acetylcholine, gamma-aminobutyric acid and L-glutamate responses. *J. Physiol.* **280**: 213-236.
- Murphy, A. D., K. Lukowiak, and W. K. Stell. 1985. Peptidergic modulation of patterned motor activity in identified neurons of *Helisoma*. *Proc. Nat. Acad. Sci. USA* **82**: 7140-7144.
- Nistri, A., and A. Constanti. 1979. Pharmacological characterisation of different types of GABA and glutamate receptors in vertebrates and invertebrates. *Prog. Neurobiol.* **13**: 117-235.

- Norekian, T. P., and R. A. Satterlie. 1991a. Acquisition phase of feeding behavior in the pteropod mollusc, *Clione limacina*. *Soc. Neurosci. Abstr.* 17: 1593.
- Norekian, T. P., and R. A. Satterlie. 1991b. Neuronal analysis of hunting behavior of the pteropod mollusc, *Clione limacina*. *J. Higher Nervous Activ.* 41: 982-997 (in Russian).
- Norekian, T. P., and R. A. Satterlie. 1993. Cerebral neurons underlying the prey capture movements in the pteropod mollusc, *Clione limacina*. I. Physiology, morphology. *J. Comp. Physiol. A* 172: 153-169.
- Oomura, Y., J. Maruhashi, N. Shimizu, and M. Kato. 1979. GABA receptors and ionic channels in *Onchidium* neurons. *Brain Res. Bull.* 4: 178-180.
- Painter, S. D. 1982. FMRFamide catch contractures of a molluscan smooth muscle: pharmacology, ionic dependence and cyclic nucleotides. *J. Comp. Physiol.* 148: 491-501.
- Richmond, J. E., A. D. Murphy, A. G. M. Bulloch, and K. Lukowiak. 1986. Evidence for an excitatory effect of GABA on feeding patterned motor activity (PMA) of *Helisoma trivolvis*. *Soc. Neurosci. Abstr.* 12: 792.
- Satterlie, R. A. 1989. Reciprocal inhibition and rhythmicity: swimming in a pteropod mollusk. Pp. 151-171 in *Neuronal and Cellular Oscillators*, J. W. Jacklet, ed. Marcel Dekker Inc., New York and Basel.
- Simmonds, M. A. 1983. Multiple GABA receptors and associated regulatory sites. *Trends Neurosci.* 6: 279-281.
- Tallman, J. F., and D. W. Gallagher. 1985. The GABA-ergic system: a locus of benzodiazepine action. *Ann. Rev. Neurosci.* 8: 21-44.
- Wagner, N. 1885. *Die Wirbellosen des Weissen Meeres: Zoologische Forschungen an der Kuste des Solowetzkischen Meerbusens in den Sommermonaten der Jahre*. Verlag Von Wilhelm Engelmann, Leipzig, Germany.
- Walker, R. J., M. J. Azanza, G. A. Kerkut, and G. N. Woodruff. 1975. The action of gamma-aminobutyric acid (GABA) and related compounds on two identified neurones in the brain of the snail, *Helix aspersa*. *Comp. Biochem. Physiol.* 50C: 147-154.
- Walker, R. J., V. A. James, and C. J. Roberts. 1981. The action of FMRFamide and proctolin on *Helix*, *Hirudo*, *Limulus* and *Periplaneta* neurones. Pp. 411-416 in *Advances in Animal and Comparative Physiology*, G. Pethes and V. L. Frenyo, eds. Pergamon, Oxford, and Akadem. Kiado, Budapest, Hungary.
- Watson, A. H. D., and M. Burrows. 1987. Immunocytochemical and pharmacological evidence for GABAergic spiking local interneurons in the locust. *J. Neurosci.* 7: 1741-1751.
- Yarowsky, P. J., and D. O. Carpenter. 1978. Receptors for gamma-aminobutyric acid (GABA) on *Aplysia* neurones. *Brain Res.* 144: 75-94.

# Glycosaminoglycans in *Anodonta californiensis*, a Freshwater Mussel

PETER HOVINGH AND ALFRED LINKER

*Research Service, Veterans Affairs Medical Center and Departments of Biochemistry and Pathology,  
University of Utah, Salt Lake City, Utah 84148*

**Abstract.** The synthesis of glycosaminoglycans (GAG) in a freshwater mussel was studied in organ culture using labeled precursors. The major GAGs synthesized were determined and characterized by chemical and enzymatic methods. They were shown to be heparin and an unusual type of heparan sulfate. Gills produced about 50% of each polymer; mantles synthesized little heparin and mostly the heparan-sulfate-like compound, which is similar to a GAG isolated previously from lobsters. No significant amounts of chondroitin sulfates were present.

Histological data showed that the sulfate-labeled GAGs were present mainly in exterior pericellular and basement membrane locations of gills and mantle. That is, they would be in contact with the external aqueous environment, suggesting a potential role in calcium transport and storage.

## Introduction

Glycosaminoglycans (GAG) constitute a group of highly charged complex polysaccharides that have a remarkable distribution in organisms. They are present from prokaryotes to vertebrates, and their main structural features appear to have been conserved during evolution. Their occurrence and distribution have been widely studied in animal species (Rahemtulla and Lovtrup, 1974; Cassaro and Dietrich, 1977; Nader *et al.*, 1983), and most of the six or so GAGs are represented in a variety of organisms. One unusual exception is heparin, which is present in some invertebrates (De Meio *et al.*, 1967; Rahemtulla and Lovtrup, 1975), and appears only sporadically in vertebrates but, with some exceptions (Gomes and

Dietrich, 1982; Hovingh *et al.*, 1986), is widely distributed in mammals.

Various important biological functions have been ascribed to GAGs (Kjellen and Lindahl, 1991)—many well-documented, others speculative. Heparin is an excellent anticoagulant when used pharmacologically, but its biological role in higher organisms is uncertain. Though heparin interacts with such biologically active materials as growth factors, cell receptors, and matrix components, its absence from the *in vivo* locations where interaction is plausible has cast doubt on the biological significance of those interactions. The heparin isolated from species of marine clams and mussels (Pejler *et al.*, 1987) has structural features and anticoagulant activity identical to the mammalian polysaccharide. The presence and potential function of heparin in clams and mussels may provide a clue to its role in vertebrates because structural consistency may imply some functional consistency.

This study had two objectives: first, to determine the presence of heparin or other GAGs in a freshwater mussel; second, to examine the exact location of these polymers in the organism as an initial step toward identifying a potential role.

## Materials and Methods

*Anodonta californiensis* Lea was collected in western Utah in autumn and spring. The animals were either utilized immediately or kept in an aquarium for up to 6 months. Organ cultures were performed in Minimum Essential Eagle Medium (Modified) with Earle's salts and glutamine (Flow Laboratory, McClean, Virginia); the pH was adjusted to 7.2 with sodium bicarbonate. The medium contained gentamicin sulfate (80 µg/ml) and 10% bovine calf serum (Orvine Laboratory, Santa Ana, CA) and was sterile-filtered before use.

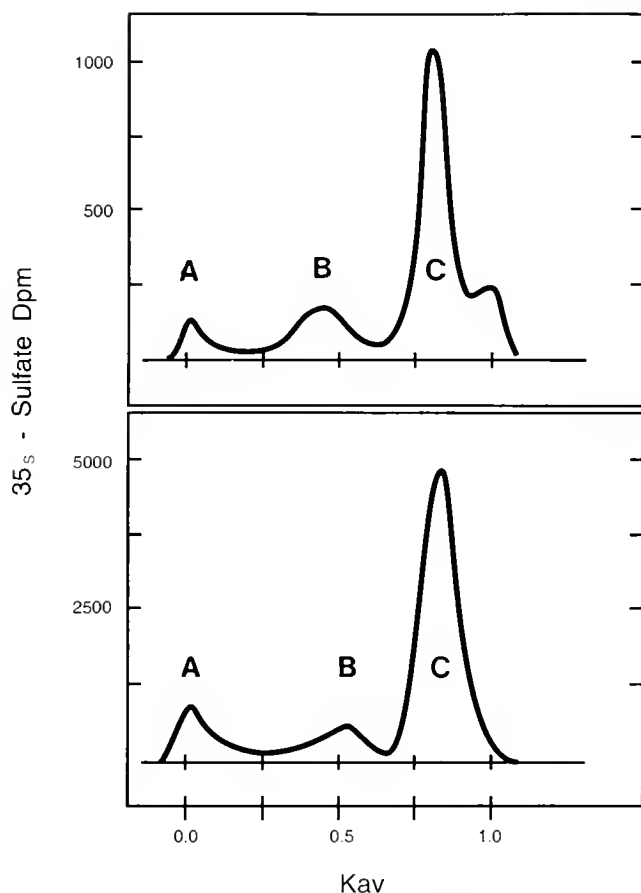


**Figure 1.** Sepharose CL-4B. Chromatography of labeled GAGs isolated from organs. Top: mantle. Bottom: gills.  $K_{av}$  of heparan sulfate with molecular weight of 11,000 daltons is 0.58.

Radiolabeled sulfate ( $\text{Na}_2^{35}\text{S}\text{O}_4$ , 370 mCi/mM),  $^3\text{H}$  glucosamine (30 mCi/mM), and sodium borotritide were obtained from NEN (Burbank, CA). Pronase and chon-

droitinase ABC were obtained from Sigma (St. Louis, MO). Heparinase and heparitinase were prepared as described previously (Linker and Hovingh, 1972); they were free of other lyases, disaccharidase, and sulfatases. For the identification of isolated GAGs, the purified heparinase and heparitinase were used at 12  $\mu\text{g}$  of enzyme protein per milliliter of 0.05 M phosphate buffer pH 7.0, at 25°C for the heparinase and at 37°C for the heparitinase. The solutions were incubated for 16 h. Chondroitinase ABC was used at 5–10 units/ml of the same buffer at 37°C and incubated for 16 h. Substrates were at 10 mg/ml. The low-pH nitrous acid method (Shively and Conrad, 1976) was also used for identification.

DEAE Sephacel, Sepharose Cl-4B, Sephadex G-50, G-25, and G-10 were obtained from Pharmacia (Piscataway, NJ) and Bio Rad AG 1-X2 from Bio Rad (Richmond, CA).

#### Chromatography and electrophoresis

Columns of Sepharose Cl-4B (1100  $\times$  10 mm) were eluted with 0.1% SDS in pH 7.5 Tris buffer containing protease inhibitors (10 mM EDTA, 10 mM N-ethylmaleimide, and 5 mM benzamidine HCl). Sephadex G-50 and G-25 columns were eluted with 0.2 M NaCl in 10% ethanol and Sephadex G-10 columns with 10% ethanol in water. DEAE Sephacel columns were eluted stepwise in increments of 0.2 M NaCl starting with 0.2 M NaCl to 1.0 M NaCl in the presence of 1% Triton X-100 in 4 M urea with the protease inhibitors described above. Bio Rad AG1  $\times$  2 columns (30  $\times$  10 mm) were eluted with 0.5 M, 1.0 M, 1.25 M, and 2.0 M NaCl.

Electrophoresis was carried out on cellulose acetate strips in pyridine:formic acid (Hovingh and Linker, 1982) at pH 3.0 for 15 min at 50 mA. Enzymatic and nitrous acid breakdown products were identified by paper elec-

**Table I**

*Distribution of  $^{35}\text{S}$ -sulfate labeled polymers from gills and mantles after elution from sepharose Cl-4B columns: a summary of three experiments*

	Peak A			Peak B			Peak C		
	Percent of sulfate label	$K_{av}^*$	$K_{av}$ after alkali	Percent of sulfate label	$K_{av}$	$K_{av}$ after alkali	Percent of sulfate label	$K_{av}$	$K_{av}$ after alkali
<i>Mantle</i>									
Expt. I	9	0.0	0.0	19	0.47	0.4–0.80	72	0.80	
Expt. II	8	0.0	0.06–0.83	8	0.50	0.54–0.77	84	0.87	0.84
Expt. III	12	0.17	0.76	43	0.53	0.76	45	0.73	0.76
<i>Gills</i>									
Expt. I	12	0.0	0.0–0.8	9	0.52	0.80	79	0.85	
Expt. II	7	0.0	0.6–0.4	8	0.52	0.45–0.74	85	0.87	0.81
Expt. III	9	0.03	ND	32	0.53	ND	59	0.87	0.76

\* A sample of an average commercial heparin had a  $K_{av}$  of 0.6–0.93, which corresponds to a molecular weight of 11,000.  $K_{av}$  is an indicator of molecular weight and determined by the formula: (elution volume minus void volume)/(total volume minus void volume).

ND = not determined.



35S - Sulfate Dpm

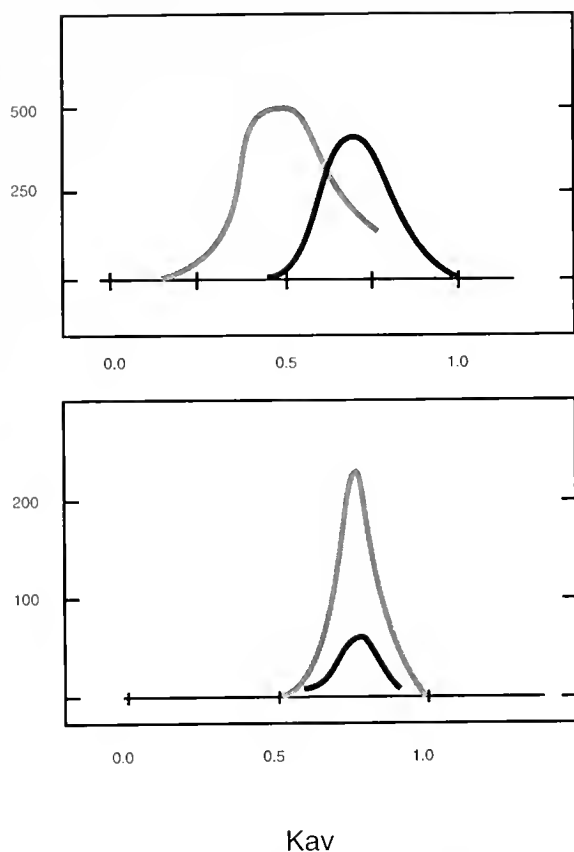


**Figure 2.** Sepharose CL-4B. Chromatography of material isolated from the peaks shown in Figure 1. Top: labeled material from gills in peak B before and after treatment with pronase. Solid line, untreated material; shaded line, pronase digested material. Bottom: labeled material from mantle in peaks A, B, C shown in Figure 1 after alkaline borohydride treatment. Material from peak A, shaded line; peak B, and peak C, solid line. Note that compared to Figure 1, material in peaks A and B shifted to a  $K_{av}$  of 0.75–0.80, whereas material in peak C (with a  $K_{av}$  of 0.75–0.80) showed no further shift.

trophoresis in 1.6 M formic acid at pH 1.6. Scintillation counting was performed on a Packard Tri Carb 1500 using Opti Fluor scintillation cocktails.

The presence of proteoglycans was determined by alkaline degradation with borotritide in 0.5 N NaOH for 16 h at 4°C or in 0.1 N NaOH for 16 h at room temperature. In this connection, the term 'free chains' (vs. proteoglycans) is used here as defining GAGs that show no change in molecular weight upon alkaline treatment; they may contain a small peptide, however.

#### Organ culture

Gills and mantles were obtained from the mussels after the adductor muscles were transected (to open the shell). Organs were placed in the medium in Falcon 3046 multiwell (35 mm) tissue culture plates (Becton Dickinson).

**Table II**

*Distribution of molluscan GAG (Fraction C) on ion-exchange chromatography and on cellulose acetate electrophoresis*

	NaCl molarity	Gills	Mantle
<i>Ion exchange</i>	1.0 M	16%	19%
	1.25 M	38%	45%
	1.5–2.0 M	46%	33%
<i>Electrophoresis</i>	Migrating as:		
	Heparan sulfate	55%	79%
	Heparin	45%	21%

[<sup>35</sup>S] sulfate alone, or with up to 50  $\mu$ Ci/ml radiolabeled glucosamine, 5  $\mu$ Ci/ml. The tissues were slowly shaken in a water bath at 25°C for 6 or 24 h and then washed with cold medium and ground in a Potter-Elvehjem tissue grinder in the presence of 1% Triton X-100 in 4 M urea containing the protease inhibitors. The ground material was added to a DEAE-Sephacel column and washed extensively with the above solution in 0.2 M NaCl. The labeled material was then eluted with the 1% Triton, 4 M

**Table III**

*Composition of radiolabeled sulfate polymers in molluscan gills and mantle*

	"Heparin"*	Percent chondroitin sulfate*	Other*
<i>Mantle</i>			
Total			
Expt I	58	0	42
Expt II	96	1	3
Fraction A			
Expt I	0	0	100
Expt II	50	0	50
Fraction B			
Expt I	21	0	79
Expt II	80	0	20
Fraction C			
Expt I	75	0	25
Expt II	98	1	1
<i>Gill</i>			
Total			
Expt I	72	4	26
Expt II	84	1	15
Fraction A			
Expt I	46	8	46
Expt II	0	0	100
Fraction B			
Expt I	29	0	71
Expt II	17	0	83
Fraction C			
Expt I	81	0	19
Expt II	86	1	13

\* Identified by heparinase, chondroitinase, and nitrous acid.

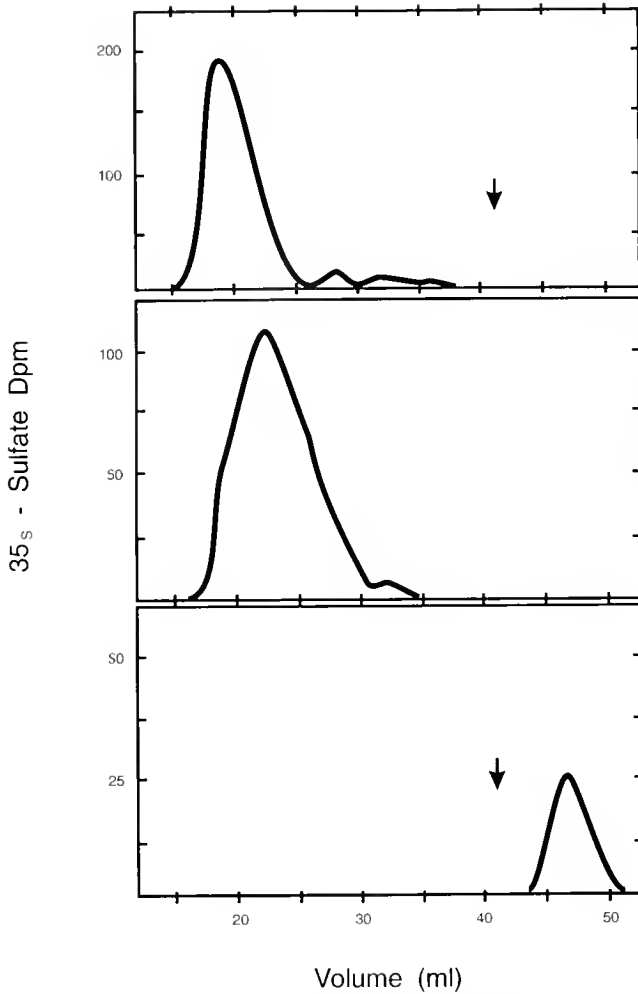


**Figure 3.** Characterization of GAGs of the mantle in peak C of Figure 1. Chromatography on Sephadex G-50 of the GAGs treated with heparinase (top) purified heparinase (middle), and nitrous acid (bottom).

urea solution containing 1.0 M NaCl and characterized further, as will be described.

*Histology*

Parts of the incubated tissues were processed in a routine manner with an Autotechnicon processor, embedded in paraffin, and sectioned. Crude flavobacterial heparinase (Linker and Hovingh, 1972) was used for the identification of sulfate-labeled material. The enzyme, at 1 mg/ml in phosphate-buffered saline, was added to the deparaffinized sections on the slides and incubated for 1 h at 25°C just prior to staining. The saline was used only in control incubations. The sections were examined by autoradiography using Kodak NTB2 emulsion and exposure for 3-5 days. They were then stained and counterstained, respectively with either Alcian blue and Congo red or with hematoxylin and eosin.

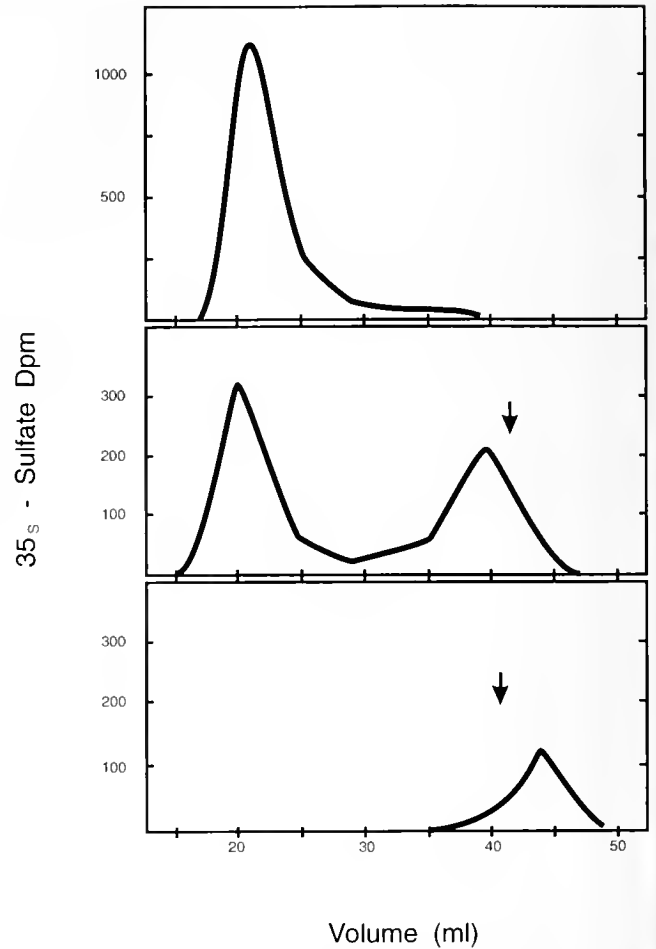


**Figure 4.** Characterization of GAGs of gills in peak C of Figure 1. Chromatography on Sephadex G-50 of the GAGs treated with heparinase (top), purified heparinase (middle), and nitrous acid (bottom).

**Results**

The labeled polymers isolated after organ culture were first examined for size, charge, and carbohydrate composition. Size distributions on Sepharose CL-4B are shown

**Table IV**

*Structural studies of molluscan "heparin" in Fraction C*

	Percent degraded (radiolabeled sulfate)		
	Heparinase	Heparinase	Nitrous Acid*
<i>Gills</i>			
Expt I	3**	52	31
Expt II	ND	27	59
<i>Mantle</i>			
Expt I	22**	13**	51
Expt II	ND	28	70

\* Material resistant to heparinase degraded further by nitrous acid.  
 \*\* No disaccharides or tetrasaccharides.  
 ND = not determined.

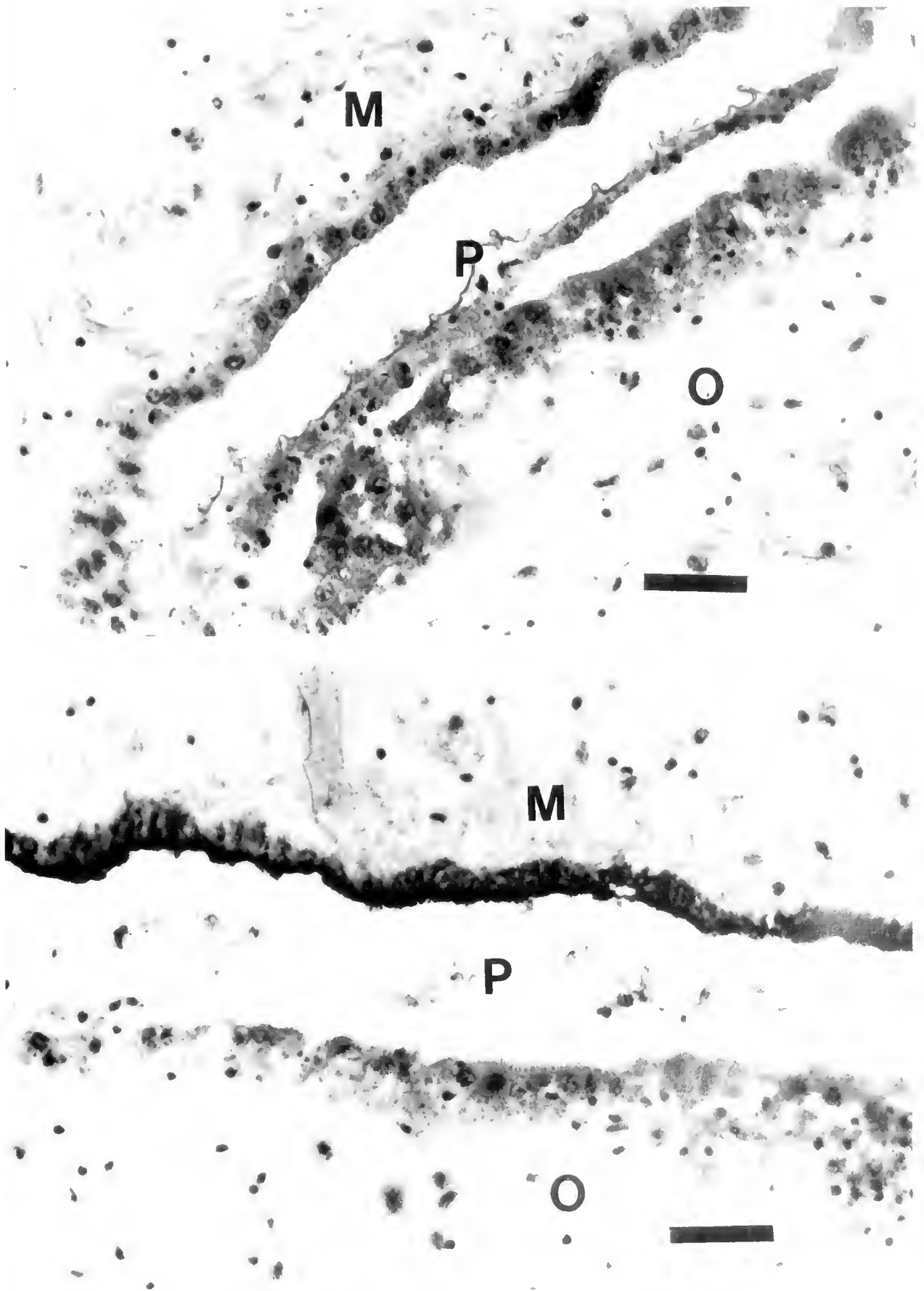
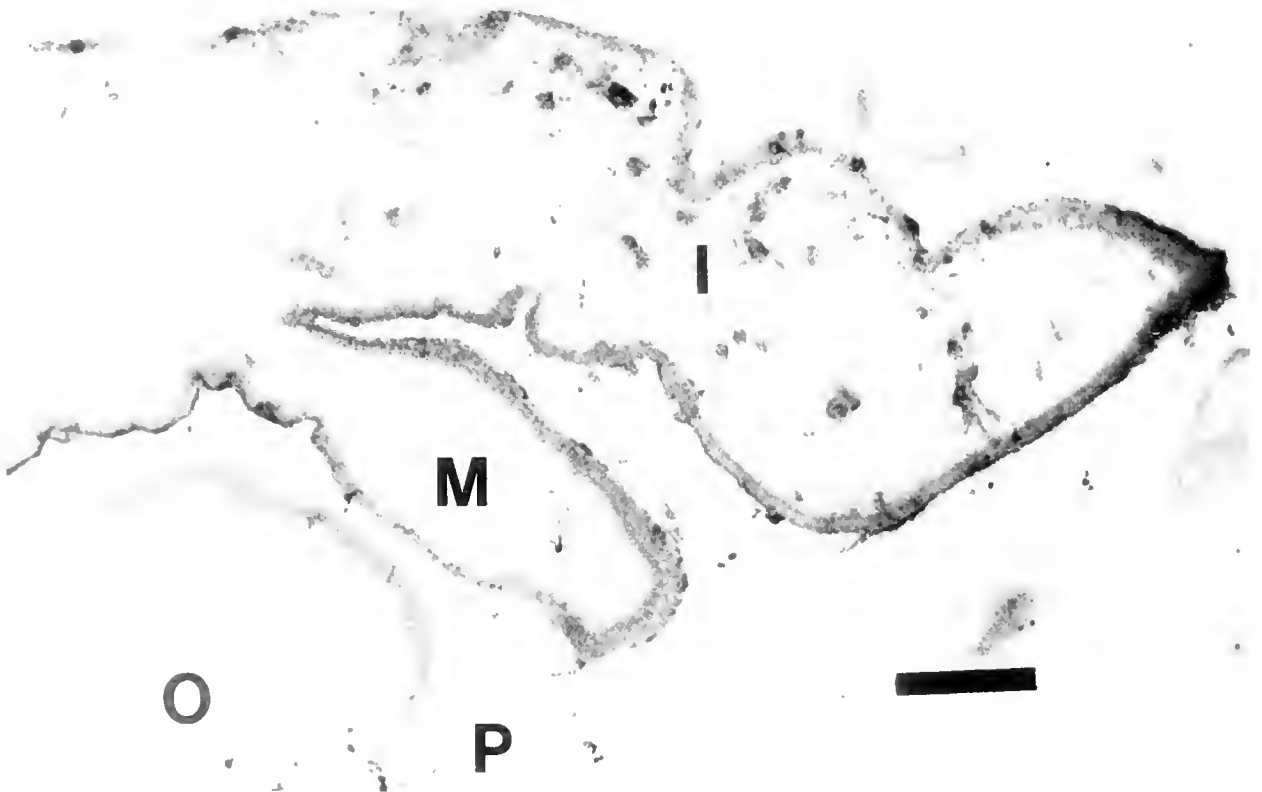
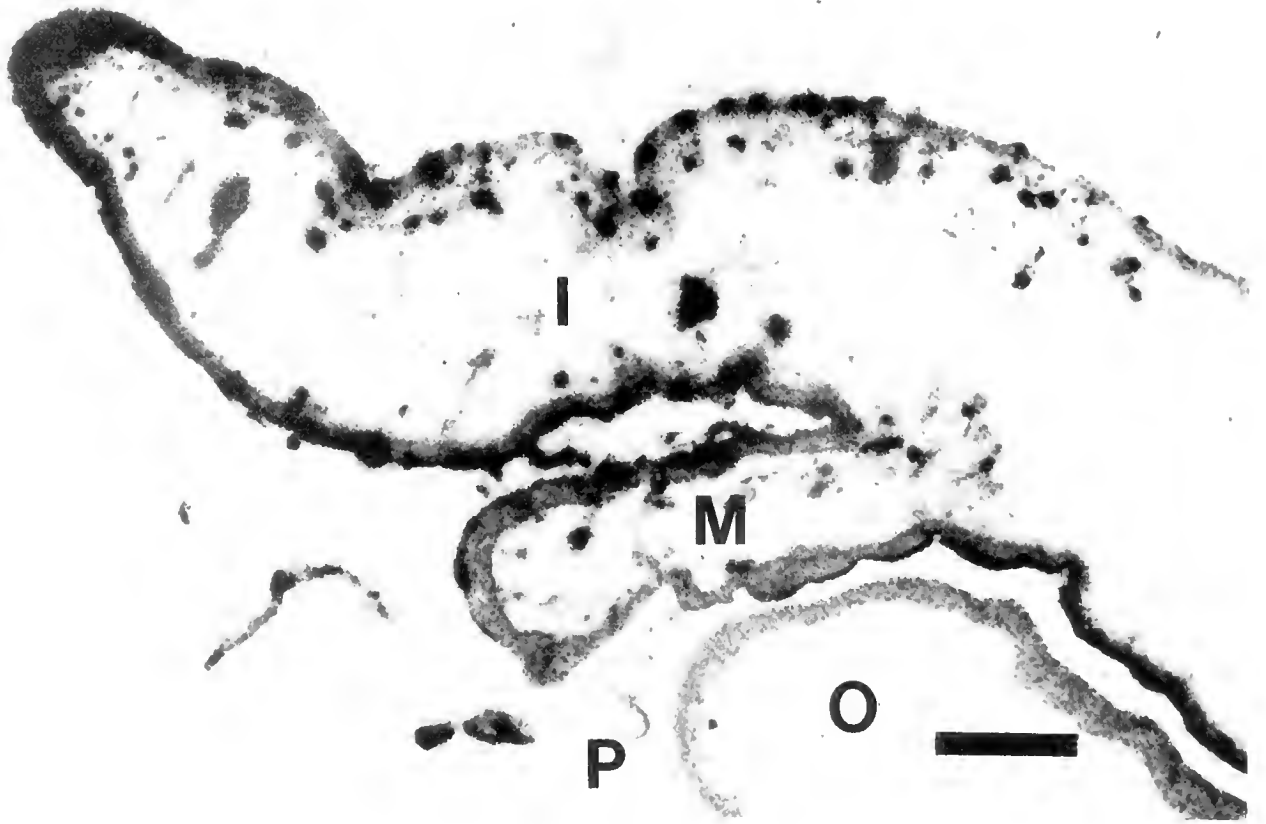


**Figure 5.** Mantle section. A view of the middle fold (M) and outer fold (O) with the periostracum (P) between the two folds. Magnification  $\times 25$ , stained with hematoxylin and eosin. Upper figure from unlabeled mantle and lower figure mantle incubated with labeled sulfate and developed for autoradiography. Bar = 50  $\mu\text{m}$ .



in Figure 1 and Table I for material from mantle and gills. Size is measured as  $K_{av}$ , an indicator of molecular weight, calculated as (elution volume - void volume)  $\div$  (total volume - void volume). Two minor and one major peak can be seen for the sulfate-labeled polymers. After pronase or alkaline borohydride treatment, most of the minor fractions A and B shifted to a  $K_{av}$  of 0.75-0.80 (similar to fraction C), indicating that a part may consist of proteoglycans (Fig. 2). Material in peak C showed no change in size after treatment, indicating that it consists of free GAG chains; this is further supported by its elution close to commercial heparin ( $K_{av} = 0.77$ ). Distribution of sulfate-labeled compounds into peaks A, B, and C is shown in Table I. The variation in distribution in the three experiments is most likely due to the physiological state of the mussels, which could vary depending on when the animals were collected and whether they were used immediately or kept in the laboratory before use. On ion exchange chromatography (AGI  $\times$  2), the fraction of peaks A and B that was resistant to alkaline borohydride and pronase eluted with 0.5 M NaCl. This fraction contained labeled sulfate and glucosamine, but was not GAG in nature because it was not degraded by heparinase, chondroitinase, or nitrous acid.

The polymers in peak C, the major fraction, were eluted from the ion exchange resin as shown in Table II. Note that a larger percentage of the GAGs from gill eluted at the highest salt concentration, indicating a higher charge content. Cellulose acetate electrophoresis confirmed the finding from ion exchange chromatography that the GAG from mantle contained a considerably higher percentage of material with a lower sulfate content, as does heparan sulfate (Table II).

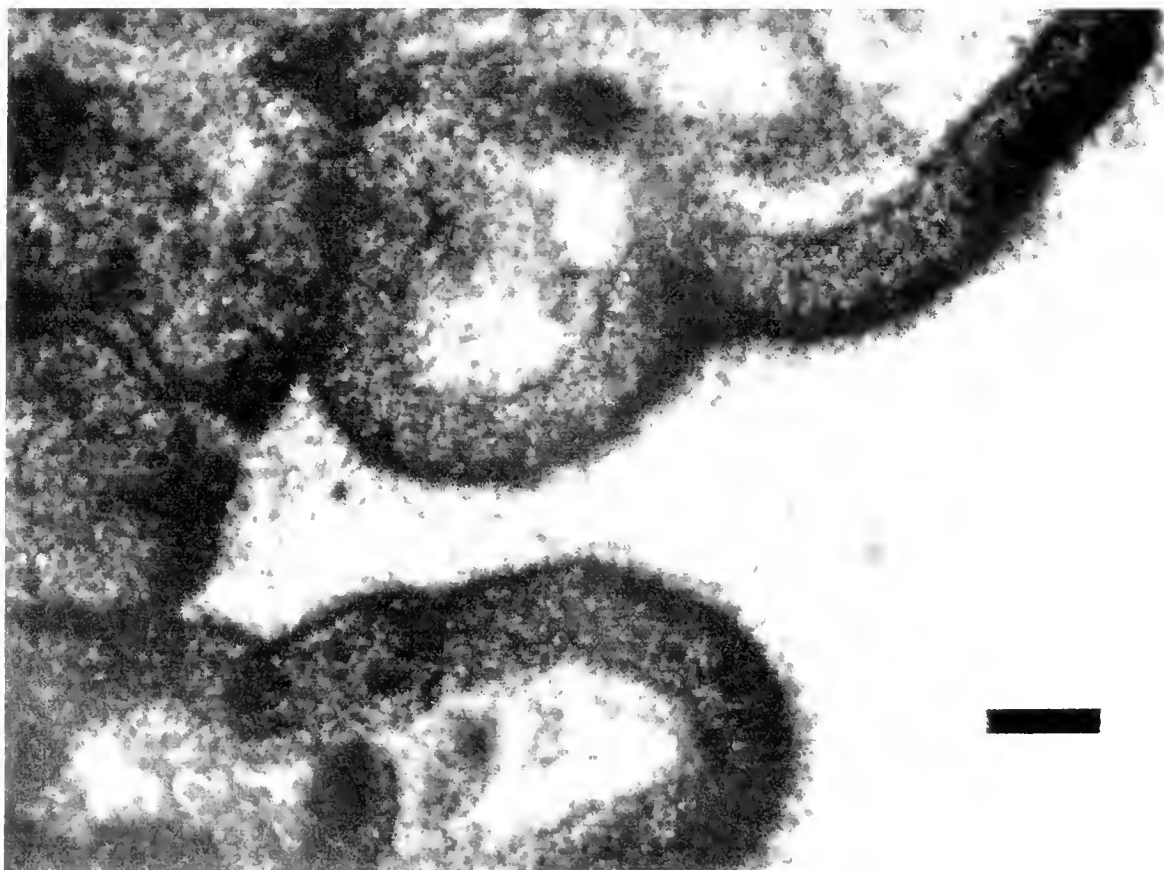
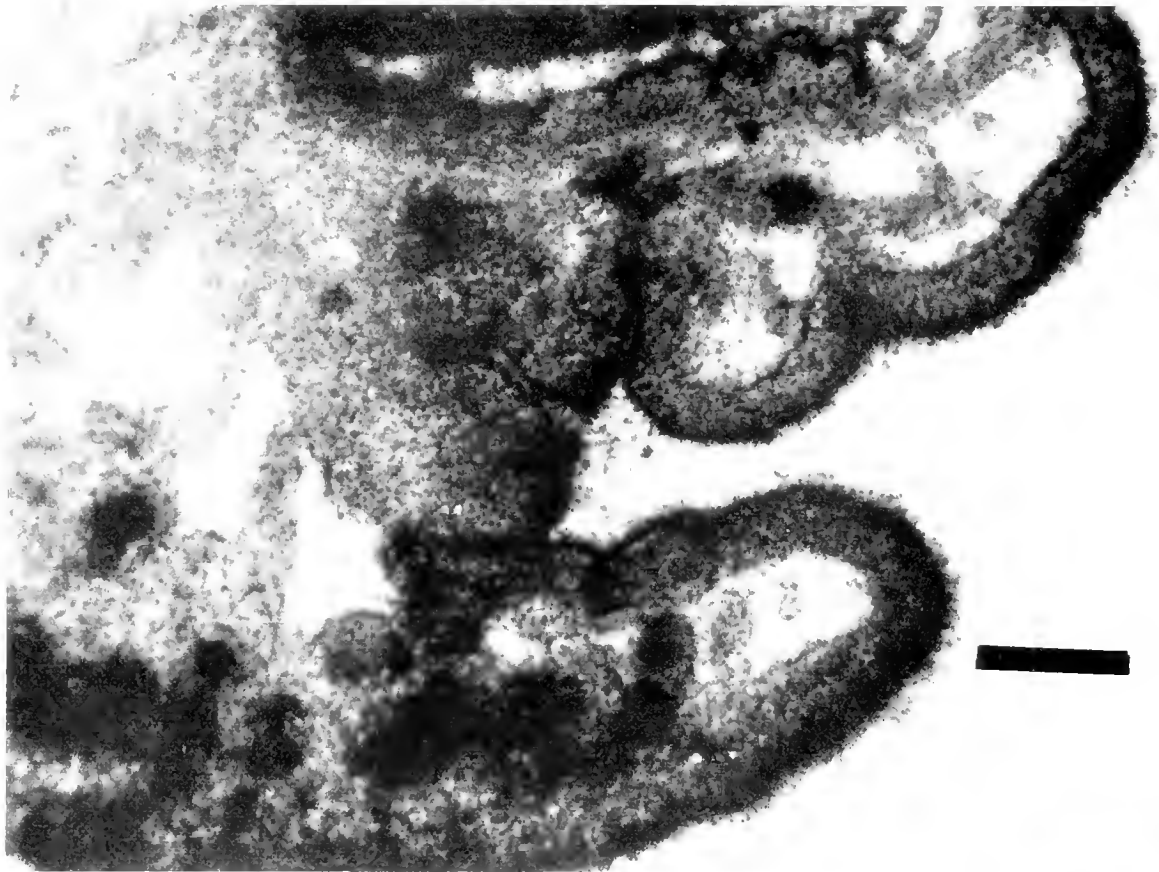
The GAG composition of sulfate- and glucosamine-labeled material in peaks A, B and C was further determined by degradation with nitrous acid, heparinase, chondroitinase ABC, and electrophoresis. As seen in Table III, the major components migrated, like heparin and heparan sulfate, with little chondroitin sulfate; but fairly substantial, though variable, amounts of non-GAG polymers in the minor peaks A and B. The variations between experiments could result from differences in the physiological states of the mussels.

Structural characteristics of material eluting in the Sepharose peak C, which migrated like heparin and heparan sulfate on electrophoresis, were examined by degradation with nitrous acid, heparinase, and heparitinase.

As shown in Figure 3 for mantle- and Figure 4 for gill-derived GAGs, nitrous acid extensively degraded the polymers present, a characteristic of heparin, which contains mainly N-sulfated glucosamine, and to a lesser extent of heparan sulfate, which usually contains about 50% N-acetyl glucosamine and is therefore degraded less extensively. The mantle GAGs were degraded to a small extent by heparitinase and heparinase; although the gill polymers were barely degradable by heparitinase, 50% was extensively degraded to low molecular weight oligosaccharides by heparinase (Figs. 3 and 4). Quantitation of the data is shown in Table IV.

The nitrous acid reaction and the specificity of the enzymes used allows some structural information to be deduced. The heparitinase does not act on standard heparin or heparin-like segments of heparan sulfate. It degrades mono- or non-sulfated sequences of heparan sulfate. The heparinase requires N-sulfate and uronic acid sulfate repeating units for activity and will therefore act well on standard heparins and on heparin-like segments of heparan sulfate, if present (Linker and Hovingh, 1972; Hovingh and Linker, 1974). That is, the mantle polysaccharides, which are degraded to small oligosaccharides by nitrous acid, must have mainly N-sulfated glucosamine and additional O-sulfate to be fairly resistant to heparitinase, but may not contain sufficient O-sulfated iduronic acid to be susceptible to heparinase. Extensive degradation by nitrous acid indicates the absence of N-acetyl. The mantle polysaccharides therefore resemble the "heparan sulfate" isolated from lobsters (Hovingh and Linker, 1982). Approximately half of the GAGs from gills are well degraded by heparinase and are resistant to heparitinase. This, combined with the finding of degradation by nitrous acid, indicates that at least half of this gill product closely resembles vertebrate heparins, but consists mostly of disulfated repeating units. Thomas (1954) reported the isolation of two types of metachromatic GAGs from mucous and tissues of the surf clam *Spisula*, with only one type having significant anticoagulant activity. The presence of sulfated non-GAG polymers (see fractions A and B) has been reported for other species (Mourao and Bastos, 1987; Mourao and Perlin, 1987). The products obtained from nitrous acid treatment consisted of mono-sulfated disaccharides and tetrasaccharides derived from di-sulfated disaccharides and tetrasaccharides in the original polymer.

**Figure 6.** Section of the outer edge of the mantle. Interior fold (I), middle fold (M), outer fold, adjacent to shell (O), periostracum (P). Magnification  $\times$  10, stained with Alcian blue and Congo red. Mantle was incubated with labeled sulfate. Lower figure: section was treated with crude heparinase before autoradiography. Upper figure: control, not treated with enzyme. Bar = 400  $\mu$ m.



## Histology

The precise location of heparin in the tissues of the mussel is prerequisite to an understanding of the role of the polymer. We therefore carried out the histological studies described below. Our main approach was to examine sections of tissues that had been incubated with  $^{35}\text{SO}_4$ -labeled precursors and to locate the labeled polymers by autoradiography. Tissues incubated without the label were used as controls when needed.

Figure 5 shows a section of the mantle. The middle fold, outer fold, and periostracum can be seen. The labeled section shows the presence of sulfated GAGs on the periphery of the epithelial cells in the middle fold but not in the outer fold. Figure 6 represents the edge of the mantle showing the interior fold, middle fold, outer fold (adjacent to shell), and periostracum. The  $^{35}\text{SO}_4$ -labeled material was largely associated with the epithelium of the interior and middle fold, but not the outer fold. The labeled polymers were almost completely removed by crude heparinase, indicating that they consist of GAGs. Furthermore, because the isolation data showed that chondroitin sulfates are present only to a minor extent, the polymers must be related to heparin. The crude heparinase used combines the activities of heparitinase and purified heparinase and also contains another enzyme (heparitinase II), which acts on segments of heparan sulfate or heparin with an intermediate sulfate content, *i.e.*, too high for heparitinase I action and too low for the heparinase (Nader *et al.*, 1990). Figure 7, at a higher magnification, shows the location of the labeled GAGs more clearly. Note the preponderance of sulfate label in the outer pericellular portion of the epithelial cells, with a trace of label at the base of the epithelia. Also note (bottom figure) the dual layer of labeled GAGs at the outer pericellular location of the epithelial cells.

Figure 8 shows the interior fold of the mantle, including mucous cells and epithelium. An unlabeled section is included as control. The label is associated largely with the mucous cells and the epithelial cells. Gill sections are shown in Figure 9. Most of the labeled GAGs are associated with the filaments and not with the water tubes. The labeled polymers were largely removed by crude heparinase, indicating that they are heparin-like GAGs. Figure 10 shows the gill filaments at a higher magnification. Note the  $^{35}\text{SO}_4$  label on the exterior pericellular surfaces of the filaments and some double membranes, which are labeled (see arrows). Some label occurs at the base of the cells.

## Discussion

The presence of GAGs in representatives of most major taxa from bacteria to mammals and the preservation of their main structural features during evolution indicates a fundamental role for these complex anionic polysaccharides in most biological systems. Some members of the six or so distinct GAGs have been shown to be present in Eubacteria (Sugahara *et al.*, 1979; Vann *et al.*, 1981; Rodriguez *et al.*, 1988); in the invertebrate phyla Porifera, Coelanterata, Annelida, Arthropoda, Mollusca, Echinodermata, and in the invertebrate members of the Chordata (Cassaro and Dietrich, 1977; Nader *et al.*, 1983; Nader *et al.*, 1984); and in all Vertebrata examined. Though the survey has not been exhaustive, the data are consistent with an extensive presence.

Among the GAGs, heparin and heparan sulfate form a subgroup of closely related but distinct polymers. These polymers are unique in that they contain N-sulfated glucosamine and have a highly variable structure. Heparin the most highly sulfated GAG, has an unusually sporadic phyletic distribution. Though it is present in some invertebrates (De Meio *et al.*, 1967; Rahemtulla and Løvtrup, 1975), heparin appears only occasionally in vertebrates (Gomes and Dietrich, 1982; Hovingh *et al.*, 1986), and though synthesized by most mammals, it is absent in rabbits and present in only small amounts in man. Heparan sulfate, on the other hand, has one of the widest distributions known. Heparin was isolated from marine bivalves in amounts adequate for detailed structural investigations. Except for some minor differences, it is very close to mammalian heparins in structure and has a high anticoagulant activity (Pejler *et al.*, 1987).

In keeping with the wide distribution of these compounds, a large variety of biological functions have been assigned to GAGs or, more precisely, to their proteoglycans. Aside from their role in vertebrate connective tissue, they appear to interact with growth factors, tissue matrix components, and cell receptors, and may play a role in cell migration, morphology, and angiogenesis (Kjellen and Lindahl, 1991).

As for heparin, it is certainly an excellent anticoagulant when used as a pharmacological agent, but its location in the animals studied (*i.e.*, most likely in the mast cell only) seems to preclude this as its true biological activity. Other well-documented *in vitro* interactions—with growth factors, cell receptors, and matrix components such as laminin or fibronectin—may not occur *in vivo*, because hep-

**Figure 7.** Section of the mantle at higher magnification. Magnification  $\times 25$ ; bar = 50  $\mu\text{m}$  (upper figure) and  $\times 40$ ; bar = 20  $\mu\text{m}$  (lower figure). Incubated with labeled sulfate. Developed for autoradiography, and stained with hematoxylin and eosin. Note the preponderance of sulfate label in the outer pericellular location of the epithelial cells and a trace of radioactivity at the base of the cells. In the bottom figure, note the dual layer of label on the outer pericellular location.



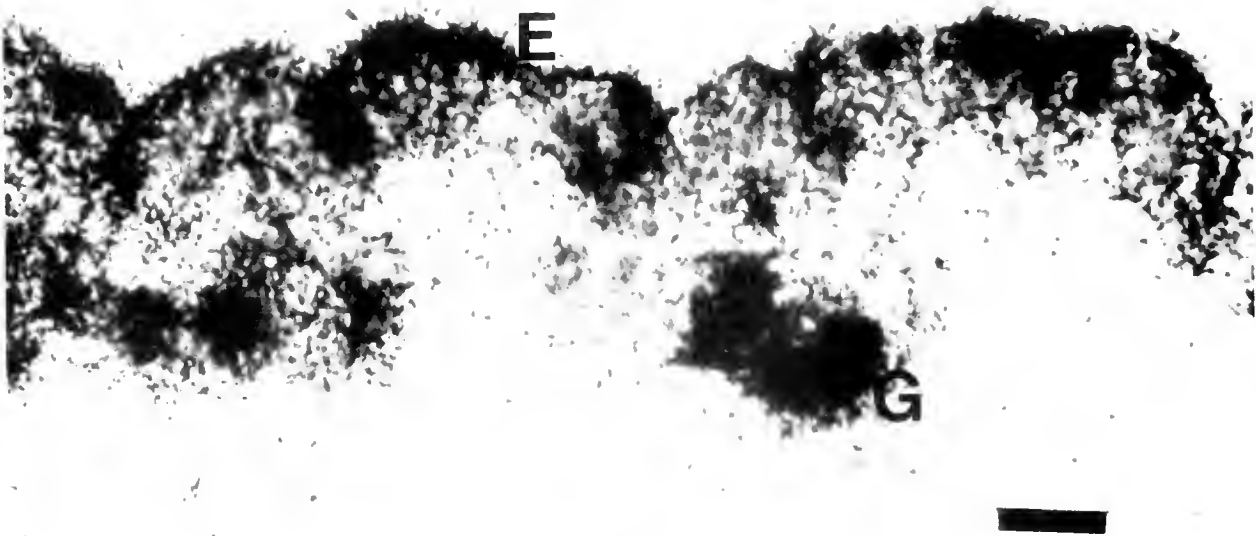
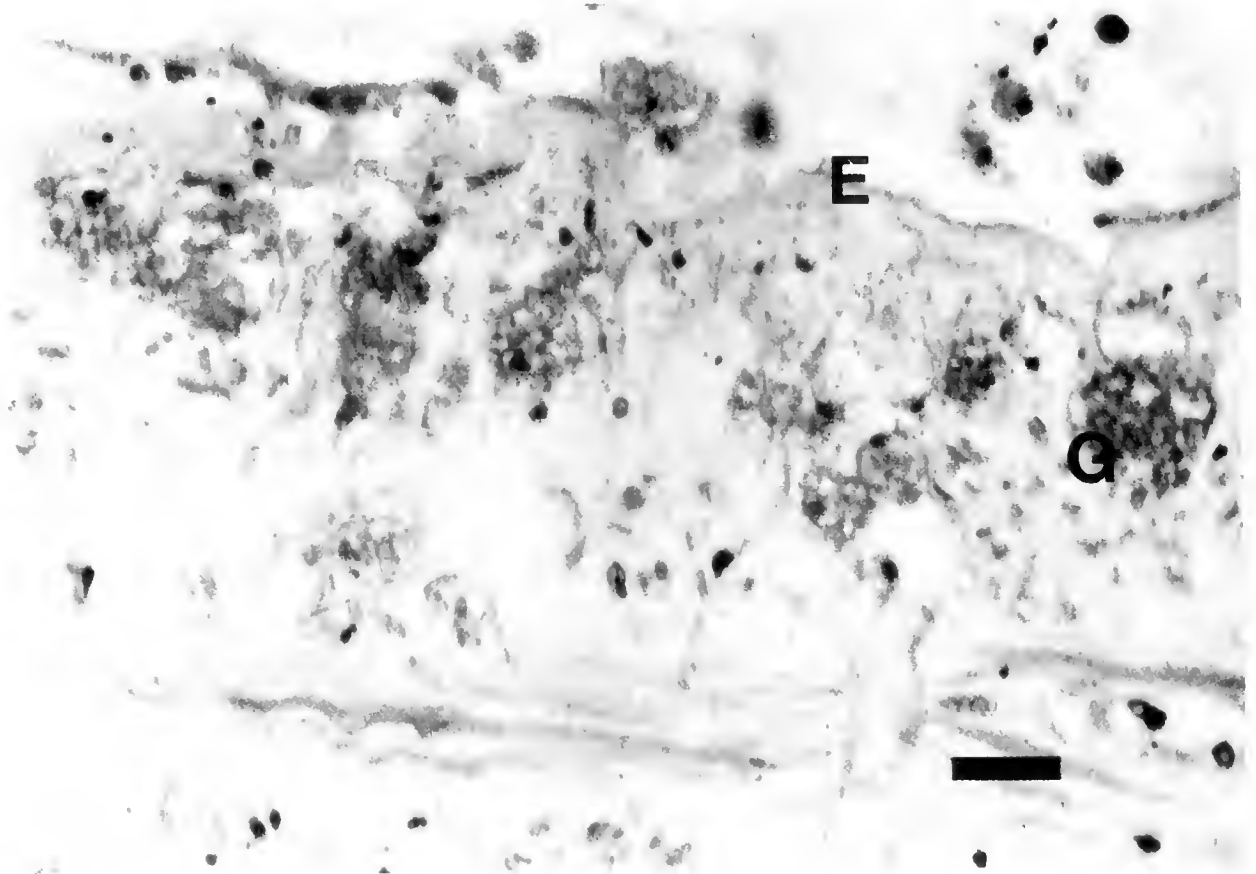


Figure 8. Section of the interior fold showing mucous cells (G) and epithelium (E). Magnification  $\times 40$ ; Bar = 20  $\mu\text{m}$ . Stained with hematoxylin and eosin after autoradiography. Upper figure: unlabeled mantle. Lower figure: incubated with radiolabeled sulfate.

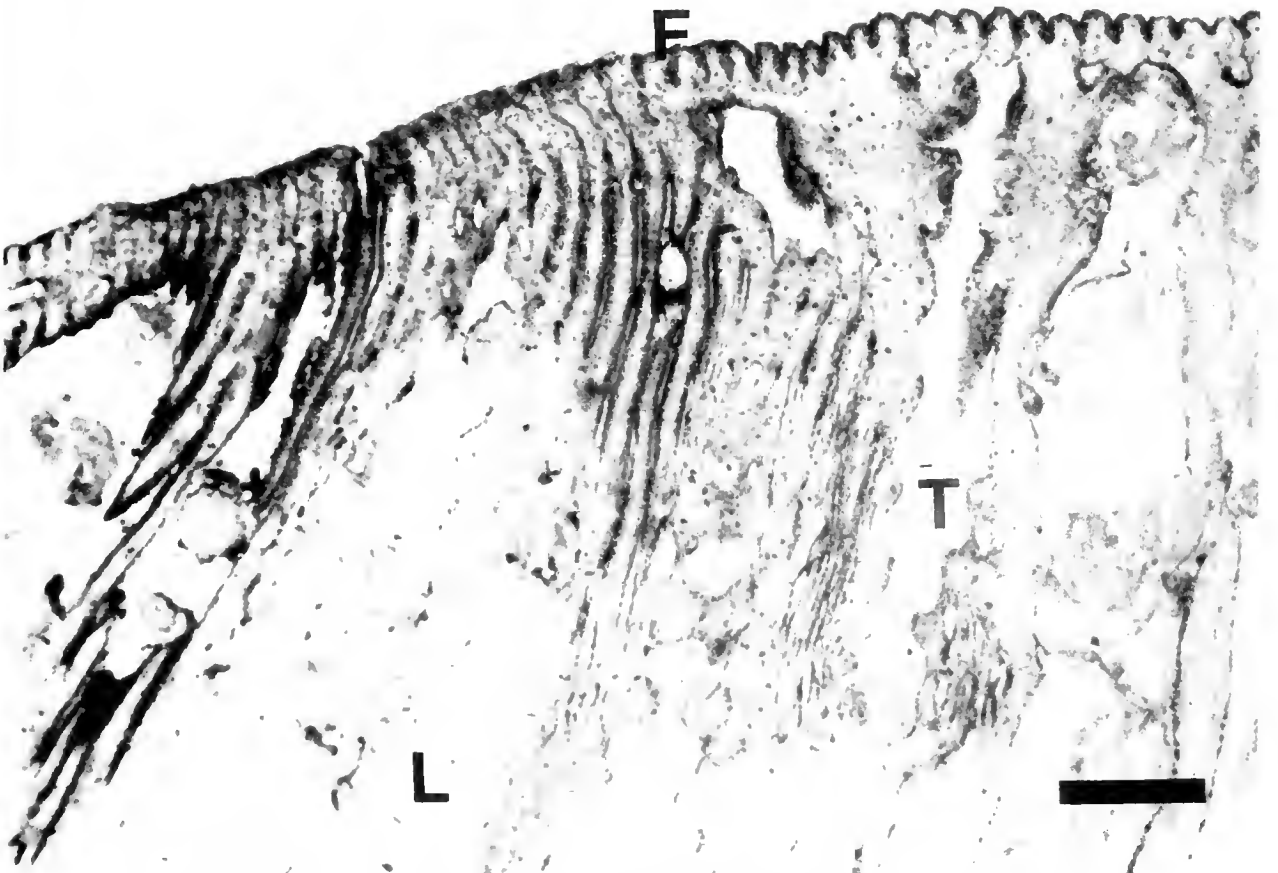
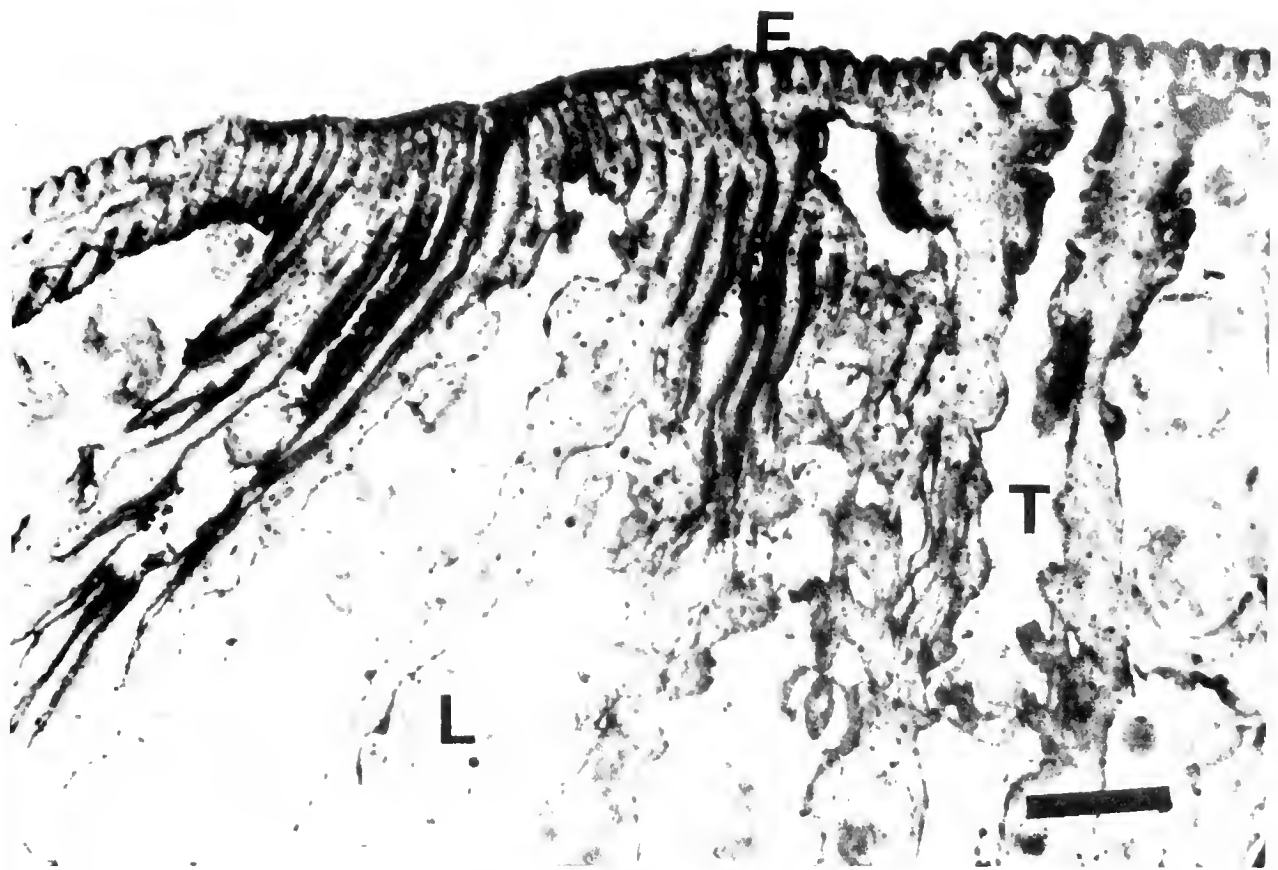
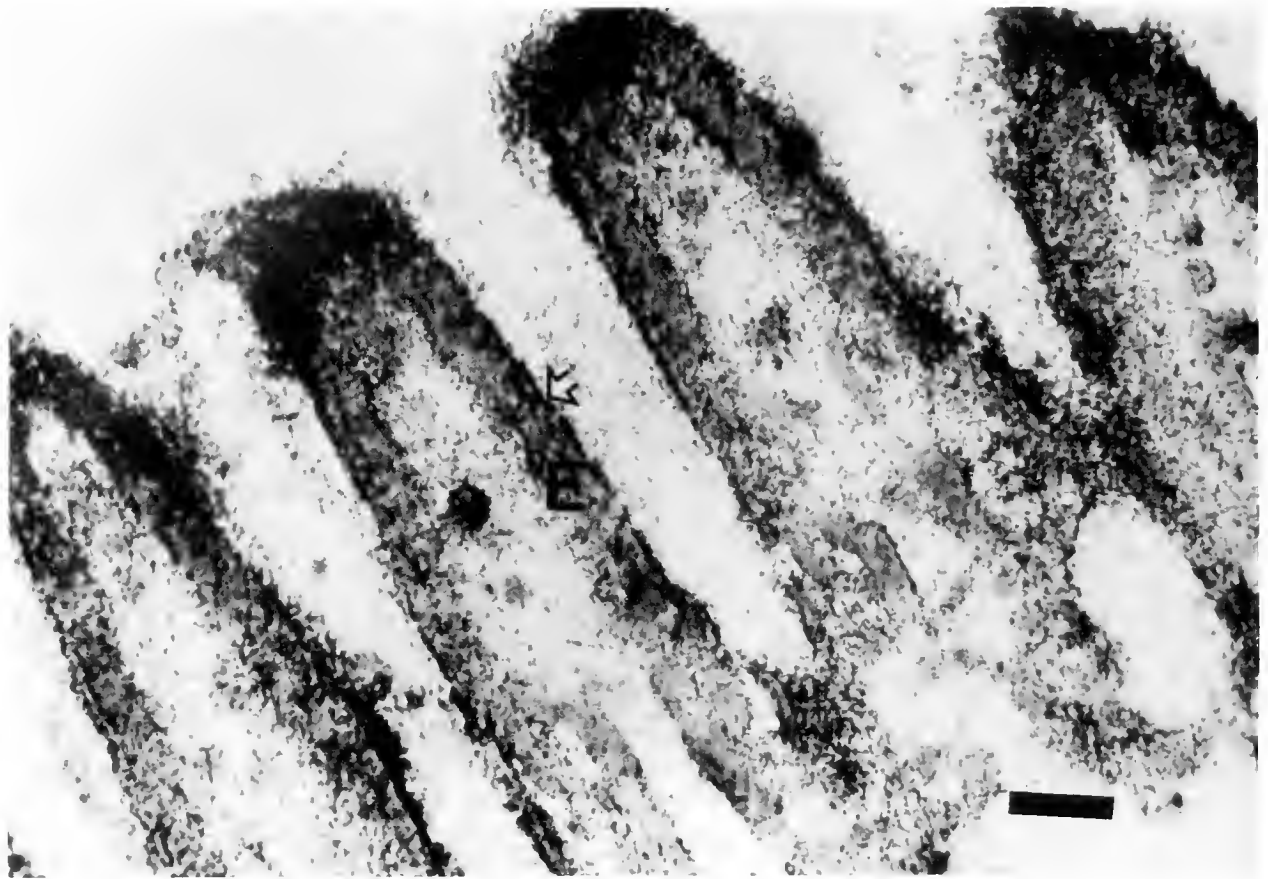


Figure 9. Section of the gills. Magnification  $\times 4$ . Bar = 400  $\mu\text{m}$ . Note filaments (F); water tubes (T), and larva (L). Stained with Alcian blue and Congo red after autoradiography. Gills were incubated with labeled sulfate. Lower figure: section was treated with crude heparinase. Upper figure: control not treated with enzyme.



**Figure 10.** Section of gills filaments. Magnification  $\times 40$ ; Bar = 20  $\mu\text{m}$ . Gills were incubated with labeled sulfate. Stained with hematoxylin and eosin after autoradiography, epithelial layer (E). Note the sulfate label on the exterior pericellular surfaces of the filaments (arrow) and the occasional double membranes which are labeled. Some label occurs at the base of the cells.

arin is not present in locations where such interactions would be plausible. Whatever the biological role of heparin may be, it is not clear, however, what other substance fulfills the same role in species that lack this apparently quite critical member of the GAG family. There is no adequate evidence that heparan sulfate substitutes for heparin in such cases. If structural consistency implies functional consistency, a study of the function of heparin or heparin-like compounds in invertebrates such as clams may give a clue to the role of these GAGs in vertebrates.

In this study we have shown the synthesis of heparin and a heparin- or heparan-sulfate-like polysaccharide in a freshwater mussel. Though the synthetic pathway may involve a proteoglycan precursor, the major final product, as in mammals, is a free GAG chain (see Table I). The data obtained by the use of specific degradative enzymes and nitrous acid treatment show that gills synthesize approximately 50% each of one polymer that shows the characteristics of a somewhat poorly sulfated heparin (see Tables II, III, and IV) and a second polymer intermediate in structure to heparan sulfate and heparin. Little heparin

appears to be synthesized in the mantle, where the major material labeled is the intermediate polymer, which seems to be closely related to a heparan-sulfate-like GAG isolated from lobsters (Hovingh and Linker, 1982). Large-scale preparation could clarify this similarity further, but *Anodonta californiensis* occurs only in small and isolated populations. Other species of *Anodonta*, or other unionid clams, are more plentiful and thus more suitable for scaling up the preparation, provided that the distribution of GAGs is similar to that in *A. californiensis*.

The histology shows the presence of heparin or heparan sulfate in the mantle and gills, *i.e.*, in the exterior pericellular and "basement membrane" locations of the epithelial cells and on the exterior surface of gill filaments; that is, in areas exposed to the aquatic medium. GAGs in general have been implicated in  $\text{Ca}^{2+}$  metabolism and calcification (Sauren *et al.*, 1992) and heparin has been shown to complex with  $\text{Ca}^{2+}$  (Grant *et al.*, 1992) and to bind strongly to L-type  $\text{Ca}^{2+}$  channels of vertebrate skeletal muscles (Knaus *et al.*, 1990). We propose a model in which heparin in mussels sequesters  $\text{Ca}^{2+}$  from the aquatic medium and

transports it across the epithelial layer in the mantle and gills (and perhaps all organs with a surface bordering the environmental water). Heparin may not actually be involved in the transport itself, but only in the sequestering of  $\text{Ca}^{2+}$  on both sides of the epithelial layer. After  $\text{Ca}^{2+}$  is transported across the epithelial layer,  $\text{Ca}^{2+}$  (without heparin) is accumulated and stored in spheroids for use in glochidia development in the gills (Silverman *et al.*, 1983, 1985, 1987) and in the calcification of the shell (Wilbur and Saleuddin, 1983). This model suggests that, as filter feeders, all bivalves (marine and freshwater), would use heparin-like GAG to efficiently sequester  $\text{Ca}^{2+}$ , whereas gastropods would obtain  $\text{Ca}^{2+}$  in their food, so that heparin (if present) may have a different role than in bivalves. The model also implies that heparin will be found on the exterior surfaces of these organisms.

The model presented here could be tested by labeling mussels *in vivo* with  $^{35}\text{S}$ , treating them and the controls with  $^{45}\text{Ca}$  and the crude Flavobacter enzymes, and following the disappearance of heparin from the epithelial surface and the incorporation of  $^{45}\text{Ca}$  from the water.

Another role for heparin may be inactivation of toxic amines present in the aquatic environment: this is analogous to a function proposed for mast-cell heparin in vertebrates. As in clams, tunicates, and sea cucumbers (Cifonelli and Mathews, 1972; Mourao and Bastos, 1987; Mourao and Perlin, 1987), sulfate-labeled material in addition to GAGs was also isolated from the mantles and gills of the *Anodonta* (see Table 3). The data obtained are similar to those in earlier reports showing that heparin and other metachromatic polymers occur in the mantle, gills, and some other organs of mussels (Thomas, 1954; Nader and Dietrich, 1989). The functions and detailed structures of these sulfated polymers are unknown, although their molecular weight is high and they may be bound to threonine (Cifonelli and Mathews, 1972).

### Acknowledgments

This study was supported by DVA Medical Research Funds. The authors would like to thank Helen C. Carney for her valuable help with histological processing and Walter R. Hoeh for discussions concerning the histological sections and the functional histology of the mantle and gills.

### Literature Cited

- Cassaró, C. M. F., and C. P. Dietrich. 1977. Distribution of sulfated mucopolysaccharides in invertebrates. *J. Biol. Chem.* **252**: 2254-2261.
- Cifonelli, J. A., and M. B. Mathews. 1972. Structural studies on spulan: a mucopolysaccharide from clams. *Connective Tissue Res.* **1**: 231-241.
- De Meio, R. H., Y.-C. Lin, and S. Narasimulu. 1967. Some aspects of the biosynthesis of mactin. *Comp. Biochem. Physiol.* **20**: 581-591.
- Gomes, P. B., and C. P. Dietrich. 1982. Distribution of heparin and other sulfated glycosaminoglycans in vertebrates. *Comp. Biochem. Physiol.* **73B**: 857-863.
- Grant, D., W. F. Long, C. F. Moffat, and F. B. Williamson. 1992. A study of  $\text{Ca}^{2+}$ -heparin complex-formation by polarimetry. *Biochem. J.* **282**: 601-604.
- Hovingh, P., and A. Linker. 1974. The disaccharide repeating-units of heparan sulfate. *Carb. Res.* **37**: 181-192.
- Hovingh, P., and A. Linker. 1982. An unusual heparan sulfate isolated from lobsters (*Homarus americanus*). *J. Biol. Chem.* **257**: 9840-9844.
- Hovingh, P., M. Piepkorn, and A. Linker. 1986. Biological implications of the structural, antithrombin affinity and anticoagulant activity relationships among vertebrate heparins and heparan sulphates. *Biochem. J.* **237**: 573-581.
- Kjellen, L., and U. Lindahl. 1991. Proteoglycans: structures and interactions. *Ann. Rev. Biochem.* **60**: 443-475.
- Knaus, H.-G., F. Scheffauer, C. Romanin, H.-G. Schindler, and H. Glossmann. 1990. Heparin binds with high affinity to voltage-dependent L-type  $\text{Ca}^{2+}$  channels: Evidence for an agonistic action. *J. Biol. Chem.* **265**: 11156-11166.
- Linker, A., and P. Hovingh. 1972. Heparinase and heparitinase from Flavobacteria. Pp. 902-911 in *Methods in Enzymology*. U. Ginsburg, ed. Academic Press, New York.
- Mourao, P. A. S., and I. G. Bastos. 1987. Highly acidic glycans from sea cucumbers: Isolation and fractionation of fucose-rich sulfated polysaccharides from the body wall of *Ludwigothurea grisea*. *Eur. J. Biochem.* **166**: 639-645.
- Mourao, P. A. S., and A. S. Perlin. 1987. Structural features of sulfated glycans from the tunic of *Styela plicata* (Chordata—Tunicata): A unique occurrence of L-galactose in sulfated polysaccharides. *Eur. J. Biochem.* **166**: 431-436.
- Nader, H. B., and C. P. Dietrich. 1989. Pp. 81-96 in *Heparin, Chemical and Biological Properties*. D. A. Lane and U. Lindahl eds. CRC Press, Florida.
- Nader, H. B., T. M. P. C. Ferreira, J. F. Paiva, M. G. L. Madeiros, S. M. B. Jeronimo, V. M. P. Paiva, and C. P. Dietrich. 1984. Isolation and structural studies of heparan sulfates and chondroitin sulfates from three species of molluscs. *J. Biol. Chem.* **259**: 1431-1435.
- Nader, H. B., M. G. L. Madeiros, J. F. Paiva, V. M. P. Paiva, S. M. B. Jeronimo, T. M. P. C. Ferreira, and C. P. Dietrich. 1983. A correlation between the sulfated glycosaminoglycan concentration and degree of salinity of the "habitat" in fifteen species of the classes Crustacea, Pelecypoda and Gastropoda. *Comp. Biochem. Physiol.* **76**: 433-436.
- Nader, H. B., M. A. Porcionatto, I. L. S. Tersariol, M. A. S. Pinhal, F. W. Oliveira, C. T. Moraes, and C. P. Dietrich. 1990. Purification and substrate specificity of heparitinase I and heparitinase II from Flavobacterium heparinum: Analyses of the heparin and heparan sulfate degradation products by  $^{13}\text{C}$  NMR spectroscopy. *J. Biol. Chem.* **265**: 16807-16813.
- Pejler, G., A. Danielsson, I. Björk, U. Lindahl, H. B. Nader, and C. P. Dietrich. 1987. Structure and antithrombin-binding properties of heparin isolated from the clams *Anomalocardia brasiliensis* and *Tivela mactroides*. *J. Biol. Chem.* **262**: 11413-11421.
- Rahemtulla, F., and S. Lovtrup. 1974. The comparative biochemistry of invertebrate mucopolysaccharides—II. Nematoda: Annelida. *Comp. Biochem. Physiol.* **49B**: 639-646.
- Rahemtulla, F., and S. Lovtrup. 1975. The comparative biochemistry of invertebrate mucopolysaccharides—IV. Bivalvia. Phylogenetic implications. *Comp. Biochem. Physiol.* **50B**: 631-635.
- Rodríguez, M.-L., B. Jann, and K. Jann. 1988. Structure and serological characteristics of the capsular K4 antigen of *Escherichia coli* 05:K4:

- H4, a fructose-containing polysaccharide with a chondroitin backbone. *Eur. J. Biochem.* **177**: 117-124.
- Sauren, Y. M. H. F., R. H. P. Mieremet, C. G. Groot, and J. P. Scherft. 1992. An electron microscopic study on the presence of proteoglycans in the mineralized matrix of rat and human compact lamellar bone. *Anatom. Record* **232**: 36-44.
- Shively, J. E., and H. E. Conrad. 1976. Formation of anhydro-sugars in the chemical depolymerization of heparin. *Biochemistry* **15**: 3932-3942.
- Silverman, H., W. T. Kays, and T. H. Dietz. 1987. Maternal calcium contribution to glochidial shells in freshwater mussels (Eulamellibranchia: Unionidae). *J. Exper. Zoology* **242**: 137-146.
- Silverman, H., W. L. Steffens, and T. H. Dietz. 1983. Calcium concretions in the gills of a freshwater mussel serve as a calcium reservoir during periods of hypoxia. *J. Exper. Zoology* **227**: 177-189.
- Silverman, H., W. L. Steffens, and T. H. Dietz. 1985. Calcium from extracellular concretions in the gills of freshwater unionid mussels is mobilized during reproduction. *J. Exper. Zoology* **236**: 137-147.
- Sugahara, K., N. B. Schwartz, and A. Dorfman. 1979. Biosynthesis of hyaluronic acid by *Streptococcus*. *J. Biol. Chem.* **254**: 6252-6261.
- Thomas, L. J., Jr. 1954. The localization of heparin-like blood anticoagulant substances in the tissues of *Spisula soldissima*. *Biol. Bull.* **106**: 129-138.
- Vann, W. F., M. A. Schmidt, B. Jann, and Jann K. 1981. The structure of the capsular polysaccharide (K5 antigen) of urinary tract-infective *Escherichia coli* 010:K5:H4. A polymer similar to desulfo-heparin. *Eur. J. Biochem.* **116**: 359-364.
- Wilbur, K. M., and A. S. M. Saleuddin. 1983. Shell formation. Pp. 235-287 in *The Mollusca*, Vol. 4. Physiology, Part 1. Academic Press, New York.

# Metabolic Rates in Early Life History Stages of Elopomorph Fishes

EDWARD PFEILER<sup>1\*</sup> AND JOHN J. GOVONI<sup>2</sup>

<sup>1</sup>Department of Biology, University of Puerto Rico, Mayagüez, Puerto Rico 00681, and

<sup>2</sup>NOAA, National Marine Fisheries Service, Southeast Fisheries Science Center, Beaufort Laboratory, Beaufort, North Carolina 28516

**Abstract.** The respiratory electron transport system (ETS) assay was used to estimate metabolic rates in four species of eel (Anguilliformes: Ophichthidae and Congridae) leptocephali (*Myrophis punctatus*, *Ophichthus* sp., *Hildebrandia flava*, and one unidentified congrid) and the bonefish (Albuliformes: Albulidae: *Albula* sp.). Wet-weight-specific ETS values in whole-body homogenates, assayed at physiological temperatures, ranged from 4–20  $\mu\text{g-at O h}^{-1}$  ( $\text{g wet wt}^{-1}$ ). Arrhenius activation energies ( $E_a$ ) ranged from 11.0–15.7  $\text{kcal mole}^{-1}$ . Both wet-weight-specific ETS activity and oxygen consumption rate increased approximately fivefold during metamorphosis of leptocephali of *Albula* sp. Wet-weight-specific ETS activity showed little change as leptocephali of *M. punctatus* transformed into glass eels, but increased about fivefold as glass eels metamorphosed into elvers. No significant difference was found in ETS activity measured in fresh early metamorphic leptocephali of *Albula* sp. and leptocephali that had been stored frozen at  $-70^\circ\text{C}$  for up to 15 months. The data suggest that metabolic rates are low in leptocephali, which implies that the demand for nutrients is also relatively low. We argue that the apparent diet of these larvae seems capable of providing a sufficient supply of nutrients under these conditions.

## Introduction

A leptocephalous larva is characteristic of marine teleost fishes (superorder Elopomorpha) comprising the orders

Albuliformes (including Notacanthiformes), Anguilliformes, Elopiformes, and Saccopharyngiformes (Robins, 1989). In addition to their distinct morphological characteristics, including the presence of a transparent, laterally compressed body composed mainly of a central core of gelatinous material (Smith, 1984), leptocephali differ from larvae of most other marine teleosts in having an extended larval period, referred to here as the premetamorphic period. This period, during which the leptocephalus increases in size as the gelatinous matrix is formed, may last from a few months within the albuliforms and elopiforms (Smith, 1980; Pfeiler *et al.*, 1988) to several years within the anguilliforms (Schmidt, 1925). The metamorphic period, during which the leptocephalus transforms into a juvenile fish, is usually completed within 2–3 weeks (Pfeiler, 1986). In addition to increased development of muscle, bone, and internal organs, metamorphosis is characterized by a decrease in size as the gelatinous matrix is broken down (Pfeiler, 1989).

The source of nutrition in premetamorphic leptocephali has puzzled biologists for decades. Most of the premetamorphic period is passed in the absence of a yolk sac (Pfeiler, 1986), and identifiable food material has not been observed in the gut of many species (for references see Pfeiler, 1989). The presence of a functional digestive system also has been questioned (Rasquin, 1955; Hulet, 1978). Premetamorphic leptocephali may be receiving nutrients by absorption of dissolved organic matter across surface epithelia and by ingestion of particulate organic matter and microscopic organisms (Pfeiler, 1986; Hulet and Robins, 1989; Otake *et al.*, 1993), but the relative contribution of these potential sources of nutrients has not been determined.

Most of the nutritional requirements of metamorphic leptocephali are thought to be provided by breakdown and utilization of organic material stored in the extracel-

Received 3 December 1992; accepted 24 June 1993.

\* Present address: Departamento de Ciencias Marinas, Instituto Tecnológico y de Estudios Superiores de Monterrey (ITESM), Campus Guaymas, Apartado Postal 484, Guaymas, Sonora 85400, Mexico.

Abbreviations: ETS, electron transport system; NADH, reduced nicotinamide adenine dinucleotide; NADPH, reduced nicotinamide adenine dinucleotide phosphate; INT, *p*-iodonitrotetrazolium violet,  $E_a$ , Arrhenius activation energy;  $V_{O_2}$ , routine oxygen consumption rate; R:ETS, ratio of wet-weight-specific  $V_{O_2}$  to ETS activity.



lular gelatinous body matrix (Rasquin, 1955; Pfeiler, 1986). Recent work (J. Govoni, unpublished data) has revealed the presence of fecal pellets and protozoans in the gut of metamorphosing eel (*Myrophis punctatus*) leptocephali; these may also provide a nutritional source.

It follows that, if the metabolic demands of premetamorphic leptocephali are low, as might be expected given their high water content and large extracellular gelatinous component (Pfeiler, 1984; Smith, 1984), these larvae should have low energy requirements overall, and thereby be capable of subsisting on the very low concentrations of dissolved organic compounds in seawater and on minute food particles. Data on oxygen consumption could help confirm this hypothesis, but obtaining undamaged premetamorphic leptocephali for determination of metabolic rates is difficult. An alternate method of estimating respiratory rates is the electron transport system (ETS) assay, which has been used in a wide variety of marine phytoplankton, zooplankton, and micronekton (Packard, 1971; Packard *et al.*, 1975; Owens and King, 1975), as well as in specific tissues such as fish liver (Smith and Chong, 1982).

The purpose of the present study was (1) to obtain ETS activity measurements on several species of anguilliform and albuliform leptocephali (premetamorphic and early metamorphic), (2) to determine the effects of assay temperature on ETS activity of leptocephali collected at different temperatures, and (3) to determine whether changes in activity occurred during metamorphosis of albuliform (*Albula* sp.) and anguilliform (*M. punctatus*) leptocephali. We also present data on oxygen consumption rates of metamorphosing leptocephali of *Albula* sp. and compare these rates with ETS activity.

## Materials and Methods

### Animals

Anguilliform leptocephali were collected from 28 January–2 February 1990 in the western North Atlantic, off the coast of North Carolina, as described by Pfeiler (1991). Water temperature at the depth of collection ranged from 12–23°C. After species identification (voucher specimens were retained [Pfeiler, 1991]), leptocephali for analysis were placed in plastic vials, immediately frozen in liquid nitrogen, and stored at –70°C.

The species identified were *Hildebrandia flava* (Goode and Bean) and one unidentified species, both from the family Congridae; and *Myrophis punctatus* Lütken and *Ophichthus* sp., both from the family Ophichthidae. Specimens of *M. punctatus* were also collected on 26 January 1990 (1830–2000 h, Eastern Standard Time) and 29 January 1992 (0100–0200) at flood tide with a plankton net suspended from a small bridge at Beaufort, North Carolina. Water temperature was 9°C. These larvae were either immediately frozen or placed in an aquarium with

running seawater at ambient temperature (9–16°C) and allowed to metamorphose to glass eels and elvers and then frozen and stored at –70°C.

Metamorphosing leptocephali of *Albula* sp. (Albuliformes: Albulidae) were collected with a beach seine in the Gulf of California at Estero del Soldado, Guaymas, Sonora, Mexico, on 4 January 1990 (water temperature = 16°C), placed in plastic bags, and immediately transferred to a freezer at –18°C. They were stored for 2 weeks at –18°C and then transferred to –70°C, where they were stored until used for ETS assays. Experiments were also conducted with fresh larvae collected on 7 and 14 March 1992 (water temperature = 19 and 23°C). The first group was held in an aquarium with running seawater at ambient temperature (19–21°C) for 9 days and allowed to metamorphose to advanced larvae; the second group of early metamorphic larvae was assayed immediately.

### Chemicals

The following chemicals were purchased from Sigma Chemical Co., St. Louis, Missouri:  $\beta$ -NADH (grade III),  $\beta$ -NADPH (type I), *p*-iodonitrotetrazolium violet (INT), polyvinylpyrrolidone, and Triton X-100. All other chemicals were of analytical grade. Water was glass distilled.

### ETS assay

ETS activity was determined both on fresh animals (*Albula* sp. only) and on animals that had been stored at –70°C for up to 15 months. Immediately before assay, frozen fish were thawed. Both thawed and fresh fish were then rinsed with distilled water, measured (total length or standard length to the nearest millimeter), and weighed (wet weight to the nearest 0.1 mg). Individual fish were homogenized in a hand-held glass homogenizer using 10–20 ml of a cold (4°C) solution containing 75  $\mu$ M MgSO<sub>4</sub>, 1.5 mg/ml polyvinylpyrrolidone, and 0.2% (v/v) of Triton X-100 in 0.1 M phosphate buffer (pH 8.5) (Solution "ETS B" of Owens and King, 1975). The homogenate was centrifuged for 10 min at 7800 *g* (4°C). One milliliter of the supernatant was immediately assayed for ETS activity according to Owens and King (1975). This method is based on the reduction, and corresponding increase in absorbance at 490 nm, of an artificial electron acceptor (INT) by the respiratory electron transport system when NADH and NADPH are used as electron donors.

Assays were conducted, in duplicate, for 20 min at temperatures ranging from 10 to 30°C. Reaction mixtures were pre-incubated for 5 min at the appropriate temperature before initiating the reaction. Absorbance readings were taken immediately after stopping the reaction. Unless indicated otherwise, ETS activity refers to micrograms of oxygen consumed per hour ( $\mu$ g-at O h<sup>-1</sup>) and is expressed on a wet weight, dry weight, or individual basis.



Dry weight and water content were determined for leptocephali of *M. punctatus* (70–77 mm total length; 0.2196–0.2868 g wet weight) and *Ophichthus* sp. (77–85 mm total length; 0.2175–0.3026 g wet weight). Three individuals of each species were rinsed, measured and weighed, and then dried to constant weight in an oven at 70°C. Water contents ranged from 92.5 to 92.9% (mean = 92.7%) for *M. punctatus* and from 90.1 to 92.1% (mean = 91.2%) for *Ophichthus* sp. Mean water contents for each species were then used to estimate dry weights of larvae assayed for ETS activity. Dry weights ( $y$ ) of leptocephali of *Albula* sp. were calculated from wet weights ( $x$ ) using the least-squares regression equation,  $y = 18.445 + 59.610x$  (Pfeiler and Luna, 1984).

### Oxygen consumption

Oxygen consumption rates were determined for metamorphosing leptocephali of *Albula* sp. The respirometer consisted of a 570-ml glass jar fitted with an oxygen electrode (Yellow Springs Instruments Model 57 Oxygen Meter) and connected to an air supply. The water was thoroughly mixed with a magnetic stir bar placed underneath a nylon net screen so as not to damage the larvae. Oxygen consumption was determined on four separate groups of larvae at different stages of metamorphosis. A group of larvae (from 9 to 21 individuals) was placed in the respirometer and allowed to acclimate for 5 min in constantly aerated seawater at ambient temperature (20–25°C). Because larvae are developing rapidly, showing a daily reduction in standard length of about 10–15% (Pfeiler, 1984), and because they are easily damaged, we chose not to use longer acclimation periods. Oxygen consumption was then followed in a closed system after shutting off the air supply. After the oxygen content decreased by 20–30% (20–60 min) the water was aerated for several minutes and then measurements were resumed. The total time ranged from 2 to 3 h and the number of intervals from 4 to 6.

Larvae adapted rapidly to the respirometer, as judged by their swimming behavior, and oxygen consumption rates (routine respiration) usually agreed well between intervals. The first interval (20–35 min), however, resulted in erratic values in three of the groups, probably because of handling stress, and was omitted. Corrections were made for oxygen consumption in seawater controls (without larvae). After the experiment, larvae were measured and weighed as described above.

### Results

Weight-specific ETS activity values for different species of leptocephali that had been stored frozen at -70°C ranged from about 4 to 20  $\mu\text{g-at O h}^{-1} (\text{g wet wt})^{-1}$  when assayed at temperatures corresponding to, or near, water temperatures at which larvae were collected (Table I).

When expressed on a dry weight basis, the ETS values ranged from 58 to 280  $\mu\text{g-at O h}^{-1} (\text{g dry wt})^{-1}$  (Table I). ETS activity was also determined on four fresh early metamorphosing larvae of *Albula* sp. (Table I). The mean value ( $\pm$  standard deviation) for wet-weight-specific activity ( $10.2 \pm 1.1 \mu\text{g-at O h}^{-1} \text{g}^{-1}$ ) was not significantly different at the 5% level (Student's  $t$  test) from the mean value for larvae of *Albula* sp. that had been stored frozen for 10–15 months ( $14.1 \pm 3.7 \mu\text{g-at O h}^{-1} \text{g}^{-1}$ ;  $N = 4$ ).

Wet-weight-specific ETS activity was determined at four temperatures (ranging from 10 to 30°C) in order to construct Arrhenius plots (not shown) for estimation of apparent activation energies ( $E_a$ ).  $E_a$  values were calculated from the slopes of the regression lines. All plots were linear ( $r > -0.993$ ).  $E_a$  values ranged from 11.0–15.7 kcal mole<sup>-1</sup>, and different adaptation temperatures had little effect on  $E_a$  in *M. punctatus* (Table II).

Changes in wet-weight-specific ETS activity were found during metamorphosis of *Albula* sp. (Fig. 1). Larvae show a pronounced shrinkage during this period, losing about 60% of their standard length (SL) in less than 2 weeks (Pfeiler, 1984). Wet-weight-specific ETS values obtained in advanced larvae near the end of metamorphosis (approximately 25 mm SL) were about 5× higher than those obtained for early metamorphic leptocephali (>50 mm SL). When the data were converted to dry-weight-specific ETS activity (data not shown) the values were about 3× higher in advanced larvae than in early larvae. The regression equation relating dry-weight-specific ETS activity ( $\mu\text{g-at O h}^{-1} [\text{g dry wt}]^{-1}$ ;  $y$ ) to standard length (mm;  $x$ ) was  $y = 512.25 - 7.04x$ ;  $r = -0.87$ ;  $N = 19$ . When expressed as total ETS activity per larva, a smaller (approximately twofold) increase in activity was observed during metamorphosis (Fig. 2). The difference in magnitude of increase in ETS activity in Figures 1 and 2 is due to the loss of approximately 75% of larval wet weight during metamorphosis (Pfeiler, 1984).

Changes in oxygen consumption rate in metamorphosing larvae of *Albula* sp. were similar to the changes seen in ETS activity; wet-weight-specific oxygen consumption increased more than fourfold, and oxygen consumption per larva increased about twofold (Table III). Because of a lack of ETS assay reagents, wet-weight-specific ETS activity values were calculated for the mean standard lengths of larvae used in the oxygen consumption experiments, using the regression equation from Figure 1. These data were then used to estimate the ratios of respiration to ETS activity (R:ETS) that are given in Table III.

Changes in wet-weight-specific ETS activity were also found during metamorphosis of *M. punctatus* (Fig. 3), although the pattern was different from that seen in *Albula* sp. As with *Albula* sp., metamorphosing leptocephali of *M. punctatus* shrink and lose wet weight during the transformation to glass eels. Wet-weight-specific ETS activity,

Table I

Weight-specific ETS activity in leptocephali expressed on a wet weight and dry weight<sup>a</sup> basis

Species	Wet wt (g)	Length <sup>b</sup> (mm)	Temperature (°C)		ETS activity			
			Water	Assay	$\mu\text{g-at O h}^{-1} \text{g}^{-1}$		$\mu\text{l O}_2 \text{h}^{-1} \text{g}^{-1}$	
					Wet wt	Dry wt	Wet wt <sup>c</sup>	Dry wt <sup>c</sup>
<i>Myrophis punctatus</i>	0.1915	67	23	23	20.4	280	246	3.37
	0.3008	78	9	10	4.2	58	51	0.70
<i>Ophichthus</i> sp.	0.2220	71	18	17	7.6	87	92	1.05
	0.2254	80	18	17	5.1	58	61	0.70
	0.2857	80	18	17	11.4	130	137	1.57
<i>Hildebrandia flava</i>	0.1868	59	21	24	6.9	—	83	—
	0.3225	67	21	23	5.3	—	64	—
Congridae (unidentified)	0.2983	76	23	23	9.8	—	118	—
<i>Albula</i> sp. (early metamorphic)	0.4738	56	16	17	12.5	127	151	1.53
	0.3815	53	16	23	19.2	177	231	2.13
	0.4130	53	16	23	13.9	133	168	1.60
	0.4351	55	16	23	10.7	105	129	1.27
	0.5917 <sup>d</sup>	56	23	23	10.7	118	129	1.42
	0.4858 <sup>d</sup>	58	23	23	8.8	90	106	1.08
	0.5681 <sup>d</sup>	56	23	23	11.3	123	136	1.48
0.6029 <sup>d</sup>	61	23	23	9.9	110	119	1.33	

<sup>a</sup> Dry weights for *M. punctatus* and *Ophichthus* sp. were calculated using mean water contents of 92.7% and 91.2%. Dry weights for *Albula* sp. were calculated from wet weights (see Materials and Methods).

<sup>b</sup> Standard length for *Albula* sp.; total length for all others.

<sup>c</sup>  $\mu\text{g-at O}$  converted to  $\mu\text{l O}_2$  at 20°C ( $0.083 \mu\text{g-at O} (\mu\text{l O}_2)^{-1}$ ).

<sup>d</sup> Data from fresh larvae; all other larvae had been stored frozen at  $-70^\circ\text{C}$  for periods ranging from 8 to 15 months.

however, showed only a small increase during this time. Wet weight continues to decrease during the transformation from glass eels to elvers, although total length remains about the same. For this reason, wet weight, instead of length, was used as the independent variable in Figures 3 and 4. The data in Figures 1 and 3 (and Figs. 2 and 4), can, however, be compared because standard length ( $x$ ) is a linear function of wet weight ( $y$ ) in metamorphosing leptocephali of *Albula* sp. ( $y = -0.145 + 0.011x$ ; Pfeiler, 1984). It is during the transformation from glass eels to elvers in *M. punctatus* that a large increase in wet-weight-specific ETS activity was seen (Fig. 3). Total ETS activity per individual decreased about twofold during metamor-

phosis of *M. punctatus* (Fig. 4), in contrast to the twofold increase in *Albula* sp. (Fig. 2).

## Discussion

Wet-weight-specific ETS values reported here for leptocephali of four anguilliform species and one albuliform agree well with those reported by Schalk (1988) for unidentified leptocephali that had not been frozen and were analyzed within 12 h of capture. This suggests that freezing larvae in liquid nitrogen immediately after capture, followed by storage at  $-70^\circ\text{C}$  for up to 15 months, resulted in little or no loss in ETS activity. In addition, we found no significant difference in ETS activity values between fresh and frozen early metamorphic leptocephali of *Albula* sp. (Table I; Figs. 1 and 2). The latter group, although stored at  $-70^\circ\text{C}$ , was not quick frozen in liquid nitrogen (see Materials and Methods). The sample size for fresh advanced metamorphic larvae of *Albula* sp. is too small ( $N = 2$ ) for statistical comparison, but ETS activity values did not differ substantially in fresh larvae compared with frozen larvae (Figs. 1 and 2).

Yamashita and Bailey (1990) also found that cold storage had little effect on ETS activity in larval walleye pollock (*Theragra chalcogramma*); they reported about a 10% loss in activity after 50 days at  $-80^\circ\text{C}$ . Substantial loss

Table II

Apparent Arrhenius activation energies ( $E_a$ ) for ETS activities in leptocephali

Species	Water Temp. (°C)	$E_a$ (kcal mole <sup>-1</sup> )
<i>Albula</i> sp.	16	11.0
<i>Hildebrandia flava</i>	21	12.2
<i>Ophichthus</i> sp.	18	12.4
<i>Myrophis punctatus</i>	12	14.9
<i>Myrophis punctatus</i>	21	15.7

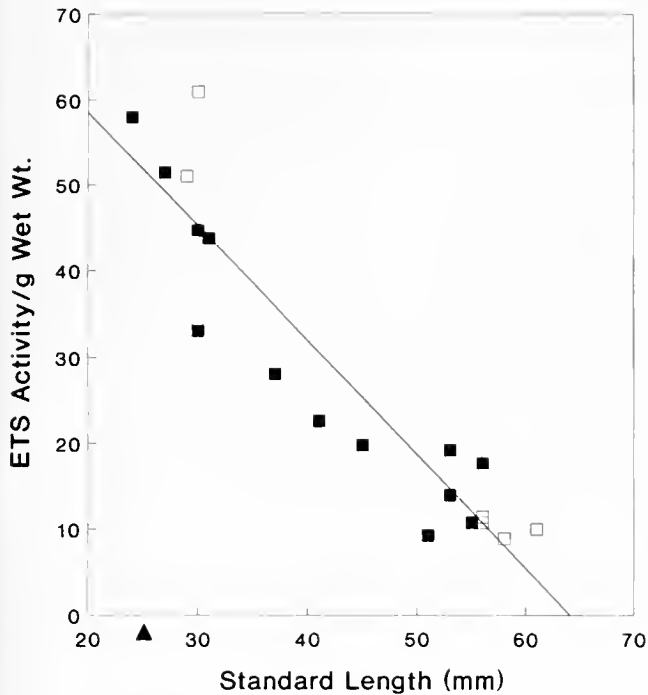


Figure 1. Change in wet-weight-specific ETS activity ( $\mu\text{g-at O h}^{-1} [\text{g wet wt}]^{-1}$ ) during metamorphosis of bonefish (*Albula* sp.) leptocephali ( $y = 85.13 - 1.33x$ ;  $r = -0.93$ ;  $N = 19$ ). Assay temperature =  $23^{\circ}\text{C}$ . Metamorphosis proceeds from right to left along the  $x$  axis because larvae decrease in length during this period (Pfeiler, 1984). The arrowhead shows the standard length at the end of metamorphosis. Open symbols are values obtained from fresh larvae; solid symbols are values obtained from frozen larvae (see Materials and Methods).

of activity would, however, be expected in damaged larvae, whether they were assayed immediately or frozen. Pelagic premetamorphic leptocephali are often dead or dying by the time the net is retrieved, and this might explain some of the variation in activity values reported here and by Schalk (1988).

The apparent activation energies ( $E_a$ ) for ETS activity of leptocephali and the lack of an effect of environmental temperature on  $E_a$  in *M. punctatus* agree well with results reported for marine plankton (Packard *et al.*, 1975).

Wet-weight-specific ETS values for leptocephali reported here and by Schalk (1988) ( $4\text{--}20 \mu\text{g-at O h}^{-1} \text{g}^{-1}$  at *in situ* temperature) are very low compared to those reported for walleye pollock larvae by Yamashita and Bailey (1990). These authors found an ETS value of  $5.82 \mu\text{O}_2 \text{h}^{-1} (\text{mg dry wt})^{-1}$  in prefeeding larvae assayed at  $6.5^{\circ}\text{C}$ . Mean ETS activity of the four fresh early metamorphic leptocephali of *Albula* sp. (Table I) was about 4 times lower ( $1.33 \mu\text{O}_2 \text{h}^{-1} (\text{mg dry wt})^{-1}$ ) for larvae adapted to, and assayed at, a much higher temperature ( $23^{\circ}\text{C}$ ). If we ignore the possibility of compensation to low temperature adaptation and assume that  $E_a$  for *Albula* sp. is not affected by adaptation temperature, the value obtained at  $23^{\circ}\text{C}$  can be converted to  $6.5^{\circ}\text{C}$  using the

equation given in Båmstedt (1980). The result ( $0.44 \mu\text{O}_2 \text{h}^{-1} (\text{mg dry wt})^{-1}$ ) is more than 10-fold lower than that found in larval walleye pollock. Part of this decrease may be a function of size differences between species; dry weights of leptocephali of *Albula* sp. were about  $10^3$  greater than those of larval walleye pollock. Yamashita and Bailey (1990) found in pollock, however, that ETS activity per individual larva is directly related to dry weight over a 10-fold range of weight. In addition, hepatic ETS activity in American plaice (*Hippoglossoides platessoides*) is a function of liver wet weight to the 0.86 power (Smith and Chong, 1982). These results suggest that differences in weight could, at most, account for only a two- to threefold decrease in ETS activity in *Albula* sp. compared with walleye pollock.

Because ETS activity is assumed to represent the maximum potential oxygen consumption rate (Owens and King, 1975), it follows that metabolic rates in leptocephali, expressed on a wet weight or a dry weight basis, are also low when compared with other fish larvae. This conclusion is valid only if the ratios of respiratory rate (R) to ETS activity (R:ETS ratio) are similar in both groups. The R:ETS ratios in leptocephali of *Albula* sp. (Table III) agree well with values reported for prefeeding and feeding larval walleye pollock, 0.27 and 0.47, respectively (Yamashita and Bailey, 1990). Early and intermediate metamorphosing leptocephali of *Albula* sp. (first two groups

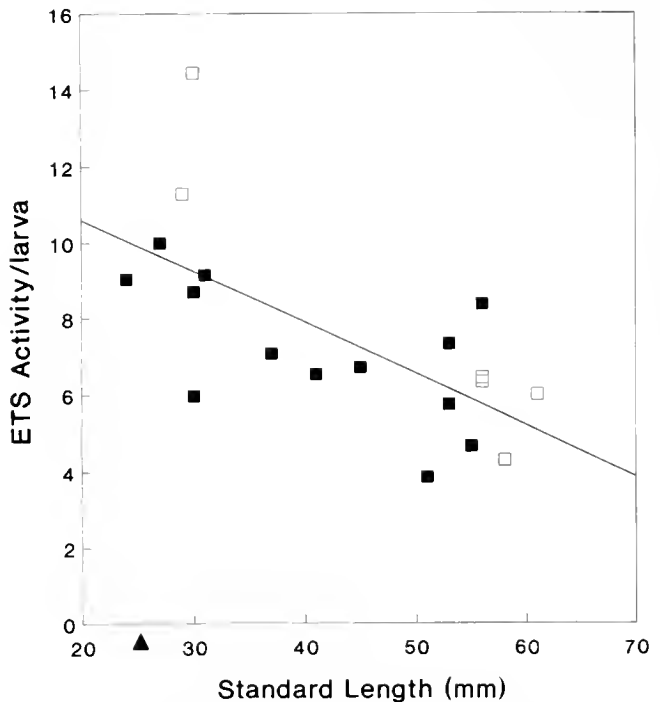


Figure 2. Change in total ETS activity ( $\mu\text{g-at O h}^{-1}$ ) during metamorphosis of bonefish (*Albula* sp.) leptocephali ( $y = 13.30 - 0.14x$ ;  $r = -0.67$ ;  $N = 19$ ). Assay temperature =  $23^{\circ}\text{C}$ . Same symbols as in Figure 1.

Table III

Oxygen consumption ( $V_{O_2}$ ) in metamorphosing *Albula sp. leptocephali*

SL <sup>a</sup> (mm)	N <sup>b</sup>	Total WW <sup>c</sup> (g)	Temp. (°C)		$V_{O_2}$ ( $\mu\text{l O}_2 \text{ h}^{-1}$ )		R:ETS <sup>d</sup>
			Run	Adapt.	per larva	per g WW	
49.4 ( $\pm 3.0$ )	9	3.9186	24-25	23	29.6	67.9	0.29
39.8 ( $\pm 3.7$ )	21	7.2587	20-21	19	31.3	90.6	0.23
33.4 ( $\pm 1.8$ )	21	5.2984	21-22	20	45.6	180.6	0.37
28.2 ( $\pm 0.8$ )	20	4.0744	24-25	21	57.3	281.1	0.49

<sup>a</sup> Mean standard length ( $\pm$  standard deviation).<sup>b</sup> N = total number of larvae in respirometer during the run.<sup>c</sup> WW = wet weight.<sup>d</sup> Ratio of wet-weight-specific  $V_{O_2}$  (R = respiration) to ETS activity (see Results).

in Table III; mean R:ETS = 0.26) are nonfeeding; the more advanced metamorphosing larvae (last two groups in Table III; mean R:ETS = 0.43) are just beginning to feed. In general, the R:ETS ratio shows species-specific differences with values of 0.50 or less (Owens and King,

1975; Schalk, 1988). In spot (*Leiostomus xanthurus*) and Atlantic menhaden (*Brevoortia tyrannus*) larvae, this ratio can be as low as 0.10 (P. Tester and L. Coston-Clements, pers. comm.).

In order for ETS activity to be of value in precisely estimating metabolic rates, the relationship between respiration and ETS activity must be determined for each species. Clearly, this is not possible for organisms that are often dead on capture. However, based on the good agreement of R:ETS ratios in larval walleye pollock and metamorphosing *Albula sp. leptocephali*, we suggest that ETS values can also be used to obtain rough estimates of res-

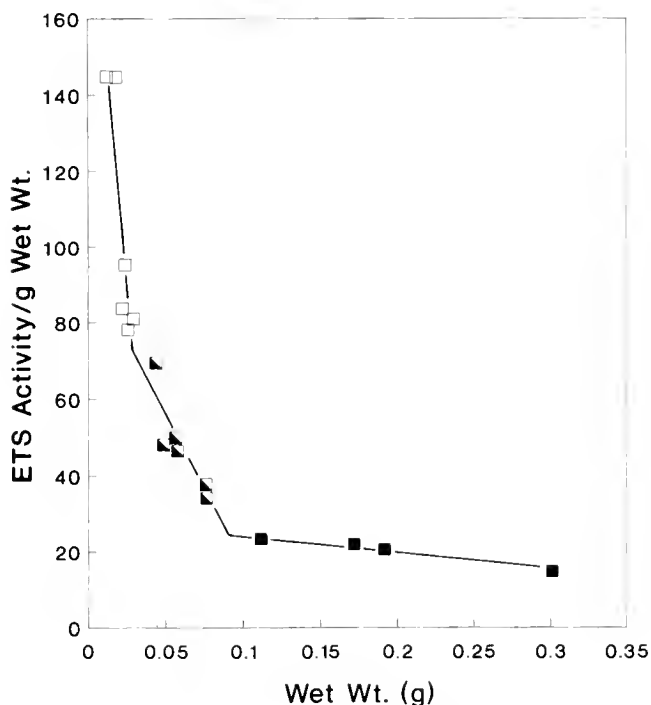


**Figure 3.** Change in wet-weight-specific ETS activity ( $\mu\text{g-at O h}^{-1} [\text{g wet wt}]^{-1}$ ) during metamorphosis in the eel, *Myrophis punctatus*. Assay temperature = 23°C. Metamorphosis proceeds from right to left along the x axis (key to symbols: solid = leptocephali; solid/open = glass eels; open = elvers). The four leptocephali, in order of decreasing wet weight, measured 78, 67, 63 and 55 mm total length; total length of glass eels and elvers ranged from 43 to 49 mm and was not related to wet weight. Regression equations are as follows: (leptocephali)  $y = 29.21 - 47.27x$ ;  $r = -0.99$ ;  $N = 4$ ; (glass eels)  $y = 94.68 - 792.58x$ ;  $r = -0.88$ ;  $N = 6$ ; (elvers)  $y = 205.56 - 4658.42x$ ;  $r = -0.88$ ;  $N = 6$ . All data were obtained from frozen individuals (see Materials and Methods).

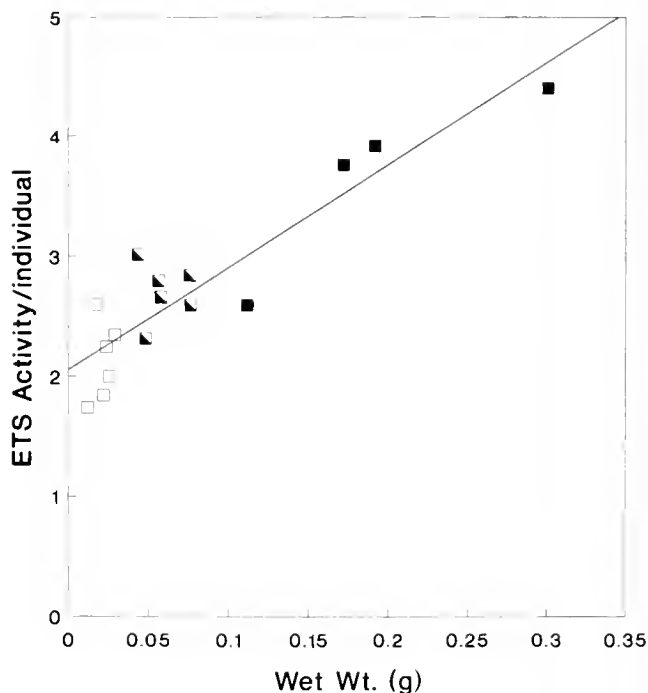


**Figure 4.** Change in total ETS activity ( $\mu\text{g-at O h}^{-1}$ ) during metamorphosis in the eel, *Myrophis punctatus* ( $y = 2.05 + 8.53x$ ;  $r = 0.91$ ;  $N = 16$ ). Assay temperature = 23°C. Same symbols as in Figure 3.

piration and, therefore, that the low ETS values obtained in premetamorphic leptocephali in this study and by Schalk (1988) indicate a low metabolic rate compared with other marine teleost larvae. The prediction would be false only if the R:ETS ratio in leptocephali was much higher than in other fish larvae, and our data suggest that it is not.

Oxygen consumption rates of early metamorphic leptocephali of *Albula* sp. (mean standard length = 49.4 mm; Table III) compare favorably with the low metabolic rates of larval lampreys of approximately the same size (Lewis and Potter, 1977), if one assumes a  $Q_{10}$  of 2 to account for differences in experimental temperature. The values for lampreys, however, represent standard respiration (*i.e.*, no activity), as compared to routine respiration (*i.e.*, minimal swimming activity) for *Albula* sp., which offers further support for the view that metabolic rates are low in leptocephali. Wet-weight-specific oxygen consumption rates increase during metamorphosis of larval lampreys (Lewis and Potter, 1977), a pattern similar to that seen in *Albula* sp. and *M. punctatus* (Figs. 1 and 3).

A low metabolic rate in leptocephali would result in a lower demand for nutrients and offer an overall survival advantage to the long-lived premetamorphic larval stage. Under these conditions the seemingly inefficient, putative feeding strategies described earlier may be capable of supplying all the nutritional requirements of these larvae.

#### Acknowledgments

We wish to thank the captain and crew of the NOAA Ship *Chapman* for their efforts in making the collection of leptocephali both enjoyable and successful. We also thank Patricia A. Tester and Linda Coston-Clements for kindly providing unpublished data, Omar Vidal for assistance in collecting bonefish leptocephali, Larry Settle for help in collecting and identifying eel leptocephali, and David Martinez for technical assistance. Travel funds for E.P. were provided by the Office for Research and External Funding, University of Puerto Rico, Mayagüez.

#### Literature Cited

- Bämstedt, U. 1980. ETS activity as an estimator of respiratory rate of zooplankton populations. The significance of variations in environmental factors. *J. Exp. Mar. Biol. Ecol.* **42**: 267-283.
- Hulet, W. II. 1978. Structure and functional development of the eel leptocephalus *Ariosoma balearicum* (De La Roche, 1809). *Phil. Trans. R. Soc. Lond., Ser. B.* **282**: 107-138.
- Hulet, W. H., and C. R. Robins. 1989. The evolutionary significance of the leptocephalus larva. Pp. 669-677 in *Fishes of the Western North Atlantic*, E. B. Böhlke, ed. Sears Foundation for Marine Research (Memoir No. 1, Part 9, Vol. 2), New Haven, CT.
- Lewis, S. V., and I. C. Potter. 1977. Oxygen consumption during the metamorphosis of the parasitic lamprey, *Lampetra fluviatilis* (L.) and its non-parasitic derivative, *Lampetra planeri* (Bloch). *J. Exp. Biol.* **69**: 187-198.
- Otake, T., K. Nogami, and K. Maruyama. 1993. Dissolved and particulate organic matter as possible food sources for eel leptocephali. *Mar. Ecol. Prog. Ser.* **92**: 27-34.
- Owens, T. G., and F. D. King. 1975. The measurement of respiratory electron-transport-system activity in marine zooplankton. *Mar. Biol.* **30**: 27-36.
- Packard, T. T. 1971. The measurement of respiratory electron-transport activity in marine phytoplankton. *J. Mar. Res.* **29**: 235-244.
- Packard, T. T., A. H. Devol, and F. D. King. 1975. The effect of temperature on the respiratory electron transport system in marine plankton. *Deep-Sea Res.* **22**: 237-249.
- Pfeiler, E. 1984. Changes in water and salt content during metamorphosis of larval bonefish (*Albula*). *Bull. Mar. Sci.* **34**: 177-184.
- Pfeiler, E. 1986. Towards an explanation of the developmental strategy in leptocephalous larvae of marine teleost fishes. *Environ. Biol. Fish.* **15**: 3-13.
- Pfeiler, E. 1989. Sensory systems and behavior of premetamorphic and metamorphic leptocephalous larvae. *Brain Behav. Evol.* **34**: 25-34.
- Pfeiler, E. 1991. Glycosaminoglycan composition of anguilliform and elopiform leptocephali. *J. Fish Biol.* **38**: 533-540.
- Pfeiler, E., and A. Luna. 1984. Changes in biochemical composition and energy utilization during metamorphosis of leptocephalous larvae of the bonefish. (*Albula*). *Environ. Biol. Fish.* **10**: 243-251.
- Pfeiler, E., M. A. Mendoza, and F. A. Manrique. 1988. Premetamorphic bonefish (*Albula* sp.) leptocephali from the Gulf of California with comments on life history. *Environ. Biol. Fish.* **21**: 241-249.
- Rasquin, P. 1955. Observations on the metamorphosis of the bonefish, *Albula vulpes* (Linnaeus). *J. Morphol.* **97**: 77-117.
- Robins, C. R. 1989. The phylogenetic relationships of the anguilliform fishes. Pp. 9-21 in *Fishes of the Western North Atlantic*, E. B. Böhlke, ed. Sears Foundation for Marine Research (Memoir No. 1, Part 9, Vol. 1), New Haven, CT.
- Schalk, P. H. 1988. Respiratory electron transport system (ETS) activities in zooplankton and micronekton of the Indo-Pacific region. *Mar. Ecol. Prog. Ser.* **44**: 25-35.
- Schmidt, J. 1925. The breeding places of the eel. *Annu. Rep. Smithsonian Inst.* **1924**: 279-316.
- Smith, D. G. 1980. Early larvae of the tarpon, *Megalops atlantica* Valenciennes (Pisces: Elopidae), with notes on spawning in the Gulf of Mexico and the Yucatan Channel. *Bull. Mar. Sci.* **30**: 136-141.
- Smith, D. G. 1984. Elopiformes, Notacanthiformes and Anguilliformes: Relationships. Pp. 94-102 in *Ontogeny and Systematics of Fishes*, H. G. Moser *et al.*, eds. American Society of Ichthyologists and Herpetologists (Special Publication 1), Allen Press, Lawrence, KS.
- Smith, J. C., and C. K. Chong. 1982. Body weight, activities of cytochrome oxidase and electron transport system in the liver of the American plaice *Hippoglossoides platessoides*. Can these activities serve as indicators of metabolism? *Mar. Ecol. Prog. Ser.* **9**: 171-179.
- Yamashita, Y., and K. M. Bailey. 1990. Electron transport system (ETS) activity as a possible index of respiration for larval walleye pollock *Theragra chalcogramma*. *Nippon Suisan Gakkaishi* **56**: 1059-1062.

# Reports of Papers Presented at the General Scientific Meetings of the Marine Biological Laboratory August 16–18, 1993

## Special Editorial Board

- |   |   |
|---|---|
| Shelley Adamo, Cornell University                             | Lionel Jaffe, Marine Biological Laboratory                                  |
| Daniel Alkon, NIH   | Daniel Johnston, Baylor College of Medicine                                 |
| Nina Stromgren Allen, Wake Forest University                  | George Langford, Dartmouth College  |
| Peter Armstrong, University of California, Davis              | John Lisman, Brandeis University  |
| William Baldrige, McMaster University                         | Rodolfo Llinás, NYU Medical Center  |
| Michael V. L. Bennett, Albert Einstein College of<br>Medicine | Enrico Nasi, Boston University School of Medicine                           |
| Timothy Bestor, Harvard Medical School                        | James Olds, NIH   |
| William Bialek, NEC Research Institute                        | Michael Paulin, University of Otago   |
| David Bodznick, Wesleyan University                           | Haohua Qian, Harvard University   |
| Robert Bullis, University of Pennsylvania                     | James Quigley, SUNY, Stony Brook  |
| Richard Chappell, Hunter College                              | Wade Regehr, University of Pennsylvania                                     |
| Neal Cornell, Marine Biological Laboratory                    | Harris Ripps, University of Illinois  |
| Charlene D'Avanzo, Hampshire College                          | Michael Sheetz, Duke University Medical Center                              |
| Linda Deegan, Ecosystems Center, MBL                          | Peter J. S. Smith, Marine Biological Laboratory                             |
| John Dowling, Harvard University                              | Antoinette Steinacker, Puerto Rico Medical Sciences<br>Campus               |
| William Eckberg, Howard University                            | Sidney Tamm, Boston University Marine Program,<br>MBL                       |
| Harvey Fishman, University of Texas Medical Branch            | Walter Troll, NYU Medical Center  |
| Kenneth Foreman, Boston University Marine Program,<br>MBL     | Steven Vogel, NIH   |
| Vladimir Gelfand, University of California, San<br>Francisco  | Dieter Weiss, University of Rostock   |
| Maria Gomez, University of Pennsylvania                       | Seymour Zigman, University of Rochester School of<br>Medicine and Dentistry |
| Richard Hill, Michigan State University                       | Conchita Zuazaga de Ortiz, University of Puerto Rico                        |
| Susan Hill, Michigan State University                         |   |

## Contents

## Feature Article

- Oldenbourg, Rudolf, Guang Mei, and Robert E. Palazzo**  
Asters in lysates of *Spisula* oocytes observed with a new type of polarized light microscope . . . . . 288

## Calcium in Development

- Eckberg, William R., Andrew L. Miller, Lisa G. Short, and Lionel F. Jaffe**  
Calcium pulses during the activation of a proto-stome egg . . . . . 289
- Miller, A. L., A. Galione, E. Karplus, and L. F. Jaffe**  
Mechanically induced calcium release from *Xenopus* cell cycle extracts . . . . . 290

## Neurobiology

- Fishman, Harvey M., and Janis Metuzals**  
Ca<sup>2+</sup>-induced axosome formation in internally dialyzed giant axons of *Loligo pealei* . . . . . 292
- Smith, P. J. S., G. G. Duthie, A. Shipley, and M. Tytell**  
Steady-state calcium efflux from *Aplysia* neurons: perturbation by H<sub>2</sub>O<sub>2</sub> and protection by stress protein, HSP70 . . . . . 293
- Rossi, David J., Gregory A. Kinney, Eric Karplus, Andrew L. Miller, Lionel F. Jaffe, and N. Traverse Slater**  
Fluorescence imaging of NMDA receptor-activated calcium influx in granule cells in thin cerebellar slices . . . . . 295
- Wang, Samuel S.-H.**  
Modeling the apparent diffusion constant of calcium ions emanating from a channel: implications for calcium wave propagation . . . . . 297
- Brady, S. T., M. Sugimori, P. L. Leopold, J.-W. Lin, D. S. Chu, and R. Llinás**  
Activity-dependent inhibition of neurotransmitter release by Brefeldin A . . . . . 299
- Lin, Shien-Fong, Rashi A. Abbas, and John P. Wiksw, Jr.**  
Magnetic localization of the origins of self-sustained oscillation in squid giant axons . . . . . 300
- Makarenko, Vladimir**  
Noise modulated persistence of the metastable state in a simulated neural network . . . . . 301

## Cell Biology and Cell Motility

- Pierson, E. S., P. J. S. Smith, A. M. Shipley, L. F. Jaffe, M. Cresti, and P. K. Hepler**  
Ca<sup>2+</sup> fluxes around pollen grains and pollen tubes of lily: normal development and effects of thermal shock, BAPTA-type buffer microinjection and depletion of boric acid from the medium . . . . . 302
- Hill, Susan Douglas, Alan M. Shipley, and Peter J. S. Smith**  
Endogenous currents during wound healing and regeneration in sabellid fanworms . . . . . 303

## Gamete Physiology and Biochemistry

- Ueno, Hiroshi, Renu Juneja, Osamu Shimomura, S. S. Koide, and Sheldon J. Segal**  
The presence of the GABA-synthesizing enzyme, glutamate decarboxylase, in *Spisula* sperm . . . 305
- Abraham, Vivek C., Andrew L. Miller, Lionel F. Jaffe, and Richard A. Fluck**  
Cytoplasmic microtubule arrays in *Oryzias latipes* (medaka) eggs during ooplasmic segregation . . 305

## Sensory Neurobiology

- Herzog, E. D., C. L. Passaglia, S. A. Dodge, N. D. Levine, and R. B. Barlow, Jr.**  
*Limulus* vision in the ocean: comparing neural and behavioral thresholds . . . . . 307
- Chappell, Richard L., and Paul Glynn**  
Equivalent sine wave frequency for interpretation of responses to frequency-swept sinusoids defined: an algorithm from studies in skate ganglion cells . 308
- Araneda, Ricardo C., and Michael V. L. Bennett**  
Electrical properties of electroreceptor cells isolated from skate ampulla of Lorenzini . . . . . 310
- Qian, Haohua, and John E. Dowling**  
GABA responses on retinal bipolar cells . . . . . 312
- Bodznick, David**  
The specificity of an adaptive filter that suppresses unwanted reafference in electrosensory neurons of the skate medulla . . . . . 312
- Lemon, William C., and Richard B. Levine**  
Role of proprioceptive input during abdominal bending-reflex motor activity in the tobacco hawkmoth *Manduca sexta* . . . . . 314
- Bayha, Keith M., Rainer Voigt, and Jelle Atema**  
A comparison of the tuning properties of chemoreceptor cells in the first and fourth walking legs of female American lobsters . . . . . 316



## Behavior

- Breithaupt, Thomas, and Jelle Atema**  
Evidence for the use of urine signals in agonistic interactions of the American lobster ..... 318
- Bushmann, Paul, and Jelle Atema**  
A novel tegumental gland in the nephropore of the lobster, *Homarus americanus*: a site for the production of chemical signals? ..... 319
- Kaplan, Liat J., Courtney Lowrance, Jennifer Basil, and Jelle Atema**  
The role of chemical and visual cues in agonistic interactions of the American lobster ..... 320
- Karavanich, Christy, and Jelle Atema**  
Agonistic encounters in the American lobster, *Homarus americanus*: Do they remember their opponents? ..... 321

## Comparative Biochemistry and Physiology

- Hill, Richard W., John W. H. Dacey, Judith E. McDowell, and Dale F. Leavitt**  
The impact of feeding by mussels and scallops on production of dimethylsulfide from marine phytoplankton ..... 322
- Beiner, John M., Christopher S. Ogilvy, and Arthur B. DuBois**  
Cerebral blood flow and ventral aortic blood pressure response during elevation of intracranial pressure in bluefish (*Pomatomus saltatrix*) ... 323
- Srimal, Subita, James P. Quigley, and Peter B. Armstrong**  
Limulin and C-reactive protein from the plasma of *Limulus polyphemus* are different proteins ..... 325
- Armstrong, Peter B., Paul M. Selzer, Niklas Ahlborg, Kerstin Morehead, Melissa Perregaux, Patricia Komuniecki, Richard Komuniecki, Subita Srimal, and Peter J. Hotez**  
Identification and partial characterization of an extracorporeal protease activity secreted by the triclad turbellariid worm, *Bdelloura candida* ... 326
- Bruning, Grace, Michael Ferkowicz, and Neal Cornell**  
Heme biosynthesis in fish and land vertebrates: enzyme and cDNA comparisons ..... 327
- Zigman, Seymour, and Nancy S. Rafferty**  
Near-UV radiation effects on dogfish (*Mustelus canis*) lens catalase and antioxidant protection ..... 328

## Estuarine Ecology

- Judge, Bryan S., Christopher A. Scholin, and Donald M. Anderson**  
RFLP analysis of a fragment of the large-subunit ribosomal RNA gene of globally distributed populations of the toxic dinoflagellate *Alexandrium* ..... 329

## Bierzuchudek, Anne, Charlene D'Avanzo, and Ivan Valiela

- Effects of macroalgae, night and day, on ammonium profiles in Waquoit Bay ..... 330

## ABSTRACTS

*In addition to the short reports contained in this issue, the following papers were also presented at the meetings. The abstracts of these papers are available from the Marine Biological Laboratory Archives.*

## Calcium in Development

- Cameron, L. A., E. Ito, D. L. Alkon, and J. L. Olds**, "Dynamic changes in intracellular free  $Ca^{++}$  after Brefeldin A treatment in sea urchin eggs as visualized by fura-2"

## Neurobiology

- Chu, D. S., J. Marsal, J. Glasi, M. Morita, M. Sugimori, and R. Llinás**, "Transmitter release in squid giant synapse: lessons from tetanus toxin"
- Marsal, J., J. Blasi, M. Morita, D. S. Chu, M. C. Wilson, M. Sugimori, and R. Llinás**, "Transmitter release in squid giant synapse: lessons from botulinum toxin A"
- Sugimori, M., M. Morita, and R. Llinás**, "The reversal potential differences for presynaptic and glutamate derived postsynaptic potentials in squid giant synapse"

## Cell Biology and Cell Motility

- Humphreys, Tom**, "Cyclosporin A attenuates allogeneic rejection reactions in the marine sponge *Microciona prolifera*"
- Langford, G. M., S. A. Kuznetsov, D. A. Johnson, D. L. Cohen, and D. G. Weiss**, "Axoplasmic organelles move toward the barbed end of actin filaments"
- Tabor, Aaron T., and Nina Stromgren Allen**, "Mechanism of gliding of the marine cyanobacterium *Spirulina subsalsa*"

## Gamete Physiology and Biochemistry

- Chang, D. C., and Pin Lu**, "Mechanisms of DNA-uptake facilitated by electrical treatments"

## Sensory Neurobiology

- Dodge, S. A., N. D. Levine, K. Longnecker, M. E. Kelly, E. D. Herzog, C. L. Passaglia, M. K. Powers, and R. B. Barlow, Jr.**, "*Limulus* vision in the ocean: behavioral thresholds for target detection"
- Farley, Lynda, and Jelle Atema**, "A comparison of changes in the olfactory organ (antennule) of the American lobster during early larval development"

**Steinacker, A., J. Monterrubio, R. Perez, A. F. Mensinger, and A. Marin,** "Pharmacological study of outward currents in toadfish semicircular canal hair cells"

#### Behavior

**Adamo, Shelley,** "Communication in cuttlefish: measuring the responses of *Sepia officinalis* to conspecific body patterns"

#### Comparative Biochemistry and Physiology

**Lutz, Gordon J., and Lawrence C. Rome,** "Built for jumping: the design of the frog muscular system"

#### Estuarine Ecology

**Duran, Robert, Michael LaMontagne, and Ivan Valiela,** "Temporal and spatial distribution of nitrous oxide flux in the Waquoit Bay estuarine system"

**Faulstich, Emilie, John Brawley, and Ivan Valiela,** "Fresh and seawater sources to a coastal pond in Waquoit Bay"

**Gribble, Kristin E.,** "Rates of decomposition estimated by  $\text{NH}_4^+$  and DIC production in anoxic estuarine sediments of Childs River, MA"

**O'Brien, Todd,** "Growth of *Fundulus heteroclitus* populations among three estuaries experiencing different rates of nutrient loading"

**Richards, Timothy, and James N. Kremer,** "Using rhodamine dye to estimate eddy diffusivity in a seaweed canopy"

Reference: *Biol. Bull.* 185: 288. (October, 1993)

## Asters in Lysates of *Spisula* Oocytes Observed with a New Type of Polarized Light Microscope Rudolf Oldenbourg, Guang Mei, and Robert E. Palazzo (Marine Biological Laboratory)

Asters consist of microtubules radiating in all directions from centrosomes, microtubule-organizing centers found in almost all animal cells. The structure of centrosomes and their mechanism of microtubule nucleation are still poorly understood. We have studied asters that formed spontaneously in cytoplasmic extracts prepared from activated eggs obtained from the surf clam *Spisula solidissima* (1). Astral birefringence was augmented, and asters were stabilized, by the addition of 3% hexylene glycol to the extract. Asters formed with the addition of hexylene glycol display a central region devoid of birefringence and contain astral rays of surprisingly uniform length (Fig. 1).

The aster image presented here was obtained using a new type of polarized light microscope ("pol-scope") that measures, at high resolution, the retardance due to specimen anisotropy irrespective of its orientation. The design of this new pol-scope, which we are developing at the Marine Biological Laboratory, is based on the traditional polarized light microscope but has two essential modifications: the specimen is illuminated with nearly circular polarized light, and the traditional compensator is replaced by two electro-optical modulators (2). A video camera and computer-assisted image analysis provide measurements of specimen anisotropy in rapid succession for all points of the image constituting the field of view. The images document fine structural and molecular organization within a thin optical section of the specimen.

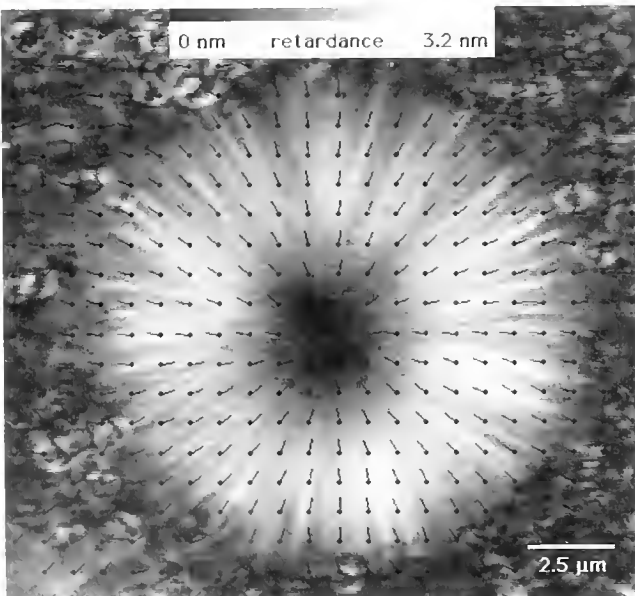


**Figure 1.** Aster in lysate prepared from clam oocytes 4 min after activation. The image represents the magnitude of measured retardance values in an array of 256 by 240 pixels of different gray levels. Retardance values range between 0 (black) and 3.2 nm (white). In addition, we indicated the measured azimuths, or orientations of the slow axis, with additional black lines in the image (see text).

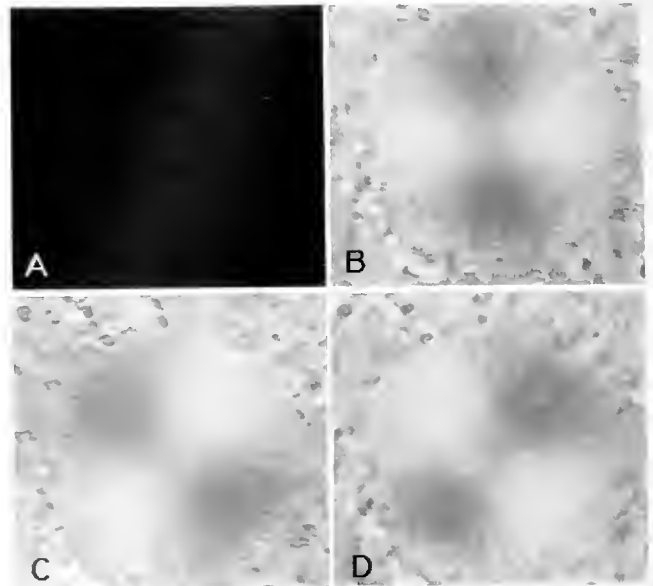


**Figure 2.** Four experimental images used to compute the aster image displayed in Figure 1. Images (A), (B), (C), and (D) were recorded sequentially, each with different voltages applied to the electro-optical modulators.

The image shown in Figure 1 was computed using four experimental images (Fig. 2) recorded with the new pol-scope equipped with a 60 $\times$ /1.4-NA Plan Apo objective lens (Nikon). Note that the computed image exhibits no orientationally dependent contrast, usually a hallmark of micrographs taken with conventional polarized light microscopes. The retardances and the azimuths were computed for every image point from the same set of four experimental images. The azimuths in Figure 1 are represented by lines with orientations between 0 $^\circ$  and 180 $^\circ$ . To reduce the complexity of Figure 1 we chose to display the azimuths on regular grid points (indicated by small closed circles) at a much lower resolution than the original measurements would permit. With the current setup of the new pol-scope, a set of four experimental images can be recorded in 0.3 s, and computation of the retardance or azimuth image takes about 15 s.

We gratefully acknowledge the support, inspiration, and guidance provided by Shinya Inoué. The instrument development is supported by the National Institutes of Health grant R01 GM49210 awarded to R.O.

### Literature Cited

1. Palazzo, R. E., J. B. Brawley, and L. I. Rebhun. 1988. *Zool. Sci.* 5: 603-611.
2. The design of the microscope will be published elsewhere. The use of electro-optical modulators in light microscopy was first introduced by Robert D. Allen and his colleagues; Allen, R. D., J. Brault, and R. D. Moore. 1963. *J. Cell Biol.* 18: 223-235.

Reference: *Biol. Bull.* 185: 289-290, (October, 1993)

### Calcium Pulses During the Activation of a Protostome Egg

William R. Eckberg<sup>1,2</sup>, Andrew L. Miller<sup>1</sup>, Lisa G. Short<sup>1,2</sup>, and Lionel F. Jaffe<sup>1</sup> (<sup>1</sup>Marine Biological Laboratory and <sup>2</sup>Department of Biology, Howard University, Washington, DC 20059)

Transient increases in free cytoplasmic  $\text{Ca}^{2+}$  pass through the cytosol of a wide variety of fertilizing deuterostome eggs and do so from the sperm entry point to its antipode. These  $\text{Ca}^{2+}$  waves

occur through the release of stored  $\text{Ca}^{2+}$ , and they provide most or all of the activating stimulus for these eggs. Based on several indirect lines of experimental evidence, it was proposed (1,2)

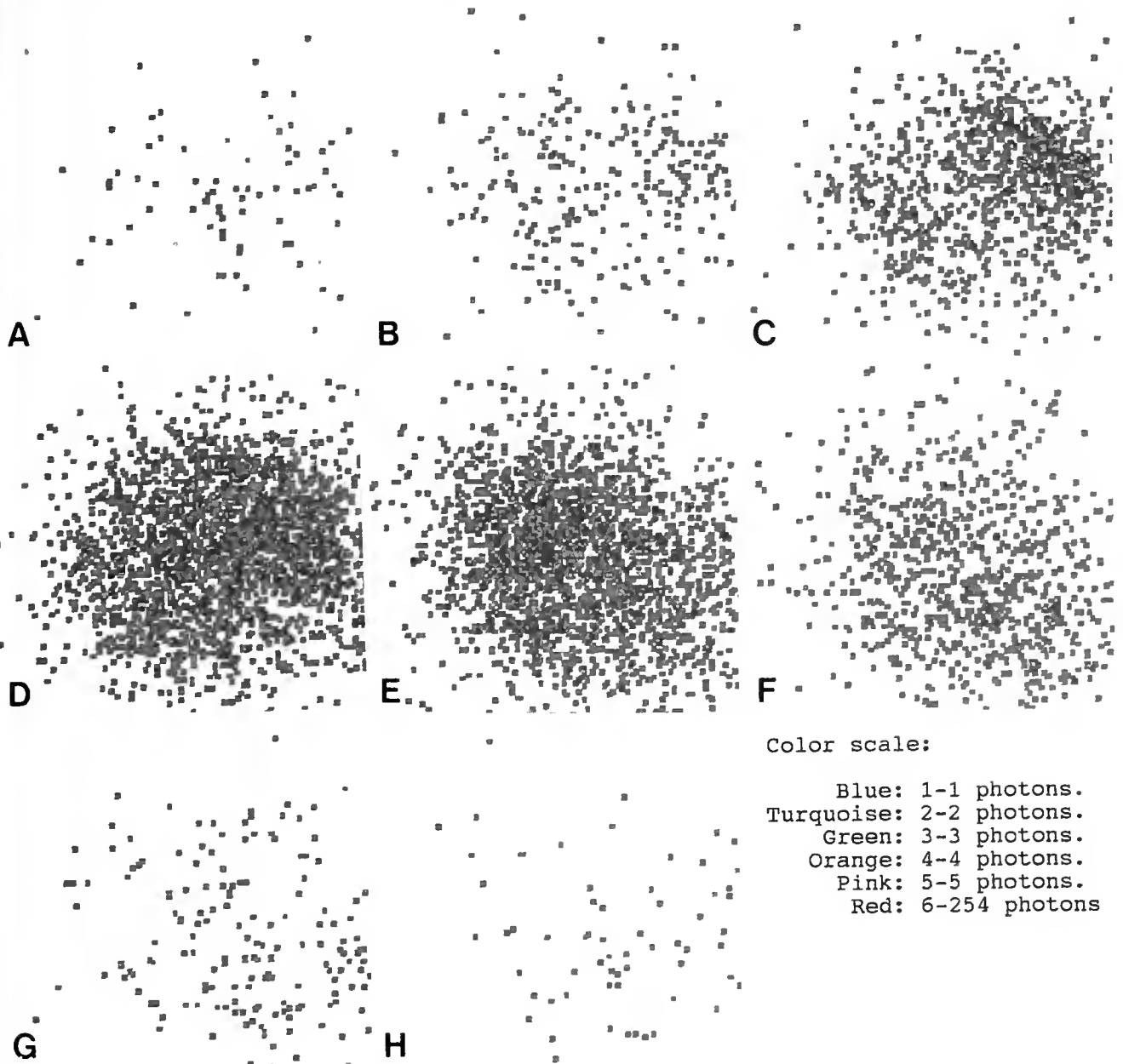


**Figure 1.** An example of a wave of  $\text{Ca}^{2+}$  release in a fertilized *Chaetopterus* egg. Panels A through H show the photons accumulated during successive 3-s intervals. This wave moves from the upper right to the lower left. Panels A and H show the resting levels before and after the wave, which took approximately 6 s to traverse the 105  $\mu\text{m}$  diameter egg, indicating a velocity of around 30  $\mu\text{m}/\text{s}$ . The eggs were injected with *f*-recombinant aequorin prior to insemination.

that protostome eggs are activated by a prolonged uptake of  $\text{Ca}^{2+}$  from the medium due to sperm-induced membrane depolarization, and that this uptake then starts an activation wave similar to those in deuterostomes, except that it moves inward from the whole surface rather than across the egg from pole to pole. To test these hypotheses, we microinjected *Chaetopterus pergamentaceus* oocytes with semisynthetic recombinant aequorins (3) and measured light emission in response to both fertilization and artificial activation by excess  $\text{K}^+$ .

Both fertilization and  $\text{K}^+$ -activation induced multiple, brief  $\text{Ca}^{2+}$  transients in the eggs (Fig. 1). Generally, the first transient was localized to one sector of the egg. This was followed by one or more global waves of  $\text{Ca}^{2+}$ . The waves passed through the egg at about  $30 \mu\text{m/s}$  (speed calculated along the cell surface to allow direct comparison with wave speeds through other cells). After the global waves, more non-propagating pulses were observed; sequential waves and pulses originated at different points on the egg surface.

These new data are consistent with the hypothesis that the activation of protostome eggs is initiated by voltage-gated entry of  $\text{Ca}^{2+}$  through much or all of the egg surface. It is likewise consistent with the hypothesis that this entry then triggers a  $\text{Ca}^{2+}$  wave through the egg. But the notion that such waves are radial is clearly incorrect. All the waves that we have seen in *Chaetopterus* moved from pole to pole like those through deuterostome eggs.

Moreover, the speed of these waves—about  $30 \mu\text{m/s}$  at room temperature—is the same as the speed exhibited by  $\text{Ca}^{2+}$  waves through 50 other, highly varied, active cells (2,4). Indeed, no clear exception to this conserved velocity is known for  $\text{Ca}^{2+}$  waves that penetrate deeply into normal cells. Since all these so-called “fast” waves are believed to be propagated by  $\text{Ca}^{2+}$ -induced  $\text{Ca}^{2+}$  release from the endoplasmic reticulum, we propose that the activation waves through *Chaetopterus* eggs are typical fast  $\text{Ca}^{2+}$  waves propagated in the same way. Moreover, the rapidity with which the pulses and waves were extinguished indicates that the eggs have powerful mechanisms with which to pump  $\text{Ca}^{2+}$  out of the cytosol.

We would like to thank Dr. Osamu Shimomura for supplying us with semisynthetic recombinant aequorins. This work was supported by NSF grants DCB-9103569 to L.F.J. and DIR-9211855 to L.F.J. and A.L.M. and by NIH HD08016 and Council for Tobacco Research, USA, Inc. grant #3378 to W.R.E.

### Literature Cited

1. Jaffe, L. F. 1985. Pp 127–165 in *Biology of Fertilization*, Vol. III, C. B. Metz and A. Monroy, eds. Academic Press, Orlando, FL.
2. Jaffe, L. F. 1991. *Proc. Natl. Acad. Sci. USA* 88: 9883–9887.
3. Shimomura, O., B. Musicki, Y. Kishi, and S. Inoué. 1993. *Cell Calcium* 14: 373–378.
4. Jaffe, L. F. 1993. *Cell Calcium* (in press).

Reference: *Biol. Bull.* 185: 290–292, (October, 1993)

## Mechanically Induced Calcium Release From *Xenopus* Cell Cycle Extracts

A. L. Miller, A. Galione, E. Karplus, and L. F. Jaffe (Marine Biological Laboratory)

We previously reported the discovery of slow ( $0.5 \mu\text{m/s}$ ) calcium waves that accompany cytokinesis in both frog and fish eggs (1,2). The low velocity of these waves shows that they are unlikely to be propagated by calcium-induced calcium release (3). So we proposed that they are propagated mechanically and belong in a small but well-documented class of  $0.3$  to  $1.0 \mu\text{m/s}$  waves that traverse a variety of cells during normal development (4,5). Such propagation does not require the influx of calcium through the plasma membrane from the extracellular medium (1). A likely candidate for an intracellular calcium repository is the cortical endoplasmic reticulum (ER), which is deformed during the organization and contraction of the contractile arc. One mechanism of release might be stretch-activated channels in the surface of the ER. In theory, the contracting actomyosin band and the cortical ER network might be connected by actin “cables” that would stretch the ER in front of the advancing furrow, releasing calcium and thus organizing and advancing the contractile band.

We sought, therefore, to induce the release of calcium mechanically from the ER in plasma-membrane-free cell cycling extracts from activated *Xenopus* eggs, and to prevent this release by adding an agent that disassembles actin microfilaments. We also sought to examine pharmacologically the nature of the

channels involved in calcium release and to compare the magnitude of mechanically induced calcium release to that induced by inositol triphosphate ( $\text{IP}_3$ ).

We used recombinant aequorin, a bioluminescent photoprotein that generates light when it binds with free calcium (6); the light was detected with a photomultiplier tube (PMT). Absolute resting levels of calcium in the extracts were determined with calcium-sensitive microelectrodes and were found to vary between  $300$  and  $400 \text{ nM}$ .

We designed and built a device that could apply reproducible deformations to a  $30\text{-}\mu\text{l}$  droplet of extract compressed to a distance of  $50 \mu\text{m}$  between two  $22\text{-mm-square}$ , #1 thickness, horizontal glass coverslips (Fig. 1A). Shear forces were applied to the extract by moving the upper coverslip with a computer-controlled servomotor equipped with a tachometer-feedback speed-control system and a digital position encoder. This device allowed us to vary the direction, velocity, and duration of applied shear in a controlled and reproducible manner. The lower coverslip was fixed above the window of the PMT; thus the light emitted on application of a shear force could be monitored over time.

Figure 1B shows the effect of applying mechanical shear to the extract, and Figure 1C illustrates how the calcium release

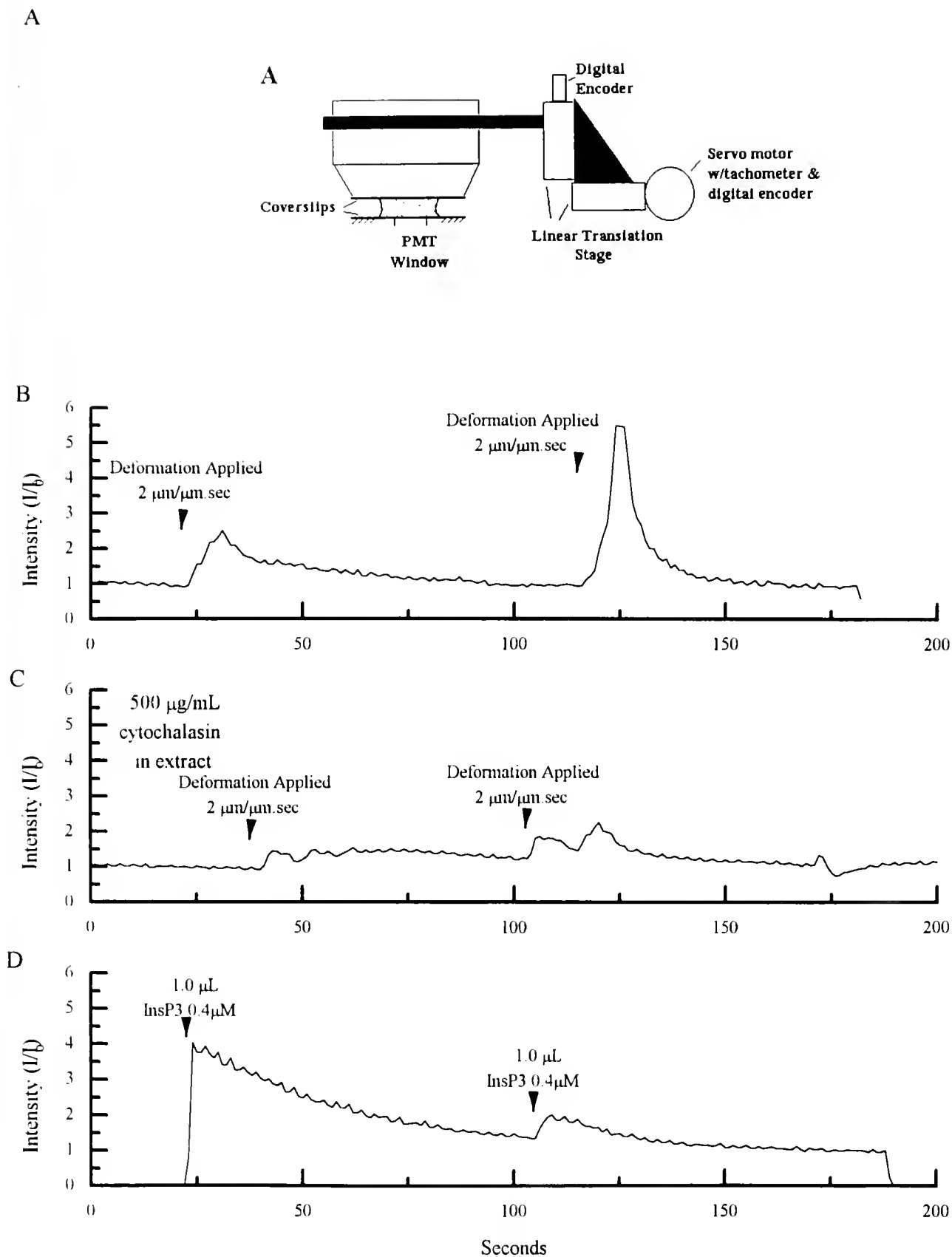


**Figure 1.** Figure 1A is a schematic diagram of the device used to apply mechanical shear to extracts. Figure 1B shows increases in luminescence resulting from the application of mechanical shear to an aequorin-loaded extract. Figure 1C illustrates how this mechanically induced calcium release can be dramatically reduced in the presence of cytochalasin (500  $\mu\text{g/ml}$ ). Figure 1D is an example of an equivalent magnitude of calcium release induced by addition of 1  $\mu\text{l}$  of  $\text{IP}_3$  (0.4  $\mu\text{M}$ ).

can be dramatically reduced in the presence of cytochalasin (500  $\mu\text{g/ml}$ ). Figure 1D illustrates the magnitude of release induced by the addition of 1  $\mu\text{l}$  of  $\text{IP}_3$  (0.4  $\mu\text{M}$ ).

The smallest rate of movement of the upper coverslip that gave a substantial calcium release was 10  $\mu\text{m/s}$ . When this is divided by the 50- $\mu\text{m}$  gap between the two coverslips, it yields a deformation rate of 2  $\mu\text{m}/\mu\text{m}\cdot\text{s}$ . We estimated that the deformation rate during furrow progression in an intact frog egg would be only 0.001  $\mu\text{m}/\mu\text{m}\cdot\text{s}$ . Thus we are applying a much greater degree of deformation to an extract than would occur naturally during cytokinesis. This difference could be accounted for by the immense differences between the cytoskeletal architectures of an intact cell and a cycling extract. The degree of deformation we applied is, however, much smaller than that which occurs in routine handling of extracts during experimental procedures; e.g., pipetting. One should be cautious, therefore, in interpreting results that could be unknowingly influenced by a mechanically induced release of calcium.

In summary, we have demonstrated that mechanical deformation of extracts induces a reproducible calcium release that is rapidly resequenced by a functional ER. In addition, the order of magnitude of this mechanical release is similar to that

induced by  $\text{IP}_3$ . This suggests that the mechanical forces applied are not merely breaking up the ER and dumping vast amounts of calcium into the cytosol, but are opening stretch-activated ER channels. Our next step will be to image mechanically induced calcium release from intact eggs.

We wish to thank Andrew Murray for providing cycling *Xenopus* extracts, Osamu Shimomura for the recombinant aequorin, and the MBL for a Herbert W. Rand Fellowship to A.G. This work was supported by NSF grants DCB 9103569 to L.F.J. and BIR 9211855 to L.F.J. and A.L.M.

### Literature Cited

1. Fluck, R. A., A. L. Miller, and L. F. Jaffe. 1991. *J. Cell Biol.* 115: 1259–1265.
2. Miller, A. L., R. A. Fluck, J. A. McLaughlin, and L. F. Jaffe. 1990. *Biol. Bull.* 179: 224a.
3. Jaffe, L. F. 1991. *Proc. Natl. Acad. Sci. USA* 88: 9883–9887.
4. Sawai, T. 1985. *Zool. Sci.* 2: 707–712.
5. Cheer, A., J.-P. Vincent, R. Nuccitelli, and G. Oster. 1987. *J. Theor. Biol.* 124: 377–404.
6. Shimomura, O., S. Inouye, B. Musicki, and Y. Kishi. 1990. *Biochem J.* 270: 309–312.

Reference: *Biol. Bull.* 185: 292–293. (October, 1993)

## Ca<sup>2+</sup>-Induced Axosome Formation in Internally Dialyzed Giant Axons of *Loligo pealei* Harvey M. Fishman (University of Texas Medical Branch at Galveston) and Janis Metzals

Axosomes are large vesicles (20–50  $\mu\text{m}$  diameter) that form by fusion of induced, smaller vesicles within 30 min after transection of cephalopod giant axons in Ca<sup>2+</sup>-containing artificial seawater (ASW) (1). Electron microscopy (Fig. 1a) shows hypertrophy of different types of membrane within cut axons and modifications of the cytoskeleton associated with these membranes. Vesiculation of glia (Schwann cells) and association of these vesicles with those of the axon are also observed. We used internal dialysis of excised giant axons of *Loligo pealei* to determine whether induced vesiculation is caused by direct structural damage (transection) or by elevated concentrations of Ca<sup>2+</sup> and other external ions.

A method for dialyzing axoplasm within a giant axon (2) was modified. The bottom of the nerve chamber (trough) incorporated a glass slide so that axons could be observed during dialysis under phase-contrast light microscopy. A 4-cm length of isolated giant nerve fiber was cannulated by the insertion of separate, collinear glass capillaries (300  $\mu\text{m}$  diameter) 3 mm into both transected ends. The ends were then tied against the outer surface of each capillary. A 160- $\mu\text{m}$  diameter dialysis tube (cellulose acetate) with porous length of 1.5 cm was advanced through the proximal glass cannula until the porous length was midway into the axon and the tip protruded from the distal cannula (Fig. 1b).

Flow through the dialysis tube was maintained at 0.5 ml/h with an infusion pump.

Control solution (lacking NaCl, CaCl<sub>2</sub>, and MgCl<sub>2</sub>) [(mM): 440 K glutamate, 2.5 EGTA-Tris, 5 TrisCl] was used as the external solution. The pH of the control and other solutions was adjusted to 7.4, and the osmolarity was kept constant at 974 mOsm by addition of glycine. Axoplasmic dialysis for 1 h with control solution produced no observable vesiculation. Addition of 3.5 mM CaCl<sub>2</sub> to the dialysate, which yielded a free [Ca<sup>2+</sup>] of 1 mM, resulted in axosome production only in the dialyzed portion of the axon 30 min to 1 h after the change of dialysate (Fig. 1c). Replacement of glutamate with Cl<sup>-</sup> in the control dialysate produced a small amount of vesiculation compared to the control. Dialysis with a divalent cation-free ASW (430 NaCl, 10 KCl, 2.5 EGTA-Tris, 5 TrisCl) produced a further increase in vesiculation over that produced by Cl<sup>-</sup>, but axosomes formed only when Ca<sup>2+</sup> was present in the dialysate at free concentrations  $\geq 100 \mu\text{M}$ . Mg<sup>2+</sup> acted similarly to Ca<sup>2+</sup> but at higher concentrations (>10 mM). The effectiveness of Ca<sup>2+</sup> in inducing axosome formation was enhanced by the presence of Na<sup>+</sup>, Cl<sup>-</sup>, and Mg<sup>2+</sup> in the dialysate; i.e., dialysis with ASW produced more axosomes than did dialysis with the control solution at the same free [Ca<sup>2+</sup>]. Thus, all ions in the extracellular fluid, except for



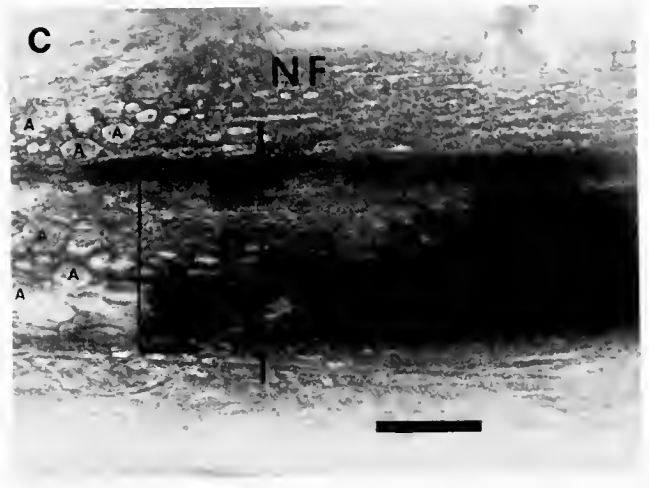
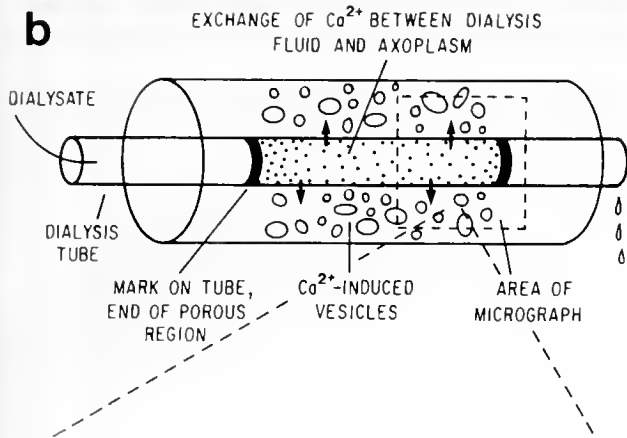
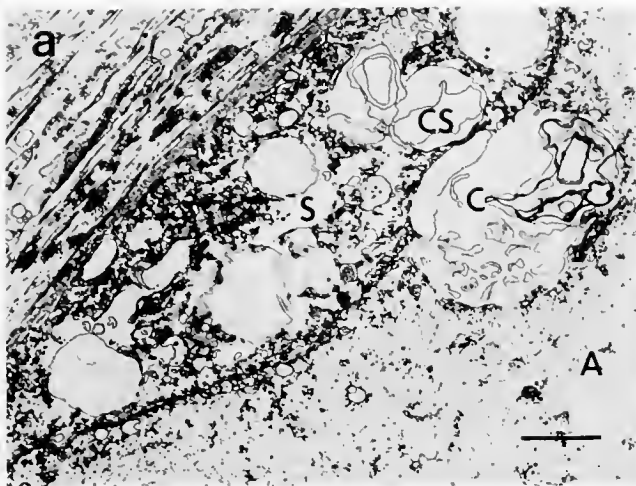


**Figure 1.** *a.* Electron micrograph survey of transverse section of squid giant nerve fiber fixed 10 min after transection in  $\text{Ca}^{2+}$ -containing ASW. This section proximal to the cut end shows spongiform membrane modifications in the axon (C) and in the Schwann cells (CS); A: axon; S: Schwann cell layer. *b.* Diagram of internal dialysis of giant axon with the porous length of dialysis tube delimited with black dye. *c.* Micrograph of portion of nerve fiber (NF) within dashed lines of diagram in *b.* 30 min after internal dialysis with control solution plus 3.5 mM  $\text{CaCl}_2$  (free  $[\text{Ca}^{2+}] = 1 \text{ mM}$ ) and control solution externally. Arrows in *c* mark the porous/non-porous transition region of the dialysis tube (DT). Notice the presence of axosomes (A) only in the porous region. Calibration bar: *a.* 1  $\mu\text{m}$ ; *c.* 100  $\mu\text{m}$ .

$\text{K}^+$ , act synergistically to maximize production. These data indicate that a short-term (min) rise in axoplasmic free  $[\text{Ca}^{2+}] \geq 100 \mu\text{M}$ , without mechanical injury to an axon, is sufficient to cause axosome generation and that  $\text{Na}^+$ ,  $\text{Cl}^-$ , and  $\text{Mg}^{2+}$  together enhance this formation.

H.M.F. thanks Dr. J. M. Russell for advice on the dialysis method. Supported by NIH (NS31256) and ONR (N00014-90-J-1137).

### Literature Cited

1. Fishman, H. M., K. P. Tewari, and P. L. Stein. 1990. *Biophys. Biochim. Acta (Biomembranes)* 1023: 421-435.
2. Mullins, L. J., and F. J. Brinley, Jr. 1991. Chapter 8 in *Squid as Experimental Animals*. D. L. Gilbert, W. J. Adelman, Jr., and J. M. Arnold, eds., Plenum, New York.

Reference: *Biol. Bull.* 185: 293-294. (October, 1993)

### Steady-State Calcium Efflux from *Aplysia* Neurons: Perturbation by $\text{H}_2\text{O}_2$ and Protection by Stress Protein, HSP70

Smith, P. J. S., G. G. Duthie<sup>1</sup>, A. Shipley, and M. Tytell<sup>2</sup> (National Vibrating Probe Facility, Marine Biological Laboratory, <sup>1</sup>the Rowett Research Institute, Scotland, and <sup>2</sup>Wake Forest University)

The control of cellular calcium levels is an integral part of cellular homeostasis, and the regional variation of the calcium ion is an important component of intracellular signaling. A compromised calcium regulation can lead to cell death by a variety of potentially destructive pathways (1). By acting on reg-

ulatory mechanisms such as the  $\text{Ca}^{2+}$ -ATPases,  $\text{Na}^+$ - $\text{Ca}^{2+}$  exchange, or the voltage-sensitive ryanodine receptor, reactive oxygen species (free radicals) can perturb the intracellular calcium balance (2). However, because free radicals are an inevitable product of normal respiration and neuronal activity, cells have

developed antioxidant systems to scavenge the radicals. The latter are also implicated in damage to the polyunsaturated component of the membrane. Failure of the scavenging systems is presumably, at least in part, responsible for some CNS disease states. Alzheimer's and Parkinson's diseases are believed to involve free radicals (3).

In this study we used the large and relatively easily cultured bag cell from the abdominal ganglion of *Aplysia californica* as a model for cellular damage. Cells were cultured as previously described (4), except that the background calcium was reduced to approximately  $50 \mu\text{mol} \cdot \text{l}^{-1}$  and  $\text{MgCl}_2$  was elevated to  $65.2 \text{mmol} \cdot \text{l}^{-1}$ . We assessed the effects of introducing  $\text{H}_2\text{O}_2$  to the culture medium, which we presume to generate free radicals, on the anatomy of the neuron *in vitro* and on the calcium efflux from the cell soma. As yet, we have not attempted to measure the production of free radicals in the medium. The efflux was measured with a calcium-selective vibrating probe (5,6). Intracellular recordings were made in a routine manner, using an Axoclamp2A. We further examined the protective effect of incubating the cells in dilutions of exogenous heat shock protein or bovine serum albumin (HSP70 & BSA:  $0.5 \mu\text{g} \cdot \text{ml}^{-1}$ ) for 2–3 h.

*Aplysia* bag cells develop extensive neurites and growth cones within days of isolation. All soma examined reveal a steady-state calcium efflux. Signals are measured to be between 5 and 20  $\mu\text{V}$ , which, within the limitations of the technique (4), equates to fluxes of about  $1 \text{pmol} \cdot \text{cm}^{-2} \cdot \text{s}^{-2}$ . Addition of  $\text{H}_2\text{O}_2$  at final concentrations of 10, 5, and  $2.5 \mu\text{mol} \cdot \text{l}^{-1}$  causes a marked perturbation of this efflux. In general, the first effect is a reduction in the efflux strength as it rapidly approaches background. This is followed by a resumed efflux equal to or greater than the original. After 1 h, however, preparations exposed to 10 or  $5 \mu\text{mol} \cdot \text{l}^{-1}$  have signals near background and in some instances can be seen to have exploded. Structurally these events are marked by blebbing of the growth cones, retraction of the neurites, and swelling of the soma. Cells incubated in BSA and then washed behaved in the same manner as the controls. Preliminary data indicate that the time course of this response is not only dose dependent but also related to the level of background calcium. Normal calcium levels of  $11 \text{mmol} \cdot \text{l}^{-1}$  cause a more rapid degeneration. Intracellular recording indicates that the membrane potential is lost at around the same time the flux returns to zero for the second time.

Cells bathed in HSP70 and then washed with low-calcium seawater show a markedly different anatomical response to the addition of  $\text{H}_2\text{O}_2$ . After 1 h of observation, no obvious change in the structure is evident, even with a  $5 \mu\text{mol} \cdot \text{l}^{-1}$  dose. Cell somas and neurites are apparently intact 24 h later. Although we have only preliminary data on the physiological response to

the  $\text{Ca}^{2+}$  flux, it also seems markedly different. In one trial, controls and HSP70-incubated cells (4 h) were exposed to  $15 \mu\text{mol} \cdot \text{l}^{-1}$  of  $\text{H}_2\text{O}_2$ . The control cells, incubated in the HSP70 solvent, lyse immediately, whereas the incubated cell monitored with the probe maintains a strong efflux signal ( $20 \mu\text{V}$ ) for at least 1 h. No anatomical damage was observed in this group.

The calcium efflux may be due to the activity of plasma ATPases, but as yet we have not identified a mechanism. The dramatic change in the calcium efflux signal and the eventual death of the cells on the addition of  $\text{H}_2\text{O}_2$ , and presumably during a free radical attack, may reflect the inactivation of ATPases and the eventual degradation of the membranes. Ultimately, however, it appears that the calcium homeostatic regulation of the cell fails. Whether such failure can occur *in vivo* is unclear, although many neurological syndromes have been associated with pro-oxidant conditions (7).

Perhaps the most important result of this study is the hitherto unreported protection that incubation in exogenous HSP70 affords cells. Proteins such as HSP70 are generated by cells in response to a diverse array of conditions and perform equally diverse roles, ranging from protein folding to pore induction (8,9). They are known to be produced after brief periods of brain and heart ischemia when highly reactive molecular species (free radicals) are frequently present (8). Although we have not identified the source of the perturbation induced by  $\text{H}_2\text{O}_2$ , a likely mechanism is via the generation of free radicals. If this proves to be the case, the use of *Aplysia* neurons, in conjunction with probe and anatomical observations, seems to offer a novel and potentially powerful method for analyzing both the degradative action of free radical attacks and the potential of protective agents.

### Literature Cited

1. Duncan, C. J. 1991. Pp. 1–9 in *Oxygen Radicals and Cellular Damage*. C. J. Duncan, ed. Cambridge University Press.
2. Duthie, G. G., and J. R. Arthur. 1993. *Free Radical Biol. Med.* **14**: 435–442.
3. Bondy, S. C., and C. P. LeBel. 1993. *Free Radical Biol. Med.* **14**: 633–642.
4. Knox, R. J., E. A. Quattrocki, J. A. Connor, and L. K. Kaczmarek. 1992. *Neuron* **8**: 883–889.
5. Kühtreiber, W. M., and L. F. Jaffe. 1990. *J. Cell Biol.* **110**: 1565–1573.
6. Smith, P. J. S., R. H. Sanger, and L. F. Jaffe. 1994. *Methods Cell Biol.* **40**. In press.
7. Duthie, G. G. 1993. *Eur. J. Clin. Nutr.* In press.
8. Welch, W. J. 1993. *Sci. Am.* **268**: 56–64.
9. Alder, G. M., B. M. Austen, C. L. Bashford, A. Mehler, and C. A. Pasternak. 1990. *Biosci. Rep.* **10**(6): 509–518.

Reference: *Biol. Bull.* 185: 295–296. (October, 1993)

## Fluorescence Imaging of NMDA Receptor-Activated Calcium Influx in Granule Cells in Thin Cerebellar Slices

David J. Rossi, Gregory A. Kinney, Eric Karplus\*, Andrew L. Miller\*, Lionel F. Jaffe\*, and N. Traverse Slater (Department of Physiology, Northwestern University Medical School and \*Marine Biological Laboratory)

In many cells, calcium regulates cell migration as well as neurite extension (1,2). Activation of the N-methyl-D-aspartate (NMDA) subtype of glutamate receptor and the associated calcium entry via NMDA-gated ion channels have been implicated in both the migration and subsequent neurite extension of cerebellar granule cells (3,4). At least two other effectors of intracellular calcium, metabotropic glutamate receptors and voltage-gated calcium channels, have also been linked to the development of cerebellar granule cells (5,6). To further assess the mechanisms by which NMDA receptors affect granule cell migration and neurite extension, the role of these receptors in controlling intracellular calcium concentrations ( $[Ca^{2+}]_i$ ) must be determined. In this study, we have examined changes in intracellular free calcium levels ( $[Ca^{2+}]_i$ ) caused by endogenous glutamate release; we have focused on the developing cerebellum, using fluorescence imaging of living granule cells in cerebellar slices maintained *in vitro*.

Parasagittal slices (150  $\mu$ m thick) of cerebellar vermis from young (postnatal days 6–16) Sprague-Dawley rats anaesthetised with Isoflurane were prepared with a vibrating tissue slicer (Vibratome). The slices were incubated for 1 h in a medium containing (in mM): NaCl 126; NaHCO<sub>3</sub> 26; NaH<sub>2</sub>PO<sub>4</sub> 1; KCl 3; CaCl<sub>2</sub> 2.5; MgCl<sub>2</sub> 2 and D-glucose 10 (gassed with 95% O<sub>2</sub>/5% CO<sub>2</sub>, pH = 7.2–7.4; osmolarity adjusted to 310 milliosmoles; 37°). After incubation, the slices were placed, for 2 h, in a solution containing the membrane-permeable calcium-sensitive fluorophores fluo-3 AM or fura-2 AM (110  $\mu$ M; Molecular Probes) dispersed in .031% Cremophor EL (Sigma). Slices were then mounted on the stage of an upright microscope (Zeiss Axioscope) and continuously perfused with a magnesium-free, bicuculline-containing (10  $\mu$ M) medium. Slices were imaged with an Attofluor ratio imaging system (Atto Instruments) equipped with 100 watt Xenon lamp; 10 nm bandpass excitation filters (334 nm, 380 nm and 488 nm); standard fluo-3 and fura-2 dichroic and barrier filter sets (Zeiss); Attofluor intensified CCD camera; and Attofluor acquisition software. Images were digitized and stored on disk.

Granule cells at all developmental stages were effectively loaded with both fluo-3 AM and fura-2 AM (Fig. 1A). In initial studies with fluo-3, the bath application of the glutamate uptake inhibitor L-alpha-aminoadipic acid (LAA, 1 mM) produced an increase of resting  $[Ca^{2+}]_i$  in all granule cells, regardless of migrational position: granule cell layer (GCL)  $2.4 \pm .3$  n = 104; molecular layer (ML)  $1.6 \pm .2$  n = 36; and external germinal layer (EGL)  $1.6 \pm .2$  n = 23 (data expressed as mean  $\pm$  S.D. fold increase). Similar increases in  $[Ca^{2+}]_i$  were produced by the bath application of 10  $\mu$ M NMDA, and both effects were blocked by the NMDA receptor antagonist DL-2-amino-5-phosphopentanoic acid (APV; 100  $\mu$ M). These results demonstrate that granule cells possess functional NMDA receptor-channels at all

developmental stages, and suggests that endogenous glutamate release tonically regulates  $[Ca^{2+}]_i$  in these neurons.

Although experiments employing the calcium-permeable ionophore A23187 indicated that cells at all developmental stages were loaded to similar levels, the ratiometric calcium fluorophore fura-2 AM was also employed, so that differences in  $[Ca^{2+}]_i$  between cells could be more accurately assessed. Surprisingly, despite the previously reported differences in spontaneous NMDA channel activity in cells during development (7), fura-2 measurements indicated that granule cells in the EGL had significantly (ANOVA  $P < .005$ ) higher resting  $[Ca^{2+}]_i$  than cells in the ML or GCL (mean  $\pm$  S.D. in arbitrary pixel units: GCL:  $60.3 \pm 22.0$  n = 279; ML:  $58.1 \pm 20.7$  n = 152; EGL:  $70.0 \pm 24.5$  n = 140; Fig. 1C). In addition, both LAA (1 mM) and NMDA (10  $\mu$ M) significantly (ANOVA  $P < .01$ ) increased  $[Ca^{2+}]_i$  in all granule cells observed (Fig. 1A–D). Furthermore, LAA produced a significantly (ANOVA  $P < .005$ ) larger rise in  $[Ca^{2+}]_i$  in postmigratory cells within the GCL than either the ML or EGL (Fig. 1D) (mean  $\pm$  S.D. in arbitrary pixel units: GCL:  $108.2 \pm 30.9$  n = 145; ML:  $91.8 \pm 31.5$  n = 80; EGL:  $91.2 \pm 34.4$  n = 70). The response to NMDA was not significantly different between layers.

We have used acetoxymethyl esters of calcium-sensitive fluorophores to simultaneously measure  $[Ca^{2+}]_i$  in cells in an intact brain slice at varying developmental stages. This approach allowed the examination of some of the mechanisms by which  $[Ca^{2+}]_i$  is regulated by NMDA receptors during development with minimal perturbations to their normal environment. The results show that resting  $[Ca^{2+}]_i$  in cerebellar granule cells is dependent on migrational position in a manner that would not be predicted by the reported (7) profile of spontaneous NMDA-gated channel activity. But, cells at all developmental stages do have functional NMDA receptors that are capable of substantially elevating  $[Ca^{2+}]_i$  (Fig. 1A–D). We have not yet determined what proportion of the rise in  $[Ca^{2+}]_i$  is due to calcium influx through the activated channel. A substantial portion of the rise in  $[Ca^{2+}]_i$  could be due to voltage-sensitive calcium channels responding to NMDA-induced depolarization. This might also explain why the observed rises in  $[Ca^{2+}]_i$  do not parallel the reported electrophysiological measures of NMDA sensitivity (7,8). Finally, at all developmental stages resting  $[Ca^{2+}]_i$  is suppressed by a tonic reuptake of endogenously released glutamate. These results support the view that NMDA receptors are involved in regulating  $[Ca^{2+}]_i$  in developing cerebellar granule cells; but suggest that there are other important contributing mechanisms.

We thank Drs. Kamran Khodakhah, Wade Regehr, and Samuel Wang for helpful discussions, and Zeiss and Attofluor for the use of their equipment. This work was supported by a grant from the Markey Program in Developmental Biology to N. T. Slater, NSF grant BIR9211855 to Lionel F. Jaffe and Andrew

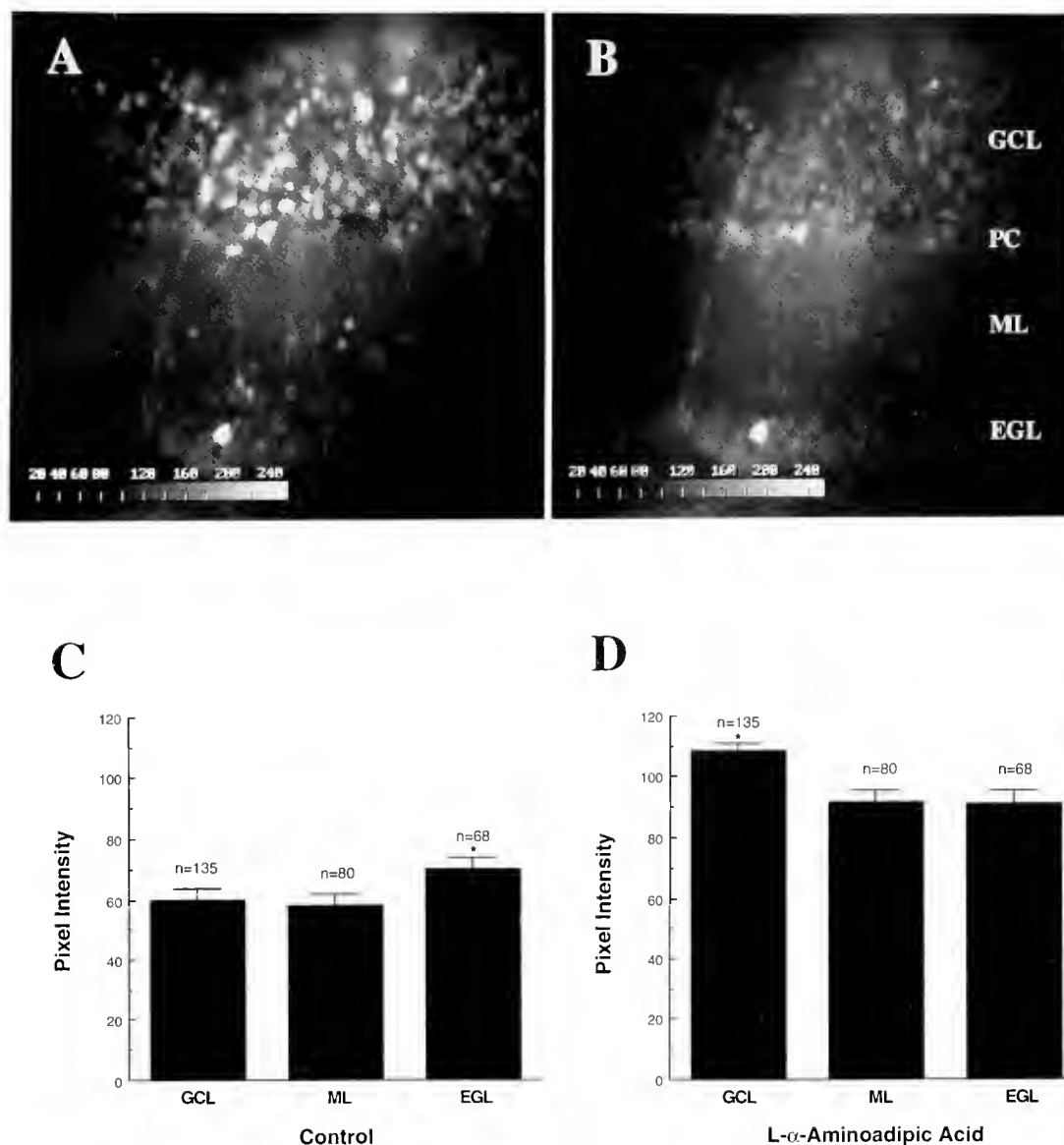


**Figure 1.** (A) Fluorescence image of a cerebellar slice showing cells loaded with fura-2 AM and excited with 380 nm wavelength light. (B) Same slice as in A in the presence of the glutamate uptake inhibitor L- $\alpha$ -aminoadipic acid (1 mM). 380 nm light excites fura-2 in the unbound state, so decreases in fluorescence indicate rises in  $[Ca^{2+}]_i$ . Cell layers are labelled. Granule cell layer (GCL); Purkinje cell layer (PC); Molecular layer (ML); External germinal layer (EGL). (C) Pixel intensity as a measure of the ratio of the response to 334 and 380 nm excitation. Each column is the mean response of at least 80 individual granule cells in the EGL, ML and GCL pooled from 7 different slices. Error bar is SEM. Asterisk indicates statistical significance ( $P < .005$ ). (D) Same as in C except in the presence of L- $\alpha$ -aminoadipic acid. All three values are significantly greater ( $P < .01$ ) than their respective control values.

L. Miller and by MBL summer fellowships awarded to David J. Rossi and Gregory A. Kinney.

#### Literature Cited

1. Stossel, T. P. 1993. *Science* 260: 1086-1094.
2. Kater, S. B., and L. R. Mills. 1991. *J. Neurosci.* 11: 891-899.
3. Cambray-Deakin, M. A., and R. D. Burgoyne. 1992. *Dev. Brain Res.* 66: 25-32.
4. Komuro, H., and P. Rakic. 1993. *Science* 260: 95-97.
5. Komuro, H., and P. Rakic. 1992. *Science* 257: 806-809.
6. Aronica, E., D. F. Condorelli, F. Nicoletti, P. Dell'Albani, C. Amico, and R. Balazs. 1993. *J. Neurochem.* 60: 559-565.
7. Rossi, D. J., and N. T. Slater. 1993. *Neuropharmacology*. In Press.
8. Farrant, M., D. Feldmeyer, S. Kobayashi, T. Takahashi, and S. G. Cull-Candy. 1993. *J. Physiol. (Lond.)* 467: 272P.

Reference: *Biol. Bull.* 185: 297–298. (October, 1993)

## Modeling the Apparent Diffusion Constant of Calcium Ions Emanating From a Channel: Implications for Calcium Wave Propagation

Samuel S.-H. Wang (Hopkins Marine Station of Stanford University, Pacific Grove, California 93950)

Ionized calcium ( $\text{Ca}^{2+}$ ) is an intracellular messenger in nearly all eukaryotic organisms. Calcium waves have been observed in many cell types, including airway epithelia, eggs, hepatocytes, exocrine pancreas, cultured glial cells, and neuronal cells. These waves travel across or between cells without slowing or getting smaller, and so cannot be generated by pure passive diffusion. Rather, the waves must be amplified locally. This leads to the questions: what substance mediates the local amplification process, and over what distance does that substance act? Here I bring together previous measurements of calcium diffusion and wave propagation to show that if calcium itself mediates amplification, it acts locally at a distance of  $0.2 \mu\text{m}$  or less.

In most calcium wave-generating preparations, the source of  $\text{Ca}^{2+}$  is an internal store that is sensitive to the second messenger inositol 1,4,5-triphosphate ( $\text{IP}_3$ ). Receptor activation leads to the activation of heterotrimeric G proteins in the plasma membrane, which in turn activate the enzyme phospholipase C to produce  $\text{IP}_3$ . In this signaling cascade, both  $\text{IP}_3$  and  $\text{Ca}^{2+}$  can contribute to the production of a regenerative calcium wave.  $\text{IP}_3$  binds to receptors in the endoplasmic reticulum, which open to allow  $\text{Ca}^{2+}$  to pass into the cytoplasm. Conversely, micromolar levels of calcium augment the activity of phospholipase C and the  $\text{IP}_3$  receptor. Therefore, the speed of calcium waves might be rate-limited by the diffusion of  $\text{IP}_3$ ,  $\text{Ca}^{2+}$ , or both, from one release site to neighboring ones, in the direction of propagation.

Previously I showed that BAPTA and its analogs, all of which have fast on-rates ( $k_+ \sim 10^8 \text{ M}^{-1}\text{s}^{-1}$ ), slow calcium wave propagation in cultured neuronal cells. In contrast, the "slow" buffer EGTA ( $k_+ \sim 10^6 \text{ M}^{-1}\text{s}^{-1}$ ) does not slow waves (1). Together, these experiments show that an exogenous buffer must bind calcium quickly if it is to impede  $\text{Ca}^{2+}$  wave propagation. This supports a mechanism for wave propagation in which the local diffusion of calcium is a rate-limiting step.

This conclusion is important in interpreting estimates of the diffusion constant (D) of the rate-limiting factor from wave front parameters. D can be inferred from measurements of the length and speed of a traveling wave by using the relation  $D = Lv + \mathcal{C}$  (2–4; J. Sneyd and L. V. Kalachev, in prep.), where  $\mathcal{C}$  is a positive correction term that depends on the specific excitatory mechanism, so that  $D > Lv$ . In agonist-evoked calcium waves in N1E-115 neuroblastoma cells, wave front analysis gives  $Lv = 140$  to  $700 \mu\text{m}^2/\text{s}$  (1). These values are near the diffusion constant of  $\text{IP}_3$  ( $280 \mu\text{m}^2/\text{s}$ ) or free calcium ( $200$ – $600 \mu\text{m}^2/\text{s}$ ), but not near the D of buffered calcium in cytoplasm ( $10$ – $20 \mu\text{m}^2/\text{s}$ ). Therefore, the estimate of D from  $Lv$  is reconcilable with calcium as the rate-limiting factor only if calcium is free, not buffered, at the time it closes the feedback loop.

The apparent slowing of calcium diffusion in cytoplasm can be explained by the presence of immobile calcium buffers that slow the movement of calcium ions by binding them (5,6). At first, when calcium ions emerge from an ion channel, they diffuse freely. Then they begin to come into equilibrium with endogenous buffers. The movement of the ions is then slowed if the

buffer is less mobile than the free calcium ion. When the ions have come into equilibrium with buffers (at long distances or after long times), the apparent rate of diffusion is the weighted average  $D_{\text{app}} = D_{\text{Ca}}f_{\text{eq}} + D_{\text{buffer}}(1 - f_{\text{eq}})$ , where  $f_{\text{eq}}$  is the fraction of calcium ions which are free at binding equilibrium,  $D_{\text{Ca}}$  is for calcium diffusing freely in cytoplasm, and  $D_{\text{buffer}}$  is for the calcium-buffer complex. A consequence of this equation is that  $D_{\text{app}}$  must lie between  $D_{\text{Ca}}$  and  $D_{\text{buffer}}$ . At low calcium levels,  $D_{\text{app}}$  has been measured to be about  $10 \mu\text{m}^2/\text{s}$  (6,7). Therefore,  $D_{\text{buffer}}$  is less than  $10 \mu\text{m}^2/\text{s}$ .  $D_{\text{buffer}}$  can also be calculated directly for elevated levels of calcium from the published data of Allbritton *et al.* (6), because they give  $D_{\text{app}}$  as a function of both free calcium and the total amount of calcium added.  $D_{\text{buffer}}$  calculated this way increases with increasing  $[\text{Ca}]_i$  and is lowest at resting levels of calcium. These low rates of buffer diffusibility are consistent with the observation that in chromaffin cells, buffers do not wash out even after extended whole-cell patch clamp recording (8). Because these numbers are so much smaller than  $D_{\text{Ca}}$ , the endogenous buffers can be regarded as immobile ( $D_{\text{buffer}} = 0$ ).

The spatial distribution of calcium ions diffusing into a non-saturating buffer can be calculated by regarding calcium ions emanating from a pore as starting in a free state and passing back and forth between free and bound states with binding and unbinding rate constants  $k_+$  and  $k_-$ .  $D_{\text{app}}$ , the apparent diffusion constant of calcium, can be calculated by considering the averaged behavior of the ions. The average fraction of ions that are free at a given time,  $f_{\text{avg}}(t)$ , is an exponential that relaxes toward binding equilibrium with time constant  $\tau = 1/(k_+ + [B]_i k_-)$  (ref. 9; Fig. 1A). Integrating  $f_{\text{avg}}(t)$  over time will give the total average amount of time that calcium ions are free. Then, for the case of an immobile buffer,

$$D_{\text{app}}(t) = \frac{D_{\text{Ca}}}{t} \int_0^t f_{\text{avg}}(t') dt' = D_{\text{Ca}}[f_{\text{eq}} + \tau(1 - f_{\text{eq}})(1 - e^{-t/\tau})/t],$$

where  $f_{\text{eq}}$  is the equilibrium value of  $f_{\text{avg}}(t)$ . Solutions of this expression for  $f_{\text{eq}} = 0.01$  (8),  $K_D = 1 \mu\text{M}$ , and various buffer on-rates are plotted in Figure 1B. Figure 1C shows these solutions for  $D_{\text{app}}$  as a function of mean distance from the channel.

Wave fronts were analyzed to obtain  $Lv$  in neuronal cells loaded with fura-2 (1) under the assumption that the fluorescence profile faithfully reflects the advancing front of excitation as it crosses a cell. Wave front length measured this way may be overestimated due to camera lag and contributions of out-of-focus light to the signal. The dotted lines at  $D = 140 \mu\text{m}^2/\text{s}$  correspond to the lowest value of  $Lv$  observed. It corresponds to a distance of  $0.25 \mu\text{m}$  for  $k_+ = 10^8 \mu\text{m}^2/\text{s}$  and  $0.9 \mu\text{m}$  for  $k_+ = 10^7 \mu\text{m}^2/\text{s}$ . Because BAPTA compounds can slow waves but EGTA cannot, the endogenous buffer probably has a fast on-rate comparable to BAPTA, and so the range of action of calcium in positive feedback is less than  $0.25 \mu\text{m}$ .

Based on these calculations, the distance over which  $\text{Ca}^{2+}$  acts to cause regenerative feedback for wave propagation is likely to

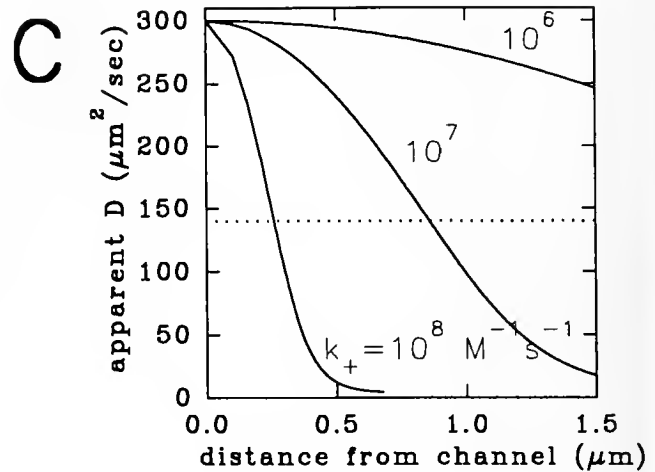
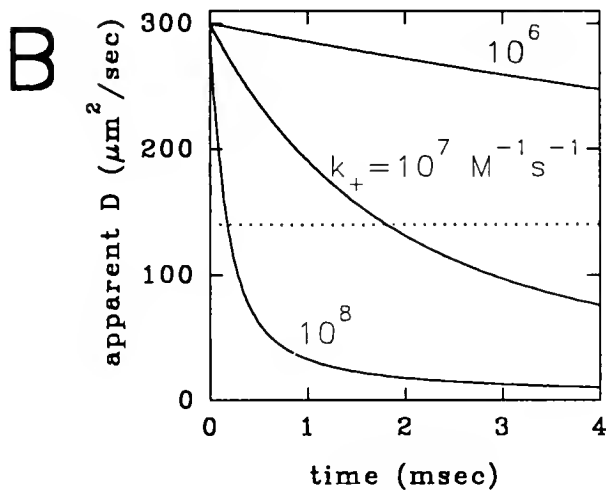
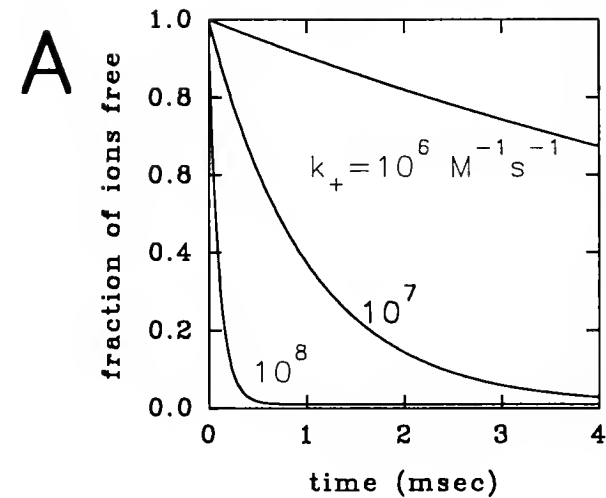


**Figure 1.** Interactions between free calcium ions and buffers. (A) Average fraction of free ions versus time for 100  $\mu\text{M}$  of a buffer with  $K_D = 1 \mu\text{M}$  and  $k_+ = 10^6, 10^7,$  or  $10^8 \text{ M}^{-1} \text{ s}^{-1}$ . (B) Apparent diffusion constant of  $\text{Ca}^{2+}$  as a function of time, assuming that the buffer is immobile and  $D_{\text{free}} = 300 \mu\text{m}^2/\text{s}$ . (C) Apparent diffusion constant of  $\text{Ca}^{2+}$  as a function of mean distance from the channel. Conversion from time to distance was done by finding the mean squared distance from the channel as a function of time:  $\langle x^2 \rangle = 2 \int_0^t D_{\text{app}}(t') dt'$ .

be less than 0.2  $\mu\text{m}$ . This is consistent with a mechanism in which, after activation,  $\text{IP}_3$  levels rise globally and  $\text{Ca}^{2+}$  from one channel diffuses to neighboring channels to act as a coagonist for further calcium release.

The upper distance limit on action of calcium depends on the theoretical analysis of calcium diffusion from a channel mouth, which assumes that the endogenous buffer is immobile, nonsaturable, and has a fast on-rate. A slower on-rate would increase the range of free calcium diffusion, as would the saturation of buffers near the channel mouth. Although experimental work has placed limits on these variables (8), more accurate measurements must be made in order to gauge the validity of the present analysis.

I am grateful to the Grass Foundation for supporting my work this summer at the Marine Biological Laboratory. I also thank

George Augustine, Partha Mitra, and Jürgen Klingauf for helpful discussions.

#### Literature Cited

1. Wang S. S.-H., and S. H. Thompson. 1993. *Soc. Neurosci. Abst.*
2. Luther, R. 1906. (transl. Arnold, R., K. Showalter, and J. J. Tyson. 1987) *J. Chem. Educ.* **64**(9): 740-742.
3. Jaffe, L. F. 1991. *Proc. Natl. Acad. Sci. USA* **88**: 9883-9886.
4. Meyer, T. 1991. *Cell* **64**: 675-676.
5. Hodgkin, A. L., and R. D. Keynes. 1957. *J. Physiol.* **138**: 253-281.
6. Allbritton, N. L., T. Meyer, and L. Stryer. 1992. *Science* **258**: 1812-1815.
7. Baker, P. F., and A. C. Crawford. 1972. *J. Physiol.* **227**: 855-874.
8. Neher, E., and G. J. Augustine. 1992. *J. Physiol.* **450**: 273-301.
9. Tsien, R. Y. 1989. *Ann. Rev. Neurosci.* **12**: 227-253.

Reference: *Biol. Bull.* 185: 299–300. (October, 1993)

### Activity-Dependent Inhibition of Neurotransmitter Release by Brefeldin A

S. T. Brady (Dept. of Cell Biology and Neuroscience, University of Texas Southwestern Medical Center, 5323 Harry Hines Blvd., Dallas, TX 75235-9111), M. Sugimori, P. L. Leopold, J.-W. Lin, D. S. Chu, and R. Llinás

The fungal metabolite Brefeldin A (BFA) disrupts membrane sorting in the Golgi complex and the endocytic and secretory compartments of nonneuronal cells (1,2) by inducing the accumulation of intermediate membranous organelles that are normally transient. The molecular mechanisms of BFA are incompletely understood, but appear to act at a step requiring a small G-protein (3,4). Because synaptic vesicles must be recycled in the presynaptic terminal (5–7), we examined actions of BFA on the electrophysiology of pre- and postsynaptic cells of the squid giant synapse at concentrations that disrupt the Golgi complex in most cells.

The actions of BFA on neurotransmitter release and synaptic vesicle recycling at the squid giant synapse were assessed by a combination of electrophysiology (8,9) and quantitative electron microscopic morphometry. Injection of BFA into the presynaptic terminals stimulated at 3 Hz produced a rapid decrease in the postsynaptic response without altering the electrical properties of the presynaptic terminal (Fig. 1). Stimulation at 0.33 Hz produced minimal changes in the postsynaptic potential over a period of 30–35 min, whereas stimulation at 3–5 Hz led to a loss of the postsynaptic response in 7–10 min.

Electron microscopic analysis of terminals injected with BFA or treated with BFA as the bathing solution showed a substantial accumulation of irregular membranous organelles in the presynaptic terminal. These organelles were significantly larger than normal synaptic vesicles; indeed, when BFA was applied in the bath, they had not reached a relative volume of about 170% of control synaptic vesicles. Control terminals that were injected with medium and stimulated in the same manner were normal in morphology and electrophysiology. BFA introduced either by injection into the presynaptic terminal or by bath application had similar effects on both the electrophysiology and morphology of the synapse. The effects of BFA were dose dependent and reversible in bath application (data not shown).

The simplest explanation for these observations is that BFA prevents the conversion of a larger membrane component to a mature synaptic vesicle. Thus, once the population of preexisting synaptic vesicles has been depleted by activity, it cannot be renewed through recycling in the presence of BFA. As a result, neurotransmitter release fails, and the postsynaptic response is lost. These observations indicate that synaptic vesicle recycling involves a unique transient component that has not been defined previously. Based on the mechanism of action of BFA in the Golgi complex, conversion of this intermediate component to a mature synaptic vesicle may require the activity of a small G-protein.

The effect of BFA on neurotransmission appears distinct from endocytic recycling in nonneuronal cells, where membranes continue to be returned to the plasma membrane (10, 11). Although G-proteins have previously been implicated in the docking of vesicles in the presynaptic terminal of the squid giant

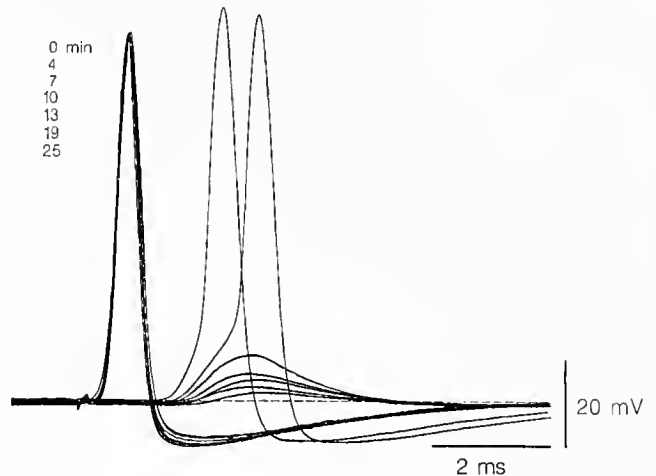


**Figure 1.** Actions of Brefeldin A on presynaptic spikes and postsynaptic response at the squid giant synapse. In this experiment, a small volume of buffer X (13) containing 180  $\mu$ M BFA was microinjected several hundred micrometers proximal to the last bifurcation of the presynaptic terminal; our standard technique was used (9,10). The terminal was stimulated at 3 Hz, and both pre- and postsynaptic spikes were recorded at 3-min intervals for about 25 min. During this time, the amplitude of the presynaptic spike showed little change, whereas the amplitude and rate of rise of the postsynaptic potentials declined dramatically, falling below threshold by 7 min after the onset of stimulation. Injection of presynaptic terminals with carrier solution had little or no effect on the postsynaptic responses, even after 25 min. Recording time intervals are listed in the upper left.

synapse (12), this is the first report of a possible role for G-proteins in the recycling of synaptic vesicles. BFA blocks secretion from the presynaptic terminal by preventing re-formation of the secretory organelle. The effects of BFA on the synaptic vesicle cycle suggest that this recycling involves unique biochemical factors specialized for the presynaptic terminal. BFA and the squid giant synapse provide a basis for identifying these unique factors involved in the recycling of synaptic vesicles and defining their mode of action.

The research described in this report was supported in part by grants to S.T.B. from the National Institutes of Health (NS23868 and NS23320), from the Council for Tobacco Research, and from the Welch Foundation; and to R.L. from the U. S. Air Force (AF 49620-92).

### Literature Cited

1. Klausner, R. D., J. G. Donaldson, and J. Lippincott-Schwartz. 1992. *J. Cell Biol.* 116: 1071–1080.
2. Pelham, H. R. B. 1991. *Cell* 67: 449–451.



3. Donaldson, J. G., D. Finazzi, and R. D. Klausner. 1992. *Nature* 360: 350-352.
4. Helms, J. B. and J. E. Rothman. 1992. *Nature* 360: 352-354.
5. Holtzman, E., A. R. Freeman, and A. Kashner. 1971. *Science* 173: 733-736.
6. Ceccarelli, B., W. P. Hurlbut, and A. Mauro. 1973. *J. Cell Biol.* 57: 499-524.
7. Heuser, J. E., and T. S. Reese. 1973. *J. Cell Biol.* 57: 315-344.
8. Llinás, R., I. Z. Steinberg, and K. Walton. 1980. *Biophys. J.* 33: 289-322.
9. Llinás, R., I. Z. Steinberg, and K. Walton. 1980. *Biophys. J.* 33: 323-352.
10. Wood, S. A., J. E. Park, and W. J. Brown. 1991. *Cell* 67: 591-600.
11. Lippincott-Schwartz, J., L. C. Yuan, C. Tipper, M. Amherdt, L. Orci, and R. D. Klausner. 1991. *Cell* 67: 601-616.
12. Hess, S. D., P. A. Doroshenko, and G. J. Augustine. 1993. *Science* 259: 1169-1172.
13. Brady, S. T., R. J. Lasek, and R. D. Allen. 1982. *Science* 218: 1129-1131.

Reference: *Biol. Bull.* 185: 300-301. (October, 1993)

### Magnetic Localization of the Origins of Self-sustained Oscillation in Squid Giant Axons Shien-Fong Lin (Vanderbilt University), Rashi A. Abbas, and John P. Wikswo, Jr.

Self-sustained oscillatory behavior has been observed in single neurons as well as in a group of neurons (1,2,3). In particular, when squid giant axons are put in a nonequilibrium environment, they may abruptly enter a state of repetitive firing exhibiting temporal and spatial order. Such a phenomenon can be described as a change from the stable resting state to a state of dissipative structure. Despite its important correlation to the generation of rhythmic behaviors in neurons, the membrane

currents in the pacemaker area have not been experimentally studied in real axons. In this report, we used toroidal current probes to measure the distribution of action currents in oscillating axons. Such a measurement provides both temporal and spatial information about action signal generation and propagation along neurons in a stable oscillatory state. A standing wave-like spatial order of the action current can be clearly demonstrated using noninvasive magnetic recording.

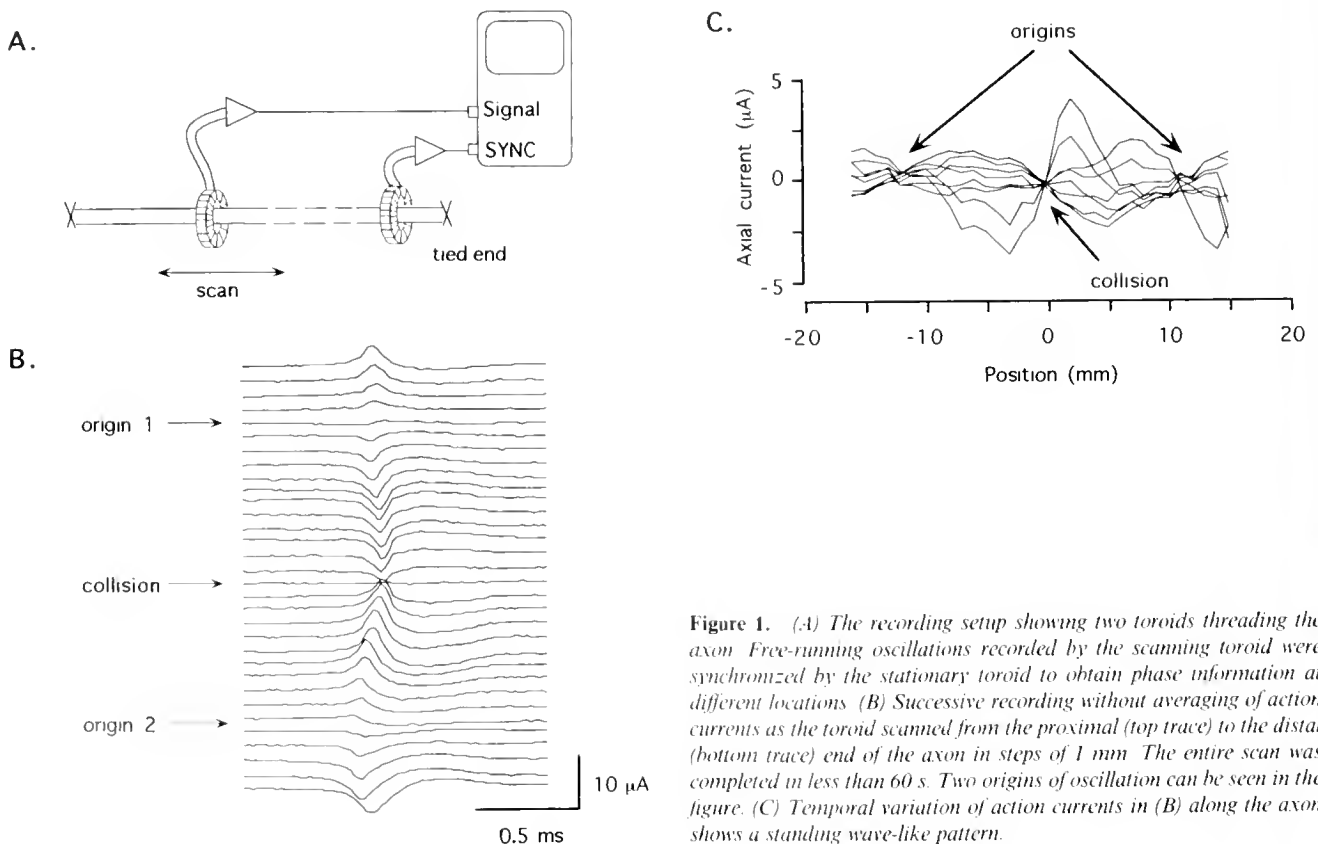


**Figure 1.** (A) The recording setup showing two toroids threading the axon. Free-running oscillations recorded by the scanning toroid were synchronized by the stationary toroid to obtain phase information at different locations. (B) Successive recording without averaging of action currents as the toroid scanned from the proximal (top trace) to the distal (bottom trace) end of the axon in steps of 1 mm. The entire scan was completed in less than 60 s. Two origins of oscillation can be seen in the figure. (C) Temporal variation of action currents in (B) along the axon shows a standing wave-like pattern.

Squid giant axons were threaded in a biomagnetic current probe mounted on a single-axis scanning stage for action current measurement (Fig. 1A). To obtain the correct phase relationship of the oscillation waveform at different locations along the axon, a second stationary toroid placed near one of the tied ends of the axon was used for synchronization. The toroidal probes were 1.25 mm wide with an outer and inner diameter of 5 mm and 2 mm, respectively.

Spontaneous oscillations of action signals were induced in the axon by changing the bathing solution from normal artificial seawater to 520 mM NaCl, 10 mM KCl, 10 mM Hepes, pH 7.4. The action currents were biphasic with two apparent peaks. We adopted the convention that an action current with a negative first phase represents propagation in the positive-axis direction. Therefore, the direction of action current propagation could be determined by the polarity of the first phase of the action currents. The oscillations maintained their stability in the amplitude and frequency for more than 30 min with a variation of less than 5%. This allowed us to perform time average on the synchronized waveforms at any fixed location, especially around the origins of oscillation where the axial currents were small.

The oscillation originated between the proximal and the distal ends, as evidenced by a reversed direction of action current propagation when the toroid was scanned along the axon. In most cases only one stable origin, located 7–17 mm from the tied end, could be observed. In about 10% of the experiments, however, there appeared to be two origins of oscillation synchronized with each other (Fig. 1B). The action signals started from these two origins propagated in opposite direction toward the middle of the axon and collided. The action current distribution in one-origin oscillations resembled the upper or lower half of Fig. 1B without collision. When the length of the axon

was reduced by ligation to less than 25 mm, the oscillations either disappeared or originated from a location closer to the geometrical center of the axon.

Spontaneous tonic oscillation was not observed when the axons were bathed in a 1:3.5 or 1:4 mixture of normal artificial seawater and 550 mM NaCl as described previously (1). Instead, phasic oscillations which lasted about 40 s could be induced by a brief current injection. The spontaneous and induced oscillations had their origins at the same locations, which were characterized by a quiescent point on the axon with no axial current. By examining the phasic relationship of action currents in the origination area, the oscillation should start with a flow of axial current away from the origination point, corresponding to an inward radial current in a zone about 4–6 mm wide centered around the origin.

Based on the experimental observations described above, the dissipative structure of squid giant axons associated with the self-sustained oscillation may have more stable ordered states than proposed earlier (1). Further studies, combining the magnetic and electric measurement, will be invaluable in characterizing normal as well as abnormal rhythmic activity in complex neural systems.

Supported by NIH grant NS 19794.

#### Literature Cited

1. Matusmoto, G., K. Aihara, and T. Utsunomiya. 1982. *J. Phys. Soc. Jpn.* **51**: 942–950.
2. Llinás, R. 1990. *Cold Spring Harb. Symp. Quant. Biol.* **55**: 933–938.
3. Angstadt, J. D., and W. O. Friesen. 1991. *J. Neurophysiol.* **66**: 1858–1873.

Reference: *Biol. Bull.* **185**: 301–302. (October, 1993)

### Noise Modulated Persistence of the Metastable State in a Simulated Neural Network

Vladimir Makarenko (*Institute for Mathematical Problems of Biology, Pushchino, Moscow Region, 142292, Russia*)

Many models simulate neural networks. The noise component of most of these models is commonly ignored, and the physiological role of noise and its effect on the behavior of the network is not seriously considered. The relatively large contribution of noise is traditionally regarded as the inevitable consequence of the great variability characteristic of the parameters and processes constituting biological systems. Most modelers treat this component as a side issue, and only a few of them approach noise as a functionally critical part of observed phenomena.

Apart from its other effects, noise is necessary for the metastability of local excitations in neural networks. Metastability can occur during the transition between two trivial steady states (*i.e.*, when no neuron in the network is excited, and when all neurons are excited) provided that the noise is under some critical value (1). Such metastability has been thought to be important to an understanding of short-term memory and related phenomena

like attention (2). But a major shortcoming of these models is that the initial excitation diffuses quickly throughout the network, and one of the steady states is therefore very rapidly achieved.

The present work is devoted to discovering how noise influences the metastability while at the same time it is dependent upon the state of the system, and how it may evolve in a deterministic neuronal system. This relationship would allow us to define a functional role of noise.

*Model.* The simulated network consists of model neurons of the integrate-and-fire type located in the nodes of a rectangular,  $60 \times 60$  lattice. Each neuron has interconnections of equivalent strength with its four nearest neighbors. In addition to input from its nearest neighbors, every neuron also has input from randomly chosen "distant" neighbors that are about two orders of magnitude more numerous than the nearest neighbors. The value of the input from "distant" neighbors has been chosen to

reflect a physiological contribution of such a subset to the collective behavior of the network. Therefore, for each neuron, the activity of its "distant" neighbors has been compared with the mean value of all such subsets in the network.

*Results of simulations.* Simulations have begun with the excitation of a localized subset of neurons in the described network. The following results appear most promising and bear close attention:

(a) In contrast with the above model, which has a metastable mode of excitatory behavior, the lifetime of the mode is increased by at least two orders of magnitude, and the initial localized excitation never diffuses over the network. The power spectrum of the temporal dynamics demonstrates a power law dependence,  $f^{-\alpha}$ , between the amplitude of the fluctuations in the level of excitation (taken as the ratio of excited neurons to the total number of neurons in the network) and the frequency of the fluctuations. In our case the analysis indicates that large fluctuations appear with a lower probability than those of low amplitude.

(b) The average topological distance (ATD) between excited elements (a measure of the minimum number of synaptic junctions that information must traverse in going from one randomly chosen element to another) is within the topological distance interval (2.2–2.3), until a steady state is approached. According to experimental data (3), the ATD in the cortex is close to this interval: about 2. This result indicates that the metastable mode is inherent only to a subset of excited elements which has an ATD reasonably close to what is found in a real biological object.

(c) The average number of excited "distant" neighbors for most neurons at the border of the group of excited neurons is larger than for most neurons inside the group. Thus, there is dynamic selectivity which operates without the synaptic modulation that usually underlies selectivity.

*Analysis and discussion:* First, what kind of approximation can be applied to the part of the input signal to each neuron that comes from "distant" neighbors? It may be regarded as Gaussian noise with amplitude  $\sigma^2 \approx S*(1 - S)$ , where  $S$  is the fraction of excited neurons. Next we can pass to a diffusion approximation (4) which leads to an interesting explanation of the persistence of the metastable mode in the system: the system moves over the stochastic potential surface, but is never able to reach a stable state, because the latter is changing its position as the system changes its level of excitation and, therefore, the amplitude of noise. Remember that the amplitude of the noise determines the location of stable states on the stochastic potential surface.

These results lead us to the following conclusion: the noise component in neural network dynamics may play, not only a destructive, but also a stabilizing role in neural activity. Indeed noise can originate naturally, not from the "imperfection" of biological systems, but rather from the interactions between different structural levels of a deterministic system.

Supported by a fellowship from the James S. McDonnell Foundation.

#### Literature Cited

1. Kirillov, A. B., and V. I. Makarenko. 1991. In *Neurocomputers and Attention II*, A. V. Holden and V. I. Kryukov, ed. Manchester University Press.
2. Little, W. A. 1974. *Math. Biosci.* 19: 101–120.
3. Clark, J. W., G. C. Littlewort, and J. Rafelski. 1986. 'Topology, structure and distance in quasirandom neural networks', preprint, University of Cape Town.
4. W. Horsthemke and R. Lefever. 1984. *Noise-Induced Transitions*, Springer Series in Synergetics, Vol. 15. Hermann Haken, ed. Springer-Verlag.

Reference: *Biol. Bull.* 185: 302–303. (October, 1993)

### **Ca<sup>2+</sup> Fluxes Around Pollen Grains and Pollen Tubes of Lily; Normal Development and Effects of Thermal Shock, BAPTA-Type Buffer Microinjection and Depletion of Boric Acid From the Medium**

*E. S. Pierson (Biologia Ambientale, University of Siena, I-53100 Siena, Italy), P. J. S. Smith, A. M. Shipley, L. F. Jaffe, M. Cresti, and P. K. Hepler*

Under favorable conditions, pollen grains germinate to form a long tubular extension, the pollen tube, through which the plant male gametes reach the egg apparatus. Cytosolic free Ca<sup>2+</sup> ions, which are distributed in a steep gradient along the growing pollen tube tip (5), are assumed to play a role in regulating the growth of the tip, the organelle movement, and the maintenance of the cytoplasmic zonation (5,6). From <sup>45</sup>Ca<sup>2+</sup> labeling (1) we know that the high Ca<sup>2+</sup> domain in the cell apex is at least partly created by a transient uptake of the ion. With the Ca<sup>2+</sup>-selective vibrating probe technique (2,9), minute Ca<sup>2+</sup> fluxes can be detected around single cells (2). Here, we have used this technique

to survey the net Ca<sup>2+</sup> flux pattern around *in vitro* germinating pollen grains and growing pollen tubes of the lily (*Lilium longiflorum* 'White Nellie'). We have also explored the effect on the net Ca<sup>2+</sup> flux of three growth-disturbing treatments: thermal shock, microinjection of 4,4'-difluoro 1,2-bis(o-aminophenoxy) ethane-N,N,N',N'-tetraacetic acid [2F-BAPTA] buffer, and depletion of boric acid from the culture medium.

Pollen tubes were grown at room temperature in a film of medium composed of 10% sucrose, 100  $\mu$ M CaCl<sub>2</sub>, 160  $\mu$ M H<sub>3</sub>BO<sub>3</sub>, 15 mM 2 n-morpholino ethane sulfonic acid buffer adjusted to pH 5.5 with KOH, and about 1% low temperature

gelling agarose.  $\text{Ca}^{2+}$  fluxes were measured according to standard procedures (2, 9), except that the tip of the electrode was vibrated inside the agarose layer, as close as possible to the cell.

Normally developing pollen grains and tubes typically showed a marked pattern of  $\text{Ca}^{2+}$  influx at the cell tip, but with great variability among cells (estimated range: 15–180  $\mu\text{V}$  after subtraction of the background value  $\approx 0 \mu\text{V}$ , at a vibration amplitude of 10  $\mu\text{m}$  and a background  $[\text{Ca}^{2+}]$  of about 100  $\mu\text{M}$ ).  $\text{Ca}^{2+}$  diffusion is obviously an important component of the total ionic current that traverses pollen tubes (10,11). No significant  $\text{Ca}^{2+}$  flux signal could be detected in the other regions of the grain. The influx magnitude appeared to be positively correlated with the growth rate (1–14  $\mu\text{m}/\text{min}$ ) of the cell. The voltage differences ( $\approx \text{Ca}^{2+}$  flux) were higher for *Lilium* pollen tubes than for *Arabidopsis* root hairs (7).

Exposure of short (10  $\mu\text{m}$ ) and long (400  $\mu\text{m}$ ) pollen tubes to a thermal shock (45°C for 10 s) immediately halted growth and concomitantly arrested  $\text{Ca}^{2+}$  influx. Moreover, large organelles, which normally were absent from the tip zone, penetrated into the apical dome. Resumption of growth, characterized by the bulging of the tip and the restoration of the organelle zonation, was in all cases accompanied by recovery of the  $\text{Ca}^{2+}$  influx.

BAPTA-type buffers possibly act as calcium shuttle buffers when they are introduced inside cells (8), dissipating or diminishing the natural calcium gradients (see reference 5 for pollen tubes). In previous work (E. S. Pierson *et al.*, in prep.) BAPTA-type buffers with a  $K_d$  between 0.2 and 4.6  $\mu\text{M}$  were found to inhibit pollen tube growth in a reversible way. In the present study we injected a low dose of 2F-BAPTA in normally growing pollen tubes to block cell growth without seriously affecting the cytoplasmic streaming. As a consequence, the  $\text{Ca}^{2+}$  flux at the cell tip fell rapidly to about zero. Spontaneous resumption of growth, probably due to the sequestration of buffer into the vacuole, proceeded together with recovery of the  $\text{Ca}^{2+}$  ionic flux.

This observation suggests that a certain level of intracellular  $\text{Ca}^{2+}$  is required for transcellular  $\text{Ca}^{2+}$  entry (positive feedback), and that this entry pathway is not directly linked to passive diffusion of the ion.

Boric acid has been reported to enhance the chemotropic response of pollen tubes to calcium (4). In preliminary experiments we progressively washed boric acid out of the culture and found that most pollen tubes burst at their tip. The cells had a normal morphology, growth behavior, and  $\text{Ca}^{2+}$  influx pattern at the moment of disruption. Explanations for the above findings are that boric acid may affect cell wall integrity or plasma membrane water permeability, rather than the  $\text{Ca}^{2+}$  flux mechanism.

This study was supported by a Traveling Fellowship from Development (1992) and an MBL Summer Fellowship (1993) to E.S.P., NIH grant P41RR01395 to L.F.J. for the National Vibrating Probe Facility, and NSF grant DCB93-04953 to P.K.H.

### Literature Cited

1. Jaffe, L. A., M. H. Weisenseel, and L. F. Jaffe. 1975. *J. Cell Biol.* 67: 488–492.
2. Kührtreiber, W. M., and L. F. Jaffe. 1990. *J. Cell Biol.* 110: 1565–1573.
3. Mascarenhas, J. P., and L. Machlis. 1964. *Plant Physiol.* 39: 70–77.
4. Miller, D. D., D. A. Callahan, D. J. Gross, and P. K. Hepler. 1992. *J. Cell Sci.* 101: 7–12.
5. Pierson, E. S., and M. Cresti. 1992. *Int. Rev. Cytol.* 140: 73–125.
6. Schiefelbein, J. W., A. Shipley, and P. Rowse. 1992. *Planta* 187: 455–459.
7. Speksnijder, J. E., D. W. Corson, C. Sardet, and L. F. Jaffe. 1989. *Dev. Biol.* 135: 182–190.
8. Smith, P. J. S., R. H. Sanger, and L. F. Jaffe. 1994. In *Methods in Cell Biology* 40. R. Nuccitelli, ed. Academic Press (in press).
9. Weisenseel, M. H., R. Nuccitelli, and L. F. Jaffe. 1975. *J. Cell Biol.* 66: 556–567.
10. Weisenseel, M. H., and L. F. Jaffe. 1976. *Planta* 133: 1–7.

Reference: *Biol. Bull.* 185: 303–304. (October, 1993)

## Endogenous Currents During Wound Healing and Regeneration in Sabellid Fanworms Susan Douglas Hill (Michigan State University), Alan M. Shipley, and Peter J. S. Smith

The concept that endogenous currents play a significant role in wound healing and regeneration has gained considerable support over the past 20 years (1, 2). It is well-documented that in urodele amphibians, an outward ionic current leaves the wound surface shortly after limb amputation (2, 3, 4) and persists at low levels until the time of blastema formation. Much of the impetus for the present interest in endogenous currents has resulted from the development of the vibrating probe by Jaffe and Nuccitelli (5), subsequently modified (6, 7), which allows precise current measurements to be made noninvasively at specific sites. We have used the vibrating probe to detect the weak voltages associated with the steady state ionic currents generated during anterior regeneration in sabellid fanworms following segment amputation.

Sabellids have remarkable powers of regeneration. Following transection at almost any level of the body, anterior-facing cuts result in the regeneration of a new head complete with branchial crown, collar, mouth, and anterior neural ganglia and connectives. Posterior amputations result in the replacement of the pygidium and the addition of new posterior segments. Immediately after amputation, muscle contractions constrict the wound surface. Within 24 h, the wound surface is usually thinly covered with epidermis. This initial phase of wound healing probably results primarily from cell migration, since few cell divisions (as detected by  $\text{H}^3$  thymidine incorporation) are observed (8). Following the initial healing, cells accumulate to form the regeneration blastema that gives rise to the new outgrowth. New branchial filaments appear as finger-like projections, and

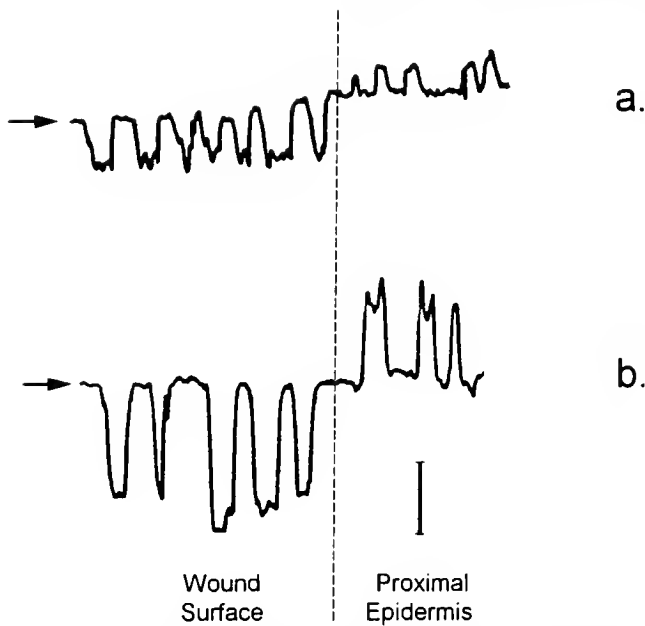


**Figure 1.** Repeated measurements of ionic current densities following transection. Both traces show repeated measurements made over a 6-min interval at the wound surface and proximal epidermis. *a.* 15 min post amputation. *b.* 1 h post amputation. Deflections below the baseline (arrows) indicate an outward current; deflections above the baseline correspond to an inward current. Reference bar =  $10 \mu\text{A}/\text{cm}^2$ .

a mouth reforms; then the filaments elongate, secondary branches appear, and the missing anterior portions of the circulatory and nervous systems differentiate. Extensive cell division is involved in blastema formation and subsequent differentiation (8).

We have used the voltage-sensitive vibrating probe technique to monitor temporal changes in the steady state ionic currents that are associated with injury, wound healing, and early regeneration in sabellid fanworms. The probe is a platinum black-tipped insulated wire electrode that responds, relative to a reference electrode, to voltage gradients produced by steady state ion movements. Probes were independently calibrated against a KCl-filled current electrode (6). Amputations and measurements were made in filtered seawater at room temperature ( $21\text{--}22^\circ\text{C}$ ). Anesthesia was not used.

Immediately following transection, we sometimes detected a strong inward current which declined rapidly and, within 5 min or less, reversed directionality. The maximum inward current that we have measured to date with a one-dimensional vibration system is  $40 \mu\text{A}/\text{cm}^2$ . Frequently this inward current was not

detected, probably because of its transient nature and the time required to position the amputation surface appropriately to allow data collection. The inward current was replaced by a persistent outward current leaving the wound site.

Sabellids are segmented worms. On transection, fluid contents and cell debris from the injured somite are released into the surrounding seawater. We suggest that the inward current which we detect corresponds to this immediate loss of body fluid and cell contents. Within moments of transection, muscles at the wound site contract, constricting the surface area of the wound and thus probably reducing loss of body fluids. It seems likely that these events are correlated with the change in current polarity observed within the first few minutes of the transection.

The outward persistent current reached a peak within approximately an hour after amputation and was accompanied by an inward current through the uninjured epidermis proximal to the wound (Fig. 1). These currents declined to less than half the maximum strength by the day after amputation. By this time, the wound surface was thinly covered with epithelium. Outward currents leaving the amputation site persisted at low levels throughout the period of wound healing and blastema formation.

The pattern of outward currents from the amputation surface accompanied by inward currents through the proximal epidermis, highest in the hours following amputation but persisting at low levels during early regenerative stages, parallels that described during amphibian regeneration (3, 4). Earlier work has implicated electrical currents in regeneration in an earthworm (9) and in a colonial hydroid (10). To our knowledge, this is the first report of extracellular electrical currents associated with whole body regeneration measured using the vibrating probe technique.

This work was supported by NIH grant P41RR01395 to the National Vibrating Probe Facility, Marine Biological Laboratory, Woods Hole, MA.

#### Literature Cited

1. Nuccitelli, R., ed. 1986. *Ionic Currents in Development*. Alan R. Liss, Inc., New York.
2. Borgens, R. B., K. R. Robinson, J. W. Vanable, Jr., and M. E. McGinnis, eds. 1989. *Electric Fields in Vertebrate Repair*. Alan R. Liss, Inc., New York.
3. Borgens, R. B., J. W. Vanable, Jr., and L. F. Jaffe. 1977. *Proc. Natl Acad Sci* 74: 4528–4532.
4. Borgens, R. B., M. E. McGinnis, J. W. Vanable, Jr., and E. S. Miles. 1984. *J. Exp. Zool.* 231: 249–256.
5. Jaffe, L. F., and R. Nuccitelli. 1974. *J. Cell Biol.* 63: 614–628.
6. Scheffey, C. 1988. *Rev. Sci. Instrum.* 59: 787–792.
7. Smith, P. J. S., and A. Shipley. 1990. *J. Exp. Biol.* 154: 371–382.
8. Hill, S. D. 1970. *Am. Zool.* 10: 101–112.
9. Moment, G. B. 1949. *J. Exp. Zool.* 112: 1–12.
10. Rose, S. M. 1972. *Dev. Biol.* 28: 274–277.

Reference: *Biol. Bull.* 185: 305. (October, 1993)

## The Presence of the GABA-synthesizing Enzyme, Glutamate Decarboxylase, in *Spisula* Sperm

Hiroshi Ueno (*Osaka Medical College*), Renu Juneja, Osamu Shimomura,

S. S. Koide, and Sheldon J. Segal

Glutamate decarboxylase (GAD) is an enzyme that produces  $\gamma$ -aminobutyric acid (GABA), an inhibitory neurotransmitter. In many mammals, both GAD and GABA appear to be colocalized in various parts of the brain, but they are also found in pancreatic  $\beta$ -cells and testis. Two cDNAs coding for GAD were recently identified in rat (1). The cDNAs are products of two different genes on chromosomes 2 and 10, which encode for GAD-67 and GAD-65, respectively. In human pancreatic  $\beta$ -cells, GAD-65 appears to be the predominant form and was recently identified as an antigen for an autoantibody produced by insulin-dependent diabetes patients (2). The presence of GAD-like immunoreactivity has also been detected in the midpiece of ejaculated human spermatozoa (3), but no further information on the significance of this observation is available.

In this communication, we report evidence for the presence of GAD-active materials in homogenates of *Spisula* sperm. Homogenates of motile sperm contain significant GAD activity (0.5 nmol CO<sub>2</sub>/min/mg protein). In addition, GAD-immunoreactive material can be identified in *Spisula* sperm homogenates. Two antibodies, AB108 and GAD-6, were used as probes for the Western blots. The former, a polyclonal antibody, recognizes GAD-67, and the latter, a monoclonal antibody, recognizes GAD-65. Each antibody is highly specific to its target GAD when mammalian brain tissues are examined. We have found that AB108 strongly stains protein bands with molecular masses estimated to be 79, 77, 58, 46, 44, and 28 kDa, and weakly stains 67 kDa band. On the other hand, GAD-6 stains bands corresponding to 76 and 28 kDa. Those bands at 77–79 and 76 kDa are somewhat larger than 67 and 65 kDa, which are observed for the mammalian GADs. The results suggest, although they are speculative, that the *Spisula* sperm GAD can be larger in size than the mammalian GADs.

We have previously found that a gossypolone-sepharose affinity column specifically absorbs surface macromolecules of *Spisula* sperm, with masses of 46, 44, and 28 kDa. This column does not, however, absorb rat GAD-65 expressed in yeast (Ueno, Kanai, Atomi, Ueda, and Tanaka, in prep.). When *Spisula* sperm proteins are passed through the gossypolone-sepharose affinity column, proteins of 79, 77, 76, and 58 kDa are not absorbed, but proteins of 46, 44, and 28 kDa are absorbed. The nonabsorbed cluster of macromolecules may be derived from sperm GAD, but further study is needed to determine whether these bands are related to GAD. Multiple bands are often observed in brain GADs from various species. For example, monkey and rat brain homogenates showed such multiple bands.

The present findings indicate that *Spisula* sperm exhibits GAD activity and contains immunoreactive GAD-like proteins. The results suggest that there may be GAD in *Spisula* sperm; thus, it raises an interesting question about the role of GABA in sperm function.

Supported by a grant from the Rockefeller Foundation (GA PS 9032). The hybridoma for GAD-6 was obtained from the Developmental Studies Hybridoma Bank maintained by the University of Iowa under contract N01-HD-6-2915 from the NICHD.

### Literature Cited

1. Erlander, M. G., N. J. K. Tillakaratne, S. Feldblum, N. Patel, and A. J. Tobin. 1991. *Neuron* 7: 91–100.
2. Baekkeskov, S., H.-J. Aanstoot, S. Christgau, A. Reetz, M. Solimena, M. Cascalho, F. Folli, H. Richter-Olesen, and P.-D. Camilli. 1990. *Nature* 347: 151–156.
3. Persson, H., M. Pelto-Huikko, M. Metsis, O. Soder, S. Brene, S. Skog, T. Hokfelt, and E. M. Ritzen. 1990. *Mol. Cell. Biol.* 10: 4701–4711.

Reference: *Biol. Bull.* 185: 305–306. (October, 1993)

## Cytoplasmic Microtubule Arrays in *Oryzias latipes* (Medaka) Eggs During Ooplasmic Segregation

Vivek C. Abraham<sup>1</sup>, Andrew L. Miller<sup>2</sup>, Lionel F. Jaffe<sup>2</sup>, and Richard A. Fluck

(<sup>1</sup>Franklin & Marshall College and <sup>2</sup>Marine Biological Laboratory)

Ooplasmic segregation in the fertilized medaka egg consists of the streaming of ooplasm toward the animal pole to form a blastodisc, the movement of oil droplets toward the vegetal pole, and the saltatory motion of small parcels toward both polar regions (1). In earlier studies we found that microtubule poisons and 5,5'-dibromo-BAPTA, a weak calcium buffer that dissipates the polar gradients of cytosolic free [Ca<sup>2+</sup>] present during segregation (4), inhibit segregation in similar ways (1, 3). In the present study, using a protocol for indirect immunofluorescence developed by Gard (5), we characterized the microtubule arrays

in medaka eggs during segregation and examined microtubule arrays in eggs injected with dibromo-BAPTA.

At regular intervals after fertilization eggs were fixed for 2–4 h at room temperature in a microtubule-stabilizing medium (3.7% formaldehyde; 0.05% glutaraldehyde; 5 mM EGTA; 1 mM MgCl<sub>2</sub>; 80 mM PIPES, pH 6.8); fixed overnight in methanol at –20°C; permeabilized with 0.5% Triton X-100; treated with 100 mM NaHB<sub>4</sub>; and incubated first with a monoclonal anti-alpha tubulin antibody (mouse, clone #DM-1A, ICN Immunobiologicals) and then with a rhodamine-labeled secondary

antibody. The eggs were examined by conventional fluorescence microscopy and also by laser scanning confocal microscopy. To correct for differences in the rate of development at different temperatures, we used a scale of normalized time ( $t_n$ ) in which cytokinesis begins at  $t_n = 1.0$  units.

In eggs fixed soon after fertilization ( $t_n = 0.02$ , Fig. 1A), we saw punctate sources of fluorescence. A loose network of microtubules, lacking any preferred orientation, was present in the interpolar regions of the egg by  $t_n = 0.16$  (Fig. 1B); and by  $t_n = 0.24$ , the density of this network had increased (Fig. 1C). A microtubule-organizing center (MTOC) was present at the animal pole, as evidenced by the convergence of microtubules into this region. At the vegetal pole of the egg, a mat consisting of mostly parallel microtubules was present during ooplasmic segregation (Fig. 1D). The parallel organization of this mat was lost by  $t_n = 1.0$ . We saw no linear elements in eggs treated with microtubule poisons or in eggs that were not incubated with the primary antibody.

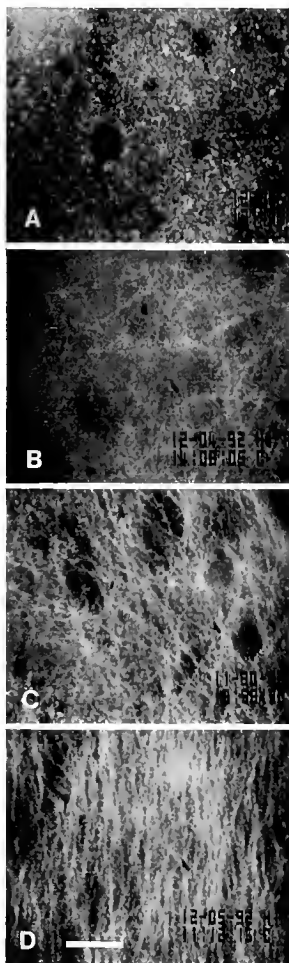


**Figure 1.** Microtubule arrays in developing medaka eggs. (A)  $t_n = 0.02$ , equatorial region. Punctate foci of fluorescence can be seen, but no linear elements are apparent. (B)  $t_n = 0.16$ , equatorial region. A loose network of microtubules, lacking any preferred orientation, can be seen. (C)  $t_n = 0.24$ , equatorial region. The number of microtubules in the interpolar ooplasm has increased. (D)  $t_n = 0.40$ , vegetal pole. A mat of parallel microtubules can be seen. Scale bar, 10  $\mu\text{m}$ .

Fertilized eggs were injected with dibromo-BAPTA (50 mM dibromo-BAPTA, tetra potassium salt; 5 mM HEPES, pH 7.3) within 8 min after fertilization. Typically, the oil droplets in the hemisphere into which the buffer was injected were dislodged from their positions and floated to the top of the egg, but the oil droplets in the hemisphere opposite the injection site appeared to be frozen in place; that is, they moved neither toward the top of the egg nor to the vegetal pole (3). We also examined control eggs into which we had injected 150 mM KCl and 5 mM HEPES, pH 7.3. All eggs were fixed at  $t_n = 0.76$ .

When we injected sufficient dibromo-BAPTA to raise the cytosolic concentration to 2.7 mM, microtubules near the animal pole no longer converged into this region as they did in control eggs, suggesting a disruption of the MTOC. However, the mat of parallel microtubules at the vegetal pole was apparently unaffected by dibromo-BAPTA. Interpolar ooplasm near the injection site contained a very sparse network of microtubules, whereas ooplasm on the opposite side of the egg, where oil droplets were frozen in place, contained a microtubule network having a density comparable to that seen in control eggs. In both regions, the proportion of very long microtubules was greater in eggs receiving dibromo-BAPTA. Eggs into which we injected 150 mM KCl were indistinguishable from untreated eggs.

In summary, we have demonstrated (a) the development of a complex pattern of cytoplasmic microtubules during ooplasmic segregation in the medaka egg and (b) the alteration of this pattern by injection of the dibromo-BAPTA. Two features of this pattern—the apparent presence of a MTOC near the animal pole and the development of an array of microtubules between fertilization and the first cleavage—have been seen in developing sea urchin (6) and *Xenopus* eggs (2, 5), and the mat of parallel microtubules at the vegetal pole of the medaka egg is very similar to the one present in *Xenopus* eggs (2). The results of the present study are consistent with the suggestion that microtubules have a role in the propulsion of oil droplets toward the vegetal pole of the medaka egg during ooplasmic segregation (1) and that cytosolic calcium gradients are important for the development of the pattern of microtubules in the medaka egg.

Supported by NSF DCB-9017210 to R. A. F., NSF DCB 9103569 to L. F. J., NSF BIR 9211855 to L. F. J. and A. L. M., and grants from Franklin and Marshall College's Hackman Scholar Program and Harry W. and Mary B. Huffnagle Fund to V. C. A. We thank Louis Kerr of the Central Microscope Facility at the Marine Biological Laboratory for his assistance in the use of the Zeiss LSM 410 confocal microscope.

### Literature Cited

1. Abraham, V. C., S. Gupta, and R. A. Fluck. 1993. *Biol. Bull.* **184**: 115–124.
2. Elinson, R. P., and J. Palecek. 1993. *Roux's Arch. Dev. Biol.* **202**: 224–232.
3. Fluck, R. A., V. C. Abraham, A. L. Miller, and L. F. Jaffe. 1992. *Biol. Bull.* **183**: 371–372.
4. Fluck, R. A., A. L. Miller, and L. F. Jaffe. 1992. *Biol. Bull.* **183**: 70–77.
5. Gard, D. L. 1991. *Dev. Biol.* **143**: 346–362.
6. Harris, P., M. Osborn, and K. Weber. 1980. *J. Cell Biol.* **84**: 668–679.



Reference: *Biol. Bull.* 185: 307-308, (October, 1993)

***Limulus* Vision in the Ocean: Comparing Neural and Behavioral Thresholds**  
*E. D. Herzog, C. L. Passaglia, S. A. Dodge, N. D. Levine, and R. B. Barlow, Jr.*  
 (Marine Biological Laboratory)

The horseshoe crab, *Limulus polyphemus*, uses vision to locate mates (1, 2). What information must the eye send to the brain for the animal to see a mate? Building on the extensive knowledge regarding the animal's visual system (3, 4) and its visually guided behavior (2), we are investigating this question with a wide range of techniques (5, 6). Here we report our technique for recording optic nerve activity *in situ* from animals moving past behaviorally significant scenes in the ocean. We also report preliminary data comparing neural and behavioral thresholds.

We conduct all experiments in about 0.5 m of water on a sandy, gently sloping beach in Woods Hole, Massachusetts, under ambient conditions. Adult male *Limulus*, about 20 cm across the carapace, are collected and maintained at the Marine Biological Laboratory. We gain access to the lateral optic nerve by cutting a 2-cm hole in the carapace, then we gently slide the uncut nerve into a sealed, nylon recording chamber affixed to the carapace (Fig. 1). We tease a single active fiber from the optic nerve and suck it into a microsuction electrode built into the recording chamber. Nerve impulses are amplified ( $10^4$  gain AC preamplifier, Electronics Shop, Rockefeller University), digitized, and recorded on a portable 80486 personal computer with Lab-view Software (National Instruments, Austin, Texas). In the laboratory, we select optic nerve fibers from ommatidia that view the world near the animal's horizon, and we use an underwater goniometer to measure their precise directions of view (optic axes). We then mount the animal on a sled and take it to the ocean.

Our strategy is to record visual responses from the "wired" animal under field conditions approximating those observed during the mating season. Behavioral experiments have shown



**Figure 1.** Chamber for recording optic nerve activity *in situ* from *Limulus* underwater. The lateral optic nerve exits the eye on the left, travels under the carapace and runs through the chamber on the right on its way to the brain. The microsuction electrode is shown inserted into the chamber from the right.

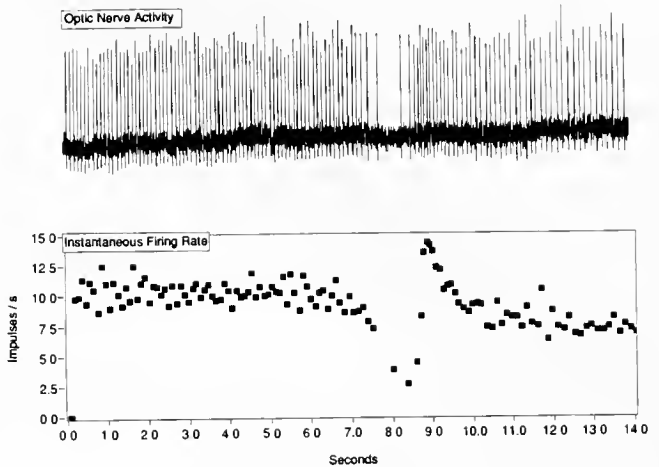


**Figure 2.** (Top). Impulse discharge recorded from a single optic nerve fiber as the animal moved past a 9" cylindrical target at a distance of 0.25 m. The animal passed the target between 7.5 and 8.5 s. (Bottom). Instantaneous firing rate of the spike train above. The nearby black target produced a robust modulation of the discharge, reducing the firing rate to about 2.5 impulses/s followed by a burst of activity at about 15 impulses/s.

that males will turn towards and make contact with targets that have been placed in the water and that are about the size of a female (1). For these experiments, we selected a black cylinder (9" diameter; 6" tall) as a visual target because we know from previous experiments how close an animal must be to this type of target to see it (7). The cylinder is a convenient target because its profile appears the same regardless of the direction of approach. We suspend the sled (with the animal) on a 2-m-long underwater track so that the lateral eyes are about 9 cm above the bottom; then we pull the sled past the visual target which is placed at various distances from the track. Optic nerve activity is recorded simultaneously on an FM tape recorder and a VCR, as well as on the portable computer. We pull the animal at about 10 cm/s (which approximates the average speed of *Limulus* locomotion), determining the precise velocity from the videotape after the experiment is completed. To measure the temporal variation in stimulus intensity during each run, a photodiode is attached to the carapace above the eye with an acceptance angle of an ommatidium and an optic axis parallel to the recorded unit.

As the animal, moving along the track, comes within 1.25 m of the target, we detect a clear modulation of the optic nerve discharge (Fig. 2). We define the neural threshold as the distance at which the target no longer evokes an audible modulation in the spike discharge. When the target is placed more than 1.25 m from the eye, the modulation in firing rate decreases to the back-

ground level recorded in control runs without a target. This neural threshold of 1.25 m is slightly less than the behavioral threshold of 1.4 m. Behavioral experiments show that males do not turn toward the 9° target when it is placed more than 1.4 m away from the animal (7).

We have previously shown that, at any given moment, as the animal moves along the track, the target at 1.4 m subtends approximately 6–12 of the 1000 receptors in the lateral eye (5). This report suggests that the modulated activity of a small population of retinal neurons transmits to the brain the information necessary for the animal to see the target.

Supported by grants from the National Science Foundation and the National Institutes of Health.

### Literature Cited

1. Barlow, R. B., Jr., L. C. Ireland, and L. Kass. 1982. *Nature* 296: 65–66.
2. Powers, M. K., R. B. Barlow, Jr., and L. Kass. 1991. *Vis. Neurosci.* 7: 179–89.
3. Ratliff, F., and H. K. Hartline. 1974. *Studies of Excitation and Inhibition in the Retina: A Collection of Papers from the Laboratories of H. Keffer Hartline*. The Rockefeller University Press, New York.
4. Barlow, R. B., Jr. 1990. *Sci. Am.* 262: 90–95.
5. Herzog, E. D., and R. B. Barlow. 1992. *Vis. Neurosci.* 9: 571–580.
6. Barlow, R. B., Jr., R. Prakash, and E. Solessio. 1993. *Am. Zool.* 33: 66–78.
7. Herzog, E. D., C. L. Passaglia, K. Longnecker, E. Boudreau, and R. B. Barlow, Jr. 1992. *Invest. Ophthalm. Vis. Sci.* (suppl.), 1157.

Reference: *Biol. Bull.* 185: 308–310. (October, 1993)

## Equivalent Sine Wave Frequency for Interpretation of Responses to Frequency-Swept Sinusoids Defined: an Algorithm From Studies in Skate Ganglion Cells

Richard L. Chappell and Paul Glynn (Hunter College and The Graduate School and University Center, CUNY)

The frequency-swept sinusoid (FSS) has proven useful in the presentation and qualitative interpretation of responses to physiological stimulation (1–4). It also played an extensive role in early sonar applications because the echo of sweep-frequency modulated signals exhibited a recognizable chirp (5). An example of responses to such stimulation from our studies of OFF pathways in the skate (*Raja erinacea*) retina (Fig. 1A) shows that extracellularly recorded (6) responses of a decrementally responding ganglion cell to FSS stimulation are a function of light adaptation time. Although intuitively helpful, results from such experiments have been difficult to quantify because the frequency is continuously changing as a function of time; thus, the time for which the frequency is determined must be carefully specified. Furthermore, the driving frequency is not the same as the apparent frequency that might be estimated by simply measuring the time between peaks, as for a regular sinusoid; nor is the driving frequency directly comparable to the frequency of regular sinusoids used in the rich literature of flicker-fusion frequency studies. Therefore, the results of FSS and regular sinusoidal stimulation have been difficult to compare. Consequently, we have derived relationships that we have used to define an equivalent sine wave frequency,  $f_E$ , representing the instantaneous slope of an FSS in terms of the frequency of a regular sinusoid of equivalent instantaneous slope having the same peak-to-peak amplitude.

Consider an FSS described by a sinusoidally driven function for which the command frequency,  $f_c$ , increases linearly with time,  $t$ , from some initial frequency,  $f_0$ , such that the command frequency is given by the relation:

$$f_c = At + f_0 \quad (1)$$

where  $A$  is a constant having the units of  $\text{Hz}^2$ , and the general form of the stimulus as a function of time,  $y(t)$ , is given by:

$$y(t) = \sin(2\pi f_c t) \quad (2)$$

where the amplitude of the stimulus is taken as 1 for convenience. Substituting for  $f_c$  from Eqn. (1) we have:

$$y(t) = \sin(2\pi(At^2 + f_0t)). \quad (3)$$

Differentiating, we obtain:

$$dy/dt = 2\pi(2At + f_0) \cos(2\pi(At^2 + f_0t)). \quad (4)$$

Observing that  $(2At + f_0)$  can be written  $(2(At + f_0 - f_0))$ , and substituting  $f_c$  from Eqn. (1), we have:

$$dy/dt = 2\pi(2f_c - f_0) \cos(2\pi f_c t) \quad (5)$$

as the instantaneous slope of the FSS at any time,  $t$ .

We note that for a regular sinusoid having a fixed frequency,  $f_c$ , which is not a function of time, the comparable expression for its slope would be simply:

$$dy/dt = 2\pi f \cos(2\pi ft). \quad (6)$$

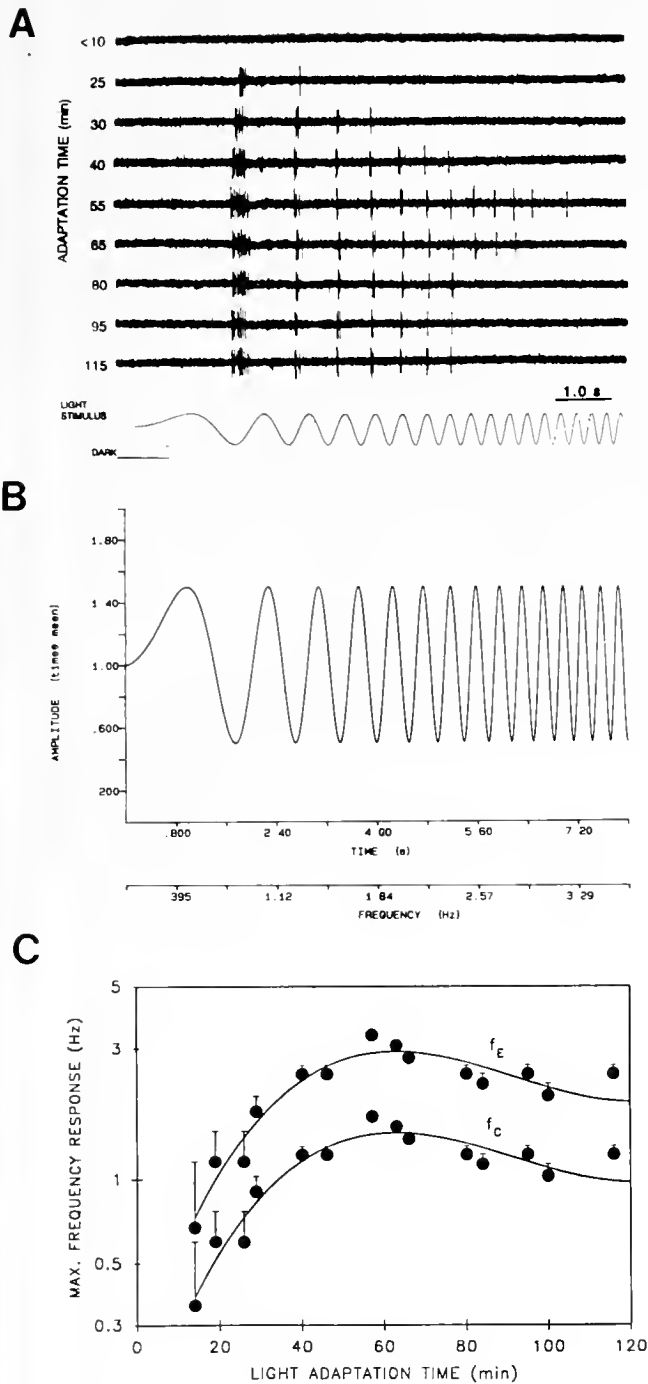


**Figure 1.** Frequency response during light adaptation in a decrementally responding skate ganglion cell after 45 min of dark adaptation. *A.* Extracellularly recorded responses to frequency-swept sinusoidal stimulation during light adaptation to a 55% modulation of a green LED light source around a mean intensity of  $0.1 \mu\text{W}/\text{cm}^2/\text{s}$ . *B.* Plot of Eqn. (2) for a frequency-swept sinusoid having the same time scale as that of the stimulus in Figure 1A. The corresponding equivalent sine wave frequency ( $f_E$ ) calculated from Eqn. (8) is plotted below the time scale for comparison. *C.* Maximum equivalent sine wave frequency (upper curve,  $f_E$ ) compared with command frequency of the frequency-swept sinusoid (lower curve,  $f_C$ ) plotted as a function of light adaptation time from the data of Figure 1A. Frequencies determined at the time the stimulus descended across the mean are plotted for this decrementally responding cell

By inspection, it can be seen from Eqn. (5) that the slope of the FSS at any given frequency is nearly double (exactly double for  $f_0 = 0$ ) the slope of a regular sinusoid having the same frequency and amplitude (Eqn. (6)). Therefore, we found it useful to define an equivalent sine wave frequency,  $f_E$ , of the FSS such that:

$$f_E = 2f_c - f_0 \quad (7)$$

or, substituting for  $f_c$  from Eqn. (1):

$$f_E = 2At + f_0. \quad (8)$$

This expression, at any time,  $t$ , in an FSS, represents the instantaneous value of the frequency of a regular sinusoid having an equivalent slope and the same peak-to-peak amplitude as the FSS. This approach to defining an equivalent sine wave frequency has some precedent in the concept of the "equivalent sine wave intensity," which has been used in underwater acoustics as a practical way to express the intensity of acoustic waves (5). Note also that the effective sine wave frequency defined here represents a special case of the more general "instantaneous frequency," which has been defined as  $1/2 \pi$  times the derivative of the argument of sinusoidal type waves (7).

An FSS, calculated from Eqn. (2) for a 50% modulation around the mean, is shown in Figure 1B. The scale along the abscissa labeled TIME indicates the time after start of the stimulus for the first 15 peaks of the stimulus shown in Figure 1A. From Eqn. (8), the equivalent sine wave frequency at each corresponding time,  $t$ , was calculated and plotted along the abscissa labeled FREQUENCY. Values of the equivalent frequency determined at the time the decremting stimulus crossed the mean were then used to plot the corresponding maximum frequency response ( $f_E$ , upper curve) from the data of Figure 1A for comparison with the FSS command frequency at that time ( $f_c$ , lower curve) in Figure 1C. Note that an upward flag marks a "bin width" spanning the higher frequencies (up to the frequency given by the next decremental crossing of the mean by the FSS stimulus) to indicate a limit of resolution in the measurement due to the nature of the stimulus.

Practically speaking, it is this equivalent sine wave frequency,  $f_E$ , as opposed to the command frequency,  $f_c$ , that may prove more relevant to the interpretation of a cell's physiological response dynamics. This is because  $f_E$  relates the rate of change of an FSS to a comparable sinusoidal stimulus while accounting for a near doubling (Eqn. (7) and Fig. 1C) of the command frequency; this relationship is especially significant for the physiological responses of rate-sensitive systems. Furthermore, the concept of frequency is defined on the basis of such periodic events, but the FSS is not periodic.

Thus, the FSS can be used quantitatively as a critical assay of changes in the frequency response of a ganglion cell during the slow process of light adaptation in the skate (6, 8). The investigator, instead of relying on subjective judgment about when flicker fusion has been reached, can allow the FSS to make its own "decisions" on when to fire an action potential. This approach may prove helpful in the study of other neuronal systems as well. Intuitively, the equivalent sine wave frequency of an FSS defined here may be thought of conveniently as approximately doubling the command frequency when considering its role in eliciting a physiological response.

Supported by NIH Grant EY00777 and ONR Grant N00014-92-J-1954.

## Literature Cited

1. Naka, K.-I., M. Sakuranaga, and R. L. Chappell. 1982. *Biomed. Res. Suppl.* 3: 131-136.
2. Chappell, R. L., K.-I. Naka, and M. Sakuranaga. 1985. *J. Gen. Physiol.* 86: 423-453.
3. Sakuranaga, M., and K.-I. Naka. 1985. *J. Neurophysiol.* 53: 411-428.
4. Naka, K.-I., R. L. Chappell, M. Sakuranaga, and H. Ripps. 1988. *J. Gen. Physiol.* 92: 811-831.
5. Horton, J. W. 1957. *Fundamentals of Sonar*. U. S. Naval Inst., Annapolis, MD.
6. Dowling, J. E., and H. Ripps. 1970. *J. Gen. Physiol.* 56: 491-520.
7. Gerlach, A. A. 1970. *Theory and Applications of Statistical Wave-Period Processing*. Gordon and Breach, New York.
8. Green, D. G., and I. M. Siegel. 1975. *Science* 188: 1120-1122.

Reference: *Biol. Bull* 185: 310-311. (October, 1993)

**Electrical Properties of Electoreceptor Cells Isolated from Skate Ampulla of Lorenzini**  
*Ricardo C. Araneda and Michael V. L. Bennett (Marine Biological Laboratory  
 and Albert Einstein College of Medicine)*

Marine elasmobranchs are extraordinarily sensitive to voltage, responding reliably to gradients of  $<1 \mu\text{V}/\text{m}$  (1). Afferent fibers from the ampullae of Lorenzini change their frequency of firing in response to  $1 \mu\text{V}$  applied across the sensory epithelium, which contains a single layer of supporting and receptor cells. Previous work on the isolated ampulla suggested that the receptors cells were capable of generating  $\text{Ca}^{2+}$  spikes and had a  $\text{Ca}^{2+}$ -activated late outward current (2). Clusin and Bennett postulated that the receptor cells were asynchronously active and generated full-sized action potentials under normal unstimulated conditions. They ascribed high sensitivity to frequent threshold crossings. A further aspect of the receptor responsiveness is the accommodation that occurs in response to DC stimuli. Over a range of  $\pm 1 \text{ mV}$ , which is 2000 times the amplitude of a threshold stimulus, the afferent discharge adapts over tens of seconds to return to the resting level of spontaneous discharge. Moreover, sensitivity to incremental stimuli recovers to near its initial level, and the receptor responds to a  $1 \mu\text{V}$  pulse superimposed on the  $1 \text{ mV}$  DC with almost the same change in discharge rate that it showed in the absence of the DC (3). Thus, the receptor retains sensitivity in the presence of well suprathreshold DC voltages of endogenous or exogenous origin.

To further understand the physiological basis of the receptor sensitivity, we acutely isolated receptor cells following papain treatment and recorded from them with patch pipettes in the whole-cell mode. Receptor cells were recognized by their single apical cilium. Recordings were made at room temperature. Under current-clamp and the recording conditions used, the resting potentials were rather low ( $-20$  to  $-40 \text{ mV}$ ) and the cells were inactive. When the cells were hyperpolarized to about  $-60 \text{ mV}$ , they generated large spikes in response to depolarizations of a few mV (Fig. 1A). They could be spontaneously active (B), and in some instances a train of induced action potentials was followed by a prolonged burst that ended spontaneously (C).

Under voltage-clamp, depolarizing steps from  $-90 \text{ mV}$  in-

duced the activation of an inward current (measured at  $5 \text{ ms}$ ) between  $-40$  and  $-20 \text{ mV}$ ; at greater depolarizations this inward current was overridden by a large outward current (Fig. 1D, upper inset, open circles in graph). Both currents showed little inactivation during a  $200\text{-ms}$  pulse. The inward current was carried by  $\text{Ca}^{2+}$  ions because it was insensitive to tetrodotoxin and replacement of  $\text{Ca}^{2+}$  by  $\text{Ba}^{2+}$  left only a non-inactivating inward current between  $-40 \text{ mV}$  and  $+5 \text{ mV}$  (Fig. 1D, lower inset, closed circles in graph). The outward current was carried by  $\text{K}^+$  because it was blocked by  $30 \text{ mM}$  tetraethylammonium in the external solution or by the inclusion of  $\text{Cs}^+$  in the recording pipette. The outward current was suppressed at large inside positive voltages, suggesting that it was  $\text{Ca}^{2+}$  activated. Block of the outward current by  $\text{Ba}^{2+}$  does not identify the  $\text{K}^+$ -channel type, because  $\text{Ba}^{2+}$  could act directly on voltage-sensitive or  $\text{Ca}^{2+}$ -activated  $\text{K}^+$ -channels or fail to substitute for  $\text{Ca}^{2+}$  at  $\text{Ca}^{2+}$ -activated channels.

In summary, the voltage-dependent conductances predicted from measurements on the intact epithelium are present, and the receptor cells are capable of generating large action potentials. Activation of  $\text{Ca}^{2+}$  occurs over a normal range compared to other cells and is not unusually voltage sensitive. We are obtaining quantitative data to simulate receptor activity computationally. We shall determine whether the computed sensitivity of many receptor cells in parallel approaches that observed physiologically.

## Literature Cited

1. Kalmijn, A. J. 1974. P. 147 in *Handbook of Sensory Physiology, Vol. 3, Electoreceptors and Other Specialized Receptors in Lower Vertebrates*, A. Fessard, ed., Springer, New York.
2. Clusin, W. T., and M. V. L. Bennett. 1979. *J. Gen. Physiol.* 73: 703.
3. Bodznick, D., G. Hjelmstad, and M. V. L. Bennett. 1993. *Jpn. J. Physiol., suppl. 1* (in press).

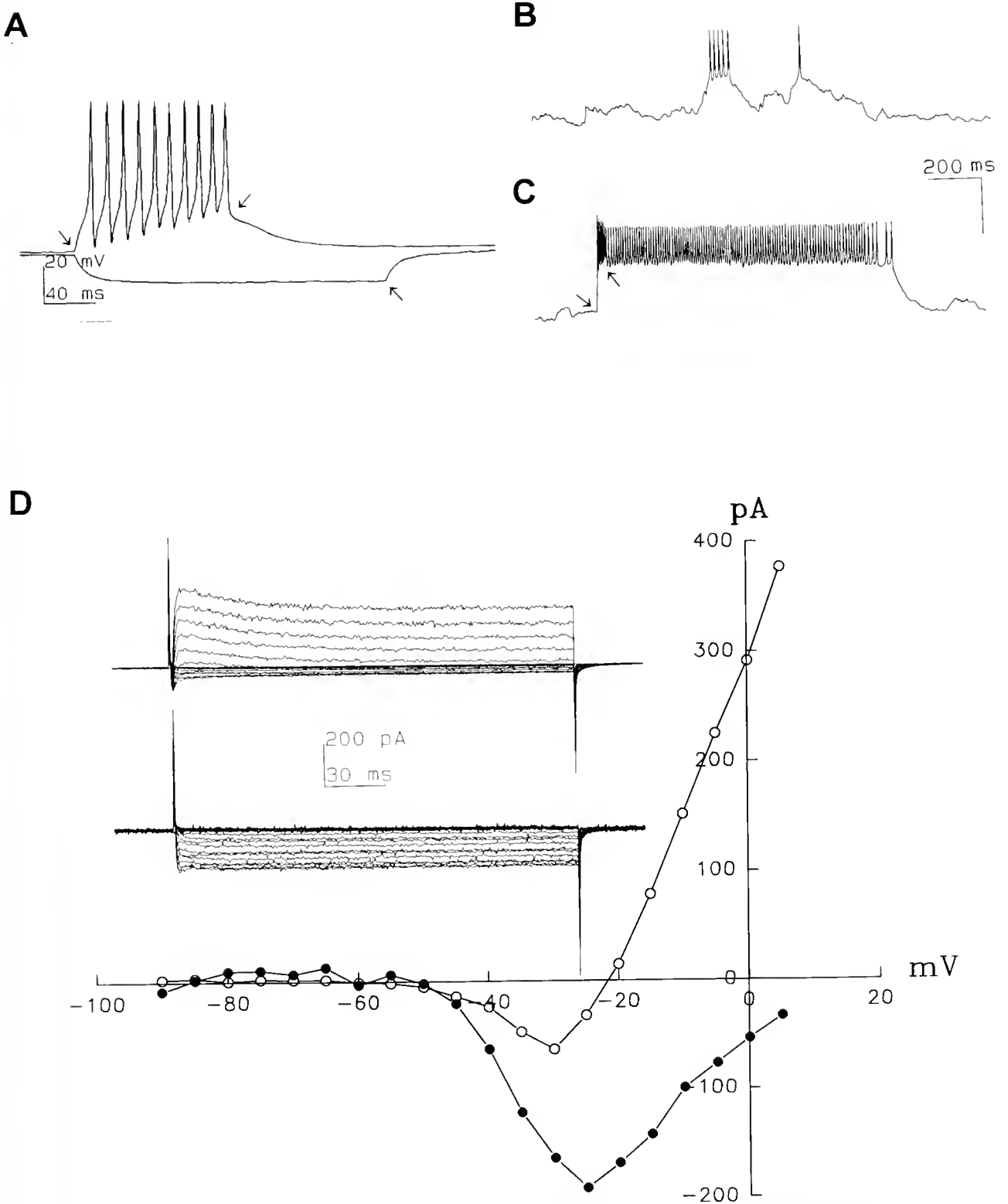


**Figure 1.** Responses of isolated receptor cells. (A) A cell was hyperpolarized to c. -60 mV; depolarization generated a train of spikes. Hyperpolarization showed that the cell was of high resistance, c. 2 GΩ. (B) Spontaneous slow depolarizations and spikes in a hyperpolarized cell. (C) In the same cell, a short train of evoked spikes was followed by a prolonged train of spikes. Arrows indicate the onset and end of the stimuli. (D) Voltage-clamp data. The insets show responses to 200 ms depolarizing pulses applied from a holding potential of -90 mV up to +5 mV at 5-mV increments in normal saline (upper) and in Ba<sup>2+</sup> saline (lower). The graph plots current at 5 ms after stimulus onset for normal saline (open circles) and for Ba<sup>2+</sup> saline (closed circles).

Reference: *Biol. Bull.* 185: 312. (October, 1993)

### GABA Responses on Retinal Bipolar Cells

Haohua Qian and John E. Dowling (*The Biological Laboratories, Harvard University*)

GABA is the main inhibitory neurotransmitter in the central nervous system. Recently, a new type of GABA receptor, termed the GABA<sub>C</sub> receptor, has been reported (1–4). Unlike the well-characterized GABA<sub>A</sub> and GABA<sub>B</sub> receptors, GABA<sub>C</sub> receptors are insensitive to both bicuculline and baclofen, and are not modulated by either the benzodiazepines or barbiturates. Although both GABA<sub>A</sub> and GABA<sub>C</sub> receptors are linked to chloride channels, a major difference between the responses of these two receptors is that GABA<sub>C</sub> responses are quite sustained, whereas GABA<sub>A</sub> responses desensitize substantially. Although GABA<sub>C</sub> receptors are especially prominent in retina (1–4), the distribution of these receptors on retinal neurons is largely unknown. The rod horizontal cells in perch retina possess only GABA<sub>C</sub> receptors, but bipolar cells in the same species appear to have both GABA<sub>A</sub> and GABA<sub>C</sub> receptors (1). In this study, the GABA responses of perch and bass bipolar cells were characterized, and the location of GABA receptors on the cells was determined.

Solitary retinal neurons were enzymatically dissociated from both white perch (*Roccus americana*) and white bass (*Morone chrysops*)–striped bass (*Morone saxatilis*) hybrid retinas. Bipolar cells were identified by their morphology. The membrane currents were recorded using either conventional or amphotericin-perforated whole-cell voltage-clamp recordings. Application of 100 μM GABA onto bipolar cells induced a chloride current that was blocked by picrotoxin. The GABA-induced currents had both transient and sustained components (Fig. 1a). The transient component was sensitive to bicuculline, whereas the more sustained component was resistant to bicuculline and resembled the sustained currents mediated by GABA<sub>C</sub> receptors in rod horizontal cells (1) (Fig. 1b). For example, the bicuculline-resistant GABA responses from the bipolar cells were unaffected by phaclofen and 2-hydroxysaclofen, GABA<sub>B</sub> receptor inhibitors, and they could not be modulated by either diazepam or pentobarbital. In the presence of 10 μM diazepam and 100 μM pentobarbital, the bicuculline-resistant GABA responses were  $0.94 \pm 0.45$  (n = 7) and  $1.10 \pm 0.25$  (n = 5) of control. Interestingly, such bicuculline-resistant GABA responses could be blocked substantially by I4AA (imidazole-4-acetic acid) (Fig. 1c), an antagonist of GABA<sub>C</sub> receptors (5). The ratio of variances to means of the currents induced by GABA was  $10.1 \pm 2.1$  pA (n = 4) in the presence of I4AA and  $3.6 \pm 0.9$  pA (n = 4) in the presence of bicuculline, suggesting a different single channel conductance for GABA<sub>A</sub> and GABA<sub>C</sub> receptors. Our results in-

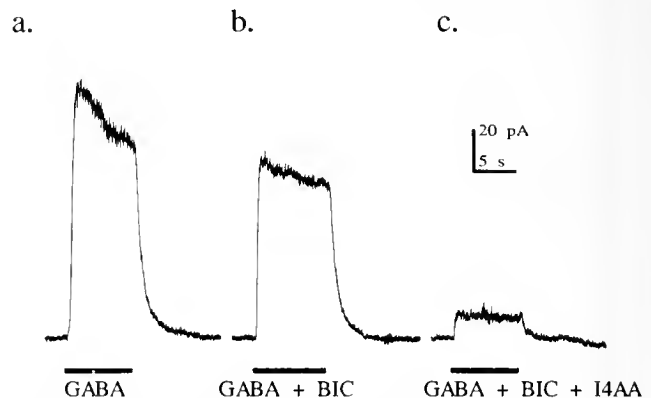


**Figure 1.** Responses of a bipolar cell to 100 μM GABA in Ringer (a), coapplied with 100 μM bicuculline (b), or coapplied with 100 μM bicuculline + 200 μM I4AA (c). The time course of application is shown by the bar under each trace. The perforated patch technique was used to record the membrane currents. Cell was held at 0 mV. Note that the GABA response of this cell was mediated predominately by GABA<sub>C</sub> receptors. An example of a bipolar cell in which GABA<sub>A</sub> receptor responses predominated is shown in Figure 3b of reference (1).

dicating that both GABA<sub>A</sub> and GABA<sub>C</sub> receptors mediate GABA responses on retinal bipolar cells. The GABA<sub>C</sub>/GABA response ratio on individual bipolar cells varied considerably, from 0.09 to 0.82, with an average value of  $0.37 \pm 0.23$  (n = 28). Local application of GABA onto dendrites or axon terminals showed that both types of GABA receptors are present on both regions of the cell. The distinct properties of these two GABA receptor types suggest they play different roles in retinal function.

H. Qian is a Grass Fellow at The Marine Biological Laboratory, Woods Hole.

#### Literature Cited

1. Qian, H., and J. E. Dowling. 1993. *Nature* 361: 162–164.
2. Feigenspan, A., et al. 1993. *Nature* 361: 159–162.
3. Cutting, G. R., et al. 1991. *Proc. Natl. Acad. Sci. U.S.A.* 88: 2673–2677.
4. Polenzani, L., et al. 1991. *Proc. Natl. Acad. Sci. U.S.A.* 88: 4318–4322.
5. Kusama, T., et al. 1993. *Br. J. Pharmacol.* 109: 200–206.

Reference: *Biol. Bull.* 185: 312–314. (October, 1993)

### The Specificity of an Adaptive Filter That Suppresses Unwanted Reafference in Electrosensory Neurons of the Skate Medulla

David Bodznick (*Wesleyan University, Middletown, CT 06457*)

The electroreceptors of elasmobranchs are subject to interference from electrical potentials created by the fish's own ventilatory movements. Electroreceptive afferents in skates are

sometimes modulated through more than half their dynamic range by ventilation. However, brain mechanisms that eliminate the self-stimulation (reafference) do occur. Second order elec-

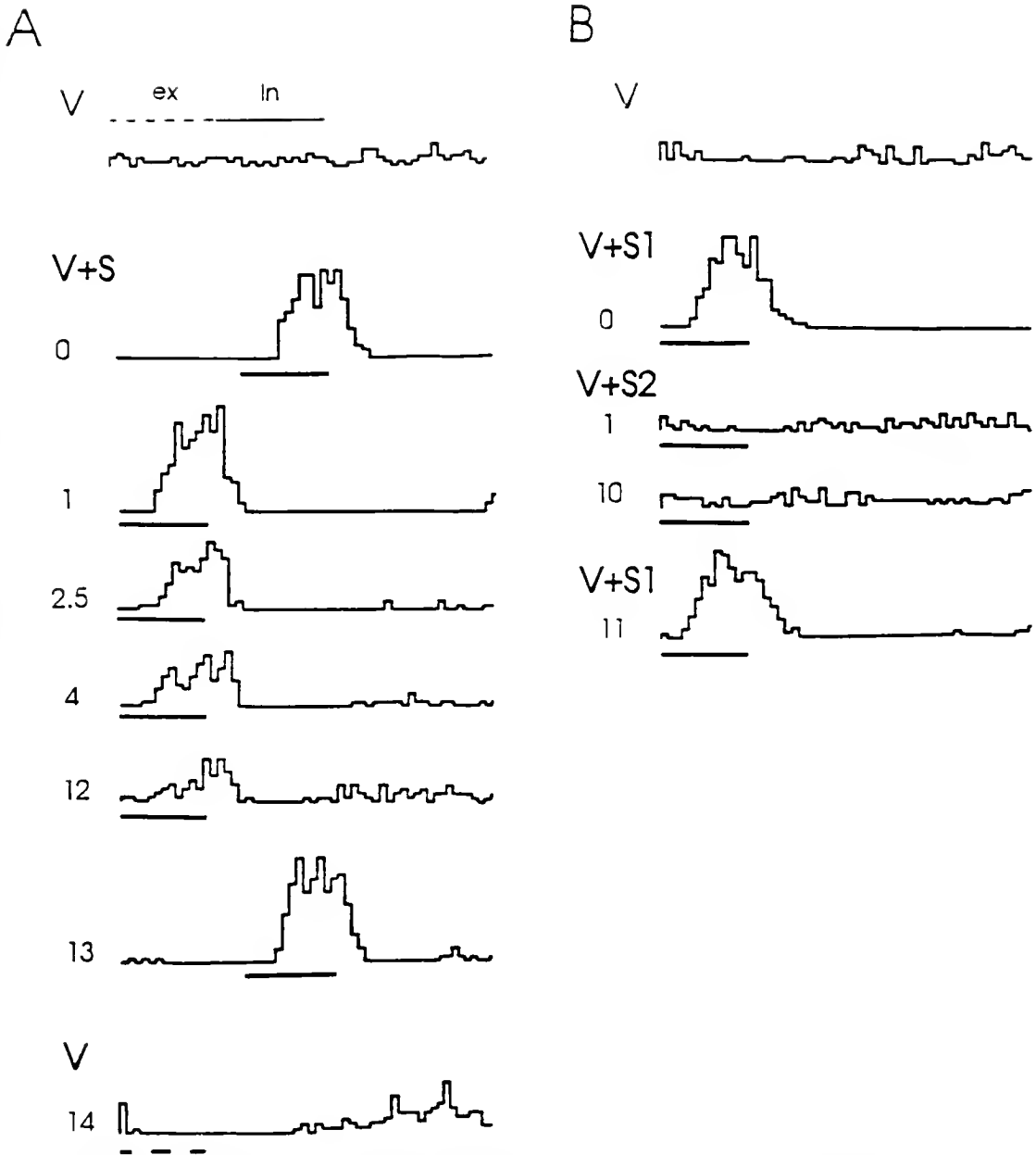


**Figure 1.** Histograms (30 trials, 1.75-s duration) of AEN activity during ventilation alone (*V*) and when an electric field stimulus is coupled to ventilation (*V* + *S*). All records are from the same neuron. Periods of exhalation (*ex*) and inhalation (*in*) are indicated (1*A*) Series of histograms presented in the order collected (times indicated in minutes) show that the AEN's response to a dipole electric field stimulus ( $2 \mu\text{V}$ ) gradually declines when the stimulus is repeatedly presented at the same time during ventilation (records at 1–12 min). However, this coupling does not affect the cell's response to the same dipole given at a different time in the ventilation cycle (compare records at 0 and 13 min). For a short time after the coupling is ended, the cell's firing during ventilation reveals an apparent cancellation signal that has developed during the coupling (compare *V* before and at 14 min). (1*B*) The spatial specificity of the adaptive filter mechanism is illustrated. *S1* is a local electric field stimulus ( $2 \mu\text{V}$ ) presented in the cell's receptive field, and *S2* is the same stimulus presented near electroreceptors outside the cell's receptive field. The repeated presentation of *S2* time locked to ventilation (1–10 min) does not reduce the cell's response to *S1* when tested at the same phase of the ventilatory cycle.

troductory neurons (called AENs), located in the dorsal nucleus of the medulla are much less affected by ventilation than the electroreceptors. They are sheltered, in part by a simple common mode rejection mechanism (1, 2, 3); *i.e.*, AENs receive separate

excitatory and inhibitory inputs from electroreceptors on different parts of the body and reject ventilatory noise, which is similar in all receptors, in favor of extrinsic stimuli that affect the receptors differentially.



Recent observations (in prep.) indicate that a separate adaptive filter mechanism further suppresses ventilatory reafference in AENs. The response of an AEN to an electric field stimulus gradually diminishes when the stimulus is repeatedly presented at the same time during the fish's ventilatory movements (Fig. 1A, traces at 1–12 min). The response to the coupled stimulus appears to be reduced by an additive mechanism. When the stimulation is abruptly stopped, the cell's firing pattern during ventilation shows the effects of an apparent cancellation signal that has developed during the coupling (Fig. 1A, compare V before and at 14 min). The source of the cancellation signal is not known but is suggested by the anatomical organization of the dorsal nucleus.

In cerebellar fashion, AEN apical dendrites extend into a molecular layer, where they receive inputs from parallel fibers and stellate interneurons carrying proprioceptive and motor command-associated signals with various temporal relationships to ventilation (4). In weakly electric mormyrid fish, a modifiable efference copy mechanism that suppresses unwanted reafference in medullary electrosensory neurons is mediated by plasticity in the synapses of a comparable molecular layer (5, 6). J. C. Montgomery and I propose (in prep.) that, in the same way, the cancellation signal in elasmobranchs is created through adjustments in synaptic strengths of the molecular layer inputs onto the AENs. Here I report further studies of the temporal and spatial specificity of this adaptive filter mechanism.

AEN activity is recorded extracellularly in spinalized, decerebrate skates (*Raja erinacea*), while ventilatory movements are simultaneously monitored (3). The temporal specificity of the filter mechanism is apparent in the observation that the coupling of a stimulus during one phase of ventilation never affects the response to the same stimulus presented at other times in the ventilatory cycle (Fig. 1A). This observation also serves as an important control, showing that the diminished response does not result from sensory fatigue or cell injury.

The spatial specificity of the learning mechanism was also

examined in several AENs. The consistent result is that, although the response to a local electric field presented to electroreceptors in an AEN's receptive field (RF) declines when coupled to ventilation for 10 to 20 min, no such effect is seen if the coupled stimulus is presented to electroreceptors outside the recorded AEN's RF. The response to a test stimulus presented in the AEN's RF at the same phase of ventilation is unaffected by such coupling (Fig. 1B). Weak, large-scale uniform electric fields, which are potent stimuli for the electroreceptors, are ineffective stimuli for many AENs because of their composite RFs. Coupling of a uniform field stimulus with ventilation also does not affect the response of such an AEN to an effective local test stimulus presented at the same phase of ventilation. This is so although the receptors of the AEN's excitatory RF are strongly activated by the uniform field.

This temporal and spatial specificity indicates that the development of the cancellation signal, and thus the adaptive filter mechanism, is specifically related to the activity of each AEN. The results are consistent with the proposed synaptic plasticity mechanism in which the learning rules are based on the temporal relationships of activity in AENs and particular molecular layer synapses.

I thank Alison Pachynski for excellent technical help. The research is funded by an NSF grant.

#### Literature Cited

1. Montgomery, J. C. 1984. *J. Comp. Physiol.* 155A: 103–111.
2. New, J. G., and D. Bodznick. 1990. *J. Comp. Physiol.* 167A: 295–307.
3. Bodznick, D., J. C. Montgomery and David J. Bradley. 1992. *J. Exp. Biol.* 171: 107–125.
4. Hjelmstad, G., G. Parks, and D. Bodznick. (in press). *Soc. Neurosci. Abst.* 19.
5. Bell, C. C. 1981. *Science* 214: 450–453.
6. Bell, C. C., A. Caputi, K. Grant, and J. Serrier. 1993. *Proc. Natl. Acad. Sci.* 90: 4650–4654.

Reference: *Biol. Bull.* 185: 314–316. (October, 1993)

### Role of Proprioceptive Input During Abdominal Bending-Reflex Motor Activity in the Tobacco Hawkmoth *Manduca sexta*

William C. Lemon and Richard B. Levine (Division of Neurobiology, University of Arizona, Tucson, AZ 85721)

Neural circuits in the abdominal nerve cord of *Manduca sexta* are responsible for a wide range of behaviors, including abdominal bending and crawling in the larva, abdominal rotation and gin trap closure in the pupa, and abdominal ruddering and egg laying in the adult. Many of the sensory neurons, interneurons, motoneurons, and muscles that are involved in producing these behaviors persist from one life stage to the next. Sensory feedback from the abdominal stretch receptor onto the neural circuits responsible for abdominal movements may modify behaviors within one life stage. Furthermore, changes in the sensory feedback between life stages may contribute to qualitative changes in the behaviors produced.

Behaviors that have been useful for examining the organization and postembryonic development of neural circuits are the abdominal bending behaviors seen during the larval and pupal stages (1–4). Although the elements of the circuit are retained from larva to pupa, the bending-reflex motor patterns in these stages are quite different. In the larva, stimulation of some of the mechanosensory hairs on the abdomen produces an ipsilateral, long burst of low frequency motoneuron activity that causes intersegmental muscles (ISM) in several segments to contract, bending the abdomen slowly toward the stimulus (4). In the pupa, the same sensory hairs have become part of large cuticular pits called 'gin traps'. Stimulation of these sensory hairs

evokes a phasic, bilaterally coordinated motor pattern causing rapid bending and subsequent straightening of the pupal abdomen (4).

Recent studies have shown that the neural elements of the abdominal stretch receptor organ persist through development,

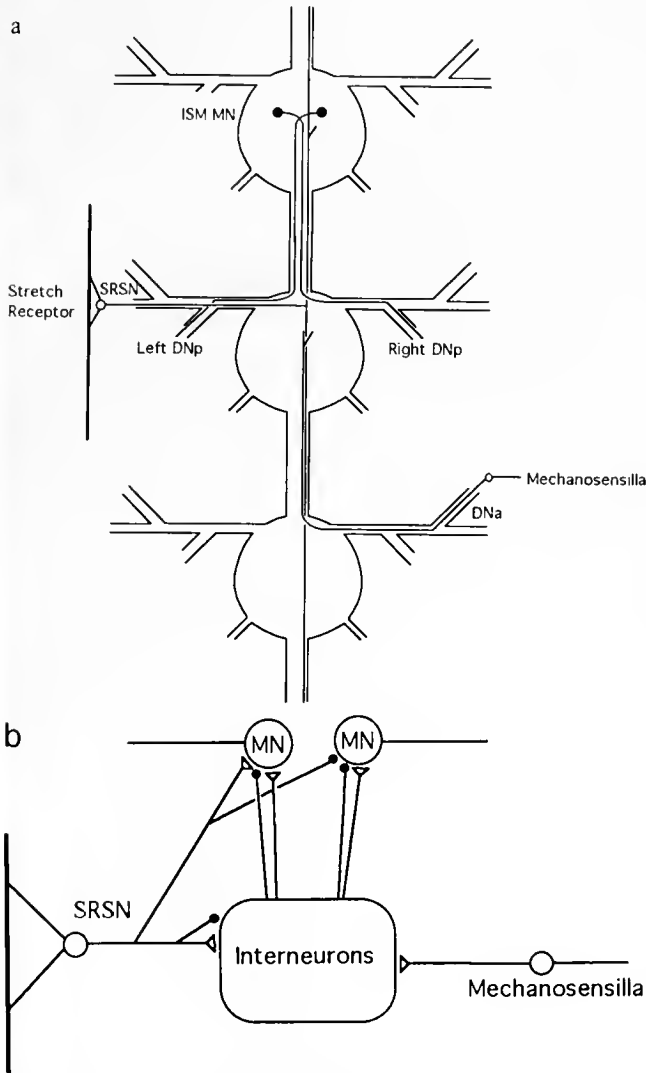


**Figure 1.** a. Diagram of a chain of ganglia in the abdominal nerve cord of *Manduca sexta*. Records of motor activity were obtained from extracellular recordings of the motor nerves innervating intersegmental muscles (left and right DNp), and from the somata of intersegmental muscle motoneurons (ISM MN). Reflexes were elicited by electrical stimulation (400 ms train of 0.1 ms, 5 V pulses at 100 Hz) of the sensory nerve (DNa) carrying afferents from mechanosensilla on the abdominal cuticle. Stretch receptor input to the reflex circuit was provided by electrical stimulation (2 s train of 1 ms, 3 V pulses at 100 Hz) of the contralateral stretch receptor sensory neuron (SRSN). b. Simplified wiring diagram of the abdominal bending circuit. Afferents from mechanosensilla project to a population of interneurons that provide excitatory (open triangles) and inhibitory (closed circles) input to motoneurons (MN). The SRSN has excitatory connections with ipsilateral motoneurons and inhibitory connections with contralateral motoneurons. The SRSN also has excitatory connections with many of the interneurons and may have inhibitory connections with some interneurons.

but that the sign and strength of synaptic connections to some motoneurons are changed (5). The stretch receptor organ in each abdominal segment contains a single muscle fiber that extends along the anterior-posterior axis, and is inserted near the anterior and posterior segment boundaries on the dorso-lateral body wall (Fig. 1a). The muscle fiber is innervated by a single motoneuron and a single sensory neuron. The dendrites of the stretch receptor sensory neuron (SRSN) are embedded in the cell membrane of the muscle fiber and transduce stretch of the muscle fiber into an increased rate of firing of the sensory neuron. The SRSN has monosynaptic and polysynaptic connections with the motoneurons innervating the ISMs responsible for abdominal bending (Fig. 1b). Semi-intact preparations of larval and pupal *M. sexta* (Fig. 1a) were used in this study to examine the role that input from the stretch receptor has on the production of stage-specific motor patterns underlying the bending reflex and the modulation of stretch receptor input by the CNS.

Stimulation of the larval SRSN alone consistently evoked a prolonged motor response that occurred after several seconds of inactivity (Fig. 2). Simultaneous stimulation of the larval sensory nerve carrying mechanosensilla afferents (dorsal nerve, anterior branch: DNa) and the SRSN produced a bending-reflex motor pattern that resembled the typical larval motor pattern evoked by DNa stimulation alone. SRSN activity did not dramatically alter the duration of the bursts of bending-reflex motor activity, nor introduce a delay to the onset of the bursts. In addition, when the abdominal bending-reflex motor pattern was elicited by DNa stimulation, the delayed excitation evoked by SRSN activity alone was absent, suggesting gating of stretch receptor input during the reflex motor activity.

Stimulation of the SRSN only in the pupa did not evoke motor activity that occurred after a period of inactivity as in the larva. However, SRSN stimulation during pupal bending-reflex motor activity consistently modulated the motor pattern produced. As seen in Figure 2, DNa stimulation alone caused a typical triphasic patterned motor response. When the DNa and contralateral SRSN were stimulated together, the strength of the first burst of activity was reduced and action potentials occurred during the subsequent hyperpolarization. The pupal bending-reflex motor pattern appears to have been modified by input from the stretch receptor.

These results indicate that during the larval bending-reflex motor patterns, the input from abdominal stretch receptors is gated. In contrast, pupal bending-reflex motor patterns appear to be modulated by stretch receptor input. These results suggest that there is a developmental change in the role that proprioceptive input plays in producing bending-reflex motor patterns.

This work was supported by a Grass Foundation Fellowship to W. C. L. and NSF BNS 11174 to R. B. L.

**Literature Cited**

1. Bate, C. M. 1973. *J. Exp. Biol.* 59: 95-107.
2. Bate, C. M. 1973. *J. Exp. Biol.* 59: 109-119.
3. Bate, C. M. 1973. *J. Exp. Biol.* 59: 121-135.
4. Waldrop, B., and R. B. Levine. 1989. *J. Comp. Physiol. A* 165: 743-753.
5. Tamarkin, D. A., and R. B. Levine. 1992. *Soc. Neurosci. Abstr.* 18: 1413.

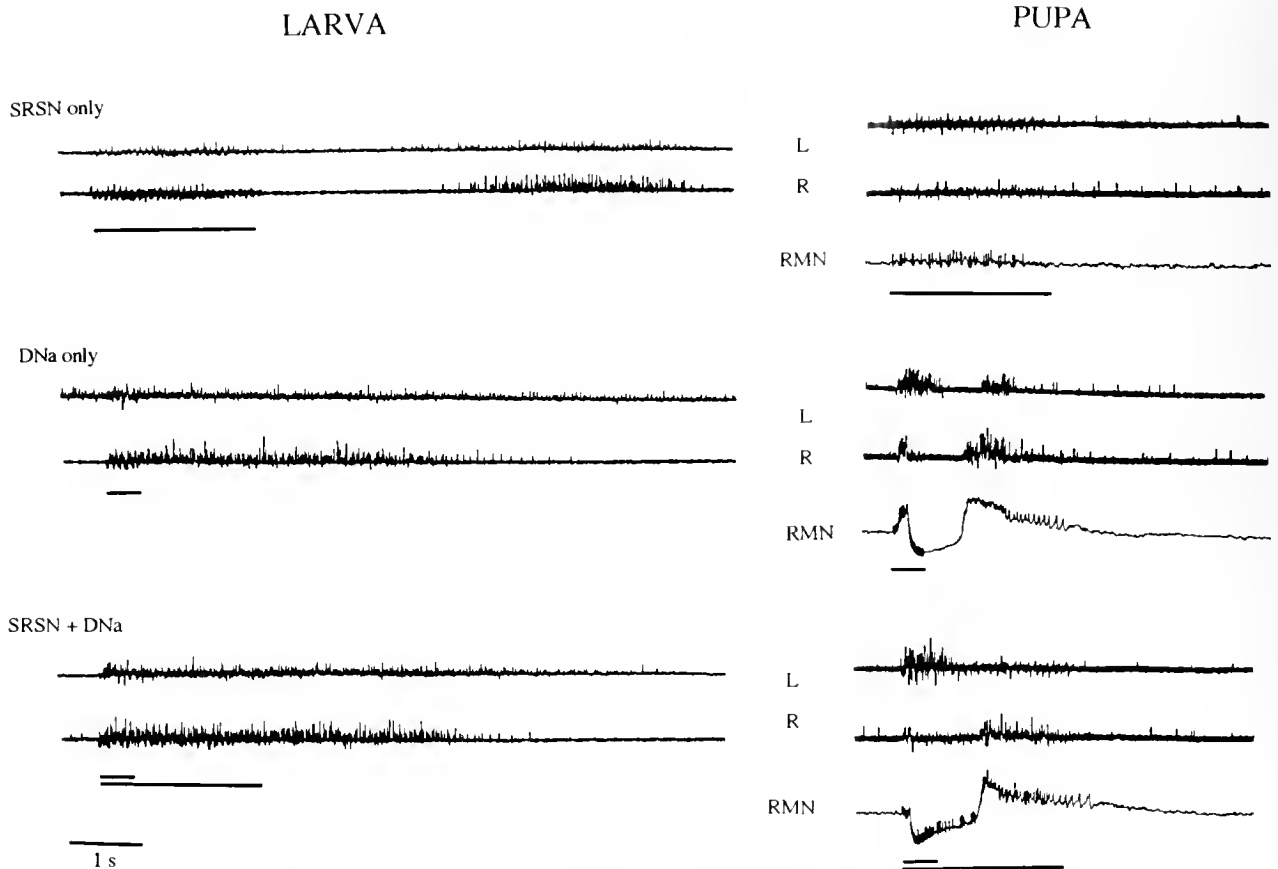


**Figure 2.** Records of bending-reflex motor activity in larval and pupal *Manduca sexta*. Larval extracellular records are responses of motor neurons in the left (L) and right (R) motor nerves innervating the intersegmental muscles (ISM). The responses are produced by electrical stimulation of the left stretch receptor sensory neuron (SRSN) alone (indicated by long bar); the right sensory nerve (DNa) carrying axons from mechanosensillae (indicated by short bar); or the stretch receptor and DNa together. When the SRSN was stimulated alone, the stimulus induced motor activity coincident with the stimulus and a long burst of motor activity that occurred after a period of inactivity (mean duration of inactivity = 3.7 s,  $n = 5$ ). Stimulation of the DNa only produced a typical, prolonged burst of activity on the stimulated side (mean duration of activity = 5.5 s,  $n = 5$ ) and weak, or no, activity on the opposite side. The response evoked by stimulation of the DNa and the SRSN was virtually the same as that evoked by DNa stimulation only, and the response evoked by SRSN stimulation alone was absent. Pupal responses to stimulation of the left DNa and the right SRSN are shown in recordings of left (L) and right (R) motor nerves and in an intracellular recording of a motoneuron innervating an intersegmental muscle on the right (RMN). Stimulation of the pupal SRSN only produced low frequency motor activity coincident with the stimulus. Stimulation of the DNa only produced a typical, triphasic patterned response in which two high frequency bursts of activity were separated by a period of inhibition. The response to simultaneous SRSN and DNa stimulation showed a weaker first burst of activity, a period of hyperpolarization during which action potentials occurred, and a high frequency second burst of activity ( $n = 4$ ).

Reference: *Biol. Bull.* 185: 316-317. (October, 1993)

### A Comparison of the Tuning Properties of Chemoreceptor Cells in the First and Fourth Walking Legs of Female American Lobsters

Keith M. Bayha, Rainer Voigt, and Jelle Atema (Boston University Marine Program, Marine Biological Laboratory)

The first and fourth pair of walking legs in the American lobster differ in morphology and behavioral function. Apart from their obvious use in walking, the first pair of walking legs are

chelated and serve in feeding behavior, *i.e.*, for grasping and transporting food to the maxillipeds and for grooming the anterior body (1). The fourth pair of walking legs is used for walking

and grooming of the posterior body (2). In the egg-bearing female, this prominently includes the grooming of the egg mass. Such behavioral differences may correlate with physiological differences in chemoreceptor function between the two leg pairs, e.g., lobsters may be able to differentiate between healthy and fouled eggs using fourth leg chemoreceptors. We therefore determined the spectral sensitivity of chemoreceptor cells in the first and fourth walking legs, focusing on chemicals present in food odor and products of bacterial degradation. Because of their egg-cleaning behavior, we used female lobsters for this initial study.

We assessed the tuning properties of chemoreceptor cells by measuring responses to single chemical stimuli; standard electrophysiological methods using suction electrodes were applied to record extracellular action potentials. From the first leg we excised the dactyl and from the fourth leg the dactyl and propus to ensure that both smooth and toothed sensilla would be present (3). The segment with the exposed nerve bundle was placed in the stimulating compartment of a two-compartment preparation chamber. The proximal end with the intact nerve bundle projecting into the recording compartment was immersed in lobster Ringer's solution. The stimulating and recording compartments were separated by a rubber plug (4). The segments were super-

fused with a carrier flow of artificial seawater (30 ml/min). Each single compound was injected as a 50  $\mu$ l aliquot into the carrier flow. The stimulation chamber was especially designed to provide thorough stimulus mixing for rapid stimulus onset and evacuation time; conductivity measurements (4) showed that the time course and dilution profiles were similar for both preparations. Single chemoreceptors were identified by their response to a mixture of 18 compounds (each at  $10^{-3}$  M; see Fig. 1). We then tested each compound separately at  $10^{-2}$  M. We evaluated cell viability with the mixture as every sixth stimulus, and we tested for mechanoreception with artificial seawater. Stimulus effectiveness was quantified as the total number of action potentials elicited in the first 5 s after stimulus injection. Action potentials from single chemoreceptors were differentiated on the basis of amplitude, wave form, and latency.

The first and fourth pairs of legs had different effective stimuli. Hind leg chemoreceptors responded best to hydroxy-L-proline, followed by glycine, methionine, glutamine, betaine, and leucine. Front leg chemoreceptors, on the other hand, responded best to ammonium chloride, followed by glutamate, lysine, leucine, betaine, and taurine. In contrast to Johnson *et al.* (4), we found no dominant population of glutamate-best cells in the front leg, but glutamate was the second-most effective stimulus. The tuning breadth of chemoreceptors in the two leg pairs was also different. Chemoreceptor cells in the hind legs were more broadly tuned than those in the front legs. Cells in the hind legs responded to between 1 and 18 stimuli, whereas cells in the front legs responded to between 1 and 10 stimuli. The H-metric, a measure of the tuning breadth, varies from 0 to 1, with 0 indicating narrow tuning and 1 indicating broad tuning (5). The H-metric mean was 0.55 for the hind legs and 0.42 for the front legs.

Our results indicate that the front and hind legs have different spectral sensitivities, which might be necessary for different behavioral functions. Whether this includes recognition of fouled eggs remains to be seen.

Supported by NSF BNS 88-12952 to J. A.

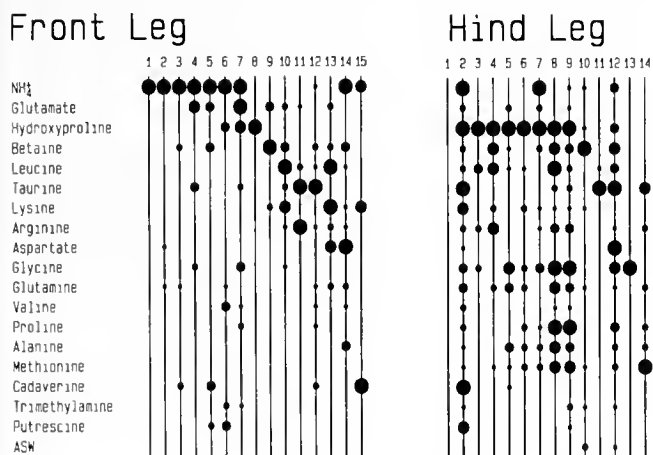


**Figure 1.** Spectral tuning properties of chemoreceptor cells in the first and fourth walking legs of female American lobsters. A continuous line indicates no response, the smallest dots indicate less than 20% of the maximum response, next largest dots between 20 and 40%, third largest dots between 40 and 60%, fourth largest dots between 60 and 80%, and the largest dots between 80 and 100%. Cells are grouped by their best stimulus and, within each group, ordered by increasing tuning breadth based on their H-metric value (5). Numbers indicate individual cells.

**Literature Cited**

1. Derby, C. D., and J. Atema. 1982. *J. Exp. Biol.* 98: 317-327.
2. Bauer, R. T. 1989. In *Functional Morphology of Feeding and Grooming in Crustacea*, F. R. Schram, ed. A. A. Balkema, Rotterdam.
3. Derby, C. D. 1982. *J. Crust. Biol.* 2: 1-21.
4. Johnson, B. R., R. Voigt, P. F. Borroni, and J. Atema. 1984. *J. Comp. Phys. A.* 155: 593-604.
5. Smith, D. V., and J. B. Travers. 1979. *Chem. Senses Flav.* 4: 215-229.

Reference: *Biol. Bull.* 185: 318. (October, 1993)

## Evidence for the Use of Urine Signals in Agonistic Interactions of the American Lobster

Thomas Breithaupt and Jelle Atema (Boston University Marine Program, Marine Biological Laboratory)

Recent experiments suggest that chemical communication is important for the recognition of dominance in the American lobster, *Homarus americanus* (1). We hypothesize that the urine of lobsters contains a dominance signal. Lobsters release urine through a paired set of nephropores on the ventral sides of the basal segments of the second antennae. Following release, the urine is blown forward by the powerful anteriorly projecting gill currents, which emerge on both body sides just below the antennal bases (2). These currents appear to be perfectly suited for carrying urine-borne chemicals from one animal to another. We wanted to test whether urine may be used as a signal in agonistic encounters. If it is a signal, we would expect that a lobster would release more urine in a social situation (*i.e.*, when at least one other lobster is present) than in a nonsocial situation (*e.g.*, when resting or when active without another lobster present).

To monitor urine release continuously without interfering with the animal, we catheterized lobsters with flexible plastic tubing. The first piece of tubing was attached with cyanoacrylate glue to the shell surfaces surrounding the nephropores. The tubing from both pores joined above the carapace of the lobster into a common tube connected with a syringe needle to a collection vial. The collection vial was a sealed transparent plastic cylinder that floated vertically on the water surface, supported by air-filled containers. Accuracy of reading was within 0.2 ml. Between January and May 1993, we measured the hourly urine production of six male and six female intermolt lobsters (76–87 mm carapace length) kept in individual 20-gallon tanks at water temperatures between 2° and 8°C. The lobsters were fed once a week, and the urine production was monitored each hour throughout the day, from 0800 h to at least 1800 h.

Each animal experienced two types of treatment (16 total trials). In the first treatment, a second male lobster (chosen from 18 different males of similar body size) was introduced into each tank for 1 h in eight separate trials. Adding a second male often resulted in fights between the lobsters. In the second treatment, the lobster was strongly disturbed by a 10 × 23 cm (lobster-sized) plate that was rapidly moved through the water towards the lobster every 10 min for 1 h. This plate produced a strong visual and mechanical stimulus that generally elicited activity including tailflips. Lobsters received treatment trials up to three times daily at randomly chosen hours; the type of treatment and order of presentation were also randomized. Urine release was compared between treatments and also between the hours before and after treatments (Fig. 1). The effect of treatments was tested with a Friedman ANOVA by ranks and subsequent Wilcoxon signed-rank tests adjusted for repeated comparisons by the Dunn-Sidak method.

The amounts of urine produced in the presence of a second male lobster were significantly higher ( $P \ll 0.001$ ) than in all other groups. We found no significant differences between any other groups.

In the presence of a conspecific, lobsters sometimes did not release any urine (36 of 96 trials). In these cases, however, no

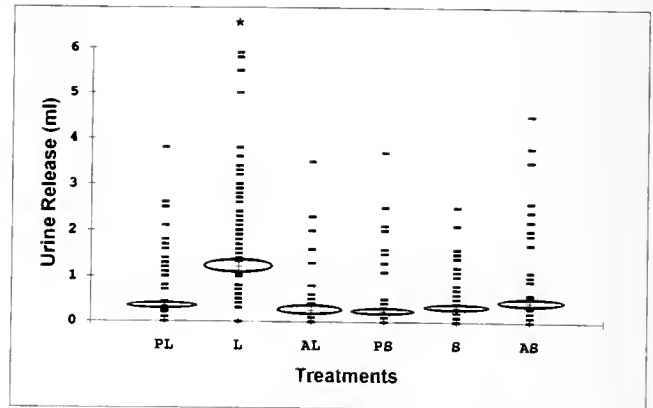


**Figure 1.** Amounts of urine released per hour by 12 lobsters. Dashes represent individual values; plus symbols encircled by ovals are mean values. The heights of the ovals indicate the standard error of the mean. Treatment groups: L = presence of second lobster; S = strong disturbance; PL, PS = hour before treatment; AL, AS = hour after treatment. Asterisk indicates significant difference ( $P \ll 0.001$ ) between the marked group and all others

aggressive behavior (as classified by Scrivener (3)) was noticed in the catheterized animals. In contrast, the highest amounts of urine (>5 ml, see Fig. 1) were released by animals that showed aggressive behavior throughout the hour a conspecific was present. The amount of urine release was not increased during disturbance treatment, which in most cases caused the lobster to tailflip away. These observations suggest that it is not physical exertion, but aggressive behavior, that caused the increased urine release. In a subsequent study we will address the question of whether there is a simple correlation between aggressive behavior and amount of urine release.

The finding that urine release is increased in agonistic encounters suggests that urine may be used as a signal. Not only the quantity but also the quality of the urine could change during agonistic interactions. We currently examine if there is a difference in the composition of the urine produced in social situations compared to nonsocial situations. It is not clear whether the signal communicates dominant status or the individual identity of a strong animal. In either case, the signal could be advantageous to both sender and receiver by helping to establish a dominance hierarchy that prevents costly fighting behavior.

Supported by NIH 2POINS25915-04A1 to J.A. and the Deutsche Forschungsgemeinschaft Br 1321/1-1 to T. B.

### Literature Cited

1. Karavanich, C., and J. Atema. 1991. *Biol. Bull.* 181: 359–360.
2. Atema, J. 1985. *Soc. Exp. Biol. Symp.* 39: 387–423.
3. Scrivener, J. C. E. 1971. *Fish. Res. Board Can. Tech. Rep.* 235: 1–128.

Reference: *Biol. Bull.* 185: 319–320. (October, 1993)

## A Novel Tegumental Gland in the Nephropore of the Lobster, *Homarus americanus*: A Site for the Production of Chemical Signals?

Paul Bushmann and Jelle Atema (Boston University Marine Program, Marine Biological Laboratory)

Evidence exists that chemical signals play an important role in lobster social behavior. Behavioral responses have been observed to both whole body odor (1) and lobster urine (2). Karavanich and Atema (3) showed that normal fighting behavior in male lobsters is disrupted if the antennular chemoreceptors are lesioned. Females are less interested in males in which urine release has been blocked (4).

Urine as a carrier in chemical communication implies that the signal consists of either general metabolic products or a unique substance or mixture, produced in a gland and released into the urine (5). Glands that may function as producers of chemical signals have been described in other species of crustaceans. Kamiguchi (6) described what he termed a "sternal gland" in the female *Palaemon pautidens*. It consists of rosettes of cells, surrounding a central lumen, and shows changes in activity closely tied to reproduction. Fontaine *et al.* (7) have described a gland in *Carcinus maenas*. This structure appears to be an exocrine gland, located in the distal section of the ureter, close to the excretory pore. Its greater development in females implies a role in sexual signaling.

In this study, a histological examination was made of the nephropore area of *Homarus americanus*. Animals were collected in the summer and fall of 1992 in the Woods Hole area. Four males and five females were examined. Two females were post molt and three were intermolt, one with eggs in her abdomen. All males were intermolt. The nephropores and the cuticle and tissue surrounding them were removed from each animal, then carefully excised under a dissecting scope and placed in Bouin's fixative for two to three days. After fixation, the tissue was decalcified in equal volumes of 50% formic acid and 0.68 M sodium citrate for two days and placed in 70% ethanol until embedding. The tissue was dehydrated and embedded in paraffin using vacuum infiltration. Cross sections (10 and 5  $\mu\text{m}$ ) were cut on a rotary microtome, working from the nephropore posteriorly. Sections were stained either with Masson's trichrome (8), consisting of Ponceau/acid fuschin, phosphotungstic acid, and aniline blue, or with Richard Allen hematoxylin and eosin.

Examination of the sections revealed two types of glandular structures. Small glands were present in all animals. Most of these glands showed a rosette structure, each rosette a cluster of 8–12 cells surrounding a central lumen, with basal nuclei. A duct was seen draining some rosettes, running from the central lumen to either the cuticle of the carapace or the lumen of the ureter. This duct was probably present in all cases, with breakage or shrinkage during preparation preventing its observation. Occasional unicellular glands were seen.

This morphology is typical of tegumental glands, well described in lobsters and other crustaceans (9, 10, 11). Some produce phenoloxidases necessary for tanning of chitinous cuticle (12). The activity of the glands seen here seemed to follow the molt cycle, staining blue in the post-molt females, with grainy cytoplasm suggesting vesicles containing secretory product. Ro-

settes from intermolt animals were smaller and less developed, staining red with little graininess. This evidence suggests that the small glands described here may function during molting, perhaps by release of phenoloxidase.

In addition to these small glands, every specimen examined possessed a large gland. This consisted of groups of rosettes, surrounded by connective tissue. Its mean length ranged from 395 to 660  $\mu\text{m}$ , with a mean of 526  $\mu\text{m}$ . The gland ran parallel to the ureter, opening into a muscular area, which abutted the lumen of the ureter, near the middle of its length. The gland was at its greatest diameter there, ranging between individuals from 86 to 500  $\mu\text{m}$ , with a mean of 225  $\mu\text{m}$ . No consistent differences were found between males and females.

Figure 1 shows a drawing of this gland in cross section, taken from a post-molt female. In this animal a duct was observed, running from the main body of the gland. It passed through a muscle mass and terminated near the distal end of the ureter.

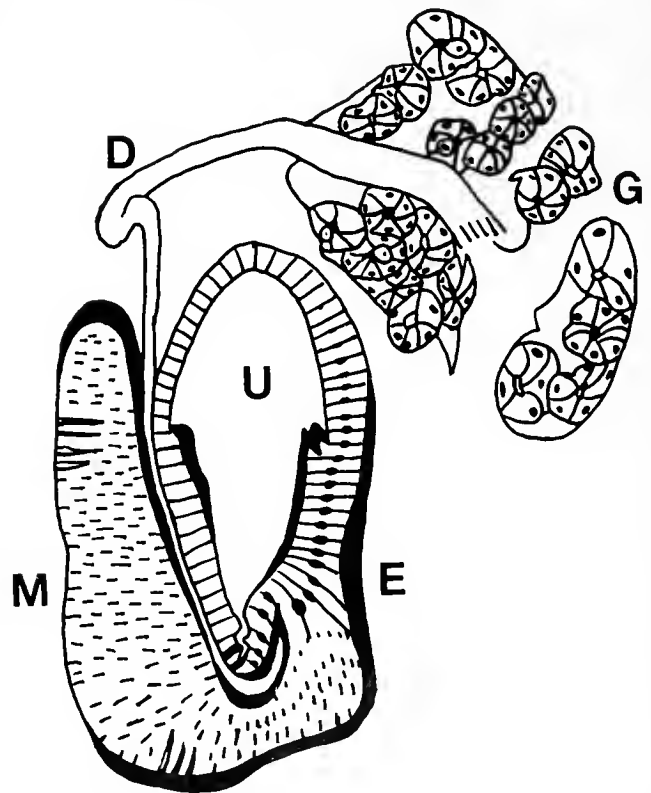


Figure 1. Drawing of a cross section of a nephropore of a post-molt female lobster. The section shown is 10  $\mu\text{m}$  in thickness, and 100  $\mu\text{m}$  posterior to the nephropore opening. Labels: G: gland; D: duct; U: lumen of ureter; E: epithelium of ureter; M: muscle surrounding ureter. Bar indicates 100  $\mu\text{m}$ .

Close examination of the termination point revealed small ducts traversing the epithelium of the ureter, suggesting that the larger duct releases product into the lumen of the ureter. These large glands stained differently than did the small glands. They stained blue in all specimens, and always showed the rosette development and grainy cytoplasm postulated to represent active cells.

In summary, lobsters possess two types of tegumental glands in the nephropore areas. The first, unicellular or individual rosettes, follows the molt cycle in activity. The second, a large mass of rosettes, seems to drain into the ureter via a common duct. It does not follow the molt cycle, appearing active in all specimens, although its large size in the post-molt female (Fig. 1) suggests some involvement in molting. Tegumental glands have been described that neither follow the molt cycle nor produce phenoloxidase, such as pleopodal cement glands (13). The large gland described here could be a novel type of tegumental gland, and is well positioned for production and release of a chemical signal, because any product would soon be excreted through the nephropore. It is possible, however, that the large gland serves another function, such as release of a bacteriostatic agent (14).

Determination of function requires behavioral, chemical, and physiological testing, and work is under way in these areas.

Supported by NIH 2POINS25915-04A1 to J. A.

### Literature Cited

1. Atema, J., and D. G. Engstrom. 1971. *Nature* 232: 2661-2663.
2. Cowan, D., and J. Atema. 1986. *J. Chem Ecol.* 12(11): 2065-2080.
3. Karavanich, C., and J. Atema. 1991. *Biol. Bull.* 181: 359-360.
4. Bushmann, P. 1993. unpublished data.
5. Dunham, P. J. 1978. *Biol. Rev.* 53: 555-583.
6. Kamiguchi, Y. 1972. *J. Fac. Sci. Hokkaido Univ. Ser. VI, Zool.* 18(3): 356-365.
7. Fontaine, M.-Th., et al. 1989. *Crustaceana* 57(2): 208-216.
8. Schreiber, P. 1964. *Zoologica* 49: 217-243.
9. Herrick, F. H. 1896. *Bull. U. S. Fish Comm.* 15: 1-252.
10. Yonge, C. M. 1932. *Proc. Roy. Soc. Lond., Ser. B.* 111: 298-329.
11. Harrison, F. W., and A. G. Humes (eds.). 1992. *Microscopic Anat. Invert.* 10: 459 pp.
12. Stevenson, R. J. 1961. *Biol. Bull.* 121: 554-560.
13. Aiken, D. E., and S. L. Waddy. 1982. *J. Crust. Biol.* 2: 315-327.
14. Talbot, P., and P. Zao. 1991. *J. Crust. Biol.* 11: 1-9.

Reference: *Biol. Bull.* 185: 320-321. (October, 1993)

## The Role of Chemical and Visual Cues in Agonistic Interactions of the American Lobster

*Liat J. Kaplan, Courtney Lowrance, Jennifer Basil, and Jelle Atema  
(Boston University Marine Program, Marine Biological Laboratory)*

When two American lobsters (*Homarus americanus*) fight in a paired agonistic encounter, one will eventually exhibit more aggressive behavior than the other and establish dominance (1, 2). Chemical, mechanical, and visual senses contribute to the outcome of these interactions, but the relative importance of each sense is not known. We thus examined the roles of vision and chemical substances (*i.e.*, urine) in agonistic encounters between lobsters.

A dominant lobster is usually larger (1) and more aggressive than a subordinate lobster. Both of these characteristics are at least partly visual, and the extent to which they determine the winner of an encounter is unknown. We therefore examined the role of vision in initial establishment of dominance. In addition, lobsters may secrete a chemical substance into their urine that communicates dominance status during fights. After dominance has been established in an initial encounter between two lobsters, the subordinate lobster will be less aggressive in subsequent fights, resulting in a decrease in fight duration. We examined whether natural urine release is necessary for the decrease in second fight duration in encounters between previously matched lobsters.

*General Procedures:* Dominance interactions were examined by pairing two lobsters in a "boxing match." Two lobsters were placed into a 340-l "boxing tank" and their interactions were recorded on videotape for 20 min. The taped record was viewed in 5-s intervals. In each interval, a rank of aggression—from -2 (extremely submissive) to 4 (extremely aggressive)—was assigned to each lobster, based on stereotypical categories of behavior

that it exhibited. Fight duration was defined as the time between first approach and the point at which the subordinate lobster stopped approaching the other animal. The percentage of intervals containing each aggression level was calculated for each fight.

*Experiment 1:* Twenty-four adult male lobsters were separated into 2 groups ("blindfold first" and "blindfold second") of 12 animals each. For the "blindfold first" group, two blindfolded lobsters were isolated in separate tanks for 48 h and then paired in a boxing match. Blindfolds were then removed and the lobsters were placed in separate communal tanks for two weeks so that their "memory" of each other would be erased (Karavanich, pers. comm.). The same pairs were then isolated for 48 h and were brought together for a second fight, without blindfolds. The "blindfold second" group underwent exactly the same procedure, except they fought first without blindfolds, then with blindfolds. Performances across groups were compared to determine whether there was a treatment order effect of blindfolding. To account for individual differences in behavior, a within-subject design was used, each animal serving as its own control.

*Experiment 2:* Four pairs of adult male lobsters were fitted with catheters attached to their nephropores (3). Each lobster was then fitted with a urine release device, and pairs were brought together for boxing matches. In first fights, the catheters were detached from the nephropores so each lobster could release its urine naturally. The lobsters (lobster A and lobster B) were then isolated from each other for 24 h; during this time their urine was collected for at least 12 h. Each pair was then matched a



second time, with catheters attached to block natural urine release. The urine collected from each lobster before the second fight was diluted 20:1 with seawater to mimic the natural dilution of urine in the gill current. During the fight, this urine was released manually from syringes connected to the urine release devices. Fifteen seconds into the fight, 5 ml of diluted urine was released for 3 s from lobster A, but only when he was facing and within one body length of his opponent, regardless of the opponent's orientation. Fifteen seconds later the same procedure was followed for lobster B. This procedure continued for the entire 20-min duration of the fight. At no time were both lobsters releasing urine simultaneously.

**Results:** In Experiment 1, there were significant differences (Kruskal-Wallis,  $P < 0.05$ ) in aggression level 1 between groups in the nonblindfolded condition and in level 2 between groups in the blindfolded condition, indicating that there was an order effect. In the blindfolded fight of the "blindfold first" group, the average percentages of levels 0 and 1 were significantly higher, and the average percentage of level 2 was significantly lower, than in the nonblindfolded fight (Wilcoxon Signed Rank,  $P < 0.05$ ), indicating that under blindfolded conditions there is diminished detection of the opponent. This could explain why the percentage of time they spent in physical contact (level 2) was lower than in nonblindfolded fights. We found no significant difference between aggression-level percentages in the first and second fights of the "blindfold second" group. No significant difference was found between the durations of first and second fights in the "blindfold first" group (first fight mean =  $520 \pm 348$  s, second fight mean =  $374 \pm 167$  s) or the "blindfold second" group (first fight mean =  $577 \pm 383$  s, second fight mean =  $378 \pm 257$  s). Finally, no significant difference was found in duration between groups for the nonblindfolded or the blindfolded condition. The finding that fight duration is not affected

when lobsters are blindfolded, despite subtle differences in fighting behavior, suggests that vision is not important in initial agonistic encounters. Because lobsters are nocturnal and learn much of their fighting behavior under relatively dark conditions, vision may be less important than the other senses.

In Experiment 2, there were subtle changes in behavior between natural and manual urine release fights; later studies will explore these trends. Durations of first (natural urine release) and second (manual urine release) fights were not significantly different (first fight mean =  $732 \pm 354$  s, second fight mean =  $858 \pm 259$  s; Student's t-test,  $P > 0.05$ ). These data indicate that the lobsters did not recognize each other, perhaps because natural urine release was blocked by catheters, in the second match of each trial. It may be that the timing of manual urine release did not mimic the natural timing. Alternatively, a cue necessary for communicating dominance may be released only during aggressive encounters and may therefore have been absent in the urine that was collected overnight and released manually. The presence of investigator-controlled squirts of the animal's nonfight urine appeared not to have a significant effect on fighting behavior.

We can therefore conclude that vision does not play an important role in the initial establishment of dominance and that natural urine release is necessary for recognition in repeated encounters.

Supported by NIH 2POINS25915-04A1 to J. A.

#### Literature Cited

1. Scrivener, J. C. E. 1971. *Fish. Res. Board Can. Tech. Rep.* 235: 1-128.
2. Karavanich, C., and J. Atema. 1991. *Biol. Bull.* 181: 359-360.
3. Lindstrom, D. 1991. MA thesis, Boston University Marine Program, Woods Hole, MA.

Reference: *Biol. Bull.* 185: 321-322. (October, 1993)

### Agonistic Encounters in the American Lobster, *Homarus americanus*: Do They Remember Their Opponents?

Christy Karavanich and Jelle Atema (Boston University Marine Program, Marine Biological Laboratory)

Dominance is important in male lobsters for many reasons. Previous studies have demonstrated that female lobsters choose to mate with locally dominant males (1, 2, 3, 4). Dominant males also obtain more desirable shelters, which they need for protection (4, 5). The dominance of a particular lobster depends on its size, sex, molt state, and previous experience (6, 7). In aquaria, lobsters will form dominance hierarchies (6, 8, 9), and highly aggressive interactions can be observed during formation of these hierarchies. Subsequently, interactions are reduced to simple approach and retreat behaviors, similar to what is observed in the field (4). The mechanisms maintaining these hierarchies are unknown, but the alternatives are that subordinates recognize aggressive state and avoid all lobsters more dominant

than themselves or lobsters recognize particular individuals and act dominant or submissive based on previous encounters.

Twenty pairs of size-matched, adult male lobsters were isolated for 48 h. Each pair was then allowed to interact in a 340-l tank for a 20-min videotaped match, during which a dominance relationship was established. After a postfight isolation of 24 h, 10 pairs were rematched against their original opponents in a second fight. In the other 10 pairs, the subordinates of the first fights were matched against an unfamiliar dominant. Each animal was assigned a relative aggression rank for each 5-s period on a scale of -2 to 4, ranked in whole number intervals. Negative numbers denoted submissive behaviors, and increasingly positive numbers indicated escalating aggression. The period necessary to establish

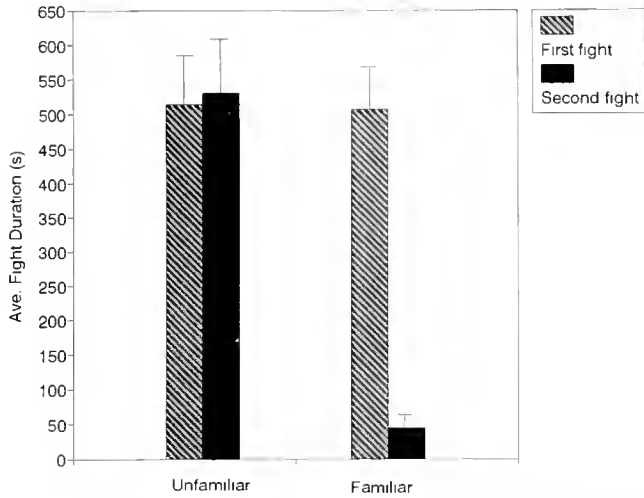


**Figure 1.** Average duration of all fights ( $\pm$ SEM). A 2-way ANOVA was performed and demonstrated a significant difference between the average duration of the fights ( $F$ -ratio = 5.04,  $P$  = .0376). The only significant difference resulted from comparing the average duration of the second fights between the familiar and unfamiliar opponent groups ( $F$ -ratio = 7.02,  $P$  = .0163).

a winner (fight duration) was determined by recording the time after which subordinates failed to show any aggression above level 1.

Subordinates rematched against former opponents "remember" the outcome of the first match: they backed away almost immediately, thus avoiding a potentially costly second fight (Fig. 1). The subordinates in these second fights rarely earned aggression ranks above level 1. When subordinates were paired against unfamiliar dominants, however, they attempted to fight their new opponents, often showing aggression levels as high as

level 4. In 3 of the 10 fights between unfamiliar opponents, the previous subordinates won the match, yet no such reversals occurred in the fights between opponents that had encountered one another previously.

Lobsters distinguish between familiar and unfamiliar opponents. That first-fight subordinates attempted to challenge a new opponent implies that dominant, aggressive state alone does not maintain a hierarchy. Preliminary studies suggest that subordinates maintained in a chronic submissive state investigate strange, dominant opponents, but are less likely to challenge them aggressively. A continual dominant or submissive state may alter internal motivation. However, such a confined situation would rarely occur naturally. Field studies have shown that although some lobsters remain in the same area, permitting repeated recognition of individuals, others are transient, allowing for encounters with unfamiliar lobsters (4, 10, 11). The results presented here suggest that submissive lobsters act conservatively when encountering familiar opponents of known, higher dominance status, but "test" the strength of unknown lobsters.

Supported by NIH 2POINS25915-04A1 to J. A.

#### Literature Cited

1. Atema, J., et al. 1979. *Mar. Behav. Physiol.* 6: 277-296.
2. Cowan, D., and J. Atema. 1990. *Anim. Behav.* 39: 1199-1206.
3. Karnofsky, E., and H. Price. 1989. *Mar. Behav. Physiol.* 15: 101-121.
4. Karnofsky, E., et al. 1989. *Biol. Bull.* 176: 239-246.
5. Jacobsen, S. 1977. Ph.D. Thesis, Boston Univ. Marine Program.
6. Scrivener, J. C. E. 1971. *Fish. Res. Board Can. Tech. Rep.* 235: 1-113.
7. Tamm, G., and S. Cobb. 1978. *Science* 200: 79-81.
8. Douglass, M. 1946. *Anat. Rec.* 96: 553.
9. Atema, J., and S. Cobb. 1980. Pp. 409-450 in *The Biology and Management of Lobsters*.
10. Pezzark, D., and D. Duggan. 1984. *Biol. Bull.* 167: 510-511.
11. Ennis, G. 1984. *Trans. Am. Fish. Soc.* 113: 330-335.

Reference: *Biol. Bull.* 185: 322-323. (October, 1993)

### The Impact of Feeding by Mussels and Scallops on Production of Dimethylsulfide From Marine Phytoplankton

Richard W. Hill (Department of Zoology, Michigan State University, East Lansing, MI 48824),  
John W. H. Dacey, Judith E. McDowell, and Dale F. Leavitt

Dimethylsulfide (DMS) originating from marine algae is implicated as an important gas in climate regulation (1, 2). Oxidation of DMS in the atmosphere forms aerosols, including cloud-condensation nuclei that increase cloud albedo (reflectivity) and thereby decrease penetration of solar radiation to the surface of the earth. A global increase in the flux of DMS to the atmosphere could cool the earth and decrease light available for photosynthesis, whereas a decrease in the DMS flux could exert opposite effects.

DMS from marine algae is derived from the decomposition of dimethylsulfoniopropionate (DMSP). Whereas some marine algae synthesize little or no DMSP, many manufacture substan-

tial quantities (3). The function of DMSP synthesis in algae is not well understood. Although DMSP is not volatile, DMS is.

Dacey and Wakeham (4) found that grazing by copepods greatly increases the rate of formation of DMS from DMSP-containing phytoplankton. Ecological processes are thus implicated in setting the rate at which DMS appears in the water column, which in turn helps determine the flux of DMS to the atmosphere.

To understand more generally the effects of phytoplanktivory on rates of DMS formation in the oceans, phytoplanktivores in addition to copepods must be studied. We therefore have examined two bivalve mollusks, the blue mussel (*Mytilus*

*edulis*) and the bay scallop (*Argopecten irradians*). These species were chosen because they can be abundant in coastal habitats, and their populations can filter large volumes of water (5).

Each study chamber was a 3.8-l jar containing 2 l of seawater. Gas in the jar was recirculated with a peristaltic pump, which drew gas from the space above the water and discharged it through an underwater bubbling stone. Preliminary tests had shown that any DMS that was formed in the jar would remain within, without leakage, for the duration of experiments.

Mussels (6–8 cm) and scallops (5–6 cm) were studied, respectively, in sets of five and two individuals/jar. Three replicate jars, plus a control jar containing seawater alone, were prepared for each species at 15–18°C. About 3 h after the jars were sealed, five aliquots (for the mussels) or six aliquots (for the scallops) of a culture of *Tetraselmis* UW474 were injected into each jar at 30–40 min intervals, for a total dose of DMSP of 2500–3000 nmol/jar. Each aliquot created a phytoplankton density of about  $10^4$  cells/ml and, in the animal-containing jars, was virtually cleared before the next addition. Cell density was kept to  $<10^4$ /ml to minimize the production of pseudofeces. After the last addition of phytoplankton, water samples were drawn periodically

for 24 h, the same duration as the copepod studies (4). Oxygen was added to replace that used metabolically.

Each water sample was filtered through a Gelman A/E glass fiber filter. Raw filtrate was assayed for DMS by cryofocusing and gas chromatography (Chromosil 330 column, Sievers 350B chemiluminescence detector). To quantify soluble DMSP, the filtrate was then incubated with cold base (KOH), which converted DMSP to DMS (6), and the assay of DMS was repeated. To quantify particulate DMSP, the filter was incubated in cold base, and the yield of DMS was measured.

Phytoplanktivory by mussels and scallops released little or no DMS from DMSP-containing phytoplankton during the first 24 h after feeding, in sharp contrast to grazing by copepods (Table I). The fate of the DMSP fed to the bivalves is not fully clear. Only 1–5% appeared as DMSP in the feces and pseudofeces, and just 0–1% appeared as soluble or particulate DMSP in the water. Significant amounts accumulated in the tissues of the bivalves but have not yet been adequately quantified.

These results show that phytoplanktivores can differ markedly in their effect on DMS release from phytoplankton. Further comparative study of phytoplanktivores will thus be required to understand the overall effect of phytoplanktivory on DMS flux in the oceans. The potential mechanisms of DMS formation during phytoplanktivory include autolysis of damaged but uningested algal cells, animal catabolism and excretion, and microbial activity in gut contents and feces. Mechanistic studies now deserve emphasis.

J. Burnett, E. Enos, D. Franks, B. Lancaster, F. Nichy, D. Radosh, S. Wigley, and Taylor Seafood made necessary contributions. Supported in part by Michigan State University, NSF OCE91-02532, and NASA NAGM-2431 and NAGW-2783.

Table I

Production of DMS during the first 24 h after grazing on DMSP-containing phytoplankton

Phytoplanktivore	Average DMS (nmol/l) accumulated in ambient water over 24 h		Average proportion (%) of ingested DMSP released as DMS in animal jars
	Animal jars	Control jar	
Mussels	9 (0.5–14)	4.5	0.7
Scallops	0 (0–0.5)	1.5	0
Copepods	204	8.4	36

DMS concentrations (nmol/l) in animal and control jars should be compared within lines, because differences in experimental detail confound comparison across lines. Ranges for animal jars are shown in parentheses for the present experiment. Data on copepods (*Labidocera aestiva* and *Centropages hamatus*) are from (4).

#### Literature Cited

1. Charlson, R. J., J. E. Lovelock, M. O. Andreae, and S. G. Warren. 1987. *Nature* 326: 655–661.
2. Falkowski, P. G., Y. Kim, Z. Kolber, C. Wilson, C. Wirick, and R. Cess. 1992. *Science* 256: 1311–1313.
3. Keller, M. D., W. K. Bellows, and R. R. L. Guillard. 1989. Pp. 167–182 in *Biogenic Sulfur in the Environment*, E. S. Saltzman and W. J. Cooper, eds.
4. Dacey, J. W. II., and S. G. Wakeham. 1986. *Science* 233: 1314–1316.
5. Kautsky, N., and I. Wallentinus. 1980. *Ophelia* Suppl. 1: 17–30.
6. Dacey, J. W. II., and N. V. Blough. 1987. *Geophys. Res. Lett.* 14: 1246–1249.

Reference: *Biol. Bull.* 185: 323–324. (October, 1993)

### Cerebral Blood Flow and Ventral Aortic Blood Pressure Response During Elevation of Intracranial Pressure in Bluefish (*Pomatomus saltatrix*)

John M. Beiner, Christopher S. Ogilvy, and Arthur B. DuBois (John B. Pierce Laboratory and Yale University School of Medicine, New Haven, CT 06519)

In mammals, blood pressure increases and the heart rate declines in response to intracranial pressures (ICP) above 40 mm Hg (1, 2). In bluefish, the threshold for the blood pressure response is zero mm Hg ICP, and tachycardia is elicited (3).

In this study we determined whether ICP reduces cerebral blood flow (CBF) and increases ventral aortic blood pressure in bluefish. Fish were anesthetized for 10 min in tricaine methanesulfonate, 50 mg/l, then set prone on a V-board above a

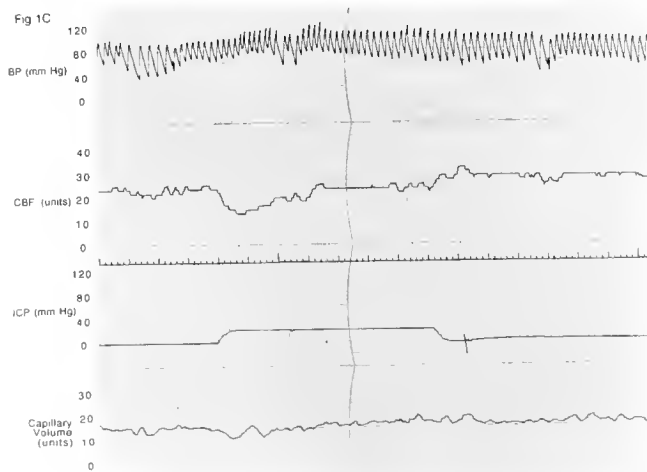
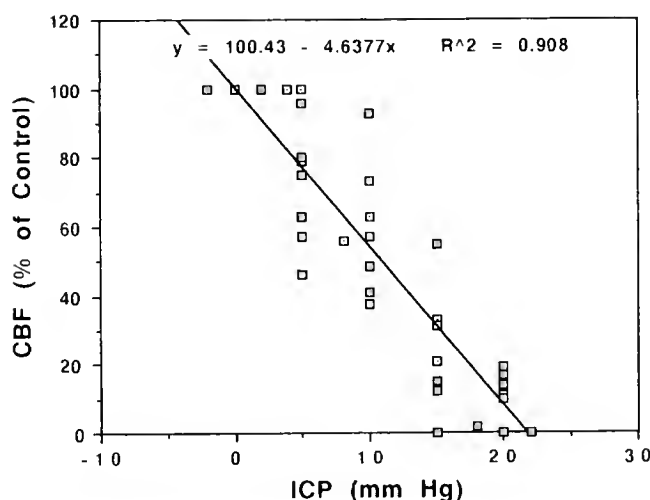
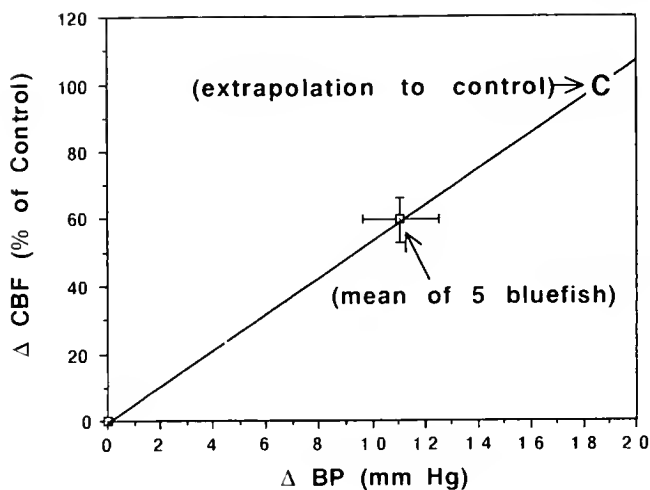


**Figure 1.** (A) Intracranial pressure (ICP) reduces cerebral blood flow (CBF) in 1 to 10 s (34 measurements in 5 bluefish). (B) Recovery from minimum cerebral blood flow ( $\Delta$ CBF) accompanying rise in ventral aortic blood pressure ( $\Delta$ BP) within 20–30 s in response to elevated intracranial pressures of 10, 15, 20, and 30 mm Hg (C) Ventral aortic blood pressure (BP) response to an increase of 20 mm Hg intracranial pressure (ICP)

wooden trough that contained a recirculating pump. Their gills were perfused with the anesthetic solution diluted 1:1 with seawater. The ventral aorta was catheterized for blood pressure measurements. Metal cranial implants were screwed into holes drilled into the right and left sides of the skull over the optic lobes. A laser-Doppler probe (Vasamedics, model P435) was inserted through one of the implants until the tip rested at the brain surface. Cerebral blood flow, volume, and velocity were measured with a model BPM 403A LaserFlo monitor. This apparatus compares favorably with  $H_2$  clearance and other blood flow measurement techniques (4, 5). The other implant was connected to a reservoir containing teleost-Ringer's solution, and pressurized with an air-filled syringe and mercury manometer. The intracranial pressure was recorded with a Statham pressure gauge. Intracranial pressure was elevated in fixed increments, from 5 to 60 mm Hg, for 30–35-second periods with five minutes recovery.

In five bluefish, elevation of ICP typically reduced CBF within seconds in proportion to ICP (Fig. 1A). At an ICP of 22 mm Hg, CBF ceased. In response, ventral aortic blood pressure increased in proportion to the increase of ICP (Fig. 1B). The increased blood pressure produced a partial or complete restoration of CBF (Fig. 1C) unless an ICP of 40 mm Hg or higher was reached, producing a maximum attainable blood pressure. Sustained elevation of ICP (20 mm Hg for 10–15 min) produced an initial reduction of brain capillary flow that was restored within 30 s by elevation of blood pressure to a new level that maintained some degree of brain capillary blood flow for the duration of the increased intracranial pressure. The blood pressure often oscillated about the elevated level.

Our conclusion is that blood pressure of bluefish is regulated by the need of these fish to supply their brains with adequate blood flow. This delivers oxygen to the brain (6). Carbon dioxide does not seem to affect the blood pressure response (7). In contrast to mammals, this control mechanism in bluefish overrides autoregulation of CBF and any other possible inhibitory mechanism in a reflex arc controlling blood pressure, such as the pseudobranch in fish (8) or baroreceptors in mammals.

Dr. Alan Hargens of NASA Ames Research Center supplied the laser-Doppler instrument for these studies.

### Literature Cited

1. Cushing, H. 1903. *Am. J. Med. Sci.* **125**: 1017–1044.
2. Ogilvy, C. S., and A. B. DuBois. 1987. *Biol. Neonate* **52**: 327–336.
3. Fox, S. H., C. S. Ogilvy, and A. B. DuBois. 1989. *Biol. Bull.* **177**: 328 (abstr.).
4. Dirnagl, U., et al. 1989. *J. Cerebral Blood Flow and Metabolism* **9**: 589–596.
5. Haberl, R., et al. 1989. *Am. J. Physiol.* **256** (Heart Circ. Physiol. **25**) H1247–H1254.
6. Fox, S. H., C. S. Ogilvy, and A. B. DuBois. 1990. *Biol. Bull.* **179**: 233 (abstr.).
7. Fox, S. H., A. B. DuBois, and C. S. Ogilvy. 1991. *Marine Biological Laboratories Archives*, October 1991 (abstr.).
8. Laurent, P. 1967. *C. R. Acad. Sci. Paris* **264**: 1879–1882.

of 35 s duration. Initially cerebral blood flow (CBF, units =  $ml\ min^{-1}$  per 100 g) falls, then slowly increases in response to a gradual increase of blood pressure, until flow is restored to approximately control levels. When ICP is released, flow shows an overshoot followed by a decline in response to bradycardia. (time interval: small ticks = 1 s)

Reference: *Biol. Bull.* **185**: 325. (October, 1993)

**Limulin and C-reactive Protein From the Plasma of *Limulus polyphemus* Are Different Proteins**  
*Subita Srimal (Molecular Biophysics Unit, Indian Institute of Science, Bangalore 560012, India),*  
*James P. Quigley, and Peter B. Armstrong*

The immune defenses of higher animals are mediated largely by cells, soluble proteins, and peptides in the blood. In the horseshoe crab, *Limulus*, immune defense activities conducted by the plasma include cytolysis of foreign cells and agglutination. The cytolytic activity is mediated in part by a *Limulus* homolog of mammalian C-reactive protein (1). The agglutinating activity is produced by a family of lectins, proteins of non-immune origin that bind to specific carbohydrates with high affinity. The best characterized lectin is limulin, which reacts with oligosaccharide chains having terminal sialic acid residues (2). Earlier reports have claimed that limulin and the *Limulus* homolog of C-reactive protein are the same protein (3, 4, 5). We report here that, contrary to these claims, limulin and C-reactive protein are different proteins, separable from each other by appropriate affinity purification steps.

Two sialic acid binding lectins homologous to limulin, *i.e.*, carcinoscorpin and tachyplesin, have been purified from the hemolymph of the horseshoe crabs *Carcinoscorpius rotundicauda* and *Tachyplesus tridentatus* (6, 7) by affinity chromatography on sialated glycoprotein-derivatized matrices. A similar strategy was applied to the purification of limulin from the hemolymph of *Limulus*, with hemagglutinating activity being determined as the minimal dilution that would agglutinate rabbit erythrocytes in buffer 1 (0.15 M NaCl, 10 mM CaCl<sub>2</sub>, 50 mM Tris pH 8.0). Limulin was purified by affinity chromatography successively on mucin- and fetuin-sepharose method as described by (8). Briefly, blood was collected from adult horseshoe crabs and allowed to clot at room temperature. The clarified serum was dialyzed against buffer 1 and passed over a bovine submaxillary mucin-sepharose column at 4°C. The bound proteins were eluted with 40 mM citrate buffer and dialyzed into buffer 1. Residual hemocyanin was removed from the limulin sample by anion exchange chromatography on DEAE-Sephadex under conditions such that limulin does not bind to the ion exchange matrix. Limulin was further purified by passage over fetuin-sepharose and the purified protein was concentrated and stored in small aliquots at -20°C. Purified limulin (1211-fold purification) had a specific activity of 25806 hemagglutination activity units/mg protein. C-reactive protein was purified from hemolymph by affinity chromatography on phosphorylethanolamine-sepharose as described previously (1).

Limulin and the *Limulus* homolog of C-reactive protein have similar subunit molecular weights, as determined by SDS-poly-

acrylamide gel electrophoresis. Limulin shows a pair of closely spaced bands at about 29 kDa, and C-reactive protein shows three closely spaced bands at about 25 kDa. The two proteins are different in their ligand specificity. C-reactive protein that had been purified on phosphorylethanolamine-sepharose failed to bind to fetuin-sepharose, and limulin purified on sialomucin- and fetuin-sepharose failed to bind to phosphorylcholine-sepharose and was recovered in the breakthrough fraction without a decrease in its hemagglutinating activity. C-reactive protein purified by elution from phosphorylethanolamine-sepharose contained a minor contaminant with a weak hemagglutinating activity. Moreover, fetuin and sialic acid both inhibited this hemagglutinating activity; therefore, the hemagglutinin contaminating the phosphorylethanolamine-sepharose-purified CRP may be limulin. Passage of C-reactive protein over fetuin-sepharose removed this minor contaminant.

C-reactive protein is present in the hemolymph at 1-5 mg/ml (3), a markedly higher concentration than limulin, which is present at 20-50 µg/ml. The concentrations of the homologous sialic-acid-binding lectins carcinoscorpin and tachyplesin in the hemolymph of *Carcinoscorpius* and *Tachyplesus* are 18-30 µg/ml (6, 7), values similar to those for limulin in *Limulus*. Thus the two important immune proteins of *Limulus* plasma, limulin and C-reactive protein, are different species.

This research was supported by Grant # MCB-218460 from the National Science Foundation.

### Literature Cited

1. Armstrong, P. B., J. P. Quigley, and M. T. Armstrong. 1993. *Mol. Immunol.* in press.
2. Kaplan, R., S. S. S. Li, and J. M. Kehoe. 1977. *Biochemistry* **16**: 4297-4303.
3. Robey, F. A., and T.-Y. Liu. 1981. *J. Biol. Chem.* **256**: 969-975.
4. Nguyen, N. Y., A. Suzuki, S. M. Cheng, G. Zon, and T.-Y. Liu. 1986. *J. Biol. Chem.* **261**: 10450-10455.
5. Nguyen, N. Y., A. Suzuki, R. A. Boykins, and T.-Y. Liu. 1986. *J. Biol. Chem.* **261**: 10456-10465.
6. Bishayee, S., and D. T. Dorai. 1980. *Biochim. Biophys. Acta* **623**: 89-97.
7. Shishigikura, F., and K. Sekiguchi. 1983. *J. Biochem.* **93**: 1539-1546.
8. Dorai, D. T., B. K. Bachhawat, S. Bishayee, K. Kannan, and D. R. Rao. 1981. *Arch. Biochem. Biophys.* **209**: 325-333.

Reference: *Biol. Bull.* 185: 326. (October, 1993)

## Identification and Partial Characterization of an Extracorporeal Protease Activity Secreted by the Triclad Turbellarid Worm, *Bdelloura candida*

Peter B. Armstrong (Department of Molecular and Cell Biology, University of California, Davis, CA 95616-8755), Paul M. Selzer, Niklas Ahlborg, Kerstin Morehead, Melissa Perregaux, Patricia Komuniecki, Richard Komuniecki, Subita Srimal, and Peter J. Hotez

*Bdelloura* is an ectoparasite found among the gill leaflets and on the cuticle of the legs of *Limulus* (1). We report here that *Bdelloura* releases into its environment a  $\text{Ca}^{+2}$ -dependent serine protease that may contribute to hook gill disease of *Limulus*. We used a small spatula and a moist paper towel to collect individual adult *Bdelloura* from freshly collected horseshoe crabs maintained in the Marine Resources Center of the Marine Biological Laboratory. About 100–200 *Bdelloura* individuals were maintained at 16°C in 10 ml seawater that had been sterilized by membrane filtration and that contained penicillin G (100 U/ml) and streptomycin sulfate (50 µg/ml). The filtered seawater was collected and replaced daily, and this *Bdelloura*-conditioned water was the source of the ectoprotease activity described in this report.

Samples of conditioned seawater were run on SDS-polyacrylamide gels that contained gelatin as described previously (2, 3). After electrophoresis, the protease activity was identified by the proteolytic clearance of the gelatin, as follows. The gel was washed in 2.5% Triton X100 to remove the SDS<sup>1</sup>, and was then incubated in 0.1 M glycine with 2 mM  $\text{CaCl}_2$ , pH 8.2, at 37°C for 12 h. The gel was then stained with Coomassie blue. Due to the presence of gelatin, the gel stained uniformly blue, except for a clear band at a position corresponding to a molecular mass of 49 kDa. This staining pattern indicates that *Bdelloura*-conditioned seawater contains a protease with molecular mass of 49 kDa that is capable of hydrolysing gelatin.

The hydrolysis of gelatin was inhibited when lanes of the gelatin gel were incubated in the presence of 5 mM PMSF or 5 mM EDTA (in the absence of  $\text{Ca}^{+2}$ ). The susceptibility to inhibition by PMSF is consistent with the identification of the protease as a serine protease, and the susceptibility to EDTA indicates that the proteolytic activity is dependent on  $\text{Ca}^{+2}$ . Leupeptin (10 µg/ml) and 0.5 mM TLCK were not inhibitory. The enzyme was active in the gelatin substrate gel at a neutral-to-basic pH and inactive at an acid pH.

The proteolytic activity of *Bdelloura*-conditioned seawater could also hydrolyze the amide substrate Boc-Leu-Gly-Arg-paranitroanilide. This activity appears also to be due to a  $\text{Ca}^{+2}$ -dependent serine protease because it was abolished by 20 mM EGTA and was 80% inhibited by 2 mM PMSF. The amidase activity was completely inhibited also by 1.7 mM benzamide, 10 µM leupeptin, and 10 µM antipain. The activity was partially inhibited by 1 mM TLCK; it was not inhibited by 0.1 mM 1, 10-phenanthroline, or 1 mg/ml SBTI. We know that the protease is produced by *Bdelloura*, and not by contaminating bacteria, because the addition of antibiotics to the seawater did not diminish the release of protease. The amount of proteolytic ac-

tivity in conditioned seawater decreased after 2–4 days, when *Bdelloura* were cultured separately from their *Limulus* hosts.

The *Bdelloura* protease appears to interact with some of the immune systems in *Limulus* hemolymph. *Bdelloura*-conditioned seawater promoted the clotting of coagulogen, the clottable protein released from stimulated blood cells (4). Normally, coagulogen is induced to clot by two specific proteolytic cleavages administered by clotting enzyme, a serine protease also released from the activated *Limulus* blood cells (4). In addition, the protease of *Bdelloura*-conditioned seawater appears to bind to  $\alpha_2$ -macroglobulin, a protease-binding protein found in the plasma of *Limulus* (5). Purified *Limulus*  $\alpha_2$ -macroglobulin was incubated with *Bdelloura*-conditioned seawater and then was chromatographed on a 100 cm column of Sephacryl S 300 HR gel filtration resin. The fractions eluted from the column were assayed for protease activity with the amide substrate. About one half of the amidase activity of *Bdelloura*-conditioned seawater co-purified with *Limulus*  $\alpha_2$ -macroglobulin after incubation with  $\alpha_2$ -macroglobulin (estimated molecular mass = 370 kDa), and the other half eluted at a position consistent with a molecular mass of approximately 40–60 kDa. All of the proteolytic activity was found at the low molecular mass elution position when *Bdelloura*-conditioned seawater that had not been exposed to  $\alpha_2$ -macroglobulin was subjected to chromatography on the S 300 column.

The egg cases and immature stages of *Bdelloura* are invasive to the gill leaflets of *Limulus*, causing lesions that are portals for the entry of bacteria and other pathogens (6, 7). The ectoproteases may facilitate the penetration of the integument of *Limulus* by *Bdelloura*. The interaction of the host's clotting system and  $\alpha_2$ -macroglobulin with the ectoproteases of the parasite may limit the extent of the damage wrought by the proteases once an individual *Bdelloura* penetrates the cuticle and contacts the hemolymph.

This research was supported by Grants # MCB 9218460 from the National Science Foundation (P. B. A.) and AI32726 from the National Institutes of Health (P. J. H.).

### Literature Cited

1. Rudloe, J. 1971. Pp. 183–185 in *The Erotic Ocean*. Thomas Y. Crowell Co., New York.
2. Quigley, J. P., R. S. Braithwaite, and P. B. Armstrong. 1993. *Differentiation*. In press.
3. Hotez, P. J., J. Haggerty, J. Hawdon, L. Milstone, H. Gamble, G. A. Schad, and F. F. Richards. 1990. *Infect. Immun.* 58: 3883–3892.
4. Iwanaga, S., T. Miyata, F. Tokunaga, and T. Muta. 1992. *Thrombos. Res.* 68: 1–32.
5. Armstrong, P. B., and J. P. Quigley. 1991. Pp. 291–310 in *Immunology of Insects and Other Arthropods*, A. P. Gupta, ed. CRC Press, Boca Raton, FL.
6. Groff, J. M., and L. Leibovitz. 1992. *Biol. Bull.* 163: 392.
7. Huggins, L. G., and J. H. Waite. 1993. *J. Exp. Zool.* 265: 549–557.

<sup>1</sup> Abbreviations: EDTA = ethylenediamine tetraacetic acid, EGTA = [ethylenbis(oxyethylenetriol)] tetraacetic acid, PMSF = phenylmethylsulfonyl fluoride, SBTI = soybean trypsin inhibitor, SDS = sodium dodecylsulfate, TLCK = L-1-tosyl-L-lysine chloromethyl ketone.

Reference: *Biol. Bull.* 185: 327. (October, 1993)

## Heme Biosynthesis in Fish and Land Vertebrates: Enzyme and cDNA Comparisons

Grace Bruning, Michael Ferkowicz, and Neal Cornell (Marine Biological Laboratory)

Heme is required by all living organisms for vital processes such as electron transport in mitochondrial oxidative phosphorylation and chloroplast photosynthesis, metabolism of hydroperoxides, transport of respiratory oxygen, and metabolism of toxicological and pharmacological chemicals as well as natural hydrophobic materials, e.g., steroid hormones. Each cell has to synthesize the heme needed for those processes. However, the rate of production must be well-regulated because excesses of either free heme or its precursors can have adverse consequences as evidenced by human porphyrias—diseases of heme metabolism that can be caused by inherited gene defects or by environmental pollutants (1).

Some regulatory features of heme biosynthesis are known. The biosynthetic pathway includes eight enzymatic reactions, and, in common laboratory species (rat, chicken), the first enzyme—5-aminolevulinic synthase (ALS)—plays the major role in determining the overall rate of heme production (2). Those animals have two forms of ALS: the erythroid type (E-ALS), which is expressed only in differentiating red blood cells, and a mitochondrial, housekeeping form (H-ALS) that occurs in almost all tissues. H-ALS is inducible by drugs and xenobiotics, e.g., barbiturates and polychlorinated biphenyls (3). Most important, heme influences the rate of its own production via feedback regulation of the tissue content of ALS, but the mechanism of that action has not been established.

Among the few studies in fish, results with rainbow trout indicated that as much as 30% of total hepatic ALS was cytoplasmic and that the hepatic activity of the biosynthetic pathway's second enzyme, aminolevulinic dehydratase (ALD), was much lower than that of ALS (4). This implied that fish heme synthesis has regulatory features that differ significantly from those in mammals. That report led us to measure the liver activity and subcellular distribution of ALS and ALD in rainbow trout, *Oncorhynchus mykiss*, and the marine teleost *Opsanus tau* (oyster toadfish). Our measurements showed that, in either fish, total liver activity of ALS is about 60-fold less than that of ALD. Subcellular distribution of hepatic ALS, measured with reference to marker enzymes for the cytoplasmic and mitochondrial compartments, indicated that this enzyme is more than 92% mitochondrial in toadfish and 100% mitochondrial in trout. These results show that rates of heme biosynthesis in teleosts, as in mammals, are limited by the activity of the mitochondrial enzyme, ALS.

Known inducers of ALS in terrestrial vertebrates include succinyl acetone, an inactivator of ALD (5), and N-methylprotoporphyrin IX and 3,5-diethoxy-carbonyl-1,4-dihydrocollidine, both of which inhibit ferrochelatase, the last of the eight enzymes (3). In cultured toadfish liver cells, the last two compounds increased ALS activity, respectively, by 7- and 3-fold. Succinyl acetone is particularly potent; at 0.5 mM it increased ALS activity of cultured toadfish liver cells by almost 20-fold, and that increase was completely blocked by 10  $\mu$ M heme added to the medium.

Similar results were obtained with cultured hepatoma cells from the topminnow, *Poeciliopsis lucida*. These inductions, and the apparent feedback action of heme, resemble regulatory phenomena observed in terrestrial vertebrates. A surprising difference, however, is that northern blots show that the induction of the fish enzyme by succinyl acetone occurs without a concomitant increase in the ALS mRNA. Thus, there probably are important posttranscriptional events in the regulation of heme biosynthesis in fish.

ALS is an enzyme of very low abundance in toadfish, as it is in other vertebrates. Consequently, recombinant DNA techniques were employed to obtain information about protein structure. We cloned cDNAs for both the E and H forms of toadfish ALS. Two criteria were used to confirm that the cDNAs encode ALS protein. One was that each cDNA gave rise to enzymatically active ALS when expressed in wild-type *E. coli*, and the other was that each was able to complement a mutation in the *hem A* strain, which otherwise cannot grow in the absence of added aminolevulinic, the product of the ALS reaction (6). The cDNAs were sequenced and have open reading frames that encode proteins with molecular weights of 65,000 and 70,000, in good agreement with the ALS subunit sizes in chickens (7), mice (8), rats (9), and humans (10). Amino acid sequence alignments indicate that two-thirds of the ALS protein at the carboxyl-terminal is highly conserved among vertebrates. That region shows 62 to 77% amino acid identity among E forms, and 80 to 82% identity among H forms of toadfish, birds, and mammals.

Further studies, in progress, will define the regulation of heme synthesis in marine fish. Our observations suggest that those studies will also help us to understand this process in humans and other mammals.

### Literature Cited

1. Moore, M. R., K. E. L. McColl, E. J. Fitzsimons, and A. Goldberg. 1990. *Blood Rev.* 4: 88–96.
2. May, B. K., I. A. Borthwick, G. Srivastava, B. A. Pirola, and W. H. Elliot. 1986. *Curr. Top. Cell. Regul.* 28: 233–262.
3. Marks, G. S., S. A. McCluskey, J. E. Mackie, D. S. Riddick, and C. A. James. 1988. *FASEB J.* 2: 2774–2783.
4. Addison, R. F., D. Fitzpatrick, and K. W. Renton. 1990. *Comp. Biochem. Physiol.* 95B: 317–319.
5. Ebert, P. S., R. A. Hess, B. C. Frykholm, and D. P. Tschudy. 1979. *Biochem. Biophys. Res. Commun.* 88: 1382–1390.
6. Sasarman, A., M. Surdeanu, and T. Horodniceanu. 1968. *J. Bacteriol.* 96: 1882–1884.
7. Riddle, R. D., M. Yamamoto, and J. D. Engel. 1989. *Proc. Natl. Acad. Sci. USA* 86: 792–796.
8. Schoenhaut, D. S., and P. J. Curtis. 1989. *Nucleic Acids Res.* 17: 7013–7028.
9. Yamamoto, M., S. Kure, J. D. Engel, and K. Hiraga. 1988. *J. Biol. Chem.* 263: 15973–15979.
10. Bawden, M. J., I. A. Borthwick, H. M. Healy, C. P. Morris, B. K. May, and W. H. Elliot. 1987. *Nucleic Acids Res.* 15: 8563.



Reference: *Biol. Bull.* 185: 328. (October, 1993)

## Near-UV Radiation Effects on Dogfish (*Mustelus canis*) Lens Catalase and Antioxidant Protection

Seymour Zigman (University of Rochester School of Medicine) and Nancy S. Rafferty (Northwestern University School of Medicine)

A disturbance of the oxidation-reduction balance in the lens is thought to be a contributing cause of cataracts.  $H_2O_2$  derived from metabolism and photochemistry disrupts this balance by increasing oxidative reactions. The resulting damage to the lens is thought to be one cause of human cataract formation. Catalase, which breaks down  $H_2O_2$  to form oxygen, is abundant in dogfish lens epithelial cells. Its activity would thus protect the lens from damage due to  $H_2O_2$  exposure. We have found that catalase activity in mammalian lens epithelial cells is inhibited by near-UV (UV-A) radiation (1, 2). The dogfish lens has high catalase activity and resists damage from levels of  $H_2O_2$  up to 0.1 mM. Thus, UV-A may decrease the capacity of the dogfish lens to resist oxidative insult due to  $H_2O_2$ . The sensitivity of catalase to near-UV energy is related to a near-UV chromophore that absorbs the radiation efficiently.

We aimed to determine whether the ability to detoxify  $H_2O_2$  in dogfish lens epithelial cells is inhibited by UV-A radiation, and whether the antioxidant  $\alpha$ -tocopherol or the free-radical-scavenger deferoxamine can protect this ability. We have previously shown that  $\alpha$ -tocopherol protects epithelial cells from near-UV-induced damage to cytoskeletal actin (3, 4).

Fresh dogfish lenses were incubated at 20°C in 20 ml of elasmobranch Ringer's medium (bicarbonate, pH 7.4) gassed with 95% air:5%  $CO_2$ . Lenses of similar weights were used, two pair per treatment; one lens from each animal served as a control, and the other was UV irradiated. The anterior surface of the lenses received about 1.5 mW/cm<sup>2</sup> of UV radiation at 360 nm (from a Woods lamp through a Pyrex beaker); this represents 80% of the total UV energy reaching to the specimens. In 14 h the lenses received 75.6 J/cm<sup>2</sup> of UV-A energy. Half of the lenses were preincubated for 6 h with either  $\alpha$ -tocopherol (0.01 mM) or deferoxamine (20 mM).

The transparency of the lenses was assessed by viewing a printed grid through them. Catalase activity was estimated by the reduction of the  $H_2O_2$  concentration of a 100  $\mu$ M solution after 30 min incubation with the lens. The concentration of  $H_2O_2$  was measured by the optical absorbance at 240 nm. The assay was calibrated with pure beef liver catalase (Sigma) in Ringer's medium (*i.e.*, Beer's assay). The lenses and their separated capsule epithelia were weighed to quantify specific catalase activities. The catalase-catalyzed reduction of  $H_2O_2$  was also visualized directly by the production of oxygen bubbles by lenses after incubation in  $H_2O_2$  for 1 h.

The qualitative findings are as follows. The images passing through UV-exposed opalescent lenses were not as sharp as those passing through the clear controls or those treated with UV plus  $\alpha$ -tocopherol. In a similar test, deferoxamine also maintained lens clarity. UV-exposed lenses untreated with  $\alpha$ -tocopherol or deferoxamine produced few oxygen bubbles in comparison with the irradiated samples with  $\alpha$ -tocopherol or deferoxamine added or with the controls. An examination by rhodamine-phalloidin fluorescence revealed that  $H_2O_2$  altered the cytoskeletal actin.

The quantitative data obtained by measuring the 240 nm absorbance loss in media containing 100  $\mu$ M  $H_2O_2$  are summarized

Table 1

Catalase activity in dogfish lens: effects of near-UV radiation and antioxidants

	Units of catalase per mg of lens capsule-epithelium <sup>+</sup>	Percent of control lens activity
a) $\alpha$ -tocopherol ( $10^{-5}$ M)		
Control	7.1	100
UV-exposed	2.5	35
Control plus $\alpha$ -tocopherol	6.4	85
UV-exposed plus $\alpha$ -tocopherol	6.4	85
b) Deferoxamine (20 mM)		
Control	14.0	100
UV-exposed	1.5	11
Control plus deferoxamine	21.7	155
UV-exposed plus deferoxamine	5.6	40

<sup>+</sup> Catalase assays were done in two separate experiments. The averages of two determinations are reported here. Deficiencies greater than 10% were observed between duplicates.

in Table 1. The controls and the UV-exposed lenses treated with  $\alpha$ -tocopherol were found to retain three times the catalase activity as UV-exposed lenses untreated with  $\alpha$ -tocopherol. With deferoxamine in the medium, UV exposure reduced the catalase activity by only 60% as compared to 90% inhibition without it. These agents protected against the UV-induced loss of lens clarity and loss of catalase activity equally. They also protected the ability of the lens to generate  $O_2$  bubbles from  $H_2O_2$ .

In summary, exposure of dogfish lenses in culture to UV-A energy less intense than that in sunlight caused lens opalescence that reduced the sharpness of images viewed through them. The opalescence was reduced by preincubation with  $\alpha$ -tocopherol (an antioxidant and free-radical scavenger) or with deferoxamine (an iron chelator that prevents OH-radical formation). The ability of the lens to break down a challenge of  $H_2O_2$  (*i.e.*, 100  $\mu$ M  $H_2O_2$ ) was impaired by UV exposure and was significantly protected by  $\alpha$ -tocopherol and deferoxamine.

Grant Support was from NIH (EY 00459) and Research to Prevent Blindness, Inc. (S. Zigman) and NIH (EY 00698; N. S. Rafferty). We would like to thank B. R. Zigman for technical assistance and for preparing the manuscript.

### Literature Cited

- Zigman, S., N. S. Rafferty, and K. Lowe. 1992. *Exp. Eye Res.* 55: 193-201.
- Zigman, S., T. Paxhia, T. McDaniel, J. Schultz, J. Reddan, J. Rafferty, and N. S. Rafferty. 1992. *Invest. Ophthalmol. & Vis. Sci.* (Suppl.) 33: 1039.
- Zigman, S., N. S. Rafferty, and R. B. Wheeler, Jr. 1991. *Biol. Bull.* 181: 341-342.
- Zigman, S., N. S. Rafferty, and S. Sooudi. 1992. *Biol. Bull.* 183: 372-373.

Reference: *Biol. Bull.* 185: 329–330. (October, 1993)

## RFLP Analysis of a Fragment of the Large-Subunit Ribosomal RNA Gene of Globally Distributed Populations of the Toxic Dinoflagellate *Alexandrium*

Bryan S. Judge (Michigan State University), Christopher A. Scholin (Monterey Bay Aquarium Research Institute), and Donald M. Anderson (Woods Hole Oceanographic Institution)

The dinoflagellate genus *Alexandrium* includes several species that produce potent neurotoxins responsible for paralytic shellfish poisoning (PSP). Commonly called "red tides," these events occur when shellfish and other marine animals consume the toxic phytoplankton as food, concentrating their toxins to levels that can cause illness and even death in consumers. PSP has been a problem for centuries in many of the world's coastal regions, but in recent years, the number of countries and areas affected has increased. This increase has been attributed in part to natural and human-assisted dispersal (1, 2). The evaluation of dispersal hypotheses depends on an understanding of the global biogeography of *Alexandrium* species, yet virtually nothing is known of their biogeography.

At the regional level, the inter- and intraspecific relationships of toxic *Alexandrium* have been assessed by morphological comparisons, isozyme electrophoresis, and toxin composition analysis (e.g., 3, 4, 5). Unfortunately, these methodologies often gave conflicting information about the relatedness of isolates of *Alexandrium* from different regions. Recently, sequence analysis of a fragment of the large-subunit ribosomal RNA gene (LsrDNA) from globally distributed *Alexandrium* isolates revealed eight distinctive classes of sequences, or "ribotypes" (6). For morphologically distinct species, such as *A. affine*, *A. minutum*, and *A. andersoni*, separate ribotypes are identified, confirming the validity of species designations based on morphology. However, for morphologically similar species within the so-called *A. tamarense/catenella* species complex (the "tamarensis group"), ribotypes appear to delineate regional populations, not morphospecies. Regarding the latter observation, isolates from the same geographic region have ribotypes that are similar, regardless of morphotype, whereas isolates from geographically distant populations display more divergent ribotypes even when the same morphospecies are compared (6).

Sequencing of LsrDNA has proven useful for assessing the inter- and intraspecific relationships of toxic *Alexandrium* strains, but it is also time consuming, tedious, and expensive. We therefore sought to develop a restriction-fragment-length polymorphism (RFLP) assay for each ribotype, to reduce analytical costs of our program of biogeographic surveys. To accomplish this goal, sequences representing each of the tamarensis group's ribotypes ("North American," "Western European," "Temperate Asian," "Tropical Asian," and "Tasmanian") and those of *A. affine*, *A. minutum*, and *A. andersoni* ("affine," "minutum," and "andersoni," respectively) were examined for restriction site polymorphisms. Based on this analysis, five restriction enzymes were selected that theoretically should distinguish each of these ribotypes, as well as "subribotypes" within the North American and Temperate Asian clusters (6).

To test the predictions, 11 isolates previously compared by LsrDNA sequencing were selected for trial RFLP analysis: (1) North American ribotype—PWO6 (*A. tamarense*); AFNFA4 (*A. fundyense*); OFO41 (*A. tamarense*); (2) Western European ribotype—WKS-1 (*A. tamarense*); (3) Temperate Asian

ribotype—OF101 (*A. catenella*); G. HOPE 1 (*A. tamarense*); (4) Tropical Asian ribotype—CU-13 (*A. tamarense*); (5) Tasmanian ribotype—ATTBO1 (*A. tamarense*); (6) "affine" ribotype—CU-1 (*A. affine*); (7) "minutum" ribotype—AMADO6 (*A. minutum*); (8) "andersoni" ribotype—TCO2 (*A. andersoni*).

Nucleic acid extractions and LsrDNA polymerase chain reaction (PCR) amplifications were performed as previously described (6). PCR-amplified LsrDNA from each isolate was then digested separately with *Nsp*-I, *Hinc*-II, *Apa*L-I, *Mse*-I, and *Afl*-III, following enzyme manufacturers' recommendations. Digestion products were resolved on 2.5% NuSieve (FMC Corp.), 1x

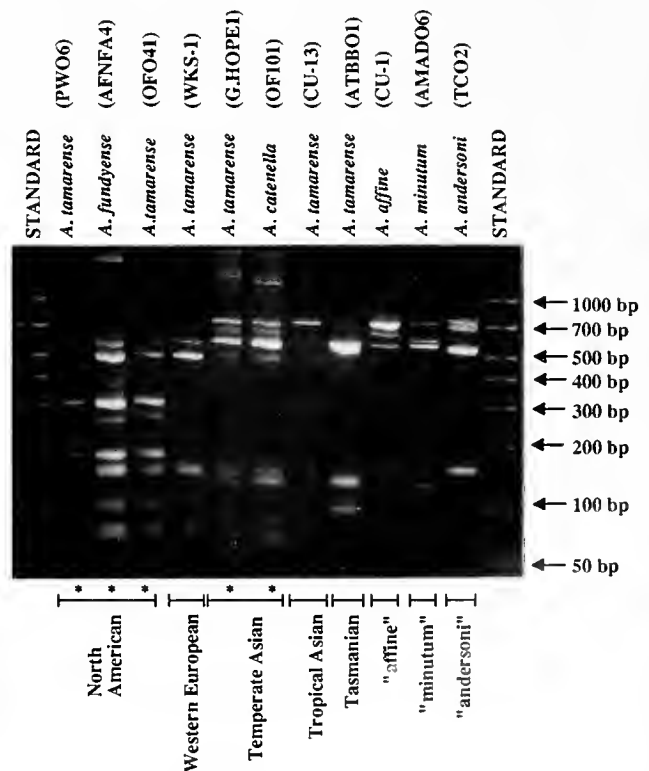


**Figure 1.** Agarose gel showing LsrDNA fragments from RFLP analysis of eleven isolates of *Alexandrium* that were digested with the restriction enzyme *Nsp*-I. Species designations are listed at the top of the figure followed by the isolate designation. Ribotype classifications, as determined from sequence analysis, are listed along the bottom of the figure. The \* represents subribotype classifications within the North American and Temperate Asian ribotypes (6). Ten restriction patterns were resolved with *Nsp*-I: one pattern each for the Western European, Tasmanian, Tropical Asian, "affine," "minutum," and "andersoni" ribotypes, and two patterns for the North American and Temperate Asian ribotypes. DNA standards are in the left and right lanes, with fragment sizes as indicated. Variability in the intensity of bands among lanes reflects differences in the amount of PCR product digested. With image enhancement, these differences were easily adjusted with the GelReader program.

TBE gels stained with ethidium bromide (7), and compared to size standards. Gel photographs were scanned, and then the National Center for Supercomputing Applications' GelReader computer program was used to identify bands indicative of restriction fragments.

Results to date demonstrate that patterns of restriction fragments delineate the major ribotypes, as well as subribotypes, represented by the 11 *Alexandrium* isolates used in this study. The most informative enzyme is *Nsp*-1, which yields 10 distinct patterns (Fig. 1). The remaining enzymes also yield restriction patterns that are useful in defining an isolate's ribotype, and in some cases subribotypes as well (data not shown). As an application of this concept, the RFLP assay employing five restriction enzymes was used to screen two uncharacterized *A. tamarense* and *A. catenella* isolates that matched two established ribotype patterns, coinciding with our predictions based on the isolates' geographic origins (data not shown). Thus, a suite of five enzymes appears to provide sufficient information to confidently assign ribotype designations to previously uncharacterized *Alexandrium* isolates.

In conclusion, implementation of the LsrDNA RFLP assay as a "front line" screening procedure of *Alexandrium* cultures will expedite their sorting and genetic characterization, and at the same time greatly reduce analytical costs per isolate. We expect this to facilitate a better understanding of the global biogeography of toxic *Alexandrium* species, hence providing a

stronger foundation from which to evaluate dispersal hypotheses (1, 2). Finally, as more isolates are examined with the RFLP technique, new ribotypes may be discovered. If so, the LsrDNA of these isolates will be sequenced, leading to a better definition of their specific characteristics, and the RFLP assay will be revised accordingly to incorporate these findings.

The technical assistance of D. M. Kulis is gratefully acknowledged. This study has been supported by funds from the Woods Hole Marine Sciences Consortium, Michigan State University, and a grant from the National Science Foundation (OCE89-11226).

### Literature Cited

1. Anderson, D. M. 1989. Pp. 11-16 in *Red Tides: Biology, Environmental Science, and Toxicology*, Okaichi, T., Anderson, D. M., and Nemoto, T., eds.
2. Hallegraeff, G. M., and C. J. Bolch. 1991. *Mar. Poll. Bull.* 22: 27-30.
3. Cembella, A. D., et al. 1987. *Biochem. Syst. and Ecol.* 15: 171-186.
4. Hayhome, B. A., et al. 1989. *Mar. Biol.* 101: 427-435.
5. Sako, Y., et al. 1990. Pp. 320-323 in *Toxic Marine Phytoplankton*, Graneli, E., Sundstrom, B., Edler, L., Anderson, D. M., eds.
6. Scholin, C. A. 1992. Analysis of toxic and non-toxic *Alexandrium* (Dinophyceae) species using ribosomal RNA gene sequences. Doctoral Dissertation, Woods Hole Oceanographic Institution.
7. Ausubel, F. M., et al., eds. 1987. Vols. 1 and 2 in *Current Protocols in Molecular Biology*.

Reference: *Biol. Bull.* 185: 330-331. (October, 1993)

## Effects of Macroalgae, Night and Day, on Ammonium Profiles in Waquoit Bay

Anne Bierzychudek, Charlene D'Avanzo, and Ivan Valiela (Marine Biological Laboratory)

We examined the vertical distribution of ammonium, a key limiting nutrient in marine ecosystems, in the water column at the Childs River, a eutrophic estuary within Waquoit Bay. Nutrient uptake by macroalgae and phytoplankton may alter ammonium concentrations between day and night. To measure changes in concentrations, vertical profiles of ammonium were sampled through the water column at dawn and dusk over bare sediments and in areas where dense macroalgal mats were present.

Data were collected by taking water samples, including water held within algal mats, at various depths with a vertical profiler on six separate days. The profiler apparatus consisted of a metal rod with tubing attached at 3-cm intervals. Samples were obtained within the algal mat and at 20- and 50-cm intervals throughout the water column. The rod was driven into the sediment on the bottom of the estuary. The tubes extended to the surface, and water samples were drawn from each depth with syringes. Ammonium concentrations of each sample were then analyzed by the indolephenol method (1).

Concentrations through the upper water column were uniformly low, with less than 2  $\mu$ M ammonium (Fig. 1). Highest ammonium concentrations occurred near the sediments, implying that nitrogen regeneration from decomposing organic

matter was the source of ammonium (Fig. 1). Within the algal mat, where advective and diffusive losses were reduced, ammonium concentrations were the highest, averaging up to 127  $\mu$ M ammonium (Fig. 1). At the top of the macroalgal mat, average concentrations ranged from 4-8  $\mu$ M ammonium, while at the same height above bare sediment, concentrations measured less than 1  $\mu$ M ammonium (Fig. 1). This was the result of advection mixing the ammonium in the water column and the algal mat retaining ammonium.

Ammonium concentrations were significantly higher at dawn than at dusk within the algal mat. At dawn there was an increase of 4-20  $\mu$ M ammonium between 147 and 180 cm depths as compared to ammonium measured at dusk (Fig. 1). Lower ammonium concentrations at dusk may be the result of plankton and macroalgae taking up ammonium during the day. At night photosynthesis stops, so uptake is reduced; regenerated ammonium is no longer completely intercepted and diffuses upward. In profiles over algal mats, a persistent ammonium peak occurred at a 120 cm depth for which we have no explanation (Fig. 1). This peak was observed in all six trials. Salinity gradients can be ruled out as causing this peak because the halocline occurred above one meter (Fig. 1).

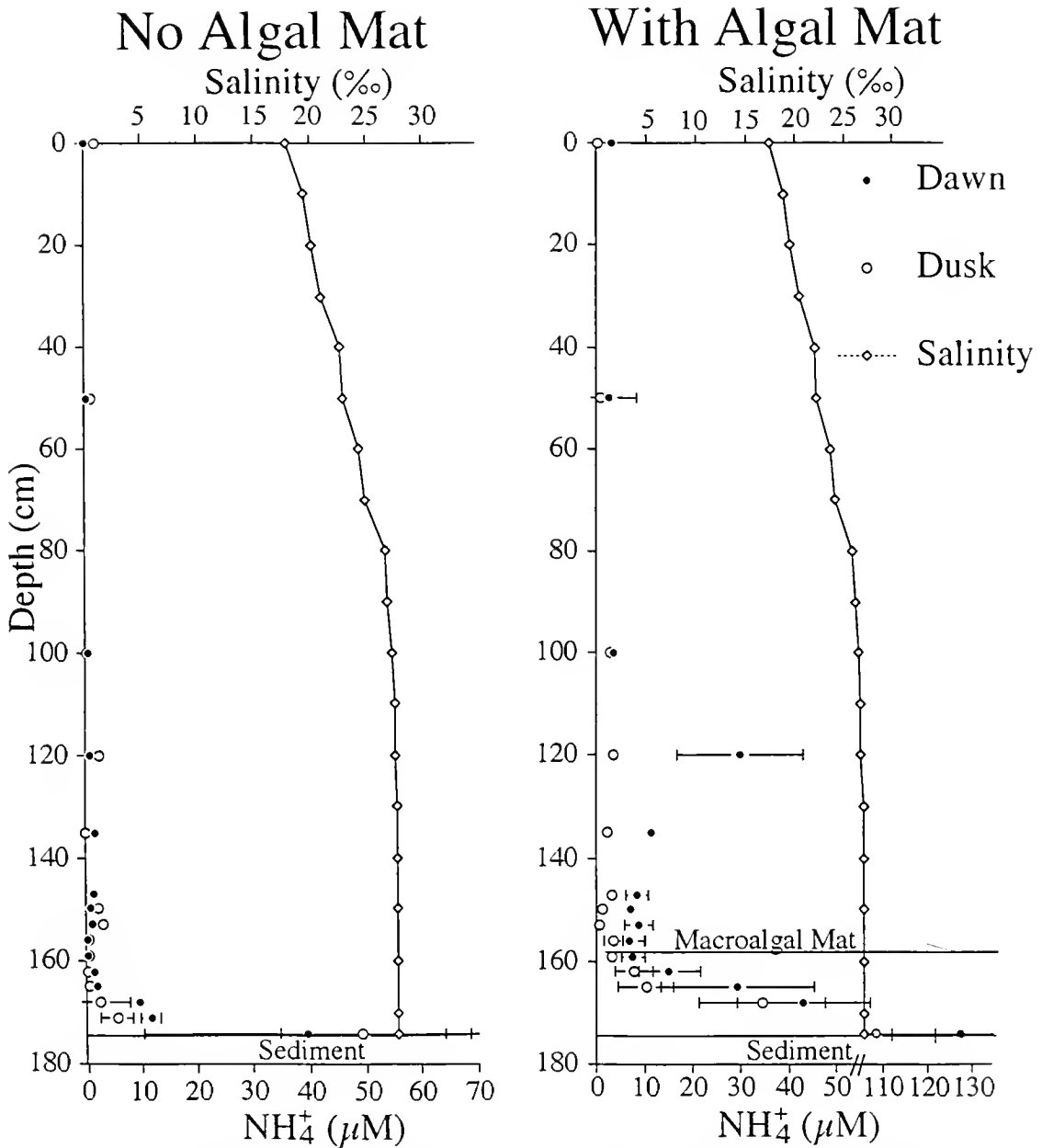


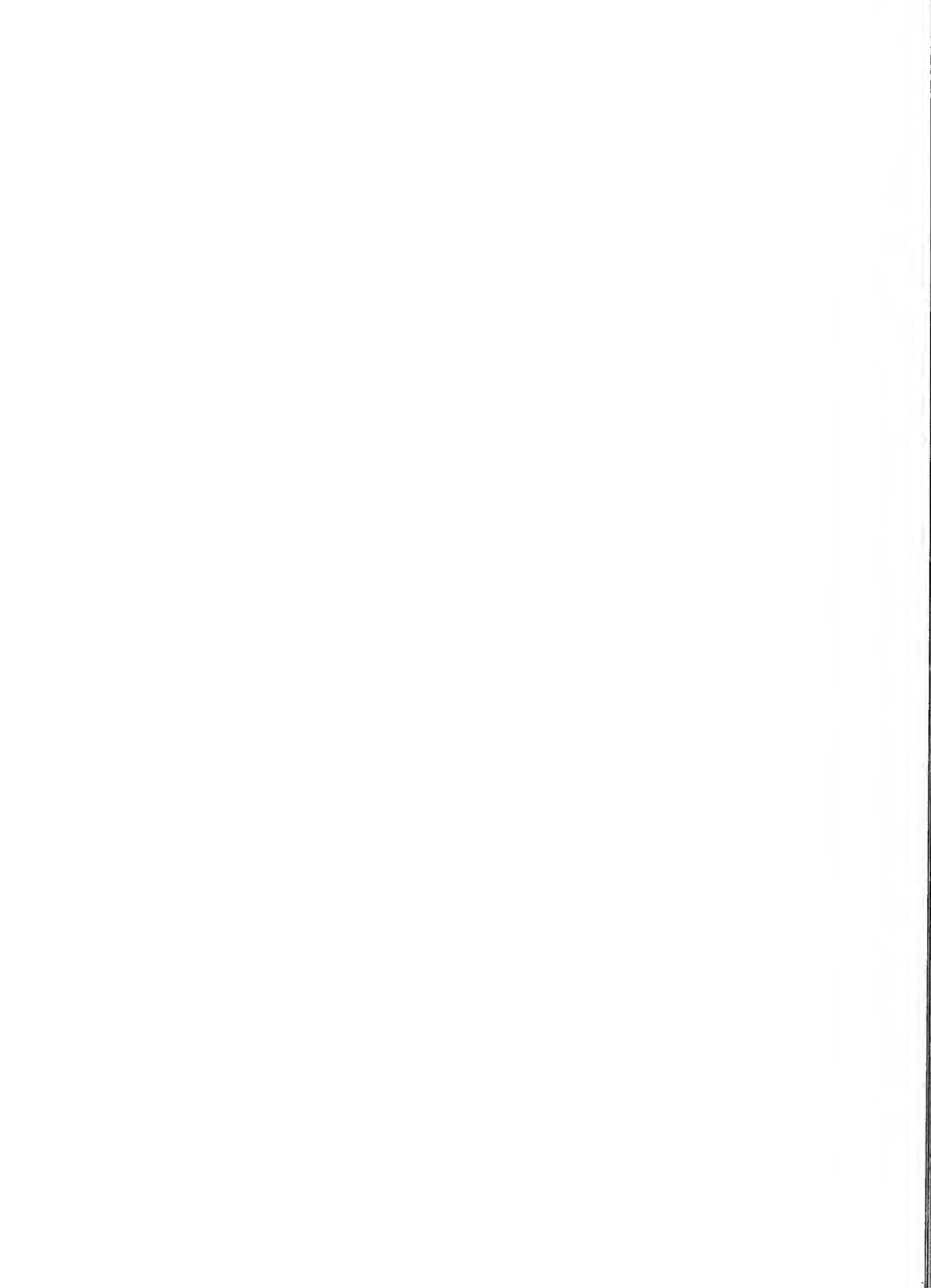
**Figure 1.** Vertical profiles of ammonium and salinity for the water columns of Waquoit Bay obtained at dawn and dusk over sites with a seaweed canopy and over bare sediment. The points are the average mean ( $\pm$  standard error) of six trials.

Overall, the profiles indicate that ammonium concentrations within macroalgal mats are higher than over bare sediment because the mat reduces water exchange, and the diurnal difference in ammonium concentrations within the mat is due to photosynthetic processes and nutrient uptake.

This work was supported by Waquoit Bay LMER.

**Literature Cited**

1. Solorzano, L. 1969. *Limnol. Oceanogr.* 12: 799.





# CONTENTS

## DEVELOPMENT AND REPRODUCTION

- McHugh, Damhnait**  
A comparative study of reproduction and development in the polychaete family Terebellidae . . . 153
- Sagi, Amir, Ellen Homola, and Hans Laufer**  
Distinct reproductive types of male spider crabs *Libinia emarginata* differ in circulating and synthesizing methyl farnesoate . . . . . 168
- Bauer, Raymond T., and Lin Jun Min**  
Spermatophores and plug substance of the marine shrimp *Trachypenaeus similis* (Crustacea: Decapoda: Penaeidae): formation in the male reproductive tract and disposition in the inseminated female . . 174
- Saperas, N., M. Chiva, N. C. Bols, D. Kulak, and H. E. Kasinsky**  
Sperm-specific basic proteins in the holocephalan fish *Hydrolagus colliei* (Chondrichthyes, Chimaeriformes) and comparison with protamines from an elasmobranch . . . . . 186
- Longo, Frank J., Lori Mathews, and Dennis Hedgecock**  
Morphogenesis of maternal and paternal genomes in fertilized oyster eggs (*Crassostrea gigas*): effects of cytochalasin B at different periods during meiotic maturation . . . . . 197
- Sousa, Mário, Rui Pinto, Pedro Moradas-Ferreira, and Carlos Azevedo**  
Histochemical studies of jelly coat of *Marthasterias glacialis* (Echinodermata, Asteroidea) oocytes . . . 215
- Sousa, Mário, and Carlos Azevedo**  
Ultrastructural histochemistry of *Marthasterias glacialis* (Echinodermata, Asteroidea) gametes before and after fertilization . . . . . 225

## ECOLOGY AND EVOLUTION

- Strathmann, R. R., L. Fenaux, A. T. Sewell, and M. F. Strathmann**  
Abundance of food affects relative size of larval and postlarval structures of a molluscan veliger . . . . . 232

## NEUROBIOLOGY AND BEHAVIOR

- Norekian, Tigran P., and Richard A. Satterlie**  
Co-activation of antagonistic motoneurons as a mechanism of high-speed hydraulic inflation of prey capture appendages in the pteropod mollusk *Chione limacina* . . . . . 240
- Norekian, Tigran P., and Richard A. Satterlie**  
FMRFamide and GABA produce functionally opposite effects on prey-capture reactions in the pteropod mollusk *Chione limacina* . . . . . 248

## PHYSIOLOGY

- Hovingh, Peter, and Alfred Linker**  
Glycosaminoglycans in *Anodonta californiensis*, a freshwater mussel . . . . . 263
- Pfeiler, Edward, and John J. Govoni**  
Metabolic rates in early life history stages of elopomorph fishes . . . . . 277
- Short Reports from the Marine Biological Laboratory's General Scientific Meetings** . . . . . 284



# THE BIOLOGICAL BULLETIN

Marine Biological Laboratory/  
Woods Hole Oceanographic Institution  
Library

JAN 14 1994

Woods Hole MA 02543



---

DECEMBER, 1993

---

Published by the Marine Biological Laboratory



# THE BIOLOGICAL BULLETIN

PUBLISHED BY  
THE MARINE BIOLOGICAL LABORATORY

Marine Biological Laboratory/  
Woods Hole Oceanographic Institution  
Library

## Associate Editors

JAN 14 1994

PETER A. V. ANDERSON, The Whitney Laboratory, University of Florida Woods Hole MA 02543

WILLIAM D. COHEN, Hunter College, City University of New York

DAVID EPEL, Hopkins Marine Station, Stanford University

J. MALCOLM SHICK, University of Maine, Orono

## Editorial Board

DAPHNE GAH FAUTIN, University of Kansas

WILLIAM F. GILLY, Hopkins Marine Station, Stanford University

ROGER T. HANLON, Marine Biomedical Institute, University of Texas Medical Branch

CHARLES B. METZ, University of Miami

K. RANGA RAO, University of West Florida

BARUCH RINKEVICH, Israel Oceanographic & Limnological Research Ltd.

RICHARD STRATHMANN, Friday Harbor Laboratories, University of Washington

STEVEN VOGEL, Duke University

SARAH ANN WOODIN, University of South Carolina

*Editor* MICHAEL J. GREENBERG, The Whitney Laboratory, University of Florida

*Managing Editor* PAMELA L. CLAPP, Marine Biological Laboratory

## DECEMBER, 1993

Printed and Issued by  
LANCASTER PRESS, Inc.

3575 HEMPLAND ROAD  
LANCASTER, PA

## THE BIOLOGICAL BULLETIN

THE BIOLOGICAL BULLETIN is published six times a year by the Marine Biological Laboratory, MBL Street, Woods Hole, Massachusetts 02543.

Subscriptions and similar matter should be addressed to Subscription Manager, THE BIOLOGICAL BULLETIN, Marine Biological Laboratory, Woods Hole, Massachusetts 02543. Single numbers, \$37.50. Subscription per volume (three issues), \$90.00 (\$180.00 per year for six issues).

Communications relative to manuscripts should be sent to Michael J. Greenberg, Editor-in-Chief, or Pamela L. Clapp, Managing Editor, at the Marine Biological Laboratory, Woods Hole, Massachusetts 02543. Telephone: (508) 548-3705, ext. 428. FAX: 508-540-6902. E-mail: pelapp@hoh.mbl.edu.

---

POSTMASTER: Send address changes to THE BIOLOGICAL BULLETIN, Marine Biological Laboratory, Woods Hole, MA 02543.

Copyright © 1993, by the Marine Biological Laboratory  
Second-class postage paid at Woods Hole, MA, and additional mailing offices.  
ISSN 0006-3185

---

## INSTRUCTIONS TO AUTHORS

*The Biological Bulletin* accepts outstanding original research reports of general interest to biologists throughout the world. Papers are usually of intermediate length (10–40 manuscript pages). A limited number of solicited review papers may be accepted after formal review. A paper will usually appear within four months after its acceptance.

Very short, especially topical papers (less than 9 manuscript pages including tables, figures, and bibliography) will be published in a separate section entitled "Research Notes." A Research Note in *The Biological Bulletin* follows the format of similar notes in *Nature*. It should open with a summary paragraph of 150 to 200 words comprising the introduction and the conclusions. The rest of the text should continue on without subheadings, and there should be no more than 30 references. References should be referred to in the text by number, and listed in the Literature Cited section in the order that they appear in the text. Unlike references in *Nature*, references in the Research Notes section should conform in punctuation and arrangement to the style of recent issues of *The Biological Bulletin*. Materials and Methods should be incorporated into appropriate figure legends. See the article by Lohmann *et al.* (October 1990, Vol. 179: 214–218) for sample style. A Research Note will usually appear within two months after its acceptance.

The Editorial Board requests that regular manuscripts conform to the requirements set below; those manuscripts that do not conform will be returned to authors for correction before review.

1. **Manuscripts.** Manuscripts, including figures, should be submitted in triplicate. (Xerox copies of photographs are not acceptable for review purposes.) The submission letter accompanying the manuscript should include a telephone number, a FAX number, and (if possible) an E-mail address for the corresponding author. The original manuscript must be typed in no smaller than 12 pitch, using double spacing (including figure legends, footnotes, bibliography, etc.) on one side of 16- or 20-lb. bond paper, 8½ by 11 inches. Please, no right justification. Manuscripts should be proofread carefully and errors corrected legibly in black ink. Pages should be numbered consecutively. Margins on all sides should be at least 1 inch (2.5 cm). Manu-

scripts should conform to the *Council of Biology Editors Style Manual*, 5th Edition (Council of Biology Editors, 1983) and to American spelling. Unusual abbreviations should be kept to a minimum and should be spelled out on first reference as well as defined in a footnote on the title page. Manuscripts should be divided into the following components: Title page, Abstract (of no more than 200 words), Introduction, Materials and Methods, Results, Discussion, Acknowledgments, Literature Cited, Tables, and Figure Legends. In addition, authors should supply a list of words and phrases under which the article should be indexed.

2. **Title page.** The title page consists of a condensed title or running head of no more than 35 letters and spaces, the manuscript title, authors' names and appropriate addresses, and footnotes listing present addresses, acknowledgments or contribution numbers, and explanation of unusual abbreviations.

3. **Figures.** The dimensions of the printed page, 7 by 9 inches, should be kept in mind in preparing figures for publication. We recommend that figures be about 1½ times the linear dimensions of the final printing desired, and that the ratio of the largest to the smallest letter or number and of the thickest to the thinnest line not exceed 1:1.5. Explanatory matter generally should be included in legends, although axes should always be identified on the illustration itself. Figures should be prepared for reproduction as either line cuts or halftones. Figures to be reproduced as line cuts should be unmounted glossy photographic reproductions or drawn in black ink on white paper, good-quality tracing cloth or plastic, or blue-lined coordinate paper. Those to be reproduced as halftones should be mounted on board, with both designating numbers or letters and scale bars affixed directly to the figures. All figures should be numbered in consecutive order, with no distinction between text and plate figures. The author's name and an arrow indicating orientation should appear on the reverse side of all figures.

4. **Tables, footnotes, figure legends, etc.** Authors should follow the style in a recent issue of *The Biological Bulletin* in

preparing table headings, figure legends, and the like. Because of the high cost of setting tabular material in type, authors are asked to limit such material as much as possible. Tables, with their headings and footnotes, should be typed on separate sheets, numbered with consecutive Roman numerals, and placed after the Literature Cited. Figure legends should contain enough information to make the figure intelligible separate from the text. Legends should be typed double spaced, with consecutive Arabic numbers, on a separate sheet at the end of the paper. Footnotes should be limited to authors' current addresses, acknowledgments or contribution numbers, and explanation of unusual abbreviations. All such footnotes should appear on the title page. Footnotes are not normally permitted in the body of the text.

5. **Literature cited.** In the text, literature should be cited by the Harvard system, with papers by more than two authors cited as Jones *et al.*, 1980. Personal communications and material in preparation or in press should be cited in the text only, with author's initials and institutions, unless the material has been formally accepted and a volume number can be supplied. The list of references following the text should be headed Literature Cited, and must be typed double spaced on separate pages, conforming in punctuation and arrangement to the style of recent issues of *The Biological Bulletin*. Citations should include complete titles and inclusive pagination. Journal abbreviations should normally follow those of the U. S. A. Standards Institute (USASI), as adopted by BIOLOGICAL ABSTRACTS and CHEMICAL ABSTRACTS, with the minor differences set out below. The most generally useful list of biological journal titles is that published each year by BIOLOGICAL ABSTRACTS (BIOSIS List of Serials; the most recent issue). Foreign authors, and others who are accustomed to using THE WORLD LIST OF SCIENTIFIC PERIODICALS, may find a booklet published by the Biological Council of the U.K. (obtainable from the Institute of Biology, 41 Queen's Gate, London, S.W.7, England, U.K.) useful, since it sets out the WORLD LIST abbreviations for most biological journals with notes of the USASI abbreviations where these differ. CHEMICAL ABSTRACTS publishes quarterly supplements of additional abbreviations. The following points of reference style

for THE BIOLOGICAL BULLETIN differ from USASI (or modified WORLD LIST) usage:

A. Journal abbreviations, and book titles, all underlined (for *italics*)

B. All components of abbreviations with initial capitals (not as European usage in WORLD LIST *e.g.*, *J. Cell. Comp. Physiol.* NOT *J. cell. comp. Physiol.*)

C. All abbreviated components must be followed by a period, whole word components *must not* (*i.e.*, *J. Cancer Res.*)

D. Space between all components (*e.g.*, *J. Cell. Comp. Physiol.*, not *J.Cell.Comp.Physiol.*)

E. Unusual words in journal titles should be spelled out in full, rather than employing new abbreviations invented by the author. For example, use *Rit Vísindafélags Íslendinga* without abbreviation.

F. All single word journal titles in full (*e.g.*, *Veliger, Ecology, Brain*).

G. The order of abbreviated components should be the same as the word order of the complete title (*i.e.*, *Proc.* and *Trans.* placed where they appear, not transposed as in some BIOLOGICAL ABSTRACTS listings).

H. A few well-known international journals in their preferred forms rather than WORLD LIST or USASI usage (*e.g.*, *Nature, Science, Evolution* NOT *Nature, Lond., Science, N.Y.: Evolution, Lancaster, Pa.*)

6. **Reprints, page proofs, and charges.** Authors receive their first 100 reprints (without covers) free of charge. Additional reprints may be ordered at time of publication and normally will be delivered about two to three months after the issue date. Authors (or delegates for foreign authors) will receive page proofs of articles shortly before publication. They will be charged the current cost of printers' time for corrections to these (other than corrections of printers' or editors' errors). Other than these charges for authors' alterations, *The Biological Bulletin* does not have page charges.

# VOLUME CONTENTS

NO. 1, AUGUST 1993

## BEHAVIOR AND BIOMECHANICS

- Drewes, Charles D., and Charles R. Fournier**  
Helical swimming in a freshwater oligochaete . . . 1
- Johnson, Amy S.**  
Sag-mediated modulated tension in terebellid tentacles exposed to flow . . . . . 10
- Trager, Geoff, and Amatzia Genin**  
Flow velocity induces a switch from active to passive suspension feeding in the porcelain crab *Petrolisthia leptochelae* (Heller) . . . . . 20

## ECOLOGY AND EVOLUTION

- Eckman, James E., and David O. Duggins**  
Effects of flow speed on growth of benthic suspension feeders . . . . . 28
- Garcia-Esquivel, Zaul, and V. Monica Bricelj**  
Ontogenetic changes in microhabitat distribution of juvenile bay scallops, *Argopecten irradians irradians* (L.), in eelgrass beds, and their potential significance to early recruitment . . . . . 42

## DEVELOPMENT AND REPRODUCTION

- Janies, Daniel A., and Larry R. McEdward**  
Highly derived coelomic and water-vascular morphogenesis in a starfish with pelagic direct development . . . . . 56
- Olson, Richard Randolph, J. Lane Cameron, and Craig M. Young**  
Larval development (with observations on spawning) of the pencil urchin *Phyllacanthus imperialis*: a new intermediate larval form? . . . . . 77

## INVERTEBRATE MORPHOLOGY AND PHYLOGENY

- Balser, Elizabeth J., Edward E. Ruppert, and William B. Jaekle**  
Ultrastructure of the coeloms of auricularia larvae

- (Holothuroidea: Echinodermata): evidence for the presence of an axocoel . . . . . 86
- Emschermann, Peter**  
Lime-twig glands: a unique invention of an Antarctic entoproct . . . . . 97

## NEUROBIOLOGY

- Westfall, Jane A., and Cornelis J. P. Grimmelikhuijzen**  
Antho-RFamide immunoreactivity in neuronal synaptic and nonsynaptic vesicles of sea anemones 109

## PHYSIOLOGY

- Baker, Shirley M., and Nora B. Terwilliger**  
Hemoglobin structure and function in the rat-tailed sea cucumber, *Paracaecum chilense* . . . . . 115
- Kreeger, D. A., and C. J. Langdon**  
Effect of dietary protein content on growth of juvenile mussels, *Mytilus trossulus* (Gould 1850) . . . 123
- Sevala, V. M., V. L. Sevala, and A. S. M. Saleuddin**  
Hemolymph insulin-like peptides (ILP) titers and the influence of ILP and mammalian insulin on the amino acid incorporation in the mantle collar *in vitro* in *Helisoma* (Mollusca) . . . . . 140

## RESEARCH NOTE

- Lohmann, Kenneth J., and Catherine M. Fittinghoff Lohmann**  
A light-independent magnetic compass in the leatherback sea turtle . . . . . 149
- Annual Report of the Marine Biological Laboratory** R1

NO. 2, OCTOBER 1993

## DEVELOPMENT AND REPRODUCTION

- McHugh, Damhnait**  
A comparative study of reproduction and development in the polychaete family Terebellidae . . . 153
- Sagi, Amir, Ellen Homola, and Hans Laufer**  
Distinct reproductive types of male spider crabs *Li-*

- bmia emarginata* differ in circulating and synthesizing methyl farnesoate . . . . . 168
- Bauer, Raymond T., and Lin Jun Min**  
Spermatophores and plug substance of the marine shrimp *Trachypenaeus similis* (Crustacea: Decapoda: Penaeidae): formation in the male reproductive tract and disposition in the inseminated female . . 174

**Saperas, N., M. Chiva, N. C. Bols, D. Kulak, and H. E. Kasinsky**

Sperm-specific basic proteins in the holocephalan fish *Hydrolagus colliei* (Chondrichthyes, Chimaeriformes) and comparison with protamines from an elasmobranch . . . . . 186

**Longo, Frank J., Lori Mathews, and Dennis Hedgecock**

Morphogenesis of maternal and paternal genomes in fertilized oyster eggs (*Crassostrea gigas*): effects of cytochalasin B at different periods during meiotic maturation . . . . . 197

**Sousa, Mário, Rui Pinto, Pedro Moradas-Ferreira, and Carlos Azevedo**

Histochemical studies of jelly coat of *Marthasterias glacialis* (Echinodermata, Asteroidea) oocytes . . . . . 215

**Sousa, Mário, and Carlos Azevedo**

Ultrastructural histochemistry of *Marthasterias glacialis* (Echinodermata, Asteroidea) gametes before and after fertilization . . . . . 225

**ECOLOGY AND EVOLUTION**

**Strathmann, R. R., L. Fenaux, A. T. Sewell, and M. F. Strathmann**

Abundance of food affects relative size of larval and postlarval structures of a molluscan veliger . . . . . 232

**NEUROBIOLOGY AND BEHAVIOR**

**Norekian, Tigran P., and Richard A. Satterlie**

Co-activation of antagonistic motoneurons as a mechanism of high-speed hydraulic inflation of prey capture appendages in the pteropod mollusk *Clione limacina* . . . . . 210

**Norekian, Tigran P., and Richard A. Satterlie**

FMRFamide and GABA produce functionally opposite effects on prey-capture reactions in the pteropod mollusk *Clione limacina* . . . . . 218

**PHYSIOLOGY**

**Hovingh, Peter, and Alfred Linker**

Glycosaminoglycans in *Anodonta californensis*, a freshwater mussel . . . . . 263

**Pfeiler, Edward, and John J. Govoni**

Metabolic rates in early life history stages of elopomorph fishes . . . . . 277

**Short Reports from the Marine Biological Laboratory's General Scientific Meetings . . . . . 284**

NO. 3, DECEMBER 1993

**EDITORIAL**

**Greenberg, Michael J.**

An animal resources section and a Marine Models Electronic Record for *The Biological Bulletin* . . . . . 333

**CELL BIOLOGY**

**Mire-Thibodeaux, Patricia, and Glen M. Watson**

Direct monitoring of intracellular calcium ions in sea anemone tentacles suggests regulation of nematocyst discharge by remote, rare epidermal cells . . . . . 335

**Murray, Thomas F., and Joseph F. Siebenaller**

Differential susceptibility of guanine nucleotide-binding proteins to pertussis toxin-catalyzed ADP-ribosylation in brain membranes of two congeneric marine fishes . . . . . 346

**Toomey, Barbara Holland, and David Epel**

Multixenobiotic resistance in *Urechis caupo* embryos: protection from environmental toxins . . . . . 355

**Chaparro, O. R., R. J. Thompson, and J. E. Ward**

*In vivo* observations of larval brooding in the Chilean oyster, *Ostrea chilensis* Philippi, 1845 . . . . . 365

**Chintala, Marnita M., and Victor S. Kennedy**

Reproduction of *Stylochus ellipticus* (Platyhelminthes: Polycladia) in response to temperature, food, and presence or absence of a partner . . . . . 373

**Gaseoigne, Lisa, and Alistair McVean**

Postembryonic growth of two peripheral sensory systems in the medicinal leech *Hirudo medicinalis* . . . . . 388

**ECOLOGY AND EVOLUTION**

**Ariani, A. P., K. J. Wittmann, and E. Franco**

A comparative study of static bodies in mysid crustaceans: evolutionary implications of crystallographic characteristics . . . . . 393

**Gardner, J. P. A., D. O. F. Skibinski, and C. D. Bajdik**

Shell growth and viability differences between the marine mussels *Mytilus edulis* (L.), *Mytilus galloprovincialis* (Lmk.), and their hybrids from two sympatric populations in S.W. England . . . . . 105

**Halanych, Kenneth M.**

Suspension feeding by the lophophore-like apparatus of the pterobranch hemichordate *Rhabdopleura nommami* . . . . . 117

## NEUROBIOLOGY AND BEHAVIOR

- Candelario-Martinez, A., D. M. Reed, S. J. Prichard, K. E. Doble, T. D. Lee, W. Lesser, D. A. Price, and M. J. Greenberg**  
SCP-related peptides from bivalve mollusks: identification, tissue distribution, and actions . . . . . 428

## PHYSIOLOGY

- Menon, Jaishri G., and Alissa J. Arp**  
The integument of the marine echiuran worm *Urechis caupo* . . . . . 440

- Shashar, N., Y. Cohen, and Y. Loya**  
Extreme diel fluctuations of oxygen in diffusive boundary layers surrounding stony corals . . . . . 455

## RESEARCH NOTE

- Schetz, John A., and Peter A. V. Anderson**  
A reevaluation of the structure in the pore region of voltage-activated cation channels . . . . . 462

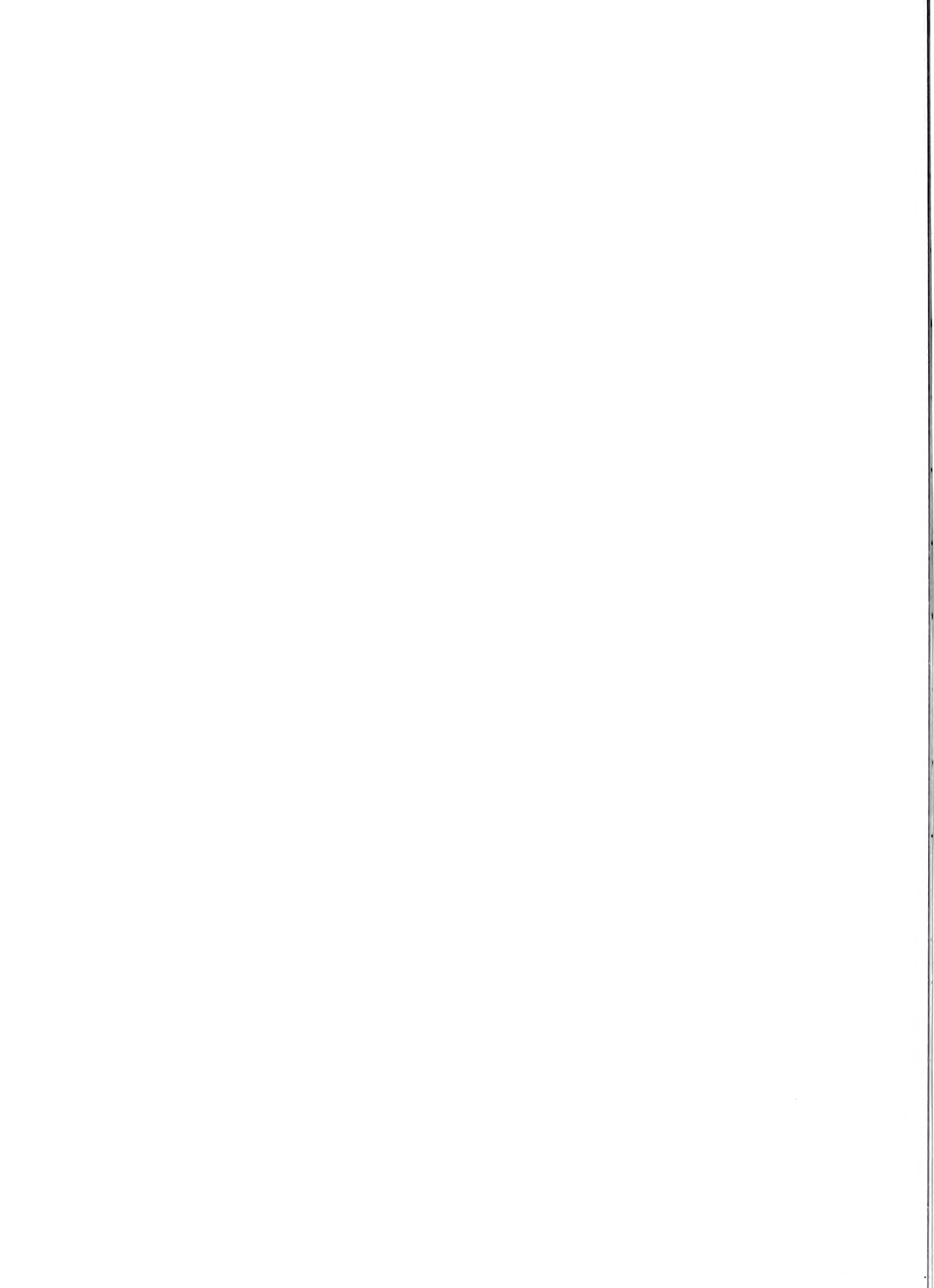
- Index to Volume 185 . . . . . 467

**Notice to Subscribers**

The 1994 subscription rate for *The Biological Bulletin* will be \$180 for the year (6 issues: \$90 for 3 issues). Back and single issues are \$37.50, and subject to availability. For additional information, please contact our subscription officer at the Marine Biological Laboratory, Woods Hole, MA 02543; tel: (508) 548-3705, ext. 428.







## An Animal Resources Section and a Marine Models Electronic Record for *The Biological Bulletin*

With the next issue of the *Biological Bulletin* (February, 1994; Volume **186**, Number 1), we inaugurate a new section of the journal devoted to nonmammalian marine organisms that serve, either altogether or in part, as experimental models in basic biological research. Of special interest will be reports on the collection and husbandry of these model organisms, the preparation of their cells or tissues, and research techniques specifically applicable to them.

This new animal resources section should help in promoting the use of marine organisms for the study of fundamental problems in biology and, if that goal is fulfilled, it should also make the road easier for the converts. To those ends, the section will:

- Present methods, new and old, in greater detail than would be possible in a typical research paper, including even the minor details that make a procedure work;
- Preserve, in some cases, years of practical experience in an organized and accessible form;
- Provide an outlet for results obtained at the Marine Resources Center of the Marine Biological Laboratory and at similar facilities throughout the world; and
- Identify widely distributed sets of models, any of which could be used to perform a given experiment, but (on the other hand) some of which may have special advantages.

Notwithstanding the compelling argument for a section on model organisms, difficulties do emerge. For example, we would expect the reports submitted to this section to be quite practical and thus to appeal to interests much narrower than those of the general readership of *The Biological Bulletin*. But presented in the aggregate, as reviews or integrated clusters of papers about a particular model, the appeal and value of these data should broaden dramatically. However, such reviews could appear only slowly (no more than two per year), whereas contributions about a variety of species and biological processes are ready or are being written *now*. In addition, these reviews, like all

others, would begin to age from the moment of their publication.

Therefore, to speed availability, solve the temporal discrepancy between contribution and print publication, and retard obsolescence, the marine resources section will be published both electronically and in print—but not necessarily in the same format or at the same time. Here is how the system will work:

- *The Biological Bulletin* and the Division of Information Systems of the Marine Biological Laboratory will establish and publish a Marine Models Electronic Record (*BB-MMER*). The database will comprise numerous subdivisions (called drawers), each characterized by both an organism (*e.g.*, *Limulus polyphemus*) and some phenomenon that it models (*e.g.*, vision). The *BB-MMER* will provide hypertext links between the drawers since, for example, horseshoe crabs are also used to study immune responses.

- Papers on marine models that are submitted (on disk, or hard copy) to *The Biological Bulletin* will be reviewed, evaluated, and edited as usual. Once accepted, these reports will be published immediately in the *BB-MMER* where they will be accessible to researchers everywhere.

- Because the reports in the *BB-MMER* will have been reviewed, they can be cited like any other paper or short report appearing in the *Bulletin*. Furthermore, each printed issue of the *Bulletin* will include a list of reports added to the *BB-MMER*, together with a brief summary of each.

- Once the contributions in a drawer have ripened, they will be retrieved and integrated, and a printed review or compendium will be produced. Conversely, once the data have been reviewed, additions to the drawer in the *BB-MMER* will keep them fresh and current. These important functions will be in the hands of a drawer-editor who will also be a member of *The Biological Bulletin* editorial board.

The possibilities for this new section of *The Biological Bulletin*, for its novel mode of publication, and for the

entrance of this nonagenarian journal into the world of cyberspace are manifest. As for the details—*e.g.*, submission, citation, access, preparation of reviews—they will be forthcoming in the February issue, and they will be widely publicized.

Note that some of the published details will be vague, and in any event, *none* of them will be carved in stone. This enterprise will evolve over several years, and we will always be interested in your ideas and comments. You

can send them to: William D. Cohen,<sup>1</sup> the associate editor for this section; Catherine N. Norton,<sup>2</sup> who heads the Division of Information Systems and will be our electronic publisher; or me.<sup>3</sup>

—Michael J. Greenberg

<sup>1</sup> W. D. Cohen (FAX: 212-772-5227; E-mail:cohen@mvaxbl.hunter.cuny.edu)

<sup>2</sup> C. N. Norton (508-540-6902; cnorton@mbi.edu)

<sup>3</sup> M. J. Greenberg (904-461-4008; michael@icbr.ifas.ufl.edu)

# Direct Monitoring of Intracellular Calcium Ions in Sea Anemone Tentacles Suggests Regulation of Nematocyst Discharge by Remote, Rare Epidermal Cells

PATRICIA MIRE-THIBODEAUX AND GLEN M. WATSON

*Department of Biology, The University of Southwestern Louisiana, Lafayette, Louisiana 70504-2451*

**Abstract.** In tentacles of sea anemones, cnidocytes and adjacent supporting cells are believed to be independent receptor-effector complexes that regulate nematocyst discharge in response to exogenous N-acetylated sugars. When sugar chemoreceptors on supporting cells are activated, nematocyst discharge is two- to threefold greater than discharge without chemosensitization. To examine the role of  $Ca^{2+}$  as a second messenger in chemodetection of sugars, we used fluo-3 to monitor  $Ca^{2+}$  levels in epidermal cells of intact anemone tentacles. Certain epidermal cells exhibit relatively high  $Ca^{2+}$  both with and without chemosensitization. With chemosensitization, a two- to threefold increase occurs in the abundance of relatively rare cells exhibiting the highest  $Ca^{2+}$  levels. Timecourses depicting abundances of these rare cells in chemosensitized specimens show positive correlations to timecourses for nematocyst discharge from chemosensitized specimens and for labeling of chemoreceptors. Cnidocyte/supporting-cell complexes discharging nematocysts are about three times more abundant than the rare cells exhibiting the highest intracellular  $Ca^{2+}$  levels. One interpretation of these data is that the  $Ca^{2+}$ -dependent regulation of nematocyst discharge occurring with chemosensitization involves intense  $Ca^{2+}$  signaling by remote, rare cells. This interpretation is inconsistent with the current model that portrays cnidocyte/supporting-cell complexes as independent effectors of nematocyst discharge.

## Introduction

Sea anemones and other cnidarians, such as jellyfishes, hydras, and corals, are simple animals that use complex

secretory products called nematocysts for prey capture, defense, and aggression. Nematocysts, consisting of intracellular capsules containing highly folded, eversible tubules, are produced in and deployed from effector cells called cnidocytes (Skaer and Picken, 1965). Cnidocytes within tentacles discharge nematocysts in response to appropriate chemical and mechanical stimulation (Pantin, 1942b; Thorington and Hessinger, 1988a, b). Discharge involves a rapid and forceful eversion of the tubule (Holstein and Tardent, 1984). Depending on the type of nematocyst, the everting tubule may penetrate the target to release potent toxins or adhere to the surface of the target (Mariscal, 1974). Although cnidocytes are abundant in tentacles, each nematocyst can be used only once (Robson, 1988). Thus, it is advantageous for the animals to control nematocyst discharge, and several cnidarians have been found to exercise such control (Pantin, 1942b; Williams, 1968; Lubbock, 1979; Thorington and Hessinger, 1988a).

In tentacles of the sea anemone *Haliplanella luciae*, nematocyst discharge is regulated, at least in part, by receptor-effector complexes composed of cnidocytes and supporting cells (Watson and Hessinger, 1989). According to the current model, chemoreceptors on supporting cells detect substances derived from suitable target organisms and sensitize mechanoreceptors to trigger discharge upon physical contact between the tentacles and the target organism. Of the chemical stimuli that modulate discharge, most is known about the effects of N-acetylated sugars. Cnidocyte/supporting-cell complexes (CSCCs) discharge nematocysts in response to both free and conjugated N-acetylated sugars. The response is dose-dependent: at optimal doses of the sugars ( $10^{-7}$  M for *Haliplanella*), a two- to threefold increase in discharge is detected compared to

that in seawater alone (Thorington and Hessinger, 1988a, b; Watson and Hessinger, 1987, 1989). The supporting-cell chemoreceptors are cycled via receptor-mediated endocytosis so that receptor number changes over time (Watson and Hessinger, 1987, 1989). Interestingly, nematocyst discharge to optimal doses of sugars also changes over time and exhibits a strong positive correlation to temporal changes in numbers of activated surface chemoreceptors.

Relatively little is known about the specific cellular interactions or intracellular processes regulating nematocyst discharge. To investigate  $\text{Ca}^{2+}$  as a second messenger in the chemodetection of sugars, we used fluo-3 to monitor  $\text{Ca}^{2+}$  levels in intact tentacles exposed to optimal levels of sugar and to seawater alone.

### Materials and Methods

#### Reagents

Bovine submaxillary mucin, type I, and rhodamine-dextran 10 s (MW = 9000) were obtained from Sigma; calcium ionophore 4-bromo A23187, fluo-3 AM, and pluronic acid F-127 were obtained from Molecular Probes.  $\text{Ca}^{2+}$ -free artificial seawater ( $\text{Ca}^{2+}$ -free ASW) was prepared in deionized water as follows: NaCl (448 mM), KCl (9 mM),  $\text{MgCl}_2 \cdot 6\text{H}_2\text{O}$  (23 mM),  $\text{MgSO}_4 \cdot 7\text{H}_2\text{O}$  (25 mM),  $\text{NaHCO}_3$  (2 mM), and EGTA (2 mM) (Sigma). Magnesium/seawater (MgSW) was prepared by dissolving 0.6 M  $\text{MgCl}_2 \cdot 6\text{H}_2\text{O}$  in deionized water and then diluting 1:1 with natural seawater.

#### Animal maintenance

Monoclonal specimens of the sea anemone *Haliplanella luciae* were cultured in Pyrex dishes containing natural seawater at 32‰ and held at 22–24°C. The anemones were maintained on a 12:12 photoperiod and fed brine shrimp nauplii (San Francisco Bay) twice weekly. Experiments were performed about 72 h after feeding.

#### Microscopy

Anemones were prepared for microscopy by anesthetizing them for 60 min in one of two media. MgSW was used for experiments in which fluo fluorescence and autofluorescence were monitored in the presence of external  $\text{Ca}^{2+}$ .  $\text{Ca}^{2+}$ -free ASW was used when  $\text{Ca}^{2+}$ -independent fluo fluorescence was monitored. These solutions served as media during labeling, washing, and viewing of the specimens.

For experiments involving fluo, whole animals were incubated in a 20- $\mu\text{M}$  fluo-3 AM solution for 40 min at 23°C and then washed twice for 10 min each. Tentacles were excised, placed on glass coverslips, and secured with glass micropipettes (tip diameters of <1 mm) by applying

gentle suction with microinjectors (Narashigi). The tentacles were viewed with an IMT2 Olympus inverted microscope using a 40 $\times$  SPlan objective (n.a. = 0.9). The fluorescence light source used was a 100-W halogen lamp set at 12 V with a Leitz power supply. This light source caused virtually no detectable radiation damage to the specimens and produced negligible autofluorescence. In contrast, preliminary work using a 100-W mercury lamp showed extensive radiation damage to specimens (the tissue rapidly deteriorated) and produced more autofluorescence. Images were taken with a cooled CCD camera (–15°C typical, 192 H  $\times$  165 V pixel array; Electrim Inc.), exposure time 20 s, and analyzed using VGACAM (Electrim Inc.) and IPPLUS software (Media Cybernetics).

For studies of morphology and organization of cells in intact tissue, excised tentacles were viewed with DIC optics (DPlanApo100UV objective [n.a. = 1.30] and BHS-2 APlanat Achromat DIC condenser [n.a. = 1.4], modified to fit the IMT-2 microscope). Video images were digitally processed using a Hamamatsu Argus 10 processor. Video recordings (8 mm) were made while focusing through the tissue to facilitate tracking of cell processes through optical sections. From these recordings, images were captured, enhanced, and analyzed using Image 1 software and hardware. To permit visualization of supporting cells and sensory cells, tentacles were depleted of cnidae by exposure to a hypotonic seawater solution prepared by diluting MgSW 1:1 with distilled water. The osmotic stress promotes cnida extrusion from tissue while leaving other cells intact for several hours.

#### Timecourse experiments for intracellular $\text{Ca}^{2+}$

Timecourse experiments were performed with unlabeled or fluo-labeled tentacles in which fluorescence was monitored in epidermal cells following exposure either to MgSW (controls) or to MgSW containing optimal doses ( $10^{-7}$  M) of mucin, a glycoprotein with many terminal N-acetylated sugars (mucin treatment). For each experiment, a single tentacle was excised, secured, and allowed to recover for 10 min in washing medium. This solution was then replaced with a fresh drop of medium appropriate for the experimental condition, and areas of the tentacle epidermis were imaged at 5-min intervals for 60 min. Specimens remained in the dark between exposures. A single image was made at each of the 13 timepoints.

#### Ascertaining $\text{Ca}^{2+}$ -dependent fluorescence and testing effects of mucin

To verify  $\text{Ca}^{2+}$ -dependent fluo fluorescence in tentacles and to test the effects of mucin on  $\text{Ca}^{2+}$ -dependent fluo fluorescence, four timecourse experiments were performed. To determine the intensity of autofluorescence,

unlabeled tentacles were imaged. To determine the intensity of fluo fluorescence in the absence of Ca<sup>2+</sup>, fluo-labeled tentacles were incubated for 1 h in 10  $\mu$ M calcium ionophore, 4-Bromo A23187, prepared in Ca<sup>2+</sup>-free ASW and then exposed to 10<sup>-7</sup> M mucin prepared in Ca<sup>2+</sup>-free ASW prior to imaging. To examine Ca<sup>2+</sup>-dependent fluo fluorescence and the effect of mucin on Ca<sup>2+</sup>-dependent fluo fluorescence, labeled tentacles were imaged in MgSW alone or after exposure to 10<sup>-7</sup> M mucin. For each of these experiments, gray-level values were recorded (from 0 to 255) for the 10 most intensely fluorescent epidermal cells at each timepoint. Means were calculated from these values and then averaged from replicate experiments to derive a mean maximum fluorescence value for each timepoint. Such derived values provided an index of the fluorescence intensity, over time, for the brightest cells per treatment, taking into account day-to-day variation between experiments.

#### *Correlation to chemoreceptor activity*

Preliminary observations suggested that fluo-labeled tentacles showed an increase in abundance of the brightest epidermal cells upon exposure to mucin. This phenomenon was examined in greater detail by counting the brightly fluorescent cells in fluo-labeled tentacles in either MgSW alone or with the addition of 10<sup>-7</sup> M mucin. A *brightly fluorescent cell* (BFC) was defined as one having a gray-level value at least 20 levels higher than the mean maximum fluorescence of the tentacle. This mean value was calculated by averaging gray-level values for the 10 most intensely fluorescent epidermal cells for each image acquired during a timecourse experiment. This step normalized data against day-to-day variations in labeling intensity. A gray-level value of 20 was selected for defining BFCs because it approximated the mean standard deviation for the mean maximum fluorescence of the tentacles used for the five replicate experiments. Data indicating number of BFCs were pooled from five replicate experiments for each condition (MgSW alone or 10<sup>-7</sup> M mucin in MgSW).

#### *Timecourse experiment for nematocyst discharge*

To measure nematocyst discharge in the absence of N-acetylated sugars, timecourse experiments were performed using the procedure described by Watson and Hessinger (1989). These results were compared to previously published timecourses for discharge following exposure to sugars (Watson and Hessinger, 1989) and to timecourses depicting the abundance of BFCs in both the absence and presence of N-acetylated sugars.

Briefly, anemones were removed from the mass culture and placed in small petri dishes filled with natural seawater. After a recovery of 3–4 h, the medium was replaced

with fresh natural seawater. After 10 min in the fresh medium, tentacles were touched with gelatin-coated test probes. Following glutaraldehyde fixation, the probes were prepared as wet mounts and the microbasic p-mastigophore nematocysts discharged into the gelatin were counted. Counts were recorded from a single field of view (10 $\times$  oculars, 40 $\times$  objective, and phase contrast optics) for each probe. For each timepoint, four replicate probes were used; one probe for each of four anemones. A mean discharge value  $\pm$  standard error was calculated by averaging data from two separate experiments for each timepoint.

#### *Identification of cells involved*

Supporting cells were identified by exploiting their ability to endocytose. Fluo-labeled tentacles were incubated in a 0.1% dextran-rhodamine/seawater solution for 15 min, rinsed quickly, and viewed immediately. Whereas fluo-3 AM is cell permeant, dextran-rhodamine is cell impermeant but may enter cells by endocytosis. With free Ca<sup>2+</sup>, fluo-3 has an excitation maximum at 506 nm, an emission maximum at 526 nm, and negligible fluorescence above approximately 600 nm (Minta *et al.*, 1989). Dextran-rhodamine has an excitation maximum at 570 nm and an emission maximum at 590 nm (Molecular Probes, Inc.). Each of the two indicators was visualized with optics to optimize excitation and emission of the desired indicator while prohibiting significant, coincidental excitation and emission of the other indicator (for fluo-3, a BP-490 excitation filter that permits transmittance between 450 and 500 nm; for dextran-rhodamine, a BP-545 + supplemental exciter filter EO-530 that permits transmittance between 500 and 570 nm and an additional R-610 barrier filter that prevents transmission of emitted light below approximately 600 nm). Because supporting cells are the only epidermal cells known to endocytose (Watson and Hessinger, 1987, 1989), paired images of double-labeled tentacles were used to determine which of the cells exhibiting fluo fluorescence were likely to be supporting cells.

#### *Ratio of BFCs to nematocysts discharged*

Specimens were exposed to seawater alone or to seawater containing 10<sup>-7</sup> M N-acetylneuraminic acid (NANA) for 10 min, then touched with gelatin-coated test probes. The average density of BFCs imaged (see above) in the epidermis of intact tentacles ( $n = 5$ ) was compared with the density of nematocysts and other cnidae discharged into test probes ( $n = 10$ ). We estimated the area of the tentacle epidermis imaged to be 2112  $\mu$ m<sup>2</sup>, half the total field of view of the camera. Areas on test probes subjectively evaluated to have the greatest number of nematocysts were scored. Microbasic p-mastigophore ne-

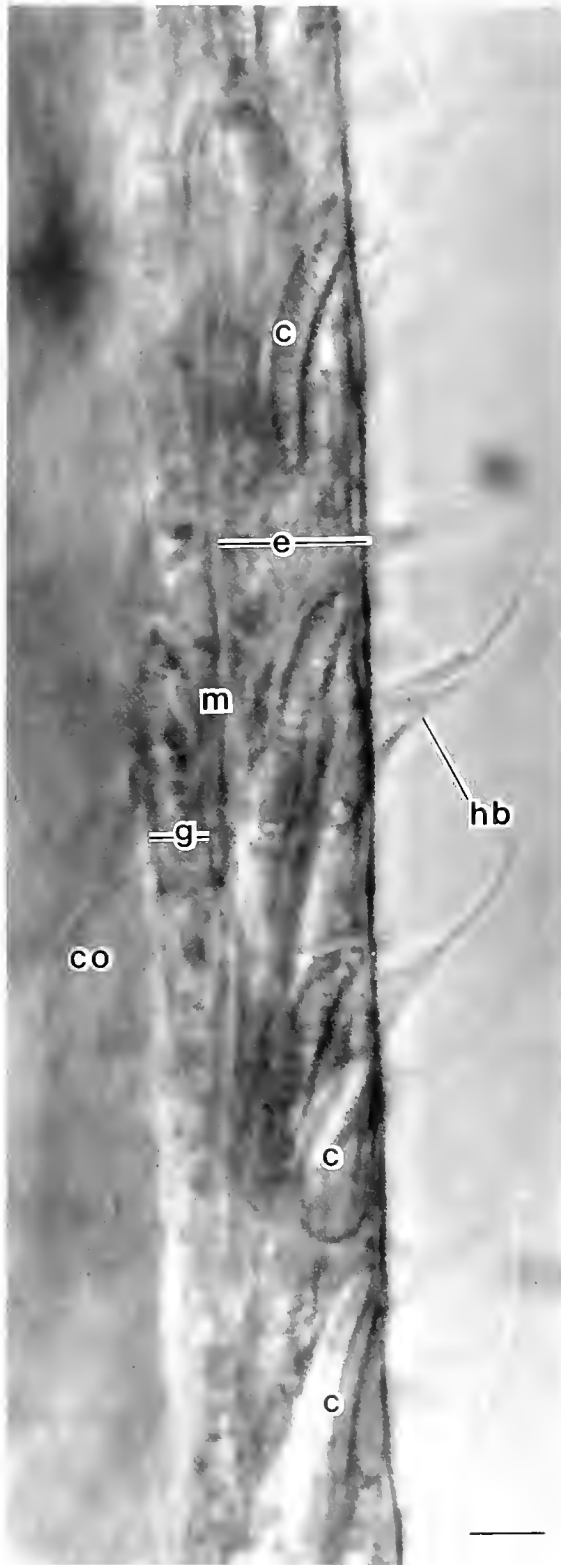


Figure 1. DIC photomicrograph of sea anemone tentacle. The epidermis (e), containing endocyte/supporting-cell complexes (CSCCs) and sensory-cell, supporting-cell complexes (SNSCs), is separated from the gastrodermis (g) by the mesoglea (m). Cnidiae within endocytes (c) of CSCCs are visible within the epidermis. Hair bundles (hb) at the apices

matocysts, spirocysts, and basitrich nematocysts were counted on the test probes within a rectangular reticule measuring  $38,880 \mu\text{m}^2$ . The mean number of nematocysts and other cnidae counted was divided by the mean number of BFCs to give a ratio. This value was multiplied by 0.054 to correct for the difference between the areas of the tentacle sampled for discharge and imaged for fluo fluorescence.

## Results

### *Morphology and organization of cells*

Sea anemone tentacles are composed of two tissue layers separated by a mostly acellular matrix called the mesoglea (Fig. 1). The epidermal layer lies adjacent to the external surface and the gastrodermal layer lines the internal cavity (the coelenteron).

Within the epidermis, supporting cells form complexes either with endocytes or with sensory cells (CSCC = endocyte/supporting-cell complex; SNSC = sensory-cell/supporting-cell complex). In each of the complexes, a single endocyte or a single sensory cell is surrounded by several supporting cells. These supporting cells contribute small-diameter ( $0.05\text{--}0.2 \mu\text{m}$ ) stereocilia to a hair bundle that protrudes from the apical surface of the complex (Peteya, 1975). In the CSCC, the endocyte contributes a single kinocilium to the hair bundle (Mariscal *et al.*, 1978). In the SNSC, the sensory cell contributes a single kinocilium and 5–10 large-diameter ( $0.2\text{--}0.5 \mu\text{m}$ ) stereocilia to the hair bundle (Peteya, 1975).

In CSCCs, endocytes are easily recognized by the presence of cnidae (microbasic p-mastigophores, basitrichs, or spirocysts); however, because cnidae are strongly birefringent, supporting cells are difficult to resolve clearly. Due to the extreme abundance of cnidae in tentacles, sensory cells and supporting cells of SNSCs are also difficult to visualize. Supporting cells and sensory cells can be better visualized in tentacles that have been depleted of cnidae (Fig. 2). From a lateral view, the apices of supporting cells are broad (approximately  $10\text{-}\mu\text{m}$  diameter) and triangular, and the bases gradually narrow into long tenuous processes that extend toward the mesoglea (Thibodeaux and Watson, 1991). Sensory cells have narrow apices (approximately  $3\text{-}\mu\text{m}$  diameter) and bases that are thought to terminate in synapses with the nerve net near the mesoglea

of CSCCs and SNSCs are apparent at the surface of the epidermis. (co = coelenteron.) This photomicrograph was taken near the base of the tentacle where the cnidae are less abundant than at the tip, making the tissue layers easier to distinguish. This specimen was fully extended, causing the cnidae to become oriented obliquely to the epidermal surface. More commonly, cnidae are oriented perpendicular to the epidermal surface (see Fig. 2B). Scale bar =  $5 \mu\text{m}$ .



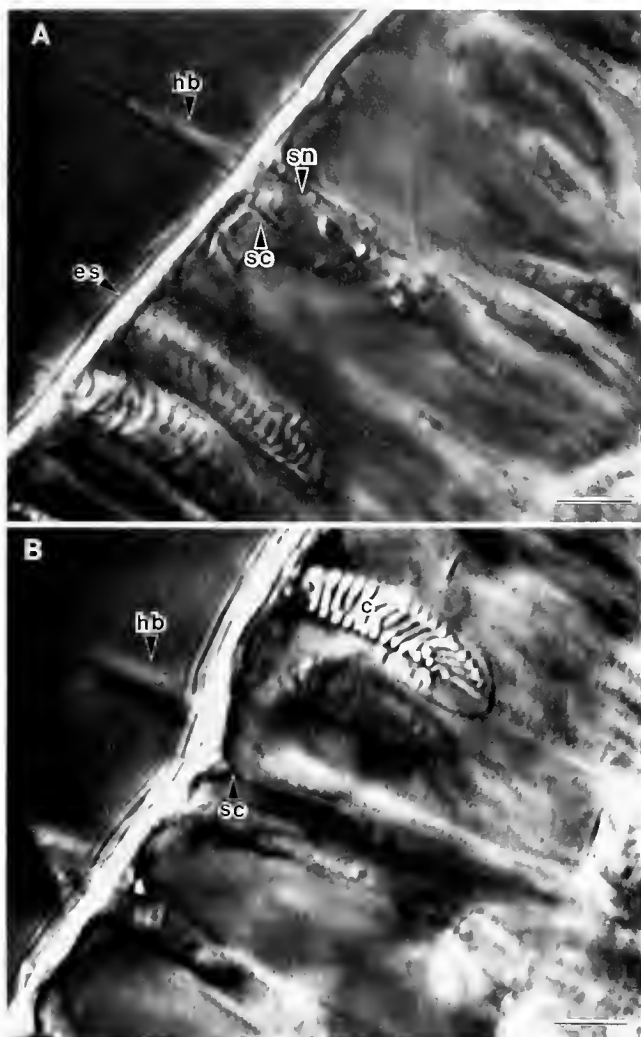


**Figure 2.** DIC video-enhanced photomicrographs of a sea anemone tentacle exposed to hypotonic medium to promote the extrusion of cnidae. Two optical sections of a SNSC: (A) The hair bundle (hb) extends into the seawater from the epidermal surface (es). Beneath the epidermal surface, the sensory cell (sn) of the SNSC and several supporting cells (sc) surrounding it extend toward the mesoglea located just beyond the border of the micrograph; (B) a deeper optical section of the same SNSC more clearly shows the triangular apex of one of the supporting cells (sc) of the SNSC. A endocyte (c) is in focus. Scale bar = 5  $\mu$ m.

(Peteya, 1975). Although CSCC involvement in the regulation of nematocyst discharge has been well characterized (Watson and Hessinger, 1989, 1992), SNSC involvement, if any, is not known.

#### *Description of fluo fluorescence*

Fluo-labeled tentacles exhibited fluorescence both in the epidermis and in the gastrodermis (Fig. 3A). Whereas autofluorescence within the gastrodermis was so intense that it overwhelmed fluo fluorescence, autofluorescence

within the epidermis did not significantly interfere with detecting Ca<sup>2+</sup>-dependent fluo fluorescence (see below). Only certain cells within the epidermis were fluorescent above autofluorescence levels; the fluorescence intensity of these cells varied somewhat, both in MgSW controls and in mucin-treated specimens. Most of the fluorescent cells occurred at the tentacle surface and had a triangular shape reminiscent of supporting cells. Less frequently, extremely bright cells were observed within the epidermis at the tentacle surface (Fig. 3A, B). The glare from the intense fluorescence made the morphology of these cells difficult to distinguish. The least common brightly fluorescent loci occurred deeper within the epidermis, often with fine processes extending toward both the epidermal surface and the mesoglea (Fig. 3A). It was not clear whether these bright loci constituted domains of cells extending to the epidermal surface or were contained within cells not in immediate contact with the surface.

#### *Identification of supporting cells*

To determine whether the triangular patterns of fluo fluorescence, described above, represented supporting cells, 30 paired images of tentacles double-labeled with fluo-3 and rhodamine-dextran were analyzed (Fig. 4). In comparisons of 380 cells, there was 80% agreement between cells endocytosing rhodamine-dextran (Fig. 4A) and those exhibiting Ca<sup>2+</sup>-dependent fluo fluorescence (Fig. 4B). To determine autofluorescence ranges, fluorescence intensity of unlabeled tentacles was measured with both fluorescein and rhodamine optics; filters were used to prevent crossover excitation and emission of the two indicators (see Materials and Methods). Only cells exhibiting values higher than autofluorescence were used in the pairwise analysis.

#### *Ca<sup>2+</sup>-dependent fluo fluorescence and mucin effect*

Fluorescence intensity was measured for the 10 brightest epidermal cells per microscopic field at each timepoint. Mean values were calculated for each timepoint of each replicate experiment. The resulting means from these replicates, averaged to give mean maximum fluorescence values (see Materials and Methods), were compared for autofluorescence, Ca<sup>2+</sup>-independent fluo fluorescence, and Ca<sup>2+</sup>-dependent fluo fluorescence in MgSW controls and in mucin-treated specimens (Fig. 5). Statistical analyses (ANOVA) of the timecourse data (considering data sets consisting of between 10 and 13 timepoints; Fig. 5) indicated heterogeneity among the means for the treatments ( $p = 2.45 \times 10^{-23}$ ). *Post hoc* comparisons (Tukey's LSD) revealed that Ca<sup>2+</sup>-dependent fluo fluorescence was significantly greater in mucin treatment than in MgSW controls ( $p = .02$ ). Additionally, autofluorescence and Ca<sup>2+</sup>-independent fluo fluorescence were comparable to each

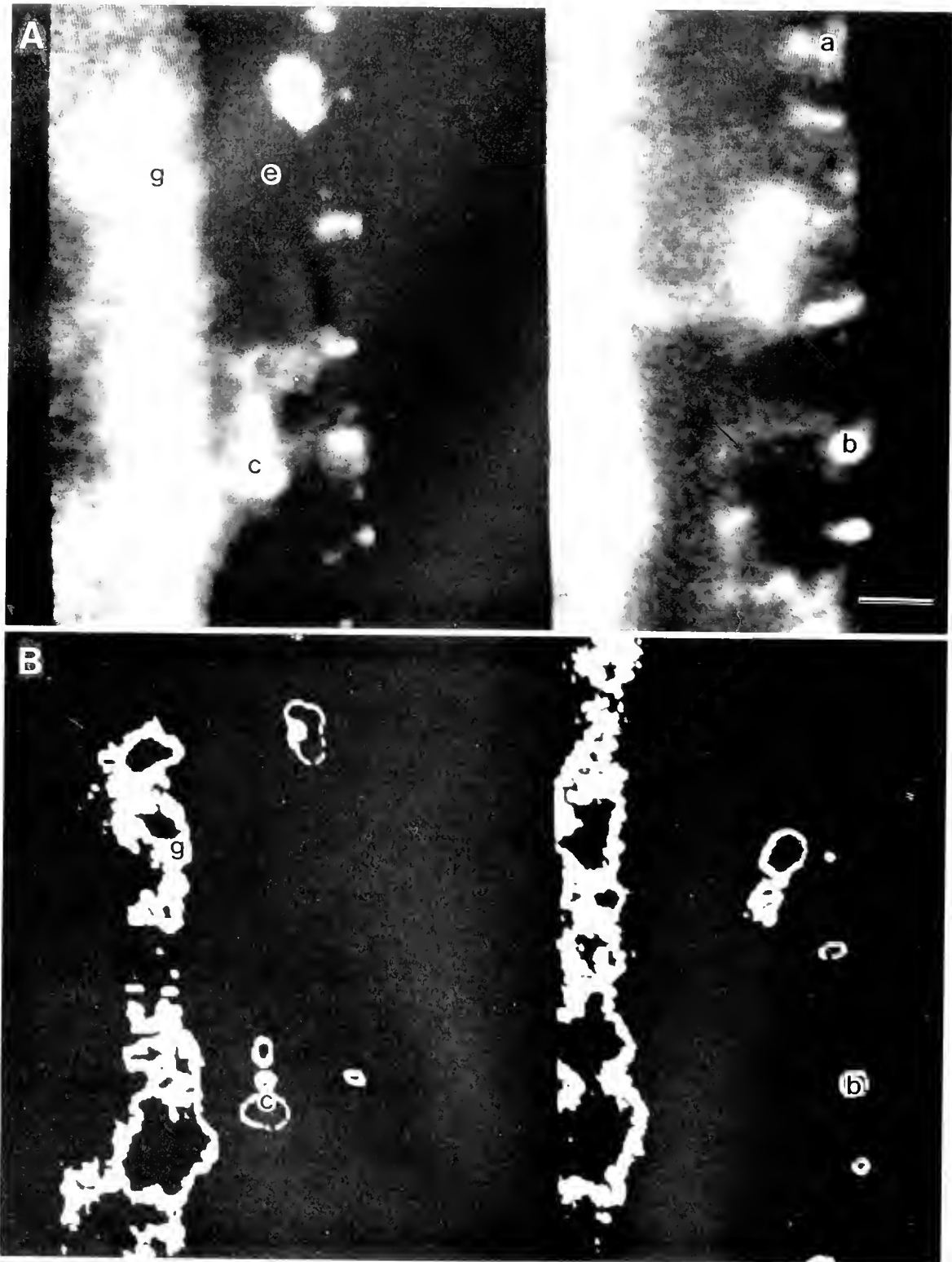


**Figure 3.** Cooled CCD photomicrographs of fluorescence from two fluo-labeled tentacles. (A) Several cells within the epidermis (e) are fluorescent, including triangular cells (a) exhibiting moderate fluorescence (see also Fig. 4A) and brightly fluorescent cells (BFCs) with intense fluorescence at (b) or beneath (c) the surface of the epidermis. The strongly autofluorescent gastrodermis (g) also is shown. Scale bar = 5  $\mu$ m. (B) Outline plots depict gray values ranging from 121 to 131 for some of the brightest fluorescent cells shown in Figure 3A. Note that the triangular cell (a) in Figure 3A was too dim to be seen in Figure 3B. For presentation, contrast was linearly enhanced using IPPLUS software.

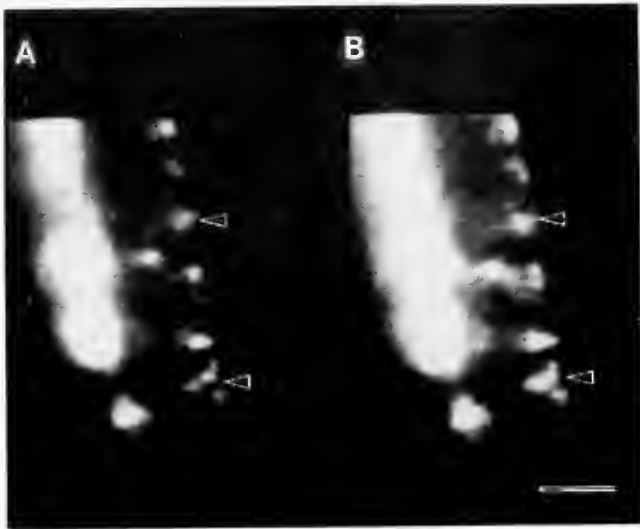


**Figure 4.** Cooled CCD paired photomicrographs of fluorescence from a fluo-labeled tentacle incubated in rhodamine dextran. (A) Rhodamine dextran fluorescence of the tentacle epidermis includes several bright loci. (B) Fluo fluorescence of the same region of the tentacle epidermis with several bright loci. Arrows indicate representative cells exhibiting fluorescence both for fluo and rhodamine-dextran. For presentation, contrast was linearly enhanced using IPPLUS software. Scale bar = 10  $\mu$ m.

other but less than Ca<sup>2+</sup>-dependent fluo fluorescence ( $p = .0002$ ).

*BFCs in mucin treatment versus MgSW controls*

To more precisely describe the difference in Ca<sup>2+</sup>-dependent fluo fluorescence attributable to the effects of mucin, total numbers of BFCs in mucin treatment were compared to BFCs in MgSW controls. Overall, BFCs were about twice as numerous in mucin-treated specimens as in control specimens. Statistical analysis (Student's *t*-test) comparing the mean number of BFCs per timepoint, computed by averaging data from five separate timecourses ( $n = 650$  cells scored per treatment), indicated that the means for the two treatments were significantly different ( $p < .05$ ).

*Correlation of BFC abundance to chemoreceptor activity*

Timecourses depicting number of BFCs in both the absence and presence of mucin were compared to timecourses depicting numbers of nematocysts discharged in both the absence and presence of mucin, and to timecourses in which supporting-cell chemoreceptors were labeled with mucin-gold (Watson and Hessinger, 1987, 1989). A strong positive correlation was found between timecourses for nematocyst discharge from mucin-treated specimens (free mucin or gold-conjugated mucin) and timecourses for mucin-gold labeling at supporting cell

surfaces (Fig. 6A and Table I). Furthermore, the time-course data for BFCs in mucin-treated specimens were positively correlated to timecourses for both nematocyst discharge from mucin-treated specimens and surface chemoreceptor labeling with mucin-gold (Figs. 6B, C, and Table I). In contrast, data for BFCs in mucin treatment showed no correlation to data for BFCs in MgSW controls or to data for nematocyst discharge from specimens in seawater alone (Table I). Additionally, timecourse data for nematocyst discharge from specimens in seawater alone showed no correlation to data for BFCs in MgSW controls or to nematocyst discharge from specimens in mucin (Fig. 6D and Table I).

*Relative abundances of BFCs and nematocysts discharged*

The mean densities of BFCs and discharged nematocysts were compared (see Materials and Methods) to provide an index of the relative abundances of BFCs and responding CSCCs. In seawater controls, the ratio of BFCs to discharged nematocysts was 1 to 3.61 when only microbasic p-mastigophores were considered. In chemosensitized specimens, this ratio was 1 to 2.85. Previous studies on nematocyst discharge have focused on microbasic p-mastigophores (*e.g.*, Watson and Hessinger, 1989) because they are easy to quantify. However, two other cnida types

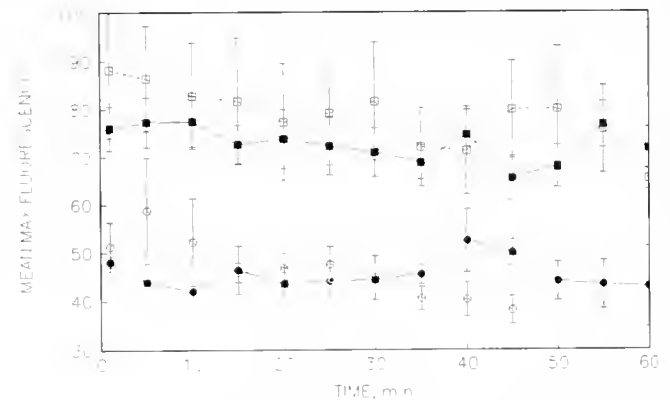


**Figure 5.** Timecourse of mean maximum fluorescence. Maximum gray values were recorded for the 10 brightest cells from digitized images collected at each time point. These values were averaged for each time point over five replicate experiments to give mean maximum fluorescence values. Timecourses for mean maximum fluorescence are shown (as gray-level values,  $\pm$ SEM) for autofluorescence (solid circles); and for fluo fluorescence in MgSW alone (solid squares); in MgSW containing 10<sup>-7</sup> M mucin (open squares); and in Ca<sup>++</sup>-free SW containing 10<sup>-7</sup> M mucin after 1 h pretreatment of specimens in 10<sup>-5</sup> M 4-bromo A23187 prepared in Ca<sup>++</sup>-free SW (Ca<sup>++</sup> independent fluo fluorescence; open circles). The results of statistical analysis of the data, including ANOVA with LSD *post hoc* comparisons of the treatments (CSS Statistica software, Tulsa) are described in the text. In all cases, significant findings are reported in the text with a maximum *p* value of .05.

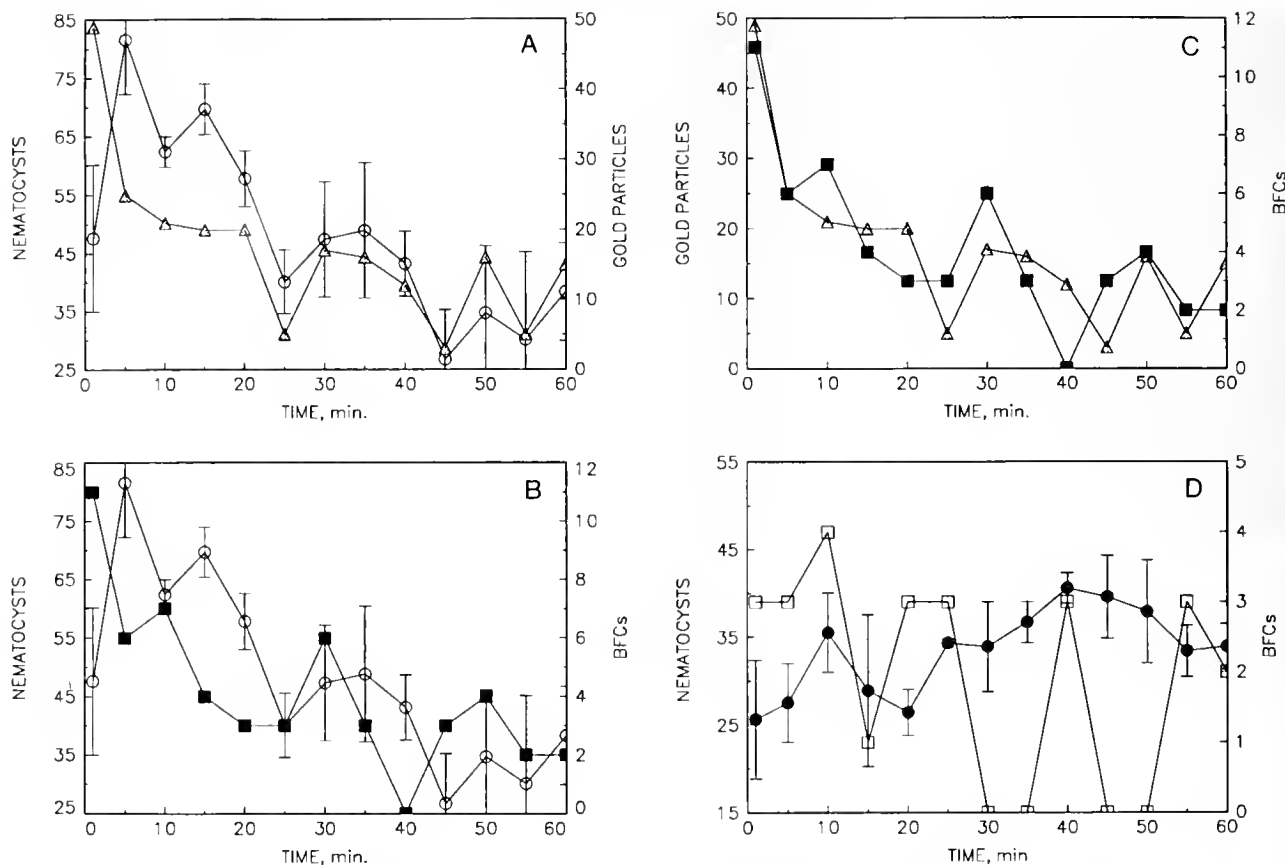


**Figure 6.** Timecourses for the abundance of mucin-gold particles observed at the apical surface of supporting cells, for the abundance of BFCs observed in the tentacle epidermis in both the presence and absence of  $10^{-7}$  M mucin, and for discharged nematocysts counted in test probes ( $\pm$ SEM) in both the presence and absence of mucin. To facilitate comparisons, timecourses are paired as follows: (A) mean nematocysts discharged within single microscopic fields ( $0.16 \text{ mm}^2$ ) of test probes upon exposure to  $10^{-7}$  M mucin (open circles) and mucin gold particles counted at the apical surface of 25 supporting cells (speckled triangles, data from Watson and Hessinger, 1989); (B) mean nematocysts discharged after exposure to  $10^{-7}$  M mucin (open circles) and BFCs counted in tentacles after exposure to  $10^{-7}$  M mucin (solid squares); (C) mucin gold particles counted at the surface of supporting cells (speckled triangles) and BFCs counted upon exposure to  $10^{-7}$  M mucin (closed squares); and (D) mean nematocysts discharged into test probes in seawater alone (closed circles) and BFCs counted in tentacles exposed to MgSW alone (open squares). The results of statistical analysis of the data using Spearman rank correlation are shown in Table 1.

occur in cnidocytes of tentacles: basitrichs and spirocysts. Although less is known about the processes involved in regulating discharge of these cnidae, they also occur in CSCCs in tentacles and routinely discharge into test probes. Spirocyst CSCCs respond to chemosensitization by N-acetylated sugars (Thorington and Hessinger, 1990). When considering all of the types of cnida discharged, the ratio of BFCs to total responding CSCCs was 1 to 8.36 in seawater controls and 1 to 6.22 following chemosensitization.

### Discussion

In this study, we used the  $\text{Ca}^{2+}$ -dependent fluorescent dye fluo-3 to directly monitor intracellular  $\text{Ca}^{2+}$  levels in

the epidermis of anemone tentacles (Fig. 3). Fluo-3 is only weakly fluorescent in the absence of  $\text{Ca}^{2+}$  and significantly increases in fluorescent intensity upon binding  $\text{Ca}^{2+}$ . We show that intracellular  $\text{Ca}^{2+}$  levels are higher in tentacles exposed to optimal levels of N-acetylated sugars (mucin treatment) than in tentacles exposed to seawater alone (MgSW controls) (Fig. 5). Furthermore, the abundance of cells exhibiting the highest  $\text{Ca}^{2+}$  levels, BFCs, is two- to threefold greater in mucin treatment than in MgSW controls. This increase in BFC abundance with mucin treatment is comparable in magnitude to the enhancement in nematocyst discharge that occurs upon exposure to mucin (Watson and Hessinger, 1987, 1989). Moreover, timecourses depicting BFC abundance in mucin-treated

Table 1

Positive correlations between fluorescence, nematocyst discharge, and chemoreceptor labeling under different conditions

Significant correlations ( $p < .05$ )	Insignificant correlations ( $p > .05$ )
BFCs mucin vs. ND mucin	BFCs seawater vs. BFCs mucin
BFCs mucin vs. ND mucin-gold	BFCs seawater vs. ND seawater
BFCs mucin vs. mucin-gold labeling	ND seawater vs. ND mucin
ND mucin vs. mucin-gold labeling	

Correlation calculated using Spearman rank analysis of data from timecourse experiments.

BFCs, brightly fluorescent cells; ND, nematocyst discharge.

specimens are positively correlated to timecourses depicting nematocyst discharge to optimal levels of mucin and to timecourses for supporting-cell chemoreceptor labeling (Figs. 6A, B, C and Table I). Although these positive correlations do not prove causal relationships between BFC abundance and CSCC responsiveness, one plausible interpretation is that BFCs are somehow involved in the Ca<sup>2+</sup>-dependent regulation of nematocyst discharge from CSCCs upon chemosensitization with N-acetylated sugars.

It is interesting, however, that in seawater alone, a few BFCs are observed in tentacles, and nematocyst discharge can be triggered at a baseline level (Fig. 6D). The co-occurrence of these two phenomena in the absence of N-acetylated sugars may indicate that BFCs are also somehow involved in controlling nematocyst discharge in seawater alone. The duration of Ca<sup>2+</sup> signaling by individual BFCs could not be determined by our methods, which incorporated relatively long exposures (20 s) and imaging of many different sites of the tentacle per timecourse experiment.

Results of morphological studies using DIC optics and of endocytosis experiments using dextran-rhodamine suggest that some cells exhibiting relatively high internal Ca<sup>2+</sup>, in both the presence and absence of mucin, are supporting cells (Fig. 4). However, it is not clear whether all cells exhibiting Ca<sup>2+</sup>-dependent fluorescence are supporting cells. This uncertainty is especially pronounced for the less common, brightest loci observed at the tentacle surface and deeper within the epidermis. In both cases, glare from intense fluorescence prevented our determining the precise morphology of the cells involved (Fig. 3).

Of the five cell types occurring at the tentacle surface (cnidocytes, supporting cells, sensory cells, two types of gland cell), we speculate that the extremely bright surface cells are components of CSCCs or SNSCs—either specialized cnidocytes and/or supporting cells, or sensory cells. Although these BFCs did not appear to possess cnidae, and therefore would not be cnidocytes, we cannot rule out the possibility that the intense fluorescence from

these cells obscured cnidae within them. Supporting cells are the most abundant epidermal cells at the tentacle surfaces because several such cells make up each CSCC and each SNSC. CSCCs are highly abundant in tentacles. If supporting cells or cnidocytes of each activated CSCC were responsible for the intense fluorescence, one would expect a higher abundance of BFCs than was observed. Therefore, if these BFCs are supporting cells, or cnidocytes, or both, of CSCCs, we suggest they are specialized in some way so that only certain ones, among the many present in the tentacle epidermis, participate in intense Ca<sup>2+</sup> signaling. These specialized CSCCs would be required to activate other CSCCs by a mechanism that would not involve extreme elevations in Ca<sup>2+</sup> levels within the secondarily activated CSCCs.

SNSCs are less abundant than CSCCs. It is possible that BFCs are supporting cells, sensory cells, or both, of SNSCs. Sensory cells are reported to be involved in nervous integration in cnidarians (Bullock and Horridge, 1965; see also Shelton, 1982; Boothby and McFarlane, 1986; Westfall, 1988; Grimmelikhuijzen *et al.*, 1990; McFarlane *et al.*, 1990). In anemone tentacles, the sensory cell is thought to be a bipolar neuron in the tentacle epidermis with a narrow dendrite that terminates apically in a cluster of large stereocilia and basally in a long, tenuous axon that connects to the nerve net (Peteya, 1975; van Marle, 1990). The location and morphology of the bright loci deeper within the epidermis suggest that these BFCs could be neurons or basal domains of surface epidermal cells. These loci occurred in the vicinity of the nerve net and commonly appeared to have fine processes extending toward the surface or mesoglea. Although all three types of cells proposed as candidates for surface BFCs (cnidocytes, supporting cells, and sensory cells) have been implicated as connecting to the nerve net, the evidence appears to be strongest for sensory cells (Westfall, 1973; Peteya, 1975; Bigger, 1982; van Marle, 1990).

The independent effector hypothesis, the classical explanation for the regulation of nematocyst discharge, portrays the cnidocyte as responding directly to mechanical and chemical stimuli by triggering discharge. In this view, the cnidocyte is both a receptor and effector cell acting independently of any nervous intervention (Parker, 1916, 1919; Parker and Van Alstyne, 1932; Pantin, 1942a, b; Ewer, 1947). Later interpretations of the hypothesis allow for some nervous intervention either to reduce or to increase discharge, depending on the physiological state of the animal. For example, in experiments assaying nematocyst discharge immediately following treatment, certain physically agitated anemones discharge more nematocysts and spirocysts than undisturbed anemones (Conklin and Mariscal, 1976). In this revision of the hypothesis, the nervous system is viewed as modulating the

overall responsiveness of the cnidocytes, which still exercise self-regulation of discharge.

More recent evidence indicates that chemoreceptors regulating discharge are located on supporting cells, and not on cnidocytes. These results have prompted another revision of the hypothesis, which suggests that discharge is regulated by complexes consisting of cnidocytes and the supporting cells surrounding the cnidocytes (CSCCs). According to this model, the CSCCs act as independent effector complexes with the supporting cells detecting chemical stimuli, such as N-acetylated sugars, and the cnidocytes responding by effecting nematocyst discharge (Thorington and Hessinger, 1988b; Watson and Hessinger, 1989). Like its predecessor, this model permits the nervous system to modulate the overall responsiveness of the CSCCs.

In this study, we present evidence that neither cnidocytes alone nor individual CSCCs are independent effectors of nematocyst discharge. Comparison of densities of BFCs and nematocysts discharged, both with and without chemosensitization, indicates that the ratio of BFCs to responding CSCCs is approximately 1 to 3 when only microbasal p-mastigophore nematocysts are considered and approximately 1 to 7 when all types of responding CSCCs are included (see Materials and Methods). We propose that relatively few cells, the BFCs, are somehow involved with CSCCs in regulating the discharge of nematocysts.

### Conclusion

We have shown that epidermal cells exhibiting relatively high  $\text{Ca}^{2+}$  levels occur in anemone tentacles both with and without chemosensitization. However, when chemoreceptors for N-acetylated sugars are activated, the number of cells that exhibit the highest  $\text{Ca}^{2+}$  levels increases two- to threefold—an enhancement comparable to that seen in nematocyst discharge upon chemosensitization. Timecourses depicting the abundance of these cells upon mucin treatment correlate to timecourses both for nematocyst discharge to mucin and for supporting-cell chemoreceptor labeling. The scarcity of the cells exhibiting the highest  $\text{Ca}^{2+}$  levels indicates that not every activated CSCC, if any, participates in this intense  $\text{Ca}^{2+}$  signaling. Although the identity of the cells exhibiting the highest  $\text{Ca}^{2+}$  levels is frequently uncertain, it appears that these few cells, using  $\text{Ca}^{2+}$  as a second messenger, are somehow involved in regulating discharge of nematocysts from many cnidocytes. This regulation occurs via specific remote control, either with or without some local control by individual CSCCs. Thus, the evidence presented here suggests a major departure from the independent effector hypothesis explaining regulation of nematocyst discharge in sea anemones.

### Acknowledgments

We are grateful to Dr. Paul G. Greenwood for critically reading an earlier version of the manuscript. This work was supported by NSF DCB-9105058 and LEQSF RDA-44 and GF-19.

### Literature Cited

- Bigger, C. H. 1982. The cellular basis of the aggressive acrorhagial response of sea anemones. *J. Morph.* **173**: 259–278.
- Boothby, K. M., and I. D. McFarlane. 1986. Chemoreception in sea anemones: Betaine stimulates the pre-feeding response in *Urticina eques* and *U. felina*. *J. Exp. Biol.* **125**: 385–389.
- Bullock, T. H., and G. A. Horridge. 1965. *Structure and Function in the Nervous System of Invertebrates*. Vol. 1. W. H. Freeman and Co., San Francisco. 798 pp.
- Conklin, E. J., and R. N. Mariscal. 1976. Increase in nematocyst and spirocyst discharge in a sea anemone in response to mechanical stimulation. Pp. 549–558 in *Coelenterate Ecology and Behavior*, G. O. Mackie, ed. Plenum Press, New York.
- Ewer, R. F. 1947. On the functions and mode of action of the nematocysts of hydra. *Proc. Zool. Soc. Lond.* **117**: 365–376.
- Grimmelikhuijzen, C. J. P., D. Graff, O. Koizumi, J. A. Westfall, and I. D. McFarlane. 1990. Neurons and their peptide transmitters in coelenterates. Pp. 95–109 in *Evolution of the First Nervous Systems*, P. A. V. Anderson, ed. Plenum Press, New York.
- Holstein, T., and P. Tardent. 1984. An ultrahigh-speed analysis of exocytosis: nematocyst discharge. *Science* **223**: 830–833.
- Lubbock, R. 1979. Chemical recognition and nematocyte excitation in a sea anemone. *J. Exp. Biol.* **83**: 283–292.
- Mariscal, R. N. 1974. Nematocysts. Pp. 129–178 in *Coelenterate Biology, Reviews and New Perspectives*, L. Muscatine and H. M. Lenhoff, eds. Academic Press, New York.
- Mariscal, R. N., E. J. Conklin, and C. H. Bigger. 1978. The putative sensory receptors associated with the cnidae of cnidarians. *Scanning Electron Microsc.* **2**: 959–966.
- McFarlane, I. D., D. Graff, and C. J. P. Grimmelikhuijzen. 1990. Peptidergic neurotransmitters in the anthozoa. Pp. 111–127 in *Evolution of the First Nervous Systems*, P. A. V. Anderson, ed. Plenum Press, New York.
- Minta, A., J. Kao, and R. Tsien. 1989. Fluorescent indicators for cytosolic calcium based on rhodamine and fluorescein chromophores. *J. Biol. Chem.* **264**: 8171–8178.
- Pantin, C. F. A. 1942a. Excitation of nematocysts. *Nature* **149**: 109.
- Pantin, C. F. A. 1942b. The excitation of nematocysts. *J. Exp. Biol.* **19**: 294–310.
- Parker, G. H. 1916. The effector system of actinians. *J. Exp. Zool.* **21**: 461–484.
- Parker, G. H. 1919. *The Elementary Nervous System*. Lippincott, Philadelphia.
- Parker, G. H., and M. A. Van Alstyne. 1932. The control and discharge of nematocysts, especially in *Metridium* and *Physalia*. *J. Exp. Biol.* **63**: 329–344.
- Peteya, D. J. 1975. The ciliary-cone sensory cell of anemones and cerianthids. *Tissue Cell* **7**(2): 243–252.
- Robson, E. A. 1988. Problems of supply and demand for cnidae in anthozoa. Pp. 179–207 in *The Biology of Nematocysts*, D. A. Hessinger and H. M. Lenhoff, eds. Academic Press, San Diego.
- Shelton, G. A. B. 1982. Anthozoa. Pp. 203–242 in *Electrical Conduction and Behaviour in "Simple" Invertebrates*, G. A. B. Shelton, ed. Oxford University Press, New York.
- Skaer, R. J., and L. E. R. Picken. 1965. The structure of the nematocyst thread and the geometry of discharge in *Corynactis viridis* (Allman). *Phil. Trans. R. Soc. Lond., Ser. B* **250**: 131–164.

- Thibodeaux, P. M., and G. M. Watson. 1991. Imaging of intracellular calcium fluxes in tentacles of a sea anemone. *Am Zool* **31**: 15a.
- Thorington, G. U., and D. A. Hessinger. 1988a. Control of cnida discharge: I. Evidence for two classes of chemoreceptor. *Biol Bull* **174**: 163-171.
- Thorington, G. U., and D. A. Hessinger. 1988b. Control of discharge: factors affecting discharge of cnidae. Pp. 233-253 in *The Biology of Nematocysts*, D. A. Hessinger and H. M. Lenhoff, eds. Academic Press, San Diego.
- Thorington, G. U., and D. A. Hessinger. 1990. Control of cnida discharge III. Sprocysts are regulated by three classes of chemoreceptors. *Biol Bull* **178**: 74-83.
- van Marle, J. 1990. Catecholamines, related compounds and the nervous system in the tentacles of some anthozoans. Pp. 129-140 in *Evolution of the First Nervous Systems*, P. A. V. Anderson, ed. Plenum Press, New York.
- Watson, G. M., and D. A. Hessinger. 1987. Receptor-mediated endocytosis of a chemoreceptor involved in triggering the discharge of cnidae in a sea anemone tentacle. *Tissue Cell* **19**: 747-755.
- Watson, G. M., and D. A. Hessinger. 1989. Cnidocytes and adjacent supporting cells form receptor-effector complexes in anemone tentacles. *Tissue Cell* **21**: 17-24.
- Westfall, J. A. 1973. Ultrastructural evidence for neuromuscular systems in coelenterates. *Am Zool* **13**: 237-246.
- Westfall, J. A. 1988. Presumed neuronematocyte synapses and possible pathways controlling discharge of a battery of nematocysts in Hydra. Pp. 41-51 in *The Biology of Nematocysts*, D. A. Hessinger and H. M. Lenhoff, eds. Academic Press, San Diego.
- Williams, R. B. 1968. Control of the discharge of cnidae in *Diadumene luciae* (Verrill). *Nature* **219**: 959.



## Differential Susceptibility of Guanine Nucleotide-binding Proteins to Pertussis Toxin-catalyzed ADP-ribosylation in Brain Membranes of Two Congeneric Marine Fishes

THOMAS F. MURRAY<sup>1</sup> AND JOSEPH F. SIEBENALLER<sup>2,\*</sup>

<sup>1</sup>College of Pharmacy, Oregon State University, Corvallis, Oregon 97331, and <sup>2</sup>Department of Zoology and Physiology, Louisiana State University, Baton Rouge, Louisiana 70803

**Abstract.** Pertussis toxin-catalyzed [<sup>32</sup>P]ADP-ribosylation was used to probe the guanine nucleotide binding regulatory proteins G<sub>i</sub> and G<sub>o</sub> in brain membranes from two scorpaenid fishes, *Sebastolobus alascanus* and *S. altivelis*. The membranes of the two species exhibit a differential sensitivity to [<sup>32</sup>P]ADP-ribosylation produced by a fixed concentration of pertussis toxin. The membranes from the deeper-living *S. altivelis* consistently incorporated more [<sup>32</sup>P]ADP than the membranes from *S. alascanus*. Proteins of 39 and 41 kDa are specifically labeled in both species, corresponding to the apparent molecular masses of the  $\alpha$  subunits of G<sub>i</sub> and G<sub>o</sub>. At 5°C the ribosylation reaction is linear for at least 7 h. The pertussis toxin concentration-response relationship was evaluated with concentrations of pertussis toxin from 0 to 100 ng/ $\mu$ l. The extent of [<sup>32</sup>P]ADP-ribosylation was quantified by autoradiography and computer-assisted image analysis. The EC<sub>50</sub> values for pertussis toxin were similar for the two species, but the maximum level of [<sup>32</sup>P]ADP-ribosylation was significantly greater in *S. altivelis* brain membranes. Because the heterotrimeric holoprotein is the substrate for ribosylation, the modulatory effects of the guanyl nucleotides GDP and GTP $\gamma$ S on the ribosylation were assessed. GDP increased [<sup>32</sup>P]ADP-ribosylation of the  $\alpha$  subunits in *S. altivelis*. Only the highest concentration tested (1000  $\mu$ M) increased [<sup>32</sup>P]ADP-ribosylation in *S. alascanus* brain membranes and only to a modest extent. Increasing concentrations of GTP $\gamma$ S suppressed [<sup>32</sup>P]ADP-ribosylation in *S. alascanus* brain membranes,

presumably by promoting dissociation of the holotrimer. GTP $\gamma$ S had much less of an effect on the *S. altivelis* brain membranes. These differences in the extent of ADP-ribosylation and the modulatory effects of guanyl nucleotides may reflect different coupling efficiencies of G proteins and receptors. The expression of the  $\alpha$  and  $\beta$  subunits of G<sub>i</sub> and G<sub>o</sub> in the two *Sebastolobus* species, the deep-sea morid teleost fish *Antimora rostrata*, and the rat were compared by Western immunoblotting of brain membranes with antipeptide antisera. Levels of G<sub>1 $\alpha$ 3</sub> were 63% higher in brain membranes of *S. altivelis* than those in *S. alascanus*. The levels of G<sub>1 $\alpha$ 1</sub>, G<sub>1 $\alpha$ 2</sub>, G<sub>o</sub> and  $\beta$ <sub>36</sub> were similar in the two species. Although the complement of G proteins identified by the array of antisera used was similar in all the species, there appears to be additional diversity of  $\alpha$  subunits in the teleost brain membranes. In fish, antiserum to G<sub>o $\alpha$</sub>  reacted with an additional 41 to 42 kDa protein that was not expressed in rat brain.

### Introduction

The hydrostatic pressures characteristic of the deep sea exert profound effects on the physiology and biochemistry of organisms in this extensive habitat (Siebenaller, 1987, 1991; Siebenaller and Somero, 1989). Among the processes affected is guanine nucleotide binding protein (G protein)-coupled transmembrane signaling (Siebenaller *et al.*, 1991; Siebenaller and Murray, 1993). In A<sub>1</sub> adenosine receptor-modulation of adenylyl cyclase in teleost brain membranes, pressure affects agonist efficacy (Siebenaller *et al.*, 1991; Siebenaller and Murray, 1993), the coupling of the receptor to adenylyl cyclase (Siebenaller *et al.*, 1991), and the enzymatic activities of components of the system,

Received 26 October 1992; accepted 30 September 1993.

\* To whom reprint requests should be addressed.



*i.e.*, adenylyl cyclase activity (Siebenaller *et al.*, 1991) and the high-affinity GTPase activity of  $\alpha$  subunits of G proteins (Siebenaller and Murray, 1993).

G proteins couple a diverse superfamily of cell surface receptor proteins (estimated at up to 1000, *e.g.*, Barinaga, 1991) to a variety of effector elements such as adenylyl cyclase, ion channels, and phospholipases (Birnbaumer *et al.*, 1990). Because G proteins are central to transmembrane signaling, physical factors, such as pressure, may be critical as selective forces influencing adaptation and shaping the functional characteristics of G proteins.

G proteins are heterotrimers and the subunits are designated  $\alpha$ ,  $\beta$ , and  $\gamma$ . The classes of G proteins are defined by the  $\alpha$  subunit type (Gilman, 1987), and further diversity of the  $\alpha$  subunits has been documented by molecular genetic techniques (*e.g.*, Simon *et al.*, 1991). The general features of the model of G protein-coupled signaling are briefly described here (see Gilman, 1987, and Birnbaumer *et al.*, 1990). Agonist-liganded receptors interact with G proteins, promoting the binding of GTP to the guanine nucleotide binding site on the  $\alpha$  subunit. GTP binding evokes a conformational change (Yi *et al.*, 1991), causing the protein to dissociate into  $\alpha \cdot$ GTP and a  $\beta\gamma$  dimer (Gilman, 1987; Birnbaumer *et al.*, 1990; Boege *et al.*, 1991). The activated  $\alpha \cdot$ GTP complex and the  $\beta\gamma$  dimer interact with the target enzyme (Gilman, 1987; Lefkowitz, 1992; Birnbaumer, 1992). Signaling is terminated by the hydrolysis of bound GTP to GDP by the intrinsic GTPase activity of the  $\alpha$  subunit and the subsequent reassociation of the  $\alpha$  and  $\beta\gamma$  subunits.

The inhibitory G protein ( $G_i$ ) plays a role in receptor-mediated inhibition of adenylyl cyclase, whereas  $G_o$  is a common G protein in brain membranes. These two classes of G proteins are specific substrates for mono-ADP-ribosylation by pertussis toxin (Katada and Ui, 1982; Gierschik, 1992). Pertussis toxin catalyzes the transfer of an ADP-ribose moiety from  $NAD^+$  to a specific cysteine four residues from the carboxyterminus of the  $\alpha$  subunit in the heterotrimer. ADP-ribosylation prevents the coupling of the modified G protein to its receptor and therefore a response to agonists (Gierschik, 1992). Because the heterotrimeric holoprotein is the substrate for ADP-ribosylation (Neer *et al.*, 1984; Van Dop *et al.*, 1984), pertussis toxin has been used to characterize the subunit aggregation state and the conformation of G proteins (*e.g.*, Yi *et al.*, 1991), as well as the interaction of receptors and G proteins (*e.g.*, van der Ploeg *et al.*, 1992).

The  $\alpha$  subunits of  $G_i$  and  $G_o$  serve as transduction elements in  $A_1$  adenosine receptor transmembrane signaling (Linden, 1991). We have used pertussis toxin-catalyzed ADP-ribosylation to probe the  $G_i$  and  $G_o$  proteins of two *Sebastolobus* species in order to identify species differences that might be correlated with the differences in the pressure sensitivity of  $A_1$  adenosine receptor-mediated inhibition

of adenylyl cyclase (Siebenaller *et al.*, 1991). These two scorpaenid fishes of the genus *Sebastolobus* have similar life histories, experience similar temperatures, but occur at different depths (Hubbs, 1926; Siebenaller and Somero, 1978). With these species, fine-scale adaptations to pressure have been delineated without the potentially confounding effects of other environmental variables or phylogenetic distance (*e.g.*, Siebenaller, 1984a, b, 1987).

We observed previously that the extent of [ $^{32}$ P]ADP-ribosylation produced by a fixed concentration of pertussis toxin is different in the two *Sebastolobus* species (Siebenaller and Murray, 1990; Siebenaller *et al.*, 1991). Brain membranes from the deeper-living *S. altivelis* incorporate more [ $^{32}$ P]ADP than *S. alascanus* membranes (Siebenaller *et al.*, 1991). Our previous work (*e.g.*, Murray and Siebenaller, 1987; Siebenaller and Murray, 1990; Siebenaller *et al.*, 1991) suggested that the coupling of G proteins to receptors would be different in species adapted to different pressure regimes; *e.g.*, the two *Sebastolobus* species that experience different pressure regimes yet have brain membranes with identical phospholipid and fatty acid compositions (Siebenaller *et al.*, 1991). A less tightly coupled and more flexible signaling complex may be required for optimal function in the more highly ordered membranes which result at the higher pressures experienced by the deeper-living *S. altivelis* (Siebenaller *et al.*, 1991; see also Casadó *et al.*, 1992; Shinitzky, 1984).

In the present study we have confirmed the difference in pertussis toxin-catalyzed incorporation of [ $^{32}$ P]ADP into the  $\alpha$  subunits of  $G_i$  and  $G_o$  of the two *Sebastolobus* species. We have tested two possible reasons for this difference in [ $^{32}$ P]ADP ribosylation: that the G-proteins of the two species are differently suitable as substrates for ribosylation (*i.e.*, that the ribosylation site of *S. altivelis* is more susceptible to pertussis toxin); or that the levels of the G protein substrates in the two species are different. We have quantified the steady state levels and subtypes of  $G_i$  and  $G_o$   $\alpha$  and  $\beta$  subunits by Western immunoblot analyses as a measure of the differential expression of subunits in the two species. To examine and characterize the coupling of G proteins to receptors in the two species, we have tested the effects of guanyl nucleotides on pertussis toxin-catalyzed ribosylation. We relate these data to differences in the coupling of the  $A_1$  adenosine receptor to adenylyl cyclase in brain membranes of the two *Sebastolobus* species.

## Materials and Methods

### Specimens

Demersal adults of *Sebastolobus* (Scorpaenidae) were collected by otter trawl off the coast of Oregon at their typical depths of abundance on two cruises of the R/V *Wecoma*. *S. alascanus* adults are common between 180

and 330 m; the adults of *S. altivelis* are found between 550 and 1300 m (Miller and Lea, 1976). Demersal *Antimora rostrata* (Moridae) were collected at their typical depths of abundance, 850–2500 m (Haedrich and Merret, 1988), off the coast of Newfoundland, Canada, on a cruise of the R/V *Gyre*. Brain tissue was dissected, frozen in liquid nitrogen at sea, and transported to the laboratory where tissues were maintained at  $-80^{\circ}\text{C}$  until used.

Frozen rat brains were obtained from Pel-Freez (Rogers, Arkansas) and forebrains were dissected following thawing of the whole brain.

#### *Preparation of brain membranes*

Membranes were homogenized with a Dounce (Pestle A) in 40 volumes of 50 mM Tris-HCl, pH 7.6 at  $5^{\circ}\text{C}$ , containing 0.3 mg/ml soybean trypsin inhibitor and 3.4 mg/ml bacitracin. The homogenate was centrifuged at  $27,000 \times g$  (0 to  $4^{\circ}\text{C}$ ) for 10 min. The pellet was resuspended in 40 volumes of buffer and recentrifuged. The pellet was resuspended in 40 volumes of buffer and used in the ribosylation assays.

The protein concentration was determined prior to experimentation to permit adjustment of the samples to equivalent protein concentrations. Protein was determined by the method of Lowry *et al.* (1951) following solubilization of the samples in 0.5 M NaOH. Bovine serum albumin (Sigma) was used as the standard.

#### *[ $^{32}\text{P}$ ]ADP ribosylation*

Pertussis toxin-catalyzed [ $^{32}\text{P}$ ]ADP ribosylation of  $\alpha$  subunits of  $G_i$  and  $G_o$  followed the procedures described in Siebenaller and Murray (1990). Pertussis toxin was activated in 100 mM Tris-HCl, pH 8.0 with 50 mM dithiothreitol for 1 h at room temperature. The 100  $\mu\text{l}$  incubation mixture routinely contained 100 mM Tris-HCl, pH 7.6 at the incubation temperature of  $5^{\circ}\text{C}$ , 25 mM dithiothreitol, 2 mM ATP, 2  $\mu\text{Ci}$  NAD, 1.5  $\mu\text{g}$  soybean trypsin inhibitor, 15  $\mu\text{g}$  bacitracin, 2  $\mu\text{g}$  pertussis toxin, and 10 to 20  $\mu\text{g}$  of membrane protein. The incubation was stopped by adding 50  $\mu\text{l}$  of stop solution (3% sodium dodecyl sulfate, 42% glycerol, 15% 2-mercaptoethanol, 200 mM Tris-HCl, pH 6.8 at  $20^{\circ}\text{C}$ ) and the mixture was boiled for 5 min. The denatured samples were subjected to sodium dodecyl sulfate polyacrylamide electrophoresis (SDS-PAGE) in 1.5 mm thick 12.5% acrylamide gels following Laemmli (1970). The gel was stained with 0.25% Serva Blue R (Serva Fine Biochemicals, Westbury, New York) in 25% 2-propanol, 10% acetic acid, destained, and dried. The dried gels were apposed to Kodak (Rochester, New York) X-Omat AR film. DuPont Cronex Lightning Plus intensifying screens were used. The developed autoradiograms were digitized and quantified with an MCID

system (Imaging Research, Inc., St. Catherine, Ontario, Canada).

#### *Immunological quantification of G proteins*

Membranes were diluted to the appropriate protein concentration and electrophoresed in Laemmli sodium dodecyl sulfate mini-gels (0.75 mm thick, 4.5% acrylamide stacking/12.5% acrylamide resolving) in a BioRad MiniProtein II electrophoresis unit. When using AS/7 antiserum to detect  $G_{i\alpha 1}$  and  $G_{i\alpha 2}$ , we supplemented the resolving gel with 4 M urea to enhance separation of these proteins. For routine assays, 10  $\mu\text{g}$  samples were diluted in  $2 \times$  Laemmli sample buffer for a final volume of 15  $\mu\text{l}$  and heated to  $95^{\circ}\text{C}$  for 3 min. Samples of each species were run on each gel.

Proteins were transferred from the gels to nitrocellulose membranes (Schleicher & Schuell, BA85, 0.45  $\mu\text{m}$ ) on a Sartoblot II-S transfer block (Sartorius). Transfer was accomplished in 12 h at 100 mA (constant current) using 25 mM Tris, 150 mM glycine, 10% methanol, pH 8.3. The nitrocellulose membrane was stained in 0.2% Ponceau S (Sigma Chemical Co.) and the polyacrylamide gels were stained with Coomassie Brilliant Blue R (Sigma) to assess completeness of transfer. After destaining in deionized water, the nitrocellulose was blocked for 1 h at room temperature with 1% nonfat dried milk (Carnation) in Tris-buffered saline (TBS: 20 mM Tris HCl, 150 mM NaCl, pH 7.5 and 0.05% Tween-20). The washed nitrocellulose membrane was incubated overnight at  $4^{\circ}\text{C}$  with primary rabbit antisera diluted 1:1000 in 1% dried milk/TBS. Following multiple washes in TBS and 1% dried milk/TBS, the blots were incubated for 2 h at room temperature with goat anti-rabbit IgG alkaline phosphatase conjugate (Sigma) diluted 1:1000 in 1% dried milk/TBS. The nitrocellulose was again washed in TBS, and then washed in alkaline phosphatase buffer (0.1 M Tris-HCl, 0.1 M NaCl, 2 mM  $\text{MgCl}_2$ , 1  $\mu\text{M}$   $\text{ZnCl}_2$ , 25 mM diethanolamine, pH 9.55). Enzyme activity was assayed using 3 mg/ml nitroblue tetrazolium chloride and 0.17 mg/ml 5-bromo-4-chloro-3-indolyl phosphate p-toluidine salt (Sigma) in alkaline phosphatase buffer. Color development was stopped after 5 to 10 min by washing with deionized water. The blots were digitized and quantified using the MCID system.

#### *Data analysis*

Statistical comparisons were made by Student's *t*-test and analysis of variance using InStat (GraphPad, San Diego, California).

#### *Reagents*

[Adenylate- $^{32}\text{P}$ ]-nicotinamide adenine dinucleotide ([ $^{32}\text{P}$ ]NAD, 31.31 Ci/mmol) was from DuPont NEN

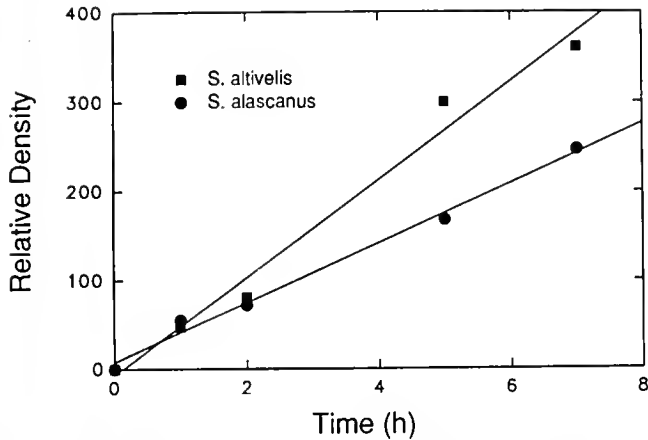


**Figure 1.** Time course of pertussis toxin-catalyzed [ $^{32}$ P]ADP-ribosylation of *Sebastolobus altivelis* (squares) and *S. alascanus* (circles) brain membranes at 5°C. Preparations were incubated with 2  $\mu$ Ci [ $^{32}$ P]NAD and 2  $\mu$ g preactivated pertussis toxin. The samples were denatured and subjected to SDS-PAGE. The dried gels were exposed to x-ray film. The relative optical density was determined by densitometric analysis of the autoradiogram. The results are from a single experiment which was replicated twice with similar results.

(Boston, Massachusetts). Pertussis toxin (islet activating protein) was from List Biological Laboratories, Inc. (Campbell, California). Water was processed through a four-bowl Milli-Q purification system (Millipore, Bedford, Massachusetts). Molecular weight standards were from BioRad. The antipeptide antisera obtained from DuPont NEN were AS/7 (recognizes  $G_{i\alpha 1}$  and  $G_{i\alpha 2}$ , Goldsmith *et al.*, 1987, 1988), EC/2 (recognizes  $G_{i\alpha 3}$  and  $G_{o\alpha}$ , Simonds *et al.*, 1989) GC/2 (recognizes  $G_{o\alpha}$ , Spiegel, 1990) and MS/1 (recognizes  $G_{\beta}$ , Goldsmith *et al.*, 1988). These antisera had been raised to deduced consensus sequence peptides of the carboxy- and amino-termini of G protein subunits of mammalian species (*e.g.*, McKenzie *et al.*, 1988; Mumby and Gilman, 1991). Other reagents were purchased from Sigma Chemical Co. (St. Louis, Missouri).

## Results

The time course of pertussis toxin-catalyzed [ $^{32}$ P]ADP-ribosylation of brain membranes from *S. altivelis* and *S. alascanus* is depicted in Figure 1. At 5°C, the labeling of G protein  $\alpha$  subunits was linear for 7 h in both species.

The pertussis toxin concentration-response relationships in both species were evaluated in a fixed 6-h incubation. Equivalent amounts of *S. altivelis* and *S. alascanus* membrane protein were loaded on SDS-polyacrylamide gels following the [ $^{32}$ P]ADP-ribosylation reaction. The dependence of [ $^{32}$ P]ADP-ribosylation on pertussis toxin concentration is shown in the autoradiogram in Figure 2. In brain membranes from both species there was no specific labeling in the absence of pertussis toxin. The extent

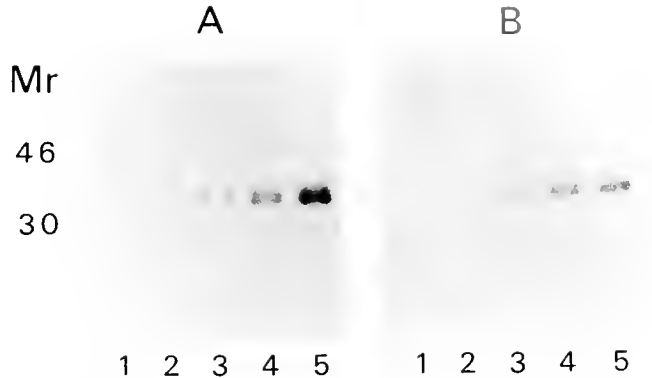


**Figure 2.** Autoradiogram of pertussis toxin-catalyzed [ $^{32}$ P]ADP-ribosylation of *Sebastolobus altivelis* (A) and *S. alascanus* (B) brain membranes. Membranes were incubated for 6 h at 5°C with 2  $\mu$ Ci [ $^{32}$ P]NAD in the presence of increasing concentrations of pertussis toxin. The concentrations of pertussis toxin used are Lane 1, 5 ng/ $\mu$ l; Lane 2, 10 ng/ $\mu$ l; Lane 3, 25 ng/ $\mu$ l; Lane 4, 50 ng/ $\mu$ l; and Lane 5, 100 ng/ $\mu$ l. The membranes were subjected to SDS-PAGE and labeled proteins were detected by autoradiography. The results are from a single representative experiment that was repeated three times.

of [ $^{32}$ P]ADP-ribosylation increased as a function of pertussis toxin concentration (5–100 ng/ $\mu$ l) in both species. The labeling was consistently greater in *S. altivelis* membranes. Proteins of 39 kDa and 41 kDa were radiolabeled in both species. Image analysis of the autoradiograms per-

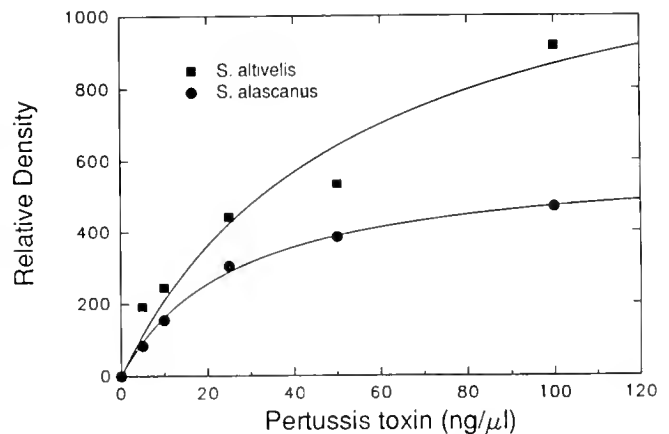


**Figure 3.** Concentration-response relationship for pertussis toxin-catalyzed [ $^{32}$ P]ADP-ribosylation of *Sebastolobus altivelis* (squares) and *S. alascanus* (circles) brain membranes for 6 h at 5°C. The curves are the best fits to the data using the logistic function:  $E = (E_{max}) / (1 + EC_{50} / [PTX])$ . E is the effect in units of relative optical density and  $E_{max}$  is the maximum effect.  $EC_{50}$  is the concentration of pertussis toxin (PTX) which produced 50% of the maximum effect, and [PTX] is the concentration of pertussis toxin. The maximum extent of [ $^{32}$ P]ADP-ribosylation in *S. altivelis* brain membranes was 2.2-fold greater than the level of [ $^{32}$ P]ADP-ribosylation in *S. alascanus* membranes. The results depicted represent the fits to pooled data from three separate experiments. The parameter estimates derived from this analysis are shown in Table I.

Table I

Analysis of pertussis toxin concentration-response relationships in *Sebastolobus altivelis* and *S. alascanus* brain membranes

Species	Pertussis toxin EC <sub>50</sub> (ng)	E <sub>max</sub> (ROD)
<i>S. alascanus</i>	26.7 ± 3	597 ± 25
<i>S. altivelis</i>	53.5 ± 27	1329 ± 325

E<sub>max</sub> units are relative optical density (ROD).

mitted quantification of the relative optical density of each lane. The resultant pertussis toxin concentration-response curves are shown in Figure 3. The maximum level of [<sup>32</sup>P]ADP-ribosylation is significantly greater in *S. altivelis* brain membranes than in *S. alascanus* membranes (Fig. 3, Table I). The EC<sub>50</sub> values for pertussis toxin in the two species were not significantly different (Table I).

The increase in the extent of pertussis toxin-induced labeling of G protein α subunits in *S. altivelis* could be due to a greater accessibility of the ribosylation sites of the G<sub>1α</sub> and G<sub>0α</sub> substrates, or to elevated quantities of G<sub>1α</sub> and G<sub>0α</sub> or G<sub>βγ</sub>. Western immunoblots were employed to quantify the levels of G protein α and β subunits in brain membranes of the two *Sebastolobus* species. For these studies, another deep-living species, *Antimora rostrata*, exemplified the pattern and diversity of immunoreactive material in brain membranes from another marine fish family (Moridae). Rat (*Rattus rattus*) brain membranes were employed as a reference to aid in identifying the immunoreactive material. Equal amounts of membrane protein from each species were loaded on gels and an array of antipeptide antisera were employed to detect G<sub>1α1</sub>, G<sub>1α2</sub>, G<sub>1α3</sub>, G<sub>0α</sub> and the β subunit. Standard curves were generated for each antiserum by varying the amount of membrane protein loaded on gels. The inten-

Table II

Quantitation of material in brain membranes of *Sebastolobus alascanus* and *S. altivelis* immunoreactive to antibodies directed against α and β subunits of G<sub>i</sub> and G<sub>o</sub>

Subunit	<i>S. alascanus</i>	<i>S. altivelis</i>
G <sub>i</sub> α <sub>1</sub>	1 (9)	1.14 ± 0.29 (8)
G <sub>i</sub> α <sub>2</sub>	1 (10)	1.09 ± 0.19 (9)
G <sub>i</sub> α <sub>3</sub>	1 (12)	1.63 ± 0.40* (12)
G <sub>o</sub> α	1 (13)	1.12 ± 0.28 (13)
β <sub>36</sub>	1 (14)	1.06 ± 0.10 (11)

The data are standardized to *S. alascanus*. The number of determinations is given in parentheses.

\* Value significantly different from the 1.00 value at  $P < 0.05$ .

sity of staining of G protein subunits was within the linear range of immunoreactivity for the results shown. Representative immunoblots for G<sub>1α1</sub>, G<sub>1α2</sub>, G<sub>1α3</sub>, and G<sub>0α</sub> are depicted in Figure 4.

Using antiserum EC/2 to detect G<sub>1α3</sub>, we observed a single band in brain membranes of the four species. This band from brain membranes of *A. rostrata* and *R. rattus* migrated as an approximately 41 kDa protein. The corresponding protein in both *Sebastolobus* species had a lesser apparent molecular mass. The intensity of staining of this protein was consistently greater (mean = 1.63-fold) in *S. altivelis* than in *S. alascanus* brain membranes (Table II). Antiserum EC/2 was raised against the carboxyterminal decapeptide of mammalian transducin-α (Goldsmith *et al.*, 1987) and crossreacts somewhat with both G<sub>0α</sub> and G<sub>1α1</sub> (Simonds *et al.*, 1989). Because only a single band was identified in each species, these bands are tentatively identified as G<sub>1α3</sub>.

Antiserum GC/2 was used to detect G<sub>0α</sub>. As shown in Figure 4, this antiserum recognized a single band of ap-

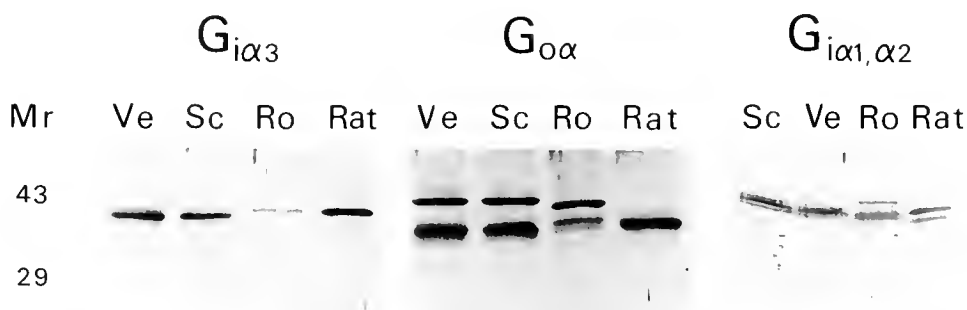
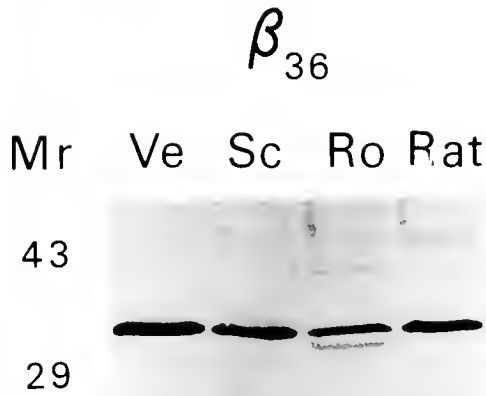


Figure 4. Immunoblots of *Sebastolobus altivelis* (Ve), *S. alascanus* (Sc), *Antimora rostrata* (Ro), and *Rattus rattus* (Rat) brain membranes obtained with peptide antisera specific for G protein α subunits. Brain membranes were subjected to SDS-PAGE, and the separated proteins were transferred to nitrocellulose membranes. Immunoblotting was performed with antiserum EC/2, selective for G<sub>1α3</sub>, antiserum GC/2, selective for G<sub>0α</sub>, and antiserum AS/7 which recognizes G<sub>1α1</sub> and G<sub>1α2</sub>. The positions of molecular weight standards are indicated.



**Figure 5.** Immunoblots of *Sebastolobus altivelis* (Ve), *S. alascanus* (Sc), *Antimora rostrata* (Ro), and *Rattus rattus* (Rat) brain membranes obtained using a peptide antiserum (MS/1) which recognizes the  $\beta$  subunit (36 kDa) of G proteins.

proximately 39 kDa in rat brain membranes, but two immunoreactive proteins were detected in all three marine fishes. In addition to a heavily stained band of approximately 39 kDa, which likely represents  $G_{\alpha c}$ , brain membranes from the marine teleosts displayed immunoreactive proteins of apparent molecular masses of 41 to 42 kDa. There were no significant differences between the two *Sebastolobus* species in the intensity of immunoreactive bands detected with the antiserum GC/2 (Table II).

The antipeptide antiserum AS/7 was used to identify  $G_{\alpha 1}$  and  $G_{\alpha 2}$ . These  $\alpha$  subunits in rat brain were readily resolved in the presence of 4 M urea in the running gel (Fig. 4). This doublet was not resolved as well in the three marine fishes, where the band tentatively identified as  $G_{\alpha 2}$  migrated somewhat slower than the corresponding protein in rat brain membranes. There were no significant differences in the levels of  $G_{\alpha 1}$  or  $G_{\alpha 2}$  between the *Sebastolobus* species (Table II).

Immunoblots of G protein  $\beta$  subunits are depicted in Figure 5. The antiserum MS/1 was used to quantify the 36 kDa  $\beta$  subunits, and the intensity of these bands did not differ significantly between the *Sebastolobus* species (Table II).

The substrate for the pertussis toxin-catalyzed ADP-ribosylation reaction is the heterotrimeric holoprotein (Neer *et al.*, 1984; Van Dop *et al.*, 1984), and as a consequence, guanyl nucleotides are capable of modulating the sensitivity of G proteins to pertussis toxin (*e.g.*, Gierschik, 1992). We therefore compared the guanyl nucleotide regulation of ADP-ribosylation in *S. altivelis* and *S. alascanus*. The aim was to examine the differential susceptibility of the G protein  $\alpha$  subunits to modification by pertussis toxin.

Increasing concentrations of guanosine 5'-diphosphate (GDP) included in the incubation with pertussis toxin augmented the extent of [ $^{32}$ P]ADP-ribosylation in *S. altivelis* brain membranes (Fig. 6). Only the highest concentration tested, 1000  $\mu$ M GDP, had an effect in *S. alascanus* brain membranes, and this effect was modest (Fig. 6).

Incubation with the nonhydrolyzable GTP analog guanosine 5'-O-(3-thiotriphosphate) (GTP $\gamma$ S) effected a marked suppression of [ $^{32}$ P]ADP-ribosylation in *S. alascanus* brain membranes (Fig. 7). [ $^{32}$ P]ADP-ribosylation of the G protein  $\alpha$  subunits of *S. altivelis* membranes was relatively insensitive to the effect of GTP $\gamma$ S (Fig. 7). The concentration-dependent inhibition of pertussis toxin-catalyzed ADP-ribosylation produced by GTP $\gamma$ S in *S. alascanus* brain membranes presumably reflects a dissociation of the  $G_i$  and  $G_o$  heterotrimers.

## Discussion

Pertussis toxin catalyzes the incorporation of significantly more [ $^{32}$ P]ADP into brain membranes of *S. altivelis* than of *S. alascanus* (Siebenaller *et al.*, 1991; Fig. 2 and 3, Table I). Although *S. altivelis* brain membranes have

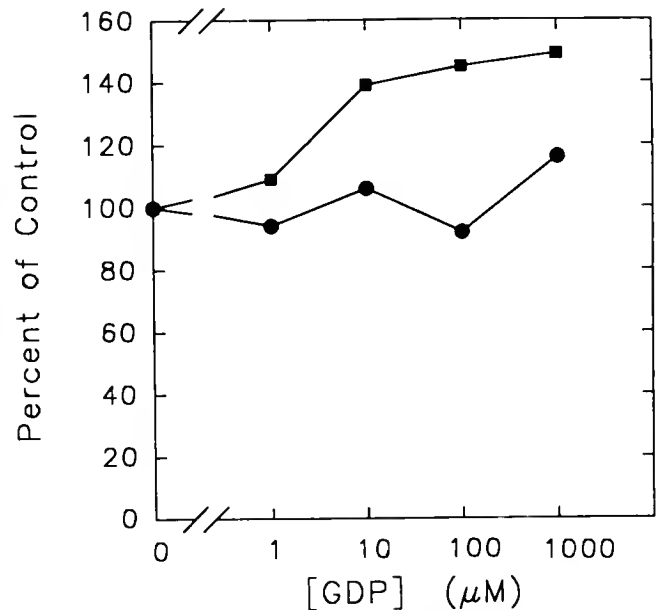


**Figure 6.** Effects of GDP on pertussis toxin-catalyzed [ $^{32}$ P]ADP ribosylation of G protein  $\alpha$  subunits in brain membranes of *S. altivelis* (squares) and *S. alascanus* (circles). Membranes were incubated with 2  $\mu$ Ci [ $^{32}$ P]NAD and 2  $\mu$ g preactivated pertussis toxin in the presence of increasing concentrations of GDP. Incubations were at 5°C for 6 h. SDS-PAGE and autoradiography were carried out as described in Materials and Methods. The ordinate values represent the relative optical density of autoradiograms expressed as % of control value determined in the absence of GDP. The results depicted are derived from a single experiment which was replicated twice with similar results.

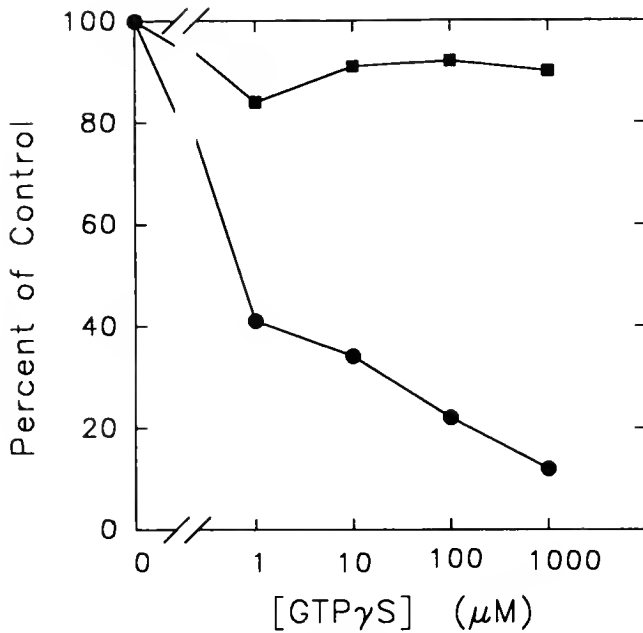


Figure 7. Effects of GTP $\gamma$ S on pertussis toxin-catalyzed [ $^{32}$ P]ADP-ribosylation of G protein  $\alpha$  subunits in brain membranes of *S. altivelis* (squares) and *S. alascanus* (circles). The methods and data presentation are as described in the legend to Figure 6.

a 63% higher level of one subtype of pertussis toxin substrate, G $_{i\alpha 3}$  (Table II), a simple increase in the amount of G protein substrates cannot adequately explain the differences between the two species. There are also qualitative differences in the pertussis toxin-catalyzed reaction; *i.e.*, the guanyl nucleotides GDP and GTP $\gamma$ S modulate the [ $^{32}$ P]ADP-ribosylation reaction differently in the membranes of the two species (Figs. 6, 7). These experiments indicate that *S. alascanus* brain membranes contain lower quantities of one type of pertussis toxin substrate, and that the ribosylation sites of the substrates are less accessible to pertussis toxin.

The differences between the two species in the guanyl nucleotide modulation of ribosylation may relate to the interactions of G $_i$  and G $_o$  with receptors. The A $_1$  adenosine receptors of *S. alascanus* brain membranes are more tightly coupled to G proteins, and a larger fraction exist coupled, than are those of *S. altivelis* (Murray and Siebenaller, 1987). This conclusion is based on the greater agonist affinity of the A $_1$  adenosine receptor and the larger fraction of receptors in the high affinity state in *S. alascanus* (Murray and Siebenaller, 1987). The present study suggests that this relatively tighter coupling may be characteristic of other receptors. Tighter receptor-G protein interactions might explain the reduced susceptibility to pertussis toxin-catalyzed ADP-ribosylation in *S. alascanus* membranes; *i.e.*, it would reduce accessibility of the carboxyterminal ADP-ribosylation site to pertussis toxin due to steric hindrance caused by the receptor.

Both the subunit aggregation state of G $_i$  and G $_o$  and interactions with other membrane components will affect the susceptibility of these G proteins to [ $^{32}$ P]ADP-ribosylation (Neer *et al.*, 1984; Van Dop *et al.*, 1984; Panico *et al.*, 1990; van der Ploeg *et al.*, 1992). The carboxyterminal region of the G protein is involved in interactions with receptors (Boege *et al.*, 1991) and may sterically hinder modification of the cysteine that is ADP-ribosylated (West *et al.*, 1985). Because guanyl nucleotides affect the aggregation state and conformation of G proteins, we compared the effects of guanyl nucleotides in modulating pertussis toxin-induced ADP-ribosylation.

GDP augmented the level of ADP-ribosylation produced by pertussis toxin to a greater extent in *S. altivelis* than in *S. alascanus* brain membranes (Fig. 6); only the highest concentration of GDP tested (1000  $\mu$ M) was effective in *S. alascanus* membranes. GDP may enhance [ $^{32}$ P]ADP-ribosylation by promoting the formation and stabilization of the substrate G $_{\alpha\beta\gamma}$  holoprotein (Birnbauer *et al.*, 1990) and by dissociating the G $_{\alpha\beta\gamma}$  holoprotein from unoccupied receptors (Panico *et al.*, 1990; van der Ploeg *et al.*, 1992). This latter action would facilitate ADP-ribosylation by relieving the steric hindrance caused by receptor coupling to heterotrimeric G proteins (van der Ploeg *et al.*, 1992). Thus, by promoting the dissociation of the unoccupied receptor-G $_{\alpha\beta\gamma}$  complex, GDP may expose the carboxyterminal cysteine residue to pertussis toxin. In *S. alascanus* brain membranes, G proteins more tightly coupled to high-affinity forms of receptors would have a reduced affinity for GDP.

In the presence of GTP $\gamma$ S, the extent of incorporation of the radiolabel into G protein  $\alpha$  subunits of *S. alascanus* brain membrane was markedly suppressed; *S. altivelis* G protein  $\alpha$  subunits were much less sensitive to this inhibitory modulation (Fig. 7). The results with *S. alascanus* membranes are in accordance with the demonstration that GTP $\gamma$ S markedly inhibits pertussis toxin-catalyzed ADP-ribosylation of a 40 kDa protein in rat glioma membranes (Milligan, 1987). GTP $\gamma$ S promoting the dissociation of G $_i$  and G $_o$  protein heterotrimers into  $\alpha \cdot$ GTP $\gamma$ S and  $\beta\gamma$  subunits may underlie this effect, although a GTP $\gamma$ S induced conformational change in G proteins has also been reported to inhibit ADP-ribosylation (Mattera *et al.*, 1987; Yi *et al.*, 1991).

Tighter association of receptors and G proteins in *S. alascanus* would result in a larger fraction of coupled receptors. This could promote, relative to uncoupled G proteins, the binding of GTP $\gamma$ S to the unoccupied guanyl nucleotide binding site, eliciting the dissociation of the G protein subunits, and a resultant decrease in [ $^{32}$ P]ADP-ribosylation. This would be less likely to occur in *S. altivelis* brain membranes inasmuch as the uncoupled population of G protein heterotrimers would be largely GDP-liganded. The modest GDP-enhancement of ADP-

ribosylation in *S. altivelis* membranes could result from the stabilization and recruitment of that fraction of G proteins that are either uncoupled or loosely coupled, and unliganded by GDP.

This reasoning is supported by several observations. First, unoccupied receptors can stimulate, albeit weakly, G protein activation; signaling is a consequence of an agonist-induced increase in the efficacy of G protein-receptor coupling (Birnbaumer *et al.*, 1990; Mukai *et al.*, 1992). Second, the high affinity states of receptors, i.e., G protein-coupled states, can be abolished by the addition of guanyl nucleotides (Mukai *et al.*, 1992). Third, solubilized receptors are often isolated precoupled with G proteins and this coupling can be disrupted by the addition of guanyl nucleotides (Leid *et al.*, 1989).

The coupling of G proteins and receptors is sensitive to the degree of membrane order (Casadó *et al.*, 1992). In porcine brain cortical membranes, increased membrane viscosity abolishes the high affinity (G protein-coupled) A<sub>1</sub> adenosine receptor state (Casadó *et al.*, 1992). In hepatocytes, membrane viscosity influences the lateral movement of components of the glucagon-G protein-adenylyl cyclase complex necessary for signal transduction (Houslay *et al.*, 1980, 1981). The brain membrane phospholipid and fatty acid compositions of the *Sebastolobus* species are identical, and the different hydrostatic pressures experienced by the species will impose different degrees of membrane order (Siebenaller, 1991). A less efficient coupling of receptors in brain membranes of the deeper-living *S. altivelis* may reflect a requirement for greater conformational flexibility and mobility for elements functioning in the more ordered membrane environment of *S. altivelis* at its *in situ* pressure. That the G<sub>i</sub> and G<sub>o</sub> proteins of *S. altivelis* membranes are better substrates for pertussis toxin-catalyzed [<sup>32</sup>P]ADP-ribosylation may reflect this greater conformational flexibility. Based on these considerations, we predict that, in addition to the A<sub>1</sub> adenosine receptor, other G protein-coupled receptor signaling complexes will be sensitive to pressure perturbation.

The precise homology of the G protein  $\alpha$  subunits in fish membrane to mammalian  $\alpha$  subunits cannot be ascertained at present, although comparisons of cloned  $\alpha$  subunit genes from a variety of organisms suggest a slow evolution of these genes, as would be expected for proteins with such important biological functions (Yokoyama and Starmer, 1992). The array of G protein subunits identified in three fishes from two families with antisera directed against mammalian consensus peptides supports the evolutionary conservation of these proteins. But the unique protein in fish brain identified with GC/2 antiserum (Fig. 4) and the altered electrophoretic mobilities of G<sub>1 $\alpha$</sub>  in the *Sebastolobus* species (Fig. 4) suggest that there may be phylogenetic diversity as well. The central role played by

G proteins in transmembrane signaling makes them an important site for adaptation to environmental parameters.

### Acknowledgments

This research was supported by ONR grant N0014-89-J-1865 and NSF grant DCB-8710155. We thank the scientific parties on the R/V *Wecoma* cruises, particularly J. M. Willis. Shiptime on the R/V *Gyre* off the coast of Newfoundland was supported by NSF grant DMB-8502857 to Dr. A. F. Riggs. We thank Drs. A. Riggs and R. Noble for their help in obtaining specimens of *Antimora rostrata*. We thank Patricia Perry, Valerie Caldwell, and Barbara Hettinger-Smith for the Western immunoblots and Ron Bouchard for photographic services.

### Literature Cited

- Barinaga, M. 1991. How the nose knows: olfactory receptors cloned. *Science* 252: 209-210.
- Birnbaumer, L. 1992. Receptor-to-effector signaling through G proteins: Roles for  $\beta\gamma$  dimers as well as  $\alpha$  subunits. *Cell* 71: 1069-1072.
- Birnbaumer, L., J. Abramowitz, and A. M. Brown. 1990. Receptor-effector coupling by G proteins. *Biochim. Biophys. Acta* 1031: 163-224.
- Boege, F., E. Neumann, and E. J. M. Helmreich. 1991. Structural heterogeneity of membrane receptors and GTP-binding proteins and its functional consequences for signal transduction. *Eur. J. Biochem.* 199: 1-15.
- Casadó, V., J. Mallol, E. I. Canela, R. Franco, and C. Lluís. 1992. Modulation of adenosine agonist [<sup>3</sup>H]N<sup>6</sup>-(R)-phenylisopropyladenosine binding to pig brain cortical membranes by changes of membrane fluidity and of medium physicochemical characteristics. *Eur. J. Pharmacol. Mol. Pharmacol.* 225: 7-14.
- Gierschik, P. 1992. ADP-ribosylation of signal-transducing guanine nucleotide-binding proteins by pertussis toxin. *Current Topics in Microbiology and Immunology* 175: 69-96.
- Gilman, A. G. 1987. G proteins: transducers of receptor-generated signals. *Ann. Rev. Biochem.* 56: 615-649.
- Goldsmith, P., P. Gierschik, G. Milligan, C. G. Unson, R. Vinitzky, H. Malech, and A. M. Spiegel. 1987. Antibodies directed against synthetic peptides distinguish between GTP-binding proteins in neutrophil and brain. *J. Biol. Chem.* 262: 14683-14688.
- Goldsmith, P., K. Rossiter, A. Carter, W. Simonds, C. G. Unson, R. Vinitzky, and A. M. Spiegel. 1988. Identification of the GTP-binding protein encoded by G<sub>3</sub> complementary DNA. *J. Biol. Chem.* 263: 6476-6479.
- Haedrich, R. L. and N. R. Merrett. 1988. Summary atlas of deep-living demersal fishes in the North Atlantic Basin. *J. Nat. Hist.* 22: 1325-1362.
- Houslay, M. D., I. Dipple, and R. F. Elliott. 1980. Guanosine 5'-triphosphate and guanosine 5'-[ $\beta\gamma$ -imido]triphosphate effect a collision coupling mechanism between the glucagon receptor and catalytic unit of adenylate cyclase. *Biochem. J.* 186: 649-658.
- Houslay, M. D., I. Dipple, and L. M. Gordon. 1981. Phenobarbital selectively modulates the glucagon-stimulated activity of adenylate cyclase by depressing the lipid phase separation occurring in the outer half of the bilayer of liver plasma membranes. *Biochem. J.* 197: 675-681.
- Hubbs, C. L. 1926. The supposed intergradation of two species of *Sebastolobus* (a genus of scorpaenoid fishes) of western America. *American Museum Novitates* 216: 1-9.



- Katada, T., and M. Ui. 1982. Direct modification of the membrane adenylate cyclase system by islet-activating protein due to ADP-ribosylation of a membrane protein. *Proc. Natl. Acad. Sci. U.S.A.* **79**: 3129-3133.
- Laemmli, U. K. 1970. Cleavage of structural proteins during the assembly of the head of bacteriophage T4. *Nature* **227**: 680-685.
- Lefkowitz, R. J. 1992. G proteins: the subunit story thickens. *Nature* **358**: 372.
- Leid, M., M. I. Schimerlik, and T. F. Murray. 1989. Agonist radioligand interactions with the solubilized porcine atrial A<sub>1</sub> adenosine receptor. *Mol. Pharmacol.* **35**: 450-457.
- Linden, J. 1991. Structure and function of A<sub>1</sub> adenosine receptors. *EASEB J.* **5**: 2668-2676.
- Lowry, O. H., N. J. Rosebrough, A. L. Farr, and R. J. Randall. 1951. Protein measurement with the Folin phenol reagent. *J. Biol. Chem.* **193**: 265-275.
- Mattera, R., J. Codina, R. D. Sekura, and L. Birnbaumer. 1987. Guanosine 5'-O-(3-thiotriphosphate) reduces ADP-ribosylation of the inhibitory guanine nucleotide-binding regulatory protein of adenyl cyclase (N<sub>i</sub>) by pertussis toxin without causing dissociation of the subunits of N<sub>i</sub>: evidence of existence of heterotrimeric *pt+* and *pt-* conformations of N<sub>i</sub>. *J. Biol. Chem.* **262**: 11247-11251.
- McKenzie, F. R., I. Mullaney, C. G. Unson, A. M. Spiegel, and G. Milligan. 1988. The use of anti-peptide antisera to probe interactions between receptors and guanine nucleotide binding proteins. *Biochem. Soc. Trans.* **16**: 434-437.
- Miller, D. J., and R. N. Lea. 1976. *Guide to the Coastal Marine Fishes of California*. California Department of Fish and Game, Sacramento.
- Milligan, G. 1987. Guanine nucleotide regulation of the pertussis and cholera toxin substrates of rat glioma C6 BU1 cells. *Biochim. Biophys. Acta* **929**: 197-202.
- Mukai, H., E. Munekata, and T. Higashijima. 1992. G protein antagonists. *J. Biol. Chem.* **267**: 16237-16243.
- Mumby, S. M., and A. G. Gilman. 1991. Synthetic peptide antisera with determined specificity for G protein  $\alpha$  or  $\beta$  subunits. *Methods Enzymol.* **195**: 215-233.
- Murray, T. F., and J. F. Siebenaller. 1987. Comparison of the binding properties of A<sub>1</sub> adenosine receptors in brain membranes of two congeneric marine fishes living at different depths. *J. Comp. Physiol.* **157**: 267-277.
- Neer, E. J., J. M. Lok, and L. G. Wolf. 1984. Purification and properties of the inhibitory guanine nucleotide regulatory unit of brain adenylate cyclase. *J. Biol. Chem.* **259**: 14222-14229.
- Panico, J., J. H. Parkes, and P. A. Liebman. 1990. The effect of GDP on rod outer segment G-protein interactions. *J. Biol. Chem.* **265**: 18922-18927.
- van der Ploeg, I., F. E. Parkinson, and B. B. Fredholm. 1992. Effect of pertussis toxin on radioligand binding to rat brain adenosine A<sub>1</sub> receptors. *J. Neurochem.* **58**: 1221-1229.
- Shinitzky, M. 1984. Membrane fluidity and cellular functions. Pp. 1-51 in *Physiology of Membrane Fluidity. Volume I*. M. Shinitzky, ed. CRC Press, Boca Raton.
- Siebenaller, J. F. 1984a. Pressure-adaptive differences in NAD-dependent dehydrogenases of congeneric marine fishes living at different depths. *J. Comp. Physiol. B* **154**: 443-448.
- Siebenaller, J. F. 1984b. Structural comparison of lactate dehydrogenase homologs differing in sensitivity to hydrostatic pressure. *Biochim. Biophys. Acta* **786**: 161-169.
- Siebenaller, J. F. 1987. Biochemical adaptation in deep-sea animals. Pp. 34-48 in *Current Perspectives in High Pressure Biology*. H. W. Jannasch, A. M. Zimmerman and R. E. Marquis, eds. Academic Press, London.
- Siebenaller, J. F. 1991. Pressure as an environmental variable: magnitude and mechanisms of perturbation. Pp. 323-343 in *Biochemistry and Molecular Biology of Fishes, Volume I*. P. W. Hochachka and T. P. Mommsen, eds. Elsevier, Amsterdam.
- Siebenaller, J. F., and T. F. Murray. 1990. A<sub>1</sub> adenosine receptor modulation of adenyl cyclase of a deep-living teleost fish, *Antimora rostrata*. *Biol. Bull.* **178**: 65-73.
- Siebenaller, J. F., and T. F. Murray. 1993. The effects of hydrostatic pressure on the low-K<sub>m</sub> GTPase in brain membranes from two congeneric marine fishes. *J. Comp. Physiol. B* (in press).
- Siebenaller, J. F., and G. N. Somero. 1978. Pressure-adaptive differences in lactate dehydrogenases of congeneric fishes living at different depths. *Science* **201**: 255-257.
- Siebenaller, J. F., and G. N. Somero. 1989. Biochemical adaptation to the deep sea. *Rev. Aquatic Sci.* **1**: 1-25.
- Siebenaller, J. F., A. F. Hagar, and T. F. Murray. 1991. The effects of hydrostatic pressure on A<sub>1</sub> adenosine receptor signal transduction in brain membranes of two congeneric marine fishes. *J. Exp. Biol.* **159**: 23-43.
- Simon, M. I., M. P. Strathmann, and N. Gautam. 1991. Diversity of G proteins in signal transduction. *Science* **252**: 802-808.
- Simonds, W. F., P. K. Goldsmith, J. Codina, C. G. Unson, and A. M. Spiegel. 1989. G<sub>2</sub> mediates  $\alpha_2$ -adrenergic inhibition of adenyl cyclase in platelet membranes: *in situ* identification with G<sub>2</sub> C-terminal antibodies. *Proc. Natl. Acad. Sci. U.S.A.* **86**: 7809-7813.
- Spiegel, A. M. 1990. Antibodies as probes of the structure and function of heterotrimeric GTP-binding proteins. Pp. 207-224 in *ADP-ribosylation Toxins and G-proteins*. J. Moss and M. Vaughan, eds. American Society of Microbiology.
- Van Dop, C., G. Yamanaka, F. Steinberg, R. D. Sekura, C. R. Manclark, L. Stryer, and H. R. Bourne. 1984. ADP-ribosylation of transducin by pertussis toxin blocks the light-stimulated hydrolysis of GTP and cGMP in retinal photoreceptors. *J. Biol. Chem.* **259**: 23-26.
- West, R. E., Jr., J. Moss, M. Vaughan, T. Liu and T.-Y. Liu. 1985. Pertussis toxin-catalyzed ADP-ribosylation of transducin: cysteine 347 is the ADP-ribose acceptor site. *J. Biol. Chem.* **260**: 14428-14430.
- Yi, F., B. M. Denker, and E. J. Neer. 1991. Structural and functional studies of cross-linked G<sub>o</sub> protein subunits. *J. Biol. Chem.* **266**: 3900-3906.
- Yokoyama, S., and W. T. Starmer. 1992. Phylogeny and evolutionary rates of G protein  $\alpha$  subunit genes. *J. Mol. Evol.* **35**: 230-238.



## Multixenobiotic Resistance in *Urechis caupo* Embryos: Protection From Environmental Toxins

BARBARA HOLLAND TOOMEY AND DAVID EPEL

*Hopkins Marine Station, Stanford University, Pacific Grove, California 93950*

**Abstract.** *Urechis caupo* is a marine worm that lives and reproduces in sediments containing a variety of potentially toxic environmental chemicals (xenobiotics). Its embryos have a multixenobiotic transporter, which is similar to the multidrug transporter in mammals, as indicated by their ability to transport a variety of moderately hydrophobic compounds such as dyes, drugs, and pesticides out of the cells. The cell membranes of the embryos contain a protein of approximately 145 kD that is immunologically related to the mammalian multidrug transport protein and that can be cross-linked by a photoactivatable substrate of the mammalian multidrug transport protein. The sediments in which the worm lives contain potential substrates for the transporter, indicating that this multixenobiotic transport activity may protect *Urechis* embryos from naturally occurring toxic compounds. Embryos of a sea urchin from a pristine environment do not have this transport activity and are sensitive to hydrophobic toxins. These data strongly support a role for multixenobiotic transport as a mechanism of protection from environmental toxins and indicate an unsuspected mode of protection in invertebrate embryos.

### Introduction

Certain organisms live and reproduce successfully in areas rich with potentially toxic environmental chemicals, yet the way in which these organisms, and especially their embryonic stages, can grow and develop normally in these habitats is not well understood. For example, sediment-dwelling and filter-feeding organisms are indiscriminately exposed to a wide variety of hydrophobic compounds that may be cytotoxic. Here we report a mechanism that may allow the embryos of the echiuran worm *Urechis caupo* to survive and develop normally in an environment that

is rich in hydrophobic compounds. This mechanism is similar to multidrug resistance (MDR) in mammalian cells and to multixenobiotic resistance (MXR) in several aquatic invertebrates. Multixenobiotic transport activity may indeed be one of several defense mechanisms that certain organisms have to help them resist natural toxins in their environment.

Multidrug resistance is a phenomenon in which cells become simultaneously resistant to several unrelated drugs, commonly through the increased expression of a membrane protein that reduces drug accumulation in the cells (reviewed in Gottesman and Pastan, 1988; Endicott and Ling, 1989; Gottesman *et al.*, 1991; Higgins, 1992). This protein, the multidrug transport protein or P-glycoprotein, is a member of a family of membrane proteins [ATP-binding cassette (ABC) transport proteins (Hyde *et al.*, 1990) or traffic ATPases (Ames and Lecar, 1992)] that are present in organisms from bacteria to humans and transport a variety of molecules using energy from ATP (McGrath and Varshavsky, 1989; Wu *et al.*, 1991; Samuelson *et al.*, 1990; Riordan *et al.*, 1989; Dudler and Hertig, 1992). The P-glycoprotein-mediated MDR confers resistance by binding drugs and transporting them out of the cells in an energy-dependent manner (Hamada and Tsuruo, 1988; Ambudkar *et al.*, 1992; Doige *et al.*, 1992; Doige and Sharom, 1992).

The substrate specificity of the mammalian multidrug transport protein has been characterized; a common feature among substrates of the transporter appears to be moderate hydrophobicity, with most substrates having both hydrophobic and positively charged domains (reviewed in Gottesman *et al.*, 1991). Although the role of the multidrug transport protein in normal tissues is not known, a variety of endogenous substrates of the transporter have been identified, including steroids (Wolf and Horwitz, 1992; Ueda *et al.*, 1992), organic chemicals (Charuk and Reithmeier, 1992; Ichikawa *et al.*, 1991),

peptides (Sharma *et al.*, 1992), and ions (Gros *et al.*, 1992). The tissue distribution of the protein suggests that it plays a normal role in the transport of metabolites and also protects certain tissues from potentially toxic compounds (Thiebaut *et al.*, 1987; Tatsuta *et al.*, 1992).

Kurelec and his colleagues (reviewed in Kurelec, 1992) found that several aquatic invertebrates have an activity similar to multidrug transport in mammals, and suggested that this activity rids the organisms of toxic environmental compounds and confers multixenobiotic resistance on these organisms (Kurelec and Pivcevic, 1989, 1991, 1992; Kurelec *et al.*, 1992; Kurelec, 1992; Cornwall *et al.*, unpublished data). Several adult invertebrates, including the sponges *Tethya aurantium*, *Geodia cydonium*, and *Verrucaria aerophoba* and the mussels *Mytilus galloprovincialis* and *Anodonta cygnea*, have xenobiotic transport activity, as evidenced by the presence of a verapamil-sensitive drug export and verapamil-sensitive drug binding in several tissues (Kurelec and Pivcevic, 1989, 1991, 1992; Kurelec *et al.*, 1992; Cornwall *et al.*, unpublished data). This transport activity is also related to the presence of a protein similar to the mammalian multidrug transport protein in sponges and mussels (Kurelec *et al.*, 1992; Waldmann *et al.*, unpublished data). In relation to pollution, Minier *et al.* (1993) found that oysters and mussels from a polluted location have a higher frequency of expression of the multixenobiotic transport protein than do oysters and mussels from a site with little pollution.

*Urechis caupo* lives and spawns in a habitat rich with naturally occurring hydrophobic compounds. Here we describe a cellular mechanism, related to MDR in mammals, that may allow the embryos to develop normally in this seemingly noxious environment. The juvenile and adult worms may also need this mechanism to inhabit the sediment. MXR may be one of several mechanisms that invertebrates can use as a defense against environmental toxins, and may be especially important in developing embryos to prevent the toxins from entering the cells and interfering with normal development.

### Materials and Methods

Adult specimens of *Urechis* were collected from a mudflat north of Moss Landing Harbor in Moss Landing, California, and maintained in glass tanks with several inches of mud and with running seawater. Fresh worms were collected every 2–3 months. *Urechis* gametes were collected and fertilized according to Gould (1967). *Strogylacentrotus purpuratus* adults were collected from the rocky intertidal shore at Point Arena, California, and the gametes were obtained and fertilized according to Leahy (1986).

#### Dye Transport Assays

To measure dye accumulation over time, embryos were incubated in filtered seawater (FSW) with 1  $\mu$ M rhoda-

mine B in the presence or absence of 22  $\mu$ M verapamil (an inhibitor of mammalian multidrug transport activity) at 16°C. At the indicated times after suspension in rhodamine with or without verapamil, an aliquot of embryos was removed and washed twice by hand centrifugation and resuspension in FSW. The fluorescence of 10 embryos was then measured within 5 min of washing. Each embryo was viewed with a 40 $\times$  water immersion lens on a Zeiss epifluorescence microscope fitted with a photosensor. An aperture was closed to a uniform diameter over each cell, and the light emitted by the cell was shunted to the photosensor. The light was then converted to a voltage that was quantified by a voltmeter and is expressed as relative fluorescence units. Error bars represent standard deviations. Unless otherwise indicated, each graph represents a single experiment.

Photographs of fluorescent dye accumulation in embryos were taken with AGFAPAN (ASA100) black and white film. Embryos were incubated in 1  $\mu$ M rhodamine in the presence or absence of verapamil as above, and at 1 h they were washed free of the drugs. The two groups of embryos were mixed together immediately prior to photography.

To measure efflux of rhodamine over time, embryos were incubated in 1  $\mu$ M rhodamine B for 1 h, after which they were washed three times with FSW and incubated in FSW or FSW + 22  $\mu$ M verapamil. At various times after the dye was washed out, aliquots of each sample were washed once with FSW, and the fluorescence of the embryos was measured as above.

To assess the affinity of the transport activity for rhodamine, embryos were incubated in rhodamine with or without 22  $\mu$ M verapamil for 1 h and washed. The fluorescence of 10 embryos was then measured as above. The concentrations of rhodamine B in FSW used were 0.01  $\mu$ M, 0.1  $\mu$ M, 1  $\mu$ M, 5  $\mu$ M, and 10  $\mu$ M.

#### Radioactive drug accumulation

To measure drug accumulation, fertilized *Urechis* eggs were incubated at 16°C in FSW containing a mixture of unlabeled forskolin and [<sup>3</sup>H]forskolin (DuPont-NEN) (0.5  $\mu$ M forskolin + 1  $\mu$ Ci of [<sup>3</sup>H]forskolin/ml of embryos; S.A. of [<sup>3</sup>H]forskolin = 26.2 Ci/mmol)  $\pm$  22  $\mu$ M verapamil or  $\pm$  10  $\mu$ M rhodamine B. Two 0.5-ml aliquots of each sample were removed after 1 h, and the embryos were washed two times by hand centrifugation and resuspension in FSW. The pellet was dissolved in 0.5 ml of 0.5 N NaOH + 5% Triton X-100 and mixed with 5 ml of Ecolume (ICN Biomedicals, Inc.). The radioactivity of the solution was measured using a liquid scintillation counter (Beckman LS-8000). The values are the average of duplicate samples, with error bars indicating the standard deviations.

### Toxicity assays

The effect of two cytotoxic drugs on cell division was measured in developing *Urechis* embryos in the presence and absence of verapamil. Fertilized eggs were incubated either in FSW  $\pm$  5  $\mu$ M verapamil, FSW + 0.2  $\mu$ M vinblastine  $\pm$  5  $\mu$ M verapamil, or FSW + 0.5  $\mu$ M vinblastine  $\pm$  5  $\mu$ M verapamil. This experiment was also done with 2  $\mu$ M or 4  $\mu$ M emetine in place of the vinblastine. The embryos were allowed to develop at 16–18°C, and the number of embryos at the 1-, 2-, 4-, 8-, and 16-cell stages was counted 3 h after fertilization for each sample. The average number of cell divisions was determined by multiplying the percentage of embryos at each stage (minus the number of embryos that did not divide in the control samples) by the number of cell divisions that had occurred to produce that stage (e.g., 4-cell stage = 2 divisions). Then the values for each cell division in each sample were added to obtain the number of cell divisions that occurred in that sample 3 h after fertilization. The average values of two experiments for vinblastine and three experiments for emetine are shown with error bars representing standard deviations.

### Western blotting

For Western blot analysis, 200  $\mu$ l of packed unfertilized eggs of *U. caupo* or *S. purpuratus* were homogenized in 200  $\mu$ l of lysis buffer (Morris *et al.*, 1991). The proteins were then solubilized by adding 100  $\mu$ l of 5% SDS and sonicating for several seconds. Tissues of the adult worm were dissected and chopped with a clean razor blade and treated in a similar manner as the eggs (a longer period of sonication and an additional 100  $\mu$ l of SDS were used to solubilize the proteins in the adult tissues). Protein concentration was determined using the BCA protein assay (Pierce), and 40  $\mu$ g of protein from each sample was then loaded onto the gel after the addition of an equal volume of mM Tris-Cl, pH 7.4, 10% sucrose, and 0.001% bromphenol blue. Proteins were separated on a 7.5% gel by SDS-PAGE, transferred to nitrocellulose (Schleicher & Schuell), and incubated first with the monoclonal antibody C219 (Centocor) and then with a goat anti-mouse antibody conjugated to alkaline phosphatase. The blots were developed using a substrate for alkaline phosphatase (nitroblue tetrazolium and 5-bromo-4-chloro-3-indolyl phosphate) (Mierendorf *et al.*, 1987).

### Photolabeling and immunoprecipitation

Substrate binding to the *Urechis* multixenobiotic transport protein was determined by a competition assay using a photoactivatable substrate to label the protein and by testing to see whether other compounds could compete for that labeling. The photolabeling and immunoprecip-

itation experiments were essentially according to Morris *et al.* (1991); visualization of labeled proteins was by autoradiography.  $^{125}$ I-6-AIPP-FSK (6-*O*-[[2-[3-(4-azido-3-[ $^{125}$ I]iodophenyl)propionamido]ethyl]carbonyl]forskolin) (Morris *et al.*, 1991) was used to photolabel the membranes. For the competition experiment, egg membranes were incubated with 40  $\mu$ M rhodamine B, 50  $\mu$ M verapamil, 100  $\mu$ M forskolin, 100  $\mu$ M 1,9 dideoxyforskolin, or 2  $\mu$ l of a chloroform:methanol extract of the sediment. For immunoprecipitation, the labeled membranes were dissolved by adding 20  $\mu$ l of 50 mM Tris (pH 7.4), 20  $\mu$ l of buffer A (2% SDS, 2 mg/ml BSA, 50 mM Tris, pH 7.4), and 200  $\mu$ l of buffer B (1.25% Triton X-100, 190 mM NaCl, 50 mM Tris, pH 7.4). They were then immunoprecipitated with 10  $\mu$ l of mdr(Ab-1) (Oncogene Science) and Protein A agarose beads (Pierce). After 2 h, the beads were washed four times with buffer C (0.1% Triton X-100, 0.03% SDS, 150 mM NaCl, 50 mM Tris, pH 7.4) and one time with buffer D (150 mM NaCl, 50 mM Tris, pH 7.4). Proteins were eluted with 35  $\mu$ l of sample buffer containing 0.5 M Tris-HCl, pH 6.8, 20% glycerol, 10% (w/v) SDS, 0.1% bromphenol blue, and 4%  $\beta$ -mercaptoethanol. Samples were run on precast 10% Tricine SDS-PAGE gels (Novex) and stained with coomassie blue; the dried gels were exposed on x-ray film.

### Sediment extraction

Sediment samples were taken from Moss Landing Harbor, California, at the same site where adult worms were collected. The sediment was frozen at  $-80^{\circ}$ C within 1 h of collection and thawed just prior to use. To obtain pore water, approximately 40 ml of wet sediment was mixed well by shaking the sediment and its associated water vigorously. The sediment was removed by centrifugation, the pore water was extracted with an equal volume of chloroform:methanol (2:1), and the organic solvent phase was removed by evaporation. As a control, seawater that was not exposed to sediment was also extracted with organic solvent as above. The dried residue from each extraction (pore water or seawater) was dissolved into 100  $\mu$ l of 95% ethanol prior to use in the dye assays. The effects of the extracts on dye transport were tested by incubating 5 ml of *Urechis* embryos in 100 nM rhodamine B in FSW  $\pm$  25  $\mu$ l of the extract (2.4) or a dilution of the extract (1.2, 0.24). As a control, embryos were incubated in dye  $\pm$  22  $\mu$ M verapamil. After 1 h, the fluorescence of the embryos in each sample was measured as above.

## Results

### Rhodamine accumulation and efflux

Multixenobiotic transport activity was measured using a fluorescence assay that follows the accumulation of rho-

damine dye, a substrate of the mammalian multidrug transporter (Neyfakh, 1988). In the absence of an inhibitor or competitive substrate of the transport activity (e.g., verapamil), there is little rhodamine accumulation (little fluorescence increase), but when the transporter is inhibited, dye accumulates in the cells (fluorescence increase). This phenomenon is seen with *Urechis* embryos. Figure 1 shows the difference in intensity of dye in *Urechis* embryos at the 2-cell stage incubated in rhodamine  $\pm$  verapamil for 1 h. Embryos in rhodamine + verapamil accumulate much more dye than embryos in rhodamine alone. To quantify this difference, measurements were made on single embryos over a 3-h period. In rhodamine alone the cells accumulate little dye. In the presence of rhodamine + verapamil, however, the fluorescence of *Urechis* embryos increases several-fold over the 3-h incubation. As shown in Figure 2A, uptake of dye in the presence of verapamil comes to an apparent equilibrium in about 1 h. Experiments with different batches of eggs showed slight variability in the fluorescence values, but the shape of the curves was the same.

In mammalian cells containing the multidrug transport protein, the accumulation of dye in the presence of verapamil is through the inhibition of this efflux pump (Fojo *et al.*, 1985), with verapamil acting as a competitive substrate or as an inhibitor. This is also true for *Urechis*. Embryos preloaded with rhodamine and washed into seawater show a rapid efflux of dye from the cells (Fig. 2B). However, in embryos washed into seawater + verapamil, this efflux of dye is retarded, as seen in the higher fluorescence of the embryos (Fig. 2B).

The *Urechis* transporter is effective at exporting low concentrations of substrate ( $1 \times 10^{-8}$  to  $5 \times 10^{-6}$  M); there is increased dye accumulation in the presence of verapamil at concentrations ranging from 10 nM to 5  $\mu$ M rhodamine B, but there is no difference in the fluorescence of embryos  $\pm$  verapamil above 5  $\mu$ M rhodamine (Fig. 3), suggesting substrate saturation above this concentration.

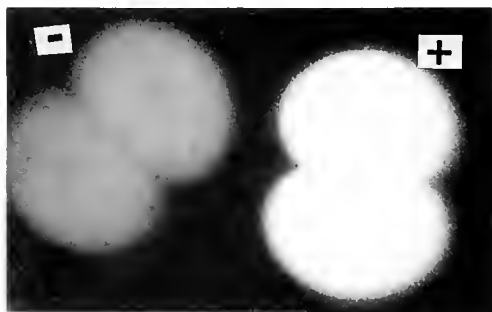


Figure 1. Photograph of *Urechis* embryos at the 2-cell stage incubated in 1  $\mu$ M rhodamine  $\pm$  22  $\mu$ M verapamil for 1 h: (-) = rhodamine without verapamil and (+) = rhodamine with verapamil. At the end of the 1-h incubation period, the embryos were quickly washed free of drugs, placed on a slide, and photographed.

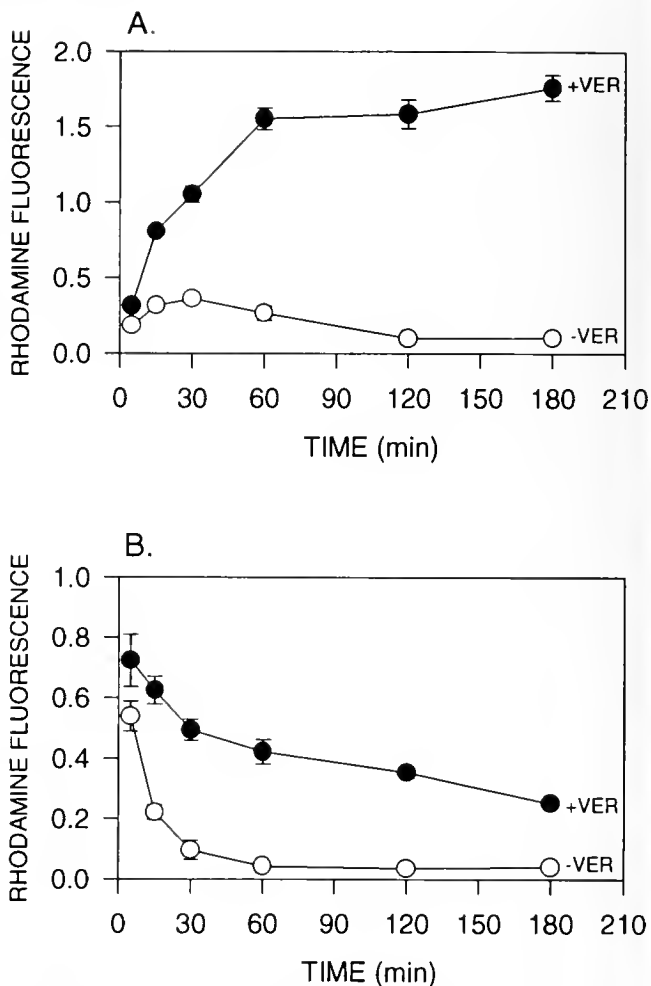
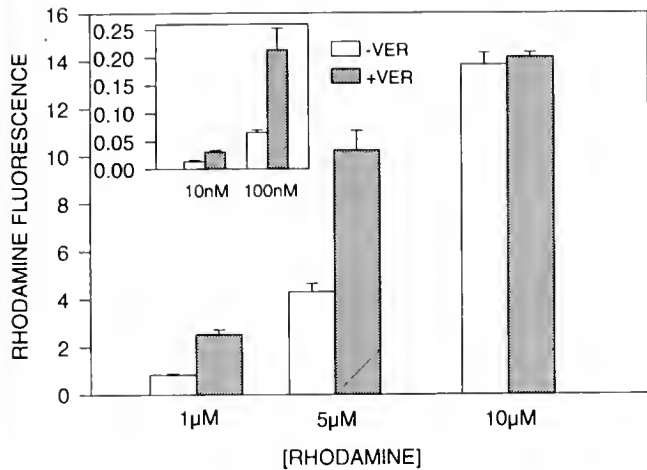


Figure 2. Accumulation and efflux of rhodamine B in *Urechis* embryos. (A) Rhodamine accumulation: Fertilized eggs were incubated in 1  $\mu$ M rhodamine B (—○—) or in rhodamine plus 22  $\mu$ M verapamil (—●—), and the fluorescence was measured at various times. (B) Rhodamine efflux: Embryos were preloaded with 1  $\mu$ M rhodamine for 1 h and washed into seawater (—○—) or seawater containing 22  $\mu$ M verapamil (—●—). Fluorescence of the cells in (B) was measured at various times after washing. Data points represent the average measurements of 10 eggs; error bars indicate standard deviations.

In addition to *U. caupo* embryos, we measured dye transport activity in embryos of the sea urchin *Strongylocentrotus purpuratus* to determine if the embryos of an organism collected from a relatively pristine environment also have this toxin defense mechanism. Figure 4 shows that, unlike *Urechis* embryos, the sea urchin embryos incubated in rhodamine have the same high fluorescence as embryos in rhodamine + verapamil.

We used competition for rhodamine export to indirectly identify substrates or inhibitors of the transport protein. Numerous drugs modulate the mammalian multidrug transporter (Hofslil and Nissen-Meyer, 1990; Ichikawa *et al.*, 1991), and many but not all of these inhibit rhodamine



**Figure 3.** Relationship between rhodamine concentration and accumulation of dye  $\pm$  verapamil. Embryos were incubated in increasing concentrations of rhodamine B  $\pm$  22  $\mu$ M verapamil for 1 h. The inset shows fluorescence values of embryos in rhodamine concentrations of 10 nM and 100 nM.

export from *Urechis* embryos. Potent inhibitors of rhodamine transport activity in embryos include verapamil, cyclosporin A, 1,9 dideoxyforskolin, forskolin, and quinidine ( $EC_{50}$ 's < 10  $\mu$ M). Emetine, promethazine ( $EC_{50}$ 's  $\sim$  20  $\mu$ M) and vinblastine ( $EC_{50}$   $\sim$  40  $\mu$ M) are less effective inhibitors, and colchicine does not affect dye transport in the embryos. (Data not shown.)

#### Radioactive drug accumulation

Multixenobiotic transport activity was also identified by assessing the accumulation of a radioactive substrate. In agreement with the fluorescence transport assay, more [ $^3$ H]forskolin accumulates in *Urechis* embryos in the presence of verapamil than in its absence (Fig. 5A). Similarly, rhodamine B inhibits the transport of [ $^3$ H]forskolin from the embryos (Fig. 5B).

#### Toxicity of drugs to developing embryos

Cell division in *Urechis* embryos incubated in vinblastine (Fig. 6A) or emetine (Fig. 6B) (substrates of the multixenobiotic transporter that inhibit cell division) is not greatly affected by low concentrations of these drugs. However, if multixenobiotic transport activity is inhibited with verapamil, the drugs now inhibit cell division as seen in Figures 6A and 6B. Verapamil had no apparent effect on the embryos during the first few cell divisions, but it caused a four- to fivefold decrease in the number of cell divisions of embryos when in combination with 0.2  $\mu$ M vinblastine and a 350-fold decrease in the cell divisions in combination with 0.5  $\mu$ M vinblastine. Embryos in 2  $\mu$ M emetine + verapamil had two- to threefold decrease

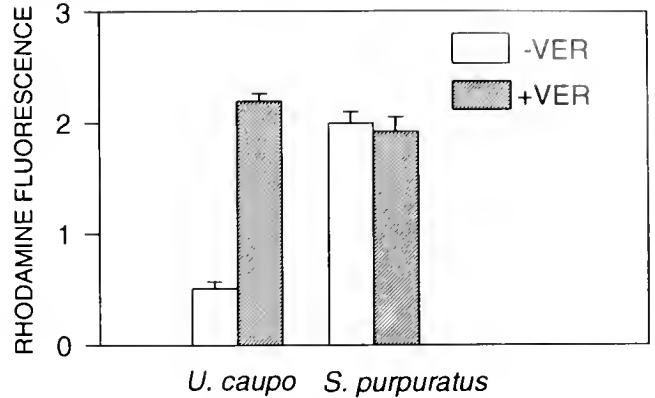


**Figure 4.** Dye transport activity in *Urechis caupo* embryos (*U. caupo*), and *Strongylocentrotus purpuratus* embryos (*S. purpuratus*). Fertilized eggs were incubated for 1 h in 1  $\mu$ M rhodamine B  $\pm$  22  $\mu$ M verapamil, washed with FSW, and the fluorescence of 10 cells was determined for each sample.

in the number of cell divisions, and embryos in 4  $\mu$ M emetine + verapamil had a fourfold decrease in the cell divisions compared with embryos in emetine alone.

#### Western blotting

A protein related to the mammalian multidrug transporter was detected in *Urechis* egg membranes as assessed by Western blot, photoaffinity labeling, and immunoprecipitation experiments (Figs. 7 and 8). A monoclonal antibody to the conserved ATP-binding region of the mammalian multidrug transport protein (C219) identifies a protein of 140 kD in *Urechis* egg membranes and whole eggs (Fig. 7A) which is not abundant in the cytoplasmic fraction of the eggs. This protein is also identified by two

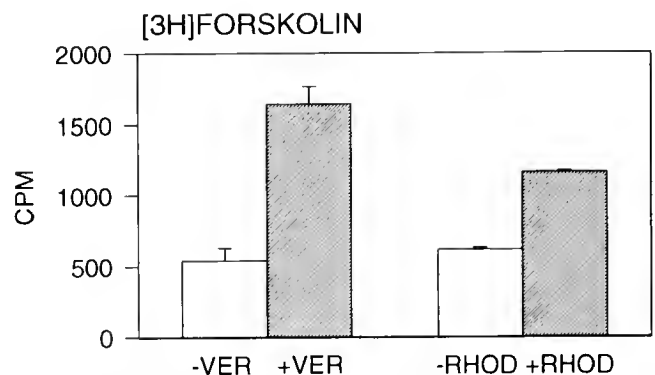


**Figure 5.** [ $^3$ H]Forskolin accumulation in *Urechis* embryos. On the left, embryos were incubated in 0.5  $\mu$ M [ $^3$ H]Forskolin  $\pm$  22  $\mu$ M verapamil for 1 h (-VER, +VER). On the right, embryos were incubated in 0.5  $\mu$ M [ $^3$ H]Forskolin  $\pm$  10  $\mu$ M rhodamine B for 1 h (-RHOD, +RHOD). The amount of radioactive forskolin in the cells was measured with a scintillation counter.

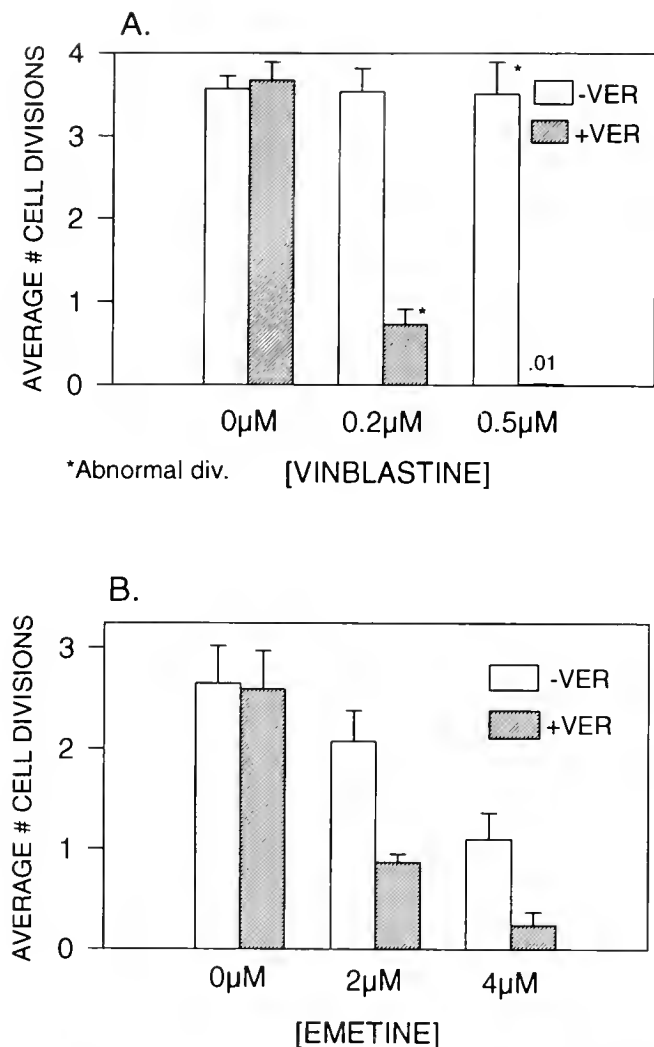


**Figure 6.** Effects of cytotoxic drugs on cell division. (A) Average number of cell divisions of embryos developing in FSW ( $0 \mu\text{M}$ ),  $5 \mu\text{M}$  verapamil ( $0 \mu\text{M}$ , hatched bar), and vinblastine at  $0.2$  and  $0.5 \mu\text{M}$   $\pm 5 \mu\text{M}$  verapamil (+verapamil = hatched bars) after 3 h. Error bars indicate standard deviations from two experiments; \* indicates that the embryos did not form normal cells upon division; .01 = the number of divisions that the embryos in  $0.5 \mu\text{M}$  vinblastine + verapamil underwent. (B) Average cell divisions of developing *Urechis* embryos in FSW ( $0 \mu\text{M}$ ),  $5 \mu\text{M}$  verapamil ( $0 \mu\text{M}$ , hatched bar), or  $2$  and  $4 \mu\text{M}$  emetine  $\pm 5 \mu\text{M}$  verapamil (+verapamil = hatched bars) after 3 h. Error bars indicate standard deviations from three experiments.

polyclonal antibodies to the mammalian multidrug transport protein [mdr(Ab-1) and 4007] (data not shown). A major band appears at 140–145 kD in all the egg samples and in the mammalian MDR cells, but there are also some minor bands that could be proteolytic fragments (smaller bands) (Schinkel *et al.*, 1991) or multiples (larger bands) of the transport protein. The C219 antibody does not label a protein in *S. purpuratus* eggs (Fig. 7A). In a control experiment in which the C219 antibody was

omitted, no bands were labeled in any of the samples (data not shown).

Western blot analysis of adult *Urechis* tissues shows that a major protein in both epidermal tissue and tissue from the anterior portion of the digestive tract stains heavily with an antibody to the mammalian multidrug transporter, but the band is lower in relative molecular mass (110 kD) than the egg or mammalian proteins (Fig. 7B).

#### Photolabeling and immunoprecipitation

A photoactivatable  $^{125}\text{I}$ -forskolin derivative labels several proteins in mammalian cells including adenylyl cyclase and the multidrug transporter (Morris *et al.*, 1991). Proteins in *Urechis* egg membranes are also labeled by this forskolin derivative, and a major labeled protein of 145 kD in *Urechis* eggs is immunoprecipitated by mdr(Ab-1) (Fig. 8A), supporting the hypothesis that this protein is related to the mammalian multidrug transport protein. The labeling of a 140-kD protein by the forskolin derivative is inhibited by unlabeled forskolin, 1,9 dideoxyforskolin, rhodamine, and verapamil (Arrow, Fig. 8B).

#### MXR substrates in the sediment

Using a competition assay similar to the inhibition of dye export by verapamil, we tested the ability of compounds from the sediments in which the worm lives to inhibit dye transport (Fig. 9). Moderately hydrophobic compounds from the interstitial seawater associated with the sediments (pore water) inhibit dye transport in *Urechis* embryos (Fig. 9). These extracted compounds are water-soluble, and thus may be available to the embryos in the natural environment, but they are not found in seawater that is not associated with sediment (Fig. 9, SWEXT.). Furthermore, these environmental chemicals affect dye transport in the embryos at concentrations similar to those in the original pore water (Fig. 9, 1.2 = 1.2-fold concentration of the pore water). Undiluted pore water without chloroform:methanol extraction contains substrates of the transporter, although the results are variable (data not shown). Finally, the compounds extracted from the sediments inhibit the binding of the  $^{125}\text{I}$ -forskolin derivative to the *Urechis* multixenobiotic transport protein (Fig. 8B; Sed. Extr.).

#### Discussion

This work demonstrates the presence of multixenobiotic transport activity in the embryos of a sediment-dwelling worm and suggests that this activity is responsible for protecting the embryos from toxic environmental compounds. In support of this role, we have shown that compounds from the sediments and some anthropogenic

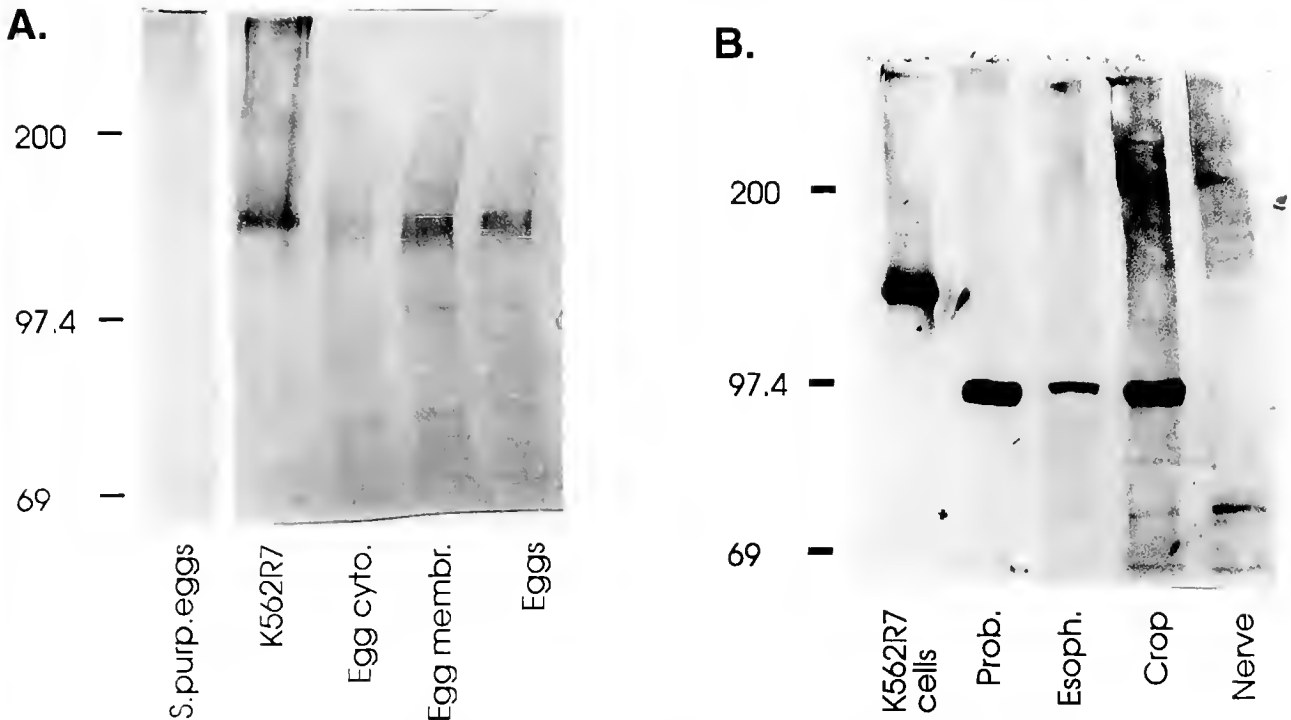


**Figure 7.** Western blot of the multixenobiotic transport protein in *Urechis* eggs and adult tissues. (A) Egg protein preparations were labeled with a monoclonal antibody to the mammalian multidrug transport protein (C219). *Urechis caupo* whole eggs (U.c. Eggs; lane 5), egg membranes (U.c. Egg membr.; lane 4) and egg cytoplasm (U.c. Egg cyto; lane 3). Mammalian K562R7 cells are an MDR+ control (K562R7 cells; lane 2). Eggs of *S. purpuratus* (S. purp. Eggs; lane 1) are a negative control. (B) Several tissues of the adult worm, including the proboscis, were labeled with C219 (Prob.; lane 2), esophagus (Esoph.; lane 3), crop (Crop; lane 4), nerve tissue (Nerve; lane 5), and K562R7 cells were again used as a positive control (K562R7 cells; lane 1).

compounds inhibit the labeling by forskolin of the multixenobiotic transport protein *in vitro* and inhibit dye efflux from *Urechis* embryos at low concentrations *in vivo*, indicating that these compounds may be substrates of a multixenobiotic transporter. Furthermore, two substrates of the transporter are more toxic to the embryos when the transport mechanism is inhibited by verapamil, suggesting a protective function.

Multixenobiotic transport activity in *Urechis* embryos is characterized by a verapamil-sensitive export of dyes and drugs similar to that found in MDR mammalian cells (Neyfakh, 1988; Hofli and Nissen-Meyer; 1989). Using an indirect assay that measures the accumulation of dye in the cells in the presence or absence of potential substrates, our data show that the embryos have the capacity to export a variety of moderately hydrophobic compounds. The relative ability of each compound to inhibit dye transport in the embryos may relate to its affinity for the transporter relative to the dye or to its ability to enter the cells and interact with the protein. Results similar to those using the dye assay are also obtained when transport is measured with radioactive forskolin (Fig. 5), thus confirming and validating the results of the dye assay.

Another type of indirect but functionally relevant transport assay was done by measuring the effects of cytotoxic substrates on the embryos. When the multixenobiotic transporter is inhibited by verapamil, the cytotoxic substrates are more effective than when the embryos develop in the substrate alone (Fig. 6). Thus, when the multixenobiotic transport mechanism cannot function, toxic substrates have a greater effect on the embryos' development.

Characterization of the membrane proteins in *Urechis* reveals a protein at 140-145 kD that is similar to the mammalian multidrug transport protein. The fact that the protein is similar in size and is labeled by three different antibodies made to the mammalian multidrug transport protein indicates that *Urechis* embryos have a protein related by sequence, structure, or both to the mammalian protein. The adult worms also have a related protein, suggesting that the MDR-like protein is present in both the embryos and adults. The two proteins may be different but related, or the size difference between the egg and adult proteins may be due to proteolysis of the adult protein or differences in protein modifications. This question will be further studied using molecular techniques.

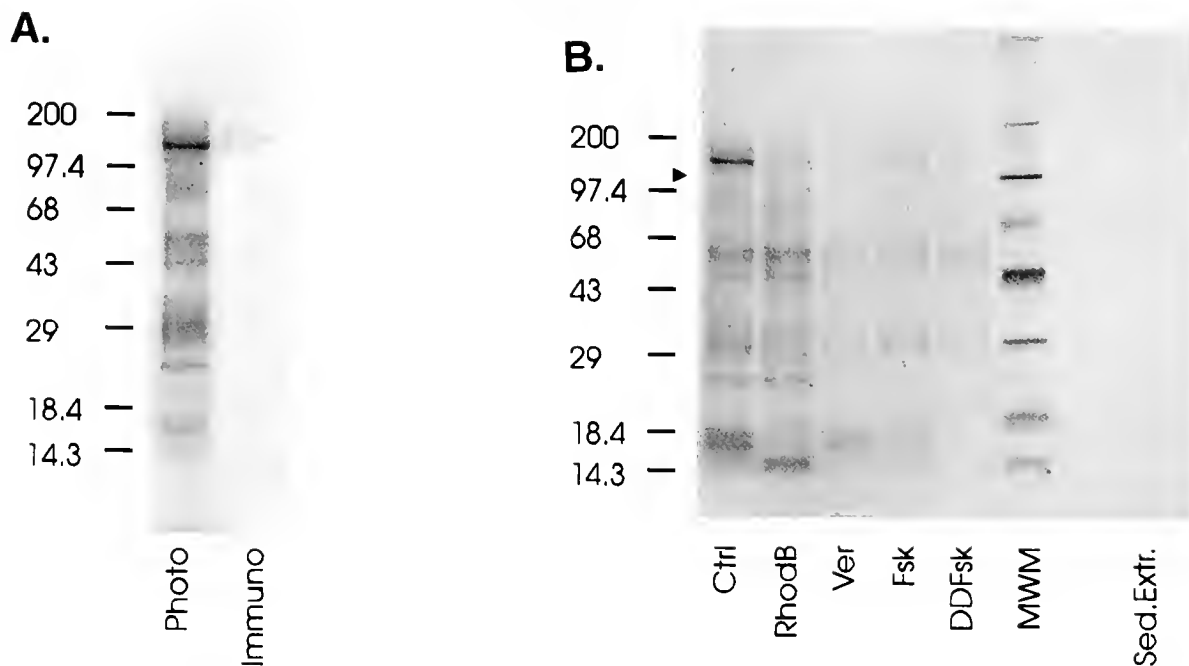


**Figure 8.** Photoaffinity labeling and immunoprecipitation: (A) *Urechis* egg membrane proteins labeled with a radioactive photoactivatable derivative of forskolin (Photo), and immunoprecipitation of the labeled proteins by an antibody to the mammalian multidrug transport protein [mdr(Ab-1)] (Immuno). (B) Egg membrane proteins were labeled with the forskolin derivative in the absence (arrow, Ctrl) and presence of an excess of unlabeled drugs: 40  $\mu$ M rhodamine B (RhodB), 50  $\mu$ M verapamil (Ver), 100  $\mu$ M forskolin (Fsk), 100  $\mu$ M 1,9 dideoxyforskolin (DDFsk), and sediment extract (Sed. Extr.).

The multixenobiotic transport protein in the eggs is also a drug-binding protein, as seen in the photolabeling experiments, showing that substrates of multixenobiotic transport activity interact directly with the 140- to 145-kD protein. This work suggests that the multixenobiotic transport protein, which is immunologically related to the mammalian multidrug transport protein, is also responsible for xenobiotic transport activity in *Urechis* embryos (*i.e.*, is responsible for the MXR phenomenon); a forskolin derivative specifically labels the *Urechis* multixenobiotic transport protein, and forskolin is a substrate for multixenobiotic transport activity.

Several of the drugs that competed for labeling of the 140-kD protein also decreased the labeling of some lower molecular weight proteins, possibly reflecting the non-specific nature of these drugs. In particular, a protein at 20–25 kD was labeled much less in the presence of excess rhodamine B, forskolin, or 1,9 dideoxyforskolin. A protein of approximately 50 kD was also labeled; this could be adenylyl cyclase, a known target of forskolin.

A possible role of the mammalian multidrug transport protein in normal tissues is the transport of toxic dietary compounds or endogenous metabolites (Thiebaut *et al.*, 1987; Charuk and Reithmeier, 1992; Wolf and Horwitz, 1992; Roninson, 1992), and it has been hypothesized that

a similar multixenobiotic transport protein may protect aquatic organisms from environmental toxins (Kurelec, 1992). *U. caupo* lives and spawns in mud flats rich with natural hydrophobic compounds, many of which adsorb to sediment particles (Yen and Tang, 1977). Although *Urechis* has planktonic larvae, they do not start swimming until several hours after fertilization and presumably proceed through the early developmental stages in close association with the mud. We have shown that the sediment in which the worm lives contains compounds that are potential substrates of the transporter (Fig. 9) and that interact with the *Urechis* multixenobiotic transport protein (compete for photolabeling, Fig. 8B). Exposure of the gel in Figure 8B on a phosphor analyzer showed several faint bands in the Sed. extr. lane, but the band at 140 kD was not labeled (data not shown), indicating that compounds in the sediment specifically inhibited photolabeling of the multixenobiotic transporter. In further support of a role for the transporter in protection from environmental toxins (*i.e.*, in conferring MXR), we have preliminary evidence indicating that *U. caupo* embryos develop normally in sediment-exposed seawater (pore water), but that embryos of *Strongylocentrotus purpuratus*, which do not have transport activity, die before they reach the gastrula stage in this pore water (data not shown).



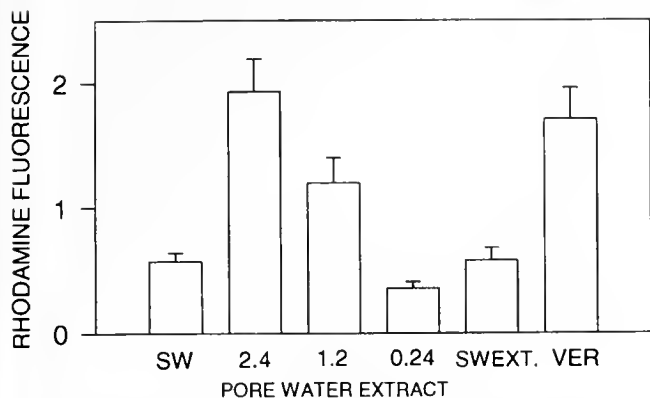


**Figure 9.** Competition for rhodamine export by pore water extract. Compounds leached from the sediments into the pore water and extracted into chloroform:methanol were used in the dye transport assay. Embryos were exposed to FSW containing 100 nM rhodamine B  $\pm$  the following compounds for 1 h before the fluorescence was measured: SW = filtered seawater; 2.4 = pore water extracted into chloroform:methanol (the organic extraction of the pore water led to a 2.4-fold concentration of compounds from the original pore water to the dye assay); 1.2 = dilution of pore water extract to a 1.2-fold concentration of pore water compounds; 0.24 = dilution of pore water extract so that the compounds are less concentrated than in the original pore water; SWEXT = seawater extracted into chloroform:methanol; VER = 22  $\mu$ M verapamil.

Many sediments are polluted with anthropogenic toxins as well as with natural hydrophobic compounds. Four moderately hydrophobic pollutants (CDEC, DCPA, pentachlorophenol, and 2-acetylaminofluorene) inhibit dye transport in *Urechis* embryos; the inhibition is similar to that produced by verapamil (Toomey and Epel, unpublished data). However, several pollutants of greater hydrophobicity (DDT, DDD, DDE, polychlorinated biphenyls, and benzo(a)pyrene) do not affect dye transport and presumably are not substrates of the transporter (Toomey and Epel, unpublished data).

All the compounds that act as substrates appear to be moderately hydrophobic, whether they are natural product drugs or manmade pollutants. Compounds of greater hydrophobicity may not be transported out of the cells; this may be because they do not enter the cells at all; because they become sequestered in the cell membrane; or because they do not interact with the transport protein, which may require substrates containing both hydrophobic and hydrophilic regions. Although these results indicate that the MXR mechanism will protect embryos from environmental toxins, this mechanism will not function if the substrates saturate the transport system. Thus, naturally occurring MXR in *Urechis* embryos and other marine organisms (Kurelec, 1992) is effective against low levels of moderately hydrophobic environmental toxins but may be ineffective against high levels of natural or anthropogenic pollutants.

Protection from a variety of toxic compounds is important for all life stages of an organism that lives and reproduces in an environment enriched with organic pollutants from natural or anthropogenic sources. Eggs and embryos are often the most sensitive stages of an organism's life, and the presence of multixenobiotic transport activity and other detoxification mechanisms may allow these embryos to survive, thus conferring multixenobiotic resistance. These protective mechanisms in both embryos and adults may account in part for the distribution of organisms and their ability or inability to live under exposure to environmental toxins. MXR could be an important first defense against moderately hydrophobic toxins that are attached to particulate matter in the organism's habitat or food supply (e.g., for sediment-dwellers or filter-feeders). Organisms that do not have MXR may be unable to live in a habitat with an abundance of hydrophobic compounds.

#### Acknowledgments

The photoaffinity labeling and immunoprecipitation experiments were carried out in the Laboratory of Molecular Pharmacology, Food and Drug Administration, Bethesda, MD, by B. H. Toomey. We thank D. Morris and K. B. Seamon for their assistance. Thanks to M. Gottesman for kind gift of 4007 antibody and K. Ross and B. Sikic for gift of K562R7 cells. Also thanks to R. Cornwall for help with pesticide experiments. We thank the following for helpful discussion or critical reading of the manuscript: S. McConnell, D. Morris, B. Rees, K. Ross, R. Schimke, B. Schomer, K. B. Seamon, B. Sikic, and R. Swezey. Special thanks to C. Patton for help in preparing the figures and to M. Paul for help with collecting and spawning *Urechis*. This work was initiated by starter grants from the Vital Spark Foundation, the Myers Oceanographic Trust, the National Science Foundation, and the Stanford Office of Technology Licensing and was supported by a grant from the Office of Naval Research.

#### Literature Cited

- Ambudkar, S. V., I. H. LeLong, J. Zhang, C. O. Cardarelli, M. M. Gottesman, and I. Pastan. 1992. Partial purification and reconstitution of the human multidrug-resistance pump: characterization of the drug-stimulatable ATP hydrolysis. *Proc. Natl. Acad. Sci. U.S.A.* 89: 8472-8476.
- Ames, G. F.-L., and H. Lecar. 1992. ATP-dependent bacterial transporters and cystic fibrosis: analogy between channels and transporters. *FASEB J.* 6: 2660-2666.
- Charnk, J. H. M., and R. A. F. Reithmeier. 1992. Interaction of P-glycoprotein with a hydrophobic component of rat urine. *Biochem. Biophys. Res. Comm.* 186: 796-802.
- Doige, C. A., and F. J. Sharom. 1992. Transport properties of P-glycoprotein in plasma membrane vesicles from multidrug-resistant Chinese hamster ovary cells. *Biochim. Biophys. Acta* 1109: 161-171.

- Doige, C. A., X. Yu, and F. J. Sharom. 1992. ATPase activity of partially purified P-glycoprotein from multidrug-resistant Chinese hamster ovary cells. *Biochim Biophys. Acta* 1109: 149-160.
- Dudler, R., and C. Hertig. 1992. Structure of an mdr-like gene from *Arabidopsis thaliana*: evolutionary implications. *J Biol Chem* 267: 5882-5888.
- Endicott, J. A., and V. Ling. 1989. The biochemistry of P-glycoprotein-mediated multidrug resistance. *Ann Rev Biochem* 58: 137-171.
- Fojo, A., A. Shin-ichi, M. M. Gottesman, and I. Pastan. 1985. Reduced drug accumulation in multiple drug-resistant human KB carcinoma cell lines. *Cancer Res* 45: 3002-3007.
- Gottesman, M. M., and I. Pastan. 1988. The multidrug transporter, a double-edged sword. *J. Biol. Chem.* 263: 12163-12166.
- Gottesman, M. M., P. V. Schoenlein, S. J. Currier, E. P. Bruggemann, and I. Pastan. 1991. Biochemical basis for multidrug resistance in cancer. Pp. 339-379 In *Biochemical Aspects of Selected Cancers* Vol. 1. T. Pretlow and T. Pretlow, eds. Academic Press.
- Gould, M. C. 1967. Echiuroid worms: *Urechis* Pp. 163-171 In *Methods in Developmental Biology*: F. H. Wilt and N. K. Wessells, eds. Thomas Y. Crowell Co., New York.
- Gros, P., F. Talbot, D. Tang-Wai, E. Bibi, and H. R. Kaback. 1992. Lipophilic cations: a group of model substrates for the multidrug-resistance transporter. *Biochemistry* 31: 1992-1998.
- Hamada, H., and T. Tsuruo. 1988. Purification of the 170- to 180-kilodalton membrane glycoprotein associated with multidrug resistance. 170- to 180-kilodalton membrane glycoprotein is an ATPase. *J Biol. Chem.* 263: 1454-1458.
- Higgins, C. F. 1992. ABC transporters: from microorganisms to man. *Ann Rev. Cell Biol.* 8: 67-113.
- Hofsl, E., and J. Nissen-Meyer. 1990. Reversal of multidrug resistance by lipophilic drugs. *Cancer Res* 50: 3997-4002.
- Hyde, S. C., P. Emsley, M. I. Hartshorn, M. M. Mimmack, U. Gileadi, S. R. Pearce, M. P. Gallagher, D. R. Gill, R. E. Hubbard, and C. F. Higgins. 1990. Structural model of ATP-binding proteins associated with cystic fibrosis, multidrug resistance and bacterial transport. *Nature* 346: 362-365.
- Ichikawa, M., A. Yoshimura, T. Sumizawa, N. Shudo, Y. Kuwazuru, T. Furukawa, and S. Akiyama. 1991. Interaction of organic chemicals with P-glycoprotein in the adrenal gland, kidney, and a multidrug-resistant KB cell. *J Biol. Chem.* 266: 903-908.
- Kurelec, B. 1992. The multixenobiotic resistance mechanism in aquatic organisms. *Crit Rev. Toxicol.* 22: 23-43.
- Kurelec, B., and B. Pivcevic. 1989. Distinct glutathione-dependent enzyme activities and a verapamil-sensitive binding of xenobiotics in a fresh-water mussel *Anodonta cygnea*. *Biochem. Biophys. Res. Comm.* 164: 934-940.
- Kurelec, B., and B. Pivcevic. 1991. Evidence for a multixenobiotic resistance mechanism in the mussel *Mytilus galloprovincialis*. *Aquat. Toxicol.* 19: 291-302.
- Kurelec, B., and B. Pivcevic. 1992. The multidrug resistance-like mechanism in the marine sponge *Fethya aurantium*. *Mar. Environ. Res.* 34: 249-253.
- Kurelec, B., S. Krea, B. Pivcevic, D. Ugarkovic, M. Bachmann, G. Insiecke, and W. E. G. Mueller. 1992. Expression of P-glycoprotein gene in marine sponges. Identification and characterization of the 125-kDa drug-binding glycoprotein. *Carcinogenesis* 13: 69-76.
- Leahy, P. S. 1986. Laboratory culture of *Strongylocentrotus purpuratus* adults, embryos, larvae. *Methods Cell Biol.* 27: 1-13.
- McGrath, J. P., and A. Varshavsky. 1989. The yeast STE6 gene encodes a homologue of the mammalian multidrug resistance P-glycoprotein. *Nature* 340: 400-404.
- Mierendorf, R. C., C. Percy, and R. A. Young. 1987. Gene isolation by screening  $\lambda$ gt11 libraries with antibodies. *Methods Enzymol.* 152: 458-469.
- Minier, C., F. Akcha, and F. Galgani. 1993. P-glycoprotein expression in *Crassostrea gigas* and *Mytilus edulis* in polluted seawater. *Comp. Biochem. Physiol.* (in press).
- Morris, D. J., L. A. Speicher, A. E. Ruoho, K. D. Tew, and K. B. Seamon. 1991. Interaction of forskolin with the P-glycoprotein multidrug transporter. *Biochemistry* 30: 8371-8379.
- Neyfakh, A. A. 1988. Use of fluorescent dyes as molecular probes for the study of multidrug resistance. *Exp. Cell Res.* 174: 168-170.
- Riordan, J. R., J. M. Rommens, B. Kerem, N. Alon, R. Rozmahel, Z. Grzelczak, J. Zielenski, S. Lok, N. Plavsic, J.-L. Chou, M. L. Drumm, M. C. Iannuzzi, F. S. Collins, and L.-C. Tsui. 1989. Identification of the cystic fibrosis gene: cloning and characterization of complementary DNA. *Science* 245: 1066-1073.
- Roninson, I. B. 1992. The role of the MDR1 (P-glycoprotein) gene in multidrug resistance *in vitro* and *in vivo*. *Biochem. Pharmacol.* 43: 95-102.
- Samuelson, J., P. Ayala, E. Orozoco, and D. Wirth. 1990. Emetine-resistant mutants of *Entamoeba histolytica* overexpress mRNAs for multidrug resistance. *Mol. Biochem. Parasitol.* 38: 281-290.
- Schinkel, A. F., M. E. M. Roelofs, and P. Borst. 1991. Characterization of the human MDR3 P-glycoprotein and its recognition by P-glycoprotein-specific monoclonal antibodies. *Cancer Res.* 51: 2628-2635.
- Sharma, R. C., S. Inoue, J. Roitelman, R. T. Schimke, and R. D. Simoni. 1992. Peptide transport by the multidrug resistance pump. *J. Biol. Chem.* 267: 5731-5734.
- Tatsuta, T., M. Naito, T. Oh-hara, I. Sugawara, and T. Tsuruo. 1992. Functional involvement of P-glycoprotein in blood-brain barrier. *J Biol Chem* 267: 20383-20391.
- Thiebaut, F., T. Tsuruo, H. Hamada, M. M. Gottesman, I. Pastan, and M. C. Willingham. 1987. Cellular localization of the multidrug-resistance gene product P-glycoprotein in normal human tissues. *Proc Natl Acad Sci. U.S.A.* 84: 7735-7738.
- Ueda, K., N. Odamura, M. Hirai, Y. Tanigawara, T. Saeki, N. Kioka, T. Komano, and R. Hori. 1992. Human P-glycoprotein transports cortisol, aldosterone, and dexamethasone, but not progesterone. *J Biol Chem.* 267: 24248-24252.
- Wolf, D. C., and S. B. Horwitz. 1992. P-glycoprotein transports corticosterone and is photoaffinity-labelled by the steroid. *Int. J. Cancer* 52: 141-146.
- Wu, C. T., M. Budding, M. S. Griffin, and J. M. Croop. 1991. Isolation and characterization of *Drosophila* multidrug resistance gene homologs. *Mol. Cell. Biol.* 11: 3940-3948.
- Yen, T. F., and J. I. S. Tang. 1977. Chemical aspects of marine sediments. Pp. 1-39 in *Chemistry of Marine Sediments* T. F. Yen, ed. Ann Arbor Science, Ann Arbor, MI.

## *In Vivo* Observations of Larval Brooding in the Chilean Oyster, *Ostrea chilensis* Philippi, 1845\*

O. R. CHAPARRO<sup>1</sup>, R. J. THOMPSON<sup>2</sup>, AND J. E. WARD<sup>3</sup>

*Ocean Sciences Centre, Memorial University of Newfoundland, St. John's, Newfoundland A1C 5S7, Canada*

**Abstract.** The Chilean oyster *Ostrea chilensis* broods its larvae within the mantle cavity. *In vivo* observations, made with an endoscope, have demonstrated that the female does not undergo gill modification before or during the brooding process. The veliger larvae move freely, have no physical connections with the tissues of the mother, and are often seen as an aggregation ("swarm") around the labial palps. The larvae show a distinct circulation pattern inside the mantle cavity of the mother. Sporadic but strong pallial currents eject larvae from the swarm and transport them between the demibranchs to the posterior region, from which some return anteriorly in the basal ciliated tracts of the gills, and others on the marginal ciliated grooves. Larvae frequently move from the basal to the marginal groove of a demibranch via the ordinary filaments, although they occasionally travel in the opposite direction, moving along the principal filaments from the marginal groove to the basal tract. The circulation of the larvae in the mantle cavity may serve to irrigate them, thereby facilitating gas exchange and suspension-feeding.

The veligers are not lecithotrophic, but readily remove and ingest particles suspended in the mantle cavity. The impact on the nutrition of the mother is not yet known, although the presence of particles in the food grooves and tracts and the transfer of material to the palps suggest that the feeding mechanism functions normally during brooding.

### Introduction

Brooding of larvae is a mode of reproduction which has evolved in many species within a variety of higher taxa (Webber, 1977; Mackie, 1984; Brahmachary, 1989), and brooding mechanisms vary considerably. Among bivalve mollusks that brood, both freshwater and marine, the larvae (embryos) are contained in the mantle cavity of the female, either in the suprabranchial or the infra-branchial chamber, but always in association with the gill. The larvae are sometimes retained in the interlamellar spaces of both demibranchs or of the inner or outer demibranchs only; alternatively, they may be confined to brood sacs, marsupia, mucous masses, or other specialized structures (Ockelmann, 1964; Solis, 1967; Franz, 1973; Mackie *et al.*, 1974; Heard, 1977; Mackie, 1984; Tankersley and Dimock, 1992, 1993). Most authors have concluded that when the larvae are brooded in specialized structures, they are restricted to those structures (Morton, 1977a; Kabat, 1985; Asson-Batres, 1988; Richard *et al.*, 1991; Tankersley and Dimock, 1992) and show little or no motility until the release period (Mackie, 1984). Several species possess brood masses, often confined by a membrane, and in others the embryos are attached to the demibranchs with byssal threads or affixed to gill papillae (Heard, 1977; Bartlett, 1979; Richardson, 1979; Kabat, 1985; Asson-Batres, 1988; Russell and Huelsenbeck, 1989). Conversely, in species that brood the larvae between the demibranchs, the larvae have been presumed to move within the mantle cavity of the mother, unattached to the maternal tissues. In some cases brooding is sequential, *i.e.*, not all eggs are fertilized at the same time, and embryos are gradually displaced ventrally in the mantle cavity as they mature (Kabat, 1985; Russell and Huelsenbeck, 1989).

The family Ostreidae is probably the most well-known marine bivalve group in which brooding behavior occurs.

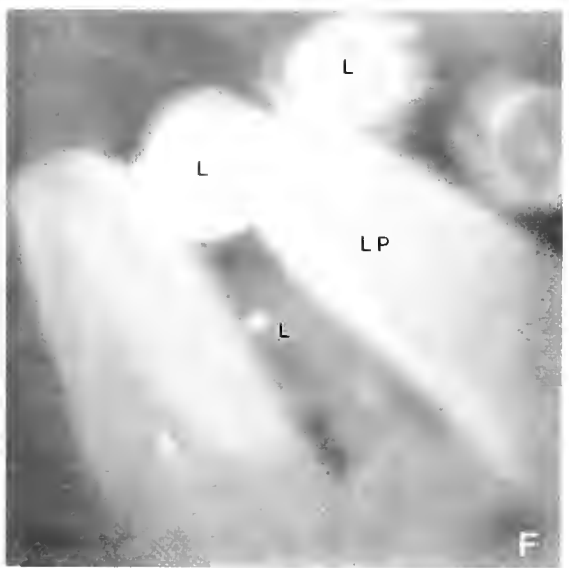
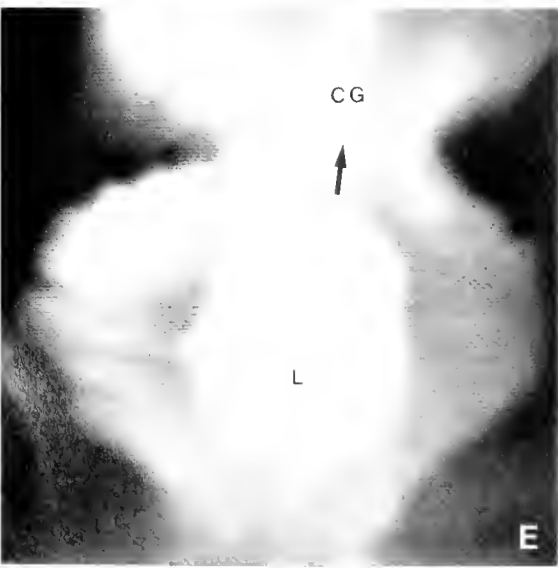
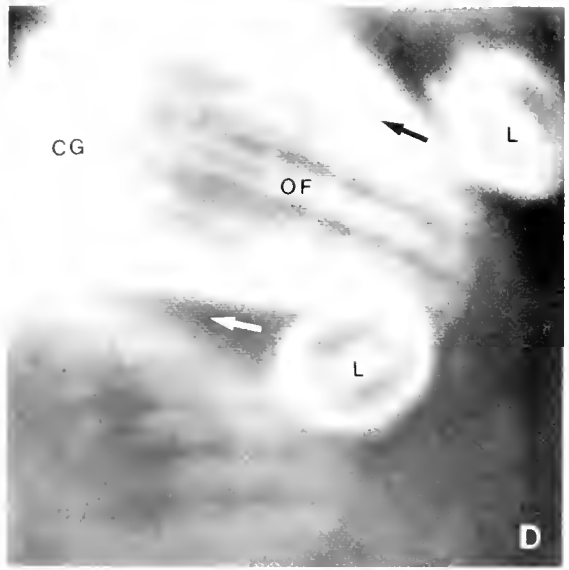
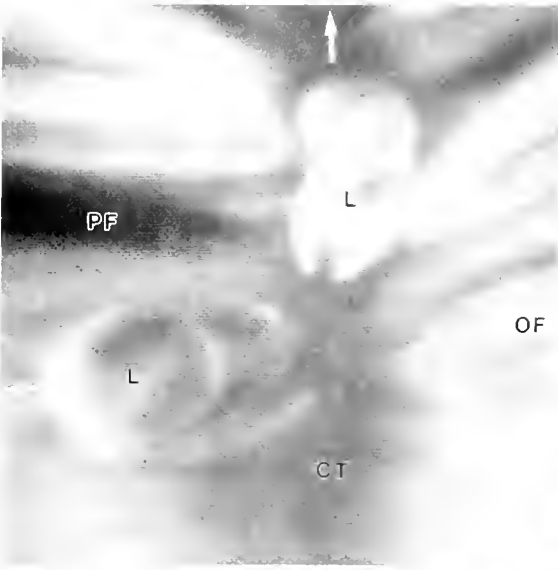
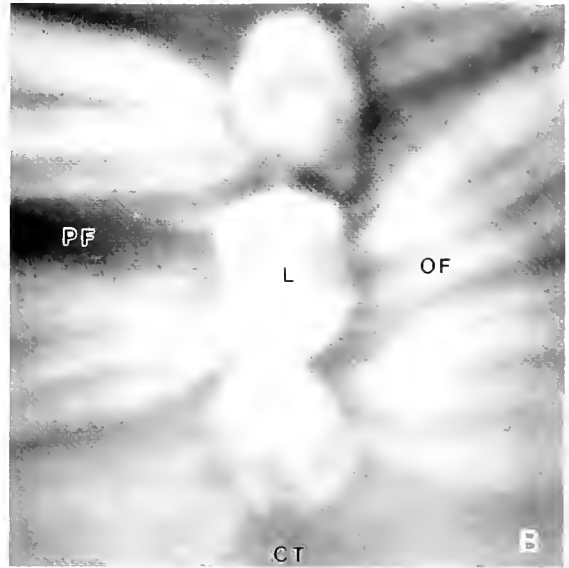
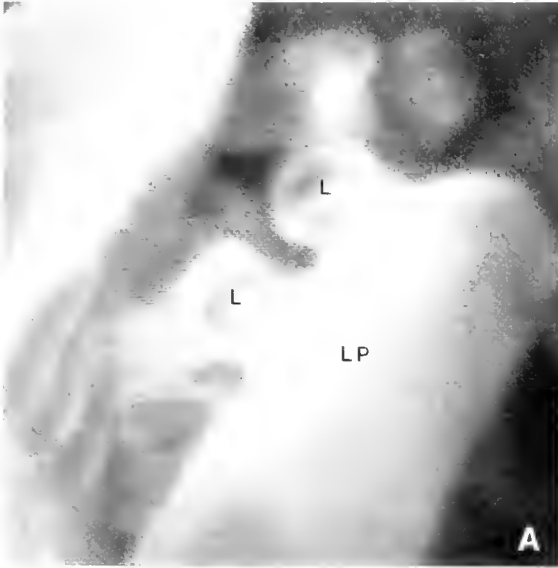
Received 22 October 1992; accepted 28 September 1993.

\* A condensed, narrated version of the video sequences is available by sending a blank VHS tape to RJT (format available is NTSC only).

<sup>1</sup> Present address: Instituto de Biología Marina, Universidad Austral de Chile, Casilla 567, Valdivia, Chile.

<sup>2</sup> Author for correspondence.

<sup>3</sup> Present address: Marine Research Group, Department of Biology, University of New Brunswick, Saint John, New Brunswick E2L 4L5, Canada.



All species of the genus *Ostrea* brood their young (Millar and Hollis, 1963; Galtsoff, 1964; Chanley and Dinamani, 1980; Fernandez Castro and Le Pennec, 1988). Moreover, the brooding takes place within the mantle cavity of the female (*i.e.*, not associated with specialized structures), and the circulation of late blastulae within the cavity has been briefly described in the crested oyster, a member of the closely related genus *Ostreola* (Nelson, 1946). Although the number of larvae produced has also been estimated for several species of brooding oysters (*e.g.*, Winter *et al.*, 1984), very little is known about the brooding process, excepting a limited amount of information for the Chilean oyster *Ostrea chilensis*, which broods the larvae for a longer time (8 weeks) than any other oyster, and releases them at a more advanced stage of development, when they are very large (>450  $\mu\text{m}$  diameter; Toro and Chaparro, 1990). These features make the Chilean oyster particularly suitable for the endoscopic studies we describe in this paper. The pediveligers settle within a few hours of being released by the mother. There is some evidence that the larvae lie on the gill of the mother or in the mantle cavity (Walne, 1963; Solis, 1967; Tomicic and Bariles, 1981; DiSalvo *et al.*, 1983; L pez, 1983), and that the loss in meat content by adult female oysters during spring and summer may be interpreted as a cost of the brooding process (Solis, 1967; Winter *et al.*, 1983).

The nature of the mother-larva relationship in brooding ostreids and the physiology of the larvae and the mother during brooding are not well understood. Among the questions that remain to be addressed are the following. How are the larvae distributed within the mantle cavity? Is there any physical connection between mother and larvae, or do the larvae swim freely inside the mantle cavity of the mother? What is the mechanism for ventilating the larvae? Is the mother able to filter while brooding? Do the larvae interfere with the feeding activity of the mother, as suggested for *Ostrea chilensis* by Winter *et al.* (1983), either physically or by competing with her for suspended particles? If the larvae do feed, what is the mechanism? In this study we addressed these questions by using an endoscope to observe living larvae of *O. chilensis* in the mantle cavity of the mother.

## Materials and Methods

Brooding females (48–60 mm long) of *Ostrea chilensis*<sup>4</sup>, an economically important species found only on the south-central coast of Chile, were obtained from the Quempill n Estuary, Chilo  Island (41° 52'S; 73° 46'W). They were transported on ice to the Marine Sciences Research Laboratory, Memorial University of Newfoundland, where they were held in natural seawater at 17°C and 27‰ S until they were examined with the endoscope. The oysters were fed daily with a variety of cultured algae. Although several of the specimens released some larvae on arrival at the laboratory, most females retained their broods without apparent ill-effects.

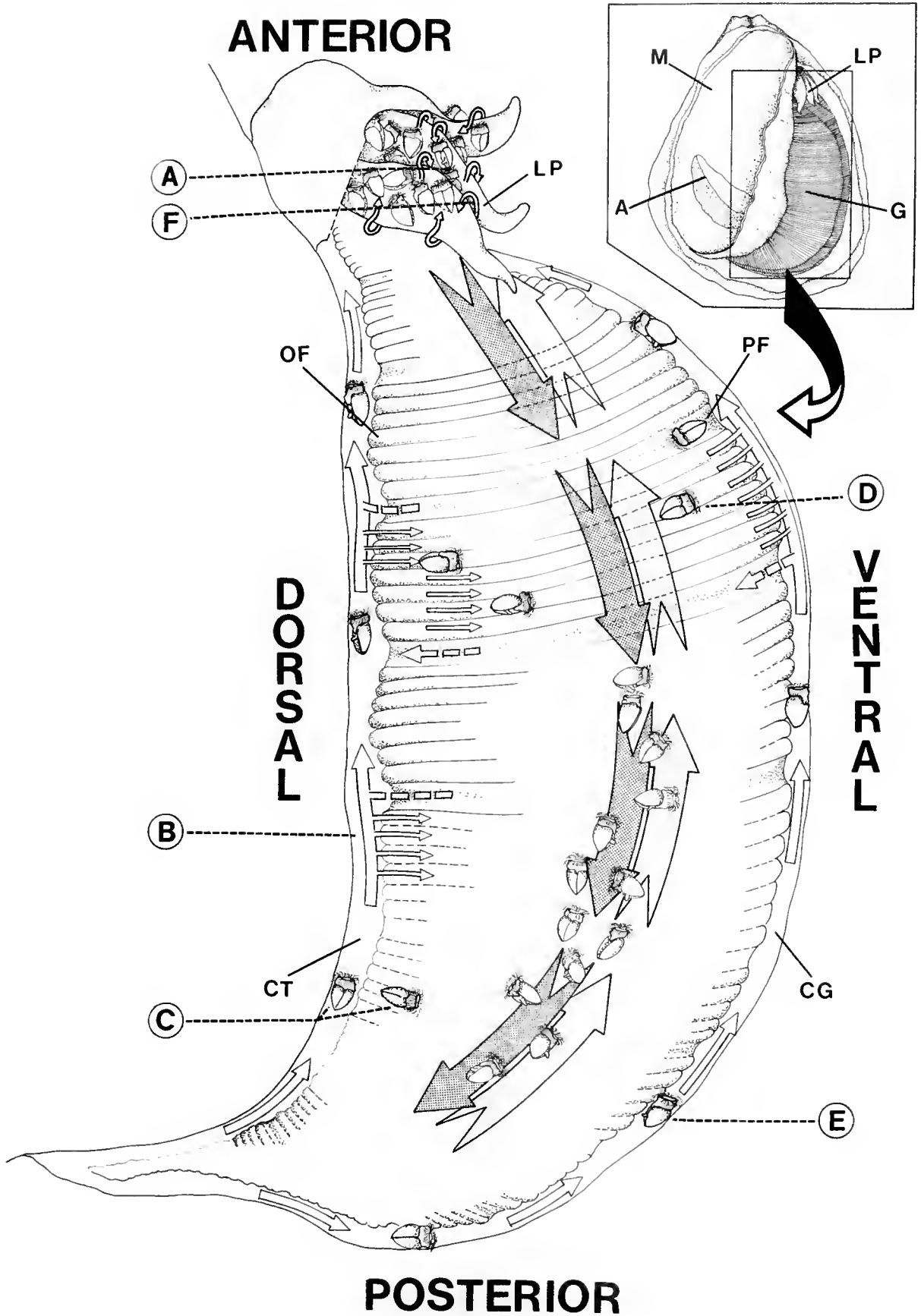
Details of the endoscope methods have been published previously (Ward *et al.*, 1991). The apparatus consisted of an endoscope (Olympus SES 1711D or Scholly 241810.045) mounted on a micromanipulator to facilitate location of the optical insertion tube (OIT; 1.7 mm diameter) within the mantle cavity of the oyster, a cold light source connected to the endoscope with a fiber-optic cable, and a CCD camera (monochrome or color; Cohu 6500 or 8210) coupled to a Hi-8 video recording system (Sony EV-S2000). For some observations, an accessory mirror was fitted to the Scholly endoscope, so that objects at 90° to the OIT could be observed. To permit insertion of the OIT into the mantle cavity, a piece of shell was trimmed from the ventral margin, care being taken to avoid damage to the mantle or other soft tissues.

Most observations were made on the eyed stage of the pediveliger (*ca.* 400  $\mu\text{m}$  diameter), although some were made on trochophores. To determine whether the larvae were capable of feeding, and whether the feeding tracts of the brooding female were able to function, nontoxic, light-reflective red plastic particles (2–10  $\mu\text{m}$  diameter) were introduced through a Pasteur pipette in the vicinity of the inhalent margin of the adult. These particles were clearly visible with the monochrome and color cameras.

<sup>4</sup> Assigned to the genus *Tiostrea* as *Tiostrea chilensis* by Chanley and Dinamani (1980) and subsequently reassigned to the genus *Ostrea* as *Ostrea (Eostrea) puelchana* by Harry (1985).

**Figure 1.** Endoscope micrographs of veliger larvae in the pallial cavity of a brooding female oyster (*Ostrea chilensis*). The diameter of each larva is about 400  $\mu\text{m}$ . (A) Swarm of larvae around the labial palps of the mother. (B) Movement of larvae anteriorly within the basal tract. (C, D) Larvae leaving the basal tract and being carried along the ordinary filaments towards the marginal groove of the demibranch. (E) A larva being transported anteriorly along the margin of the demibranch. (F) Larvae returning to the swarm between the labial palps. These micrographs are represented diagrammatically in Figure 2.

L = larva; CT = ciliated tract (basal tract); CG = ciliated groove (marginal groove); OF = ordinary filament; PF = principal filament; LP = labial palp. Arrows indicate direction of movement of larvae.



To determine whether brooding oysters can distinguish between their own larvae and other particles of similar size (biogenic and nonbiogenic), we introduced into the mantle cavity Sephadex beads (175–350  $\mu\text{m}$  diameter) or eggs of the limpet *Crepidula dilatata* (150–300  $\mu\text{m}$  diameter). The oysters were then examined periodically with the endoscope for about 24 h to establish the fate of these particles. Feces and pseudofeces from each oyster were also examined.

### Results and Discussion

No physical connections between mother and larvae were detected, and the gill of the mother did not appear to be modified for brooding, nor was there any evidence of special structures in which larvae could be held. Likewise, the larvae were not adapted for adhesion to any part of the adult. Rather, they were observed free in the interdemibranchial spaces and between and around the labial palps, as well as being transported on the ciliary tracts of the gill. These observations are consistent with those of Kabat (1985), who found no anatomical modifications of the gill in *Transemella tantilla* (Veneridae), and suggested that the larvae are not attached to the mother's gills.

The larvae of *O. chilensis* were always located within the infrabranchial chamber, never the suprabranchial, and were prevented from leaving the mantle cavity only by the interdigitating processes of the mantle margin. In other brooding species of bivalve mollusks, individual larvae or small groups are often enveloped by a membrane, which may prevent the premature release of the larvae from the mantle cavity (Bartlett, 1979; Richardson, 1979).

In our study of brooding *O. chilensis*, a large aggregation of larvae (which we term a "swarm") was always observed closely associated with the palps (Fig. 1A, F; Fig. 2A, F). According to Hopkins (1936), the larvae of *O. lurida* also lie adjacent to the labial palps and at the anterior margin of the gill. In the Chilean oyster, we noted that the tips of the palps appeared to manipulate the larvae, keeping the swarm constantly in motion. This palp action may serve to remove mucus, which appears to build up on the larvae as a result of their close proximity to the gill, especially the food grooves, and may also facilitate irrigation of the larvae in a region where they are concentrated.

The larvae circulated within the mantle cavity of the mother in a clearly defined pattern (Figs. 2, 3). At irregular intervals, some of the larvae close to the palps were ejected from the swarm and moved posteriorly by a strong water current produced intermittently by the mother, as described by Nelson (1946) for blastulae (92–105  $\mu\text{m}$  diameter) of the crested oyster *Ostreola equestris*. There was also a weaker counter-current which transported suspended larvae anteriorly. The resultant force was in a posterior direction; the overall impression was of a "sloshing" motion, alternating between the strong posteriorly directed current and the weaker anteriorly directed current. The larvae returned to the palp region via the basal ciliary tracts and the marginal grooves, where they were commonly seen aligned one behind the other (Fig. 1B, E; Fig. 2B, E).

The highest larval fluxes were observed in the basal tract. Some of the larvae were carried from the basal tract to the marginal groove via the frontal tracts of the ordinary filaments (Fig. 1C, D; Fig. 2C, D). In such instances, each larva usually lay within a single plical fold, and contacted the frontal cilia on the ordinary filaments of the two adjacent plicae, which transported it ventrally; on reaching the gill margin, the larva was directed anteriorly towards the palps, presumably by cilia on the crests of the groove (Fig. 1E; Fig. 2E). Occasionally, a larva was observed moving on the frontal surface of the gill along the principal filament of a plical groove, towards the basal tract. The mean velocity of the larvae was 471  $\mu\text{m s}^{-1}$  in the basal tracts and 141  $\mu\text{m s}^{-1}$  in the marginal grooves (measurements made at 17°C). These values are consistent with those obtained at 11–13°C for food particles (approximately 5  $\mu\text{m}$  diameter) transported by the same means in the eastern oyster *Crassostrea virginica*, viz. 413–697  $\mu\text{m s}^{-1}$  in the basal groove and 101–193  $\mu\text{m s}^{-1}$  in the marginal groove (Ward *et al.*, 1993). Thus the brooded larvae of *O. chilensis* are moved anteriorly in the basal tracts and marginal grooves by the same mechanism as the food particles, which are much smaller. Furthermore, the aggregation of larvae around the labial palps of the mother is maintained, in part, through the transportation of larvae by ciliary action on the gill, a mechanism which was not apparent to Hopkins (1936) when he observed

**Figure 2.** Schematic lateral view of a single demibranch and the labial palp region of *Ostrea chilensis*, showing the circulation pattern followed by the larvae in a brooding female. The orientation follows the convention that the buccal region is anterior. To be consistent with the terminology followed by most students of ostreids, the text refers to the basal tract rather than the dorsal groove, and to the marginal groove rather than the ventral groove. Circled letters correspond to the endoscope micrographs in Figure 1. Broad arrows show the direction in which larvae are transported by currents in the mantle cavity (dark arrow = strong flow producing resultant movement in a posterior direction; light arrow = weaker counter-flow in an anterior direction, producing a "sloshing" action). Thin arrows show the routes taken by larvae that are in contact with the gill; broken arrows indicate that larval transport is intermittent.

A = adductor muscle; G = gill; LP = labial palps; M = mantle; CT = ciliated tract (basal tract); CG = ciliated groove (marginal groove); OF = ordinary filament; PF = principal filament.



concentrations of larvae around the palps of brooding *O. lurida*.

While returning from the posterior region of the mantle cavity to the anterior region, the larvae were constantly in motion, but normally remained in contact with the gill. Larvae located within the swarm, or moving posteriorly in the mantle current, rotated and oscillated continuously, using their vela. Circulation of the larvae through the mantle cavity, however, was achieved by the currents generated by the mother, because larval transport in a posterior direction ceased when the mother stopped pumping, even though the velar ciliary tracts remained active. Furthermore, movement in an anterior direction was not influenced by the orientation of the active velum.

Because their eggs are relatively large, oysters of the genus *Ostrea* are often believed to be lecithotrophic (Mackie, 1984). Gallardo (1989) considered the larvae of *O. chilensis* to be lecithotrophic, a view supported by the observation of DiSalvo *et al.* (1983) that they do not ingest microalgae when reared outside the mantle cavity of the mother. Our *in vivo* endoscopic examination of larvae of the Chilean oyster, however, showed that red plastic particles drawn into the mantle cavity by the mother were captured by the vela and were visible in the stomachs of the larvae. Mucus strings containing red particles were occasionally seen adhering to the larvae, but we could not determine whether the larvae were ingesting these mucus-bound particles. The larva, at least during the brooding pediveliger stage, is clearly capable of ingesting suspended particles, which is consistent with the suggestion by Solis (1973) that the larva is planktotrophic during the short pelagic phase.

We conclude that the brooded larvae obtain food indirectly from the mother by removing particles suspended in the mantle cavity and possibly by ingesting the mucus string from the food grooves. Such modes of feeding have not been reported previously for bivalve species, although Buroker (1985) has suggested that brooded oyster veligers (*Ostrea* spp.) can feed in the ventilatory current of the mother. Mackie (1979) has postulated a similar feeding mechanism for the larvae of some freshwater bivalves (Pisidiidae), in which the mother removes particles from the incoming water current, and the extramarsupial larvae may secondarily filter the water that has passed through the gill ostia of the mother.

Some bivalve species seem to transfer nutrients directly from the mother to the larvae during the brooding period. For example, larvae may obtain nutrients from maternal tissues (Purchon, 1968), from mucus secreted by cells in the interlamellar septa (Wood, 1974), from secretions of the hypobranchial gland (Morton, 1978), from epithelial secretions of the interfilamentar and interlamellar junctions (Morton, 1977b), or from branchial papillae to which the embryos adhere (Bartlett, 1979). Furthermore, ele-

ments such as calcium may be transferred to embryos maintained in brood chambers (Tankersley and Dimock, 1992).

According to Solis (1967), the meat content of Chilean oysters decreases during winter, spring, and summer. The weight losses in winter and spring can be attributed to low food availability and to spawning, respectively, but during summer spawning is complete and food availability is high. The loss of body weight in summer occurs during the brooding period, and has been attributed to a reduced feeding capability resulting from the presence of the larval brood (Winter *et al.*, 1983). The proposed mechanism was physical interference by the larvae in the normal functioning of the gill, rather than competition for food between the mother and the larvae. Our observations with the endoscope showed clearly that the larvae were removing particles from suspension in the mantle cavity of the brooding female, and that there was no apparent interference with the feeding process of the mother. Thus the larvae were concentrated around the palps and in the basal tracts and marginal food grooves of the gill, yet particle retention by the gill filaments appeared to be unimpeded. Furthermore, the particles intercepted by the gill moved to the basal and marginal tracts in the usual way (Ward *et al.*, 1993), and mucus-bound particle strings were observed being transported from the marginal grooves to the labial palps, despite the presence of larvae in these channels. In fact, larvae were often observed adhering to the mucus string and being carried across the marginal gill-palp junction to the palps themselves. Whether feeding by the larvae significantly diminishes the food available to the mother, thereby reducing energy input, and whether the presence of the brood, especially the swarm around the palps, may reduce the efficiency with which the brooding female can process food particles, are possibilities that remain to be tested.

Higher energy costs may also contribute to weight loss during the brooding period. During brooding, the clearance rate of the female may increase to compensate for the retention of particles by the larvae; there would be an energy cost associated with such a response. There may also be a significant cost to the mother in generating the currents that transport the larvae through the pallial cavity. Some studies have considered the energy costs associated with brooding in marine invertebrates. For example, brooding sea stars continually manipulate and aerate the young, and the energy allocated to reproduction may therefore be partitioned between gonad development and brood handling (Menge, 1974, 1975). Brooding octopods expel water from the mantle cavity more frequently than nonbrooding individuals, because the former irrigate their egg masses (Brahmachary, 1989); presumably additional energy costs are incurred through this behavior.

Brooding Chilean oysters distinguished between their own larvae and large foreign particles introduced into the



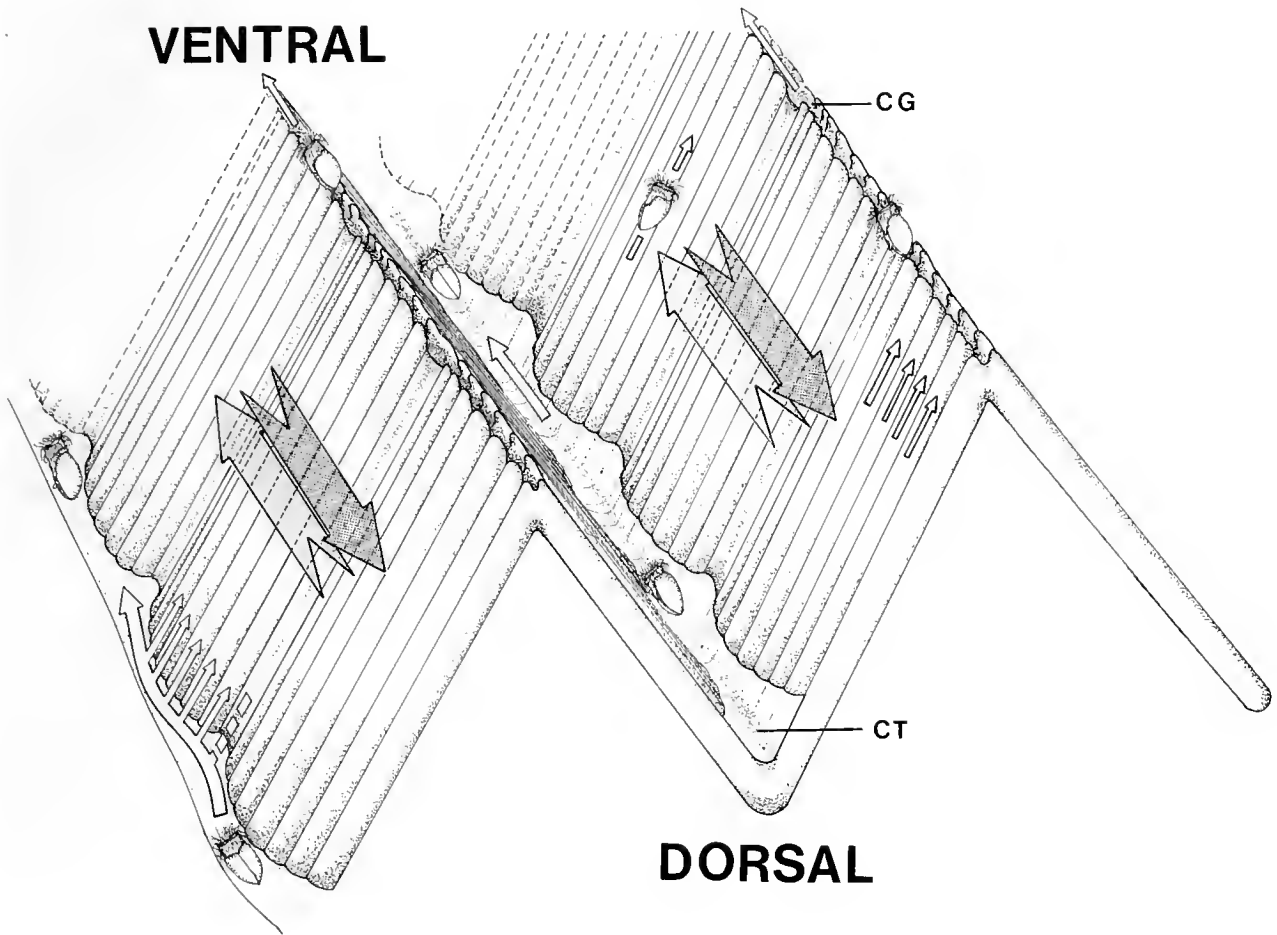


Figure 3. Schematic representation of two adjacent demibranchs in *Ostrea chilensis* (posterior view), showing the circulation of larvae between them. Symbols as in Figure 2.

mantle cavity, whether the latter were biogenic (eggs of *Crepidula dilatata*, 150–300  $\mu\text{m}$  diameter) or nonbiogenic (Sephadex beads 175–350  $\mu\text{m}$  diameter). Most of the Sephadex beads were eliminated as pseudofeces by the mother, but some were detected in the feces. Discrimination between Sephadex beads and larvae did not appear to be perfect, however, because intact larvae and fragments of larvae were sometimes found in the feces alongside Sephadex particles, although these ingested larvae may have been individuals that the mother identified as non-viable. *Crepidula* eggs were observed in the pseudofeces of the mother, but never in the feces, perhaps because they were completely digestible.

This paper is the first attempt to understand the brooding process in the Chilean oyster. We have shown that the veliger larvae can move freely in the mantle cavity of the mother, exhibiting a well-defined circulation pattern that may serve to facilitate gas exchange and perhaps to maximize contact with suspended particles, because the veligers are able to feed. We have preliminary observations suggesting that trochophore larvae are brooded in a similar manner to veligers. Nevertheless, some questions remain

unanswered. What is the impact of the brooding process on the physiological condition of the mother? In particular, is the mother's food intake significantly reduced during brooding, and what proportion of the food collected by the mother is ingested by the larvae? These and related issues are currently being addressed as we assess the advantages and disadvantages of brooding as a mode of reproduction in this species.

#### Acknowledgments

This work was supported by an operating grant to R.J.T. from the Natural Sciences and Engineering Research Council of Canada, by funding from the Canadian Centre for Fisheries Innovation, and by scholarships to O.R.C. from the International Development Research Centre (Canada) and the Ocean Production Enhancement Network, one of the National Centres of Excellence supported by the Government of Canada. We also acknowledge support to O.R.C. from the Fondo Nacional de Desarrollo Científico y Tecnológico (FONDECYT-Chile 1930364) and from the International Foundation for Science (IFS Sweden).

## Literature Cited

- Asson-Batres, M. A. 1988. Reproduction and growth of the brooding bivalve *Transennella tantilla* Veliger 30(3): 257-266.
- Bartlett, B. R. 1979. The possible role of gill filament papillae in the development of the brooding bivalve, *Parastarte triquetra* Am. Zool. 19(3): 957.
- Brahmachary, R. L. 1989. Mollusca. Pp. 280-348 in *Reproductive Biology of Invertebrates II Part A Fertilization, Development, and Parental Care*. K. G. Adiyodi and R. G. Adiyodi, eds. Wiley-Interscience, New York.
- Buroker, N. E. 1985. Evolutionary patterns in the family Ostreidae: larviparity vs. oviparity. *J. Exp. Mar. Biol. Ecol.* 90: 233-247.
- Chanley, P., and P. Dinamani. 1980. Comparative descriptions of some oyster larvae from New Zealand and Chile, and a description of a new genus of oyster, *Tiostrea* New Zealand *J. Mar. Freshwater Res.* 14(2): 103-120.
- DiSalvo, L. H., E. Alarcón, and E. Martínez. 1983. Induced spat production from *Ostrea chilensis* Philippi 1845 in mid-winter. *Aquaculture* 30: 357-362.
- Fernandez Castro, N., and M. Le Penec. 1988. Modalities of brooding and morphogenesis of larvae in *Ostrea puelchana* (D'Orbigny) under experimental rearing. *J. Mar. Biol. Assoc. U. K.* 68: 399-407.
- Franz, D. R. 1973. Ecology and reproduction of a marine bivalve *Myssella planulata* Biol. Bull. 144: 93-106.
- Gallardo, C. S. 1989. Patrones de reproducción y ciclo vital en moluscos marinos bénticos; Una aproximación ecológica evolutiva. *Medio Ambiente* 10(2): 25-35.
- Galtsoff, P. S. 1964. The American oyster *Crassostrea virginica* Gmelin. *U.S. Fish Wildl. Serv. Fish. Bull.* 64: 480 pp.
- Harry, H. W. 1985. Synopsis of the supraspecific classification of living oysters (Bivalvia: Gryphaeidae and Ostreidae). *Veliger* 28(2): 121-158.
- Heard, W. H. 1977. Reproduction of fingernail clams (Sphaeriidae: *Sphaerium* and *Musculum*). *Malacologia* 16(2): 421-455.
- Hopkins, A. E. 1936. Ecological observations on spawning and early larval development in the olympia oyster (*Ostrea lurida*). *Ecology* 17(4): 551-566.
- Kabat, A. R. 1985. The allometry of brooding in *Transennella tantilla* (Gould) (Mollusca: Bivalvia). *J. Exp. Mar. Biol. Ecol.* 91: 271-279.
- Lépez, M. I. 1983. El cultivo de *Ostrea chilensis* en la zona Central y Sur de Chile. *Mem. Asociación Latinoamericana de Acuicultura* 5(2): 117-127.
- Mackie, G. L. 1979. Dispersal mechanisms in Sphaeriidae (Mollusca: Bivalvia). *Bull. Am. Malacol. Union* 1979: 17-21.
- Mackie, G. L. 1984. Bivalves. Pp. 351-418 in *The Mollusca, Vol. 7, Reproduction*, A. S. Tompa, N. H. Verdonk, and J. Van Den Biggelaar, eds. Academic Press, Orlando, FL.
- Mackie, G. L., S. U. Qadri, and A. H. Clarke. 1974. Development of brood sacs in *Musculum securis* (Bivalvia: Sphaeriidae). *Nautilus* 88: 109-111.
- Menge, B. A. 1974. Effect of wave action and competition on brooding and reproductive effort in the seastar, *Leptasterias hexactis* Ecology 55: 84-93.
- Menge, B. A. 1975. Brood or broadcast? The adaptive significance of different reproductive strategies in the two intertidal sea stars *Leptasterias hexactis* and *Pisaster ochraceus*. *Mar. Biol.* 31: 87-100.
- Milnik, R. H., and P. J. Hollis. 1963. Abbreviated pelagic life of Chilean and New Zealand oysters. *Nature* 197: 512-513.
- Morton, B. 1977a. The occurrence of inflammatory granulomas in the ctenidial marsupium of *Corbicula fluminea* (Mollusca: Bivalvia): a consequence of larval incubation. *J. Invert. Pathol.* 30: 5-14.
- Morton, B. S. 1977b. The population dynamics of *Corbicula fluminea* (Bivalvia: Corbiculacea) in Plover Cove Reservoir, Hong Kong. *J. Zool.* 181: 21-42.
- Morton, B. S. 1978. The biology and functional morphology of *Philobrya munita* (Bivalvia: Philobryidae). *J. Zool.* 185: 173-196.
- Nelson, T. C. 1946. Circulation of embryos in the branchial chamber of *Ostrea cristata* Anat. Rec. 94: 355.
- Ockelmann, K. W. 1964. *Turtonia minuta* (Fabricius), a neotenous veneracean bivalve. *Ophelia* 1: 121-146.
- Purchon, R. D. 1968. *The Biology of the Mollusca*. Pergamon Press, Oxford.
- Richard, P. E., T. H. Dietz, and H. Silverman. 1991. Structure of the gill during reproduction in the unionids *Anodonta grandis*, *Ligumia subrostrata*, and *Carunculina parva texasensis*. *Can. J. Zool.* 69: 1744-1754.
- Richardson, M. G. 1979. The ecology and reproduction of the brooding antarctic bivalve *Lissarca mularis* Br. *Antarct. Surv. Bull.* 49: 91-115.
- Russell, M. P., and J. P. Huelsenbeck. 1989. Seasonal variation in brood structure of *Transennella confusa* (Bivalvia: Veneridae). *Veliger* 32(3): 288-295.
- Solis, I. 1967. Observaciones biológicas en ostras (*Ostrea chilensis* Philippi) en Pullinque. *Biol. Pesquera, Chile* 2: 51-82.
- Solis, I. 1973. Valoración de colectores de larvas de ostras, *Ostrea chilensis* Philippi en Pullinque. *Biol. Pesquera, Chile* 6: 5-23.
- Tankersley, R. A., and R. V. Dimock. 1992. Quantitative analysis of the structure and function of the marsupial gills of the freshwater mussel *Anodonta cataraeta* Biol. Bull. 182: 145-154.
- Tankersley, R. A., and R. V. Dimock. 1993. Endoscopic visualization of the functional morphology of the ctenidia of the unionid mussel *Pyganodon cataraeta* Can. J. Zool. 71: 811-819.
- Tomicic, J. K., and J. Bariles. 1981. Manual de guía para el cultivo de la ostra (*Ostrea chilensis*) en la 2a. región de Chile. Univ. de Antofagasta. 73 pp.
- Toro, J. E., and O. R. Chaparro. 1990. Conocimiento biológico de *Ostrea chilensis* Philippi 1845. Impacto y perspectivas en el desarrollo de la ostricultura en Chile. Pp. 231-264 in *Cultivo de moluscos en América Latina*, A. Hernandez, ed. Memorias Segunda reunión grupo trabajo técnico, Ancud, Chile, Noviembre 1989.
- Walne, P. R. 1963. Breeding of the Chilean oyster (*Ostrea chilensis* Philippi) in the laboratory. *Nature* 197: 676.
- Ward, J. E., P. G. Beninger, B. A. MacDonald, and R. J. Thompson. 1991. Direct observations of feeding structures and mechanisms in bivalve molluscs using endoscopic examination and video image analysis. *Mar. Biol.* 111: 287-291.
- Ward, J. E., B. A. MacDonald, R. J. Thompson, and P. G. Beninger. 1993. Mechanisms of suspension-feeding in bivalves: resolution of current controversies by means of endoscopy. *Limnol. Oceanogr.* 38: 265-272.
- Webber, H. H. 1977. Gastropoda: Prosobranchia. Pp. 1-77 in *Reproduction of Marine Invertebrates*, IV, A. C. Giese and J. S. Pearse, eds. Academic Press, NY.
- Winter, J. E., C. S. Gallardo, J. Araya, J. E. Toro, and A. Gleisner. 1983. Estudios en la ostricultura Quempillén, un estuario del Sur de Chile. Parte II. La influencia de los factores ambientales sobre el crecimiento y los periodos de reproducción en *Ostrea chilensis*. *Mem. Asociación Latinoamericana de Acuicultura* 5(2): 145-159.
- Winter, J. E., J. E. Toro, J. M. Navarro, G. S. Valenzuela, and O. R. Chaparro. 1984. Recent developments, status, and prospects of molluscan aquaculture on the Pacific coast of South America. *Aquaculture* 39: 95-134.
- Wood, E. M. 1974. Development and morphology of the glochidium larva of *Anodonta cygnea* (Mollusca: Bivalvia). *J. Zool.* 173: 1-13.

# Reproduction of *Stylochus ellipticus* (Platyhelminthes: Polycladida) in Response to Temperature, Food, and Presence or Absence of a Partner

MARNITA M. CHINTALA<sup>1</sup> AND VICTOR S. KENNEDY

*University of Maryland System, Horn Point Environmental Laboratory, P.O. Box 775,  
Cambridge, Maryland 21613*

**Abstract.** The common polyclad turbellarian *Stylochus ellipticus* is an important and abundant predator of young oysters, *Crassostrea virginica*, in Chesapeake Bay. Laboratory experiments revealed that higher temperature and starvation negatively affected flatworm size. Egg production, adjusted for flatworm area, was not significantly affected by flatworm size, nor by increasing number of egg batches produced. In addition, there was no significant statistical effect of higher temperature and starvation on egg production, although there were some instances of diminished egg production under these conditions. Flatworms did react to higher temperature and starvation by significantly decreasing the number of days that elapsed before egg laying began. Overall, more larvae would be produced at 21°C than at 30°C, by fed flatworms than starved flatworms, and by solitary flatworms than paired flatworms. When isolated animals were alternately fed and starved for five-week periods over a 20-week experimental period at 21°C, 56% of individuals continued to deposit eggs, although the number of eggs laid and embryo hatching success declined with time. *Stylochus ellipticus* individuals can maintain a relatively high reproductive effort despite reduction in available food. Thus, this species would appear to be a "capital" breeder, relying on stored energy to produce eggs.

## Introduction

The free-living flatworm *Stylochus ellipticus* (Girard) is usually found in littoral and sublittoral habitats (Hyman, 1940, 1951; Loosanoff, 1956) and is common on

U.S. Atlantic and Gulf of Mexico coasts. It occurs at low to moderate salinities (Pearse and Wharton, 1938; Landers and Rhodes, 1970) over a wide temperature range. This flatworm is an active predator of eastern oyster spat [*Crassostrea virginica* (Gmelin)] and barnacles of various species in Chesapeake Bay and its tributaries (Webster and Medford, 1961; Shaw, 1967; Christensen, 1973). Natural oyster mortality has been associated with flatworm density in Chesapeake Bay (Webster and Medford, 1961). Raft-cultured oyster spat have been heavily preyed upon by the flatworm in Chesapeake Bay (Christensen, 1973) and in Massachusetts (Provenzano, 1961).

The reproductive pattern and life history of *S. ellipticus* are poorly understood. For example, *S. ellipticus* is hermaphroditic, but is generally thought to be cross-fertilizing (Hyman, 1940, 1951; Prudhoe, 1985) because the male and female copulatory organs are separate (Prudhoe, 1985). However, because the male and female genital pores are close together, self-fertilization (which occurs among other groups of flatworms) may be possible (Prudhoe, 1985).

While holding individuals of *S. ellipticus* separately in petri dishes early in this study, we noticed that they kept laying eggs. There appeared to be no information in the literature on the need for continued contact with other flatworms to maintain production of eggs, fertilized or not. In addition, there was a lack of information on the effects of environmental factors on reproduction in this species. Consequently, we undertook exploratory laboratory studies to examine how late spring and late summer temperatures, being fed or starved, and the presence or absence of a potential sexual partner ("status") affected reproduction in *S. ellipticus*. Evidence presented here reveals that individuals are fecund even in the face of high

Received 14 February 1992; accepted 27 September 1993.

<sup>1</sup> Present address: Institute of Marine & Coastal Sciences, P. O. Box 231, Rutgers University, New Brunswick, New Jersey 08903.

temperature, starvation, and the lack of a partner, with about 93–100% (median values) of the eggs produced eventually hatching.

## Materials and Methods

### *General procedures*

Flatworms were collected in the spring and summer by dredging oysters and oyster shells from oyster bars in the Choptank River (a tributary of central Chesapeake Bay). Salinities in the river ranged between 10 and 16 ppt during the study. Flatworms were held singly in the dark in 85-mm petri dishes at ambient salinity and room temperature for 24–48 h after collection. Apparently healthy individuals were then measured and used in the experiments (again, in 85-mm petri dishes) described below. In the paired experiments, flatworms were placed with worms of the same relative size. The flatworms were then assigned haphazardly to the respective treatments.

To avoid injury to specimens, we measured the size (area) of each flatworm, with as little disturbance as possible, by observing it through a dissection microscope while it crawled in a petri dish placed on graph paper (Lytwyn and McDermott, 1976). Low-intensity light induced movement away from the light. Length (anterior-posterior axis) and width (perpendicular to the anterior-posterior axis) were measured in terms of the number of graph squares covered while the animal was fully extended, with the number of graph squares subsequently converted to  $\text{mm}^2$ . Because these animals are elastic when moving, a surface area estimate of length times width was thought to be preferable to a length measurement alone. The replicability of this area measurement was determined at the start of the study by measuring each of seven animals twice, with a resultant 4% deviation from the mean. We measured adult flatworms weekly to monitor growth or shrinkage ("degrowth"; Calow and Woollhead, 1977) during the experiments; size changes are presented as the area when a treatment or an experiment ended expressed as a percentage of the area at the start.

During experiments, we checked the petri dishes every 48 h for the presence of eggs and changed the water (and food if flatworms had been fed). Because it is difficult to control the amount of food offered in experiments on small aquatic carnivores, we chose to offer one consistent amount of food to some flatworms and none to others in these exploratory experiments. Thus, flatworms that were fed were given a piece of fresh oyster body tissue (one piece for solitary flatworms; two for pairs; gills were not included in the tissue) that was about  $4 \text{ mm}^2$  in size. In many instances, the food was consumed within 48 h. Uneaten food was discarded and replaced with fresh tissue (we have no data on possible declines in oxygen tension as uneaten food decayed). If egg masses were present, the

flatworm(s) was (were) moved to a new dish. We designate the number of eggs laid by a flatworm or pair of flatworms during a 48-h period as a "batch," and note that the disturbances associated with changing water and dishes may have interrupted egg-laying episodes.

The effects of experimental manipulations were assessed by determining change in flatworm area, as well as the following estimators of reproductive effort: number of flatworms that laid eggs, number of days to the laying of the first batch, number of batches per flatworm or flatworm pair, number of eggs per batch, and percentage of embryos hatching in each batch. All mean values are reported  $\pm 1$  standard error of the mean except when percentages are involved; in those instances the median and range are reported. On occasion, flatworms crawled out of the water onto the covers of the petri dishes and desiccated, and a few were found dead of unknown causes in the water. Data from these animals were not used, but the mortalities are reported.

When eggs were present, they were teased off the petri dish with a paint brush and preserved with formalin for later enumeration. A subsample of 50–100 eggs was allowed to remain in each dish so we could monitor hatching success. We counted the number of eggs in the subsample by microscopic examination, and returned the subsample to its rearing regime of darkness, salinity, and temperature until hatching occurred. Water was changed every 2 days. Embryos that showed no signs of development after 7 days (embryos usually hatched 5–7 days after eggs were laid), nor the rotating motion characteristic of pre-hatch behavior, were considered to be nonviable, allowing us to determine hatching success of that subsample, and by extension, of the batch from which it was derived.

All embryos in the preserved sample were counted, or, if numbers were high, were estimated by subsampling. At the start of the experiments, the accuracy of subsample estimates was checked by first counting the number of embryos in a subsample on a Sedgewick-Rafter slide and multiplying the count by the volume (estimated in a graduated cylinder) of the entire sample, and then by counting the entire sample. A 7% deviation from the mean resulted, so we used this subsampling procedure throughout our studies. Average egg number in all experiments is reported to the nearest hundred eggs, with standard errors rounded to the nearest ten.

The size range of experimental flatworms was high (5–338  $\text{mm}^2$ ), so in some instances we attempted to adjust for this variation by dividing the number of eggs produced during the experiments by the surface area of solitary worms at the start of an experiment (we call this the "initial size") to provide an area-specific estimate of egg production. This was not done for paired worms because we did not know which flatworm of a pair had laid the eggs.

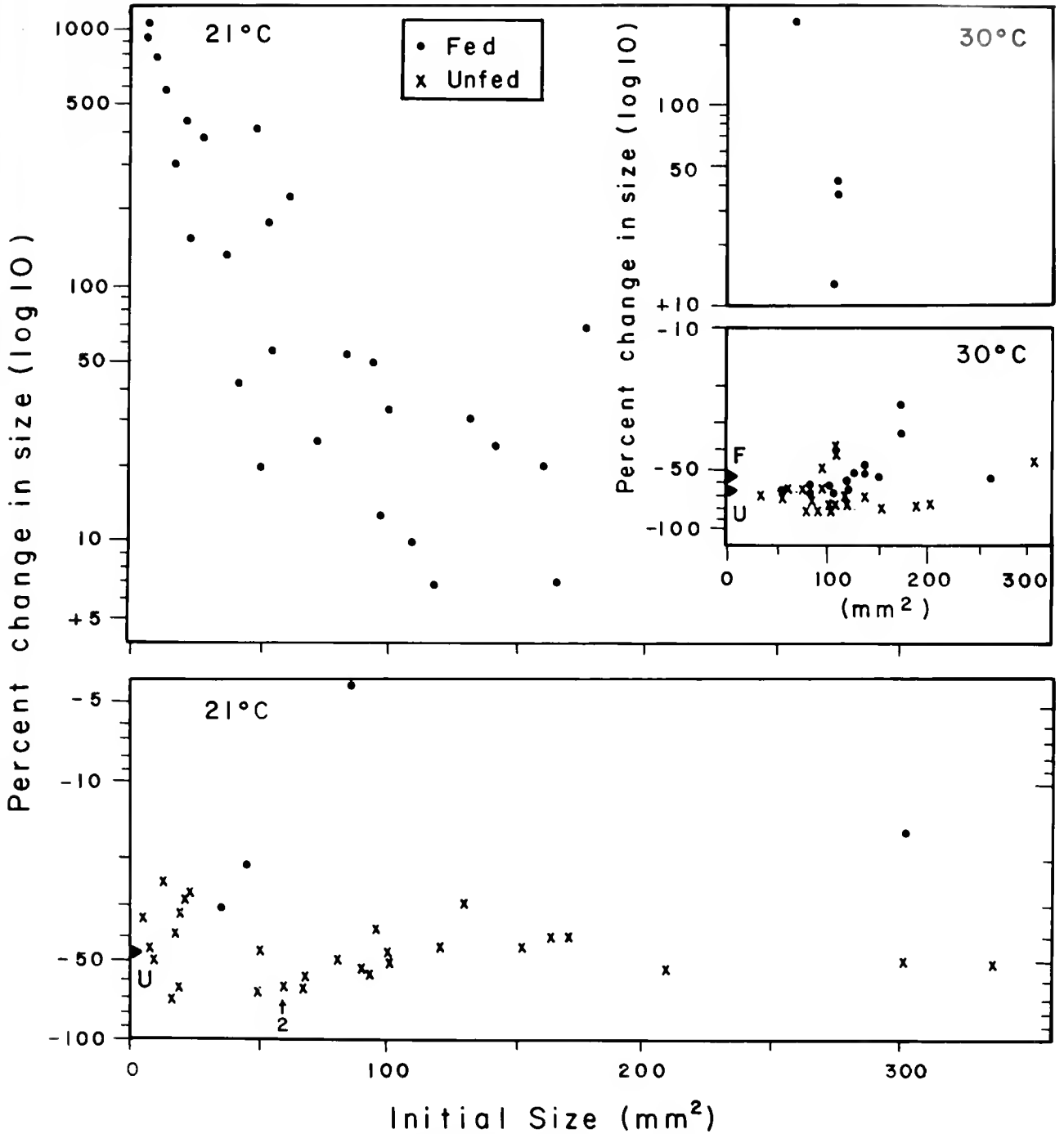
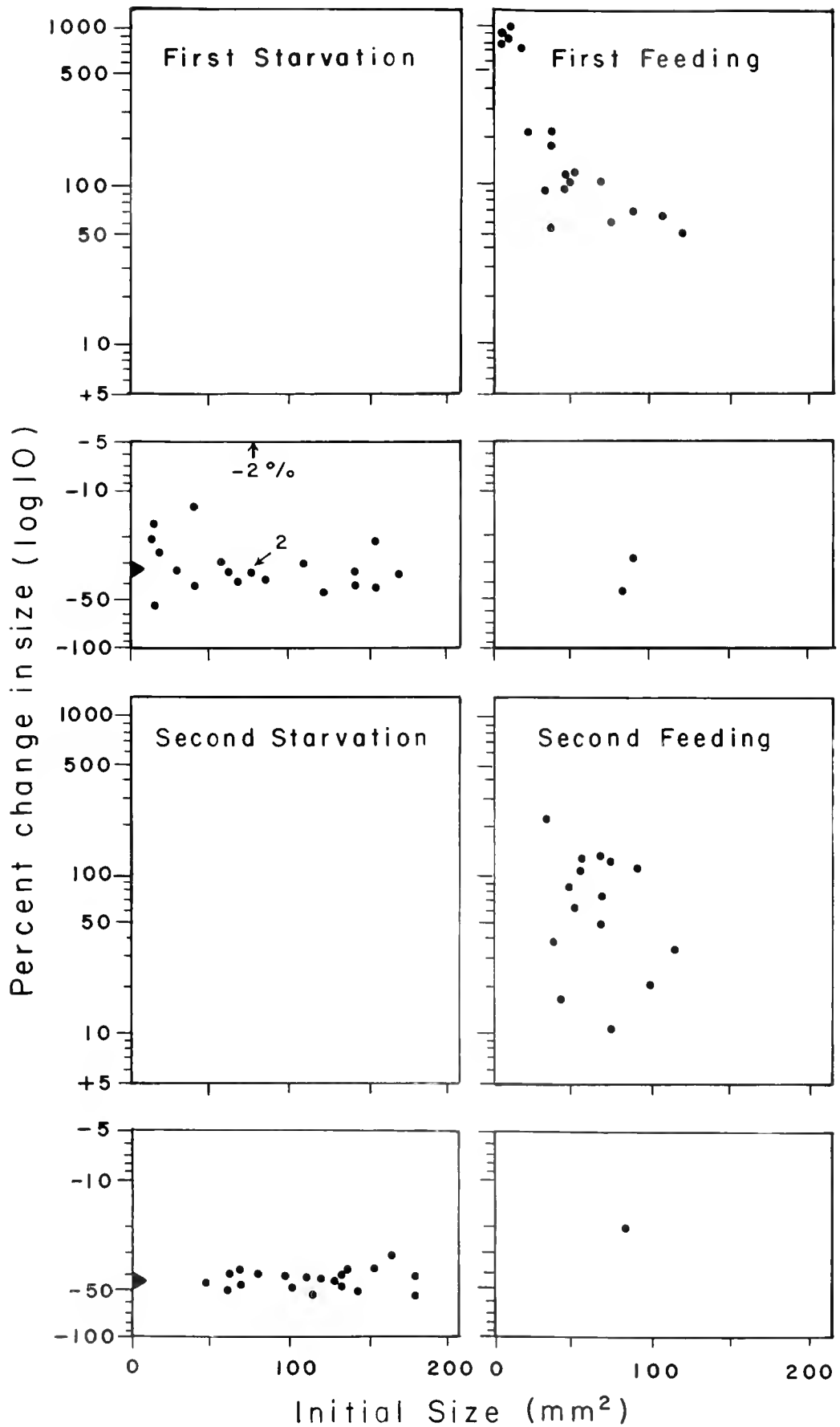


Figure 1. Experiment A Percentage increase (+) or decrease (-) in size (length  $\times$  width) of solitary *Stylochus ellipticus* in relation to temperature (21°, 30°C) and food (fed, unfed) for 5-week periods. Note that the scale breaks across the main figure (21°C data) and inset figure (30°C data) indicate transition between growth (+) and degrowth (-). Arrowheads on the y-axes indicate average decrease in size for unfed (U) animals at 21°C and for fed (F) and unfed (U) animals at 30°C (inset). Numeral (2) in lower panel at 21°C indicates where data for two animals coincide.



Data were analyzed by a split-level ANOVA (Experiment A, below) because the experiments were run at different times of the year and by regular ANOVA (Experiment B, below) on SAS (Hendrix *et al.*, 1982). An  $F_{\max}$  test was used to determine homogeneity of variances, and normality of the data was determined by stem leaf diagrams of the residuals and normal probability plots on SAS. Any data that did not meet these assumptions were transformed prior to analysis. Statistical comparisons were declared to be significant at the  $P < 0.1$  level in Experiment A because the high variability among the data and the limits of sample sizes in some instances undoubtedly resulted in a low power of the test (Peterman, 1990). We used a significance level of  $P < 0.05$  in Experiment B.

*Experiment A: Effects of temperature, food, and presence or absence of a partner*

In 1987, flatworm reproduction was assessed over arbitrarily selected 5-week periods in the dark under two feeding regimes (fed, unfed), at two temperatures (21°C, a late spring temperature, and 30°C, a high late summer temperature), and with and without partners. Thus at each temperature (21° and 30°) there were four treatments to which flatworms were haphazardly assigned: fed flatworms held singly or in size-matched pairs; unfed flatworms held singly or in pairs. Treatments at 21°C were made in spring and summer 1987. Treatments at 30°C were made in summer 1987 when field temperatures reached 29°C. All animals used in a 5-week period began a treatment at the same time and were observed every 48 h until they died or the 5-week period ended. A total of 103 single individuals and 45 pairs of flatworms survived the 5-week exposure. No animals were used more than once. Reproductive effort was measured as described earlier, except where noted in the results. It was not possible to ascertain if one or both animals in a pair had laid the eggs in any batch present in culture dishes after 48 h. Thus, for paired animals, we divided the number of eggs in any batch they produced by two to allow for a comparison with egg production by solitary animals.

*Experiment B: Effects of temporal variations in food supply and absence of a partner*

During spring and summer 1987, an attempt was made to determine how sensitive solitary flatworms were to long-term isolation and starvation, as evidenced by changes in

reproductive effort. Twenty-one flatworms were collected in April, measured, and held singly in the dark at 21°C. They were starved for 5 weeks to attempt to deplete any egg supply that might have been produced before capture (a 5-week period was used for symmetry with Experiment A). The water was changed every 48 h, but the logistical effort that went into initiating Experiment A prevented data collection during this initial 5-week period of Experiment B. The flatworms were then fed for 5 weeks, starved for 5 weeks, then fed again for 5 weeks to estimate their resilience to such changes. Data were collected and analyzed as in Experiment A. The four 5-week periods were designated First Starvation Period (only degrowth data collected), First Feeding Period, Second Starvation Period, and Second Feeding Period, respectively.

## Results

*Stylochus ellipticus* laid eggs whether food or a partner were present or not. Egg diameter ranged from 61 to 74  $\mu\text{m}$  ( $\bar{x} \pm \text{S.E.} = 68.5 \pm 0.45 \mu\text{m}$ ;  $n = 50$ ). Numbers of eggs within a batch (unadjusted for flatworm size) ranged from 125 to 85,600 for paired flatworms (these numbers were not divided by two) and from 295 to 39,300 for individuals. Up to 14 batches were produced (in the latter instance by a 93  $\text{mm}^2$  individual that also laid the most eggs—156,000 distributed over the 14 batches).

Mortality in Experiment A varied from 0 to 23% at 21°C and from 22 to 78% at 30°C, with no clear pattern of mortality associated with feeding state or presence or absence of a partner. Mortality was 19% at the end of 20 weeks at 21°C in Experiment B.

*Size-related observations*

Before we consider the main subject of the influence of temperature, food, and presence or absence of a partner on reproductive effort, we examine some findings that involve flatworm size. For Experiment A, our data are for solitary animals because it was not possible to distinguish between individual members of most pairs in order to follow their growth or degrowth.

*Size changes in solitary flatworms.* Starvation, accumulated exposure to stress, and high temperature had negative effects on flatworm growth.

At 21°C in Experiments A and B, most fed flatworms increased in area, whereas all unfed flatworms shrank

**Figure 2.** Experiment B Percentage increase (+) or decrease (–) in size (length  $\times$  width) of solitary *Stylochus ellipticus* at 21°C, under conditions of successive periods of starvation (First), feeding (First), starvation (Second), and feeding (Second), with each period being 5 weeks long. Note that the scale breaks across all four panels indicate transition between growth (+) and degrowth (–). Arrowheads on the y-axes of the starvation periods indicate average decrease in size. In the First Starvation panel, one animal decreased only 2% in size, and numeral (2) indicates where data for two other animals coincide.

(Figs. 1, 2). Fed animals that were smallest at the start of the experiments had the greatest increase in growth (up to about 1000% over their initial size); percentage change in growth declined with increasing initial size for fed animals. In terms of accumulated exposure to stressors, in Experiment B (Fig. 2), flatworms that survived the initial 5-week period of starvation grew more during the 5-week First Feeding Period (range of about 50–1000% increase over their initial size) than those in the Second Feeding Period (range of about 10–200% increase in size).

At 21°C in Experiments A and B, degrowth was relatively constant across the initial size range of unfed animals, with an average percentage change in size of -48% in Experiment A (Fig. 1) and -31% and -44% by the end of the First Starvation Period and Second Starvation Period of Experiment B, respectively (Fig. 2).

High temperature during Experiment A affected growth negatively, especially in concert with starvation. At 30°C, most fed individuals shrank (average decrease = -56%; Fig. 1, inset) in contrast to only four fed animals at 21°C (Fig. 1). As happened at 21°C, unfed flatworms at 30°C shrank at a relatively constant rate across the experimental size range, but degrowth occurred to a greater extent at 30°C (average decrease = -68%; Fig. 1, inset) than at 21°C (average decrease = -48%; Fig. 1).

*Number of batches of eggs and flatworm size.* Most flatworms smaller than 40 mm<sup>2</sup> produced no batches of eggs (Figs. 3, 4). There was a slight tendency for number of batches to increase with increasing area, but this was statistically significant only for the unfed animals at 30°C (a high stress condition) in Experiment A (Fig. 3).

*Egg production and flatworm size.* In Experiments A and B, especially for fed animals, the average area-specific number of eggs (*i.e.*, adjusted for flatworm area) produced per batch for solitary flatworms appeared to decline as initial area of the flatworms increased (Figs. 5, 6). However, this apparent decline was not statistically significant for any group.

#### Egg production and number of batches

Variability about the average area-specific number of eggs produced per batch was high in both experiments (Figs. 7, 8). Individual analysis of variance of the four sets of data in Experiment A (two temperatures; fed and unfed) and the three in Experiment B (First and Second Feeding, Second Starvation) revealed no significant differences in area-specific egg production per batch for any of the seven experimental conditions, undoubtedly because of this high variability in egg production.

#### Egg production and stressors

The overall (or grand mean) egg production in Experiments A and B was negatively affected by stress, with high

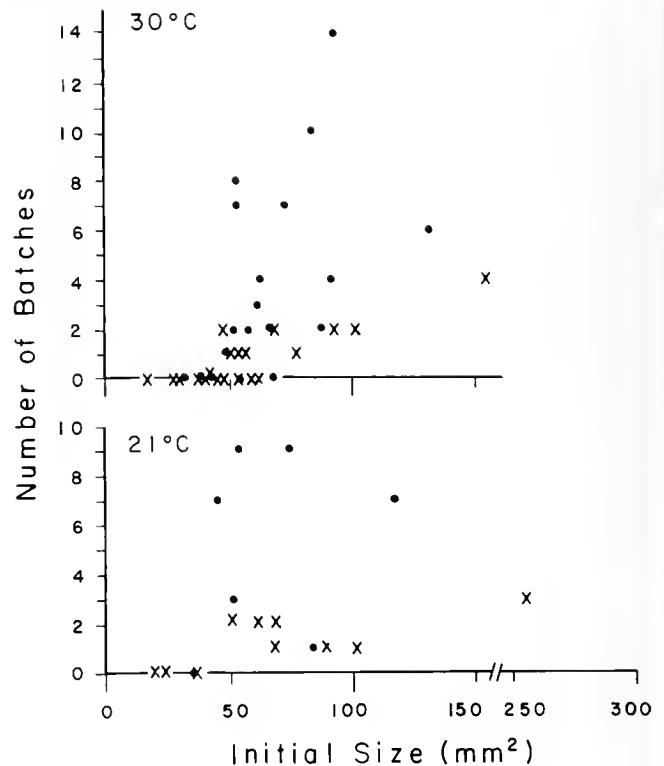


Figure 3. Experiment A. Number of batches of eggs in relation to initial size (length  $\times$  width) of fed (●) or unfed (×) solitary *S. ellipticus* after 5 weeks at 21° and 30°C.

temperature and lack of food generally depressing egg production in Experiment A, as did two starvation periods in Experiment B. In Experiment A, fed individuals produced an overall average of 150 eggs mm<sup>-2</sup> per batch at 21°C and 82 eggs mm<sup>-2</sup> per batch at 30°C (Fig. 7). In contrast, unfed individuals produced an overall average of 45 eggs mm<sup>-2</sup> per batch at 21°C and 55 eggs mm<sup>-2</sup> per batch at 30°C (Fig. 7). Experiment B flatworms produced an overall average of 163 eggs mm<sup>-2</sup> per batch during First Feeding (F<sup>1</sup>, Fig. 8), a value similar to the 150 eggs mm<sup>-2</sup> per batch reported above for fed individuals at 21°C in Experiment A. As stress accumulated, Experiment B flatworms produced an overall average of only 52 eggs mm<sup>-2</sup> per batch during Second Feeding (F<sup>2</sup>, Fig. 8), after having experienced two periods of starvation; they produced only 26 eggs mm<sup>-2</sup> per batch on average during the Second Starvation period (U, Fig. 8).

#### Experiment A: Effects of temperature, food, and presence or absence of a partner

Split-level ANOVA of our data grouped by four attributes (number of batches, days to first batch, percent



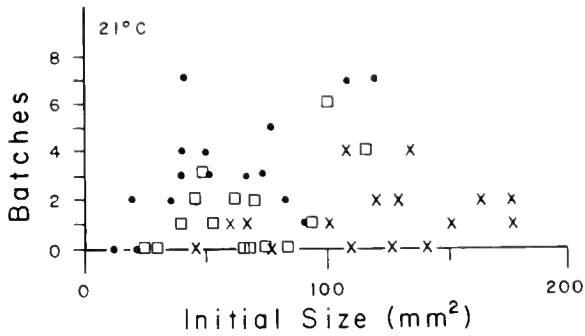


Figure 4. Experiment B Number of batches of eggs in relation to size (length · width) of 16 solitary individuals of *Stylochus ellipticus* at 21°C. Animals had been starved for 5 weeks, then fed for 5 weeks (●), starved for 5 more weeks (□), then fed for 5 weeks (×). Initial size refers to size at the start of each of the 5-week periods. Only 15 square symbols are presented for second feeding flatworms because one animal's size was not recorded (it produced no eggs).

hatch, eggs per batch) produced complicated results (Table I). Because these experiments were made during different months (March–August), we performed a covariate analysis with day of the year to determine if the results were affected by time of year the experiment was performed. For two attributes (number of batches and percent hatch)

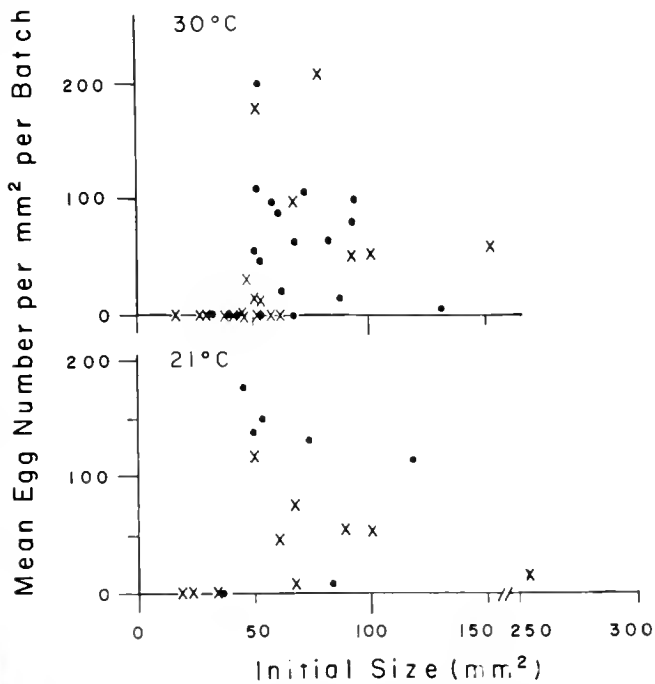


Figure 5. Experiment A Average number of eggs produced per batch by solitary individuals of *Stylochus ellipticus*, adjusted for initial flatworm size at the start of the experiment and plotted in relation to initial size. Data are for flatworms fed (●) or starved (×) for 5 weeks at 21°C or 30°C.

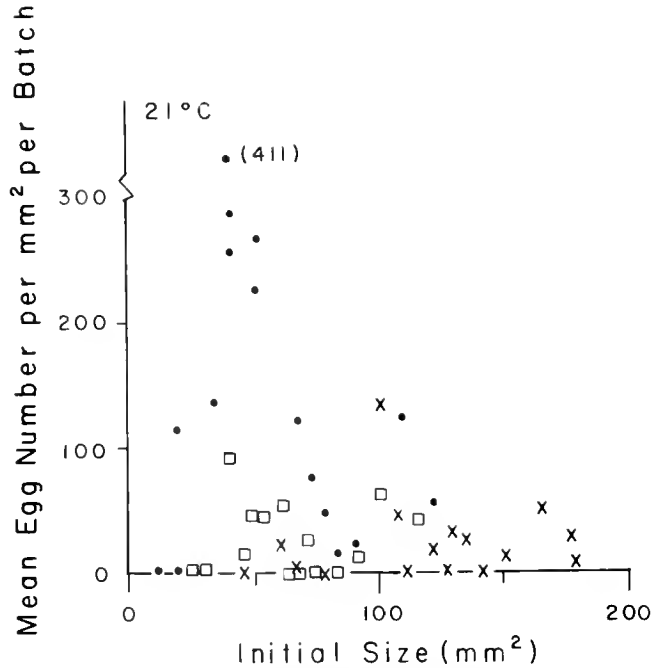


Figure 6. Experiment B Average number of eggs produced per batch by 16 solitary individuals of *Stylochus ellipticus*, adjusted for initial flatworm size at the start of the experiment and plotted in relation to size. Animals had been starved for 5 weeks, then fed for 5 weeks (●), starved for 5 more weeks (□), then fed for 5 weeks (×). Initial size refers to size at the start of each of the 5-week periods. Only 15 square symbols are presented for second feeding flatworms because one animal's size was not recorded (it produced no eggs).

there was a significant effect ( $P \leq 0.1$ ) due to day of year (Table I). It is difficult to determine the reasons for the differences in number of batches because the four-way interaction of day of year \* status \* temp \* food was significant ( $P \leq 0.1$ ) for that attribute (Table I). Day of year combined with factors like temperature and status showed a significant effect ( $P \leq 0.1$ ) on percent hatch. An examination of the interactive effects on flatworm reproduction of temperature, feeding, and status, independent of day, showed they were insignificant, except for number of eggs per batch (Table I).

Temperature effects on flatworm reproduction were the most pronounced of the three manipulations. Values for the percent of flatworms (solitary or paired) laying eggs were generally higher at 21°C than at 30°C, but the average time to produce a first batch of eggs was significantly faster at 30°C than at 21°C (Tables II, III). The average number of batches produced was similar between the two temperatures for solitary animals, and fewer at 30°C when paired. There was a tendency for unfed solitary and paired animals at 30°C to lay more eggs per batch than at 21°C. Hatching success remained high (median values of 93–100%) under all conditions. In these comparisons for solitary and paired flatworms, statistically significant differ-

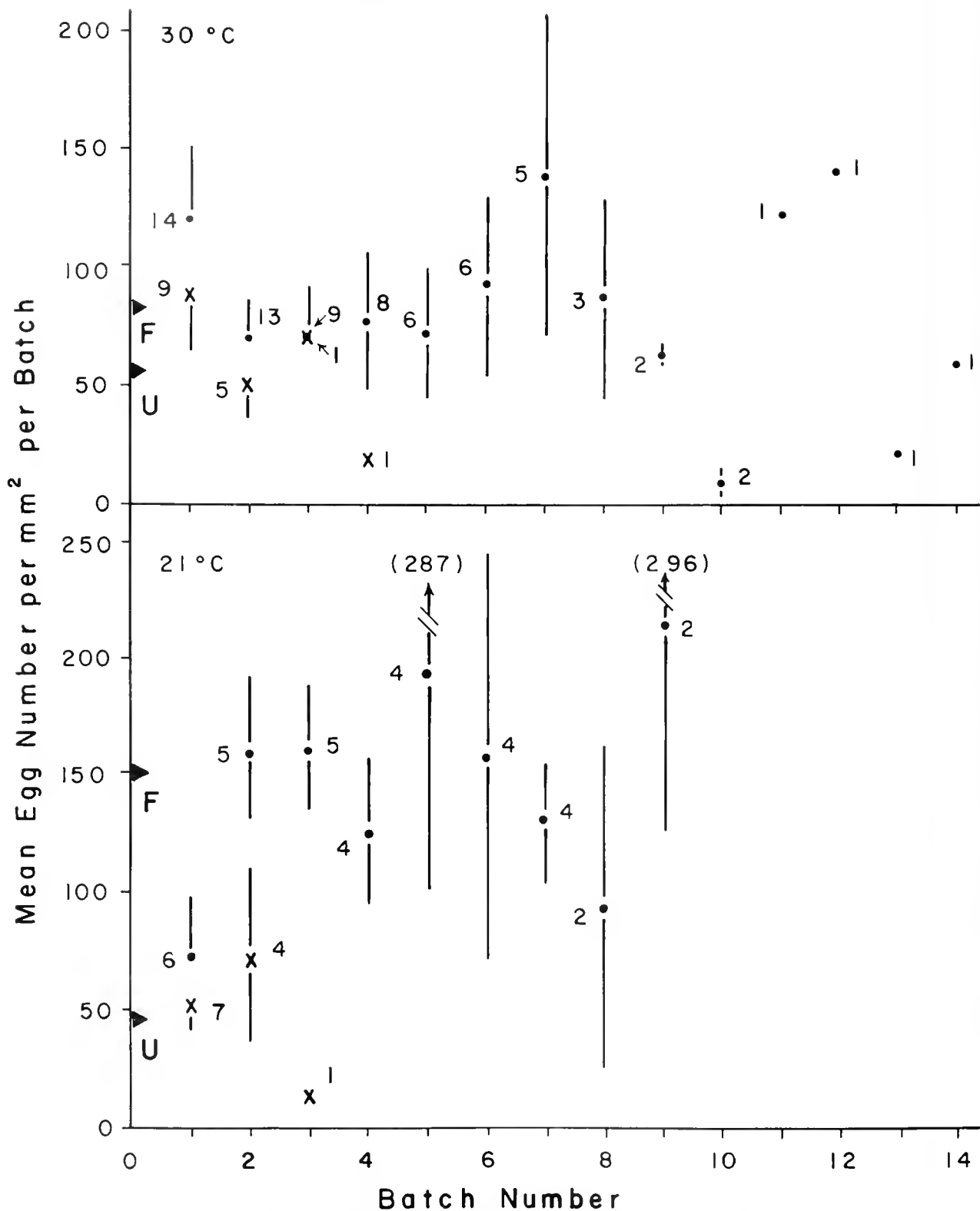
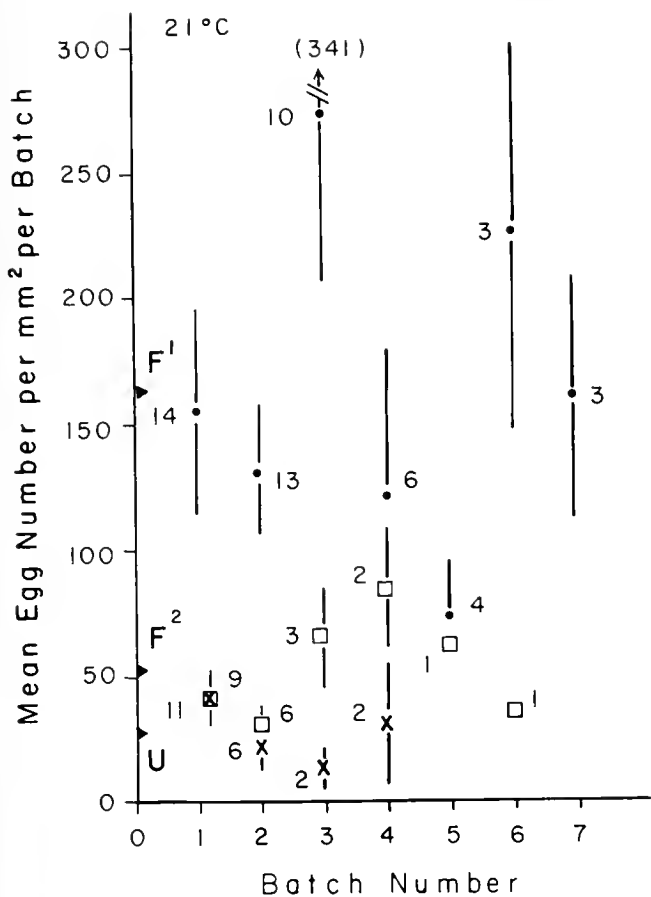


Figure 7. Experiment 1. Average number ( $\pm 1$  SE) of eggs produced per batch by solitary individuals of *Stylochus ellipticus*, adjusted for flatworm size at the start of the experiment and plotted in relation to batch number. Data are for flatworms fed (●) or starved (x) for 5 weeks at 21°C or 30°C. Number of flatworms producing a batch are indicated. Arrowheads on the x-axis indicate grand means of eggs produced per batch under the experimental conditions of being fed (F) or unfed (U).



**Figure 8.** Experiment B Average number ( $\pm 1$  SE) of eggs produced per batch by 16 solitary individuals of *Stylochus ellipticus*, adjusted for flatworm size at the start of the experiment and plotted in relation to batch number. Number of flatworms producing a batch are indicated. Animals had been starved for 5 weeks, then fed for 5 weeks (●, first feeding), starved for 5 more weeks (○, second starvation), then fed for 5 weeks (□, second feeding). Arrowheads on the y-axis indicate grand means of eggs produced per batch under the experimental conditions of first feeding (F<sup>1</sup>), second starvation (U), or second feeding (F<sup>2</sup>).

ences ( $P \leq 0.1$ ) between temperatures occurred only in days to first batch (Table I).

We multiplied the average number of eggs per batch by the average number of batches produced, and multiplied the resultant estimate of total eggs laid by the median hatching percentage to derive an estimate of total larvae that would be produced in each treatment (Tables II, III). Except for unfed solitary flatworms, more larvae would result at 21°C than at 30°C.

Food availability also affected the reproductive activities of *S. ellipticus*. The proportion of animals that produced no batches was about twice as high for unfed animals (30% at 21°C; 53% at 30°C) than for fed animals (14% at 21°C; 26% at 30°C) (Fig. 3); note that the proportion producing no batches whether unfed or fed was about twice as high at 30°C as at 21°C. Lack of food had a

statistically significant effect ( $P \leq 0.1$ ) on the onset of egg laying, with days to first batch generally declining with starvation (Tables II, III). We estimated that fed flatworms (paired or solitary) would produce more eggs than would unfed flatworms over the course of time, resulting in the production of more larvae despite a sometimes higher percentage of hatching for unfed flatworms (Tables II, III).

Solitary flatworms sometimes took longer average times than paired to produce their first batch of eggs (Tables II, III), but time differences over the range of experiments were not statistically significant for status (Table I). Average numbers of batches also were not significantly different between paired and solitary flatworms. Paired *S. ellipticus* individuals laid from 1.5 to 3.5 times fewer eggs per batch (recall that the number of eggs produced by a pair has been halved for this comparison) and consequently produced fewer larvae than solitary animals (Tables II, III); this difference was statistically significant ( $P \leq 0.1$ ).

*Experiment B: Effects of temporal variations in food supply and absence of a partner*

When flatworms were held singly at 21°C for twenty weeks, 56% were still able to lay eggs when the experiment

**Table I**

*Experiment A Statistically significant results of manipulations based on split-level ANOVA*

Attribute	Source	Type III SS	F-Value
Number of batches	Temp	27.25	4.53*
	Food	101.35	16.83**
	Day	31.68	5.26*
	Day*Status	49.59	10.47**
	Day*Food	29.75	6.28*
	Day*Temp*Food	13.03	2.75 <sup>2</sup>
	Day*Status*Temp*Food	22.47	4.74*
Days to first batch	Temp	13.46	29.10**
	Food	2.70	5.83*
Percent hatch	Status	1285.86	8.63**
	Temp	750.21	5.03*
	Food	2010.29	13.49**
	Day	765.91	5.14*
	Day*Status	1125.75	7.83**
	Day*Temp	1030.48	7.17**
	Day*Status*Temp	922.56	6.42*
Eggs/batch	Status	514462964.99	19.17**
	Food	86836259.36	3.24 <sup>2</sup>
	Status*Food	79686364.38	2.97 <sup>2</sup>
	Temp*Food	180828017.83	6.74*

<sup>2</sup>“Type III SS” refers to the sum-of-squares value. In the F-value column, significant values are indicated as  $P \leq 0.1$  (\*),  $P \leq 0.05$  (\*) or  $P \leq 0.01$  (\*\*). “Status” refers to presence or absence of a partner; “Food” to presence or absence of food; “Temp” to 21° or 30°C; “Day” to day of the year for experiments within a treatment. Degrees of freedom for all comparisons were 1.

Table II

Experiment A. Data for nine separate sets of observations on reproductive effort for solitary *Stylochus ellipticus* that survived, fed and unfed at 21°C and 30°C, for a 5-week period

Attribute	Solitary									
	Fed				Unfed					
	21°C		30°C		21°C		30°C			
1. Sample size after 5 weeks	24	7	9	10	23	7	3	9	11	
2. Number laying eggs (%)	17 (71)	6 (86)	5 (56)	9 (90)	11 (52)	5 (71)	2 (67)	5 (56)	4 (36)	
3. $\bar{X}$ Days to first batch	14.6 ± 2.3	10.3 ± 3.2	3.2 ± 0.8	2.9 ± 0.4	10.4 ± 2.5	8.2 ± 2.5	3.0 ± 1.0	2.8 ± 0.8	4.0 ± 0.8	
4. $\bar{X}$ Number of batches	2.9 ± 0.5	6.0 ± 1.3	5.6 ± 1.5	4.9 ± 1.4	2.8 ± 0.5	1.6 ± 0.2	2.0 ± 1.0	2.2 ± 0.5	1.3 ± 0.3	
5. $\bar{X}$ Eggs per batch	ND	9400 ± 1200	5300 ± 1280	7000 ± 1000	ND	4200 ± 920	4600 ± 1630	5500 ± 1380	7800 ± 2510	
6. Total eggs, thousands (row 4 × row 5)	ND	56	30	34	ND	7	9	12	10	
7. Percent hatch										
range	0-100	72-100	49-100	35-100	48-100	66-100	100	94-100	94-100	
median	97	99	97	99	99	98	100	98	98	
8. Total larvae, thousands (row 6 × row 7, median)	ND	55	29	34	ND	7	9	12	10	

Values are mean ± S.E. ND = eggs not counted.

ended, even after 20 weeks of alternate starvation and feeding (Table IV). In two instances, flatworms did not lay their first batch of eggs until after they were starved for the second time and then had been fed, *i.e.*, weeks 16-20 of the experiment.

In Experiment B, the percentage of flatworms laying eggs declined with time (Table IV). For attributes 3, 4, and 7, but not attribute 5, there was no significant difference between the First Feeding Period and the Second Feeding Period. Likewise, there was no significant difference between the Second Starvation Period and the Second Feeding Period for all four attributes except days to first batch (Table IV). The average number of batches produced per flatworm during the Second Starvation Period (1.9) was significantly lower than the numbers during the First Feeding Period (3.9) but not during the Second Feeding Period (2.4), in agreement with the decline in batch production with starvation in Experiment A (Tables II, III). Two flatworms in the First Feeding Period, five in the Second Starvation Period, and six in the Second Feeding Period produced no eggs (Fig. 4). The average number of eggs per batch decreased with time, so that the calculated total output of eggs decreased significantly ( $P \leq 0.05$ ) from about 36,000 eggs during the First Feeding Period to about 9000 in the Second Feeding Period.

Over the three experimental periods, the median percentage of eggs that hatched into viable larvae remained

between 93 and 97%, with hatching success varying directly with feeding. As a result, as the total number of eggs changed with experimental conditions, the calculated total number of larvae also changed (Table IV).

The results of Experiment B (Table IV) can be compared with those for solitary flatworms at 21°C in Experiment A (Table II). At the end of the First Feeding Period in Experiment B, the percent laying eggs, the average number of days to first batch production, the average number of batches, the average number of eggs per batch, and the median percent hatching success (Table IV) were within the ranges of, or were similar to, values in Experiment A for the two sets of fed animals at 21°C (Table II). This was true also when results from the Second Starvation Period in Experiment B (Table IV) were compared with data for three sets of starved animals at 21°C in Experiment A (Table II), except for average hatching success which was lower in Experiment B. Values for attributes for the Second Feeding Period in Experiment B (Table IV) were lower (except for average number of days to first batch) than for fed flatworms at 21°C in Experiment A (Table II). Total egg and larval production at the end of 20 weeks was much less in Experiment B (Table IV) than in Experiment A after 5 weeks at 21°C (Table II). The overall similarities in attribute responses between fed animals in Experiment A and in Experiment B (First Feeding Period) and between starved animals from the two ex-

Table III

Experiment A: Data for five separate sets of observations on reproductive effort for paired *Stylochus ellipticus* that survived, fed and unfed at 21°C and 30°C, for a 5-week period

Attribute	Paired				
	Fed		Unfed		
	21°C	30°C	21°C	30°C	
1. Sample size after 5 weeks	6	9	6	13	11
2. Number laying eggs (%)	5 (83)	6 (67)	5 (83)	12 (92)	7 (64)
3. $\bar{X}$ Days to first batch	9.8 ± 2.7	4.7 ± 1.9	6.0 ± 2.5	5.3 ± 1.6	2.9 ± 0.9
4. $\bar{X}$ Number of batches	6.8 ± 2.0	4.5 ± 1.0	2.8 ± 1.1	4.0 ± 0.6	1.7 ± 0.4
5. $\bar{X}$ Eggs per batch <sup>a</sup>	4200 ± 610	2200 ± 400	2400 ± 760	3000 ± 600	3700 ± 1170
6. Total eggs, thousands (row 4 × row 5)	29	10	7	12	6
7. Percent hatch range	62–100	26–100	93–100	65–100	65–100
median	97	93	99	98	98
8. Total larvae, thousands (row 6 × row 7, median)	28	9	7	12	6

Values are mean ± S.E.

<sup>a</sup> Adjusted by dividing by two to allow comparison with solitary flatworms.

periments indicate that the patterns uncovered in the two experiments are indeed repeatable and not specific to a single experiment.

Summary of results

Our experiments produced complex results, so we summarize the significant findings here. Higher temperature and starvation negatively affected flatworm growth (Figs. 1, 2). When fed, smaller flatworms grew proportionately more than did larger flatworms; all unfed animals tended to shrink to a proportionately similar extent, with higher temperature and accumulated exposure to starvation associated with greater degrowth (Figs. 1, 2). The number of batches of eggs produced (Figs. 3, 4) and (when egg production was adjusted for area of solitary flatworms) the average number of eggs produced per batch (Figs. 5, 6) were not significantly affected by initial area of the flatworms. Similarly, the average number of eggs produced per batch, adjusted for flatworm area, did not change significantly as more batches were produced (Figs. 7, 8).

There was no significant statistical effect of higher temperature and starvation on egg production, although there were some instances of diminished egg production under these conditions (Figs. 7, 8; Tables II–IV). Flatworms did react to higher temperature and starvation by significantly decreasing the number of days that elapsed before egg laying began (Tables II–IV). Overall, more larvae would be produced at 21°C than at 30°C (Tables II, III), by fed flatworms than by starved flatworms (Tables II–IV), and

by solitary flatworms than by paired flatworms (Tables II, III).

Discussion

Flatworms in our experiments increased or decreased in surface area relative to the availability of food. Pearse and Wharton (1938) found in Florida that fed *S. ellipticus* (which they called *Eustylochus meridionalis*) could grow from an average of 1.4 to 5.2 mm (n = 5) in 17 days in March, and that starved *Stylochus frontalis* experienced an average 30% decrease in size from November 18 to March 5, a slightly lower percentage than we found. In our study, smaller, fed animals grew the most proportionally, while larger flatworms grew the least. In Experiment B, the lessened growth in the Second Feeding Period compared with growth in the First Feeding Period (Fig. 2) may have resulted from the accumulated stress of two periods of starvation, or from increasing age of the flatworms; the lack of continuously fed controls hinders a conclusion.

Flatworms that were held for a long period under stress (lack of food, high temperature) could produce many eggs while at the same time undergoing degrowth (Tables II–IV). This may be an indication that the flatworms diverted resources from growth and maintenance to reproduction, resulting in a decreased body size. A similar strategy has been reported in mollusks (Havenhand and Todd, 1989). If the cost of reproduction results in an inability of the reproducing adult to meet all its energy requirements from

Table IV

Experiment B Data for reproductive effort of solitary *Stylochus ellipticus* held at 21°C for 20 weeks under alternating feeding and starvation regimes of 5 weeks each

Attribute	First feeding	Second starvation	Second feeding
1. Sample size after each 5-week period	21	20	16
2. Number laying eggs (%)	14 (67)	11 (55)	9 (56)
3. $\bar{X}$ Days to first batch	12.4 ± 2.04 <sup>z</sup>	6.2 ± 1.69	13.0 ± 3.55 <sup>z</sup>
4. $\bar{X}$ Number of batches	3.9 ± 0.53 <sup>z</sup>	1.9 ± 0.34 <sup>y</sup>	2.4 ± 0.56 <sup>z</sup>
5. $\bar{X}$ Eggs per batch	9200 ± 1100	4000 ± 800 <sup>z</sup>	3700 ± 650 <sup>z</sup>
6. Total eggs, thousands (row 4 × row 5)	36	8	9
7. Percent batch range	5–100	12–100	29–100
median	97 <sup>z</sup>	93 <sup>y</sup>	94 <sup>z</sup>
8. Total larvae, thousands (row 6 × row 7, median)	35	7	8

Values are means ± S.E. Values with like superscripts for attributes 3, 4, 5, and 7 are not significantly different at  $P \leq 0.05$ .

input energy, the deficit may be made good in *S. ellipticus*, as in triclads, from the catabolism of tissue or degrowth (Woollhead and Calow, 1979). This capacity for degrowth may be especially important during the reproductive period if food supply is reduced through inter- and intra-specific competition for food (Woollhead, 1983).

Life history features such as how much resource to put into reproduction must be the outcome of compromises between conflicting demands (Grahame and Branch, 1985). The most prominent life-history compromise involves the cost of reproduction, with costs paid in survival or in future reproduction (Stearns, 1989). For *S. ellipticus*, the reproductive effort of the flatworm is maintained while the flatworm decreases in size, rather than ceasing at the same time that size is being maintained.

*Stylochus ellipticus* was able to produce numerous fertile eggs whether solitary or paired, fed or unfed, and at 21° or 30°C. In this it appears to differ from many other turbellarians that are reported by Henley (1974) to show rapid regressive changes in their reproductive systems under adverse environmental conditions.

*Stylochus ellipticus* in Chesapeake Bay has the potential to be reproductively active in spring, summer, and early autumn, based on the fact that it was able to produce eggs at both 21°C and 30°C. Flatworms produced eggs in our study from March through August (we did not examine

them in other months). In Florida, Pearse and Wharton (1938) found *S. ellipticus* to continue to lay eggs when brought into the laboratory in winter and spring, but there appears to be no information on the effects of the lower temperatures of the northern winter on gametogenesis and reproduction.

The fact that reproductive output of *S. ellipticus* (as measured by total eggs and larvae produced) was usually greater for animals at 21°C than 30°C in our study suggests that the optimal period for reproduction in nature is most likely spring or autumn when field temperatures are lower than in summer. Dumont and Schorreels (1990) likewise found 20°C to be the optimum temperature for reproduction in the turbellarian *Mesostoma lingua*.

There are limited spawning data available for other species of *Stylochus*. Two species show evidence of prolonged spawning for six months or more, i.e., *S. mediterraneus* in Italy (Galleni *et al.*, 1980) and *S. inimicus* (?) in Taiwan (Kuo *et al.*, 1984). This is also true for other polyclads, including *Pseudostylochus ostreophagus* (Woelke, 1957) and *Notoplana acticola* (Thum, 1974; see also Kato, 1940). However, *S. zebra* only produces eggs from June through August (Lytwyn and McDermott, 1976).

We have no data on how long *S. ellipticus* can survive in nature, but we collected individuals all year round in the Choptank River, Maryland (unpub. data), as did Pearse and Wharton (1938) at some stations in Florida. Large flatworms (>200 mm<sup>2</sup>) were not collected in the Choptank River from about November to March (Chintala, 1987), so it is possible that *S. ellipticus* is an annual species. *S. zebra* can live in the laboratory for over one year, although there is a lower abundance in nature after the summer reproductive period (Lytwyn and McDermott, 1976). Galleni *et al.* (1980) found *S. mediterraneus* in mussel beds year round, although the flatworms were rare in winter and spring. On the other hand, *Pseudostylochus ostreophagus* in Washington died in nature and in the laboratory during the midsummer of three successive years (Woelke, 1957).

Even after twenty weeks of isolation, 56% of the flatworms in Experiment B were still able to produce viable eggs. Thus, even though these animals may be non-self-fertilizing (Hyman, 1940, 1951; Prudhoe, 1985), and are thought to be internally fertilized (Pearse and Wharton, 1938; Giese and Kanatani, 1987), they were still reproductively active. If they do not self-fertilize, then either there must be some mechanism of sperm storage or else these animals could produce eggs capable of parthenogenic development when necessary in adverse conditions, such as when mates are absent. Self-fertilization is thought to be uncommon in Turbellaria because the male and female reproductive systems are largely separate, although a few triclads are parthenogenic (Gosner, 1971). It is possible

that sperm retention is the alternative mode used by these flatworms, because *S. ellipticus* has a seminal receptacle in which sperm could be stored (Prudhoe, 1985). *S. ellipticus* could be like the Pacific Coast species *Notoplana acticola* in which sperm is present in the seminal receptacle throughout the year, suggesting either that copulation occurs throughout the year or that sperm are readily stored for extended periods of time (Thum, 1974).

The eggs of *S. ellipticus* and some other species of *Stylochus* are relatively small in comparison with those of *S. zebra* and other polyclads (Table V). This small size is accompanied in *S. ellipticus* by the shortest development period before hatching reported for stylochids, and by the potential to produce tens of thousands of eggs per batch, with numerous batches possible. The small egg size and high fecundity, coupled with the short developmental period and extended breeding period, indicate that *S. ellipticus* is well adapted to resisting environmental stressors encountered in its estuarine habitat.

There was a distinct pattern in the flatworms' egg laying response to potential stressors (*i.e.*, high temperature, no food) and the condition of isolation. Earlier egg laying was significantly associated with increased temperature or decreased food, which could result in the animals contributing to the gene pool before they could possibly succumb to the effects of the high summer temperatures or, especially, to starvation. Perhaps this is because there is little point in withholding energy from reproduction if the adult is not likely to survive long enough to reproduce

at a later stage (Grahame and Branch, 1985). In addition, even though the flatworms responded to stress by de-growth, they may not have decreased the amount of material needed to maintain egg viability as reflected by the high hatching success of eggs over most stress conditions. For example, the percent of eggs hatching for solitary unfed individuals at 30°C was about as high as or higher than for unfed animals at 21°C and similar for fed animals at both temperatures (Table II). All these events suggest that when adult *S. ellipticus* are exposed to stress, they at least maintain the effort of producing young. Nevertheless, a variety of factors may determine when reproduction occurs, and at times these factors may conflict so that no single general cue for reproduction emerges (Grahame and Branch, 1985).

The concept of compensation means that if allocation to one function increases, then allocations to others will decrease (Grahame and Branch, 1985). Whether physiological compensations exist depends on the organism and what sort of breeding cycle it has. Two extremes on a continuum are "income" and "capital" breeders (Stearns, 1989). An income breeder uses its current income for reproductive investment, whereas a capital breeder stores energy that can be mobilized later for reproduction (Stearns, 1989). *S. ellipticus* resembles a capital breeder in that it can produce eggs while unfed, relying on stored energy.

Solitary flatworms sometimes took longer average times than paired flatworms to produce eggs, but the data were

Table V

Size and number of eggs laid in a batch, and length of time before hatching occurs for polyclad Turbellaria

Species	Egg number	Egg size (µm)	Development period (days)	T (°C)	Reference
<i>Stylochus ellipticus</i>	63-42,800 (pair) 295-39,300 (individual)	61-74	5-7	21	This study
<i>S. aomori</i>	—	95-105	8	"early summer"	Kato (1940)
<i>S. frontalis</i>	919-18,028	—	11	28	Pearse and Wharton (1938)
(= <i>mimicus</i> )	<sup>a</sup>	—	10-17	26	Kuo <i>et al</i> (1984)
<i>S. mediterraneus</i>	—	—	8	22	Bytinski-Salz (1935)
			8-10		Galleni <i>et al.</i> (1980)
<i>S. uniporis</i>	—	85-95	8	"early summer"	Kato (1940)
<i>S. zebra</i>	220-487 <sup>b</sup>	200-220	14	25.5	Lytwyn and McDermott (1976)
			17	22	
<i>Euplana gracilis</i>	25-400	85-100	7	21	Christensen (1971)
<i>Notoplana australis</i>	"several hundred"	120-125	12-14	20-22	Anderson (1977)
<i>Pseudostylochus ostreophagus</i>	3373-88,332 <sup>c</sup>	147	30-34	15-17	Woelke (1957)

T—incubation temperature. RT = room temperature (not stated). Egg numbers reported for *Stylochus ellipticus* pairs in this study have been divided by two.

<sup>a</sup> Largest produced 450,000 eggs in seven batches; smallest produced 93,000 in four batches.

<sup>b</sup> Maximum number over 23 days was 9549 eggs.

<sup>c</sup> Number of eggs laid in a season (March-October).

not consistent enough to suggest that the presence of a partner stimulates egg laying. The number of eggs laid per flatworm was significantly higher for solitary than for paired animals; however, the number of eggs per batch was not significantly different. This suggests that the solitary animals might decrease size more and put the same amount of effort into reproduction as do animals that are paired. Another possibility is that when animals are paired, both reduce their allocation of resources to reproduction or only one animal does the egg laying. The fact that a solitary individual produces significantly more eggs is intriguing. If, when populations are low in nature, the lack of stimulation by other flatworms causes solitary individuals to lay more eggs, then the population could grow. The presence of a partner would not lead to a concomitant increase in fecundity, thus stabilizing the population.

Although *S. ellipticus* reacted to perturbations in food supply by growing or shrinking, it continued to put much effort into reproduction. In this it resembles semelparous species that put more effort into reproduction than do iteroparous species (Calow and Woollhead, 1977; Woollhead and Calow, 1979; Woollhead, 1983). Semelparous species also are less sensitive to perturbations in food supply and continue their reproductive output despite reductions in food supply. Or, *S. ellipticus* could be like the gastropod *Nassarius pauperatus*, which produces more eggs when food is short, thus shifting from iteroparity to semelparity when future adult survival is threatened (McKillup and Butler, 1979). However, our data are only preliminary and more work is required to answer the question about semelparity in *S. ellipticus*.

### Acknowledgments

We acknowledge the technical advice of Dr. D. Bonar and Dr. W. M. Kemp, the statistical guidance of Dr. L. Douglass, the logistical assistance of M. Maddox and M. Clayton, the artwork of D. Kennedy, and the criticism of the manuscript by Drs. S. Alspach, J. McDermott, D. Penry and D. Weston, Ms. D. Goldbach, and three referees. This paper is based on work submitted for the M.S. degree in the Marine, Estuarine and Environmental Sciences Program, University of Maryland System. Partial support was provided by the University of Maryland Sea Grant Program. Contribution No. 2482 of the University of Maryland System Center for Environmental and Estuarine Studies.

### Literature Cited

- Anderson, D. T. 1977. The embryonic and larval development of the turbellarian *Notoplana australis* (Schmada, 1859). (Polycladida: Leptoplanidae). *Aust J Mar Freshwater Res* 28: 303-310.
- Bytinski-Salz, H. 1935. Un polyclado (*Stylochus pilidium* Lang) danoso ai parcu ostricoh. *Thalassia* 2: 1-24.
- Calow, P., and A. S. Woollhead. 1977. The relationship between ration, reproductive effort and age-specific mortality in the evolution of life-history strategies—some observations on freshwater triclads. *J. Anim. Ecol.* 46: 765-781.
- Chintala, M. M. 1987. Reproduction and feeding of *Stylochus ellipticus* (Girard), a predator of juvenile oysters. M.S. thesis. University of Maryland. College Park. 75 pp.
- Christensen, D. J. 1971. Early development and chromosome number of the polyclad flatworm *Euplana gracilis*. *Trans. Am. Microsc. Soc.* 90: 457-463.
- Christensen, D. J. 1973. Prey preference of *Stylochus ellipticus* in Chesapeake Bay. *Proc. Natl. Shellfish. Assoc.* 63: 35-38.
- Dumont, H. J., and S. Schorreels. 1990. A laboratory study of the feeding of *Mesostoma lingua* (Schmidt) (Turbellaria: Neorhabdococla) on *Daphnia magna* Straus at four different temperatures. *Hydrobiologia* 198: 79-89.
- Galleni, L., P. Tongiorgi, E. Ferrero, and U. Salghetti. 1980. *Stylochus mediterraneus* (Turbellaria: Polycladida), predator on the mussel *Mytilus galloprovincialis* Mar. Biol. 55: 317-326.
- Giese, A. C., and H. Kanatani. 1987. Maturation and spawning. Pp. 251-329 in A. C. Giese, J. S. Pearse, and V. B. Pearse, eds. *Reproduction of Marine Invertebrates, Volume IX: General Aspects: Seeking Unity in Diversity*. Blackwell Scientific Publications, Palo Alto, CA, and The Boxwood Press, Pacific Grove, CA.
- Gosner, K. L. 1971. *Guide to the Identification of Marine and Estuarine Invertebrates: Cape Hatteras to the Bay of Fundy*. Wiley-Interscience, New York. Pp. 169-172.
- Grahame, J., and G. M. Branch. 1985. Reproductive patterns of marine invertebrates. *Oceanogr Mar Biol. Ann. Rev.* 23: 373-398.
- Havenhand, J. N., and C. D. Todd. 1989. Reproductive effort of the nudibranch molluscs *Adalaria proxima* (Alder & Hancock) and *Onchidoris muricata* (Müller); an evaluation of techniques. *Functional Ecol.* 3: 153-163.
- Hendrix, L. J., M. W. Carter, and D. T. Scott. 1982. Covariance analysis with heterogeneity of slopes in fixed models. *Biometrics* 38: 641-650.
- Henley, C. 1974. Platyhelminthes (Turbellaria). Pp. 267-343 in A. C. Giese and J. S. Pearse, eds. *Reproduction of Marine Invertebrates, Volume I: Acoelomate and Pseudocoelomate Metazoans*. Academic Press, New York.
- Hyman, L. H. 1940. The polyclad flatworms of the Atlantic Coast of the United States and Canada. *Proc. U.S. Nat. Mus.* 89: 449-495.
- Hyman, L. H. 1951. *The Invertebrates: Platyhelminthes and Rhynchocoela*, Vol. II. McGraw-Hill, New York. 547 pp.
- Kato, K. 1940. On the development of some Japanese polyclads. *Jpn. J. Zool.* 8: 537-573.
- Kuo, G.-H., Y.-S. Lin, H.-C. Chen, and C.-F. Lo. 1984. Disease and mortalities of cultured marine fish and shellfish in Taiwan. Pp. 173-192 in *Proceedings of ROC-Japan Symposium on Mariculture*, I. C. Liao and R. Hirano, eds. TML Conference Proceedings I. Tungking Marine Laboratory, Taiwan.
- Landers, W. S., and E. W. Rhodes, Jr. 1970. Some factors influencing predation by the flatworm, *Stylochus ellipticus* (Girard), on oysters. *Chesapeake Sci.* 11: 55-60.
- Loosanoff, V. L. 1956. Two obscure oyster enemies in New England waters. *Science* 123: 1119-1120.
- Lytwyn, M. W., and J. J. McDermott. 1976. Incidence, reproduction and feeding of *Stylochus zebra*, a polyclad turbellarian symbiont of hermit crabs. *Mar. Biol.* 38: 365-372.
- McKillup, S. C., and A. J. Butler. 1979. Modification of egg production and packaging in response to food availability by *Nassarius pauperatus*. *Oecologia* 43: 221-231.
- Pearse, A. S., and G. W. Wharton. 1938. The oyster "leech," *Stylochus mimicus* Palombi, associated with oysters on the coasts of Florida. *Ecol. Monogr.* 8: 605-655.



- Peterman, R. M. 1990.** Statistical power analysis can improve fisheries research and management. *Can. J. Fish. Aquat. Sci.* **47**: 2–15.
- Provenzano, A. J., Jr. 1961.** Effects of the flatworm *Stylochus ellipticus* (Girard) on oyster spat in two salt water ponds in Massachusetts. *Proc. Natl. Shellfish Assoc.* **50**: 83–88.
- Prudhoe, S. 1985.** *A Monograph on Polyclad Turbellaria*. Oxford University Press, London, 259 pp.
- Shaw, W. N. 1967.** Seasonal fouling and oyster setting on asbestos plates in Broad Creek, Talbot County, Maryland, 1963–65. *Chesapeake Sci.* **8**: 228–236.
- Stearns, S. C. 1989.** Trade-offs in life-history evolution. *Funct. Ecol.* **3**: 259–268.
- Thum, A. B. 1974.** Reproductive ecology of the polyclad turbellarian *Notoplana acticola* (Boone, 1929) on the central California Coast. Pp. 431–445 in N. W. Riser and M. P. Morse, eds. *Biology of the Turbellaria*. McGraw-Hill, New York.
- Webster, J. R., and R. Z. Medford. 1961.** Flatworm distribution and associated oyster mortality in Chesapeake Bay. *Proc. Natl. Shellfish Assoc.* **50**: 89–95.
- Wolke, C. E. 1957.** The flatworm *Pseudostylochus ostreophagus* Hyman, a predator of oysters. *Proc. Natl. Shellfish Assoc.* **47**: 62–66.
- Woolhead, A. S. 1983.** Energy partitioning in semelparous and iteroparous triclads. *J. Anim. Ecol.* **52**: 603–620.
- Woolhead, A. S., and P. Calow. 1979.** Energy-partitioning strategies during egg production in semelparous and iteroparous triclads. *J. Anim. Ecol.* **48**: 491–499.

## Postembryonic Growth of Two Peripheral Sensory Systems in the Medicinal Leech *Hirudo medicinalis*

LISA GASCOIGNE AND ALISTAIR MCVEAN

*Department of Biology, Royal Holloway and Bedford New College, University of London, Egham, Surrey TW20 OEX, UK*

**Abstract.** The midbody segments of *Hirudo medicinalis* have two types of sensory cilia that project from the skin into the surrounding water. These are the proposed mechanosensory S cilia and the putative chemosensory G cilia. The cells bearing these cilia are clustered together into structures known as sensilla. The skin of each midbody segment is externally divided into five annuli. Fourteen large sensilla carrying S and G cilia are found on the central annulus of each segment. Small sensilla carrying only G cilia are found on all five annuli. In this paper we show a positive correlation between the size of a neural sensillum and the number of S and G cilia it contains. Any one leech contains a range of sizes of neural sensilla, but the average area increases with the weight of the leech. In contrast, the annular sensilla show only a modest increase in size with leech weight.

### Introduction

In both vertebrates (Glucksmann, 1951) and invertebrates (Truman, 1984), during development the final number of cells in the adult nervous system is reduced by cell death. In the ventral horn of the lumbar spinal cord of the frog, as many as 75% of the cells die within 64 days after the hind limbs have emerged (Hughes, 1961). Death of motoneurons in the sphinx moth reduces the number of cells in the adult abdominal ganglia (Truman and Schwartz, 1980). The leech central nervous system is no exception to this process. In *Haemopsis marmorata*, the mean number of cells in each ganglion is reduced, over the first 20 days of development, by selective cell death (Stewart and Macagno, 1984).

Some peripheral sensory systems mature through a similar process of cell deletion. Every mammalian species studied loses 50–90% of its retinal ganglion cells (Finlay

and Pallas, 1989). Cell numbers can, however, also increase during postembryonic development. In fish and amphibia, the eyes and the brain grow continuously throughout the life of the animal. New retinal ganglion cells are supplied with synaptic targets by simultaneous growth of the tectum. In insects, new peripheral sensory structures can be added without new cells being added centrally. All insects studied add new chemoreceptors at each additional molt (Chapman, 1982), and new sensory hairs are added to the cerci of crickets at each instar (Murphy and Chiba, 1990). In the medicinal leech, it is possible to compare the postembryonic development of three sensory systems that transduce stimuli at the skin. These are the contact mechanoreceptors whose cell bodies are located within the ganglia (Nicholls and Baylor, 1968); the chemoreceptors on the lips, which consist of multiciliated cells (Elliott, 1987); and the singly ciliated mechanoreceptors that respond to water motion (Friesen, 1981; Young *et al.*, 1981). Both sets of ciliated receptor cells have cell bodies located within the skin; their cilia are known as G cilia and S cilia, respectively (Philips and Friesen, 1982). S cilia range in length from 3 to 9  $\mu\text{m}$ ; G cilia from 1 to 2  $\mu\text{m}$ . Sensillum 1 has only short S cilia, whereas other sensilla have long whip-like cilia (DeRosa and Friesen, 1981). So far there is no evidence that the multiciliated afferents in the midbody segments are chemoreceptors.

The cell bodies of the ciliated mechanoreceptors are located, in each segment, on 14 discrete neural sensilla (Fig. 1) that appear, under the dissecting microscope, as pale grey patches. Water flow distorts the cilia (Fig. 2a), setting up action potentials that are transmitted to the central nervous system without an intervening synapse (Philips and Friesen, 1982; Gascoigne and McVean, 1991). Each body segment is externally divided into five annuli. The neural sensilla lie on the central, or neural, annulus. The neural sensilla also carry some chemosen-

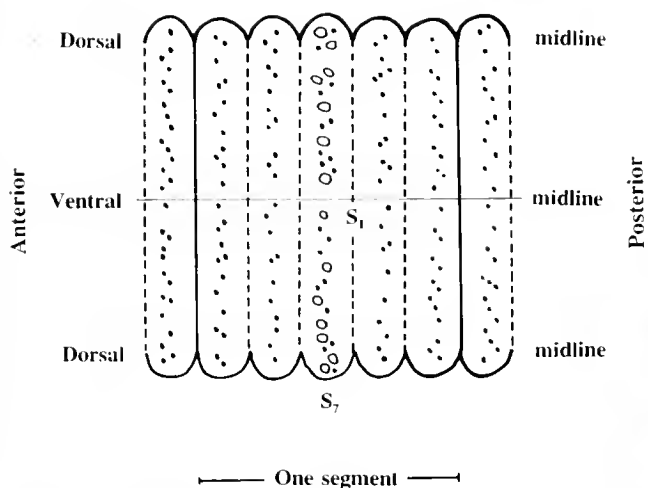


Figure 1. Distribution of neural and annular sensilla on the skin of a typical midbody segment. The skin has been cut along the dorsal midline and pinned flat. There are 14 neural sensilla (clear ellipsoids) on each neural annulus and a variable number of annular sensilla (filled ellipsoids) distributed over all five annuli. The most ventral ( $S_1$ ) and most dorsal ( $S_7$ ) sensilla are labeled.

sory G cilia (DeRosa and Friesen, 1981), but small (annular) sensilla (Fig. 2b) with only G cilia are also found on both the central annulus and the other four annuli of each segment (McVean *et al.*, 1990). Unlike the neural sensilla, the annular sensilla are variable in number and position: they are also more numerous (McVean *et al.*, 1990).

Embryogenesis in *Hirudo medicinalis* is complete after 30 days. Neurogenesis and cell death in the central nervous system are complete after 12 days, after which the number of mechanosensory cells in the segmental ganglia becomes fixed (DeReimer and Macagno, 1989). Yet leeches continue to grow postembryonically; the largest leeches we used in this study were about 230 times heavier than the smallest leeches. These facts raise the following questions. Do S and G cilia-bearing cells maintain their initial density in the skin by postembryonic recruitment of additional sensory cells as the leech grows, or are the numbers of ciliated cells, like those of the centrally located neurons, fixed at 12 days? If, on the other hand, the numbers of ciliated cells in the sensilla change as the leech grows, do the annular and neural sensilla change in the same way?

To answer these questions, we examined the change in diameter of the neural and annular sensilla in juvenile, postjuvenile, and mature adult leeches, having first established that there is a positive correlation between the area of a neural sensillum and the number of cilia in it.

## Materials and Methods

### Animals

Adult *Hirudo medicinalis*, approximately 6 months old, and unfed juveniles, 3 weeks old, were obtained from

Biopharm (UK) Ltd. and maintained in filtered pond water at 12°C.

### SEM preparation

We started with a single batch of 20 three-week-old leeches. Two leeches from this batch were anesthetized by immersion in leech Ringer (Muller *et al.*, 1981) con-

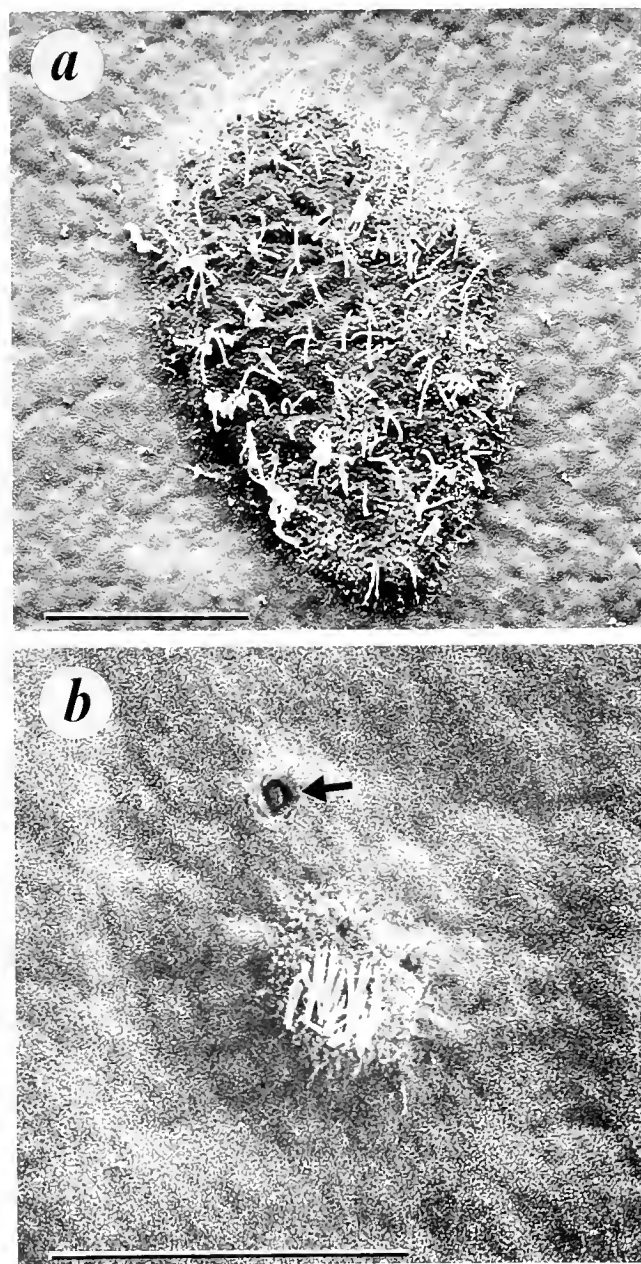
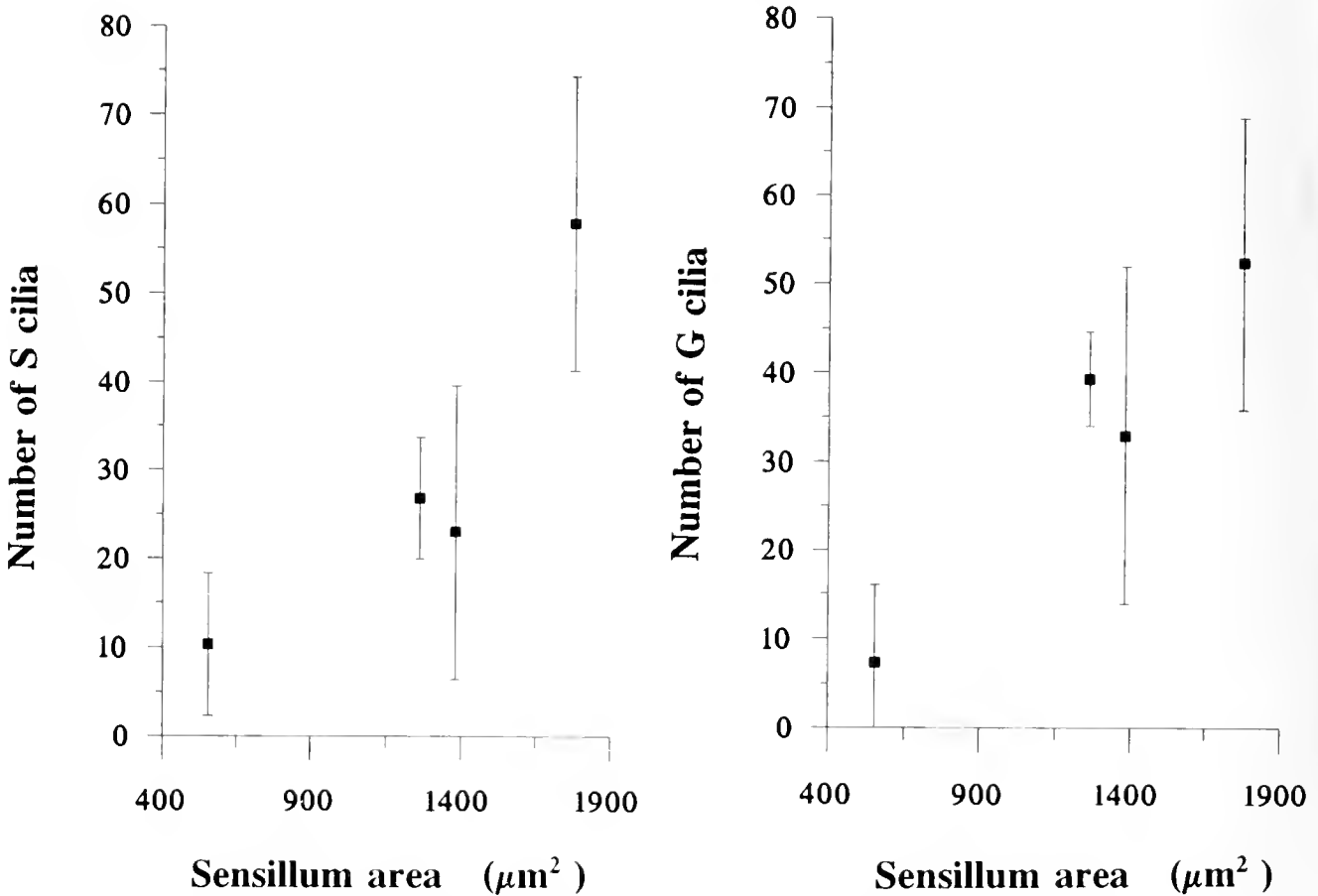


Figure 2. Scanning electron micrograph of a neural (a) and an annular (b) sensillum. Both S and G cilia are present on the neural sensilla, but the annular sensilla carry only G cilia. In the living animal, both neural and annular sensilla are raised above the surface of the skin on circular mounds. The arrow shows a pore, which are often associated with annular sensilla. Scale bars 20  $\mu\text{m}$ .



**Figure 3.** The number of S cilia (left) or G cilia (right) in a sensillum is directly correlated with sensillum size. Data are from four leeches whose weights ranged from 94 to 2600 mg. Each point represents the mean ( $\pm 1$  SD) for 10 neural sensilla from each leech. The sensilla were selected at random.

taining 8% ethanol and then weighed after their body surface was dried. The leeches were spread out, dorsal side uppermost, and pinned onto sheets of dental wax. We used a large number of pins around the perimeter in an effort to stretch the body wall evenly. Mucus was removed by rinsing the surface of the skin in 8% ethanol. Preparations were fixed in 3% glutaraldehyde in 0.1 M Sorensen's phosphate buffer, pH 7.2, for 2 h, dehydrated through a graded series of ethanol, and critical-point dried. Preparations were mounted on stubs, splutter coated with gold palladium, and viewed in a Cambridge S-100 scanning electron microscope. We inspected adjacent midbody segments in the region of the genital openings and measured the diameter of sensilla visible on their ventral surface. When searching for sensilla, we viewed the surface of the skin at a magnification of 750 $\times$  and checked the identity of possible sensilla at higher magnification. Searching started midventrally; the stub was moved one frame at a time, working from the posterior edge of the annulus to the anterior edge, at which point the stub was moved one frame away from the midline and the search continued in the opposite direction.

This procedure was repeated with two more leeches from the original batch at weekly intervals for a further 7 weeks (10th postembryonic week). The remaining leeches were fed, to satiation, in their 11th postembryonic (PE) week. Two of these were examined in their 12th PE week, and the last two leeches were fed a second time in the 13th PE week and their sensilla measured in the 15th PE week.

A further six leeches were prepared for scanning electron microscopy. Two were large adults (4148 and 5454 mg) used to confirm that neural sensilla continue to grow beyond the 15th PE week. The other four leeches (94 and 1430 mg) were used to define the relationship between the area of a sensillum and the number of externally ciliated cells it contains. Adult leeches were prepared by first removing their body contents and then dividing the skin into anterior and posterior halves. Fixation and preparation was then as for juvenile leeches.

### Results

Tissue shrinkage in leech skin due to fixation has been estimated to be 16–29% (DeRosa and Friesen, 1981; El-

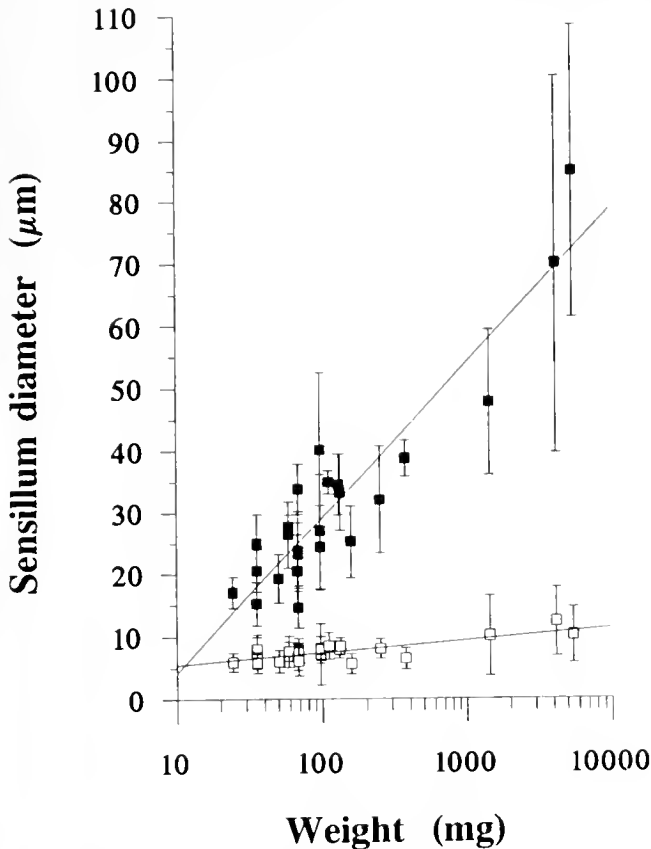


Figure 4. Mean ( $\pm 1$  SD) of neural (■) and annular (□) sensilla on midbody segments of leeches of different weights plotted against log weight of the leech. The size of both neural and annular sensilla is directly correlated with the size of the leech, but the size increase of the annular sensilla over this weight range is small compared with the size increase of the neural sensilla over the same weight range. A line of best fit is drawn through each set of data points.

liott, 1987). Measurements of sensilla dimensions are therefore relative rather than absolute.

#### *Relationship between sensillum area and number of cilia*

We measured the major and minor diameter of 10 annular sensilla and 10–31 neural sensilla in each of four leeches whose weights ranged from 94 to 2600 mg. We counted the number of S and G cilia in the neural sensilla and the number of G cilia in the annular sensilla (G cilia from one cell become clumped together during preparation for scanning electron microscopy, and each clump was counted as one). For the neural sensilla, area was positively correlated with number of both S ( $r^2 = 0.79$ ) and G ( $r^2 = 0.95$ ) cilia (Fig. 3). Annular sensilla varied little in diameter between leeches (Fig. 4). DeRosa and Friesen (1981) found similar numbers of S cilia per sensillum, but our numbers for G cilia are higher than theirs.

#### *Sensillum size in postembryonic to adult leeches*

After demonstrating a positive correlation between the area of a neural sensillum and the number of S and G cilia it contains, we used the diameter of both neural and annular sensilla as an indirect measure of the number of S and G ciliated cells in leeches whose weights spanned a range from immediately postembryonic to large adult. We measured the major diameter of 176 neural sensilla and 712 annular sensilla in 23 leeches weighing from 24 to 5450 mg. Over this weight range, leech weight is positively correlated with the diameter of both neural ( $r^2 = 0.89$ ) and annular ( $r^2 = 0.78$ ) sensilla (Fig. 4). Though significant, the growth of annular sensilla is small. The ratio between the average area of the annular sensilla in the smallest and largest leech was 1:4, and the similar ratio for the neural sensilla was 1:24.

The area of the neural sensilla in any one leech varies and is positively correlated with the number of ciliated cells it contains (Fig. 5).

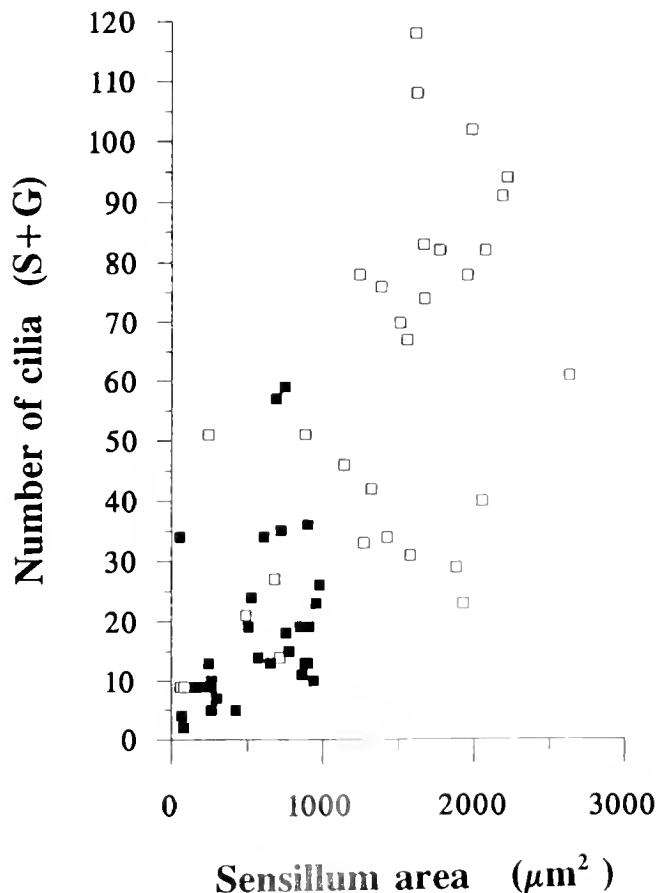


Figure 5. The size of the neural sensilla in any one leech is variable. Here the numbers of S and G cilia are plotted against sensillum area for two leeches of different weights. ■ = 500 mg leech. □ = 2600 mg leech. The sizes of the neural sensilla in these two leeches overlap.

## Discussion

We have shown positive correlations between the area of a neural sensillum and the number of S and G cilia that it contains and between the weight of a leech and the diameter of its neural sensilla. Over the range that we considered, the weight of the leech increased about 230 times, the area of the neural sensilla increased about 24 times, and the area of the annular sensilla increased about 4 times. We conclude that, as leeches grow, the neural sensilla increase in area as more S and G cilia are added.

New G-cilia-bearing cells clearly are recruited into the neural sensilla, so their number is not fixed by the end of embryogenesis. The modest growth in the area of the annular sensilla may be compensated for by the addition of new annular sensilla. Because the skin was invariably coated with patches of mucus, we were unable to assess the number of annular sensilla for any one leech.

The increase in the number of chemoreceptors and mechanoreceptors in insects with successive instars is well documented (Murphey and Chiba, 1990; Chapman, 1982). The total number of olfactory pegs and contact chemoreceptor pegs in the cockroaches *Leucophaea maderae* and *Periplaneta americana* increases dramatically at each instar, but the density of both types of sensory receptors remains constant. Only in the adult male does the density double (Chapman, 1982).

During insect development there is a dynamic relationship between the number of peripheral sensory cells and the structure of the dendritic arbor of the interneuron onto which the sensory cells synapse. When a cercus was removed from embryonic grasshoppers that had completed 60% of their development, the medial giant interneuron developed 30% fewer dendritic branches (Shankland *et al.*, 1982).

Our data suggest that new peripheral sensory cells continue to be added throughout the life of the leech. Because the S-cilia-bearing cells probably synapse directly onto T cells as well as onto first order interneurons (Gascoigne and McVean, 1991), the increase in size of the T cell arbor in larger leeches (DeReimer and Macagno, 1989) may partly reflect increased demands for synaptic space by the peripheral sense organs.

Other authors (Peinado, 1988; Peinado *et al.*, 1990) have shown that new axons are added to peripheral nerves after embryogenesis is complete, surmising that these additions were from sensory structures. We have confirmed that new sensory structures are added to the skin of the leech after embryogenesis and, because these must communicate with the central nervous system via axons, they must contribute to the new axon complement observed by Peinado *et al.* (1990). We have also shown that new sensory structures are added throughout adult life. Although the additions include both S and G ciliated sensory

structures, the pattern of development is different for the cells within annular and neural sensilla.

## Literature Cited

- Chapman, R. F. 1982. Chemoreception: the significance of receptor numbers. Pp. 247-356 in *Advances in Insect Physiology*, Vol. 16, M. J. Berridge, J. E. Treherne, and V. B. Wigglesworth, eds. Academic Press.
- DeReimer, S. A., and E. R. Macagno. 1989. Quantitative studies on the growth of neuronal arbors. Pp. 11-31 in *Perspectives in Neural Systems and Behaviour*, T. J. Carew and D. B. Kelly, eds. Alan R. Liss.
- DeRosa, S. Y., and W. O. Friesen. 1981. Morphology of leech sensilla: observations with a scanning electron microscope. *Biol. Bull.* 160: 383-393.
- Elliott, E. J. 1987. Morphology of chemosensory organs required for feeding in the medicinal leech. *J. Morph.* 192: 181-187.
- Finlay, B. L., and S. L. Pallas. 1989. Control of cell number in the developing mammalian visual system. *Prog. Neurobiol.* 32: 207-234.
- Friesen, W. O. 1981. Physiology of water motion detection in the medicinal leech. *J. Comp. Physiol.* 92: 255-275.
- Gascoigne, L., and A. R. McVean. 1991. Water movement sensitive cells in leech C.N.S. *Phil. Trans. R. Soc. Lond. B* 332: 261-270.
- Gluecksmann, A. 1951. Cell deaths in normal vertebrate ontogeny. *Biol. Rev.* 26: 59-86.
- Hughes, A. F. 1961. Cell degeneration in the larval ventral horn of *Xenopus laevis* (Dandini). *J. Embryol. Exp. Morphol.* 9: 269-284.
- McVean, A. R., L. Gascoigne, and A. Page. 1990. The external structure and distribution of sensilla in the medicinal leech. *Acta Zool.* 71: 161-167.
- Muller, K. J., J. G. Nicholls, and G. S. Stent. 1981. *Neurobiology of the Leech*. Cold Spring Harbour Laboratory.
- Murphey, R. K., and A. Chiba. 1990. Assembly of the cricket cercal sensory system: genetic and epigenetic control. *J. Neurobiol.* 21: 120-137.
- Nicholls, J. G., and D. A. Baylor. 1968. Specific modalities and receptive fields of sensory neurons in C.N.S. of the leech. *J. Neurophysiol.* 31: 740-756.
- Peinado, A. 1988. Axon guidance and fasciculation in the peripheral nervous system of the leech *Hirudo medicinalis*. Ph.D. Thesis, Columbia University.
- Peinado, A., B. Zipser, and E. R. Macagno. 1990. Segregation of afferent projections in the central nervous system of the leech *Hirudo medicinalis*. *J. Comp. Neurol.* 301: 232-242.
- Philips, C. E., and W. O. Friesen. 1982. Ultrastructure of the water-movement-sensitive sensilla in the medicinal leech (*Hirudo medicinalis*). *J. Neurobiol.* 13: 473-486.
- Stewart, R. R., and E. Macagno. 1984. The development of segmental differences in cell number in the CNS of the leech. *Soc. Neurosci. Abstr.* 10: 512.
- Shankland, M., D. Bentley, and C. S. Goodman. 1982. Afferent innervation shapes the dendritic branching pattern of the medial giant interneuron in grasshopper embryos raised in culture. *Dev. Biol.* 92: 507-520.
- Truman, J. W. 1984. Cell death in invertebrate nervous systems. *Ann. Rev. Neurosci.* 7: 171-188.
- Truman, J. W., and L. M. Schwartz. 1980. Peptide hormone regulation of programmed death of neurons and muscle in an insect. In *Peptides. Integrators of Cell and Tissue Functions*. Soc. Gen. Physiol. Series, Vol. 25, F. E. Bloom, ed. Raven Press, New York.
- Young, S. R., R. D. Dedwylder, and W. O. Friesen. 1981. Response of the medicinal leech to water waves. *J. Comp. Physiol. A* 144: 111-116.

# A Comparative Study of Static Bodies in Mysid Crustaceans: Evolutionary Implications of Crystallographic Characteristics

A. P. ARIANI<sup>1</sup>, K. J. WITTMANN<sup>2</sup>, AND E. FRANCO<sup>3</sup>

<sup>1</sup>*Dipartimento di Zoologia, Università di Napoli, Via Mezzocannone 8, I-80134 Napoli, Italia;*

<sup>2</sup>*Institut für Allgemeine Biologie, Universität Wien, Schwarzschanerstrasse 17, A-1090 Vienna,*

*Austria; and* <sup>3</sup>*Dipartimento di Scienze della Terra, Università di Napoli,*

*Via Mezzocannone 8, I-80134 Napoli, Italia*

**Abstract.** We studied the mineral composition of statoliths in 154 species belonging to 55 genera of Mysidae. Fluorite (CaF<sub>2</sub>) was found in 86% of Recent species, vaterite (CaCO<sub>3</sub>) in 9%, and no crystalline component in 5%. Seven samples of fossil statoliths from Upper Miocene deposits were exclusively calcite (CaCO<sub>3</sub>).

Vaterite has the peak of occurrence in fresh water, fluorite in the photic zone of marine waters, and organic statoliths in oceanic deep waters. With respect to population numbers in the different aquatic biota, vaterite prevails in freshwater species and fluorite is dominant among species in all brackish to marine environments.

The occurrence of CaCO<sub>3</sub> in fresh to brackish waters coincides with fossil records and biogeographical observations. The Ponto-Caspian region is the center of abundance for Recent CaCO<sub>3</sub>-precipitating species. The rich brackish to freshwater fauna in this region probably has its roots in the brackish Paratethys, where a rich fossil material of calcareous mysid statoliths is known from Upper Miocene sediments.

Morphological and scarce palaeontological evidence suggests that the earliest (Carboniferous to Jurassic) Mysidacea were mainly oceanic shrimps without statocysts; these were followed by (benthopelagic) animals with non-mineralic organic statoliths. With the colonization of coastal to littoral areas by benthopelagic to benthic forms, mineralic statoliths were formed by precipitation of fluorite. Among the modern Mysidae, a special development occurred (in the Miocene) in the Ponto-Caspian region

where CaCO<sub>3</sub> statoliths appeared in brackish to freshwater forms.

As in vertebrates, the patterns of mineral composition of static bodies in the Mysidae reflect both anatomical and ecophysiological differences.

## Introduction

The hard parts of animals consist of a variety of minerals, some of which occur in static organs (statocysts) as components of the static bodies, statoliths, or otoliths (Lowenstam, 1981). Carlström (1963) first showed that in vertebrates, the mineral composition of otoliths provides evolutionary information: the primitive forms (Agnatha) have phosphatic otoliths, but in the Gnathostomata, all endogenous otoliths consist of calcium carbonate. The form of the latter varies from vaterite in primitive bony fishes (Chondrostei Acipenseroidea) to more stable polymorphs—aragonite in advanced bony fishes and amphibians, both aragonite and calcite in reptiles, and only calcite in birds and mammals. Later investigations (Marmo *et al.*, 1983; Gauldie, 1990) modified only the details of this picture.

By analogy to the investigations on vertebrates, we sought to identify possible evolutionary implications of the mineral composition of statoliths in a group of invertebrates. Unlike most crustaceans, which have exogenous static bodies, mysid shrimps of the family Mysidae have large endogenous statoliths in a pair of statocyst chambers on the base of the tail fan. The statocysts serve as the primary equilibrium organs for these small shrimps, which spend a substantial portion of their lives swimming. Each statocyst chamber contains a single statolith, a

moveable dense body, which transmits gravitational and inertial forces as primary stimuli to attached sensory hairs. Besides controlling body position, the statocysts are also involved in stabilizing the visual perceptive field (Neil, 1975). In addition to gravity, light is important for the control of body position and swimming plane in mysids (Jander, 1962).

Mysid statoliths are of interest because in most species they consist of fluorite ( $\text{CaF}_2$ ), a mineral that rarely occurs in the hard parts of organisms (Bethe, 1895; Lowenstam and McConnell, 1968). It may be of equal interest that certain species possess statoliths made of vaterite (Ariani *et al.*, 1981, 1983), a metastable polymorph of  $\text{CaCO}_3$  that is rare in organisms and almost unknown from geologic systems. Fossil statoliths, however, consist of calcite (Voicu, 1974, 1981), the most common and stable phase of crystalline calcium carbonate.

During the last decade the following picture was obtained on the basis of a relatively modest number of extant species: statoliths composed of fluorite in the majority of marine species; vaterite in some representatives of the tribe Mysini, mainly in brackish to freshwater forms; and non-mineralic material in a few mesopelagic forms (Ariani *et al.*, 1983; Wittmann *et al.*, 1993). These results prompted the present large-scale study of the ecological, biogeographic, and evolutionary implications of crystallographic characteristics in a rich collection of material covering a broad range of taxonomic relationships, environments, and geographical areas.

### Materials and Methods

The mysids were collected during the last two decades by means of plankton or bottom nets in fresh to marine waters around the globe. Materials were either fixed in 70% alcohol or briefly placed in a solution of 4–5% formaldehyde in ambient water, then transferred to 70% alcohol. Materials were examined a few hours to several years after collection. In some cases, especially for euryhaline species, specimens from different natural populations were examined. We studied 179 populations belonging to 154 species and 55 genera of extant mysids and also examined seven samples of fossil statoliths from Upper Miocene deposits of various parts of the Paratethys. Mysid statoliths from these sediments were assigned to the Recent genus *Paramysis* by Voicu (1981) and later transferred to the Miocene genus *Sarmysis* by Maissuradze and Popescu (1987).

Statoliths of extant species were mechanically removed from the endopods of uropods and briefly washed in distilled water. Statolith diameter was calculated as the geometric mean of apparent length and width in ventral view. Body length was measured with a micrometer eyepiece from the tip of the rostrum to the telson. We measured

both body length and diameter from adults of both sexes: 5–20 individuals for most species, or only 1–4 specimens for very rare species. From the sediment samples we measured 5–10 fossil statoliths at each location.

In 96 extant species and 7 fossil samples, the mineral composition of crystalline components was determined by x-ray diffraction analysis on whole statoliths. The standard grinding of the samples to powder was not necessary because all crystalline statoliths gave clear diffraction patterns due to spherulitic microcrystal arrangement visible by transmitted light. Statoliths were glued with collodion to the tip of glass fibers. In the case of very small statoliths, up to four of them were put together on the same fiber. Diffraction patterns were recorded with a 114.6-mm Debye-Scherrer camera using Ni-filtered  $\text{Cu-K}\alpha$  radiation; working conditions: 40 kV, 30 mA, recording time 8–12 h. Diffractions that gave no lines were repeated with 24-h exposure.

In 102 species, a less expensive and faster method of mineral determination was used, as proposed by Wittmann *et al.* (1993). This method, which we call WSA, uses  $\text{CH}_3\text{COOH}$  treatment and inspection of crystal aggregates with polarization, scanning microscopy, or both, to identify statoliths by means of their chemical and physical characteristics. The four known types of statolith composition are distinguished without error, but new types may not always be detected or may not be well identified. From two to five statoliths of each species were examined. In 44 species both methods (X + WSA) were used and gave identical results.

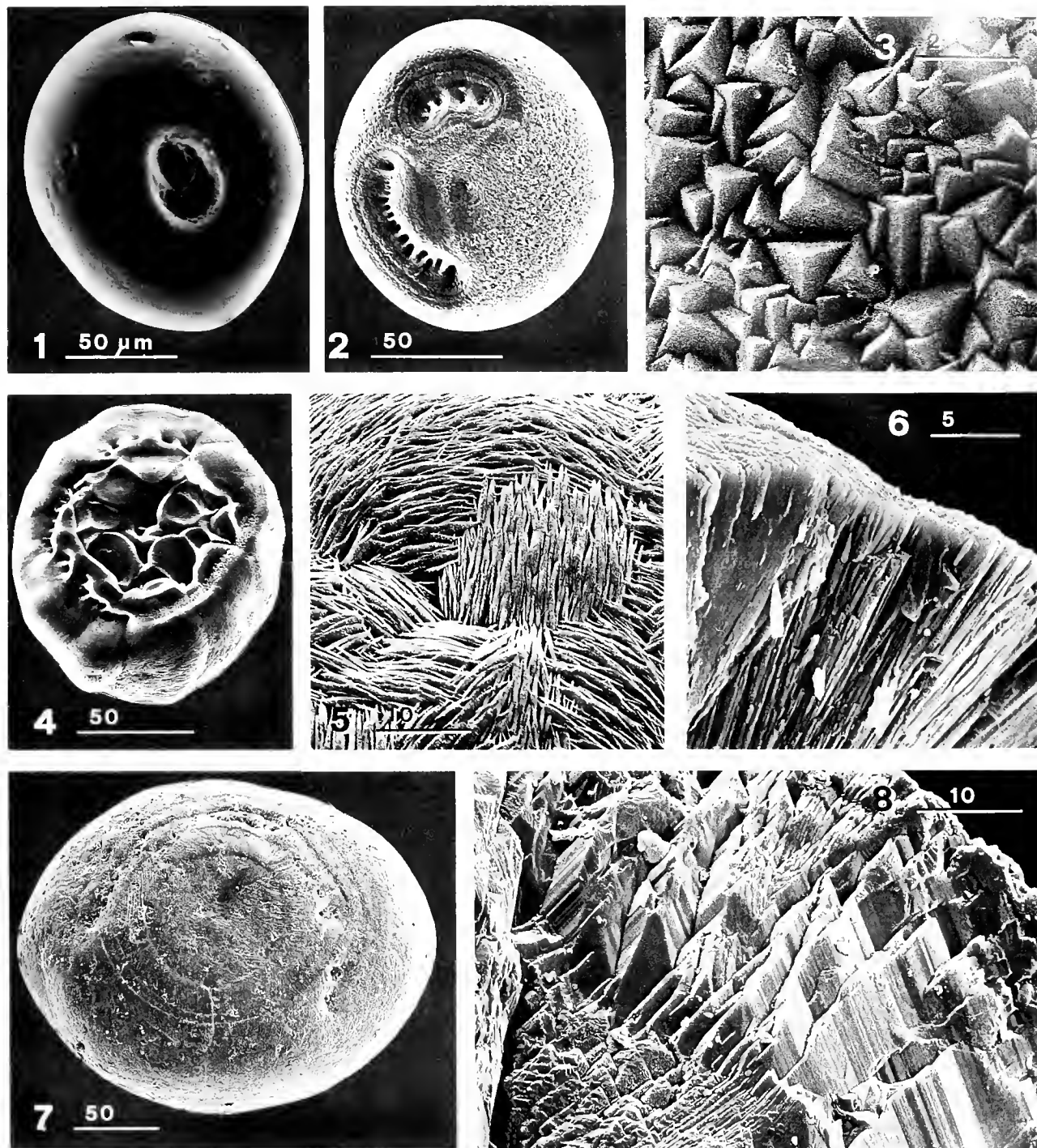
Micrographs were obtained with a Cambridge Stereoscan scanning electron microscope (SEM) or with a JEOL SEM 35CF on parts or entire statoliths coated with gold. For qualitative SEM microanalysis, statoliths were briefly washed in distilled water twice and then air dried and carbon coated. Statoliths of 2–6 individuals in 10 species were analyzed with a LINK AN 10000 system. Elements with an order number  $\geq 9$  were recorded.

### Results

The types of statoliths we identified were noncrystalline (organic) (Fig. 1), fluorite (Figs. 2, 3), vaterite (Figs. 4–6), and calcite (Figs. 7, 8). Eighty-six percent of Recent statoliths were mineralized with fluorite and only 9% with vaterite; 5% had no crystalline component (Table I). All fossil statoliths consisted of calcite (Table II).

Some statoliths gave no diffraction patterns—these showed elastic consistency and shrinkage due to desiccation. When observed in the animal, they resembled the spherical organic matrix that appears during the first stage of statolith formation (Ariani *et al.*, 1982). Fluorite showed its typical cubic habit (Fig. 3) at the statolith surface. Vaterite usually appeared as a patchwork of scales, needles,





Figures 1-8. Mineral types of statoliths of Recent and fossil Mysidae: scanning electron micrographs of entire statoliths in ventral to ventrolateral view

Figure 1. Noncrystalline statolith of *Borcomysis megalops*, center malformed due to desiccation

Figure 2. Fluorite statolith of *Paramysis arenosa*

Figure 3. *P. arenosa*, cubic habit of fluorite on ventral surface.

Figure 4. Vaterite statolith of *Paramysis helleri*

Figure 5. *P. helleri*, aggregates of vaterite on dorsal surface.

Figure 6. *P. helleri*, lamellar habit of vaterite on fracture surface.

Figure 7. Fossil statolith from Upper Miocene sediments in the Oas Basin.

Figure 8. Fossil statolith, crystal habit of calcite on fracture surface.

Table 1

Crystalline components of statoliths in Recent Mysidae

Species	Locality, remarks	Salinity ‰	Depth (m)	Body length <sup>1</sup> (mm)	Statol. diam. <sup>1</sup> (µm)	Method <sup>2</sup>	Crystall. component
Subfam. Boreomysinae							
<i>Boreomysis arctica</i> (Kroyer)	Korsfjorden, Norway	35	200	21	170	X + WSA	None
<i>Boreomysis brucei</i> W. Tattersall	Weddell Sea, Antarctic	35	980-990	35	110	WSA	None
<i>Boreomysis megalops</i> Sars	Tyrrhenian Sea, off Sardinia	36	330-400	11	160	X + WSA	None
	Hjeltefjord, Norway	35	260	13	150	X-ray	None
<i>Boreomysis microps</i> Sars	Biscay Depth, NE-Atlantic	35	500-1000	14	120	X + WSA	None
<i>Boreomysis sphaerops</i> Li	N-Pacific, off Japan	35	≤850	22	200	WSA	None
<i>Boreomysis tridens</i> Sars	Norway, continental shelf	35	520	26	130	X-ray	None
Subfam. Siriellinae							
<i>Siriella acquiremis</i> Hansen	N-Pacific, off Christmas Island	35	Surface	8	310	X-ray	Fluorite
<i>Siriella anomala</i> Hansen	Batbatan, Philippines	35	10	10	290	X-ray	Fluorite
<i>Siriella armata</i> (M.-Edw.)	Gulf of Trieste, Adriatic	32-36	0-1	15	240	X + WSA	Fluorite
<i>Siriella brevicaudata</i> Paulson	Gulf of Aqaba, Red Sea	42	1-2	5	90	WSA	Fluorite
<i>Siriella castellabatensis</i> Ariani & Spagnuolo	Gulf of Salerno, Tyrrhenian Sea	38	<30	7	130	X-ray	Fluorite
<i>Siriella clausi</i> Sars	Gulf of Salerno, Tyrrhenian Sea	38	<30	6	150	X-ray	Fluorite
	Lake Faro, Sicily	33	<5	5	120	X-ray	Fluorite
<i>Siriella gracilis</i> Dana	Gulf of Aden, NE-Indian Ocean	36	Surface	5	130	WSA	Fluorite
	N-Pacific, off Philippines	34-35	Surface	5	130	WSA	Fluorite
<i>Siriella inornata</i> Hansen	Philippines, Batbatan	33-34	Coastal	11	190	WSA	Fluorite
<i>Siriella jaltensis gracilipes</i> Nouvel	Gulf of Salerno, Tyrrhenian Sea	38	<60	9	190	X + WSA	Fluorite
<i>Siriella longipes</i> Nakazawa	Kominato, Japan	33-35	20	14	250	X + WSA	Fluorite
<i>Siriella norvegica</i> Sars	Istria, N-Adriatic Sea	36	1	8	160	WSA	Fluorite
<i>Siriella pacifica</i> Holmes	Aqua Verde Bay, Gulf of California	35	10	10	230	X-ray	Fluorite
<i>Siriella roosevelti</i> W. Tattersall	Charles I., Galapagos Islands	35	10	7	170	WSA	Fluorite
<i>Siriella thompsoni</i> M.-Edw.	Gulf of Aden, NE-Indian Ocean	36	Surface	9	260	WSA	Fluorite
	Argentinian Basin, S-Atlantic	35	Surface	10	190	WSA	Fluorite
	N-Pacific, off Philippines	34-35	Surface	7	190	X-ray	Fluorite
<i>Siriella trispina</i> Li	East China Sea	33-35	Surface	10	190	WSA	Fluorite
<i>Siriella vulgaris rostrata</i> W. Tattersall	Philippines, Batbatan	33-34	Surface	7	170	WSA	Fluorite
Subfam. Rhopalophthalminae							
<i>Rhopalophthalmus terrantalisis</i> O. Tattersall	Algoa Bay, South Africa	10-34	0-6	14	200	X + WSA	None
Subfam. Gastrosaccinae							
<i>Anchialina agilis</i> (Sars)	Gulf of Salerno, Tyrrhenian Sea	38	20	6	70	X-ray	Fluorite
<i>Anchialina oculata</i> Hoenigman	Gulf of Salerno, Tyrrhenian Sea	38	<60	5	60	WSA	Fluorite
<i>Gastrosaccus mediterraneus</i> Bacescu	Adriatic, near Brindisi, littoral	38	0	7	80	X + WSA	Fluorite
<i>Gastrosaccus roscoffensis</i> Bacescu	English Channel, near Roscoff	35	<20	8	80	X-ray	Fluorite
<i>Gastrosaccus sanctus sanctus</i> (van Beneden)	Gulf of Salerno, Tyrrhenian Sea	32-38	2-16	8	70	X + WSA	Fluorite
<i>Gastrosaccus sanctus widhalmi</i> Bacescu	Black Sea, Romania	17	2	10	90	WSA	Fluorite
<i>Gastrosaccus spinifer</i> (Goes)	German Bight, North Sea	34-35	50-60	14	90	WSA	Fluorite
<i>Haplostylus bacescui</i> Hatzakis	Gulf of Salerno, Tyrrhenian Sea	38	12-19	8	130	X + WSA	Fluorite

Table I (Continued)

Species	Locality, remarks	Salinity ‰	Depth (m)	Body length <sup>1</sup> (mm)	Statol. diam. <sup>1</sup> ( $\mu$ m)	Method <sup>2</sup>	Crystall. component
Subfam. Gastrosaccinae							
(Continued)							
<i>Haplostylus lobatus</i> (Nouvel)	Gulf of Salerno, Tyrrhenian Sea	38	30-40	8	120	X + WSA	Fluorite
<i>Haplostylus magnilobatus</i> (Bacescu & Schiceke)	Gulf of Naples, Tyrrhenian Sea	36	35-40	8	100	X-ray	Fluorite
<i>Haplostylus normani</i> (Sars)	Gulf of Salerno, Tyrrhenian Sea	38	12-20	7	130	WSA	Fluorite
Subfam. Mysinae, tribe							
Erythropini							
<i>Imblyops abbreviata</i> (Sars)	Hjeltefjord, Norway	35	260	11	230	X + WSA	Fluorite
<i>Imblyops antarctica</i> O. Tattersall	Weddell Sea, Antarctic	35	470	14	200	WSA	Fluorite
<i>Imblyops tattersalli</i> Zimmer	Weddell Sea, Antarctic	35	520	25	360	WSA	Fluorite
<i>Caesaromysis hispida</i> Ortmann	N-Pacific, off Japan	34	$\leq$ 1060	9	110	X-ray	Fluorite
<i>Dactylamblyops hodgsoni</i> Holt & Tattersall	Weddell Sea, Antarctica	35	400-600	21	300	X + WSA	Fluorite
<i>Dactylamblyops iii</i> Nouvel & Lagardere	N-Pacific, off Japan	34	$\leq$ 1300	9	230	X-ray	Fluorite
<i>Dactylamblyops murrayi</i> W. Tattersall	N-Pacific, off Japan	34	$\leq$ 480	12	230	X-ray	Fluorite
<i>Erythroops elegans</i> (Sars)	Gulf of Salerno, Tyrrhenian Sea	38	16	3	120	X + WSA	Fluorite
<i>Erythroops microps</i> (Sars)	Rockall Trough Area, N-Atlantic	35	700	7	170	X-ray	Fluorite
<i>Erythroops neapolitana</i> Colosi	Adriatic, Dalmatia	38	200	5	130	X-ray	Fluorite
<i>Erythroops serrata</i> (Sars)	Hjeltefjord, Norway	35	260	9	180	X-ray	Fluorite
<i>Euchaetomera</i> <i>glyphidophthalmica</i> Illig	N-Pacific, off Japan	35	$\leq$ 1050	5	210	X-ray	Fluorite
<i>Euchaetomera tenuis</i> Sars	N-Pacific, off Japan	35	$\leq$ 1250	9	240	WSA	Fluorite
<i>Euchaetomera typica</i> Sars	N-Pacific, off Japan	35	$\leq$ 950	7	180	X-ray	Fluorite
<i>Euchaetomera zurstrasseni</i> (Illig)	Weddell Sea, Antarctica	35	140-300	8	210	WSA	Fluorite
<i>Holmestella affinis</i> Li	Honshu, Japan	34-35	72	11	300	X-ray	Fluorite
<i>Illigiella brevisquamosa</i> (Illig)	Honshu, Japan	33-34	280	8	160	X-ray	Fluorite
<i>Katerythroops oceanae</i> Holt & Tattersall	N-Pacific, off Japan	34-35	$\leq$ 680	8	90	X-ray	Fluorite
<i>Meterythroops microphthalma</i> W. Tattersall	Sea of Japan	34	570-730	18	340	X + WSA	Fluorite
<i>Meterythroops picta</i> Holt & Tattersall	Rockall Trough Area, N-Atlantic	35	1500-2000	12	150	X-ray	Fluorite
<i>Paramblyops brevirostris</i> O. Tattersall	N-Pacific, off Japan	34	$\leq$ 1300	13	140	X-ray	Fluorite
<i>Pseudamblyops conicops</i> Li	Weddell Sea, Antarctic	35	350-380	15	280	WSA	Fluorite
<i>Pseudomma affine</i> Sars	N-Pacific, off Japan	34	$\leq$ 1300	11	110	X-ray	Fluorite
<i>Pseudomma armatum</i> Hansen	Hjeltefjord, Norway	35	260	8	130	X + WSA	Fluorite
<i>Pseudomma belgicae</i> (Hansen) [in Holt & Tatt.]	Weddell Sea, Antarctic	35	250	21	290	WSA	Fluorite
<i>Pseudomma japonicum</i> Murano	Weddell Sea, Antarctic	35	240	9	220	WSA	Fluorite
<i>Pseudomma latiphthalmum</i> Murano	Honshu, Japan	33-35	72	4	90	X-ray	Fluorite
<i>Pseudomma roseum</i> Sars	Honshu, Japan	33-35	280	6	90	X-ray	Fluorite
<i>Feraterthroops robusta</i> (Birstein & Tchindonova)	Honshu, Japan	33-35	280	6	90	X-ray	Fluorite
<i>Pseudomma roseum</i> Sars	Fensfjord, Norway	35	460	14	190	X-ray	Fluorite
<i>Feraterthroops robusta</i> (Birstein & Tchindonova)	N-Pacific, off Japan	34	$\leq$ 1440	5	100	WSA	Fluorite
Subfam. Mysinae, tribe							
Leptomysini							
<i>Intichthomysis notudana</i> Fenton	Beach near Hobart, SE-Tasmania	35	Coastal	9	240	WSA	Fluorite

Table 1 (Continued)

Species	Locality, remarks	Salinity ‰	Depth (m)	Body length <sup>1</sup> (mm)	Statol. diam. <sup>1</sup> (µm)	Method <sup>2</sup>	Crystall. component
Subfam. Mysinae, tribe							
Leptomysini (Continued)							
<i>Leptomysis buergii</i> Bacescu	Gulf of Taranto, Ionian Sea	38	5	8	230	X + WSA	Fluorite
<i>Leptomysis gracilis</i> (Sars)	Gulf of Biscay, NE-Atlantic	35	90	9	190	WSA	Fluorite
<i>Leptomysis heterophyla</i> Wittmann	Istria, N-Adriatic Sea	34-37	17	8	190	WSA	Fluorite
<i>Leptomysis linguva adriatica</i> Wittmann	Gulf of Taranto, Ionian Sea	38	2	6	180	X + WSA	Fluorite
<i>Leptomysis linguva marioni</i> (Gourret)	Gulf of Naples, Tyrrhenian Sea	35-37	8-12	7	190	WSA	Fluorite
<i>Leptomysis mediterranea atlantica</i> Wittmann	Gulf of Biscay, NE-Atlantic	35	<10	11	240	WSA	Fluorite
<i>Leptomysis mediterranea mediterranea</i> Sars	Gulf of Salerno, Tyrrhenian Sea	28-36	2-4	9	270	WSA	Fluorite
<i>Leptomysis megalops</i> Zimmer	Gulf of Biscay, NE-Atlantic	35	180	9	220	X-ray	Fluorite
<i>Leptomysis posidoniae</i> Wittmann	Gulf of Naples, Tyrrhenian Sea	35-37	12	7	180	X + WSA	Fluorite
<i>Leptomysis truncata sardica</i> (Sars)	Gulf of Naples, Tyrrhenian Sea	35-37	1-2	9	230	WSA	Fluorite
<i>Leptomysis truncata truncata</i> (Heller)	Gulf of Trieste, N-Adriatic Sea	32-36	0-1	8	230	WSA	Fluorite
<i>Metamysidopsis swifti</i> Bacescu	Tampa Bay, Florida	35	20	6	110	X-ray	Fluorite
<i>Mysidetes insignis</i> (Sars)	Hjeltefjord, Norway	35	260	16	270	X-ray	Fluorite
<i>Mysidetes parva</i> Zimmer	Adriatic, near Ancona	37	225	9	230	X-ray	Fluorite
<i>Mysidetes posthon</i> Holt & Tattersall	Weddell Sea, Antarctic	35	400-500	28	340	WSA	Fluorite
<i>Mysidopsis acuta</i> Hansen	S-Atlantic, off Falkland Islands	34	≤150	10	260	WSA	Fluorite
<i>Mysidopsis almyra</i> Bowman	Everglades, Florida	10	1	7	160	WSA	Fluorite
<i>Mysidopsis bahia</i> Molenok	Lab. tanks, from Gulf of Mexico	30	Coastal	7	110	X-ray	Fluorite
<i>Mysidopsis bigelowi</i> W. Tattersall	NW-Atlantic, off North Carolina	32	23	6	190	WSA	Fluorite
<i>Mysidopsis gibbosa</i> Sars	Gulf of Trieste, Adriatic	36	22	3	120	X + WSA	Fluorite
<i>Notomysis australiensis</i> (W. Tattersall)	St. Vincent Gulf, South Australia	35	9-11	10	310	X-ray	Fluorite
<i>Paraleptomysis hanyulensis</i> (Bacescu)	Gulf of Salerno, Tyrrhenian Sea	38	16	7	230	X + WSA	Fluorite
<i>Paraleptomysis dimorpha</i> Wittmann	Cape Lopez area, Gabon, W-Africa	34	60-70	7	160	WSA	Fluorite
<i>Prionomysis</i> sp.	Storm Bay, Hope Beach, SE-Tasmania	35	Coastal	9	310	X-ray	Fluorite
<i>Pseudomysis dactylops</i> W. Tattersall	Honshu, Japan	33-35	275	13	200	X + WSA	Fluorite
<i>Pyroleptomysis rubra</i> Wittmann	Gulf of Eilat, Red Sea	42	Coastal	5	150	WSA	Fluorite
<i>Tenagomysis tasmaniae</i> Fenton	Gulf of Trieste, Adriatic Derwent River, SE-Tasmania	34-37 35	6 Coastal	7 9	200 230	X-ray WSA	Fluorite Fluorite
Subfam. Mysinae, tribe Mysini							
<i>Acanthomysis dybowskii</i> li	Bering Sea	33	37	22	450	WSA	Fluorite
<i>Acanthomysis japonica</i> (Marukawa)	Kominato, Japan	30-34	Coastal	11	290	WSA	Fluorite
<i>Acanthomysis longicornis</i> (M.-Edw.)	Gulf of Trieste, Adriatic	36	10-28	5	120	X + WSA	Fluorite
<i>Acanthomysis macropsis</i> (W. Tattersall)	San Francisco Bay	34	9	11	200	WSA	Fluorite
<i>Acanthomysis mitsukurii</i> li	Tateyama Bay, Japan	30-34	20	9	180	X-ray	Fluorite
<i>Acanthomysis nakazatoii</i> li	Tateyama Bay, Japan	30-34	20	14	240	X-ray	Fluorite

Table 1 (Continued)

Species	Locality, remarks	Salinity ‰	Depth (m)	Body length <sup>1</sup> (mm)	Statol. diam. <sup>1</sup> (µm)	Method <sup>2</sup>	Crystall. component
Subfam. Mysinae, tribe Mysini							
<i>(Continued)</i>							
<i>Acanthomysis tamarai</i> It	Tateyama Bay, Japan	30–34	Coastal	11	270	WSA	Fluorite
<i>Anisomysis tjamai</i> Nakazawa	Heta, Japan	30–34	Surface	7	120	WSA	Fluorite
<i>Anisomysis mansrubri</i> Bacescu	Gulf of Aqaba, Red Sea	42	0–3	5	100	WSA	Fluorite
<i>Anisomysis</i> sp.	N-Red Sea, near Sharm el Sheikh	42	1–2	3	60	WSA	Fluorite
<i>Antarctomysis maxima</i> (Hansen) [in Holt & Tatt.]	Weddell Sea, Antarctic	35	300–490	60	690	X + WSA	Fluorite
<i>Antarctomysis ohluni</i> Hansen	Weddell Sea, Antarctic	35	≤850	64	560	X + WSA	Fluorite
<i>Antromysis cenotensis</i> Creaser	Cave of Tzab-Nah, Yucatan, Mexico	0	1	3	60	X-ray	Vaterite
<i>Diamysis bahirensis</i> (Sars)	Lake of Tunis	38	1	4	130	X-ray	Vaterite
	Gulf of Naples, Tyrrhenian Sea	37	20	5	120	X + WSA	Vaterite
	Piccolo river, Apulia, S-Italy	11–13	1	7	140	X + WSA	Vaterite
	San Pietro river, Apulia, S-Italy	3–5	1	7	140	X-ray	Vaterite
	Lake Deransko, Bosnia- Hercegovina	0	0–1	7	160	X-ray	Vaterite
<i>Diamysis pengoi</i> (Czerniavsky)	Danube Delta, Romania	0	3	9	180	X-ray	Fluorite
<i>Hemimysis abyssicola</i> Sars	Hjeltefjord, Norway	35	260	11	170	X-ray	Fluorite
<i>Hemimysis anomala</i> Sars	Northern Baltic Sea, Finland	<7	Lower litt.	7	160	WSA	Vaterite
<i>Hemimysis lamornae</i> <i>lamornae</i> (Couch)	Norway, Kristineberg	35	15	5	110	WSA	Fluorite
<i>Hemimysis lamornae</i> <i>mediterranea</i> Bacescu	Gulf of Naples, Tyrrhenian Sea	37	1–3	6	130	X + WSA	Fluorite
<i>Hemimysis speluncola</i> Ledoyer	N-Adriatic, near Rovinj	37	2	7	130	X-ray	Fluorite
<i>Holmesimysis costata</i> (Holmes)	Monterey Bay, California	35	20	10	170	X-ray	Fluorite
<i>Idiomysis tsumamali</i> Bacescu	Gulf of Eilat, Red Sea	38	30	3	110	X-ray	Fluorite
<i>Kanommatomysis schieckei</i> Bacescu	N-Red Sea, near Sharm el Sheikh	42	1–2	3	120	WSA	Fluorite
<i>Katamysis warpachowskyi</i> Sars	Danube Delta, Romania	0	3	8	100	X-ray	Vaterite
<i>Limnomysis benedeni</i> Czerniavsky	Lake Sinoe, Danube Delta	2	0–1	10	160	WSA	Vaterite
	Danube in Vienna	0	0–1	9	150	X + WSA	Vaterite
<i>Mesopodopsis aegyptia</i> Wittmann	Island of Lesbos, Aegean Sea	39	3	6	170	WSA	Fluorite
<i>Mesopodopsis orientalis</i> (W. Tattersall)	Banica, Philippines	7	Surface	7	180	WSA	Fluorite
<i>Mesopodopsis slabberi</i> (van Beneden)	Lake of Tunis	38–40	1	9	160	X-ray	Fluorite
	Gulf of Taranto, Ionian Sea	35	1	9	120	WSA	Fluorite
	Penzé Estuary, English Channel	4–17	<1	11	190	WSA	Fluorite
	Costinesti, Black Sea	13	2	11	190	WSA	Fluorite
	Lake Sinoe, Danube Delta	2	0–1	10	170	X-ray	Fluorite
<i>Mesopodopsis wooldridget</i> Wittmann	Algoa Bay, South Africa	10–34	3	10	170	X + WSA	Fluorite
<i>Mysidium columbiae</i> (Zimmer)	Stann Creek District, Belize	35	1	6	130	WSA	Fluorite
<i>Mysidium integrum</i> W. Tattersall	English Harbour, Antigua, W-Indies	35	2	6	130	X + WSA	Fluorite
<i>Mysis litoralis</i> (Banner)	Arctic Ocean, off P. Barrow, Alaska	35	20	12	170	WSA	Fluorite
<i>Mysis mixta</i> Lilljeborg	Massachusetts Bay	10	1	13	280	X-ray	Fluorite
<i>Mysis relicta</i> Lovén	Lake near Drottningholm, Sweden	0	20	12	180	X + WSA	Fluorite
	Green Lake, Wisconsin	0	55–120	18	220	X-ray	Fluorite

Table 1 (Continued)

Species	Locality, remarks	Salinity ‰	Depth (m)	Body length <sup>1</sup> (mm)	Statol. diam. <sup>1</sup> (µm)	Method <sup>2</sup>	Crystall. component
Subfam. Mysinae, tribe Mysini							
(Continued)							
<i>Neomysis americana</i> (Smith)	Oregon Inlet, North Carolina	32–34	Coastal	8	200	WSA	Fluorite
<i>Neomysis integer</i> (Leach)	Baltic Sea, Askö I., Sweden	7	0–1	11	220	X + WSA	Fluorite
<i>Neomysis japonica</i> Nakazawa	Tokyo Bay	<15	1	13	190	X-ray	Fluorite
<i>Neomysis mercedis</i> Holmes	San Francisco Bay	35	10–14	11	200	WSA	Fluorite
<i>Neomysis rayii</i> (Murdoch)	San Francisco Bay	34	9	28	380	WSA	Fluorite
<i>Paramesopodopsis rufa</i> Fenton	Derwent River, SE-Tasmania	35	Coastal	10	210	X-ray	Fluorite
<i>Paramysis arenosa</i> (Sars)	Gulf of Salerno, Tyrrhenian Sea	38	4–16	6	140	X + WSA	Fluorite
	Firth of Lorne, Scottish Sea	32–35	0–1	7	130	X-ray	Fluorite
<i>Paramysis bacscoti</i> Labat	Guernsey, Channel Islands	35	10	7	180	X-ray	Vaterite
<i>Paramysis helleri</i> (Sars)	S-Adriatic, near Brindisi	38	1	7	140	X + WSA	Vaterite
	Small creek near Split, Dalmatia	0	<1	9	150	WSA	Vaterite
<i>Paramysis intermedia</i> (Czerniavsky)	Danube Delta, Romania	0	0–1	11	140	X + WSA	Vaterite
<i>Paramysis kessleri sarsi</i> (Derjavin)	Danube Delta, Romania	0	0–1	5	140	X-ray	Vaterite
<i>Paramysis kroeyeri</i> (Czerniavsky)	Lake Uluabat, NW-Turkey	0	0–1	9	140	X-ray	Vaterite
<i>Paramysis lacustris tanattica</i> (Martinov)	Danube Delta, Romania	0	3	14	160	X + WSA	Vaterite
<i>Paramysis noveli</i> Labat	Small river, Roscoff, Eng. Channel	5–33	0	9	180	X-ray	Vaterite
<i>Paramysis pontica</i> Bacescu	Altintas Bay, Marmara Sea	19	35	8	180	X-ray	Vaterite
<i>Praunus flexuosus</i> (Müller)	Roscoff, English Channel	26–35	0	18	180	X + WSA	Fluorite
<i>Praunus inermis</i> (Rathke)	Firth of Lorne, Scottish Sea	32–35	1–5	11	180	WSA	Fluorite
<i>Praunus neglectus</i> (Sars)	Roscoff, English Channel	26–35	1	19	320	WSA	Fluorite
<i>Proneomysis perminuta</i> Li	Tateyama Bay, Japan	33–35	Coastal	7	210	WSA	Fluorite
<i>Proneomysis toriumi</i> Murano	Tateyama Bay, Japan	33–35	Coastal	9	180	WSA	Fluorite
<i>Schistomysis assimilis</i> (Sars)	Gulf of Salerno, Tyrrhenian Sea	24–37	2–6	9	290	X + WSA	Vaterite
	Lagoon near Caorle, Gulf of Venice	11	0	9	230	WSA	Vaterite
<i>Schistomysis kervillei</i> (Sars)	North Sea, German coast	35	<50	13	240	WSA	Fluorite
<i>Schistomysis ornata</i> (Sars)	Gulf of Biscay, NE-Atlantic	35	<100	12	280	X-ray	Fluorite
<i>Schistomysis spiritus</i> (Norman)	English Channel, near Roscoff	35	10	12	210	X + WSA	Fluorite
<i>Taphromysis bowman</i> Bacescu	Wakulla, Florida	10	1	8	120	WSA	Fluorite
<i>Taphromysis louisianae</i> Banner	Blackwater River, Florida	1	<2	9	120	WSA	Fluorite
<i>Tasmanomysis oculata</i> Fenton	Catamaran River, SE-Tasmania	35	Coastal	11	200	WSA	Fluorite
<i>Troglomysis vjetrenicensis</i> Stammer	Cave of Vjetrenica, Hercegovina	0	0–1	13	150	X-ray	Fluorite
Subfam. Mysinae, tribe Heteromysini							
<i>Heteromysis formosa</i> Smith	Narragansett Bay, Rhode Island	32	Coastal	6	130	X + WSA	Fluorite
<i>Heteromysis mayana</i> Brattegard	Coral reef aquarium, Smith, Inst.	35	Coastal	4	90	X-ray	Fluorite
<i>Heteromysis microps</i> (Sars)	Gulf of Naples, Tyrrhenian Sea	35–37	3	6	110	WSA	Fluorite
<i>Heteromysis</i> sp.	Weddell Sea, Antarctic	35	210–250	17	140	WSA	Fluorite
Subfam. Mysidellinae							
<i>Mysidella typica</i> Sars	Hjeltefjord, Norway	35	260	6	100	X + WSA	Fluorite
<i>Mysidella</i> sp.	Weddell Sea, Antarctic	35	280	7	70	WSA	Fluorite

<sup>1</sup> Values are the means of statoliths from either 5–20 or (for very rare species) 1–4 adult male and female specimens.<sup>2</sup> X-ray = X-ray diffraction; WSA = the WSA method (Wittmann *et al.*, 1993); X + WSA = both methods.

Table II

Crystalline components of statoliths of Mysidae Mysini from Miocene (Upper Volhynian to Lower Bessarabian) sediments of the brackish Paratethys

Location	Diameter <sup>1</sup> ( $\mu\text{m}$ )	Method <sup>2</sup>	Crystalline component
Carpathian Foredeep, Machów, Poland	190	X-ray	Calcite
Carpathian Foredeep, Berca, Romania	200	X-ray	Calcite
Carpathian Foredeep, Dacic Basin, Romania	220	X-ray	Calcite
Oas Basin, Transylvania, Romania	230	X-ray	Calcite
Transylvanian Basin, Ocna Mures, Romania	190	X + WSA	Calcite
Eastern Caucasian Foredeep, Tul'skaya, former USSR	180	X + WSA	Calcite
Kerch Peninsula, Kop- Takyl, former USSR	210	X + WSA	Calcite

<sup>1</sup> Values are the means of 5–10 statoliths.

<sup>2</sup> X-ray = X-ray diffraction; X + WSA = both X-ray diffraction and the WSA method (Wittmann *et al.*, 1993).

or lens-like aggregates (Fig. 5), but occasionally occurred as nodules. Fractures of both fluorite and vaterite statoliths showed scales in a spherulitic arrangement (Fig. 6). Fractures and, less frequently, surfaces of fossil statoliths showed characteristic calcite crystal forms (Fig. 8).

In noncrystalline (*Rhopalophthalmus terranatalis*), fluorite (*Leptomysis lingvura adriatica*, *Mesopodopsis slabberi*, *Neomysis integer*), and vaterite (*Diamysis bahirensis*, *Limnomysis benedeni*) statoliths, no difference in mineral composition was found between freshly caught individuals and conspecific material that had been stored for several years.

Noncrystalline statoliths appeared to be confined to the subfamilies Boreomysinae and Rhopalophthalminae. Fluorite statoliths were characteristic of Siriellinae, Gastrosaccinae, Mysidellinae, and most Mysinae. Vaterite statoliths were restricted to certain representatives of the tribe Mysini (Mysinae). In *Diamysis*, *Paramysis* (Figs. 2–6), *Schistomysis*, and *Hemimysis*, congeneric species showed either fluorite or vaterite.

In spite of the large interspecific variability, no intraspecific variations in mineral type were found (Table I). This was true for extremely euryhaline species (*Paramysis helleri*, *Diamysis bahirensis*, and *Mesopodopsis slabberi*) and for distant populations of *Siriella thompsoni* (South Atlantic, northeast Indian Ocean, and North Pacific), *Meterythroptis picta* (North Atlantic and North Pacific), and *Mysis relicta* (northern Europe and North America). Similarly, no differences were found between the sexes or between left and right statoliths.

The ecological distribution of statolith mineral composition is summarized in Table III. Noncrystalline statoliths were found from brackish water (*Rhopalophthalmus*) to the deep sea (*Boreomysis*), with the greatest numbers in depths of 201–2000 m. The frequency of fluorite mineralization increased from freshwater to marine environments, with a maximum in the photic zone (0–200 m). On the contrary, vaterite was most common in fresh water and completely absent in the deep sea (Table IIIa). With respect to frequency of mineral types in different biota (Table IIIb), vaterite prevailed in freshwater organisms but fluorite was the dominant form in all remaining aquatic biota.

The microanalytical determinations gave only qualitative results. More elements were recorded in noncrystalline and fluorite statoliths than in vaterite statoliths. Species studied were *Boreomysis megalops* (Na, Mg, S, Ca), *B. microps* (Mg, Si, S, Cr, Fe, Ni), and *Rhopalophthalmus terranatalis* (Mg, S, Ca, Fe, Cu) with noncrystalline statoliths; *Katerythroptis oceanae* (F, Mg, Si, P, S, Ca, Zn), *Pseudomna latiphalmmum* (F, Mg, P, S, Ca, Cr, Zn), *Idiomysis tsurnamali* (F, P, Ca), and *Paramysis arenosa* (F, K, Ca) with fluorite; *P. lacustris tanaitica* (P, S, Ca, Cu), *Schistomysis assimilis* (P, S, Ca), and *Limnomysis benedeni* (P, S, Ca) with vaterite. In *S. assimilis* the presence of Ni and Cu varied between populations (present in Gulf of Venice; absent in Gulf of Salerno) and among individuals ( $n = 6$ ). In *L. benedeni* the presence of Cu varied among individuals ( $n = 4$ ).

## Discussion

Our study covers about 17% of the extant species described worldwide for the family Mysidae; this includes

Table III

Occurrence (% populations) of mineral types of mysid statoliths in different aquatic biota

A. Percentages of biota with respect to mineral types					
Type	n	Freshwater %	Brackish %	Marine 0–200 m %	Marine 201–2000 m %
Noncrystalline	8	0	13	13	75
Fluorite	150	3	7	65	24
Vaterite	21	43	33	24	0

B. Percentages of mineral types with respect to biota					
Type	Freshwater n = 14	Brackish n = 19	Marine 0–200 m n = 104	Marine 201–2000 m n = 42	
Noncrystalline %	0	5	1	14	
Fluorite %	36	58	94	86	
Vaterite %	64	37	5	0	

34% of the genera and all subfamilies. All oceans and shelf areas of all continents are represented. Special emphasis is placed on zoogeographically important areas such as the Black Sea, the Mediterranean, the Red Sea, the Caribbean, Japan, Tasmania, and the Antarctic. Species are littoral, coastal, or oceanic (epi-, meso-, and bathypelagic); estuarine, limnic, or cave dwelling. Results are thus highly representative of the mysid fauna of the world, with the reservation that European species are overrepresented.

Three main types of statoliths were identified: those without crystalline components (organic statoliths), and those mineralized with either fluorite or calcium carbonate (vaterite or calcite).

As in other x-ray diffraction studies, qualitative microanalysis was used to provide supplementary information. The determinations showed a high diversity of trace elements. When a mysid molts, its statocyst cavity is open to ambient water; therefore, we cannot exclude the possibility that the presence of some elements in marine and brackish-water species is a residual of sea salt that has been enclosed during statolith formation. The presence of sulfur in most statoliths coincides with the finding of sulfated mucopolysaccharides in fluorite statoliths (Espeel, 1987). In *Boreomysis microps*, the absence of calcium in the noncrystalline statoliths further indicates their nonmineralic composition. The absence of fluorine in all examined vaterite statoliths suggests that vaterite and fluorite statoliths have different mineralization patterns.

Noncrystalline statoliths are characteristic of the Boreomysinae and the Rhopalophthalminae, two subfamilies considered primitive among Mysidae (Tattersall and Tattersall, 1951; Schlacher *et al.*, 1992).

Fluorite precipitation represents the most frequent mineral-forming process occurring in statocysts of Mysidae. It remains unclear why these animals are bearing the expense of concentrating fluorine, an element present in small quantities (1.3 mg/l) in seawater (35‰) and almost absent in fresh water. This is especially remarkable if one considers the large size of vaterite statoliths, which have diameters about 1–4% of the body length.

Mineralization with  $\text{CaCO}_3$  is common in both Recent and fossil statoliths. The noteworthy aspect of this very common form of biomineralization is that extant forms produce vaterite. Precipitation of this hexagonal metastable polymorph of crystalline  $\text{CaCO}_3$  may have biological significance by favoring rapid statolith formation after each molt (Ariani *et al.*, 1981). In fact, vaterite is often precipitated during the regeneration of the aragonitic shells of mollusks, when sudden mobilization of calcium is necessary (Watabe *et al.*, 1976). Considering the metastable nature of vaterite and the absence of calcite in Recent species, it seems likely that calcite in fossil specimens was

formed by phase transformation of vaterite during or after the process of fossilization. Voicu (1981) assigned Miocene calcite statoliths to *Paramysis*, a genus that precipitates vaterite in Recent forms of the Black Sea area (Table I). His assumption that the Recent species *Paramysis kroeyeri* and *P. kessleri sarsi* produce calcite was not confirmed by our finding of vaterite in both species.

Conspecific populations from different geographical areas and different biota show identical crystallographic characteristics (Table I); thus mineral composition of statoliths appears to be a definite specific character. The presence of an organic matrix in all types of statoliths (Wittmann *et al.*, 1993) suggests that the mineral type is matrix mediated and under genetic control, as in fish otoliths (Gauldie, 1986). Genes controlling the mineral type of vertebrate otoconia have important functions in the physiology of the inner ear (Mulligan and Gauldie, 1989). These observations render discussions on the adaptive meaning of mineral type rather difficult, because natural selection may act via complex epigenetic patterns.

In contrast to the similarity of mineral type on the intraspecific level, either vaterite or fluorite may be found when congeneric species or closely related genera of the tribe Mysini are compared. Table III confirms the dominant role of vaterite in fresh water and of fluorite in seawater. The finding (Enbysk and Linger, 1966) of fluorite statoliths in subfossil shelf sediments of northwestern America fits this picture. Vaterite statoliths are rare in marine water. All marine forms with vaterite statoliths also inhabit brackish or fresh waters (Table I). According to Voicu (1981), in seawater the function of the static organ demands the precipitation of a mineral with a greater specific gravity (fluorite, 3.2) than in fresh water (calcite, 2.7; we add vaterite, 2.5). Ariani *et al.* (1983) note that the precipitation of fluorine in fresh water may be difficult or impossible when fluorine concentrations are low. Nevertheless, four freshwater species, *Mysis relicta*, *Taphromysis louisianae*, *Diamysis pengoi*, and *Troglo-mysis vjetrenicensis*, precipitate fluorite. This is especially remarkable for *D. pengoi* and *T. vjetrenicensis*, because they are closely related to *D. bahirensis*, an extremely euryhaline form that occurs mainly in brackish waters and produces vaterite. The ecological meaning of this situation is still obscure.

Biogeographical correlations may be established based on the fact that vaterite statoliths are found only in two groups of closely related genera of Mysini, the 'Diamysis group' (*Diamysis*, *Limnomysis*, and *Antromysis*) and the 'Paramysis group' (*Paramysis*, *Katamysis*, and *Schistomysis*). Both groups are characterized by features of antennal scale and male pleopods. Vaterite is found in *Hemimysis*, which shows intermediate morphological features. Most Recent vaterite-forming species inhabit the Ponto-Caspian region (Table I), where calcareous mysid



statoliths largely occur (Voicu, 1974; Fuchs, 1979) in Miocene deposits of the brackish Paratethys. The Caribbean genus *Antromysis* does not fit this pattern, but it is a vicariant of the European genus *Diamysis*.

The biogeography of calcareous statoliths and their predominant role in fresh water are mutually dependent. About one-third of the world fauna of freshwater Mysidae is endemic to the Ponto-Caspian region, where the Danube river alone is inhabited by 10 species. Vaterite is found in 78% species ( $n = 9$ ; see Table 1) of the tribe Mysini in the Black Sea including adjacent waters. Based on faunal composition, a similar value is expected for the Caspian Sea. Corresponding values are 30% ( $n = 10$ ) for the Mediterranean, 17% ( $n = 24$ ) for the Atlantic, and 0% ( $n = 22$ ) for all remaining seas and oceans of the globe. From species composition in the Baltic, we expect that vaterite is found only in species introduced by man (Köhn, 1992) from the Ponto-Caspian (*Hemimysis anomala*, *Limnomysis benedeni*, and *Paramysis lacustris*).

The earliest fossil records of Mysidacea are Lophogastrida (or nearly so) from Carboniferous to Jurassic sediments (see compilation in Tattersall and Tattersall, 1951). Most Recent forms belonging to this suborder have an oceanic life habit. Together with several small families (Petalophthalmidae, Stygiomysidae, and Lepidomysidae) within the suborder Mysida, they have conserved the ancestral mysidacean morphotype, characterized by seven pairs of brood plates, (nearly) unmodified male pleopods, and the absence of statocysts.

No early fossil records are available for the species-rich family Mysidae, which has statocysts in the endopods of uropods as its most important autapomorphic feature. As discussed by Schlacher *et al.* (1992), the subfamilies Boreomysinae (pelagic) and Rhopalophthalminae (benthopelagic) have conserved certain plesiomorphic features such as subdivided exopods of uropods and biramous and many-segmented male pleopods or, as in Boreomysinae, seven pairs of brood plates. In both subfamilies, the statoliths are exclusively noncrystalline (Table 1). The apparent correlation with plesiomorphic characters suggests that organic statoliths may have preceded mineralic ones. The probable ancestral status of nonmineralized statoliths is also supported by the observations of Ariani *et al.* (1982) on the ontogenetic development of calcareous statoliths.

The late appearance of mineralic statoliths in fossil history (Lower Miocene according to Voicu, 1981) points to a post-Cretaceous origin of modern Mysidae (Siriellinae, Gastrosaccinae, Mysinae, and Mysidellinae), which are characterized by two to three pairs of brood plates, reduced pleopods in females, and specialized pleopods in males. Most Recent species have fluorite statoliths (Table 1); these constitute the bulk of the benthopelagic to benthic forms inhabiting coastal and littoral zones of all oceans.

Our evolutionary scheme is aligned with the theoretical considerations of Buddenbrock (1914) on the biological meaning of static organs in crustaceans. Besides control of body position, the main adaptive value of such organs is support of visual orientation in the complex spatial structure found in benthopelagic to benthic habitats; this function is less important in oceanic habitats where orientation towards light source is paramount. In fact, Neil (1975) gave experimental evidence that the statocysts of mysids stabilize the visual perceptive field through statocyst modulation of the optokinetic eyestalk movements. Biometrical observations by Wittmann *et al.* (1990) fit this concept by showing that, on the average, blind mysids or those with reduced eyes have smaller statoliths than those with well-developed eyes.

Both the scarcity of mysid statoliths outside Paratethyan sediments and the biogeography of Recent species suggest that  $\text{CaCO}_3$  statoliths developed in fresh to brackish waters of the Ponto-Caspian region during the Miocene. A large marine to brackish basin, the Paratethys, covered the region during that period. In the late Miocene, salinities gradually decreased in peripheral areas such as the Vienna Basin (Fuchs, 1979). During the Pleistocene, conditions in the Black Sea area varied between completely freshwater during glaciations and brackish during interglacial periods (Hsü, 1978). These events may have favored the evolution of a rich brackish to freshwater fauna.

The few vaterite-forming species outside the Ponto-Caspian (Table 1) have close relatives there and thus are probably of the same origin. Such relationships are obvious for certain members of the *Diamysis* group (Wittmann, 1992). The problem arises, however, that most vaterite-forming species have close relatives that form fluorite. The occurrence of both mineral types in congeneric species of *Hemimysis*, *Diamysis*, *Paramysis*, and *Schistomysis* suggests that vaterite evolved from fluorite in at least four parallel lines. The only reasonable explanation appears to be homoiology—that is, analogy on the basis of homology: the common ancestors may have evolved physiological or morphological predispositions favoring a phylogenetically rapid shift of statolith mineral composition from fluorite to calcium carbonate.

Statolith crystallography in the Mysidae seems to reflect two elements: first, the morphological differentiation between two primitive subfamilies, the Boreomysinae and the Rhopalophthalminae, with organic statoliths and all remaining taxa with mineralized statoliths; and second, ecophysiological differences between marine forms with fluorite and freshwater forms with vaterite. These elements offer parallels to those advanced by Carlström (1963) for the vertebrates, where the mineral composition of otoliths reflects first, the anatomical division in two main groups, the Agnatha with phosphate and the Gnathostomata with carbonate; and second, the differentiation between cold-

blooded forms with aragonite or vaterite and warm-blooded ones with calcite. The more recent discovery of calcite in certain amphibians (Marmo *et al.*, 1983) suggests that the appearance of calcite may rather mark the transition from an aquatic to a terrestrial mode of life.

### Acknowledgments

We are greatly indebted to members of the "Mysid Research Group" for exchange or donation of mysid material: T. E. Bowman (Washington), T. Brattegard (Blomsterdalen), G. Fenton (Hobart), J. Mauchline (Oban), S. M. Lussier (Narragansett), M. Murano (Tokyo), J. C. Sorbe (Arcachon), and T. Wooldridge (Port Elizabeth). We also thank G. Voicu (Bucarest) for the generous donation of fossil statoliths. The Division of Ultrastructure, Zool. Inst. Vienna, and Lab. Micr. Elettronica, Dip. Sci. Terra (Naples), kindly provided scanning electron microscopy and microanalytical facilities. Part of the material was collected during the Antarctic expedition ANT VIII/5 of the RV *Polarstern*.

### Literature Cited

- Ariani, A. P., F. Marmo, G. Balsamo, and E. Franco. 1981. Vaterite in the statoliths of a mysid crustacean (*Diamysis bahrensis*). *Annuaire Ist. Mus. Zool. Univ. Napoli* 24: 69-78.
- Ariani, A. P., F. Marmo, G. Balsamo, G. Cesaro, and N. Maresca. 1982. Prime osservazioni sullo sviluppo degli statoliti di Crustacea Misidacei. *Annuaire Ist. Mus. Zool. Univ. Napoli* 25: 327-341.
- Ariani, A. P., F. Marmo, G. Balsamo, E. Franco, and K. J. Wittmann. 1983. The mineral composition of statoliths in relation to taxonomy and ecology in mysids. *Rapp. Comm. Int. Mer Médit.* 28(6): 333-336.
- Bethe, A. 1895. Die Otocyste von *Mysis*. *Zool. Jb. Anat. Ontog.* 8: 544-564.
- Buddenbrock, W. von. 1914. Über die Orientierung der Krebse im Raum. *Zool. Jb. Allg. Zool.* 34: 479-514.
- Carlström, D. 1963. A crystallographic study of vertebrate otoliths. *Biol. Bull.* 125: 441-463.
- Enbysk, B. J., and F. L. Linger. 1966. Mysid statoliths in shelf sediments off Northwest America. *J. Sediment. Petrol.* 36: 839-840.
- Espeel, M. F. 1987. On the fine structure of the statolith and the caudal statocyst gland of the mysid shrimp *Neomysis integer* (Leach, 1814) (Crustacea, Mysidacea). *Meded. K. Acad. Wet., Lett. Sch. Kunst. België* 49(1): 95-109.
- Fuchs, R. 1979. Das Vorkommen von Statolithen fossiler Mysiden (Crustacea) im obersten Sarmatien (O-Miozän) der Zentralen Paratethys. *Beitr. Paläont. Österreich* 6: 61-69.
- Gauldie, R. W. 1986. Vaterite otoliths from chinook salmon (*Oncorhynchus tshawytscha*). *New Zealand J. Mar. Freshw. Res.* 20: 209-217.
- Gauldie, R. W. 1990. Vaterite otoliths from the opah: *Lampris immaculatus* and two species of sunfish, *Mola mola* and *M. ramsayi*. *Acta Zool.* 71(4): 193-199.
- Hsu, K. J. 1978. When the Black Sea was drained. *Sci. Am.* 238(5): 53-63.
- Jander, R. 1962. The swimming plane of the crustacean *Mysidium gracile* (Dana). *Biol. Bull.* 122: 380-390.
- Köhn, J. 1992. Mysidacea of the Baltic Sea—state of the art. Pp. 5-23 in *Taxonomy, Biology and Ecology of (Baltic) Mysids (Mysidacea, Crustacea)*. J. Köhn, M. B. Jones, and A. Moffat, eds. Univ. Rostock.
- Lowenstam, H. A. 1981. Minerals formed by organisms. *Science* 211: 1126-1131.
- Lowenstam, H. A., and D. McConnell. 1968. Biologic precipitation of fluorite. *Science* 162: 1496-1498.
- Maissuradze, L. S., and G. Popescu. 1987. Carpatho-Caucasian comparative study of Sarmatian Mysids. *D. S. Inst. Geol. Geofiz.* 72-73(3): 75-80.
- Marmo, F., G. Balsamo, and E. Franco. 1983. Calcite in the statoconia of amphibians. A detailed analysis for the frog *Rana esculenta*. *Cell Tissue Res.* 233: 35-43.
- Mulligan, K. P., and R. W. Gauldie. 1989. The biological significance of the variation in crystalline morph and habit of otoconia in elasmobranchs. *Copeia* 1989(4): 856-871.
- Neil, D. M. 1975. Statocyst control of eyestalk movements in mysid shrimps. *Fortschr. Zool.* 23:98-109.
- Schlacher, T. A., K. J. Wittmann, and A. P. Ariani. 1992. Comparative morphology and actinopaleontology of mysid statoliths (Crustacea, Mysidacea). *Zoomorphology* 112: 67-79.
- Tattersall, W. M., and O. S. Tattersall. 1951. *The British Mysidacea*. Ray Society, Publ. 136, London. 460 pp.
- Voicu, G. 1974. Identification des Mysidés fossiles dans les dépôts du Miocène supérieur de la Paratéthys Centrale et Orientale et leur importance paléontologique, stratigraphique et paléogéographique. *Geol. Carpath.* 25: 231-239.
- Voicu, G. 1981. Upper Miocene and Recent mysid statoliths in Central and Eastern Paratethys. *Micropaleontology* 27: 227-247.
- Watabe N., V. R. Meenakshi, P. L. Blackwelder, E. M. Kurtz, and D. G. Dunkelberger. 1976. Calcereous spherules in the gastropod *Pomacea paludosa*. Pp. 283-308 in *The Mechanisms of Mineralization in the Invertebrates and Plants*. N. Watabe and K. M. Wilbur, eds. Univ. South Carolina Press, Columbia.
- Wittmann, K. J. 1992. Morphogeographic variations in the genus *Mesopodopsis* Czerniavsky with descriptions of three new species (Crustacea, Mysidacea). *Hydrobiologia* 241: 71-89.
- Wittmann, K. J., A. P. Ariani, and A. Stanzione. 1990. Implicazioni tassonomiche ed ecologiche di alcune caratteristiche biometriche degli statoliti dei Misidacei. *Oebalia* 16-2(Suppl.): 805-807.
- Wittmann, K. J., T. A. Schlacher, and A. P. Ariani. 1993. Structure of Recent and fossil mysid statoliths (Crustacea, Mysidacea). *J. Morphol.* 215: 31-49.

# Shell Growth and Viability Differences Between the Marine Mussels *Mytilus edulis* (L.), *Mytilus galloprovincialis* (Lmk.), and Their Hybrids From Two Sympatric Populations in S.W. England

J. P. A. GARDNER<sup>1\*</sup>, D. O. F. SKIBINSKI<sup>1</sup>, AND C. D. BAJDIK<sup>2</sup>

<sup>1</sup>*School of Biological Sciences, University College of Swansea, Singleton Park, Swansea, SA2 8PP, Great Britain, and* <sup>2</sup>*49-2625 Hemlock Street, Vancouver, British Columbia, V6H 2V6, Canada*

## Introduction

**Abstract.** Mussels were collected at high and low shore locations from two *Mytilus edulis*/*Mytilus galloprovincialis* populations. Croyde Bay and Whitsand Bay, in S.W. England. Genotype-dependent length-at-age values were determined. At high and low shore locations at both sites, *M. edulis*-like mussels had significantly smaller length-at-age values than *M. galloprovincialis*-like and putative F1 hybrid individuals. The putative F1 hybrids exhibited length-at-age values between those of the parental types, but much closer to those of *M. galloprovincialis*-like rather than *M. edulis*-like individuals.

Genotype frequencies as a function of age were determined and relative viability coefficients estimated from comparisons of genotype frequencies of young versus old mussels. At high and low shore locations at both sites, the relative viability coefficient of *M. galloprovincialis*-like individuals was greater than that of *M. edulis*-like mussels. Putative F1 hybrids at both sites had relative viability coefficients intermediate between those of the parental types. These data indicate that the length-dependent variation in allozyme frequencies that characterizes sympatric populations can be attributed to a small but significant genotype-dependent difference in length-at-age values, but mostly to large and highly significant differences in viability.

Hybrid zones have been defined as "interactions between genetically distinct groups of individuals resulting in at least some offspring of mixed ancestry. Pure populations of the two genetically distinct groups are found outside of the zone of interaction" (Harrison, p. 72, 1990). As such, hybrid zones are thought to represent cases of partial (incomplete) reproductive or genetic isolation between two related species, semi-species or conspecifics. The dynamics of hybrid zones are of considerable interest from an evolutionary point of view because such zones often play important roles in models of speciation (reviewed by Hewitt, 1988).

The role of selection in the maintenance of hybrid zones has been emphasized in several reviews (Moore, 1977; Barton and Hewitt, 1985, 1989; Hewitt, 1988, 1989; Harrison, 1990). The traditional view, and the one with the most evidence to support it, is that hybrid zones are maintained by a balance between dispersal (immigration) and selection against hybrids (individuals of mixed ancestry). In this case it is more appropriate to think of hybrid zones as tension zones (Barton and Hewitt, 1985, 1989) because reduced hybrid fitness is independent of the environment. Individuals of mixed ancestry are considered to be less fit than parental types because the parental co-adapted gene complexes, which presumably evolved in response to localized selection outside the hybrid zone, are broken up by recombination within the hybrid zone. New gene combinations resulting from hybridization and recombination are considered to be less adapted to the environment (and to interaction and functioning with each other) than are the parental gene com-

Received 12 December 1990; accepted 30 September 1993.

\* Current address: Ocean Sciences Centre, Marine Sciences Research Laboratory, Memorial University of Newfoundland, St. John's, Newfoundland, A1C 5S7, Canada.

plexes. Hybrids are therefore less fit and thus are selected against. Indeed, Harrison (1990) cites 20 examples of hybrid zones involving plants, insects, fish, amphibians, reptiles, birds, and mammals in which individuals of mixed ancestry have reduced fitness compared with parental types.

Moore (1977) proposed an alternative model of hybrid zone maintenance (see also Moore and Buchanan, 1985; and Moore and Koenig, 1986). This is the geographically bounded hybrid superiority model, which suggests that, within the limited environment of the hybrid zone, hybrids have a selective advantage compared to parental types when environmental factors determine relative fitness. Because the parental types are adapted to environments outside the hybrid zone, the habitat in which the hybrid zone is located is more favorable for hybrids. So far, the only evidence that supports this model comes from avian species in which adult dispersal is limited. For example, Moore and Buchanan (1985) note that their results from the Northern Flicker (woodpecker) zone are more consistent with the hybrid superiority theory than with the hybrid unfitness model. Hewitt (1988), however, suggests that the evidence does not permit this model to be distinguished from other explanations (*e.g.*, tension zones or environmental zones).

In S.W. England, sympatric populations of *Mytilus edulis* (the blue mussel) and *Mytilus galloprovincialis* (the Mediterranean mussel) exhibit a strong positive correlation between shell length and gene frequency at two allozyme loci (*Est-D* and *Odh*). Larger mussels tend to be *M. galloprovincialis*-like; that is, they possess alleles at highest frequency in pure *M. galloprovincialis* populations (Skibinski, 1983; Gardner and Skibinski, 1988). This relationship is also found in other regions of the British Isles (Skibinski and Roderick, 1991). Two hypotheses have been investigated to explain the length-dependent allozyme variation observed in hybrid populations. The first—historical change, with *M. edulis* replacing *M. galloprovincialis*—has been rejected (Gardner and Skibinski, 1988). The second—differential growth rates—was not supported by the results of transplant experiments with mussels from S.W. England (Skibinski, 1983; Skibinski and Roderick, 1989); however, *in situ* growth in sympatric mussel populations has not been studied previously. A third possibility, that differential viability causes the length-dependent allozyme variation, has also not been tested.

Investigators of the *Mytilus* contact zone in S.W. England have long thought that the hybrid zone in this area is maintained by selection, but that this selection is not principally against hybrids (Skibinski and Beardmore, 1979; Skibinski et al., 1983). Skibinski and Beardmore (1979) noted that intergradation, although extensive at many sites, is often not complete, which suggests that some genotypes of mixed ancestry have a selective advantage

over *M. edulis*. The geographic distribution of sites with high genetic mixing is consistent with the hypothesis that individuals of mixed ancestry do have an advantage over at least one of the parental types in some environments (Skibinski and Beardmore, 1979; Skibinski et al., 1983). Furthermore, it was suggested that any temporal stability exhibited by the hybrid zone might result from the superior fitness of the hybrids and intergrades (Skibinski and Beardmore, 1979). In this paper, we explore these ideas further by the study of genotype-dependent viability and shell growth of mussels from two sympatric populations in S.W. England.

The objectives of our study are twofold. First, we seek to explain the length-dependent change of allozyme frequencies in sympatric populations by examining differences in genotype-dependent shell growth and viability. The use of shell-sectioning techniques permitted us to determine annual growth increments. By comparing year classes, we estimated the relative mortality of different genotypes within two hybrid populations. Second, we use the viability data to address the question of how the mussel hybrid zone is structured and maintained.

We found substantial differences in viability and small but significant differences in growth favoring *M. galloprovincialis* and individuals of mixed ancestry. The evidence suggests that these differences contribute to the variation in length-dependent allele frequency that was reported in earlier studies, and that selection against *M. edulis*-like mussels plays an important role in maintaining the hybrid zone.

## Materials and Methods

In March 1987, mussels were collected at high and low shore locations from two sympatric *M. edulis*/*M. galloprovincialis* populations in S.W. England: Croyde Bay, north Devon, and Whitsand Bay, south Cornwall. These are the same locations used for previous collections (Skibinski, 1983; Gardner and Skibinski, 1988, 1990a, b). Four groups of mussels were analyzed—CHS, CLS, WHS, and WLS—where C stands for Croyde, W for Whitsand, HS for high shore, and LS for low shore. Mussels were collected from areas of the low and high shore at Croyde approximately 2.2 m and 3.5 m above chart datum (CD), and at Whitsand approximately 2.5 m and 3.8 m above CD.

In both populations, *M. edulis* numerically dominates among smaller mussels (<30 mm), whereas *M. galloprovincialis* dominates among larger mussels (>30 mm) (Skibinski, 1983; Gardner and Skibinski, 1988). Thus, it is hard to obtain small *M. galloprovincialis* and large *M. edulis*. To increase the numbers of these types of mussels for analysis, and to keep other diagnostic techniques such as starch gel electrophoresis to a minimum, large samples

of mussels were collected and sorted according to shell morphology, which is partially diagnostic for differences between *M. edulis* and *M. galloprovincialis* (Seed, 1972, 1974; Skibinski, 1983). The morphological criteria that were employed included shell height and shell curvature (both greater in *M. galloprovincialis*), the presence or absence of an anterior beak (present in *M. galloprovincialis*), and the profile of the shell (more rounded and convex in *M. galloprovincialis*).

A total of 7302 mussels with lengths of at least 20 mm were collected and sorted. For each location (CHS sample size = 1123; CLS = 1700; WHS = 2313; and WLS = 2166) the mussels were sorted into two size groups, 20–35 mm and >35 mm. Each size group was sorted according to shell morphology into three classes, “*M. edulis*-like,” “*M. galloprovincialis*-like,” and “intermediate.” Each phenotypic group was sorted according to size into two groups, “small” and “large,” a boundary size being chosen such that approximately 50% of mussels fell above and 50% below the boundary, selection being made by eye. The sorting process yielded 12 categories (two quantitative size classes  $\times$  three phenotype classes  $\times$  two qualitative size classes) for CLS, WHS, and WLS. Because of the limited numbers of large (>35 mm) mussels at CHS, all individuals >35 mm ( $n = 20$ ) were retained as one group with no subselection. Thus, there were seven categories for CHS and twelve each for CLS, WHS, and WLS. For all four locations, 25 mussels were picked at random from each category ( $n = 20$  for mussels >35 mm at CHS) for starch gel electrophoresis and length-at-age estimations. Table I illustrates the sorting procedure for mussels of WLS. The number of mussels subject to electrophoresis was 170 at CHS and 300 each at CLS, WHS, and WLS. Samples were either analyzed immediately or stored at  $-70^{\circ}\text{C}$  for subsequent analysis.

Starch gel electrophoresis was performed on digestive gland dissected from each animal and prepared as described by Gardner and Skibinski (1988). Two allozyme loci, esterase-D (EST-D; EC 3.1.1.1) and octopine dehydrogenase (ODH; EC 1.5.1.11) were assayed, because these two loci show large allele frequency differences between *M. edulis* and *M. galloprovincialis* (Skibinski, 1983; Sanjuan *et al.*, 1990). To aid in data analysis, the compound allele system described by Skibinski (1983) was used. At a given locus, the compound *E* allele is obtained by pooling those alleles that are at highest frequency in “pure” *M. edulis*, and the compound *G* allele is obtained by pooling those alleles that are at highest frequency in “pure” *M. galloprovincialis*. Thus, for two polymorphic loci such as *Est-D* and *Odh*, there are nine dilocus genotype combinations ranging from the most *M. edulis*-like (*E/E E/E*), through the intermediate or putative F1 hybrid (*E/G E/G*) to the most *M. galloprovincialis*-like (*G/G G/G*). For the rest of the paper, the terms *galloprovincialis*, *ed-*

*ulis*, and hybrid refer to *M. galloprovincialis*-like (*G/G G/G*), *M. edulis*-like (*E/E E/E*), and putative F1 hybrid (*E/G E/G*) individuals of sympatric populations, without implying that these are truly pure types, but with the understanding that distinctive phenotype differences exist between the groups (*e.g.*, Skibinski *et al.*, 1978a, b; Beaumont *et al.*, 1989).

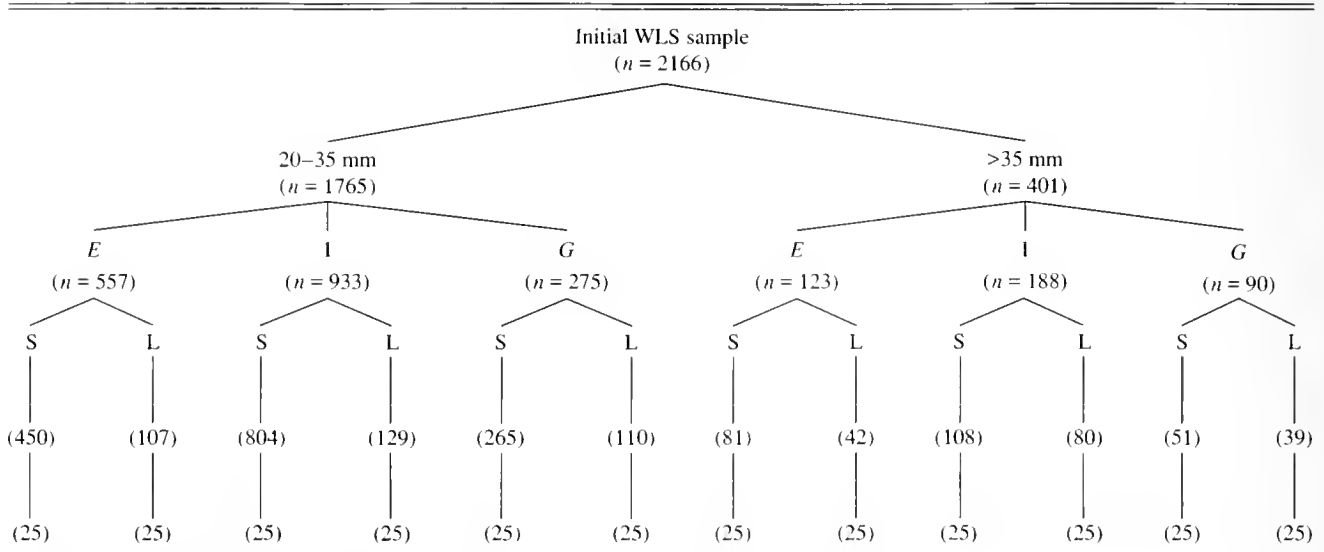
We focused upon only three (*E/E E/E*, *E/G E/G* and *G/G G/G*) of the nine genotypes because these represent the two extremes (both parental genotypes) and the intermediate (putative F1 hybrid), and consequently growth and viability differences between these groups are likely to be as great as any that occur within the zone of sympatry. Furthermore, these three genotypes represent between 65 and 70% of the total number of individuals within each population, making them of considerable importance in numerical terms alone. This does not imply that the other six genotypes are unimportant or occur at such low frequency that they are insignificant, but simply reflects the advantage of working with genotypes that are well represented in both populations and have arguably the most potential (at least initially) to provide data on fitness differences within the zone of sympatry. Obviously, the ability to differentiate between *edulis*, *galloprovincialis*, and hybrid individuals is important in identifying growth and viability differences between these types. However, because of introgression in these populations (*e.g.*, Skibinski, 1983; Skibinski *et al.*, 1983; Gardner and Skibinski, 1988), pure individuals or genuine F1 hybrids might not exist, and thus would not be detectable, regardless of the number of genetic markers used.

The allozymes selected provide a strong indication of background genotype in mussels from sympatric populations. For example, *G/G G/G* individuals from sympatric populations are morphologically and electrophoretically very similar to *M. galloprovincialis* from pure allopatric populations, just as *E/E E/E* individuals from sympatric populations most closely resemble *M. edulis* from pure allopatric populations (*e.g.*, Grant and Cherry, 1985; Sanjuan *et al.*, 1990).

Shell lengths ( $\pm 0.1$  mm) of all mussels typed by electrophoresis were recorded. Shells were sectioned to establish that age determination from external check marks could be performed accurately. A valve from each of 155 randomly chosen individuals from all four locations was thin-sectioned, and an acetate peel replica was prepared (*e.g.*, Lutz, 1976; Richardson *et al.*, 1979). The number of internal annual growth bands was counted, and the distance from the umbo to each mark was measured to provide length-at-age data. The processes of counting the annual bands from the acetate peels and from the exterior of the valve were carried out independently to minimize bias in the results. When a peel or the valve from which it was derived could not be scored with total confidence,

Table I

The sorting procedure used to obtain 12 groups of 25 mussels each (where possible) for analysis, as exemplified by the Whitsand low shore (WLS) sample



E = *edulis* mussels; I = intermediate mussels; G = *galloprovincialis* mussels; S = small; L = large.

the data pair was discarded (there was no evidence of a nonrandom factor explaining which data pairs could or could not be accurately scored). Nine of 65 mussels were incorrectly aged, eight by  $\pm 1$  year, and one by 2 years. Regression analysis of the number of annual growth rings from the acetate peel against the number estimated from the valve exterior was carried out, the two being highly correlated ( $R^2 = 0.908$ ;  $n = 65$ ;  $P < 0.001$ ).

The ages of all remaining nonsectioned mussels were determined by examination of external growth marks. Each mussel provided length-at-age data for a minimum of 4 years of age up to a maximum of 13 years of age, with an average of about 6–7 years. Data were analyzed by univariate ANOVA of each length-at-age category. This analysis is based on minimal assumptions, the results are easily interpretable and biologically meaningful, and maximum information can be extracted from the data set because a large proportion of the values can be used. This is a conservative approach, so that if significant length-at-age differences are observed it can be assumed that they represent genuine differences. A slight loss of statistical power is associated with this approach, but this is offset by the advantages described above. To control for the multiple testing involved with this approach, we used the Bonferroni test, which compensates for the increased probability of Type I error rate (the sequential Bonferroni test, which is less conservative than the standard Bonferroni test [Rice, 1989], gave identical results). With the Bonferroni procedure, the alpha level (nominally  $\alpha = 0.05$ ) is divided by the total number of tests made

of the same hypothesis, which at CHS, WHS, and WLS was 10 each, giving an acceptance value of  $\alpha = 0.005$  at these locations; and at CLS was 8, giving an acceptance value of  $\alpha = 0.00625$  at this location. We employed the univariate option of the PROC GLM (General Linear Model) subroutine of SAS (SAS Institute, 1987) with the Ryan-Einot-Gabriel-Welsch multiple range test (REGWQ option) to locate between-subject effects. The REGWQ multiple range test is particularly appropriate because it controls the experimentwise Type I error rate (Day and Quinn, 1989). The data were tested for normality using the Shapiro-Wilkes statistic: transformations were unnecessary because the data were normally distributed.

Best-fit growth curves were derived from polynomial regression computed by the PROC GLM procedure of SAS (e.g., MacDonald and Thompson, 1985, 1988), which has an advantage over the von Bertalanffy function in that it does not impose asymptotic behaviour (Roff, 1980; MacDonald and Thompson, 1985). A cubic polynomial best explained variation in the growth curves following stepwise significance testing of each newly added term (e.g., Sokal and Rohlf, 1981, p. 673).

Following electrophoresis and age determination, data from the mussels of the four locations were tabulated according to age and dilocus genotype to permit estimation of age-dependent genotype frequencies. An example is given in Table II. The predicted frequency of each genotype of any age in the initial random sample was estimated, taking into account, and adjusting for, the sorting procedure described above. For example, using the data

Table II

The method used to estimate genotype frequencies as exemplified by data from Whitsand low shore (WLS)

Age (yr)	20-35 mm category (n = 1765 mussels collected)			>35 mm category (n = 401 mussels collected)		
	Dilocus genotype					
	<i>E/E E/E</i>	<i>E/G E/G</i>	<i>G/G G/G</i>	<i>E/E E/E</i>	<i>E/G E/G</i>	<i>G/G G/G</i>
0	32	3	1			
1	27	6	3			
2	21	10	8			
3	9	13	17	5	10	19
4				2	12	20
5				1	18	28
6				0	8	14
7				1	4	7
Subtotal	89	32	29	9	52	88
Total		150			149	

*E/E E/E* = *edulis* mussels; *E/G E/G* = putative F1 mussels; *G/G G/G* = *galloprovincialis* mussels.

from Table II, the predicted frequency of 3-year-old *G/G G/G* mussels among all 3-year-old mussels in the WLS sample is

$$\frac{(17 \times 1765/150) + (19 \times 401/149)}{(9 + 13 + 17) \times (1765/150) + (5 + 10 + 19) \times (401/149)} = 0.456$$

In the above equation, the numerator estimates the number of 3-year-old *G/G G/G* mussels in the 1765 + 401 total, and the denominator estimates the total number of 3-year-old mussels of all genotypes in the same total.

## Results

The results of the ANOVA for the high and low shore locations at Croyde are given in Table III, and for the two locations at Whitsand in Table IV. Data are presented for mussels up to the maximum age at which all three genotypes co-occur. Thus, although data were available for certain genotypes up to length-at-age 13 years, these were not included if the same data were not available for any other genotype. All four locations have a similar pattern of between-subject (genotype) effects throughout the analyses. Among the youngest individuals of the three genotypes, length-at-age values are not significantly different, but at age 4 years and older significant differences are apparent. Nonsignificant differences between the genotypes among the oldest age classes may be partially attributable to the small sample sizes for these oldest mussels. Where significant between-subject effects exist at CHS, CLS, and WLS, the *E/G E/G* and *G/G G/G* genotypes exhibit nonsignificant length-at-age differences

throughout their life spans, whereas the *E/E E/E* mussels have statistically lower mean length-at-age values than both these genotypes. Where significant between-subject effects exist at WHS, the *G/G G/G* mussels have significantly greater mean length-at-age values than the *E/G E/G* individuals (at ages 7, 8, and 9 years). From age 3 years onwards, one or, more usually, both of the *E/G E/G* and *G/G G/G* genotypes have significantly greater length-at-age values than the *E/E E/E* mussels. The maximum difference in length-at-age values between the three genotypes (*i.e.*, maximum minus minimum value regardless of genotype) is also presented in each table. Length-at-age differences among older individuals are smaller than those observed among intermediate-aged mussels, which suggests that, on average, individuals that live the longest, regardless of genotype, have similar length-at-age values. Thus, among the *edulis* mussels, individuals that exhibit greatest maximum longevities also exhibit greatest length-at-age values at all ages.

Growth curves fitted by polynomial regression (Fig. 1) are very similar between genotypes for mussels of less than 4 years of age, but diverge thereafter. The standardized polynomial partial regression coefficients (up to the cubic term) for each growth line and the  $R^2$  values, which give an indication of how well each line fits the observed data, are given in Table V.

High or low shore location within a site has a pronounced effect upon growth (comparisons of growth were based upon tests of differences in the linear parameter of the cubic regression models). At Croyde, the three genotypes all have greater length-at-age values in the low shore than in the high shore; this difference is nonsignificant for



Table III

Analysis of variance, with significant Ryan-Einot-Gabriel-Welsch multiple range test results, of mean length-at-age data for mussels from Croyde high and low shore

Age (yr)	E/E E/E mean length (mm)	E/G E/G mean length (mm)	G/G G/G mean length (mm)	Max. diff. (mm)	N	P	REGWQ
CHS							
1	5.58	5.67	5.59	0.09	94	0.9720 <sup>NS</sup>	
2	10.08	10.83	10.46	0.75	94	0.4011 <sup>NS</sup>	
3	15.25	16.23	15.76	0.98	94	0.3910 <sup>NS</sup>	
4	19.62	20.99	20.97	1.79	94	0.0707 <sup>NS</sup>	
5	22.75	25.00	25.33	2.58	87	0.0013*	G/G = E/G > E/E
6	24.64	28.16	28.55	3.91	72	0.0001*	G/G = E/G > E/E
7	25.63	31.68	30.91	6.05	47	0.0001*	E/G = G/G > E/E
8	26.36	34.10	32.78	7.74	30	0.0001*	E/G = G/G > E/E
9	29.03	35.53	33.40	6.50	19	0.0013*	E/G = G/G > E/E
10	30.15	36.73	33.20	6.58	11	0.0312 <sup>NS</sup>	
CLS							
1	6.54	6.78	6.74	0.24	130	0.6721 <sup>NS</sup>	
2	13.44	13.02	13.28	0.42	130	0.7986 <sup>NS</sup>	
3	20.72	20.48	20.95	0.23	130	0.8065 <sup>NS</sup>	
4	25.45	27.23	26.73	1.78	127	0.0034*	E/G = G/G > E/E
5	29.41	31.08	30.96	1.67	108	0.0038*	G/G > E/E
6	32.86	34.60	34.34	1.74	88	0.0127 <sup>NS</sup>	
7	35.70	36.09	36.28	0.58	62	0.9110 <sup>NS</sup>	
8	37.76	38.70	39.22	1.46	37	0.5803 <sup>NS</sup>	

N = number of individuals; P = significance level following Bonferroni test; NS = nonsignificant following Bonferroni test; \* = significant following Bonferroni test at alpha = 0.05/k (where k = number of tests); REGWQ = Ryan-Einot-Gabriel-Welsch multiple range test results; CHS = Croyde high shore; CLS = Croyde low shore; E/E E/E, E/E = *edulis* mussels; E/G E/G, E/G = putative F1 mussels; G/G G/G, G/G = *galloprovincialis* mussels.

the E/G E/G genotype only (CHS vs. CLS: E/E E/E,  $t = 13.951$ ,  $df = 129$ ,  $P < 0.001$ ; E/G E/G,  $t = 3.290$ ,  $df = 22$ ,  $P > 0.05$ <sup>NS</sup>; G/G G/G,  $t = 10.484$ ,  $df = 65$ ,  $P < 0.001$ : all significance levels given in this paragraph were determined after Bonferroni test; i.e., if  $P = 0.05/14 = 0.00357$  or less, the result is significant). Even the greatest length-at-age values at CHS (the E/G E/G genotype) are less than the greatest length-at-age values (the E/E E/E genotype) at CLS (CHS E/G E/G vs. CLS E/E E/E:  $t = 17.826$ ,  $df = 74$ ,  $P < 0.001$ ). At Whitsand, each genotype has greater length-at-age values in the low shore than in the high shore; this difference is nonsignificant only for the putative F1 hybrids (WHS vs. WLS: E/E E/E,  $t = -9.502$ ,  $df = 144$ ,  $P < 0.001$ ; E/G E/G,  $t = 1.229$ ,  $df = 46$ ,  $P > 0.05$ <sup>NS</sup>; G/G G/G,  $t = -3.405$ ,  $df = 32$ ,  $P < 0.002$ ). The greatest length-at-age values at WHS (the G/G G/G genotype) are less than the greatest length-at-age values (the E/E E/E genotype) at WLS, although WHS G/G G/G length-at-age values are slightly lower at ages < 4 years and slightly greater at ages > 4 years than WLS E/E E/E values (WHS G/G G/G vs. WLS E/E E/E,  $t = 6.604$ ,  $df = 100$ ,  $P < 0.001$ ). Comparison of length-at-age data between the site locations indicates that values at WHS and at WLS are greater than those at CHS and

at CLS respectively (CHS vs. WHS: E/E E/E,  $t = 4.399$ ,  $df = 127$ ,  $P < 0.001$ ; E/G E/G,  $t = 4.292$ ,  $df = 25$ ,  $P > 0.05$ <sup>NS</sup>; G/G G/G,  $t = 0.416$ ,  $df = 32$ ,  $P > 0.05$ <sup>NS</sup>; CLS vs. WLS: E/E E/E,  $t = 4.779$ ,  $df = 146$ ,  $P < 0.001$ ; E/G E/G,  $t = 0.513$ ,  $df = 43$ ,  $P > 0.05$ <sup>NS</sup>; G/G G/G,  $t = 4.059$ ,  $df = 65$ ,  $P < 0.001$ ). Thus, as reported for other *Mytilus* populations (e.g., Dickie *et al.*, 1984; Mallet *et al.*, 1987), site explains as much, if not more, of the variation in growth as is explained by genotype.

At all locations, genotype frequency as a function of age describes a sigmoidal pattern (Tables VI and VII). The frequency of *edulis* is highest among the youngest mussels, whereas the hybrids and *galloprovincialis* both occur at very low frequencies. With increasing age, the frequency of *edulis* decreases, whereas the frequencies of hybrids and *galloprovincialis* increase. Regression analysis of arcsine squareroot transformed compound E allele frequency (to transform a sigmoidal to a linear relationship, Sokal and Rohlf, 1981) as a function of age describes a negative linear relationship that is significant at CHS ( $R^2 = 0.869$ ,  $n = 8$ ,  $P < 0.001$ ), CLS ( $R^2 = 0.966$ ,  $n = 8$ ,  $P < 0.001$ ), WHS ( $R^2 = 0.823$ ,  $n = 8$ ,  $P < 0.001$ ) and WLS ( $R^2 = 0.736$ ,  $n = 9$ ,  $P < 0.01$ ) (Figs. 2 and 3). The mean slope of the equation for Croyde mussels is not signifi-



Table IV

Analysis of variance, with significant Ryan-Einot-Gabriel-Welsch multiple range test results, of mean length-at-age data for mussels from Whitsand high and low shore

Age (yr)	<i>E/E E/E</i> mean length (mm)	<i>E/G E/G</i> mean length (mm)	<i>G/G G/G</i> mean length (mm)	Max. diff. (mm)	<i>N</i>	<i>P</i>	REGWQ
<b>WHS</b>							
1	6.18	6.22	6.23	0.05	98	0.9913 <sup>NS</sup>	
2	10.99	11.91	11.69	0.92	98	0.2429 <sup>NS</sup>	
3	16.01	18.07	17.49	2.06	98	0.0149 <sup>NS</sup>	
4	20.63	23.49	23.61	2.98	98	0.0002*	<i>G/G = E/G &gt; E/E</i>
5	24.08	28.38	29.36	5.28	97	0.0001*	<i>G/G = E/G &gt; E/E</i>
6	27.02	31.85	33.97	6.97	88	0.0001*	<i>G/G = E/G &gt; E/E</i>
7	29.85	34.48	37.92	8.07	60	0.0001*	<i>G/G &gt; E/G &gt; E/E</i>
8	34.18	36.19	40.39	6.21	35	0.0001*	<i>G/G &gt; E/G = E/E</i>
9	35.72	38.60	42.18	6.46	25	0.0043*	<i>G/G &gt; E/G = E/E</i>
10	40.15	40.02	44.40	4.38	12	0.2051 <sup>NS</sup>	
<b>WLS</b>							
1	7.08	6.94	6.47	0.61	129	0.4947 <sup>NS</sup>	
2	13.25	13.48	13.65	0.40	129	0.8193 <sup>NS</sup>	
3	19.32	20.12	20.71	1.39	129	0.2092 <sup>NS</sup>	
4	24.67	26.57	27.21	2.54	129	0.0136 <sup>NS</sup>	
5	28.50	32.26	33.95	5.45	116	0.0001*	<i>G/G = E/G &gt; E/E</i>
6	31.93	36.75	38.51	6.58	90	0.0001*	<i>G/G = E/G &gt; E/E</i>
7	33.61	39.99	42.32	8.71	67	0.0001*	<i>G/G = E/G &gt; E/E</i>
8	35.80	43.28	45.27	9.47	35	0.0015*	<i>G/G = E/G &gt; E/E</i>
9	39.00	44.74	45.94	6.94	19	0.2817 <sup>NS</sup>	
10	45.30	46.67	49.50	4.20	10	0.5705 <sup>NS</sup>	

*N* = number of individuals; *P* = significance level following Bonferroni test; NS = nonsignificant following Bonferroni test; \* = significant following Bonferroni test at  $\alpha = 0.05/k$  (where *k* = number of tests); REGWQ = Ryan-Einot-Gabriel-Welsch multiple range test results; WHS = Whitsand high shore; WLS = Whitsand low shore; *E/E E/E*, *E/E = edulis* mussels; *E/G E/G*, *E/G = putative F1* mussels; *G/G G/G*, *G/G = galloprovincialis* mussels.

cantly different from that for Whitsand mussels (mean  $\pm$  SD of  $-10.842 \pm 4.343$ ,  $n = 2$ , at Croyde;  $-9.246 \pm 0.771$ ,  $n = 2$ , at Whitsand;  $t = -0.210$ ,  $df = 33$ ,  $P > 0.05$ ).

A relative viability coefficient for each genotype (Table VIII) was calculated from the data in Tables VI and VII. A genotype frequency estimate among young mussels ( $GF_{\text{young}}$ ) was obtained from the mean genotype frequency of the first three years for which data were available. For example, for *E/E E/E* mussels of CHS, this value is the mean of the frequency values for individuals of ages 4, 5, and 6 years (*i.e.*,  $[0.93 + 0.97 + 0.97]/3 = 0.957$ ) shown in Table VII. For *E/G E/G* mussels of CLS, the value is the mean genotype frequency of individuals of ages 3, 4, and 5 years (*i.e.*,  $[0 + 0 + 0.08]/3 = 0.027$ ) shown in Table VII. Similarly, the genotype frequency among the oldest individuals ( $GF_{\text{old}}$ ) was calculated as the mean for the last three years for which data were available. For example, for all genotypes at CHS, this is the mean frequency of 9, 10, and 11 years of age; for all genotypes at CLS, it is the mean frequency of 8, 9, and 10 years of age. Mean gene frequencies were calculated to reduce the

problem of small sample sizes among the youngest and oldest mussels. Comparison of gene frequencies estimated in this way could lead to conservative estimates of viability compared with values obtained using the youngest and oldest individuals owing to the pooling of data from three year classes. However, the greatest rate of change in genotype frequencies occurs among mussels of intermediate ages and not among the oldest or youngest mussels used for this calculation. In each case, an absolute viability coefficient was obtained by dividing  $GF_{\text{old}}$  by  $GF_{\text{young}}$ . Relative viability coefficients were obtained by dividing each absolute viability coefficient by the highest observed value of all absolute viability coefficients among the three genotypes to give one relative viability coefficient value of 1.000 and two others as proportions of 1.000. The relative viability coefficients calculated in this way should not be confused with coefficients estimated for the interval from zygote to reproductive maturity, but they nevertheless give some indication of relative viability and mortality during much of adult life. At all four locations, the relative viability coefficient of *galloprovincialis* is much higher than that of *edulis* (Table VIII).

## Discussion

In S.W. England, *M. galloprovincialis* is presumed to be at the northernmost limit of its distribution (Seed, 1971; Gosling, 1984). For sites in England, it may therefore be predicted that the endemic cold-water *M. edulis* form should have a growth advantage over the warm-water *M. galloprovincialis* form. At  $<20^{\circ}\text{C}$  in the laboratory, Seed (1971) found that *M. edulis* grew up to four times faster than *M. galloprovincialis* from Rock, S.W. England. However, he was doubtful if these differences would be maintained under natural conditions. Using a larger data set taken from mussels, since their settlement, had been growing at high and low shore locations in two hybrid populations in S.W. England, we have shown that *galloprovincialis* has a small but significant growth advantage over *edulis*.

The negative correlation between *E* allele frequency and age lends support to the third hypothesis, advanced by Skibinski (1983), that differential mortality acts against the more numerous and smaller *edulis*. The most pronounced changes in length-dependent allele frequencies occur at older ages (8–9 years at CHS and WHS, 6–8

Table V

Parameters of the polynomial regressions for genotype-dependent best-fit growth curves

Location	Genotype	Intercept	Linear term	Square term ( $\times 10$ )	Cubic term ( $\times 10$ )	$R^2$
CHS	<i>E/E E/E</i>	-1.842	7.590	-6.697	0.228	0.898
	<i>E/G E/G</i>	-0.293	6.041	-1.647	-0.069	0.947
	<i>G/G G/G</i>	-1.708	7.064	-3.485	0.002	0.944
CLS	<i>E/E E/E</i>	-3.102	10.350	-9.716	0.410	0.953
	<i>E/G E/G</i>	-1.151	7.632	0.014	-0.462	0.951
	<i>G/G G/G</i>	-3.074	10.138	-7.913	0.235	0.956
WHS	<i>E/E E/E</i>	-0.146	6.554	-4.319	0.169	0.896
	<i>E/G E/G</i>	-2.301	8.528	-5.768	0.152	0.920
	<i>G/G G/G</i>	-1.062	6.866	-1.165	-0.113	0.943
WLS	<i>E/E E/E</i>	-1.648	9.161	-7.914	0.311	0.866
	<i>E/G E/G</i>	-1.016	7.890	-2.154	-0.097	0.921
	<i>G/G G/G</i>	-2.344	8.796	-3.449	-0.032	0.934

CHS, CLS = Croyde high shore, Croyde low shore; WHS, WLS = Whitsand high shore, Whitsand low shore; *E/E E/E* = *edulis* mussels; *E/G E/G* = putative F1 mussels; *G/G G/G* = *galloprovincialis* mussels;  $R^2$  = coefficient of determination.

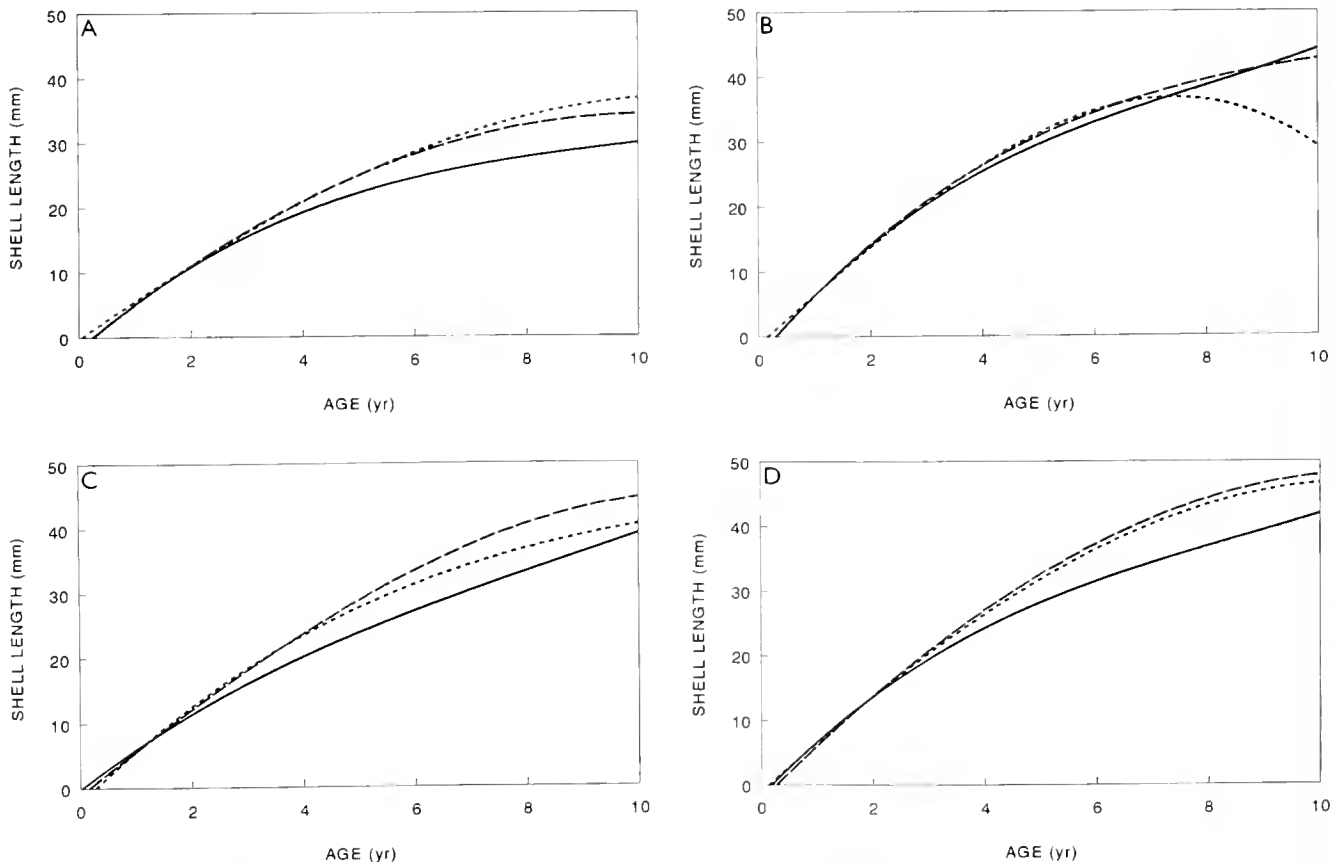


Figure 1. Best-fit polynomial growth curves for *edulis* (*E/E E/E*) (solid line), F1 hybrid (*E/G E/G*) (dotted line), and *galloprovincialis* (*G/G G/G*) (broken line) mussels, at (A) Croyde high shore, (B) Croyde low shore, (C) Whitsand high shore, and (D) Whitsand low shore.

Table VI

Predicted genotype frequencies as a function of age (calculated from electrophoretic and external annual shell check mark data) for mussels from Croyde (see Table II for further explanation)

Age (yr)	CHS			N	CLS			N
	E/E E/E	E/G E/G	G/G G/G		E/E E/E	E/G E/G	G/G G/G	
3	—	—	—	—	1.00	0	0	3
4	0.93	0	0.07	7	1.00	0	0	19
5	0.97	0.03	0	14	0.90	0.08	0.02	20
6	0.97	0.02	0.01	25	0.82	0.03	0.15	26
7	0.73	0.16	0.11	17	0.29	0.29	0.42	25
8	0.74	0.19	0.07	11	0.27	0.08	0.65	15
9	0.37	0	0.63	9	0.05	0	0.94	14
10	0.47	0.53	0	6	0	0	1.00	8
11	0.19	0	0.81	4	—	—	—	—
Total				93				130

CHS, CLS = Croyde high shore, Croyde low shore; E/E E/E = *edulis* mussels; E/G E/G = putative F1 mussels; G/G G/G = *galloprovincialis* mussels; N = number of mussels.

years at CLS and at WLS: Tables VI and VII), whereas the most pronounced differences in length-at-age values occur earlier (significant differences exist by 4 years of age at CLS and WHS, and by 5 years at CHS and WLS). Differential growth therefore begins several years before the greatest differences in genotype frequencies are generated, so that differential growth cannot be solely responsible for the length-dependent changes in allele frequencies. Thus, small but significant differences in length-at-age values are insufficient by themselves to explain the pronounced decrease in compound E allele frequency, even though the growth differences must contribute (slightly) to this phenomenon.

Significant differences in length-at-age values are observed at age 4 years and older and among intermediate-aged, but not the very oldest, mussels. This can be partially explained by the small sample sizes of the oldest mussels, but examination of the maximum difference in length-at-age indicates that this parameter increases with age, reaches its greatest values at intermediate ages, and then decreases among the oldest age classes. A threefold explanation for this can be advanced. First, up to about 4 years of age, length-at-age values are not significantly different between the genotypes, and viability differences are small (e.g., Gardner and Skibinski, 1988; Figs. 2 and 3 of the present paper). Second, at intermediate ages, signifi-

Table VII

Predicted genotype frequencies as a function of age (calculated from electrophoretic and external annual shell check mark data) for mussels from Whitsand (see Table II for further explanation)

Age (yr)	WHS			N	WLS			N
	E/E E/E	E/G E/G	G/G G/G		E/E E/E	E/G E/G	G/G G/G	
3	—	—	—	—	1.00	0	0	4
4	1.00	0	0	1	0.65	0.35	0	8
5	1.00	0	0	9	0.98	0	0.02	26
6	0.96	0.04	0	28	0.84	0.14	0.02	23
7	0.73	0.10	0.17	25	0.72	0.25	0.03	29
8	0.72	0.18	0.10	10	0.47	0.42	0.11	18
9	0.33	0.16	0.51	13	0.15	0.25	0.60	9
10	0.33	0.33	0.34	3	0	0.56	0.44	7
11	0	0.58	0.42	4	0.33	0.67	0	3
12	0.49	0.28	0.23	3	—	—	—	—
13	0	0.56	0.44	2	—	—	—	—
Total				98				127

WHS, WLS = Whitsand high shore, Whitsand low shore; E/E E/E = *edulis* mussels; E/G E/G = putative F1 mussels; G/G G/G = *galloprovincialis* mussels; N = number of mussels.

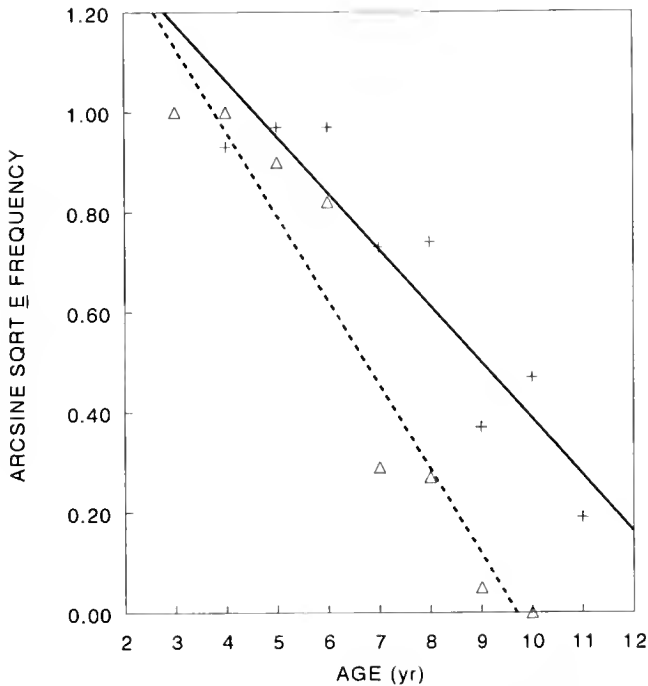


Figure 2. Arcsine square root compound *E* allele frequency as a function of age at Croyde high shore (+ and solid line) and Croyde low shore ( $\Delta$  and broken line).

cant length-at-age differences exist between the genotypes. It is at this stage that viability differences between the genotypes are most pronounced, resulting in greatest differential mortality of *edulis* mussels. Third, following this period of maximum differential mortality, the oldest surviving mussels exhibit nonsignificant differences in length-at-age values. Thus, during the second stage, the highest mortality rates are experienced by the *edulis* individuals with the lowest viabilities (and also the smallest length-at-age values), resulting in the significant differences in mean length-at-age values observed at this time. The *edulis* with (by definition) the highest viabilities (and the greatest length-at-age values) survive this period so that among the oldest age classes, when viability differences are once again less pronounced, there are no significant differences in length-at-age values. The positive association between length-at-age values and viability among the *edulis* individuals can be explained in one of two ways. One, the association is noncausal, resulting from, for example, pleiotropy (e.g., Falconer, 1989). Two, it is causal, and occurs because increased shell length offers a refuge from predators (Gardner and Skibinski, 1991) and confers a fitness advantage in terms of increased byssal strength of attachment to the substrate, which decreases the chance of being dislodged from the rock face and swept out to sea (Gardner and Skibinski, 1991; Willis and Skibinski, 1992).

Based on genotype frequency differences between young and old mussels, relative viability coefficients were calculated that demonstrate a high selective mortality against *edulis*. Increasingly more evidence points to the conclusion that strong selection is common in natural populations (Endler, 1986), and that selection coefficients in hybrid zones can also be very large (e.g., Dowling and Moore, 1985; Barton and Hewitt, 1985; Hewitt, 1988). The relative viability coefficients estimated in this study indicate that selection against *edulis* is indeed strong—at all four locations *edulis* had viability coefficients that are orders of magnitude smaller than those of *galloprovincialis*. The extent of the coefficient differences between *edulis* and *galloprovincialis* is strong support for the hypothesis of differential viability (Skibinski, 1983) as an explanation for the pattern of length-dependent allele frequencies.

Mussels reproduce by external fertilization, producing pelagic larvae that are almost all immigrants at the time of settlement (Tracey et al., 1975). Because components of fitness such as viability and fecundity are much lower in *edulis* than in *galloprovincialis*, considerable immigration of *edulis* spat is required to maintain the genetic structure of these populations, which are characterized by a very high frequency of *edulis* among the smallest and youngest mussels (Skibinski, 1983; Gardner and Skibinski, 1988). Furthermore, this genetic structure is apparently stable in the short term (over a period of 6 years), an

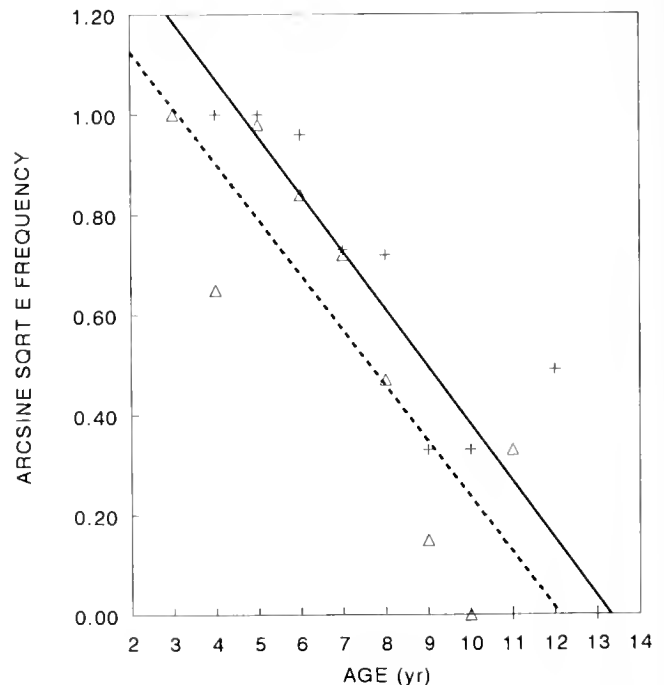


Figure 3. Arcsine square root compound *E* allele frequency as a function of age at Whitsand high shore (+ and solid line) and Whitsand low shore ( $\Delta$  and broken line).

Table VIII

Genotype-dependent relative viability coefficients for high and low shore locations at Croyde and Whitsand, calculated from the data of age-dependent variation given in Tables VII and VIII

	CHS			CLS		
	E/E E/E	E/G E/G	G/G G/G	E/E E/E	E/G E/G	G/G G/G
GF <sub>young</sub>	0.957	0.017	0.027	0.967	0.027	0.007
GF <sub>old</sub>	0.343	0.177	0.480	0.107	0.027	0.863
Absolute viability	0.358	10.412	17.778	0.111	1.000	123.286
Relative viability	0.020	0.586	1.000	0.001	0.008	1.000

	WHS			WLS		
	E/E E/E	E/G E/G	G/G G/G	E/E E/E	E/G E/G	G/G G/G
GF <sub>young</sub>	0.987	0.013	0.001*	0.877	0.117	0.007
GF <sub>old</sub>	0.163	0.473	0.363	0.160	0.493	0.347
Absolute viability	0.165	36.385	363.000	0.182	4.213	49.571
Relative viability	0.0005	0.100	1.000	0.004	0.085	1.000

CLS, CHS = Croyde low shore, Croyde high shore; WLS, WHS = Whitsand low shore, Whitsand high shore; E/E E/E = *edulis* mussels; E/G E/G = putative F1 mussels; G/G G/G = *galloprovincialis* mussels; GF<sub>young</sub>, GF<sub>old</sub> = gene frequencies among the young and old mussels; \* = actual mean value of zero, assumed value of 0.001.

interval representing a minimum 50% turnover in population numbers (Gardner and Skibinski, 1988). Thus our data (Gardner and Skibinski, 1988, 1990a, and this paper) indicate that these sympatric *Mytilus* populations in S.W. England are maintained by a balance between the differential viability acting against *edulis* and the predominance of *edulis* spat among immigrants. One reason for a very low proportion of *galloprovincialis* spat, despite their pronounced viability advantage over *edulis*, is that *M. galloprovincialis* reaches its northernmost limit in S.W. England and is apparently restricted from successfully settling further north by the lower seawater temperatures. This is indeed the case for most other warm-water Mediterranean forms that extend this far north (Yonge, 1949).

The mechanism responsible for greater *edulis* mortality is thought to involve genotype-dependent differences in strength of attachment of the byssus (Gardner and Skibinski, 1991; Willis and Skibinski, 1992). At both Croyde and Whitsand, at all shell lengths, *edulis* are more easily removed from the substrate than *galloprovincialis* of the same length. This results in part from morphological differences between the two mussel types and is consistent with evolutionary trends observed in lineages of byssally attached bivalves (Yonge and Campbell, 1968). Differences attributable to wave exposure have been reported in the ecological distributions of the two mussel types in S.W. England (Skibinski, 1983; Gardner and Skibinski, 1988), the Atlantic coast of France (Seed, 1972), and southern Ireland (Gosling and Wilkins, 1981) where *galloprovincialis* frequency is positively correlated with increasing wave exposure. At the microgeographic level

among sympatric populations in S.W. England, *galloprovincialis* frequency is greatest in the high shore and least in the low shore; this distribution is significantly correlated with site-specific variability in wave action (Skibinski, 1983; Gardner and Skibinski, 1988). Thus, differences in strength of attachment between the two species are consistent with the relationship between wave exposure and the ecological distribution of the two mussel types (Gardner and Skibinski, 1991).

#### Acknowledgments

We thank Drs. Ray Thompson and Bruce MacDonald for comments on the manuscript, and Eric Roderick, Donna Gardner, and Paul Schembri for technical assistance. This research was supported in part by a NERC Studentship to JPAG.

#### Literature Cited

- Barton, N. H., and G. M. Hewitt. 1985. Analysis of hybrid zones. *Ann Rev Ecol Syst* 16: 113-148.
- Barton, N. H., and G. M. Hewitt. 1989. Adaptation, speciation and hybrid zones. *Nature* 341: 497-503.
- Beaumont, A. R., R. Seed, and P. Garcia-Martinez. 1989. Electrophoretic and morphometric criteria for the identification of the mussels *Mytilus edulis* and *M. galloprovincialis*. Pp. 251-258 in *Reproduction, Genetics and Distributions of Marine Organisms*, J. S. Ryland and P. A. Tyler, eds. Proc. 23rd European Marine Biology Symposium, University of Wales, Swansea. Olsen and Olsen, Fredensborg, Denmark.
- Day, R. W., and G. P. Quinn. 1989. Comparisons of treatments after an analysis of variance in ecology. *Ecol Monogr* 59: 433-463.

- Dickie, L. M., P. R. Boudreau, and K. R. Freeman. 1984. Influences of stock and site on growth and mortality in the blue mussel (*Mytilus edulis*). *Can. J. Fish. Aquat. Sci.* **41**: 134-140.
- Dowling, T. E., and W. S. Moore. 1985. Evidence for selection against hybrids in the Family Cyprinidae (Genus *Notropis*). *Evolution* **39**: 152-158.
- Endler, J. A. 1986. Natural selection in the wild. *Monographs in Population Biology*, 21. Princeton University Press, Princeton, NJ.
- Falconer, D. S. 1989. *Introduction to Quantitative Genetics*. 3rd ed. Longman Scientific and Technical, Harlow, England.
- Gardner, J. P. A., and D. O. F. Skibinski. 1988. Historical and size-dependent genetic variation in hybrid mussel populations. *Heredity* **61**: 93-105.
- Gardner, J. P. A., and D. O. F. Skibinski. 1990a. Genotype-dependent fecundity and temporal variation of spawning in hybrid mussel (*Mytilus*) populations. *Mar. Biol.* **105**: 153-162.
- Gardner, J. P. A., and D. O. F. Skibinski. 1990b. Thermostability differences of allozyme loci in *Mytilus edulis*, *M. galloprovincialis* and hybrid mussels. *Mar. Ecol. Prog. Ser.* **64**: 99-105.
- Gardner, J. P. A., and D. O. F. Skibinski. 1991. Biological and physical factors influencing genotype-dependent mortality in hybrid mussel populations. *Mar. Ecol. Prog. Ser.* **71**: 235-243.
- Gosling, E. M. 1984. The systematic status of *Mytilus galloprovincialis* in western Europe: a review. *Malacologia* **25**: 551-568.
- Gosling, E. M., and N. P. Wilkins. 1981. Ecological genetics of the mussels *Mytilus edulis* and *Mytilus galloprovincialis* on Irish coasts. *Mar. Ecol. Prog. Ser.* **4**: 221-227.
- Grant, W. S., and M. I. Cherry. 1985. *Mytilus galloprovincialis* Lmk. in Southern Africa. *J. Exp. Mar. Biol. Ecol.* **90**: 179-191.
- Harrison, R. G. 1990. Hybrid zones: windows on evolutionary process. *Oxf. Surv. Evol. Biol.* **7**: 69-128.
- Hewitt, G. M. 1988. Hybrid zones—natural laboratories for evolutionary studies. *Trends Ecol. Evol.* **3**: 158-167.
- Hewitt, G. M. 1989. The subdivision of species by hybrid zones. Pp. 85-110 in *Speciation and Its Consequences*, D. Otte and J. Endler, eds. Sinauer Associates, Sunderland, MA.
- Lutz, R. A. 1976. Annual growth patterns in the inner shell of *Mytilus edulis*. *J. Mar. Biol. Ass. U.K.* **56**: 723-731.
- MacDonald, B. A., and R. J. Thompson. 1985. Influence of temperature and food availability on the ecological energetics of the giant scallop *Placopecten magellanicus*. I. Growth rates of shell and somatic tissue. *Mar. Ecol. Prog. Ser.* **25**: 279-294.
- MacDonald, B. A., and R. J. Thompson. 1988. Intraspecific variation in growth and reproduction in latitudinally differentiated populations of the giant scallop *Placopecten magellanicus*. *Biol. Bull.* **175**: 361-371.
- Mallet, A. L., C. E. A. Carver, S. S. Coffen, and K. R. Freeman. 1987. Winter growth of the blue mussel *Mytilus edulis* L.: importance of stock and site. *J. Exp. Mar. Biol. Ecol.* **108**: 217-228.
- Moore, W. S. 1977. An evaluation of narrow hybrid zones in vertebrates. *Quart. Rev. Biol.* **52**: 263-277.
- Moore, W. S., and D. B. Buchanan. 1985. Stability of the Northern Flicker hybrid zone in historical times: implications for adaptive theory. *Evolution* **39**: 135-151.
- Moore, W. S., and W. D. Koenig. 1986. Comparative reproductive success of yellow-shafted, red-shafted and hybrid flickers across a hybrid zone. *The Auk* **103**: 42-51.
- Rice, W. R. 1989. Analyzing tables of statistical tests. *Evolution* **43**: 223-225.
- Richardson, C. A., D. J. Crisp, and N. W. Runham. 1979. Tidally deposited growth bands in the shell of the common cockle *Cerastoderma edule* (L.). *Malacologia* **18**: 277-290.
- Roff, D. A. 1980. A motion for the retirement of the von Bertalanffy function. *Can. J. Fish. Aquat. Sci.* **37**: 127-129.
- Sanjuan, A., H. Quesada, C. Zapata, and G. Alvarez. 1990. On the occurrence of *Mytilus galloprovincialis* Lmk. on the N.W. coast of the Iberian Peninsula. *J. Exp. Mar. Biol. Ecol.* **143**: 1-14.
- SAS Institute. 1987. *SAS/STAT Guide for Personal Computers*. Release 6.03 ed. Cary, NC.
- Seed, R. 1971. A physiological and biochemical approach to the taxonomy of *Mytilus edulis* L. and *Mytilus galloprovincialis* (Lmk.). *Cah. Biol. Mar.* **12**: 291-322.
- Seed, R. 1972. Morphological variations in *Mytilus* from the French coasts in relation to the occurrence and distribution of *Mytilus galloprovincialis* (Lmk.). *Cah. Biol. Mar.* **13**: 357-384.
- Seed, R. 1974. Morphological variations in *Mytilus* from the Irish coasts in relation to the occurrence and distribution of *Mytilus galloprovincialis* (Lmk.). *Cah. Biol. Mar.* **15**: 1-25.
- Skibinski, D. O. F. 1983. Natural selection in hybrid mussel populations. Pp. 283-298 in *Protein Polymorphism: Adaptive and Taxonomic Significance*, G. S. Oxford and D. Rollinson, eds. Systematics Association Special Volume 24, Academic Press, London.
- Skibinski, D. O. F., and J. A. Beardmore. 1979. A genetic study of intergradation between *Mytilus edulis* and *Mytilus galloprovincialis*. *Experientia* **35**: 1442-1444.
- Skibinski, D. O. F., and E. E. Roderick. 1989. Heterozygosity and growth in transplanted mussels. *Mar. Biol.* **102**: 73-84.
- Skibinski, D. O. F., and E. E. Roderick. 1991. Evidence of selective mortality in favour of the *Mytilus galloprovincialis* Lmk phenotype in British mussel populations. *Biol. J. Linn. Soc.* **42**: 351-366.
- Skibinski, D. O. F., M. Ahmad, and J. A. Beardmore. 1978a. Genetic evidence for naturally occurring hybrids between *Mytilus edulis* and *Mytilus galloprovincialis*. *Evolution* **32**: 354-364.
- Skibinski, D. O. F., J. A. Beardmore, and M. Ahmad. 1978b. Genetic aids to the study of closely related taxa of the genus *Mytilus*. Pp. 469-486 in *Marine Organisms: Genetics, Ecology and Evolution*, B. Battaglia and J. A. Beardmore, eds. Plenum Press, New York.
- Skibinski, D. O. F., J. A. Beardmore, and T. F. Cross. 1983. Aspects of the population genetics of *Mytilus* (Mytilidae: Mollusca) in the British Isles. *Biol. J. Linn. Soc.* **19**: 137-183.
- Sokal, R. R., and F. J. Rohlf. 1981. *Biometry*. 2nd ed. W. H. Freeman and Company, San Francisco.
- Tracey, M. L., N. F. Bellet, and C. D. Gravem. 1975. Excess homozygosity and breeding population structure in the mussel *Mytilus californianus*. *Mar. Biol.* **32**: 303-311.
- Willis, G. L., and D. O. F. Skibinski. 1992. Variation in strength of attachment to the substrate explains differential mortality in hybrid mussel (*Mytilus galloprovincialis* and *M. edulis*) populations. *Mar. Biol.* **112**: 403-408.
- Yonge, C. M. 1949. *The Sea Shore*. Collins, New Naturalist Series, London.
- Yonge, C. M., and J. I. Campbell. 1968. On the heteromyarian condition in the Bivalvia with special reference to *Dreissena polymorpha* and certain Mytiliacea. *Trans. R. Soc. Edinb.* **68**: 21-43.

# Suspension Feeding by the Lophophore-like Apparatus of the Pterobranch Hemichordate *Rhabdopleura normani*

KENNETH M. HALANYCH

*Department of Zoology, University of Texas at Austin, Austin, Texas 78712\*, Bermuda Biological Station for Research, 17 Biological Lane, Ferry Reach, GE01, Bermuda, and Friday Harbor Laboratories, University of Washington, 620 University Road, Friday Harbor, Washington 98250*

**Abstract.** Selective forces acting on feeding mechanisms have played an important role in the evolution of metazoans. To develop a more accurate understanding of the evolution of feeding within the deuterostome and lophophorate clades, I used video analysis and electron microscopy to examine suspension-feeding behavior and ciliation patterns in *Rhabdopleura normani*, a pterobranch hemichordate. In *R. normani*, local reversals of ciliary beat capture food particles, and the normal feeding activity does not involve the use of mucus to capture particles. Also, several different methods of particle rejection are identified. Lateral, frontal, and frontolateral ciliary bands, which are composed of cilia 8–13  $\mu\text{m}$  in length, are present on the tentacles. In *R. normani* from Bermuda, ciliated perforations occur along the length of the arms, specifically between the bases of adjacent tentacles. These structures are previously undescribed in suspension-feeding organisms. My findings are consistent with the hypothesis that the tentaculated arms of pterobranchs are homologous to the lophophores of brachiopods, phoronids, and bryozoans. The similarities in the feeding biology of these groups are discussed.

## Introduction

The course of evolution within a taxon can be greatly influenced by selective forces on feeding mechanics and morphology. The classic examples of the Cichlidae (Liem, 1973) and Darwin's finches (Darwin, 1972; Grant, 1986) demonstrate that major shifts in diet and food acquisition

can occur in a relatively short time. Feeding morphology and methods of feeding may also be correlated with the origin and divergence of phyla. To determine whether this is the case, I am analyzing the evolution of feeding within the deuterostome and lophophorate clades. Because information about the feeding of both deuterostome and lophophorate taxa is essential to this analysis, this paper will focus on pterobranch hemichordates.

Pterobranchs are a class of marine hemichordates that suspension feed with ciliated tentacles. Unfortunately, our knowledge of pterobranch feeding biology is very limited. Gilmour (1979) and Stebbing and Dilly (1972) provided some observations on the feeding of living *Rhabdopleura compacta*, and Lester (1985) commented on *Cephalodiscus gracilis* feeding. In the pterobranch *Rhabdopleura normani*, I examined the flow of water around the tentacles, the method of particle capture, methods of particle rejection, and the ciliation pattern of the tentacles. Because some workers assert that the pterobranch feeding apparatus is homologous to the lophophore of brachiopods, bryozoans, and phoronids (Hyman, 1959; Gilmour, 1979; Hoverd, 1985; Lester, 1985; Dilly *et al.*, 1986; Nielsen, 1987), my findings are compared to reports on these taxa (Strathmann, 1973; Gilmour, 1978). There are several similarities between these groups, including patterns of ciliation, use of ciliary reversal in particle capture, similar rejection mechanisms, and similar morphologies.

*R. normani* is a colonial sessile organism that lives on the underside or protected regions of hard substrates (e.g., rocks, coralline rubble, concrete slabs). The entire adult animal is approximately 3 mm in length with tentaculated arms that are 1.5 mm long. A coenecium is secreted by the cephalic shield which also serves a locomotory func-

Received 28 September 1992; accepted 24 September 1993.

\* Present address.

tion similar to a molluscan foot. The individuals within the coenecium occupy separate compartments but are connected by an organic stolon. *R. normani* in Bermuda is found in shallow water areas (1–10 m in depth) that are characterized by high flow and limited particulate matter content.

### Materials and Methods

I collected *Rhabdopleura normani* from subtidal areas by free diving under The Causeway bridge in Bermuda, and transported them to Bermuda Biological Station for Research for subsequent observation (see Lester, 1988, for a description of the Bermudan *R. normani*). Feeding was observed with a Wild dissecting scope and a Panasonic video camera. Zooids were examined both within, and removed from, their tubes. Because the zooids were very sensitive to vibrations, I also observed individuals relaxed in a 1:1 mixture of 7.5% MgCl<sub>2</sub> and filtered seawater. This method of relaxation had no noticeable effect on ciliary function or mechanics. Zooids were fed a combination of carbon particles and calcium carbonate particles that varied in size from 10 to 200  $\mu\text{m}$  and were easily ingested. I also used the algae *Dunaliella tertiolecta* (approximately  $4 \times 10 \mu\text{m}$ ) and *Tetraselimis chuii* (approximately  $7 \times 13 \mu\text{m}$ ) to track particle movement and capture. Particle motions were also recorded on video tape so that they could be assessed more accurately.

For microscopy, several specimens were relaxed and preserved in either one-third strength Bouin's fixative or 1% glutaraldehyde. Scanning electron microscopy (SEM) specimens were post-fixed with 2% osmium tetroxide, dehydrated in ethanol, and transferred to 2,2-dimethoxypropane before being critical-point dried in carbon dioxide. The specimens were then sputter coated with a gold palladium alloy, and observed with a JEOL-JSM35 scanning microscope. TEM specimens were post-fixed in 2% osmium tetroxide, dehydrated in ethanol, and transferred to propylene oxide before being embedded in an Epon-Araldite mixture. A Siemens Elmiskop IA transmission microscope was used to examine thin sections, and standard light microscopy techniques were used with thick sections.

### Results

The suspension-feeding apparatus of *R. normani* consists of numerous tentacles attached to each of two arms. Depending on the contractile state of the zooid, the arms of average mature zooids range from 500 to 1500  $\mu\text{m}$  in length, and 45 to 120  $\mu\text{m}$  in width. The tentacles are 200–500  $\mu\text{m}$  in length and 10–15  $\mu\text{m}$  in diameter. A commissure of tissue connecting adjacent tentacles near their bases (further described below) creates a series of perforations along the length of the arm. To feed, the zooid moves to

the tube aperture, primarily by means of the cephalic shield, and then perches on the rim of the aperture with the anterior lobe of the cephalic shield overhanging the rim of the tube. The role of the cephalic shield in feeding is unclear, but the dense ciliation on the dorsal surface of the shield suggests its involvement in particle manipulation near the mouth. The zooid extends the two feeding arms in line with the tube (*i.e.*, straight extension), but several individuals were observed to curl their arms posteriorly. Once extended, the arms were spread slightly to form a 30–35° angle when viewed from the frontal surface of the arm (Fig. 1). The tentacles are extended such that the profile of an arm viewed end on is V-shaped. Individuals not treated with MgCl<sub>2</sub> showed active tentacle flicking behavior. I was not able to ascertain whether this behavior was involved in either particle rejection or particle capture.

### Morphology

Both SEM and light microscopy reveal four distinct bands of cilia running longitudinally along each ten-

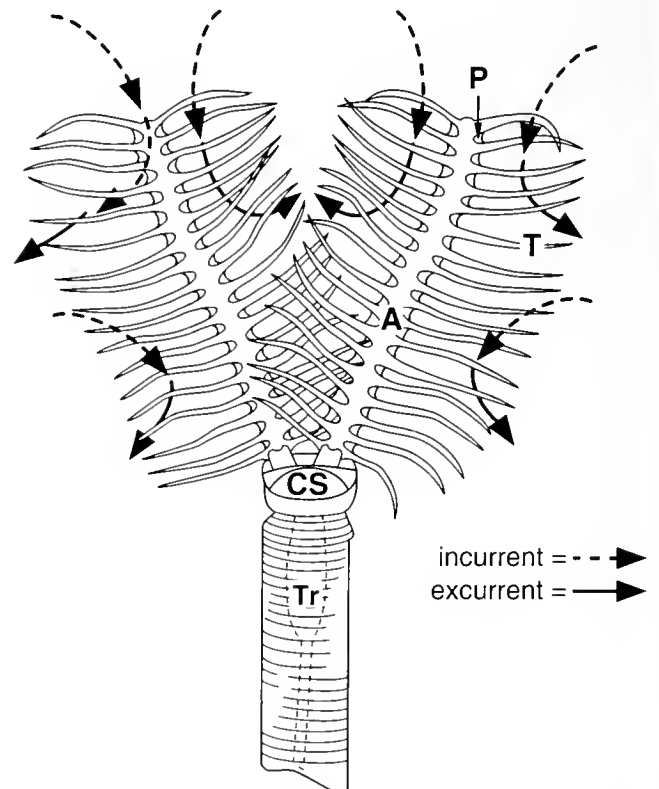


**Figure 1.** The gross morphology and the feeding position of a zooid is shown from an anterior perspective (the arms are topologically dorsal). The tentacular apparatus consists of two main parts, tentacles and arms. The general incurrent flow of water across the feeding apparatus passes from the frontal ciliated surface of the arms and tentacles to the abfrontal surface. The water is then moved posteriorly away from the apparatus as excurrent flow. Broken arrows depict unfiltered water and solid arrows depict filtered water. A—arm, CS—cephalic shield, P—perforation, T—tentacle, Tr—trunk.



tacle. Prominent lateral cilia, 10–13  $\mu\text{m}$  in length, make up two of the ciliated bands (Fig. 2a). My findings confirm Nielsen's (1987) report that these bands are composed of two rows of monociliated cells. Two additional rows of single cilia are present in the frontolateral position of the tentacles (Fig. 2b). These cilia are slightly shorter, about 8–10  $\mu\text{m}$ . Finally some sparse frontal cilia (8–10  $\mu\text{m}$ ) are also present. There are no ciliated tracts on the abfrontal surface of the tentacle. All three types

of ciliated bands are represented in Figure 2c, which is a TEM of a tentacle in cross-section. Microvilli completely cover the tentacle as well as the frontal surface of the arm (Fig. 2d). My findings corroborate those of Gilmour (1979) in *R. compacta* and Dilly *et al.* (1986) in *Cephalodiscus gracilis*.

The frontal surface of the arms is densely ciliated throughout its length (Fig. 3a). I was not able to discern whether these cilia formed one large ciliated

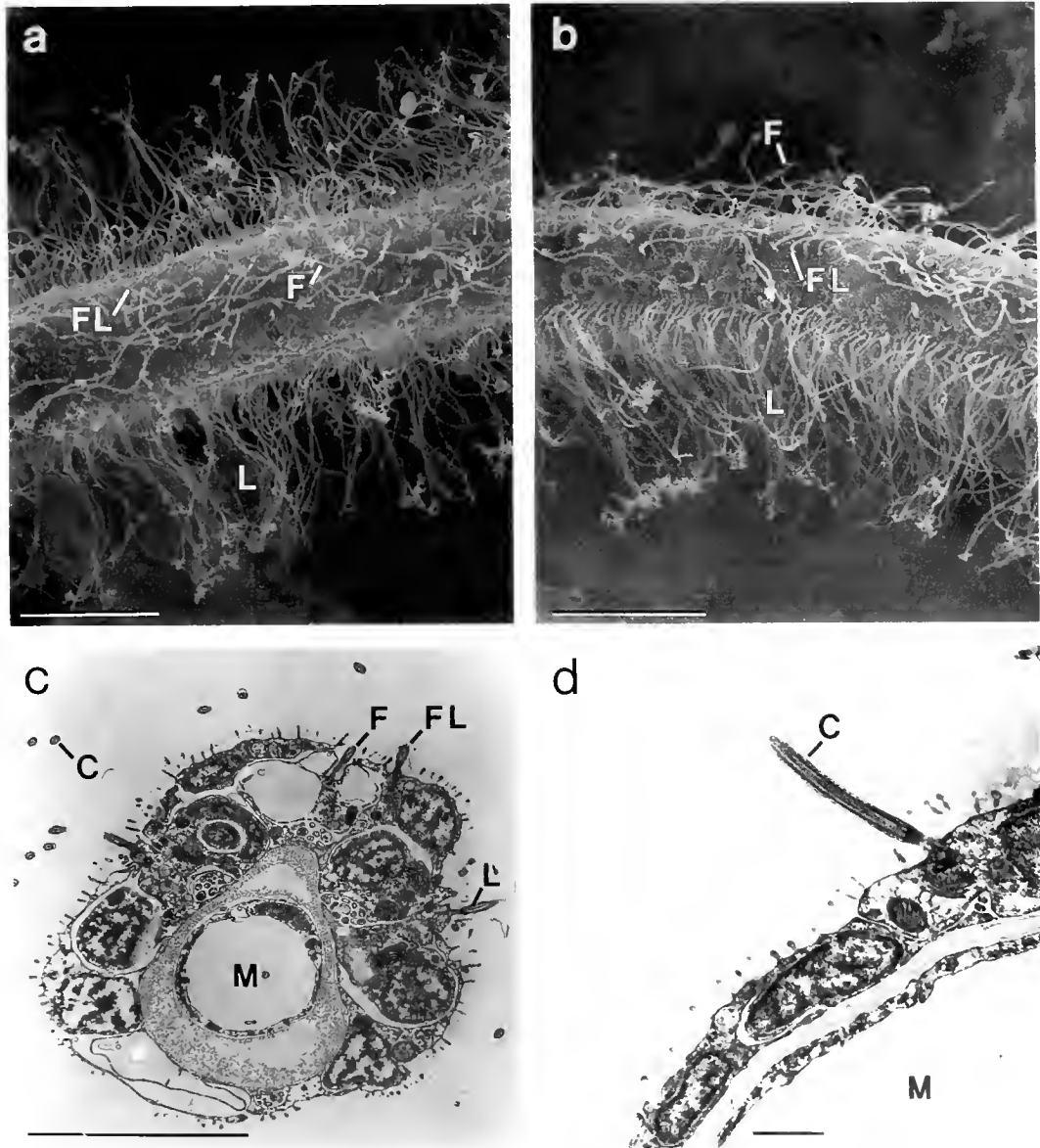


**Figure 2.** Ciliation patterns on the tentacle and arm of *Rhabdopleura normani*. (A) SEM of tentacle in frontal view reveals the ciliary pattern (scale bar = 10  $\mu\text{m}$ ). (B) SEM of tentacle in lateral view (scale bar = 10  $\mu\text{m}$ ). (C) TEM of tentacle in cross section (scale bar = 10  $\mu\text{m}$ ). A frontal and a right frontolateral cilium are shown, but the corresponding left frontolateral cilium is not. (D) TEM of the arm in cross section showing the frontal surface. Note the numerous microvilli (scale bar = 1  $\mu\text{m}$ ). C—cilium, F—frontal cilia, FL—frontolateral cilia, L—lateral cilia, M—mesocoelom.

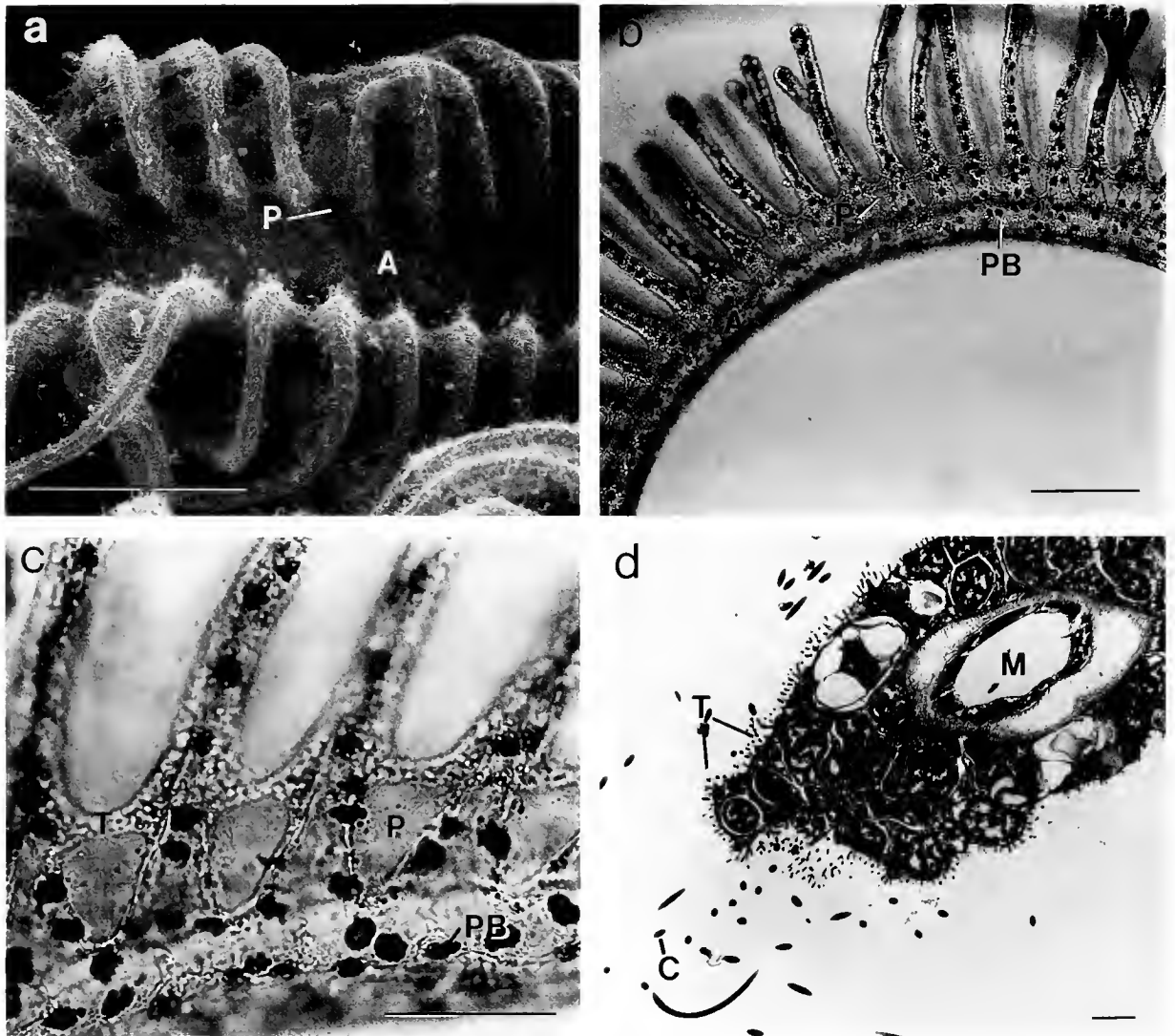


**Figure 3.** Perforations at the base of the tentacles. (A) A frontal view of the arm (SEM) showing the dense ciliation and the ciliated perforations between the bases of the tentacles (scale bar = 100  $\mu$ m). (B) A light micrograph of an arm viewed from the side showing the distribution of the pigmented bodies and the location of the perforations (scale bar = 100  $\mu$ m). (C) A light micrograph of the ciliated perforations at high magnification (scale bar = 50  $\mu$ m). (D) A tentacular cross section (TEM) that partially includes the tissue bridge delimiting the perforation. Cross sections of cilia along the length of the bridge are also obvious (scale bar = 1  $\mu$ m). A—arm, C—cilium, P—perforation, PB—pigmented body, M—mesocoelom, T—tissue commissure.

tract or several smaller ciliated fields. Because of their orientation when viewed with the SEM and light microscope, the cilia were difficult to measure; nevertheless, they appeared to be about 10–12  $\mu$ m in length.

Perforations are present between the bases of adjacent tentacles and are formed by a commissure of tissue that connects the tentacles (Fig. 3b). These perforations are 10–25  $\mu$ m in height and 10–14  $\mu$ m in width (Fig. 3c). The commissure that delimits the distal por-

tion of each hole is composed of cellular components (Fig. 3d) and cilia are present along the rim of the aperture. Presumably, the flow of water around the arm and tentacle bases is affected by this series of perforations.

Dark pigmented bodies (Fig. 3b, c) and cilia are distributed over the entire epidermis of *R. normani*. These bodies are especially visible in the tentaculated region where the surrounding tissue is translucent, but their function and composition are not known.

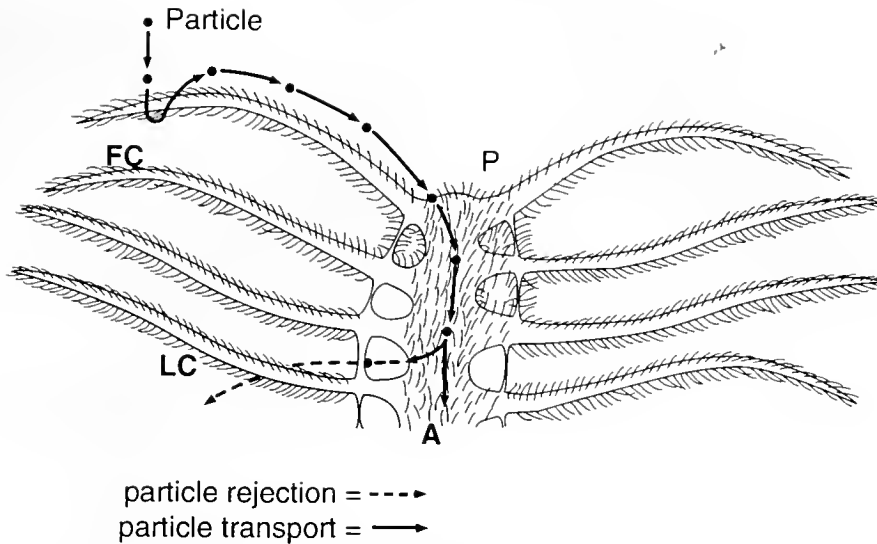


**Figure 4.** Particles are captured by local reversal in beat of the lateral cilia. Particles are then transported down the tentacle to the arm by the frontal and frontolateral cilia. Once on the arm, the particle can be rejected through one of the perforations, or sent to the mouth for ingestion. Note: in this diagram, the number of cilia on the feeding apparatus has been reduced to increase the clarity. A—arm, FC—frontal and frontolateral cilia, LC—lateral cilia, P—perforation.

### Feeding

The direction and position of water currents generated by the zooids were determined as follows. Small colonies of zooids,  $\leq 10$  cm in diameter, were placed in eight-inch finger bowls with standing filtered seawater. Zooids removed from their tubes were treated in a similar manner, but no more than 10 individuals were examined in a four-inch finger bowl or a 15-mm petri dish. Particles were added to the water distal to the arm and above the frontal tentacular surface of a mature zooid in normal feeding posture. The movement of the particles was indicative of the flow of water near the feeding apparatus. In both intact zooids and zooids removed from their tubes, the water currents generated by the metachronal beating of lateral cilia are toward the frontal ciliated surface of the arms and tentacles, between and perpendicular to the tentacles, and then away from the zooid's abfrontal tentaculated surface (Fig. 1). Even though a current produced by the frontal surface of the ciliated arm is not obvious, observations of particle capture, particle transport, and ciliation suggest that a current is generated down the length of the arm in a distal-to-proximal direction.

The particles captured by zooids ranged in size from 9 to 70  $\mu\text{m}$ , but additional work is needed to determine the size range of particles that are actually ingested. As the water currents carry the particles between the tentacles, lateral cilia capture the particles and transfer them to the frontal side of the tentacle. In several cases, the particles captured are seen to change or reverse direction abruptly and bounce onto the frontal surface of the tentacle. This

observation indicates that some particles are captured by a local reversal of beat by the lateral cilia and not by impingement on the cilia (see Hart, 1991, for a more detailed description of particle capture by ciliary reversal). Once on the frontal surface, the particle is transported down the length of a tentacle by the frontolateral and frontal cilia, then quickly transferred to the ciliated tract of the arm, and transported down the arm directly to the mouth (Fig. 4). Particle transport on the arm is perpendicular to and much more rapid than that on the tentacles. There is no evidence of mucus in normal feeding (*i.e.*, during particle capture and transport down the tentacles and arms), and the independent motion of particles further suggests that mucus is not used.

Figure 5 shows a video montage of a particle being captured by ciliary reversal near the base of a tentacle. While this particular event did not occur further out on the tentacle, as is typical (see Fig. 4), the abrupt change in particle direction indicative of ciliary reversal is evident. However, observing a capture by ciliary reversal is dependent upon the angle at which the particle path is viewed; *i.e.*, the degree with which a particle changes direction is determined by the viewing angle.

To control for this bias, two categories of observation for particle capture are scored. In both cases, the mechanism of particle capture is ciliary reversal. The first category is characterized strictly by a change of  $\geq 90^\circ$  in the particle's path. Using this criterion, ciliary reversals are observed to occur in 19.9% of all capture events by the entire feeding apparatus, and 23.5% of captures by the

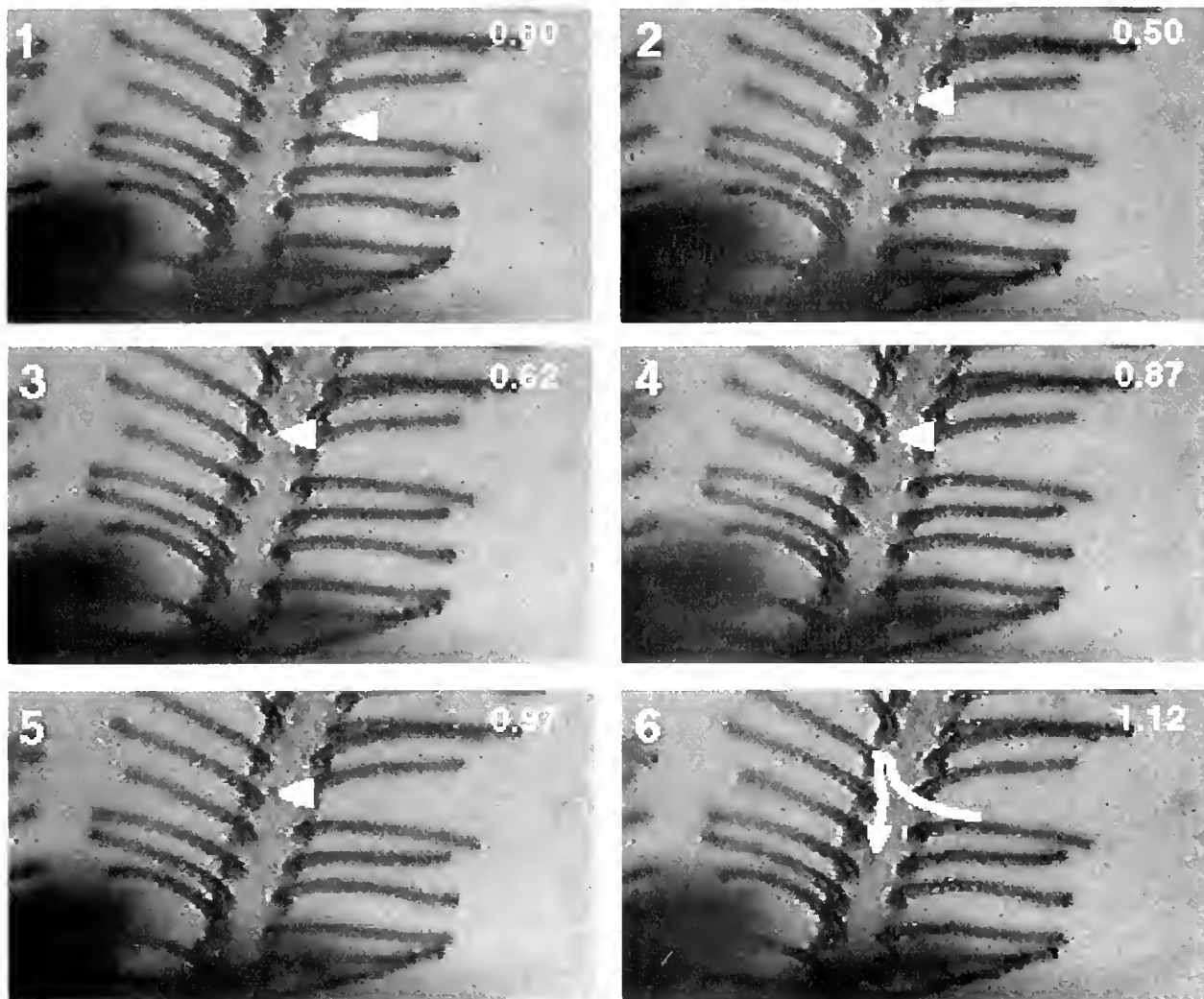


**Figure 5.** Ciliary reversal. This figure is a montage of frames taken from a video tape of *Rhabdopleura normani* feeding. The arrow heads point to a particle that is pulled down into the feeding apparatus by water vortices (1–2), contacts a tentacle at the base (3), and then immediately reverses direction and is transported down the tentacle and arm toward the mouth (4–6). The arrow in frame six indicates the particle path. The elapsed time in seconds is shown in the upper right of each frame.

tentacles (Table 1). These observations are highly credible since this criterion for identifying a ciliary reversal event is conservative. Thus, explanation by alternative hypotheses (e.g., impingement on the cilia, sieving by the cilia) can be excluded. The second category of particle captures, which is less restrictive, is defined by a sudden  $30^\circ$  to  $90^\circ$  change in particle direction. Such events occurred in 53.9% of all particle captures and 63.9% of those by the tentacles.

Furthermore, direct observation with a compound light microscope confirmed that the ciliary beat is altered when particles contact the lateral cilia. Individual zooids were placed in a depression slide under the microscope, and algal particles were added. Even though the particle path

could not be accurately followed due to the magnification, when the particle contacted the cilia a change of beat was evident.

In addition to particle capture by the tentacles, the frontal ciliated surface of the arm captures particles directly, though I was unable to determine whether ciliary beat was altered when particles were captured in this fashion. Although direct capture by the arm occurs infrequently, it still accounted for a noticeable portion, 15.6%, of all particles captured.

Thus, the total number of ciliary reversal events (category 1 and category 2) observed was 104 out of 141 capture events, or 73.8% of all observed events. If just the captures by ciliary reversal on the tentacle are analyzed (because

Table I

## Particle capture

	Number of particles captured	% of particles captured	% of particles captured by tentacles
Capture on tentacles by a $\geq 90^\circ$ change in particle's path	28	19.9%	23.5%
Capture on tentacles by a sudden $30^\circ$ to $90^\circ$ change in particle's path	76	53.9%	63.9%
Capture on tentacles by a $< 30^\circ$ change in particle's path	15	10.6%	12.6%
Particle capture on the arms	22	15.6%	—
Total	141		

the occurrence of ciliary reversal during captures by the arms could not be substantiated), 87.4% (104 out of 119) of all tentacular capture events are due to ciliary reversal. In 12.6% of all particle capture events that occurred on the tentacles, ciliary reversals were not observed. Although the captures of these particles may have occurred by ciliary reversal, other mechanistic hypotheses of particle capture cannot be ruled out.

As water passed over the tentacles, the proportion of particles that were captured and the proportion that were ingested varied from near 0% to almost 100%, depending upon particle concentration, particle type, and duration of the feeding experiment. These proportions were lowest when particle concentration was high and when the feeding experiment was long ( $\geq 1$  h). Also, algal particles were more efficiently cleared and more often ingested than the artificial food particles.

The ciliated perforations apparently have no direct function in particle capture. During my analysis, no particles were ever observed to be captured or trapped by the cilia around these perforations and then transported towards the mouth.

## Particle rejection

Particle rejection occurs when a particle is actively captured and released at some point prior to ingestion. In *R. normani*, I observed four types of particle rejection. The data in Table II are representative of *R. normani* feeding, in that the largest category of particles are those ingested, and the four different types of particle rejection mechanisms are observed. Fifty percent of the particles rejected are merely captured on the tentacles, transferred to the frontal side of the tentacle, and then discharged or lost.

Also, the frontal surface of the tentacles can transport large particles distally via the frontolateral and frontal cilia, and expel them at the tentacle tip. This observation, which occurred in 9.7% of the rejections, is consistent with Gilmour's (1979) findings in *R. compacta*. Gilmour also reported that mucus is involved in rejection in *R. compacta*, but water currents quickly carry particles away in *R. normani* and the particles move independently, indicating that mucus is not involved in transport along the tentacles.

In the third type of particle rejection, particles may be lost during transfer from the tentacle to the arm. While I have interpreted this behavior as particle rejection, it might just as easily be seen as an inefficiency in particle transfer.

The last type of particle rejection, accounting for 31.9% of such observations, involves the perforated tentacular structures. As particles are transported down the arm, they may be suddenly shuffled off at a  $45$ – $90^\circ$  angle and released through one of the many perforations found between the tentacle bases. Figure 4 shows a schematic of this event, and Figure 6 shows a video montage of this type of rejection. In observing live animals, the passage of the particle under the tissue commissure and through the perforation can clearly be seen. Because cilia can only beat in one plane, I hypothesize that two types of cilia (*i.e.*, those involved in particle transport towards the mouth, and those involved in particle transport toward the perforations) are present on the frontal surface of the arm to account for this peculiar particle motion.

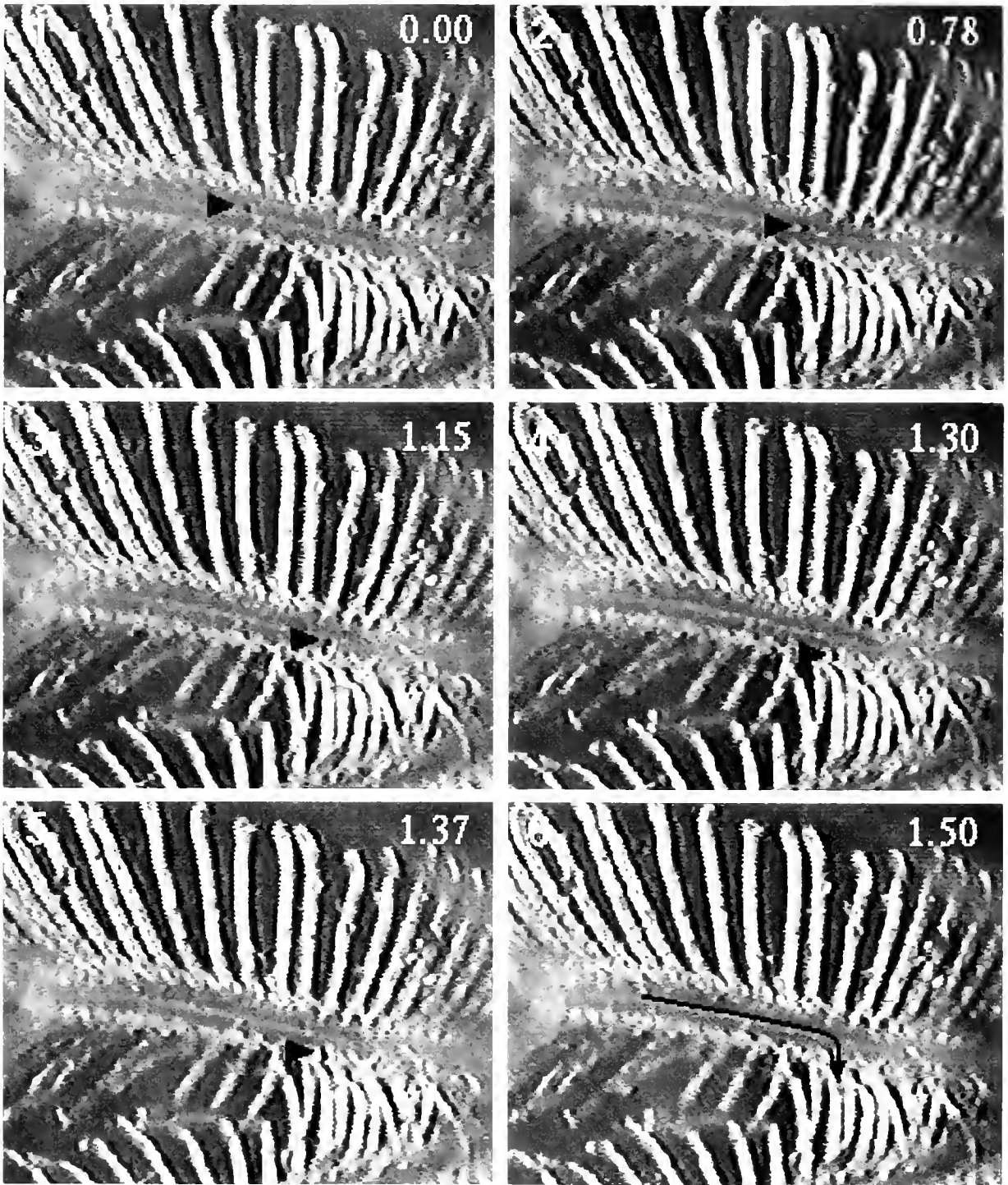
Infrequently, larger particles become lodged in the apertures at the tentacle base. Because this occurs only when zooids are flooded with a high concentration of particles, it may be an artifact. As the concentration of particles presented increases and the fouling of the feeding apparatus occurs, rejection through the perforations and by distal transport of particles along the tentacles accounts for a much greater percentage of particle rejection events. Moreover, when the feeding apparatus is very fouled, particles become stationary temporarily, and the tentaculated

Table II

## Fate of captured particles

	Number of captured particles	% of particles	% of particles not ingested
Ingested	69	48.9%	—
Loss from tentacle	36	25.5%	50.0%
Distal transport off tentacle	7	5.0%	9.7%
Loss during arm-tentacle transfer	6	4.3%	8.3%
Through perforation	23	16.3%	31.9%
Total	141		





**Figure 6.** Particle rejection. The arrowheads in this figure point to a food particle that is traveling down the length of the arm towards the mouth (1-2). The particle abruptly changes direction (3) and is shuffled off at a 90° angle through a perforation (4-6). The arrow in frame six indicates the particle path. The elapsed time in seconds is shown in the upper right of each frame.

arms secrete mucus to facilitate the removal of fouling particles.

### Discussion

#### *Impingement or reversal*

The actual method of particle capture by the lophophorates and other deuterostome groups is currently the source of a controversy in the literature. Are particles captured by an impingement process (Gilmour, 1978, 1979), or is a local reversal of ciliary beat used to capture particles (Strathmann, 1973; Strathmann and Bonar, 1976; Hart, 1991)? Gilmour (1979) and Stebbing and Dilly (1972) both reported that impingement is the main method of particle capture by pterobranchs. However, an impingement hypothesis cannot explain several of my observations. Namely, particles quickly change or reverse direction at angles  $\geq 90^\circ$ , and particles bounce from the lateral cilia to the frontal surface of the tentacle. An impingement hypothesis postulates that such movements should not occur. Furthermore, as Strathmann (1973) has argued, food particles are only slightly denser than the water, so it is doubtful that food particles could cross flow lines with sufficient force to allow impingement on the cilia. Gilmour (1978) has also suggested that impingement is the main mechanism of particle capture in lophophorates, but this is contrary to both my own unpublished data and Strathmann's (1973) observations of these taxa.

The conclusion that a ciliary reversal mechanism is used by pterobranchs is an inference based on particle motion. Previous studies validate such an inference. Using cinefilms, reversal ciliary beats associated with particle capture have been directly observed in pluteus larva of echinoids (Strathmann *et al.*, 1972) and in adult bryozoans (Strathmann, 1982), and I have observed altered ciliary beat in pterobranchs. Also, Hart (1990) pharmacologically manipulated calcium channels to demonstrate that particle capture in echinoderm larvae is dependent on ciliary reversal.

However, an impingement mechanism for particle capture by pterobranchs cannot be completely ruled out. Because only 23.5% of those particles captured on pterobranch tentacles demonstrated obvious ciliary reversal, the use of an impingement mechanism as well is conceivable. When the tentaculated arms were flooded with high particle concentrations and became fouled, particles often appeared "stuck," possibly by impingement on the cilia, and surrounded with mucus. Because this event was observed only when the tentaculated arms were fouled, I interpreted it as a cleaning mechanism and not a particle-capture mechanism.

The distribution of animals that use ciliary reversal extends beyond the lophophorates and pterobranchs. The larvae of enteropneusts (Strathmann and Bonar, 1976)

and echinoderms (Strathmann, 1971; Hart, 1991) use ciliary reversal mechanisms, which, however, have not been identified in protostome organisms. Curiously, the cilia involved in ciliary reversal in these taxa are usually 20–30  $\mu\text{m}$  long compared to the 10–13  $\mu\text{m}$  long cilia of pterobranchs. The use of ciliary reversal to capture food can also be dependent on the life-history stage. For example, ciliary reversal mechanisms have not been demonstrated in adult forms of enteropneusts or echinoderms, and, while ciliary reversal is present in adult bryozoans, the cyphonautes larva uses sieving instead (Strathmann and McEdward, 1986; McEdward and Strathmann, 1987).

#### *Pterobranchs versus lophophorates*

The feeding apparatuses of pterobranchs, brachiopods, bryozoans, and phoronids have several similar attributes (Table III). At a gross morphological level, the feeding structure is a ring of tentacles that surrounds the oral region and is invaded by mesocoelom. This superficial similarity was recognized by early workers who initially allied pterobranchs with the Bryozoa within the "Lophopea" (Allman, 1869).

Table III

#### *Feeding apparatus similarities\**

	Pter	Phor	Brac	Bryo
1) Extensions of the mesocoelom invade the tentacles.	+	+	+	+
2) Lateral, frontal, and frontolateral ciliary bands are present on the tentacles.	+	+	+	+
3) Lateral cilia generate a water current between and perpendicular to the tentacles that draws water from the frontal surface to the abfrontal surface.	+	+	+	+
4) A local reversal of ciliary beat is used to capture food particles.	+	+	+	+
5) Particles are transported by the frontal and frontolateral cilia down the tentacle.	+	+	+	+
6) Mucus is not used in normal feeding activity.	+	+	+	+
7) Particles are rejected by distal transport along the frontal surface of the tentacle.	+	+	+	+
8) Tentacles are innervated.	+	+	+	+/-
9) Tentacles contain blood vessels.	+	+	+/-	-

\* Data obtained from Hyman (1959), Nielsen (1987), Strathmann (1973), Gilmour (1978, 1979), Reed and Cloney (1977), Smith (1973), and my own unpublished results.

But the similarities extend beyond gross morphology to structure and function. In all four taxa, the tentacles have lateral, frontolateral, and frontal ciliary bands (Strathmann, 1973; Nielsen, 1987). The lateral cilia generate a flow of water around the feeding apparatus that draws water from the frontal surface, moves the water between and perpendicular to the tentacles, and then passes it abfrontally away from the feeding apparatus (Strathmann, 1973). In the case of brachiopods, the presence of the valves causes the water current to be redirected after it has passed through the tentacular region. As the water passes between the tentacles, particles are captured with the lateral bands of cilia by a local reversal of ciliary beat. After particle capture, the frontal and frontolateral cilia transport particles proximally down the frontal side of the tentacle without the use of mucus.

The particle-rejection mechanism, in which large particles are moved distally along the tentacles, is similar among the lophophorates and the pterobranchs. This particular mechanism often involves the use of mucus in bryozoans, brachiopods, and phoronids (Strathmann, 1973; pers. obs.). Although I did not observe mucus used in this manner under normal conditions, it has been reported in pterobranchs (Gilmour, 1979) and is seen when the tentaculated arms are sufficiently fouled. Additional structural similarities, such as extensions of the blood vascular system and the nervous system into the tentacles, have been observed in the pterobranchs, phoronids, and brachiopods (Hyman, 1959; Dilly *et al.*, 1986; Halanych, unpub.).

Earlier workers (Hyman, 1959; Gilmour, 1979; Hoverd, 1985; Lester, 1985; Dilly *et al.*, 1986; Nielsen, 1987) postulated a possible homology among the tentacles of pterobranchs and the lophophore, and my findings are consistent with that notion. Furthermore, whereas any one of the above characteristics may be found in other suspension-feeding organisms (*e.g.*, polychaetes), the entire suite of characters (nos. 1–7 in Table III) is unique to pterobranchs, phoronids, brachiopods, and bryozoans. Without a phylogeny to determine character evolution, one cannot, however, infer whether these commonalities are due to a shared evolutionary history or due to similar selective pressures on sessile tentaculated suspension-feeders.

There are two differences between *R. normani* and lophophorates. First, pterobranch cilia are much shorter than those of brachiopods, bryozoans, and phoronids. To confirm this finding I examined *Cephalodiscus gracilis* from the same locality in Bermuda. The cilia of *C. gracilis* are also 10–13  $\mu\text{m}$  long, and I found no cilium longer than 15  $\mu\text{m}$ . Second, the ciliated perforations found in Bermuda specimens of *R. normani* are unique. *C. gracilis* has no similar structures at the base of its tentacles, nor is any similar structure reported in the literature. Although

these structures are used in particle rejection, their effect on flow around the feeding apparatus is unclear.

These differences and similarities between the lophophorates and pterobranchs continue to generate many interesting hypotheses about how evolution has shaped the ability of organisms to acquire food. When the molecular phylogeny of these groups has finally been completed by this and other laboratories, many of these hypotheses can be directly tested, and thus provide a much more lucid understanding of early metazoan evolution.

### Acknowledgments

I thank the directors and staff of The Bermuda Biological Station for Research, Inc. and Friday Harbor Laboratories. The following provided helpful comments and constructive criticism; P. N. Dilly, M. Hart, G. Freeman, D. M. Hillis, C. M. Pease, C. Cunningham, and an anonymous reviewer. Figures were drawn by Janet Young. The research reported here was supported by a Bermuda Biological Station for Research Grant-in-aid of Research, Sigma Xi Grant-in-aid, The Lerner-Gray Fund of Marine Research of the American Museum of Natural History, and The Hartmann Fellowship through the Department of Zoology at the University of Texas. The scanning electron microscopy was conducted at Friday Harbor Laboratories, The University of Washington, and the transmission electron microscopy was conducted with the aid of Bob Riess at The University of Texas.

### Literature Cited

- Allman, G. 1869. On *Rhabdopleura*. *Q. J. Microsc. Sci.* **1X**: 57–63.
- Darwin, C. 1972. Chapter XVII in *The Voyage of the Beagle*. Bantam Books, Inc., New York.
- Dilly, P. N., U. Welsch, and G. Rehkamper. 1986. Fine structure of tentacles, arms, and associated coelomic structures of *Cephalodiscus gracilis* (Pterobranchia, Hemichordata). *Acta Zool. (Stockh.)* **67**: 181–191.
- Gilmour, F. H. J. 1978. Ciliation and function of the food-collecting and waste-rejecting organs of lophophorates. *Can. J. Zool.* **56**: 2142–2155.
- Gilmour, F. H. J. 1979. Feeding in pterobranch hemichordates and the evolution of gill slits. *Can. J. Zool.* **57**: 1136–1142.
- Grant, P. R. 1986. *Ecology and Evolution of Darwin's Finches*. Princeton University Press, Princeton, New Jersey.
- Hart, M. W. 1990. Manipulating external  $\text{Ca}^{2+}$  inhibits particle capture by planktotrophic echinoderm larvae. *Can. J. Zool.* **68**: 2610–2615.
- Hart, M. W. 1991. Particle captures and the method of suspension feeding by echinoderm larvae. *Biol. Bull.* **180**: 12–27.
- Hoverd, W. A. 1985. Histological and ultrastructural observations of the lophophore and larvae of the brachiopod, *Notosaria nigricans* (Sowerby 1846). *J. Nat. Hist.* **19**: 831–850.
- Hyman, L. H. 1959. *The Invertebrates: Smaller Coelomate Groups, Chaetognatha, Hemichordata, Pogonophora, Phoronida, Ectoprocta, Brachiopoda, Sipunculida, The Coelomate Bilateria*. McGraw-Hill Book Company, New York.
- Lester, S. M. 1985. *Cephalodiscus* sp. (Hemichordata: Pterobranchia): observations of functional morphology, behavior and occurrence in shallow water around Bermuda. *Mar. Biol.* **85**: 263–268.



- Lester, S. M. 1988. Ultrastructure of adult gonads and development and structure of the larvae of *Rhabdopleura normani* (Hemichordata: Pterobranchia). *Acta Zool. (Stockh.)* **69**: 95-109.
- Liem, K. F. 1973. Evolutionary strategies and morphological innovations: Cichlid pharyngeal jaws. *Syst. Zool.* **22**: 425-441.
- McEdward, L. R., and R. R. Strathmann. 1987. The body plan of the cyphonautes larva of bryozoans prevents high clearance rates: comparison with the pluteus and a growth model. *Biol. Bull.* **172**: 30-45.
- Nielsen, C. 1987. Structure and function of metazoan ciliary bands and their phylogenetic significance. *Acta Zool. (Stockh.)* **68**: 205-262.
- Reed, C. G., and R. A. Cloney. 1977. Brachiopod tentacles: ultrastructure and functional significance of the connective tissue and myo-epithelial cells in *Terebratalia*. *Cell. Tiss. Res.* **185**: 17-42.
- Smith, L. W. 1973. Ultrastructure of the tentacles of *Flustrellidra hispida* (Fabricius). In *Living and Fossil Bryozoa: Recent Advances in Research*. G. P. Larwood, ed. Academic Press, New York.
- Stebbing, A. R. D., and P. N. Dilly. 1972. Some observations on living *Rhabdopleura compacta* (Hemichordata). *J. Mar. Biol. Assoc. U. K.* **52**: 443-448.
- Strathmann, R. R. 1971. The feeding behavior of planktotrophic echi-noderm larvae: mechanisms, regulation, and rates of suspension feeding. *J. Exp. Mar. Biol. Ecol.* **6**: 109-160.
- Strathmann, R. R. 1973. Function of lateral cilia in suspension feeding lophophorates (Brachiopoda, Phoronida, Ectoprocta). *Mar. Biol.* **23**: 129-136.
- Strathmann, R. R. 1982. Cinefilms of particle capture by induced local changes of beat by lateral cilia of a bryozoan. *J. Exp. Mar. Biol. Ecol.* **62**: 225-236.
- Strathmann, R. R., T. L. Jahn, and J. R. C. Fonseca. 1972. Suspension feeding by marine invertebrate larvae: clearance of particles by ciliated bands of a rotifer, pluteus, and trochophore. *Biol. Bull.* **142**: 505-519.
- Strathmann, R. R., and D. Bonar. 1976. Ciliary feeding of tornaria larvae of *Ptychodera flava* (Hemichordata: Enteropneusta). *Mar. Biol.* **34**: 317-324.
- Strathmann, R. R., and L. R. McEdward. 1986. Cyphonautes' ciliary sieve breaks a biological rule of inference. *Biol. Bull.* **171**: 694-700.

## SCP-Related Peptides From Bivalve Mollusks: Identification, Tissue Distribution, and Actions

A. CANDELARIO-MARTINEZ<sup>1</sup>, D. M. REED, S. J. PRICHARD, K. E. DOBLE,  
T. D. LEE\*, W. LESSER, D. A. PRICE, AND M. J. GREENBERG<sup>2</sup>

*The Whitney Laboratory, University of Florida, St. Augustine, Florida 32086-8623, and \*Division of Immunology, Beckman Research Institute of the City of Hope, Duarte, California 91010-0269*

**Abstract.** The SCPs<sup>3</sup> are a small peptide family, characterized in gastropods, and implicated in the control of the cardiovascular system and the muscles involved in feeding and gut motility. We aimed to determine the manifestation of this peptide family in the class Bivalvia. Acetone extracts of whole bivalves were fractionated by high pressure liquid chromatography (HPLC), and reactive peaks were identified by radioimmunoassay (RIA). After purification, sequencing, and analysis by mass spectroscopy, three peptides were identified in the clam *Mercentaria mercenaria*: IAMSFYFPRMamide, AMSFYFPRMamide, and YFAFPRQamide<sup>4</sup>. SCP-related peptides from two other species were also sequenced: APKYFYFPRMamide and SAFYFPRMamide from an oyster, *Crassostrea virginica*; and AMSFYFPRMamide

(identical to one of the clam peptides) from a cockle, *Dinocardium robustum*. The tissue distribution and pharmacological actions of the clam SCPs were determined in *M. mercenaria*, as follows. The levels of peptide in extracts of 12 tissues were estimated by RIA. The largest concentrations of SCP occur in the palps and the visceral ganglia; the levels in the cerebral and pedal ganglia, the rectum, intestinal typhlosole, and gills were substantially lower; and the smallest amounts were found in the heart and the style sac typhlosoles. Immunohistochemistry revealed many cell bodies in the periphery of the ganglia and fibers in the neuropil. Immunoreactive, varicose fibers also occur in the typhlosoles of the intestine and style sac, and in the rectum, gill, and palps. The atrioventricular valves, but not the atria or ventricle proper, contain immunoreactive fibers. Synthetic clam SCPs were assayed on the rectum, the typhlosoles of the intestine and style sac, and the ventricle, all isolated in an organ bath. At low to moderate doses, the SCPs relaxed the muscles of the rectum; higher doses had biphasic actions. The muscles of the intestinal and style sac typhlosoles were relaxed, and spontaneous rhythmicity was slowed by the SCPs. Most ventricles were unresponsive. We conclude that the SCPs isolated in bivalves—though distinctive—are true homologs of those in gastropods. Moreover, the bivalve peptides also serve similar roles, controlling feeding and digestion, and perhaps even cardioactivity.

Received 12 May 1993; accepted 28 September 1993.

<sup>1</sup> Present address: Department of Physiology, Biophysics and Neurosciences, CINVESTAV, Ave. IPN 2508, Col. San Pedro Zacatenco, México, D. F. 07300, Mexico.

<sup>2</sup> To whom correspondence should be addressed.

<sup>3</sup> The logogram 'SCP,' its plural 'SCPs,' and the phrase 'SCP-related peptides' refer to a well-studied family of molluscan peptides. The initials were originally the abbreviation of the phrase 'small cardioactive peptides,' a designation for a peak of cardioexcitation in ganglion extracts of *Helix aspersa* that eluted relatively late from Sephadex G15 (Lloyd, 1978; discussed at length in Price *et al.*, 1990). Although the logogram SCP is widely used and recognized, the phrase 'small cardioactive peptides' no longer describes accurately the diverse functions of this peptide family or even the size of its members. To avoid confusion—since this paper is primarily *not* about cardioactivity—we avoid reference to the original abbreviation in the text or the title. Of course, the original meanings of names or symbols commonly lose their relevance and usage, in science (*e.g.*, substance P) as well as other endeavors (*e.g.*, ITT).

<sup>4</sup> The one-letter abbreviations of the amino acids are used to display all peptide sequences: A = Ala; D = Asp; E = Glu; F = Phe; G = Gly; I = Iso; K = Lys; L = Leu; M = Met; N = Asn; P = Pro; Q = Gln; R = Arg; S = Ser; W = Trp; Y = Tyr.

### Introduction

Several years ago, two SCPs were isolated from *Aplysia californica* and *A. brasiliana*, respectively, and sequenced: SCP<sub>A</sub> (ARPGYLAFPRMamide) (Lloyd *et al.*, 1987), and SCP<sub>B</sub> (MNYLAFPRMamide) (Morris *et al.*, 1982). A genetic analysis in *A. californica* showed that both peptides

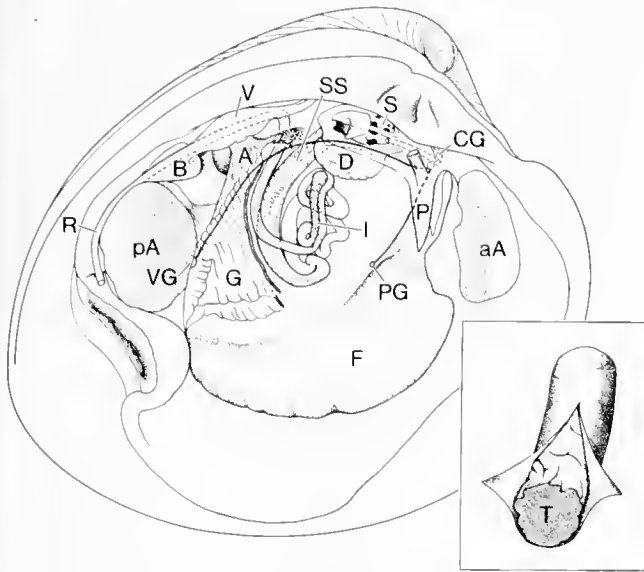


**Figure 1.** A diagram of *Mercenaria mercenaria* on the half-shell. The tissues, and particularly the parts of the mid-gut, utilized in these experiments are indicated. The segment of the intestine (I) that was used is stippled; the inset is an enlargement of that segment showing the typhlosole (T) within. The nervous system of this clam was thoroughly described by Loveland (1963). Abbreviations: A, atrium; aA, anterior adductor muscle; B, bulbus arteriosus; CG, cerebral ganglion; D, digestive gland; F, foot; G, gill (mostly cut away); I, intestine; P, palp; pA, posterior adductor muscle; PG, pedal ganglion; R, rectum; S, stomach; SS, style sac; T, typhlosole; V, ventricle; VG, visceral ganglion.

are processed from a common precursor (Mahon *et al.*, 1985). More recently, a pair of SCPs was also found in *Helix aspersa*: one of them is SCP<sub>B</sub>, and the other is the

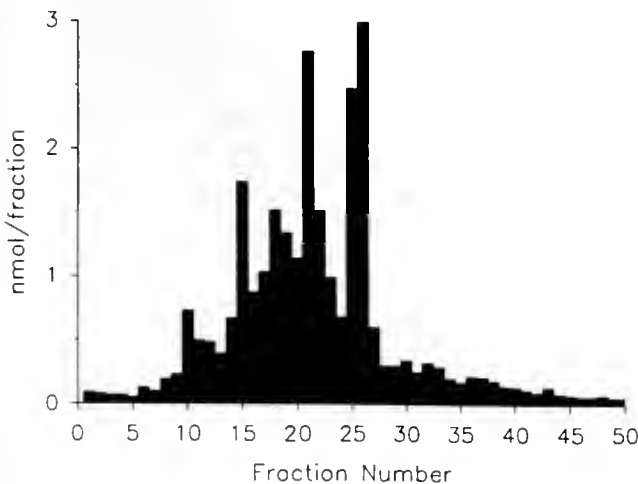


**Figure 2.** Immunoreactivity profile from the initial HPLC fractionation of a whole-clam extract. The extract was loaded onto a Prep-10 Octyl column (10 × 100 mm, 4 ml/min) and eluted with a gradient of acetonitrile (16–40% over 30 min) in water with 0.1% trifluoroacetic acid. Fractions were collected every half minute.

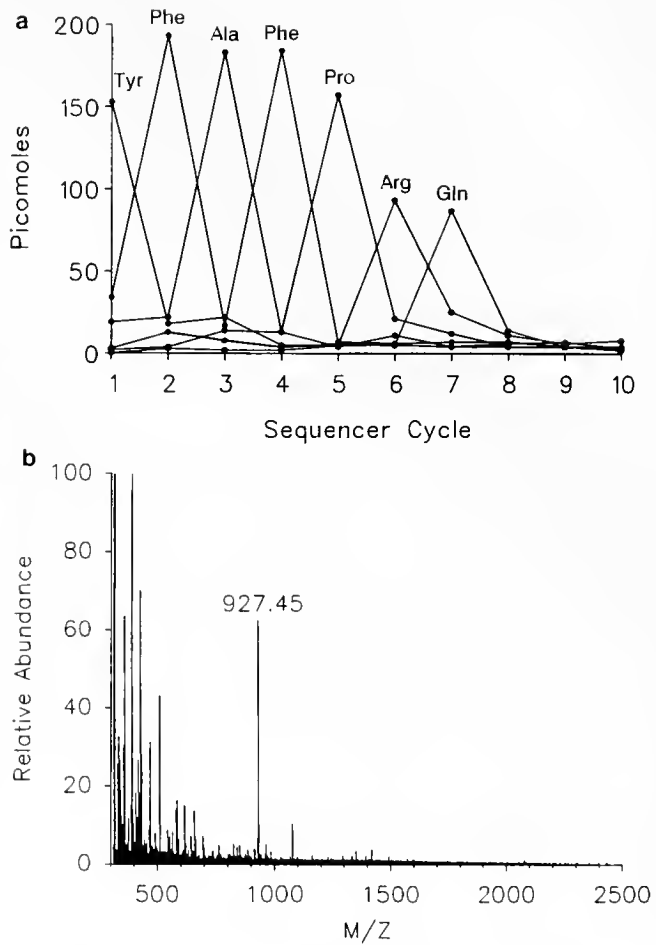


**Figure 3.** Identification of YFAFPRQamide from the earliest eluting SCP-like immunoreactive peak (fraction 10) in Figure 2. a. The yields of the pertinent amino acid derivatives at each cycle are plotted, and the most abundant amino acid is identified. b. FAB mass spectrum of this peak with the observed 927.45 molecular ion.

nonapeptide SGYLAFPRMamide (Price *et al.*, 1990). All of these peptides, as well as others from gastropods (Price *et al.*, 1989), have a common heptapeptide amide (–YLAFPRMamide) at the C-terminal.

The two SCPs from *Aplysia* have identical biological activities in that genus: they increase the amplitude and frequency of beat of the isolated heart (Lloyd *et al.*, 1985), regulate gut motility (Lloyd *et al.*, 1988), and enhance the amplitude of contraction of the accessory radula closer muscle, which is involved in biting (Lloyd *et al.*, 1984; Richmond *et al.*, 1986; reviewed by Weiss *et al.*, 1992).

The heart of the pulmonate snail *Helix aspersa* (Morris *et al.*, 1982; Price *et al.*, 1990) and that of the terrestrial slug *Limax maximus* (Prior and Welsford, 1989) are also potentially stimulated by the SCPs. SCP<sub>B</sub> also stimulates the isolated esophagus of the snail (Morris *et al.*, 1982) and, indeed, most studies of the SCPs in pulmonate snails and slugs (as in *Aplysia* and other opisthobranchs) have fo-

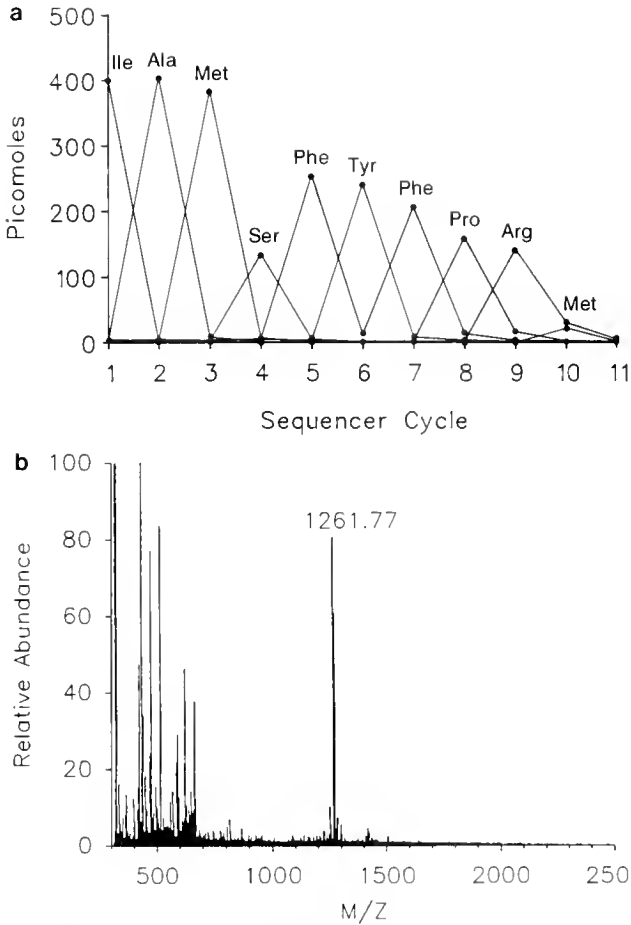


**Figure 4.** Identification of IAMSFYFPRMamide from the most retained SCP-like immunoreactive peak (fractions 25–27) in Figure 2. a. The levels of pertinent amino acid derivatives at each cycle are plotted, and the amino acid assigned to each position is shown. b. FAB mass spectrum of this peak with the prominent molecular ion 1261.77.

cused on the stimulation of feeding and gut motility (Murphy *et al.*, 1985; Lloyd and Willows, 1988; Willows *et al.*, 1988; Prior and Welsford, 1989; and Krajniak *et al.*, 1989).

We sought to learn whether, and to what extent, the structure and functions of the SCPs are retained in the Bivalvia, a class of mollusks that has been diverging from the Gastropoda since the early Cambrian (Pojeta *et al.*, 1973). We report here the isolation and sequencing of SCP analogs from the venerid clam, *Mercentaria mercenaria*, from another heterodont, the giant Atlantic cockle *Dinocardium robustum*, as well as from a pteriomorph, the eastern oyster *Crassostrea virginica*. In *M. mercenaria*, we have also determined the tissue distributions of the clam peptides and have demonstrated their actions on the musculature of several isolated organs. Preliminary reports of these data have been published (Price *et al.*, 1989; Candelario *et al.*, 1990a; Candelario *et al.*, 1990b).

## Materials and Methods

### Animals

Quahogs (*Mercentaria mercenaria*) and eastern oysters (*Crassostrea virginica*) were obtained from the inland waters adjacent to Marineland, Florida. Giant cockles (*Dinocardium robustum*) were obtained from the beach in the same locality. The bivalves were maintained in flowing, natural seawater until they were needed, except that only freshly collected animals were used for immunohistochemistry.

### Peptide characterization

Between 1 and 10 whole shucked animals, or batches of 10 or 20 pieces of particular tissues, were prepared for high pressure liquid chromatography (HPLC) as described previously (Price *et al.*, 1990). The only exception to the published procedure is that the acetone extraction was limited to overnight (about 16 h) to minimize oxidation;

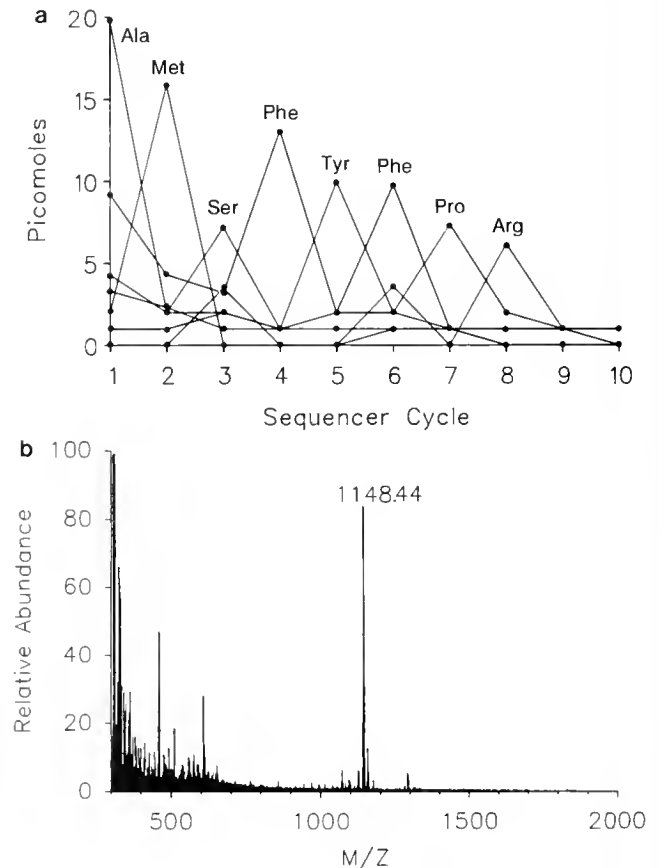


**Figure 5.** Identification of AMSFYFPRMamide from the fourth peak (fractions 21–22) in Figure 2. a. The levels of pertinent amino acid derivatives at each cycle are plotted, and the amino acid assigned to each position is shown. b. FAB mass spectrum of this peak with observed 1148.44 molecular ion.

**Table 1**

Distribution of SCP-related immunoreactivity in tissues of the clam *Mercenaria mercenaria*

Tissue	p mole/g wet wt*
Palps (480, 450)	465
Visceral ganglia	426
Cerebral ganglia	250
Pedal ganglia	200
Gills (178, 170)	174
Rectum	170
Intestinal typhlosole	115†
Mantle (113, 96)	105
Foot (40, 30)	35
Adductor muscles (23, 22, 60)	35
Style sac typhlosole	9†
Heart	9

\* Tissues from 10† or 20 animals were pooled, weighed, extracted in acetone, evaporated, and the aqueous portion fractionated by HPLC with analysis by RIA. The immunoreactivities of the peak fractions were added to produce the value indicated. Where more than one extract was tested, the means are reported in the right-hand column and the individual values are in parentheses.

*i.e.*, the peptides were expected to be similar to gastropod SCPs and to contain multiple methionine residues.

After the acetone was removed and the extract filtered, the resulting clarified aqueous solution was loaded on a Prep10 Aquapore Octyl column (1.0 × 15 cm; Applied

Biosystems) and eluted with an aqueous acetonitrile gradient containing trifluoroacetic acid (TFA; 0.1% throughout). The fractions were analyzed by radioimmunoassay (RIA; Price *et al.*, 1990). Each immunoreactive peak (consisting of one to three fractions) was further purified on a Spheri-5 RP18 (4.6 × 220 mm), or an Aquapore Octyl RP300 (2.1 × 220 mm) column. In addition to aqueous acetonitrile gradients, we also used aqueous isopropanol gradients, all containing 0.1% TFA.

In some cases, the fractions were treated with H<sub>2</sub>O<sub>2</sub> (50 μl of 30%/ml) for 15 min to oxidize the methionyl residues of the peptides before re-chromatography (see Price *et al.*, 1990). In other cases, fractions were dried and incubated with dimethylsulfide (30 μl), TFA (50 μl), and trifluoromethanesulfonic acid (TMFSA; 10 μl) for 3 h (basically following the Applied Biosystems "low" conditions for TFMSA deprotection of synthetic peptides, but leaving out *m*-cresol) to reduce possible methionine sulfoxide residues. After the 3-h incubation, the fraction was diluted with deionized water and loaded onto the HPLC.

The purified peaks were analyzed by fast atom bombardment mass spectrometry (FABms; method in Bulloch *et al.*, 1988), by automated sequencing, and usually by both techniques. FABms and some sequencing was carried out at the Immunology Division of the Beckman Research Institute; most sequencing was done at the University of Florida Protein Core facility.

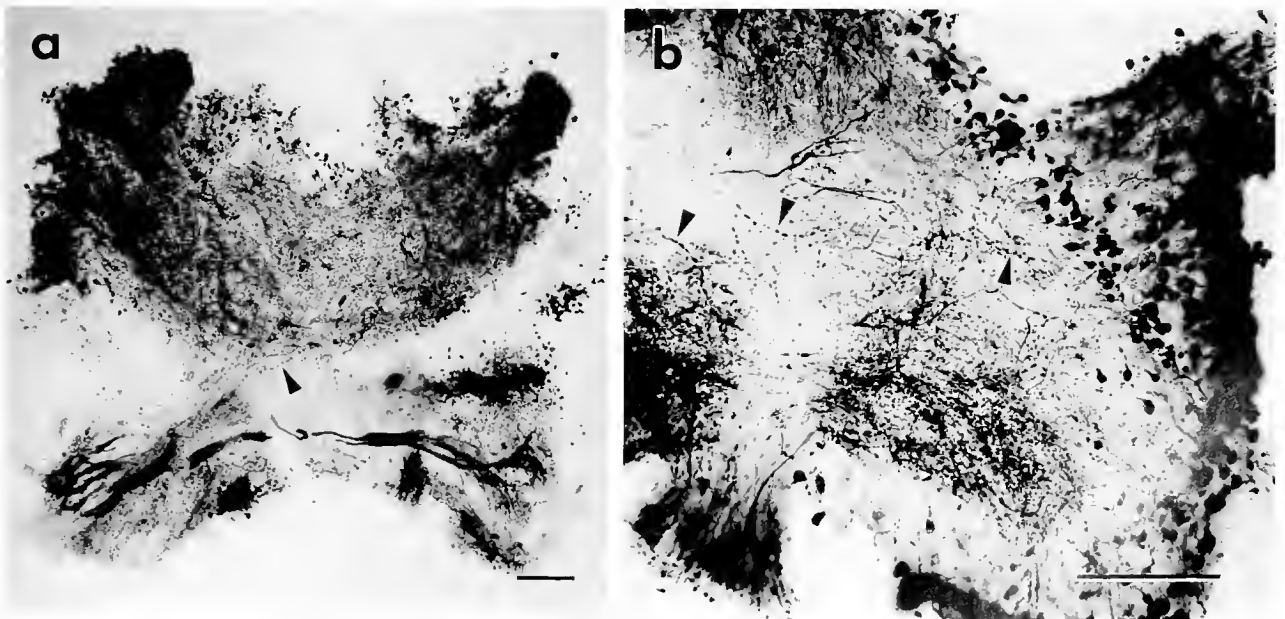


**Figure 6.** Frontal sections through the visceral (a) and cerebral (b) ganglia of *Mercenaria mercenaria* showing the distribution of neuronal cell bodies and fibers containing SCP-like immunoreactivity. The sections were stained by the PAP technique. Arrowheads indicate varicose fibers in the neuropil. Scale bars: 50 μm.

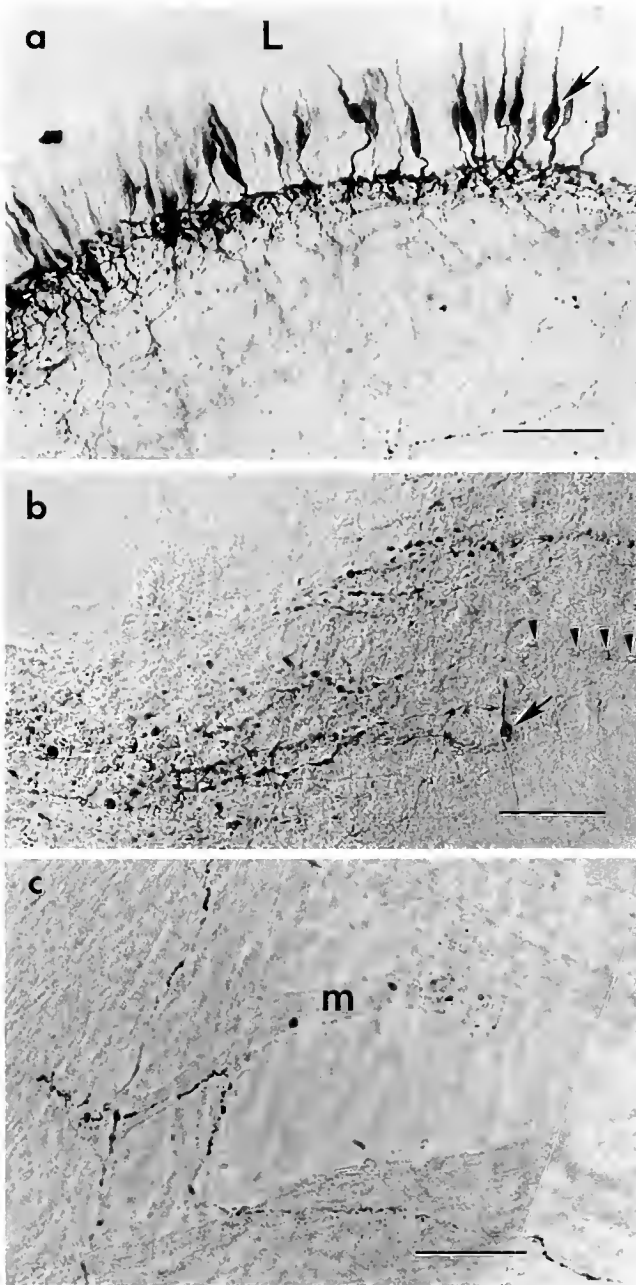


**Figure 7.** Differential interference contrast images of longitudinal sections through three regions of the digestive tract of *Mercenaria mercenaria*. The sections were stained by the PAP method. a. The surface of the style sac typhlosole shows SCP-like immunoreactivity within apparent sensory cells (arrow) that project toward the lumen (L). The bases of these cells join a network of varicose fibers, also stained. b. The wall of the intestine contains a network of varicose fibers and neuronal cell bodies (arrow) stained with SCP-like immunoreactivity. The network also includes cells that do not stain (arrowheads). c. Immunoreactive neural fibers in close association with muscle cells (m) in the wall of the rectum. Scale bars: 50  $\mu$ m.

### Immunohistochemistry

The three ganglia (visceral, pedal, and cerebral), as well as the rectum, the typhlosoles of the intestine and style sac, the gills, and the palps, were excised from *M. mercenaria*. The tissues were fixed and sectioned, as described below. They were then stained, either by indirect immunofluorescence or by the three-step peroxidase-antiperoxidase (PAP) method (Beltz and Burd, 1989).

**Immunofluorescence.** The tissues were fixed in Bouin's solution, embedded in paraffin (Humason, 1967), and sectioned at 6–8  $\mu$ m. The primary antibody, a monoclonal, was raised against SCP<sub>B</sub> (Masinovsky *et al.*, 1988), and diluted 1:50 in a solution of 0.1 M phosphate buffered saline (PBS), 1% Triton X-100, and 3% normal goat anti-serum at 4°C. The sections were incubated in this antibody solution for 12–18 h, rinsed with PBS for 30 min, and then stained with goat-anti-mouse IgG and IgM (both conjugated to fluorescein isothiocyanate) for 2 h at room temperature.

**The PAP method.** The protocol of Lesser and Greenberg (1993) was followed. The tissues were fixed overnight in 4% paraformaldehyde and then embedded in 12% gelatin dissolved in PBS. Sections (100  $\mu$ m) were cut with a Vibratome (Series 1000; TPI, Inc.), and the gelatin was melted away. The sections were rinsed, and the nonspecific binding was blocked by treatment for 1 h with antibody diluent (3% Triton X-100, 5% normal goat serum, 3% bovine serum albumin in 0.1 M phosphate buffer). The sections were incubated overnight in primary antibody (1:50), rinsed, incubated overnight in goat-anti-mouse antiserum (1:100), rinsed again, incubated overnight in mouse-PAP (1:100), rinsed, incubated for 20 min in 0.5% DAB (3,3'-diaminobenzidine tetrahydrochloride; Sigma), and developed in H<sub>2</sub>O<sub>2</sub>. The reaction was quenched with phosphate buffer. The slides were dehydrated in a series of alcohols and xylene and mounted in Permount (Fisher) under coverslips.

**Controls.** Some sections were incubated with SCP<sub>B</sub> antibody that had been preincubated with peptide for 24 h; *i.e.*, aliquots of antibody were individually preincubated with AMSFYFPRMamide (an endogenous clam peptide; see Results), with SCP<sub>B</sub>, or with FMRFamide at 10<sup>-4</sup> M. For some other sections, the SCP<sub>B</sub> antibody was omitted from the primary incubation solution. The control sections were incubated with the secondary antiserum at the same time as the experimentals. Some sections were stained with a FMRFamide antiserum provided by Dr. E. Weber; this was a positive control.

### Bioassays

**Rectum.** As described by Greenberg and Jegla (1963), the pericardial cavity was opened and the ventricular muscle teased away to expose the transcardiac segment

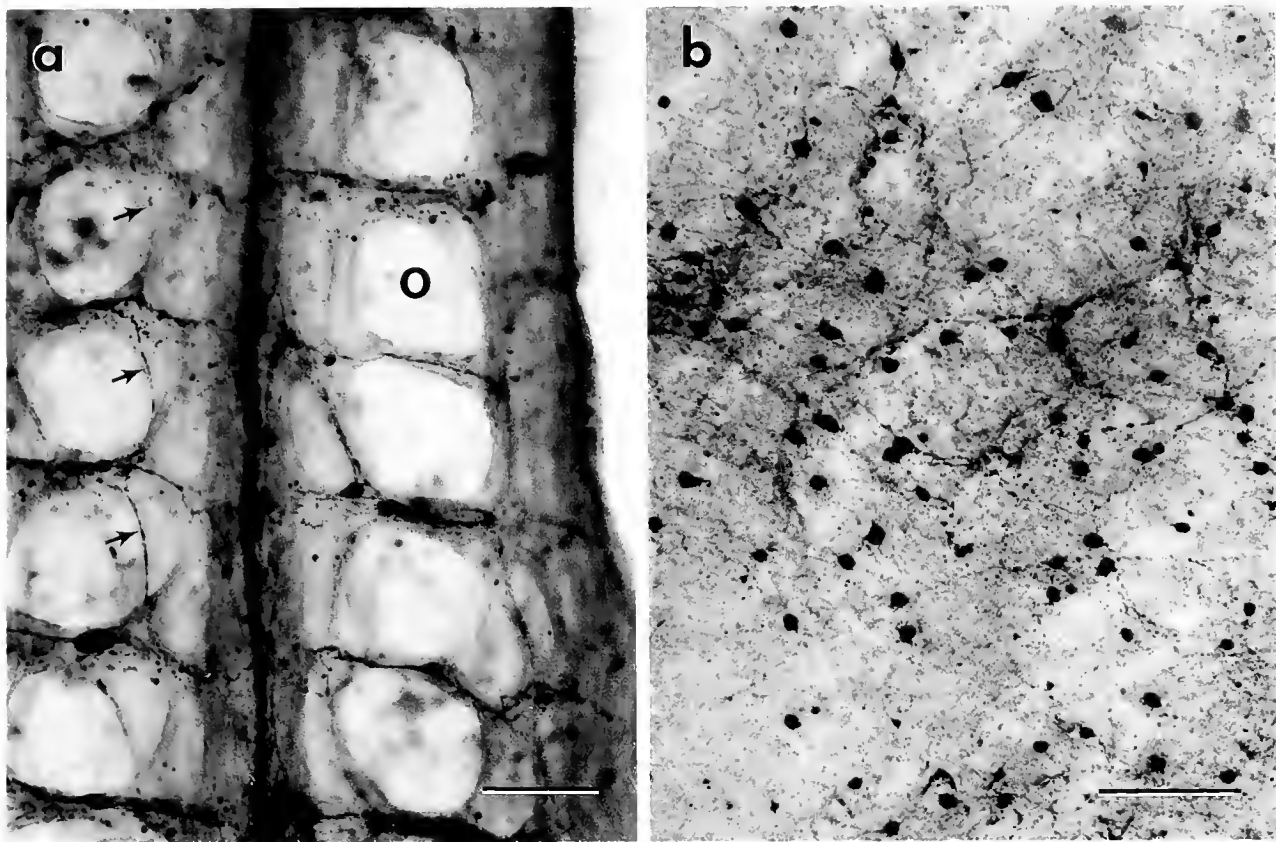


**Figure 8.** Frontal sections through the gill (a) and palp (b) of *Mercenaria mercenaria*. a. Gill: SCP-like immunoreactivity appears within neurons associated with the musculature of the ostia (O); note the iterated pattern of innervation (one example indicated by arrows). b. Palp: note numerous cell bodies and a dense network of varicose fibers containing SCP-like immunoreactivity. Scale bars: 50  $\mu$ m.

of the rectum (Fig. 1). The muscular tube was ligated anterior to the bulbus arteriosus and posterior to the digestive gland, and was cut free distal to the ligations. The isolated rectum was suspended in a 5-ml aerated organ bath between a force transducer (Grass FT.03) and a stainless steel hook immersed in the bath. The tissue was superfused with natural seawater and aerated. Tension changes were recorded with an ink-writing oscillograph (Grass Model 7). Drugs were added directly to the bath; the doses are expressed as molar concentrations in the medium.

*Typhlosoles of the intestine and style sac.* These sections of the digestive tract both lie within the visceral mass of the clam (Fig. 1) and were prepared as follows. A shallow incision was made just through the epidermis on the right side of the visceral mass, from below the heart to the anterior adductor. Along this incision, the muscular body wall was peeled toward the foot, while being separated from the underlying adherent tissue. This procedure revealed two parallel segments of intestine covered with a thin layer of gonad, which was teased away. The wall of the intestine is extremely thin and delicate and ill-suited

for bioassay. But when the intestinal wall was slit open, a large, firm typhlosole was revealed (Fig. 1 inset). A centimeter of this typhlosole was easily excised and the isolated tissue suspended in an organ bath, as described above for the rectum. We always used the typhlosole from the most posterior of the two parallel intestinal segments (Fig. 1).

The style sac contains two flaplike, longitudinal typhlosoles that separate it from the midgut. A segment of the sac close to the stomach was cut open, and the typhlosoles were removed, suspended in an organ bath, and used for bioassay.

*Heart.* The isolated heart of the clam was prepared according to the classical method of Welsh and Taub (1948).

## Results

### Peptide sequences

*Mercenaria mercenaria.* In the initial HPLC fractionation of clam extract, the immunoreactivity eluted between 5 and 15 min (fractions 10–30; Fig. 2); the active fractions were divided into 3 to 5 pools for further puri-



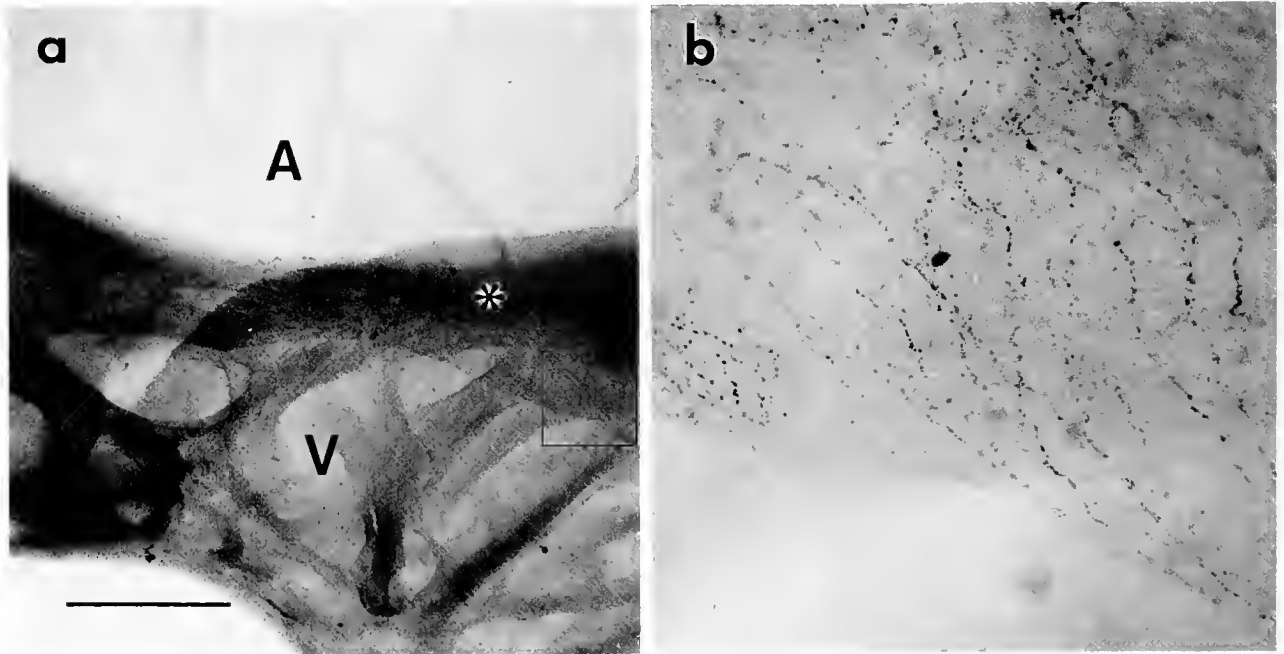


**Figure 9.** Wholemount of the atrioventricular region of the heart. (a) SCP-like immunoreactivity occurs only in varicose neuronal fibers in the valves (\*); no immunoreactivity was seen in the atrial (A) or ventricular (V) musculature. (b) An enlargement of the boxed area in (a) showing varicose fibers in the valve. Scale bar: 500  $\mu\text{m}$ .

fication. Most of these pools yielded more than one final pure peak of immunoreactivity. All of the final peaks were analyzed by FABms, and the most abundant peaks were sequenced as well. Two distinct sequences were found: YFAFPRQ and IAMSIFYPRM. The sequence YFAFPRQ (Fig. 3a) was obtained from the earliest eluting peak of immunoreactivity (fraction 10 in Fig. 2). It was associated with a 927.45 molecular ion (Fig. 3b), in good agreement with the value calculated for YFAFPRQamide (927.44); this indicated that the peptide is present as the amide and not the free acid.

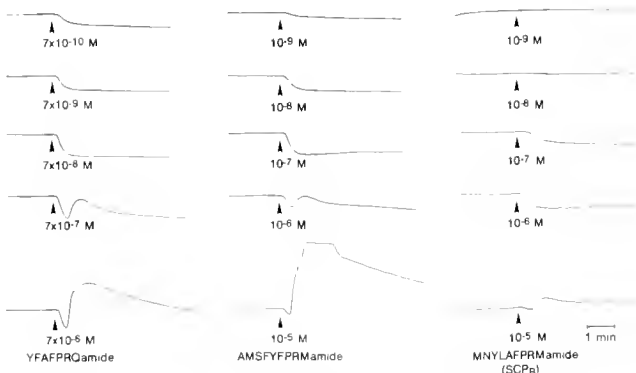


**Figure 10.** Dose-dependent responses of isolated clam rectums to two SCPs from the clam and one from gastropods (SCP<sub>B</sub>). Doses were delivered at the arrowheads.

The sequence IAMSIFYPRM (Fig. 4a) is primarily found in the most retained peak (fractions 25–27 in Fig. 2), which contains the unoxidized form (molecular ion 1261.77; Fig. 4b). But oxidized forms (molecular ions of 1277.78 and 1293.75) can be isolated from the earlier peaks (especially fractions 18 and 19 in Fig. 2). AMSFYPRM, a truncated version of IAMSIFYPRM, was sequenced (Fig. 5a) from the fourth peak (fractions 21 and 22 in Fig. 2; molecular ion, 1148.44, Fig. 5b); it also occurs in earlier peaks in oxidized forms (molecular ions, 1164.52 and 1180.44). Three ions corresponding to very low levels of even shorter forms were found in the two earliest peaks: 1077.56, MSFYPRMamide; 946.47, SFYPRMamide; and 859.51, FYFPRMamide. These three peptides are probably artifacts arising during purification. All of the ions associated with the series of peptides related to IAMSIFYPRMamide correspond to the amidated forms rather than the free acids.

*Dinocardium robustum*. Only one purified peak from this cockle was analyzed, and it yielded the sequence AMSFYPRM. The associated molecular ion (1148.37) was in good agreement with that calculated for AMSFYPRMamide (1148.54)—one of the peptides found in *M. mercenaria*. As in the clam, molecular ions for all fragments of this peptide, down to oxidized FYFPRMamide (875.49), were identified in *D. robustum*. Furthermore, a molecular ion of 927.46 was found, sug-



gesting that *Dinocardium*—like *Mercenaria*—contains YFAFPRQamide. The possibility that the longer *Mercenaria* peptide (IAMSFYFPRMamide) also occurs in *Dinocardium* has not been examined.

*Crassostrea virginica*. Two immunoreactive peaks were recovered from this oyster, and they contained material enough for both sequence and FAB/MS analyses. Two distinct sequences were obtained, and their associated molecular ions indicated that the peptides are amidated: *i.e.*, APKYFYFPRMamide (1318.81) and SAFYFPRMamide (1017.58).

#### Distribution

Acetone extracts from the different tissues of the clam were fractionated by HPLC and analyzed for SCP-related peptides by RIA. The elution patterns of the immunoreactivity were essentially those seen in the whole animal, and the same peptides were present, as deduced by FAB/MS. The amount of immunoreactivity varied from tissue to tissue, and the values for each could be sorted roughly into four classes (Table 1). The visceral ganglia and palps contained the highest levels, and they were substantially higher than those of the cerebral and pedal ganglia, the rectum, and the gills. Some tissues had very low levels of SCP-like immunoreactivity, and the heart was among them.

#### Immunohistochemistry

*Central ganglia*. The cortex of the visceral, cerebral, and pedal ganglia, particularly around the bases of the connectives and nerves, contain many immunoreactive ovoid cell bodies (about  $15 \times 10 \mu\text{m}$ ). In all three ganglia, a meshwork of stained fibers, some varicose, is present in the central neuropil; the density of these fibers is not uniform (Fig. 6).

*Peripheral structures*. Immunoreactive fibers, some of them varicose, are present in all of the tissues examined: the style sac typhlosole (Fig. 7a), intestinal typhlosole (Fig. 7b), rectum (Fig. 7c), gill (Fig. 8a), and palps (Fig. 8b). In the rectum, particularly, these fibers were very clearly associated with the musculature (Fig. 7c). A few small cell bodies (about  $5 \mu\text{m}$ ) were also observed in the periphery (*e.g.*, Figs. 7c, 8b). Immunoreactive fibers in the heart were restricted to the atrioventricular valves (Fig. 9a, b).

*Controls*. When the primary antibody was either not applied or was preincubated with AMSFYFPRMamide or SCP<sub>B</sub>, staining was abolished. Staining persisted, however, when the primary antibody was preincubated with FMRFamide. The controls were the same for both staining methods.

#### Bioassay

The three novel peptides identified in *M. mercenaria* were synthesized and tested for their effects on isolated

rectums and hearts of the clam. The effects of IAMSFYFPRMamide were indistinguishable from those of AMSFYFPRMamide, so only the latter peptide and YFAFPRQamide were tested on the typhlosoles of the intestine and style sac.

*Rectum*. Sixteen preparations were tested, most of them quiescent. The effect of low to moderate doses of the clam SCPs was a prompt relaxation of the rectum (Fig. 10); the threshold was  $10^{-10}$ – $10^{-9}$  M. When higher doses ( $10^{-6}$ – $10^{-5}$  M) were applied, a biphasic response (*i.e.*, relaxation followed by contraction) was observed. Compared with the actions of AMSFYFPRMamide or its Ile<sup>1</sup> analog, YFAFPRQamide produced a stronger relaxation and a weaker contraction. SCP<sub>B</sub>, the gastropod peptide, also decreased the tone of the rectum, but was much less potent than the endogenous bivalve peptides; threshold was about  $10^{-8}$  M (Fig. 10).

Since acetylcholine (ACh) also relaxes the clam rectum with a threshold of  $3 \times 10^{-9}$ – $3 \times 10^{-8}$  M (Greenberg and Jegla, 1963), the SCPs might be acting presynaptically to release ACh. But the addition of  $10^{-5}$  M benzoquinonium chloride (an ACh antagonist) to the bath did not alter the response of the rectum to the SCPs.

The effect of 5-HT ( $10^{-6}$  M) on the clam rectum is a large contracture, sometimes accompanied by rhythmic "beating" (Greenberg and Jegla, 1963; Doble and Greenberg, 1982). In five experiments, the SCP-like peptide YFAFPRQamide was applied after the effect of 5-HT had developed (Fig. 11). Under these conditions, YFAFPRQamide usually relaxed the 5-HT contracture, and then either augmented the rhythmical contractions or reduced them. These combined actions were extraordinarily variable.

*Intestinal typhlosole*. We tested 18 strips of intestinal typhlosole, and unlike the rectum, all displayed slow, regular, rhythmical activity with a frequency of 2–7 contractions per minute. The effects of the two SCPs tested (AMSFYFPRMamide and YFAFPRQamide) were similar: both reduced the frequency and force of contraction, as well as the tone of the preparation (Fig. 12). YFAFPRQamide seems to be more potent; its threshold is  $10^{-8}$  M compared with  $3 \times 10^{-7}$  M for AMSFYFPRMamide.

In preliminary experiments, 5-HT increased both the basal tone of the preparation and the frequency of contractions (threshold, about  $3 \times 10^{-7}$  M); FMRFamide had a similar effect, but at a slightly higher threshold ( $10^{-6}$  M); and ACh seemed to have a biphasic effect, as it does on the rectum, but never at a dose below  $3 \times 10^{-6}$  M. These effects were modest, except at very high concentrations.

*Style sac typhlosoles*. Of the eight preparations tested, six exhibited rhythmic activity, particularly after the application of peptides. Of the two SCPs tested,

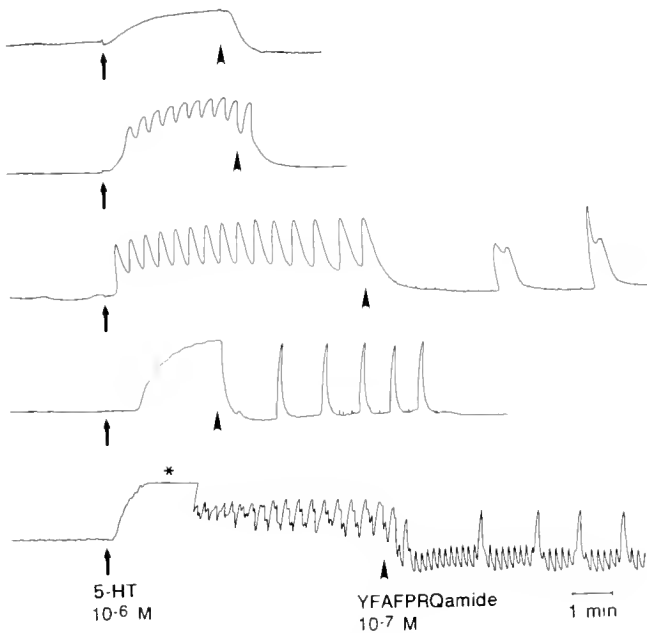


**Figure 11.** Responses of isolated clam rectums to YFAFPRQamide in the presence of 5-hydroxytryptamine (5-HT). The preparations were first stimulated with 5-HT (arrow). When the effect was established (contracture with or without rhythmical activity), the peptide was added (arrowhead). \*Recording off-scale; baseline adjusted.

YFAFPRQamide was again more potent: it inhibited rhythmicity transiently at  $10^{-9}$  M, and relaxed the tissue at  $10^{-8}$  M. These effects were also produced by AMSFYFPRMamide, but at doses about 3- to 10-fold higher (Fig. 13).

**Heart.** The effects of the SCP-related peptides were tested on 42 isolated hearts. More than half of the preparations were either not affected ( $10^{-7}$ – $10^{-4}$  M), or an effect appeared that could not be repeated. The rest of the hearts responded reliably to the SCPs. The threshold action was an inhibition of beat amplitude (threshold,  $10^{-7}$ – $10^{-6}$  M). At higher doses, beat and tone increased transiently, and the heart was finally arrested, usually in diastole. Acceptable dose-response relationships were seen in only five or six experiments.

### Discussion

We have isolated and sequenced three SCP-related peptides in the venerid clam *Mercenaria mercenaria*: IAMSFYFPRMamide, AMSFYFPRMamide, and YFAFPRQamide. The latter two peptides were also identified in the cockle *Dinocardium robustum*. But two quite different SCP-like sequences were found in the eastern oyster *Crassostrea virginica* (Table II). The features of these bivalve peptides are best evaluated with reference to an SCP-like sequence found in a mussel, *Mytilus edulis* (Fujisawa

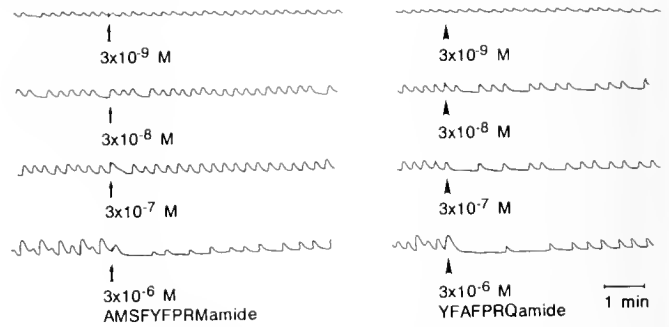


**Figure 12.** Dose-dependent effects of two clam SCPs on the isolated typhlosole of the clam intestine. Doses were delivered at the arrows or arrowheads.

et al., 1993), as well as six sequences identified in various gastropods (Lloyd et al., 1987; Price et al., 1989; Price et al., 1990). The total set includes 12 peptides from 13 species (Table II).

The bivalve SCPs as a group, including peptides from both pteriomorphs and heterodonts, are clearly distinct from the gastropod peptides. All but one of the gastropod SCPs—from a selection of species representing all three subclasses—contain the C-terminal heptapeptide -YLAFPRMamide, and the substitution of an isoleucyl residue for a leucyl in *Littorina irrorata* is a conservative one. In contrast, the bivalve peptides are much more diverse, and none of them has fewer than two substitutions with respect to the gastropod C-terminal heptapeptide. Indeed, in two of these peptides—YFAFPRQamide (in *M. mercenaria*) and APNFLAYPRLamide (in *M. edulis*)—the terminal methionine is replaced.

The high pharmacological potency of YFAFPRQamide, and the similarity of its effect on the clam gut to that of AMSFYFPRMamide and the gastropod peptide

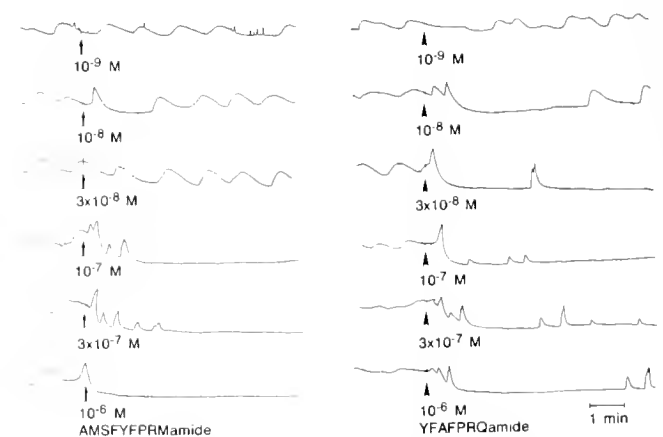


**Figure 13.** Dose-dependent responses of isolated segments of the style sac typhlosole to two clam SCPs. Doses were delivered at the arrows or arrowheads.

Table II

Sequences and species distribution of known molluscan SCPs

CLASS SEQUENCES <sup>a</sup>	Subclass Species <sup>b,c</sup>		
<b>BIVALVIA</b>	<u>Pteriomorphia</u>	<u>Heterodonta</u>	
A P N <u>F</u> L A <u>Y</u> P R <u>L</u> a	<i>Med</i> <sup>1</sup>		
A P K <u>Y</u> F <u>Y</u> F P R M a	<i>Cvi</i>		
S <u>A</u> F <u>Y</u> F P R M a	<i>Cvi</i>		
I A M <u>S</u> F <u>Y</u> F P R M a		<i>Mme</i>	
A M <u>S</u> F <u>Y</u> F P R M a		<i>Mme, Dro</i>	
<u>Y</u> F A F P R Q a		<i>Mme, Dro</i>	
<b>GASTROPODA</b>	<u>Prosobranchia</u>	<u>Opisthobranchia</u>	<u>Pulmonata</u>
S G Y L A F P R M a			<i>Has</i> , <sup>2</sup> <i>Lst</i> , <sup>3</sup> <i>Spe</i> , <sup>3</sup> <i>Htr</i> , <sup>3</sup> <i>Bgl</i> , <sup>3</sup>
M N Y L A F P R M a		<i>Abr</i> , <sup>4</sup> <i>Aca</i> <sup>5</sup>	<i>Has</i> , <sup>2</sup> <i>Spe</i> <sup>3</sup>
S Q G Y L A F P R M a			<i>Htr</i> , <sup>3</sup> <i>Bgl</i> <sup>3</sup>
A R P G Y L A F P R M a		<i>Aca</i> <sup>6</sup>	
S Q P Y <u>I</u> A F P R M a	<i>Lir</i> <sup>3</sup>		
N Y L A F P R M a	<i>Tha</i> <sup>3</sup>		

<sup>a</sup> The residues in the standard gastropod C-terminal heptapeptide (-YLAFPRMa) are in bold italics; residues that are different from the standard are underlined. a = amide.

<sup>b</sup> Species abbreviations: first letter of genus plus first two letters of species:

<i>Abr</i> , <i>Aplysia brasiliana</i>	<i>Lir</i> , <i>Littorina irrorata</i>
<i>Aca</i> , <i>Aplysia californica</i>	<i>Lst</i> , <i>Lymnaea stagnalis</i>
<i>Bgl</i> , <i>Biomphalaria glabrata</i>	<i>Med</i> , <i>Mytilus edulis</i>
<i>Cvi</i> , <i>Crassostrea virginica</i>	<i>Mme</i> , <i>Mercenaria mercenaria</i>
<i>Dro</i> , <i>Dinocardium robustum</i>	<i>Spe</i> , <i>Siphonaria pectinata</i>
<i>Has</i> , <i>Helix aspersa</i>	<i>Tha</i> , <i>Thais haemastoma</i>
<i>Htr</i> , <i>Helisoma trivolvis</i>	

<sup>c</sup> References:

- <sup>1</sup> Fujisawa *et al.*, 1993
- <sup>2</sup> Price *et al.*, 1990
- <sup>3</sup> Price *et al.*, 1989
- <sup>4</sup> Morris *et al.*, 1982
- <sup>5</sup> Mahon *et al.*, 1985
- <sup>6</sup> Lloyd *et al.*, 1987

SCP<sub>B</sub> (MNYLAFPRMamide; Table II), suggest that the substitution of a Gln for a Met at the C-terminal carries little apparent functional penalty. Further, the structural features critical for the function of the clam SCPs seem not to be confined to the C-terminal. Notwithstanding the high potency of YFAFPRQamide on clam gut, Gln may not be an effective replacement for Met in general. Indeed, very high doses of YFAFPRQamide are required for activity on the heart of *Helix aspersa*, (W. Lesser, personal communication), whereas SCP<sub>B</sub> is a highly potent excitor of this preparation (Price *et al.*, 1990). So the structure-activity relations of the gastropod heart may be very different from those of the bivalve gut.

In *M. mercenaria*, the number of SCP-like peptides that are primary products of precursor processing remains uncertain. We have isolated and sequenced three peptides; but no more than two SCPs have been found in any other species (Table II), and the preprohormone

in *Aplysia californica* includes only one copy each of SCP<sub>B</sub> and SCP<sub>A</sub> (Mahon *et al.*, 1985). Furthermore, two of the peptides we have identified (IAMSFYFPRMamide and AMSFYFPRMamide) differ only by the occurrence or lack of a single isoleucine residue at the N-terminal. Thus, the shorter peptide, AMSFYFPRMamide, might well be a degradation product. Indeed, we have identified, by their molecular ions, a series of peptides representing successive deletions at the N-terminal down to FYFPRMamide. Still, the SCP precursor of *Aplysia* is the only one known, so we cannot rule out the possibility that both IAMSFYFPRMamide and AMSFYFPRMamide are, with YFAFPRQamide, primary processing products of one or more preprohormones. This issue will only be resolved when the mRNAs encoding the clam or cockle precursors have been identified and sequenced.

The distribution and pharmacological actions of a peptide are often indicative of its role in the animal. For example, the visceral ganglia, containing roughly twice as much SCP as either the cerebral or pedal ganglia, innervate the posterior sections of the mantle, the somatic musculature, and the gut, as well as the gills and the renopericardial organs (Loveland, 1963). Of these potential targets, the gills, intestine, and rectum contain about a quarter of the amount of SCP in the visceral ganglia. Moreover, immunoreactive fibers are present in the rectal musculature, the intestinal typhlosole, and the gills. Finally, the clam SCPs are also biologically active, not only on the gut musculature, as reported here, but on the cilia of isolated gill demibranchs (L. F. Gainey, Jr., personal communication). These findings suggest that one role of the SCPs in *M. mercenaria* is to regulate feeding and gut motility, as in gastropods (see Prior and Welsford, 1989; Lloyd, 1989; and Weiss *et al.*, 1992).

Other data are less supportive of this notion, or are incomplete. The style sac typhlosoles contain very low levels of peptide, yet immunoreactive neural fibers are clearly evident, and the SCPs reduce rhythmic activity and relax the tissue at low doses. In contrast, the palps, which are innervated from the cerebral ganglia, contain very high levels of SCPs and, again, the peptide has been localized to a network of neurons. But the palps are complex organs, with both sensory and motor (muscular, ciliary, and secretory) functions. In the absence of an appropriate bioassay, the roles of the SCPs in this tissue remain enigmatic.

The pharmacology of the bivalve midgut has never before been examined, and rhythmical muscular activity of the typhlosole has not previously been reported. Indeed, the notion that digested food and feces are moved through the midgut by cilia is widely accepted (*e.g.*, Morton, 1983). Our results suggest that the typhlosole plays a role in moving material through the gut. The relative ease with which this tissue is prepared and the regularity of its contractions suggest that further studies of its regulation will be possible.

Belying the original meaning of 'SCP' (see footnote 3), the clam heart contains very low levels of SCP-related immunoreactivity and is poorly responsive to the synthetic peptides, with a threshold at least 100 times higher than those of gastropod hearts. But nerve fibers containing SCP-related immunoreactivity do occur in the atrioventricular valves, and isolated valves treated with YFAFPRQamide contract and begin to beat rhythmically (N. A. Pennell and W. Lesser, personal communication). In conclusion, the SCPs may play a cardioregulatory role in the clam, perhaps limited to the valves, but certainly unlike that in *Helix aspersa* (Price *et al.*, 1990; Lesser and Greenberg, 1993) or *Aplysia californica* (Lloyd *et al.*, 1985; Skelton *et al.*, 1992).

## Acknowledgments

We thank A. O. D. Willows for the gift of the monoclonal antibody for SCP<sub>B</sub> and E. Weber for providing an antiserum for FMRFamide. This work was supported by the Grass Foundation (A. C.-M.), by the National Institutes of Health (HL28440, M. J. G. and D. A. P., HL08371, W.L.), and by the REU program of NSF (D. M. R. and S. J. P.). Peptide sequence analysis and peptide synthesis were provided by the Protein Chemistry Core Facility of the Interdisciplinary Center for Biotechnology Research, University of Florida. This is Contribution No. 308 from the Tallahassee, Sopchoppy & Gulf Coast Marine Biological Association.

## Literature Cited

- Beltz, B. S., and G. D. Burd. 1989. *Immunocytochemical Techniques: Principles and Practice*. Cambridge Scientific Publications, Massachusetts. 182 pp.
- Bulloch, A. G. M., D. A. Price, A. D. Murphy, T. D. Lee, and H. N. Bowes. 1988. FMRFamide peptides in *Helisoma*: identification and physiological actions at a peripheral synapse. *J. Neurosci.* **8**: 3459-3469.
- Candelario, A., D. A. Price, K. E. Doble, and M. J. Greenberg. 1990a. Isolation and identification of SCPs in bivalved molluscs. *Soc. Neurosci. Abstr.* **16**: 550.
- Candelario, A., S. J. Prichard, W. Lesser, K. E. Doble, D. A. Price, and M. J. Greenberg. 1990b. Neurohormonal modulation of the gut and feeding organs of the clam. *Am. Zool.* **30**: 29A.
- Doble, K. E., and M. J. Greenberg. 1982. The clam rectum is sensitive to FMRFamide, the enkephalins and their common analogs. *Neuropeptides* **2**: 157-167.
- Fujisawa, Y., I. Kubota, K. Nomoto, H. Minakata, Y. Yasuda-Kamatani, T. Ikeda, and Y. Muncoka. 1993. A *Mytilus* peptide related to the small cardioactive peptides (SCPs): structure determination and pharmacological characterization. *Comp. Biochem. Physiol.* **104C**: 469-475.
- Greenberg, M. J., and T. C. Jegla. 1963. The action of 5-hydroxytryptamine and acetylcholine on the rectum of the venus clam, *Mercenaria mercenaria*. *Comp. Biochem. Physiol.* **9**: 275-290.
- Humason, G. L. 1967. *Animal Tissue Techniques*. 2nd ed. Freeman, San Francisco, CA.
- Krajniak, K. G., M. J. Greenberg, D. A. Price, K. E. Doble, and T. D. Lee. 1989. The identification, localization, and pharmacology of FMRFamide-related peptides and SCP<sub>B</sub> in the penis and crop of the terrestrial slug, *Limax maximus*. *Comp. Biochem. Physiol.* **94C**: 485-492.
- Lesser, W., and M. J. Greenberg. 1993. Cardiac regulation by endogenous small cardioactive peptides and FMRFamide-related peptides in the snail *Helix aspersa*. *J. Exp. Biol.* **178**: 205-230.
- Lloyd, P. E. 1978. Distribution and molecular characteristics of cardioactive peptides in the snail, *Helix aspersa*. *J. Comp. Physiol.* **128**: 269-276.
- Lloyd, P. E. 1989. Peripheral actions of the SCPs in *Aplysia* and other gastropod molluscs. *Am. Zool.* **29**: 1265-1274.
- Lloyd, P. E., and A. O. D. Willows. 1988. Multiple transmitter neurons in *Tritonia* II. Control of gut motility. *J. Neurobiol.* **19**: 55-67.
- Lloyd, P. E., I. Kupfermann, and K. R. Weiss. 1984. Evidence for parallel actions of a molluscan neuropeptide and serotonin in mediating arousal in *Aplysia*. *Proc. Natl. Acad. Sci. U.S.A.* **81**: 2934-2937.

- Lloyd, P. E., I. Kupfermann, and K. R. Weiss. 1985. Two endogenous neuropeptides (SCP<sub>A</sub> and SCP<sub>B</sub>) produce a cAMP-mediated stimulation of cardiac activity in *Aplysia*. *J. Comp. Physiol.* **156**: 659-667.
- Lloyd, P. E., I. Kupfermann, and K. R. Weiss. 1987. The sequence of small cardioactive peptide A: a second member of a class of neuropeptides in *Aplysia*. *Peptides* **8**: 179-184.
- Lloyd, P. E., I. Kupfermann, and K. R. Weiss. 1988. Central peptidergic neurons regulate gut motility in *Aplysia*. *J. Neurophysiol.* **59**: 1613-1626.
- Loveland, R. E. 1963. Some aspects of cardio-regulation in *Mercenaria mercenaria*. Thesis, Dept. of Biology, Harvard University.
- Mahon, A. C., P. E. Lloyd, K. R. Weiss, I. Kupfermann, and R. H. Scheller. 1985. The small cardioactive peptides A and B of *Aplysia* are derived from a common precursor molecule. *Proc. Natl. Acad. Sci. U.S.A.* **82**: 3925-3929.
- Masinovsky, B., S. C. Kempf, J. S. Callaway, and A. O. D. Willows. 1988. Monoclonal antibodies to the molluscan small cardioactive peptide SCP<sub>B</sub>: Immunolabeling of neurons in diverse invertebrates. *J. Comp. Neurol.* **273**: 500-515.
- Morris, H. R., M. Panico, A. Karplus, P. E. Lloyd, and B. Riniker. 1982. Elucidation by FAB-MS of the structure of a new cardioactive peptide from *Aplysia*. *Nature* **300**: 643-645.
- Morton, B. 1983. Feeding and digestion in Bivalvia. Pp. 65-147 in *The Mollusca, Vol. 5, Physiology Part 2*. A. S. M. Saleuddin and K. M. Wilbur, eds. Academic Press, New York.
- Murphy, A. D., K. Lukowiak, and W. K. Stell. 1985. Peptidergic modulation of patterned motor activity in identified neurons of *Helisoma*. *Proc. Natl. Acad. Sci. U.S.A.* **82**: 7140-7144.
- Pojeta, J., Jr., B. Runnegar, and J. Kriz. 1973. *Fordilla troyensis* Barande: the oldest known pelecypod. *Science* **180**: 866-868.
- Price, D. A., D. M. Reed, K. E. Doble, T. D. Lee, and M. J. Greenberg. 1989. The distribution of SCP peptides in molluscs. *Soc. Neurosci. Abstr.* **15**: 737.
- Price, D. A., W. Lesser, T. D. Lee, K. E. Doble, and M. J. Greenberg. 1990. Seven FMRFamide-related and two SCP-related cardioactive peptides from *Helix*. *J. Exp. Biol.* **154**: 421-437.
- Prior, D. J., and I. G. Welford. 1989. The role of small cardioactive peptide, SCP<sub>B</sub>, in the regulatory responses of terrestrial slugs. *Am. Zool.* **29**: 1255-1263.
- Richmond, J. E., A. G. M. Bulloch, and K. Lukowiak. 1986. Peptidergic modulation of a neuromuscular junction in *Aplysia*: bioactivity and immunocytochemistry. *Brain Res.* **370**: 159-164.
- Skelton, M., A. Alevizos, and J. Koester. 1992. Control of the cardiovascular system of *Aplysia* by identified neurons. *Experientia* **48**: 809-817.
- Weiss, K. R., V. Brezina, E. C. Cropper, S. L. Hooper, M. W. Miller, W. C. Probst, F. S. Vilim, and I. Kupfermann. 1992. Peptidergic co-transmission in *Aplysia*: functional implications for rhythmic behaviors. *Experientia* **48**: 456-463.
- Welsh, J. H., and R. Faub. 1948. The action of choline and related compounds on the heart of *Venus mercenaria*. *Biol. Bull.* **95**: 346-353.
- Willows, A. O. D., P. E. Lloyd, and B. Masinovsky. 1988. Multiple transmitter neurons in *Tritonia*. III. Modulation of central pattern generator controlling feeding. *J. Neurobiol.* **19**: 69-86.

# The Integument of the Marine Echiuran Worm *Urechis caupo*

JAISHRI G. MENON AND ALISSA J. ARP

*Department of Biology, San Francisco State University, 1600 Holloway Avenue,  
San Francisco, California 94132*

**Abstract.** During low tide, the burrow water of the marine echiuran worm *Urechis caupo* becomes hypoxic, and hydrogen sulfide concentrations reach levels that would be toxic to most animals. Integument morphology in *U. caupo* is evaluated as an exchange surface and as a permeation barrier. Adaptive features include the rugose nature of the epidermis, which increases the surface area for oxygen uptake, and the thick muscular body wall, which provides a chief motive power in creating peristaltic movements along the body wall to ventilate the burrow. The epidermis is covered by a cuticle and contains two types of mucus-secreting cells: orthochromatic and metachromatic. Underlying connective tissue and three muscle layers form the bulk of the body wall. The integument does not present a significant structural barrier to permeation, although the mucus secreted by the epidermal cells may retard sulfide entry. Ultrastructural studies suggest three possible mechanisms that *U. caupo* may use to counteract the toxic effects of sulfide at the integumentary surface: metabolism of symbiotic bacteria embedded in the innermost cuticle layer and grouped together in the superficial epidermis, dying off of peripheral, sulfide-exposed cells, and oxidation of sulfide at specialized, iron-rich, lysosomal organelles termed sulfide oxidizing bodies.

## Introduction

Invertebrate integuments are morphologically and biochemically diverse but, because they are located at the interface of the organism with its environment, have common adaptive and protective functions. They provide physical protection for internal organs, regulate the exchange of materials between the organism and its envi-

ronment, and act as a barrier to the ingress of various environmental agents.

Environmental hydrogen sulfide, produced by both natural and industrial sources, poisons aerobic respiration by binding to cytochrome c oxidase (National Research Council, 1979). No marine animal has been shown to be impermeable to ambient sulfide, and a variety of sulfide detoxification mechanisms have been reported (reviewed in Somero *et al.*, 1989), including the secretion of a mucus coat that buffers sulfide entry into the priapulid worm *Halicryptus spinulosus* (Oeschger and Janssen, 1991).

Although sulfide levels less than 1  $\mu M$  are fatal to most organisms, the marine worm *Urechis caupo* lives in mud and sand flats with sulfide levels of 25–30  $\mu M$  (Arp *et al.*, 1992) and is freely permeable to sulfide (Julian and Arp, 1992). The cytochrome c oxidase activities of the tissues of *U. caupo* are as sensitive to sulfide as homologous enzymes of other animals (Powell and Arp, 1989), indicating that this worm must either protect sensitive cytochromes in the body wall integument or tolerate anaerobic metabolism. Eaton and Arp (1993), however, have demonstrated that living worms rely primarily on aerobic respiration when exposed to sulfide, and various physiological adaptations that enable sulfide tolerance and detoxification have been reported (Arp *et al.*, 1992; Menon and Arp, 1992a,b; Arp, 1991; Powell and Arp, 1989).

Several early studies of the body wall of *U. caupo* (Newby, 1941) and other echiuran worms (Jameson, 1899; Jose, 1964) provide only limited information about histology and none, of course, about the ultrastructure of the cells that constitute the integument. The intent of this study was to examine the structure and histochemistry of the integument of *U. caupo* and, in particular, to evaluate its role as a protective organ or exchange surface in an animal living in the physiologically challenging environment of the marine mudflat. We report ultrastructural

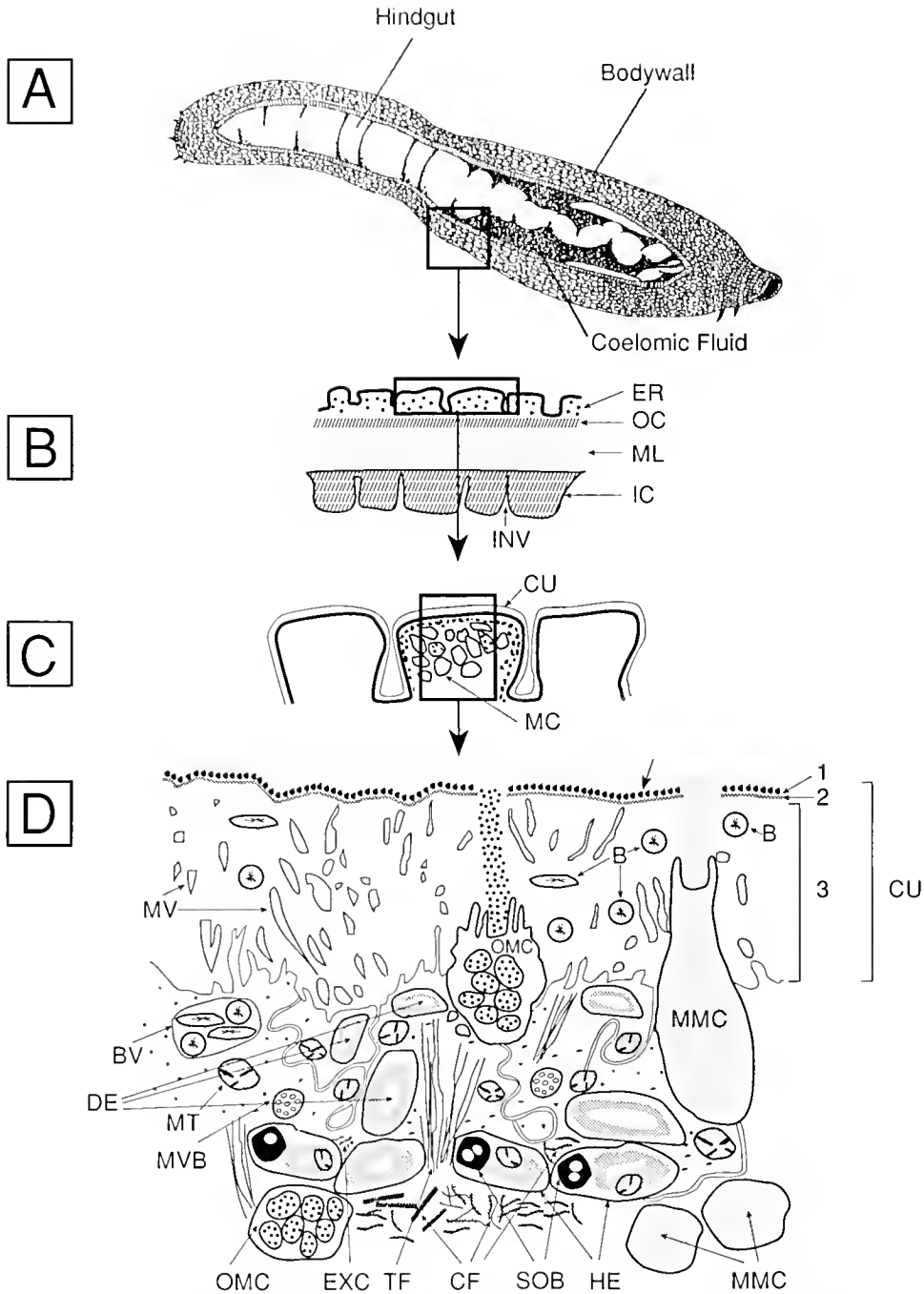
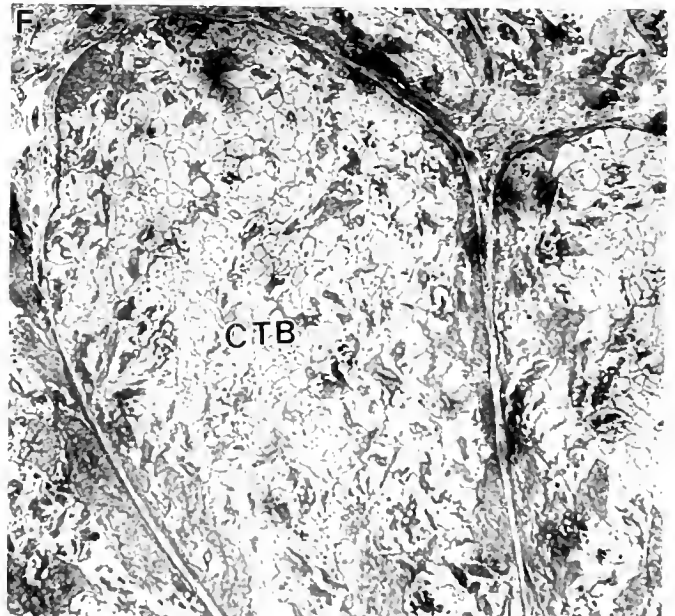
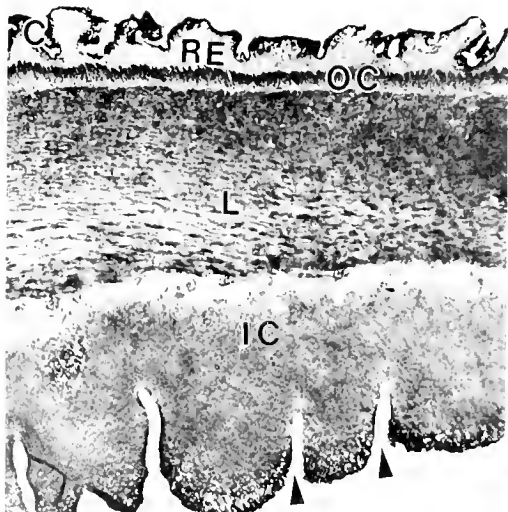
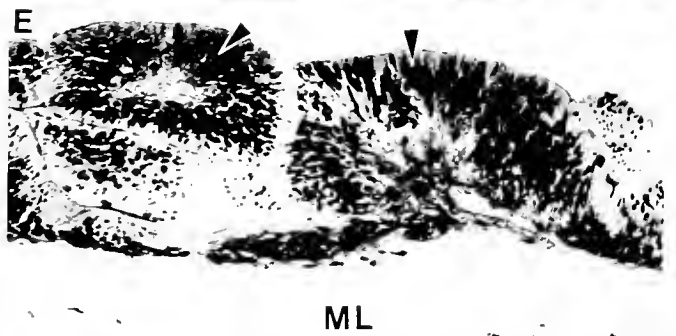
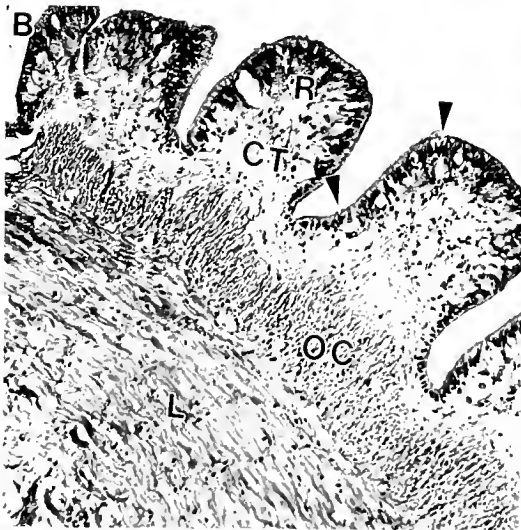
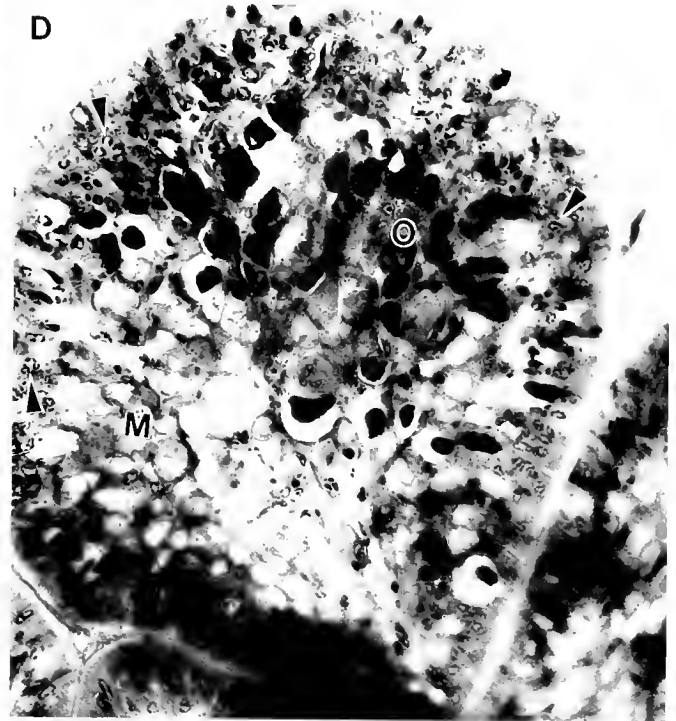
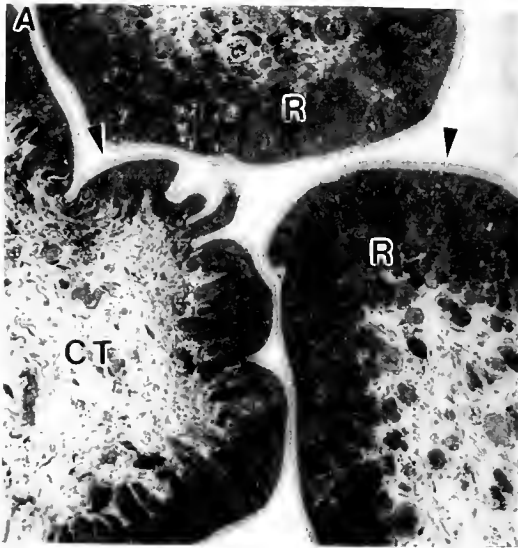


**Figure 1.** Schematic diagram of the gross anatomy and body wall structure of *Urechis caupo*. (A) Body plan and internal anatomy. (B) Schematic diagram of a 5  $\mu\text{m}$  thick paraffin section of the body wall showing rugose epidermis (ER) followed by three muscle layers: outer circular muscle layer (OC), middle longitudinal muscle layer (ML), and innermost circular muscle layer (IC) showing invaginations (INV) at regular intervals. (C) Schematic representation of 0.5–1.0  $\mu\text{m}$  thick plastic section showing rugae of the epidermis with mucus cells (MC) covered by a thin cuticle (CU). (D) Schematic representation of the ultrastructure of the epidermis at a magnification of about 13,000. Note that the cuticle (CU) is made up of three layers: (1) an outer layer consisting of epicuticular projections covered by fuzzy mucus (arrow) derived from metachromatic mucus cells (MMC). (2) a middle layer that is thin and granular, and (3) an innermost layer, which is the largest, and contains many microvilli (MV) and bacteria (B). Two types of mucus cells are evident in the epidermis: orthochromatic (OMC) and metachromatic (MMC). Groups of bacteria occur inside vacuoles (BV) in the superficial epidermal layers. Numerous mitochondria (MT), tonofilaments (TF), and multivesicular bodies (MVB) are present in the deeper layers of the epidermis. Healthy epidermal cells (HE) often have lysosomal sulfide oxidizing bodies (SOB) which possess empty vacuoles. Dying epidermal cells (DE) show condensed cytoplasm and a loss of organelles. The extracellular matrix (EXC) is composed of collagen fibers (CF) with a beaded appearance.







evidence suggesting that *U. caupo* may protect the integumentary surface from the toxic effects of sulfide by secretion of mucus, metabolic activity of symbiotic bacteria, dying-off of peripheral, sulfide-exposed cells, and oxidation of sulfide at specialized lysosomal organelles.

### Material and Methods

*U. caupo* individuals weighing 25 to 55 g were collected from Princeton Harbor, Elkhorn Slough, and Bodega Bay, California, during low tides. Animals were treated in one of three ways and then examined. Freshly collected worms were used within one day of capture from the natural environment. Laboratory-maintained worms were kept for 2 weeks to 4 months on the bottom of aerated aquaria free of sediment. These worms were not housed in artificial tubes, which has no effect on survival rate in the laboratory (authors' unpub. obs.). Sulfide-exposed worms were placed in respirometers, and oxygenated seawater was circulated through the chamber. Sulfide from a deoxygenated 8 mM sodium sulfide ( $\text{Na}_2\text{S} \cdot 9\text{H}_2\text{O}$ ) stock solution, buffered with 125 mM imidazole and titrated with concentrated HCl to a final pH of approximately 6.8, was introduced with a peristaltic pump into the line just before the respirometer. Sulfide and oxygen levels in the respirometer were continuously monitored with electrodes that led to a data collection system (Arp *et al.*, 1992; Eaton and Arp, 1993).

Prior to dissection, the coelom of each animal was injected with muscle relaxant (0.4 M  $\text{MgCl}_2$ , 0.5 ml/g body weight), and the animal was left in water containing 0.4 M  $\text{MgCl}_2$  until it had completely relaxed. Once relaxed, the body wall was cut open through a longitudinal incision in the mid-dorsal line. For light microscopy, body wall samples from three different regions were taken: the anterior region just behind the mouth, the middle region, and the posterior region. The tissues were fixed in either Bouin's fixative or 10% formalin for 24 h, dehydrated in an ethanol series (70%, 100%), cleared in toluene, and embedded in paraffin. Thick sections (5  $\mu\text{m}$ ) were cut, mounted on slides, and stained with hematoxylin and eosin for routine histology.

For electron microscopy, body wall samples were taken from the mid-dorsal region and fixed in 3% glutaraldehyde in 0.1 M cacodylate buffer, with 0.4 M NaCl to maintain the proper osmolarity (Holland and Neilson, 1978). Three 10-min rinses were carried out in the same solution without glutaraldehyde. Postfixation was for 30 min in 1% osmium tetroxide in 0.1 M cacodylate buffer (pH 7.3) with 0.4 M NaCl. All samples were rapidly dehydrated in an ethanol series (50%, 70%, 95%, 100%), and specimens were transferred to propylene oxide and embedded in Eponate 12 resin (Ted Pella). Semi-thin sections (0.5–1.0  $\mu\text{m}$ ) were stained with toluidine blue for light microscopy. Sections in the pale gold to silver range were cut with a diamond knife on a Sorvall MT2 ultramicrotome, double stained with uranyl acetate and lead citrate, and observed under a Zeiss EM 10 operating at 60 kV.

Bacterial densities in the cuticles of two worms from each of the following treatments were estimated: freshly collected worms from Bodega Bay; laboratory-maintained animals in sulfide-free water; and sulfide-exposed worms in the laboratory. One grid was taken from each specimen, and 15 electron micrographs of different areas were photographed at the same magnification. Bacteria observed in photomicrographs at a final magnification of 32,000 were counted.

To demonstrate mucopolysaccharides, the following histochemical methods were performed with appropriate controls (Bancroft and Stevens, 1977). Paraffin sections were stained with periodic acid-Schiff's (PAS) for mucopolysaccharides; diastase treatment followed by PAS for glycogen; PAS in conjunction with alcian blue 8GX to distinguish neutral mucins from acidic mucins; alcian blue staining at pH 0.5 and 2.5 to confirm the sulfated and carboxylated mucins; methylation and saponification with alcian blue (pH 2.5) and critical electrolyte concentration with alcian blue (pH 2.5) to differentiate sulfated from carboxylated mucopolysaccharides; and toluidine blue and azure A for showing metachromasia and acidic mucopolysaccharides.

After calibration with a stage micrometer, an ocular micrometer and a whipple disc were used on the micro-

**Figure 2.** (A) Tangential section of epidermal rugae (R). Epidermal cells covered by a cuticle (arrows) and stained with PAS showing the presence of mucopolysaccharides. Underlying connective tissue (CT) does not show PAS positive reaction. 1  $\mu\text{m}$  Epoxy section.  $\times 220$ . (B) Transverse section of epidermis showing rugae (R), underlying connective tissue (CT), and the outer circular (OC) and middle longitudinal (L) muscle layers. Note darkly stained nuclei on the periphery of epidermis (arrows). 5  $\mu\text{m}$  paraffin section. Hematoxylin and eosin stain.  $\times 110$ . (C) Transverse section of the body wall showing rugose epidermis (RE), followed by three muscle layers: outer circular (OC), middle longitudinal (L) and inner circular (IC). The innermost layer shows deep invaginations (arrows) at regular interval. 10  $\mu\text{m}$  frozen section. Hematoxylin and eosin.  $\times 20$ . (D) Epidermal rugae at a higher magnification. Two types of mucus-secreting cells are evident: orthochromatic (O), which are darkly stained, and metachromatic (M) showing a fine reticulate pattern. Note cells with pyknotic nuclei at the periphery of the epidermis (arrows). 1  $\mu\text{m}$  Epoxy section. Toluidine blue stain.  $\times 220$ . (E) Transverse section of epidermis showing the presence of acidic mucopolysaccharides in the rugae (arrows). Underlying muscle layers (ML) do not react with stain. 5  $\mu\text{m}$  paraffin section. Alcian blue stain.  $\times 110$ . (F) Transverse section passing through the anterior region of the body at the proboscis showing connective tissue bundles (CTB). 1  $\mu\text{m}$  Epoxy section. Toluidine blue.  $\times 570$ .

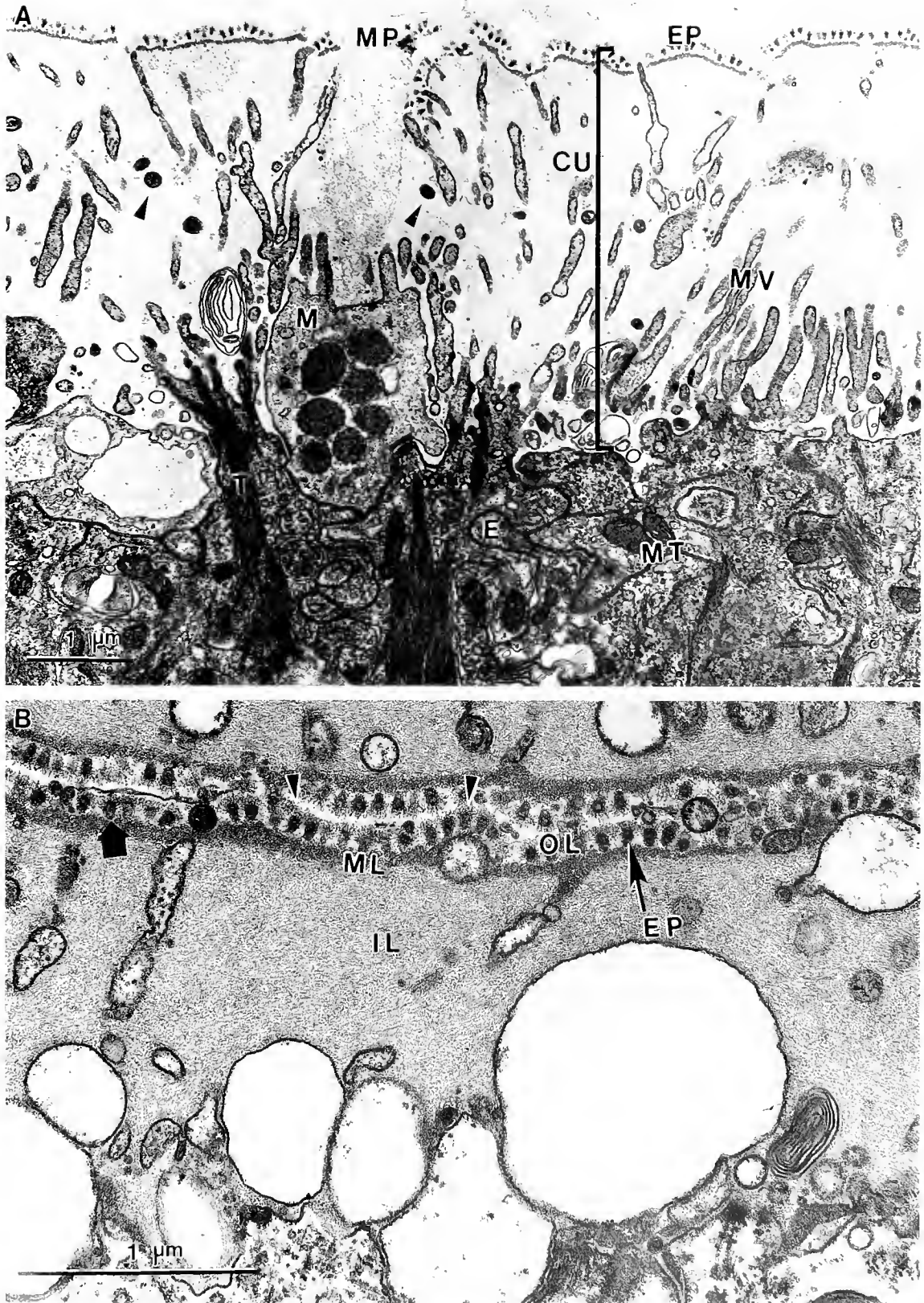


Figure 3. (A) Overview of the epidermis showing the cuticle (CU) with epicuticular projections (EP) in the outermost layer, scattered bacteria (arrows) and microvilli (MV) in the innermost layer, a mucus-secreting cell (M) discharging mucus through the mucus pore (MP), tonofibrils (T), and numerous mitochondria

scope to count the number of mucus cells per 0.2 mm<sup>2</sup> area in 0.5 to 1.0  $\mu$ m thick plastic sections of the epidermis of freshly collected and laboratory-maintained animals (Gona, 1979). The terminology of Gona (1979) for the color of mucus cells after staining with toluidine blue has been adopted. Counts were made from three to five mid-dorsal body regions of animals. Dying epidermal cells in sulfide-free (laboratory-maintained) and sulfide-exposed (freshly collected and exposed to sulfide in the laboratory) animals were distinguished under the light microscope by their intensely basophilic nuclei and loss of cytoplasm, and were counted. The body wall epidermis of sulfide-exposed animals was grazed with a sharp razor blade in the mid-dorsal region prior to sulfide exposure, and the mucus or dying cells in the sample counted (control). The worms were then allowed to heal in the aquaria for 4 to 5 days, and were then placed in a flow-through aquarium with oxygenated seawater containing 50 to 70  $\mu$ M sulfide for 48 to 78 h (Arp *et al.*, 1992). A second epidermal sample was taken about 1 cm from the original sample and the cells counted (experimental).

Results are presented as the mean  $\pm$  the standard deviation of the mean. Statistical tests were accepted as significant for  $P < 0.05$ . Fixed effects analysis of variance (ANOVA) was employed to test for significant differences between animal treatments (Zar, 1984).

## Results

An overview of the structure of the integument of *U. caupo* is shown diagrammatically in Figure 1, at the light microscopic level in Figure 2, and at the ultrastructural level in Figure 3A. The surface of the body wall integument is traversed by fine irregular channels that form a rugose surface (Fig. 1B, 2B, C). The epidermis is covered by an outermost cuticle that harbors prokaryotic cells (Fig. 1D, 3A, 4). The epidermis contains two types of columnar mucus-secreting cells (Fig. 1D, 2D). Another type of cell present in the superficial layers of the epidermis is characterized by large, pyknotic, and intensely basophilic nuclei with chromatin material dispersed toward the nuclear membrane (Fig. 2D, arrows). Unusual cytolysosomes are present in many of the epidermal cells as well (Fig. 1D, 7, 8). Subjacent to the epidermis is a thin layer of connective tissue (Fig. 2A, B), and below it are three distinct muscle layers: an outer circular, a middle longitudinal, and an innermost circular muscle layer (Fig. 2C). The innermost layer shows invaginations at regular intervals (Fig. 2B, C, arrows). The anterior body wall in the region

of the proboscis has additional connective tissue bundles (Fig. 2F), and the posterior body wall in the region of the anus has a thicker muscle layer than does the anterior and middle body wall.

Ultrastructural observations indicate that the integumentary cuticle consists of three layers. The outermost layer is composed of membrane-bound and regularly arranged epicuticular projections that show a definite substructure of an electron-dense lining surrounding a central core (Fig. 3A, B). The epicuticular projections arise from the exposed tips of the microvilli, which are cytoplasmic extensions of epidermal cell membranes and are present in the innermost layer of cuticle (Fig. 3A). Covering the epicuticular projections are fine strands of mucus material forming the supracuticular mucus coat (Fig. 3B). The fuzzy nature of this mucus material is ultrastructurally similar to the contents of the metachromatic mucus cells (see below), suggesting that this cell type is the origin of the mucus coat. The middle layer, on which epicuticular projections rest, is slightly electron dense (Fig. 3A, B). The innermost layer is the largest, and is composed of thin and loosely arranged fibers interspersed with abundant microvilli (Fig. 3A, B). Closely applied to the inner surface of the base of the microvilli is a prominent bundle of supporting tonofilaments that extend a considerable distance (Fig. 3A). Numerous mitochondria are concentrated in the most superficial epidermal layers (Fig. 3A).

Extracellular, rod-shaped cells of a structure typical of gram-negative bacteria occur scattered between the tips of microvilli in the cuticular matrix (Fig. 3A, 4A, B), as well as in groups of 4 to 5 enclosed in vacuoles near the surface of the epidermis (Fig. 4A, C). Cuticular and epidermal bacterial are similar in size, ranging from 0.22 to 1.80  $\mu$ m. In both cases, the bacterial nature of these cells is confirmed by the presence of a typical diffuse reticulum of DNA threads, the absence of a distinct nucleus, and by the double cell wall with an inner amorphous zone (Fisher, 1990). Bacterial densities vary significantly depending upon treatment ( $P < 0.05$ ). Freshly collected worms from Bodega Bay, California (a high sulfide site; Arp *et al.*, 1992) have high bacterial densities ( $8.97 \pm 2.48$ ), laboratory-maintained worms have the lowest bacterial densities ( $5.67 \pm 0.99$ ), and worms exposed to 50 to 70  $\mu$ M sulfide in the laboratory for 48 to 72 h have the highest bacterial densities ( $15.07 \pm 1.98$ ).

The mucus-secreting cells of the epidermis are large and ovoid. Based on their staining properties with the metachromatic stains toluidine blue and azure A, two

(MT) in the epidermal cells (E). (B) Higher magnification showing details of the cuticle lining of two adjacent rugae. The outermost layer (OL) shows epicuticular projections (EP) with an electron-dense lining surrounding a central core (arrow). This layer is covered with a fuzzy mucus coat (arrow heads), followed by a thin and electron-dense middle layer (ML), and largest innermost layer (IL) made up of thin fibers.

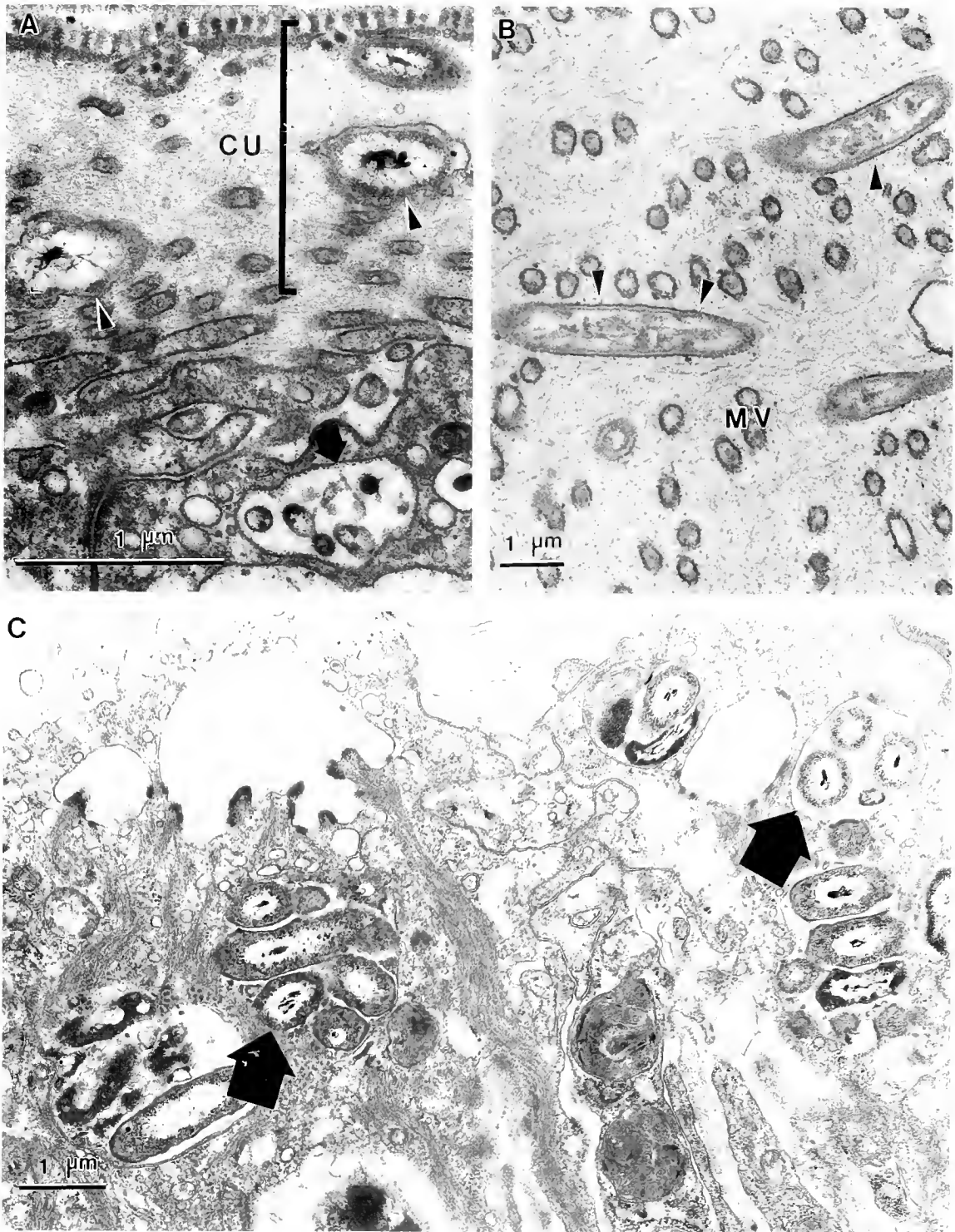


**Figure 4.** (A) Ultrastructure of the cuticle (CU) and part of the superficial epidermis with solitary bacteria (arrow heads) in the innermost layer of the cuticle and a group of bacteria within a vacuole (arrow) in the superficial epidermal layer. (B) Higher magnification reveals the double cell wall (arrow heads) of solitary bacteria and diffuse chromatin material with microvilli (MV) cut in cross sections. (C) Epidermis of a sulfide-exposed worm showing abundant bacteria grouped in vacuoles (arrows) in the outermost region of the epidermis.

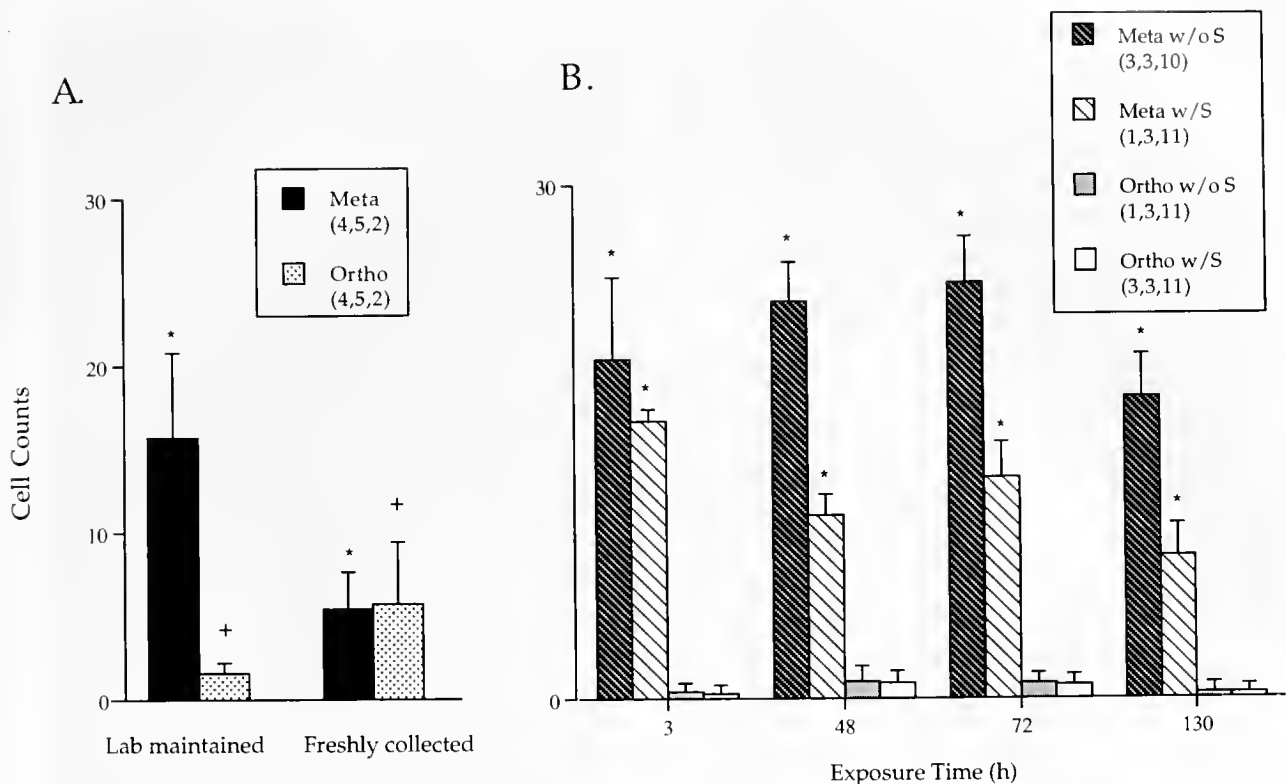


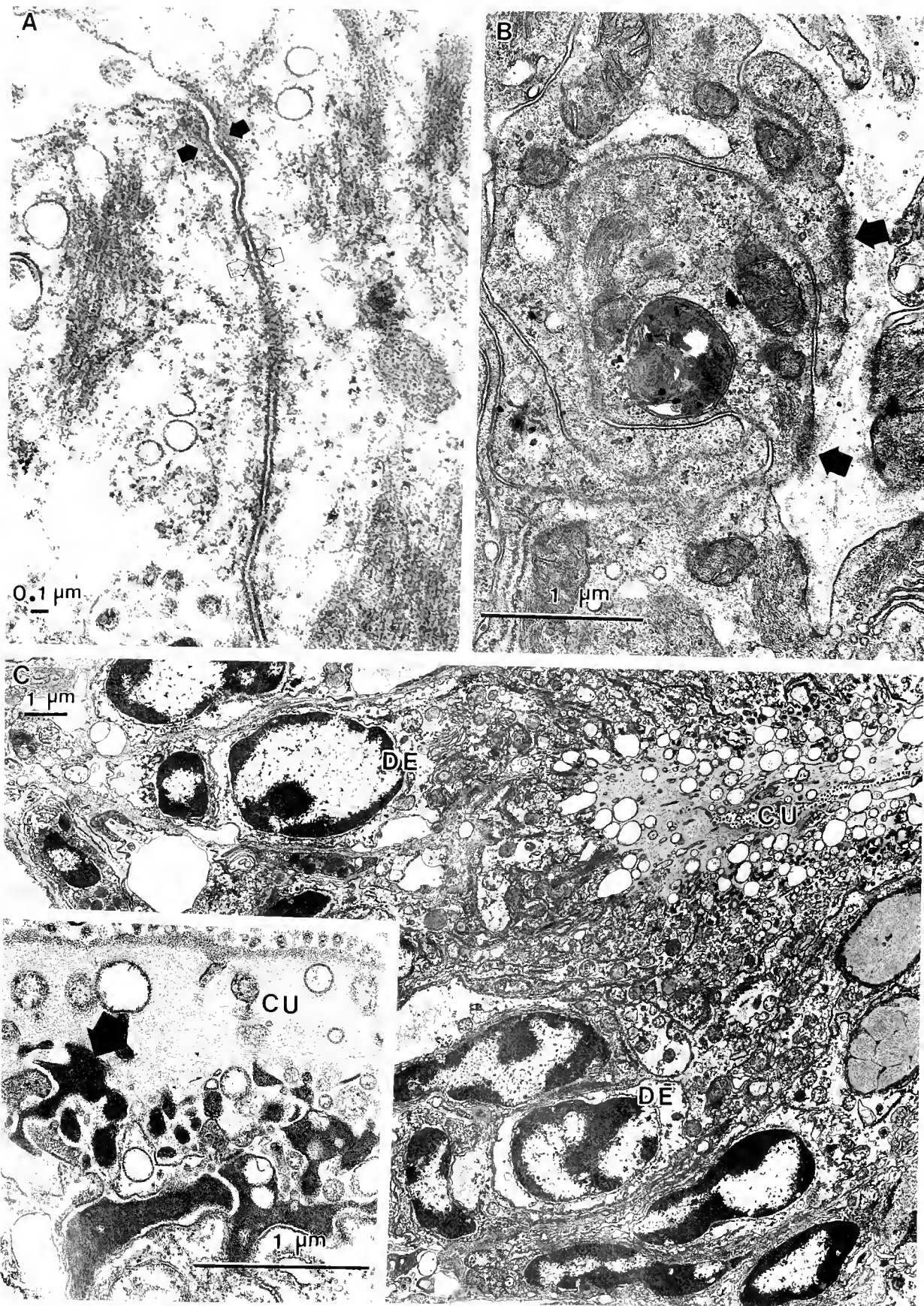
**Figure 5.** The number (mean  $\pm$  SD) of mucus cells in the epidermal surface of *Urechis caupo* present in a 0.2 mm<sup>2</sup> field under light microscopy. (A) The number of mucus cells in the epidermal surface of freshly collected animals and animals maintained in sulfide-free seawater in the laboratory for two to three weeks. (B) The number of mucus cells in the epidermal surface of animals maintained in sulfide-free seawater in the laboratory for one to four months, compared to the number of mucus cells in the epidermal surface of the same animals after exposure to 45 to 110  $\mu$ M sulfide in the laboratory. Metachromatic cell counts from freshly collected animals and sulfide-exposed animals were significantly lower than those of the laboratory-maintained animals, and orthochromatic cell counts from freshly collected animals were significantly higher than those of the laboratory-maintained animals. Orthochromatic cell counts from laboratory-maintained animals were not significantly altered with sulfide exposure. Numbers in parentheses are the number of worms sampled, followed by the number of body regions examined, and the number of fields counted per region. Data bars with like symbols (asterisks and crosses) are significantly different ( $P < 0.05$ ).

types of mucus-secreting cells are evident: orthochromatic mucus cells identified by the presence of discrete blue granules, and metachromatic cells identified by the presence of pink strands or a very fine reticulum within the mucus cell cavity. Animals freshly collected from the environment during low tide had very few purple to pink metachromatic cells filled with mucus ( $5.4 \pm 2.2$ ; Fig. 5A) and more empty metachromatic cells ( $14.1 \pm 5.4$ ; data not shown). Animals maintained in sulfide-free seawater in the laboratory for 3–4 weeks had significantly higher numbers of full metachromatic cells than did freshly collected worms ( $15.7 \pm 5.1$ ; Fig. 5A,  $P < 0.05$ ) and negligible numbers of empty metachromatic cells. Sulfide exposure in the laboratory resulted in a significant decrease in the number of metachromatic cells at all exposure times (Fig. 5B;  $P < 0.05$ ; the initial numbers of metachromatic cells in this group are higher than the laboratory-maintained group in Figure 5A because these animals had been kept

in the laboratory longer, 2–4 months). Orthochromatic mucus-secreting cell counts in animals maintained in sulfide-free seawater in the laboratory for 3–4 weeks were significantly lower ( $1.6 \pm 0.6$ ; Fig. 5A) than cell counts from freshly collected worms ( $5.7 \pm 3.7$ ;  $P < 0.05$ ; Fig. 5A). However, animals exposed to sulfide in the laboratory showed no significant change in the number of orthochromatic cells (Fig. 5B). Animals collected from the other two sites revealed similar patterns in the distribution and type of mucus-secreting cells (data not shown).

Histochemical techniques employed to distinguish the types of mucopolysaccharides indicate the presence of neutral and acidic substances in the epidermis. When PAS is used in conjunction with alcian blue, the epidermal cells stain with alcian blue and do not respond to the subsequent PAS treatment, thus distinguishing the neutral mucin from acidic mucins. The acid moiety of mucus is composed of carboxyl or sulfated groups, or a combination





of both, and these groups were distinguished by the following tests. Strong reactions with alcian blue at pH 2.5 indicate the presence of both carboxylated and sulfated mucopolysaccharides. Furthermore, positive staining at pH 0.5 indicates the presence of sulfated mucins. The critical electrolyte concentration-alcian blue staining at low molarity (0.06 M) gave an intense reaction, indicating the presence of both types of acidic mucins (Scott and Dorling, 1965). At higher molarity (0.5 M and 0.9 M), the epidermal cells yield a positive reaction, again showing the presence of sulfated mucins. The restoration of alcian blue staining, which occurred after high temperature combined with methylation and then saponification, also indicates the presence of carboxymucins (Spicer and Lillie, 1959). With the metachromatic dyes, toluidine blue and azure A, certain cells of the epidermis appear to be strongly metachromatic, indicating the presence of acidic mucus.

The epidermis of *U. caupo* contains three junctional specializations: (1) zonula adherens are typically present at the cuticular surface of epidermal cells (Fig. 6A); (2) septate intercellular junctions, which have less distinct septa traversing the cleft between epithelial cells, lie basal to zonula adherens (Fig. 6A); and (3) hemidesmosomes, which consist of plaques of electron-dense cytoplasm, may be present anywhere from zonula adherens to extracellular matrix (Fig. 6B). A prominent extracellular matrix, underlying the epidermis, consists of fine fibrils of collagen but is not organized into layers. Fibrils are oriented in all directions and do not display prominent cross-banding, although they have a slightly beaded appearance (not shown here).

Another cell type is present in the superficial layers of epidermis immediately below the cuticle of *U. caupo* (Figs. 6C, 7A, 8). In freshly collected worms, these cells exhibit the following characteristics of cell death: *e.g.*, a large nucleus-cytoplasmic ratio, condensed and vacuolated cytoplasm, chromatin material aggregated in large compact masses that border the nuclear membrane, and the loss of cellular organelles (Figs. 6C, 8). In some areas, chromatin or cytoplasmic material is broken down into fragments and appears to be in the process of extrusion from the cell (Fig. 6C, inset). Similar cells from the same tissue from laboratory-maintained animals, or deeper within the tissues of freshly collected worms, appear healthy, with visible cell organelles and less electron-dense chromatin material (Figs. 7A, 8). Dying cells, distinguished at the

light microscopic level by their intensely basophilic nuclei and loss of cytoplasm, were counted in a similar manner to mucus cells. Freshly collected animals from all three sites had significantly higher numbers of dying cells than laboratory-maintained animals ( $33.52 \pm 3.01$  and  $17.02 \pm 2.99$  per  $0.2 \text{ mm}^2$  area, respectively;  $n = 10$  worms, 5 regions per worm, 1 area per region;  $P < 0.05$ ), and laboratory-maintained animals exposed to 50 to 70  $\mu\text{M}$  sulfide for 48 to 78 h had significantly higher numbers of dying cells than before the exposure ( $32.65 \pm 2.98$  and  $15.20 \pm 1.36$  per  $0.2 \text{ mm}^2$  area, respectively;  $n = 4$  worms, 5 regions per worm, 1 area per region;  $P < 0.05$ ).

The cytoplasm of healthy superficial epidermal cells contains abundant cytolysosomes that show a partially lamellated pattern (Figs. 7A, B; 8). These bodies are composed primarily of iron and silicate, possibly in a paracrystalline array that may be responsible for their lamellated appearance (authors' unpublished X-ray micro analysis). They often possess empty vacuoles characteristic of mineral deposits and are close to mitochondria and occasionally bacteria (Fig. 8 and inset). Additionally, groups of electron-dense, swollen mitochondria are often observed surrounding secondary lysosomes (Fig. 7B inset), and cytolysosome density increases in sulfide-exposed worms (authors' unpub. obs.).

## Discussion

Adaptive features of the integument of *U. caupo* for life in a periodically hypoxic and sulfidic habitat include the rugose nature of the epidermis, which increases the surface area for oxygen uptake, and the thick muscular body wall, which provides a chief motive power in creating peristaltic movements along the body wall to drive ventilatory and feeding currents through the burrow. The integument does not present a significant structural barrier to permeation, although the mucus secreted by the epidermal cells may retard sulfide entry. Ultrastructural studies suggest three possible mechanisms that *U. caupo* may use to various degrees to counteract the toxic effects of this naturally occurring environmental poison at the integumentary surface: metabolism of symbiotic bacteria, dying off of peripheral, sulfide-exposed cells, and oxidation of sulfide at lysosomal sulfide oxidizing bodies.

Sulfide exists in marine systems predominantly as  $\text{H}_2\text{S}$  and  $\text{HS}^-$ . Both are highly permeable, small molecules that

**Figure 6.** (A) Adjacent epidermal cells display specialized junctions such as zonula adherens (closed arrows) and septate junctions (open arrows). (B) Hemidesmosomes showing electron-dense cytoplasmic plaques on either side of the cells (arrows). (C) Epidermal cells below the cuticle (CU) of a freshly collected animal (sulfide-exposed) with dying epidermal cells (DE) exhibiting condensed cytoplasm, no visible cellular organelles, and chromatin material aggregated in the nuclear periphery. Inset: ultrastructure of a dying epidermal cell below the cuticle (CU) showing disintegration of the chromatin or cytoplasmic material (arrow).

easily diffuse through membranes via paracellular or transcellular routes (Powell *et al.*, 1979; Julian and Arp, 1992). Permeation of an integument by some molecules can be prevented by morphologically identifiable barriers such as tight junctions, a fibrous or mineralized cuticle, and the presence of lipids (Lillywhite and Maderson, 1988). *U. caupo* has three types of intercellular junctions—zonula adherens, macula adherens (desmosomes), and septate junctions—structures similar to those reported in several invertebrates (Coggeshall, 1966; Tyler, 1984). Tight junctions have not been reported in invertebrate epidermis except for tunicates; septate junctions substitute for tight junctions which are comparatively leaky and offer low resistance to diffusion (Lillywhite and Maderson, 1988). These features may explain why the body wall of this worm presents no significant permeability barrier to sulfide. Additionally, the numerous mitochondria in the epidermal cells immediately below the cuticle suggests that there is active absorption and direct transport of substances from the environment (Richards and Arme, 1979, 1980; Jouin and Gaill, 1990).

The integument of *U. caupo* is composed of simple columnar glandular cells covered by a cuticle. Underlying the epidermis are connective and muscular tissues that form the bulk of the body wall. There are two types of glandular mucus-secreting cells histologically distinguished as orthochromatic (granular) and metachromatic (reticulate) that secrete mucus of an acidic and neutral nature. The cuticle, as revealed by its ultrastructure, is covered by a thin film of mucus derived from the metachromatic cells. The formation of sulfated mucopolysaccharides for the mucus coat in *U. caupo* may use sulfide present in the environment. Vetter (1985) reported the incorporation of sulfur into normal organic compounds, such as the sulfur amino acids, mucopolysaccharides and sulfolipids, in clams from sulfidic habitats.

Metachromatic cells in freshly collected (sulfide-exposed) worms are reduced in number relative to those in the sulfide-free animals, and distinct empty metachromatic cells are present; empty metachromatic cells were not detected in worms from any other treatment. These animals are likely to be exposed to sulfide in the environment and may have empty metachromatic cells due to the recent secretion of mucus in response to sulfide or other physiological or ecological factors such as burrow friction in the natural environment. Sulfide exposure in the laboratory resulted in a decrease in metachromatic mucus cells and a noticeable increase in mucus production (authors' unpub. obs.). These data suggest that mucus is secreted in response to sulfide exposure and may reduce sulfide entry. The priapulid worm *Halicyptus spinulosus* has been reported to detoxify sulfide by trapping it in an iron-containing mucus that is secreted by associated epibacteria and rapidly turns the body wall black (Oeschger and Janssen, 1991). Although mucus may interact with

sulfide at the body surface in *U. caupo*, there is no color change or evidence of a sulfide-trapping mechanism. Orthochromatic mucus-secreting cells were significantly more abundant in freshly collected animals and less prevalent in sulfide-free or sulfide-exposed laboratory-maintained animals. These cells may be involved in mucus secretion for burrow lubrication and mating (Richards, 1974) and may not be used while the worm is maintained out of a burrow in the laboratory.

The innermost layer of the cuticle and superficial epidermal region harbors extracellular, rod-shaped cells of a structure typical of gram-negative bacteria. The bacteria often have electron-transparent regions similar to those reported by Cavanaugh *et al.* (1981) in *Riftia pachyptila* trophosome, and these regions may have contained sulfur inclusions prior to fixation. A preliminary assay for the primary enzyme responsible for carbon dioxide fixation, ribulose-1,5-biphosphate carboxylase-oxygenase (RuBPCase), showed mean activity levels of 0.0018 IU/g in homogenized samples of *U. caupo* body wall (pers. comm. A. E. Anderson, Oregon State University). These levels are similar to those reported in pogonophoran tube worms, the bivalve *Calymptogena elongata* and several thyasirid clams (Somero *et al.*, 1989). Although further biochemical data are needed, the close proximity of bacteria to the external environment and the preliminary evidence of RuBPCase activity suggest that the symbionts metabolize chemoautotrophically, fueled by low levels of reduced sulfur compounds from the environment.

The extracellular location and size of the bacterial symbionts in *U. caupo* are similar to those described from several marine invertebrates from mildly reducing sediments (Felbeck *et al.*, 1983; Fisher, 1990). Their consistent abundance under the cuticle of *U. caupo* indicates a significant functional relationship. Symbiont-containing hosts usually possess a reduced digestive system (Fisher, 1990), but *U. caupo* not only has bacterial symbionts, but also a well-differentiated alimentary canal and an elaborate filter-feeding behavior (Fisher and MacGinitie, 1928; Judd and Arp, 1992). Thus, these worms are not sulfide-dependent; their symbionts probably provide sulfide detoxification rather than significant nutrition (Powell and Somero, 1986; Gaill *et al.*, 1988).

Epidermal cells situated just below the cuticle in sulfide-exposed individuals of *U. caupo*, appear to be dying, whereas the epithelial cells of laboratory-maintained worms, or cells from the deeper layers of the epidermis, appear healthy. These dying cells may be in the process of controlled cell death, or apoptosis, as characterized by the loss of cell organelles, condensation of the cytoplasm and nuclear chromatin, followed by fragmentation of the nucleus (Ojcius *et al.*, 1991). Dying cells in *U. caupo* go through two distinct deletion stages characteristic of apoptosis: nuclear and cytoplasmic disintegration, followed by shedding from epidermal surfaces as described



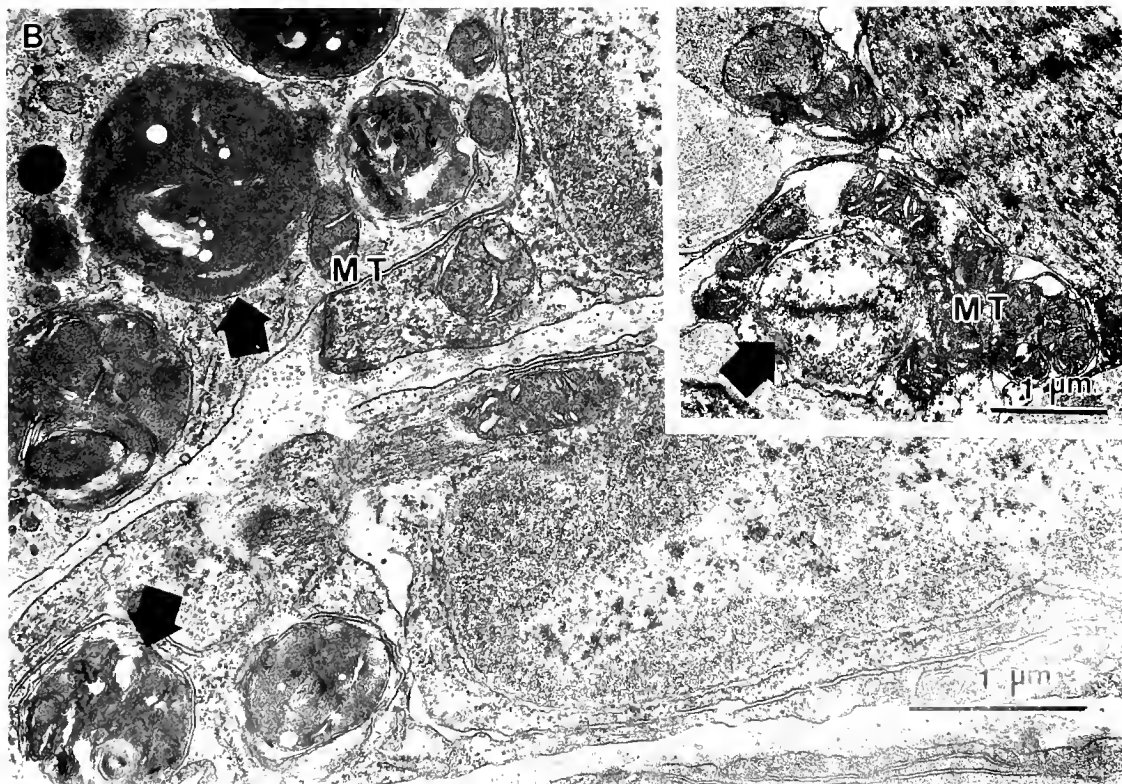
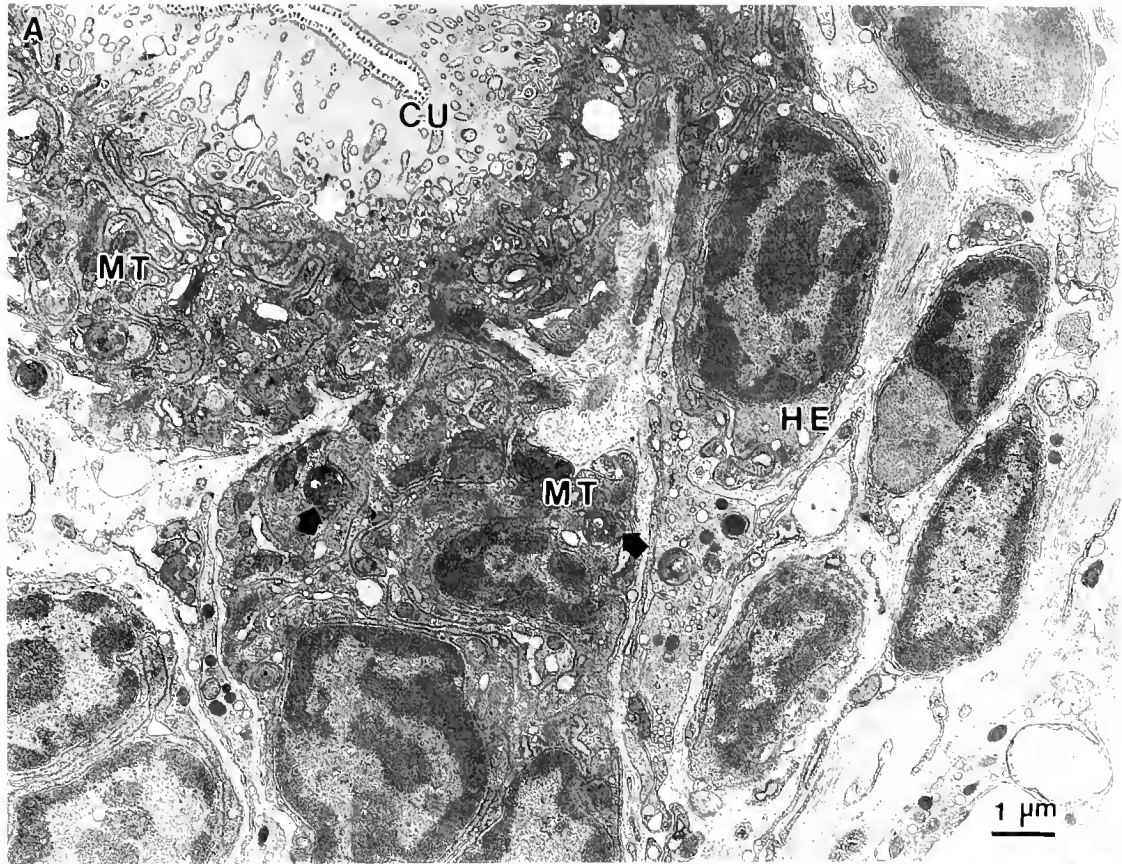


Figure 7. (A) Epidermis from a laboratory-maintained animal showing healthy epidermal cells (HE) below the cuticle (CU) with numerous mitochondria (MT), cytolysosomes (arrows), and a fair amount of cytoplasm. (B) Ultrastructure of epidermal cells showing numerous lysosomal sulfide-oxidizing bodies (arrows) and mitochondria (MT). Inset, ultrastructure of mitochondria from a sulfide-exposed worm showing altered morphology and close proximity to a cytolysosome (arrow).

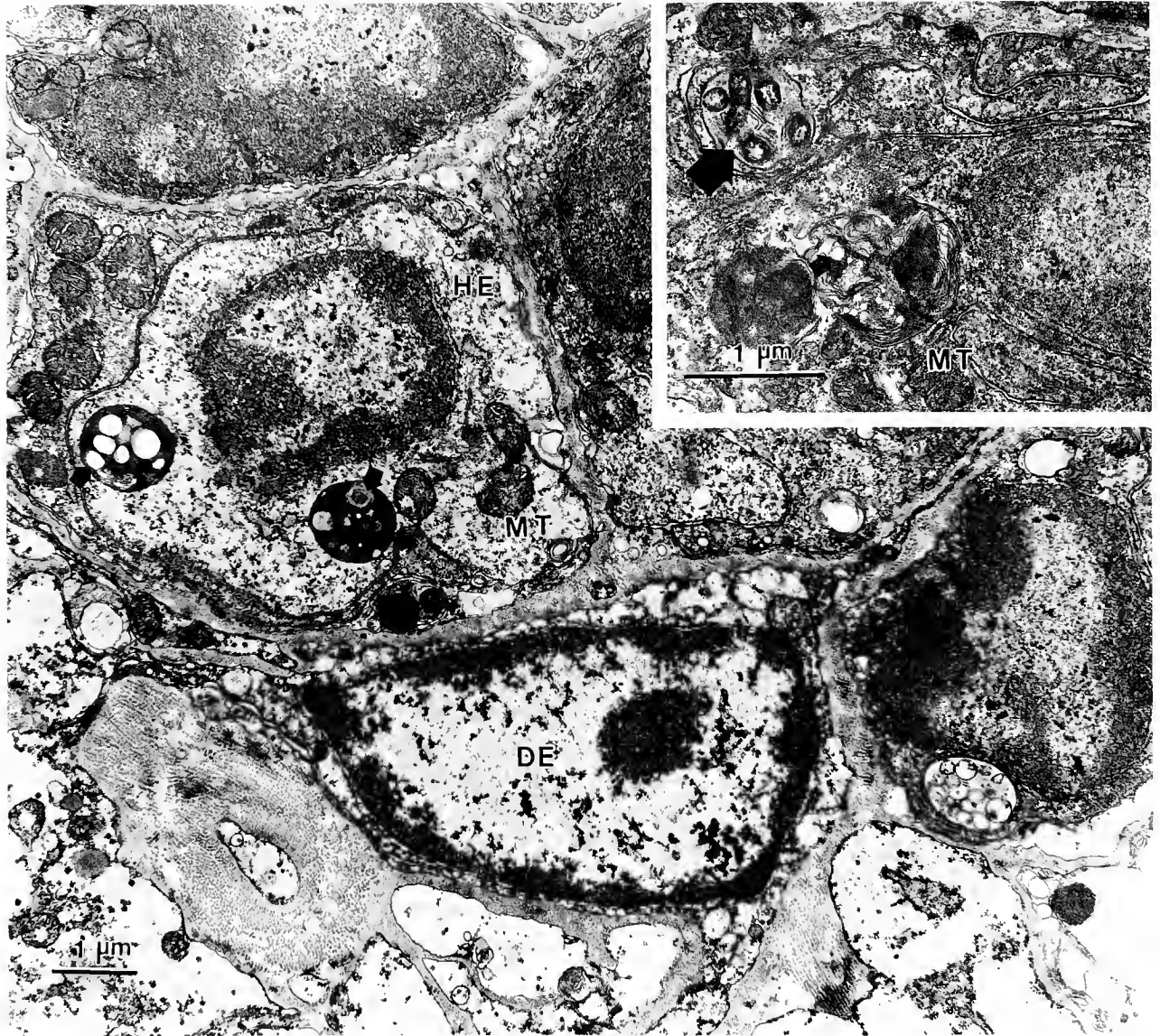


Figure 8. Epidermal cells from the deeper layers of body wall showing a few healthy cells (HE) containing lysosomal sulfide oxidizing bodies with inclusions (arrows) in close proximity to mitochondria (MT), and a dying cell (DE) with a pyknotic nucleus, condensed cytoplasm, and loss of organelles. Inset: higher magnification of the lysosomal sulfide oxidizing bodies showing inclusions (small arrow) in close proximity to mitochondria (MT) and bacteria (large arrow).

by Young (1987) in sunburned mammalian skin. Changes in intracellular concentrations of smaller molecules or ions (possibly sulfide molecules in *U. caupo*) have been shown to trigger apoptosis (Wyllie *et al.*, 1980). Differences in the number of dying cells between freshly collected animals, animals exposed to sulfide in the laboratory, and animals maintained in a sulfide-free environment in the laboratory, suggest that these cells increase in number in response to sulfide. This suggests that sulfide-sequestering subcuticular epidermal cells of *U. caupo* may die and be sloughed-off, thus eliminating sulfide from the organism.

Alternatively, rapid cell turnover may simply be a non-specific response to sulfide toxicity (rather than a discrete sulfide elimination mechanism) that occurs on the outside, or sulfide-exposed, surface of the animal's body, or cells may be dying in response to the mechanical abrasion associated with the burrow habitat of the animal.

Healthy epidermal cells lying below the dying cells contain structures morphologically similar to specialized organelles termed sulfide-oxidizing bodies. Sulfide oxidizing bodies were originally observed and described in *Solemya reidi* by Powell and Somero (1985) and have

also been reported in the hindgut of *U. caupo* (Menon and Arp, 1992b). These specialized lysosomal structures are predominantly composed of iron and often lie in close proximity to mitochondria and bacteria, suggesting a possible connection to sulfide-driven mitochondrial ATP production or bacterial nutrition (Felbeck, 1983; Powell and Somero, 1985, 1986; O'Brien and Vetter, 1990; Oeschger and Vetter, 1992).

Mitochondria in the epidermis of *U. caupo* collected from high sulfide environments or exposed to sulfide in the laboratory are unusually electron dense, swollen, and clumped together near cytolysosomes, and cytolysosome density increases in sulfide-exposed worms. Electron-dense ferritin-containing iron particles have been reported from mammalian lysosomes that phagocytose red blood cells, and the transformation or incorporation of damaged mitochondria into cytolysosomes is a common method by which mitochondria are eliminated from the body (Muirden and Rogers, 1978; Ghadially 1982). In *U. caupo*, these putative sulfide oxidizing bodies may scavenge mitochondria or coelomic fluid heme and secondarily use it for sulfide detoxification by binding sulfide or accelerating sulfide oxidization in a manner similar to that reported for the worms' coelomic fluid heme compound, hematin (Powell and Arp, 1989; Arp, 1991; Arp *et al.*, 1992; Menon and Arp, 1992b). Theoretically, the binding or oxidation of sulfide to nontoxic forms of sulfur in peripheral body tissues would prevent the penetration of this aerobic poison to vital muscle tissues. The relationship between heme iron, mitochondria, and lysosomal sulfide oxidizing bodies in *U. caupo* is currently under investigation.

### Acknowledgments

This research was supported by NSF DCB-891776 and IBN 9218732 grants to AJA. Dr. A. Anderson generously performed the preliminary RuBPCase assay for us, and the X-ray micro analysis was assisted by Dr. A. Z. Mason. We are grateful to Dr. Nick Holland for initial consultation, to Dr. Gregory Antipa for use of the EM facilities, and to Gregg Lum and Richard Simpson for technical support. Computer graphics are by Diane Fenster. We thank Drs. Stephen Gardiner and David Julian for critical review of the manuscript.

### Literature Cited

- Arp, A. J. 1991. The role of heme compounds in sulfide tolerance in the echiuran worm *Urechis caupo*. In *Structure and Function of Invertebrate Oxygen Proteins*, Vinogradov and Kapp, eds. Springer-Verlag, New York.
- Arp, A. J., B. M. Hansen, and D. Julian. 1992. The burrow environment and coelomic fluid characteristics of the echiuran worm *Urechis caupo* from three northern California population sites. *Mar Biol* 13: 613-623.
- Bancroft, J. D., and A. Stevens. 1977. In *Theory and Practice of Histological Techniques*. Churchill Livingstone, Edinburgh, London and New York.
- Cavanaugh, C. M., S. L. Gardiner, M. L. Jones, H. W. Jannasch, and J. B. Waterbury. 1981. Prokaryotic cells in the hydrothermal vent tube worm *Riftia pachyptila* Jones: possible chemoautotrophic symbionts. *Science* 213: 340-342.
- Coggeshall, R. E. 1966. A fine structural analysis of the epidermis of the earthworm, *Lumbricus terrestris* L. *J. Cell Biol.* 28: 95-108.
- Eaton, R., and A. J. Arp. 1993. Aerobic respiration during sulfide exposure in the marine echiuran worm, *Urechis caupo*. *Physiol. Zool.* 66(1): 1-19.
- Felbeck, H. 1983. Sulfide oxidation and carbon fixation by the gutless clam *Solemya reidi*: an animal-bacterial symbiosis. *J. Comp. Physiol.* 152: 3-11.
- Felbeck, H., G. Liebecz, R. Dawson, and O. Giere. 1983. CO<sub>2</sub> fixation in tissues of marine oligochaetes (*Phalloidrihts leudodermatus* and *P. planus*) containing symbiotic, chemoautotrophic bacteria. *Mar. Biol.* 75: 187-189.
- Fisher, W. K., and G. E. MacGinitie. 1928. The natural history of an echiurid worm. *Ann. Mag. Nat. Hist.* 10: 204-213.
- Fisher, C. R. 1990. Chemoautotrophic and methanotropic symbioses in marine invertebrates. *Crit. Rev. Aquat. Sci.* 2: 399-436.
- Gaill, F., D. Desbruyeres, and L. Laubier. 1988. Morphological relationships between the "Pompeii worms" and their epibiotic bacteria. *Oceanol. Acta* 8: 147.
- Gaill, F., D. Herbage, and L. Lepescheux. 1991. A discrete Helicoid of collagenous fibrils: the cuticle of deep-sea hydrothermal vent worms (*Riftia pachyptila*). *Matrix* 11: 197-205.
- Ghadially, F. N. 1982. *Ultrastructural Pathology of the Cell and Matrix*. 2nd edition. Butterworths, London. Pp. 176.
- Gona, O. 1979. Mucous glycoproteins of teleostean fish: a comparative histochemical study. *Histochem. J.* 11: 709-718.
- Holland, N. D., and K. H. Neilson. 1978. The fine structure of the echinoderm cuticle and the subcuticular bacteria of echinoderms. *Acta Zool.* 59: 169-185.
- Jameson, H. L. 1899. Contributions to the anatomy and histology of *Thalassema neptuni* Gaertner. *Zool. Jahrb. Ab. f. Anat., Bd.* 12, S: 535-566.
- Jose, K. V. 1964. The morphology of *Acanthobonellia pitotensis* N. Sp., a bonellid from the Gulf of Kutch, India. *J. Morphol.* 115: 53-68.
- Jouin, C., and F. Gaill. 1990. Gills of hydrothermal vent annelids: structure, ultrastructure and functional implications in two alvinellid species. *Progr. Oceanogr.* 24: 59-69.
- Judd, J. R., and A. J. Arp. 1992. The feeding behavior, food availability and digestive physiology of *Urechis caupo*. *Am. Zool.* 32: 125A.
- Julian, D., and A. J. Arp. 1992. Sulfide permeability in the marine invertebrate *Urechis caupo*. *J. Comp. Physiol. B* 162: 59-67.
- Lillywhite, H. B., and P. F. A. Maderson. 1988. The structure and permeability of integument. *Am. Zool.* 28: 945-962.
- Menon, J. G., and A. J. Arp. 1992a. Symbiotic bacteria may prevent sulfide poisoning of the body wall of *Urechis caupo*. *Am. Zool.* 32: 59A.
- Menon, J. G., and A. J. Arp. 1992b. Morphological adaptations of the respiratory hindgut of a marine echiuran worm. *J. Morphol.* 214: 131-138.
- Muirden, K. D., and K. Rogers. 1978. Electron microscopy and synovial pathology. *Aust. N.Z. J. Med. Suppl.* 18: 20-24.
- National Research Council, Subcommittee on Hydrogen Sulfide, Division of Medical Sciences. 1979. *Hydrogen Sulfide*. University Park Press, Baltimore.
- Newby, W. W. 1941. The development and structure of the slime net glands of *Urechis*. *J. Morphol.* 69: 303-316.

- O'Brien, J., and R. D. Vetter. 1990. Production of thiosulfate during sulphide oxidation by mitochondria of the symbiont containing bivalve *Solemya reidi*. *J. Exp. Biol.* **149**: 133-148.
- Oeschger, R., and H. H. Janssen. 1991. Histological studies on *Halicryptus spinulosus* (Priapulida) with regard to environmental hydrogen sulfide resistance. *Hydrobiologia* **222**: 1-12.
- Oeschger, R., and R. D. Vetter. 1992. Sulfide detoxification and tolerance in *Halicryptus spinulosus* (Priapulida): a multiple strategy. *Mar. Ecol. Progr. Ser.* **86**: 167-179.
- Ojcus, D. M., A. Zychlinsky, L. M. Zheng, and D. Young. 1991. Ionophore-induced apoptosis: role of DNA fragmentation and calcium fluxes. *Exp. Cell Res.* **197**: 43-49.
- Powell, E. N., M. A. Crenshaw, and R. M. Reigher. 1979. Adaptations to sulfide in the meiofauna of the sulfide system. I. 35S-sulfide accumulation and the presence of a sulfide detoxification system. *J. Exp. Mar. Biol. Ecol.* **37**: 57-76.
- Powell, M. A., and G. N. Somero. 1985. Sulfide oxidation occurs in the animal tissue of the gutless clam, *Solemya reidi*. *Biol. Bull.* **169**: 164-181.
- Powell, M. A., and G. N. Somero. 1986. Adaptations to sulfide by hydrothermal vent animals: sites and mechanisms of detoxification and metabolism. *Biol. Bull.* **171**: 274-290.
- Powell, M. A., and A. J. Arp. 1989. Hydrogen sulfide oxidation by abundant nonhemoglobin heme compounds in marine invertebrates from sulfide rich habitats. *J. Exp. Zool.* **249**: 121-132.
- Richards, K. S. 1974. The ultrastructure of the orthochromatic mucous cells of some British lumbricids (Annelida). *J. Zool.* **174**: 575-590.
- Richards, K. S., and C. Arme. 1979. Transintegumentary uptake of amino acids in the lumbricid earthworm *Eisenia foetida*. *Comp. Biochem. Physiol.* **64A**: 351-356.
- Richards, K. S., and C. Arme. 1980. Transintegumentary uptake of D-galactose, D-fructose and 2-deoxy-D-glucose by the lumbricid earthworm *Lumbricus rubellus*. *Comp. Biochem. Physiol.* **66A**: 209-214.
- Somero, G. N., A. E. Anderson, and J. J. Childress. 1989. Transport, metabolism, and detoxification of hydrogen sulfide in animals from sulfide-rich marine environments. *CRC Crit. Rev. Aquat. Sci.* **1**: 591-614.
- Scott, J. E., and J. Dorling. 1965. Differential staining of acid glycosaminoglycans (mucopolysaccharides) by alcian blue in salt solution. *Histochemie* **5**: 221-233.
- Spicer, S. S., and R. D. Lillie. 1959. Saponification as a means of selectively reversing the methylation blockade of tissue basophilia. *J. Histochem. Cytochem.* **7**: 123-125.
- Tyler, S. 1984. Invertebrates. Pp. 121-122 in *Biology of the Integument*. Springer-Verlag, Berlin.
- Vetter, R. D. 1985. Elemental sulfur in the gills of three species of clams containing chemoautotrophic symbiotic bacteria, a possible inorganic energy storage compound. *Mar. Biol.* **88**: 33-42.
- Wyllie, A. H., J. F. R. Kerr and A. R. Currie. 1980. Cell death: the significance of apoptosis. *Int. Rev. of Cytol.* **68**: 251-306.
- Young, A. R. 1987. The sunburn cell. *Photodermatology* **4**: 127-134.
- Zar, J. H. 1984. *Biostatistical Analysis*. Prentice-Hall, Englewood Cliffs, New Jersey.

# Extreme Diel Fluctuations of Oxygen in Diffusive Boundary Layers Surrounding Stony Corals

N. SHASHAR<sup>1,2,\*</sup>, Y. COHEN<sup>3</sup>, AND Y. LOYA<sup>1</sup>

<sup>1</sup>Tel Aviv University, Department of Zoology, George S. Wise Faculty of Life Sciences, Tel-Aviv, 69978, Israel, <sup>2</sup>The Interuniversity Institute of Eilat, P. O. B 469, Eilat 88103, Israel, and <sup>3</sup>Division of Microbial and Molecular Ecology, Life Science Institute, Hebrew University of Jerusalem, 91904, Israel

**Abstract.** The diffusive boundary layers surrounding sessile marine organisms have been implicated in controlling an organism's metabolism and growth. We studied boundary layers surrounding hermatypic corals by monitoring oxygen concentrations on a submillimetric scale. Oxygen concentration within the boundary layers varied from supersaturation during the day to anoxia at night, although the ambient water composition remained constant. Detailed mapping and oxygen measurements revealed diel oxygen fluctuations from supersaturation (373% air saturation) in the light to complete oxygen depletion at darkness in the massive coral *Favia favaus*. Exposure to a 5-cm/s current reduced the boundary layer thickness from 2.44 mm to 1.90 mm, allowing more rapid oxygen exchange across the diffusive boundary layer. Similar patterns were found in the branching coral *Stylophora pistillata*. In massive corals, the thickness of the diffusive boundary layer was negatively correlated with the size of the polyp. We suggest that the distribution of corals in areas of differential turbulence is related to the thickness of the diffusive boundary layers surrounding them.

## Introduction

Oligotrophic tropical marine waters experience relatively small diel chemical changes. Hence, coral reefs in tropical waters are exposed, on a macro-scale, to a relatively constant chemical milieu. Yet the metabolic activities of macro- as well as microorganisms may cause con-

siderable changes in the chemical composition of their near surroundings. Diffusion limitations in the stagnant layer around the organisms may induce the development of diffusive boundary layers (DBL) in proximity to the surface of the organisms. In the marine environment, intense metabolic activity can result in niches of sharp gradients of solute concentrations in the DBLs; these have been found in benthic sediments (Gundersen and Jørgensen, 1990), over hypersaline microbial mats (Revsbech *et al.*, 1983; Jørgensen and Des Marais, 1990), in planktonic organisms such as Foraminifera (Jørgensen *et al.*, 1985), and in marine snow (Alldredge and Cohen, 1987).

Diffusive boundary layers, their development, and their relationships with momentum boundary layers have been extensively studied (Revsbech and Jørgensen, 1976; Jørgensen and Des Marais, 1990; Patterson, 1992a). In seawater, most biologically important small molecules and ions such as O<sub>2</sub>, CO<sub>2</sub>, and Ca<sup>++</sup> have a similar Schmidt number (Sc) of about 500 (Patterson *et al.*, 1991; Patterson, 1992b). Schmidt number is correlated to the ratio between the thickness of the DBL (d) and that of the momentum boundary layer ( $\delta$ ) as  $d/\delta = Sc^{-0.33}$ . Because the thickness of the momentum boundary layer over a given surface at a given flow does not depend on the solute measured, the thicknesses of the DBLs for these metabolically important small molecules are very similar (Patterson, 1992b). Therefore, by measuring the concentration profile of one of these solutes, one can estimate the DBL thickness for the others. The development of O<sub>2</sub> micro-sensors caused researchers to favor O<sub>2</sub> concentration measurements, occasionally accompanied by other measurements such as pH (Jørgensen *et al.*, 1985; Alldredge and Cohen, 1987) or N<sub>2</sub>O concentration (Revsbech *et al.*, 1988).

Received 22 October 1992; accepted 22 September 1993.

\*Present address: Department of Biological Science, University of Maryland Baltimore County, Catonsville, MD 21228.



Like many other sessile marine organisms, corals are oxyconformers; they lack the ability to actively ventilate their external surface and thus enhance the exchange of solutes with their surroundings (Shick, 1990; Patterson, 1992a). However, unlike most other animals, hermatypic corals have endosymbiotic algae. Through the activity of these symbionts, hermatypic corals experience  $O_2$  and  $CO_2$  fluxes resembling those known from free-living algae. The balance between photosynthesis by the symbiotic algae and respiration by animal and algae, both occurring within the coral tissue, causes shifts from net efflux to net uptake of  $O_2$  and  $CO_2$ . Uptake and excretion of other solutes such as  $Ca^{+2}$  and  $NH_4^+$  occur in both passive and active transport (Crossland and Barnes, 1974; Burris, 1983; D'Elia and Cook, 1988). While studying the dynamics of solute exchange, the resistance of the water within the DBL must be taken into account. In freshwater amphibians, the DBL resistance was found to be similar to or greater than that of the animal skin (Pincler and Feder, 1990; Feder and Booth, 1992). Therefore, the thickness of the DBL may control the flux rates of solutes between the coral and its surrounding (Patterson *et al.*, 1991; Patterson, 1992b).

In hermatypic corals, high rates of solute exchange are limited by the coral's external skeleton to the direction of the open water. Thus it is possible to map and study the DBL surrounding the coral polyp (the individual module of the colony) on a two-dimensional scale. Hence, corals present a good, though complicated, model for study of the effects of structure and changes in the DBL on the metabolism of sessile marine animals and plants. By correlating DBL changes to the activity of other members of the coral community, and to environmental factors such as exposure to light and water flow, we may improve our understanding of the adaptations and distribution patterns sessile marine organisms employ to cope with these metabolic confinements.

### Materials and Methods

Corals were collected from a coral reef in front of the H. Steinitz Marine Biology Laboratory, in the Gulf of Eilat, Red Sea, from depths of 5–7 m. At 6 m depth, maximal light intensity (measured in microEinsteins, where  $1 \mu E = 1 \mu mol$  of photons) reached  $980 \mu E \cdot m^{-2} \cdot s^{-1}$ . Coral colonies (up to 15 cm in diameter) and surrounding substrate were cut and transferred to the laboratory. Corals were submerged in seawater throughout their handling. After collection, corals were placed in experimental aquaria and held in position by attaching the surrounding substrate to a glass base. Corals were set in running seawater for 6 h and then aerated for an additional 3 h. Aeration was maintained throughout the experiments.

Oxygen concentrations were measured using combined oxygen microelectrodes with sensing tips 10–200  $\mu m$  in

Table 1

Thickness of oxygen diffusive boundary layer (DBL) in stony corals

Coral species	DBL thickness (mm)	Polyp width (mm)
Massive		
<i>Platygyra lamellina</i>	4.00	>10*
<i>Favia fava</i>	2.44	$8.8 \pm 1.0$
<i>Favites pentagona</i>	1.75	$8.7 \pm 1.6$
<i>Porites lobata</i>	1.50	$1.9 \pm 0.3$
Branching		
<i>Stylophora pistillata</i>	3.09	$0.9 \pm 0.1$

DBL thickness was determined as the distance, perpendicular to the opening of the polyps' oral disk, in which oxygen concentration differed from that in the external water mass by more than 10% (Jørgensen and Des Marais, 1990). Measurements were conducted in the dark and in calm seawater.

\* *Platygyra lamellina* is a brain coral, and the size of the opening over the polyps increases as the coral grows.

diameter (Revsbech and Jørgensen, 1976). The extremely low oxygen consumption by these electrodes enabled accurate measurements to be made without stirring the water. Microelectrodes were calibrated against seawater flushed to equilibrium with nitrogen, air, or oxygen. Oxygen concentrations in the calibration chambers were determined using the Winkler-Iodometric method (Taras *et al.*, 1971). Oxygen concentration profiles were measured perpendicular to the coral tissue at vertical intervals of 0.10–0.25 mm. DBL thickness was determined as the distance at which oxygen concentration differed from that of the external water mass by more than 10% (Jørgensen and Des Marais, 1990). Oxygen profiles through the diffusion boundary layers were measured in several species of stony corals, followed by detailed measurements of oxygen profiles in the massive coral *Favia fava* and the branching coral *Stylophora pistillata*. With these two coral species, series of vertical oxygen profiles were measured in the light and in the dark, at horizontal intervals of 0.1–0.5 mm, and contour maps of oxygen concentrations within the DBL were constructed.

To evaluate the effect of water motion on the DBL, a 5-cm/s current was created in the aquaria by using a magnetic stirrer. Current velocity was measured at a distance of 1 cm perpendicular to the oxygen measurement point by tracing small suspended particles. This flow velocity is the average velocity of the strong currents measured off the laboratory in Eilat, excluding wave currents (A. Genin, pers. comm.). Oxygen profiles were measured when corals were exposed to this current in the dark. Contour maps of oxygen concentration were constructed from these profiles as well.

To define oxygen concentration within the coral skeleton, a hole 1 mm in diameter was drilled 5 cm into the

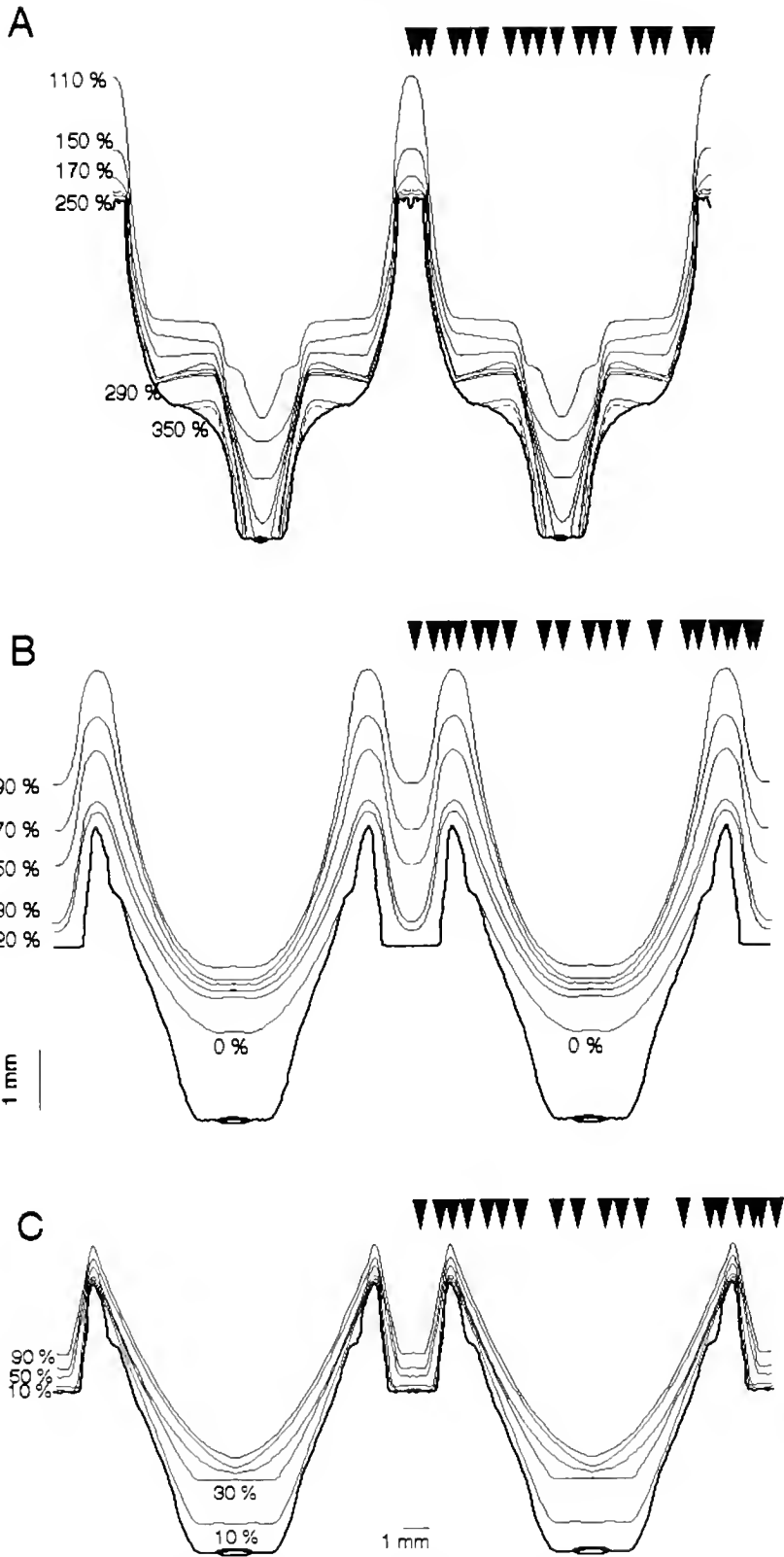
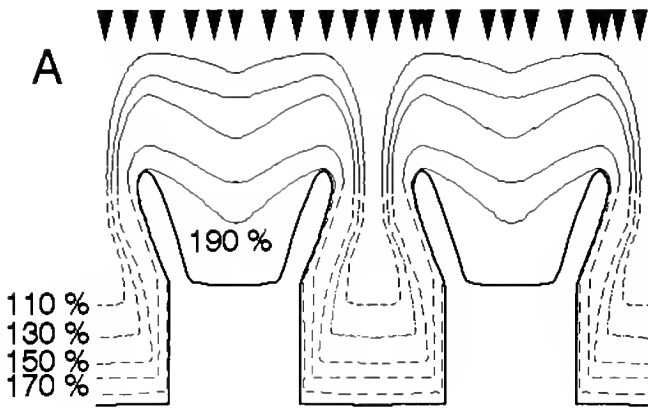


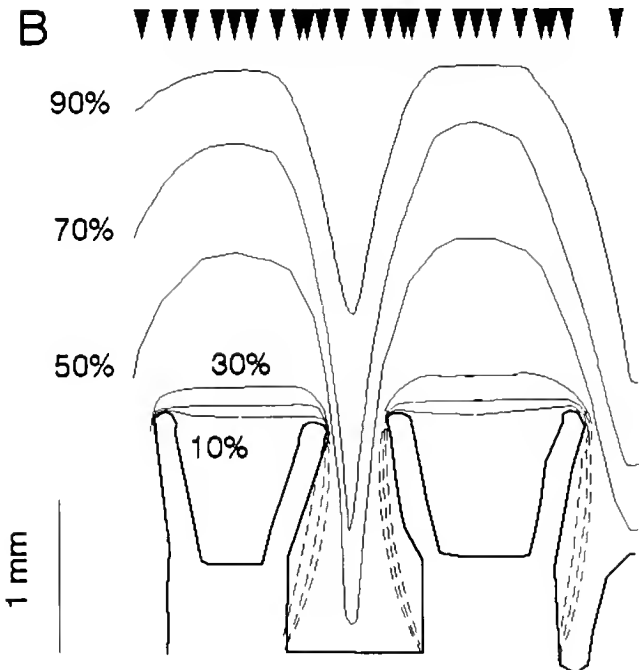
**Figure 1.** Contour maps of the oxygen boundary layers surrounding *Favia javus* coral polyps. Each map was constructed from measurements of oxygen profiles taken from 10 different colonies. Arrows indicate points of profile measurements. Tissue surface is marked in bold lines. Dashed lines mark estimated values where continuous measurements were not possible. For better illustration, maps were duplicated by left symmetry. (A) Oxygen boundary layer under light conditions of  $980 \mu\text{E} \cdot \text{m}^{-2} \cdot \text{s}^{-1}$ . (B) Oxygen boundary layer in darkness. (C) Oxygen boundary layer under a 5-cm/s current, in darkness.



skeleton of a living *F. favius* coral. The hole was cleaned with a gentle water jet. The oxygen concentration was measured within the hole in total darkness. 1 h after the light was turned off.

To evaluate the rate of oxygen production, oxygen concentration was monitored at the opening of a polyp of *S. pistillata* coral during shifts from light to darkness. The microelectrode was positioned 0.5 mm perpendicular to the opening of the oral disk, and between the coral tentacles, for at least 5 min. in the light. The light was not turned off until the tentacles were extended and not affected by the electrode. Oxygen concentration was recorded continuously.

Light intensity, provided by a Scott KL-1500 light source equipped with a fiber optic, was  $980 \mu\text{E} \cdot \text{m}^{-2} \cdot \text{s}^{-1}$  in all experiments. Light was measured using a Li-Cor Li-1000 light meter with an underwater, cosine corrected,  $2\pi$  sensor.



## Results

A defined oxygen DBL was identified in all stony corals examined (Table 1). In darkness and in calm seawater, the thickness of the oxygen boundary layers, as measured perpendicular to the opening of the polyp's oral disk, varied from 4.00 mm in *Platygyra lamellina* to 1.50 mm in *Porites lobata*. In the massive corals tested, corals having a larger calyx tended to have a thicker DBL (Table 1).

Detailed measurements on *F. favius* and *S. pistillata* yielded the contour maps presented in Figures 1 and 2. These measurements revealed the existence of diffusive boundary layers completely encompassing each coral. Oxygen depletion was extreme during darkness, when oxygen concentration dropped to 10% of air saturation ( $22 \mu\text{M}$ ) in *S. pistillata* (Fig. 2.B) and to total anoxia in *F. favius* (Fig. 1.B). When corals were exposed to a light intensity of  $980 \mu\text{E} \cdot \text{m}^{-2} \cdot \text{s}^{-1}$ , supersaturation of oxygen was measured at 191% air saturation ( $420 \mu\text{M}$ ) in *S. pistillata* (Fig. 2.A) and 373% air saturation ( $820 \mu\text{M}$ ) in *F. favius* (Fig. 1.A). In the smaller polyped coral *S. pistillata*, the DBL extended into the surrounding water beyond the polyp tentacles.

Even in a current of 5 cm/s, a DBL was continuously present (Figs. 1 and 2.C). Though not changing the minimal oxygen concentration at the surface of the coral tissue (anoxia in *F. favius* and 10% of air saturation in *S. pistillata*), exposure to this current reduced the thickness of the DBL (Fig. 3) from 2.44 mm to 1.90 mm in *F. favius*

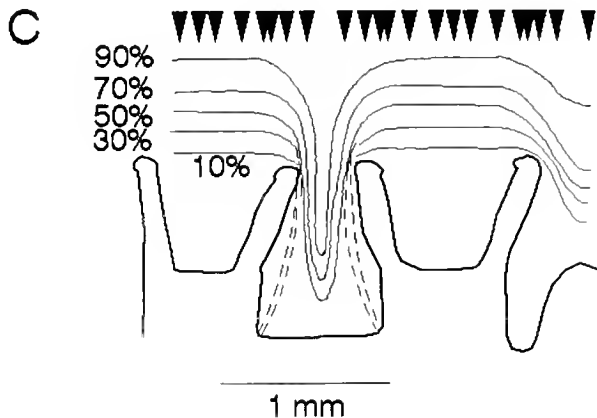


**Figure 2.** Contour maps of the oxygen boundary layers surrounding *Stylophora pistillata* coral polyps. Each map was constructed from measurements of oxygen profiles taken from 10 different colonies. Further details are as in the legend to Figure 1 (symmetry duplication was not used).



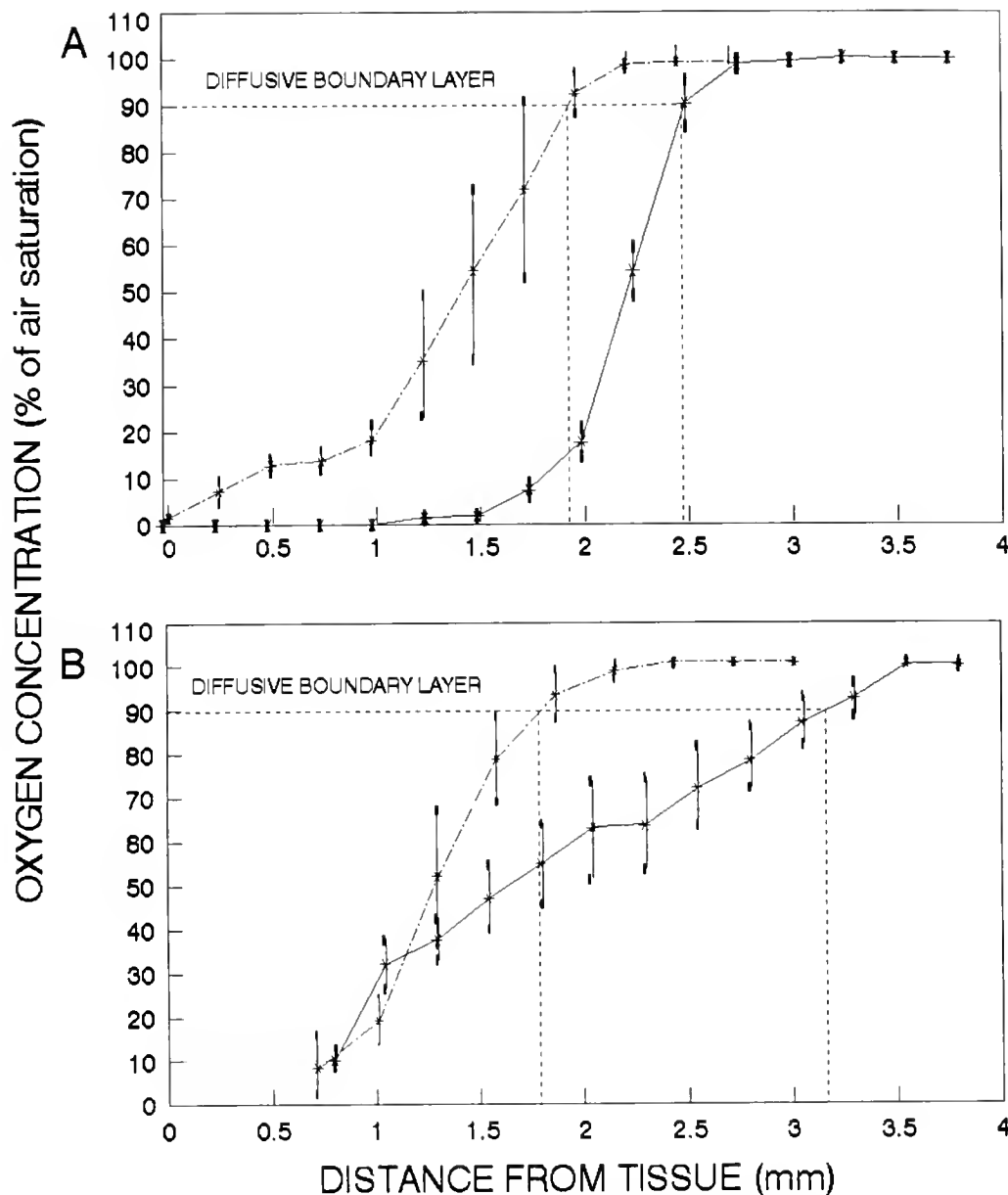


Figure 3. Oxygen concentrations perpendicular to the oral disk opening of the corals *Favia fava* (A) and *Stylophora pistillata* (B) in calm water (continuous lines) and with a 5-cm/s current (dashed lines). Means  $\pm$  SD: n: A-calm = 4, A-current = 3, B-calm = 5, B-current = 7.

and from 3.09 mm to 1.80 mm in *S. pistillata*. Although the 5-cm/s current reduced the thickness of the DBL, it remained laminar and the iso-oxic profiles in the boundary layers remained continuous.

Measurements made in a hole drilled into the coral skeleton of an *F. fava* coral showed that, in the dark, hypoxia (13% air saturation) extended throughout the entire depth of the hole, and a defined DBL was present outside it.

When corals were shifted from light to darkness, oxygen concentrations within the diffusive boundary layer changed from supersaturation to anoxia within less than

1 min. From the initial slope of the decline in oxygen concentration, we calculated the oxygen residence time (the time needed for consumption of the excess oxygen, reducing the concentration from its level in the light to its level in the surrounding seawater, in the dark) to be 4.3 s (Fig. 4).

### Discussion

Like other sessile organisms, corals create a distinct microhabitat considerably different from the water sur-

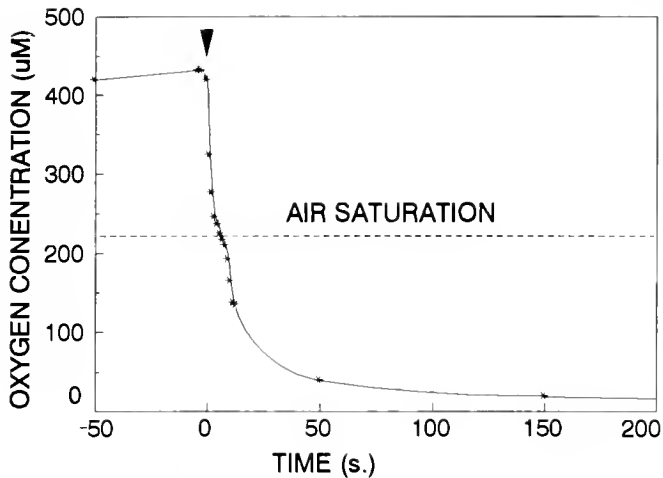


**Figure 4.** Changes in oxygen concentration measured between the tentacles, at a 0.5-mm distance perpendicular to the opening of the polyps' oral disk, of a *Stylophora pistillata* coral, as it was shifted from light to darkness (arrow indicates light turned off).

rounding them (Schiller and Herndl, 1989). The diffusive boundary layers describe some of the unique properties of this microhabitat. In these layers, oxygen concentrations fluctuate from supersaturation during the day to hypoxia during the night.

Two processes regulate oxygen concentration: oxygenic photosynthesis by the corals' symbiotic zooxanthellae and by endolithic photosynthetic organisms, and oxygen consumption due to respiration of the entire coral head community. The short time scale during which changes in oxygen concentrations occur indicates that the light regime is the main factor affecting the balance between respiration and photosynthesis, and thus dictating the oxygen concentration close to the coral. Other processes such as tentacle movement and water exchange within the polyp require a longer time, and were not found to be directly coupled to the fluctuations in oxygen concentration. In the field, oxygen supersaturation may develop soon after sunrise, and oxygen depletion may occur soon after sunset. Therefore, corals and endolithic algae must be adapted to function at both very low and very high oxygen concentrations. High specific activities of the enzymes superoxide dismutase, catalase, and ascorbate peroxidase have been found in isolated zooxanthellae, in coral host tissue, and in endolithic algae (Shick and Dykens, 1985; Lesser and Shick, 1989; Matta and Trench, 1991; Shashar and Stambler, 1992). These enzymes may protect the organisms against the toxic effects of elevated oxygen concentrations. In addition to possible toxic effects, high oxygen concentrations from photosynthesis will increase host respiration (Shick, 1990) and may reduce photosynthetic rates in algal symbionts. The high oxygen concentrations are expected to be coupled with  $\text{CO}_2$  depletion and high

pH levels (Shashar and Stambler, 1992). Both result in lower rates of net carbon photoassimilation. The enzyme carbonic anhydrase, found in the animal tissue and in the symbiotic zooxanthellae (Weis *et al.*, 1989), may partly reduce the enhanced photorespiration.

At night, corals are exposed to extreme internal oxygen depletion. During that time, they extend their tentacles into the water column. As has been suggested for several cnidarians (Shick *et al.*, 1979; Shick, 1990; Patterson, 1992b), the extended tentacles, by increasing the polyps' surface-to-volume ratio and exposed surface area, can enhance diffusion rates across the DBL and reduce oxygen limitation during darkness.

Currents considerably reduced the thickness of the diffusive boundary layer, although the DBL remained continuous, surrounding the surfaces of the entire coral. The thickness of the DBL for most small metabolically important molecules and ions is very similar (Patterson, 1992b). Therefore, the effect of currents on the oxygen DBL should be analogous to their effect on the DBLs of other small molecules such as  $\text{CO}_2$  and  $\text{Ca}^{++}$ . In stony corals, diffusion rates of  $\text{CO}_2$ ,  $\text{O}_2$  and  $\text{Ca}^{++}$  have been postulated to limit photosynthesis, respiration, and calcification, respectively (Kanwisher and Wainwright, 1967; Weis *et al.*, 1989). The flux rates of oxygen and other solutes through the boundary layer can be expressed by the steepness of their concentration gradients. Higher current velocities allow more rapid solute exchange through the thinner diffusive boundary layer, probably supporting higher rates of respiration, photosynthesis, calcification, and overall growth (Jokiel, 1978; Dennison and Barnes, 1988; Patterson and Sebens, 1989).

The boundary layers can affect other organisms living within the coral head (Vogel, 1981; Atkinson, 1992). Eukaryotic endolithic algae found in stony corals survive by maintaining an overall low metabolic rate and utilizing enzymes such as catalase and carbonic anhydrase (Shashar and Stambler, 1992). Boring macroorganisms may avoid severe fluctuations in oxygen concentration by creating strong microcurrents that can alter the boundary layer in the vicinity of the boring animal. Microcurrents of 1.9–4.0 cm/s have been measured at the exhalant siphon of the boring bivalve *Lithophaga lessepsiana* (Y. Loya and J. R. Strickler, unpublished data). Because *L. lessepsiana* heavily infects the coral *S. pistillata*, these microcurrents may significantly reduce the effect of the boundary layer on both coral and bivalve.

The effect of the boundary layer on the coral and its inhabitants may in turn determine the coral reef community structure. A thick DBL may limit a coral's tolerance to low current areas or to extreme light intensities. In comparing the thickness of DBLs in large-polyped and small-polyped corals, our results sustain Patterson's (1992a) assumption that the thickness of the DBL is pro-

portional to organism size. We predict that small-polyped corals, with thinner diffusive boundary layers, will be more abundant in reef habitats characterized by low currents, whereas large-polyped corals will be more abundant in reef areas of higher turbulence. The community structure and zonation patterns in Eilat support this prediction (Loya and Slobodkin, 1971; Loya, 1972). As examples, the small-polyped coral *Porites lutea* is the primary species at a depth of 30 m, where the water is relatively calm; and the large-polyped *Platygyra lamellina* is most abundant and has the largest colony size at depths less than 3 m, where the water is more turbulent.

Corals grow under various light and flow conditions. This wide range of external conditions combines with specific behavior such as extension of tentacles, secretion of mucus, and creation of local microcurrents to shape the boundary layer surrounding the colony. Further studies of solute transport mechanisms through the DBL in other sessile organisms, as well as more information about the exact reactions of different coral species to diffusion limitations, are needed to increase our understanding of the ways sessile aquatic organisms cope with their extremely fluctuating environment.

#### Acknowledgments

We thank Mr. Offir Tchelet for his invaluable assistance and Dr. T. W. Cronin for his lengthy support. Comments by several referees greatly improved this paper, and we are grateful for them. This research was supported by a fellowship from the Tel Aviv University; by a grant from the Israel Ministry of Science and Technology, and GSF, Munich, Germany; and by the Moshe Shilo Center for Marine Biogeochemistry. N.S. was partly supported by the H. Steinitz Foundation and the Wolf Foundation.

#### Literature Cited

- Aldredge, A. L., and Y. Cohen. 1987. Can microscale chemical patches persist in the sea? Microelectrode study of marine snow, fecal pellets. *Science* 235: 689-691.
- Atkinson, M. J. 1992. Productivity of Enewetak Atoll reef flats predicted from mass transfer relationships. *Continental Shelf Res.* 12(7/8): 799-807.
- Burris, R. H. 1983. Uptake and assimilation of  $^{15}\text{NH}_4$  by a variety of corals. *Mar Biol* 75: 151-155.
- Crossland, C. J., and D. J. Barnes. 1974. The role of metabolic nitrogen in coral calcification. *Mar Biol* 28: 325-332.
- D'Elia, C. F., and C. B. Cook. 1988. Methylamine uptake by zooxanthellae-invertebrate symbioses: insights into host ammonium environment and nutrition. *Limnol Oceanogr* 33(5): 1153-1165.
- Dennison, C. W., and D. J. Barnes. 1988. Effect of water motion on coral photosynthesis and calcification. *J Exp Mar Biol Ecol* 115: 67-77.
- Feder, M. E., and D. T. Booth. 1992. Hypoxic boundary layer surrounding skin-breathing aquatic amphibians: occurrence, consequences and organismal responses. *J Exp Biol* 166: 237-251.
- Gundersen, J. K., and B. B. Jorgensen. 1990. Microstructure of diffusive boundary layers and the oxygen uptake of the sea floor. *Nature* 345: 604-607.
- Jokiel, P. 1978. Effects of water motion on coral reefs. *J Exp Mar Biol Ecol* 33: 87-97.
- Jorgensen, B. B., J. Erez, N. P. Revsbech, and Y. Cohen. 1985. Symbiotic photosynthesis in the planktonic foraminifer *Globigerinoides sacculifer* (Bardy), studied with microelectrodes. *Limnol Oceanogr* 30(6): 1253-1267.
- Jorgensen, B. B., and D. J. Des Marais. 1990. The diffusive boundary layer of sediments: oxygen microgradients over a microbial mat. *Limnol Oceanogr* 35(6): 1343-1355.
- Kanwisher, J., and S. A. Wainwright. 1967. Oxygen balance in some reef corals. *Biol Bull* 133: 378-390.
- Lesser, M. P., and J. M. Shick. 1989. Photoadaptation and defenses against oxygen toxicity in the zooxanthellae from natural populations of symbiotic cnidarians. *J Exp Mar Biol Ecol* 134: 129-141.
- Loya, Y. 1972. Community structure and species diversity of hermatypic corals at Eilat, Red Sea. *Mar Biol* 13: 100-123.
- Loya, Y., and L. B. Slobodkin. 1971. The coral reefs of Eilat (Gulf of Eilat, Red Sea). *Symp Zool Soc Lond* 28: 117-139.
- Matta, J. L., and R. K. Trench. 1991. The enzymatic response of the symbiotic dinoflagellate *Symbiodinium microadriaticum* (Freudenthal) to growth *in vitro* under varied oxygen tensions. *Symbiosis* 11: 31-45.
- Patterson, M. R. 1992a. A mass transfer explanation of metabolic scaling relations in some aquatic invertebrates and algae. *Science* 255: 1421-1423.
- Patterson, M. R. 1992b. A chemical engineering view of cnidarian symbioses. *Am Zool* 32: 566-582.
- Patterson, M. R., and K. P. Sebens. 1989. Forced convection modulates gas exchange in cnidarians. *Proc Natl Acad Sci U S A* 86: 8833-8836.
- Patterson, M. R., K. P. Sebens, and R. R. Olson. 1991. *In situ* measurements of flow effects on primary production and dark respiration in reef corals. *Limnol Oceanogr* 36: 936-948.
- Pinder, A. W., and M. E. Feder. 1990. Effect of boundary layers on cutaneous gas exchange. *J Exp Biol* 154: 67-80.
- Revsbech, N. P., and B. B. Jorgensen. 1976. Microelectrodes: their use in microbial ecology. *Adv Microb Ecol* 9: 293-352.
- Revsbech, N. P., B. B. Jorgensen, T. H. Blackburn, and Y. Cohen. 1983. Microelectrode studies of the photosynthesis and  $\text{O}_2$ ,  $\text{H}_2\text{S}$  and pH profiles of a microbial mat. *Limnol Oceanogr* 28(6): 1062-1074.
- Revsbech, N. P., L. P. Nielsen, P. B. Christensen, and J. Sorensen. 1988. Combined oxygen and nitrous oxide microsensor for denitrification studies. *Appl Environ Microbiol* 54(9): 2245-2249.
- Schiller, C., and G. J. Herndl. 1989. Evidence of enhanced microbial activity in the interstitial space of branched corals: possible implications for coral metabolism. *Coral Reefs* 7: 179-184.
- Shashar, N., and N. Stambler. 1992. Endolithic algae within corals—life at an extreme environment. *J Exp Mar Biol Ecol* 163: 277-286.
- Shick, J. M. 1990. Diffusive limitation and hyperoxic enhancement of oxygen consumption in zooxanthellae, sea anemones, zoanthids and corals. *Biol Bull* 179: 148-158.
- Shick, J. M., and J. A. Dykens. 1985. Oxygen detoxification in algal-invertebrate symbioses from the Great Barrier Reef. *Oecologia* 66: 33-41.
- Shick, J. M., W. I. Brown, E. G. Dolliver, and S. R. Kayar. 1979. Oxygen uptake in sea anemones: effects of expansion, contraction, and exposure to air and the limitation of diffusion. *Physiol Zool* 52(1): 50-62.
- Taras, M. J., A. E. Greenberg, R. D. Hoak, and M. C. Rand. 1971. Pp. 477-481 in *Standard Methods for Examination of Water and Waste Water*. American Public Health Ass.
- Vogel, S. 1981. Pp. 152-153 in *Life in Moving Fluids*. Willard Grant Press. Boston.
- Weiss, V. M., G. J. Smith, and L. Muscatine. 1989. A  $\text{CO}_2$  supply mechanism in zooxanthellae cnidarians: role of carbonic anhydrase. *Mar Biol* 100: 195-202.

## A Reevaluation of the Structure in the Pore Region of Voltage-Activated Cation Channels

JOHN A. SCHETZ\*<sup>1,2</sup> AND PETER A. V. ANDERSON<sup>1,2,3</sup>

<sup>1</sup>The Whitney Laboratory and Departments of <sup>2</sup>Neuroscience and <sup>3</sup>Physiology, University of Florida, St. Augustine, Florida 32086

Members of the Voltage-Sensitive Cation Channel (VSCC) superfamily form highly selective voltage-gated pores in excitable membranes. These pores are thought to be formed from the extracellular loops that interconnect transmembrane segments 5 and 6 in each of the four domains that constitute the channel. Each of these loops is currently modeled as consisting of two short segments, SS1 and SS2, that are linked by a hairpin turn to form an antiparallel structure. In this study, the hypothesized  $\beta$ -turn in the S5-S6 loop of each of 80 domains from the VSCC superfamily (26 different channel isoforms) were identified and located on the basis of their significant local maxima for  $\beta$ -turn propensity ( $P_{\text{beta}}$ ). Significant  $\beta$ -turns were identified in all 80 sequences, but they are shifted, and lie in the region currently defined as the SS2  $\beta$ -strand. This location of the  $\beta$ -turn is incompatible with an antiparallel  $\beta$ -sheet structure of the pore. The region identified here as forming the turn corresponds to the ion selective determinants in the pore, implying that the turn imparts some of the ionic selectivity of each channel.

Voltage-sensitive potassium ( $K^+$ ), sodium ( $Na^+$ ), and calcium ( $Ca^{++}$ ) channels form a superfamily of cation channels (VSCC). In each case, the functional channel is thought to be a tetrameric structure that creates a highly selective, voltage-gated pore. In  $Na^+$  and  $Ca^{++}$  channels, the channel tetramer is formed by four homologous domains (I–IV) in one large protein. In  $K^+$  channels, the functional tetramer is formed from four separate, single domain proteins that are homologous to each of the four domains in  $Na^+$  and  $Ca^{++}$  channels.

The hydrophobicity profile of individual domains in the eel  $Na^+$  channel, the first VSCC cloned (1), suggests

that each domain consists of six separate transmembrane-spanning alpha helices (S1–S6) that are interconnected by extracellular and cytoplasmic loops. Point and cassette mutations have been used to alter the ionic selectivity of different channel types (2, 3, 4). Furthermore, point mutations, photoaffinity labeling, and antibody mapping have been used to identify regions of channels that are sensitive to agents that act at the internal (5) and external surfaces (5–9) of the membrane. In all of these studies, the S5-S6 loop has been identified as a strong candidate for the pore-forming region of the channel (10). Current models of all members of the VSCC family cloned to date portray this region—variously termed the 'p' region (9), the H5 region (2), or the SS1-SS2 region (5, 11, 12)—as consisting of two short, antiparallel structures (SS1 and SS2), linked by a hairpin turn (13, 14, 19), that dip into the lipid membrane to form the lining of the pore. In the case of  $K^+$  channels, the antiparallel structures are thought to be  $\beta$ -strands linked by a  $\beta$ -hairpin turn (13–15).

Tight turns (hairpins,  $\beta$ -turns, reverse turns) within proteins are defined as nonrepetitive pieces of structure that have a particular succession of different backbone dihedral angles ( $\phi$  and  $\psi$ ) around the  $\alpha$ -carbon (16). The influence of a particular amino acid residue within the quartet of amino acids that typically forms a turn structure is more pronounced than that in repetitive structures ( $\alpha$ -helices or  $\beta$ -sheets), where the backbone dihedral angles are the same. For instance, the energy and packing constraint for type II  $\beta$ -turns results in a strong preference for glycine at the third position in the quartet, and proline in position two (16). This positional preference for certain amino acids within the quartet (17), and the preference for hydrophilic amino acids in any position within the turn (18), allows turn structures to be predicted with higher certainties than  $\alpha$ -helices or  $\beta$ -sheets. However, in the eel (19) and rat brain II (13)  $Na^+$  channels, the residues that

Received 21 September 1993; accepted 30 September 1993.

\* Address correspondence to this author at The Whitney Laboratory, 9505 Ocean Shore Blvd, St. Augustine, FL 32086.

Table 1

Turn probabilities in the S5-S6 pore-forming regions of VSCCs assigned on the basis of significant local maxima for  $P_{\text{bend}}$

Channel/domain	Sequence	$P_{\text{turn}}$	$P_{\text{bend}} \times 10^4$	Source/Tissue
Na <sup>+</sup> /I (bend)	TQDY	1.135	1.890	Squid
	AQDY	1.060	1.316	Uterine
	TQDC	1.148	1.931	Rat heart I, Skm II
	TQDF	1.000	0.981	Fly <i>para</i> , brain I and II
	QDYW	1.135	1.550	Eel, brain III, Skm $\mu$ I
	LDYW	1.038	1.277	<i>Cyanea</i> , fly DCS1
Na <sup>+</sup> /II (turn/bend)	CGEW	1.112	1.629	Fly <i>para</i> and DSC1, squid, eel, brain I, II, III, heart I, Skm I, Skn II, uterine
	CGKW	1.180	1.523	<i>Cyanea</i>
Na <sup>+</sup> /III (bend)	FNGW	1.170	1.554	Uterine
	FKGW	1.033	2.153	Eel, brain I, II & III, heart I, Skm I, Skm II
	FEGW	0.965	1.123	Fly DSC1, squid
	LEGW	0.962	1.161	<i>Cyanea</i>
Na <sup>+</sup> /IV (turn/bend)	SAGW	1.152	2.894	Fly <i>para</i> and DSC1, brain I, II & III, Skm I, heart I, eel, squid
	STGW	1.228	4.112	Skm II
	AAGW	0.960	1.447	<i>Cyanea</i>
	FAGW	0.945	1.423	Uterine
Ca <sup>++</sup> /I (bend)	MEGW	0.965	1.295	Rabbit brain BI, cardiac & skeletal, human $\beta$ -pancreatic, rat aorta
	TESW	1.023	1.077	Carp
Ca <sup>++</sup> /II (turn/bend)	GEDW	1.180	1.829	Rabbit brain BI, cardiac & skeletal, human $\beta$ -pancreatic, rat aorta
	GEEW	1.000	0.787	Carp
Ca <sup>++</sup> /III (bend)	FEGW	0.965	1.123	Rabbit cardiac & skeletal, human $\beta$ -pancreatic, carp, rat aorta
	GEGW	1.205	1.942	Brain BI
Ca <sup>++</sup> /IV (turn/bend)	CATG	1.092	1.119	Rabbit cardiac & skeletal, human $\beta$ -pancreatic, rat aorta
	SATG	1.153	0.901	Rabbit brain BI
	ATGE	0.980	0.788	Carp
K <sup>+</sup> (turn/bend)	GYGD	1.430	1.020	<i>Shaker</i> A and B, DRK1, RCK1, RCK4, mbk1, <i>Shaw</i> , <i>Shah</i>

Amino acid tetrapeptide sequences are written with the 1-letter amino acid code. Residue in the stippled regions corresponds to the region previously defined as SS2. Residues in bold are predicted to form a turn on the basis of both a high  $P_{\text{turn}}$  and a high  $P_{\text{bend}}$ .

Turn regions were predicted by the method of Chou and Fasman (17). Two software routines, PC-Gene (Intelligenetics) and MSeq (University of Michigan), were used to calculate  $P_{\text{turn}}$  and  $P_{\text{bend}}$  for each sequence of four consecutive amino acids within the S5-S6 loops from a total of 80 ion channel domains (12 Na<sup>+</sup>, 6 Ca<sup>++</sup> and 8 K<sup>+</sup> channels). Turns are represented here as amino acid quartets, but the position of the turn in some isoforms is shifted one residue. To reflect these shifts in the position of the turn, in Table III, the consensus motifs of Na<sup>+</sup> channel domain I and Ca<sup>++</sup> channel domain VI are represented as five spaces instead of the four that constitute the turn. Sequence information used for this analysis is available in the cited literature or in Genbank.

are predicted to form the turn between SS1 and SS2 include leucine, isoleucine, and valine—the least likely amino acids to be found in a turn region (17, 18, 20). This raises concerns as to the validity of assigning a turn to this location. In the case of K<sup>+</sup> channels, one model (14) has the proposed turn consisting of only three amino acids, and another (15) locates the turn further towards the N-terminal of the protein to

accommodate the antiparallel  $\beta$ -sheet model. In the first case, the assignment of a turn is suspect, because three amino acid turns, unless they are described as G1  $\beta$ -bulges, constitute gamma tight turns, which are very rare (16). In the second model, the amino acids involved (TMTT) are not predicted to be turns by any standard criteria, including those of Chou and Fasman (17).

Turns exert a major influence on the three-dimensional structure of a protein (16), and if the S5-S6 loop forms the pore of the channel and is a major determinant of ion selectivity and pharmacology, the geometry of this loop, and specifically the location of any turns within it, must be identified. Only then can the structure and function of this important class of proteins be correlated. The questionable assignment of  $\beta$ -hairpin turns to their current positions in the linker between the proposed SS1 and SS2 segments prompted us to search for probable turn sequences within the pore region.

An initial search for  $\beta$ -turns—regions with a significant local maximum ( $P_{\text{bend}}$ ) and a significant  $P_{\text{turn}}$  (17)—revealed that 61% of the 80 pore-forming regions examined contain a clearly significant (assignable) turn. The additional 39% contain a significant turn probability based on  $P_{\text{bend}}$  alone. Almost all the residues within these putative turns (89%) occur in what is currently defined as the SS2  $\beta$ -sheet (Table I). This trend is illustrated in Figure 1, which plots  $P_{\text{bend}}$  for each quartet of amino acids in S5-S6 loops from (a) a  $\text{Na}^+$  channel (Rat Brain II, domain IV), (b) a  $\text{Ca}^{++}$  channel (rabbit skeletal muscle, domain II), and (c) a Shaker  $\text{K}^+$  channel. One hundred percent of the amino acids in the quartets that constitute the assigned turns in domains III and IV of the 12  $\text{Na}^+$  channels examined and 100% of the residues assigned as turns in domains I, II, and III of the 8  $\text{Ca}^{++}$  channels are found in SS2 (Table II). In domains I and II of  $\text{Na}^+$  channels

respectively, 85% and 75% of the residues assigned to the turn occurred in SS2 (Table II). One hundred percent of the amino acids in turn quartets in the 8  $\text{K}^+$  channels examined occurred in SS2 (Table II). The only assigned turn that clearly does not occur in what is currently defined as SS2 is in domain IV of  $\text{Ca}^{++}$  channels (Table II).

Despite low interfamilial sequence identity, the amino acids that form the hairpin turns are remarkably conserved across the VSCC superfamily (Table III). Of the identified tetrapeptide turns, 81% include a glycine (G); and of the 13 amino acid quartets that lack a glycine, 12 occur in domain I of  $\text{Na}^+$  channels. Furthermore, 64% of the assigned turns have a tryptophan (W) in the fourth position and a glycine (G) elsewhere in the tetrapeptide.

The methods used in this study clearly identify regions of high turn probability (significant  $P_{\text{bend}}$ ) in 100% of the S5-S6 loops examined. With the exception of domain IV of  $\text{Ca}^{++}$  channels, the tight turns we identified were all shifted, relative to other models (14, 15) by about 2–5 residues (Fig. 1, Table I) toward the C-terminal. The other obvious structural feature revealed by this study is that turns within these loops are often (55%) characterized by a glycine (G) at position 3 in the quartet, and frequently (70%) by a tryptophan (W) at position 4.  $\text{K}^+$  channel turns are an exception in that they contain no tryptophans and the four amino acids that form the turn are absolutely conserved (Table I).

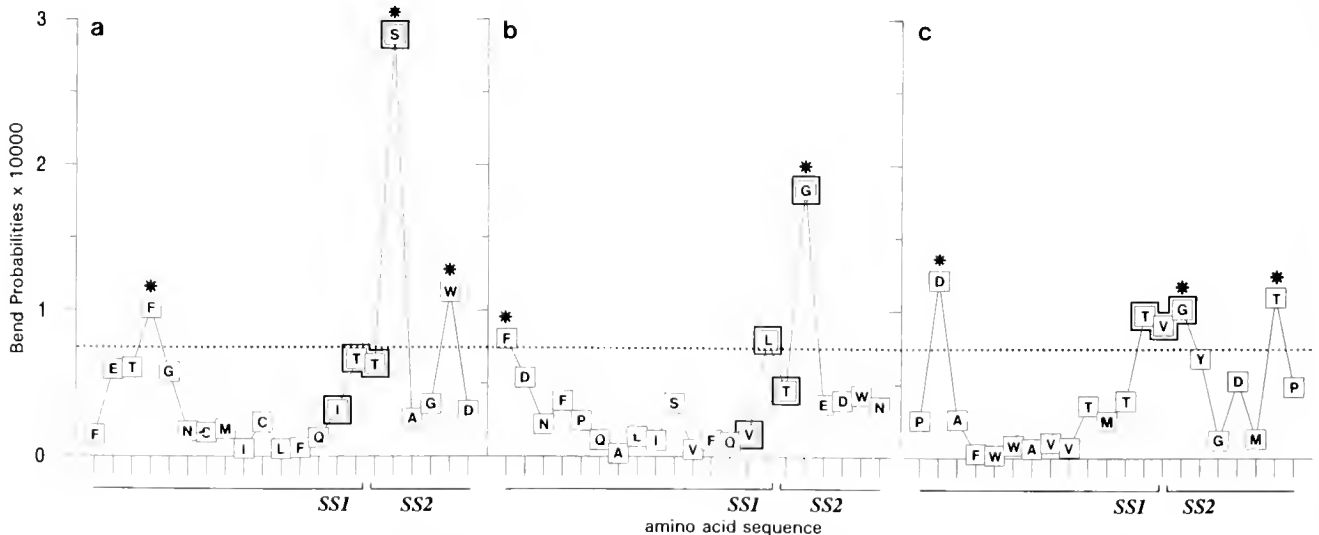


**Figure 1.** Turn probabilities ( $P_{\text{bend}}$ ) for amino acid quartets within the S5-S6 loops of representative domains from VSCCs, as predicted by the method of Chou and Fasman (17). (a) Rat Brain II  $\text{Na}^+$  channel domain IV, (b) rabbit skeletal muscle  $\text{Ca}^{++}$  channel domain II, and (c) Shaker A  $\text{K}^+$  channel monomer. Amino acids are depicted as squares labeled with the single-letter amino acid code. Asterisks denote the first amino acid in the quartet with a significant  $P_{\text{bend}}$  and a significant  $P_{\text{turn}}$ . The boxes around the amino acids that form the  $\beta$ -hairpin turns in current models (13) have double outlines. SS1-SS2 regions are drawn such that the end of SS1 and the beginning of SS2 are centered on the previously proposed " $\beta$ -hairpin" turn. The dotted line indicates the significance level for  $P_{\text{bend}}$ .

Table II

Percentage of residues in identified turns that occur in SS2

	Domain				Total
	I	II	III	IV	
12 Na <sup>+</sup> channel isoforms (coelenterate ≥ primate)	85% (48)	75% (48)	100% (48)	100% (48)	90% (192)
6 Ca <sup>++</sup> channel isoforms (fish ≥ mammal)	100% (24)	100% (24)	100% (24)	29% (24)	82% (96)
8 K <sup>+</sup> channel isoforms (insect ≥ primate)	100% (32)				100% (32)

The numbers in each block correspond to a percentage derived from the number of occurrences divided by the total number possible. The numbers in parentheses are the total number possible.

This shift in the position of the tight turn in the S5-S6 loop has major implications for the presumed structure of this region of the channel. If the turn region is shifted towards the C-terminal of the S5-S6 loop, then the SS1  $\beta$ -sheet would be slightly longer than currently envisaged, and the region previously defined as the SS2  $\beta$ -strand would consist of only a few amino acids or, in the case of K<sup>+</sup> channels, there would be no SS2 region (no second  $\beta$ -strand). More important, since SS2 is actually a turn region and not a  $\beta$ -strand, the SS1-SS2 loop could not form the antiparallel  $\beta$ -sheet motif that is so conceptually attractive for modeling the lining of the pore.

Although our analyses provide no information as to whether a lengthened SS1 region forms an  $\alpha$ -helix,  $\beta$ -sheet, or random coil, the extended SS1 region would be long enough to reach to the cytoplasmic surface of the membrane but, in the case of K<sup>+</sup> channels, not long enough to return to the extracellular surface. Thus, we view the pore-forming regions as loops dipping into the membrane for only a short distance, with the remainder of the pore

being formed by residues projecting from the inner surface of the protein.

This model does not immediately reconcile our results with those obtained from experiments designed to locate the internal (5) and external (21) TEA binding sites on K<sup>+</sup> channels. Two residues on the Shaker A K<sup>+</sup> channel, T441 (internal) and T449 (external), are particularly critical for internal and external TEA binding, respectively. However, internal (and external) TEA block is only weakly voltage-dependent, implying that the residues involved in TEA binding are located close to the internal and external ends of the membrane potential gradient, *i.e.*, close to the internal and external surfaces of the membrane. This finding was interpreted as indicating that the intervening segment of amino acids (SS2) must exist as a  $\beta$ -sheet because an  $\alpha$ -helix composed of eight amino acids would not span the required width of the membrane potential gradient. The presence of a turn between T441 (internal site) and T449 (external site) further reduces the distance between them, suggesting that the internal site would have to be further into the voltage gradient of the pore than the voltage dependency of TEA block would indicate. However, internal TEA binds only to channels in their open configuration (22). The precise location and accessibility of T441 in the closed configuration of the channel is unknown, but T441 may translocate to a more cytoplasmic location, consistent with the electrophysiological data, once the conformational change that opens the channel has occurred. Studies of VSCC conformational changes following channel opening suggest that voltage-independent conformational changes occur in both potassium (23) and sodium channels (24), and that these conformational shifts can be quite large (*i.e.*, 1300 Å<sup>3</sup> and 40–60 Å<sup>3</sup>, respectively).

The structure proposed here is consistent with the results of mutational experiments (2, 3, 4, 12) which imply that residues in the S5-S6 loop are determinants of ion selectivity and several aspects of the pharmacology of the

Table III

Conservation of amino acids in the putative tetrapeptide turn regions

	Domain				Total
	I	II	III	IV	
12 Na <sup>+</sup> channel isoforms	25%	75%	50%	50%	50%
Strict consensus motif	--D--	CG-W	--GW	--GW	
Loose consensus motif	-qD-w	CGkW	f-GW	-aGW	
6 Ca <sup>++</sup> channel isoforms	50%	75%	75%	75%	69%
Strict consensus motif	-E-W	GE-W	-EGW	-ATG	
Loose consensus motif	-EgW	GEdW	fEGW	-ATGE	
8 K <sup>+</sup> channel isoforms	100%				100%
Strict consensus motif	GYGD				

The lower case amino acids in the loose consensus motif are conserved in all but one of the isoforms from each family tested (see Table I).



different channels (6–9, 25–30). Further support for these arguments comes from an examination of cyclic nucleotide-gated channels. These nonselective cation channels have no clearly assignable turns in their putative pore-forming regions (data not shown). Cyclic nucleotide-gated channels differ notably from voltage-activated K<sup>+</sup> channels in that they bear a two-amino-acid deletion in an otherwise highly conserved pore-forming region (31). This deletion, which has been identified as the basis for the lack of ion selectivity of cyclic nucleotide-gated channels (31), actually occurs in the region we have identified as a turn in K<sup>+</sup> channels, implying that ion selectivity is conferred by some aspect of the turn.

### Acknowledgments

Supported by NIMH training grant #MH15737, NSF grant 9109155, and the American Heart Association, Florida affiliate. We thank Drs. H. Robert Guy, Christopher Miller, and Robert M. Greenberg for helpful comments and discussions.

### Literature Cited

- Noda, M., S. Shimizu, T. Tanabe, T. Takai, T. Kayano, T. Ikeda, T. Hideo, H. Nakayama, Y. Kanaoka, N. Minamino, K. Kangawa, H. Matsuo, M. Raftery, T. Hirose, S. Inayama, H. Hayashida, T. Miyata, and S. Numa. 1984. Primary structure of *Electrophorus electricus* sodium channel deduced from cDNA sequence. *Nature* **312**: 121–127.
- Yool, A. J., and T. L. Schwartz. 1991. Alteration of ionic selectivity of a K<sup>+</sup> channel by mutation of the H5 region. *Nature* **349**: 700–704.
- Heinemann, S. H., H. Terlau, W. Stühmer, K. Imoto, and S. Numa. 1991. Calcium channel characteristics conferred on the sodium channel by single mutations. *Nature* **356**: 441–443.
- Tang, S., G. Mikala, A. Bahinski, A. Yatani, and T. L. Schwartz. 1993. Molecular localization of ion selectivity sites within the pore of a human L-type cardiac calcium channel. *J. Biol. Chem.* **268**: 13026–13029.
- Yellen, G., M. Jurman, T. Abramson, and R. MacKinnon. 1991. Mutations affecting internal TEA blockade identify the probable pore-forming region of a K<sup>+</sup> channel. *Science* **251**: 939–942.
- Tejedor, F. J., and W. A. Catterall. 1988. Site of covalent attachment of alpha-scorpion toxin derivatives in domain I of the sodium channel alpha subunit. *Proc. Natl. Acad. Sci.* **85**: 8742–8746.
- Thomsen, W. J., and W. A. Catterall. 1989. Localization of the receptor site for alpha-scorpion toxins by antibody mapping: implications for sodium channel topology. *Proc. Natl. Acad. Sci.* **86**: 10161–10165.
- MacKinnon, R., and C. Miller. 1989. Mutant potassium channels with altered binding of charybdotoxin, a pore-blocking peptide-inhibitor. *Science* **245**: 1382–1385.
- MacKinnon, R., L. Heginbotham, and T. Abramson. 1990. Mapping the receptor site for charybdotoxin, a pore-blocking potassium channel inhibitor. *Neuron* **5**: 767–771.
- Stevens, C. F. 1991. Making a submicroscopic hole in one. *Nature* **349**: 657–658.
- Guy, R. H. 1990. Models of voltage- and transmitter-activated membrane channels based on their amino acid sequences. In *Monovalent Cations in Biological Systems*. CRC Press, Boca Ration, Florida. 31 pp.
- Hartmann, H. A., G. E. Kirsch, J. A. Drewe, M. Tagliatalata, R. H. Joho, and A. M. Brown. 1991. Exchange of conduction pathways between two related K<sup>+</sup> channels. *Science* **251**: 942–944.
- Guy, R. H., and F. Conti. 1990. Pursuing the structure and function of voltage-gated channels. *Trend Neurosci.* **13**: 201–206.
- Durell, S. R., and R. H. Guy. 1992. Atomic scale structure and functional models of voltage-gated potassium channels. *Biophys. J.* **62**: 238–250.
- Bogusz, S., A. Boxer, and D. D. Busath. 1992. An SS1-SS2  $\beta$ -barrel structure for the voltage-activated potassium channel. *Protein Eng.* **5**: 285–293.
- Richards, J. 1981. The anatomy and taxonomy of protein structure. In *Advances in Protein Chemistry*, C. B. Anfinsen, J. T. Edsall, and F. M. Richards, eds. Academic Press, New York. 167 pp.
- Chou, P., and G. Fasman. 1978. Empirical predictions of protein conformation. *Ann. Rev. Biochem.* **47**: 251–276.
- Rose, G. D. 1978. Prediction of chain turns in globular proteins on a hydrophobic basis. *Nature* **272**: 586–590.
- Guy, R. H., and P. Seetharamulu. 1986. Molecular model of the action potential sodium channel. *Proc. Natl. Acad. Sci.* **83**: 508–512.
- Kuntz, I. D. 1972. Protein folding. *J. Am. Chem. Soc.* **94**: 4009–4012.
- MacKinnon, R., and G. Yellen. 1990. Mutations affecting TEA block and ion permeation in voltage-activated K<sup>+</sup> channels. *Science* **47**: 276–279.
- Armstrong, C. M. 1966. Time course of TEA<sup>+</sup>-induced anomalous rectification in squid giant axons. *J. Gen. Physiol.* **50**: 491–503.
- Bezanilla, F., V. A. Parsegian, and J. Zimmerberg. 1988. Solute inaccessible aqueous volume changes during opening of the potassium channel of the squid axon. *Biophys. J.* **53**: 545a.
- Conti, F. 1986. The relationship between electrophysiological data and thermodynamics of ion channel conformations. P. 3 in *Ion Channels in Neural Membranes*, J. M. Ritchie, R. D. Keynes, and L. Bolis, eds. Alan R. Liss, New York.
- Striessnig, J., H. Glossmann, and W. A. Catterall. 1990. Identification of a phenylalkylamine binding region within the  $\alpha 1$  subunit of skeletal muscle Ca<sup>2+</sup> channels. *Proc. Natl. Acad. Sci.* **87**: 9108–9112.
- Striessnig, J., B. J. Murphy, and W. A. Catterall. 1991. Dihydropyridine receptor of L-type Ca<sup>2+</sup> channels: identification of binding domains for [<sup>3</sup>H](+)-PN200-110 and [<sup>3</sup>H]jazidopine within the  $\alpha 1$  subunit. *Proc. Natl. Acad. Sci.* **88**: 10769–10773.
- Terlau, H., S. H. Heinemann, W. Stühmer, M. Pusch, F. Conti, K. Imoto, and S. Numa. 1991. Mapping the site of block by tetrodotoxin and saxitoxin of sodium channel II. *Fed. Eur. Biophys. Soc.* **293**: 93–96.
- Pusch, M., M. Noda, W. Stühmer, S. Numa, and F. Conti. 1991. Single point mutations of the sodium channel drastically reduce the pore permeability without preventing its gating. *Eur. Biophys. J.* **20**: 127–133.
- Satin, J., J. W. Kyle, M. Chen, P. Bell, L. Cribbs, H. A. Fozzard, and R. B. Rogart. 1992. A mutant of TTX-resistant cardiac sodium channels with TTX-sensitive properties. *Science* **256**: 1202–1205.
- Backx, P. H., D. T. Yue, J. H. Lawrence, E. Marban, and G. F. Tomaselli. 1992. Molecular localization of an ion-binding site within the pore of mammalian sodium channels. *Science* **257**: 248–250.
- Heginbotham, L., T. Abramson, and R. MacKinnon. 1992. A functional connection between the pores of distantly related ion channels as revealed by mutant K<sup>+</sup> channels. *Science* **258**: 1152–1155.

## INDEX

### A

- A comparative study of reproduction and development in the polychaete family Terebellidae, 153
- A comparative study of static bodies in mysid crustaceans: evolutionary implications of crystallographic characteristics, 393
- A comparison of the tuning properties of chemoreceptor cells in the first and fourth walking legs of female American lobsters, 316
- A light-independent magnetic compass in the leatherback sea turtle, 149
- A novel tegumental gland in the nephropore of the lobster, *Homarus americanus*: a site for the production of chemical signals? 319
- A reevaluation of the structure in the pore region of voltage-activated cation channels, 462
- ABBAS, RASHI A., see Shien-Fong Lin, 300
- ABRAHAM, VIVEK C., ANDREW L. MILLER, LIONEL F. JAFFE, AND RICHARD A. FLUCK, Cytoplasmic microtubule arrays in *Oryzias latipes* (medaka) eggs during ooplasmic segregation, 305
- Abundance of food affects relative size of larval and postlarval structures of a molluscan veliger, 232
- Acrosome, 225
- Activity-dependent inhibition of neurotransmitter release by Brefeldin A, 299
- ADP-ribosylation, 346
- Aggression, 320, 321
- Agonistic encounters in the American lobster, *Homarus americanus*. Do they remember their opponents? 321
- Agonistic interactions, 318
- AHLBORG, NIKLAS, see Peter B. Armstrong, 326
- Alexandrium*, 329
- Algal effects on ammonium, 330
- Amino acids, 316
- Aminolevulinic synthase, 327
- Ammonium concentrations (day/night), 330
- Ampulla of Lorenzini, 312
- An animal resources section and a Marine Models Electronic Record for *The Biological Bulletin*, 333
- ANDERSON, DONALD M., see Bryan S. Judge, 329
- ANDERSON, PETER A. V., see John A. Schetz, 462
- Anodonta*, 262
- Antarctic benthos, 97
- Antho-RFamide immunoreactivity in neuronal synaptic and nonsynaptic vesicles of sea anemones, 109
- Anthopleura elegantissima*, 109
- Aplysia*, 293
- ARANEDA, RICARDO C., AND MICHAEL V. L. BENNETT, Electrical properties of electroreceptor cells isolated from skate ampulla of Lorenzini, 310
- Argopecten*, 42
- ARIANI, A. P., K. J. WITTMANN, AND E. FRANCO, A comparative study of static bodies in mysid crustaceans: evolutionary implications of crystallographic characteristics, 393
- ARMSTRONG, PETER B., PAUL M. SELZER, NIKLAS AHLBORG, KERSTIN MOREHEAD, MELISSA PERREGAUX, PATRICIA KOMUNIECKI, RICHARD KOMUNIECKI, SUBITA SRIMAL, AND PETER J. HOTEZ, Identification and partial characterization of an extracorporeal protease activity secreted by the triclad turbellariid worm, *Bdelloura candida*, 326
- ARMSTRONG, PETER B., see Subita Srimal, 325

- ARP, ALISSA J., see Jaishri G. Menon, 440
- Asteroidea, 56
- Asters in lysates of *Spisula* oocytes observed with a new type of polarized light microscope, 288
- ATEMA, JELLE, see Christy Karavanich, 321; Keith M. Bayha, 316; Liat J. Kaplan, 320; Paul Bushmann, 319; Thomas Breithaupt, 318
- Attachment behavior, 42
- Auricularia larval coeloms, 86
- Axocoel, 86
- AZEVEDO, CARLOS, see Mario Sousa, 215, 225

### B

- Bag cells, 293
- BAJDIK, C. D., see J. P. A. Gardner, 405
- BAKER, SHIRLEY M., AND NORA B. TERWILLIGER, Hemoglobin structure and function in the rat-tailed sea cucumber, *Paracaudina chilensis*, 115
- BALSER, ELIZABETH J., EDWARD E. RUPPERT, AND WILLIAM B. JAECKLE, Ultrastructure of the coeloms of auricularia larvae (Holothuroidea: Echinodermata): evidence for the presence of an axocoel, 86
- BARLOW, R. B., JR., see E. D. Herzog, 307
- Barnacle, 28
- BASIL, JENNIFER, see Liat J. Kaplan, 320
- BAUER, RAYMOND T., AND LIN JUN MIN, Spermatophores and plug substance of the marine shrimp *Trachypenaeus similis* (Crustacea: Decapoda: Penaeidae): formation in the male reproductive tract and disposition in the inseminated female, 174
- BAYHA, KEITH M., RAINER VOIGT, AND JELLE ATEMA, A comparison of the tuning properties of chemoreceptor cells in the first and fourth walking legs of female American lobsters, 316
- BEINER, JOHN M., CHRISTOPHER S. OGILVY, AND ARTHUR B. DUBOIS, Cerebral blood flow and ventral aortic blood pressure response during elevation of intracranial pressure in bluefish (*Pomatomus saltatrix*), 323
- BENNETT, MICHAEL V. L., see Ricardo C. Araneda, 310
- BIERZYCHUDEK, ANNE, CHARLENE D'AVANZO, AND IVAN VALIELA, Effects of macroalgae, night and day, on ammonium profiles in Waquoit Bay, 330
- Biogeography, 393
- Biomagnetism, 300
- Biomechanics, 10
- Biom mineralization, 393
- Bipolar cells, 308
- Birefringence, 288
- Bivalve, 123, 322
- Blood pressure regulation, 323
- Body wall, 440
- BODZNICK, DAVID, The specificity of an adaptive filter that suppresses unwanted reafference in electrosensory neurons of the skate medulla, 312
- BOLS, N. C., see N. Saperas, 186
- Boundary layer, 455
- BRADY, S. T., M. SUGIMORI, P. L. LEOPOLD, J.-W. LIN, D. S. CHU, AND R. LLINÁS, Activity-dependent inhibition of neurotransmitter release by Brefeldin A, 299
- Brain membranes, 346

- BREITHAAPT, THOMAS, AND JELLE ATEMA. Evidence for the use of urine signals in agonistic interactions of the American lobster, 318
- BRICELJ, V. MONICA. see Zaul Garcia-Esquivel, 42
- Brooding behavior, 365
- BRUNING, GRACE, MICHAEL FERKOWICZ, AND NEAL CORNELL. Heme biosynthesis in fish and land vertebrates: enzyme and cDNA comparisons, 327
- Bryozoan, 28
- BUSHMANN, PAUL, AND JELLE ATEMA. A novel tegumental gland in the nephropore of the lobster, *Homarus americanus*: a site for the production of chemical signals? 319

## C

- C-reactive protein, 325
- Ca<sup>++</sup>-imaging, 335
- Ca<sup>2+</sup>-activated K<sup>+</sup> currents, 312
- Ca<sup>2+</sup> current, 312
- Ca<sup>2+</sup> fluxes around pollen grains and pollen tubes of lily: normal development and effects of thermal shock. BAPTA-type buffer microinjections and depletion of boric acid from the medium, 302
- Ca<sup>2+</sup>-induced axome formation in internally dialyzed giant axons of *Loggia pealei*, 292
- Ca<sup>2+</sup> waves, 289
- Calcite, 393
- Calcium, 290, 295, 335
- buffers, 297, 305
  - carbonate, 393
  - diffusion, 297
  - ion flux, 302
  - pulses during the activation of a protostome egg, 289
  - regulation, 293
  - waves, 297
- Calcium-dependent serine protease, 326
- Calcium-induced vesiculation, 292
- CAMERON, J. LANE. see Richard Randolph Olson, 77
- CANDALARIO-MARTINEZ, A., D. M. REED, S. J. PRICHARD, K. E. DOBLE, T. D. LEE, W. LESSER, D. A. PRICE, AND M. J. GREENBERG. SCP-related peptides from bivalve mollusks: identification, tissue distribution, and actions, 428
- Cardioactivity, 428
- Catalase, 328
- Cellulose acetate electrophoresis, 215
- Cerebellar granule cells, 295
- Cerebral blood flow and ventral aortic blood pressure response during elevation of intracranial pressure in bluefish (*Pomatomus saltatrix*), 323
- Chaetopterus*, 289
- CHAPARRO, O. R., R. J. THOMPSON, AND J. E. WARD. *In vivo* observations of larval brooding in the Chilean oyster, *Ostrea chilensis* Philippi, 1845, 365
- CHAPPELL, RICHARD L., AND PAUL GLYNN. Equivalent sine wave frequency for interpretation of responses to frequency-swept sinusoids defined: an algorithm from studies in skate ganglion cells, 308
- Chemical signal, 318, 319
- Chemoreception, 316
- Chemoreceptors, 335
- Chilean oyster, 365
- CHINTALA, MARNITA M., AND VICTOR S. KENNEDY. Reproduction of *Stylochus ellipticus* (Platyhelminthes: Polycladia) in response to temperature, food, and presence or absence of a partner, 373
- CHIVA, M., see N. Saperas, 186
- Chondrichthyes*, 186
- CHU, D. S., see S. T. Brady, 299
- Clam, 428
- Co-activation of antagonistic motoneurons as a mechanism of high-speed hydraulic inflation of prey capture appendages in the pteropod mollusk *Clione limacina*, 240
- Coelom, 56
- COHEN, Y., see N. Shashar, 455

- CORNELL, Neal. see Grace Bruning, 327
- Cortical vesicles, 225
- Crassostrea*, 232, 428
- CRESTI, M., see E. S. Pierson, 302
- Crustacea, 20, 168
- Cuticle, 440
- Cytochalasin B, 197
- Cytochemistry, 225
- Cytoplasmic Ca<sup>2+</sup>, 289
- Cytoplasmic microtubule arrays in *Oryzias latipes* (medaka) eggs during ooplasmic segregation, 305

## D

- D'AVANZO, CHARLENE. see Anne Bierzychudek, 330
- DACEY, JOHN H., see Richard W. Hill, 322
- Defense, 355
- Deposit feeding, 10
- Dermochelys*, 149
- Development, 77, 295
- Dialysis of giant axon, 292
- Dietary protein, 123
- Differential growth and viability, 405
- Differential susceptibility of guanine nucleotide-binding proteins to pertussis toxin-catalyzed ADP-ribosylation in brain membranes of two congeneric fishes, 346
- Dimethylsulfide, 322
- Direct development, 56
- Direct monitoring of intracellular calcium ions in sea anemone tentacles suggests regulation of nematocyst discharge by remote, rare epidermal cells, 335
- Distinct reproductive types of male spider crabs *Libinia emarginata* differ in circulating and synthesizing methyl farnesoate, 168
- DOBLE, K. E., see A. Candelario-Martinez, 428
- DODGE, S. A., see E. D. Herzog, 307
- Dominance, 321
- DOWLING, JOHN E., see Haohua Qian, 312
- DREWES, CHARLES D., AND CHARLES R. FOURTNER. Helical swimming in a freshwater oligochaete, 1
- Drug, 10
- DUBOIS, ARTHUR B., see John M. Beiner, 323
- DUGGINS, DAVID O., see James E. Eckman, 28
- DUTHIE, G. G., see P. J. S. Smith, 293
- Dying cells, 440

## E

- Echinoderm, 77, 115
- ECKBERG, WILLIAM R., ANDREW L. MILLER, LISA G. SHORT, AND LIONEL F. JAFFE. Calcium pulses during the activation of a protostome egg, 289
- ECKMAN, JAMES E., AND DAVID O. DUGGINS. Effects of flow speed on growth of benthic suspension feeders, 28
- Ecology, 393
- Eelgrass, 42
- Effect of dietary protein content on growth of juvenile mussels, *Mytilus trossulus* (Gould 1850), 123
- Effects of flow speed on growth of benthic suspension feeders, 28
- Effects of macroalgae, night and day, on ammonium profiles in Waquoit Bay, 330
- Egg and sperm structure, 197
- Elasmobranch, 186, 312
- Electrical properties of electroreceptor cells isolated from skate ampulla of Lorenzini, 310
- Electron Transport System (ETS) assay, 276
- Electronic *Biological Bulletin*, 333
- Electroreception, 312
- Elevated intracellular calcium, 292
- Elvers, 276
- Embryo, 355

Embryology, 77  
 EMSCHERMANN, PETER, Lime-twig glands: a unique invention of an Antarctic entoproct, 97  
 Endogenous currents during wound healing and regeneration in sabellid fanworms, 303  
 Endoplasmic reticulum, 290  
 Endoscopy, 365  
 Entoprocta, 97  
 EPEL, DAVID, see Barbara Holland Toomey, 355  
 Epidermis, 440  
 Equivalent sine wave frequency for interpretation of responses to frequency-swept sinusoids defined: an algorithm from studies in skate ganglion cells, 308  
*Eupolyommia*, 10  
 Evidence for the use of urine signals in agonistic interactions of the American lobster, 318  
 Extreme diel fluctuations of oxygen in diffusive boundary layers surrounding stony corals, 455  
 Extrusive glands, 97

## F

*Favia fava*, 455  
 Feeding, 232, 240, 248, 417  
 Feeding and digestion, 428  
 FENAUX, L., see R. R. Strathmann, 232  
 FERKOWICZ, MICHAEL, see Grace Bruning, 327  
 Fertilization, 197, 225, 289  
 FISHMAN, HARVEY M., AND JANIS METUZALS, Ca<sup>2+</sup>-induced axome formation in internally dialyzed giant axons of *Logigo pealei*, 292  
 Flow speed, 28  
 Flow velocity induces a switch from active to passive suspension feeding in the porcelain crab *Petrolisthes leptochelae* (Heller), 20  
 FLUCK, RICHARD A., see Vivek C. Abraham, 305  
 Fluorescence imaging of NMDA receptor-activated calcium influx in granule cells in thin cerebellar slices, 295  
 Fluorite, 393  
 FMRFamide and GABA produce functionally opposite effects on prey-capture reactions in the pteropod mollusk *Chione hincma*, 248  
 FORTNER, CHARLES R., see Charles D. Drewes, 1  
 FRANCO, E., see A. P. Ariani, 393  
 Free radicals, 293  
 Frequency-swept sinusoid, 310

## G

G proteins, 346  
 GABA, 248, 305  
 GABA pharmacology, 308  
 GABA responses on retinal bipolar cells, 312  
 GALIONE, A., see A. L. Miller, 290  
 Gametes, 225  
 GARCIA-ESQUIVEL, ZAUL, AND V. MONICA BRICELI, Ontogenetic changes in microhabitat distribution of juvenile bay scallops, *Argopecten irradians irradians* (L.), in eelgrass beds, and their potential significance to early recruitment, 42  
 GARDNER, J. P. A., D. O. F. SKIBINSKI, AND C. D. BAJDIK, Shell growth and viability differences between the marine mussels *Mytilus edulis* (L.), *Mytilus galloprovincialis* (Lmk.), and their hybrids from two sympatric populations in S. W. England, 405  
 GASCOIGNE, LISA, AND ALISTAIR MCVFAN, Postembryonic growth of two peripheral sensory systems in the medicinal leech *Hirudo medicinalis*, 388  
 GENIN, AMATZIA, see Geoff Trager, 20  
 G<sub>1</sub>, 346  
 Glass eels, 276  
 Glutamate decarboxylase (GAD), 305  
 Glycosaminoglycans, 215, 225, 262  
 Glycosaminoglycans in *Anodonta californensis*, a freshwater mussel, 262

GLYNN, PAUL, see Richard L. Chappell, 308  
 G<sub>0</sub>, 346  
 GOVONI, JOHN J., see Edward Pfeiler, 276  
 GREENBERG, M. J., see A. Candelario-Martinez, 428  
 GREENBERG, MICHAEL J., An animal resources section and a Marine Models Electronic Record for *The Biological Bulletin*, 333  
 GRIMMELIKHUIZEN, CORNELIS J. P., see Jane A. Westfall, 109  
 Growth, 28, 232, 373  
 Growth of sensilla, 388  
 Gut motility, 428

## H

Hairpin turn, 462  
 HALANYCH, KENNETH M., Suspension feeding by the lophophore-like apparatus of the pterobranch hemichordate *Rhabdopleura normani*, 417  
 HEDGECOCK, DENNIS, see Frank J. Longo, 197  
 Helical swimming in a freshwater oligochaete, 1  
 Heme biosynthesis in fish and land vertebrates: enzyme and cDNA comparisons, 327  
 Hemichordata, 417  
 Hemoglobin structure and function in the rat-tailed sea cucumber, *Paracaudina chilensis*, 115  
 Hemolymph insulin-like peptides (ILP) titers and the influence of ILP and mammalian insulin on the amino acid incorporation in the mantle collar *in vitro* in *Helisoma* (Mollusca), 140  
 Heparin, 262  
 HEPLER, P. K., see E. S. Pierson, 302  
 HERZOG, E. D., C. L. PASSAGLIA, S. A. DODGE, N. D. LEVINE, AND R. B. BARELOW, JR., *Limulus* vision in the ocean: comparing neural and behavioral thresholds, 307  
 Highly derived coelomic and water-vascular morphogenesis in a starfish with pelagic direct development, 56  
 HILL, RICHARD W., JOHN H. DACFY, JUDITH E. MCDOWELL, AND DALE F. LEAVITT, The impact of feeding by mussels and scallops on production of dimethylsulfide from marine phytoplankton, 322  
 HILL, SUSAN DOUGLAS, ALAN M. SHIPLEY, AND PETER J. S. SMITH, Endogenous currents during wound healing and regeneration in sabellid fanworms, 303  
 Histochemical studies of jelly coat of *Marthasterias glacialis* (Echinodermata, Asteroidea) oocytes, 215  
 Histochemistry, 215  
 Holocephali, 186  
 Holothuroidea, 86, 115  
 HOMOLA, ELLEN, see Amir Sagi, 168  
 HOJEC, PETER J., see Peter B. Armstrong, 326  
 HOVINGH, PETER, AND ALFRED LINKER, Glycosaminoglycans in *Anodonta californensis*, a freshwater mussel, 262  
 Hybrid mussel populations, 405  
*Hydrolagus*, 186

## I

Identification and partial characterization of an extracorporeal protease activity secreted by the triclad turbellariid worm, *Bdellonva candida*, 326  
 Immunogold, 109  
 Immunolocalization, 248  
*In vivo* observations of larval brooding in the Chilean oyster, *Ostrea chilensis* Philippi, 1845, 365  
 Insect, 314  
 Insemination, 174  
 Insulin-like peptides, 140  
 Integument, 440  
 Intracellular Ca<sup>++</sup>, 335  
 Intracranial pressure, 323  
 Invertebrate larvae, 77  
 Ionic currents, 303

## J

- JAECKLE, WILLIAM B., see Elizabeth J. Balsler, 86  
 JAFFE, L. F., see A. L. Miller, 290; E. S. Pierson, 302; David J. Rossi, 295; Vivek C. Abraham, 305; William R. Eckberg, 289  
 JANIES, DANIEL A., AND LARRY R. MCEWARD. Highly derived coelomic and water-vascular morphogenesis in a starfish with pelagic direct development, 56  
 Jelly coat, 215  
 JOHNSON, AMY S., Sag-mediated modulated tension in terebellid tentacles exposed to flow, 10  
 JUDGE, BRYAN S., CHRISTOPHER A. SCHOLIN, AND DONALD M. ANDERSON, RFLP analysis of a fragment of the large-subunit ribosomal RNA gene of globally distributed populations of the toxic dinoflagellate *Alexandrium*, 329  
 JUNEJA, RENU, see Hiroshi Ueno, 305  
 Juvenile scallops, 42

## K

- K<sup>+</sup>, N<sup>+</sup>, Ca<sup>+</sup> channels, 462  
 KAPLAN, LIAT J., COURTNEY LOWRANCE, JENNIFER BASIL, AND JELLE ATEMA, The role of chemical and visual cues in agonistic interactions of the American lobster, 320  
 KARAVANICH, CHRISTY, AND JELLE ATEMA, Agonistic encounters in the American lobster, *Homarus americanus*: Do they remember their opponents? 321  
 KARPLUS, E., see A. L. Miller, 290; David J. Rossi, 295  
 KASINSKY, H. E., see N. Saperas, 186  
 KENNEDY, VICTOR S., see Marnita M. Chintala, 373  
 KINNEY, GREGORY A., see David J. Rossi, 295  
 KOIDE, S. S., see Hiroshi Ueno, 305  
 KOMUNIECKI, PATRICIA, see Peter B. Armstrong, 326  
 KOMUNIECKI, RICHARD, see Peter B. Armstrong, 326  
 KREEGER, D. A., AND C. J. LANGDON, Effect of dietary protein content on growth of juvenile mussels, *Mytilus trossulus* (Gould 1850), 123  
 KULAK, D., see N. Saperas, 186

## L

- LANGDON, C. J., see D. A. Kreeger, 123  
 Larva, 232  
 Larval development (with observations on spawning) of the pencil urchin *Phyllacanthus imperialis*: a new intermediate larval form? 77  
 Laser doppler flowmetry, 323  
 LAUFER, HANS, see Amir Sagi, 168  
 LEAVITT, DALE F., see Richard W. Hill, 322  
 Lectin, 325  
 LEE, T. D., see A. Candelario-Martinez, 428  
 Leech, 388  
 LEMON, WILLIAM C., AND RICHARD B. LEVINE, Role of proprioceptive input during abdominal bending-reflex motor activity in the tobacco hawkmoth *Manduca sexta*, 314  
 Lens, 328  
 LEOPOLD, P. L., see S. T. Brady, 299  
 Leptocephali, 276  
 LESSER, W., see A. Candelario-Martinez, 428  
 LEVINE, N. D., see E. D. Herzog, 307  
 LEVINE, RICHARD B., see William C. Lemon, 314  
*Labinia emarginata*, 168  
 Life history evolution, 153  
 Light adaptation, 310  
 Lime-twig glands: a unique invention of an Antarctic entroproct, 97  
 Limulin and C-reactive protein from the plasma of *Limulus polyphemus* are different proteins, 325  
*Limulus polyphemus*, 307, 325, 326  
*Limulus* vision in the ocean: comparing neural and behavioral thresholds, 307  
 LIN, J.-W., see S. T. Brady, 299

- LIN, SHIEN-FONG, RASHI A. ABBAS, AND JOHN P. WIKSWO, JR., Magnetic localization of the origins of self-sustained oscillation in squid giant axons, 300  
 LINKER, ALFRED, see Peter Hovingh, 262  
 LINÁS, R., see S. T. Brady, 299  
 Lobster, 316, 318, 320, 321  
 Locomotion, 1  
 LOHMANN, CATHERINE M. FITTINGHOFF, see Kenneth J. Lohmann, 149  
 LOHMANN, KENNETH J., AND CATHERINE M. FITTINGHOFF LOHMANN, A light-independent magnetic compass in the leatherback sea turtle, 149  
 LONGO, FRANK J., LORI MATHEWS, AND DENNIS HEDGECOCK, Morphogenesis of maternal and paternal genomes in fertilized oyster eggs (*Crassostrea virginica*): effects of cytochalasin B at different periods during meiotic maturation, 197  
 Lophophore, 417  
 LOWRANCE, COURTNEY, see Liat J. Kaplan, 320  
 LOYA, Y., see N. Shashar, 455  
 Lysosome, 440

## M

- Magnetic localization of the origins of self-sustained oscillation in squid giant axons, 300  
 Magnetic orientation, 149  
 Magnetoreception, 149  
 MAKARENKO, VLADIMIR, Noise modulated persistence of the metastable state in a simulated neural network, 301  
 Male reproductive types, 168  
 Mandibular organ, 168  
 Mantle, 140  
 Marine fish, 327  
 Marine Models Electronic Record, 333  
 MATHEWS, LORI, see Frank J. Longo, 197  
 Mating, 174  
 McDOWELL, JUDITH E., see Richard W. Hill, 322  
 MCEWARD, LARRY R., see Daniel A. Janies, 56  
 MCHUGH, DAMHNAIT, A comparative study of reproduction and development in the polychaete family Terebellidae, 153  
 MCVEAN, ALISTAIR, see Lisa Gascoigne, 388  
 Mechanically induced calcium release from *Xenopus* cell cycle extracts, 290  
 MEI, GUANG, see Rudolf Oldenbourg, 288  
 Meiotic maturation, 197  
 MENON, JAISHRI G., AND ALISSA J. ARP, The integument of the marine echiuran worm *Urechis caupo*, 440  
*Mercenaria*, 428  
 Metabolic rates in early life history stages of elopomorph fishes, 276  
 Metachromatic, 440  
 Metamorphosis, 276  
 Metastability, 301  
 Methyl farnesoate, 168  
 METUZALS, JANIS, see Harvey M. Fishman, 292  
 Microcapsule, 123  
 Microtubules, 305  
 MILLER, A. L., A. GALIONE, E. KARPLUS, AND L. F. JAFFE, Mechanically induced calcium release from *Xenopus* cell cycle extracts, 290  
 MILLER, ANDREW L., see David J. Rossi, 295; Vivek C. Abraham, 305; William R. Eckberg, 289  
 MIN, LIN JUN, see Raymond T. Bauer, 174  
 MIRE-THIBODEAUX, PATRICIA, AND GLEN M. WATSON, Direct monitoring of intracellular calcium ions in sea anemone tentacles suggests regulation of nematocyst discharge by remote, rare epidermal cells, 335  
 Model, 462  
 Modeling the apparent diffusion constant of calcium ions emanating from a channel: implications for calcium wave propagation, 297  
 Mollusca, 140, 240, 248  
 MORADAS-FERREIRA, PEDRO, see Mario Sousa, 215

- MOREHEAD, KERSTIN, see Peter B. Armstrong, 326  
 Morphogenesis of maternal and paternal genomes in fertilized oyster eggs (*Crassostrea virginica*): effects of cytochalasin B at different periods during meiotic maturation, 197  
 Morphotypes, 168  
 Motoneurons, 240, 248  
 Mucus, 440  
 Multidrug resistance, 355  
 Multixenobiotic resistance in *Urechis caupo* embryos: protection from environmental toxins, 355  
 MURRAY, THOMAS F., AND JOSEPH F. SIEBENALLER, Differential susceptibility of guanine nucleotide-binding proteins to pertussis toxin-catalyzed ADP-ribosylation in brain membranes of two congeneric marine fishes, 346  
 Mussel, 123, 262  
 Mysidacea, 393

## N

- Near-UV radiation effects on dogfish (*Mustelus canis*) lens catalase and antioxidant protection, 328  
 Nematocyst discharge, 335  
 Nephropore, 319  
 Neural network, 301  
 Neurobiology, 314  
 Neuronal vesicles, 109  
 Neurotransmitter release, 299  
 Noise modulated persistence of the metastable state in a simulated neural network, 301  
 NORKIAN, TIGRAN P., AND RICHARD A. SATTERLIE, Co-activation of antagonistic motoneurons as a mechanism of high-speed hydraulic inflation of prey capture appendages in the pteropod mollusk *Clione limacina*, 240  
 NORKIAN, TIGRAN P., AND RICHARD A. SATTERLIE, FMRamide and GABA produce functionally opposite effects on prey-capture reactions in the pteropod mollusk *Clione limacina*, 248  
 Nuclei, 186  
 Nutrition, 123

## O

- ODH activity, 42  
 OGILVY, CHRISTOPHER S., see John M. Beiner, 323  
 OLDENBOURG, RUDOLF, GUANG MEI, AND ROBERT E. PALAZZO, Asters in lysates of *Spisula* oocytes observed with a new type of polarized light microscope, 288  
 OLSON, RICHARD RANDOLPH, J. LANE CAMERON, AND CRAIG M. YOUNG, Larval development (with observations on spawning) of the pencil urchin *Phyllacanthus imperialis*: a new intermediate larval form? 77  
 Ommatidium, 307  
 Ontogenetic changes in microhabitat distribution of juvenile bay scallops, *Argopecten irradians irradians* (L.), in eelgrass beds, and their potential significance to early recruitment, 42  
 Oocyte, 215  
 Ooplasmic segregation, 305  
 Optic nerve, 307  
 Orientation, 149  
 Orthochromatic, 440  
 Oscillation, 300  
 Oxygen consumption, 276  
 Oxygen, 197, 455  
 Oyster, 232, 428

## P

- PALAZZO, ROBERT E., see Rudolf Oldenbourg, 288  
 Parasitic flatworm, 326  
 Particle capture, 417  
 PASSAGLIA, C. L., see E. D. Herzog, 307

- Penaeidae, 174  
 Peptide sequence, 428  
 PERREGAUX, MELISSA, see Peter B. Armstrong, 326  
 PFEILER, EDWARD, AND JOHN J. GOVONI, Metabolic rates in early life history stages of elpomorphic fishes, 276  
 Phytoplanktivory, 322  
 PIERSON, E. S., P. J. S. SMITH, A. M. SHIPLEY, L. F. JAFFE, M. CRESTI, AND P. K. HEPLER,  $Ca^{2+}$  fluxes around pollen grains and pollen tubes of lily: normal development and effects of thermal shock, BAPTA-type buffer microinjections and depletion of boric acid from the medium, 302  
 PINTO, RUI, see Mario Sousa, 215  
 Podocytes, 86  
 Polarized light microscope, 288  
 Pollen, 302  
 Polychaeta, 10, 153, 303  
 Polyelad flatworm, 373  
 Pore, 462  
 Postembryonic growth of two peripheral sensory systems in the medicinal leech *Hirudo medicinalis*, 388  
 PRICE, D. A., see A. Candelario-Martinez, 428  
 PRICHARD, S. J., see A. Candelario-Martinez, 428  
 Pronuclear development, 197  
 Protamines, 186  
 Protostome, 289  
 Pterobranch, 417

## Q

- QIAN, HAOHUA, AND JOHN E. DOWLING, GABA responses on retinal bipolar cells, 312  
 QUIGLEY, JAMES P., see Subita Srimal, 325

## R

- RAFFERTY, NANCY S., see Seymour Zigman, 328  
 Ratfish, 186  
 Red tides, 329  
 REED, D. M., see A. Candelario-Martinez, 428  
 Regeneration, 303  
 Reproduction of *Stylochus ellipticus* (Platyhelminthes: Polyeladia) in response to food, temperature, and presence or absence of a partner, 373  
 Retina, 307, 308  
 RFLP analysis of a fragment of the large-subunit ribosomal RNA gene of globally distributed populations of the toxic dinoflagellate *Alexandrium*, 329  
 Role of proprioceptive input during abdominal bending-reflex motor activity in the tobacco hawkmoth *Manduca sexta*, 314  
 ROSSI, DAVID J., GREGORY A. KINNEY, ERIC KARPLUS, ANDREW L. MILLER, LIONEL F. JAFFE, AND N. TRAVERSE SLATER, Fluorescence imaging of NMDA receptor-activated calcium influx in granule cells in thin cerebellar slices, 295  
 Rugae, 440  
 RUPPERT, EDWARD E., see Elizabeth J. Balsler, 86

## S

- Sag-mediated modulated tension in terebellid tentacles exposed to flow, 10  
 SAGI, AMIR, ELLEN HOMOLA, AND HANS LAUFER, Distinct reproductive types of male spider crabs *Libinia emarginata* differ in circulating and synthesizing methyl farnesoate, 168  
 SALEUDDIN, A. S. M., see V. M. Sevala, 140  
 SAPERAS, N., M. CHIVA, N. C. BOLS, D. KULAK, AND H. E. KASINSKY, Sperm-specific basic proteins in the holocephalan fish *Hydrolagus collieri* (Chondrichthyes, Chimaeriformes) and comparison with protamines from an elasmobranch, 186  
 SATTERLIE, RICHARD A., see Tigran P. Norekian, 240, 248

- SCHETZ, JOHN A., AND PETER A. V. ANDERSON, A reevaluation of the structure in the pore region of voltage-activated cation channels, 462
- SCHOLIN, CHRISTOPHER A., see Bryan S. Judge, 329
- SCP-related peptides from bivalve mollusks: identification, tissue distribution, and actions, 428
- Sea anemone, 109, 335
- Sea cucumber, 115
- Sea turtle, 149
- Sea urchin, 335
- Sebastolobus alascanus*, 346
- Sebastolobus altivelis*, 346
- Sediment, 355
- SEGAL, SHELDON J., see Hiroshi Ueno, 305
- Selection, 405
- SELZER, PAUL M., see Peter B. Armstrong, 326
- Sensory cues, 320
- Sensory processing, 312
- Serpulid, 28
- SEVALA, V. L., see V. M. Sevala, 140
- SEVALA, V. M., V. L. SEVALA, AND A. S. M. SALEUDDIN, Hemolymph insulin-like peptides (ILP) titers and the influence of ILP and mammalian insulin on the amino acid incorporation in the mantle collar *in vitro* in *Helisoma* (Mollusca), 140
- SEWELL, A. T., see R. R. Strathmann, 232
- Sex and the single flatworm, 373
- SHASHAR, N., Y. COHEN, AND Y. LOYA, Extreme diel fluctuations of oxygen in diffusive boundary layers surrounding stony corals, 455
- Shell growth, 140, 405
- Shell growth and viability differences between the marine mussels *Mytilus edulis* (L.), *Mytilus galloprovincialis* (Lmk.), and their hybrids from two sympatric populations in S. W. England, 405
- Shell regeneration, 140
- SHIMOMURA, OSAMU, see Hiroshi Ueno, 305
- SHIPLEY, A. M., see E. S. Pierson, 302; P. J. S. Smith, 293; Susan Douglas Hill, 303
- SHORT, LISA G., see William R. Eckberg, 289
- Shrimp, 174
- SIEBENALLER, JOSEPH F., see Thomas F. Murray, 346
- Skate, 312
- Skate retinal ganglion cell, 310
- SKIBINSKI, D. O. F., see J. P. A. Gardner, 405
- SLATER, N. TRAVERSE, see David J. Rossi, 295
- SMITH, P. J. S., G. G. DUTHIE, A. SHIPLEY, AND M. TYTELL, Steady-state calcium efflux from *Aplysia* neurons: perturbation by H<sub>2</sub>O<sub>2</sub> and protection by stress protein, HSP70, 293
- SMITH, P. J. S., see E. S. Pierson, 302; Susan Douglas Hill, 303
- SOUSA, MARIO, AND CARLOS AZEVEDO, Ultrastructural histochemistry of *Marthasterias glacialis* (Echinodermata, Asteroidea) gametes before and after fertilization, 225
- SOUSA, MARIO, RUI PINTO, PEDRO MORADAS-FERREIRA, AND CARLOS AZEVEDO, Histochemical studies of jelly coat of *Marthasterias glacialis* (Echinodermata, Asteroidea) oocytes, 215
- Sperm-specific basic proteins in the holocephalan fish *Hydrolagus collieri* (Chondrichthyes, Chimaeriformes) and comparison with protamines from an elasmobranch, 186
- Spermatophores and plug substance of the marine shrimp *Trachypenaeus similis* (Crustacea: Decapoda: Penaeidae): formation in the male reproductive tract and disposition in the inseminated female, 174
- Spermiogenesis, 186
- Spisula* sperm, 305
- Squid giant axon, 300
- SRIMAL, SUBITA, JAMES P. QUIGLEY, AND PETER B. ARMSTRONG, Limulin and C-reactive protein from the plasma of *Limulus polyphemus* are different proteins, 325
- SRIMAL, SUBITA, see Peter B. Armstrong, 326
- Starfish, 215, 225
- Starvation, 373
- Statoliths, 393
- Stony coral, 455
- STRATHMANN, M. F., see R. R. Strathmann, 232
- STRATHMANN, R. R., L. FENAUX, A. T. SEWELL, AND M. F. STRATHMANN, Abundance of food affects relative size of larval and postlarval structures of a molluscan veliger, 232
- Stress protein, 293
- Stretch receptor, 314
- Stretch-activated channels, 290
- Stylochus ellipticus*, 373
- Stylophora pistillata*, 455
- SUGIMORI, M., see S. T. Brady, 299
- Sulfide oxidizing body, 440
- Superfamily, 462
- Suspension feeding, 10, 20, 28, 417
- Suspension feeding by the lophophore-like apparatus of the pterobranch hemichordate *Rhabdopleura normani*, 417
- Swimming behavior, 1
- Symbiotic bacteria, 405
- Synapse, 109, 299
- Synaptic vesicle recycling, 299

## T

- Tegumental gland, 319
- Temperature, 373
- Terebellidae, 10, 153
- Terwilliger, Nora B., see Shirley M. Baker, 115
- The impact of feeding by mussels and scallops on production of dimethylsulfide from marine phytoplankton, 322
- The integument of the marine echinuran worm *Urechis caupo*, 405
- The presence of the GABA-synthesizing enzyme, glutamate decarboxylase, in *Spisula* sperm, 305
- The role of chemical and visual cues in agonistic interactions of the American lobster, 320
- The specificity of an adaptive filter that suppresses unwanted reafference in electrosensory neurons of the skate medulla, 312
- Thelycum, 174
- THOMPSON, R. J., see O. R. Chaparro, 365
- TOOMEY, BARBARA HOLLAND, AND DAVID EPEL, Multixenobiotic resistance in *Urechis caupo* embryos: protection from environmental toxins, 355
- Toxin, 355
- Trachypenaeus similis*, 174
- TRAGER, GEOFF, AND AMATZIA GENIN, Flow velocity induces a switch from active to passive suspension feeding in the procelarian crab *Petrolisthes leptochelus* (Heller), 20
- TYTELL, M., see P. J. S. Smith, 293

## U

- UENO, HIROSHI, RENU JUNEJA, OSAMU SHIMOMURA, S. S. KOIDE, AND SHELDON J. SEGAL, The presence of the GABA-synthesizing enzyme, glutamate decarboxylase, in *Spisula* sperm, 305
- Ultrastructural histochemistry of *Marthasterias glacialis* (Echinodermata, Asteroidea) gametes before and after fertilization, 225
- Ultrastructure of the coeloms of auricularia larvae (Holothuroidea: Echinodermata): evidence for the presence of an axocoel, 86
- Ultraviolet radiation, 328
- Urchin, 77
- Urechis caupo*, 355, 440

## V

- VALIELA, IVAN, see Anne Bierzychudek, 330
- Vas deferens, 174
- Vaterite, 393
- Veliger, 232
- Vertical distribution, 42

Vertical profiles of ammonium, 330  
Vibrating ion probe, 302  
VOIGT, RAINER, see Keith M. Bayha, 316  
Voltage-gated ion channel, 462

**W**

WANG, SAMUEL S.-H., Modeling the apparent diffusion constant of calcium ions emanating from a channel: implications for calcium wave propagation, 297  
WARD, J. E., see O. R. Chaparro, 365  
Water flow, 20  
Water-vascular system evolution, 56  
WATSON, GLEN M., see Patricia Mire-Thibodeaux, 335

WESTFALL, JANE A., AND CORNELIS J. P. Grimmelikhuijzen, Antho-RFamide immunoreactivity in neuronal synaptic and nonsynaptic vesicles of sea anemones, 109  
WIKSWO, JOHN P., JR., see Shien-Fong Lin, 300  
WITTMANN, K. J., see A. P. Ariani, 393

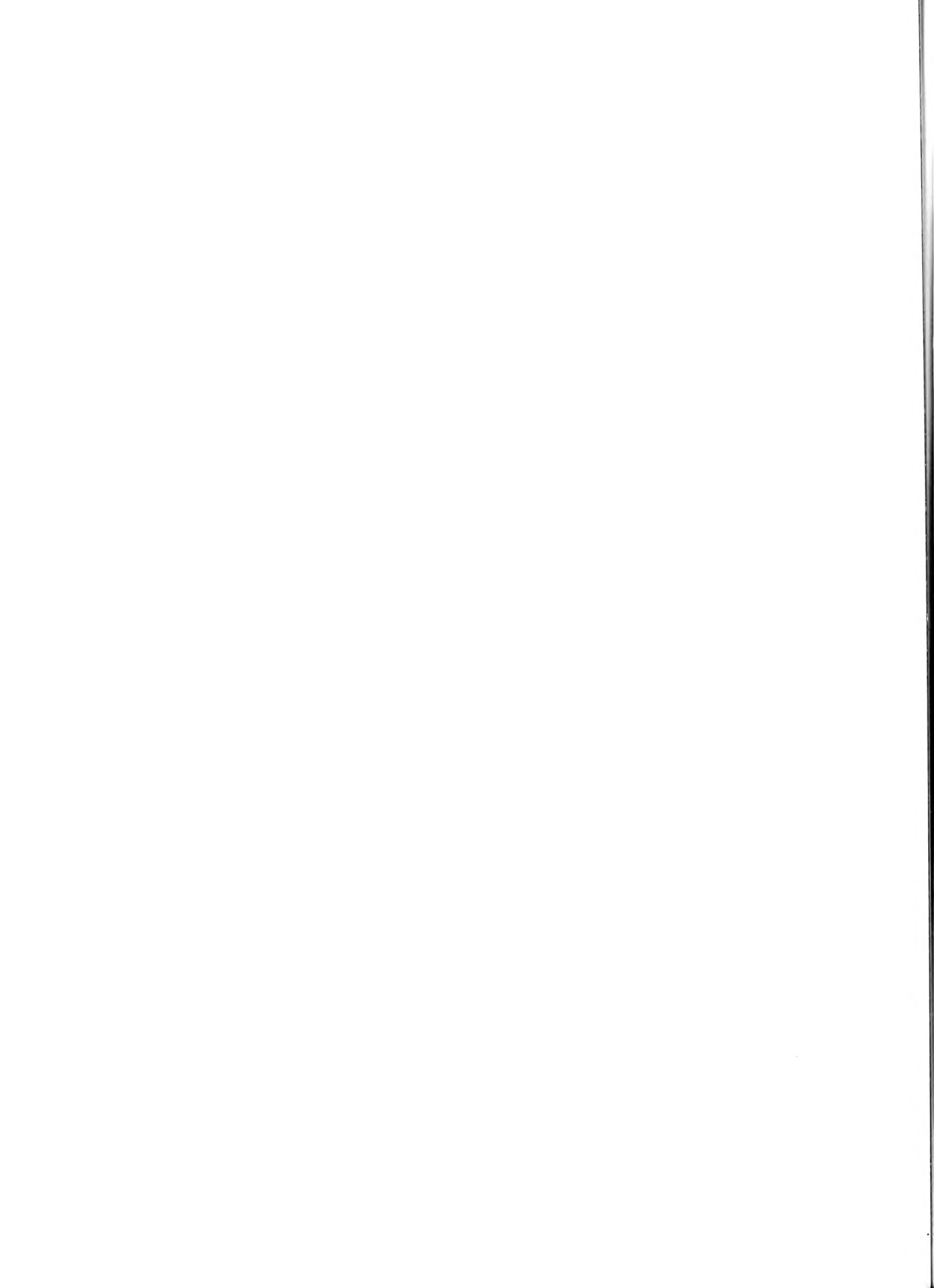
**Y**

YOUNG, CRAIG M., see Richard Randolph Olson, 77

**Z**

ZIGMAN, SEYMOUR, AND NANCY S. RAFFERTY, Near-UV radiation effects on dogfish (*Mustelus canis*) lens catalase and antioxidant protection, 328









2 - 1  
~~525~~ 58

## CONTENTS

### EDITORIAL

- Greenberg, Michael J.**  
An animal resources section and a Marine Models  
Electronic Record for *The Biological Bulletin* . . . . . 333

### CELL BIOLOGY

- Mire-Thibodeaux, Patricia, and Glen M. Watson**  
Direct monitoring of intracellular calcium ions in  
sea anemone tentacles suggests regulation of ne-  
matocyst discharge by remote, rare epidermal cells . . . . . 335
- Murray, Thomas F., and Joseph F. Siebenaller**  
Differential susceptibility of guanine nucleotide-  
binding proteins to pertussis toxin-catalyzed ADP-  
ribosylation in brain membranes of two congeneric  
marine fishes . . . . . 346
- Toomey, Barbara Holland, and David Epel**  
Multixenobiotic resistance in *Urechis caupo* embryos:  
protection from environmental toxins . . . . . 355
- Chaparro, O. R., R. J. Thompson, and J. E. Ward**  
*In vivo* observations of larval brooding in the Chilean  
oyster, *Ostrea chilensis* Philippi, 1845 . . . . . 365
- Chintala, Marnita M., and Victor S. Kennedy**  
Reproduction of *Stylochus ellipticus* (Platyhelminthes:  
Polycladia) in response to temperature, food, and  
presence or absence of a partner . . . . . 373
- Gascoigne, Lisa, and Alistair McVean**  
Postembryonic growth of two peripheral sensory  
systems in the medicinal leech *Hirudo medicinalis* . . . . . 388

### ECOLOGY AND EVOLUTION

- Ariani, A. P., K. J. Wittmann, and E. Franco**  
A comparative study of static bodies in mysid crus-  
taceans: evolutionary implications of crystallo-  
graphic characteristics . . . . . 393

- Gardner, J. P. A., D. O. F. Skibinski, and C. D. Bajdik**  
Shell growth and viability differences between the  
marine mussels *Mytilus edulis* (L.), *Mytilus gallopro-  
vincialis* (Lmk.), and their hybrids from two sym-  
patric populations in S.W. England . . . . . 401
- Halanych, Kenneth M.**  
Suspension feeding by the lophophore-like appa-  
ratus of the pterobranch hemichordate *Rhabdo-  
pleura normani* . . . . . 411

### NEUROBIOLOGY AND BEHAVIOR

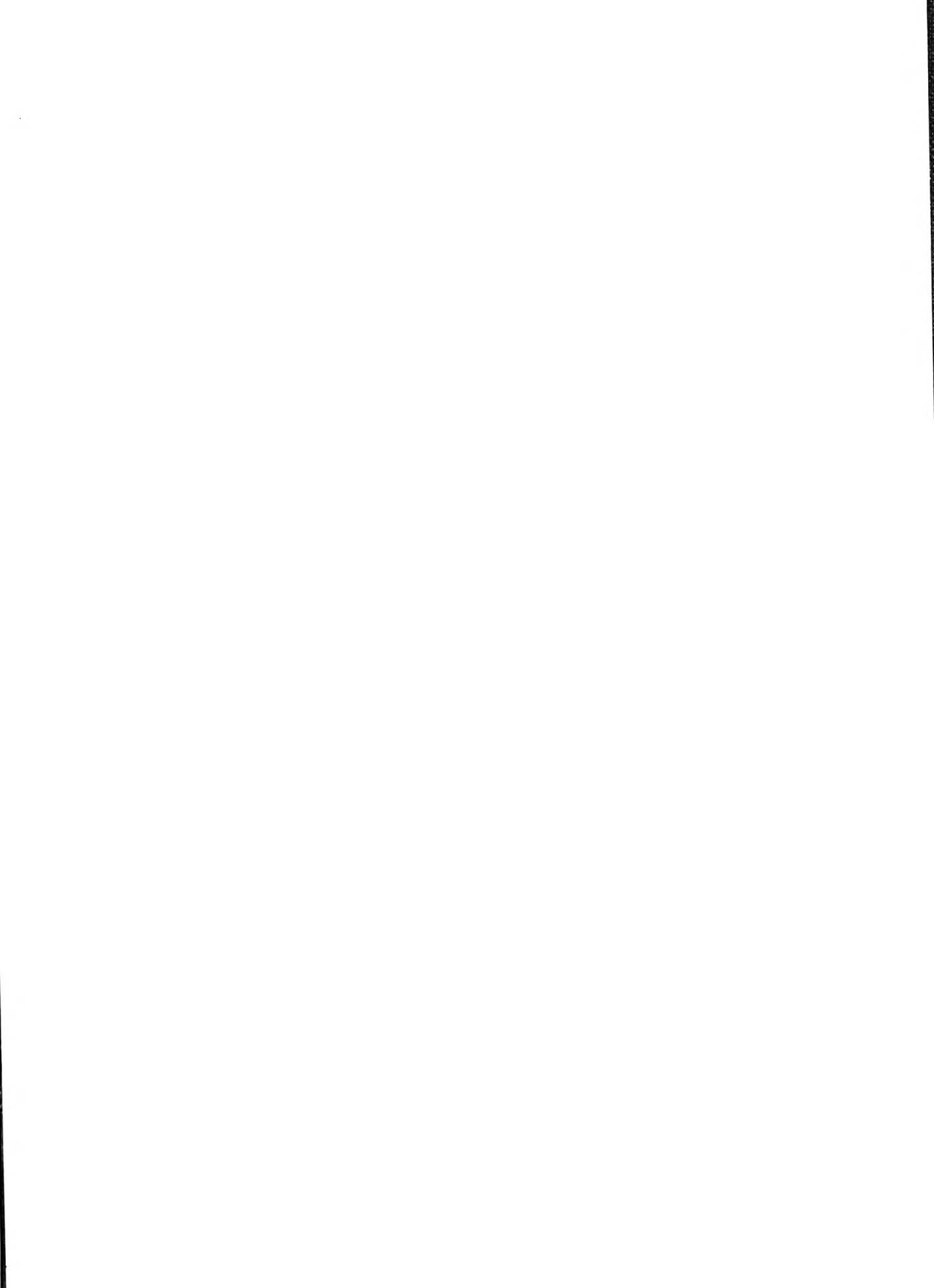
- Candelario-Martinez, A., D. M. Reed, S. J. Prichard,  
K. E. Doble, T. D. Lee, W. Lesser, D. A. Price, and  
M. J. Greenberg**  
SCP-related peptides from bivalve mollusks: iden-  
tification, tissue distribution, and actions . . . . . 421

### PHYSIOLOGY

- Menon, Jaishri G., and Alissa J. Arp**  
The integument of the marine echiuran worm  
*Urechis caupo* . . . . . 441
- Shashar, N., Y. Cohen, and Y. Loya**  
Extreme diel fluctuations of oxygen in diffusive  
boundary layers surrounding stony corals . . . . . 451

### RESEARCH NOTE

- Schetz, John A., and Peter A. V. Anderson**  
A reevaluation of the structure in the pore region  
of voltage-activated cation channels . . . . . 461
- Index to Volume 185 . . . . . 461





MBL WHOI LIBRARY



WH 1B2P 2



